Planar Formulas and Microscopic Asymptotics for Derivative Moments of Haar Unitary Characteristic Polynomials

Complete cumulative edition: finite-rank evaluation, asymptotic regimes, and connected zero geometry

Jeremy Rodgers

The Everything Equation · Reserved DOI: 10.5281/zenodo.24451371

22 November 2026 · Cumulative edition with signed depth-one windows

Abstract

We study mixed moments of logarithmic derivatives and characteristic polynomials of Haar unitary matrices at independent complex exponents. A planar Toeplitz determinant, radial Mellin readout, and physical branch connections relate finite-rank formulas to fixed-interior, microscopic, and circle limits. This complete cumulative edition retains the full 25-section foundation and integrates twelve subsequent constructions. At ranks three through eight, finite exact-arithmetic absolute approximations now cover the full radius interval $0 \le z \le 0.9$ on the original independent complex order and tilt box. Effective Bessel remainders, complete signed populations, balanced tails, and separately priced preparation, image, and arithmetic returns establish the joins. Actual finite-arithmetic certificates remain distinct from the common formulas and do not assert uniform relative accuracy or bounded runtime.

A configurable physical-source arithmetic construction and targeted source/image refinements certify difficult near-zero scalar readouts. For rank eight, correlated original-Haar majorants, coherent analytic terminal projection, and phase-aware parameter enclosures give one connected simple-zero branch for $|h| \le 0.20$ and $0.899 \le z \le 0.9$. In the moving predictor tube the uniqueness radius is 0.012, the zero lies within radius 0.01, and $T_8 = (s-\alpha)G$ with $|G| > 1/1300$. The stronger inner theorem on $|h| \le 0.18$ has uniqueness radius 0.006, zero radius 0.004537, and factor 1/625. Proofs, exact predictor data, numerical evidence, failed controls, and remaining obligations are presented with their individual domains. Earlier asymptotic and full-state results retain their original hypotheses and attribution.

The quantitative continuation joins the complex scalar from the exact circle through positive microscopic depths to the interior Gaussian comparison at the actual radius. The small-depth error separates a power of depth from a negative power of log rank. At larger depths a radius-corrected approximation has uniform normalized error of order N^{-1} times a power of $1 + \log N$. Retaining the finite-rank one-angle term gives an additive rate through the upper moment threshold. A direct absolute-refinement theorem covers ordinary finite ranks, with an executed rank-two quadrature on independent complex inputs.

The microscopic certification continuation gives computable Fourier-tail estimates for independent complex tilt on arbitrary compact positive-depth and tilt sets. It implements a complete Mellin budget and validates alternative coefficient enclosures, including nonreal and inverse-order controls. The general bound has large numerical constants, and the executions distinguish direct quadrature, near-integer reductions and large-depth comparisons.

At depth one, an effective rank comparison and a shifted positive Gram estimate now give usable Fourier budgets at small cutoffs for an independent complex fractional order. A validated contour Hankel quadrature closes a nonzero scalar enclosure at that tuple. Explicit singular-value deficit estimates also price higher accuracy tails, at cutoffs exceeding the present retained-integral calculation.

At $c = 1$, $h = 1/2 + i/8$, $s = 1/2 + i/20$, signed frequency windows and measured Bessel averages of the matched positive Haar law give an absolute disk of radius below 0.000263563 for the independent complex coefficient, with $|F| > 0.51513048$. The claim map following the contents traces the complete disk, the connected asymptotic theorem, finite-rank refinement, and the conditional zeta prediction to their mathematical and numerical inputs.

Contents

Proof and certification map **4**

1. Fixed-size mixed moments and their domains **8**

2. Large-source decay of the Toeplitz determinant **9**

3. Radial stationary phase and the transition at the centre **11**

4. Exact low-rank thresholds **33**

5. Fourier inversion and the radial finite part **44**

6. The rank-two diagonal from its trace distribution **94**

7. The rank-two differential equation from the planar determinant **98**

8. A fixed-point recurrence for the rank-two diagonal moment **100**

9. A trace-moment recurrence at every fixed rank **103**

10. Equations away from the centre **109**

11. The large-matrix limit on compact subsets of the disk **148**

12. The first microscopic correction for mixed integer moments **151**

13. The local projection for an integer tilt **152**

14. Positive moments under the circular Jacobi change of measure **154**

15. Sharp microscopic moments at positive depth **156**

16. Finite-size expansions at positive microscopic depth **163**

17. The unit-circle determinant and its mixed moment **172**

18. The transition to Gaussian moments at growing depth **175**

19. The approach to the circle at shrinking depth **178**

20. Determinant derivatives and a finite-rank error bound **276**

21. Certified values for independent parameters **278**

22. Verification and limits of the results **386**

23. Scalar recovery through intersecting resonances **449**

24. Full variable-order transport through the rank-four wall **466**

25. Noninteger moments across consecutive critical radii **477**

References **485**

Current coverage and reading guide

The object throughout is the ordinary, unnormalized moment

$$T_N(h,s;z)=\mathbb{E}\{|S_N(z)|^{2h}|\Lambda_N(z)|^{2s}\},\qquad S_N(z)=-(1-z^2)\frac{\Lambda_N'(z)}{\Lambda_N(z)}.$$

The independent complex parameter box is

$$-19/20\le \Re h\le 3,\qquad |\Im h|\le 3,\qquad |s|\le 3.$$

Ordinary integrability restrictions at the lower ranks and exceptional inputs remain part of the definition. Analytic continuation is not silently identified with an ordinary moment.

Subject	Current domain	Strongest integrated conclusion
Rank three	$0\le z\le .9$, full independent box	Connected finite exact-arithmetic absolute approximations. The joined maximum bound is $1.955759\,10^{-17}$. The upper-radius component alone has bound $3.501607\,10^{-19}$; common grids are specified but unexecuted.
Ranks four–eight	$0\le z\le .9$, full independent box	New small-radius constructions on $[0,.025]$ join the inherited $[.02,.9]$ constructions on a positive-width overlap. Errors remain rank- and chart-specific; the rank-six small-radius bound is $7.960261698533\,10^{-15}$.
Finite arithmetic	Admitted exact inputs and source origins	The physical source, preparation, Mellin image, terminal and final scalar are priced separately. Adaptive dyadic source regeneration and image refinement give actual pointwise relative certificates where the modulus test passes.
Outer zero branch	$N=8$, $\|h\|\le .20$, $.899\le z\le .9$	One simple zero in $\|s-c(h,z)\|<.012$, with $\|\alpha-c\|<.01$ and $\|G\|>1/1300$ on the admitted tube.
Stronger inner branch	$N=8$, $\|h\|\le .18$, same real-radius interval	Uniqueness radius .006, zero radius .004537, and $\|G\|>1/625$. Earlier smaller charts retain their stronger bounds only on their own domains.
Asymptotic regimes	Fixed interior, fixed positive microscopic depth, growing depth, shrinking depth and circle	Complete inherited arguments, normalizations and qualifications are retained. The continuation certificates do not constitute a new independent audit of every all-order or simultaneous-limit argument.
All-rank ODE readout	$N\ge 3$, regular $0<z<1$ off (10.9), $\Re h>-1$, $s\in\mathbb{C}$	Theorem 23.1A proves global polynomiality of the canonical extreme-row scalar row $Q_{N,z}(h,s)$ through all normal-jet resonances $\rho=1,\dots,2H$, lifting Theorem 23.2 and Proposition 25.5's regular-exit scalar readout without supplementary ODE coordinates. It does not cover excluded radii (10.9), supply higher-rank numerical conditioning bounds, identify Grover's elliptic formula, or prove zeta claims.

Uniform absolute approximation, an executed scalar certificate, a zero-existence theorem and a practical runtime guarantee are different claims. The first three are supplied on the domains stated above; universal relative certification and bounded runtime over the entire programme remain open. Physical zeros preclude a uniform positive modulus floor. The exact external elliptic expression attributed to Grover remains an identification obligation; the paper's own low-rank formulas are retained.

The complete November 17 mathematical body is retained in its original order. Subsequent arguments are integrated into Sections 3–5 and 21–22, without renumbering the inherited theorems. A letter before a new

theorem, equation or local section number identifies the following construction. For example, Q2.1 is the correlated positive-source comparison, and the proof criterion Q4.1 is used with the outer and stronger inner executed inequalities in Q7. All these identifiers refer to arguments printed in this volume, not to missing reports.

Identifier	Integrated construction
R	Effective rank-three critical-radius resolution
C	Rank-three centre-to-critical coverage
U	Rank-three upper-radius completion
O	Odd-rank small-radius source and contour
E	Even-rank balanced-population resolution
A	Unified finite arithmetic, adaptive source and exact characteristic moment
Z	Noninteger zero continuation and local modulus geometry
T	Regularized real-radius source transport
M	Moving-centre connected zero atlas
J	Joint complex-order and real-radius predictor
N	Near-zero source reconstruction and refreshed order circle
Q	Correlated source majorants and coherent terminal continuation

Statements about what was unproved, unexecuted or next at an intermediate stage describe that construction's evidence boundary. The table above gives the cumulative status. In particular, the earlier generic rank-three and small-radius absolute-coverage gaps are closed by U, O and E; the tighter near-zero query left in J is repaired by N; the .17 complex-order boundary in N is extended by Q.

This edition integrates recovered mathematical sources and recorded verification evidence. Its new checks concern preservation, exact input transcription, internal references, compilation and rendering. Recorded physical computations and independent audits retain their original provenance; they are not presented as freshly rerun research calculations.

Proof and certification map

The five claims below concern the normalized large-rank limit, the ordinary finite-rank expectation, a height average over zeta, and the all-rank finite-size scalar readout. For each claim the mathematical input and the scope of the numerical comparison are given together.

1. From the circle to the interior, at large rank. Put $p = s^2 + 2h$, $d = 1 - z^2$, $c = Nd$ and $F_N = N^{-p}\mathbb{E}[|\Lambda_N'|^{2h}|\Lambda_N|^{2(s-h)}]$. On each compact subset of $\Re s > -1/2$, $-1 < \Re h < \Re s + 1/2$, the quantitative depth theorem in Section 19 gives (19.Q1), with the circle comparison in Section 19. At $0 \le c \le b$, the approximation by $F(c)$ has additive error $O_K(\log(e+N)^{-\eta})$, and $F(c) - F(0) = O_K(c^\beta)$ with $F(0) = g_s\mathcal{C}(s,h)$. At $b/2 \le c \le N$ one approximates $c^p F_N$ by $c^p F(c) + \mathcal{G}_z - \mathcal{G}_1$, with additive error $O_K((1+\log N)^A/N)$. The common interval is $[b/2, b]$. The positive-depth coefficient comes from Theorem 16.4, the Gaussian comparison at the actual radius from Theorem 18.2, and the circle limits from Theorems 19.8 and 19.10. The general constants depend on the compact. The Schur comparison in Section 19 proves the positive-integer derivative-diagonal identity from a common finite Schur polynomial. The evaluations in verification_new/integer_overlap.json test the integer specialization. They supply no numerical uniform constant on a two-complex-parameter compact.

2. The independent complex coefficient at depth one. Use $c = 1$, $h = 1/2 + i/8$, $s = 1/2 + i/20$. The limit in the preceding paragraph is the Mellin readout of the unnormalized circularly averaged source (15.5)–(15.7), with the positive-depth scaling c^{-2h}. The chain to an actual disk has three steps. First, the origin jets (Section 19, validated jets) and the keyhole Hankel estimates (K1)–(K4) in Section 19, keyhole quadrature pay for the finite part and each retained annulus. Second, (19.D1) compares the original complex transform at a specified rank on a finite band. Angular integration gives (19.D4), and (19.D5) prices the residual after the signed polynomial contribution is placed in the center, as shown in Section 19, finite-rank comparison and integrated Bessel tail. Third, the window certificate in Section 22 prices the changed complement. Signed complex bands enter the center and the additional measured real-tilt Bessel averages enter the absolute error bound. Both

calculations keep their respective Haar normalizations. The baseline operands are listed in verification_depthon e/complete_R8_repriced_centered.json. The package's RESTART.md identifies the final window receipt and replay command. The applicable relative test is $E/(\ell - E) \le 10^{-10}$, with $\ell \le |m|$ and $\ell > E$ for $D(m, E)$. The finite-rank extrapolation and the exterior scalar in Section 22, executed depth-one disks are floating comparisons. The rational Schur and real Hermite checks are in verification_window/positive_controls.json. The independent positive-measure check at $h = s = 1/2$ in verification_window/audit_real_half.json measures five real Bessel averages and gives $0.5102186 < F(1; 1/2, 1/2) < 0.5145490$.

3. Finite ranks one through eight. For each exact input with $-19/20 \le \Re h \le 3$, $|\Im h| \le 3$, $|s| \le 3$, and $0 \le z \le 0.9$, the direct Haar theorem in Section 21 gives arbitrarily small absolute enclosures of T_N on its ordinary domain. All h, s are admitted at rank one. Rank two at $z = 0$ requires $\Re h > -1/2$. At other rank-two radii, and at ranks three through eight, the condition is $\Re h > -1$. Shrinking the small-mark cutoff, angular cells and arithmetic errors yields pointwise relative termination at nonzero values. Zeros have absolute enclosures and require separate evidence for exact recognition. Section 21 gives a faster rank-two construction. The executed dispatcher cases in verification_new/dispatch_receipts.json and the direct fallback in verification_new/fallback_audit.json have different costs. The quantitative checks in Section 22 identify the independent series, finite-polynomial, and Haar-orthogonality checks for the individual cases. Uniform running time over the parameter box is open.

4. What reaches the critical line of zeta. For fixed real $a \ge 0$, $k > 0$, write $L = \log(T/(2\pi))$. The final zeta comparison in Section 19 predicts $a_{\mathrm{arith}}(k) L^{k^2+2k} F(2a; k, k)$ for the height average of $|\zeta'(1/2 + a/L + it)|^{2k}$ over $[T, 2T]$. At $a = 0$ the same notation uses $F(0; k, k) = g_k \mathcal{C}(k, k)$. The Euler product and transfer assumptions are displayed in the zeta-comparison subsection of Section 19. The positive-integer Schur check and Section 19's exact-circle comparison concern the CUE factor. An arithmetic factor, a joint microscopic distribution comparison and integrability sufficient to pass to moments are separate number-theoretic inputs. Zero locations alone do not provide them. For independent complex orders the proposed observable is $|\zeta'|^{2h} |\zeta|^{2(s-h)}$; negative orders also demand control near the corresponding zeros.

5. All-rank finite-size scalar readout through normal-jet resonances. Distinct from the large-rank programme in items 1–2, Theorem 23.1A in Section 23 proves that at every rank $N \ge 3$ and every regular interior radius $0 < z < 1$ off (10.9), the canonical extreme-row scalar row $Q_{N,z}(h, s)$ of Theorem 10.6 has zero residue along every normal-jet resonance hyperplane $\rho = 1, \dots, 2H$ on all $d = \binom{N+3}{3}$ coordinates, and is globally polynomial of explicit bidegree in (h, s). This lifts Theorem 23.2 to all $N \ge 3$ and discharges Proposition 25.5's normal-divisor scalar readout obligation at regular exits, while showing why Theorem 23.1's zero-injection shortcut is valid at $N = 3, 4$ and fails for $N \ge 5$. Two-prime and exact rank-five checks test the construction; the theorem itself is proved algebraically and makes no claim at excluded radii (10.9), for Grover's elliptic expression, or about zeta moments.

Method of comparison. Theorem 3.2 of J. Rodgers, *The ordinary Riemann Hypothesis argument in the supplied Lean source* (22 November 2026, DOI 10.5281/zenodo.24433884), which credits the underlying argument to Levent Alpöge and Claude, isolates the complement of a transform window explicitly in (13)–(14). Lemmas 14.2–14.3 price truncation and contour contributions in a different transform, and Sections 17–18 identify the exact premises of a terminal claim. Here this suggests the window decomposition and the arrangement of this map. The estimates used in the depth-one disk are the CUE estimates above.

Quantitative continuation. The depth ranges and error estimates and the upper-threshold residual appear in Section 19. The direct Haar evaluator gives arbitrary absolute finite-size refinement. The inherited discussion below records the earlier scope of the individual constructions.

Observable and normalization. For normalized Haar measure on $U(N)$, let $\Lambda_N(z) = \det(I - zU)$, $d = 1 - z^2$, $S_N = -d\Lambda_N'/\Lambda_N$, and

$$T_N(h, s; z) = \mathbb{E}\{|S_N|^{2h} |\Lambda_N|^{2s}\}, \qquad 0 \le z < 1.$$

Here s is the independent tilt and h is the moment order. On the diagonal $T_N(h, h; z) = d^{2h} \mathbb{E}|\Lambda_N'(z)|^{2h}$. At depth $c = Nd$, S_N is already the microscopic statistic. An additional factor N^{-s^2} normalizes the tilted mass. This distinction matters for both inverse moments and complex tilts.

Foundation, scope and attribution. Sections 1–6 give the proofs of the fixed-rank formulas used here, including the Gaussian prescription in Section 5. The starting statements and the history of their reconstruction are documented in the accompanying research note. Sections 7–17 and 20 retain the previous finite-size and fixed-depth arguments. The fixed-interior limit is due to Simm and Wei. For higher integer-order derivative moments both inside the unit disc (contingency-table sums) and near the unit circle (determinants with Kostka-number weights), see Alexander Grover, Francesco Mezzadri, and Nick Simm, *Higher order derivative moments of CUE characteristic polynomials and the Riemann zeta function*, arXiv:2604.03051 (2026); Section 12 and the positive-integer diagonal comparison in Section 19 use their finite integer determinant (Theorem 2.9) and compare leading asymptotics directly against our independent-complex-exponent framework. Separately, Alexander Grover's expository video provided the original inspiration for our $N = 3$ investigation; our rank-three elliptic reductions (Propositions 9.2 and 10.2A) are established on their own explicit slices and have not been shown to coincide with his particular displayed elliptic expression. Further published inputs are cited where used.

Sections 10, 16, 18, 19 and 21 give the further results. Section 16 starts with the compact-source and integer-tilt derivations. A disk automorphism then places both complementary Fourier spaces on fixed half-lines. An expansion of their relative multiplier controls the entire physical frequency plane at real tilt. Complex interpolation at several matrix sizes transfers the expansion to arbitrary independent complex tilt and to the densities themselves. At growing depth the comparison with a translated Gaussian is exponentially accurate also at complex tilt. At shrinking depth two nearby eigenangles determine the leading density of the rescaled mark near zero. Theorems 19.7–19.11 and Proposition 19.12 extend the circle readout to independent complex tilt and resolve the depth scale transverse to its limiting line. Theorems 19.13–19.15 distinguish transport of the circle density from the explicit two-angle correction at a resolved imaginary mark. Propositions 19.16–19.19 treat the integrated tail, higher planar bands and weak limits at the one-angle front and the first planar fold. A single near eigenangle controls the upper critical logarithm and the supercritical normalization. Theorems 10.6–10.9 give the reduced radius system and the connection across singular radii. Proposition 10.10 constructs full-vector starting values and validates a short transfer. Theorem 21.5 and Corollary 21.6 give independent scalar enclosures and a uniform polynomial truncation budget. Propositions 21.7–21.8 supply inverse-order benchmarks and a validated critical crossing. Theorems 10.12–10.13 and Proposition 10.14 give validated full-state transport, singular germs and compatible scalar rows. Propositions 21.9–21.10 report the complete crossings and the parameter-set enclosure. Theorems 10.15–10.17, Proposition 21.11 and Theorem 21.12 give the parameter-uniform transport, the order-disk connection, the rank-four singular column and the complete error budgets. Section 22 records the preceding verification history. Section 23 proves scalar recovery through normal-jet resonances, crosses their intersections with exceptional connection orders, and gives separate executable and reference error bounds. Its final theorem gives a scalar computation through several critical radii at positive integer orders. Section 24 develops the one-pair variable-order construction and its executions. Section 25 transports noninteger rank-five states through consecutive radii.

All-rank normal-jet resonance cancellation. Distinct from the lead asymptotic programme of Section 19, Theorem 23.1A resolves the algebraic normal-jet resonance obstruction of the four-mode finite-rank system (Theorem 10.6) at every rank $N \geq 3$ and every regular interior radius $0 < z < 1$ outside the exceptional set (10.9). Explicit complexified pinch-simplex solutions of the two-dimensional displacement system, together with squared Weyl Vandermonde vanishing, show that every apparent normal-jet pole $\rho \in \{1, \dots, 2H\}$ of the canonical extreme-row scalar row has zero residue on every coordinate of $\mathbb{C}^d$, so the numerator row $Q_{N,z}(h, s)$ is globally polynomial in (h, s) of explicit bidegree and requires no supplementary normal-jet ODE coordinates. This lifts the analytic scalar readout of Theorem 23.2 to all ranks $N \geq 3$ and discharges the regular-exit normal-divisor scalar readout requirement in Proposition 25.5, while explaining why Theorem 23.1's zero-injection shortcut works at ranks three and four and fails from rank five onward. It is strictly a finite-rank algebraic theorem on regular interior radii: it does not cover excluded radii in (10.9), supply higher-rank numerical conditioning bounds, identify Grover's particular elliptic expression, or prove any statement about Riemann zeta moments.

Finite-rank evaluation in the November 17 foundation. Proposition 5.2 expresses the moment through equally spaced frequencies. Sections 8–10 use the rank-two inverse strip, the rank-three elliptic laws and the signed expansion at the centre to evaluate very small positive radii. Theorems 21.16–21.17 give continuous parameter regions on both sides of critical radii and separate absolute from relative accuracy. Section 22 records the independent source checks and the remaining upper-radius cases.

Outer-radius continuation. Theorems 5.3 and 21.18 couple the angular source and the inverse-order frequency

tail. Proposition 21.19 gives the pointwise arithmetic certificate. Section 21 also gives a faster estimated evaluation and Theorem 21.20, a zero of the rank-eight moment that persists under independent tilt perturbations. The new rank-three calculations accompany the elliptic formulas in §10. The earlier critical-radius and large-size results retain their domains.

Prepared-source continuation. Sections 5 and 21 retain a signed physical projection through the change of sampling rate. Its concentration bound controls the actual folded angular mass. A change of polynomial basis stabilizes strongly negative tilt, and a restricted critical-radius construction uses eigenvalue repulsion on the resonant configurations. The new finite-rank work uses the Haar law and the sampling identity directly. Section 22 gives timed cold runs, warm orders and independent original-angle checks.

Critical-radius continuation. Theorem 21.25 now gives a connected exact-arithmetic scalar approximation on $4 \le N \le 8$, $.02 \le z \le .9$ through all positive critical trace radii, throughout the original independent complex order and tilt box. It uses closed-cell bounds on the same physical source, with a justified join to the outer formula. The finite-arithmetic evaluator has been executed at exact walls, adjacent radii, parameter boundaries, small positive radii and the representation switch. These computations remain pointwise certificates, separate from the uniform truncation theorem.

Propositions 3.2–3.3 give explicit paired-saddle corrections. Propositions 4.3–4.6 construct a rank-three source partition and bound its conditional singularities; its general numerical quadrature remains estimated. Propositions 5.14–5.18 retain the local preparation and folded-frequency information needed by the wider scalar bounds. The full predecessor paper and its hypotheses are preserved. The new fixed-size computations do not independently audit the major microscopic or circle-limit theorems, and the precise external elliptic-formula comparison remains open. Section 22 gives the new execution record, failures, repairs and target-coverage ledger.

Identification and operations. The source is the specified Haar ensemble with its tilt. Its Fourier determinant records the full planar mark and its circular average identifies its radial measure by uniqueness of Fourier transforms after rotation averaging. For integrable powers this identifies the moment. Recovering it from bounded frequencies, a limit of sources, or a finite numerical approximation requires quantitative estimates. For each operation we give the necessary bound at the point of use.

Operation	Information retained	Estimate that permits the readout
Fixed-size radial inversion	Bessel mean and integer jets	Oscillatory tails and origin subtraction, Sections 2–5
Inverse microscopic power	Full planar mark under a positive tilt	Two-sided density control near zero, Section 15
Finite-size corrections	Both exterior Fourier spaces and their relative phase	Trace-norm expansion, interpolation in the tilt, and weighted Fourier inversion, Section 16
Vary depth together with size	Dependence of the source on c and N	Frequency estimates for growing depth, probability estimates for shrinking depth, Sections 18–19
Density of a rare off-line value	Two signed angles, their mutual repulsion, two exterior sums and the finite Barnes mass	Uniform coarea and circle insertions in Section 19
Independent finite-rank parameters	Interior algebraic weight and integration cycle	Exact annihilating relations, Section 10
Passage through a critical trace value	Both analytic continuations of the same incoming physical angular solution	Their phase-weighted sum, or its order derivative at resonance, Sections 10 and 22
Certified numerical readout	Separate rounding, truncation and modulus bounds	Sections 20–21, Section 23 and their accompanying replays

1. Fixed-size mixed moments and their domains

Let U have normalized Haar measure on $U(N)$, let λ_j denote its eigenvalues, and take z real with $0 \le z < 1$. Define

$$\Lambda_N(z) = \det(I - zU), \qquad S_N(z) = \sum_{j=1}^{N} \frac{(1-z^2)\lambda_j}{1 - z\lambda_j} = -(1-z^2)\frac{\Lambda_N'(z)}{\Lambda_N(z)}.$$

For complex h, s define the expectation, in its domain of absolute integrability on $U(N)$,

$$T_N(h, s; z) = \mathbb{E}\,[|S_N(z)|^{2h}|\Lambda_N(z)|^{2s}].$$

Positive bases use the real logarithm. Values on Haar-null zero sets can be assigned arbitrarily. The diagonal $s = h$ recovers the derivative moment multiplied by $(1-z^2)^{2h}$.

Theorem 1.1 (fixed-size moment formulas).

Write $D_N(\zeta)$ for the determinant in (1.1), and $\Phi(\rho)$ for its circular average, also denoted $\bar{\varphi}(\rho)$. The radial Mellin formula (5.3), the Gaussian planar limit (5.2), and the derivative formula (5.4) hold on the following domains. Each finite lower entry a denotes the strict inequality $\operatorname{Re} h > a$. The derivative column also requires $\operatorname{Re} h < 1$ before applying Laplacians.

Matrix size and location	Absolute moment	Mellin and Gaussian limits	Derivative limit
$N \ge 3$, $0 \le z < 1$	-1	-1	-1
$N = 2$, $0 < z < 1$	-1	-1	$-3/4$
$N = 2$, $z = 0$	$-1/2$	$-1/2$	$-1/2$
$N = 1$, $0 < z < 1$	all h	-1	$-1/2$
$N = 1$, $z = 0$	all h	$-3/4$	$-1/4$

At nonnegative integer h, the Mellin formula is evaluated by its removable limit, which gives the integer moment. For $N = 2$, $0 < z < 1$, the Mellin tail alone exists even for $-5/4 < \operatorname{Re} h \le -1$. The table describes equality with the ordinary Haar expectation. Estimates are for fixed N. On compact parameter sets in the interior of each stated regime the proof yields locally uniform estimates. In a conditionally convergent region, integrating a planar kernel means truncating to disks centered at zero.

The Fourier determinant and its mixed derivatives

For a single eigenangle put $f_z(\lambda) = (1-z^2)\lambda/(1-z\lambda)$ and define

$$g_\zeta(\theta) = |1 - ze^{i\theta}|^{2s} \exp\big(i \operatorname{Re}(\bar{\zeta} f_z(e^{i\theta}))\big), \qquad \widehat{g}_\zeta(k) = \frac{1}{2\pi}\int_0^{2\pi} g_\zeta(\theta) e^{-ik\theta}\, d\theta.$$

The Toeplitz matrix has constant entries along each diagonal. Weyl's eigenangle formula (Meckes, Theorem 3.1) and expansion of the two Vandermonde determinants by permutations give the Heine identity

$$D_N(\zeta) = \det[\widehat{g}_\zeta(j-k)]_{j,k=0}^{N-1} = \mathbb{E}\,[|\Lambda_N(z)|^{2s} e^{i \operatorname{Re}(\bar{\zeta} S_N(z))}]. \tag{1.1}$$

Indeed, the Vandermonde square against product measure $d\theta/(2\pi)$ carries the factor $1/N!$. Permuting the integration variables collapses one permutation sum into $N!$, leaving the determinant of the Fourier integrals. This fixes the source normalization and its sign. Reversing the sign only sends ζ to $-\zeta$ and leaves the circular average unchanged.

The Taylor coefficients required by the theorem can be obtained from the determinant itself. Replace the exponential in g_ζ by $\exp(uf_z + v\tilde{f}_z)$, for independent complex u, v, and denote the resulting determinant by $H_N(u, v)$. Compactness gives an entire function of both variables and

$$T_N(j, s; z) = (j!)^2[u^j v^j]H_N(u, v), \qquad a_j = \frac{(-1)^j}{4^j}[u^j v^j]H_N(u, v).$$

For any prescribed j, this coefficient uses only terms of bidegree at most (j, j) in the entries; here a_j are the radial Taylor coefficients of the circularly averaged source $\Phi(\rho) = \sum_{j\geq 0} a_j \rho^{2j}$ defined in Section 5. This gives the integer data appearing in the non-integer moment formula.

Support.

The transformation $w = (\lambda - z)/(1 - z\lambda)$ gives $S_N = Nz + \sum_j w_j$ with $|w_j| = 1$. The support of the untilted law is the circle $|x - z| = 1$ at $N = 1$ and the closed disk $|x - Nz| \leq N$ at $N \geq 2$. For two unit vectors their possible sums fill the disk of radius two. Adding a unit vector to a disk of radius $r \geq 1$ fills the disk of radius $r + 1$, by rotation and the triangle inequality in both directions. The entire image is support because configurations with distinct angles have strictly positive density, are dense, and every open neighborhood of an image point has an open nonempty inverse image. The strictly positive weight for each real tilt preserves this support. In determinant language the entire Fourier transform determines this positive measure. The same bound follows from its exponential type, but that bound by itself gives only containment. The proof of equality above uses the eigenangle realization of the displayed determinant.

2. Large-source decay of the Toeplitz determinant

Fix an integer $N \geq 1$. Throughout this subsection $0 \leq z < 1$ is real, $s \in \mathbb{C}$, and $|v|^{2s} = \exp(s \log |v|^2)$ for $v \neq 0$. Use the Fourier convention

$$D_N(\zeta) = \mathbb{E}\left[|\Lambda_N(z)|^{2s} \exp\{i \operatorname{Re}(\bar{\zeta} S_N(z))\}\right].$$

Write $\zeta = \rho u$, with $|u| = 1$ and $\rho > 0$. For nonnegative integers n, m with $n + m = N$ set

$$P_{nm} = \frac{n^2 + m^2}{2}, \qquad d_{nm} = n - m, \qquad S_{nm}(u) = Nz + d_{nm}u, \qquad F_n = \frac{\prod_{j=1}^n j!}{n!}, \quad F_0 = 1.$$

For any nonnegative derivative orders a, b, define

$$C_{nm}(u) = \frac{(1 - z^2)^{N^2+2Ns}\, 4^{nm} F_n F_m}{(2\pi)^{N/2}} |1 + zu|^{-2n(N+s)} |1 - zu|^{-2m(N+s)} \exp\left(\frac{i\pi}{4}(m^2 - n^2)\right),$$
$$C_{nm}^{a,b}(u) = C_{nm}(u) \left(\frac{i\overline{S_{nm}(u)}}{2}\right)^a \left(\frac{iS_{nm}(u)}{2}\right)^b.$$

A factor to the power zero is one, also when $S_{nm} = 0$.

Proposition 2.1 (directional stationary phase).

Put $p_N = \min_{n+m=N} P_{nm}$. Uniformly in u and on compact subsets of $[0, 1) \times \mathbb{C}$ in (z, s), as $\rho \to \infty$,

$$\partial_\zeta^a \partial_{\bar{\zeta}}^b D_N(\rho u) = \rho^{-p_N} \sum_{\substack{n+m=N \\ |n-m|\leq 1}} C_{nm}^{a,b}(u) e^{i\rho(Nz \operatorname{Re} u + n - m)} + O(\rho^{-p_N - 1}). \tag{2.1}$$

Here $p_N = N^2/4$ for even N and $p_N = (N^2 + 1)/4$ for odd N. In particular, with a constant depending also on N, a, b and the compact set,

$$|\partial_\zeta^a \partial_{\bar\zeta}^b D_N(\zeta)| \le C(1+|\zeta|)^{-p_N}.$$

The expansion with $a = b = 0$ has a nonzero leading coefficient for every balanced saddle. Derivatives may annihilate one or more leading contributions.

Proof.

The disk automorphism $w = (\lambda - z)/(1 - z\lambda)$ has inverse $\lambda = (z + w)/(1 + zw)$ on the unit circle. Direct subtraction and differentiation give

$$\frac{(1-z^2)\lambda}{1-z\lambda} = z + w, \qquad 1 - z\lambda = \frac{1-z^2}{1+zw},$$
$$\lambda_j - \lambda_k = \frac{(1-z^2)(w_j - w_k)}{(1+zw_j)(1+zw_k)}, \quad d\arg\lambda = \frac{1-z^2}{|1+zw|^2}\, d\arg w.$$

Using the Haar unitary eigenangle density, with $w_j = e^{it_j}$ and $\Delta(w) = \prod_{j<k}(w_k - w_j)$, gives

$$D_N(\rho u) = \frac{(1-z^2)^{N^2+2Ns} e^{i\rho N z \operatorname{Re} u}}{N!(2\pi)^N} \int_{[0,2\pi]^N} e^{i\rho \sum_j \operatorname{Re}(\bar u w_j)} |\Delta(w)|^2 \prod_j |1+zw_j|^{-2(N+s)}\, d^N t. \tag{2.2}$$

Wirtinger differentiation before substituting $\zeta = \rho u$ multiplies the integrand by $(i\bar S_N/2)^a (iS_N/2)^b$, with $S_N = Nz + \sum_j w_j$. The resulting amplitudes are smooth. All their derivatives of a fixed order are bounded on the compact parameter sets above, since $|1 + zw| \ge 1 - z$.

Rotate $w_j = ue^{ix_j}$. The phase $\sum_j \cos x_j$ has precisely the 2^N critical points $x_j = 0, \pi$. If n of the coordinates are 0 and m are π, the critical value is $n - m$ and the Hessian is diagonal with n entries -1 and m entries $+1$. Away from the critical points, repeated integration by parts gives arbitrary inverse powers of ρ. Near each critical point, choose local Morse coordinates $y_j = 2\sin((x_j - x_j^*)/2)$. The phase becomes

$$n - m - \frac{1}{2}\sum_+ y_j^2 + \frac{1}{2}\sum_- y_j^2.$$

The lowest-degree homogeneous term of the squared Vandermonde is

$$4^{nm}\Delta(y_+)^2\Delta(y_-)^2, \qquad \deg = n(n-1) + m(m-1).$$

Indeed, each mixed pair has squared separation 4 and each same-sign pair contributes $(y_k - y_j)^2$ to lowest order. The Jacobian in the new coordinates equals one at the origin. If the derivative multiplier vanishes there, the displayed homogeneous term of the full amplitude has zero coefficient.

Stationary phase now gives the saddle order $\rho^{-[N+n(n-1)+m(m-1)]/2} = \rho^{-P_{nm}}$. The coefficient follows from the Gaussian Vandermonde integral

$$\int_{\mathbb{R}^r} e^{-\sum x_j^2/2} \Delta(x)^2\, d^r x = (2\pi)^{r/2} \prod_{j=1}^{r} j!.$$

For completeness, expand each Vandermonde in monic probabilists' Hermite polynomials. Orthogonality reduces the integral of the product of the two determinants to $r!$ times the product of their squared norms $\sqrt{2\pi}\, j!$ for $0 \le j < r$. Replacing the real Gaussian coefficient 1 by v, $\operatorname{Re} v > 0$, multiplies the answer by $v^{-r^2/2}$, first for positive v by scaling, then throughout the half-plane by analytic continuation. The limits $v \to +i$ and $v \to -i$ supply the Fresnel factors $e^{-i\pi n^2/4}$ and $e^{i\pi m^2/4}$. The smooth weight at the critical point and the $N!/(n!m!)$ choices of its labels give exactly $C_{nm}^{a,b}(u)$.

In each localized expansion only integer corrections ρ^{-j} occur after $\rho^{-P_{nm}}$, since odd-degree Gaussian moments vanish. The smooth-amplitude stationary-phase expansion (Vasy, *Stationary Phase Lemma*) is uniform in the stated parameters to every finite order. Its remainder has this uniformity also after any fixed number of angular derivatives once the factor $e^{i\rho Nz\,\mathrm{Re}\,u}$ has been removed: after rotation the interior phase is independent of u. Balancing n, m minimizes P_{nm}, and every unbalanced value exceeds the minimum by at least one. This proves (2.1); boundedness for $\rho \le 1$ follows directly from the compact integral. □

Frequencies of the leading saddles

For even N there is a single balanced saddle class. Its directional frequency is $Nz\,\mathrm{Re}\,u$. It vanishes in every direction at $z = 0$ and on the two imaginary rays for every real $z > 0$. For odd N the balanced frequencies are $Nz\,\mathrm{Re}\,u \pm 1$. Both undifferentiated coefficients are nonzero, and at least one frequency is nonzero, although one can vanish. At $z = 0$ with even N every positive-order source derivative has zero leading coefficient because $S_{N/2,N/2} = 0$. Thus the common derivative estimate is an upper bound. As normalization checks, $(N, z) = (1, 0)$ gives $J_0(\rho)$ and $(N, z) = (2, 0)$ gives $J_0(\rho)^2 + J_1(\rho)^2 \sim 2/(\pi\rho)$.

3. Radial stationary phase and the transition at the centre

Proposition 3.1 (radial expansion and uniform angular average). Let $\bar\varphi(\rho) = (2\pi)^{-1}\int_0^{2\pi} D_N(\rho e^{i\theta})\,d\theta$. For fixed $z > 0$, the angular phase in (2.2) is $Nz\cos\theta$, and its stationary points are $0, \pi$. Write $\epsilon = +1, -1$ for these points, respectively. Combining the torus expansion with one-dimensional stationary phase gives the all-orders asymptotic expansion

$$\bar\varphi(\rho) \sim \sum_{n+m=N}\sum_{\epsilon=\pm1} e^{i(d_{nm}+\epsilon Nz)\rho}\,\rho^{-P_{nm}-1/2}\sum_{j\ge0} c_{nm,\epsilon,j}\rho^{-j}, \qquad c_{nm,\epsilon,0} = \frac{C_{nm}(\epsilon)e^{-i\epsilon\pi/4}}{\sqrt{2\pi Nz}}. \tag{3.1}$$

The meaning of the expansion is by finite total order. Keeping all terms with exponent below a given order leaves a remainder bounded at that order. This follows either by applying stationary phase jointly in $(x_1, \dots, x_N, \theta)$ after rotation, where the phase splits exactly, or from the uniform smooth angular amplitudes in the preceding proof. The expansion and its differentiated versions are uniform for z in compact subsets of $(0, 1)$. Applying the joint proof after ρ-differentiation proves termwise asymptotics for any fixed number of radial derivatives. At coincident frequencies the coefficients must be added; cancellations can suppress the first power at a given frequency. At $z = 0$ rotational invariance gives $\bar\varphi(\rho) = D_N(\rho)$, so there is no angular $\rho^{-1/2}$ factor. Uniformly continuing (3.1) to $z = 0$ would require a different asymptotic treatment of the angular integral.

Multiplication by ρ^{-2h-1} gives the powers for the tail integrand of the radial moment formula (5.3). Its frequencies are $n-m\pm Nz$ and its powers before integer corrections are $-2h-1-(n^2+m^2+1)/2$. The determinant fixes the coefficients of this asymptotic expansion. A numerical fit and a finite truncation each require an error estimate.

Uniformity through the small-z transition

One can retain the angular integral and allow $t = Nz\rho$ to have any size. Define

$$\mathcal{J}_t[f] = \frac{1}{2\pi}\int_0^{2\pi} e^{it\cos\theta} f(\theta)\,d\theta, \qquad A_{nm}(\theta) = C_{nm}(e^{i\theta}).$$

On every compact parameter set $0 \le z \le z_* < 1$, $s \in K \subset \mathbb{C}$, the more uniform leading formula is

$$\bar\varphi(\rho) = \rho^{-p_N}\sum_{|n-m|\le1,\ n+m=N} e^{i(n-m)\rho}\,\mathcal{J}_{Nz\rho}[A_{nm}] + O_K\Big(\rho^{-p_N-1}(1+Nz\rho)^{-1/2}\Big), \qquad \rho \ge 1. \tag{3.2}$$

To see this, remove $e^{it\cos\theta}$ before taking the remainder of the directional expansion. The remainder has C^1 angular norm bounded by $C_K\rho^{-p_N-1}$ because the rotated torus phase is independent of θ. For any C^1 periodic f, $|\mathcal{J}_t[f]| \le C(1+t)^{-1/2}\|f\|_{C^1}$ when $t \ge 0$. For $t > 1$ remove arcs of length $O(t^{-1/2})$ about $0, \pi$ and bound their

contributions directly. On the complementary arcs integrate by parts with $(it(-\sin\theta))^{-1}\partial_\theta$. The boundary term and the integral involving $|\cos\theta|/(t\sin^2\theta)$ are $O(t^{-1/2})$, and the term involving f' is $O(t^{-1}\log(2+t))$. This proves (3.2).

The leading angular integrals have an absolutely convergent Bessel representation

$$\mathcal{J}_t[A_{nm}] = \sum_{k\in\mathbb{Z}} i^k J_k(t)\widehat{A}_{nm}(k), \qquad \widehat{A}_{nm}(k) = \frac{1}{2\pi}\int_0^{2\pi} A_{nm}(\theta)e^{-ik\theta}\,d\theta.$$

For any $\delta > 0$ with $z_* e^\delta < 1$, $|\widehat{A}_{nm}(k)| \le C_{\delta,K}e^{-\delta|k|}$: factor the weights into powers of $1 \pm ze^{i\theta}$ and $1 \pm ze^{-i\theta}$, take the analytic logarithms from their convergent power series, and shift the contour by $\pm i\delta$. Since $|J_k(t)| \le 1$ for integer k and real t, truncating this Fourier sum to $|k| \le L$ incurs error at most $2C_{\delta,K}e^{-\delta(L+1)}/(1-e^{-\delta})$ in the angular integral, uniformly in t. This expansion treats the transition $Nz\rho \sim 1$. Quantitative evaluation also requires effective constants for the full radial remainder and a separate accuracy test.

A paired saddle correction at and near a critical radius

After the same exact Möbius change and rotation used in the paper, the source is

$$\Phi(r) = \frac{d^{N^2+2Ns}}{N!(2\pi)^{N+1}}\int e^{irG}\prod_j g(x_j+\phi)^{-N-s}\prod_{j<k} 4\sin^2\frac{x_j-x_k}{2}\,dx\,d\phi,$$

where $G = Nz\cos\phi + \sum_j \cos x_j$, $g(t) = 1 + 2z\cos t + z^2$, and $d = 1 - z^2$. For $z > 0$, all stationary points are nondegenerate and have coordinates zero or π. Group their opposite-direction pairs by the number m of eigenangle signs agreeing with the direction. Put

$$\ell = N - m, \quad a = Nz, \quad b = \ell - m, \quad \omega = a - b, \quad P = \frac{m^2+\ell^2+1}{2}, \quad \theta = \frac{\pi}{4}(\ell^2 - m^2 - 1),$$

$$B_m = \frac{\binom{N}{m}4^{m\ell}(\prod_{j=1}^m j!)(\prod_{j=1}^\ell j!)}{N!(2\pi)^{(N+1)/2}\sqrt{a}}\,\frac{d^{N^2+2Ns}}{(1+z)^{2m(N+s)}(1-z)^{2\ell(N+s)}},$$

$$K_m = \frac{b(1-2m\ell)-a^{-1}}{8} - (N+s)z\left[\frac{m^2+m/a}{(1+z)^2} + \frac{\ell^2-\ell/a}{(1-z)^2}\right].$$

Proposition 3.2 (the first correction for paired radial saddles). The local contribution of this population is

$$\Phi_m(r) = 2B_m r^{-P}\left[\cos(\omega r+\theta) - \frac{K_m}{r}\sin(\omega r+\theta)\right] + O(r^{-P-2}).$$

The remainder is uniform on compact sets of $z \in (0,1)$ and complex s, with fixed rank. Summing over all populations gives the full source expansion; the nonstationary complement is smaller than any prescribed algebraic power. This assertion is an asymptotic theorem with unspecified compact-dependent constant. The code does not turn its big-O into a numerical certificate.

Proof. At $\phi = 0$, write the agreeing variables as u_j, the opposite ones as $\pi + v_j$, and the direction as t. The phase begins

$$G = \omega - \tfrac{1}{2}(at^2 + \sum u_j^2 - \sum v_j^2) + \tfrac{1}{24}(at^4 + \sum u_j^4 - \sum v_j^4) + O(|(u,v,t)|^6).$$

The leading Vandermonde is $4^{m\ell}\Delta(u)^2\Delta(v)^2$. Fresnel continuation of the Gaussian Mehta integrals gives phase $e^{i\theta}$ and amplitude $B_m r^{-P}$. The opposite-direction saddle has the same complex preparation, with phase and Fresnel signs reversed. It is not obtained by conjugating the tilt.

For a squared-Vandermonde Gaussian of dimension q and quadratic parameter τ, the needed normalized moments are

$$\mathbb{E}\sum x_j^2 = q^2/\tau, \quad \mathbb{E}(\sum x_j)^2 = q/\tau, \quad \mathbb{E}\sum x_j^4 = q(2q^2+1)/\tau^2.$$

In the agreeing group $\tau = ir$; in the opposite group $\tau = -ir$. The direction has second moment $-i/(ar)$. Quadratic preparation terms give the two displayed $-(N+s)z$ contributions to K_m. The quadratic Vandermonde correction is $(m-\ell)(N^2+2m\ell-1)/12$, times i/r. The quartic phase gives $[-3/a - m(2m^2+1) + \ell(2\ell^2+1)]/24$, also times i/r. Their sum is $[b(1-2m\ell) - a^{-1}]/8$. The first saddle therefore has relative factor $1 + iK_m/r$, and the second $1 - iK_m/r$; summing proves the formula. A smooth cutoff around each stationary point and ordinary stationary phase justify the expansion and its compact uniformity. The amplitude's same-sign Vandermonde vanishes to its stated homogeneous order, which is retained throughout this calculation.

At a critical radius $z = b/N > 0$, $\omega = 0$. If N and m are odd, $\cos\theta = 0$, so the first nonoscillatory term cancels exactly. At rank three's first wall,

$$K_1 = -(49+15s)/8, \qquad \Phi_{\mathrm{res}}(r) = \frac{49+15s}{\pi^2}\frac{d^{9+6s}}{(1+z)^{2(3+s)}(1-z)^{4(3+s)}}r^{-4} + O(r^{-6}), \quad z = 1/3.$$

Here the next even relative order also cancels by opposite-saddle parity. The coefficient is nonzero on $|s| \le 3$, since $|49+15s| \ge 4$. This is a cancellation of the resonant component, not a statement that the entire source lacks other oscillatory r^{-3} terms.

A computable correction for an independent source check

The original-angle reference uses a smooth beta window. Let $V \sim \mathrm{Beta}(16,16)$, $L = R(.55+.45V)$. A continuous windowed tail for a frequency ω is

$$H_q(\omega; R) = \mathbb{E}[L^{-q}E_{q+1}(-i\omega L)], \quad H_q(0;R) = \frac{(.55R)^{-q}}{q}\,{}_2F_1(q,16;32;-9/11).$$

Here E_ν is the generalized exponential integral, approached from the positive Laplace half-plane. This representation is continuous at zero frequency. Substitution of the paired expansion gives, with $q = P + 2h$,

$$C(h)B_m\{e^{i\theta}H_q(\omega) + e^{-i\theta}H_q(-\omega) + iK_m[e^{i\theta}H_{q+1}(\omega) - e^{-i\theta}H_{q+1}(-\omega)]\}.$$

This correction does not fit the desired midpoint. It is calculated from (N, z, s, h) and the analytically derived coefficients. The incomplete gamma kernel is evaluated with 192-bit Acb arithmetic, but the window quadrature and asymptotic remainder are not certified. Thus the complete corrected reference is labelled **estimated**, despite enclosed special-function calls.

This explicit calculation is a new derivation in this continuation; no priority claim is made. The effective remainder problem is separate from the rigorous localized bounds in Section 5.

The next resonant coefficient at rank three

The paired expansion admits a useful additional explicit term at the lowest positive critical radius. This is a coefficient calculation for the same Haar-defined source, not a fit to the computed moment. It does not provide a usable numerical remainder constant by itself.

Proposition 3.3 (rank-three resonant pair). At $N = 3$, $z = 1/3$, set

$$\mathcal{P}_s = \frac{(1-z^2)^{9+6s}}{(1+z)^{2(3+s)}(1-z)^{4(3+s)}}, \qquad Q(s) = 2097s^3 + 21084s^2 + 67983s + 70940.$$

Use real logarithms in these powers of positive real numbers. The contribution of the resonant opposite-direction saddle pair to the radial source satisfies

$$\Phi_{\mathrm{res}}(r) = \frac{\mathcal{P}_s}{\pi^2}\left[(49+15s)r^{-4} - \frac{3Q(s)}{128}r^{-6}\right] + O_{\mathcal{K}}(r^{-8}),$$

uniformly for s in any fixed compact subset $\mathcal{K}$ of $\mathbb{C}$. The other sign populations of the full source are not included in this formula. In particular they may have oscillatory r^{-3} contributions.

Proof. Write $p = 3 + s$. In the first saddle use the scaled agreeing variable u, the two opposite variables v, w, and the direction t. The quadratic Fresnel form has covariances $(-i, i, i, -i)$ in that order, and its leading Vandermonde is $(v-w)^2$. Let $\mathcal{G}$ be the corresponding normalized Wick functional with that Vandermonde retained. It is computed by independent Gaussian monomial contractions followed by division by $\mathbb{E}_0(v-w)^2 = 2i$. Thus odd moments vanish, and the even one-variable moment with covariance τ is $(2k-1)!!\,\tau^k$. This defines an exact algebraic functional; it is not a probability measure with complex covariance.

The logarithm of the scaled amplitude and phase, after removing the quadratic part and the leading Vandermonde, is $r^{-1}L_1 + r^{-2}L_2 + r^{-3}L_3 + O(r^{-4})$. Put $q = u + t$, $q_1 = v + t$, $q_2 = w + t$. Its coefficients are

$$\begin{aligned} L_j = {} & -p\{a_j q^{2j} + b_j(q_1^{2j} + q_2^{2j})\} + d_j(v-w)^{2j} + e_j\{(u-v)^{2j} + (u-w)^{2j}\} \\ & + \frac{i(-1)^{j+1}}{(2j+2)!}(u^{2j+2} - v^{2j+2} - w^{2j+2} + t^{2j+2}), \qquad 1 \le j \le 3, \end{aligned}$$

where, with $A = 3/16$ and $B = 3/4$,

$$\begin{aligned} (a_1, a_2, a_3) &= (-A, A/12 - A^2/2, -A/360 + A^2/12 - A^3/3), \\ (b_1, b_2, b_3) &= (B, -B/12 - B^2/2, B/360 + B^2/12 + B^3/3), \\ (d_1, d_2, d_3) &= (-1/12, -1/1440, -1/90720), \\ (e_1, e_2, e_3) &= (-1/4, -1/96, -1/1440). \end{aligned}$$

These follow respectively by expanding the two preparation factors, $2\log[\sin(x/2)/(x/2)]$, $2\log\cos(x/2)$, and the phase. No same-sign Vandermonde is dropped. Applying the Wick functional gives

$$\begin{aligned} \mathcal{G}(L_1) &= -\frac{i(15p+4)}{8}, \\ \mathcal{G}(L_2 + L_1^2/2) &= -\frac{27p(17p+1)}{128}, \\ \mathcal{G}(L_3 + L_1L_2 + L_1^3/6) &= \frac{3i}{1024}(2097p^3 + 2211p^2 - 1902p + 128). \end{aligned}$$

Each equality is a finite polynomial identity under the stated monomial rule; `rank3_saddle_cubic.py` computes it in exact rational arithmetic. At this saddle the leading factor is $iB_s r^{-3}$, with $B_s = 4\mathcal{P}_s/\pi^2$. The opposite saddle has leading factor $-iB_s r^{-3}$ and reverses the sign of every odd relative coefficient. It has the same s, not its complex conjugate. The even relative terms therefore cancel. If the third relative coefficient is written $-iK_3$, then

$$K_3 = -\frac{3}{1024}(2097p^3 + 2211p^2 - 1902p + 128).$$

The retained pair coefficients are $-2B_sK_1$ at r^{-4} and $2B_sK_3$ at r^{-6}, which give the displayed formula after $p = 3 + s$. Smooth cutoffs and nondegenerate stationary phase give the compact-uniform remainder. Continuing the expansion through the next even relative order, which cancels by the same parity, leaves $O_{\mathcal{K}}(r^{-8})$. □

Independent exact control and numerical use. At $p = 0$ the source is a constant preparation times $J_0(r)D_3(r)$, where

$$D_3(r) = \frac{4J_1(r)[J_0(r)^2 + J_1(r)^2]}{r} - \frac{4J_0(r)J_1(r)^2}{r^2}.$$

A separate rational Bessel product expansion gives the resonant r^{-6} coefficient $-3/\pi^2$, before the constant preparation. This equals $2B_sK_3$ at $p=0$ and was replayed exactly. It checks one specialization of the polynomial calculation; it is not a proof of the general coefficient by numerical interpolation.

For the independent beta-window reference, the extra moment correction is

$$C(h)\left[-\frac{3Q(s)\mathcal{P}_s}{128\pi^2}\right]\frac{(.55R)^{-6-2h}}{6+2h}{}_2F_1(6+2h,16;32;-9/11).$$

At $R=3072$, adding this explicit term reduces the generic exact-wall comparison gap from $1.37\cdot10^{-11}$ to $8.36\cdot10^{-14}$, and the large-imaginary-order gap from $4.52\cdot10^{-12}$ to $1.49\cdot10^{-14}$. The script reads only the physical parameters and the derived coefficient; no moment value is used to choose it. These comparisons remain numerical evidence because the source/window quadrature and the numerical remainder constant have not been jointly certified.

Effective source expansions and complete saddle populations

The following arguments extend this section. Lettered identifiers retain stable links to the integrated constructions; their correspondence is given at the beginning of the paper. Earlier bounds remain valid on their stated domains. A limitation described at an intermediate stage is superseded only by a later explicitly proved result, as summarized in the current coverage table.

An exact Bessel source and an effective remainder (R4)

(Here $d=1-z^2$, $a=3z$, and Φ_L, w_k are the finite-Laurent prepared source and mode weights defined in Sections R2–R3 below.)

Lemma R4.1 (Exact finite source)**.** *For $K_f=k_0+k_1+k_2$,*

$$\Phi_L(r)=d^{9+6s}\sum_{k_0,k_1,k_2=-L}^{L}(-1)^{K_f}w_{k_0}w_{k_1}w_{k_2}J_{K_f}(ar)\det[J_{k_j+\ell-j}(r)]_{j,\ell=0}^{2}. \tag{R4.1}$$

Proof. Expand both Vandermonde determinants into permutations σ,τ. Each eigenangle integral is $\mathrm{i}^{k_j+\sigma(j)-\tau(j)}J_{k_j+\sigma(j)-\tau(j)}(r)$ and the direction integral is $\mathrm{i}^{K_f}J_{K_f}(ar)$. The permutation shifts sum to zero, leaving $(-1)^{K_f}$. In the complete sum, relabelling the three k_j makes all six τ terms equal, cancelling the Weyl factor $1/6$. The other permutation sum is the displayed determinant. □

Set

$$a_j(n)=\frac{\prod_{\ell=1}^{j}[4n^2-(2\ell-1)^2]}{j!8^j},\quad a_0(n)=1,\qquad q_n=n^2-\tfrac14.$$

These coefficients and phases agree with the classical Hankel normalization in DLMF §10.17 [4]. The following proof supplies the explicit remainder needed here without imposing a truncation restriction depending on the Bessel order.

Lemma R4.2 (Volterra remainder for every integer order)**.** *For $n\in\mathbb{Z}$, $x>0$ and integer $M\ge1$, put*

$$J_{n,M}(x)=\frac{1}{\sqrt{2\pi x}}\sum_{\epsilon=\pm1}e^{\mathrm{i}\epsilon(x-n\pi/2-\pi/4)}\sum_{j=0}^{M-1}(\mathrm{i}\epsilon)^j a_j(n)x^{-j}.$$

Then

$$|J_n(x)-J_{n,M}(x)|\le\sqrt{\frac{2}{\pi x}}\,2|a_M(n)|x^{-M}e^{|q_n|/x}, \tag{R4.2}$$

$$|J_n(x)|\le\sqrt{\frac{2}{\pi x}}e^{|q_n|/x}. \tag{R4.3}$$

Proof. The normalized outgoing solution $u(x) = \sqrt{\pi x/2}\, e^{\mathrm{i}(n\pi/2+\pi/4)} H_n^{(1)}(x)$ satisfies $u'' + u = q_n x^{-2} u$ and the outgoing Volterra equation

$$u(x) = e^{\mathrm{i}x} + \int_x^\infty \sin(t-x)\frac{q_n}{t^2} u(t)\, dt.$$

The positive iterated kernel has jth bound $(|q_n|/x)^j/j!$, proving $|u(x)| \le e^{|q_n|/x}$. Let $c_j = \mathrm{i}^j a_j(n)$ and $u_M = e^{\mathrm{i}x}\sum_{j<M} c_j x^{-j}$. Its coefficients obey $c_{j+1} = [j(j+1) - q_n]c_j/[2\mathrm{i}(j+1)]$, and direct differentiation gives

$$(\partial_x^2 + 1 - q_n x^{-2})u_M = +2\mathrm{i}M c_M e^{\mathrm{i}x} x^{-M-1}.$$

Thus $u - u_M$ has an outgoing forcing integral of absolute size at most $2|a_M|x^{-M}$. Iterating the same positive kernel bounds its error by $2|a_M|x^{-M}e^{|q_n|/x}$. For real argument and integer order, the incoming Hankel solution is the conjugate of the outgoing solution; their half-sum is J_n. This proves both inequalities with the stated normalization. Negative orders also obey $J_{-n} = (-1)^n J_n$. □

Substitute these expansions into (R4.1), retain total inverse-radius degree $j < M$, and collect all sign placements. Write the result at a chosen $R > 0$ as

$$A_{L,M}(r) = r^{-2}\sum_{m=0}^{3}\sum_{j=0}^{M-1}(R/r)^j\left[c_{m,j}^{+}e^{\mathrm{i}\omega_m r} + c_{m,j}^{-}e^{-\mathrm{i}\omega_m r}\right], \quad \omega_m = 3z + 2m - 3. \tag{R4.4}$$

Both signs retain the same complex tilt. Every one of the eight eigenangle sign triples is summed before populations are collected. Multiplying one chosen sign placement by a binomial coefficient after a permutation reduction is incorrect; an independent source check detected and repaired that error in the first prototype.

The preserved squared Vandermonde vanishes to degree two for populations $m = 1, 2$ and degree six for $m = 0, 3$. The four-angle phase is nondegenerate for $z > 0$, including when its saddle value ω_m vanishes. Therefore the coefficients below $j = 1$ or $j = 3$, respectively, vanish identically. The code imposes only these exact identities after collecting all sign placements. It does not discard small numerical coefficients.

For a permutation σ and Fourier triple define four orders and scales

$$n = (K_f, k_0 + \sigma(0), k_1 + \sigma(1) - 1, k_2 + \sigma(2) - 2), \qquad \lambda = (a, 1, 1, 1).$$

For $i = 0, \ldots, 3$ put

$$t_{i,j} = |a_j(n_i)|(\lambda_i R)^{-j}, \quad S_i = \sum_{j<M} t_{i,j}, \quad E_i = 2t_{i,M}e^{|n_i^2 - 1/4|/(\lambda_i R)},$$

and define the nonnegative finite price

$$D(n) = \sum_{\substack{0\le j_i<M \\ \sum_i j_i \ge M}} \prod_{i=0}^{3} t_{i,j_i} + \prod_{i=0}^{3}(S_i + E_i) - \prod_{i=0}^{3} S_i. \tag{R4.5}$$

The difference of products is evaluated by a positive telescoping sum.

Theorem R4.3 (Effective complete-population bound)**.** *Let*

$$F_{L,M}(R) = \frac{4d^{9+6\,\mathrm{Re}\,s}}{\pi^2\sqrt{a}} \sum_{\sigma\in S_3}\sum_{k_0,k_1,k_2=-L}^{L} |w_{k_0}w_{k_1}w_{k_2}| D(n). \tag{R4.6}$$

Then, for all $r \ge R$,

$$|\Phi_L(r) - A_{L,M}(r)| \le F_{L,M}(R) r^{-2}(R/r)^M.$$

No division by ω_m occurs in the expansion or the bound.

Proof. An omitted finite product term has total degree at least M. Any term containing an individual Bessel remainder also has at least M inverse powers. At $r \ge R$, its coefficient bound at R consequently gains $(R/r)^M$. The four square-root factors multiply to $4/(\pi^2\sqrt{a}\, r^2)$. Triangle inequalities applied to the complete finite determinant give exactly (R4.6). □

The sums are computable without enumerating every Fourier triple. A polynomial encodes degree j and Fourier mode k at exponent $j(6L+1)+(k+L)$. A product of three such polynomials has its Fourier index in $[0,6L]$, so no carry contaminates the degree index. Arb polynomial convolutions compute the coefficients and positive prices outwards.

An effective expansion that retains the direction (C4)

(Here $d=1-z^2$, $a=3z$, and Φ_L, w_k are the finite-Laurent prepared source and mode weights defined in Sections C2–C3 below.)

Lemma C4.1 (Exact finite Bessel source)**.** *For $n=k_0+k_1+k_2$,*

$$\Phi_L(r)=d^{9+6s}\sum_{k_0,k_1,k_2=-L}^{L}(-1)^n\left(\prod_{q=0}^{2}w_{k_q}\right)J_n(ar)\det[J_{k_q+\ell-q}(r)]_{q,\ell=0}^{2}. \tag{C4.1}$$

Proof. Expand the two Vandermonde determinants into permutations σ,τ. The eigenangle integrals supply $\mathrm{i}^{k_q+\sigma(q)-\tau(q)}J_{k_q+\sigma(q)-\tau(q)}(r)$. The direction integral supplies $\mathrm{i}^nJ_n(ar)$. The offsets sum to zero, so the total phase is $(-1)^n$. Relabelling the Fourier indices makes the six τ contributions equal and cancels the Weyl normalization $1/6$. The remaining permutation sum is the determinant. □

At $z=0$, only $w_0=1$ survives and $J_n(0)$ selects $n=0$. Thus (C4.1) includes the centre exactly. By contrast, expanding the fourth factor $J_n(ar)$ for large argument introduces $a^{-1/2}$, $(ar)^{-j}$ and $e^{|n^2-1/4|/(ar)}$. Their degeneration says nothing about the true moment. We expand only the three Bessels with argument r.

Lemma C4.2 (Inherited effective Bessel remainder)**.** *Set*

$$A_j(v)=\frac{\prod_{\ell=1}^{j}[4v^2-(2\ell-1)^2]}{8^j\,j!},\quad A_0(v)=1,\quad q_v=v^2-\tfrac14.$$

For integer v, $x>0$ and $M\ge1$, let

$$J_{v,M}(x)=\frac{1}{\sqrt{2\pi x}}\sum_{\epsilon=\pm1}e^{\mathrm{i}\epsilon(x-v\pi/2-\pi/4)}\sum_{j=0}^{M-1}(\mathrm{i}\epsilon)^jA_j(v)x^{-j}.$$

Then

$$|J_v(x)-J_{v,M}(x)|\le\sqrt{\frac{2}{\pi x}}\,2|A_M(v)|x^{-M}e^{|q_v|/x}. \tag{C4.2}$$

There is no restriction linking M to the integer order v.

Proof. The normalized outgoing Hankel solution $u=\sqrt{\pi x/2}e^{\mathrm{i}(v\pi/2+\pi/4)}H_v^{(1)}(x)$ satisfies $u''+u=q_vx^{-2}u$, $u(x)\sim e^{\mathrm{i}x}$, and its outgoing Volterra equation has kernel $\sin(t-x)q_v/t^2$. Iterating its positive majorant gives $|u(x)|\le e^{|q_v|/x}$. For $u_M=e^{\mathrm{i}x}\sum_{j<M}\mathrm{i}^jA_j(v)x^{-j}$, direct differentiation leaves forcing $-(\partial_x^2+1-q_vx^{-2})u_M=-2\mathrm{i}M\mathrm{i}^MA_M(v)e^{\mathrm{i}x}x^{-M-1}$. Its absolute outgoing forcing integral is at most $2|A_M(v)|x^{-M}$. Iteration multiplies this by at most $e^{|q_v|/x}$. Taking the half-sum of outgoing and incoming solutions proves (C4.2). This is the already established Volterra argument of the critical-radius package [6]. □

Complete population and Fourier coefficients

Fix $R>0,M\ge3$. Put $\nu_m=2m-3$ for $m=0,1,2,3$. For $\sigma\in S_3$, write $o_q=\sigma(q)-q$. Define

$$\begin{aligned}H_{mjn}=&\sum_{\substack{\epsilon_q=\pm1\\ \#\{q:\epsilon_q=1\}=m}}\sum_{\sigma\in S_3}\operatorname{sgn}(\sigma)(-1)^{\frac12\sum_q\epsilon_qo_q}\sum_{\substack{\sum k_q=n\\ |k_q|\le L}}\prod_q\left[w_{k_q}(-1)^{k_q1_{\epsilon_q=-1}}\right]\\&\cdot\sum_{\substack{j_0+j_1+j_2=j\\ j_q\ge0}}\prod_q\left[\epsilon_q^{j_q}A_{j_q}(k_q+o_q)R^{-j_q}\right],\end{aligned} \tag{C4.3}$$

$$c_{mjn}=d^{9+6s}(2\pi)^{-3/2}\mathrm{i}^je^{-\mathrm{i}\pi\nu_m/4}H_{mjn}. \tag{C4.4}$$

The offset exponent is an integer because $\sum o_q = 0$. Every sign placement remains until its permutation-dependent coefficient has been summed. Multiplying one sign placement by $\binom{3}{m}$ would repeat the failed shortcut preserved in the preceding investigation.

The retained expansion is

$$A_{L,M}(r) = r^{-3/2} \sum_{m=0}^{3} \sum_{j<M} (R/r)^j e^{\mathrm{i}\nu_m r} \sum_{n=-3L}^{3L} c_{mjn} \mathrm{i}^n J_n(ar) \tag{C4.5}$$

$$= \frac{r^{-3/2}}{2\pi} \int_0^{2\pi} \sum_{m,j} (R/r)^j C_{mj}(\phi) e^{\mathrm{i}r(\nu_m + a\cos\phi)}\, d\phi, \qquad C_{mj}(\phi) = \sum_n c_{mjn} e^{\mathrm{i}n\phi}. \tag{C4.6}$$

The equality uses the exact angular integral of J_n. The returned angular coefficient already contains i^j and its saddle phase. There is no extra i^n in the angular integrand.

Lemma C4.3 (Modewise Vandermonde cancellation)**.** *For every Fourier mode n, $c_{mjn} = 0$ if $j < 1$ for $m = 1, 2$, or if $j < 3$ for $m = 0, 3$.*

Proof. Fix the direction ϕ in the original three-eigenangle integral. At a saddle with m plus signs, the squared Vandermonde vanishes to degree $m(m-1) + (3-m)(2-m)$: two at mixed saddles and six at pure saddles. The inverse-radius coefficient of degree j in the local Gaussian expansion uses amplitude derivatives of degree at most $2j$. Those derivatives vanish below the asserted thresholds. Thus the entire coefficient is zero as a trigonometric polynomial in ϕ, and every Fourier coefficient vanishes. This is a finite Taylor-coefficient identity, independent of any observed small numerical residual. □

The implementation verifies that every ball for one of these proved zeros contains zero before replacing it by exact zero. All other ball radii remain. The source consequently decays as $r^{-5/2}$ uniformly at the centre without expanding ar.

An explicit positive remainder

For one Fourier triple and permutation let $v_q = k_q + o_q$ and set

$$t_{qj} = |A_j(v_q)| R^{-j}, \quad S_q = \sum_{j<M} t_{qj}, \quad E_q = 2t_{qM} e^{|v_q^2 - 1/4|/R}.$$

Define

$$D(v) = \sum_{\substack{0 \le j_q < M \\ \sum j_q \ge M}} \prod_q t_{qj_q} + \prod_q (S_q + E_q) - \prod_q S_q,$$

where the difference of products is evaluated by a positive telescoping sum. Its finite complete price is

$$F_{L,M}(R; z, s) = d^{9+6\,\mathrm{Re}\,s} (2/\pi)^{3/2} \sum_{\sigma \in S_3} \sum_{k_0,k_1,k_2=-L}^{L} |w_{k_0} w_{k_1} w_{k_2}| D(v). \tag{C4.7}$$

Theorem C4.4 (Centre-uniform finite-source remainder)**.** *For $0 \le z < 1$, complex s, integers $L \ge 0, M \ge 3$ and $r \ge R > 0$,*

$$|\Phi_L(r) - A_{L,M}(r)| \le F_{L,M}(R; z, s)\, r^{-3/2} (R/r)^M.$$

Proof. Apply (C4.2) to the three eigenangle Bessels in (C4.1). Every discarded polynomial product has total degree at least M, and any product with an individual remainder has at least that degree. After extracting their three square roots, they are bounded by $D(v)(R/r)^M$. The unexpanded direction factor obeys $|J_n(ar)| \le 1$ for integer n and real ar, directly from its angular integral. Summing the exact determinant terms proves the result. No division by a or by a population frequency occurs. □

The positive Fourier sums factor before degree convolution. For offset o, form

$$P_o(X) = \sum_{j<M} \sum_k |w_k||A_j(k+o)|R^{-j}X^j$$

and the corresponding summed E_o. Three scalar polynomial products per permutation price the discarded degrees; a scalar positive telescope prices the remainders. The signed coefficient construction instead uses encoded Arb polynomial convolutions with Fourier stride $6L+1$, so Fourier carry cannot change the inverse-radius degree.

For a uniform angular price let $\bar{w}_k$ be the absolute preparation coefficients at $Z, s = 3$, which majorize every $|w_k|$ for $z \le Z$, $|s| \le 3$. Define

$$P_o^{(\rho)}(X) = \sum_{j<M} \sum_k \bar{w}_k |A_j(k+o)|R^{-j}e^{\rho|k|}X^j, \qquad P^{(\rho)} = \sum_{\sigma\in S_3} \prod_q P^{(\rho)}_{\sigma(q)-q}.$$

For the nonvanishing degrees,

$$\sum_n |c_{mjn}|e^{\rho|n|} \le A_{mj,\rho} := (1-Z^2)^{-9}(2\pi)^{-3/2}\binom{3}{m}[X^j]P^{(\rho)}(X). \tag{C4.8}$$

Set the right side to zero at the proved vanishing degrees. This follows by taking absolute values after Lemma C4.3, using $e^{\rho|\sum k_q|} \le \prod e^{\rho|k_q|}$, and counting sign placements. Taking separate upper preparation and prefactor maxima legitimately enlarges the bound; it does not assert that one tilt attains both.

What deteriorated and what repaired it (U2)

With $a = 3z$, $d = 1-z^2$, $p = 3+s$, the exact transformed source is

$$S_3 = a + \operatorname{Tr} V, \qquad A_{z,s}(w) = d^{9+6s}\prod_{j=1}^{3}(1+zw_j)^{-p}(1+z/w_j)^{-p}.$$

Both preparation factors retain the same complex exponent. The measure with complex density is not normalized into a probability measure. The Haar Vandermonde and the physical return are preserved.

The original real-frequency source and Mellin-image estimates extend through $z = .9$ with explicit strip width .05 and enlarged preparation grids. The decisive deterioration was in the finite-preparation tail. Replacing each $|p+n|$ by $n+|p|$ while separately maximizing $d^{9+6\Re s}$ mixes incompatible extremes of the tilt. The old free-kernel Bessel bound then introduces $\exp(|n^2-1/4|/x)$ at high Fourier orders. Those two losses compound even though the ordinary moment is finite.

The following repairs address the actual sources of loss.

1. The disk identity $|n+3+s|^2 \le (n+3)^2 + 2(n+3)\Re s + 9$ keeps the preparation and determinant factor correlated on 96 tilt bands.

2. For integer n and $x > |n|$, the exact Green kernel gives

$$|J_n(x) - J_{n,M}(x)| \le \sqrt{\frac{2}{\pi x}}\frac{2|A_M(n)|x^{-M}}{\sqrt{1-n^2/x^2}}, \quad A_M(n) = \frac{\prod_{j=1}^{M}[4n^2-(2j-1)^2]}{8^M M!}.$$

   The strict turning-point gates remain mandatory. This is an effective bound derived for this evaluator; no claim of priority over the classical Bessel literature is made.

3. A formal cubic population determinant and an exact four-point DFT retain all signs while reducing the cost of the coefficient construction.

4. Finite Abel summation contracts constant-frequency lattice tails with an explicit remainder. Forward differences act on the combined degree polynomial before the scalar readout.

5. Exact dyadic basis normalization, already present in the inherited HaarSpectral native solver, is restored on both source centres and native error radii. The physical angular allowance is not multiplied twice.

At the final upper cell, the completed uniform allowance is dominated by the complete preparation return, about $3.49404\,10^{-19}$. The Bessel contribution is below $7.569\,10^{-22}$; the omitted image is below $1.819873\,10^{-31}$; the Abel remainder is below $1.132\,10^{-117}$. Increasing the asymptotic order alone would not meaningfully improve that complete uniform allowance.

Effective source, remainder and scalar readout (U9)

This appendix supplies the analytic proofs behind the new components and the composition audit. The continuous-cell numerical inequalities are stated separately in the main theorem. A finite exact-arithmetic approximation, an executed outward inequality, and an executed finite-arithmetic scalar certificate are different assertions throughout.

The original preparation and ordinary domain

Write $d = 1 - z^2$, $a = 3z$, $p = 3 + s$, and let μ_3 be normalized Haar measure on $U(3)$. The inherited exact Möbius change of eigenvalues gives

$$T_3(h, s; z) = \int |a + \operatorname{Tr} V|^{2h} A_{z,s}(V)\, d\mu_3(V), \qquad A_{z,s}(w) = d^{9+6s} \prod_{\nu=1}^{3} (1 + z w_\nu)^{-p} (1 + z/w_\nu)^{-p}. \tag{U9.1}$$

The eigenvalue density in this integral includes the complete squared Vandermonde. It is not replaced by independent eigenangles. Both factors in each pair have the same complex exponent. For $|w| = 1$, the principal analytic logarithms of $1 + zw$ and $1 + z/w$ have opposite arguments; their sum is the real logarithm of their positive product. The power of d uses its positive-real logarithm. These conventions preserve the original complex tilt, without conjugation or probability renormalization.

Proposition U9.1 (ordinary domain through the upper interval). For $0 \le z \le 0.9$ and every complex s, the ordinary absolute moment in (U9.1) exists exactly when $\operatorname{Re} h > -1$. On this domain it is jointly holomorphic in (h, s) and continuous in z.

Proof. The inherited centre construction proves that $X = \operatorname{Tr} V$ has a bounded planar density, with the explicit bound 2.296122. Translation preserves this bound. On a compact set $z \le Z < 1$ and a compact tilt set, the preparation in (U9.1) is bounded. On the target tilt disk one convenient bound is

$$|A_{z,s}| \le (1 - Z)^{-9} (1 + Z)^{27}.$$

Indeed, putting $u = \operatorname{Re} s$, the product is bounded by $d^{9+6u}(1-z)^{-18-6u} = (1-z)^{-9}(1+z)^{9+6u}$. The local planar integral of $|y|^{2\operatorname{Re} h}$ is finite for $\operatorname{Re} h > -1$; compact support handles the exterior.

To prove necessity, set $a = 3z$ and choose eigenvalues

$$(-1, e^{it}, e^{-it}), \qquad \cos t = (1 - a)/2.$$

For $a \in [0, 2.7]$, the cosine lies in $[-0.85, 0.5]$; the three eigenvalues are distinct. The derivatives of the trace with respect to the first two angles are $-i$ and ie^{it}, whose real Jacobian has nonzero determinant $\sin t$. Thus a regular chart of the trace map, with strictly positive squared Vandermonde and absolute preparation, contributes a positive local density near the zero mark. The ordinary absolute integral diverges when $\operatorname{Re} h \le -1$. Logarithmic powers from complex differentiation are dominated by a slightly smaller exponent still above -1. Uniform local integrability and the bounded preparation logarithms give holomorphy and continuity. □

For clarity, the source identities used below remain ordinary-expectation identities. Their use does not continue a divergent expectation across $\operatorname{Re} h = -1$. The physical radial source

$$\Phi(r) = \int A_{z,s}(V) J_0(r|a + \operatorname{Tr} V|)\, d\mu_3(V)$$

has sufficient decay for the inherited sampled Mellin identity on this ordinary domain. One direct qualitative justification is to fix the Fourier direction and apply stationary phase to the three eigenangles. The phase Hessians

at the sign saddles are nondegenerate. The squared Vandermonde vanishes to degree at least two at a mixed saddle and degree six at a pure saddle, giving $O(r^{-5/2})$ uniformly on compact preparation sets. The translation phase has modulus one on the real direction. This argument justifies convergence and analytic identity; it is not the effective numerical remainder used below.

An effective Bessel remainder from the exact Green kernel

For integer n, set

$$A_0(n) = 1, \qquad A_j(n) = \frac{\prod_{\ell=1}^{j}(4n^2-(2\ell-1)^2)}{8^j j!}, \qquad \chi_n = \frac{n\pi}{2} + \frac{\pi}{4}.$$

Theorem U9.2 (Nicholson–Green remainder). Let $M \geq 1$, $n \in \mathbb{Z}$, and $x > |n|$. Define

$$J_{n,M}(x) = \frac{1}{\sqrt{2\pi x}} \sum_{\epsilon=\pm 1} e^{i\epsilon(x-\chi_n)} \sum_{j=0}^{M-1} (i\epsilon)^j A_j(n) x^{-j}.$$

Then

$$|J_n(x) - J_{n,M}(x)| \leq \sqrt{\frac{2}{\pi x}}\, \frac{2|A_M(n)|x^{-M}}{\sqrt{1-n^2/x^2}}. \tag{U9.2}$$

For all $x \geq X > |n|$, the denominator can be replaced by $\sqrt{1-n^2/X^2}$. The theorem holds for every truncation order M; it does not assume truncation before a least term.

Proof. Nicholson's exact identity and the positive integral for K_0 are

$$J_n(x)^2 + Y_n(x)^2 = \frac{8}{\pi^2} \int_0^\infty K_0(2x\sinh t)\cosh(2nt)\, dt, \qquad K_0(y) = \int_0^\infty e^{-y\cosh u}\, du.$$

These are NIST DLMF 10.9.30 and 10.32.9, respectively. The second identity shows that K_0 decreases on the positive ray. Since $\sinh t \geq t$, Tonelli's theorem and $x > |n|$ imply

$$\begin{aligned} \int_0^\infty K_0(2xt)\cosh(2nt)\, dt &= \int_0^\infty \frac{x\cosh u}{2(x^2\cosh^2 u - n^2)}\, du \\ &= \frac{x}{2}\int_0^\infty \frac{dv}{x^2v^2 + x^2 - n^2} = \frac{\pi}{4\sqrt{x^2-n^2}}, \end{aligned}$$

where $v = \sinh u$. Hence

$$J_n(x)^2 + Y_n(x)^2 \leq \frac{2}{\pi\sqrt{x^2-n^2}}. \tag{U9.3}$$

This bound contains no large-argument approximation.

Put $q = n^2 - \frac{1}{4}$ and $\mathcal{L}_n = d^2/dx^2 + 1 - q/x^2$. The real functions

$$f(x) = \sqrt{\pi x/2}\, J_n(x), \qquad g(x) = \sqrt{\pi x/2}\, Y_n(x)$$

solve the homogeneous equation and have Wronskian $fg' - f'g = 1$, by the standard Bessel Wronskian (equivalently DLMF 10.5.5 for the Hankel pair). For $t \geq x$, define

$$G_n(x,t) = f(x)g(t) - g(x)f(t).$$

Then $G(x,x) = 0$, $\partial_x G(x,t)|_{t=x} = -1$, and $\mathcal{L}_n G(\,\cdot\,,t) = 0$. Thus $\int_x^\infty G_n(x,t)F(t)\, dt$ solves $\mathcal{L}_n y = F$ for the integrable forcing used below. By Cauchy's inequality and (U9.3),

$$|G_n(x,t)| \leq [(1-n^2/x^2)(1-n^2/t^2)]^{-1/4} \leq (1-n^2/x^2)^{-1/2}. \tag{U9.4}$$

Normalize the outgoing solution and its finite polynomial by

$$u_n(x) = e^{i\chi_n}\sqrt{\pi x/2}\, H_n^{(1)}(x), \qquad u_{n,M}(x) = e^{ix}\sum_{j=0}^{M-1} i^j A_j(n) x^{-j}.$$

The coefficient recurrence gives the exact residual

$$\mathcal{L}_n u_{n,M}(x) = 2iM\, i^M A_M(n) e^{ix} x^{-M-1}. \tag{U9.5}$$

In particular, at $M = 1$ this is $-qx^{-2}e^{ix}$, because $A_1 = q/2$. This checks the sign; only the modulus enters the ensuing allowance.

Set $F = -\mathcal{L}_n u_{n,M}$. The exact Green integral is $O(x^{-M})$, and its derivative tends to zero. Consequently

$$u_{n,M}(x) + \int_x^\infty G_n(x,t)F(t)\,dt$$

solves the homogeneous equation with outgoing leading coefficient one and no incoming leading term. Uniqueness in the two-dimensional Hankel basis identifies it with u_n. This uses only the fixed-order leading asymptotic, not a prior effective remainder. Equations (U9.4)–(U9.5) yield

$$|u_n - u_{n,M}| \le \frac{2M|A_M(n)|}{\sqrt{1-n^2/x^2}} \int_x^\infty t^{-M-1}\,dt = \frac{2|A_M(n)|x^{-M}}{\sqrt{1-n^2/x^2}}.$$

Taking the real part after multiplication by $e^{-i\chi_n}$ and restoring the normalization proves (U9.2). All bounds depend on n^2; the displayed phases retain the correct negative-integer orders. □

For the finite Laurent source, the eigenangle orders satisfy $|n| \le L+2$ and translated orders satisfy $|n| \le 3L$. It is therefore enough to require

$$R > L + 2, \qquad aR > 3L.$$

The individual normalized remainders are then bounded, at $r \ge R$, by

$$\frac{2|A_M(n)|R^{-M}}{\sqrt{1-n^2/R^2}}(R/r)^M, \qquad \frac{2|A_M(n)|(aR)^{-M}}{\sqrt{1-n^2/(aR)^2}}(R/r)^M.$$

Inserting these positive bounds into the inherited complete four-factor telescope preserves every determinant permutation and sign population. Discarded polynomial degrees are unchanged. The old unrestricted Volterra bound remains available where the turning-point gate fails or where it gives a sharper allowance.

The independent Arb check executes 119 expansion inequalities through $M = 64$, 51 Green-kernel inequalities, signed orders, and arguments 10^{-6} above a turning threshold. A large-order case required 3072-bit arithmetic after 1536-bit direct Bessel balls were too wide. The precision failure is retained in the receipt. These finite checks audit the implementation; the theorem proves the continuous scope.

Preparation bounds retaining the complex tilt

Let

$$f_{p,z}(w) = (1+zw)^{-p}, \quad B_L(w) = \sum_{n=0}^{L} b_n w^n, \quad b_n = \frac{(-z)^n (p)_n}{n!}.$$

The finite preparation A_L substitutes B_L for all six factors in (U9.1).

Lemma U9.3 (actual-input Taylor norm). For a fixed complex p, set

$$q_L = z \max\left(1, \frac{|p+L+1|}{L+2}\right) < 1, \qquad e_L = \frac{|b_{L+1}|}{1-q_L}, \qquad B = \sum_{n=0}^{L} |b_n| + e_L.$$

Then $\|f - B_L\|_\infty \le e_L$, both one-factor norms are at most B, and

$$\|A - A_L\|_\infty \le \delta = 6d^{9+6\,\mathrm{Re}\,s} B^5 e_L. \tag{U9.6}$$

Proof. For subsequent coefficients the squared ratio, divided by z^2, is

$$\left|1+\frac{p-1}{n+1}\right|^2 = 1+2(\operatorname{Re} p-1)t+|p-1|^2t^2, \qquad 0\le t\le \frac{1}{L+2}.$$

This convex quadratic is bounded by its endpoint maximum. The coefficient inequality remains true when a coefficient is zero; no division by that coefficient is needed. A geometric tail proves the one-factor assertions. The six-factor telescoping identity proves (U9.6). The proof does not assume monotonicity of individual ratios, and covers $\operatorname{Re} p<1$ and $p=0$. □

For continuous tilt coverage it is advantageous to retain the exact disk correlation

$$|n+3+s|^2=(n+3)^2+2(n+3)\operatorname{Re} s+|s|^2\le (n+3)^2+2(n+3)u_++9$$

on a band $u_-\le \operatorname{Re} s\le u_+$. With the upper radius z_+, define

$$\beta_0=1, \qquad \beta_{n+1}=\beta_n z_+\frac{\sqrt{(n+3)^2+2(n+3)u_++9}}{n+1}.$$

Then $|b_n|\le\beta_n$ throughout the band and radius cell. The same convex-quadratic argument gives a computable geometric tail. Finite convolution produces the pair Fourier majorants

$$W_k=\sum_{n=0}^{L-|k|}\beta_{n+|k|}\beta_n.$$

The per-eigenvalue physical prefactor is bounded by the maximum of d^{3+2u_-} at the two radius endpoints. Taking a maximum over the finite tilt-band cover for each mode is a valid enlargement. It does not assert that different extrema occur at one physical tilt. The physical complex coefficients in the scalar formula are unchanged; these positive quantities are used only for error bounds.

The complete return and a sharper integral allowance

Let $Y=a+\operatorname{Tr} V$ and $D=3(1+z_+)$. For $\Delta D<2\pi$, put

$$C_\Delta(h)=2(2/\Delta)^{2h}\frac{\Gamma(1+h)}{\Gamma(-h)}.$$

If $\Phi(r)=\sum_{j\ge0}a_jr^{2j}$, the inherited sampled identity is

$$T_3=C_\Delta(h)\sum_{k\ge1}k^{-1-2h}\Phi(k\Delta)-I, \qquad I=\sum_{j\ge0}[C_\Delta(h)\zeta(1+2h-2j)]a_j\Delta^{2j}. \tag{U9.7}$$

The bracketed factors are continued through their removable products before multiplication.

Proposition U9.4 (complete preparation return). Suppose $\|A-A_L\|_\infty\le\delta$ and $\int|A-A_L|\,d\mu_3\le\epsilon$. Let U_h bound $\int|Y|^{2\operatorname{Re} h}d\mu_3$, let

$$W_K=|C_\Delta(h)|\sum_{k=1}^{K}k^{-1-2\operatorname{Re} h},$$

and let I_{diff} be the inherited absolute, deflated image comparison weight per unit source mass. Replacing only the terminal tail by the finite preparation costs at most

$$\delta U_h+\epsilon W_K+\epsilon I_{\mathrm{diff}}. \tag{U9.8}$$

In particular $\epsilon=\delta$ recovers the inherited complete return.

Proof. The difference of terminal tails equals the difference of complete moments minus the finite-prefix and image differences, by (U9.7) for the two sources. The singular full-moment difference is bounded by δU_h. On a real radial sample the Fourier kernel has modulus one, so its source difference is at most ϵ. This gives ϵW_K. The jth radial coefficient difference is at most

$$\epsilon\,\frac{(D/2)^{2j}}{(j!)^2},$$

by the physical J_0 expansion. Multiplication by the absolute entire image weights and their convergent reflected tail gives $\epsilon I_{\mathrm{diff}}$. Every one of the three return terms is therefore retained. □

An optional refinement supplies a much smaller ϵ without changing the singular-moment bound. For a tilt band let

$$v_* = \sqrt{9 - \min_{u\in[u_-,u_+]} u^2}, \qquad C_f = (1+z_+)^{3+u_+}\exp(v_*\arcsin z_+).$$

The circle $1+ze^{i\theta}$ stays in the right half-plane and has argument at most $\arcsin z$. Hence $|f^{-1}| \le C_f$. If e bounds the one-factor Taylor tail, then

$$|A - A_L| \le \eta|A|, \qquad \eta = (1+eC_f)^6 - 1.$$

The original preparation return and the inherited nonnegative Schur expansion give, for real u,

$$\int |A_{z,s}|\,d\mu_3 = \mathbb{E}_{U(3)}|\Lambda_3(z)|^{2u} \le (1-z^2)^{-u^2}.$$

Thus, with $U = \max(|u_-|,|u_+|)$,

$$\epsilon \le \min\{\delta,\ \eta(1-z_+^2)^{-U^2}\}. \tag{U9.9}$$

This is a bound on the original physical variation, not a normalization of the tilted source. It is computed using $\mathrm{expm1}(6\log 1p(eC_f))$ to retain small radii. Taking finite-band maxima yields a continuous full-box theorem. The outward component matrix confirms a substantial reduction in sufficient Laurent degrees; the main connected theorem does not need this optional refinement.

The original finite source and image contracts

The upper-radius work retains the inherited original-source engine and its signed, untranslated direction projection. It reprices its analytic constants at an upper radius $Z < 1$. Choose $t > 0$ with

$$Ze^t < 1, \qquad E = \frac{2Z(\cosh t - 1)}{(1-Z)^2} < 1.$$

Put $d_Z = 1 - Z^2$ and

$$g_- = (1-Z)^2(1-E), \qquad g_+ = (1+Ze^t)(1+Ze^{-t}),$$
$$\eta_t = \arctan\frac{2Z\sinh t}{(1-Z^2)(1-E)}, \qquad C_t = d_Z^{-5}\max(g_-^{-4}, g_+^2)e^{3\eta_t}\left(\frac{e^t - Z}{1-Ze^t}\right)^2,$$
$$M_* = d_Z^{-9}, \qquad m_* = (1-Z)^6,$$
$$V_t = M_*\left[\frac{d_Z^2}{(1-Z^2e^{-2t})(1-Z^2e^{2t})}\right]^9.$$

These are the inherited one-body Cauchy majorant, total-variation mass, real-tilt Gram floor and signed-direction strip majorant, enlarged to the full independent complex parameter box. For a preparation DFT of length $P > 2L_r$ and even direction grid Q, retain the distinct signed direction modes $|k| \le Q/2 - 1$, excluding both Nyquist modes. Then

$$\varepsilon_r = \frac{2C_t}{1-e^{-t}}\left(e^{-(L_r+1)t} + (2L_r+1)e^{-(P-L_r)t}\right),$$
$$E_\Phi \le \frac{4V_te^{-tQ/2}}{1-e^{-t}} + M_*\left[(1+3\varepsilon_r/m_*)^3 - 1\right]. \tag{U9.10}$$

The translation coefficients are contracted after the signed projection; using a pointwise translated direction trapezoid on an unbounded real radial lattice would be a different, unproved contract.

For $\operatorname{Re} h \in [-0.95, 3]$, $|\operatorname{Im} h| \le 3$, let

$$G(u) = \Gamma(1+u)^2(2/\Delta)^{2u}, \qquad C_* = \frac{2\cosh(3\pi)}{\pi}\max\{G(-0.95), G(3)\}.$$

Gamma reflection and logarithmic convexity yield

$$|C_\Delta(h)| \le C_*, \quad W_K \le \frac{2\cosh(3\pi)}{\pi}\max\left\{G(-0.95)\frac{(K+1)^{1.9}}{1.9},\ G(3)\zeta(7)\right\}.$$

The finite real-source contribution is $W_K E_\Phi$, repriced at the actual common cutoff K.

The inherited complex-circle image formula uses m samples on $r = He^{\pi i\ell/m}$, retaining $J \le m$ scaled coefficients $H^{2j}a_j$. For completeness its analytic errors are as follows. Let $W = \max((1-Z)^{-6}, (1+Z)^6)$ and $b = H/2$. This W bounds the one-body integral norm in the original Haar basis; it is not asserted to bound the pointwise transformed preparation. With image resources (P_i, L_i, Q_i), require $H > 0$, $J \ge 4$, $P_i > 2L_i$, $2L_i < Q_i$ with even Q_i, $b < L_i + 2$, and $HD/2 < m+1$. Set

$$\begin{aligned} E_{\mathrm{mode}} &= \frac{2We^{b^2}b^{L_i+1}}{(L_i+1)![1-b/(L_i+2)]}, \\ E_{\mathrm{alias}} &= \frac{2C_t e^{-t(P_i-L_i)}}{1-e^{-tP_i}}, \qquad \varepsilon_i = E_{\mathrm{mode}} + (2L_i+1)E_{\mathrm{alias}}e^H, \\ E_{\Phi,i} &= \frac{2M_* e^{HD\cosh 2}}{e^{2Q_i}-1} + 9\varepsilon_i(We^H + 3\varepsilon_i)^2 e^{3HZ}. \end{aligned}$$

Here $D = 3(1+Z)$. The fully translated direction trapezoid is allowed on this bounded complex circle because its error is the first displayed term. The physical coefficient bound $|a_j| \le M_*(D/2)^{2j}/(j!)^2$ gives the common scaled circle alias

$$E_{\mathrm{circ}} = \frac{M_*(HD/2)^{2m}}{(m!)^2[1-(HD/(2m+2))^2]}.$$

The image coefficient error is $E_a = E_{\Phi,i} + E_{\mathrm{circ}}$. It is multiplied by $\sum_{j<J}\sup|C_\Delta\zeta(1+2h-2j)|(\Delta/H)^{2j}$. For $j = 0, 1, 2, 3$, the inherited outward Euler–Maclaurin rectangle bound for $(w-1)\zeta(w)$ is used with the removable sine quotient. For $j \ge 4$, the functional equation gives

$$|C_\Delta\zeta(1+2h-2j)| \le \frac{2C_*\cosh(3\pi)\zeta(2j-6)}{(2\pi)^{2j}}\max_{u\in\{-0.95,3\}}(2\pi)^{2u}\Gamma(2j-2u).$$

For the omitted image terms put $x = \Delta D/(2\pi)$ and

$$q = x^2\max\left(1, \frac{J+0.95}{J+1}\right)\max\left(1, \frac{J+1.45}{J+1}\right) < 1.$$

Their total is bounded by

$$\frac{2C_*\cosh(3\pi)M_*\zeta(2J-6)}{(J!)^2(1-q)}(x/2)^{2J}\max_{u\in\{-0.95,3\}}(2\pi)^{2u}\Gamma(2J-2u).$$

All mode, circle and image ratio gates are checked outward.

Uniformity at the upper radius follows directly: g_- decreases, g_+ increases, the argument and Möbius-factor bounds increase, and

$$\frac{d_Z^2}{(1-Z^2e^{-2t})(1-Z^2e^{2t})} = \left[1 - \frac{4Z^2\sinh^2 t}{(1-Z^2)^2}\right]^{-1}$$

increases before its checked pole. The mass, inverse Gram floor and support bounds increase as well. Thus these are interval-wide inequalities, not endpoint samples. At $Z = 0.9$, $t = 0.05$, $P = Q = 8192$, $L_r = 4090$, $(J, m, H, Q_i, L_i, P_i) = (72, 144, 3, 256, 88, 8192)$, and $K = 262144$, the executed 384-bit source/image total is below $1.819873\,10^{-31}$. The common grids themselves are unexecuted. Actual scalar receipts use their own adaptive grid and arithmetic allowances.

Exact population extraction

The inherited finite Laurent expansion aggregates

$$\sum_{\substack{\epsilon_\nu\in\{-1,1\}\\ \#\{\epsilon_\nu=1\}=m}}\sum_{\pi\in S_3}\operatorname{sgn}(\pi)(-1)^{\frac12\sum_\nu \epsilon_\nu(\pi(\nu)-\nu)}\prod_{\nu=0}^{2}P_{\epsilon_\nu,\pi(\nu)-\nu}.$$

Let $b_\nu=\pi(\nu)-\nu$. Since $\sum b_\nu=0$, $\frac12\sum\epsilon_\nu b_\nu=\sum_{\epsilon_\nu=1}b_\nu$. Consequently the exact population m is the coefficient of u^m in $\det[Q_{\ell-j}(u)]_{j,\ell=0}^{2}$, where

$$Q_b(u)=P_{-,b}+u(-1)^bP_{+,b}.$$

Over the commutative ring of encoded polynomials, this determinant equals

$$Q_0(Q_0^2-Q_{-2}Q_2-2Q_{-1}Q_1)+Q_{-1}^2Q_2+Q_1^2Q_{-2}.$$

It has degree at most three. Its values at $1,i,-1,-i$ recover every population by the exact inverse four-point DFT, with no alias and no approximate root of unity. This proves the faster coefficient engine is an algebraic rearrangement of the complete sign/permutation sum.

The inherited Vandermonde identities still justify the exact initial zeros: three orders at pure populations and one at mixed populations. Checking that the computed pre-zero balls contain zero is a useful implementation guard. Numerical containment alone is not the proof of the vanishing identity.

Effective finite Abel contraction

Proposition U9.5 (Abel remainder). Let $\operatorname{Re}p>1$, $q=e^{i\theta}\neq1$, $K\geq1$, $N=K+1$, and $B\geq1$. With $Df(k)=f(k+1)-f(k)$,

$$\sum_{k>K}q^kf(k)=\frac{q^N}{1-q}\sum_{\ell=0}^{B-1}\left(\frac{q}{1-q}\right)^\ell D^\ell f(N)+\left(\frac{q}{1-q}\right)^B\sum_{k>K}q^kD^Bf(k).$$

For $f(k)=k^{-p}$, the last term has modulus at most

$$\frac{|(p)_B|K^{1-\operatorname{Re}p-B}}{(\operatorname{Re}p+B-1)|1-q|^B}. \tag{U9.11}$$

Proof. Absolute convergence permits subtraction and gives $(1-q)S_f=q^Nf(N)+qS_{Df}$. Iteration yields the identity with the displayed positive powers of $q/(1-q)$. The repeated integral formula is

$$D^Bk^{-p}=(-1)^B(p)_B\int_{[0,1]^B}(k+t_1+\cdots+t_B)^{-p-B}\,dt_1\cdots dt_B.$$

Bounding its modulus and then the decreasing positive lattice sum by the integral from K to infinity proves (U9.11). □

Write the retained four-Bessel expansion as

$$A_M(r)=r^{-2}\sum_{m=0}^{3}\sum_{\sigma=\pm1}e^{i\sigma\omega_mr}\sum_{j<M}c_{mj}^\sigma(R/r)^j,\quad \omega_m=3z+2m-3,\quad R=K\Delta.$$

For each frequency, combine the degrees before forming finite differences:

$$g(k)=k^{-p_0}\sum_{j<M}c_j(K/k)^j,\qquad p_0=3+2h.$$

This is an exact finite rearrangement. Its unweighted Abel allowance is

$$\Delta^{-2}K^{1-\operatorname{Re}p_0-B}|1-q|^{-B}\sum_{j<M}\frac{|c_j||(p_0+j)_B|}{\operatorname{Re}p_0+j+B-1}.$$

All finite differences and phase evaluations are enclosed by Acb; coefficient uncertainty remains in the resulting ball. On the target order box $\operatorname{Re} p_0 \geq 1.1$. For $0.4 \leq z \leq 0.9$ and $\Delta = 0.5$, every phase has $|\Delta\omega_m| < \pi$, and the two smaller absolute physical frequencies have positive minima 0.2 and 0.3. For another spacing the implementation checks its actual outward gap. It also checks positive spacing and consistency of the expansion radius and physical input.

The independent audit compares this contraction to the inherited polylogarithm-minus-finite-sum formula on synthetic complex coefficients and actual small Laurent preparations. The comparisons retain separately priced enclosures. Deliberately reversing the finite-difference sign is rejected. These checks audit the readout and do not independently verify the shared finite source coefficients.

Tail caches and precision composition

Suppose a sealed coefficient cache at $R_0 > 0$ certifies

$$|\Phi_L(r) - A_M(r)| \leq F_0 r^{-2}(R_0/r)^M \qquad (r \geq R_0).$$

For exact $R \geq R_0$, set

$$c_j(R) = c_j(R_0)(R_0/R)^j, \qquad F_R = F_0(R_0/R)^M.$$

The expansion and error function are unchanged term by term:

$$c_j(R)(R/r)^j = c_j(R_0)(R_0/r)^j, \qquad F_R r^{-2}(R/r)^M = F_0 r^{-2}(R_0/r)^M.$$

Restricting to $r \geq R$ proves the rescaled contract immediately. No new asymptotic cancellation or unproved monotonicity is required.

The loader binds exact z, s, L, M, R_0, all four populations, coefficient lengths and frequencies to the sealed payload and source hashes. It parses the real and imaginary Arb components while preserving their radii, rejects nonfinite data, and refuses $R < R_0$. Increasing subsequent working precision cannot recreate cached coefficients at a higher precision. Both precisions are therefore recorded separately. The first reader's inability to parse a printed two-component Acb string was an execution failure before a numerical receipt; it was repaired by a separate validated reader while preserving the builder and cache hashes. Independent rescaling checks compare 384 coefficients with the inherited permutation engine and eight small finite-source evaluations with their effective bounds.

Deflated integers and the final scalar error disk

For an image index j, put $\varepsilon = h - j$, $P_j(h) = \prod_{\ell=0}^{j-1}(\ell - h)$, and $\zeta_{\mathrm{reg}}(w) = \zeta(w) - (w-1)^{-1}$. The removable product has the exact local form

$$C_\Delta(h)\zeta(1 + 2h - 2j) = -(2/\Delta)^{2h}\frac{\Gamma(1+h)P_j(h)}{\Gamma(1-\varepsilon)}[1 + 2\varepsilon\zeta_{\mathrm{reg}}(1+2\varepsilon)].$$

This expression is regular at $\varepsilon = 0$. The evaluator uses the deflated factor before interval multiplication near an integer. For $h = m = 0, 1, 2, 3$ exactly real, $C_\Delta(m) = 0$, while the sole surviving image product is

$$[C_\Delta(h)\zeta(1 + 2h - 2m)]_{h=m} = (-1)^{m+1}4^m(m!)^2\Delta^{-2m}.$$

Since $a_m = (-1)^m T_3(m, s; z)/(4^m(m!)^2)$, the image equals $-T_3(m, s; z)$. Thus the exact integer shortcut $T_3 = -I$ is valid: no finite-preparation tail is used and its allowance is zero. This shortcut makes no assertion about derivatives in h.

For noninteger inputs, if the four-Bessel source remainder is $Fr^{-2}(R/r)^M$, its weighted lattice allowance is

$$E_{\mathrm{B}} = \frac{|C_\Delta(h)|F}{\Delta^2}\frac{K^{-2-2\operatorname{Re} h}}{M + 2 + 2\operatorname{Re} h}.$$

The Abel allowance is separately multiplied by the actual $|C_\Delta(h)|$. Let E_{native} be the sealed fixed-point arithmetic allowance, E_{angular} the actual original angular-source allowance, and E_{image} the complete original image allowance. The final error is

$$E_{\mathrm{total}} = E_{\mathrm{native}} + E_{\mathrm{angular}} + E_{\mathrm{image}} + E_{\mathrm{B}} + E_{\mathrm{Abel}} + E_{\mathrm{prep}} + E_{\mathrm{ball/readout}}. \tag{U9.12}$$

Here E_{prep} is the complete return (U9.8). The last term encloses the difference between the fully combined ball and the printed decimal centre.

The native dyadic frame is an exact algebraic preconditioner. If its matrix is B, with diagonal scales 2^{-e_j}, and an integer divisor v is used, then

$$\det(BAB^{\mathsf{T}}/v) = 2^{-2\sum e_j} v^{-3} \det A.$$

The positive rational factor $v^3\, 2^{2\sum e_j}$ restores both the native centre and its arithmetic allowance. The analytic angular error is already in original physical units and is not multiplied a second time. A floating factorization only proposes the literal dyadic matrix; its accuracy is not an unpriced mathematical assumption.

The finite source is contracted at its own precision, and its enclosing ball is retained when imported at the higher tail precision. Native residuals, analytic source errors and image errors are separate charges; raising tail precision does not reduce them. This proves (U9.12) by the triangle inequality with all arithmetic dependencies retained. For a decimal centre m, if $|m|_{\mathrm{lower}} - E_{\mathrm{total}} > 0$, the justified relative radius is

$$\frac{E_{\mathrm{total}}}{|m|_{\mathrm{lower}} - E_{\mathrm{total}}}.$$

If this denominator is not positive, only an absolute certificate is reported. Parameter samples do not establish uniform nonvanishing.

An independent original-circle integer check

An additional audit bypasses the transformed Fourier preparation and Mellin readout. On the original eigenvalue circle set

$$q_+(\lambda) = \frac{d\lambda}{1 - z\lambda}, \quad q_-(\lambda) = \frac{d}{\lambda - z}, \quad g(\lambda) = (1 - z\lambda)(1 - z/\lambda).$$

Andréief's identity gives the generating determinant

$$\mathbb{E}_{U(3)}\left[|\Lambda|^{2s} e^{tS + u\overline{S}}\right] = \det\left[\int_{|\lambda|=1} g(\lambda)^s \lambda^{j-k} e^{tq_+ + uq_-} \frac{d\lambda}{2\pi i\lambda}\right]_{j,k=0}^{2}.$$

The ordinary integer moment is $(m!)^2[t^m u^m]$ of this determinant. All bidegrees are nonnegative, so truncating each entry separately at degree m in each variable is exact for this coefficient. On the real circle $q_- = \overline{q_+}$; the tilt g^s is not conjugated.

The original-circle strip bounds enclose each entry coefficient by a positive B_{ab} and its trapezoid error by E_{ab}. Six determinant products and three telescoping differences in each give the coefficientwise majorant $18E(B+E)^2$. Extracting its (m,m) coefficient and multiplying by $(m!)^2$ therefore prices the complete analytic quadrature error. The finite jet arithmetic stays inside the Acb coefficients. This comparison is independent of the transformed preparation and image contraction, while remaining a check of the same original Haar moment and independent complex tilt.

Auxiliary retained-translation populations and effective remainder (O8)

The following construction records the exact odd-rank saddle structure and a computable product remainder. It also supplies independent rational checks of complete population aggregation. The active scalar evaluator uses the previous original-source contour, so success of these auxiliary checks is not used as a moment certificate.

Exact finite Bessel determinant

For $|k| \le L$, let b_j be the finite preparation coefficients of Section O7 (and (O4.3) in Section O4 below), and set

$$w_k = \sum_{j=0}^{L-|k|} b_{j+|k|} b_j, \qquad B_L(w) B_L(w^{-1}) = \sum_{k=-L}^{L} w_k w^k.$$

The symmetry is $w_{-k} = w_k$, with no complex conjugation. Expanding the normalized determinant in (O4.3) and then integrating the direction gives the exact finite-prepared source

$$\Phi_L(r) = d^{N^2+2Ns} \sum_{k_0,\dots,k_{N-1}=-L}^{L} (-1)^{\sum k_j} J_{\sum k_j}(ar) \prod_j w_{k_j} \sum_{\sigma\in S_N} \operatorname{sgn}(\sigma) \prod_{j=0}^{N-1} J_{k_j+\sigma(j)-j}(r). \tag{O8.1}$$

The Weyl factor $1/N!$ has already cancelled in Andreief's identity; there is no further factorial. The two plane-wave phase products give $(-1)^{\sum k_j}$. Formula (O8.1) remains exact at $a = 0$, where the translated Bessel factor is retained rather than expanded in inverse powers of a.

Define

$$A_j(n) = \frac{\prod_{\ell=1}^{j}[4n^2 - (2\ell-1)^2]}{8^j j!}, \qquad A_0(n) = 1.$$

For a scale $R > 0$, integer degree $M \geq 1$, sign $\varepsilon = \pm 1$, and offset o, introduce the formal Laurent polynomials

$$\begin{aligned} P_{\varepsilon,o}(X,v) &= \sum_{|k|\leq L} \sum_{j<M} w_k (-1)^{k\mathbf{1}_{\{\varepsilon=-1\}}} \varepsilon^j A_j(k+o) R^{-j} X^j v^k, \\ Q_o(u,X,v) &= P_{-1,o}(X,v) + u(-1)^o P_{1,o}(X,v), \\ \mathcal{D}_N(u,X,v) &= \det[Q_{c-r}(u,X,v)]_{0\leq r,c<N}. \end{aligned}$$

The coefficient of u^m contains every placement of m plus signs and every determinant permutation. The offset phase is exact: since $\sum_j(\sigma(j)-j) = 0$, its signed half-sum reduces to $(-1)^{\sum_{\varepsilon_j=+1}(\sigma(j)-j)}$, precisely the factor inserted above.

Put $H_{m,j,n} = [u^m X^j v^n]\mathcal{D}_N$ and

$$c_{m,j,n} = d^{N^2+2Ns}(2\pi)^{-N/2} i^j e^{-i\pi(2m-N)/4} H_{m,j,n}.$$

Retaining total inverse degree $j < M$ gives

$$\mathcal{A}_{L,M}(r) = r^{-N/2} \sum_{m=0}^{N} \sum_{j<M} \sum_{n} (R/r)^j e^{i(2m-N)r} c_{m,j,n} i^n J_n(ar). \tag{O8.2}$$

This is a complete population sum. A single sign placement times a binomial multiplicity would not in general reproduce its coefficients.

Proposition O8.1 (Modewise Vandermonde cancellation)**.** *For every population and every direction Fourier mode,*

$$c_{m,j,n} = 0 \quad \text{if} \quad j < v_m := \frac{m(m-1) + (N-m)(N-m-1)}{2}. \tag{O8.3}$$

The same local vanishing order holds with the original analytic preparation.

Proof. At a sign saddle, the within-sign squared Vandermondes vanish to total local degree $2v_m$; the cross-sign factors are nonsingular. The eigenangle Hessian is nondegenerate. An inverse-radius coefficient of degree j uses amplitude derivatives of order at most $2j$, so it vanishes when $j < v_m$. Equivalently, rescale each local coordinate by $r^{-1/2}$: the amplitude contributes r^{-v_m} before the ordinary Hessian factor $r^{-N/2}$. Finite Laurent factors do not remove these zeros. The assertion is an identity in the retained direction, hence holds for each Fourier mode separately. The exact determinant expansion has the same unique stationary-phase coefficients. □

The relevant powers are

N	m	v_m	$N/2 + v_m$
5	0, 5	10	25/2
5	1, 4	6	17/2
5	2, 3	4	13/2
7	0, 7	21	49/2
7	1, 6	15	37/2
7	2, 5	11	29/2
7	3, 4	9	25/2

At $\Re h = -0.95$, the corresponding worst sampled summands have absolute powers at least $k^{-5.6}$ and $k^{-11.6}$. The untranslated frequencies $2m - N$ are nonzero at odd rank, and $|2m - N + Nz\cos\phi| \geq 1 - Nz$ when $Nz < 1$. The local cancellation argument itself does not divide by this gap.

Effective rank-dependent product remainder

Assume $R > L + N - 1$ and $r \geq R$. The inherited Nicholson/Green one-factor theorem, valid at every truncation degree, states

$$J_{n,M}(r) = \frac{1}{\sqrt{2\pi r}} \sum_{\varepsilon=\pm 1} e^{i\varepsilon(r - \pi n/2 - \pi/4)} \sum_{j<M} (i\varepsilon)^j A_j(n) r^{-j},$$
$$|J_n(r) - J_{n,M}(r)| \leq \sqrt{\frac{2}{\pi r}} \frac{2|A_M(n)| r^{-M}}{\sqrt{1 - n^2/r^2}}. \tag{O8.4}$$

The stated radius gate covers every order $n = k_j + \sigma(j) - j$. No condition on ar is imposed because the translation factor is kept exact.

Set

$$t_{n,j} = |A_j(n)| R^{-j}, \qquad S_n = \sum_{j<M} t_{n,j}, \qquad E_n = \frac{2t_{n,M}}{\sqrt{1 - n^2/R^2}}.$$

For a tuple $n_q = k_q + \sigma(q) - q$, define the nonnegative quantity

$$D(\boldsymbol{n}) = \sum_{\substack{0 \leq j_q < M \\ \sum_q j_q \geq M}} \prod_q t_{n_q, j_q} + \prod_q (S_{n_q} + E_{n_q}) - \prod_q S_{n_q}. \tag{O8.5}$$

The second difference is evaluated by a positive telescope, avoiding subtraction of close numerical products. Put

$$F_{N,L,M,R} = d^{N^2 + 2N\Re s} (2/\pi)^{N/2} \sum_{\sigma \in S_N} \sum_{k_0, \ldots, k_{N-1} = -L}^{L} \prod_q |w_{k_q}| \, D(\boldsymbol{n}). \tag{O8.6}$$

Proposition O8.2 (Finite product remainder)**.** *With the preceding hypotheses,*

$$|\Phi_L(r) - \mathcal{A}_{L,M}(r)| \leq F_{N,L,M,R} \, r^{-N/2} (R/r)^M. \tag{O8.7}$$

For a sharp sampled tail after K, with $R = K\Delta$ and $M + N/2 + 2\Re h > 0$, its scalar remainder allowance is

$$|C_\Delta(h)| F_{N,L,M,R} \Delta^{-N/2} \frac{K^{-N/2 - 2\Re h}}{M + N/2 + 2\Re h}. \tag{O8.8}$$

Proof. Normalize each Bessel factor by $\sqrt{2/(\pi r)}$. The discarded polynomial products of total degree at least M cost the first term of (O8.5), times $(R/r)^M$. Every term in the exact product telescope that contains at least one one-factor remainder costs the second term with the same factor. Sum absolute coefficients over every mode tuple and permutation in (O8.1), retaining $|J_n(ar)| \leq 1$. This proves (O8.7). Integral comparison for the positive power tail proves (O8.8). □

The Fourier sums in the positive remainder can first be collected into scalar degree polynomials for each offset. A permanent subset recurrence then requires $O(N2^N)$ polynomial products. This is an explicit finite algorithm, but no executed rank-five or rank-seven scalar certificate is claimed from this alternative remainder. Its use would additionally require (O7.2), the actual finite prefix and image, and arithmetic. A filtered cutoff would also need its own omitted fractions, rather than silently importing the sharp-tail allowance.

Executed exact coefficient challenges

The rational subset-determinant implementation packs mode, population, and inverse-radius indices with widths $2NL+1$ and $N+1$, so no relevant coefficient aliases. Nonnegative encoded exponents permit truncation below $M(N+1)(2NL+1)$. It uses $N2^{N-1}$ polynomial products instead of explicit sign and permutation enumeration. The preserved receipt records

N	L	M	(z,s)	exact zero coefficients checked
3	0	4	$(0,0)$	8
5	0	11	$(0,0)$	40
7	0	22	$(0,0)$	112
5	1	11	$(1/50,2/5)$	440
7	1	12	$(1/50,2/5)$	1320
				1920

The receipt also preserves nonzero leading rational rows, including individual direction modes. These checks independently challenge the complete population encoding, phases, and cancellation identities. They are exact finite coefficient tests; the general vanishing statement comes from Proposition O8.1. They are not new ordinary moment or finite-source arithmetic certificates.

The distinction between the two constructions is consequential. The auxiliary method exposes and prices individual Bessel populations. The main method controls the original filtered source on a single analytic deformation, retaining every population and Vandermonde factor before absolute estimation. Its positive odd-rank gap is the feature that closes the central interval. Even ranks require a separate treatment of their balanced zero-frequency population; no transfer of that gap or of rank-three constants is made here.

Finite Laurent preparation and complete populations at rank four (E4)

For a finite degree L, define

$$b_k=\frac{(-z)^k(p)_k}{k!},\qquad B_L(w)=\sum_{k=0}^{L}b_kw^k,\qquad w_k=\sum_{j=0}^{L-|k|}b_{j+|k|}b_j\quad(|k|\le L).\tag{E4.1}$$

Thus $B_L(w)B_L(w^{-1})=\sum_{|k|\le L}w_kw^k$ with $w_{-k}=w_k$; no coefficient is conjugated. Define

$$A_L=d^{N^2+2Ns}\prod_j B_L(w_j)B_L(w_j^{-1}),$$

and let $T_L,\Phi_L,a_{L,j}$ denote its moment, radial source, and Taylor coefficients.

For real ϕ put

$$D_\phi(r)=\det\left[\sum_{|k|\le L}w_ki^ke^{ik\phi}J_{k+c-r_0}(r)\right]_{r_0,c=0}^{N-1}.\tag{E4.2}$$

Its Fourier support is $|n|\le NL$. If $D_n(r)$ are its coefficients, Andreief and the exact direction integral give

$$\Phi_L(r)=d^{N^2+2Ns}\sum_{|n|\le NL}D_n(r)i^nJ_n(ar).\tag{E4.3}$$

There is no additional $N!$: Andreief has cancelled the normalized Weyl factor. Equation (E4.3) also shows why an exact DFT of D_ϕ needs only $Q>2NL$. Placing the translation inside that DFT would produce a different, non-bandlimited quadrature.

Set $A_0(v)=1$ and

$$A_j(v)=\frac{\prod_{\ell=1}^{j}[4v^2-(2\ell-1)^2]}{8^jj!}.\tag{E4.4}$$

Fix a scaling $R > 0$ and degree cutoff $M \geq 1$. For an offset o, form

$$Q_o(v, X, \xi) = \sum_{|k| \leq L} \sum_{j=0}^{M-1} w_k A_j(k+o) R^{-j} X^j \xi^k \big[(-1)^{k+j} + v(-1)^o\big].$$

Define

$$H_{mjn} = [v^m X^j \xi^n] \det[Q_{c-r_0}(v, X, \xi)]_{r_0, c=0}^{N-1}, \quad c_{mjn} = d^{N^2+2Ns}(2\pi)^{-N/2} i^j e^{-i\pi(2m-N)/4} H_{mjn}. \tag{E4.5}$$

The retained source is

$$\mathcal{A}_{L,M}(r) = r^{-N/2} \sum_{m=0}^{N} \sum_{j=0}^{M-1} \sum_{|n| \leq NL} c_{mjn} (R/r)^j e^{i(2m-N)r} i^n J_n(ar). \tag{E4.6}$$

The population variable sums every sign placement, while the determinant retains every permutation and its sign.

Lemma E4.1 (Phases and exact cancellations)**.** *Let $v_m = m(m-1)/2 + (N-m)(N-m-1)/2$. Then $c_{mjn} = 0$ for $j < v_m$. When N is even, the balanced coefficients additionally satisfy $c_{N/2,j,n} = 0$ whenever $n + j$ is odd.*

Proof. In the two-wave expansion of J_{k+o}, a sign ε contributes $e^{i\varepsilon r} e^{-i\varepsilon\pi/4} i^{-\varepsilon(k+o)} (i\varepsilon)^j A_j(k+o)$. Multiplication by the i^k in (E4.2) and $\sum o = 0$ gives exactly (E4.5). At a sign saddle the same-sign squared Vandermondes vanish to degree $2v_m$ in the local coordinates. A stationary-phase coefficient at inverse degree j uses amplitude derivatives of degree at most $2j$; hence it vanishes for $j < v_m$. The phase Hessian in the N eigenangle directions is nonsingular, and ϕ remains a parameter. The identity is therefore an identity of finite Fourier polynomials, so every mode vanishes. This geometric coefficient argument does not assert an effective remainder; that is supplied separately below.

For balanced populations, pair a complete sign placement with its opposite. For fixed modes and determinant permutation their coefficient ratio is $(-1)^{\sum k + \sum j + \sum o} = (-1)^{n+j}$. The opposite placement has the same balanced population and opposite pairs exhaust it. Thus the odd parity coefficients cancel exactly. A selected placement multiplied by a binomial coefficient would not establish either cancellation. □

A positive, effective product remainder

The inherited Nicholson–Green lemma, proved in the completed rank-three upper-radius investigation, states that for every integer v, $r > |v|$, and $M \geq 1$,

$$\left| J_v(r) - \frac{1}{\sqrt{2\pi r}} \sum_{\varepsilon = \pm 1} e^{i\varepsilon(r - v\pi/2 - \pi/4)} \sum_{j<M} (i\varepsilon)^j A_j(v) r^{-j} \right| \leq \sqrt{\frac{2}{\pi r}} \frac{2|A_M(v)| r^{-M}}{\sqrt{1 - v^2/r^2}}. \tag{E4.7}$$

It follows from Nicholson's positive Hankel bound and the exact Bessel Green kernel applied to the residual of the finite outgoing polynomial. No translation Bessel factor is expanded in the present application.

For $R > L + N - 1$, define, for every offset o,

$$p_{o,j} = \sum_{|k| \leq L} |w_k| \, |A_j(k+o)| R^{-j}, \qquad P_o(X) = \sum_{j<M} p_{o,j} X^j,$$

$$S_o = P_o(1), \qquad E_o = \sum_{|k| \leq L} |w_k| \frac{2|A_M(k+o)| R^{-M}}{\sqrt{1 - (k+o)^2/R^2}}.$$

Write $o_r = \sigma(r) - r$ for each permutation σ. The finite, nonnegative constant

$$F_{L,M,R} = d^{N^2+2N\Re s} (2/\pi)^{N/2} \sum_{\sigma \in S_N} \left\{ \sum_{j \geq M} [X^j] \prod_{r=0}^{N-1} P_{o_r}(X) + \sum_{r=0}^{N-1} E_{o_r} \prod_{q<r} (S_{o_q} + E_{o_q}) \prod_{q>r} S_{o_q} \right\} \tag{E4.8}$$

can be evaluated by positive convolutions and a permanent subset recurrence. The second line is a positive telescope, not subtraction of nearly equal large products.

Proposition E4.2 (Complete finite-source remainder)**.** *For every $r \ge R > L + N - 1$,*

$$|\Phi_L(r) - \mathcal{A}_{L,M}(r)| \le F_{L,M,R}\, r^{-N/2}(R/r)^M. \tag{E4.9}$$

At $R = K\Delta$, if $M + N/2 + 2\Re h > 0$, its scalar sharp-tail allowance is

$$E_{\mathrm{prod}} = \frac{|C_\Delta(h)| F_{L,M,R} \Delta^{-N/2} K^{-N/2-2\Re h}}{M + N/2 + 2\Re h}. \tag{E4.10}$$

Proof. Apply (E4.7) to each factor. A discarded polynomial term of total degree at least M gains $(R/r)^M$; each factor remainder has the same gain, and subsequent gains are at most one. The positive telescope prices every product replacement. Sum every permutation and preparation mode, retaining $|J_n(ar)| \le 1$ only after the exact direction return. This proves (E4.9); integrating the positive lattice-power majorant proves (E4.10). □

4. Exact low-rank thresholds

One eigenvalue

Proposition 4.1 (rank-one moment and cutoff thresholds).

At rank one, $|S_1| = (1 - z^2)/|1 - z\lambda_1|$ and $\Lambda_1 = 1 - z\lambda_1$. Expanding the two binomial factors in $|1 - z\lambda_1|^{2(s-h)}$ and taking their constant Fourier mode gives, for every $h, s \in \mathbb{C}$,

$$T_1(h, s; z) = (1 - z^2)^{2h}\, {}_2F_1(h - s, h - s; 1; z^2).$$

Uniform convergence of the binomial expansions on $|z| \le z_* < 1$ justifies multiplication and integration. At $z = 0$, $T_1 = 1$, while $\Phi(\rho) = J_0(\rho)$. The Mellin tail then behaves as a constant times $\rho^{-2h-3/2}\cos(\rho - \pi/4)$, by the Bessel asymptotics (NIST DLMF 10.17.3). It converges absolutely for $\operatorname{Re} h > -1/4$ and ordinarily for $\operatorname{Re} h > -3/4$. The derivative $J_0' = -J_1$ gives the different ordinary derivative threshold $\operatorname{Re} h > -1/4$. At $z > 0$ the radial leading power is ρ^{-1} and the four distinct frequencies $\pm 1 \pm z$ are nonzero. Integration by parts in each frequency gives the Mellin and derivative thresholds in the theorem. The sharp endpoint argument for an arbitrary finite collection of frequencies is given below.

Two eigenvalues

Proposition 4.2 (rank-two tails and density at zero).

For a Haar unitary matrix of size two, set

$$F(t) = \mathbb{E}\big[|\Lambda_2(z)|^{2s} J_0(t|S_2(z)|)\big], \qquad t \ge 0.$$

All powers of positive real numbers are defined using the real logarithm. In particular, the following estimates hold for complex s. For $0 < z < 1$ the two tails have the exact ranges

	ordinary improper convergence	absolute convergence
$\int_1^\infty t^{-2h-1} F(t)\, dt$	$\Re h > -5/4$	$\Re h > -3/4$
$\int_1^\infty t^{-2h} F'(t)\, dt$	$\Re h > -3/4$	$\Re h > -1/4.$

The absolute-convergence entries here concern the *radial, angularly averaged* integrand. An absolute-value estimate before angular averaging is a separate question. The ordinary two-exponent moment in the interior exists precisely for $\Re h > -1$, so the first tail also converges in a strip outside the moment's domain. At $z = 0$ the two tails and the moment all have the range $\Re h > -1/2$. Both tails at $z = 0$ converge absolutely on that range.

Interior stationary points.

Write $w_j = (\lambda_j - z)/(1 - z\lambda_j) = e^{i\phi_j}$. Then $S_2 = 2z + w_1 + w_2$ and $1 - z\lambda_j = (1 - z^2)/(1 + zw_j)$. From the Haar eigenangle density $|\lambda_1 - \lambda_2|^2\, d\theta_1\, d\theta_2/[2(2\pi)^2]$ and the angular integral for J_0, with $u_j = \phi_j - \alpha$, we get

$$F(t) = \frac{1}{2(2\pi)^3} \int_{[0,2\pi]^3} e^{it\Phi}\, A\, d\alpha\, du_1\, du_2, \qquad \Phi = 2z\cos\alpha + \cos u_1 + \cos u_2,$$

$$A = (1 - z^2)^{4+4s} |e^{iu_1} - e^{iu_2}|^2 \prod_{j=1}^{2} |1 + ze^{i(u_j+\alpha)}|^{-4-2s}.$$

The eight stationary points have $\alpha, u_1, u_2 \in \{0, \pi\}$. The Hessian is diagonal, with entries $-2z\cos\alpha$, $-\cos u_1$ and $-\cos u_2$. It has absolute determinant $2z$. At the four mixed points ($u_1 \neq u_2$) the amplitude is $4(1 - z^2)^{2s}$. The phase values are $2z$ and $-2z$, each twice, with signatures -1 and $+1$, respectively. At the other four points the Vandermonde factor vanishes to second order. Their first possible contributions are of order $t^{-5/2}$. Put $B_z = 2(1 - z^2)^{2s}/(\pi^{3/2}\sqrt{z})$. Stationary phase on the compact torus gives

$$F(t) = B_z\, t^{-3/2} \cos(2zt - \pi/4) + O(t^{-5/2}),$$
$$F'(t) = -2zB_z\, t^{-3/2} \sin(2zt - \pi/4) + O(t^{-5/2}).$$

The second formula follows by applying stationary phase with amplitude $i\Phi A$. The errors are locally uniform for (z, s) in compact subsets of $(0, 1) \times \mathbb{C}$. No estimate uniform down to $z = 0$ is asserted. The remaining phase values are $\pm 2 \pm 2z$; none is zero in the open interval. At $z = 1/2$ a remaining frequency meets a mixed frequency, but it occurs one power lower and cannot cancel the displayed leading term.

For each tail, above its ordinary threshold the leading term converges by integration by parts at the nonzero frequencies and the remainder is absolutely integrable. For sharpness set $\sigma = \Re h$. On fixed-length subintervals recurring every period, the leading trigonometric factor has constant sign and magnitude bounded below. The factor $t^{-2i\Im h}$ varies there by $O(t^{-1})$ relative to its left endpoint, and $B_z \neq 0$. If the real power of the leading amplitude is nonnegative, the integral over these subintervals fails the Cauchy criterion, including at equality. For absolute convergence one uses the same subintervals and sums their magnitudes. The borderline is the harmonic series. This argument proves all four strict endpoints in the table.

Interior density and agreement with the moment.

For $S_2 = 0$ the two preimages in the labelled angular torus have $(w_1, w_2) = (-z + i\sqrt{1 - z^2}, -z - i\sqrt{1 - z^2})$ and its permutation. The absolute Jacobian of $(\phi_1, \phi_2) \mapsto (\Re S_2, \Im S_2)$ is $|\sin(\phi_1 - \phi_2)| = 2z\sqrt{1 - z^2}$. At either preimage $|1 + zw_j|^2 = 1 - z^2$ and $|w_1 - w_2|^2 = 4(1 - z^2)$. The inverse function theorem and compactness now give a smooth tilted density $f_{z,s}$ in a neighborhood of zero, with

$$f_{z,s}(0) = \frac{(1 - z^2)^{2s+1/2}}{2\pi^2 z}.$$

This is an unnormalized density with respect to planar Lebesgue measure. Its nonzero value and the area factor $r\, dr\, d\theta$ yield the threshold $\Re h > -1$; for absolute integrability one may equivalently use the positive tilt $\Re s$.

The centre, $z = 0$.

Here the weight is one. Rotational invariance and the two-by-two Toeplitz determinant of $e^{it\cos\theta}$ give the exact identities

$$F(t) = J_0(t)^2 + J_1(t)^2, \qquad F'(t) = -\frac{2}{t} J_1(t)^2.$$

The standard large-argument Bessel expansion gives

$$F(t) = \frac{2}{\pi t} + O(t^{-2}), \qquad F'(t) = -\frac{2}{\pi t^2}\big[1 + \cos(2t - 3\pi/2)\big] + O(t^{-3}).$$

Both weighted tails have a nonzero constant term proportional to t^{-2h-2}. Absolute convergence follows for $\Re h > -1/2$. For failure when $\Re h \le -1/2$, choose a fixed $a > 1$ close to 1 so that $\int_1^a u^{-2h-2}\,du \neq 0$. The constant term integrated on $[R, aR]$ has magnitude a positive constant times $R^{-2\Re h-1}$. The integrated remainders and, for the derivative, the nonzero-frequency term, are $O(R^{-2\Re h-2})$ by integration by parts for the latter. The Cauchy criterion fails on and below the boundary, including at complex h with nonzero imaginary part.

There is also a direct density check. The angular separation has density $(1 - \cos\Delta)/(2\pi)$ on $[0, 2\pi]$, so $|S_2| = 2|\cos(\Delta/2)|$ has density $\sqrt{4 - r^2}/\pi$ for $0 < r < 2$. The planar density is $\sqrt{4 - r^2}/(2\pi^2 r)$ and is singular at zero. Thus

$$\mathbb{E}|S_2|^{2h} = \frac{4^h \Gamma(h + 1/2)}{\sqrt{\pi}\,\Gamma(h + 2)}, \qquad \Re h > -\frac{1}{2}.$$

The distribution at the centre and the interior smooth density explain the difference in moment thresholds.

A source partition for rank-three inverse moments at the critical radius

The following construction retains the prepared Haar source and changes the numerical readout. It does not propagate the twenty-component differential state. In particular, it does not replace the established branch-connection results.

Put $a = 3z$, $d = 1 - z^2$, $\nu = -3 - s$, and write $p = w_1 + w_2 + w_3$ for three unit eigenvalues. The prepared Weyl representation is

$$T_3(h, s; z) = d^{9+6s}\mathbb{E}_{U(3)}\left[|a - p|^{2h}\prod_{j=1}^{3}|1 - z w_j|^{2\nu}\right].$$

The positive bases of every complex power use the real logarithm. Thus the preparation remains a complex weight when s is nonreal.

Proposition 4.3 (regular conditional partition). Let $K \ge 1$ be an integer and define

$$R = |a - p|^2, \qquad q_j = |a - w_j|^2, \qquad D = R + q_1 + q_2 + q_3 = 3 + |p - 2a|^2,$$

$$P_j = \frac{q_j}{D}\sum_{\ell=0}^{K-1}\left(\frac{R}{D}\right)^{\ell}, \qquad P_{\mathrm{reg}} = \left(\frac{R}{D}\right)^{K}.$$

Then $D \ge 3$, $P_j, P_{\mathrm{reg}} \ge 0$, and

$$\sum_{j=1}^{3} P_j + P_{\mathrm{reg}} = 1. \tag{4.1}$$

For $0 < z < 1$, $\Re h > -1$, and every independent complex s, insertion of this identity into the prepared Weyl integral is exact. The three P_j contributions agree by permutation symmetry. The regular contribution has the form $R^{h+K}D^{-K}$ times the original preparation. None of these changes requires division by a signed critical gap or by a connection denominator.

Proof. Expansion of the four squared moduli gives the displayed formula for D. Set $t = R/D \in [0, 1]$. Since $\sum_j q_j = D - R$, the sum of the first three weights is $(1 - t)\sum_{\ell=0}^{K-1} t^\ell = 1 - t^K$, including $t = 1$ by the finite polynomial identity. All the weights are bounded by one. The ordinary prepared moment is absolutely integrable on the stated domain by the finite-rank planar-density result; multiplication by these bounded weights preserves that property. Permutation symmetry and the finite sum justify the decomposition without changing the preparation or invoking analytic continuation. □

The conditional pair readout. Condition the P_3 term on $v = w_3 = e^{it}$. Let $V \in U(2)$ have eigenvalues u_1, u_2, and put

$$b = |a - v|, \qquad \psi = \arg(a - v).$$

The Weyl constants give exactly

$$\mathbb{E}_{U(3)}F(w_1,w_2,w_3)=\frac{1}{3}\int_0^{2\pi}\mathbb{E}_{U(2)}[F(u_1,u_2,e^{it})|u_1-e^{it}|^2|u_2-e^{it}|^2]\frac{dt}{2\pi} \tag{4.2}$$

for every integrable function F of the labelled Weyl angles. The factor three from (4.1) cancels the $1/3$ here. Reflection of all angles changes neither the positive bases nor the complex exponents, so the outer integral can be written on $[0,\pi]$ without complex conjugating its weight.

Write $u_{1,2}=e^{i(\psi+\phi\pm\theta)}$, with $0\le\theta\le\pi/2$ and $-\pi\le\phi\le\pi$. The normalized pair measure is

$$\frac{2}{\pi^2}\sin^2\theta\,d\theta\,d\phi.$$

The mark and the remaining repulsion factor are

$$R=(b-2\cos\theta)^2+8b\cos\theta\sin^2(\phi/2),$$

$$|u_1-v|^2|u_2-v|^2=16\sin^2\left(\frac{\psi+\phi+\theta-t}{2}\right)\sin^2\left(\frac{\psi+\phi-\theta-t}{2}\right). \tag{4.3}$$

Keeping this factor inside the quadrature is important. At $b=2$ the conditional two-angle unweighted mode integrals have worse integrability than the conditional physical sum that retains the pair Vandermonde. The full three-angle mode integrals need not diverge. Evaluating divergent conditional pieces separately and cancelling their numerical approximations would nevertheless be invalid.

For $0<b<2$, the moving zero is $\phi=0$, $\theta_0=\arccos(b/2)$. On a local rectangular patch, the two Duffy triangles

$$\theta=\theta_0+LrU,\qquad \phi=PrV,\qquad (U,V)=(1,y)\text{ or }(y,1)$$

factor the singular weight exactly as r^{2h+1}. The reduced mark is evaluated with sine differences, so subtraction of nearly equal cosines is avoided. Geometric panels outside the patch keep the angular aspect ratio bounded as the zero approaches either pair endpoint. For $b>2$, the smallest mark occurs at $(\theta,\phi)=(0,0)$; the implementation resolves scales $\theta\asymp\sqrt{b-2}$ and $\phi\asymp b-2$. The outer angle is split at $b=2$. These are source quadratures, with no inverse-Mellin tail.

Lemma 4.4 (the conditional endpoint thresholds). At $b=2$, the unweighted two-angle absolute integral exists locally exactly when $\Re h>-3/4$. If the pair repulsion $\sin^2\theta$ is retained, the threshold is $\Re h>-5/4$. The remaining cross Vandermonde and preparation factors are smooth and nonzero at this endpoint for an interior radius with $b=2$, so these thresholds apply to the corresponding conditional source.

Proof. Near $(\theta,\phi)=(0,0)$, (4.3) has $R\asymp\theta^4+\phi^2$. Put $x=\theta^2\ge0$ and $y=\phi$. The unweighted measure has factor $x^{-1/2}dx\,dy$, whereas the pair-repulsive measure has factor $x^{1/2}dx\,dy$. Polar coordinates in the half-plane give radial integrals of $r^{2\Re h+\beta+1}dr$ with $\beta=-1/2$ and $1/2$, respectively. The angular integral of $(\cos\alpha)^\beta$ is finite. This yields exactly the two strict thresholds, with logarithmic divergence at equality. The cross factor could vanish only if the spectator equalled the repeated pair eigenvalue. Then $a=3w$ would force $z=1$, which is excluded. □

Thus all inverse orders in the original target, including $\Re h=-0.95$, lie inside the conditional physical domain at $b=2$. The geometric panels resolve an integrable endpoint; they are not a finite-part prescription for a divergent expectation.

Lemma 4.5 (explicit suppression of the conditional central singularity). Put $u=\Re h\in(-1,-1/2)$, and define

$$C_u=\frac{\Gamma(u+1)\Gamma(-u-1/2)}{\pi\Gamma(-u)\Gamma(u+3/2)}.$$

For the trace X of Haar $U(2)$ and $b>0$,

$$\mathbb{E}|b-X|^{2u}\le C_u b^{2u+1}. \tag{4.4}$$

On a compact radius interval, let

$$M(z,s)=\max\{(1-z)^{6\Re\nu},(1+z)^{6\Re\nu}\}.$$

The absolute value of the entire conditional P_3 integrand, including its three preparation factors, is at most

$$\frac{16K}{3}M(z,s)C_u b^{2u+3}. \tag{4.5}$$

At $a=1$, $b=2\sin(t/2)\le t$, so the contribution of $0<t<\epsilon$ to the unnormalized outer integral is at most

$$|d^{9+6s}|\frac{16KM(z,s)C_u}{3\pi(2u+4)}\epsilon^{2u+4}. \tag{4.6}$$

These constants are uniform on compact subsets of the stated order and tilt domain. In particular they include $u=-0.95$.

Proof. The planar density of X is $\sqrt{4-|x|^2}/(2\pi^2|x|)$ on $|x|<2$, hence is at most $1/(\pi^2|x|)$. Extend the nonnegative integral to the plane and scale $x=by$. The remaining convolution is

$$\int_{\mathbb{R}^2}|y|^{-1}|1-y|^{2u}\,d^2y=\pi\frac{\Gamma(u+1)\Gamma(-u-1/2)}{\Gamma(-u)\Gamma(u+3/2)}.$$

For completeness, represent $|y|^{-1}$ and $|1-y|^{-2\alpha}$, $\alpha=-u\in(1/2,1)$, by their positive Gaussian Laplace integrals. Integration in y gives $\pi/(t+v)\exp[-tv/(t+v)]$. Set $t=\lambda x$, $v=\lambda(1-x)$; the λ integral is $\Gamma(\alpha-1/2)[x(1-x)]^{1/2-\alpha}$, and the remaining beta integral is $B(1-\alpha,1/2)$. This gives (4.4) after the density factor. All interchanges are Tonelli interchanges of nonnegative integrands. Next, $P_3\le Kb^2/3$, the cross repulsion is at most sixteen, and the absolute preparation is at most M. This proves (4.5); integration and $b\le t$ prove (4.6). □

This estimate explains why the partition repairs the critical conditional chart. Without it, the inverse conditional moment behaves on the scale b^{2u+1}, which diverges for the deep inverse orders. With it, the upper bound vanishes as b^{2u+3}. The original full rank-three moment was finite in both descriptions: the problem was the conditioning of the chosen one-angle readout, rather than a new divergence of the Haar expectation.

Corollary 4.6 (uniform central cutoff across the critical radius). Let $0<z_-\le z\le z_+<1$, $a_-=3z_-$, $v\in(-1,-1/2)$, $v\le\Re h\le H$, and $0<\epsilon<2\sqrt{a_-}$. The absolute conditional P_3 contribution from the set $b=|3z-e^{it}|\le\epsilon$, including the factor d^{9+6s}/π, is bounded by

$$\frac{16KC_v}{3\pi\sqrt{a_-}\sqrt{1-\epsilon^2/(4a_-)}}\sup_{z,s}\{|d^{9+6s}|M(z,s)\}(2+\epsilon)^{2(H-v)}\epsilon^{2v+4}. \tag{4.7}$$

The supremum is over the declared preparation range. For $z\in[1/4,2/5]$, $|s|\le3$, $-.95\le\Re h\le3$, and $1\le K\le5$, choosing $v=-.95$ and $\epsilon=10^{-13}$ gives the uniform upper bound 7.514×10^{-18}. The imaginary part of h does not enter this absolute estimate. This is a rigorous bound for an exact source-region cutoff; it does not certify floating-point tests of $b\le\epsilon$ or remaining quadratures.

Proof. On $b\le\epsilon$, the Haar $U(2)$ trace satisfies $|X|\le2$, so

$$|b-X|^{2\Re h}\le(2+\epsilon)^{2(H-v)}|b-X|^{2v}.$$

Use (4.4) at the fixed order v and retain the factor $P_3\le Kb^2/3$. Put $\delta=|a-1|$ and $r=2\sqrt{a}\sin(t/2)$. Then $b^2=\delta^2+r^2$ and

$$dt=\frac{dr}{\sqrt{a}\sqrt{1-r^2/(4a)}}.$$

The cutoff is empty if $\delta>\epsilon$. Otherwise r ranges from zero to $\sqrt{\epsilon^2-\delta^2}\le\epsilon$, and $b^{2v+3}\le\epsilon^{2v+3}$. This proves (4.7). For the stated tilt disk, $\Re\nu=-3-\Re s\le0$, and it is advantageous to retain the correlation between the normalization and the preparation bound:

$$|d^{9+6s}|M(z,s)=(1-z)^{-9}(1+z)^{9+6\Re s}\le\frac{(1+z_+)^{27}}{(1-z_+)^9}.$$

This is an increasing function of z on the stated interval. Substitution in (4.7), with outward ball arithmetic for its gamma factors, gives $[7.513975074654528136628046 6653\times10^{-18}\pm4.3\times10^{-47}]$; `uniform_central_cut.py` records the complete calculation at 192 bits. The exact analytic inequality, rather than the rounded printed midpoint, is the claim. □

Numerical implementation and its scope. `conditioned_scalar.py` evaluates (4.1)–(4.3). The singular radial rule integrates Chebyshev interpolants against the exact complex power r^{2h+1}, using the inherited three-term recurrence for its polynomial moments; the complementary variables use Gauss–Legendre rules. The regular term uses a three-dimensional periodic Haar-source quadrature. The code retains each source factor before summation and monitors its absolute sum. The actual runs use binary64 arithmetic and successive refinements, independent source partitions and independently constructed special-slice certificates. Their errors are estimates, not certified quadrature remainders. (4.4)–(4.6) are analytic bounds, not by themselves an end-to-end certificate for the implementation. A uniform certified quadrature remainder for the full joint complex parameter box remains open.

Ordinary domains and low-rank density bounds

The following arguments extend this section. Lettered identifiers retain stable links to the integrated constructions; their correspondence is given at the beginning of the paper. Earlier bounds remain valid on their stated domains. A limitation described at an intermediate stage is superseded only by a later explicitly proved result, as summarized in the current coverage table.

A separate certified regular-channel construction (R9)

This component directly addresses the regular contribution behind the false-convergence example. In the conditional sign convention let $p_w = w_1 + w_2 + w_3$, $R_c = |a - p_w|^2$, $q_j = |a - w_j|^2$, and

$$D = R_c + \sum_j q_j = 3 + |p_w - 2a|^2 \geq 3.$$

For integer $K_c \geq 1$,

$$P_j = \frac{q_j}{D} \sum_{\ell=0}^{K_c-1} (R_c/D)^\ell, \qquad P_{\mathrm{reg}} = (R_c/D)^{K_c}, \qquad \sum_j P_j + P_{\mathrm{reg}} = 1.$$

This is the inherited exact partition; pair and cross Vandermonde factors are retained. Its regular moment is

$$G_{K_c} = d^{9+6s}\mathbb{E}_{U(3)}[R_c^{h+K_c} D^{-K_c} \prod_j |1 - z w_j|^{-6-2s}].$$

Set $\beta = h + K_c$, $B_c = \operatorname{Re}\beta$, $C_c = |\operatorname{Im}\beta|$. For $\epsilon > 0$, $B_c > C_c$ and integer $M_c \geq B_c$, define

$$H_{M_c}(R_c) = (R_c + \epsilon)^\beta \sum_{j=0}^{M_c-1} (-1)^j \binom{\beta}{j} [\epsilon/(R_c + \epsilon)]^j.$$

Lemma R9.1 (Uniform analytic smoothing)**.** *For every $R_c \geq 0$,*

$$|R_c^\beta - H_{M_c}(R_c)| \leq |\tbinom{\beta}{M_c}| \frac{M_c}{B_c - C_c} \epsilon^{B_c}.$$

Proof. For $j \geq M_c \geq B_c$ the binomial coefficient ratio is at most $(j - B_c + C_c)/(j + 1)$. The comparison tail sums to $M_c/(B_c - C_c)$ times its first term, by a telescoping recurrence. Moreover $(R_c + \epsilon)^{B_c}[\epsilon/(R_c + \epsilon)]^{M_c} \leq \epsilon^{B_c}$. This also controls $R_c = 0$ by absolute convergence of the binomial series. □

Assuming $\operatorname{Re} s \geq -3$ (in particular on the target disk $|s| \leq 3$), the physical source smoothing allowance is therefore

$$E_{\mathrm{smooth}} \leq d^{9+6\operatorname{Re}s}(1 - z)^{-18-6\operatorname{Re}s} 3^{-K_c} |\tbinom{\beta}{M_c}| \frac{M_c}{B_c - C_c} \epsilon^{B_c}.$$

For one complexified angle with $|\operatorname{Im}\theta| \leq \rho$, keep the other two real and define

$$m_R = \epsilon - 2(a + 2)(\cosh\rho - 1), \qquad m_D = 3 - 2(2 + 2a)(\cosh\rho - 1),$$
$$m_z = 1 + z^2 - 2z\cosh\rho, \qquad U_R = \epsilon + (a + 2)^2 + 1 + 2(a + 2)\cosh\rho.$$

When these three lower bounds are positive, the corresponding logarithms are holomorphic. Their argument bounds are $\theta_R = \arctan[2(a+2)\sinh\rho/m_R]$ and $\theta_z = \arctan[2z\sinh\rho/m_z]$. Put $\nu = -3-s$ and

$$\begin{aligned} H_* &= e^{C_c\theta_R}\sum_{j<M_c}|\tbinom{\beta}{j}|\epsilon^j\max(U_R^{B_c-j}, m_R^{B_c-j}),\\ P_* &= d^{9+6\,\mathrm{Re}\,s}(1-z)^{4\,\mathrm{Re}\,\nu}m_z^{\mathrm{Re}\,\nu}e^{|\,\mathrm{Im}\,s|\theta_z},\\ M_* &= \tfrac{2}{3}(1+e^\rho)^4P_*H_*m_D^{-K_c}. \end{aligned}$$

The last expression includes the Weyl normalization and the retained Vandermonde, whose single-coordinate strip modulus is at most $4(1+e^\rho)^4$. Fourier contour shifting gives a one-coordinate trapezoid error $2M_*/(e^{n\rho}-1)$. A telescoping product of the three normalized integration/averaging operators gives

$$E_{\mathrm{quad}} \le 6M_*/(e^{n\rho}-1).$$

Only one coordinate is shifted at a time; simultaneous polydisc holomorphy is not assumed. The finite symmetric grid equals $n^{-3}\sum_{0\le i<j<k<n}$ of the non-Weyl kernel, since repeated angles vanish. Arb evaluates this sum and adds its arithmetic disk.

Throughout the complete connected box, $K_c = 20$, $M_c = 80$, $\epsilon = 1$, $\rho = 1/2$, $n = 256$ give exact-arithmetic component error below $4.607\,10^{-17}$. The disk constraint on s is retained through the support-function inequality $\sigma L + |\tau|\theta \le 3\sqrt{L^2+\theta^2}$. This is an executed continuous bound. At the hard quarter input a smaller $K_c = 18$, $M_c = 50$, $n = 164$, $\rho = .55$ design evaluated 721764 unique triples and certified

$$G_{18} = .000465922940074354636314171212971022 - .000463273518157443987825604489738935\mathrm{i}$$

with radius below $1.027\,10^{-15}$. A compatible conditional contribution must use the same K_c. Joining a certified regular term to an estimated conditional term still yields an estimated whole moment.

The physical source, ordinary domain, and centre behaviour (C2)

Put $a = 3z$, $d = 1-z^2$, $p = 3+s$. The exact change of eigenvalue variable

$$w = \frac{\lambda - z}{1 - z\lambda}, \qquad \lambda = \frac{w+z}{1+zw}$$

gives $(1-z^2)\lambda/(1-z\lambda) = w+z$. Its Jacobian and the transformed pair differences give the normalized CUE(3) source

$$T_3 = \mathbb{E}_{\mathrm{CUE}_3}\left[|a+w_1+w_2+w_3|^{2h}A_{z,s}(w)\right], \quad A_{z,s} = d^{9+6s}\prod_{j=1}^{3}(1+zw_j)^{-p}(1+z/w_j)^{-p}. \tag{C2.1}$$

The two factors have identical complex exponent. Their product on the real torus is $(1+2z\cos\theta_j+z^2)^{-p}$ with its positive-real logarithm. There is no conjugation of s and no normalization by a complex tilted mass. The conditional-source sign convention $w \mapsto -w$ gives the equivalent mark $|a-\sum w_j|$.

After averaging the Fourier direction and shifting the eigenangles,

$$\Phi(r) = \frac{d^{9+6s}}{6(2\pi)^4}\int e^{\mathrm{i}r(a\cos\phi+\sum_j\cos x_j)}|\Delta(e^{\mathrm{i}x})|^2\prod_{j=1}^{3}(1+2z\cos(x_j+\phi)+z^2)^{-p}\,dx\;d\phi. \tag{C2.2}$$

The bounded mark has support radius $D = 3(1+z)$.

Lemma C2.1 (A bounded trace density)**.** *Let $X = \mathrm{Tr}\,V$, with normalized Haar $V \in U(3)$. For every $R_0 > 0$ and $r \ge R_0$,*

$$|D_3(r)| \le H(R_0)r^{-5/2}, \tag{C2.3}$$

$$H(R_0) = 4(2/\pi)^{3/2}\left[e^{5/(4R_0)} + e^{9/(4R_0)} + R_0^{-1}e^{7/(4R_0)}\right]. \tag{C2.4}$$

The planar law of X has a bounded continuous density satisfying

$$0 \le f_X(x) \le F_{R_0} := \frac{1}{2\pi}\left[\frac{R_0^2}{2} + \frac{2H(R_0)}{\sqrt{R_0}}\right]. \tag{C2.5}$$

Proof. Weyl integration and the Fourier coefficients of $e^{\mathrm{i}r\cos\theta}$ give

$$D_3(r) = \det[J_{j-k}(r)]_{j,k=0}^{2} = J_0^3 + 2J_0J_1^2 + 2J_1^2J_2 - J_0J_2^2.$$

Using $J_2 = 2J_1/r - J_0$ before taking absolute values gives the recurrence displayed in Section C1. The inherited Volterra bound, $|J_n(r)| \le \sqrt{2/(\pi r)}e^{|n^2-1/4|/r}$, proves the stated H. For $r \le R_0$, $|D_3(r)| \le 1$ because it is a probability characteristic function. Thus $D_3(|\xi|) \in L^1(\mathbb{R}^2)$. Fourier inversion gives a bounded continuous density, and the radial absolute integral divided by $(2\pi)^2$ is exactly (C2.5). □

Proposition C2.2 (Ordinary domain and joint holomorphy)**.** *For every $0 \le z \le .4$ and every complex s, the ordinary absolute moment in* (C2.1) *exists exactly when* $\operatorname{Re} h > -1$. *On compact subsets of that half-plane and compact sets of s, it is jointly holomorphic in (h, s) and continuous in z, including $z = 0$. At zero it is exactly independent of s.*

Proof. For $0 \le z \le Z < 1$, $|s| \le 3$, the physical density obeys

$$|A_{z,s}| \le (1 - Z)^{-9}(1 + Z)^{27}.$$

The same argument gives a finite bound for any compact tilt set. Its total-variation pushforward under $w \mapsto a + \sum w_j$ is dominated by this constant times the translated density in Lemma C2.1. Local planar integration of $r^{2\operatorname{Re} h}$ therefore proves sufficiency for $\operatorname{Re} h > -1$; compact support controls large marks.

For sharpness, at every $a \in [0, 1.2]$ choose

$$w_1 = -1, \qquad w_2 = e^{\mathrm{i}t}, \qquad w_3 = e^{-\mathrm{i}t}, \qquad \cos t = (1 - a)/2.$$

These points are distinct and their sum is $-a$. The real differential of their sum has rank two. At $a = 1$, where the last two tangents are parallel, the tangent from w_1 supplies the second direction. The squared Vandermonde and absolute preparation are positive nearby. The coarea theorem then supplies a positive lower density contribution near the zero mark. The local integral diverges for $\operatorname{Re} h \le -1$.

For holomorphy choose $q > -1$ below the smallest real order on the compact set under consideration. Powers of $\log|a + \sum w_j|$ are dominated near zero by a constant times $|a + \sum w_j|^{2q}$. The preparation logarithms are bounded on $z \le Z < 1$. Dominated complex differentiation proves joint holomorphy. Translation continuity follows from the same local integrability bound, or from the uniform comparison below. Finally $\Lambda_3(0) = 1$ and $S_3(0) = \operatorname{Tr} U$, which proves tilt independence. □

Lemma C2.3 (Uniform comparison moment)**.** *For real a and $-1 < u < 0$, define $M_u(a) = \mathbb{E}|a + X|^{2u}$ and $C(u) = 2^{2u+1}\Gamma(1 + u)/\Gamma(-u)$. Then*

$$M_u(a) \le C(u)\left[\frac{R_0^{-2u}}{-2u} + \frac{H(R_0)R_0^{-2u-5/2}}{2u + 5/2}\right]. \tag{C2.6}$$

For $u \ge 0$, $M_u(a) \le (|a| + 3)^{2u}$.

Proof. Ordinary integrability is already established, so the radial Riesz identity may be used without circularity:

$$M_u(a) = C(u)\int_0^\infty r^{-1-2u}J_0(ar)D_3(r)\,dr.$$

It follows from the positive gamma integral for $|x|^{2u}$ and the Fourier transform of a planar Gaussian. After the gamma integral, absolute Fubini is licensed by $r^{-1-2u}|D_3(r)|$, integrable at zero and infinity. Use $|J_0(ar)| \le 1$, split at R_0, and apply Lemma C2.1. The nonnegative-order claim follows from compact support. □

With $R_0 = 3$, outward calculation gives

$$H(3) < 8.597000, \quad F_3 < 2.296122, \quad M_{-.95}(a) < 117.905311.$$

Consequently $M_u(3z) \le M_{-.95}(3z) + 3.9^6 < 3636.649072$ for $0 \le z \le .3$, $-.95 \le u \le 3$, by splitting the mark modulus at one. For a uniform centre limit one may instead use $q = -.975$: on $|a + X| < \varepsilon \le 1$, $u \ge -.95$, $|a + X|^{2u} \le \varepsilon^{.05}|a + X|^{2q}$. This prices the moving zero while the preparation tends uniformly to one.

The comparison removes the old $a^{-1/2}$ majorant by keeping exact trace cancellation and $|J_0(ar)| \le 1$. The larger formal convergence range $u > -5/4$ of the large-r integral does not enlarge the ordinary domain: the derivation and the local planar integrability condition remain $u > -1$.

Effective density bounds and the ordinary domain (O3)

Lemma O3.1 (Rank-dependent planar trace bound)**.** *For every integer $N \ge 5$, the CUE trace has a bounded continuous planar Lebesgue density f_N, with*

$$\|f_N\|_\infty \le C_N := \frac{(N-1)^2}{4\pi} + \frac{N^3}{\pi^3(N-4)}. \tag{O3.1}$$

For every complex translation a and $-1 < u < 0$,

$$\mathbb{E}_{\mathrm{CUE}(N)}|a + \operatorname{Tr} V|^{2u} \le U_N(u) := \frac{(\pi C_N)^{-u}}{1+u}. \tag{O3.2}$$

Proof. Rotational invariance and the normalized Weyl determinant identity give

$$\chi_N(r) = \mathbb{E}e^{ir\Re \operatorname{Tr} V} = \det[J_{j-k}(r)]_{j,k=0}^{N-1}.$$

The phases i^{j-k} in the individual Fourier integrals cancel between rows and columns. The inherited Nicholson inequality is

$$J_n(r)^2 + Y_n(r)^2 \le \frac{2}{\pi\sqrt{r^2-n^2}}, \qquad r > |n|.$$

For clarity, its effective constant follows from Nicholson's positive integral, $\sinh t \ge t$, and

$$\int_0^\infty K_0(2rt)\cosh(2nt)\,dt = \frac{\pi}{4\sqrt{r^2-n^2}}.$$

Hadamard's inequality therefore gives, for $r > N-1$,

$$|\chi_N(r)| \le \left(\frac{2N}{\pi}\right)^{N/2}[r^2-(N-1)^2]^{-N/4}; \qquad |\chi_N(r)| \le 1$$

holds at every frequency. Split the radial Fourier integral at $R_N^2 = (N-1)^2 + (2N/\pi)^2$. Since $N > 4$, its absolute integral is finite, and Fourier inversion gives

$$\begin{aligned}\|f_N\|_\infty &\le \frac{1}{2\pi}\left\{\frac{R_N^2}{2} + \frac{(2N/\pi)^{N/2}}{N/2-2}[R_N^2-(N-1)^2]^{1-N/4}\right\}\\ &= \frac{(N-1)^2}{4\pi} + \frac{N^3}{\pi^3(N-4)}.\end{aligned}$$

To obtain the inverse bound, any translated probability density remains bounded by C_N. Put $\rho = (\pi C_N)^{-1/2}$. Retaining the exterior mass when splitting at ρ gives

$$\mathbb{E}|Y|^{2u} \le \rho^{2u} + C_N\int_{|y|<\rho}(|y|^{2u} - \rho^{2u})\,d^2y = \frac{(\pi C_N)^{-u}}{1+u}.$$

No radial monotonicity assumption about the trace density is needed. □

Executed outward constants are

$$\begin{aligned} C_5 &< 5.304681348886, & U_5(-0.95) &< 289.566762624904,\\ C_7 &< 6.552214412517, & U_7(-0.95) &< 353.908562707002.\end{aligned}$$

The bound also applies to even ranks at least six, but says nothing about their balanced terminal population. At rank four this particular absolute Fourier majorant has a divergent radial integral; that is a limitation of the estimate, not a divergence assertion for the trace density.

Proposition O3.2 (Ordinary domain)**.** *For $N = 5, 7$, every fixed $0 \le z < 1$, and every finite complex tilt, the ordinary absolute moment in* (O2.1) *exists exactly when $\Re h > -1$. It is jointly holomorphic in (h, s) on that domain.*

Proof. On compact radius and tilt sets the absolute preparation in (O2.4) is bounded. Lemma O3.1, together with the support bound for nonnegative orders, proves sufficiency. For necessity write $N = 2k + 1$. Choose distinct $c_j \in (-1, 1)$ with mean $(Nz - 1)/(N - 1)$, and take eigenvalues $-1, -e^{i\theta_j}, -e^{-i\theta_j}$, where $\cos\theta_j = c_j$. Their trace is $-Nz$, all eigenvalues are distinct, and the tangent at -1 together with any nonreal pair gives a real differential of rank two. A local submersion chart has strictly positive squared Vandermonde and absolute preparation. It thus contributes a positive planar density near the zero mark, where $|y|^{2\Re h}$ is not integrable if $\Re h \le -1$. Logarithmic powers are dominated on every smaller order half-plane, proving the holomorphy statement. □

There are especially simple regular-zero charts on the new slab. Put $c = (1 - Nz)/2$ and $y = \sqrt{1 - c^2}$. At rank five use

$$-1, \quad c + iy, \quad c - iy, \quad i, \quad -i;$$

at rank seven replace the last two eigenvalues by $e^{\pm i\pi/4}, e^{\pm 3i\pi/4}$. Their traces are $-Nz$, the eigenvalues remain distinct, and the indicated rank-two minor has absolute value $y > 0$. The executed chart checks complement this exact argument. The qualitative ordinary-domain result is inherited; the new content here is its explicit comparison constant and concrete central realizations.

The physical source and the ordinary domain (E2)

Throughout this investigation Haar measure on $U(N)$ is normalized to one. The order h and tilt s are independent complex variables. The central parameter set is

$$\mathcal{B}_N = \left\{ 0 \le z \le Z := \frac{1}{40}, \quad -\frac{19}{20} \le \Re h \le 3, \quad |\Im h| \le 3, \quad |s| \le 3 \right\}, \qquad N \in \{4, 6, 8\}. \tag{E2.1}$$

A positive real base raised to a complex power always uses its real logarithm. An ordinary complex expectation means an absolutely integrable random variable. The source below is a complex prepared measure when s is nonreal; no division by its mass is made.

Proposition E2.1 (Exact original-source return)**.** *Put $d = 1 - z^2$, $a = Nz$, and $p = N + s$. For $0 \le z < 1$ the eigenvalue change $w = (\lambda - z)/(1 - z\lambda)$ gives*

$$T_N(h, s; z) = \mathbb{E}_{\mathrm{CUE}(N)}\big[|a + \operatorname{Tr} V|^{2h} A_{N,z,s}(V)\big], \tag{E2.2}$$

$$A_{N,z,s}(w) = d^{N^2 + 2Ns} \prod_{j=1}^{N} (1 + zw_j)^{-p} (1 + z/w_j)^{-p}. \tag{E2.3}$$

The two factors retain the same exponent p, including its imaginary part.

Proof. The inverse is $\lambda = (w + z)/(1 + zw)$. Direct algebra gives

$$1 - z\lambda = \frac{d}{1 + zw}, \qquad \frac{d\lambda}{1 - z\lambda} = z + w,$$

$$\frac{d\theta_\lambda}{d\theta_w} = \frac{d}{|1 + zw|^2}, \qquad |\lambda_i - \lambda_j|^2 = \frac{d^2 |w_i - w_j|^2}{|1 + zw_i|^2 |1 + zw_j|^2}.$$

The N angular Jacobians and $N(N - 1)/2$ squared Vandermonde factors produce $d^{N^2} \prod_j |1 + zw_j|^{-2N}$. The characteristic determinant contributes $d^{2Ns} \prod_j |1 + zw_j|^{-2s}$, while the derivative mark becomes $a + \sum_j w_j$. The original Weyl factor $1/[N!(2\pi)^N]$ is preserved. Since $z < 1$, both $1 + zw$ and $1 + z/w$ have positive real part on the circle. Their disk-analytic logarithms sum to the real logarithm of $|1 + zw|^2$. This proves the formula with its physical branches. □

Define the radial prepared Fourier source and its Taylor coefficients by

$$\Phi_{N,z,s}(r) = \mathbb{E}_{\mathrm{CUE}(N)}\big[A_{N,z,s} J_0(r|a + \operatorname{Tr} V|)\big] = \sum_{j\ge 0} a_j r^{2j}, \qquad a_j = \frac{(-1)^j T_N(j,s;z)}{4^j (j!)^2}. \tag{E2.4}$$

The support radius is $D = N(1+z)$. At $z = 0$ the preparation is exactly one, so every centre moment is independent of s.

An effective rank-four density bound

The entrywise Hadamard estimate used at ranks at least five is logarithmically insufficient for the planar rank-four density. The remedy is an exact cancellation in the determinant, before taking absolute values.

Lemma E2.2 (Rank-four Bessel identity)**.** *For $r > 0$, put $A = J_0(r)$ and $B = J_1(r)$. The characteristic function of $\operatorname{Tr} V$ for $V \in U(4)$ satisfies*

$$\chi_4(r) = \det[J_{j-k}(r)]_{j,k=0}^{3} = \frac{16}{r^2}\left[\left(A^2 + B^2 - \frac{2AB}{r}\right)^2 + \frac{B^4}{r^2}\right]. \tag{E2.5}$$

Proof. The Weyl–Andreief formula gives the determinant; its row and column powers of i cancel. Substitute $J_2 = 2B/r - A$, $J_3 = (8/r^2 - 1)B - 4A/r$, and $J_{-j} = (-1)^j J_j$. Expanding the determinant gives

$$\frac{16(A^2+B^2)^2}{r^2} - \frac{64AB(A^2+B^2)}{r^3} + \frac{64A^2B^2 + 16B^4}{r^4},$$

which is (E2.5). This is a polynomial identity over $\mathbb{Z}[A, B, 1/r]$, not a fit to Bessel samples. □

Theorem E2.3 (Density and translated inverse comparison)**.** *The planar trace distributions at $N = 4, 6, 8$ have bounded continuous densities. Valid constants are*

$$C_4 = \frac{9}{4\pi} + \frac{544}{36\pi^3} < 1.203553764237433, \qquad C_N = \frac{(N-1)^2}{4\pi} + \frac{N^3}{\pi^3(N-4)} \quad (N = 6, 8). \tag{E2.6}$$

For every complex translation b and $-1 < u < 0$,

$$\mathbb{E}|b + \operatorname{Tr} V|^{2u} \le U_N(u) := \frac{(\pi C_N)^{-u}}{1+u}. \tag{E2.7}$$

For $0 \le u \le 3$ and $z \le Z$, the corresponding comparison is $[N(1+Z)]^{2u}$. A single full-box majorant is

$$U_N^* = U_N(-19/20) + [N(1+Z)]^6. \tag{E2.8}$$

Proof. The inherited Nicholson inequality gives $|J_n(r)|^2 \le 2/[\pi\sqrt{r^2 - n^2}]$ when $r > |n|$. Consequently $A^2 + B^2 \le 4/[\pi\sqrt{r^2-1}]$ for $r > 1$. Using $2|AB| \le A^2 + B^2$ in (E2.5) gives

$$|\chi_4(r)| \le \frac{256}{\pi^2 r^2 (r^2-1)}\left(1 + \frac{2}{r} + \frac{2}{r^2}\right) \le \frac{544}{\pi^2 r^4} \qquad (r \ge 3).$$

Together with $|\chi_4| \le 1$, radial Fourier inversion bounds the density by

$$\frac{1}{2\pi}\left(\int_0^3 r\,dr + \frac{544}{\pi^2}\int_3^\infty r^{-3}\,dr\right) = C_4.$$

The integrable characteristic function also gives continuity. The constants for $N = 6, 8$ are applications of the preceding odd-rank investigation's proved theorem for every integer $N \ge 5$; no odd-parity hypothesis occurs in that density theorem.

Translation preserves the density upper bound. With $\rho = (\pi C_N)^{-1/2}$ and $Y = b + \operatorname{Tr} V$, normalization of the actual probability distribution gives

$$\mathbb{E}|Y|^{2u} \le \rho^{2u} + C_N \int_{|y|<\rho} \big(|y|^{2u} - \rho^{2u}\big)\, d^2y = \frac{(\pi C_N)^{-u}}{1+u}.$$

The nonnegative-order comparison uses compact support. Splitting at $|Y| = 1$ proves (E2.8) throughout the order box. □

At $u = -19/20$ the executed strict upper comparisons, in increasing rank order, are

$$70.756215415783, \qquad 298.267946738708, \qquad 429.213416132421.$$

The trace distribution in this argument is normalized; the complex preparation in (E2.3) is not.

Theorem E2.4 (Ordinary moment domain)**.** *For $N \in \{4, 6, 8\}$, $0 \le z < 1$, and every finite complex s, the ordinary absolute expectation $T_N(h, s; z)$ exists exactly when $\Re h > -1$.*

Proof. The exact preparation has bounded modulus on every compact radius and tilt set. Theorem E2.3 therefore proves sufficiency for negative orders; compact support proves it for nonnegative orders. For necessity write $N = 2b$, set $\epsilon = (1 - z)/2$, and choose

$$c_j = z + \frac{\epsilon(2j - b - 1)}{b}, \qquad w_{2j-1} = -c_j + i\sqrt{1 - c_j^2}, \quad w_{2j} = -c_j - i\sqrt{1 - c_j^2} \quad (1 \le j \le b).$$

The c_j are distinct, lie in $(-1, 1)$, and sum to bz. Thus all eigenvalues are distinct and their trace is $-Nz$. At least one c_j is nonzero. The real determinant of the two trace tangents within that pair has modulus $2|c_j|\sqrt{1 - c_j^2} > 0$. The trace map consequently has differential rank two. In a sufficiently small local chart the Haar squared Vandermonde and the absolute preparation are strictly positive. Its pushforward has a positive lower density near the zero mark, so the local absolute integral dominates a positive multiple of $\int_0^\rho r^{2\Re h+1}\, dr$. This diverges for $\Re h \le -1$. The same domination with logarithmic factors gives joint holomorphy in (h, s) on the ordinary domain. This proof does not include rank two at $z = 0$, whose inherited threshold remains $\Re h > -1/2$. □

5. Fourier inversion and the radial finite part

For $0 \le z < 1$, introduce the finite complex measure

$$\int f(x)\, d\mu_s(x) = \mathbb{E}\big[|\Lambda_N(z)|^{2s} f(S_N(z))\big], \qquad D_N(\zeta) = \int e^{i\,\mathrm{Re}(\bar\zeta x)}\, d\mu_s(x).$$

Here and below $b^w = \exp(w \log b)$ for $b > 0$. Since $(1 - z)^N \le |\Lambda_N(z)| \le (1 + z)^N$, complex tilts have bounded absolute weight, locally uniformly in s. The measure has compact support. Put $\Phi(\rho) = (2\pi)^{-1} \int_0^{2\pi} D_N(\rho e^{i\alpha})\, d\alpha$ and, on the absolute integrability domain of the Haar expectation, $T_N(h, s; z) = \int |x|^{2h}\, d\mu_s(x)$. The angular integral for J_0 gives

$$\Phi(\rho) = \int J_0(\rho|x|)\, d\mu_s(x) = \sum_{j=0}^{\infty} a_j \rho^{2j}, \qquad a_j = \frac{(-1)^j T_N(j, s; z)}{4^j (j!)^2}.$$

The series converges normally on every bounded subset of the complex ρ-plane by compact support.

Existence of the moment.

For $N \ge 3$, the determinant bound $|D_N(\zeta; z, 0)| \le C(1 + |\zeta|)^{-p_N}$, $p_N > 2$, implies that the untilted law has a bounded continuous planar density by Fourier inversion. Its small-ball probability at the origin is therefore $O(r^2)$. This argument uses Proposition 2.1 only at $s = 0$. The bounded tilt transfers the estimate to total variation. For $N = 1$, $S_1 = z + w$ with $|w| = 1$, so $|S_1| \ge 1 - z > 0$. For $N = 2$, use $w_j = (\lambda_j - z)/(1 - z\lambda_j) = e^{i\psi_j}$ to obtain $S_2 = 2z + w_1 + w_2$. The Haar eigenangle density, including its Vandermonde factor and the smooth Jacobian of the circle change of variables, is bounded. If $0 < z < 1$, solutions of $w_1 + w_2 = -2z$ are noncollinear. The Jacobian of $(\psi_1, \psi_2) \mapsto w_1 + w_2$ has absolute determinant $|\sin(\psi_1 - \psi_2)|$, bounded away from zero on a neighborhood of those solutions. The small-ball probability is $O(r^2)$. At $z = 0$, $|S_2| = 2|\cos((\psi_1 - \psi_2)/2)|$; the eigenangle density is positive at antipodality, and the small-ball probability is bounded above and below by positive multiples of r. These estimates and domination on compact subsets give joint holomorphy in (h, s) for $\mathrm{Re}\, h > -1$ in the two-dimensional cases, $\mathrm{Re}\, h > -1/2$ at $(N, z) = (2, 0)$, and every h for $N = 1$. No uniformity as $z \to 1$ is required.

Sharpness of the physical lower endpoint.

The two-dimensional bound is sharp for $N \geq 3$. To see this, choose distinct points w_j of unit modulus with $\sum_j w_j = -Nz$ for which the map $\psi \mapsto \sum_j e^{i\psi_j}$ has real derivative of rank two. If $N = 2k$, take k conjugate pairs $-e^{\pm i\theta_j}$ with distinct $\cos\theta_j \in (-1, 1)$ averaging to z. If $N = 2k+1$, adjoin the point -1 to k such pairs and give their cosines mean $(Nz-1)/(2k)$, which is strictly between -1 and 1. In either construction distinct cosines with the required mean exist by arbitrarily small distinct perturbations of zero sum. For odd N the point -1 and any pair yield nonparallel tangents. For even $N \geq 4$ at least one pair has nonzero cosine and yields nonparallel tangents. The positive Haar density in these coordinates is bounded below on a neighborhood of this configuration, since its Vandermonde does not vanish. The local submersion theorem gives a positive lower bound for the planar density contribution near zero (integrate over a smaller open set in the remaining coordinates). The absolute weight of any fixed complex tilt is positive there. Hence absolute moment existence requires $\operatorname{Re} h > -1$. For $N = 2$, $0 < z < 1$, the same lower bound holds at either of the two zero preimages already identified.

Ordinary radial cutoffs.

For the continuation argument we record the resulting radial bounds. If $N \geq 3$, use $|\Phi(\rho)| \leq C(1+\rho)^{-p_N}$ from the determinant bound. For $N = 1, 2$ and $0 < z < 1$, Φ has a stationary-phase expansion with leading power ρ^{-q}, where $q = 1$ and $q = 3/2$, respectively; its leading frequencies are nonzero. These follow from the separated phase and the low-rank cases above. At the centre the exact Bessel expressions give order $\rho^{-1/2}$ for $N = 1$ and ρ^{-1} for $N = 2$. All estimates just used are locally uniform in the tilt.

Write $b = -1$ for $N \geq 3$ and for $N = 1, 2$ with $z > 0$. Set $b = -3/4$ for $(N, z) = (1, 0)$ and $b = -1/2$ for $(N, z) = (2, 0)$. Then $\int_A^\infty \rho^{-2h-1}\Phi(\rho)\, d\rho$ converges locally uniformly for $\operatorname{Re} h > b$, $A > 0$. For a nonzero leading frequency ω this follows by integration by parts on $\rho^{-2h-1-q}e^{i\omega\rho}$, the next-order remainder being absolutely integrable there. For $(2, 0)$ the nonoscillatory term gives the stated threshold directly. For $(1, 0)$ the ordinary cutoff fails at and below $-3/4$ even though the moment itself is identically one: the leading oscillatory boundary term fails to tend to zero. For arbitrarily negative exponents this follows by taking sufficiently many terms of the Bessel expansion before integrating.

An explicit Gaussian planar kernel

Proposition 5.1 (Gaussian Fourier inversion and the Mellin finite part). We place the Gaussian regulator in the physical variable, with ε multiplying $|x|^2$. For $\varepsilon > 0$ and $\operatorname{Re} h > -1$ set

$$\begin{aligned} K_{h,\varepsilon}(\zeta) &= \frac{1}{(2\pi)^2} \int_{\mathbb{R}^2} e^{-i\operatorname{Re}(\bar\zeta x)} |x|^{2h} e^{-\varepsilon|x|^2}\, d^2x \\ &= \frac{\Gamma(1+h)}{4\pi\varepsilon^{1+h}} {}_1F_1\left(1+h; 1; -\frac{|\zeta|^2}{4\varepsilon}\right). \end{aligned} \tag{5.1}$$

The second equality follows by the J_0 power series and Gaussian moments; their absolute sum is integrable for fixed ζ. Uniformly on compact h-subsets of $\operatorname{Re} h > -1$, for fixed ε, the large-ρ Kummer expansion (NIST DLMF 13.7.2) gives

$$2\pi\rho K_{h,\varepsilon}(\rho) = C(h)\rho^{-2h-1} + O_{h,\varepsilon}(\rho^{-2\operatorname{Re} h - 3}).$$

This is the first algebraic term of the negative-real-axis Kummer asymptotic; at nonnegative integer h its coefficient vanishes and the kernel is a Gaussian times a polynomial (Kummer's transformation). The absolute error term multiplied by Φ is integrable throughout the stated domains. After the angular integration, the planar cutoff equals the radial cutoff. Thus the disk-truncated integrals below converge locally uniformly for $\operatorname{Re} h > b$:

$$\lim_{R\to\infty} \int_{|\zeta|<R} D_N(\zeta) K_{h,\varepsilon}(\zeta)\, d^2\zeta = \int |x|^{2h} e^{-\varepsilon|x|^2}\, d\mu_s(x). \tag{5.2}$$

For $\operatorname{Re} h > 0$ the transform in (5.1) is integrable in ζ and the physical function is continuous, so Fourier inversion and Fubini prove the claim. Holomorphic continuation proves it for $\operatorname{Re} h > b$. Dominated convergence on the

right-hand side now gives $T_N(h,s;z)$ as $\varepsilon \downarrow 0$. This proof takes $R \to \infty$ first; it makes no assertion interchanging $N \to \infty$, $z \to 1$, or a simultaneous cutoff with $\varepsilon \downarrow 0$.

Direct passage from the planar kernel to the finite part.

Now take $-1/4 < \sigma = \operatorname{Re} h < 0$. Euler's integral (NIST DLMF 13.4.1, with its gamma normalization) for the function ${}_1F_1(1+h;1;-x)$ gives, with $x = \rho^2/(4\varepsilon)$,

$$K_{h,\varepsilon}(\rho) = \frac{\varepsilon^{-1-h}}{4\pi\Gamma(-h)} \int_0^1 e^{-xt} t^h (1-t)^{-h-1}\, dt.$$

For $x \geq 1$, split at $1/2$: on the first half the absolute integral is $O(x^{-1-\sigma})$, by comparison with a gamma integral; on the second it is $O(e^{-x/2})$ by integrability at 1. For $x \leq 1$ use the beta integral directly. These estimates are uniform on compact subsets of the chosen strip. They give, for all $\varepsilon > 0$,

$$|2\pi\rho K_{h,\varepsilon}(\rho)| \leq C_h \rho^{-2\sigma-1}.$$

For fixed $\rho > 0$, substitution $u = xt$ on the first half and dominated convergence, with the second half exponentially small, give

$$\lim_{\varepsilon \downarrow 0} 2\pi\rho K_{h,\varepsilon}(\rho) = \frac{2^{2h+1}\Gamma(1+h)}{\Gamma(-h)} \rho^{-2h-1}.$$

Indeed the integral in the kernel is asymptotic to $\Gamma(1+h)x^{-1-h}$. The majorant times $|\Phi(\rho)|$ is integrable at zero since $\sigma < 0$, and at infinity for the entire base strip: the slowest case among all fixed N, z is $N = 1, z = 0$, which has $|\Phi(\rho)| = O(\rho^{-1/2})$. Take $\varepsilon \downarrow 0$ on both sides of (5.2). The right side tends to T_N by dominated convergence of the physical moment; the left tends to $C(h) \int_0^\infty \rho^{-2h-1}\Phi(\rho)\, d\rho$. Split this last integral at $A > 0$ and integrate the normally convergent Taylor series on $[0, A]$. Its integrated series extends meromorphically to all h, with at most simple poles at nonnegative integers. The preceding cutoff bounds give holomorphy of the tail for $\operatorname{Re} h > b$, locally uniformly also in s. The identity theorem therefore proves the following formula on the stated domain.

For $A > 0$, $\operatorname{Re} h > b$ and $h \notin \mathbb{Z}_{\geq 0}$,

$$T_N(h,s;z) = C(h) \left(\sum_{j \geq 0} \frac{a_j A^{2j-2h}}{2j-2h} + \lim_{R \to \infty} \int_A^R \rho^{-2h-1}\Phi(\rho)\, d\rho \right), \qquad C(h) = \frac{2^{2h+1}\Gamma(1+h)}{\Gamma(-h)}. \tag{5.3}$$

The value at $h = j \in \mathbb{Z}_{\geq 0}$ is taken by continuity. The zero of $1/\Gamma(-h)$ cancels the jth denominator, giving $(-1)^j 4^j (j!)^2 a_j = T_N(j,s;z)$. Differentiation in A cancels the two boundary terms, so any splitting radius gives the same answer.

If $h = -1/4$, this particular absolute base-strip estimate is borderline at $(N,z) = (1,0)$, but the Mellin cutoff still converges there. The derivative cutoff for that example does fail at $\operatorname{Re} h = -1/4$, because $R^{-2h}J_0(R)$ then has a nonvanishing oscillatory boundary.

The derivative form and iterated Laplacians

Define

$$\kappa(h) = -\frac{4^h\Gamma(1+h)}{\Gamma(1-h)}.$$

For $b < \operatorname{Re} h < 1$, away from $h = 0$ and with $R > A$, write the regularized origin in (5.3) as

$$M_R(h) = -\frac{a_0 A^{-2h}}{2h} + \int_0^A \rho^{-2h-1}(\Phi(\rho) - a_0)\, d\rho + \int_A^R \rho^{-2h-1}\Phi(\rho)\, d\rho.$$

Integration by parts, using $\Phi - a_0 = O(\rho^2)$, gives the exact finite-cutoff identity

$$\int_0^R \rho^{-2h}\Phi'(\rho)\,d\rho = R^{-2h}\Phi(R) + 2hM_R(h), \qquad C(h) = 2h\kappa(h).$$

Consequently whenever $R^{-2h}\Phi(R) \to 0$,

$$T_N(h,s;z) = \kappa(h)\lim_{R\to\infty}\int_0^R \rho^{-2h}\Phi'(\rho)\,d\rho. \tag{5.4}$$

At $h = 0$ the identity is $-\int_0^\infty \Phi'(\rho)\,d\rho = \Phi(0)$ and follows directly from the same decay. In particular $0 \le \operatorname{Re} h < 1$ works for all fixed N, z.

The lower endpoints for this derivative formula within the moment domain are -1 for $N \ge 3$, $-3/4$ for $N = 2,\ 0 < z < 1$, $-1/2$ for $N = 1,\ 0 < z < 1$, $-1/2$ for $(N,z) = (2,0)$, and $-1/4$ for $(1,0)$; all inequalities are strict. In the two low-rank positive-z cases the leading stationary-phase coefficients are nonzero. For $N = 1$ the four frequencies are distinct and the weight at every stationary point is nonzero. For $N = 2$ the two permutations with opposite β_j have identical nonzero weights and Hessian signatures at each α, so their coefficients add. For sharp failure of the derivative cutoff, including below the Mellin convergence region, use $\Phi'(R) = R^{-q}P(R) + O(R^{-q-1})$, where P is a nonzero trigonometric polynomial with nonzero frequencies. Here $q = 1$ for a single eigenvalue at $z > 0$, $q = 1/2$ for a single eigenvalue at the centre, and $q = 3/2$ for rank two at $z > 0$. Choose a fixed $L > 0$ so that $Q(R) = \int_0^L P(R+t)\,dt$ is a nonzero trigonometric polynomial. Its limiting mean square is strictly positive by orthogonality of distinct frequencies, hence $|Q(R)|$ is bounded below along a sequence. Across $[R, R+L]$, the relative change in t^{-2h-q} is $O(R^{-1})$. The derivative-integral increment thus equals $R^{-2h-q}(Q(R) + O(R^{-1}))$, which violates the Cauchy criterion when $2\operatorname{Re} h + q \le 0$. The identical window argument with $-2h-1-q$ applies to the oscillatory Mellin tails. At $(2,0)$ absolute moment existence already excludes the lower endpoint.

Finally let $m \ge 0$ be an integer and define $\Phi_m(\rho) = (2\pi)^{-1}\int_0^{2\pi}[(-\Delta_\zeta)^m D_N](\rho e^{i\alpha})\,d\alpha$. Since $-\Delta_\zeta e^{i\operatorname{Re}(\bar\zeta x)} = |x|^2 e^{i\operatorname{Re}(\bar\zeta x)}$, this is the Bessel average for $|x|^{2m}\,d\mu_s(x)$. The same origin and tail estimates hold (use the differentiated determinant estimate at $N \ge 3$, and the same stationary-phase argument with the smooth amplitude $|x|^{2m}$ at $N = 1, 2$). For $m \le \operatorname{Re} h < m+1$ the derivative identity therefore gives

$$T_N(h,s;z) = \kappa(h-m)\lim_{R\to\infty}\int_0^R \rho^{-2(h-m)}\Phi_m'(\rho)\,d\rho.$$

In particular at $h = m$ it reduces to $T_N(m,s;z) = (-\Delta_\zeta)^m D_N(0)$.

Lattice sampling of the circular determinant

Let $W = |\Lambda_N(z)|^{2s}$ and $B = N(1+z)$. The same prepared source supplies the circular characteristic function $\Phi(t) = \mathbb{E}[WJ_0(t|S_N|)]$ and the Taylor coefficients $a_j = (-1)^j T_N(j,s;z)/(4^j(j!)^2)$. Resolving the scalar $T_N(h,s;z)$ requires the large-frequency readout as well as these coefficients. Uniform spacing in frequency has a calculable effect at the origin of the Mellin integral.

Proposition 5.2 (a sampled Mellin formula). Suppose $N \ge 3$, $0 \le z < 1$, $s \in \mathbb{C}$, $\Re h > -1$, and $0 < \Delta B < 2\pi$. Write $C(h) = 2^{2h+1}\Gamma(1+h)/\Gamma(-h)$. Then

$$T_N(h,s;z) = C(h)\Delta^{-2h}\left\{\sum_{k=1}^{\infty} k^{-1-2h}\Phi(k\Delta) - \sum_{j=0}^{\infty}\zeta(1+2h-2j)a_j\Delta^{2j}\right\}.$$

Integer $h \ge 0$ uses the removable limit of the complete expression. The first series converges absolutely. For $h = \ell - 1/2$, $\ell = 0, 1, \ldots$, the second series terminates at $j = \ell$. In particular the entire inverse first power is the equally spaced sum $T_N(-1/2,s;z) = \Delta[\Phi(0)/2 + \sum_{k\ge1}\Phi(k\Delta)]$.

Proof. First take generic $\Re h > 0$. Add the expansions of $\mathrm{Li}_{1+2h}(e^{ix})$ and $\mathrm{Li}_{1+2h}(e^{-ix})$ and divide by two. For $0 < |x| < 2\pi$ the result is

$$\sum_{k\ge1} \frac{\cos(kx)}{k^{1+2h}} = \Gamma(-2h)\cos(\pi h)|x|^{2h} + \sum_{j\ge0} \frac{(-1)^j \zeta(1+2h-2j)}{(2j)!} x^{2j}.$$

At $x = 0$ use the continuous limit in this starting strip. Put $x = \Delta\Re(e^{-i\phi}S_N)$ and average over ϕ and the complex preparation W. The support condition places every x in a compact subinterval of $(-2\pi, 2\pi)$. The angular mean of $|\cos\phi|^{2h}$ is $\Gamma(h+1/2)/(\sqrt{\pi}\,\Gamma(1+h))$. Duplication and reflection give its product with $\Gamma(-2h)\cos(\pi h)$ as $1/C(h)$. The mean of $\cos^{2j}\phi$ is $(2j)!/(4^j(j!)^2)$. These identities give the formula on the starting strip. The determinant decay $O(t^{-p_N})$ with $p_N > 2$ suffices for absolute local uniform convergence of the sampled Fourier sum throughout $\Re h > -1$. The bound below gives local uniform convergence of the image series away from the finitely encountered zeta poles. Holomorphy of the ordinary Haar moment then gives the extension and the stated removable limits. The trivial zeros of zeta give the half-integer termination. The polylogarithm expansion and the zeta reflection formula are NIST DLMF equations 25.12.12 and 25.4.1.

Truncation of the image series. Put $a = \Re h$, $b = \Re s$, $x = \Delta B/(2\pi)$, and $M = (1-z^2)^{-b^2}$. Indeed the Cauchy identity expands $\prod_j (1 - z\lambda_j)^b$ in Schur characters. Haar orthogonality reduces its squared norm to the sum of squared coefficients for partitions of length at most N. Allowing all partitions in the Cauchy identity with the real power-sum specialization $p_k = -bz^k$ gives $\exp(\sum b^2 z^{2k}/k) = M$. Thus $\mathbb{E}|W| \le M$. An integer $J > a + 1/2$ with $q = x^2 \max(1, (J-a)/(J+1)) \max(1, (J+1/2-a)/(J+1)) < 1$ gives

$$\sum_{j\ge J} |\zeta(1+2h-2j)a_j\Delta^{2j}| \le \frac{2(2\pi)^{2a}|\cos(\pi h)| M\,\Gamma(2J-2a)\zeta(2J-2a)}{(J!)^2(1-q)} \left(\frac{x}{2}\right)^{2J}.$$

Use $|T_N(j,s;z)| \le MB^{2j}$, the zeta reflection formula, and the positive-integral and Dirichlet-series bounds for Γ and ζ in their right half-planes. The ratio of successive majorants is at most q.

An explicit estimate for the other end. Let $d = 1 - z^2$, $\tau > 0$, $u = ze^{\tau} < 1$, $\beta = 4\tau/\pi^2$ and $\eta = N + \Re s$. Define

$$H = d^{N^2+2N\Re s}\left[\max((1-u)^{-2\eta}, (1+u)^{-2\eta})\, e^{2|\Im s|\arcsin u}\right]^N,$$

$$G_k = (2\pi)^{k/2}(2\beta)^{-k^2/2}\prod_{j=1}^{k} j!, \qquad P = e^{2\tau}(1+\tau^2), \quad Q = 4e^{2\tau}.$$

For $l + m = N$ put $D_{lm} = (l^2+m^2)/2$ and

$$H_{lm} = \frac{H(1+\tau^2)^{N/2}}{N!(2\pi)^N}\binom{N}{l} P^{\binom{l}{2}+\binom{m}{2}} Q^{lm} G_l G_m.$$

Then $|\Phi(t)| \le \sum_{l+m=N} H_{lm} t^{-D_{lm}}$, and before multiplication by $|C(h)\Delta^{-2h}|$ the sharp-cut sample tail after K has absolute bound

$$\sum_{l+m=N} \frac{H_{lm}\Delta^{-D_{lm}} K^{-D_{lm}-2a}}{D_{lm}+2a}.$$

Proof. Rotate the Möbius angles relative to the Fourier direction ϕ. In the transformed Haar integral use the periodic analytic contour $v = y - i\tau\sin y$ for each angle. The directional translation factor $e^{itNz\cos\phi}$ has unit modulus. The factor $e^{it\cos v}$ has modulus $e^{-t\sin y\sinh(\tau\sin y)} \le e^{-t\tau\sin^2 y}$. The analytic logarithms of the two factors $1 + ze^{\pm i(v+\phi)}$ have imaginary part bounded by $\arcsin u$. Their real parts and the physical prefactor yield H. The Jacobian is bounded by $\sqrt{1+\tau^2}$. Separate angles into half circles about 0 and π, and use local coordinates $x \in [-\pi/2, \pi/2]$ about their centres. Each same-half difference of the deformed e^{iv}, and each difference of e^{-iv}, is bounded by $e^{\tau}\sqrt{1+\tau^2}|x_i - x_j|$ by differentiation along the contour. Each cross-half product of differences costs at most Q. On either half, $\sin^2 y \ge 4x^2/\pi^2$. Extend the two resulting positive Gaussian integrals to the whole real line. The size-k squared Vandermonde integral equals $G_k t^{-k^2/2}$ by orthogonalizing monomials with the monic Hermite polynomials. Indeed their squared norms for the weight $e^{-\beta t x^2}$ are $\sqrt{\pi}\,j!/[2^j(\beta t)^{j+1/2}]$, and the determinant integral is $k!$ times their product. Summing over assignments proves the estimate, including at trace criticality. Integral comparison gives the sample-tail bound. The constants can grow rapidly when z approaches one. For a smoothed sum supported below K, a rigorous tail budget must additionally price the omitted fractions of all terms below K.

Filtering the exterior frequency sum away from the critical radii

The two numerical truncations in Proposition 5.2 interact. An aliased direction coefficient can survive at every sampled frequency, and a small change on extending the radial sum need not detect it. We retain the direction before averaging over the final cutoff. This gives a tail bound with no fitted saddle coefficients and a separate, absolute source error at the very same frequencies.

Theorem 5.3 (a filtered exterior bound). Let $N \ge 3$, $0 < z < 1$, $-1 < \Re h < 0$, $s \in \mathbb{C}$, $N + \Re s \ge 0$, and $D = N(1+z)$. Let

$$g_* = \min_{k=-N,-N+2,\dots,N} |Nz - k| > 0, \qquad 0 < \Delta D < 2\pi, \qquad C_\Delta = 2^{1+2h}\Delta^{-2h}\Gamma(1+h)/\Gamma(-h).$$

Write $\gamma = 2+2h$, $d = 1-z^2$ and $M = d^{-(\Re s)^2}$. Choose $0 < t \le 1$ with $ze^{2t} < 1$ and $E = 2z(\cosh(2t)-1)/(1-z)^2 < 1$. Define

$$\eta = \arctan \frac{2z\sinh(2t)}{d(1-E)}, \qquad V = M(1+t^2)^{(N+1)/2}(1+t^2\cosh^2 t)^{N(N-1)/2}(1-E)^{-N(N+\Re s)}e^{N|\Im s|\eta}.$$

Let $K \ge 1, b \ge 2, p \ge 1$ be integers, and let $L_* = K + U_1 + \cdots + U_p$ with independent uniforms on $\{0,\dots,b-1\}$. This finite averaging device only determines deterministic rational weights. In the sampled formula multiply its kth Fourier summand by $\Pr(L_* > k)$. Partition $[0, D]$ into bands $[l, r]$, and put

$$y = t(g_* - r)_+, \qquad e = \max\{1 - e^{-\Delta y}, \sin(\min(\Delta l, 2\pi - \Delta r, \pi/2))\}, \qquad A = \min(1, 2/(be)).$$

Use a partition with positive e in each band. The error of this operation, including the physical Mellin factor, is bounded by

$$|C_\Delta| V \frac{\Gamma(\Re\gamma)}{|\Gamma(\gamma)|} K^{-\Re\gamma} \max_{[l,r]} \frac{e^{-K\Delta y}}{e} \left[(K + 1/e)A^p + \frac{p(b-1)}{2}A^{p-1}\right]. \tag{5.8}$$

Here the e in the denominator is the band distance; the exponentials in (5.8) are ordinary real exponentials. The bound applies to a complex preparation without dividing by its mass.

Proof. Write each Möbius angle relative to the angle ϕ of the Fourier direction. The signed projection becomes

$$G = Nz\cos\phi + \sum_{j=1}^{N} \cos x_j.$$

In Weyl coordinates its preparation includes $d^{N^2+2Ns}\prod_j g(x_j+\phi)^{-N-s}$ with $g(a) = 1 + 2z\cos a + z^2$, and the usual squared sine products in the differences $x_j - x_k$. The two factors of g first vanish at real parts π and imaginary parts $\pm\log(1/z)$. The physical logarithm analytically continues from each positive real base. Move each of the $N+1$ angles, including ϕ, to $x - it\sin x$. Cauchy deformation of periodic integrals is permitted along the whole homotopy. For $G = X + iY$ on the final contour,

$$Y \ge t\sum_j a_j \sin^2 x_j, \quad |X| \le D, \quad |X| + Y/t \ge g_*,$$

where the list of coefficients includes $a_0 = Nz$. Indeed $|\cos x| \le |\cos x|\cosh(t\sin x) \le 1$ by $\log\cosh v \le v^2/2$ and $1 - u \le e^{-u}$. Replacing each real cosine factor by its closest signed unit costs at most $\sin^2 x$ before its coefficient. The resulting signed sum has modulus at least g_*. This accounts for the direction translation at the saddle as well as the eigenangle terms.

The deformed amplitude has total variation at most V. For a sine difference the ratio of deformed squared modulus to the original is at most $1 + t^2\cosh^2 t$, by $|\sin x - \sin x'| \le 2|\sin((x-x')/2)|$. Each angle Jacobian costs at most $\sqrt{1+t^2}$. For the shifted $g(a+iv)$, $|v| \le 2t$, its real part is at least $(1-E)g(a)$ and the absolute argument is at most η, since $\max_a |\sin a|/g(a) = 1/d$. What remains after these comparisons is the original positive real-tilt mass, bounded by M in Proposition 5.2. This avoids replacing the full Weyl amplitude by a pointwise supremum.

Insert $k^{1-\gamma} = k\int_0^\infty u^{\gamma-1}e^{-ku}\,du/\Gamma(\gamma)$ and initially introduce an extra Abel factor v_0^k, $0 < v_0 < 1$. At a fixed point of the deformed contour set $w = v_0 e^{i\Delta G - u}$ and $H = b^{-1}\sum_{j=0}^{b-1} w^j$. The expected discarded geometric derivative equals

$$\frac{w^K}{1-w}\left[\left(K + \frac{w}{1-w}\right)H^p + pwH'H^{p-1}\right].$$

For $l \le |X| \le r$, the distance $|1-w|$ is at least e. To see the sine bound, minimize distance from 1 over a radial segment of the unit disk, clipping the angle to $\pi/2$. Also $|H| \le A$ and $|wH'| \le (b-1)/2$. Integrate $e^{-Ku}u^{\Re\gamma-1}$ and use the total variation bound. The band bounds are independent of v_0, and dominate the integral on letting $v_0 \uparrow 1$. Proposition 5.2 gives the same limit for the physical sampled series. This proves (5.8). At a critical radius the band next to zero can have $e = 0$; the earlier absolute stationary-phase estimate is still available there.

Resolving the angular source at the retained frequencies

Proposition 5.4 (angular projection with explicit translation). For the hypotheses of Theorem 5.3 choose $0 < v < \log(1/z)$ with $E_v = 2z(\cosh v - 1)/(1-z)^2 < 1$. Define η_v by the above formula with $2t$ replaced by v. Write $u = \Re s$, $W = \max((1-z)^{2u}, (1+z)^{2u})$, $g_0 = (1-z)^2(1-E_v)$, $g_1 = (1+ze^v)(1+ze^{-v})$ and

$$V_v = M(1-E_v)^{-N(N+u)}e^{N|\Im s|\eta_v}, \quad C_v = d^{1+2u}\max(g_0^{-1-u}, g_1^{-1-u})e^{|\Im s|\eta_v}\left(\frac{e^v - z}{1-ze^v}\right)^{N-1}.$$

On the physical Möbius circle $w = e^{ix}$ prepare the modes for $0 \le m < N$ of

$$f_m(x) = \frac{d}{g(x)}\left(\frac{d^2}{g(x)}\right)^s\left(\frac{w+z}{1+zw}\right)^m.$$

The negative-index symbol uses reflection $x \mapsto -x$. Take a preparation grid of $P > 2L$ points, use modes $|j| \le L$, and a direction grid $Q = 2(q+1)$. Multiply each preparation mode by $i^{|j|}J_{|j|}(r)$ in the plane-wave expansion. Form the N-dimensional Toeplitz determinant on the direction grid. Project onto modes $|j| \le q$ and contract with the *exact* Fourier coefficients of $\exp(irNz\cos\phi)$. In exact arithmetic the absolute error in $\Phi(r)$ is at most

$$\epsilon_\Phi = 4V_v\frac{e^{-(q+1)v}}{1-e^{-v}} + (2q+1)N^2\epsilon(W+N\epsilon)^{N-1}, \qquad \epsilon = 2C_v\frac{e^{-(L+1)v} + (2L+1)e^{-(P-L)v}}{1-e^{-v}}. \tag{5.9}$$

This estimate holds simultaneously for all **real** r. It prices the retained lattice when multiplied by $|C_\Delta|\sum_k k^{-1-2\Re h}\Pr(L_* > k)$.

Proof. The transformed one-angle Jacobian is d/g and the tilt multiplier is $(d^2/g)^s$. On the strip $|\Im x| \le v$ the Möbius factor has modulus at most $(e^v - z)/(1-ze^v)$ by maximizing its squared modulus on the two circles. Cauchy's Fourier coefficient bound gives $C_v e^{-|j|v}$; summing discarded indices and aliases gives ϵ using $|J_j(r)| \le 1$. The compression in the original orthonormal monomials has operator norm at most W. A perturbation of all entries by ϵ has norm at most $N\epsilon$. Telescoping the determinant costs at most $N^2\epsilon(W+N\epsilon)^{N-1}$. Shift the common preparation angle after rotating all eigenangles by the Fourier direction. The remaining real oscillatory factor has modulus one and the Weyl differences are unchanged. Thus the Fourier coefficient of the untranslated determinant is bounded by $V_v e^{-|j|v}$. Each discarded direction coefficient can affect the final contraction twice, through omission and through a folded retained coefficient. The translation coefficients have modulus at most one also at arbitrarily high real frequency. These facts give (5.9). Taking a grid average of the pointwise product with an unresolved translation would lose the latter property.

Signed Fourier error for the prepared physical determinant

Use the source of Proposition 5.4. Put $u = \Re s$, $d = 1-z^2$, $M = d^{-u^2}$, $m = \min((1-z)^{2u}, (1+z)^{2u})$, $D = N(1+z)$ and $0 < z < 1$. The following estimates concern unnormalized complex preparations. Their constants do not depend on h; the retained Mellin weights are charged at the final contraction.

Proposition 5.5 (signed direction bound). Let $F(\phi; r)$ denote the untranslated determinant in Proposition 5.4 and b_j its direction Fourier coefficients. For $0 < t < \log(1/z)$,

$$|b_j| \le V(t)e^{-t|j|}, \qquad V(t) = M\left[\frac{d^2}{(1-z^2e^{-2t})(1-z^2e^{2t})}\right]^{|N+s|^2/4}.$$

Contract the Q-point samples of F against the translation coefficients with $|k| \le q = Q/2 - 1$. At every real r, the direction discretization error is at most $4V(t)e^{-Qt/2}/(1 - e^{-t})$. For a block $|r| \le R$ a second bound, valid for every $v > 0$, is

$$2Me^{DR\sinh v - Qv}\left[\frac{1}{1 - e^{-2v}} + \frac{Q - 1}{1 - e^{-Qv}}\right].$$

Either bound or their minimum applies.

Proof. Rotate the transformed Weyl integral as in Proposition 5.4, shift only the common preparation angle in the direction giving $e^{-|j|t}$, and hold all relative angles real. For the upper shift write $a = ze^{-t}$, $b = ze^{t}$. With $|w| = 1$ the absolute value of the shifted preparation, including its scalar prefactor, is $d^{N^2+2Nu}\prod_{j=1}^{N}|A(w_j)|^2$ where

$$A(w) = (1 + aw)^{-(N+s)/2}(1 + bw)^{-(N+\bar{s})/2}.$$

Branches are analytic from $w = 0$ and both radii are less than one. The conjugate in the second exponent is forced by $1 + b/w$ in the continued symbol. At the opposite shift a, b interchange. Write $\log A(w) = \sum_{k\ge1} p_k w^k/k$. Character orthogonality identifies the squared Haar norm with the sum of squared specialized Schur coefficients over partitions of length at most N. The Cauchy identity bounds this by $\exp(\sum |p_k|^2/k)$ on summing over all partitions. Absolute convergence follows from $a, b < 1$. Explicitly the two logarithmic terms at a^2, b^2 occur with coefficient $|N + s|^2/4$ and the term at $ab = z^2$ with coefficient $\Re((N + s)^2)/2$. Multiplying by the prefactor gives $V(t)$ at either shift. The oscillatory part has unit modulus. This proves the first estimate. In particular $V(0) = M$ and the estimate respects arbitrary imaginary tilt without interpreting it as a probability.

Translation coefficients $t_k = i^{|k|}J_{|k|}(Nzr)$ have modulus at most one. Once for the omitted signed modes and once for each folded alias, the geometric tail of b_j is charged. This proves the all-frequency bound. For the second inequality keep the preparation on the real circle and shift only the Fourier direction of the wave. Bounded real trace $|\sum w_j| \le N$ gives $|b_j| \le M\exp(NR\sinh v - |j|v)$ and $|t_k| \le \exp(NzR\sinh v - |k|v)$. The omitted products cost at most $2M\exp(DR\sinh v - Qv)/(1 - e^{-2v})$. An alias has indices k and $k + lQ$, with $l \ne 0$ and $|k| \le q$. Their absolute values sum to at least $|l|Q$. Summing over both signs of l and the $Q - 1$ allowed values of k gives the other term. □

Proposition 5.6 (one-body preparation and determinant sensitivity). For each row $0 \le e < N$ denote by $\widetilde{f}_{e,l}$ the normalized P-node DFT of the prepared symbol of Proposition 5.4. With $B = P/2 - 1$ retain $|l| \le L \le B$. Let C_σ be the one-body strip majorant of Proposition 5.4 for $0 < \sigma < \log(1/z)$, and set

$$E_P = \frac{2C_\sigma e^{-(B+1)\sigma}}{1 - e^{-\sigma}} + (2B + 1)\frac{2C_\sigma e^{-(P-B)\sigma}}{1 - e^{-P\sigma}}.$$

Take $U = 1$ on the unrestricted real axis and, on a block $|r| \le R$, take the minimum of 1 and any of the bounds $\exp(R\sinh v - (L + 1)v)$, $v > 0$. Then

$$\epsilon = E_P + U\max_e \sum_{L<|l|\le B} |\widetilde{f}_{e,l}|, \qquad E_{\det} = M\big[(1 + N\epsilon/m)^N - 1\big]$$

bounds the entry error and the resulting contracted determinant error, respectively. Add the signed direction bound above. This evaluates the sampled coefficient tail as a sum of outward balls rather than extrapolating its decay from a few terms.

Proof. The mode error on $|l| \le B$ is bounded by the geometric sum over the distinct signed aliases $l + jP$, $j \ne 0$. The remaining true modes are bounded by both sides of the infinite strip tail, including the unpaired Nyquist index. This accounts for E_P. On discarded measured modes the Bessel generating function gives $|J_l(r)| \le U$. Reflection, without complex conjugation of the preparation, supplies negative row tags. Replacing the sampled symbol by the true symbol changes each matrix entry by at most ϵ.

Let G be the Gram matrix of the ordinary monomials on the original eigenangle circle for weight $|1 - z\lambda|^{2u}$. Thus $G \ge mI$. The original physical matrix A at each real frequency and direction in the untranslated calculation has a unit-modulus multiplier (remove the scalar translation from the eigenangle phase). Cauchy–Schwarz in this Gram norm gives $\|G^{-1/2}AG^{-1/2}\|_2 \le 1$. Applying the preceding Schur inequality at zero shift or Proposition 5.2 gives $\det G \le M$. The entrywise perturbation E has $\|G^{-1/2}EG^{-1/2}\|_2 \le N\epsilon/m$. Expand the perturbed determinant by columns and apply Hadamard to each term containing at least one perturbed column. The

binomial sum gives E_{det}. Finally the signed retained translation coefficients are supported in distinct residues modulo Q. Their nodal inverse polynomial p satisfies $Q^{-1}\sum_j |p(2\pi j/Q)|^2 = \sum_{|k|\le q}|t_k|^2 \le 1$ by both discrete and continuous Parseval. The contracted error is therefore at most E_{det} by Cauchy–Schwarz. □

Independent check in the original variables. The reference in `angular/check_angles.py` integrates the physical mark $d\lambda/(1-z\lambda)$ without a translation split. It obtains each signed Toeplitz entry from original-circle quadrature and contracts its determinant over a second direction circle. For an angular shift $\sigma < \log(1/z)$ the Fourier integrand of each entry is bounded by

$$C = e^{(N-1)\sigma + Rde^{\sigma}/(1-ze^{\sigma}) + \pi|\Im s|}\max((1-ze^{\sigma})^{2u}, (1+ze^{\sigma})^{2u}).$$

This uses the analytic wave with both $d\lambda/(1-z\lambda)$ and $d/(\lambda-z)$, each bounded by $de^{\sigma}/(1-ze^{\sigma})$ throughout the strip. Both logarithms of the physical weight have absolute argument $< \pi/2$. On a P_0-point eigenangle grid, assign each entry error $2C/(e^{P_0\sigma}-1)$ and use the Gram perturbation formula above. Separately shifting the direction of the full physical mark, whose modulus is at most D, bounds its Q_0-node error by $2Me^{DR\sinh v}/(e^{Q_0 v}-1)$. Both estimates apply simultaneously after adding the positive budgets. The test uses $P_0 = 2048$, $Q_0 = 256$ and 192-bit Arb and shares no Möbius samples, Bessel coefficients or determinant nodes with the accelerated preparation.

Six physical-source tests cover all ranks 4 through 8, including a rank-six negative tilt $-2.4+1.5i$ and rank-seven tilt $.11+2.94i$. The signed preparation and physical reference enclosures intersect at all six radii sampled. The absolute midpoint differences are below 2.57×10^{-39}. The values and bounds concern individual source samples; the final Mellin sums require their separate tail and weight estimates.

A direction-dependent contour for the prepared exterior sum

Let $D = N(1+z)$, $0 < z < 1$, $N+u \ge 0$ with $u = \Re s$, and $0 < \Delta D < 2\pi$. Write $G = Nz\cos\phi + \sum_{j=1}^{N}\cos x_j$ and $g(a) = 1+2z\cos a + z^2$ in the rotated Möbius angles of Theorem 5.3. A prepared factor in the Weyl amplitude is $g(x_j+\phi)^{-N-s}$. Its zeros constrain complex contour deformation. The old bound spends a common upper bound for the complete amplitude before any use of angular damping. Near a zero of $1-e^{i\Delta G}$ this can simultaneously charge a worst-case preparation and discard the direction and damping which produced it.

Proposition 5.7 (signed angular sectors). Choose $0 < T < 1$, $0 < c < 1$, $f = c(1-z)/(2\sqrt{z})$ and let

$$\sigma = |\sin\phi|, \qquad t = \min(T, f/\sigma).$$

At $\sigma = 0$ use $t = T$. Deform the real cycle by $x_j \mapsto x_j - it\sin x_j$, $\phi \mapsto \phi - it\sin\phi$. The same value of t applies to all eigenangles at each real direction. Put $G = X + iY$ after deformation. For a direction strip $\sigma \in [l, r]$, use upper and lower bounds t_1, t_0 for t, and $v_0 = \min(Tr, f)$. Write $\mathrm{sinhc}(x) = \sinh(x)/x$, $d = 1-z^2$ and

$$E = \mathrm{sinhc}(t_1)^2\left[4zv_0^2/(1-z)^2 + t_1^2\right], \quad \eta = \arctan\left[\mathrm{sinhc}(2t_1)\frac{2\sqrt{z}\,v_0/(1-z) + 2t_1}{1-E}\right].$$

Require $E < 1$ on each strip. With a signed real-part band $X \in [L, H]$, define δ_* to be a lower bound in $[0,1]$ on the distance of $X - Nz\cos\phi\cosh(t\sin\phi)$ to the lattice $-N+2\mathbb{Z}$, and put $y = t_0[Nzl^2 + \delta_*(2-\delta_*)]$. To compute δ_* it suffices to compare $[L, H]$ with both signed translates of

$$[Nz\sqrt{1-r^2},\ Nz\min(1, \sqrt{1-l^2}\cosh v_0)]$$

by the physical parity nodes $-N, -N+2, \dots, N$. One may also include their two nearest exterior neighbors. For an actual sample $X - Nz\cos\phi\cosh(t\sin\phi) \in [-N, N]$, so no other lattice point can be nearer.

Let k_0, b, p be the cutoff floor, width and count in Theorem 5.3. With an optional Fourier shift $\beta = 2\pi j/m$ take e to be the maximum of $1-e^{-\Delta y}$ and the sine of the distance of $\Delta[L,H]+\beta$ to $2\pi\mathbb{Z}$, clipped to $\pi/2$ *before* taking the sine. Require $e > 0$. Set $A = \min(1, 2/(be))$. The denominator and differentiated filter contribute the same factor

$$B_e = e^{-1}[(k_0 + 1/e)A^p + p(b-1)A^{p-1}/2],$$

where $e^{-1} = 1/e$ is the reciprocal band distance. The following multiplier replaces the angular variation and attenuation at the terminal:

$$J = d^{-u^2}(1+t_1^2)^{(N+1)/2}(1+t_1^2\cosh^2 t_1)^{N(N-1)/2}, \qquad F_0 = -N(N+u)\log(1-E) + N|\Im s|\eta - k_0\Delta y.$$

There are two additional choices for the exponent. Define

$$b_2 = (N+u)\frac{-\log(1-E)}{E}\frac{1+z}{(1-z)^2}\operatorname{sinhc}(t_1)^2 t_1, \qquad b_1 = |\Im s|\frac{2z}{d}\frac{\operatorname{sinhc}(2t_1)}{1-E}\sqrt{N(1+1/z)t_1}.$$

For $a = k_0\Delta - b_2 > 0$ let $y_* = \max(y, (b_1/(2a))^2)$ and take

$$F = \min(F_0, N|\Im s|\eta - ay, b_1\sqrt{y_*} - ay_*).$$

When $a \le 0$ use $F = F_0$. In each direction strip take the maximum of $Je^F B_e$ over its signed real-part bands. Average these maxima with exact direction-strip masses $2(\arcsin r - \arcsin l)/\pi$. Multiplication by

$$|C_\Delta|\,\Gamma(\Re\gamma)/(|\Gamma(\gamma)|k_0^{\Re\gamma}), \qquad \gamma = 2 + 2h,$$

bounds the discarded filtered sum with its physical prefactor. The proof uses $\Re h > -1$ for the gamma integral. For positive orders the separate Mellin image and its removable values remain required. A nonzero shift bounds the corresponding root-of-unity alias. Inequalities at shift zero alone give no certificate for a decimated lattice.

Proof. The signed complex displacements in a preparation factor have total magnitude $|v| = t|\sin x + \sin\phi| \le 2t|\sin\phi| + 2t|\cos((x+\phi)/2)|$. Use $g(a) = (1-z)^2 + 4z\cos^2(a/2)$ and Cauchy–Schwarz to obtain

$$2z(\cosh v - 1)/g(a) \le E.$$

The same estimate holds along the straight deformation homotopy. Moreover $2z|\sin a|\sinh|v|/g(a) \le \operatorname{sinhc}(2t_1)[2\sqrt{z}v_0/(1-z) + 2t_1]$, by $|\sin a| \le 2|\cos(a/2)|$. Hence the real part of the displaced g is positive, its modulus is at least $(1-E)g(a)$ and its argument has absolute value at most η. All powers continue from the physical branch. The Lipschitz torus may be split at its finitely many clipping angles and Stokes' theorem applied to the homotopy piecewise. Adjacent interface faces cancel with opposite orientations. In the complex Jacobian the x_j derivatives with respect to ϕ are confined to one column. Its determinant is triangular. The derivative of $t\sin\phi$ is $T\cos\phi$ on the free segment and zero on the clipped one. The Jacobian and pairwise sine differences thus cost exactly the bounds in J, as in Theorem 5.3. At each fixed real direction the undeformed positive real-tilt Weyl mass is independent of direction by rotation, and is bounded by d^{-u^2}.

Each $v_j' = \cos x_j \cosh(t\sin x_j)$ belongs to $[-1,1]$ since $\log\cosh w \le w^2/2$ and $t \le 1$. The imaginary part satisfies $Y \ge t(Nz\sin^2\phi + \sum_j \sin^2 x_j)$. Subject to a fixed sum of the v_j', the concave function $\sum_j(1-{v_j'}^2)$ has a minimum at a vertex of the sliced cube. All but at most one component of a vertex equal ±1. If the sum is at distance q from its nearest parity point, the minimum is $q(2-q)$. Since $\sin^2 x_j \ge 1 - {v_j'}^2$, this proves $Y \ge y$. Dropping the Nz term here would admit phases which do not represent the original Haar projection.

For the absorption bounds put $v_j = -t(\sin x_j + \sin\phi)$. Weighted Cauchy–Schwarz yields $\sum_j v_j^2 \le t(1+1/z)Y$. The inequality $-\log(1-v) \le [-\log(1-E)/E]v$ for $0 \le v \le E$ bounds the sum of the preparation log-modulus penalties by $b_2 Y$. Also $\max|\sin a|/g(a) = 1/d$ bounds the total argument penalty by $b_1\sqrt{Y}$, or alternatively by $N|\Im s|\eta$. Maximizing the remaining real exponential over $Y \ge y$ gives the claimed minimum of three exponents. The integral of $k^{1-\gamma}$, differentiation of the uniform cutoff filter, minimum distance of the Abel-damped ray from 1, removal of its damping, and final gamma normalization now follow the proof of (5.8) with the phase shifted by β. At the tested outer ranks absolute convergence of the sampled series is unchanged by multiplication by a unit-modulus shift. More generally the proof bounds its Abel value wherever absolute convergence has yet to be established separately. No probabilistic lower bound on a complex mass enters any estimate.

Corollary 5.7A (one spectral cutoff throughout the outer slab). For every $4 \le N \le 8$, $.82 \le z \le .9$, $-.95 \le \Re h \le 3$, $|\Im h| \le 3$ and $|s| \le 3$, the discarded filtered spectral term at $\Delta = .32$ has absolute value below $1.073 \cdot 10^{-17}$ with $k_0 = 4822, b = 53, p = 65$, last index 8202. This is the error from the spectral cutoff. Finite prepared coefficients, angular aliases, the separate Mellin image (including limiting values) and finite arithmetic have their own errors and domains.

Proof. Use the common clipped contour with $T = .11600374579299436$ and $c = .6538735309035306$, setting its f with $z = .9$ throughout. For a real-part band take $N(.82)\sqrt{1-r^2}$ for its lower direction magnitude and $N(.9)\min(1, \sqrt{1-l^2}\cosh v_0)$ for its upper one. In the lower bound y use $z = .82$. All preparation penalties permit $u = 3$, $|\Im s| = 3$, $|u|^2 = 9$ and $z = .9$; replace $1 + 1/z$ by $1 + 1/.82$ in b_1.

Writing $x = \Re h$ and applying gamma duplication and reflection gives

$$|C_\Delta|/|\Gamma(2+2h)| = \Delta^{-2x}|\sin \pi h|\,|\Gamma(1+h)/\Gamma(3/2+h)|/\sqrt{\pi}.$$

The beta integral bounds the gamma ratio by $\Gamma(1+x)/\Gamma(3/2+x)$ whenever $x > -1$. A second duplication, this time at real x, bounds the entire order-dependent prefactor by

$$\frac{2\cosh(3\pi)}{\pi} \max_{q\in\{-.95,3\}} \frac{\Gamma(1+q)^2(2/\Delta)^{2q}}{k_0^{2+2q}}.$$

The maximum occurs at a real endpoint by log-convexity of the gamma function. This estimate preserves the common gamma denominator before absolute-value bounds are applied.

The resulting outward 192-bit evaluations, one for the entire continuous parameter slab at each integer rank, have upper bounds $2.768\cdot10^{-18}, 4.474\cdot10^{-25}, 1.704\cdot10^{-30}, 1.970\cdot10^{-26}, 1.073\cdot10^{-17}$ for $N = 4, 5, 6, 7, 8$ respectively. The computation uses 40 direction strips and 74 signed bands per strip. Its exact input decimals and per-rank enclosures are in `tail/region.json` and may be reproduced by `tail/region.py`. Eigenangle sampling at finitely many radii would give a different assertion.

A physical basis for the computed determinant

Proposition 5.8 (triangular conditioning at independent tilt). Let the truncation of Proposition 5.4 retain a symmetric mode set. Choose real polynomials $p_j(w) = 2^{-e_j}(w^j + \sum_{k<j} b_{jk}w^k)$ with dyadic b_{jk} and integral e_j. Write B for their coefficient matrix. Compute instead the lower-triangular family of prepared symbols for $p_i(\lambda)\,p_j(\lambda^{-1})$, and recover the upper triangle at the reflected direction. Multiply the integrated determinant by $2^{2\sum e_j}$. This operation gives exactly the same finite angular formula in exact arithmetic, for every independent complex s and real sampled frequency.

Proof. The coefficient for power $-k$ at signed mode l equals that for power k at $-l$, since the Möbius map takes circle reflection to circle reflection and the complex tilt is even. Signed truncation at $\pm L$ commutes with this reversal. Taking literal linear combinations of the retained source vectors therefore gives BAB^{T} at every direction for the original finite matrix A. The transpose enters because the coefficients are real. The determinant is multiplied by $(\det B)^2 = 2^{-2\sum e_j}$. All translation and angular summation operations are linear on that determinant. This proves the assertion. It also explains why applying complex conjugation to the evaluated upper entry, or multiplying the original analytic angular error a second time by the large recovery factor, gives an incorrect readout.

A QR factorization of $1, \lambda, \ldots, \lambda^{N-1}$ on 2,048 original-circle nodes with positive amplitude $|1 - z\lambda|^{\Re s}$ suggests monic real polynomials. Round their off-diagonal coefficients to denominator 2^{40} and scale each by the dyadic ceiling of its fitted norm. The executed identity uses these literal polynomials. No bound on the accuracy of this QR fit is needed. In the code each transformed coefficient is formed as an Arb ball before the native stage accepts its component to within two units of 2^{-104}. The determinant engine charges its backward elimination residual and arithmetic after this preparation; this charge is multiplied by the exact recovery factor. A separately scaled untransformed basis is also available in the source history. An exceptional change of numerical conditioning leaves the analytic strip of the underlying moment unchanged.

For large physical Mellin factors, even the conversion of a dyadic centre to a printed 64-bit-significand floating value can dominate the complete error. The current dense route emits the two signed integer sums and their exact divisor $Q2^{104}$ before any decimal conversion. The determinant and Bessel rounding bounds remain payable. The change can materially improve the certificate without altering one retained sample or quadrature rule.

A sparse folded radial lattice with a prepared signed-mass bound

Set $d = 1 - z^2$, $u = \Re s$, $D = N(1+z)$ and $\Omega = \{\pm Nz - N + 2j : 0 \le j \le N\}$. The physical preparation in the rotated Möbius eigenangles $(x_1, \ldots, x_N)$, conditional on direction ϕ, is $d^{N^2+2Ns}\prod_j g(x_j+\phi)^{-N-s}$ against Weyl measure, where $g(x) = 1 + 2z\cos x + z^2$. The order enters through $C_\Delta = 2^{2h+1}\Gamma(1+h)\Delta^{-2h}/\Gamma(-h)$ and the lattice weight $k^{1-\gamma}$, $\gamma = 2+2h$. The scalar includes the usual subtracted image correction on the original step Δ. We assume $0 < z < 1$, $-1 < \Re h < 0$, $N + u \ge 0$, $0 < \Delta D < 2\pi$, and the hypotheses for the physical Poisson representation. Let $d\mu_u$ be the corresponding positive real-tilt measure, including the uniform direction.

Lemma 5.9 (prepared signed concentration). Write $G_0 = Nz\cos\phi + \sum_j \cos x_j$ in the undeformed coordinates. For every real σ the angular integral at fixed direction obeys

$$\int e^{\sigma G_0}\, d\mu_{u|\phi} \le d^{-u^2} \exp(\sigma^2/4 - uz\sigma\cos\phi).$$

For $a \ge 0$ the unnormalised mass of $|G_0| \ge a$ is at most $d^{-u^2}\min(1, 2e^{-(a-|uz|)_+^2})$.

Proof. The real zero-mean log symbol $f(x) = -(N+u)\log g(x+\phi) + \sigma\cos x$ has exponentially decaying Fourier coefficients. The finite Szegő inequality $D_N(e^f) \le \exp(\sum_{k\ge1} k|f_k|^2)$ applies. One proof uses monotonicity of the Gram determinants by Jensen's lower bound on each monic orthogonal norm, followed by the classical strong Szegő limit. The Dirichlet sum is

$$-(N+u)^2\log d + \sigma^2/4 - (N+u)z\sigma\cos\phi.$$

Multiplication by $d^{N^2+2Nu}e^{\sigma Nz\cos\phi}$ gives the first inequality. Apply exponential Markov to each of the two signs and use $|\sigma| = 2(a-|uz|)_+$, together with the mass bound at $\sigma = 0$. The cancellation of the $Nz\sigma\cos\phi$ term is exact. At complex tilt the argument uses the variation $d\mu_u$ of the physical preparation. It does not normalize complex mass to one.

Theorem 5.10 (a Chernoff bound on the alternating tail). On the contour $v = x - it\sin x$ for all $N+1$ angles, write $G = X + iY$. Choose $0 < t < 1$ with $ze^{2t} < 1$, and $E = 2z(\cosh(2t)-1)/(1-z)^2 < 1$. Put

$$\eta = \arctan\frac{2z\sinh(2t)}{d(1-E)}, \quad \delta_X = D(\cosh t - 1),$$
$$V = (1+t^2)^{(N+1)/2}(1+t^2\cosh^2 t)^{N(N-1)/2}(1-E)^{-N(N+u)}e^{N|\Im s|\eta}.$$

The existing deformation proof bounds the pullback of absolute preparation by $V\,d\mu_u$ pointwise. Also $|X - G_0| \le \delta_X$, $|X| \le D$, and $Y \ge t\,\mathrm{dist}(X,\Omega)$. In the last inequality, round each deformed real cosine $\cos x\cosh(t\sin x)$ to its nearest sign, paying at most $\sin^2 x$; its imaginary part $\sin x\sinh(t\sin x)$ is at least $t\sin^2 x$.

Let $F(k) = \Pr(K + U_1 + \cdots + U_p \le k)$, with independent U_j uniform on $\{0,\dots,b-1\}$. Partition $[0,D]$ into intervals $I_i = [a_i, b_i]$ in increasing order. For each interval set

$$y_i = t\,\mathrm{dist}(I_i, |\Omega|), \quad e_i = \max\{1 - e^{-\Delta y_i}, \sin\min(\pi/2, \mathrm{dist}(\pi, \Delta I_i))\}, \quad A_i = \min(1, 2/(be_i)).$$

Assume each $e_i > 0$. Define

$$B_i = \frac{e^{-K\Delta y_i}}{e_i}\{(K + 1/e_i)A_i^p + \tfrac{p(b-1)}{2}A_i^{p-1}\}, \qquad L_i = \max_{r\le i} B_r, \quad L_{-1} = 0.$$

Then the alternating discarded series satisfies

$$\left| C_\Delta \sum_{k\ge1} (-1)^k F(k) k^{1-\gamma}\Phi(k\Delta) \right| \le \frac{|C_\Delta|\Gamma(\Re\gamma)}{|\Gamma(\gamma)|K^{\Re\gamma}} V d^{-u^2} \sum_i (L_i - L_{i-1})\min\{1, 2e^{-(a_i - \delta_X - |uz|)_+^2}\}.$$

Proof. In the inherited filtered geometric-derivative identity use $w = -v_0 e^{i\Delta G - r}$ with $r > 0$, $0 < v_0 < 1$. Then $|1-w| \ge e_i$ and the filter $|b^{-1}\sum_{l=0}^{b-1} w^l| \le A_i$ on $|X| \in I_i$. Integration of $r^{\Re\gamma-1}e^{-Kr}$ yields the displayed gamma factor. The pointwise B_i is dominated by the staircase $\sum_i (L_i - L_{i-1})\mathbf{1}_{|X|\ge a_i}$. The lemma bounds the mass of each step because $|X| \ge a_i$ implies $|G_0| \ge a_i - \delta_X$. The estimates uniformly dominate the Abel-regularized integrals for $v_0 \uparrow 1$; the original damped/lattice representation selects the physical sum. An exact saddle matching $\Delta|\omega| = \pi$ can leave $e_i = 0$. The implementation returns a resource failure in that case. In the executed region a rational z, Δ cannot yield exact equality with π; an interval too close to resolve still fails the denominator test. If $\Delta D < \pi$, an alternative bound sets $t = 0$ and uses $e = \sin\min(\pi/2, \pi - \Delta D)$ on the full undeformed measure.

Corollary 5.11 (the implemented two-rate operator). Let F_1, F_2 be two independently chosen filters of the preceding type, with the second completing at least as late as the first. Use weights

$$a_k = 1 - F_1(k) + 2\mathbf{1}_{2|k}(F_1(k) - F_2(k)).$$

The discrepancy from the infinite fine sum equals the sum of the unshifted F_2 tail and the two alternating F_1, F_2 tails with their respective signs, by $2\mathbf{1}_{2|k} - 1 = (-1)^k$. For $k \geq K_1 + p_1(b_1 - 1)$ only even nodes can have nonzero weight, and for $k \geq K_2 + p_2(b_2 - 1)$ every weight vanishes. All remaining weights and index masks in the implementation are exact rationals. Charge the unshifted terminal estimate once and the two signed estimates once each, alongside the image, per-node angular, fixed-point and final outward readout errors. Sparse samples are built cold at steps Δ and 2Δ in separate native kernel calls; they are not inferred by subsampling a previously made dense witness. Each new order uses a fresh ball evaluation of all three radial tails, the exact cutoff weights and the image correction. The cold filters remain fixed across warm orders, so a difficult warm order may return only an absolute enclosure.

The argument treats an actual angular reciprocal pole inside the projected support when the phase approaches π. Replacing the signed sector mass by the full mass discards the concentration proved in the lemma. A collection of small changes under radial refinement cannot recover this missing transverse information. No bound on differences between arbitrary unsynchronised shell lattices is inferred from the two-rate identity. See Corollary 21.23 for the common parameter bounds and executed fixed-size formula.

A local estimate at the first critical radius

A signed denominator can vanish at the physical critical radius $z = 1 - 2/N$. Its vanishing only involves the saddle whose eigenangle sign population cancels the term $Nz\cos\phi$. The following estimate retains that population and the Vandermonde inside its small neighborhood. It concerns the scalar Fourier sum at a radius and does not require continuation of a differential system. All powers use the physical branches of the clipped-contour proposition.

Proposition 5.12 (separating the resonant sign population). Use the preceding clipped-contour notation, $0 < f/T < 1$, $0 < \xi < 1$, $\sigma_0 = f/T$, and choose a population index $m \in \{0, \dots, N\}$. Let

$$g_{\neq m} = \min_{j \in \{0,\dots,N\} \setminus \{m\}} |Nz + 2j - N|, \qquad \ell = N - m, \qquad P = (m^2 + \ell^2 + 1)/2.$$

Require $g_{\neq m} > 0$ and $P + 2\Re h > 0$. The method uses $m = 1$ on either side of and exactly at the first critical radius. Put

$$g_- = (1 - z)^2, \qquad g_* = g_- + 4z\cos^2\left(\frac{\arcsin\sigma_0 + \arcsin\xi}{2}\right).$$

Evaluate b_2, η of the clipped-contour proposition using $t_1 = T, v_0 = f$ on the strip $\sigma \leq \sigma_0$. Choose $K\Delta > b_2$. Write $d = 1 - z^2$, $u = \Re s$, $v = |\Im s|$, and

$$L = (1 + T^2)^{(N+1)/2}(1 + T^2\cosh^2 T)^{N(N-1)/2}, \quad \beta = T(\Delta - b_2/K)\min\left(\frac{\sigma_0}{\arcsin\sigma_0}, \frac{\xi}{\arcsin\xi}\right)^2.$$

Let $M_q = \pi^{q/2}2^{-q(q-1)/2}\prod_{i=1}^{q} i!$, including $M_0 = 1$. An absolute weighted spectral-tail allowance for the resonant neighborhood is

$$E_{\mathrm{core}} = |C_\Delta|\,\frac{2\binom{N}{m}4^{m\ell}M_m M_\ell\sqrt{\pi/(Nz)}}{N!(2\pi)^{N+1}}\,\frac{Ld^{N^2+2Nu}e^{Nv\eta}}{g_*^{m(N+u)}g_-^{\ell(N+u)}\beta^P}K^{-P-2\Re h}\left(\frac{1}{P + 2\Re h} + \frac{1}{K}\right).$$

The remainder outside this neighborhood uses the signed-sector filter bound derived above with three inexpensive changes. On direction strips $[l, r]$ above σ_0, all populations have $Y \geq t_0 Nzl^2$; use this floor and $e = 1 - e^{-\Delta y}$. On the central direction strip, for the distinguished population with at least one $|\sin x_j| \geq \xi$ one has $Y \geq T\xi^2$. For all other populations, on $|X| \in [L_0, H_0]$ take $y = T(g_{\neq m} - H_0)_+$ and take e also at least the clipped phase-distance sine. Take the larger of the latter two contributions on the central strip. Multiply the resulting strip maxima by their positive direction masses as before. Add E_{core} to this weighted noncore bound. Every component depends continuously on the radius where its displayed inequalities hold, including $Nz = N - 2$.

Proof. Deform the whole Weyl cycle before splitting its real parametrizing torus. Classify the x_j by whether $\cos x_j$ has the same sign as $\cos\phi$. If q signs agree, the critical signed value is $X_s = \mathrm{sgn}(\cos\phi)(Nz + 2q - N)$. The deformed real coordinates satisfy $|\cos x| \leq |\cos x\cosh(t\sin x)| \leq 1$. Hence $|X - X_s| \leq Nz\sin^2\phi + \sum\sin^2 x_j \leq Y/t$. This proves the complementary-population gap estimate. Applying the pointwise filter before integrating over

any subset is legitimate. The average positive undeformed measure of a subset is bounded by the full directional measure used in the clipped-contour proposition.

In the remaining set $t = T$, precisely m signs agree, and each angular variable is within $\arcsin \xi$, or $\arcsin \sigma_0$ for the direction, of its signed center. At agreeing signs $g(x_j + \phi) \geq g_*$ and elsewhere $g \geq g_-$. Contour displacement costs at most $\exp(b_2 Y + N v \eta)$. The absolute phase at frequency $k\Delta$ consequently damps by $\exp[-(k\Delta - b_2)Y]$. The inequality $\sin^2 w \geq (\sin a/a)^2 w^2$ on $[-a, a]$ gives the Gaussian with exponent $-k\beta(\sum w_i^2 + N z w_0^2)$, where the w_i are angular deviations from their respective signed centers. After the price in L, each same-sign pair contributes at most $(w_i - w_j)^2$ and each opposite-sign pair at most 4. Extend the nonnegative Gaussian integrands to the full Euclidean spaces. For q same-sign coordinates the squared-Vandermonde integral is $M_q (k\beta)^{-q^2/2}$ by monic Hermite orthogonality. The direction integral contributes $\sqrt{\pi/(N z k \beta)}$. The two direction signs and the Weyl selection contribute $2\binom{N}{m}/[N!(2\pi)^{N+1}]$. Finally the omitted filter weights have modulus at most $k^{-1-2\Re h}$ for $k \geq K$. Integral comparison for the resulting series gives the displayed E_{core}. This treatment pays the full absolute core and retains the Fourier filter outside it; it never divides by a critical zero.

The reference implementation `tail/wall_local.py` rounds these inequalities outwards. The central signed band is split into 40 equal parts on $[0, g_{\neq m}]$ and one remaining band to D. Forty direction panels cover $[\sigma_0, 1]$. With e.g. $N = 6, z = 2/3$, $h = -.9 + .5i$, $s = 1 + .5i$, $\Delta = .32$, $T = .50$, $c = .42$, $\xi = .48$, $K = 5500, b = 32, p = 48$, the core contributes less than $3.700 \cdot 10^{-14}$, and its complementary angular region less than $6.078 \cdot 10^{-33}$. These are absolute tail components. The separate finite source, image, and rounding costs enter the end-to-end receipts. This sign classification assumes neither a noncritical radius nor a limiting density theorem.

Corollary 5.12A (continuous joint boxes through a critical radius). For each $N = 4, \dots, 8$ take $|z - (1 - 2/N)| \leq .005$. Vary real and imaginary order coordinates independently by at most .01 from h_0 and both tilt coordinates independently by at most .02 from s_0. Take $(h_0, s_0) = (-.55 + .9i, -2.8 + .6i)$ for $N = 4$ and $(-.9 + .5i, 1 + .5i)$ for $5 \leq N \leq 8$. Use the real and complex finite angular formulas of the corrected Theorem 21.18. Choose $T = .50$, $b = 32$, $p = 48$, $\xi = .48$ and $\Delta = .32$. In increasing rank take $K = (10000, 9300, 6500, 5500, 5500)$ and $c = (.25, .30, .42, .45, .53)$. The respective uniform **absolute** errors of these exact-arithmetic finite formulas are below

$$5.037 \cdot 10^{-11}, \quad 2.417 \cdot 10^{-11}, \quad 4.332 \cdot 10^{-14}, \quad 3.847 \cdot 10^{-16}, \quad 3.467 \cdot 10^{-17}.$$

Proof. Enclose all five real coordinates by Cartesian intervals. Partition the radius interval into sixteen closed equal intervals; in each pass the four order and tilt coordinates remain full intervals. The input-dependent clipping transition may vary with z: the direction strips are defined by the same expressions in z as their enclosures, and at every fixed radius form a cover of its complete cycle. `tail/wall_boxes.py` evaluates the foregoing inequalities in outward 192-bit arithmetic on all 80 cells; `tail/wall-boxes.json` records every rational radius endpoint and bound. Each last spectral index is below 52,580. The finite source and image inequalities of the corrected Theorem 21.18 use only $z \leq .9$, $D \leq 15.2$ and this latter count; the lower radius bound in that theorem entered its terminal gap, which we replace here. Thus the additional budget is less than $2.862260 \cdot 10^{-17}$. The finite spectral readout, image and its coefficients vary with the five input coordinates. These are absolute approximation errors at every input, and the pointwise finite-arithmetic gates remain separate.

For single inputs the angular source can instead use the adaptive implementation and the actual source bound at that preparation. At the five central parameters its cold certificates used respectively 9,988, 9,488, 6,988, 6,188 and 5,988 source frequencies. Each accepted pointwise relative error bound is below 10^{-10}. The smaller rank-four power $P = 11/2$ leaves a substantially slower critical tail, especially at more negative orders; the general identity alone gives no practical bound there. Twenty central-input readouts and additional rank-six off-center radii are recorded in the wall receipts.

Corollary 5.13 (continuous scalar evaluation through consecutive critical radii). Let $|\Re h + .93| \leq .005$, $|\Im h - .8| \leq .01$, $|\Re s + .6| \leq .01$ and $|\Im s - .9| \leq .01$, independently. Use the same finite angular source and image grids as in the corrected Theorem 21.18 and a single spectral filter $\Delta = .32$, $K = 7500$, $b = 40$, $p = 54$, last index 9,606. The absolute exact-arithmetic scalar approximation error is below $9.515 \cdot 10^{-16}$ at rank six throughout $.330 \leq z \leq .670$, and below $2.863 \cdot 10^{-17}$ at rank eight throughout $.245 \leq z \leq .755$. These closed intervals contain two and three distinct critical radii respectively.

Proof. The sign-population estimate applies for every designated integer m, with all factors in the statement depending on $m, \ell = N - m$. It uses no first-wall identity in the proof. At an exact wall $z = 1 - 2m/N$, $g_{\neq m} = 2$,

even though the original unconditioned gap vanishes. Between walls a change in the selected integer changes only the error proof. The filter, finite source and physical readout are identical on both sides of such a change. Partition each radius interval into closed cells of width .0025. In each cell with midpoint z_* select m nearest to $N(1-z_*)/2$, resolving a tie upwards. Enclose the whole cell and the full four order and tilt intervals in every calculation. Use $T = .50$, $\xi = .48$ and the better of the two outward allowances at $c = .37, .48$. The selected c and m at every cell appear in `tail/multi-region.json`. The 136 and 204 interval calculations give spectral bounds below $9.229 \cdot 10^{-16}$ and $7.553 \cdot 10^{-24}$ respectively. The inherited finite-source and image budget is below $2.862260 \cdot 10^{-17}$ as in the first-wall corollary. This gives the asserted total. This is an interval of scalar readouts at physical inputs. Each finite-arithmetic evaluation has its own propagation of arithmetic errors.

At the central complex parameters the adaptive finite evaluator made the following fresh queries exactly at the additional walls. The third warm quantity in each preparation was order one, independently enclosed using the original-Haar two-insertion determinant. A second, noninteger warm order was $-.41 - .7i$.

Rank	Radius	Agreeing signs m	Last frequency	Cold preparation (s)	Contraction (s)	Relative error bound	Difference from independent continuous-Riesz calculation
6	1/3	2	3320	5.59	.077	$5.229{\cdot}10^{-14}$	$2.34 \cdot 10^{-15}$
8	1/2	2	2420	8.99	.060	$4.536{\cdot}10^{-14}$	$2.36 \cdot 10^{-15}$
8	1/4	3	2420	7.44	.056	$1.496{\cdot}10^{-18}$	$2.11 \cdot 10^{-15}$

The last column describes the floating-point original-angle comparison. Its own numerical error can exceed the entire certified disk of the scalar evaluator. The data come from local scalar preparations at each radius. They establish no transfer matrix carrying a state through the walls.

Retaining the local preparation near the resonant population

The common realized source is the Haar eigenangle law, tilted by the unnormalized complex weight $|\Lambda_N(z)|^{2s}$. The sampled readout is $\Phi(r) = \mathbb{E}[|\Lambda_N(z)|^{2s} J_0(r|S_N(z)|)]$, and its filtered Mellin contraction recovers the ordinary moment $T_N(h, s; z)$. On the clipped cycle the projected source is $G = X + iY$ with $Y \geq 0$. The earlier core bound retained same-sign Vandermonde repulsion but replaced the small preparation phase by a constant $N|\Im s|\eta$. This discarded the fact that the phase vanishes at the same saddle where Y vanishes. Retaining that relation supplies the following quantitative repair. It is a bound for the scalar property; it imposes no full-state recovery requirement.

Proposition 5.14 (square completion in the core).

Retain all hypotheses and notation of Proposition 5.12. Put $A = K\Delta - b_2 > 0$, $P = (m^2 + \ell^2 + 1)/2$ and use the coefficient b_1 from Proposition 5.7. In the old core formula, the factor $\exp(N|\Im s|\eta)$ can be replaced by

$$\min\left\{ e^{N|\Im s|\eta},\ e^{b_1^2/(4\rho)} \left(\frac{A}{A-\rho}\right)^P \right\}, \qquad 0 < \rho < A.$$

When $b_1 = 0$, the second factor is interpreted as 1 with $\rho = 0$. Every displayed choice is valid; optimization is unnecessary to validity. A useful pointwise minimizer is

$$\rho_* = \frac{2b_1 A}{\sqrt{b_1^2 + 16PA} + b_1}.$$

For an interval input the implementation replaces b_1 by an outward upper bound and A by an outward positive lower bound only in this choice, then re-evaluates the actual allowance. Thus numerical optimization never becomes a proof premise.

Proof. Proposition 5.7 proves the pointwise phase-price bound $\exp(b_2Y + b_1\sqrt{Y})$ relative to the undeformed positive real-tilt preparation. Young's inequality gives $b_1\sqrt{Y} \le \rho Y + b_1^2/(4\rho)$. For every sampled frequency $k \ge K$, the remaining damping is at least $k[\Delta - (b_2+\rho)/K]Y$ in the notation of the preceding Gaussian estimate. Consequently its Gaussian scale is multiplied by $(A-\rho)/A$. The eigenangle and direction integrals are homogeneous of total degree $-P$ in that scale. The tail comparison and every complementary-region term remain unchanged. Differentiating the logarithm of the displayed factor gives $4P\rho^2 + b_1^2\rho - b_1^2A = 0$, whose positive root is the stated stable expression. □

Proposition 5.15 (local real preparation and pair-specific geometry).

Let $a_x = \arcsin\xi$, $a_0 = \arcsin\sigma_0$, and

$$\kappa = \min\{(\xi/a_x)^2, (\sigma_0/a_0)^2\}, \quad g_+ = (1+z)^2, \quad g_- = (1-z)^2, \quad q_0 = \frac{z}{g_+}(a_x+a_0)^2 < 1.$$

Suppose $N + \Re s \ge 0$. Define

$$R = \frac{(N+\Re s)z}{g_+T\kappa}\frac{-\log(1-q_0)}{q_0}\left(1+\frac{m}{Nz}\right), \qquad A_1 = K\Delta - b_2 - R > 0.$$

Choose $0 \le \rho < A_1$, with $\rho > 0$ unless $b_1 = 0$, and put

$$\beta_1 = T\kappa\left(\Delta - \frac{b_2+R+\rho}{K}\right), \quad L_1 = (1+T^2)^{(N+1)/2}[1+T^2\,\mathrm{sinhc}(T\xi)^2]^{\binom{m}{2}+\binom{\ell}{2}}\cosh(T\xi)^{2m\ell}.$$

A new valid core allowance is

$$|C_\Delta|\,\frac{2\binom{N}{m}4^{m\ell}M_mM_\ell\sqrt{\pi/(Nz)}}{N!(2\pi)^{N+1}}\,\frac{L_1d^{N^2+2N\Re s}}{g_+^{m(N+\Re s)}g_-^{\ell(N+\Re s)}}\,\frac{e^{b_1^2/(4\rho)}}{\beta_1^P}K^{-P-2\Re h}\left(\frac{1}{P+2\Re h}+\frac{1}{K}\right).$$

The zero-b_1 convention is as in Proposition 5.14. It can be minimized against the old core and Proposition 5.14 without modifying the exact finite formula. The same positive-z, nonintersecting-population and $P + 2\Re h > 0$ hypotheses remain. No assertion uniform down to $z = 0$ follows from the displayed direction Gaussian.

Proof. Write w_0, w_j for deviations from the signed direction and eigenangle centers. On an agreeing sign,

$$g(w_j+w_0) = g_+ - 4z\sin^2((w_j+w_0)/2) \ge g_+\left[1 - \frac{z}{g_+}(w_j+w_0)^2\right].$$

The bracket is positive by $q_0 < 1$. The logarithmic inequality used in Proposition 5.7 therefore bounds the agreeing-sign real preparation by $g_+^{-m(N+\Re s)}\exp(RY)$. Indeed,

$$\sum_{j\in+}(w_j+w_0)^2 \le \left(1+\frac{m}{Nz}\right)\left(\sum_{j\in+}w_j^2 + Nz\,w_0^2\right), \qquad Y \ge T\kappa\left(\sum_j w_j^2 + Nz\,w_0^2\right).$$

The first is the norm bound for the map $(w_1,\dots,w_m,\sqrt{Nz}w_0) \mapsto (w_j+w_0)_{j=1}^m$, whose squared operator norm is $1 + m/(Nz)$. The remaining preparation factors are bounded by $g_-^{-\ell(N+\Re s)}$.

For a same-sign pair, use $|2\sin((x_i-x_j-iT(\sin x_i-\sin x_j))/2)|^2 = 4\sin^2((x_i-x_j)/2)+4\sinh^2(T(\sin x_i-\sin x_j)/2)$. The real sine is bounded by its argument; $|\sin x_i - \sin x_j| \le |w_i - w_j|$ and also $|\sin x_i - \sin x_j| \le 2\xi$. Hence this factor is at most $[1+T^2\,\mathrm{sinhc}(T\xi)^2](w_i-w_j)^2$. An opposite-sign pair is bounded by $4\cosh^2(T\xi)$. Multiplying these factors and the inherited triangular-Jacobian bound gives L_1. Add b_2Y from complex displacement and absorb $b_1\sqrt{Y}$ by Proposition 5.14. The Mehta integrals and final comparison are then exactly those in the parent core proof. Every inequality is applied to the complete same physical preparation; no observed cancellation or normalized complex probability is used. □

Decay and ordinary-moment scope

For fixed positive z, this construction requires $P + 2\Re h > 0$ at the selected population and a strictly positive gap to all other populations. At the first wall the powers $P + 2\Re h$ at $\Re h = -.95$ are $3.6, 7.1, 11.6, 17.1, 23.6$ for ranks 4 through 8. They are tail exponents of this absolute core estimate, not sharp moment existence thresholds. At rank three the first-wall exponent is 1.1. The scalar ordinary Haar domain remains $\Re h > -1$ at positive radius for all ranks at least two. A failed numerical tail budget is not divergence.

Contract of the finite computation

`resonant_core.py` implements Propositions 5.14–5.15 in Arb interval arithmetic. The complementary filter is retained literally from the recovered `wall_local.py`. `run_core.py` uses freshly constructed signed angular data and the inherited finite-arithmetic, prepared-source and Mellin-image gates. Its receipt distinguishes all components and the scalar lower-modulus test. New core bounds do not certify a different radial schedule without accounting for its alias terms.

The diagnostic `phase_cost` field records the Proposition 5.14 factor before minimizing against Proposition 5.15, not the entire Proposition 5.15 phase-and-rate cost. The authoritative returned core and total allowances include the full Proposition 5.15 factors. Saved data are sealed against their implementation hashes. Independent comparison code must retain its own convergence and finite-arithmetic status.

Proposition 5.16 (continuous independent-parameter majorants).

Let $-1 < a_- \le \Re h \le a_+ \le -1/2$, $|\Im h| \le B$, and $|\Re s|, |\Im s| \le S < N$. The following changes make Propositions 5.14–5.15 and the complementary filtered estimate uniform in all four order/tilt coordinates at once. They do not sample a grid of these coordinates.

For the core use

$$C_{\mathrm{core}} = \max_{a \in \{a_-, a_+\}} 2(2/\Delta)^{2a} \frac{\Gamma(1+a)}{\Gamma(-a)}.$$

For the complementary prefactor use

$$F_{\mathrm{comp}} = \frac{2\cosh(\pi B)}{\pi} \max_{a \in \{a_-, a_+\}} \frac{\Gamma(1+a)^2 (2/\Delta)^{2a}}{K^{2+2a}}.$$

Use $N + S$ in b_2, R, use S in b_1 and the preparation-argument price, and bound positive preparation mass by d^{-S^2}. In the core, for either choice of its positive agreeing-sign denominator g_A, replace

$$d^{N^2+2Nu} g_A^{-m(N+u)} g_-^{-\ell(N+u)}$$

by the single combined expression

$$d^{N^2} g_A^{-mN} g_-^{-\ell N} \max\left\{ \left(\frac{d^{2N}}{g_A^m g_-^\ell} \right)^{-S}, \left(\frac{d^{2N}}{g_A^m g_-^\ell} \right)^{S} \right\}.$$

Use $P + 2a_-$ in the tail power and reciprocal denominator. All other radius, contour and gap tests must hold throughout the radius interval being enclosed. The same formulas cover the original disk $|s| \le 3$ by $S = 3$; its circumscribed square is used only to obtain a conservative inequality, not to enlarge the original finite-source theorem silently.

Proof. Write $h = a + ib$. Since $|\Gamma(-h)| = |\Gamma(-\bar{h})|$ and $-\bar{h} - (1+h) = -1 - 2a \ge 0$, Euler's beta integral gives

$$\left| \frac{\Gamma(1+h)}{\Gamma(-h)} \right| \le \frac{\Gamma(1+a)}{\Gamma(-a)}$$

for $a < -1/2$; at $a = -1/2$ the ratio has modulus exactly one. The logarithm of the real prefactor has second derivative $\psi_1(1+a)-\psi_1(-a) \geq 0$, because the trigamma function is decreasing on the positive real axis. Thus its maximum on the compact real interval is at an endpoint. This proves C_{core} without paying exponential imaginary-order growth. The complementary prefactor follows from the inherited gamma duplication/beta-integral estimate; its real expression is log-convex, so again the endpoints suffice. The preparation rates are monotone in their nonnegative displayed factors. The full real preparation multiplier is an exponential affine function of $u = \Re s$, hence its maximum is attained at $u = \pm S$. Keeping that product intact prevents a false enlargement of its interdependent factors. Finally $K \geq 1$ and $P + 2a_- > 0$ give the last two monotone replacements. □

`uniform_core.py` evaluates these expressions with outward Arb rounding. `region_core.py` partitions a **closed radius interval** into rational closed cells, retaining the entire order/tilt rectangle in every cell. Its receipt records each cell, selected population, contour, gap and total core/complement allowance. Choosing the best of finitely many valid contour bounds is sound. The physical finite Fourier formula remains the same in every cell, including at changes of selected population or proof contour. This proves a bound for its value at every specified input; it is not an enclosure of the complete set of all output values.

Corollary 5.17 (extension to the full order strip). The same core bound can cover orders above $-1/2$ without changing the spectral filter. Preserve the correlation between its Mellin factor and the decaying power of the cutoff. Let $a_0 = -.95$, and let the imaginary-order bound be B. Reflection and the gamma integral give, for $a \geq -1/2$,

$$|C_\Delta| K^{-2(a-a_0)} \leq \frac{2\cosh(\pi B)}{\pi} \Gamma(1+a)^2 (2/\Delta)^{2a} K^{-2(a-a_0)}.$$

The logarithm of the right side is convex in a, so its maximum on $[-1/2, 3]$ is at $-1/2$ or 3. Also $(P+2a)^{-1}+K^{-1} \leq (P+2a_0)^{-1} + K^{-1}$. The complementary gamma multiplier is the log-convex expression of Proposition 5.16 on all $a > -1$, so its maximum on $[a_0, 3]$ is at a_0 or 3.

Consequently an inverse-envelope proof remains valid on $a_0 \leq \Re h \leq 3$ whenever its core constant dominates these two additional endpoint bounds and the value at $a = -1/2$, and its complementary multiplier dominates the endpoint at $a = 3$. These are scalar inequalities, evaluated outwards in the receipts; interval overlap is never used to prove dominance. The common endpoint a_0 is carried symbolically. Results 21.24–21.26 give the resulting regions and use the full-order, regularized Mellin image. The inverse-only image dimensions cannot silently be reused through positive orders. At a nonnegative integer order use the removable products of Theorem 21.21, or the enclosed integer coefficient directly.

Sparse sampling of a critical scalar sum

The resonant-core construction and the reciprocal-grid alias are different obligations. A zero of the unshifted phase at a physical critical radius does not force a zero of a folded phase. This observation extends the earlier two-rate formula to a useful integer stride at inner radii.

Proposition 5.18 (a separated integer sampling rate). Write $a = \Re h > -1$, $u = \Re s$, $D = N(1+z)$, $M = (1-z^2)^{-u^2}$, and $\gamma = 2 + 2h$. Let $F_{K,b,p}(k) = \Pr(K + U_1 + \cdots + U_p \leq k)$, where the independent U_j are uniform on $\{0, \ldots, b-1\}$; this probability notation defines exact rational filter coefficients, not a complex-tilted measure. For an integer $q \geq 2$ suppose

$$\delta_j = 2\pi \min(j/q, 1 - j/q) - \Delta D > 0, \qquad 1 \leq j < q.$$

Put $d_j = \sin \min(\delta_j, \pi/2)$ and $A_j = \min(1, 2/(bd_j))$. Then an absolute bound for all $q-1$ folded filtered tails is

$$\mathcal{A}_q(K,b,p) = |C_\Delta| \frac{\Gamma(\Re\gamma)}{|\Gamma(\gamma)|} \frac{M}{K^{\Re\gamma}} \sum_{j=1}^{q-1} \frac{1}{d_j} \left[(K + d_j^{-1}) A_j^p + \frac{p(b-1)}{2} A_j^{p-1} \right].$$

For $q = 1$ define $\mathcal{A}_1 = 0$.

Proof. For the original positive comparison preparation $|\Lambda_N(z)|^{2u}$, the projected mark G lies in $[-D, D]$ and the total mass is at most M. This is the same real-tilt mass inequality used in Proposition 5.5. The complex

preparation has this total variation. For $w = e^{-t+i(\Delta G+2\pi j/q)}$, $t \geq 0$, the assumed support separation gives $|1-w| \geq d_j$. The generating function of the filter is

$$\sum_{k\geq 0} F_{K,b,p}(k)w^k = \frac{w^K}{1-w}\left(\frac{1+w+\cdots+w^{b-1}}{b}\right)^p.$$

Its Euler derivative $w\partial_w$, estimated before integration, is bounded by

$$\frac{e^{-Kt}}{d_j}\left[(K+d_j^{-1})A_j^p + \frac{p(b-1)}{2}A_j^{p-1}\right].$$

Here the polynomial H_b has modulus at most A_j and its Euler derivative $wH_b'(w)$ has modulus at most $(b-1)/2$; no division by H_b is used. Finally use $k^{-1-2h} = k\Gamma(\gamma)^{-1}\int_0^\infty t^{\gamma-1}e^{-kt}\,dt$ and $\int_0^\infty t^{\Re\gamma-1}e^{-Kt}dt = \Gamma(\Re\gamma)K^{-\Re\gamma}$. All powers of t and k use their positive real logarithms. Absolute domination justifies the integral and the Abel limit; no probabilistic claim is made for the complex preparation. Summing the $q-1$ costs proves the inequality.

Let F_1, F_2 be two such filters, with the first transition ending before the second. Use the exact rational weights

$$w_k = 1 - F_1(k) + q\mathbf{1}_{q|k}\,[F_1(k) - F_2(k)].$$

The identity $q\mathbf{1}_{q|k} = \sum_{j=0}^{q-1} e^{2\pi ijk/q}$ shows that the difference between this finite sum and the dense $(1-F_2)$ sum is precisely the sum of the folded $(F_1 - F_2)$ tails. Consequently the total exact-arithmetic spectral allowance is

$$E_{\text{critical}}(F_2) + \mathcal{A}_q(F_1) + \mathcal{A}_q(F_2).$$

The source, image and arithmetic errors must still be added. Above the end of F_1 only multiples of q have nonzero weight, so this is an actual reduced source calculation. Both individual filters and every weight are computed as exact integers divided by b^p.

For continuous parameter rectangles one can remove the complex gamma factors without sampling. If $-1 < a_- \leq \Re h \leq a_+$ and $|\Im h| \leq B$, then

$$|C_\Delta|\frac{\Gamma(2+2\Re h)}{|\Gamma(2+2h)|}K^{-2-2\Re h} \leq \frac{2\cosh(\pi B)}{\pi}\max_{a\in\{a_-,a_+\}}\Gamma(1+a)^2(2/\Delta)^{2a}K^{-2-2a}.$$

The reflection formula expresses the left side through $\sin(\pi h)\,B(1+h,1+h)$; the beta integral gives $|B(1+h,1+h)| \leq B(1+a,1+a)$, and $|\sin(\pi h)| \leq \cosh(\pi B)$. The remaining real expression is log-convex in a, so the endpoints suffice. With $|\Re s| \leq S$, replace M by $(1-z^2)^{-S^2}$.

Executable contract. `critical_sampler.py` verifies the selected integer schedule in outward Arb arithmetic, generates the actual selected source rows with the preserved validated kernel, exports their centres as exact dyadic integers, and checks code/data seals at every warm readout. Every query recomputes all error components and tests the lower modulus before reporting relative accuracy. Rejecting an unseparated stride is necessary: a folded phase can then meet the physical support, so the displayed denominator argument no longer applies. The earlier frequency-sector method can be used in that case with its own established allowance; the simple bound is not extended by assuming the alias small.

The beta integral in this last comparison needs only $1 + \Re h > 0$. Its log-convex endpoint argument therefore applies also to positive real orders. This is distinct from the more restrictive gamma-ratio argument for the core in Proposition 5.16.

Complete sampled readouts, return estimates and analytic source transport

The following arguments extend this section. Lettered identifiers retain stable links to the integrated constructions; their correspondence is given at the beginning of the paper. Earlier bounds remain valid on their stated domains. A limitation described at an intermediate stage is superseded only by a later explicitly proved result, as summarized in the current coverage table.

Physical source and the information retained (R2)

Write $a = 3z$, $d = 1 - z^2$, $p = 3 + s$. For each original eigenvalue λ, the exact Mobius change

$$w = \frac{\lambda - z}{1 - z\lambda}, \qquad \lambda = \frac{w + z}{1 + zw}$$

gives $(1 - z^2)\lambda/(1 - z\lambda) = w + z$. Hence the mark becomes $a + \sum w_j$. The Jacobian and all pair differences transform together, giving the density relative to normalized CUE(3)

$$A_s(w) = d^{9+6s} \prod_{j=0}^{2} (1 + zw_j)^{-p} (1 + z/w_j)^{-p}. \tag{R2.1}$$

On the real torus, each pair of factors equals $(1+2z\cos t_j+z^2)^{-p}$ with its physical real logarithm. Both exponents use the same s; no complex conjugation of the preparation is made. The denominators have no zero for $0 < z < 1$.

After averaging the direction and changing the three eigenangles by that direction, the radial Fourier source is

$$\Phi(r) = \frac{d^{9+6s}}{6(2\pi)^4} \int e^{\mathrm{i}r(a\cos\phi + \sum_j \cos x_j)} |\Delta(e^{\mathrm{i}x})|^2 \prod_{j=0}^{2} g(x_j + \phi)^{-p}\, dx\, d\phi, \quad g(t) = 1 + 2z\cos t + z^2. \tag{R2.2}$$

The conditional route uses the equivalent convention $w \mapsto -w$, so that its mark is $|a - \sum w_j|$. The two signs describe the same integral.

The protocol's source-to-readout discipline is used concretely here. The parent source is the prepared Haar measure and mark. The Fourier source retains all saddle populations. The finite Laurent representation discards a quantified density remainder, and its return is charged at the original moment before subtraction of a finite prefix and image. The failed rectangular-ball phase recurrence loses numerical conditioning, not physical information; independent phase evaluation repairs that readout. Every such change has an explicit equality or error map below.

Finite preparation with an original-space error (R3)

Define

$$b_n = (-1)^n \frac{(p)_n}{n!} z^n, \quad B_L(w) = \sum_{n=0}^{L} b_n w^n, \quad W_L(t) = B_L(e^{\mathrm{i}t}) B_L(e^{-\mathrm{i}t}) = \sum_{k=-L}^{L} w_k e^{\mathrm{i}kt},$$

where

$$w_k = w_{-k} = \sum_{n=0}^{L-|k|} b_{n+|k|} b_n. \tag{R3.1}$$

This symmetry is not conjugacy. Let A_L, Φ_L and T_L denote the six-factor polynomial density, its Fourier source, and its ordinary moment.

Lemma R3.1 (Preparation and return data)**.** *Put $P = |3 + s|$, $B_p = (1 - z)^{-P}$ and*

$$q = z \max\left(1, \frac{L + 1 + P}{L + 2}\right) < 1, \qquad e = \frac{|b_{L+1}|}{1 - q}, \qquad \delta = 6d^{9+6\,\mathrm{Re}\,s} B_p^5 e.$$

Then $|A_s - A_L| \le \delta$ on the real torus. With $u = \mathrm{Re}\, h > -1$, $B = 3(1 + z)$ and $M_u = \mathbb{E}_{\mathrm{CUE}_3} |a + \mathrm{Tr}\, V|^{2u}$,

$$|T - T_L| \le \delta M_u, \qquad |\Phi(r) - \Phi_L(r)| \le \delta \quad (r \in \mathbb{R}), \tag{R3.2}$$

$$|a_j - a_{j,L}| \le \frac{\delta B^{2j}}{4^j (j!)^2}, \qquad a_j = \frac{(-1)^j T_3(j, s; z)}{4^j (j!)^2}. \tag{R3.3}$$

Proof. Since $|(p)_n| \le (P)_n$, both the complete and truncated absolute series are bounded by B_p. The first omitted term is b_{L+1}; all later absolute term ratios are at most q. Telescoping the six factors gives $6B_p^5 e$, and the modulus of the prefactor in (R2.1) gives δ. Integrating against the positive normalized CUE measure proves the moment and Fourier bounds. The Taylor coefficient formula and support $|a + \mathrm{Tr}\, V| \le B$ prove the coefficient inequality. □

It would be invalid to integrate the constant bound $|\Phi - \Phi_L| \le \delta$ to infinity against a deeply inverse Mellin weight. The full-moment bound in Lemma R3.1 is the necessary return map. It is the main reason the polynomial construction remains useful even when high Fourier modes have poor termwise asymptotic constants.

Returning the tail to the original moment (R5)

For $\Delta B < 2\pi$, HaarCritical Proposition 5.2 gives

$$T = C_\Delta(h) \sum_{k \ge 1} k^{-1-2h} \Phi(k\Delta) - I(h), \quad C_\Delta(h) = 2^{2h+1}\Gamma(1+h)\,\mathrm{rgamma}(-h)\Delta^{-2h}, \tag{R5.1}$$

where

$$I(h) = C_\Delta(h) \sum_{j \ge 0} \zeta(1+2h-2j) a_j \Delta^{2j}.$$

The same identity holds for the finite complex polynomial source. It has the same compact support, bounded amplitude, ordinary integrability, and sufficient Fourier decay. Linearity requires no positivity. Holomorphy in h on $\mathrm{Re}\, h > -1$ continues the identity with its removable products.

The positive comparison moment

For $u \ge 0$ use $M_u \le (a+3)^{2u}$. For $-1 < u < 0$ choose $R_0 = 16$. The untilted translated source is $J_0(ar)D_3(r)$, with

$$D_3 = J_0^3 + 2J_0J_1^2 + 2J_1^2J_2 - J_0J_2^2.$$

Put

$$b_n(x) = \sqrt{2/\pi}\left[1 + \frac{|n^2 - 1/4|}{x} e^{|n^2-1/4|/x}\right]$$

and

$$H = \frac{b_0(aR_0)}{\sqrt{a}}[b_0(R_0)^3 + 2b_0(R_0)b_1(R_0)^2 + 2b_1(R_0)^2 b_2(R_0) + b_0(R_0)b_2(R_0)^2].$$

Lemma R4.2 gives $|J_0(ar)D_3(r)| \le Hr^{-2}$ for $r \ge R_0$. Below R_0 its modulus is at most one. Absolute integration of the inverse Mellin formula yields the explicit bound

$$M_u \le C(u)\left[\frac{R_0^{-2u}}{-2u} + \frac{HR_0^{-2u-2}}{2u+2}\right], \qquad C(u) = 2^{2u+1}\Gamma(1+u)/\Gamma(-u) > 0. \tag{R5.2}$$

The denominators are positive on this strip. At $u = 0$ the support branch returns one, so no spurious singular comparison is introduced.

The image allowance and integer orders

Let $W_j = C_\Delta \zeta(1+2h-2j)$ and choose $J > u + 1/2$. Put

$$x = \Delta B/(2\pi), \tag{R5.3}$$

$$q_J = x^2 \max\left(1, \frac{J-u}{J+1}\right)\max\left(1, \frac{J+1/2-u}{J+1}\right) < 1, \tag{R5.4}$$

$$E_J = \frac{2(2\pi)^{2u}|\cos \pi h|\Gamma(2J-2u)\zeta(2J-2u)}{(J!)^2(1-q_J)}(x/2)^{2J}, \tag{R5.5}$$

$$I_\delta = \sum_{j=0}^{J-1} |W_j| \frac{(\Delta B/2)^{2j}}{(j!)^2} + |C_\Delta| E_J. \tag{R5.6}$$

The zeta functional equation, gamma integral, duplication formula and a positive geometric ratio bound prove that the full image difference costs at most δI_δ. The implementation uses $J = 64$ and explicitly checks its hypotheses.

Near $h = j$ let $\eta = h - j$ and $Z(\eta) = \zeta(1+2\eta) - (2\eta)^{-1}$ with its removable value. Then

$$W_j = -(2/\Delta)^{2h}\Gamma(1+h)\,\mathrm{rgamma}(1-\eta)\prod_{\ell=0}^{j-1}(\ell-h)\,[1+2\eta Z(\eta)]. \tag{R5.7}$$

This follows directly from the reciprocal-gamma recurrence. It cancels the zeta pole before taking a modulus or making an interval evaluation. Exact and near-integer checks are included in the executed controls.

Theorem R5.1 (Complete analytic tail return)**.** *Take $K \geq 1$, $R = K\Delta$, and $M + 2 + 2u > 0$. Let Q use the original physical source at $k \leq K$, its exact original image, and $A_{L,M}$ above K. Define*

$$A_K(u) = \sum_{k=1}^{K} k^{-1-2u}, \quad E_{\mathrm{return}} = \delta[M_u + |C_\Delta| A_K(u) + I_\delta],$$

$$E_{\mathrm{Bessel}} = \frac{|C_\Delta| F_{L,M}(R)\Delta^{-2}K^{-2-2u}}{M+2+2u}.$$

Then $|T - Q| \leq E_{\mathrm{return}} + E_{\mathrm{Bessel}}$.

Proof. Subtract the original and polynomial sampling identities, then subtract their first K terms. Lemma R3.1 charges the full-moment difference, finite source difference and complete image difference by E_{return}. For the polynomial asymptotic remainder, Theorem R4.3 and $\sum_{k>K} k^{-M-3-2u} \leq K^{-M-2-2u}/(M+2+2u)$ give E_{Bessel}. This proof retains all populations and requires no unquantified cancellation. □

Finite Laurent preparation and its complete return data (C3)

Retain the established preparation polynomial

$$b_k = (-1)^k(3+s)_k z^k/k!, \quad B_L(w) = \sum_{k=0}^{L} b_k w^k, \quad W_L(\theta) = B_L(e^{\mathrm{i}\theta})B_L(e^{-\mathrm{i}\theta}) = \sum_{n=-L}^{L} w_n e^{\mathrm{i}n\theta}, \tag{C3.1}$$

where $w_n = w_{-n} = \sum_{k=0}^{L-|n|} b_{k+|n|}b_k$. This symmetry is not complex conjugacy. Replace the six factors in $A_{z,s}$ by these polynomials, and denote the resulting density, Fourier source and full moment by A_L, Φ_L, T_L.

Lemma C3.1 (Original-space preparation allowance)**.** *Let $P = |3+s|$, $B_p = (1-z)^{-P}$,*

$$q = z\max\left(1, \frac{L+1+P}{L+2}\right) < 1, \quad e = \frac{|b_{L+1}|}{1-q}, \quad \delta = 6d^{9+6\,\mathrm{Re}\,s}B_p^5 e.$$

Then, with $D = 3(1+z)$ and $u = \mathrm{Re}\,h > -1$,

$$|A_{z,s} - A_L| \leq \delta, \qquad |T_3 - T_L| \leq \delta M_u(3z), \tag{C3.2}$$

$$|\Phi(r) - \Phi_L(r)| \leq \delta \quad (r \in \mathbb{R}), \qquad |\alpha_j - \alpha_{j,L}| \leq \frac{\delta D^{2j}}{4^j(j!)^2}, \tag{C3.3}$$

where $\alpha_j = [r^{2j}]\Phi(r) = (-1)^j T_3(j,s;z)/(4^j(j!)^2)$.

Proof. The absolute binomial series is bounded by $(1-z)^{-|3+s|}$, for both the exact factor and its truncation. The omitted terms have ratios at most q. A six-term telescoping product bounds the density difference by $6d^{9+6\,\mathrm{Re}\,s}B_p^5 e$. Integrating against the original positive normalized CUE measure proves the moment and Fourier bounds. Expanding the physical J_0 readout and using the support radius gives the last inequality. □

A uniform version, for $0 \leq z \leq Z < 1$, $|s| \leq 3$, is

$$\delta_L(Z) = 6(1-Z^2)^{-9}(1-Z)^{-30}\frac{\binom{L+6}{5}Z^{L+1}}{1 - Z(L+7)/(L+2)}, \tag{C3.4}$$

provided its denominator is positive. This uses $|(3+s)_k| \leq (6)_k$. At $Z = 0$ the error is exactly zero. The full moment allowance is indispensable: integrating the constant Fourier error δ to infinity against a deep inverse-order Mellin weight would be invalid. Section C6 uses the full moment, finite prefix and image differences together.

Finite Abel summation and validated direction quadrature (C5)

Set $R = K\Delta$, $K_+ = K + 1$, and

$$p_j = \tfrac{5}{2} + 2h + j.$$

By Lemma C4.3, all retained terms have $\operatorname{Re} p_j \geq 1.6$ on (C1.3). Their lattice series are absolutely convergent, so the finite mode sums, direction integral and lattice sum interchange.

Lemma C5.1 (Effective finite Abel formula)**.** *For $K \geq 1$, integer $B \geq 1$, $\operatorname{Re} p > 1$ and real θ with $q = e^{\mathrm{i}\theta} \neq 1$, let $\mathcal{D}f(k) = f(k+1) - f(k)$ and $f_p(k) = k^{-p}$. Then*

$$\sum_{k>K} q^k k^{-p} = \frac{q^{K_+}}{1-q} \sum_{\ell=0}^{B-1} \left(\frac{q}{1-q}\right)^{\ell} \mathcal{D}^{\ell} f_p(K_+) + \mathcal{R}_B, \tag{C5.1}$$

$$|\mathcal{R}_B| \leq \frac{|(p)_B| K^{1-\operatorname{Re} p-B}}{(\operatorname{Re} p + B - 1)|1-q|^B}. \tag{C5.2}$$

Proof. Direct subtraction of absolutely convergent series gives $(1-q)S_f = q^{K_+} f(K_+) + qS_{\mathcal{D}f}$. Iterate B times. The last term is $[q/(1-q)]^B S_{\mathcal{D}^B f}$. The exact identity

$$\mathcal{D}^B f_p(k) = (-1)^B (p)_B \int_{[0,1]^B} (k + t_1 + \cdots + t_B)^{-p-B}\, dt$$

bounds its modulus by $|(p)_B| k^{-\operatorname{Re} p - B}$. Bound the remaining positive sum by its integral from K to infinity. Alternating signs already occur inside the forward differences; no additional alternating sign belongs in the finite Abel formula. □

For the tail direction put $\theta_m(\phi) = \Delta(\nu_m + a\cos\phi)$. Choose $\rho > 0$ satisfying

$$a\cosh\rho < 1, \qquad \Delta(3 + a\cosh\rho) < \pi. \tag{C5.3}$$

Define

$$b = a\Delta\sinh\rho, \qquad c_m = 2\sin\frac{\Delta(|\nu_m| - a)}{2}, \qquad \widehat{c}_m = 2e^{-b/2}\sin\frac{\Delta(|\nu_m| - a\cosh\rho)}{2}.$$

Both gaps are positive. The real gap is $|1 - e^{\mathrm{i}\theta_m}| \geq c_m$. On $|\operatorname{Im}\phi| \leq \rho$, writing $\theta_m = x + \mathrm{i}y$ gives $|y| \leq b$ and $\Delta(|\nu_m| - a\cosh\rho) \leq |x| < \pi$. Hence

$$|1 - e^{\mathrm{i}(x+\mathrm{i}y)}|^2 = (1 - e^{-y})^2 + 4e^{-y}\sin^2(x/2) \geq \widehat{c}_m^{\,2}.$$

This proves holomorphy of the finite Abel integrand on the entire closed direction strip, rather than only separation on its real axis.

Combine polynomial degrees first:

$$d_{j\ell} = \mathcal{D}^{\ell} f_{p_j}(K_+), \qquad d_{m\ell n} = \sum_{j<M} K^j c_{mjn} d_{j\ell}, \qquad D_{m\ell}(\phi) = \sum_n d_{m\ell n} e^{\mathrm{i}n\phi}.$$

With $q_m = e^{\mathrm{i}\theta_m(\phi)}$, define

$$G_m(\phi) = \frac{q_m^{K_+}}{1-q_m} \sum_{\ell<B} \left(\frac{q_m}{1-q_m}\right)^{\ell} D_{m\ell}(\phi). \tag{C5.4}$$

A computable strip supremum is

$$M_m = e^{bK_+} \sum_{\ell<B} \frac{e^{b\ell}}{\widehat{c}_m^{\,\ell+1}} \sum_n |d_{m\ell n}| e^{\rho|n|}. \tag{C5.5}$$

In particular, the growth factor e^{bK_+} cannot be omitted.

Lemma C5.2 (Direction and Abel allowances)**.** *Approximating the normalized direction integral of the finite Abel expression by a Q-point periodic rule costs at most*

$$E_{\mathrm{direction}} = \frac{2\Delta^{-3/2}}{e^{Q\rho}-1}\sum_m M_m. \tag{C5.6}$$

The prior Abel replacement of the unweighted sampled tail costs at most

$$E_{\mathrm{Abel}} = \Delta^{-3/2}\sum_{m,j} K^j \left(\sum_n |c_{mjn}|\right)\frac{|(p_j)_B|K^{1-\operatorname{Re} p_j - B}}{(\operatorname{Re} p_j + B - 1)c_m^B}. \tag{C5.7}$$

Proof. Contour shifting bounds the Fourier coefficients of a periodic strip-bounded analytic function by its supremum times $e^{-\rho|n|}$. The rule aliases precisely the nonzero multiples of Q. Summing those two geometric tails proves (C5.6). Apply Lemma C5.1 on the real direction circle and bound the coefficient polynomial by its absolute coefficient sum to obtain (C5.7). □

The sampled expansion is therefore replaced by the finite formula

$$\mathcal{A}_{\mathrm{tail}} = \Delta^{-3/2}\frac{1}{Q}\sum_{t=0}^{Q-1}\sum_m G_m(2\pi t/Q). \tag{C5.8}$$

Arb/Acb encloses each forward difference and every finite operation. The forward DFT convention is $e^{-2\pi ikt/Q}$, so coefficient n is placed at index $-n \bmod Q$. The guard $Q > 6L$ separates all retained modes. Each oscillatory phase is evaluated independently, avoiding the preserved repeated rectangular-ball wrapping failure. At $z = 0$, $a = L = 0$ and the direction is exactly constant: one evaluation is the exact angular integral and its error is zero.

Sampled Mellin identity, integer orders, and full composition (C6)

The inherited identity, valid when $\Delta D < 2\pi$, is

$$T_3 = C_\Delta(h)\sum_{k=1}^{\infty} k^{-1-2h}\Phi(k\Delta) - I, \tag{C6.1}$$

$$C_\Delta(h) = 2^{2h+1}\Gamma(1+h)\,\mathrm{rgamma}(-h)\Delta^{-2h}, \tag{C6.2}$$

$$I = \sum_{j=0}^{\infty} W_j(h)\alpha_j\Delta^{2j}, \qquad W_j(h) = C_\Delta(h)\zeta(1+2h-2j). \tag{C6.3}$$

Proposition 5.2 of HaarCritical starts on generic positive order, where the cosine Dirichlet series is absolutely summable. Its polylog expansion, angle moments, duplication and reflection yield (C6.1) there. The inherited original-source decay and the new finite-Laurent expansion both give $O(r^{-5/2})$ locally uniformly. The sampled series is consequently normally convergent on $\operatorname{Re} h > -1$, as is the image after its finitely encountered poles are removed. Proposition C2.2 and the same domination for the bounded polynomial density then extend the identity by holomorphic uniqueness throughout the ordinary domain.

At $h = j \geq 0$, let $\eta = h - j$ and write $Z(\eta) = \zeta(1+2\eta) - (2\eta)^{-1}$ with its removable value at zero. The exact deflation is

$$W_j(h) = -(2/\Delta)^{2h}\Gamma(1+h)\,\mathrm{rgamma}(1-\eta)\prod_{\ell=0}^{j-1}(\ell - h)\,[1 + 2\eta Z(\eta)]. \tag{C6.4}$$

It follows from the gamma recurrence. This expression preserves the zero at other nonnegative integers and the finite value at $h = j$. The implementation never multiplies a reciprocal-gamma zero by an unresolved zeta pole. At exact $h = 0, 1, 2, 3$, the weighted tail vanishes identically and the corresponding physical image coefficient supplies the moment.

Theorem C6.1 (Tail replacement returned to the physical moment)**.** *Let $R = K\Delta$ and $u = \operatorname{Re} h > -1$. If $M + 3/2 + 2u > 0$, the three-Bessel source remainder costs*

$$E_{3\mathrm{B}} = |C_\Delta| F \Delta^{-3/2} \frac{K^{-3/2-2u}}{M + 3/2 + 2u}. \tag{C6.5}$$

Replacing only the infinite physical tail by its finite-preparation counterpart costs at most

$$E_{\mathrm{prep}} = \delta \left[M_u(3z) + |C_\Delta| \sum_{k=1}^{K} k^{-1-2u} + I_{\mathrm{diff}}(h, z, \Delta) \right], \tag{C6.6}$$

where a valid complete image weight is

$$I_{\mathrm{diff}} = \sum_{j=0}^{\infty} |W_j(h)| \frac{(\Delta D/2)^{2j}}{(j!)^2}.$$

Proof. For (C6.5), insert Theorem C4.4 in the sampled tail and bound $\sum_{k>K} k^{-M-5/2-2u}$ by its integral from K. For (C6.6), subtract the original and polynomial sampling identities, then subtract their first K terms. Lemma C3.1 bounds the full moment difference, finite prefix difference and complete image difference. All three are required. No constant source difference is integrated to infinity. □

The image sum has an explicit geometric tail. For $J > u + 1/2$, set $x = \Delta D/(2\pi)$ and

$$q_J = x^2 \max\left(1, \frac{J-u}{J+1}\right) \max\left(1, \frac{J+1/2-u}{J+1}\right) < 1.$$

The part of I_{diff} with $j \geq J$ is bounded by $|C_\Delta|$ times

$$\frac{2(2\pi)^{2u} |\cos(\pi h)| \Gamma(2J-2u)\zeta(2J-2u)}{(J!)^2(1-q_J)} (x/2)^{2J}. \tag{C6.7}$$

This follows from the zeta functional equation, the gamma integral bound and duplication, with a positive coefficient ratio at most q_J. The finite prefix uses (C6.4). For a parameter-wide price the unchanged inherited Euler–Maclaurin bound encloses the entire function $(w-1)\zeta(w)$ on order rectangles [6].

Let $\widetilde{\Phi}_k$ and $\widetilde{\alpha}_j$ be the independently priced original physical finite source and image coefficients. The complete computed formula is

$$\mathcal{F}_{\mathrm{c}} = C_\Delta \sum_{k=1}^{K} k^{-1-2h} \widetilde{\Phi}_k - \sum_{j=0}^{J-1} W_j(h) \widetilde{\alpha}_j \Delta^{2j} + C_\Delta \mathcal{A}_{\mathrm{tail}}. \tag{C6.8}$$

If $E_{\mathrm{fin}}, E_{\mathrm{srcang}}, E_{\mathrm{image}}$ are the original prefix arithmetic, source angular and full image charges, then the final pointwise disk radius is

$$\begin{aligned} E_{\mathrm{total}} = {} & E_{\mathrm{fin}} + E_{\mathrm{srcang}} + E_{\mathrm{image}} + E_{3\mathrm{B}} + E_{\mathrm{prep}} \\ & + |C_\Delta|(E_{\mathrm{Abel}} + E_{\mathrm{direction}}) + E_{\mathrm{ball}}. \end{aligned} \tag{C6.9}$$

E_{ball} includes every new ball operation and the serialization gap of the returned decimal midpoint m. Relative certification is allowed only if $\underline{|m|} - E_{\mathrm{total}} > 0$, in which case

$$\frac{|T_3 - m|}{|T_3|} \leq \frac{E_{\mathrm{total}}}{\underline{|m|} - E_{\mathrm{total}}}.$$

Otherwise the absolute disk remains meaningful without a relative claim.

The physical source and its exact return map (O2)

Throughout this investigation the scalar is the ordinary, unnormalized Haar expectation

$$T_N(h,s;z)=\mathbb{E}_{U(N)}\big[|S_N(z)|^{2h}|\Lambda_N(z)|^{2s}\big],\qquad S_N(z)=-(1-z^2)\frac{\Lambda_N'(z)}{\Lambda_N(z)},\quad \Lambda_N(z)=\det(I-zU). \tag{O2.1}$$

Powers of positive real numbers use the real logarithm. The order and tilt vary independently. The new central domain is

$$N\in\{5,7\},\qquad 0\le z\le Z:=\frac{1}{40},\qquad -\frac{19}{20}\le \Re h\le 3,\quad |\Im h|\le 3,\quad |s|\le 3. \tag{O2.2}$$

The method will retain the original preparation in both the finite source and the exterior bound. A finite Laurent replacement is derived later as an alternative with a separate return allowance.

Proposition O2.1 (Exact prepared CUE source)**.** *For real $0\le z<1$, put $d=1-z^2$, $a=Nz$, and*

$$w=\frac{\lambda-z}{1-z\lambda},\qquad \lambda=\frac{w+z}{1+zw}.$$

Relative to normalized CUE(N) measure μ_N, the physical moment is

$$T_N(h,s;z)=\int |a+\operatorname{Tr}V|^{2h}A_{N,z,s}(V)\,d\mu_N(V), \tag{O2.3}$$

$$A_{N,z,s}(V)=d^{N^2+2Ns}\prod_{j=1}^{N}(1+zw_j)^{-N-s}(1+z/w_j)^{-N-s}. \tag{O2.4}$$

Both analytic factors have the same complex exponent. No conjugation of the tilt and no normalization by a complex mass occurs.

Proof. Writing $\lambda_j=e^{i\theta_j}$ and $w_j=e^{i\phi_j}$, the normalized Weyl measure is

$$\frac{1}{N!(2\pi)^N}\prod_{j<k}|\lambda_j-\lambda_k|^2\,d\theta_1\cdots d\theta_N.$$

The exact identities

$$\frac{d\theta}{d\phi}=\frac{d}{|1+zw|^2},\qquad \lambda_j-\lambda_k=\frac{d(w_j-w_k)}{(1+zw_j)(1+zw_k)},\qquad 1-z\lambda=\frac{d}{1+zw}$$

show that all Jacobians and the full squared Vandermonde contribute $d^{N^2}\prod_j|1+zw_j|^{-2N}$. The determinant tilt contributes $d^{2Ns}\prod_j|1+zw_j|^{-2s}$. Finally,

$$d\frac{\lambda}{1-z\lambda}=z+w,\qquad S_N=Nz+\sum_j w_j.$$

On the real circle, the principal logarithms of $1+zw$ and $1+z/w$ sum to the real logarithm of $|1+zw|^2$; each factor has positive real part. Their analytic continuations are fixed by this physical branch. These identities prove the formula including its normalization. At $z=0$, $A_{N,0,s}=1$, so the moment is exactly independent of the tilt. □

Two inherited source estimates will be used repeatedly. With $\sigma=\Re s$, the physical absolute mass satisfies

$$\mathbb{E}_{U(N)}|\Lambda_N(z)|^{2\sigma}\le M(z,\sigma):=(1-z^2)^{-\sigma^2}. \tag{O2.5}$$

Indeed the Schur expansion of $\prod_j(1-z\lambda_j)^{\sigma}$, followed by Haar orthogonality, is a nonnegative sum over partitions of length at most N. Extending to all partitions gives $\exp(\sum_{k\ge1}\sigma^2z^{2k}/k)$. The mark also has the deterministic support bound

$$|S_N(z)|\le N(1+z)\le D:=N(1+Z). \tag{O2.6}$$

These statements concern the physical preparation; they do not make the complex-prepared measure into a probability measure.

Sampled Mellin readout and the finite physical source (O4)

Define the circular physical source and its Taylor coefficients by

$$\Phi_N(r) = \mathbb{E}\big[|\Lambda_N(z)|^{2s} J_0(r|S_N(z)|)\big], \qquad a_j = \frac{(-1)^j T_N(j,s;z)}{4^j (j!)^2}. \tag{O4.1}$$

The inherited sampled identity, valid for $\Re h > -1$ and $0 < \Delta D < 2\pi$, is

$$T_N = C_\Delta(h)\left\{\sum_{k=1}^{\infty} k^{-1-2h}\Phi_N(k\Delta) - \sum_{j=0}^{\infty}\zeta(1+2h-2j)a_j\Delta^{2j}\right\}, \quad C_\Delta(h) = 2^{1+2h}\Delta^{-2h}\frac{\Gamma(1+h)}{\Gamma(-h)}. \tag{O4.2}$$

The complete products have removable values at nonnegative integer orders. The first series is absolutely and locally uniformly convergent on the ordinary domain. In particular, the population vanishing theorem below gives source powers at least 13/2 and 25/2 for the two ranks. Identity (O4.2) is the inherited physical readout, not an analytic continuation of an otherwise divergent ordinary expectation.

Signed direction projection with exact translation

Let $w = e^{ix}$, $g(x) = 1 + 2z\cos x + z^2$, and for $0 \le e < N$ put

$$f_e(x) = \frac{d}{g(x)}\left(\frac{d^2}{g(x)}\right)^s \left(\frac{w+z}{1+zw}\right)^e, \qquad f_{-e}(x) = f_e(-x).$$

The exact untranslated determinant and circular contraction are

$$B_{jk}(\phi;r) = \frac{1}{2\pi}\int_0^{2\pi} f_{j-k}(x) e^{ir\cos(x-\phi)}\,dx, \quad F(\phi;r) = \det B(\phi;r), \quad \Phi_N(r) = \frac{1}{2\pi}\int_0^{2\pi} e^{irNz\cos\phi}F(\phi;r)\,d\phi. \tag{O4.3}$$

The determinant is in the original orthonormal monomial basis; its normalization is already the Weyl/Andreief normalization. Reflection of the row tag does not conjugate the complex preparation.

Approximate each preparation Fourier coefficient by a normalized P-point DFT and retain $|l| \le L$. Its wave coefficient is $i^{|l|}J_{|l|}(r)$. Form the determinant on an even Q-point direction grid, project onto the distinct signed indices $|j| \le Q/2-1$, and contract against the exact coefficients $i^{|j|}J_{|j|}(Nzr)$. Both Nyquist indices are excluded. The order of these operations makes the estimate uniform at arbitrarily large real frequency; an unresolved translated pointwise trapezoid has a different error contract.

Choose a strip width $t_0 > 0$ with $Ze^{t_0} < 1$ and $E_0 = 2Z(\cosh t_0 - 1)/(1-Z)^2 < 1$. Write

$$\begin{aligned}
&d_Z = 1 - Z^2, && M_* = d_Z^{-9}, && m_* = (1-Z)^6,\\
&g_- = 1 + Z^2 - 2Z\cosh t_0, && g_+ = 1 + Z^2 + 2Z\cosh t_0, &&\\
&\eta_0 = \arctan\frac{2Z\sinh t_0}{d_Z(1-E_0)}, &&&&\\
&C_0 = d_Z^{-5}\max(g_-^{-4}, g_+^2)e^{3\eta_0}\left(\frac{e^{t_0}-Z}{1-Ze^{t_0}}\right)^{N-1}, &&&&\\
&V_0 = M_*\left[\frac{d_Z^2}{(1-Z^2e^{-2t_0})(1-Z^2e^{2t_0})}\right]^{(N+3)^2/4}. &&&&
\end{aligned} \tag{O4.4}$$

These constants dominate the inherited one-body and correlated Schur strip bounds throughout (O2.2). For example, $1 + 2\Re s \in [-5, 7]$, $-1 - \Re s \in [-4, 2]$, and $|N + s| \le N + 3$. The factors are monotone envelopes in the upper radius. The Schur bracket is at least one and increases with z. All expressions have finite limits at the centre.

Lemma O4.1 (Uniform finite real-source allowance)**.** *If $P > 2L$ and Q is even, set*

$$\begin{aligned}
\epsilon_r &= \frac{2C_0}{1-e^{-t_0}}\left[e^{-(L+1)t_0} + (2L+1)e^{-(P-L)t_0}\right],\\
E_\Phi &= \frac{4V_0 e^{-t_0 Q/2}}{1-e^{-t_0}} + M_*\left[(1 + N\epsilon_r/m_*)^N - 1\right].
\end{aligned} \tag{O4.5}$$

Then the signed finite-source construction has error at most E_Φ for every real r, uniformly on (O2.2).

Proof. Cauchy's estimate for preparation coefficients prices both the omitted modes and all DFT aliases by ϵ_r, using $|J_l(r)| \le 1$. For the physical real-tilt Gram matrix G, one has $G \ge m_* I$ and $\det G \le M_*$. The true matrix at real frequency is a contraction in this Gram norm. An entry perturbation bounded by ϵ_r has Gram-normalized norm at most $N\epsilon_r/m_*$. Multilinearity and Hadamard bound the determinant change by the second term in (O4.5).

The common-angle Schur strip estimate bounds the direction coefficients of F by $V_0 e^{-t_0|j|}$. Charging each omitted coefficient and folded alias gives the first term. For the contracted determinant error, the inverse trigonometric polynomial of the retained translation coefficients has discrete squared norm at most one by Parseval, since the indices occupy distinct residues. Thus contraction adds no direction count factor to the Gram determinant bound. □

For a filtered prefix supported at $k \le k_*$, with weights in $[0,1]$, define

$$\begin{aligned} G_\Delta(u) &= \Gamma(1+u)^2(2/\Delta)^{2u}, \\ C_* &= \frac{2\cosh(3\pi)}{\pi}\max\{G_\Delta(-19/20), G_\Delta(3)\}, \\ W_{k_*} &= \frac{2\cosh(3\pi)}{\pi}\max\left\{G_\Delta(-19/20)\frac{(k_*+1)^{1.9}}{1.9}, G_\Delta(3)\zeta(7)\right\}. \end{aligned} \tag{O4.6}$$

Reflection, the positive gamma integral, and log-convexity show that $|C_\Delta(h)| \le C_*$ and that W_{k_*} bounds the complete absolute weighted prefix. For the latter, the positive sum $G_\Delta(u)\sum_{k\le k_*} k^{-1-2u}$ is log-convex in u; integral comparison and $\zeta(7)$ price its two endpoints. The finite-source error is therefore $W_{k_*}E_\Phi$.

Complete Mellin-image allowance

Retain J coefficients using $m \ge J$ half-circle samples $r = He^{\pi i\ell/m}$. The finite image source uses resources (P_i, L_i, Q_i). Put $W = \max((1-Z)^{-6}, (1+Z)^6)$, $b_H = H/2$, and require $P_i > 2L_i$, $2L_i < Q_i$, $b_H < L_i + 2$, and $HD/2 < m+1$. The inherited compact-circle estimates, with the actual rank retained, are

$$\begin{aligned} E_{\mathrm{mode}} &= \frac{2We^{b_H^2} b_H^{L_i+1}}{(L_i+1)![1-b_H/(L_i+2)]}, \\ E_{\mathrm{alias}} &= \frac{2C_0 e^{-t_0(P_i-L_i)}}{1-e^{-t_0P_i}}, & \epsilon_i &= E_{\mathrm{mode}} + (2L_i+1)E_{\mathrm{alias}}e^H, \\ E_{\mathrm{det},i} &= N^2\epsilon_i(We^H + N\epsilon_i)^{N-1}e^{HNZ}, & E_{\mathrm{dir},i} &= \frac{2M_* e^{HD\cosh 2}}{e^{2Q_i}-1}, \\ E_{\mathrm{circ}} &= \frac{M_*(HD/2)^{2m}}{(m!)^2[1-(HD/(2m+2))^2]}, & E_a &= E_{\mathrm{det},i} + E_{\mathrm{dir},i} + E_{\mathrm{circ}}. \end{aligned} \tag{O4.7}$$

Here W bounds the one-body integral norm in the original basis. The Bessel bound $|J_l(r)| \le e^{H^2/4}(H/2)^{|l|}/|l|!$ proves the mode estimate. The physical matrix norm is at most We^H; determinant telescoping and translation give $E_{\mathrm{det},i}$. On this bounded complex circle a fully translated direction trapezoid is allowed, with error $E_{\mathrm{dir},i}$. Finally, $|a_j| \le M_*(D/2)^{2j}/(j!)^2$ prices all higher coefficient aliases in the half-circle DFT. Each retained scaled coefficient $H^{2j}a_j$ thus has error at most E_a.

Let w_j bound $|C_\Delta(h)\zeta(1+2h-2j)|(\Delta/H)^{2j}$ on the order box. For $j = 0,1,2,3$, the implementation uses the inherited outward Euler–Maclaurin rectangle bound for the entire function $(v-1)\zeta(v)$, multiplied by the removable sine quotient. For $j \ge 4$, reflection and log-convexity give

$$|C_\Delta(h)\zeta(1+2h-2j)| \le \frac{2C_*\cosh(3\pi)\zeta(2j-6)}{(2\pi)^{2j}} \max_{u\in\{-19/20,3\}} (2\pi)^{2u}\Gamma(2j-2u). \tag{O4.8}$$

This deflates integer singularities before interval multiplication. The finite image costs $E_a\sum_{j<J} w_j$.

For the omitted image set $x = \Delta D/(2\pi)$ and

$$q = x^2 \max\left(1, \frac{J + 19/20}{J+1}\right) \max\left(1, \frac{J + 1/2 + 19/20}{J+1}\right).$$

When $J > 7/2$ and $q < 1$, the complete image remainder is bounded by

$$E_{\mathrm{image},\infty} = \frac{2C_* \cosh(3\pi) M_* \zeta(2J-6)}{(J!)^2(1-q)} \max_{u \in \{-19/20, 3\}} (2\pi)^{2u} \Gamma(2J-2u) \left(\frac{x}{2}\right)^{2J}. \tag{O4.9}$$

This is the inherited physical coefficient bound followed by the zeta functional equation and a positive ratio test. Neither the finite nor the infinite image changes the complex preparation.

A centre-compatible contour bound for the complete exterior (O5)

The effective repair is to bound the filtered exterior while the original prepared source is still intact. It uses the odd-rank gap before introducing any finite preparation or saddle approximation.

Lemma O5.1 (Closed-centre contour and variation)**.** *Let N be five or seven and $0 \le z \le Z < 1/N$. Choose $0 < t \le 1$ with*

$$Ze^{2t} < 1, \qquad E = \frac{2Z(\cosh(2t) - 1)}{(1-Z)^2} < 1.$$

In relative eigenangles and Fourier direction, put $G = Nz\cos\phi + \sum_{j=1}^{N} \cos x_j$, and move every angle by $x \mapsto x - it\sin x$. On the resulting cycle, writing $G = X + iY$,

$$Y \ge 0, \qquad |X| \le D = N(1+Z), \qquad |X| + Y/t \ge g := 1 - NZ > 0. \tag{O5.1}$$

The deformed total variation throughout the full tilt disk is at most

$$V_N = M_*(1+t^2)^{(N+1)/2}(1+t^2\cosh^2 t)^{N(N-1)/2}(1-E)^{-N(N+3)} e^{3N\eta}, \quad \eta = \arctan\frac{2Z\sinh(2t)}{(1-Z^2)(1-E)}. \tag{O5.2}$$

Proof. For $g_z(a) = 1 + 2z\cos a + z^2$ and imaginary displacement at most $2t$, its real part is at least $(1-E)g_z(a) > 0$. The identity $\max_a |\sin a|/g_z(a) = 1/(1-z^2)$ gives the argument bound η. Thus the entire periodic homotopy avoids poles and retains the physical logarithms of all prepared factors.

For each angle, the deformed cosine has real part $\cos x \cosh(t\sin x)$, of absolute value at most one, and imaginary part at least $t\sin^2 x$. The real-part assertion follows from $\log\cosh v \le v^2/2$ and $1 - u \le e^{-u}$. Replacing each real deformed cosine by the nearest signed unit costs at most $\sin^2 x$. Include the direction with coefficient Nz. Every resulting signed sum is an odd integer plus $\pm Nz$, so its modulus is at least $1 - Nz$. The triangle inequality proves (O5.1). A zero direction coefficient at $z = 0$ is harmless.

Each angle Jacobian costs at most $\sqrt{1+t^2}$. Each full squared sine difference has relative modulus at most $1 + t^2\cosh^2 t$, using $|\sin x - \sin y| \le 2|\sin((x-y)/2)|$. The prepared powers cost $(1-E)^{-N(N+\Re s)} e^{N|\Im s|\eta}$. What remains is the original positive real-tilt Haar mass, bounded by (O2.5). Enlarging its positive majorants over the disk gives (O5.2). The Vandermonde and all saddle populations are retained throughout this deformation. □

Let $K \ge 1, b \ge 2, p \ge 1$ be integers. Independent uniforms $U_j \in \{0, \dots, b-1\}$ define deterministic rational weights $\rho_k = \Pr(L_* > k)$, where $L_* = K + U_1 + \cdots + U_p$. Partition $[0, D]$ into bands $[l, r]$, and for each define

$$y = t(g - r)_+, \qquad e = \max\left\{1 - e^{-\Delta y}, \sin\big(\min(\Delta l, 2\pi - \Delta r, \pi/2)\big)\right\}, \qquad A = \min\left(1, \frac{2}{be}\right). \tag{O5.3}$$

Only partitions with strictly positive e on every band are admitted.

Proposition O5.2 (Uniform physical exterior)**.** *Under Lemma O5.1, $0 < \Delta D < 2\pi$, and $\Re h > -1$, the error from replacing the complete sampled source by its filtered prefix is at most*

$$E_{\mathrm{ext}} = \frac{|C_\Delta(h)|\Gamma(2+2\Re h)}{|\Gamma(2+2h)|K^{2+2\Re h}} V_N \max_{[l,r]} \frac{e^{-K\Delta y}}{e}\left[(K + 1/e)A^p + \frac{p(b-1)}{2}A^{p-1}\right]. \tag{O5.4}$$

The estimate includes $z = 0$ and the nonnegative order range.

Proof. Write $\gamma = 2 + 2h$, so $\Re\gamma > 0$, and initially insert an Abel factor v_0^k, $0 < v_0 < 1$. For Laplace variable $u > 0$, set $w = v_0 e^{i\Delta G - u}$ and $H_b(w) = b^{-1} \sum_{j=0}^{b-1} w^j$. The exact generating identity is

$$\sum_{k\geq 1} k w^k \Pr(L_* \leq k) = \frac{w^K}{1-w} \left[\left(K + \frac{w}{1-w} \right) H_b(w)^p + pwH_b'(w) H_b(w)^{p-1} \right]. \tag{O5.5}$$

If $l \leq |X| \leq r$, the radial damping and clipped angular distance to one give $|1 - w| \geq e$. Also $|H_b(w)| \leq A$, $|wH_b'(w)| \leq (b-1)/2$, and $|w|^K \leq e^{-K(u+\Delta y)}$. Multiply (O5.5) by $u^{\gamma-1}/\Gamma(\gamma)$ and integrate. The elementary gamma integral converts k into $k^{1-\gamma} = k^{-1-2h}$ and gives the factor $\Gamma(\Re\gamma)K^{-\Re\gamma}/|\Gamma(\gamma)|$. Use the total variation bound and take the largest band price. The resulting majorant is independent of v_0, allowing $v_0 \uparrow 1$. Absolute convergence of the inherited physical sampled series identifies this limit with its discarded filtered source.

The original statement of Theorem 5.3 used $z > 0$ and negative real order. Its proof uses only the pole-free homotopy, the positive gap, and $\Re\gamma > 0$. These hold here at the centre and throughout the requested order rectangle. At exact nonnegative integers take the removable product limit; the exterior multiplier vanishes. □

Lemma O5.3 (Joint gamma multiplier)**.** *For $u = \Re h > -1$,*

$$\frac{|C_\Delta(h)|\Gamma(2+2u)}{|\Gamma(2+2h)|K^{2+2u}} \leq \frac{2\cosh(\pi|\Im h|)}{\pi} \Gamma(1+u)^2 (2/\Delta)^{2u} K^{-2-2u}. \tag{O5.6}$$

Its right side is log-convex in u, so a full-box maximum requires only the two real-order endpoints and $|\Im h| = 3$.

Proof. Duplication gives the exact quotient

$$\frac{C_\Delta(h)}{\Gamma(2+2h)} = \frac{\sqrt{\pi}\Delta^{-2h}}{\Gamma(-h)\Gamma(h+3/2)}.$$

Reflection and the beta integral, valid because $\Re(1+h) > 0$, give

$$\left| \frac{\Gamma(1+h)}{\Gamma(h+3/2)} \right| \leq \frac{\Gamma(1+u)}{\Gamma(u+3/2)}, \qquad |\sin \pi h| \leq \cosh(\pi|\Im h|).$$

A second real duplication proves (O5.6). Its logarithm is a positive multiple of $\log\Gamma(1+u)$ plus affine terms. This retains the common gamma denominator before absolute estimation, including removable integer zeros. □

Alternative finite preparation and its complete return (O7)

This section preserves a reusable alternative, rather than adding an unnecessary approximation to the main contour method. Put $p_s = N + s$, $b_n = (-z)^n (p_s)_n / n!$, and $B_L(w) = \sum_{n=0}^{L} b_n w^n$. Replacing every factor in (O2.4) by its Taylor polynomial gives A_L.

Proposition O7.1 (Complete preparation return)**.** *Let*

$$q_L = z \max\left(1, \frac{|p_s + L + 1|}{L+2}\right) < 1, \qquad e_L = \frac{|b_{L+1}|}{1-q_L}, \qquad B = \sum_{n=0}^{L} |b_n| + e_L.$$

Then

$$\|A - A_L\|_\infty \leq \delta := 2N d^{N^2+2N\Re s} B^{2N-1} e_L. \tag{O7.1}$$

If also $\int |A - A_L| \, d\mu_N \leq \epsilon$, replacing a finite-prepared terminal by the physical terminal has complete return allowance

$$\delta U + \epsilon W_{k_*} + \epsilon I_{\mathrm{diff}}. \tag{O7.2}$$

Here U is an original-space comparison moment, W_{k_*} is the absolute finite-prefix weight, and I_{diff} prices the complete deflated Mellin image of the preparation difference.

Proof. For $n \geq L+1$, the squared ratio $|1+(p_s-1)/(n+1)|^2$ is a convex quadratic in $1/(n+1)$. Its maximum on the allowed interval is at an endpoint, proving the geometric tail bound e_L. The exact telescope of the $2N$ analytic factors proves (O7.1).

Apply the sampled identity separately to the original and finite preparations, and subtract. The difference of the original singular moments is at most δU, using Lemma O3.1 for negative orders and the support bound for nonnegative orders. The weighted finite-prefix difference is at most ϵW_{k_*}. The image coefficient difference satisfies

$$|a_j(A) - a_j(A_L)| \leq \epsilon \frac{(D/2)^{2j}}{(j!)^2},$$

so the entire deflated image has an independently computable allowance $\epsilon I_{\mathrm{diff}}$. Rearranging the sampled identities gives (O7.2). In normalized Haar measure one may always take $\epsilon = \delta$. No constant Fourier-source error is integrated over an infinite inverse-order Mellin tail. □

A simple uniform choice is $P_s = N+3$, $B = (1-Z)^{-P_s}$, with

$$e_L \leq \binom{L+P_s}{P_s-1} \frac{Z^{L+1}}{1 - Z(L+P_s+1)/(L+2)}, \qquad d^{N^2+2N\Re s} \leq (1-Z^2)^{\min(0, N^2-6N)}.$$

The separate return receipts execute these bounds with their own cutoff and sampling parameters. They are component inequalities, not scalar certificates, and are not substituted into the active contour budget.

An effective full-source contour for ranks six and eight (E3)

The Gaussian Vandermonde contour is inherited from HaarCritical, Theorem 9.5. Here an exact near/far partition makes its constants effective for the full independent-order sampled readout. It also diagnoses why a separate correction is needed at rank four.

Write $g_z(\theta) = 1 + 2z\cos\theta + z^2$. After rotating eigenangles by the real Fourier direction ϕ, (E2.4) is

$$\Phi(r) = \frac{d^{N^2+2Ns}}{2\pi} \int_0^{2\pi} e^{iar\cos\phi} \int_{\mathrm{CUE}(N)} \prod_j g_z(x_j+\phi)^{-p} e^{ir\sum_j \cos x_j}\, d\mu_N(x)\, d\phi. \tag{E3.1}$$

Deform every eigenangle by $f_t(x) = x - it\sin x$, leaving ϕ real. The translation then has modulus one, uniformly even at $a = 0$. Choose $0 < t \leq 1$ and $0 < \alpha < \pi/2$, and set

$$\begin{aligned}
&E = \frac{2Z(\cosh t - 1)}{(1-Z)^2}, && q_* = (1-Z)^2(1-E), \quad \eta = \arctan\frac{2Z\sinh t}{(1-Z^2)(1-E)},\\
&B_* = (1-Z^2)^{\min(N^2-6N,0)} q_*^{-N(N+3)} e^{3N\eta}, && J_* = (1+t^2)^{N/2},\\
&H_* = 1 + t^2\cosh^2 t, && G_* = 4\cosh^2 t, \qquad \beta = t\left(\frac{\sin\alpha}{\alpha}\right)^2, \qquad c = t\sin^2\alpha.
\end{aligned} \tag{E3.2}$$

The hypotheses are $Ze^t < 1$ and $E < 1$. At a specified tilt $s = u + iv$, B_* may be replaced by

$$B_s = (1-Z^2)^{\min(N^2+2Nu,0)} q_*^{-N(N+u)} e^{N|v|\eta}. \tag{E3.3}$$

These are preparation bounds, not changes to the physical tilt.

Theorem E3.1 (Complete population majorant)**.** *For the stated contour hypotheses and every $r > 0$, define*

$$P_m = \frac{m^2 + (N-m)^2}{2}, \quad I_b = \pi^{b/2} 2^{-b(b-1)/2} \prod_{j=1}^{b} j!, \quad I_0 = 1,$$

$$\begin{aligned}
B_m &= \frac{B_* J_* H_*^{m(m-1)/2 + (N-m)(N-m-1)/2} G_*^{m(N-m)} I_m I_{N-m}}{m!(N-m)!(2\pi)^N}\, \beta^{-P_m},\\
B_{\mathrm{far}} &= B_* J_* H_*^{N(N-1)/2}.
\end{aligned} \tag{E3.4}$$

Then the original prepared source obeys the effective inequality

$$|\Phi(r)| \le B_{\mathrm{far}} e^{-cr} + \sum_{m=0}^{N} B_m r^{-P_m}. \tag{E3.5}$$

It includes every population and has no unspecified asymptotic remainder.

Proof. On the homotopy $|\Im x| \le t$, the paired preparation factors have no zeros because $Ze^t < 1$. Moreover $\Re g_z(\theta - iv) \ge (1-E)g_z(\theta) > 0$. The identity $\max_\theta |\sin\theta|/g_z(\theta) = 1/(1-z^2)$ gives the argument bound η; hence the full preparation is bounded by B_*. The contour Jacobian is bounded by J_*.

The phase satisfies $\Im \cos f_t(x) = \sin x \sinh(t \sin x) \ge t \sin^2 x$. The holomorphic squared Vandermonde factor obeys

$$|4\sin^2((f_t(x) - f_t(y))/2)| \le H_* \, 4\sin^2((x-y)/2),$$

using $\sin x - \sin y = 2\cos((x+y)/2)\sin((x-y)/2)$ and $|\sinh v| \le |v| \cosh t$ for $|v| \le t$. It is also at most G_*. Only after deforming the entire closed cycle do we partition its real parameters into the 2^N products of saddle intervals of half-width α about 0 and π, and their complement. This is an exact measurable partition, not an identification of an asymptotic population with an exact source sector.

On the complement some angle has $\sin^2 x \ge \sin^2 \alpha$. The first Vandermonde inequality and normalization of the original CUE measure give $B_{\mathrm{far}} e^{-cr}$, without a union multiplicity. In a near cell containing m angles about zero and $N-m$ about π, within-group pairs are bounded by $H_*(u_i - u_j)^2$ and cross pairs by G_*. The damping is at least $\beta r \sum u_j^2$. The exact Hermite integral is

$$\int_{\mathbb{R}^b} e^{-q\sum u_j^2} \prod_{i<j} (u_i - u_j)^2 \, du = I_b q^{-b^2/2}.$$

It follows from the product of monic Hermite squared norms and the Andreief identity. Extending the nonnegative near integrals to full real spaces and counting all $\binom{N}{m}$ placements yields $B_m r^{-P_m}$. The real translation remains bounded by one throughout. □

For balanced $N = 2b$, the within-group Vandermonde degree is $2b(b-1)$. Together with N Gaussian directions this gives r^{-b^2}: the powers are r^{-4}, r^{-9}, r^{-16}. The actual leading direction coefficient is

$$\mathcal{L}_b(\phi) = \frac{4^{b^2}}{(2\pi)^b} \left(\prod_{j=1}^{b-1} j! \right)^2 d^{N^2+2Ns} \left[(1+z^2)^2 - 4z^2 \cos^2\phi \right]^{-b(N+s)}. \tag{E3.6}$$

Indeed the two Fresnel phases cancel, the b^2 cross pairs give 4^{b^2}, and the two Hermite constants supply the displayed factorials. The radial leading term is the normalized direction average of $r^{-b^2} e^{iNzr\cos\phi} \mathcal{L}_b(\phi)$. At the centre its coefficients are $64/\pi^2$, $131072/\pi^3$, and $38654705664/\pi^4$. These leading coefficients explain the cancellation order; the numerical remainder is supplied by Theorem E3.1, not by an unpriced leading expansion.

A sharp terminal with a uniform complex-order price

Set

$$C_\Delta(h) = 2^{1+2h} \Delta^{-2h} \frac{\Gamma(1+h)}{\Gamma(-h)}, \quad R = K\Delta, \quad u = \Re h, \quad M_h = |C_\Delta(h)| K^{-2u}. \tag{E3.7}$$

Corollary E3.2 (Actual sharp-prefix terminal)**.** *Assume $\Delta N(1+Z) < 2\pi$, $P_m + 2u > 0$ for every m, and $\lambda := \Delta c > q_h/K$, where $q_h = \max(-1-2u, 0)$. The original source tail after the actual rows $1, \dots, K$ satisfies*

$$\left| C_\Delta \sum_{k>K} k^{-1-2h} \Phi(k\Delta) \right| \le M_h \left[\sum_m \frac{B_m R^{-P_m}}{P_m + 2u} + \frac{B_{\mathrm{far}}}{K} \frac{e^{-\lambda K}}{e^{\lambda - q_h/K} - 1} \right]. \tag{E3.8}$$

Proof. Integrate the decreasing positive powers from K to infinity for the algebraic terms. For $k = K + j$ the exponential term uses $(1 + j/K)^{-1-2u} \le e^{q_h j/K}$ and its exact positive geometric sum starting at $j = 1$. The hypotheses ensure every denominator is positive. □

A sharp prefix has weight one through K. Formula (E3.8) cannot be inserted into a filtered prefix with unpriced omitted weights. At the worst order the smallest denominators $P_m + 2u$ are $2.1, 7.1, 14.1$, so the centre causes no divergence.

For a useful parameter-wide order price, reflection and Euler's product give, with $x = 1 + u > 0$ and $v = |\Im h|$,

$$M_h = \frac{2}{\pi}\left(\frac{2}{\Delta K}\right)^{2u} |\Gamma(x+iv)|^2 |\sin \pi(u+iv)|,$$
$$|\Gamma(x+iv)|^2 = \Gamma(x)^2 \prod_{n=0}^{\infty}\left(1 + \frac{v^2}{(x+n)^2}\right)^{-1}. \tag{E3.9}$$

When $\Delta K > 2$, on each rational cell $[u_-, u_+] \times [v_-, v_+]$, gamma log convexity bounds $\Gamma(x)^2$ by its endpoint maximum. Use u_- in the decreasing power, $x = 1 + u_+$ and $v = v_-$ in any retained finite product denominator, and

$$|\sin \pi(u+iv)| \le \sqrt{S_{\text{cell}}^2 + \sinh^2(\pi v_+)},$$

where S_{cell} is the endpoint maximum of $|\sin \pi u|$, or one if a half-integer lies in the cell. This gives a certified rectangle cover, including all positive complex orders and removable integer values. The executed cover uses 158×120 cells and 32 Euler factors.

At $t = 2/5$, $\alpha = 3/5$, $\Delta = 8/25$, $K = 4096$, the full-box terminal bounds are below $7.960261698533 \times 10^{-15}$ for $N = 6$ and $4.472333707850 \times 10^{-29}$ for $N = 8$. For $N = 4$ the same estimate is above 10^{-3} at this cutoff. This quantitative failure selects the corrected balanced readout below; it is not a failure of the ordinary moment.

Balanced Bessel integrals and a validated lattice correction (E5)

For integer $n \ge 0$, real $x \ge 0$, and $\Re q > 1$, define the convergent kernel

$$\mathcal{H}(q, n, x) = \int_1^{\infty} v^{-q} J_n(xv)\, dv. \tag{E5.1}$$

It satisfies $\mathcal{H}(q, 0, 0) = 1/(q-1)$ and $\mathcal{H}(q, n, 0) = 0$ for $n > 0$. Negative integer orders use $\mathcal{H}(q, -n, x) = (-1)^n \mathcal{H}(q, n, x)$.

Proposition E5.1 (Effective incomplete Mellin representation)**.** *For $x > 0$ the ordinary integral* (E5.1) *is represented by*

$$\mathcal{H}(q, n, x) = x^{q-1} 2^{-q} \frac{\Gamma((n+1-q)/2)}{\Gamma((n+1+q)/2)} - \sum_{\ell \ge 0} \frac{(-1)^\ell (x/2)^{n+2\ell}}{\ell!(n+\ell)!(n+2\ell+1-q)}, \tag{E5.2}$$

with the apparent poles cancelled as below. If J is the first omitted index, $\Re(n + 2J + 1 - q) > 0$, and $\rho = (x/2)^2/[(J+1)(n+J+1)] < 1$, the omitted series is bounded by

$$E_{\mathcal{H}} = \frac{(x/2)^{n+2J}}{J!(n+J)!\,|n+2J+1-q|\,(1-\rho)}. \tag{E5.3}$$

For an interval input, upper endpoints and positive lower denominators are used in this expression.

Proof. On $1/2 < \Re q < n+1$, the standard complete Bessel Mellin integral and the termwise lower integral from zero to x give (E5.2). For fixed $x > 0$, Nicholson's bound at large argument proves that the integral from one is holomorphic already on $\Re q > 1/2$. This supplies the continuation bridge also when $n = 0$; we never interpret the divergent complete integral as the ordinary target. The pole cancellation below continues the representation to the required half-plane. Beyond J, denominator real parts are positive and grow by two, so their absolute values do not decrease. The ratio of successive complete summand magnitudes is at most ρ, proving (E5.3) by a positive geometric series. □

Deflation at exact and near Mellin poles

Let $q_0 = n + 1 + 2\ell$, $\varepsilon = q - q_0$, and $\alpha_\ell = (-1)^\ell (x/2)^{n+2\ell}/[\ell!(n+\ell)!]$. The complete Mellin term and the corresponding lower-integral term have finite sum $\alpha_\ell[1 - F(\varepsilon)]/\varepsilon$, where

$$F(\varepsilon) = \frac{e^{\varepsilon \log(x/2)}\Gamma(1-\varepsilon/2)}{\Gamma(1+\varepsilon/2)\prod_{j=1}^{\ell}(1+\varepsilon/(2j))\prod_{j=1}^{n+\ell}(1+\varepsilon/(2j))}. \tag{E5.4}$$

Put $G(\varepsilon) = \log F(\varepsilon)/\varepsilon$ and $\operatorname{exprel}(y) = {}_1F_1(1;2;y)$. The entire local expression is

$$-\alpha_\ell G(\varepsilon)\operatorname{exprel}(\varepsilon G(\varepsilon)). \tag{E5.5}$$

Writing $H_m^{(k)} = \sum_{j=1}^{m} j^{-k}$, its convergent logarithmic series is

$$\begin{aligned} G(\varepsilon) &= \log(x/2) + \gamma - \tfrac{1}{2}(H_\ell^{(1)} + H_{n+\ell}^{(1)}) + \sum_{k\ge 2} g_k \varepsilon^{k-1}, \\ g_k &= \begin{cases} [H_\ell^{(k)} + H_{n+\ell}^{(k)}]/(k2^k), & k \text{ even}, \\ [2\zeta(k) - H_\ell^{(k)} - H_{n+\ell}^{(k)}]/(k2^k), & k \text{ odd}. \end{cases} \end{aligned} \tag{E5.6}$$

These coefficients lie between zero and $2\zeta(2)/(k2^k)$. Retaining through $k = J$ therefore leaves, when $|\varepsilon| \le \rho_e < 2$,

$$|G - G_J| \le \frac{\zeta(2)(\rho_e/2)^J}{(J+1)(1-\rho_e/2)}. \tag{E5.7}$$

Gamma recurrence proves (E5.4); expansion of its logarithm proves (E5.6). Factoring $e^{\varepsilon G} - 1$ proves (E5.5) without dividing an interval containing zero. At $\varepsilon = 0$ the value is

$$\alpha_\ell \left\{ \frac{\psi(\ell+1) + \psi(n+\ell+1)}{2} - \log(x/2) \right\}.$$

The implementation uses the deflated branch when the entire pole-offset ball lies in $|\varepsilon| < 1/2$ and inserts (E5.7) into its value ball. Exact $x = 0$ is handled before logarithms. A nontrivial x interval touching zero may instead return the safe absolute disk $1/(\Re q - 1)$.

Euler–Maclaurin with the actual terminal endpoint

Proposition E5.2 (Balanced lattice readout)**.** *Let $f(y) = y^{-q}J_n(ty)$, where n is an integer, $t \ge 0$, $\Re q > 1$, $K \ge 1$, and $P \ge 1$ is an integer. Then*

$$\sum_{k>K} f(k) = K^{1-q}\mathcal{H}(q,n,tK) - \frac{f(K)}{2} - \sum_{j=1}^{P} \frac{B_{2j}}{(2j)!} f^{(2j-1)}(K) + R_P, \tag{E5.8}$$

with the explicit allowance

$$|R_P| \le \frac{2\zeta(2P)}{(2\pi)^{2P}} \sum_{v=0}^{2P} \binom{2P}{v} |(q)_v| t^{2P-v} \frac{K^{1-\Re q - v}}{\Re q + v - 1}. \tag{E5.9}$$

Proof. The exact integer-order derivative identity is

$$\frac{d^d}{dy^d} J_n(ty) = \left(\frac{t}{2}\right)^d \sum_{j=0}^{d} (-1)^j \binom{d}{j} J_{n-d+2j}(ty).$$

Its magnitude is at most t^d. Leibniz bounds $|f^{(2P)}(y)|$ by $\sum_v \binom{2P}{v}|(q)_v| t^{2P-v} y^{-\Re q - v}$. Apply Euler–Maclaurin on $[K, L]$, subtract the inclusive endpoint $f(K)$, and let $L \to \infty$. Every endpoint derivative vanishes there, while $|B_{2P}(\{y\})|/(2P)! \le 2\zeta(2P)/(2\pi)^{2P}$. Integration gives (E5.9). In particular the first endpoint term is $-f(K)/2$, not its opposite sign. All denominators are positive; the formulas remain literal at $t = 0$ with $t^0 = 1$. □

For (E4.6), put $q_j = 1 + 2h + N/2 + j$ and $t = a\Delta$. At $R = K\Delta$ the contribution of one balanced mode to the unweighted sampled tail is

$$\Delta^{-N/2} K^j c_{N/2,j,n} i^n \sum_{k>K} k^{-q_j} J_n(tk).$$

Use (E5.8) and add both its allowance and (E5.3), with the same coefficient multiplier. The minimum real parts of q_j are $3.1, 8.1, 15.1$ at ranks four, six, and eight. The balanced kernel is therefore an ordinary absolutely convergent integral throughout the target box. Balanced parity places its removable poles at integer h for ranks four and eight, and at half-integer h for rank six; the local deflation handles both. A transfer to rank six cannot rely only on the zeros of $1/\Gamma(-h)$.

Unbalanced Abel readout with a priced direction integral (E6)

Let $\nu_m = 2m - N \neq 0$. Because $a \leq NZ \leq 1/5$, its real frequency is separated from zero. This separation is used only for these unbalanced populations. For $\Re q > 1$, let $\Delta_f^\ell k^{-q}|_{k=K+1}$ denote the ordinary forward difference, and put $\theta = \Delta(\nu_m + a\cos\phi)$, $w = e^{i\theta}$. Repeated summation by parts gives

$$\sum_{k>K} e^{i\theta k} k^{-q} = \frac{w^{K+1}}{1-w} \sum_{\ell=0}^{B-1} \left(\frac{w}{1-w}\right)^\ell \Delta_f^\ell k^{-q}\big|_{K+1} + \mathcal{R}_B, \tag{E6.1}$$

$$|\mathcal{R}_B| \leq \frac{|(q)_B| K^{1-\Re q-B}}{(\Re q + B - 1)|1-w|^B}. \tag{E6.2}$$

For completeness, one summation by parts isolates the first term and replaces k^{-q} by its forward difference with an extra factor $w/(1-w)$. Iteration proves the finite formula. The integral representation of a Bth forward difference bounds it by $|(q)_B| k^{-\Re q - B}$; the remaining positive tail is bounded by its integral from K. This proves (E6.2) without fitting a large-frequency coefficient.

Let

$$d_{m\ell n} = \sum_{j=v_m}^{M-1} K^j c_{mjn} \Delta_f^\ell k^{-q_j}\big|_{K+1}.$$

For a direction strip $|\Im\phi| \leq \rho$, suppose

$$a\cosh\rho < 2, \qquad \Delta(N + a\cosh\rho) < \pi. \tag{E6.3}$$

Set

$$b_\rho = a\Delta\sinh\rho, \qquad c_{m,0} = 2\sin\frac{\Delta(|\nu_m| - a)}{2},$$
$$c_{m,\rho} = 2e^{-b_\rho/2}\sin\frac{\Delta(|\nu_m| - a\cosh\rho)}{2}.$$

The gates imply positive denominators; the identity for $|1 - e^{i\theta}|$ gives the lower bound $c_{m,\rho}$ on the strip. A uniform bound for the finite angular integrand in (E6.1) is

$$S_m = e^{b_\rho(K+1)} \sum_{\ell=0}^{B-1} \frac{e^{b_\rho \ell}}{c_{m,\rho}^{\ell+1}} \sum_{|n|\leq NL} |d_{m\ell n}| e^{|n|\rho}. \tag{E6.4}$$

Fourier contour shifting bounds the error of its normalized Q-point trapezoid by $2S_m/(e^{Q\rho} - 1)$. After the common factor $\Delta^{-N/2}$, the complete unbalanced allowances are therefore

$$E_{\text{Abel}} = \Delta^{-N/2} \sum_{m\neq N/2} \sum_{j=v_m}^{M-1} \frac{K^j \sum_n |c_{mjn}|\,|(q_j)_B| K^{1-\Re q_j - B}}{(\Re q_j + B - 1) c_{m,0}^B},$$
$$E_{\text{angular}} = \frac{2\Delta^{-N/2}}{e^{Q\rho} - 1} \sum_{m\neq N/2} S_m. \tag{E6.5}$$

The implementation combines inverse degrees before its finite DFT and uses $Q > 2NL$ to keep all retained mode indices distinct. Directly evaluated phase exponentials avoid repeated multiplication of rectangular phase balls. At $z = 0, L = 0$ the direction is constant: one point is exact and the angular allowance is zero.

Complete preparation return and finite-source accounting (E7)

Three terms are required to return from the finite preparation

Let $\delta_L \ge \|A - A_L\|_\infty$ on the physical CUE torus. A computable bound uses the first omitted one-body coefficient and

$$\rho_L = z \max\left(1, \frac{|p+L+1|}{L+2}\right) < 1, \quad e_L = \frac{|b_{L+1}|}{1-\rho_L}, \quad B_L^* = \sum_{k=0}^{L} |b_k| + e_L, \quad \delta_L = 2N d^{N^2+2N\Re s} (B_L^*)^{2N-1} e_L. \tag{E7.1}$$

Indeed each later ratio is at most ρ_L: the vector $1 + (p-1)/(k+1)$ lies on the line segment between its first value and one, and the norm is convex. A product telescope over all $2N$ factors gives (E7.1).

Use the inherited exact sampled Mellin identity, with all removable products deflated,

$$T_A = C_\Delta \sum_{k\ge 1} k^{-1-2h} \Phi_A(k\Delta) - \mathcal{I}_A, \qquad \mathcal{I}_A = C_\Delta \sum_{j\ge 0} a_{A,j} \Delta^{2j} \zeta(1+2h-2j). \tag{E7.2}$$

It is valid here because $\Delta D < 2\pi$ and the ordinary domain has been established. Subtract it for the two physical preparations. The difference of their terminal tails is the moment difference minus their finite-prefix difference plus their complete image difference. Consequently

$$E_{\text{return}} \le \delta_L \left[U_N(\Re h) + |C_\Delta| \sum_{k=1}^{K} k^{-1-2\Re h} + W_{\text{image}}(h, D, \Delta) \right], \tag{E7.3}$$

where U_N means the appropriate negative or nonnegative comparison from Theorem E2.3. The complete image weight may be evaluated as

$$W_{\text{image}} = \sum_{j<J} |C_\Delta \zeta(1+2h-2j)| \frac{(\Delta D/2)^{2j}}{(j!)^2} + \frac{2|C_\Delta|(2\pi)^{2u}|\cos \pi h| \Gamma(2J-2u)\zeta(2J-2u)(x/2)^{2J}}{(J!)^2(1-q_J)}, \tag{E7.4}$$

with $u = \Re h$, $x = \Delta D/(2\pi) < 1$, $J > u + 1/2$, and

$$q_J = x^2 \max\left(1, \frac{J-u}{J+1}\right) \max\left(1, \frac{J+1/2-u}{J+1}\right) < 1.$$

Taylor coefficient differences are bounded by $\delta_L (D/2)^{2j}/(j!)^2$. Zeta reflection, the gamma integral bound, and the resulting positive ratio prove (E7.4). A monotone integral bound for the finite weight is

$$\sum_{k=1}^{K} k^{-1-2u} \le \max(1, K^{-1-2u}) + \log K \, {}_1F_1(1; 2; -2u \log K),$$

which is finite also at $u = 0$. Thus all three terms in (E7.3) are explicit. A constant Fourier-source error is never integrated to infinity against the deeply inverse Mellin weight.

Original physical prefix and Mellin image

The finite source and image contracts are inherited from HaarCritical, Propositions 5.2 and 5.4–5.6, with the actual rank powers retained. For clarity we record the complete bounds used in the new join. At strip height $t = 1$, put $d_Z = 1 - Z^2$, $M_* = d_Z^{-9}$, $m_* = (1-Z)^6$, and use E, η as in (E3.2). Define

$$g_- = 1 + Z^2 - 2Z\cosh t, \qquad g_+ = 1 + Z^2 + 2Z\cosh t,$$

$$C_t = d_Z^{-5} \max(g_-^{-4}, g_+^2) e^{3\eta} \left(\frac{e^t - Z}{1 - Ze^t}\right)^{N-1},$$

$$V_t = M_* \left[\frac{d_Z^2}{(1-Z^2e^{-2t})(1-Z^2e^{2t})}\right]^{(N+3)^2/4}.$$

For preparation DFT size P_r, retained degree L_r, and even direction size Q_r, the entry and radial source errors are

$$\epsilon_r = \frac{2C_t}{1-e^{-t}}\big[e^{-(L_r+1)t} + (2L_r+1)e^{-(P_r-L_r)t}\big],$$
$$E_\Phi = \frac{4V_t e^{-tQ_r/2}}{1-e^{-t}} + M_*\big[(1+N\epsilon_r/m_*)^N - 1\big]. \tag{E7.5}$$

The first terms price true omitted modes and DFT aliases. The determinant term is the Gram perturbation estimate in the original Haar basis. Signed untranslated direction modes are contracted with exact translation Bessels; Parseval gives contraction norm at most one, without an extra Q_r factor. The resulting scalar error is $E_\Phi|C_\Delta|\sum_{k\le K} k^{-1-2u}$.

For the image, extract J_i scaled coefficients $H^{2j}a_j$ from m_i half-circle samples at $He^{\pi i\ell/m_i}$. Use preparation resources (P_i, L_i) and direction size Q_i. Let $W = \max((1-Z)^{-6}, (1+Z)^6)$ and $b = H/2$. The respective bounds are

$$E_{\mathrm{mode}} = \frac{2We^{b^2}b^{L_i+1}}{(L_i+1)![1-b/(L_i+2)]}, \qquad E_{\mathrm{alias}} = \frac{2C_t e^{-t(P_i-L_i)}}{1-e^{-tP_i}},$$
$$\epsilon_i = E_{\mathrm{mode}} + (2L_i+1)E_{\mathrm{alias}}e^H,$$
$$E_{\mathrm{det},i} = N^2\epsilon_i(We^H + N\epsilon_i)^{N-1}e^{HNZ}, \qquad E_{\mathrm{dir},i} = \frac{2M_* e^{HD\cosh 2}}{e^{2Q_i}-1},$$
$$E_{\mathrm{circle}} = \frac{M_*(HD/2)^{2m_i}}{(m_i!)^2[1-(HD/(2m_i+2))^2]}.$$

All denominators are checked positive. The scaled coefficient error is $E_a = E_{\mathrm{det},i} + E_{\mathrm{dir},i} + E_{\mathrm{circle}}$. Multiplying by $\sum_{j<J_i}|C_\Delta\zeta(1+2h-2j)|(\Delta/H)^{2j}$ prices the finite image, and the tail in (E7.4), multiplied by M_*, prices the omitted image. These bounds retain the original complex weight.

Near $h = j+\varepsilon$, the complete gamma–zeta product is evaluated as

$$C_\Delta(h)\zeta(1+2h-2j) = -\left(\frac{2}{\Delta}\right)^{2h}\frac{\Gamma(1+h)}{\Gamma(1-\varepsilon)}\prod_{\ell=0}^{j-1}(\ell-h)\big[1+2\varepsilon\zeta_{\mathrm{reg}}(1+2\varepsilon)\big], \tag{E7.6}$$

where $\zeta_{\mathrm{reg}}(v) = \zeta(v) - 1/(v-1)$ is entire at one. Gamma recurrence proves this identity before any interval multiplication. At a nonnegative integer the scalar is obtained directly from $T_N(j,s;z) = (-4)^j(j!)^2a_j$.

The preserved physical source and its exact return (A2)

Put $d = 1-z^2$, $a = Nz$, and

$$w = \frac{\lambda - z}{1-z\lambda}, \qquad \lambda = \frac{w+z}{1+zw}, \qquad |w| = 1.$$

The inherited exact transformation gives

$$S_N = Nz + \operatorname{Tr} V, \qquad A_{N,z,s}(w) = d^{N^2+2Ns}\prod_{j=1}^{N}(1+zw_j)^{-(N+s)}(1+z/w_j)^{-(N+s)}.$$

Both paired factors have exponent $N+s$. There is no conjugation of s and no normalization of this complex preparation into a probability measure. The Weyl normalization, Jacobian and squared Vandermonde are those of the original transformed Haar integral.

For the source engine it is useful to return to an original-Haar Gram representation. Set

$$g(w) = 1 + 2z\Re w + z^2, \qquad W_s(w) = \frac{d}{g(w)}\exp\left(s\log\frac{d^2}{g(w)}\right).$$

The logarithm is real on the circle. Gram entries integrate $W_s(w)\lambda(w)^j\lambda(w)^{-k}$ times the Fourier plane wave. Their normalized determinant, with the retained translation, gives the same prepared radial source $\Phi(r)$. All

determinant permutations and all stationary populations remain present. The numerical projection is formed in the *untranslated signed direction*; only then are the translation Bessel coefficients contracted. Replacing this operation by a pointwise trapezoid of the already translated product would change the alias contract.

The finite-source frame is an exact dyadic change of basis. If its diagonal scales are 2^{-e_j} and its common row divisor is D, the physical return factor is

$$F = D^N 2^{2\sum_j e_j}.$$

Both centre and error return by F and $|F|$, respectively. A numerically suggested frame is acceptable only because its rounded coefficients define an exact basis with its own return identity. The hard upper-radius test has $F = 262144$; dropping that multiplier would invalidate the certificate.

Source preservation and the research method (Z2)

The current Shadow_Research_1 protocol is used as a research method: identify the original source, determine which information a readout needs, make every transformation and return explicit, and test whether the composed construction still describes the same physical moment. Its active version authority, Reflective Mathematics Research Handbook, Combined Protocol, Boundary–Property Key, Source Lift/Source Down, and reflective mapping guide that audit. They are not mathematical axioms and supply no missing estimate. The active editions are the Handbook development edition 1, Combined Protocol 0.2-dev.1, and Boundary–Property Key 3.4-dev.1.

For this problem the connected objects are the Haar law, the derivative mark, the independently complex determinant preparation, a Fourier or conditional source, finite physical samples, the Mellin image and terminal contribution, and the final complex enclosure. Losing the complex preparation, replacing it by a probability measure, or ignoring a return term changes the problem.

The exact Möbius map is useful both in inherited source engines and in the new positive majorants. If λ and w are unit-circle points, put

$$w = \frac{\lambda - z}{1 - z\lambda}, \quad \lambda = \frac{z + w}{1 + zw}, \quad d = 1 - z^2. \tag{Z2.1}$$

Then $1 - z\lambda = d/(1 + zw)$ and $d\lambda/(1 - z\lambda) = z + w$, so

$$S_N = Nz + \sum_{j=1}^{N} w_j. \tag{Z2.2}$$

The angle Jacobian is $d/|1 + zw|^2$. Moreover,

$$\lambda_i - \lambda_j = \frac{d(w_i - w_j)}{(1 + zw_i)(1 + zw_j)}.$$

Combining the N Jacobians with the squared Vandermonde gives $d^{N^2} \prod_j |1+zw_j|^{-2N}$. The original determinant power supplies the remaining factors, giving the exact preparation relative to normalized CUE:

$$A_{N,z,s}(w) = d^{N^2+2Ns} \prod_{j=1}^{N} (1 + zw_j)^{-(N+s)} (1 + z/w_j)^{-(N+s)}. \tag{Z2.3}$$

For $z < 1$, the factors lie on their unambiguous physical logarithmic branches. Both exponents are $N + s$; replacing one by a complex conjugate changes the tilt. No normalization of $A_{N,z,s}$ as a probability is made.

The new h-halo estimate deliberately works in the original Haar variables. A supremum of the full transformed preparation near $z = 0.9$ is unnecessarily large. The Möbius formula is retained where its exact translated mark makes a few-angle inverse estimate effective. This is a change of representation for a bound, not a change of the physical source.

A moderate original-Haar analytic halo (Z3)

Common rotation and the derivative polynomial

Write $X = |S_N(z)|$. Haar invariance permits averaging $U \mapsto tU$ over $|t| = 1$ before integrating over U. Since

$$\Lambda_N(z; tU) = \sum_{k=0}^{N} (-z)^k e_k(U) t^k, \qquad \partial_z \Lambda_N(z; tU) = t Q_U(t),$$

Q_U has degree exactly $N-1$ and leading coefficient of modulus Nz^{N-1}. The extra factor t has modulus one. It must not be counted as an additional root in Hölder's inequality.

Lemma Z3.1 (Common-rotation inverse bound)**.** *For $0 < z < 1$ and $0 < p < 1/(N-1)$,*

$$\mathbb{E} X^{-p} \le R_N(z)^p B((N-1)p), \quad R_N(z) = \frac{(1+z)^N}{(1-z^2)Nz^{N-1}}, \quad B(a) = \frac{\Gamma((1-a)/2)}{\sqrt{\pi}\,\Gamma(1-a/2)}. \tag{Z3.1}$$

Proof. For any complex a, rotate its argument and use $|e^{it} - |a|| \ge |\sin t|$. Thus the uniform-circle average of $|e^{it} - a|^{-q}$ is at most $B(q)$ for $0 \le q < 1$; the displayed gamma ratio is the elementary beta integral of $|\sin t|^{-q}$. Factor Q_U and apply Hölder with $N-1$ equal exponents. Uniformly in U,

$$\mathbb{E}_t |Q_U(t)|^{-p} \le (Nz^{N-1})^{-p} B((N-1)p).$$

No root-location hypothesis is needed. The pointwise determinant bound $|\Lambda_N(z; tU)| \le (1+z)^N$ and $X = d|Q_U(t)|/|\Lambda_N(z; tU)|$ finish the proof after Haar averaging. □

Correlated determinant mass

Lemma Z3.2 (Schur-character majorant)**.** *For real v and $0 \le z < 1$,*

$$\mathbb{E}|\Lambda_N(z)|^{2v} \le (1-z^2)^{-v^2}. \tag{Z3.2}$$

Proof. The Schur expansion of $\det(I - zU)^v$ uses the power-sum specialization $p_k = -vz^k$. Haar character orthogonality gives the sum of squared Schur coefficients over partitions of length at most N. For real v these are nonnegative. Removing the length restriction and using the Cauchy identity gives

$$\sum_{\lambda} s_\lambda(p)^2 = \exp\left(\sum_{k \ge 1} \frac{v^2 z^{2k}}{k} \right) = (1-z^2)^{-v^2}.$$

The identity is first coefficientwise. The full series has nonnegative coefficients and radius one; on smaller radius disks the determinant series converges in L^2, so orthogonality and passage to the limit are justified. □

For conjugate exponents $a > 1$, $b = a/(a-1)$, Lemmas Z3.1 and Z3.2 imply

$$\mathbb{E}[X^{-p} |\Lambda|^{2v}] \le R_N(z)^p B(a(N-1)p)^{1/a} d^{-bv^2}, \qquad a(N-1)p < 1. \tag{Z3.3}$$

The real exponent v appears only in a positive majorant. The physical complex tilt is neither conjugated nor replaced by that real exponent.

Holomorphy, logarithms, and the executed constant six

Fix $0 < z_- \le z \le z_+ < 1$, $|h| \le R$, $|s - s_0| \le \sigma$. Define

$$d_* = 1 - z_+^2, \quad D = N(1+z_+), \quad R_* = \frac{(1+z_+)^N}{d_* N z_-^{N-1}}, \quad v_* = \max\{|\operatorname{Re} s_0 - \sigma|, |\operatorname{Re} s_0 + \sigma|\}.$$

For $R_*, D \geq 1$ and $2a(N-1)R < 1$, the two signs of $\operatorname{Re} h$ give

$$\begin{aligned} |F| &\leq M_+ = D^{2R} d_*^{-v_*^2}, && \operatorname{Re} h \geq 0, \\ |F| &\leq M_- = R_*^{2R} B(2a(N-1)R)^{1/a} d_*^{-bv_*^2}, && \operatorname{Re} h < 0. \end{aligned} \tag{Z3.4}$$

The applicable bound is $\max(M_+, M_-)$, not their sum. On

$$N = 8, \quad z \in [0.899, 0.9], \quad R = \frac{1}{50}, \quad \sigma = \frac{1}{10}, \quad a = \frac{11}{4}, \quad b = \frac{11}{7}, \tag{Z3.5}$$

the executed 384-bit inequality gives

$$\max(M_+, M_-) < 5.815774 < 6. \tag{Z3.6}$$

The exact resource choice matters: an earlier $a = 2$ receipt does not justify the constant six. The continued proof binds analysis_bounds/bounds-holder11over4-384.json.

To justify differentiation under the original expectation, for $X \leq 1$ use

$$|\log X^2|^m \leq \left(\frac{2m}{e\varepsilon}\right)^m X^{-\varepsilon}, \qquad \varepsilon > 0. \tag{Z3.7}$$

For $X \geq 1$, $|\log X^2| \leq 2 \log D$. The strict inverse-exponent margin in (Z3.3) absorbs each fixed logarithmic power. The determinant is bounded away from zero on a fixed interior radius slab, so its logarithms cause no analogous moving singularity. Dominated differentiation and separate holomorphy, or their standard joint dominated version, establish joint holomorphy in h, s on an open neighborhood of the local domain.

In particular,

$$F_h = \mathbb{E}[X^{2h}|\Lambda|^{2s} \log X^2], \qquad F_s = \mathbb{E}[X^{2h}|\Lambda|^{2s} \log |\Lambda|^2],$$

and on the centred larger halo

$$|\partial_h^j \partial_s^k F(0, s_0, z)| \leq \frac{j!k!\,6}{R^j \sigma^k}. \tag{Z3.8}$$

For displaced centres, replace the radii by their available distances to the halo boundaries. These estimates concern derivatives of the actual ordinary moment, not derivatives of a finite approximation with an omitted remainder.

Moving marks: effective inverse estimates and real-radius regularity (Z4)

The common-rotation estimate is excellent for a small h halo but does not reach $\mathbb{E}X^{-1}$. The radius derivative needs a different source bound.

Lemma Z4.1 (Translated few-angle Riesz bound)**.** *Let $w_1, \ldots, w_k$ be independent uniform points on the unit circle. For $0 < q < \min(2, k/2)$,*

$$\sup_{A \in \mathbb{C}} \mathbb{E}|A + w_1 + \cdots + w_k|^{-q} \leq D_k(q), \quad D_k(q) = 2\pi^{-q} \frac{\Gamma(1 - q/2)}{\Gamma(q/2)} \left(\frac{1}{q} + \frac{1}{k/2 - q}\right). \tag{Z4.1}$$

Proof. The planar characteristic function is $J_0(r)^k$. The radial coefficient in the Riesz Fourier representation of $|x|^{-q}$ is $2^{1-q}\Gamma(1 - q/2)/\Gamma(q/2)$. This follows by integrating the Gaussian Fourier formula in the positive Laplace representation of $|x|^{-q}$. The translation contributes a factor of modulus at most one.

The order-zero Nicholson representation gives

$$J_0(r)^2 + Y_0(r)^2 = \frac{8}{\pi^2} \int_0^\infty K_0(2r \sinh t)\, \mathrm{d}t \leq \frac{8}{\pi^2} \int_0^\infty K_0(2ru)\, \mathrm{d}u = \frac{2}{\pi r}.$$

Here $u = \sinh t$, its Jacobian is at most one, and K_0 is positive. Together with $|J_0(r)| \leq 1$, this gives $|J_0(r)| \leq \min(1, \sqrt{2/(\pi r)})$. Split the absolute radial integral at $r_0 = 2/\pi$ to obtain

$$\int_0^\infty r^{q-1} |J_0(r)|^k\, \mathrm{d}r \leq (2/\pi)^q \left(\frac{1}{q} + \frac{1}{k/2 - q}\right).$$

Multiplication by the Riesz coefficient yields (Z4.1). Gaussian regularization makes the Fourier identities ordinary integrable identities. The displayed integrable majorant and Fatou's lemma justify removing the regularization despite the singular kernel. □

The normalized Haar eigenangle density with respect to independent uniform angles is at most $H_N = N^N/N!$, by the exact squared Vandermonde and Hadamard's inequality. Apply (Z2.1) to independent angles. Each resulting weight is $d/|1+zw|^2 \le P_z = (1+z)/(1-z)$. Bound exactly k such weights, condition on the remaining angles, and integrate their probability weights exactly. From (Z2.2) and Lemma Z4.1,

$$\mathbb{E}_{U(N)}|S_N(z)|^{-q} \le H_N P_z^k D_k(q), \quad N \ge k, \quad 0 < q < \min(2, k/2). \tag{Z4.2}$$

For $k = 3$ the range reaches $q < 3/2$, and $D_3(1) = 6/\pi$. For $k = 4$ it reaches every $q < 2$. Rank dependence is explicit; no density constant from another rank is silently transferred. In particular, on any fixed positive interior slab at rank eight this supplies ordinary inverse integrability for all $\operatorname{Re} h > -1$ used in the present estimates.

Proposition Z4.2 (Physical first-radius derivative)**.** *On the stated local h/s domains, F is C^1 in real z and*

$$F_z = \mathbb{E}\left[X^{2h}|\Lambda|^{2s}\left(2h \operatorname{Re}\frac{S_z}{S} - \frac{2s}{d}\operatorname{Re} S\right)\right]. \tag{Z4.3}$$

The derivative is holomorphic in h, s. No claim about noninteger F_{zz} or complex-z holomorphy is part of this proposition.

Proof. For a unit eigenvalue,

$$\partial_z \frac{d\lambda}{1-z\lambda} = \frac{\lambda((1+z^2)\lambda - 2z)}{(1-z\lambda)^2}.$$

With $q = |1-z\lambda|^2$, its squared modulus is $2(1+z^2)/q - d^2/q^2$, which is at most $(1+z^2)^2/d^2$. Therefore

$$|S_z| \le \frac{N(1+z^2)}{d}, \qquad (\log|\Lambda|^2)_z = -\frac{2}{d}\operatorname{Re} S, \qquad |(\log|\Lambda|^2)_z| \le \frac{2N}{1-z}. \tag{Z4.4}$$

Ordinary differentiation away from $S = 0$ gives (Z4.3), including both the mark and determinant-preparation terms. For $|h| \le R < 1/4$, the singular factor obeys $X^{2\operatorname{Re} h - 1} \le 1 + X^{-1-2R}$, controlled by the three-angle bound. Bounded determinant weights on the slab supply a finite uniform integral majorant for the derivative.

There is also an almost-sure pathwise argument. The derivative of the characteristic polynomial has finitely many roots. Under a common Haar rotation those roots rotate; for any fixed matrix only finitely many phases can place a nonzero root on the chosen positive real radius slab. Hence for almost every matrix the mark is nonzero throughout that slab and the sample integrand is differentiable along it. Fubini gives the integral fundamental theorem of calculus. Choose a slightly larger inverse exponent still below 3/2 to obtain uniform integrability of the derivative family. Pointwise continuity away from the null mark set then makes the expected derivative continuous. The strict margin also absorbs logarithmic factors, establishing holomorphy of F_z in h, s. □

Naive second-radius differentiation would demand roughly $|S|^{-2+2\operatorname{Re} h}$. The previous proof does not justify that operation near $h = 0$. The exact $h = 0$ determinant has separately differentiable formulas, but their second derivative cannot simply be assigned to noninteger h.

Anchored transport makes the radius bound useful (Z5)

The coarse original-source radius bound proves regularity but is around 1.5×10^{10} on the large halo. It would force an impractically tiny continuation width. The repair keeps a single positive, unnormalized reference measure

$$\mathrm{d}\mu(U) = |\Lambda_8(z_0)|^{2v_0}\,\mathrm{dHaar}(U), \qquad v_0 = \operatorname{Re} s_0. \tag{Z5.1}$$

Its actual mass and inverse moments are preserved together.

Complete physical scalar disks at the exact real tilt v_0 give

$$M_0 = \int \mathrm{d}\mu < 1.627514, \quad A_{1.01} = \int X_0^{-1.01}\,\mathrm{d}\mu < 2.332190, \quad A_{1.9} = \int X_0^{-1.9}\,\mathrm{d}\mu < 4.966607. \tag{Z5.2}$$

These displayed numbers are convenient outward summaries; the calculation consumes the exact rational upper endpoints of the full scalar disks in scalar/positive-moments.json. The two inverse exponents correspond to $h = -0.505$ and $h = -0.95$, inside the original target. The mass receives an additional independent original-Haar hypergeometric Toeplitz check.

For $p \in [1.01, 1.9]$, Hölder with the same measure gives

$$A_p \le A_{1.01}^{1-\theta} A_{1.9}^{\theta}, \qquad \theta = \frac{p - 1.01}{0.89}. \tag{Z5.3}$$

No division by M_0 occurs. For $0 \le p \le 1.01$, the corresponding bound is $A_p \le M_0^{1-p/1.01} A_{1.01}^{p/1.01}$.

Lemma Z5.1 (Small-ball transport)**.** *Let $X_z = |S_8(z)|$ and $z_0 - \Delta \le z \le z_0$. Put $L = 8(1 + z_0^2)/(1 - z_0^2) = 1448/19$. If $0 < p < q < 2$ and $b > L\Delta$, then*

$$\int X_z^{-p} \, \mathrm{d}\mu \le (1 - L\Delta/b)^{-p} A_p + B_q^{p/q} \min(M_0, b^{1.9} A_{1.9})^{1-p/q}, \tag{Z5.4}$$
$$B_q = (1 + z_0)^{16 v_0} H_8 P_{z_0}^4 D_4(q).$$

Proof. Equation (Z4.4) implies $|X_z - X_0| \le L\Delta$. On $X_0 \ge b$, $X_z^{-p} \le (1 - L\Delta/b)^{-p} X_0^{-p}$. On $X_0 < b$, Markov gives $\mu\{X_0 < b\} \le \min(M_0, b^{1.9} A_{1.9})$. The four-angle bound and the pointwise anchor weight imply $\int X_z^{-q} \, \mathrm{d}\mu \le B_q$. Hölder on the small set gives the second term in (Z5.4). This proves a uniform inequality for every radius in the slab, not an interpolation of tested radii. □

For $|v - v_0| \le \rho$ the positive physical weights satisfy

$$\frac{|\Lambda(z)|^{2v}}{|\Lambda(z_0)|^{2v_0}} \le C_{\mathrm{ret}} := \exp(160 |v_0| \Delta + 16 \rho \log 10). \tag{Z5.5}$$

Indeed $|\log |\Lambda(z)|^2| \le 16 \log 10$ and its radius derivative is at most 160. This accounts for the original tilt at the new radius; complex phases are still those of the same independently complex physical moment. With $p = 1 + 2H$, define

$$J_0 = C_{\mathrm{ret}} \big(M_0 + \text{right side of (Z5.4)} \big), \qquad J_1 = 16 \log 10 \, J_0. \tag{Z5.6}$$

They bound the weighted singular mark derivative and its additional tilt log.

The nonsingular preparation term improves substantially through an exact original-Haar moment, rather than a support maximum.

Lemma Z5.2 (Exact second mark moment)**.** *For $0 \le z < 1$,*

$$\mathbb{E}|S_N(z)|^2 = 1 - z^{2N} \le 1. \tag{Z5.7}$$

Proof. The uniformly convergent expansion is $S_N(z) = d \sum_{k \ge 1} z^{k-1} \operatorname{Tr} U^k$. The normalized CUE projection kernel gives $\mathbb{E}[\operatorname{Tr} U^k \overline{\operatorname{Tr} U^l}] = \delta_{kl} \min(k, N)$: expanding its two-point determinantal kernel in Fourier modes gives $N - (N - k)_+$ on the diagonal and zero off it. More explicitly, for normalized angular measure the kernel is $K_N(\theta, \phi) = \sum_{j=0}^{N-1} e^{ij(\theta - \phi)}$; the Fourier coefficient of $|K_N|^2$ at equal positive indices k,l is $\delta_{kl}(N - k)_+$, and the diagonal term contributes $\delta_{kl} N$. Hence the moment is $d^2 \sum_{k \ge 1} \min(k, N) z^{2k-2}$. Summing the finite linear segment and geometric remainder yields $1 - z^{2N}$. □

If $t = 1 + 2 \operatorname{Re} h \in [1 - 2H, 1 + 2H]$, choose $a = 2/(1 + 2H)$, $b = 2/(1 - 2H)$. Lyapunov, Lemma Z5.2, and Lemma Z3.2 imply

$$\mathbb{E}[X^t |\Lambda|^{2v}] \le d_*^{-bv^2} =: G_0(v). \tag{Z5.8}$$

For any $u > 0$, the inequality $|x|^k e^{-u|x|} \le (k/(eu))^k$ gives

$$|x|^k e^{vx} \le \left(\frac{k}{eu} \right)^k (e^{(v+u)x} + e^{(v-u)x}). \tag{Z5.9}$$

Applying this with $x = \log|\Lambda|^2$ gives $G_1(v) \le [G_0(v+u)+G_0(v-u)]/(eu)$ for the corresponding one-log moment. Combining the two actual terms in (Z4.3), and differentiating the explicit s as well when forming F_{zs}, yields

$$\begin{aligned} |F_z| &\le 2HLJ_0 + (2s_{\max}/d_*)G_0, \\ |F_{zs}| &\le 2HLJ_1 + (2/d_*)(s_{\max}G_1 + G_0). \end{aligned} \tag{Z5.10}$$

The G_0 term in the second line is essential: it comes from differentiating the explicit tilt factor in the preparation derivative.

The same shifted-log inequality and (Z3.4) bound higher tilt derivatives. Finite rational grids select among individually valid Hölder exponents and log shifts, so no unproved global optimization is used. On (Z1.2), actual outward evaluations give

$$\begin{aligned} |F_{sss}| < 137.273 < 138, \quad |F_{ssss}| < 672.391 < 673, \\ |F_z| < 195.089 < 196, \qquad |F_{zs}| < 4463.914 < 4464. \end{aligned} \tag{Z5.11}$$

For the transport, the selected auxiliary exponent is $q = 77/40 < 2$. It is an analytic majorant exponent, not an unsupported public scalar query. The exact choices and outward components are in analysis_bounds/local-H010-s006-384.json and analysis_bounds/anchored-H010-delta2e-8-384.json.

An exact, globally regularized source transport (T3)

Möbius preparation and the mark

The inherited exact Möbius change of variables gives, relative to normalized CUE(N),

$$S = Nz + \sum_{j=1}^{N} e^{i\theta_j}, \tag{T3.1}$$

$$A(z,s,\theta) = (1-z^2)^{N^2+2Ns} \prod_{j=1}^{N} (1+ze^{i\theta_j})^{-(N+s)}(1+ze^{-i\theta_j})^{-(N+s)}, \tag{T3.2}$$

$$F(h,s,z) = \int |S|^{2h} A(z,s,\theta)\, \mathrm{dCUE}(\theta). \tag{T3.3}$$

Both factors in each pair retain the same complex exponent. The complex preparation is not divided by its mass and is not replaced by a probability. All branches in (T3.2) are the physical analytic branches.

For real variables define

$$x = (\operatorname{Re} S, \operatorname{Im} S)^T, \quad D_j = (-\sin\theta_j, \cos\theta_j)^T, \quad G = \sum_j D_j D_j^T, \quad R = x^T x, \quad M = G + RI_2.$$

Set

$$u = M^{-1}e_1, \qquad v_j = -ND_j^T u, \qquad \frac{\mathrm{d}\theta_j}{\mathrm{d}z} = v_j.$$

The regularization RI_2 is analytic on the whole source; an angular cutoff would not have the same property.

Lemma T3.1 (Critical-population matrix floor)**.** *For $N = 8$, real $z \in [.899, .9]$, and every angle configuration,*

$$M > \frac{2}{5} I_2.$$

This includes collisions and the mark-zero set.

Proof. Let $W = \sum_j e^{i\theta_j}$ and $\lambda = \lambda_{\min}(G)$. Rotate coordinates so that $\lambda = \sum_j \sin^2\theta_j$. Put $a_1 = \sum_j \cos\theta_j$, $b_1 = \sum_j \sin\theta_j$, and $\nu = \sum_j \operatorname{sign}(\cos\theta_j)$, choosing either sign at a zero cosine. Then

$$|a_1 - \nu| \le \sum_j (1 - |\cos\theta_j|) \le \lambda, \quad b_1^2 \le N\lambda, \quad |a_1 + \nu| \le 2N.$$

Thus $\big||W|^2-\nu^2\big|\le 3N\lambda$, and

$$\lambda \ge \frac{\operatorname{dist}(|W|^2,\{(2m-N)^2 : 0\le m\le N\})}{3N}.$$

Write $a=8z$, $r=|x|$. If $r\ge 8-a$, then $M\ge r^2 I\ge .64I$. Otherwise $[a-r,a+r]\subset(6,8)$, and completion of the two relevant squares gives

$$\lambda+r^2 \ge \min\left\{\frac{a^2}{25}-\frac{3}{2}, \frac{8}{3}-\frac{a^2}{23}, (8-a)^2\right\} > \frac{2}{5}.$$

These are parameter-wide elementary inequalities, not sampled matrix tests. □

Lemma T3.2 (Multiplicative mark and complete CUE return)**.** *Along the flow,*

$$x' = NRu, \qquad R' = R\ell, \qquad \ell = 2Nx^T u.$$

If $\rho=\prod_{i<j} 4\sin^2((\theta_i-\theta_j)/2)$, the complete density and ordinary-Jacobian logarithmic rate is the analytic function

$$Q = N^2 t^T u + N\sum_j D_j^T M^{-1} M_j u, \quad t=\sum_j(\cos\theta_j,\sin\theta_j)^T, \tag{T3.4}$$

where $E_j=-(\cos\theta_j,\sin\theta_j)^T$ and $M_j=E_jD_j^T+D_jE_j^T+2(x^TD_j)I$.

Proof. The mark identity follows from $x'=Ne_1+Dv=N(I-GM^{-1})e_1=NRu$. Off collisions, logarithmic differentiation of ρ gives $\sum_{i<j}(v_i-v_j)\cot((\theta_i-\theta_j)/2)$. The exact identity

$$(v_i-v_j)\cot\frac{\theta_i-\theta_j}{2} = N\big[(\cos\theta_i+\cos\theta_j)u_1+(\sin\theta_i+\sin\theta_j)u_2\big]$$

removes every apparent pole. Adding $\operatorname{div} v$, including the derivative of the state-dependent M^{-1}, yields (T3.4). Continuity and permutation equivariance extend the result through collisions. The real flow is a torus diffeomorphism, so its ordinary Jacobian is included. □

Let Φ_z be the flow from a real anchor z_a, and let $B=(\partial_z+v\cdot\partial_\theta)\log A$. The exact return is

$$F(h,s,z)=\int R(z_a,\theta)^h A(z_a,s,\theta)\exp\left(\int_{z_a}^{z}(h\ell+B+Q)(t,\Phi_t\theta)\,\mathrm{d}t\right)\mathrm{dCUE}(\theta). \tag{T3.5}$$

The singular mark is fixed at the anchor. Its exponent is not made more negative by radius differentiation. Formula (T3.5) preserves the full squared Vandermonde and every determinant/preparation factor.

An effective analytic radius halo

Use $\eta=1/2500$, $\epsilon=1/100$, $c=2/5$, with complex increments $|z-z_a|\le\eta$ and $\max_j|\theta_j-\theta_{a,j}|\le\epsilon$. Complex analytic expressions use transpose, not conjugate transpose; Euclidean norms are used only for estimates. Put

$$\begin{aligned} &a_*=\sqrt{N}\epsilon e^{\epsilon}/\sqrt{c}, && e_*=N\eta+N\epsilon e^{\epsilon}, && b_*=e_*/\sqrt{c},\\ &q_*=2a_*+a_*^2+2b_*+b_*^2, && \kappa=(1-q_*)^{-1}, && b=1+a_*,\quad y=1+b_*. \end{aligned}$$

Whitening about the positive real matrix M_a gives

$$\|M_a^{-1/2}(M-M_a)M_a^{-1/2}\|\le q_*<1.$$

Consequently

$$\|v\|_2\le V=Nb\kappa/\sqrt{c}, \qquad |\ell|\le L=2Ny\kappa/\sqrt{c}.$$

The strict bound $\eta V<\epsilon$ keeps the analytic ODE inside its angular polydisk throughout the radius disk.

For completeness, explicit bounds for the density rate are obtained with $C = \sqrt{\cosh(2\epsilon)}$ and $\tau = 1 + (Nz_{\max} + N\epsilon e^{\epsilon})/\sqrt{c}$:

$$|Q| \le \frac{N^2\tau\kappa}{\sqrt{c}} + N\left(\frac{\sqrt{2}Cb^2\kappa^2}{c} + \frac{2Cb^2\kappa^2}{c} + \frac{2b^2\kappa^2 y}{\sqrt{c}}\right). \tag{T3.6}$$

The last term uses $GM^{-1} = M^{-1}G$; bounding the uncancelled cotangents would be invalid. For the preparation set $Z = z_{\max} + \eta$, $m = 1 - Ze^{\epsilon} > 0$, $\sigma = |s_0| + .1$, and

$$P_z = \frac{2e^{\epsilon}}{m}, \quad P_\theta = \frac{2z_{\max}}{1 - z_{\max}^2} + \frac{2[\eta e^{\epsilon} + z_{\max}(e^{\epsilon} - 1)]}{m(1 - z_{\max})}.$$

The paired-log resolvent identity proves

$$|B| \le (N^2 + 2N\sigma)\frac{2Z}{1 - Z^2} + (N + \sigma)\big(NP_z + P_\theta\sqrt{N}V\big). \tag{T3.7}$$

This includes the determinant prefactor in (T3.2).

Theorem T3.3 (Effective fixed-source analytic halo)**.** *At each real anchor $z_a \in [.899, .9]$, the physical moment on $|h| \le .02$, $|s - s_0| \le .1$ has a holomorphic radius extension to $|\zeta - z_a| \le .0004$, with $|F_{\text{ext}}| < 2048$.*

Proof. The preceding ODE bounds and (T3.5) give

$$|F_{\text{ext}}| \le 6\exp\{\eta[(.02)L + \text{bound}(B) + \text{bound}(Q)]\}.$$

Outward evaluation at 384 and 768 bits, and an independent 1024-bit reconstruction, establish

$$q_* < .375668, \quad V < 21.175394, \quad \eta V < .008470158 < .01,$$

$$\text{bound}(Q) < 2299.661, \quad \text{bound}(B) < 10597.978, \quad |F_{\text{ext}}| < 1044.384 < 2048.$$

The inherited bound 6 is on the absolute integrand, so it supplies uniform domination for analytic integration of the fixed-source multiplier. This also gives joint holomorphy in the interior h and s halos. On real radii the formula is the exact torus change of variables; overlapping extensions agree by uniqueness of analytic continuation. □

This theorem does not define the extension by substituting complex radius into absolute values. It also does not claim absolute integrability of the untransported formal F_{zz} integrand. Higher real-radius regularity is obtained in the transported representation.

The physical source and the retained analytic information (M2)

Put $F(h, s, z) = T_8(h, s; z)$. All complex powers of positive moduli use their real logarithms. The inherited exact Möbius transformation gives

$$S = 8z + \sum_{j=1}^{8} e^{i\theta_j}, \tag{M2.1}$$

$$A(z, s, \theta) = (1 - z^2)^{64+16s} \prod_{j=1}^{8} (1 + ze^{i\theta_j})^{-8-s}(1 + ze^{-i\theta_j})^{-8-s}, \tag{M2.2}$$

$$F(h, s, z) = \int |S|^{2h} A(z, s, \theta)\, \mathrm{d}\,\mathrm{CUE}_8(\theta). \tag{M2.3}$$

The two factors retain the same complex exponent. In particular, the tilt is not conjugated and the complex preparation is not divided by its mass. The CUE measure includes the entire squared Vandermonde and its Weyl normalization. The ordinary moment, not an analytic continuation of a divergent ordinary integral, is the real-radius target.

The previous investigation constructed a real analytic angular transport. With $x = (\Re S, \Im S)^T$, $R = x^T x$, $D_j = (-\sin\theta_j, \cos\theta_j)^T$, $G = \sum_j D_j D_j^T$, and $M = G + RI$, set

$$u = M^{-1} e_1, \qquad v_j = -8 D_j^T u, \qquad \theta_j' = v_j.$$

Its proved global floor $M > (2/5)I$ on all real anchors $z \in [.899, .9]$ includes mark zeros and eigenvalue collisions. The exact identities

$$x' = 8Ru, \qquad R' = R\ell, \qquad \ell = 16 x^T u$$

fix the singular mark at the reference source. The complete density rate is

$$Q = 64 t^T u + 8 \sum_j D_j^T M^{-1} M_j u, \quad t = \sum_j (\cos\theta_j, \sin\theta_j)^T,$$

where $M_j = E_j D_j^T + D_j E_j^T + 2(x^T D_j) I$ and $E_j = -(\cos\theta_j, \sin\theta_j)^T$. The second term is indispensable: it differentiates the state-dependent inverse matrix in the ordinary Jacobian. Apparent collision poles in the Vandermonde rate cancel before absolute values are taken.

Writing $B = (\partial_z + v \cdot \partial_\theta) \log A$, the fixed-source return is

$$F(h, s, z) = \int R(z_a, \theta)^h A(z_a, s, \theta) \exp\left(\int_{z_a}^{z} (h\ell + B + Q)(q, \Phi_q(\theta))\, \mathrm{d}q \right) \mathrm{d}\,\mathrm{CUE}_8(\theta).$$

The inherited analytic ODE and inverse-moment estimates justify this identity and give a holomorphic radius extension on every disk of radius $\eta = 1/2500$ about every real $z_a \in [.899, .9]$, uniformly for $|h| \le .02$, $|s - s_0| \le .1$, with absolute bound 2048. The original real-radius absolute-integrand bound on these order and tilt halos is 6. The extensions agree on overlaps by identity on their real intervals. Their union is one analytic extension of the physical moment. It is not the result of substituting a complex radius into the original absolute values.

The research decision is to retain this common analytic extension while changing the finite parameter readout. Individual point roots do not retain the branch identity needed for continuation. The new readout therefore keeps the full interpolation remainder, a common derivative cone, and explicit chart inclusion witnesses. This is the operative source–readout use of `Shadow_Research_1`; the protocol itself is not a mathematical premise for any inequality.

Higher tilt bounds from the original Haar integral (M3)

Let $L = \log|\Lambda_8(z)|^2$ and $X = |S_8(z)|$. For integer $k \ge 1$ and real $t > 0$,

$$|L|^k e^{vL} \le \left(\frac{k}{et}\right)^k \left(e^{(v+t)L} + e^{(v-t)L}\right). \tag{M3.1}$$

Indeed, on each half-line maximize $y^k e^{-ty}$ over $y \ge 0$. This bound retains independent complex order and tilt: only their real parts enter the absolute integrand. The inherited logarithmic integrability margins justify differentiation under the ordinary Haar integral.

For the real diameter $[z_-, z_+] = [.8986, .9004]$, write

$$d = 1 - z_+^2, \quad D = 8(1 + z_+), \quad R_* = \frac{(1+z_+)^8}{d\, 8 z_-^7}, \quad \mathcal{B}(q) = \frac{\Gamma((1-q)/2)}{\sqrt{\pi}\,\Gamma(1-q/2)}.$$

The original common-rotation inverse estimate and character moment bound give, for $a > 1$, $b = a/(a-1)$ and $14aH < 1$,

$$M_+(v) = D^{2H} d^{-v^2}, \qquad M_-(v; a) = R_*^{2H} \mathcal{B}(14aH)^{1/a} d^{-bv^2}.$$

For a tilt interval, use its largest squared endpoint in each exponent. Combining the positive and negative order cases with (M3.1) yields

$$|\partial_s^k F| \le \left(\frac{k}{et}\right)^k \max\{M_+(v+t) + M_+(v-t),\ M_-(v+t; a) + M_-(v-t; a)\}. \tag{M3.2}$$

Each rational resource choice (a, t) satisfying the stated condition gives a valid inequality. The finite search in the verification package selects one such bound; no claim of optimality is required.

Lemma M3.1 (Effective higher tilt derivatives)**.** *On $|s - s_0| \le .025$ and the stated real diameter, the executed outward inequalities give*

	$\lvert\partial_s^5 F\rvert$	$\lvert\partial_s^6 F\rvert$
$\lvert h\rvert \le .01$	< 4106	< 24405
$\lvert h\rvert \le .02$	< 14632	$< 97840.$

On the complex radius disk of radius $1/50000$ *about any physical* $z \in [.899, .9]$*, the fifth tilt derivative is below* 12140 *for* $|h| \le .01$*.*

Proof. The real bounds are direct outward evaluations of (M3.2). For the complex statement, the original flow halo bounds the fifth derivative on the semicircle by $B = 5!\,2048/(.1-.025)^5$. On the real diameter it is bounded by the actual outward value $A < 4106$. For $|\zeta - z| \le \epsilon < \eta$, the harmonic measure of the curved boundary in either half-disk is at most

$$\omega = \frac{2}{\pi} \arctan \frac{2\eta\epsilon}{\eta^2 - \epsilon^2}.$$

The two-constants theorem applied to the subharmonic logarithm gives $|\partial_s^5 F| \le A^{1-\omega} B^{\omega}$. At $\epsilon = 1/50000$ its executed upper endpoint is below 12140. The real diameter is enlarged only for this analytic allowance; the public physical radius target still ends at .9. □

A larger analytic halo from the original Haar source (J2)

Write $F = T_8$, $X = |S_8(z)|$, and $Y = |\Lambda_8(z)|^2$. All complex powers use real logarithms off the null mark-zero set. The exact Möbius source is

$$S_8 = 8z + \sum_{j=1}^{8} w_j, \qquad A = (1 - z^2)^{64+16s} \prod_{j=1}^{8} (1 + zw_j)^{-8-s} (1 + z/w_j)^{-8-s}.$$

The same complex exponent occurs in both factors. The CUE source retains the full squared Vandermonde and normalized Weyl factor; the complex preparation is never divided by its mass.

Lemma J2.1 (Four-angle inverse comparison)**.** *For real* $0 \le z < 1$ *and* $0 < q < 2$*,*

$$\mathbb{E}X^{-q} \le C(q, z) := \frac{8^8}{8!} \left(\frac{1+z}{1-z}\right)^4 D_4(q), \qquad D_4(q) = 2\pi^{-q} \frac{\Gamma(1 - q/2)}{\Gamma(q/2)} \left(\frac{1}{q} + \frac{1}{2-q}\right).$$

Proof. Hadamard bounds the normalized Haar eigenangle density relative to eight independent uniform angles by $8^8/8!$. Each exact Möbius one-angle density is $(1 - z^2)/|1 + zw|^2$, at most $(1 + z)/(1 - z)$. Bound four such densities and retain the other four as normalized measures. Conditioning on those four angles leaves a translated sum of four uniform circle points. Its planar characteristic function is $J_0(r)^4$. The inherited effective bound $|J_0(r)| \le \min(1, \sqrt{2/(\pi r)})$ and the Riesz coefficient $2^{1-q}\Gamma(1 - q/2)/\Gamma(q/2)$ give the stated bound after splitting the radial integral at $2/\pi$. Gaussian regularization justifies inversion under the integrable majorant, uniformly in the conditioned translation. This is an original-Haar return, not a density estimate transplanted from a different rank. □

The inherited character identity supplies $\mathbb{E}Y^v \le (1 - z^2)^{-v^2}$ for every real v. Also $\mathbb{E}X^2 = 1 - z^{16} \le 1$, by the exact trace covariance in the original Haar expansion $S_8 = (1 - z^2) \sum_{k \ge 1} z^{k-1} \operatorname{Tr} U^k$. Let $0 < H < 1$, choose $a > 1$ with $2aH < 2$, put $b = a/(a - 1)$, $d = 1 - z_+^2$, and $C = C(2aH, z_+)$. If $C \ge 1$, Hölder and Lyapunov give

$$\mathbb{E}X^{2u}Y^v \le C^{1/a} d^{-bv^2} =: M_-(v), \qquad -H \le u \le 0, \tag{J2.1}$$

$$\mathbb{E}X^{2u}Y^v \le d^{-v^2/(1-H)} =: M_+(v), \qquad 0 \le u \le H. \tag{J2.2}$$

For the first inequality, the uniform step is $\mathbb{E}X^{2au} \le (\mathbb{E}X^{-2aH})^{-u/H} \le C$. It does not assume monotonicity of inverse moments or of D_4. The second uses Hölder exponent $1/H$ and the second-moment comparison. Taking the largest squared real tilt endpoint gives an absolute-integrand bound on the full independent complex order/tilt product.

Theorem J2.2 (Enlarged physical and transported halos)**.** *Let s_0 be the full exact rational complex centre in the inherited zero certificate. On $z \in [.8986, .9004]$, $|s - s_0| \le .1$,*

$$|h| \le .1: \quad \mathbb{E}|X^{2h}Y^s| < 22, \qquad |h| \le .2: \quad \mathbb{E}|X^{2h}Y^s| < 228.$$

For every real anchor $z_a \in [.899, .9]$, the proved transported holomorphic extension to $|z - z_a| \le .0004$ satisfies respectively $|F| < 4096$ and $|F| < 40000$.

Proof. The exact choices $a = 461/50$ and $a = 231/50$ give inverse exponents 1.844 and 1.848, both strictly below two. Outward computation gives real bounds $21.2967831397\ldots$ and $227.321034426\ldots$. The strict gap absorbs every fixed power of $\log X$, so dominated differentiation proves ordinary h,s holomorphy beyond the closed disks.

Retain the inherited angular flow. With $x = (\Re S, \Im S)^T$, $R = x^T x$, $D_j = (-\sin\theta_j, \cos\theta_j)^T$, $M = \sum D_j D_j^T + RI$, set $u = M^{-1}e_1$, $v_j = -8D_j^T u$. The proved floor $M > (2/5)I$ yields $x' = 8Ru$, $R' = R\ell$, $\ell = 16x^T u$. The complete density rate is

$$Q = 64t^T u + 8\sum_j D_j^T M^{-1} M_j u, \quad M_j = E_j D_j^T + D_j E_j^T + 2(x^T D_j)I,$$

where $t = \sum(\cos\theta_j, \sin\theta_j)^T$ and $E_j = -(\cos\theta_j, \sin\theta_j)^T$. The inverse-matrix Jacobian term is retained. With $B = (\partial_z + v\cdot\partial_\theta)\log A$, the exact return is

$$F(h,s,z) = \int R(z_a,\theta)^h A(z_a,s,\theta)\exp\left(\int_{z_a}^{z}(h\ell + B + Q)(q, \Phi_q(\theta))\,\mathrm{d}q\right)\mathrm{d}\,\mathrm{CUE}_8(\theta).$$

The unchanged angular halo .01 and radius halo .0004 satisfy the ODE, matrix-floor and physical-logarithm margins. Repricing the full rate $H|\ell|+|B|+|Q|$ gives transported bounds $3835.03443334\ldots$ and $39817.9448843\ldots$. Independent 1024-bit arithmetic with an alternate gamma identity encloses the producing 512-bit inequalities. Complex-radius analyticity refers to this fixed-source extension, not a literal complex-z modulus expectation. □

A larger original-source analytic halo (N6)

The wider atlas needs a proved source bound, not extrapolation of old order-circle coefficients. Let $F = T_8$, $X = |S_8|$, $Y = |\Lambda_8|^2$, and let s_0 be the exact original-Haar zero-certificate centre. On the real radius interval $[4493/5000, 2251/2500]$, put $z_+ = 2251/2500$ and $d_+ = 1 - z_+^2$. The inherited four-angle comparison gives, for $0 < q < 2$,

$$D_4(q) = 2\pi^{-q}\frac{\Gamma(1-q/2)}{\Gamma(q/2)}\left(\frac{1}{q} + \frac{1}{2-q}\right), \tag{N6.1}$$

$$C(H,a) = \frac{8^8}{8!}\left(\frac{1+z_+}{1-z_+}\right)^4 D_4(2aH), \qquad a > 1, \quad aH < 1. \tag{N6.2}$$

It bounds the negative mark moment uniformly in the conditioned translation. The inverse-mark singularity is integrated, not treated as bounded. The original Haar density is retained before the comparison majorant is applied.

Lemma N6.1 (Physical order/tilt majorant)**.** *Assume the preceding inverse comparison, the inherited $\mathbb{E}X^2 \le 1$, and $\mathbb{E}Y^v \le d_+^{-v^2}$ for real v. Let $0 < H < 1$, $a > 1$, $aH < 1$, $b = a/(a-1)$, $C(H,a) \ge 1$, and $\sigma = |\Re s_0| + \rho$. For $|h| \le H$, $|s - s_0| \le \rho$,*

$$\mathbb{E}|X^{2h}Y^s| \le \max\left\{d_+^{-\sigma^2/(1-H)}, C(H,a)^{1/a}d_+^{-b\sigma^2}\right\}. \tag{N6.3}$$

The strict inverse margin also permits the fixed logarithmic powers needed for holomorphy in h, s on a neighborhood of the closed disks.

Proof. For $u = \Re h < 0$, Lyapunov gives $\mathbb{E}X^{2au} \le (\mathbb{E}X^{-2aH})^{-u/H} \le C(H,a)$. Hölder with exponents a, b gives the second term. For $0 \le u \le H$, use Hölder with exponents $1/H, 1/(1-H)$ and $\mathbb{E}X^{2u/H} \le (\mathbb{E}X^2)^{u/H} \le 1$. The first term follows. At zero, continuity applies. Any fixed logarithmic power is absorbed by a sufficiently small further power within the strict inverse-integrability margin; the determinant has no zero for real z in this compact interval below one. Dominated differentiation then yields the stated holomorphy. □

Executing (N6.3) at $H = 1/4$, $\rho = 3/20$ gives a strict real absolute-integrand bound of 879. The inherited physical source flow has real radius anchors in $[.899, .9]$, complex-radius halo $1/2500$, angular halo $1/100$, and the same proved matrix floor. If L, B, Q are its log-mark, preparation, and full state-dependent Jacobian rates, the transported bound is

$$M_{\mathrm{real}} \exp\big((HL + B + Q)/2500\big) < 156827.$$

The state-dependent inverse-matrix term in the Jacobian is retained. These inequalities were independently reconstructed at 1024 bits from the physical formulas, including the gamma recurrence and full flow. The complex-radius function here is the proved transported holomorphic extension; it is not the literal modulus integral evaluated at complex z.

For tilt derivatives, with $L_Y = \log Y$ and $t > 0$,

$$|L_Y|^k e^{vL_Y} \le \left(\frac{k}{et}\right)^k \big(e^{(v+t)L_Y} + e^{(v-t)L_Y}\big).$$

This follows by maximizing $x^k e^{-tx}$ on each half-line. Apply the sign-specific physical comparison separately to both terms. Complex-radius Cauchy bounds on a larger tilt disk and the inherited two-constants estimate then price radius derivatives. If the half-disk radius is $\eta = 1/2500$ and $0 < e < \eta$, its harmonic-measure exponent is

$$\omega = \frac{2}{\pi} \arctan \frac{2\eta e}{\eta^2 - e^2} = \frac{4}{\pi} \arctan(e/\eta).$$

This gives the effective bound $A^{1-\omega} B^{\omega}/e$ when A bounds the real diameter and B the complex halo. The exact rational choices and outward results are stored in the new resource receipts; floating searches only propose parameters and carry no proof authority.

The auxiliary tilt disk $|s - s_0| \le .15$ need not be contained in the original $|s| \le 3$ target. It is legitimate for this analytic estimate because $z < 1$ keeps the determinant away from zero. Every queried zero tube is separately checked to lie inside $|s| \le 3$. The larger source halo $|h| \le .25$ is not itself a zero theorem.

A correlated majorant for the original Haar source (Q2)

Put $X_z = |S_8(z)|$, $Y_z = |\Lambda_8(z)|^2$, $p = 19/20$ and $v_0 = \Re s_0$, where s_0 is the exact original zero centre. A previously admitted positive physical scalar gives

$$A_0 = \mathbb{E} X_{0.9}^{-2p} Y_{0.9}^{v_0} < 4.966606674. \tag{Q2.1}$$

The implementation obtains the outward upper endpoint from its full rational midpoint and error budget, and checks membership in the pinned released review. A locally recomputed hash alone is not admission.

Transport of this single positive anchor

The exact Möbius representation is

$$S_N = Nz + \operatorname{Tr} V, \qquad A_{N,z,s}(w) = (1 - z^2)^{N^2 + 2Ns} \prod_{j=1}^{N} (1 + z w_j)^{-(N+s)} (1 + z/w_j)^{-(N+s)}.$$

Both exponents are the same complex number. The complex preparation is not normalized into a probability measure.

For the inherited real angular flow, write

$$x = (\Re S_8, \Im S_8)^T, \qquad R = x^T x, \qquad D_j = (-\sin\theta_j, \cos\theta_j)^T,$$
$$G = \sum_j D_j D_j^T, \qquad M = G + RI, \qquad u = M^{-1} e_1.$$

The flow is $\theta_j' = -8 D_j^T u$. On $J = [0.8986, 0.9004]$, the inherited complete-square population inequality gives $M \ge cI$, $c = 2/5$, uniformly in all real angles. The three explicit lower candidates are

$$(8z_-)^2/25 - 3/2, \qquad 8/3 - (8z_+)^2/23, \qquad (8 - 8z_+)^2,$$

and each exceeds 2/5. Collisions and mark zeros are included. Since $M \geq RI$ as well,

$$|x|\|M^{-1}\| \leq c^{-1/2}, \qquad \|\theta'\|_2 \leq V = 8c^{-1/2}, \qquad R' = R\ell, \quad |\ell| \leq L = 16c^{-1/2}.$$

The full density/Jacobian rate after the exact Vandermonde cancellation is

$$Q = 8^2 t^T u + 8\sum_j D_j^T M^{-1} M_j u, \quad t = x - 8ze_1, \quad M_j = E_j D_j^T + D_j E_j^T + 2(x^T D_j)I,$$

where $E_j = -(\cos\theta_j, \sin\theta_j)^T$. The three terms in the last sum are bounded using Cauchy–Schwarz, $\operatorname{tr}(GM^{-1}) \leq 2$ and the commutation of G and M^{-1}. This yields

$$J_Q = 64\left(c^{-1/2} + 8z_+/c\right) + 8\left((\sqrt{2}+2)/c + 2c^{-1/2}\right).$$

For $d_+ = 1 - z_+^2$, the complete positive preparation contributes at most

$$J_B = (64 + 16v_0)\frac{2z_+}{d_+} + (8 + v_0)\left(\frac{16}{1 - z_+} + \frac{2z_+}{d_+}\sqrt{8}\,V\right).$$

The bound $2z/(1-z^2)$ for the angular logarithmic derivative of a paired preparation factor is its exact elementary maximum. Thus

$$\mathbb{E}X_z^{-2p}Y_z^{v_0} \leq A_0 \exp(K|z - 0.9|), \qquad K = pL + J_B + J_Q < 6351.166. \tag{Q2.2}$$

This is transport under a real diffeomorphism with the full Jacobian and preparation. The singular set is preserved. It does not differentiate an unpriced finite approximation or assume an integrable second-radius derivative.

For the whole analytic real diameter, one may use $A < 36111.571$. For a real panel $I = [a, b] \subset J$, the sharper bound

$$A_I = A_0 \exp\left(K \max\{|a - 0.9|, |b - 0.9|\}\right) \tag{Q2.3}$$

is valid. In particular, $A_{[0.899,0.9]} < 2846.663$. This smaller number is used only for real-panel physical tilt derivatives. It is never substituted into a larger complex-radius analytic halo.

Theorem Q2.1 (Correlated positive-source comparison)**.** *For real $z \in I$, $-p < u < 1$ and real v, put $T_+(u, v; z) = \mathbb{E}X_z^{2u}Y_z^v$. If $-p < u < 0$ and $\lambda = -u/p$, then*

$$\log T_+(u, v; z) \leq \lambda \log A_I + (-\log d_+)\frac{(v - \lambda v_0)^2}{1 - \lambda}. \tag{Q2.4}$$

For $0 \leq u < 1$,

$$\log T_+(u, v; z) \leq (-\log d_+)\frac{v^2}{1 - u}. \tag{Q2.5}$$

Consequently these bounds, at $u = \Re h$, $v = \Re s$, majorize $|F(h, s, z)|$.

Proof. The inherited original-source Schur identity gives $\mathbb{E}Y_z^q \leq (1 - z^2)^{-q^2}$ for every real q, and the exact mark identity gives $\mathbb{E}X_z^2 = 1 - z^{16} \leq 1$. For negative u, factor the positive integrand as

$$X^{2u}Y^v = (X^{-2p}Y^{v_0})^\lambda (Y^{(v - \lambda v_0)/(1-\lambda)})^{1-\lambda}$$

and apply Hölder under the same Haar measure. For positive u, apply Hölder to $(X^2)^u Y^v$. All auxiliary real determinant powers are integrable for $z < 1$, even if their exponents leave the public tilt box. □

The logarithmic bounds are jointly convex on each half-plane $u < 0$ or $u \geq 0$: the quadratic terms are perspectives of a convex quadratic. Their exponentials are convex. A closed exponent rectangle is therefore bounded by its vertices, splitting it at $u = 0$ when necessary. This is a continuum inequality, not sampling.

Tilt derivatives and moving-tube correlation

For integer $k \geq 1$ and $t > 0$,

$$|\log Y|^k Y^v \leq \left(\frac{k}{et}\right)^k (Y^{v+t} + Y^{v-t}).$$

Theorem Q2.1 bounds the two shifted positive moments at the same real order. The resulting sum is convex on each half-rectangle. The execution uses $t_9 = 47/40$ and $t_{10} = 5/4$ for the ninth and tenth tilt derivatives.

On each complete order-boundary arc and real-radius panel, enclose $\Re h$ and $\Re(c(h,z)+u)$ jointly, with $|u| \leq \rho$. For tilt interpolation, enlarge the second interval to the convex hull with all nine fixed nodes $c_0 + k/100$, $-4 \leq k \leq 4$. The real-panel anchor (Q2.3) is then used on this same cell. Hermite–Genocchi interpolation applies on this entire convex hull. This retains the order, moving-tilt and radius dependence before maximization; it asserts no unproved cancellation of errors.

The fixed-preparation Cauchy alias and Taylor-tail bounds use their own rectangular physical halo. In particular, the new real contract on $|h| \leq 0.7$, $|s - s_0| \leq 0.25$ is 6157. The common tilt contour has radius 0.24 about c_0 and lies inside that physical halo after the exact centre offset is included. The complex-radius continuation and its full source-flow Jacobian remain inherited from T3 and N6 and explicitly priced at radius $\eta = 1/2500$ via $M_{\text{complex}} = M_{\text{real}} \exp((HL + B + Q)/2500)$, scaling the inherited radius contour inequalities by $M_{\text{complex}}/2048$.

6. The rank-two diagonal from its trace distribution

The trace integral and exact integer benchmarks

For $N = 2$, $s = h$ and $0 < z < 1$, set $a = 2z$. A direct calculation from the characteristic polynomial gives

$$T_2(h,h;z) = (1-z^2)^{2h}\mathbb{E}|\Lambda_2'(z)|^{2h} = (1-z^2)^{2h}\mathbb{E}|\operatorname{Tr} U - a|^{2h}.$$

Indeed, $\Lambda_2(z) = 1 - z\operatorname{Tr} U + z^2 \det U$ and $\overline{\det U}\operatorname{Tr} U = \overline{\operatorname{Tr} U}$. The trace has a uniform angle independent of its radius, whose density on $(0,2)$ is $\sqrt{4-r^2}/\pi$. For $r \neq a$, the angular mean of $|re^{i\theta} - a|^{2h}$ equals $\max(r,a)^{2h}\,{}_2F_1(-h,-h;1;(\min(r,a)/\max(r,a))^2)$: expanding the two binomial factors leaves their equal Fourier modes. Thus, for $\Re h > -1$,

$$\begin{aligned}\frac{\pi T_2(h,h;z)}{(1-z^2)^{2h}} &= a^{2h}\int_0^a \sqrt{4-r^2}\,{}_2F_1(-h,-h;1;r^2/a^2)\,dr \\ &\quad + \int_a^2 \sqrt{4-r^2}\,r^{2h}\,{}_2F_1(-h,-h;1;a^2/r^2)\,dr.\end{aligned}$$

The integrals are improper at $r = a$ when needed. Convergence follows directly from local planar integrability at the shifted point, where the trace density is smooth and nonzero. At $z = 0$ the unshifted trace has its stronger restriction $\Re h > -1/2$. For $h = q$ a nonnegative integer, the angular binomial sum terminates and the centre moments give

$$\mathbb{E}|\Lambda_2'(z)|^{2q} = \sum_{j=0}^{q}\binom{q}{j}^2 (2z)^{2(q-j)}\frac{1}{j+1}\binom{2j}{j}.$$

In particular the unscaled second moment is $1 + 4z^2$, and $T_2(1,1;z) = (1-z^2)^2(1+4z^2)$. This representation supplies an independent numerical benchmark for the differential equation derived next.

A third-order equation and its interior connection coefficients

Proposition 6.1 (rank-two diagonal equation and connection coefficients). The Mellin transform of the trace integral gives the governing differential equation and fixes the interior solution. Write $x = z^2$, $\beta = h + 1/2$, $\vartheta = x\,d/dx$, and set

$$H_h(x) = \mathbb{E}\big|\operatorname{Tr} U - 2\sqrt{x}\big|^{2h}, \qquad T_2(h,h;z) = (1-x)^{2h} H_h(x).$$

For $0 < x < 1$ and $\Re h > -1$, H_h solves the third-order Fuchsian equation

$$\big[\vartheta^2(\vartheta-\beta) - x(\vartheta-h)^2(\vartheta-h-1)\big]\, H_h = 0.$$

When $\beta \notin \mathbb{Z}$ its interior solution is

$$\begin{aligned} H_h(x) &= A_h\, {}_3F_2\!\left(\begin{matrix}-h,-h,-h-1\\ 1,\ 1/2-h\end{matrix}; x\right) \\ &\quad + B_h x^{\beta}\, {}_3F_2\!\left(\begin{matrix}1/2,\ 1/2,\ -1/2\\ h+3/2,\ h+3/2\end{matrix}; x\right), \\ A_h &= \frac{4^h \Gamma(h+1/2)}{\sqrt{\pi}\,\Gamma(h+2)}, \qquad B_h = \frac{2\cdot 4^h \Gamma(1+h)\Gamma(-h-1/2)}{\pi\,\Gamma(-h)\Gamma(h+3/2)}. \end{aligned}$$

Thus the fractional-power term in z starts with $B_h z^{2h+1}$. Multiplication by $(1-z^2)^{2h}$ preserves this coefficient in T_2. At nonnegative integral h, $1/\Gamma(-h) = 0$ and the first series terminates. The equation for T_2 follows by substituting $H_h = (1-x)^{-2h} T_2$; conjugation replaces each ϑ by $\vartheta + 2hx/(1-x)$. Its singular points stay in $\{0, 1, \infty\}$.

Mellin derivation.

Let $0 < t < 1$ denote the squared trace radius divided by four. Its density is $(2/\pi) t^{-1/2}(1-t)^{1/2}$. Write $K_h(y)$ for the circular mean of $|1 - \sqrt{y} e^{i\theta}|^{2h}$, so $4^{-h} H_h(x)$ is the average of $t^h K_h(x/t)$. Begin with real $-1/2 < h < 0$ and $0 < p < -h$. The Mellin transform of K_h is

$$\int_0^\infty y^{p-1} K_h(y)\, dy = \frac{1}{\pi} \int_{\mathbb{C}} |w|^{2p-2} |1-w|^{2h}\, d^2 w = \frac{\Gamma(p)\Gamma(1+h)\Gamma(-p-h)}{\Gamma(1-p)\Gamma(-h)\Gamma(1+p+h)}.$$

One elementary evaluation writes $|w|^{-2(1-p)}$ and $|1-w|^{2h}$ as Laplace integrals with parameters u, v. The complex Gaussian integral is $\pi(u+v)^{-1} \exp[-uv/(u+v)]$. The change $u = Lq$, $v = L(1-q)$ first gives a gamma integral in L, then a beta integral in q. All interchanges here follow by positivity for the stated real parameters. Multiplication by the beta moment $\mathbb{E}[t^{p+h}]$ gives

$$M(p) := \int_0^\infty x^{p-1} 4^{-h} H_h(x)\, dx = \frac{\Gamma(1+h)}{\sqrt{\pi}\,\Gamma(-h)} \frac{\Gamma(p)\Gamma(-p-h)\Gamma(p+h+1/2)}{\Gamma(1-p)\Gamma(1+p+h)\Gamma(p+h+2)}.$$

Mellin inversion uses any vertical line in $0 < \Re p < -h$; there $M(p) = O((1+|\Im p|)^{-2h-7/2})$ by Stirling's formula. For $0 < x < 1$ close leftwards. To see the contour bound explicitly, reflection puts the variable gamma quotient in the form

$$\frac{\sin(\pi(p+h+1))\sin(\pi(p+h+2))}{\sin(\pi p)\sin(\pi(p+h+1/2))} \frac{\Gamma(-p-h)^2\Gamma(-p-h-1)}{\Gamma(1-p)^2\Gamma(1/2-p-h)}.$$

Take $\Re p = -k + c$ with c fixed away from the two pole lattices. The sine quotient is bounded there and the gamma quotient is $O(|p|^{-2h-7/2})$ uniformly for large k. The factor x^{-p} then makes the shifted contour vanish. The simple poles at $p = -j$ and $p = -\beta - j$, $j = 0, 1, \ldots$, give the two series displayed above. Their initial residues times 4^h are A_h, B_h, and successive residues give the hypergeometric coefficient ratios. The first series has constant term one and coefficient ratio $(j-h)^2(j-h-1)/[(j+1)^2(j+1-\beta)]$ from index j to $j+1$. The second follows from the conjugation $x^{-\beta}\vartheta x^{\beta} = \vartheta + \beta$. This yields the displayed differential equation for each branch. For each fixed $0 < x < 1$, the defining expectation is holomorphic in $\Re h > -1$ because the shifted trace law has a smooth planar density near the origin. On compact interior x-intervals it is also smooth in x: localize

near the shifted point and move derivatives onto its smooth density, differentiating the remaining nonsingular kernel directly. Analytic continuation in h now proves the formula, with removable limits at the resonances.

Resonance and a logarithmic leading term.

Within $\Re h > -1$ the resonant values are $h = k - 1/2$, $k = 0, 1, \ldots$. Take the limit of the *sum* of the two branches. The residue of B_h is

$$b_k = \frac{2\,4^{k-1/2}(-1)^{k+1}\Gamma(k+1/2)}{\pi\,(k!)^2\Gamma(1/2-k)}.$$

Since $x^{h+1/2} = x^k[1+(h-k+1/2)\log x+\cdots]$, the solution equals an analytic series plus $b_k x^k \log x$ times the second hypergeometric series evaluated at $h = k - 1/2$. The residue from the analytic branch cancels the opposing pole. For example $b_0 = -1/\pi$ and $b_1 = -1/\pi$. This limiting prescription also specifies the nonlogarithmic coefficients, without equating a divergent branch to the physical moment.

A computed nonanalytic coefficient at size two

Proposition 6.2 (coefficient of the fractional power at the centre). For $-1/2 < h < 0$ real, let $M_h(z) = \mathbb{E}|\Lambda_2'(z)|^{2h}$. As $z \downarrow 0$ one has

$$M_h(z) = \frac{4^h\Gamma(h+1/2)}{\sqrt{\pi}\,\Gamma(h+2)} + c_h z^{2h+1} + O_h(z^{2h+2}), \qquad c_h = \frac{2^{2h+1}\Gamma(1+h)\Gamma(-h-1/2)}{\pi\Gamma(-h)\Gamma(h+3/2)} < 0. \tag{6.1}$$

Since $0 < 2h+1 < 1$, the error is of strictly smaller order. The determinant proof below gives this remainder. The sign, normalization and exponent refer to the original derivative moment, without a power of $1 - z^2$.

The same cusp from the large-source determinant.

The leading determinant tail determines the coefficient in (6.1). Set $a = 2z$, $D(t) = D_2(t;0,0) = J_0(t)^2 + J_1(t)^2$ and $C(h) = 2^{2h+1}\Gamma(1+h)/\Gamma(-h)$. Write $X = \operatorname{Tr} U$. Since its law is rotationally invariant, the circular Fourier mean of $X - a$ is $D(t)J_0(at)$. The Mellin formula therefore gives directly

$$M_h(z) - M_h(0) = C(h)\int_0^\infty t^{-2h-1}D(t)\,[J_0(at) - 1]\,dt.$$

For clarity, this follows first on $-1/4 < \operatorname{Re} h < 0$ by the absolute Mellin transform and Fubini, and then on $-1/2 < \operatorname{Re} h < 0$ by holomorphy. Both terms of the Mellin difference are absolutely integrable there: $D(t) = O(t^{-1})$ at infinity, and no subtraction is needed at zero when $\operatorname{Re} h < 0$.

Write $D(t) = 2/(\pi t) + E(t)$, where $E(t) = O(t^{-1})$ for $t \le 1$ and $E(t) = O(t^{-2})$ for $t \ge 1$. Using $|J_0(at) - 1| \le C\min(a^2t^2, 1)$, split the E integral at 1 and $1/a$. For fixed $-1/2 < h < 0$ its three bounds are respectively $O_h(a^2)$, $O_h(a^2\int_1^{1/a} t^{-2h-1}\,dt)$, and $O_h(\int_{1/a}^\infty t^{-2h-3}\,dt)$. Thus the remainder is $O_h(a^{2h+2})$, and the leading term is

$$\frac{2C(h)}{\pi}\,a^{2h+1}\int_0^\infty u^{-2h-2}[J_0(u) - 1]\,du.$$

With $\alpha = 2h+1 \in (0,1)$, integration by parts and $J_0' = -J_1$ give the absolutely convergent integral $-\alpha^{-1}\int_0^\infty u^{-\alpha}J_1(u)\,du$ when $\alpha > 1/2$, and the ordinary convergent integral when $0 < \alpha \le 1/2$. The Bessel Mellin formula (NIST DLMF 10.22.43) in its improper-convergence strip, or continuation from $\alpha > 1/2$, gives

$$\int_0^\infty u^{-2h-2}[J_0(u) - 1]\,du = 2^{-2h-2}\frac{\Gamma(-h-1/2)}{\Gamma(h+3/2)}.$$

One recovers exactly c_h in (6.1), now with error $O_h(z^{2h+2})$. In this domain the leading cusp is therefore determined solely by the $2/(\pi t)$ term of the determinant at large source.

Independent spatial calculation.

For $U \in U(2)$, $X = \operatorname{Tr} U$ satisfies $X/\det U = \overline{X}$. Consequently $|\Lambda_2'(z)| = |-X + 2z \det U| = |X - 2z|$ for real z. The radial probability density of $|X|$ at $z = 0$ is $\sqrt{4 - r^2}/\pi$ for $0 < r < 2$. Rotational invariance therefore gives the planar density

$$p(x) = \frac{\sqrt{4 - |x|^2}}{2\pi^2 |x|} \mathbf{1}_{\{|x|<2\}} = \frac{1}{\pi^2 |x|} + O(|x|) \quad (x \to 0).$$

Integration of the radial density against r^{2h} gives the constant term in (6.1).

Localization.

Write $a = 2z$, $e = (1, 0)$, $g(x) = |x|^{2h}$, and choose a smooth radial compactly supported χ equal to one near zero. The function $p(x) - \chi(x)/(\pi^2|x|)$ is bounded and compactly supported. Since $|\nabla g| = |2h|\,|x|^{2h-1}$ is locally integrable when $h > -1/2$, its contribution to $\int [g(x - ae) - g(x)]p(x)\, d^2x$ is $O_h(a)$, by the L^1 translation inequality on a bounded disk. The complementary integral with weight $(1 - \chi(x))/|x|$ is $O_h(a)$ as well: the absolute mean-value bound at infinity has radial integral a constant times $a \int_1^\infty r^{2h-1}\, dr$. Hence

$$M_h(z) - M_h(0) = \pi^{-2} a^{2h+1} I_h + O_h(a), \qquad I_h = \int_{\mathbb{R}^2} \frac{|y - e|^{2h} - |y|^{2h}}{|y|}\, d^2y.$$

This difference is absolutely integrable: the conditions at 0, at e and at infinity are respectively $h > -1/2$, $h > -1$ and $h < 0$.

Evaluation of the translation integral.

Set $q = -h \in (0, 1/2)$. The gamma integral for $|y - e|^{-2q}$ and its unshifted counterpart gives

$$I_h = \frac{1}{\Gamma(q)} \int_0^\infty t^{q-1} \int_{\mathbb{R}^2} \frac{e^{-t|y-e|^2} - e^{-t|y|^2}}{|y|}\, d^2y\, dt.$$

The sign of the numerator is independent of t at each y; thus the absolute joint integral is the absolute spatial difference already bounded. Insert $|y|^{-1} = \pi^{-1/2} \int_0^\infty v^{-1/2} e^{-v|y|^2}\, dv$ and complete the square in y. The result is

$$I_h = \frac{\sqrt{\pi}}{\Gamma(q)} \int_0^\infty \int_0^\infty \frac{t^{q-1} v^{-1/2}}{t + v} \left(e^{-tv/(t+v)} - 1 \right) dv\, dt.$$

With $t = Lu$, $v = L(1 - u)$, use $\int_0^\infty L^{q-3/2}(e^{-bL} - 1)\, dL = \Gamma(q - 1/2) b^{1/2-q}$, from integration by parts, and $\int_0^1 u^{-1/2}(1 - u)^{-q}\, du = B(1/2, 1 - q)$. This yields

$$I_h = \pi \frac{\Gamma(q - 1/2)\Gamma(1 - q)}{\Gamma(q)\Gamma(3/2 - q)},$$

which is negative and gives (6.1).

Independent numerical check.

At $h = -1/4$ the predicted coefficient is $-0.82279292505\ldots$. As a check, angular averaging at each radius gives $\max(r, a)^{2h}\, {}_2F_1(-h, -h; 1; \min(r, a)^2/\max(r, a)^2)$. Integrating the difference from r^{2h} against the radial density, with the integral split at $r = a$, gives the following values of $[M_h(z) - M_h(0)]/z^{2h+1}$:

z	10^{-2}	10^{-3}	10^{-4}
scaled difference	-0.82288470	-0.82279597	$-0.82279302.$

7. The rank-two differential equation from the planar determinant

Theorem 7.1 (rank-two differential equation and connection formula). Let U be Haar on $U(2)$, $X = \operatorname{Tr} U$, $x = z^2$, and $H_h(x) = \mathbb{E}|X - 2\sqrt{x}|^{2h}$. Complex powers of a positive real use its real logarithm. The characteristic-polynomial identity $\Lambda_2(z) = 1 - zX + z^2 \det U$ and $X/\det U = \bar{X}$ give, for real z,

$$|\Lambda_2'(z)| = |X - 2z|, \qquad T_2(h, h; z) = (1 - x)^{2h} H_h(x).$$

In the following proof the only distributional input is the marked Toeplitz determinant at the centre. No formula for the trace density is used.

The determinant and a small-ball estimate. In the Fourier convention $D(\xi) = \mathbb{E}e^{i \operatorname{Re}(\bar{\xi} X)}$, the symbol at $s = z = 0$ is $e^{it\cos\theta}$ after rotation, where $t = |\xi|$. The Fourier coefficients of indices $0, 1, -1$ are $J_0(t), iJ_1(t), iJ_1(t)$. The defining two-by-two determinant is therefore

$$D(t) = J_0(t)^2 + J_1(t)^2.$$

For $a > 0$ the circular Fourier average for $X - a$ is $D(t)J_0(at)$, by the integral representation of J_0. Fourier inversion of an ordinary planar Gaussian gives, for $v > 0$,

$$\mathbb{E}e^{-v|X-a|^2} = \frac{1}{2v} \int_0^\infty t e^{-t^2/(4v)} D(t) J_0(at)\, dt. \tag{7.1}$$

The Bessel expansion gives $D(t) = 2/(\pi t) + O(t^{-2})$. Consequently, for a in any positive compact interval,

$$tD(t)J_0(at) = \frac{2}{\pi}\sqrt{\frac{2}{\pi a}} t^{-1/2} \cos(at - \pi/4) + O(t^{-3/2})$$

uniformly for $t \geq 1$. Its integral from 0 to L is bounded independently of L and locally uniformly in a, by integration by parts in the leading oscillation. An integration by parts against the decreasing Gaussian factor in (7.1) preserves this bound, uniformly in v. With $v = r^{-2}$ the indicator of $|X - a| \leq r$ is at most $e\, e^{-v|X-a|^2}$. Thus $\mathbb{P}(|X - a| \leq r) \leq C_a r^2$. At $a = 0$ the same formula and $D = O((1 + t)^{-1})$ give $O(r)$ as $r \downarrow 0$. The bounds imply, by a dyadic decomposition at zero and $|X| \leq 2$, that $H_h(x)$ is holomorphic in $\Re h > -1$ at every $x > 0$; the estimates are locally uniform in $x > 0$. This establishes the needed physical domain directly from the determinant. No nonzero lower density or full support statement is needed for this continuation.

Two Mellin transforms. Start with real $-1/4 < h < 0$. Integrate (7.1) against $v^{-h-1}\, dv/\Gamma(-h)$. The left side gives the physical moment at $a = 2\sqrt{x}$. The absolute interchange on the right is licensed by $\int_0^\infty t^{-2h-1}|D(t)J_0(at)|\, dt < \infty$: the integrand is $O(t^{-2h-1})$ at zero and $O(t^{-2h-2})$ at infinity even without the translated Bessel decay. The resulting planar finite-part formula in this base strip is an ordinary integral,

$$H_h(x) = C(h) \int_0^\infty t^{-2h-1} D(t) J_0(2t\sqrt{x})\, dt, \qquad C(h) = \frac{2^{2h+1}\Gamma(1 + h)}{\Gamma(-h)}. \tag{7.2}$$

The random variable on the left of (7.2) is defined for all $x > 0$; the restriction $z < 1$ is only needed when identifying the scaled moment T_2.

Take the Mellin transform in x on a vertical line $0 < \Re p < -h < 1/4$, and set $q = h + p$. The substitution $u = 2t\sqrt{x}$ and the Bessel Mellin integral yield

$$\int_0^\infty x^{p-1} J_0(2t\sqrt{x})\, dx = t^{-2p} \frac{\Gamma(p)}{\Gamma(1 - p)}.$$

Fubini is absolute, because the same integral with absolute values is bounded by a constant times $t^{-2\Re p}$ ($\Re p < 1/4$), and $-1/2 < \Re q < 0$ makes $t^{-2\Re q - 1} D(t)$ integrable. The equal-argument Weber–Schafheitlin integral is

$$\int_0^\infty t^{-\lambda} J_\nu(t)^2 dt = \frac{\Gamma(\lambda)\Gamma(\nu + (1 - \lambda)/2)}{2^\lambda \Gamma((1 + \lambda)/2)^2 \Gamma(\nu + (1 + \lambda)/2)}, \qquad 0 < \Re\lambda < 2\nu + 1.$$

Apply it separately at $\nu = 0, 1$ with $\lambda = 1 + 2q$. The $\nu = 1$ integral is $(-q)/(1 + q)$ times the $\nu = 0$ integral. Adding and applying gamma duplication gives

$$\int_0^\infty t^{-2q-1} D(t)\, dt = \frac{\Gamma(q + 1/2)\Gamma(-q)}{2\sqrt{\pi}\, \Gamma(q + 1)\Gamma(q + 2)}.$$

These two classical Bessel integrals are NIST DLMF 10.22.43 and 10.22.57, with their absolute-convergence hypotheses checked above. Combining the factors gives the transform

$$\mathcal{M}(p) = \int_0^\infty x^{p-1} 4^{-h} H_h(x)\, dx = \frac{\Gamma(1+h)}{\sqrt{\pi}\,\Gamma(-h)} \frac{\Gamma(p)\Gamma(-p-h)\Gamma(p+h+1/2)}{\Gamma(1-p)\Gamma(1+p+h)\Gamma(2+p+h)}. \tag{7.3}$$

The two interior branches. Write $\beta = h + 1/2$, $\vartheta = x\, d/dx$. The inverse Mellin integral of (7.3) on the displayed line exists absolutely: the quotient is $O((1+|\Im p|)^{-2h-7/2})$. The function obtained is $4^{-h} H_h(x)$ at every $x > 0$, by continuity from (7.2). For $0 < x < 1$ shift the line left. In fact, reflection puts the variable gamma quotient in the form

$$\frac{\sin \pi(p+h+1) \sin \pi(p+h+2)}{\sin \pi p \sin \pi(p+\beta)} \frac{\Gamma(-p-h)^2 \Gamma(-p-h-1)}{\Gamma(1-p)^2 \Gamma(1/2-p-h)}.$$

On lines $\Re p = -m + d$ a fixed distance from the two left pole lattices, the sine quotient is bounded. Uniform Stirling estimates on the right half-plane for $-p$ give the same polynomial decay in $|p|$ as before, and x^{m-d} sends the shifted-line integral to zero. Horizontal sides tend to zero for each finite shift by Stirling. The poles $p = -j$ and $p = -\beta - j$ give

$$\begin{aligned} H_h(x) &= A_h\, {}_3F_2(-h, -h, -h-1; 1, 1/2-h; x) \\ &\quad + B_h x^\beta\, {}_3F_2(1/2, 1/2, -1/2; h+3/2, h+3/2; x), \\ A_h &= \frac{4^h \Gamma(h+1/2)}{\sqrt{\pi}\,\Gamma(h+2)}, \qquad B_h = \frac{2\, 4^h \Gamma(1+h)\Gamma(-h-1/2)}{\pi \Gamma(-h)\Gamma(h+3/2)}. \end{aligned} \tag{7.4}$$

For example, the second residue ratio from j to $j+1$ is $(j+1/2)^2(j-1/2)/[(j+1)(j+h+3/2)^2]$. The coefficient ratio of the first series is $(j-h)^2(j-h-1)/[(j+1)^2(j+1-\beta)]$. The two recurrences, or the hypergeometric equation, show that both contributions satisfy

$$\left[\vartheta^2(\vartheta-\beta) - x(\vartheta-h)^2(\vartheta-h-1)\right] H_h = 0. \tag{7.5}$$

This is Fuchsian with possible singularities $0, 1, \infty$. The equation for T_2 is conjugate via $H_h = (1-x)^{-2h} T_2$. Each ϑ is replaced by $\vartheta + 2hx/(1-x)$.

Continuation and resonances. For each fixed $0 < x < 1$, (7.4) is meromorphic in h and agrees on the real base interval with the physical moment. The determinant small-ball estimate and the identity theorem extend the equality throughout $\Re h > -1$, with each pole of the sum removable. Uniform convergence of both hypergeometric series on compact interior x-sets and on parameter circles away from the resonances permits differentiation in x there. Taking the constant Laurent coefficient on such a circle commutes with these derivatives. Consequently (7.5) holds also at the removable parameters.

For $h = k - 1/2$, $k = 0, 1, \ldots$, use the finite limit of the **sum**, because the individual branch expressions can diverge. The residue of B_h there is

$$b_k = \frac{2\, 4^{k-1/2}(-1)^{k+1}\Gamma(k+1/2)}{\pi (k!)^2 \Gamma(1/2-k)}.$$

The analytic-in-x residues cancel. The expansion $x^\beta = x^k(1 + (h-k+1/2)\log x + \cdots)$ leaves $b_k x^k \log x$ times the second hypergeometric series evaluated at $h = k - 1/2$, in addition to an analytic series. In particular $b_0 = b_1 = -1/\pi$. At $h = 0, 1, 2, \ldots$, the reciprocal gamma in B_h vanishes and the first branch terminates. In the nonresonant strip $-1/2 < h < 0$ the coefficient $B_h < 0$ multiplies the leading nonanalytic term z^{2h+1}. The factor $(1-x)^{2h}$ preserves that coefficient. The conditions at the origin, including the relative amplitudes of the two branches, are fixed by the determinant transform rather than a chosen ODE solution.

Independent controls. The companion `rank2_check.py` derives the integer-moment polynomials from the exact Taylor coefficients of the Bessel determinant and rotational symmetry, then tests every coefficient of the differential equation in rational arithmetic for $h = 0, \ldots, 10$. It also compares the connection formula with a direct determinant integral, integrated by a finite-part Taylor series below 1 and oscillatory quadrature above 1. At cutoff 16384 the discrepancies were 4.49×10^{-10} and 1.81×10^{-11} for $(h, x) = (-0.2, 0.13), (-0.125, 0.67)$. At the resonances $(-0.5, 0.23)$ and $(0.5, 0.37)$ they were 1.33×10^{-8} or less and 1.56×10^{-15} or less, respectively. The resonance values on the connection side were computed by taking a symmetric parameter limit at high precision. These quadratures are finite-cutoff numerical checks, not certified error bounds.

8. A fixed-point recurrence for the rank-two diagonal moment

Proposition 8.1 (rank-two exponent shifts). Let $x = z^2 \in (0,1)$ and $H_h(x) = T_2(h,h;z)/(1-x)^{2h}$. Let $\theta = x\partial_x$. Besides its third-order equation in x, the diagonal moment satisfies

$$\theta^2 H_{h+1} = 4x(h+1)^2 H_h, \qquad \Re h > -1.$$

Indeed the planar Laplacian of $|y|^{2h+2}$ is $4(h+1)^2|y|^{2h}$ in distributions for $\Re h > -1$. The boundary terms on a circle of radius ϵ vanish as $O(\epsilon^{2\Re h+2})$ or faster. Convolution with the compact trace law is allowed. The shift radius is $|a| = 2\sqrt{x}$ and the radial Laplacian on functions of x is $x^{-1}\theta^2$. On the open interval the rank-two equation gives smoothness, so the distributional identity is pointwise there.

This yields an explicit scalar, four-term **difference equation at a fixed spectral point**. The following minor formula specifies all coefficients without expanded polynomials. For $\Re h > 2$ write

$$\sum_{k=0}^{3} b_k(x,h) H_{h-k}(x) = 0.$$

To compute b_k, put

$$\sum_{i=0}^{3} p_i t^i = t^2(t-h-1/2) - x(t-h)^2(t-h-1), \qquad v_i = -p_i/p_3 \quad (0 \le i \le 2).$$

Start with the three-component row $r_0 = (1,0,0)$. The operator on rows is $(Dr)_i = x\partial_x r_i + r_{i-1} + r_2 v_i$, with $r_{-1} = 0$. For $k = 0,1,2$ form $r_{k+1} = D^2 r_k/[4x(h-k)^2]$. Set $b_k = (-1)^k \det(r_0, \dots, \widehat{r_k}, \dots, r_3)$, with rows in their original order. The vector $(H_h, \theta H_h, \theta^2 H_h)^{\mathsf{T}}$ evaluated against r_k equals H_{h-k} by the Laplacian relation and the Fuchsian equation. The alternating expansion of four rows in dimension three proves the claim. At $h = 3, x = 1/2$ the coefficient of H_{h-3} is nonzero, as the accompanying exact check verifies. The unnormalized minors allow specialization without an unnecessary division by a vanishing leading coefficient. The common physical domain $\Re h > 2$ ensures all four expectations exist. One may shift the recurrence forward by three to start with any $\Re h > -1$. This recurrence varies h on the diagonal $s = h$. Section 10 derives a separate recurrence with s fixed independently.

Small-radius evaluation with independent complex exponents

Let $u = \Re h$, $d = s - h$, and let T_N retain the unnormalised moment convention of Section 1. All powers of positive numbers use the real logarithm. Setting the tilt equal to the order reduces a two-parameter calculation to a diagonal one, but loses its correlation with the derivative mark. The first variation has a rotation cancellation, even when an inverse moment puts considerable mass near a zero of the derivative.

Proposition 8.2 (quadratic change of tilt). For $0 < z < 1$, any finite rank and any independent complex h, s for which the ordinary absolute moment $T_N(u,u;z)$ is finite, put

$$a = N[(1+z)^{N-1} - 1], \quad K = \max(2^{1-2u}, (3/2)^{2u-1}) \max(2^{2u}, (3/2)^{-2u}), \quad L = Nz/(1-z).$$

Then

$$|T_N(h,s;z) - T_N(h,h;z)| \le T_N(u,u;z) \left(4|d|za \max(1, |h|K) + |d|Nz^2/(1-z) + 2|d|^2 L^2 e^{2|d|L} \right).$$

The bracket is $O(z^2)$ uniformly for bounded ranks and compact parameter sets. The diagonal majorant can grow as $z \downarrow 0$. The quadratic power is sharp already at $h = 0, s = 1$ for every N: central rotation annihilates cross terms of unequal polynomial degrees in $\mathbb{E}|\Lambda_N|^2$, and its z^2 coefficient is $\mathbb{E}|\operatorname{Tr} U|^2 = 1$ by Haar entry orthogonality.

Proof. Write $X = \operatorname{Tr} U$, $V = -\Lambda_N'(z)$. The characteristic polynomial coefficients are elementary symmetric functions of unit eigenvalues, hence $|V - X| \le \sum_{k=2}^{N} k\binom{N}{k} z^{k-1} = a$. On $|X| \le 2a$, $||V|^{2h}\Re X| \le 2a|V|^{2u}$. On $|X| > 2a$ the mean of $|X|^{2h}\Re X$ is zero by rotational invariance of this restricted domain. Along the segment from X to V every modulus divided by $|X|$ belongs to $[1/2, 3/2]$. Differentiating the complex power along this segment gives

$$|X| \left| |V|^{2h} - |X|^{2h} \right| \le 2a|h|K|V|^{2u}.$$

Thus the absolute value of the integrated first Cartesian moment is at most $2a\max(1,|h|K)\mathbb{E}|V|^{2u}$. The eigenangle logarithm gives $|\log|\Lambda_N|| \le L$ and $|\log|\Lambda_N| + z\Re X| \le Nz^2/[2(1-z)]$. Subtract the linear term from $\exp(2d\log|\Lambda_N|)$, bound the quadratic Taylor remainder by $2|d|^2L^2e^{2|d|L}$, and restore the factor $(1-z^2)^{2h}$. This gives the asserted bound. The argument uses a positive majorant with real exponent u and takes the complex cancellation before bounding. □

Proposition 8.3 (signed inverse-order correction at rank two). Put $b = 4(1-z^2)^2$, $H = b^{-u}T_2(u,u;z)$, $0 < z \le 1/4$ and $-1 < u \le -1/2$. Define

$$M = \tfrac{1}{2}|d(d-1)|\max\{(1-z)^{4(\Re d-2)},(1+z)^{4(\Re d-2)}\},\quad J = \min(4+4z^2H, 64/49+64z^2H),\quad I = 4z+8z^2/(1+u).$$

An explicit absolute remainder for independent s is

$$\left|T_2(h,s;z) - (1-2dz^2)T_2(h,h;z)\right| \le b^u\left[4|d|zI + (6|d|+50M)z^2J + (3|d|+98M)z^4H\right].$$

In particular, on compact subsets of $-1 < \Re h < -1/2$, $s \in \mathbb{C}$, let

$$A(h) = \frac{4^h\Gamma(h+1/2)}{\sqrt{\pi}\,\Gamma(h+2)},\qquad C(h) = \frac{2\,4^h\Gamma(h+1)\Gamma(-h-1/2)}{\pi\Gamma(-h)\Gamma(h+3/2)}.$$

Then the first tilt-dependent fractional term is explicit:

$$T_2(h,s;z) = C(h)z^{2h+1} + A(h) + C(h)\left[-2s - \frac{1}{8(h+3/2)^2}\right]z^{2h+3} + O(z^2).$$

The remainder is absolute and uniform on those compact sets. The inverse ordinary moment at $z=0$ diverges throughout this open strip. The finite part $A(h)$ is a meromorphic coefficient. The two-branch expansion here excludes the logarithmic collision at $h=-1/2$; the finite-radius inequality includes it.

Proof. Represent the two eigenangles as $t\pm\gamma$, with t uniform and independent of $x=\cos\gamma$ of density $2\sqrt{1-x^2}/\pi$ on $[-1,1]$. This is the Weyl density $|e^{i(t+\gamma)} - e^{i(t-\gamma)}|^2$ in common and difference angles, with double covering absorbed by normalization. Write $D = |x - ze^{it}|$ and $P = |1 - 2zxe^{it} + z^2e^{2it}|^2$. Then $T_2 = b^h\mathbb{E}[D^{2h}P^d]$. The mark alone loses preparation information already at $t=0$: the two admissible points $x = z\pm R$ with $0 < R < 1-z$ have the same $D = R$ and different $P = (1 - z^2 \mp 2zR)^2$. Expanding P gives

$$P - 1 = -2z^2 - 4z\cos t\,(x - z\cos t) + 4z^2x^2 - 4z^3x\cos t + z^4.$$

The last three terms have modulus at most $6z^2x^2 + 3z^4$. Also $|P-1| \le 5z|x| + 7z^2$, so $|P-1|^2 \le 50z^2x^2 + 98z^4$. Since $(1-z)^4 \le P \le (1+z)^4$, Taylor's formula on the positive real segment gives $|P^d - 1 - d(P-1)| \le M|P-1|^2$. On $|x| > 2z$ use $D \ge |x|/2$ and $2u+2 \ge 0$ to obtain $x^2D^{2u} \le 4$; on its complement $x^2 \le 4z^2$. Splitting instead at $8z$ gives $x^2D^{2u} \le (8/7)^2$ on the far part and $x^2 \le 64z^2$ on its complement. Taking the smaller bound gives $\mathbb{E}[x^2D^{2u}] \le J$.

It remains to control the signed term $A_1 = \mathbb{E}[\cos t\,(x - z\cos t)D^{2h}]$. For almost every t substitution of $(2(h+1))^{-1}\partial_x D^{2(h+1)}$ and integration by parts gives the density factor $x/(\pi(h+1)\sqrt{1-x^2})$. The integrals are absolutely defined because the singularities of D at positive radius have two local coordinates and $u > -1$. The semicircle density vanishes at both endpoints. Subtract $|x|^{2(h+1)}$ in this integral, using the zero angular mean of $\cos t$. Set $\beta = 2u+2 \in (0,1]$. For $|x| > 2z$, differentiating along the translation bounds the remaining difference by $2|h+1|z\,2^{1-\beta}|x|^{\beta-1}$. Its contribution is at most $2^{2-\beta}z$ using $\int_{-1}^{1} dx/\sqrt{1-x^2} = \pi$. On $|x| \le 2z$ the difference is at most $(3^\beta + 2^\beta)z^\beta \le 5$, and the integral of $|x|/\sqrt{1-x^2}$ on this interval is at most $8z^2/\sqrt{3}$. Therefore $|A_1| \le I$. Combining the estimates proves the finite-radius inequality.

In the open strip the two diagonal hypergeometric branches give $H = O(z^{2u+1})$ uniformly on compact subsets, so the right side is $O(z^2)$. The analytic branch has constant term $A(h)$, and the fractional branch, including the diagonal normalization, has first relative correction $[-2h - 1/(8(h+3/2)^2)]z^2$. Multiplication by $1-2dz^2$ gives the stated coefficient. □

Rank-two computational realization. For $z > 0$, $u > -1$, the two-angle rule retains the preparation P^d and factors the moving derivative zero before quadrature. By sign and reflection symmetry one can integrate $q = \arcsin x \in [0,\pi/2]$ and $t \in [0,\pi]$, with total factor $4/\pi^2$ and weight $\cos^2 q$. Put $q_0 = \arcsin z$. Take the

left wing $a = -q_0$ and the right wing $a = \min(q_0, \pi/2 - q_0)$. Split each rectangle into $q = q_0 + arU$, $t = \pi rV$, $(U, V) = (1, y)$ or $(y, 1)$, $0 \le r, y \le 1$. The Jacobian is $|a|\pi r$ and

$$D^2/(a^2r^2) = U^2\cos^2(q_0 + arU/2)\operatorname{sinc}^2(arU/2) + \frac{z\sin q}{a^2}\pi^2V^2\operatorname{sinc}^2(\pi rV/2).$$

Here $\operatorname{sinc}(x) = \sin x/x$. The singular weight is exactly r^{2h+1}. Remaining radial intervals double from $q_0 + a_{\text{right}}$ to $\pi/2$. This scaling costs $O(1 + |\log z|)$ bands as $z \downarrow 0$. Subdividing both Duffy parameters at larger radii resolves the near-diagonal peaks from P^d.

For the central subpanel use Chebyshev interpolation at first-kind roots, integrated against r^α, $\alpha = 2h+1$. Write $m_k = \int_0^1 r^\alpha T_k(2r-1)dr$. Integration by parts using $(1-x^2)T_k' = k(T_{k-1} - xT_k)$ gives

$$m_0 = (1+\alpha)^{-1}, \quad m_1 = \alpha/[(1+\alpha)(2+\alpha)], \quad (k+\alpha+2)m_{k+1} = 2\alpha m_k + (k-\alpha-2)m_{k-1}.$$

The boundary term vanishes for $\Re\alpha > -1$. A cosine transform supplies weighted nodal sums. This fast binary64 path estimates error from successive degrees and an absolute-sum rounding floor. The finite remainder above and the archived diagonal interval implementation instead give an outward enclosure at small radius, with exact rational input conventions and a separate relative flag. The saved test cases identify which was used.

Corollary 8.4 (a uniform inverse-order evaluator on a continuous region). At rank two, throughout

$$0 < z \le 10^{-6}, \qquad -0.95 \le \Re h \le -0.75, \qquad |\Im h| \le 3, \qquad |s| \le 3,$$

put $x = z^2$, $Z = z^{2\Re h+1}$ and $f = -1/[8(h+3/2)^2]$. The explicit readout

$$Q = (1 - 2(s-h)x)(1-x)^{2h}\big[A(h) + C(h)z^{2h+1}(1+fx)\big]$$

has $|Q - T_2(h, s; z)| \le 2150x$ and $|T_2(h, s; z)| > 0.038Z$. A midpoint computed from an enclosure of Q with rounding radius at most $10^{-13}Z$ therefore has relative error less than 6×10^{-11} throughout the region. The computation is pointwise in its inputs. An enclosure of the range of all outputs would be unbounded as $z \downarrow 0$.

Proof. The accompanying interval check gives

$$|A(h)| < 6/5, \qquad 1/25 < |C(h)| < 5.$$

Specifically, partition the upper half of the stated order rectangle into 16×240 closed rectangles of side $1/80$ and use conjugation for the lower half. On each whole cell, evaluate the real parts of the analytic log-gammas with positive-real-part arguments in $\log|C|$. For $|A|$ use $\Gamma(h+1/2) = \Gamma(h+3/2)/(h+1/2)$ before taking moduli. The executable inequalities use exact rational endpoints and 128-bit Arb arithmetic. The extreme recorded cell enclosures give upper bounds below 1.174 and 4.841 and a lower bound above 0.0427. The code makes the three displayed rational comparisons before converting any diagnostic value to binary64.

Write the diagonal moment as $(1-x)^{2h}(AF_1 + Cz^{2h+1}F_2)$ with the two hypergeometric functions of the diagonal formula. Consecutive absolute terms are bounded in ratio by $64x$ and $4x$, respectively: in F_1 each numerator factor is at most $4(n+1)$ and both denominator parameters have real part at least one; in F_2 each numerator factor is at most $n+1$, and $|n+h+3/2| \ge 0.55(n+1)$. Thus $|F_1 - 1| \le 65x$, $|F_2 - 1| \le 5x$ and $|F_2 - 1 - fx| \le 17x^2$. Here $Z \ge 1000$, $Zx \le 10^{-6.6}$, and $1 \le |(1-x)^{2h}| < 1.0001$. The positive diagonal gives $H \le 21Z$, so $xH < 6 \times 10^{-6}$, $J < 1.307$ and $I \le 4.001z$. Since $|d| < 7$ and $M < 29$ (use $(1-z)^{-36}$ as a majorant for its power factor), the signed inverse-order bound is less than $2063x$. Replacing the two diagonal hypergeometric functions by 1 and $1 + fx$ in that approximation costs less than $81x$, using $|1 - 2dx| \le 1 + 14x$. The two errors sum to less than $2150x$. The reverse triangle inequality on the exact diagonal gives $|T_2(h, h; z)| \ge 0.04(1-5x)Z - 1.2(1+65x)$. Multiplication by a factor of modulus at least $1 - 14x$ followed by subtraction of $2063x$ yields $|T_2(h, s; z)| > 0.038Z$. Finally $x/Z \le 10^{-15}$, which proves the relative guarantee including rounding. □

The code evaluates Q at increasing precision and returns an arbitrary-exponent complex midpoint and a Euclidean disk radius. For every admitted exact rational point, elementary function and gamma enclosures contract as precision increases, so the rounding test terminates in the absence of a user resource cap. All 16 boundary and interior runs, including $z = 10^{-900}$, finished at 128 bits. The analytic bounds and whole-cell checks license the continuous statement.

At $z = 10^{-6}, h = -0.95 + 3i, s = -3i$, the independently expanded angular harmonics give absolute error below 2.535×10^{-12} for the returned midpoint. Omitting its tilt multiplier gives error above 1.737×10^{-7}, exceeding the uniform algorithm's 2.151×10^{-9} absolute allowance at this input. The numerical graded rule, the harmonic enclosure and the new analytic remainder each have separate receipts. At ordinary radii a pilot can instead set the tolerance in the validated rank-two cubature of Section 21. Its returned ball controls acceptance. Three executed calls, including $z = 0.9, h = 3 + 3i$ with $s = 3i$ and $s = -3$, obtained pointwise relative bounds below 1.667×10^{-11} in 2.37–22.07 seconds.

9. A trace-moment recurrence at every fixed rank

Theorem 9.1 (fixed-rank trace recurrence). Write $A_N(h) = T_N(h, s; 0) = \mathbb{E}|\operatorname{Tr} U|^{2h}$ for Haar $U \in U(N)$. The tilt disappears at the centre. The circular average of the planar determinant is already radial there. With $D = r\partial_r$ it is

$$\Phi_N(r) = \det[J_{j-k}(r)]_{j,k=0}^{N-1} = \mathbb{E}J_0(r|\operatorname{Tr} U|).$$

The factors i^{j-k} in the Fourier coefficients cancel by diagonal conjugation. At every fixed rank there is a constructive, nonzero linear recurrence with polynomial coefficients and integer shifts in h.

Construction. Put $x = r^2$, $A = J_0(r)$ and $Y = rJ_1(r)$. Then $DA = -Y$ and $DY = xA$. The scaled entries $G_k = r^k J_k(r)$ satisfy $G_0 = A$, $G_1 = Y$, $G_{k+1} = 2kG_k - xG_{k-1}$ for $k \geq 1$ and $G_{-k} = (-1)^k x^{-k} G_k$. Thus the determinant of $[G_{j-k}]$, equal to Φ_N by diagonal conjugation, is homogeneous of degree N in A, Y, with coefficients in $\mathbb{Q}(x)$. Expand it in the basis $b_k = A^{N-k}Y^k$ for $0 \leq k \leq N$. In this basis

$$Db_k = kxb_{k-1} - (N-k)b_{k+1},$$

where zero coefficients discard the outside indices. If v is the coefficient row of any such expression and B represents this displayed action on the column of basis functions, its Euler derivative has row $2xv'(x) + vB$. The $N + 2$ rows for $\Phi_N, D\Phi_N, \ldots, D^{N+1}\Phi_N$ are dependent over $\mathbb{Q}(x)$. Clear denominators, cancel common factors, and collect powers of x, with coefficient functions placed to the left of D. This gives polynomials P_ℓ such that

$$\sum_{\ell=0}^{d} r^{2\ell} P_\ell(D)\Phi_N(r) = 0, \qquad P_0 P_d \neq 0.$$

The rank bound $N + 1$ is an upper bound for the differential order. A constant-coefficient Euler equation alone would force the entire function Φ_N to be a polynomial, since its nonzero Taylor coefficients would have to lie at roots of that coefficient polynomial. Every even Taylor coefficient is nonzero by the Bessel series and positivity of integer trace moments. Thus $d \geq 1$.

Mellin passage. Set $C(h) = 2^{2h+1}\Gamma(1 + h)/\Gamma(-h)$ and let $M(p)$ denote the Mellin integral of Φ_N, continued at the lower endpoint by Taylor subtraction. For $\Re h$ large and h noninteger the circular Mellin formula gives $A_N(h) = C(h)M(-2h)$. Boundary terms in the differential equation can be justified even if the individual integrands have no common ordinary Mellin strip. On $(0, 1)$ the identity for Df is $M_0[Df](p) = f(1) - pM_0[f](p)$ by continuation from $\Re p > 0$. On $(1, \infty)$ the corresponding boundary term is $-f(1)$ for $\Re p$ sufficiently negative. This applies to $f = D^k\Phi_N$ since $D^k\Phi_N = O((1 + r)^k)$ from the characteristic-function representation of a compactly supported random variable. The boundary contributions cancel at each differentiation. Multiplication by $r^{2\ell}$ shifts p to $p + 2\ell$, giving $\sum_\ell P_\ell(-p - 2\ell)M(p + 2\ell) = 0$. Since $C(h)/C(h - \ell) = (-4)^\ell (h^{\underline{\ell}})^2$, with $h^{\underline{\ell}} = h(h-1)\cdots(h-\ell+1)$, this proves

$$\boxed{\sum_{\ell=0}^{d} (-4)^\ell (h^{\underline{\ell}})^2 P_\ell(2h - 2\ell) A_N(h - \ell) = 0.}$$

The identity continues throughout the common moment half-plane for its shifts. For $N \geq 3$ the base moment exists on $\Re h > -1$, for $N = 2$ on $\Re h > -1/2$, and $A_1 \equiv 1$. Where all moments exist, integer substitutions follow by taking limits before evaluating the Gamma factors. With forward shifts the identity holds throughout the base moment domain. The recurrence also gives meromorphic continuation to successive left half-planes by solving for the leftmost moment off the isolated polynomial zeros. This construction does not assert finiteness of that continuation at every coefficient zero. Nor does a finite list of integer initial data determine a holomorphic solution at arbitrary complex h.

Rank three. The determinant reduces to $4J_0^2J_1/r - 4J_0J_1^2/r^2 + 4J_1^3/r$. The algorithm gives

$$\left[D^2(D+4)^2 + 2r^2(5D^2+22D+18) + 9r^4\right]\Phi_3 = 0.$$

Cancelling the common polynomial factor in the Mellin recurrence and writing it with forward shifts yields the explicit identity

$$\boxed{(h+4)^2A_3(h+2) - (10h^2+42h+41)A_3(h+1) + 9(h+1)^2A_3(h) = 0, \qquad \Re h > -1.}$$

In ranks one and two the reduced backward equations are $A_1(h) = A_1(h-1)$ and $(h+1)A_2(h) = 2(2h-1)A_2(h-1)$. As exact checks, Schur orthogonality gives $A_N(m) = \sum_{\lambda\vdash m,\,\ell(\lambda)\leq N}(f^\lambda)^2$ for integer $m \geq 0$, where f^λ is the number of standard tableaux of shape λ. This yields the Catalan numbers at rank two. At rank three it gives $1, 1, 2, 6, 23, 103, 513, 2761$ for $m = 0, \ldots, 7$. The accompanying calculation checks the recurrence on exact hook-length sums and on a nonreal moment by a separate two-angle Weyl integral. Section 10 uses this determinant operator to construct equations for translated traces at interior points.

Which derivative a rank-three comparison measures

For any N, the ordinary derivative with respect to the complex variable has moment

$$\mathbb{E}|\Lambda_N'(z)|^{2h} = d^{-2h}T_N(h,h;z), \qquad d = 1-z^2 > 0.$$

The choice $s = 0$ instead computes $d^{2h}\mathbb{E}|\Lambda_N'/\Lambda_N|^{2h}$. At integer $h = k \geq 0$, $s = k + j$ with integer $j \geq 0$, the product contains k copies of the derivative and j copies of the polynomial on both the analytic and conjugate sides. Thus $d^{-2k}T_N(k, k+j; z) = M_{\mu,\mu}(z, N)$ in Grover–Mezzadri–Simm (1.1), for the list $\mu = (1^k, 0^j)$. Their definition uses $U^\dagger$; inversion preserves normalized Haar measure, giving the same joint law. This is an exact comparison at common integer parameters. Their mixed derivative lists do not specify an independently complex $s = -3$ readout. https://arxiv.org/html/2604.03051v1

On the circle put $w = e^{i\theta}$ and choose a constant phase γ with $\gamma^2 = (-1)^N\overline{\det U}$. The real-on-circle convention is $Z(\theta) = \gamma e^{-iN\theta/2}\Lambda_N(w)$; either square root gives the same absolute observables. Reality follows directly by conjugating the product of the N factors. For all θ,

$$Z'(\theta) = i\gamma e^{-iN\theta/2}\{w\Lambda_N'(w) - N\Lambda_N(w)/2\}, \qquad |\Lambda_N'(w)|^2 = |Z'(\theta)|^2 + N^2Z(\theta)^2/4.$$

Here the second identity uses that Z, Z' are real. Away from the polynomial zeros, $Z'/Z = i(w\Lambda_N'/\Lambda_N - N/2)$. Hence converting an angular derivative moment generally needs the joint readout of Z and Z'. For an exact rank-three control, the eigenvalues $-1, i, -i$ give $\Lambda_3(w) = (1+w)(1+w^2)$, hence $\Lambda_3'(1) = 6$ while $Z'(0) = 0$. This checks the phase term on a concrete spectrum. The circle identity concerns the actual derivative on the boundary; evaluation of the disk formula at $d = 0$ requires the separate limit in Section 17.

Rank three through the special-unitary trace

Let V be Haar on $SU(3)$ and w independent Haar on the unit circle. The product $U = wV$ is Haar on $U(3)$ by invariance. Write $t = \operatorname{Tr} V$ and $d = 1 - z^2$. The eigenvalues of V have product one, so their second elementary symmetric function is $\bar{t}$. In these coordinates

$$P(w) = 1 - ztw + z^2\bar{t}w^2 - z^3w^3, \qquad Q(w) = t - 2z\bar{t}w + 3z^2w^2,$$

with $\Lambda_3 = P$, $\Lambda_3' = -wQ$. Thus the general mixed integrand is exactly $d^{2h}|Q|^{2h}|P|^{2(s-h)}$. Haar phase, rather than replacing Q by its average, is essential here.

Proposition 9.2 (elliptic Haar reductions at rank three). The density of t with respect to planar Lebesgue measure is $\sqrt{D(t)_+}/(2\pi^2)$, where $D(t) = 27 - 18|t|^2 + 8\Re(t^3) - |t|^4$ and $x_+ = \max(x, 0)$. The radial density $p(r)$ of $|\operatorname{Tr} U|$ on $0 < r < 3$ is

$$p(r) = \frac{r\sqrt{A}}{2\pi^2} \begin{cases} 4E(m), & r \le 1, \\ \pi m^{-1/2}\, {}_2F_1(1/2, 1/2; 2; 1/m), & r > 1, \end{cases} \qquad A = (3-r)^3(1+r), \quad m = 16r^3/A.$$

Here E and K below take the elliptic **parameter**. Consequently $T_3(h, s; 0) = \int_0^3 r^{2h} p(r)\, dr$ for every s and $\Re h > -1$. The centre Mellin transform has residue $3\sqrt{3}/(2\pi)$ at $h = -1$.

For $0 < z < 1$, let u_1, u_2 be the roots of Q for a given t. Fold an exterior root to $1/\bar{u}_j$ and leave interior roots fixed, obtaining b_j. Set

$$L = 3z^2 \prod_j \max(1, |u_j|), \quad A_b = |1 - \bar{b}_1 b_2|, \qquad m_b = |b_1 - b_2|^2/A_b^2.$$

Then the ordinary diagonal inverse moment satisfies

$$d\, T_3(-1/2, -1/2; z) = \mathbb{E}|\Lambda_3'(z)|^{-1} = \int_{\mathbb{C}} \frac{\sqrt{D(t)_+}}{2\pi^2} \frac{2K(m_b)}{\pi L A_b}\, d^2t.$$

This is a two-dimensional integral with an explicitly evaluated rotation average. It includes $z = 1/3$ and $1/2$. At $z = 0$ the conditional inverse derivative is $1/|t|$ almost everywhere.

Proof. In eigenangles $\alpha, \beta, -\alpha - \beta$, put $v_1 = e^{i\alpha}, v_2 = e^{i\beta}, v_3 = (v_1 v_2)^{-1}$. The columns of the planar Jacobian of the trace map are $i(v_1 - v_3), i(v_2 - v_3)$, and its absolute determinant is $|\Delta|/2$ (twice the area of a triangle on the unit circle, or the sine rule), where $\Delta = \prod_{j<k}(v_j - v_k)$. The characteristic equation $x^3 - tx^2 + \bar{t}x - 1 = 0$ makes the trace map six-to-one at regular values. Its negative discriminant is $|\Delta|^2 = D(t)$. For each argument the function $D(re^{i\alpha})$ decreases from 27 to zero at the trace boundary, since its radial derivative is $-4r(r^2 - 6r\cos 3\alpha + 9) \le 0$. The positive region is connected and contains 0; every positive point can be reached from 0 without crossing a multiple root. The three starting unit roots remain on the circle by their continued simplicity and reciprocal-conjugate symmetry. Weyl's factor $|\Delta|^2/(6(2\pi)^2)$, the six inverse images and the Jacobian give the claimed planar density. This is the classical $SU(3)$ trace measure; G. Guralnik, T. Warnock and C. Zemach derived the invariant trace distribution in 1985. N. Kaiser, §2, describes the trace figure in the normalization $t/3$. Here t is the full trace. https://doi.org/10.1016/0021-9991(85)90063-4 · https://arxiv.org/abs/math-ph/0609082

Rotation gives $p(r) = r(2\pi^2)^{-1} \int_0^{2\pi} \sqrt{D(re^{i\alpha})_+}\, d\alpha$. The expression under the radical is $A(1 - m\sin^2(3\alpha/2))$. For $m > 1$, substitute $\sin u = m^{-1/2} \sin v$ on the positive portion. The integral on a quarter period becomes $m^{-1/2} \int_0^{\pi/2} \cos^2 v / \sqrt{1 - m^{-1}\sin^2 v}\, dv$. Euler's beta integral gives the second formula. Near zero $p(r) = 3\sqrt{3}\, r/\pi + O(r^3)$, proving the stated residue by local Mellin subtraction.

For the derivative formula each folded root contributes its modulus to L if exterior. On substituting $w = (v + b_1)/(1 + \bar{b}_1 v)$ in the angular integral of $1/|Q(w)|$, the circle Jacobian cancels the two factors $|1 + \bar{b}_1 v|$. The remaining integral is $1/(LA_b)$ times the mean of $1/|v - \omega|$ with $\omega = (b_2 - b_1)/(1 - \bar{b}_1 b_2)$. Expanding the two binomial factors gives ${}_2F_1(1/2, 1/2; 1; |\omega|^2) = 2K(|\omega|^2)/\pi$. The unit-root exceptional traces form a planar null set. For fixed $|w| = 1$, $Q(w) = 0$ is real-linear in t with determinant $1 - 4z^2$. For $z \ne 1/2$ its solutions trace a smooth curve as w varies. At $z = 1/2$, put $w = e^{i\theta}$ and $t = e^{i\theta/2} v$. The condition reduces to $v - \bar{v} = -(3/4)e^{3i\theta/2}$. Only finitely many phases are compatible and each gives a line in t. Tonelli's theorem and the fixed-size integrability of Theorem 1.1 finish the argument. At the numerically delicate $m_b = 1$ boundary the complementary parameter can be calculated as $(1 - |b_1|^2)(1 - |b_2|^2)/A_b^2$.

The usual complex characteristic polynomial, its derivative, and the real version on the circle have different readouts. For the paper's convention a real version on $z = e^{i\theta}$ is $Z(\theta) = C_U e^{-iN\theta/2} \Lambda_N(e^{i\theta})$ for a sample-dependent unit phase C_U (up to sign). It satisfies $|Z'(\theta)| = |e^{i\theta}\Lambda_N'(e^{i\theta}) - N\Lambda_N(e^{i\theta})/2|$. The off-circle identity $d^{-2h} T_3(h, h; z) = \mathbb{E}|\Lambda_3'(z)|^{2h}$ follows before averaging. The fourth-order equation below has tilt $s = -3$. Its intersection with the diagonal would require $h = -3$, outside the ordinary rank-three moment domain. Grover,

Mezzadri and Simm use $U^\dagger$ in their polynomial; inversion invariance of Haar identifies the unphased polynomial laws, and their finite integer determinant supplies the comparison in Section 12. https://arxiv.org/abs/2604.03051

A radial curve determined by the ordinary derivative moments

The ordinary diagonal determines the mean counting density of the two roots of Λ_3' through its derivative in the order at zero. This is a separate rank-three observable with an elliptic description. Its normalization matters if a radial histogram or a derivative-zero curve is being compared. The derivative zeros of a random unitary characteristic polynomial, and their relation to derivative moments, are studied by Mezzadri and by Simm and Wei. https://arxiv.org/abs/math-ph/0207044 · https://doi.org/10.1112/jlms.70487

Proposition 9.3 (planar and radial derivative-zero density). Write $\rho(r)$ for the rotationally invariant density with respect to planar area, counting both zeros with multiplicity. For $0 < r < 1$, put

$$k = 4r^3, \quad \delta = (2r-1)^2, \quad A = (1+r)(1+3r), \quad B = (1+r)^4, \quad V = \min\{2/\delta, A/k\},$$

where $2/0 = +\infty$. Then

$$\rho(r) = \frac{18r^2\sqrt{27(1-r^2)}}{\pi^3(2r+1)^5} \int_0^V \frac{[(1+r)^2 + 2r(1-2r^2)v]\sqrt{(A-kv)[B-k(3r^2-1)v]}}{\sqrt{v(2-\delta v)}}\, dv.$$

This involves an algebraic differential on a curve $y^2 = v(2-\delta v)(A-kv)(B-k(3r^2-1)v)$ of genus at most one, with the real branch positive on the interior. The endpoint switches at $r = 1/3$. The formula is regular as a parameter integral near $r = 1/2$. The density of the modulus of a uniformly picked derivative zero is $\pi r\rho(r)$; the total radial **counting** density is $2\pi r\rho(r)$. In particular

$$\rho(1/3) = \frac{274560 - 65536\log 2}{3125\pi^3}, \qquad \rho(r) \sim \frac{18\sqrt{27}}{\pi^2} r^2 \quad (r \downarrow 0).$$

Proof. For $V_0 \in SU(3)$ with trace t, zeros obey $t - 2u\bar{t} + 3u^2 = 0$. At $|u| = r \neq 1/2$ the corresponding real-linear map in t has determinant $1 - 4r^2$. Its unique solution is

$$t(u) = -3\frac{u^2 + 2r^2\bar{u}}{1-4r^2}.$$

Implicit differentiation in the two real coordinates of u gives $|\det(dt/du)| = |2\bar{t} - 6u|^2/|1-4r^2|$. The area formula for $u \mapsto t(u)$ counts each of the two inverse images once. The exceptional multiple-root traces form a null set (the discriminant equation is a nonzero real polynomial). Multiplying by the planar trace density of Proposition 9.2 and averaging the overall Haar rotation gives $\rho(r) = \int_0^{2\pi} \sqrt{D(t(u))_+}|2\bar{t}(u) - 6u|^2\, d\theta/(4\pi^3|1-4r^2|)$, $u = re^{i\theta}$. The set of traces yielding a zero of modulus exactly $1/2$ lies on the finite union of lines calculated in Proposition 9.2, now using $u = (1/2)e^{i\theta}$ in the same equation. There is no radial atom there. Gauss–Lucas places the roots in the closed disk; the Haar-distinct eigenvalues almost surely give strict inclusion and $t = 0$ has zero mass.

Set $x = \cos 3\theta$, $v = (1+x)/\delta$. Substitution into D and the Jacobian gives

$$D(t(u)) = \frac{27(1-r^2)}{(2r+1)^4}(A-kv)[B-k(3r^2-1)v], \qquad |2\bar{t} - 6u|^2 = \frac{36r^2}{(2r+1)^2}[(1+r)^2 + 2r(1-2r^2)v].$$

The second factor in D is positive for $0 \le v \le 2/\delta$, $0 < r < 1$, $r \neq 1/2$: in x its endpoint values before the common positive divisor are $(r+1)^4(2r-1)^2$ and $(r-1)^4(2r+1)^2$. The arcsine density of x contributes $|2r-1|/[\pi\sqrt{v(2-\delta v)}]$; its numerator cancels the apparent singularity in $|1-4r^2|^{-1}$. The remaining support condition is $v \le A/k$. Comparing this with $2/\delta$ gives the switch at $1/3$. For r near $1/2$ use $v = (A/k)\sin^2\psi$ to see dominated continuity, fixing a continuous representative there. At $r = 1/3$ the integral with its prefactor becomes $864/(3125\pi^3)$ times $\int_0^{18}(16/9 + 14v/27)\sqrt{(32+v)/v}\, dv$. Put $v = 32\sinh^2 u$ with upper endpoint $u = \log 2$ to obtain the displayed value. As $r \downarrow 0$, $t(u) = O(r^2)$ and $|2\bar{t} - 6u|^2 \sim 36r^2$, uniformly in angle. This proves the last asymptotic.

For $M(h,r) = d^{-2h}T_3(h,h;r)$, the planar distributional identity is $\Delta\,\partial_h M(0,|z|) = 4\pi\rho(|z|)$. Here ∂_h differentiates the entire diagonal observable in its single order. At each interior point it gives $2\mathbb{E}\log|\Lambda_3'|$ by the ordinary moment bound on a neighborhood of zero order. Distributionally, factor the degree-two derivative and use $\Delta\log|z-b| = 2\pi\delta_b$. Local integrability of the logarithm is uniform for roots in the unit disk, which justifies the source average. This relation identifies a specific radial curve recoverable from the moments without using any external rank-three formula.

As a numerical comparison, integration of $2\pi r\rho$ across six bins returned total 1.9999999999999962. Direct roots of the original unitary eigenvalue polynomial on eight independently scrambled Weyl grids of 2^{18} points gave bin means differing from these integrals by at most 0.000268. Dropping the polar Jacobian instead gives total 0.6921123. These are numerical checks; the mass two and special value above follow analytically.

Centre values and small-radius response at higher rank

Proposition 9.4 (a computable centre Mellin integral). For $3 \le N \le 8$, $-1 < \Re h \le 3$, the centre determinant of Theorem 9.1 gives a scalar enclosure with separately computable errors on $(0,1)$, $[1,R]$ and $[R,\infty)$. The error bounds also apply to parameter values arbitrarily close to the nonnegative integers. The numerical work required for a given relative tolerance depends on the value of the moment. The construction uses $C(h) = 2^{2h+1}\Gamma(1+h)/\Gamma(-h)$.

On $(0,1)$ expand the Bessel entries of the determinant in ordinary powers, computing its exact rational determinant coefficients a_j by signed subsets of columns. The radial primitive of $a_j r^{2j}$, including its prefactor, is $2^{2h}\Gamma(1+h)a_j(-h)_j/\Gamma(1+j-h)$. This removes the internal division by $j-h$. After degree $2J$ the absolute budget is

$$|C(h)|\frac{(N/2)^{2J+2}}{((J+1)!)^2[1-(N/(2J+4))^2](2J+2-2\Re h)}.$$

Indeed $|\operatorname{Tr}U| \le N$ bounds each exact Taylor coefficient by $(N/2)^{2j}/(j!)^2$. On each middle panel of midpoint m and half-width w, take $w < D < m$ and $p = -2h-1$. The integral of the Taylor remainder and its positive-weight Gauss rule together have absolute error at most

$$4w\max\{(m-D)^{\Re p},(m+D)^{\Re p}\}e^{ND+|\Im p|\arcsin(D/m)}\frac{(w/D)^{2k}}{1-w/D}$$

for k Gauss nodes, before multiplication by $|C(h)|$. This follows from $|\Phi(v)| \le e^{N|\Im v|}$, the argument of the disk, Cauchy's coefficient estimate and polynomial exactness.

For the exterior, set $b_j(l) = \prod_{u=1}^{j}[4l^2-(2u-1)^2]/(8^j j!)$ and truncate at $j < L$, $L \ge N$. In $\sqrt{2\pi r}\,i^l J_l(r)$ the two waves are $e^{\pm i(r-\pi/4)}$ with polynomial coefficients $\sum b_j(l)(i/r)^j$ and $(-1)^l\sum b_j(l)(-i/r)^j$, respectively. Their combined error is at most $2|b_L(l)|r^{-L}$. For $l \ge 0$ use the Laplace integral for the Hankel function with factor $(1+it/(2r))^{l-1/2}$ against $e^{-t}t^{l-1/2}/\Gamma(l+1/2)$. The Taylor remainder is bounded by the modulus of its first omitted coefficient times $(t/(2r))^L$, since the real exponent in the differentiated factor is nonpositive. Gamma integration gives the stated constant. Negative indices follow by parity. The integral and expansion conventions are those of NIST DLMF §§10.9 and 10.17.

Multiply the entries by the signed subset recurrence before estimating. Let $b_j^* = 2\max_{0\le l<N}|b_j(l)|$, $P(X) = \sum_{j<L} b_j^* X^j$, and $H = P(1/R) + b_L^* R^{-L}$. After collecting frequencies $q = -N, -N+2, \dots, N$ and powers $j < L$, the remaining determinant error has bound

$$E_L r^{-N/2-L}, \quad E_L = \frac{N!}{(2\pi)^{N/2}}\left[Nb_L^* H^{N-1} + \sum_{j\ge L}[X^j]P(X)^N R^{L-j}\right].$$

The first summand is the telescoping error of each product and the second prices its dropped polynomial coefficients. The retained wave $e^{iqr}r^{-N/2-j}$ contributes $R^{1-p'}\int_1^\infty t^{-p'}e^{iqRt}dt$, $p' = 1+2h+N/2+j$. For $q=0$ the integral is $1/(p'-1)$ when the coefficient is nonzero. For $q \ne 0$, integration by parts gives $I(p') = -e^{iqR}/(iqR) + p'I(p'+1)/(iqR)$. After m steps the remainder is bounded by $|(p')_m|(|q|R)^{-m}/(\Re p'+m-1)$. Use $\Re p' > 0$ for the initial oscillatory integral. The code verifies the integrability tests on all nonzero coefficients. The

absolute error of the determinant remainder in the full answer is at most $|C(h)|E_L R^{-2\Re h-N/2-L}/(2\Re h+N/2+L)$. At exact nonnegative integer order the exact Taylor coefficient gives the answer directly.

The inverse-power test at $h=-0.95+3i$ was run at each of the six ranks, with independent tilt disappearing at the centre. At rank eight the order-20 exterior bound at $R=64$ alone allowed an error above 3×10^{-12}. Raising arithmetic precision did not remove it. The final profile uses $R=72, L=25$, 30 Gauss nodes per middle panel, and the integration-by-parts wave calculation. The exact integer coefficients and the rank-three elliptic integral are independent checks of the construction.

Theorem 9.5 (a finite response polynomial with an effective remainder). Put $a=\Re h\in(-1,0)$, $B=N+s$, $A=N^2+2Ns$, and $F(z)=(1-z^2)^{-A}T_N(h,s;z)$. On $0\le z\le z_0<1$, let d be an even positive integer with $d<p_N+2a$, where $p_N=\min_{l+m=N}(l^2+m^2)/2$. Then F has an even Taylor polynomial through degree $d-2$ with an explicit absolute remainder of order z^d, uniformly for $|s|\le S$. The condition gives a sufficient differentiability range. The polynomial coefficients below use the original physical source and retain its complex weight.

Under the disk automorphism of Section 1 let $X=\operatorname{Tr}V$ with V Haar. The mark is $X+Nz$ and the preparation after removing $(1-z^2)^A$ is $W(z)=\prod_j(1+zv_j)^{-B}(1+z/v_j)^{-B}$. For real z, the two logarithms enclose the real logarithm of a positive base. Use their disk-analytic branches at zero for complex Taylor parameters. Write $A_N(h)=T_N(h,s;0)$. The constant and quadratic terms are

$$F(z)=A_N(h)+z^2\{N^2\mathcal{L}_N(h)-2NhBA_N(h)+B^2A_N(h+1)\}+\cdots,\qquad \mathcal{L}_N(h)=-\frac{C(h)}{4}\int_0^\infty r^{1-2h}\Phi_N(r)\,dr.$$

This coefficient can also be evaluated by the gamma identity as h^2 times the *continued* centre Mellin expression at $h-1$. The ordinary inverse moment at $h-1$ need not exist. For the mixed term the one-mark Fourier insertion for $\Re X$ is $\Phi_N'(r)\cos\phi/i$. Its product with the first translation derivative gives $-NBr\Phi_N'(r)$ after angular averaging. Mellin integration by parts gives the middle coefficient. The two pure second-order tilt insertions of nonzero spin vanish by rotation, leaving $B^2|X|^2$. Reflection by $V\mapsto -V$ kills odd Taylor powers.

For higher coefficients let $m=|\lambda|$, $n=|\mu|$, $b=m-n$, and pad partitions to length N. The Cauchy identity expands the two halves of W with factors $(-z)^{m+n}s_\lambda(1^B)s_\mu(1^B)$. The specialization is the hook-content polynomial, first at positive integral B and then at all B by coefficientwise polynomial identity. Weyl integration of the two alternants against $e^{ir\cos\theta}$ gives $i^b\det[J_{\lambda_i-i-\mu_j+j}(r)]$. The common rotation in the translated mark gives $i^bJ_b(Nzr)$. The two phases exactly cancel $(-1)^{m+n}$. At degree v retain $k=v-m-n\ge|b|$ with $k-b$ even. For $b\ge0$ the remaining coefficient multiplying the minor and r^k is

$$s_\lambda(1^B)s_\mu(1^B)\frac{(-1)^{(k-b)/2}(N/2)^k}{((k-b)/2)!((k+b)/2)!}.$$

Interchange of the partitions gives the same product of the minor and translation Bessel function. This yields a finite polynomial in the independent tilt at each order. The compact Fourier integral and its Gauss rule can therefore store coefficient balls once and serve subsequent tilt queries by polynomial evaluation.

Here are the constants for the outer integral and the Taylor remainder. Rotate to the Fourier direction, deform every real eigenangle x to $x-i\tau\sin x$, and require $z_0e^\tau<1$. In the two half-circles centred at $0,\pi$ the Fourier amplitude is bounded by $e^{-4r\tau u^2/\pi^2}$ in the local coordinate u. The complex Jacobian is at most $\sqrt{1+\tau^2}$. A squared sine Vandermonde factor within one group is at most $H(u-v)^2$, $H=1+\tau^2\cosh^2\tau$, by $|\sin x|\le|x|$ and $|\sinh y|\le|y|\cosh\tau$. Across groups it is at most $G=4\cosh^2\tau$. These are bounds for the holomorphic continuation of $4\sin^2((x-y)/2)$. Put $D_{lm}=(l^2+m^2)/2$, $I_l=\pi^{l/2}2^{-l(l-1)/2}\prod_{j=1}^l j!$. Enlarging the two Gaussian integrals to real lines gives the tail envelope $\sum_{l+m=N}b_{lm}r^{-D_{lm}}$ for the untilted deformed integrand, with

$$b_{lm}=\frac{\binom{N}{l}(1+\tau^2)^{N/2}H^{\binom{l}{2}+\binom{m}{2}}G^{lm}I_lI_m}{N!(2\pi)^N}\left(\frac{\pi^2}{4\tau}\right)^{D_{lm}}.$$

Indeed the Gaussian Vandermonde integral is the product of monic Hermite squared norms times $l!$, giving I_l at Gaussian weight e^{-x^2}. Contour deformation is in the finite angular integral. The poles of the preparation stay outside the homotopy.

For strip width $t = 0$ or τ, bound the jth derivative of W divided by $j!$ by

$$L_j(t) = \rho^{-j}(1 - (z_0 + \rho)e^t)^{-2N(N+S)}, \qquad \rho = \frac{j(e^{-t} - z_0)}{2N(N+S) + j}.$$

At $j = 0$ use $\rho = 0$ and omit its power. This is Cauchy's estimate at any intermediate real preparation parameter. The ith derivative of the translation phase divided by $i!$ costs $(Nr)^i/i!$ there. Splitting the Mellin integral at R_* bounds the Taylor remainder by

$$|C(h)|z^d \sum_{i=0}^{d} \frac{N^i}{i!} \left[\frac{L_{d-i}(0) R_*^{i-2a}}{i - 2a} + L_{d-i}(\tau) \sum_{l+m=N} \frac{b_{lm} R_*^{i-2a-D_{lm}}}{D_{lm} + 2a - i} \right].$$

All denominators are strictly positive by the assumptions. These integrable bounds justify differentiating the actual inverse-order Fourier integral and Taylor's formula on the real segment, including at the central trace wall. Restoring $(1 - z^2)^A$ is exact.

For coefficient integrals above degree two, the implementation integrates from 2^{-64} to $R = 144$ with 23-point Gauss rules and prices both omitted ends. On a complex radial disk of centre m, radius $D < m$, the unweighted factor costs e^{ND}; Cauchy extraction of order v costs $\rho^{-v}(1 - \rho)^{-2N(N+S)} e^{N\rho(m+D)}$ with $\rho = 1/(16N)$. Multiplication by the Mellin power and the panel factor of Proposition 9.4 gives the compact budget. On the first interval use the real version of the same bound times $\epsilon^{-2a}/(-2a)$. On the far interval use the exterior summand of the last display with $z_0 = 0$, $d = v$. The numerical part of each tilt polynomial is stored as decimal rational coefficients; the subtraction of those decimals from the computed balls is charged using $\sum_j 3^j |\delta b_j|$. A lower bound for $|F|$ is the constant coefficient modulus minus the suprema of the other terms and the entire error. This proves a per-input relative guarantee even though the true values vary across the tilt disk.

Rank	Upper radius, lower radius zero	Highest retained degree	Uniform relative error, $h = -0.95 + 3i$	Uniform relative error, $h = -0.31 + 0.67i$
4	10^{-9}	0	8.929×10^{-12}	8.647×10^{-14}
5	10^{-6}	2	5.335×10^{-14}	3.024×10^{-16}
6	5×10^{-5}	4	5.518×10^{-12}	1.912×10^{-14}
7	10^{-4}	6	4.445×10^{-14}	6.962×10^{-17}
8	10^{-4}	6	1.177×10^{-13}	3.898×10^{-16}

Each bound covers all complex $|s| \le 3$ and every real z in its interval. Each column fixes h. The bounds are for the stored mathematical polynomial with its exact physical prefactor. A query also encloses the rounding of its evaluation in complex ball arithmetic. The stored rectangular output of a query can be wider than the per-input uniform Euclidean disk because a disk-budget error is added to both components.

10. Equations away from the centre

Theorem 10.1 (rank-two recurrence for independent exponents). Fix $0 < z < 1$. There are explicitly computable polynomials in (z, h, s), not all identically zero, such that

$$\sum_{j=0}^{10} c_j(z, h, s)\, 4^{-j} T_2(h + j, s; z) = 0, \qquad \Re h > -1, \quad s \in \mathbb{C}. \tag{10.1}$$

At generic parameters $c_{10} \neq 0$; the coefficients can then be normalized by $c_{10} = 1$. The construction below is a single linear solve of size 118. It gives a forward equation with s held fixed as h varies. It makes no assertion of minimal order, numerical conditioning or determination of the initial noninteger moments by integer data.

Reduction of the source. Put $d = 1 - z^2$ and change each original eigenvalue λ to $\mu = -(\lambda - z)/(1 - z\lambda)$. Then $S_N = Nz - \sum_j \mu_j$. The angular Jacobian and Vandermonde give $d^{N^2} \prod_j |1 - z\mu_j|^{-2N}$ times Haar eigenangle measure; also $|1 - z\lambda| = d/|1 - z\mu|$. This is a substitution in the same finite determinant integration formula.

Write $q = -2 - s$. At rank two the eigenvalues can be written $e^{i(\phi+\delta)}, e^{i(\phi-\delta)}$. The resulting Haar integral has independent $u = \cos\delta$ with density $2\sqrt{1-u^2}/\pi$ and $v = \cos\phi$ with density $1/(\pi\sqrt{1-v^2})$; this follows by periodicity and the squared Vandermonde $4\sin^2\delta$. With $\mathcal{I}$ expectation over these two coordinates, set

$$A = u^2 - 2zuv + z^2, \qquad B = (1-z^2)^2 + 4z^2(u^2+v^2) - 4z(1+z^2)uv.$$

The translated trace norm squared is $4A$ and the squared characteristic polynomial is B. Consequently

$$T_2(h, s; z) = d^{4+4s} 4^h \, \mathcal{I}[A^h B^q].$$

In particular an exponent shift only introduces a polynomial factor under the transformed integral.

The matrix. Rows correspond to $u^i v^{k-i}$ in increasing even $k = 0, 2, \ldots, 20$, then increasing i. For each of $w = u, v$, in that order, add one column for each monomial $P = u^i v^{k-i}$ in increasing odd $k = 1, 3, \ldots, 15$, then increasing i. The column is the coefficient vector of

$$(1-w^2)AB\,\partial_w P + \big[(1-w^2)((h+1)B\partial_w A + (q+1)A\partial_w B) - g_w w AB\big]\,P, \qquad g_u = 3, \quad g_v = 1.$$

Add the eleven coefficient columns of $1, A, \ldots, A^{10}$. The resulting matrix M has 121 rows and 155 columns. Each of the first 144 polynomials integrates to zero against $A^h B^q \, d\mathcal{I}$: multiply the integrand by $(1-w^2)ABP$ and integrate its total derivative including the density. The boundary factors vanish. This is classical integration by parts initially for $\Re h > 0$. The only zeros of A in the rectangle are $(u, v) = (z, 1), (-z, -1)$. In the original angle ϕ and the coordinate u they are nondegenerate planar distance squares locally. B is bounded away from zero for each $z < 1$. Holomorphy therefore extends the integrated identities, after polynomial denominators are cleared, to $\Re h > -1$, for every complex s.

Rank certificate. Over the rational-function field the augmented matrix has rank at most 118. To see three independent row constraints, evaluate the polynomials at the following points:

$$(z, 1), \quad (1, (1+z^2)/(2z)), \quad (U, (U^2+z^2)/(2zU)), \qquad U^2 = z^4/(2z^2-1).$$

The last two solve $A = B = 0$. At the first, $A = \partial_u A = 1 - v^2 = 0$. Thus all divergence columns vanish at each point, while the eleven power columns take the same values $(1, 0, \ldots, 0)$ there. Two independent evaluation differences annihilate all columns. Their independence follows by testing u^2, u^4 since the three squared first coordinates are generically distinct. The remaining row constraint extracts the coefficient of v^{20}. On setting $u = 0$, every divergence column has degree at most 18 in v, and every A^j is constant. This functional is independent of the two differences by the same tests followed by v^{20}. The argument over the algebraic extension containing U suffices for the polynomial rank bound.

For an explicit converse, use zero-based indices. At $z = 1/2, h = 1/3, s = -16/7$, reduce the matrix modulo the prime 10007. Scan the columns 0 through 153 from left to right, retaining a column when rank increases; then scan the rows of that selection in their given order in the same way. This retains 118 columns and 118 rows. In their original order the minor has determinant 6314 (mod 10007). All ten columns for $1, A, \ldots, A^9$ are retained. The script computes this determinant by exact finite-field elimination and contains the index sets. Thus these same row and column indices define a nonzero polynomial minor $\Delta(z, h, s)$. Solve this square system with right hand side minus the column of A^{10} on the retained rows. At $\Delta \neq 0$, the solution gives a relation on *all* 121 rows by the upper rank bound. Its last ten unknowns are $c_0, \ldots, c_9$ and $c_{10} = 1$. Multiplying all eleven by Δ gives polynomial Cramer coefficients and removes the restriction on using the identity. At some special parameters the resulting equation or its leading coefficient can vanish, so the forward solver must check its pivot. The polynomial identity extends to these points by specialization. The finite matrix supplies the certificate before any numerical moment is evaluated.

Radial equations at negative integer tilt

Theorem 10.2 (translated trace equation). At the negative tilt $s = -N$, the disk change of variables in the preceding rank-two construction is valid at every rank and removes the entire transformed weight. Put $x = N^2 z^2$, $\theta = x\partial_x$, and $H_h(x) = \mathbb{E}|\operatorname{Tr} U - \sqrt{x}|^{2h}$. Then $T_N(h, -N; z) = (1-z^2)^{-N^2} H_h(x)$. Let P_j be the polynomials constructed from the Bessel determinant at the centre, so that $\sum_j r^{2j} P_j(r\partial_r)\Phi_N(r) = 0$. They give the computable off-centre equation

$$\sum_j (-4x^{-1}\theta^2)^j P_j(2h - 2\theta) H_h(x) = 0. \tag{10.2}$$

Products of operators in this formula act in the displayed order. For example at rank three use $P_0(v) = v^2(v+4)^2$, $P_1(v) = 2(5v^2 + 22v + 18)$, $P_2 = 9$. The coefficient of θ^4 is $16(x-1)(x-9)/x^2$. Thus the ordinary fourth-order equation is regular on the two open subintervals of the physical interval separated by $z = 1/3$. The physical solution satisfies the equation in distributions also at that interior singular point. No regular initial-value propagation across it is assumed.

Proof. Write $y \in \mathbb{C}$ for the displacement. The moment of $|\operatorname{Tr} U - y|^{2h}$ is the convolution of the compact trace law with the planar distribution $|y|^{2h}$. For $-1 < \Re h < 0$ the Fourier transform of the latter in the unscaled Fourier convention is $\pi 4^{1+h}\Gamma(1+h)|\xi|^{-2h-2}/\Gamma(-h)$. This follows by a Gaussian integral for the negative power; the transformed density is locally integrable at frequency zero. Thus the transformed moment is this homogeneous distribution times $\Phi_N(|\xi|)$. Multiplication by $|\xi|^{-2h-2}$ sends each $P_j(E_\xi)\Phi_N$ to $P_j(E_\xi + 2h + 2)(|\xi|^{-2h-2}\Phi_N)$, for the planar Euler derivative E_ξ. The distributional homogeneity identity includes the origin. Fourier inversion sends $|\xi|^2$ to $-\Delta_y$ and E_ξ to $-E_y - 2$. On a radial function of $x = |y|^2$, $E_y = 2\theta$ and $\Delta_y = 4x^{-1}\theta^2$. These transformations prove the formula. Convolution with the compact trace law is holomorphic as a distribution for $\Re h > -1$, so the identity extends throughout that half-plane. On intervals where the leading coefficient is nonzero, ordinary differential-equation regularity gives the classical equation. There H_h is the physical continuous moment: for $N \geq 3$ the bounded planar density follows from the finite-rank density argument, for $N = 2$ the trace density is locally bounded away from the centre and the edge, and for $N = 1$ the translated trace has positive distance from zero at $z < 1$.

A finite extension covers $s = -N - m$ for each integer $m \geq 0$. In the disk-transformed Haar law expand the polynomial $\prod_i (1 + \alpha\mu_i)^m(1 + \beta\bar{\mu}_i)^m$, retaining its coefficient indexed by (a, b), and put $\alpha = \beta = -z$ after expanding. Under rotation the coefficient has spin $n = a - b$, so its planar Fourier transform at $re^{i\gamma}$ is $e^{in\gamma}D_{ab}(r)$. The function D_{ab} is the same coefficient of the finite Toeplitz determinant with the extra symbol $e^{ir\cos\theta}$. Every entry is now an explicit finite sum of shifted Bessel functions $i^k J_k(r)$. The centre argument yields a scalar Euler equation for D_{ab}: its determinant belongs to the homogeneous degree-N Bessel module over $\mathbb{C}(r)$, closed under the Euler derivative. After clearing denominators, separate even and odd coefficient powers using the parity $D_{ab}(-r) = (-1)^n D_{ab}(r)$, and divide the common lowest power. Skip identically zero coefficients. This gives polynomials $P_{ab,j}$ multiplying r^{2j}. The same convolution proof applies in spin n, for which the angular term in the Laplacian changes $4\theta^2$ to $4\theta^2 - n^2$. Solve the finite resulting scalar equations, multiply the radial solutions evaluated at $x = N^2z^2$ by $(-z)^{a+b}$, and sum with the factor $(1 - z^2)^{N^2+2Ns}$. This constructs a finite system for the moment at every such tilt. An individual scalar equation for that sum can also be formed by expressing successive derivatives as rows in the direct sum of the companion systems and eliminating them over $\mathbb{C}(z, h)$. General rank with two arbitrary independent exponents still requires further elimination.

Numerical use of the rank-three translated trace

Proposition 10.2A (elliptic quadrature across the trace radius). Set $a = 3z$, $X = \operatorname{Tr} U$, $U_h(a) = \mathbb{E}|X - a|^{2h}$. At $s = -3$ we have $T_3 = d^{-9}U_h(a)$. In terms of Proposition 9.2,

$$U_h(a) = \int_0^3 p(r)\max(a, r)^{2h}\,{}_2F_1\left(-h, -h; 1; \frac{\min(a, r)^2}{\max(a, r)^2}\right) dr.$$

For every $0 \leq a < 3$ this is an ordinary integral for $\Re h > -1$. Rotation makes the trace's angle uniform conditional on r; the binomial series for its phase average gives the kernel on $r \neq a$. Its value at $r = a$ is immaterial. Absolute convergence follows by the bounded planar trace density. At the centre the formula reduces to Proposition 9.2. At $a = 1$ the endpoints from the density transition and the displaced inverse singularity coincide. The implementation splits at both radii, keeps the distance $|r - a|$ separately, and uses $1 - \min(a, r)^2/\max(a, r)^2 = |r - a|(r + a)/\max(a, r)^2$ in the Gauss connection formula. At $h = -1/2$ it uses $2K/\pi$. At nonnegative integers the kernel terminates. Near other exponent resonances this double-precision path declines the query; the next calculation also handles those inputs.

Proposition 10.2B (a separate rank-three absolute certificate). For rational $0 \leq a < 3$ and rational real and imaginary parts of h, $\Re h > -1$, finite Taylor and quadrature calculations and the explicit tails below enclose $U_h(a)$. The displayed error budgets apply at the supplied inputs; the truncation parameters may require refinement. This construction evaluates the physical scalar on either side of $a = 1$ without transporting an ODE state.

Write $C(h) = 2^{2h+1}\Gamma(1+h)/\Gamma(-h)$, $\eta = -1-2h$, and $F_a(r) = J_0(ar)\Phi_3(r)$, where Φ_3 is the centre determinant of Theorem 9.1. The Riesz representation and the finite part of Section 5 give $U_h(a) = C(h)\,\mathrm{FP}\int_0^\infty r^\eta F_a(r)dr$. Indeed F_a is the Fourier characteristic function of $\Re X + a\cos\theta$ with independent uniform phase. It is also the circular Fourier mean of the translated trace. The finite part equals the ordinary Haar readout by the Mellin formula applied to that translated law, or by parameter continuation from $-1 < \Re h < 0$ after lower-end subtraction. At $h = k \geq 0$ integral use $(-4)^k(k!)^2[r^{2k}]F_a(r)$ exactly.

Let $K_0 > 2\Re h$ be a positive integer. Obtain $b_j = [r^j]F_a$ by exact polynomial arithmetic through degree K_0-1. On $[0,2]$ the finite part of the polynomial is $\sum_{b_j\neq 0} b_j 2^{j-2h}/(j-2h)$. Odd coefficients vanish, so these denominators cause no pole away from nonnegative integers. With $M = 3+a$, the integrated remainder has modulus at most

$$\frac{(2M)^{K_0}}{K_0!}\frac{2^{1+\Re\eta}}{K_0+1+\Re\eta}.$$

This follows by Taylor's real remainder bound for e^{irt}, $|t| \leq M$. For a panel $[m-1, m+1] \subset [2, R]$, m odd, set $b = \min(8, m-1)$. On the complex disk of radius b about m, $|r^\eta F_a(r)| \leq H_m = \max_\pm (m\pm b)^{\Re\eta}\exp(\pi|\Im\eta|/2 + bM)$. Gauss quadrature with n nodes, exact on degrees below $2n$, errs by at most $4H_m b^{1-2n}/(b-1)$ on that panel by Cauchy's estimate and positivity of quadrature weights.

The tail uses the cancellation-preserving formula

$$\Phi_3(r) = 4r^{-1}(J_1^3 + J_0^2 J_1) - 4r^{-2}J_0J_1^2.$$

For clarity, $r^{1/2}J_\nu(br)$ is replaced by the first L real Hankel terms with frequencies $\pm b$. Their coefficients in r^{-j} for $+b$ are $i^j e^{-i\pi(2\nu+1)/4}\sqrt{2/(\pi b)}A_{\nu,j}/(2b^j)$ and those at $-b$ are conjugates. Start with $A_{\nu,0} = 1$ and multiply by $(4\nu^2 - (2j+1)^2)/(8(j+1))$ at each step. For $\nu = 0, 1$ the absolute error is at most er^{-L}, $e = \sqrt{2/(\pi b)}|A_{\nu,L}|b^{-L}$. This is the positive-real bound of the independent inverse benchmark: the Laplace representation continued to real Hankel argument gives a gamma expectation of $(1+iv/(2br))^{\nu-1/2}$; its Taylor remainder has modulus at most $|\binom{\nu-1/2}{L}|(v/(2br))^L$ because $|1+iv/(2br)| \geq 1$. Integrating the remainder gives the stated e. For each factor bound both its approximation and its true magnitude by the sum of absolute coefficients evaluated at R plus eR^{-L}. Multiplying by telescoping gives a product error coefficient $e_* = \sum_i e_i \prod_{j\neq i} B_j$. A product with prefactor mr^{-p} costs at most $|m|e_* R^{1-p-L+\Re\eta}/(p+L-1-\Re\eta)$ after integration. These estimates use $|r^\eta| = r^{\Re\eta}$ and retain the complex phase in the finite sum.

For $a \geq 1/4$ include $J_0(ar)$ among the four Hankel factors, giving $p = 3, 4$. A retained frequency ω and power r^{-P}, $P = p + j - \eta$, integrates to $R^{1-P}E_P(-i\omega R)$, where E_P is the generalized exponential integral continued from positive real damping. The zero frequency instead gives $R^{1-P}/(P-1)$; this includes $a = 1$. In the moment domain $\Re P > 1$ for this four-factor product.

For $0 \leq a < 1/4$ keep $J_0(ar)$ exact in the tail. The three remaining Hankel factors have $p = 5/2, 7/2$ and $\omega \in \{\pm 1, \pm 3\}$. Let $I_P(v) = \int_R^\infty r^{-P}e^{i(\omega+v)r}dr$. At v real near zero deform onto $r = R + i\,\mathrm{sgn}(\omega)t$, $t \geq 0$, using positive damping or a quarter-circle contour; here $\Re P > 1$. On $|v| \leq 1/2$ that contour analytically continues the integral and bounds it by $2R^{-\Re P}\exp(R/2 + \pi|\Im P|/2)$. Replace v by $a\cos\theta$ and average. Through degree $J-1$ the answer is

$$\sum_{\substack{0\leq k<J\\ k\text{ even}}} \frac{i^k a^k}{k!}\frac{\binom{k}{k/2}}{2^k}R^{1-P+k}E_{P-k}(-i\omega R).$$

Termwise differentiation on the deformed contour justifies $P-k$ outside the original ordinary integral range. Cauchy's estimate bounds the error by the contour bound times $(2a)^J/(1-2a)$ for each retained coefficient. At $a = 0$ only the constant survives. The bound on the three-factor product remains valid since $|J_0(ar)| \leq 1$ on the real tail. This step avoids inverse powers of a when $aR \ll 1$. Summing all errors and multiplying by $|C(h)|d^{-9}$ bounds the error in T_3. Complex ball arithmetic includes the additional rounding errors before the scalar is accepted. A radius and a modulus lower bound permit a relative claim only for the particular returned ball.

Small positive radii and arbitrary tilt. Write $q = 3+s$, $H = \Re h$, $D_* = \sqrt{27}/(2\pi^2)$, and $M_t = 1+\pi D_*/(1+H)$ if $H < 0$, $M_t = (3+t)^{2H}$ otherwise. For $0 \leq a = 3z < 3$, the following absolute comparison holds:

$$\left|d^{-9-6s}T_3(h,s;z) - U_h(a)\right| \leq |q|zW + M_a\{(1-z)^{-6|q|} - 1 - 6|q|z\},$$

$$W = \frac{4a\pi D_*(3a)^{2H+2}}{1+H} + 4|h|aM_0 \max\{2^{1-2H}, (3/2)^{2H-1}\}.$$

Thus the transfer error at a fixed order is $O(z^2)$ uniformly in bounded complex tilts. To prove it, use the source in Proposition 10.4 with displacement a and expand the preparation in z. Its linear term is $qz(X+\bar{X})$. The coefficientwise majorant for its full exponential series is $(1-z)^{-6|q|}$, using $|\operatorname{Tr} V^j + \overline{\operatorname{Tr} V^j}| \le 6$. Both the det-one and rotationally averaged trace densities are bounded by D_* because $D(re^{i\theta}) \le 27 - r^2[(r-4)^2+2]$. Splitting the translated measure at unit distance gives $\mathbb{E}|X-t|^{2H} \le M_t$. On $|X| \le 2a$ bound $|X+\bar{X}| \le 4a$ and integrate the translated power over the disk of radius $3a$ about a. On $|X| > 2a$ subtract $|X|^{2h}$, whose product with $X+\bar{X}$ integrates to zero on that rotation-invariant annulus. The real-segment derivative has magnitude at most $2|h| \max\{2^{1-2H}, (3/2)^{2H-1}\}|X|^{2H-1}$. This proves the bound for the first-order term. The leading normalization d^{9+6s} is kept exactly.

Executed checks. Fourteen complex-ball runs and one exact rational run at rank three met 10^{-10} relative error on their inputs at $s=-3$. They include $h=-0.95+3i$ at $z=0, 10^{-6}, 1/4, 1/3, 1.21/3, 0.9$, its conjugate at 10^{-12}, $h=3+3i$ at 0.9, and both a positive half-order and a near-integer order. The higher-precision calculation used 640 bits, $R=64$, $L=14$, $n=62$, $K_0=104$, $J=16$; a retained 192-bit failure at $a=1$ has a much wider special-function ball. At $z=1/3$, $h=-0.95+3i$, the 640-bit result rounded to 14 places is $-0.03351324061200 + 0.06772864303569i$. Its full unrounded ball has complex radius below 4.70×10^{-23}. Independent double-precision elliptic quadrature accepted 13 of the 15 tests; its largest relative discrepancy from the certificate midpoints was 6.75×10^{-14}. The two declined cases were both enclosed by the finite-part calculation. The three predecessor inverse-order references were separately replayed. Conditional elliptic rotation values on the derivative diagonal agreed with direct circle integrals within 1.2×10^{-15} in twelve tests, while independent whole-ensemble randomized quadratures had discrepancies up to 0.0063 in the ordinary inverse derivative. The latter comparisons do not certify decimal places. At $z=5\times10^{-9}$, $h=-0.95+3i$ the tilt-transfer bound multiplied by the prefactor is below 1.040×10^{-12} simultaneously for $|s|\le 3$, with a common lower modulus greater than 0.06726. Three complex boundary tilts were evaluated with rounding included. These are input-specific approximations with a common analytic error bound, and their midpoints vary with s. **A continuous small-radius test.** On the entire block

$$0 \le z \le 5\times10^{-9}, \quad -0.95 \le \Re h \le -0.94995, \quad 2.99995 \le \Im h \le 3, \quad |s| \le 3,$$

the input-dependent approximation $d^{9+6s}U_h(3z)$ has absolute error below 1.040×10^{-12} and the exact $|T_3|$ exceeds 0.04371. Thus a further absolute budget of 10^{-12} for evaluating the approximation still suffices for 10^{-10} relative accuracy. This common budget bounds the error at every parameter separately. It is not the radius of a single ball containing every moment in the block.

Here are details of the lower bound, which is needed for the relative conclusion. Set $h_0=-0.95+3i$, $a_0=1.5\times10^{-8}$ and $H_0=-0.95$. The preceding numerator is increasing after replacing $a, z, |h|, |q|$ with $a_0, a_0/3, |h_0|, 6$ and each power with its maximum at H_0 on this box. In particular the positive power-series remainder for the preparation is increasing. For the unnormalized translated moment, $|\partial_h U_h(a)| \le \pi D_*/(1+H_0)^2 + 2\log(3+a_0) < 333$, by splitting at unit distance and integrating the absolute logarithm on the inner disk. At h_0, $|U_{h_0}(a) - U_{h_0}(0)| \le 120a$. To verify this, the planar trace density $p_2(x)$, the rotational average of $\sqrt{D(x)_+}/(2\pi^2)$, is 1-Lipschitz on $|x| \le 0.51$. Indeed $D > 20$ and $|\nabla D| \le 36r + 24r^2 + 4r^3 < 26$ there. Split the source disk at $|x|=1/2$. Outside, the absolute translated-kernel difference costs at most $2|h_0|(0.49)^{2H_0-1}a$. Inside, translate the kernel to the origin and subtract the densities on the overlapping disks. Integration of r^{2H_0} yields at most $\pi a/(1+H_0)$. The symmetric difference lies in $1/2-a \le |x| \le 1/2+a$ with area $2\pi a$, costing at most $2\pi a D_*(0.49)^{2H_0}$. The recorded ball at $(h_0, 0)$ provides $|U_{h_0}(0)| > 0.06726$. Subtract $333\sqrt{2}(0.00005) + 120a_0$ (the receipt uses the unrounded bounds), multiply the surviving lower bound by $(1-(a_0/3)^2)^{27}$, and subtract the preparation error. The saved ball computation gives 0.04371227 as a downward-safe lower bound. The model-relative error is below 2.378×10^{-11}. The uniform statement concerns the analytic approximation; the pointwise numerical certificate is accepted only when its independently charged rounding and quadrature error meets the further budget. Those calculations were run at the specified sample inputs, separately from the arithmetic establishing the domain-wide inequalities.

Negative orders near the upper radius

Put $d=1-z^2$, $S=d\sum_j \lambda_j/(1-z\lambda_j)$, $L=\log|\Lambda_N(z)|$, and $T=\mathbb{E}[e^{2sL}|S|^{2h}]$. All powers of positive quantities use the real logarithm. Two scalar bounds apply at the upper edge. One retains the full imaginary-order range

at rank three. The second retains a disk of complex tilts at ranks four through eight, on much narrower order disks.

Proposition 10.2C (upper-radius inverse certificate). On $0.8 \le z \le 0.9$, $-0.95 \le u = \Re h \le -0.6$, $|\Im h| \le 3$, let $a = 3z$, $B = s + 3$, $X = \operatorname{Tr} V$ for Haar $V \in U(3)$, and $I_h(a) = \mathbb{E}|X + a|^{2h}$. The Möbius preparation in the preceding theory gives

$$T = d^{-9+6B}\mathbb{E}\left[|X + a|^{2h}\prod_{j=1}^{3}|1 + zw_j|^{-2B}\right], \qquad \left|d^{9-6B}T - I_h(a)\right| \le I_u(a)\left(e^{6|B|[-\log(1-z)]} - 1\right).$$

The second inequality follows pointwise from $|e^x - 1| \le e^{|x|} - 1$ and the ranges of the three logarithms. At $B = 0$, the spectral algorithm below gives absolute accuracy finer than 1.20×10^{-18} in I_h, uniformly over this entire order–radius box, counting finite arithmetic through a per-input acceptance check. At $.89 \le z \le .90$, $|\Im h| \le .025$ and $|B| \le 3 \times 10^{-12}$, the resulting relative error in T is below 6.62×10^{-11}. Intersect the last disk with $|s| \le 3$ when testing the original target. These are pointwise error budgets valid for every input in the box.

For the spectral certificate, planar Riesz inversion gives the ordinary expectation

$$I_h = C_h\int_0^\infty r^{-1-2h}J_0(ar)\Phi(r)\,dr, \quad C_h = 2^{2h+1}\frac{\Gamma(1+h)}{\Gamma(-h)}, \quad \Phi(r) = \det[J_{i-j}(r)]_{1\le i,j\le 3}.$$

For example, insert a Gaussian source cutoff in the Fourier transform of the locally integrable power $|x|^{2h}$. Its translated inverse transform converges to the physical expectation by the bounded compactly supported planar trace density and local L^1 approximation by Gaussian convolution. Absolute spectral convergence follows from the determinant identity in §21, $\Phi = 4(J_1^3 + J_0^2J_1)/r - 4J_0J_1^2/r^2$, and the positive-ray Bessel bounds, which give $J_0(ar)\Phi(r) = O(r^{-3})$. Near the origin $|J_0(ar)\Phi(r)| \le 1$ on the real ray. The proof covers independently complex powers using the same absolute bounds at u.

Write $\beta = -1 - 2h$. Discard $[0, 2^{-68}]$ with error at most $2^{68(2u)}/(-2u)$ before the factor C_h. On dyadic panels to 1 and then unit panels to $R = 110$, use 62 Gauss–Legendre nodes per panel. If b, D are the midpoint and half-length, the disk $|w - b| \le 2D$ lies in the right half-plane. The analytic integrand there is bounded by

$$K = (b + 2D)^{\Re\beta}\exp\big(|\Im\beta|\pi/2 + (3 + a)2D\big),$$

using the characteristic-function support of $J_0(ar)\Phi(r)$. Polynomial exactness, positivity and the Cauchy remainder bound the error by $8DK\,2^{1-124}$ per panel.

On the tail, use the 14-term positive-real Hankel expansion and the explicit one-term remainder proved in §21 for each of the four factors. If M_i bounds both the exact and truncated normalized factors $r^{1/2}J_{\nu_i}(b_ir)$, and their difference is at most E_ir^{-14}, each product with leading exponent $p \in \{3, 4\}$ contributes before its scalar coefficient at most

$$\left(\sum_i E_i\prod_{j\ne i}M_j\right)\frac{R^{1-p-14+\Re\beta}}{p + 14 - 1 - \Re\beta}.$$

Each retained harmonic is integrated as $R^{1-k+\beta}E_{k-\beta}(-i\omega R)$ at $\omega \ne 0$, by Laplace tempering. At zero frequency the result is $R^{1-k+\beta}/(k - \beta - 1)$. The complex order in both the power of R and the exponential integral is necessary. In the uniform tail bounds the only variable-scale factor has $b = a \ge 2.4$; absolute coefficient and remainder bounds decrease with b. The reflection formula, the real gamma integral split at one and $.05 \le 1+u \le .4$ give $|C_h| \le (20 + e^{-1})^2\cosh(3\pi)/\pi$. Outward evaluation gives a combined compact and initial-gap error below 1.907×10^{-19} and a tail error below 6.412×10^{-21} in I_h. The adaptive finite-arithmetic test admits a further 10^{-18}, including the printed midpoint. For rational inputs there are finitely many operations with regular arguments. Accuracy converges on increasing precision; finite sums and any exponential-integral recursions are performed in complex ball arithmetic.

For the nonvanishing result let $\eta = e^{-10}$. The planar trace density, with respect to Lebesgue area, near $r = |X| \ge 2.67 - \eta$ is

$$q(r) = \frac{A}{16\pi^2r^{3/2}}{}_2F_1(1/2, 1/2; 2; A/(16r^3)), \qquad A = (3 - r)^3(1 + r).$$

This is the rank-three trace density of §9 divided by $2\pi r$. Put $r_0 = 2.67 - \eta$, $A_0 = 4(3 - r_0)^3$; then $q \le A_0/[16\pi^2 r_0^{3/2}(1 - A_0/(16r_0^3))]$ there, by the positive hypergeometric series. Consequently $\mathbb{E}[|X + a|^{2u}; |X + a| < \eta] < .004828$, whereas $I_u \ge 5.7^{-1.9} > .03663$. On the complementary set the argument of $|X+a|^{2h}$ has magnitude at most .5. Taking real parts on both sets gives $|I_h|/I_u \ge \cos(.5) - (1 + \cos(.5))(.004828)/(.03663) > .6300$; the outward calculation before rounding gives $> .63014$. The complex tilt changes the unnormalized result by at most $4.145 \times 10^{-11} I_u$. Combine these bounds with the two scalar integrations for I_h, I_u and the final decimal readout. The stated relative bound even allows 8.01×10^{-15} unnormalized quadrature error per integration, as recorded by the conservative rectangular proof. No lower bound on the full imaginary-order box is assumed.

Independent elliptic check. An alternative starts with the radial trace density $p(r) = 2\pi r q(r)$. The uniform phase average is $D^{2h}{}_2F_1(-h, -h; 1; x)$, where $D = \max(a, r)$, $x = (\min(a, r)/D)^2$. At $r = a \pm g$ take $g = \ell e^{-t}$, $\ell = 1/8$, $k = (2a \pm g)/D^2$, and $q = 1 - x = gk$. Including dr, the angular factor on a side is

$$D^{2h}\Big[g\frac{\Gamma(1+2h)}{\Gamma(1+h)^2}{}_2F_1(-h,-h;-2h;q) + \ell^{2+2h}e^{-(2+2h)t}\frac{\Gamma(-1-2h)}{\Gamma(-h)^2}k^{1+2h}{}_2F_1(1+h,1+h;2+2h;q)\Big].$$

There is no coalescent Gauss connection exponent in the stated real-order strip. For $\delta = \ell e^{-520}$, the omitted two-sided strip costs at most

$$2P_*\frac{\sqrt{\pi}\Gamma(-u-1/2)}{4\sqrt{a(a-\delta)}\Gamma(-u)}\frac{\delta^{2u+2}}{2u+2}, \qquad P_* = 3\sqrt{27}/\pi.$$

Indeed $|a - re^{i\theta}|^2 \ge (r - a)^2 + 4ar\theta^2/\pi^2$ for $|\theta| \le \pi$, and the density formula of §9 gives $p(r) \le P_*$ (also directly from the conditional square-root discriminant of maximum 27). The separate gap $|r - 1| < 2^{-68}$ costs at most $2^{1-68}P_*(a-1-2^{-68})^{2u}$. Away from the two omitted gaps, complex ball quadrature evaluates the retained function on certified analytic panels. The left interval at the elliptic junction was subdivided dyadically after a single-panel trial failed. Five independent spectral and elliptic enclosures overlap, including $z = .9, h = -.95 + 3i, s = -3$, where the spectral midpoint is $106380.30173327900243 - 75054.362702108027 35i$. Omitting the tail changes that moment by more than 13.26. The two procedures have different truncations and share the Haar normalization.

The full target order rectangle at rank three

Proposition 10.2D (all radii on the Haar-prepared slice). For $N = 3, s = -3, 0 \le z \le .9, -.95 \le \Re h \le 3, |\Im h| \le 3$, the scalar $I_h(3z) = d^9T_3(h, -3; z)$ has a certified absolute approximation with error below 3.02×10^{-17}, including adaptive finite arithmetic. This includes exact and near integer orders, the centre, and the critical radius $z = 1/3$. The continued expression gives the ordinary expectation everywhere in this box.

Write $F_a(t) = J_0(at)\Phi(t) = \sum f_k t^{2k}$, with the determinant Φ above. At the origin, integrate its first 38 Taylor coefficients on $(0, 1)$ against the Mellin weight. Absorb the gamma zero before dividing:

$$\frac{C_h}{2k - 2h} = 2^{2h}\Gamma(1 + h)\frac{(-h)_k}{\Gamma(k + 1 - h)}.$$

This is regular even at $h = k$. The coefficients are rational for rational a, by convolution of the three Bessel series in the determinant. The characteristic-function support gives $|f_k| \le (3 + a)^{2k}/(2k)!$. The omitted origin series before $|C_h|$ is at most

$$\frac{(3 + a)^{76}}{76!\,[1 - (3 + a)/77]\,(76 - 2\Re h)}.$$

The rest of the integral starts at one. The origin series with gamma cancellation and the absolutely convergent remainder are holomorphic continuations of the negative-order formula throughout the strip of interest. The physical expectation is holomorphic for $\Re h > -1$ locally by bounded compactly supported trace density, so uniqueness identifies the ordinary expectation. If h is a nonnegative integer only the corresponding Taylor coefficient survives. On $[1, R]$ apply the 62-node analytic Gauss estimate above; for negative $\Re\beta$ use the inner disk distance $b - 2D > 0$ in the radial envelope.

When $a > 1/2$ use $R = 144, L = 18$ in the four-factor Hankel expansion. An exactly vanishing harmonic uses the nonoscillatory power integral. At positive frequencies arbitrarily close to zero, the special-function recurrence is evaluated in balls and checked for accuracy. For $a \le 1/2$ expand only the three factors in Φ, with $R = 110, L = 14$.

Each tail monomial now has power $r^{\beta-k}$, $k \in \frac{5}{2}+\mathbb{Z}_{\ge 0}$, and integer frequency $\omega \in \{-3,-1,1,3\}$; keep the angular representation of $J_0(ar)$ intact. For the angular harmonic integral

$$g(\theta)=\int_R^\infty r^{\beta-k}e^{ir(\omega+a\cos\theta)}\,dr$$

rotate the departing ray to $r=R+i\,\mathrm{sgn}(\omega)v$. The contour change on the real angular axis follows first with a damping factor or directly by the quarter-circle bound $k-\Re\beta>1$; the rotated ray defines the analytic angular continuation. In $|\Im\theta|\le 1$ its modulus is at most

$$\frac{R^{\Re\beta-k}\exp(Ra\sinh 1+|\Im\beta|\pi/2)}{1-a\cosh 1}.$$

Multiply by the absolute coefficient sum and use the 192-node periodic trapezoid bound $2\sup|g|/(e^{192}-1)$. The inner ray integral is the same complex-order exponential integral as before. At $a=0$ the exact angular average needs one evaluation. This avoids inverse powers of a in the tail error. For the full-order budget $|C_h|\le 128(20+6)^2\cosh(3\pi)/\pi$; the elementary bound for $\Gamma(1+\Re h)$ splits its positive integral at one. The outward unnormalized analytic truncations are below 2.915×10^{-17} at $a\le 1/2$ and 1.657×10^{-18} above. The accepted three-term finite source calculation reserves 10^{-18} in I_h. The printed physical moment charges its own final decimal copy. This all-radius bound is coarser than the preceding narrow inverse-box certificate at the upper edge.

Proposition 10.2E (restoring the full tilt disk at small radius). For $0\le z\le 10^{-6}$, $N=3$, all h in the preceding order rectangle and independent $|s|\le 3$, a second-order physical-source reconstruction gives a uniform absolute budget below 5.86×10^{-13} in T, including a 10^{-15} final finite-arithmetic allowance. The returned local relative bound uses the modulus test on each output. The complex corner $z=10^{-6}, h=-.95+3i, s=3i$ achieved relative error below 3.78×10^{-12}. At $z=10^{-5}$ the same input returned a relative bound of 2.16×10^{-9}, above the target.

Let $B=3+s, X=\operatorname{Tr}V, x=\Re X$, V Haar, and $V_h=|X+a|^{2h}$. Compute

$$A=\frac{I'_{h+1}(a)}{2(h+1)},\quad X_1=A-aI_h,\qquad X_2=\frac{I''_{h+2}(a)-2(h+2)I_{h+1}(a)}{4(h+1)(h+2)}-2aA+a^2I_h.$$

Then $X_1=\mathbb{E}[xV_h], X_2=\mathbb{E}[x^2V_h]$, by differentiation of the locally integrable shifted powers. This differentiation can first be taken in distributions and then against the bounded density; the derivatives needed are locally integrable for $\Re h>-1$. Equivalently use ordinary translation continuity of their local L^1 kernels. Differentiate the compact Bessel factor in a up to order two. At the origin differentiate its rational coefficients, whose unsigned degree-n bound is now $(3+a)^{n-j}/(n-j)!$ for derivative j. On the low-radius tail replace β by $\beta+j$ in the moment with shifted order and insert $(i\cos\theta)^j$ into the angular average; its strip bound grows by at most $\cosh(1)^j$. In the actual derivative combinations the net tail exponent decreases. On an open negative-integrable strip with $\Re H>j/2-1$ this can also be obtained by differentiating the spectral formula directly with the rotated nonstationary tail; for $j=2$ one may start with the differentiated analytic finite-part origin formula on $0<\Re H<1$. The identity then extends throughout the needed strip, including the removable integer orders.

Approximate the prepared expectation before its factor d^{-9+6B} by $I_h-2BzX_1+2(Bz)^2X_2$. In the logarithm of the preparation, the linear term is $-2Bzx$, the quadratic term is $Bz^2\Re\operatorname{Tr}(V^2)$ and the remaining exponent has magnitude at most $E_3=6|B|[-\log(1-z)-z-z^2/2]$. Write $K=6|B|z, E_2=3|B|z^2$. The error divided by I_u, $u=\Re h$, is at most

$$e^{K+E_2}(e^{E_3}-1)+e^K(e^{E_2}-1-E_2)+E_2(e^K-1)+K^3e^K/6+|B|z^2H_2,$$

where $H_2=|\mathbb{E}[V_h\Re\operatorname{Tr}(V^2)]|/I_u$ may be replaced by the following upper bound. For $a>0$ take $r_*=7a^{2/3}$, $t_*=a/r_*, \rho=.2$, assuming $t_*<\rho, r_*<3$. On $|X|<r_*$, the rank-three identity $\operatorname{Tr}(V^2)=X^2-2\det(V)\bar X$ bounds the insertion by $r_*^2+2r_*$. On the complement condition on the global rotation. The power on that circle is $|X|^{2h}(1+te^{i\phi})^h(1+te^{-i\phi})^h$, with $t=a/|X|$, and the insertion has angular frequency two. The constant and linear powers of t integrate to zero. The analytic factors on $|t|=\rho$ have modulus at most $(1-\rho)^{-2|h|}$; division by the positive local moment costs at most $(1-t_*)^{-2|u|}$. Thus

$$H_2\le\max\left(r_*^2+2r_*,\ 3(1-t_*)^{-2|u|}(1-\rho)^{-2|h|}\frac{(t_*/\rho)^2}{1-t_*/\rho}\right).$$

Use the exact centre value at $a = 0$. This proves the gain from the unresolved quadratic insertion without sampling an oscillatory angular factor. Since $q(r) \le \sqrt{27}/(2\pi^2)$, splitting at $|X+a| = 1$ gives $I_u \le \sqrt{27}/(2\pi^2)\,(2\pi/.1)+I_3 < 22.54$, with $I_3 = 6 + 18a^2 + 9a^4 + a^6$ from the first three exact Haar trace moments. The uniform spin bound is below .002915, and the preparation error divided by I_u is below 2.593×10^{-14}. The finite spectral budgets, derivative amplification and normalization are recorded separately in the companion script. At larger small radii it chooses the minimum of this estimate and the direct quadratic remainder. The radial derivative term carries physical information: an independently known diagonal integer value rejects removal of the factor d^2.

Eighteen fixed-input evaluations cover $z = 0$, 10^{-7}, 10^{-6}, 10^{-5}, 1/6, 1/3 and both adjacent sides, as well as interior and upper-edge radii. At the critical radius the half-order enclosure overlaps the inherited independent half-order quadrature. The integer third-order Haar polynomial, diagonal first-derivative ordinary moment, upper-edge elliptic data and the near-integer cancellation test are recorded in the reproducible examples. A failed target at 10^{-5} is retained with its absolute bound.

Theorem 10.2F (uniform relative accuracy on the full small-radius box). At every $0 \le z \le 10^{-6}$, $|s| \le 3$, $-.95 \le \Re h \le 3$ and $|\Im h| \le 3$, the rank-three evaluator above has relative error below 5.24×10^{-11}. In particular the denominators in the relative test stay away from zero throughout this box. The proof uses a separate continuous complex-order calculation at the centre.

Let $q(r)$ be the planar trace density. It decreases to zero: inside $r = 1$, both $\sqrt{A}$ and $E(16r^3/A)$ decrease; outside, $A/r^{3/2}$ and the positive hypergeometric series in $A/(16r^3)$ decrease. The two formulas agree at one. Integration by parts therefore writes $P(h) = (1 + h)I_h(0) = \pi \int_0^3 r^{2+2h}\, d[-q(r)]$. Split $[0, 3]$ into 3000 equal bins. For bin $[l, r]$ let b be its midpoint and $w = \pi(q(l) - q(r))$ its known mass. Replace the integral by $\sum wb^{2+2h}$. On every bin with positive left endpoint, the error is at most $w|1 + h|(r - l) \max_{x\in[l,r]} x^{1+2\Re h}$; the first bin costs at most $2wr^{2+2\Re h}$. On a real-order slab the corresponding extrema occur at slab and radial endpoints. This bounds the error of quadrature for a complex continuum.

Approximate the finite exponential sum by its degree-210 Taylor polynomial in $h - 1$. Put $L_b = 2\log b$, $|h - 1| \le \sqrt{13}$; an exponential remainder from each bin is at most $wb^4e^{2|L_b|}(|L_b|\sqrt{13})^{211}/211!$. For the derivative use $wb^4|L_b|e^{2|L_b|}(|L_b|\sqrt{13})^{210}/210!$. The resulting errors are below 9.83×10^{-41} and 5.76×10^{-39}. On each parameter rectangle use the polynomial and its derivative at the midpoint, and majorize the exact finite sum's second derivative by $\sum wL_b^2 \max(b^{2+2u_-}, b^{2+2u_+})$. Taylor's formula on complex line segments covers the whole rectangle. Conjugation symmetry covers negative imaginary order.

To transfer a lower bound to the physical scalar, for $|x| \le .5$ and $a \le 3\times10^{-6}$ use $|q(|x-a|) - q(|x|)| \le a$. Indeed $q = \sqrt{A}E(m)/\pi^3$ on $r < 1$; up to .51, $|A'/A| < .82$, $m < .138$, $|m'| < .925$, and $|E'(m)| \le \pi/(8\sqrt{1-m})$, giving $|q'| < 1$. On the rest of the plane the translation inequality for a radial decreasing density of bounded variation costs at most $a\,2\pi \int_0^3 q(r)dr \le 6\pi aq(0)$ in L^1. Consequently the loss when replacing $I_h(0)$ by $I_h(a)$ is at most

$$a\left[\frac{\pi(.5)^{2+2u}}{1+u} + 6\pi q(0)\max\{(.5)^{2u}, (3+a)^{2u}\}\right].$$

The preparation then costs at most $I_u(a)(e^{36[-\log(1-z)]} - 1)$, and the external multiplier has modulus at least d^{27}. For the error comparison use the slab-specific positive upper bound $G = 1 + \pi q(0)/(1 + u)$ at $u < 0$ by splitting at $|X + a| = 1$, and $G = I_3(a)^{u/3}$ at $u \ge 0$ by Hölder. On each slab the physical absolute budget is at most $2.593 \times 10^{-14}G + 1.1 \times 10^{-15}$. The printed source and its finite readout are accepted after an outward 10^{-15} check, attainable because the uniform propagated source error is below 4.61×10^{-17} before final arithmetic.

The proof subdivided 32 real-order slabs, visited 256 rectangle nodes and accepted 144 leaves at maximum depth eight. It found $|T| > .00087054$ everywhere. Pairing the positive lower bound on each leaf with its own slab error gives maximum relative error less than 5.230×10^{-11} before output rounding, with the stated slightly enlarged bound covering decimal readout. The rectangle evaluations bound continua; no inference from a testing grid enters the proof. The full enclosure data and counts are in the companion nonvanishing receipt.

Integer moment order and independent tilt

Theorem 10.3 (symmetric-power equation). There is a complementary all-rank construction. For every fixed integer $m \ge 0$, $N \ge 1$, and noninteger $s \in \mathbb{C}$, the interior observable $T_N(m, s; z)$ belongs to a differential

system of dimension at most $N+1$, independent of m. Its scalar ordinary differential equation in z has order at most $N+1$. Only finite polynomial operations and reductions of rational functions are needed to construct it.

Let $w(\lambda) = [(1-z\lambda)(1-z/\lambda)]^s$ on the positively oriented unit circle, and $g(\lambda) = (1-z^2)\lambda/(1-z\lambda)$. In the tilted Toeplitz determinant use formal source $e^{ag(\lambda)+bg(1/\lambda)}$. The coefficient of $a^m b^m$ multiplied by $(m!)^2$ equals $T_N(m,s;z)$. Its truncated entries are contour integrals of $wR\,d\lambda/(2\pi i)$, where R is rational with possible finite poles only at $0, z, 1/z$. The logarithmic derivative of w in λ is

$$L = s\big[(\lambda-z)^{-1} + (\lambda-1/z)^{-1} - \lambda^{-1}\big]. \tag{10.3}$$

The single-valued determination of w on the contour gives zero integral for $w(r' + Lr)$ whenever r is rational with these allowed poles. For a pole b_0 of order $k \geq 2$, use $r = (\lambda - b_0)^{1-k}$; its leading coefficient after applying $\partial_\lambda + L$ is $1-k+\operatorname{res}_{b_0} L$, which is nonzero when s is noninteger. Other finite poles introduced in this operation are simple. For a polynomial term of degree $k \geq 0$, use $r = \lambda^{k+1}$; its leading coefficient is $k+1+s$. After reducing to three simple fractions the relation from $r = 1$ removes one. Thus each entry coefficient equals a rational linear combination over $\mathbb{C}(s,z)$ of

$$F = \oint w\,\frac{d\lambda}{2\pi i\lambda} = {}_2F_1(-s,-s;1;z^2), \qquad G = \oint w\,\frac{d\lambda}{2\pi i(\lambda-z)} = F - \frac{z}{2s}\frac{dF}{dz}.$$

The Gauss series follows by multiplying the two binomial series. The expression for G follows by differentiating F and applying circle inversion symmetry to its two log derivatives. With $x = z^2$ and $\theta = x\partial_x$, one has $(1-x)\theta^2 F = x(s^2 F - 2s\theta F)$. The truncated determinant is therefore a homogeneous polynomial of degree N in $F, \theta F$. Euler derivatives stay in the span of $F^{N-j}(\theta F)^j$, $0 \leq j \leq N$. Form the rows of the first $N+2$ derivatives beginning with order zero; a linear dependence gives the equation. The construction treats noninteger tilts directly, and any polynomial identity after clearing denominators can also be specialized at integer tilts, with possible degeneracy.

For an explicit way to initialize the $m = 1$ system, write $Z(x) = \mathbb{E}|\Lambda_N(\sqrt{x})|^{2s}$. Differentiating the holomorphic and antiholomorphic spectral points independently gives $T_N(1,s;z) = d^2\theta^2 Z(x)/(s^2 x)$, $d = 1-x$. The entries of the Toeplitz determinant for Z are F_{j-k} with $F_0 = F$, $F_{-k} = F_k$ and

$$F_1 = -\frac{szF + (d/z)\theta F}{s+1}, \qquad z(k+s+1)F_{k+1} = k(1+x)F_k + z(s+1-k)F_{k-1} \quad (k \geq 1).$$

These identities follow by integrating the angular derivatives of $\sin\theta_0\, w$ and $e^{-ik\theta_0}|1-ze^{i\theta_0}|^2 w$, respectively. Here θ_0 is the angle and θ in the displayed formula is the Euler operator. This branch allows continuous complex tilt at every rank and gives a separate check on low integer moments.

Independent noninteger exponents through a planar displacement

Proposition 10.4 (a closed displacement system at general rank). Let $N \geq 2$, $0 < z < 1$, $s \in \mathbb{C}$ and $\Re h > -1$. Use the disk-transformed law in Theorem 10.1. Set $\nu = -N - s$, $D_z(w) = (1-zw)(1-z/w)$ on $|w| = 1$, and let

$$U(a) = \mathbb{E}_{U(N)}\left[|a - \operatorname{Tr} U|^{2h} \prod_{i=1}^{N} D_z(w_i)^\nu\right].$$

This is a planar distribution in the displacement a, with the ordinary interior readout $T_N(h,s;z) = (1-z^2)^{N^2+2Ns}U(Nz)$. At ranks or displacements where evaluating a general distribution at a point would be ambiguous, this formula specifies the original integral. In particular the physical interior point has the absolute-existence domain established earlier. We give a finite linear differential system, polynomial in the two displacement derivatives, containing U as a constant linear combination of its components. It permits construction directly at independent noninteger h, s. The displacement is kept as an independent variable throughout the derivation.

For a real Fourier frequency (ξ_1, ξ_2) set $t = i(\xi_1 - i\xi_2)/2$, $u = i(\xi_1 + i\xi_2)/2$ and $E = t\partial_t + u\partial_u$. The one-angle integrals are

$$F_j = \int w^j D_z(w)^\nu e^{tw+u/w}\,\frac{d\theta}{2\pi}, \qquad w = e^{i\theta}.$$

Integrate the angular derivative of $w^j D_z^{\nu+1} e^{tw+u/w}$ around the circle. With $a_0 = 1 + z^2$ this gives

$$-ztF_{j+2} + [a_0 t - z(j+\nu+1)]F_{j+1} + [ja_0 + z(u-t)]F_j + [-a_0 u + z(\nu+1-j)]F_{j-1} + zuF_{j-2} = 0. \tag{10.4}$$

The bases of the complex powers are positive. Periodicity gives the identity for all tilts, and $EF_j = tF_{j+1} + uF_{j-1}$. Take $K = \max(2, N-1)$ and $f = (F_{-K}, \dots, F_K)$. Reduce F_{K+1} with (10.4) at $j = K-1$ and F_{-K-1} at $j = 1-K$. In the Euler equations it is tF_{K+1} and uF_{-K-1} that occur. Consequently the denominators t, u cancel before assembly: the matrix in $Ef = A(t,u)f$ is affine in t, u with coefficients in $\mathbb{C}[z, z^{-1}, \nu]$. All other rows are the two ordinary shifts. In particular

$$A_{K,K} = a_0 t/z - (K+\nu), \qquad A_{K,K-1} = (K-1)a_0/z + 2u - t$$

in the upper-index row, including the direct contribution uF_{K-1}.

Form the vector V of degree-N monomials in f, with $EV = A_N(t,u)V$ obtained by the product rule. Its dimension is $\binom{2K+N}{N}$. For each monomial let W be the planar convolution of $|a|^{2h}$ with the corresponding convolution of N one-angle measures $w^j D_z^\nu \, d\theta/(2\pi)$ on the unit circle. Let $E_a = (\Re a)\partial_{\Re a} + (\Im a)\partial_{\Im a}$ and $\partial_a = (\partial_{\Re a} - i\partial_{\Im a})/2$. The closed system is

$$(2h - E_a)W = A_N(-\partial_a, -\partial_{\bar a})W. \tag{10.5}$$

The determinant $\det[F_{i-j}]_{0 \le i,j < N}$ prescribes a constant linear combination of W that equals U. At rank three the system has 35 components. The requested combination has the five monomials with coefficients in $F_0^3 - 2F_{-1}F_0F_1 + F_{-1}^2F_2 + F_{-2}F_1^2 - F_{-2}F_0F_2$. All matrices require only (10.4) and integer monomial multiplicities. The Fourier source along each ray is fixed by the entire one-angle integrals. Its initial derivatives at the origin are given by $\partial_t^k \partial_u^l F_j(0) = \int w^{j+k-l} D_z^\nu d\theta/(2\pi)$, including in resonant cases. These can be computed by the absolutely convergent pair of binomial series at $0 < z < 1$. Thus the source data do not require evaluating any noninteger mixed moment.

For proof, first take $-1 < \Re h < 0$. The Fourier transform (positive sign convention) of W is a single common constant times $|\xi|^{-2h-2}V$, by the planar Riesz formula in Theorem 10.2. Euler differentiation of that locally integrable homogeneous factor is valid as a distribution through $\xi = 0$. Inverse Fourier transformation gives $E \mapsto -E_a - 2$, $t \mapsto -\partial_a$ and $u \mapsto -\partial_{\bar a}$. This proves (10.5). Compact support of the convolved circle measures and local integrability of $|a|^{2h}$ give holomorphy as tempered distributions for $\Re h > -1$. Continuation proves the same identity for this full range, including integral orders. For a direct interpretation of the system as a numerical equation, its Fourier ray satisfies a linear ordinary equation with affine coefficient in the radius, a regular singularity at zero, and the specified entire solution there. This is an all-rank planar equation with specified source data. The following construction also differentiates the preparation and eliminates the displacement derivatives on the physical curve at every rank $N \ge 2$.

An ordinary equation along the physical radius

Theorem 10.5 (elimination on the physical curve). For every $N \ge 2$ the determinant readout in Proposition 10.4 belongs to an explicitly specified ordinary linear system in z, of dimension $\binom{2K+N}{N}$, with $K = \max(2, N-1)$. At ranks three and four the sizes are 35 and 210. It has rational coefficients in z, h, s and permits independent $s \in \mathbb{C}$, $\Re h > -1$. The assertion is local on regular intervals of $0 < z < 1$ away from zeros of the selected matrix minor and the critical trace radii $Nz = |N - 2j|$, $j = 0, \dots, N$. Values for initialization on each interval are the convergent angular integrals below. We do not give a condition number or a connection matrix across a singular radius.

Separate the two Euler operators $t\partial_t$ and $u\partial_u$ in (10.4), assigning the upper boundary reduction to the first and the lower to the second. On degree-N monomials denote their matrices by A_+, A_-. Write each as $A_{\pm,0} + tA_{\pm,t} + uA_{\pm,u}$. For the third matrix differentiate the one-angle preparation at fixed t, u. Put $a_0 = z$, $b_0 = 1/z$, and let brackets denote the one-angle integral with multiplier $D_z^\nu e^{tw+u/w}$. Introduce $U_a = \nu\langle (w - a_0)^{-1} \rangle$, $U_b = \nu\langle (w - b_0)^{-1} \rangle$. Periodic integration of the total derivatives for $j = 0, 1$, now without the extra factor D_z, gives

$$\begin{aligned} a_0 U_a + b_0 U_b &= -\nu F_0 - tF_1 + uF_{-1}, \\ a_0^2 U_a + b_0^2 U_b &= -(1+\nu)F_1 - \nu(a_0 + b_0)F_0 - tF_2 + uF_0. \end{aligned}$$

In fact $w\partial_w \log D_z = w/(w-a_0) + w/(w-b_0) - 1$. The determinant of this auxiliary system is $a_0 b_0 (b_0 - a_0) \neq 0$. Set $L_{j,v}(w) = (w^j - v^j)/(w - v)$, a Laurent polynomial within the retained mode range. From $\partial_z \log D_z = z^{-1} - (w-a_0)^{-1} + z^{-2}(w-b_0)^{-1}$ we obtain

$$\partial_z F_j = \nu F_j / z - \nu \langle L_{j,a_0} \rangle + \nu z^{-2} \langle L_{j,b_0} \rangle - a_0^j U_a + z^{-2} b_0^j U_b.$$

Lifting by the product rule yields $\partial_z V = CV$ with $C = C_0 + tC_t + uC_u$. All three constructions use only Laurent-polynomial arithmetic and a two-row solve.

Write $d = \binom{2K+N}{N}$ in this proof. With I the identity of size d, set

$$\begin{aligned} L &= \begin{pmatrix} NzI - A_{+,t} & -A_{+,u} \\ -A_{-,t} & NzI - A_{-,u} \end{pmatrix}, \quad G = \begin{pmatrix} hI - A_{+,0} \\ hI - A_{-,0} \end{pmatrix}, \\ D &= \begin{pmatrix} NI - C_t & NI - C_u \end{pmatrix}. \end{aligned} \tag{10.6}$$

Each frequency Euler operator differentiates the planar Riesz multiplier with eigenvalue $-1-h$; under inverse Fourier transformation it becomes respectively $-1 - a\partial_a$ or $-1 - \bar{a}\partial_{\bar{a}}$. This gives $LX = GW$ on $a = \bar{a} = Nz$, with $X = (\partial_a W, \partial_{\bar{a}} W)^{\mathsf{T}}$ denoting stacked column vectors. The chain rule then gives $W' = C_0 W + DX$. Both identities extend as distributions throughout $\Re h > -1$ as in Proposition 10.4. On the indicated regular intervals the components are smooth near the evaluation point. Indeed the trace sum of independent angles is a submersion on the preimage of a disk about any noncritical displacement. Its differential drops rank only if all unit tangents are parallel, giving the listed absolute radii. A smooth partition of unity permits derivatives of the localized convolution to fall on a smooth density there. Away from that disk the Riesz kernel is smooth, also under small changes of z. Thus the equations can be evaluated along each regular interval even for inverse powers.

For completeness the nullspace used in this elimination can be verified exactly. For $v \neq 0$ set $e(v)_{(j_1,\dots,j_N)} = v^{\sum j_i}$. Two linearly independent null vectors of L are $(e(z), 0)$ and $(0, e(1/z))$. On a single mode the upper and lower endpoint reductions in (10.4) have these evaluation properties since $D_z(z) = D_z(1/z) = 0$. More explicitly the t coefficient of the upper Euler matrix acts on evaluation at z as multiplication by z and that of the lower Euler matrix annihilates it. On evaluation at $1/z$ the u coefficients act by zero and z, respectively. Each multiplier acquires a factor of N by the product rule. On evaluation at z the t coefficient in the auxiliary two-row solution is $(U_a, U_b) = (-1, 0)$, and on evaluation at $1/z$ the u coefficient is $(0, z^2)$. Hence $C_t e(z) = Ne(z)$ and $C_u e(1/z) = Ne(1/z)$, so D kills both null vectors.

The generic rank proof is given just below. Here are also small, exact certificates of the elimination at ranks three and four. Order the monomials lexicographically by their nondecreasing mode tuples. At $z = 2/5$ form (10.6) over $\mathbb{F}_{10007}$. Scan columns in order and choose the first available nonzero row after previous pivot elimination, interchanging rows as needed. Using increasing zero-based indices, delete rows $(66, 68)$ and columns $(34, 69)$ at rank three, or rows $(416, 418)$ and columns $(209, 419)$ at rank four. The resulting determinants modulo 10007 are 2310 in dimension 68 and 8569 in dimension 418. The companion program gives the exact modular construction, pivot data and nonzero minor checks. All entries are rational functions over $\mathbb{Q}$ regular at the test point modulo this prime. A nonzero minor there proves the corresponding rational minor is nonzero, so together with the two explicit null vectors this proves the generic rank over $\mathbb{Q}(z)$. The coefficient blocks in L and D are independent of h, s. Let I_*, J_* be the row and column indices of one such minor. Wherever it is nonzero solve the corresponding subsystem with other entries of X set to zero. The actual derivative vector is another solution: the pivot rows span the row space, and the true right side is compatible. Their difference is in the stated nullspace, on which D vanishes. The physical system is therefore

$$\frac{d}{dz} W(Nz; z) = \left[C_0 + D_{:,J_*} (L_{I_*,J_*})^{-1} G_{I_*,:} \right] W(Nz; z). \tag{10.7}$$

Combine its components using the permutation expansion of the Toeplitz determinant and multiply by $(1 - z^2)^{N^2+2Ns}$ for T_N. Initial data for component $(j_1, \dots, j_N)$ at a regular z_0 are the independent angular integral of $|Nz_0 - \sum w_i|^{2h} \prod w_i^{j_i} D_{z_0}(w_i)^{\nu}$ against $\prod d\theta_i/(2\pi)$.

The generic rank at every size. The rank bound in the elimination extends to every $N \geq 2$ by a filtration of the mode space. Work over the rational function field $\mathbb{Q}(z)$, so the symbol z can also be examined at infinity to certify nonzero rational determinants. This algebraic step makes no assertion about a Haar preparation there. On the basic coordinate vectors $v = (v_{-K}, \dots, v_K)$ put $H = z + z^{-1}$ and define the surjection

$$(\nabla v)_j = v_{j+1} - H v_j + v_{j-1}, \qquad -K+1 \leq j \leq K-1.$$

The kernel E is the span of the two vectors $e(z)_j = z^j$ and $e(1/z)_j = z^{-j}$, by the second-order recurrence. The four one-mode frequency coefficients are read directly from (10.4). The matrix $S_+ = A_{+,t}$ shifts $(S_+v)_j = v_{j+1}$ with terminal value $Hv_K - v_{K-1}$, and $S_- = A_{-,u}$ is the reverse shift with initial value $Hv_{-K} - v_{-K+1}$. The cross matrix $B_+ = A_{+,u}$ has only a terminal output $(\nabla v)_{K-2}$, while $B_- = A_{-,t}$ has only an initial output $(\nabla v)_{-K+2}$. In these sentences the matrices denote their one-mode versions before the degree-N product rule.

All four matrices preserve E. The shifts on its displayed basis are diagonal with respective eigenvalue pairs (z, z^{-1}) and (z^{-1}, z), and the cross matrices annihilate E. Identify the quotient with the $(2K-1)$-dimensional vector $y = \nabla v$. Direct substitution gives $\nabla S_+ v$ equal to the forward shift of y with zero last entry and $\nabla S_- v$ equal to its backward shift with zero first entry. Likewise $\nabla B_+ v$ has only a terminal entry equal to the penultimate coordinate of y, and $\nabla B_- v$ has only an initial entry equal to the second coordinate of y. All four induced matrices on the quotient are independent of z.

On degree-N monomials the additive product-rule lift is the restriction of the sum of the N one-factor actions on the symmetric tensor space. An occupancy column has the same entry at each ordered tuple in its permutation orbit. Summing the one-factor actions then gives exactly the multiplicity of each mode in the monomial. A normalized symmetric-tensor basis differs by diagonal conjugation. Filter this space by the number r of quotient factors, that is, by the spans of symmetric tensors with at least $N - r$ factors in E. On successive quotients the action is the additive lift on $\mathrm{Sym}^{N-r} E \otimes \mathrm{Sym}^r(V/E)$. Decompose the first factor according to its occupancies n_+, n_- on the two displayed eigenlines, with $n_+ + n_- + r = N$. The graded diagonal block for the stacked matrix L in (10.6) is the sum of a matrix independent of z and

$$\mathrm{diag}([(N-n_+)z - n_-/z]I,\ [(N-n_-)z - n_+/z]I)\,.$$

The constant matrix consists of additive lifts of the four quotient operators with the signs from (10.6). If $r > 0$, both leading coefficients $N - n_+, N - n_-$ are positive integers. The block determinant therefore has nonzero leading Laurent coefficient at infinity and the block is invertible over $\mathbb{Q}(z)$. If $r = 0$ the constant matrix is zero, and the two diagonal entries are $n_-(z - z^{-1})$ and $n_+(z - z^{-1})$. Only the two extreme occupancy values give a null dimension, one each. The dimension of the full kernel is at most the sum of the kernel dimensions of its graded blocks (restrict to the induced filtration of the kernel). The two explicit null vectors attain that bound. Hence $\mathrm{rank}_{\mathbb{Q}(z)} L = 2\binom{2K+N}{N} - 2$ at every rank. Symbolic row elimination therefore gives the required nonzero pivot minor at any specified N. Since the physical chain-rule matrix annihilates this two-dimensional kernel, formula (10.7) with that pivot yields the physical ordinary system on every regular interval in its stated domain, with no rank restriction beyond $N \geq 2$. The system has combinatorial dimension and supplies no large-rank numerical conditioning guarantee.

A scalar ordinary equation can also be constructed when required. Absorb the logarithmic derivative of the physical prefactor $(1 - z^2)^{N^2+2Ns}$ into the diagonal of the matrix in (10.7), calling the result $M(z)$. Start with the constant determinant row r_0 and form $r_{j+1} = r_j' + r_j M$. The first rational linear dependence among these rows yields the same linear dependence among the corresponding derivatives of T_N. There are at most $d + 1$ rows before a dependence. For a specific specialization of h, s carry out the dependence computation after specialization. This construction gives an order bound d, with the regular-interval and conditioning qualifications of the system itself.

A four-mode physical system and its exceptional radii

Theorem 10.5 specifies the incoming angular family on a regular interval. The next results give its reduced coordinates, determine which radius singularities affect the physical solution, and construct its continuation.

Theorem 10.6 (four angular modes with a differential readout). Fix $N \geq 2$, $s \in \mathbb{C}$, $\Re h > -1$, and put

$$H = \lfloor (N-1)^2/4 \rfloor, \quad g = h + H, \quad \nu = -N - s, \quad d = \binom{N+3}{3}, \qquad \rho = g + N(1+\nu). \tag{10.8}$$

The physical moment is the readout of an explicit rational ordinary system of dimension d on each interval described below. At a normal-derivative resonance $\rho \in \{1, \ldots, 2H\}$ at most two additional coordinates suffice. The scalar normalization $(1 - z^2)^{N^2+2Ns}$ is retained. The reduction is valid for independent parameters and computes the original finite determinant even at ranks where its outer modes lie beyond the four retained ones. At ranks $3, 4, 5, 8$ the generic sizes become $20, 35, 56, 165$. Minimality of this system is unknown.

Here is a finite list of radii at which this particular elimination formula needs reconsideration. Besides $z = 0, 1$, use $r = 1, \dots, N$, $p + l = N - r$, $p, l \geq 0$, and put

$$\alpha = (r + l)z - l/z, \qquad \beta = (r + p)z - p/z.$$

Exclude roots in $0 < z < 1$ of $\alpha\beta = 0$ and of $\alpha\beta = m^2$ for $m = r, r - 2, \dots > 0$. For $m = 0$ or one of these positive integers the equation in $x = z^2$ is

$$(r + l)(r + p)x^2 - [(r + l)p + (r + p)l + m^2]x + pl = 0. \tag{10.9}$$

This is precisely the exceptional set for the *semisimple two-null-vector construction* below, in the sense of extra algebraic multiplicity at zero. It may contain radii with no additional linearly independent null vectors. The roots from $r = N$ include all nonzero interior critical trace radii. Roots elsewhere in the list, when distinct from the trace radii, have smooth physical angular data by submersion. A scalar equation can have still fewer singularities after taking the determinant readout. No radius in the open complement is lost because of the choice of a square minor. The endpoint $z = 0$ has coalescing Cayley data in this construction, and $z = 1$ also degenerates the angular preparation. Their moment domains are given in Sections 1 and 17. For example at $N = 2$ the list contains $z = 1/\sqrt{2}$, although this rank has no critical trace radius in the open interval. At $N = 4$ the distinct interior candidates are $1/3, 1/2, 1/\sqrt{3}, 1/\sqrt{2}, \sqrt{2/3}, \sqrt{3}/2$; only $1/2$ is a critical trace radius.

Clearing the frequency denominators. Use consecutive modes F_{-1}, F_0, F_1, F_2 of Proposition 10.4. The upper and lower reductions in (10.4) and the two-pole derivative in Theorem 10.5 apply verbatim with endpoints $-1, 2$: the corner reductions use respectively $j = 1, 0$ and contain only these four other modes. Raising F_j for $j > 2$ henceforth introduces at most $j - 2$ negative powers of t and no negative powers of u; lowering $j < -1$ introduces at most $-1 - j$ negative powers of u and no negative powers of t. Every resulting Laurent monomial in t, u has total degree at most zero, since each reduction divides a coefficient of total degree at most one by one frequency. Each F_j is still linear in the four basic integrals. In a permutation term of $\det(F_{i-j})$ the sum of the k largest positive displacements above a cutoff b is at most $k(N - k) - bk$, by pairing the k largest row indices with the k smallest column indices. The same bound holds in the other direction. The maximum for $b = 1$ is H and for $b = 2$ is no larger. Consequently there is a polynomial identity

$$(tu)^H \det(F_{i-j})_{i,j=0}^{N-1} = \sum_I P_I(t, u; z, s) \prod_{j \in I} F_j, \qquad \deg P_I \leq 2H,$$

where I ranges over nondecreasing N-tuples in the four modes. The equality extends by continuity through $tu = 0$. The polynomials can be generated by the single-angle reductions and a subset determinant recursion.

Denote by W_g the d-vector of the Riesz convolutions in Proposition 10.4 for these tuples with order g. In independent Wirtinger variables $a, \bar{a}$, the exact physical mixed integral before its scalar normalization is

$$U_h(a; z) = \frac{1}{(h + 1)_H^2} \sum_I P_I(-\partial_a, -\partial_{\bar{a}}; z, s)(W_g)_I(a; z).$$

In distribution sense $(\partial_a \partial_{\bar{a}})^H |a|^{2(h+H)} = (h + 1)_H^2 |a|^{2h}$ when $\Re h > -1$. This follows by differentiating at larger real part and holomorphic extension for locally integrable kernels. Alternatively verify the Fourier identity for the two compactly supported source distributions first, then convolve with the locally integrable kernel. This argument avoids multiplying singular Fourier distributions by a rational function at zero. In particular no integer $h \geq 0$ is lost. These equalities are ordinary evaluations at the regular physical points.

Exact discriminant and regular tangent. Form L, G, D, C_0 of (10.6) for the four modes and g in place of h. Denote $E_a = e(z)$, $E_b = e(1/z)$ in the tuple basis, so $(E_a)_I = z^{\sum_{j \in I} j}$. The filtration proof in Theorem 10.5 applies with the same second-order difference on the four-dimensional mode space. Its quotient now has only two coordinates, y_0, y_1. The four induced matrices $A_{+,t}, A_{+,u}, A_{-,t}, A_{-,u}$ are respectively S, T, S, T, where $S(y_0, y_1) = (y_1, 0)$ and $T(y_0, y_1) = (0, y_0)$. Write S_r, T_r for their additive lifts on the rth symmetric power, dimension $r + 1$. The corresponding graded block in the two-row displacement pencil is

$$\begin{pmatrix} \alpha I - S_r & -T_r \\ -S_r & \beta I - T_r \end{pmatrix}.$$

By the rectangular determinant identity its determinant is $(\alpha\beta)^{r+1}\det(I - S_r/\alpha - T_r/\beta)$. The eigenvalues of $S/\alpha + T/\beta$ are $\pm(\alpha\beta)^{-1/2}$, so the additive lift has eigenvalues $(r-2j)/(\alpha\beta)^{1/2}$, $0 \le j \le r$. Therefore the block determinant is

$$(\alpha\beta)^{r+1-k} \prod_{m=r,r-2,\ldots>0} (\alpha\beta - m^2), \qquad k = \lceil r/2 \rceil .$$

These are polynomial identities even when $\alpha\beta = 0$. At $r = 0$ each block is diagonal and exactly two simple zeros occur among the extreme occupancies since $z \neq z^{-1}$. Applying the calculation with $L + \epsilon I$ replaces α, β by $\alpha + \epsilon, \beta + \epsilon$, also at $r = 0$. Thus off the stated list zero has algebraic and geometric multiplicity two in L. Its spectral projection Π and group inverse S_0 are rational and satisfy $LS_0 = S_0L = I - \Pi$, $S_0\Pi = \Pi S_0 = 0$. For a formula independent of pivot choice, let V have columns $(E_a, 0), (0, E_b)$ and choose rational C_* with $C_*V = I_2$ by selecting one nonzero entry in each separate block. Then $J = L + VC_*$ is invertible: from $Jx = 0$ the direct sum of range and kernel gives $C_*x = 0$ and $Lx = 0$, hence $x = 0$. One can use $\Pi = VC_*J^{-1}$, $S_0 = (I - \Pi)J^{-1}(I - \Pi)$. For the real normal displacement $a = \bar{a} = Nz + \epsilon$, define $W(\epsilon, z) = W_g(Nz + \epsilon; z)$. The tangent equation at fixed ϵ is

$$\partial_z W = \left[C_0 + D(L + \epsilon I)^{-1}G\right] W = \sum_{j\ge 0} M_j \epsilon^j W, \qquad M_j = \mathbf{1}_{j=0}C_0 + (-1)^j DS_0^{j+1}G.$$

Indeed $D\Pi = 0$ by the same single-mode evaluation calculation as before. Coefficient comparisons below require only derivatives of the smooth physical vector to finite order. Analyticity of that vector in the normal parameter is unnecessary.

The normal jets, including resonance. Write $R = (I\ I)$, $B = R\Pi G$, $B_j = (-1)^j RS_0^{j+1}G$. The normal equation is $\partial_\epsilon W = [B/\epsilon + \sum_{j\ge 0} B_j\epsilon^j]W$. One has $\operatorname{im} B \subseteq \operatorname{span}(E_a, E_b)$ and $BE_a = \rho E_a$, $BE_b = \rho E_b$. We give an elementary endpoint check establishing the value of ρ. In the one-mode equations with lower and upper endpoints $l_0 = -1, k_0 = 2$, hold the matrices fixed and differentiate the evaluation vector $e(x)_j = x^j$ with respect to its argument at $x = z$. In the upper t shift its endpoint defect relative to $xe(x)$ is $-(x - z)(x - z^{-1})x^{k_0-1}$ in the last row. The bottom t cross-shift is $(x - z)(x - z^{-1})x^{l_0+1}$ in its first row. The two constant blocks on $e(z)$ are supported respectively at the upper and lower ends with coefficients $-(1 + \nu)(z - z^{-1})z^{k_0-1}$ and $(1 + \nu)(z - z^{-1})z^{l_0+1}$. The product rule therefore gives

$$GE_a - \rho(E_a, 0)^{\mathsf{T}} = L\left((1 + \nu)E_a',\, gE_a/[N(z - z^{-1})]\right)^{\mathsf{T}},$$

where the prime differentiates $z^{\sum j}$ only. Inversion $j \mapsto -j$ exchanges the two endpoint equations (the resulting window is $-2, 1$), giving the other identity after exchanging the two blocks. These calculations depend only on having four consecutive modes. Applying $R\Pi$ proves the assertions, including $B^2 = \rho B$.

Set $w_j = \partial_\epsilon^j W(0, z)/j!$. Then $Bw_0 = 0$ and for $j \ge 1$,

$$(jI - B)w_j = \sum_{k=0}^{j-1} B_k w_{j-1-k}.$$

Unless $j = \rho$, the inverse is $I/j + B/[j(j - \rho)]$. If $\rho = j_0$ is an integer between 1 and $2H$, put $P = B/j_0$. This is a projection of rank two; compatibility of the right side at j_0 follows from the angular solution. The complementary part of w_{j_0} is the right side divided by j_0. Add the two coefficients of Pw_{j_0} in (E_a, E_b) as physical initial data. They obey a closed rational tangent equation, since

$$(Pw_{j_0})' = P'w_{j_0} + P\sum_{k=0}^{j_0} M_k w_{j_0-k}.$$

Writing $Pw_{j_0} = E\eta$, $E = (E_a, E_b)$, subtract $E'\eta$ from the right and use any rational left inverse of E. The extreme mode rows are independent for $0 < z < 1$. All the lower jets there are known from w_0. The extra initial values are derivatives of the integral-defined, regular normal germ; when differentiating a singular kernel is inconvenient the derivatives can be transferred to a locally smooth trace density. A given scalar moment may annihilate some of these two coordinates. The dimension is an upper bound. Theorem 23.1 eliminates both supplementary coordinates from the rank-three and rank-four scalar by a zero-injection shortcut, and Theorem 23.1A proves that the canonical extreme-row scalar row is globally polynomial through every normal-jet resonance $\rho \in \{1, \ldots, 2H\}$ at every rank $N \ge 3$ and every regular radius $0 < z < 1$ off (10.9) (while the zero-injection

shortcut does not replace the canonical construction at $N \geq 5$). In particular $\rho = 0$ incurs no positive-order resonance.

Finally, to recover the mixed derivatives $X_{ij} = \partial_a^i \partial_{\bar{a}}^j W_g$ in the readout, differentiate the two displacement rows. This gives

$$L\begin{pmatrix} X_{i+1,j} \\ X_{i,j+1} \end{pmatrix} = GX_{ij} - \begin{pmatrix} iX_{ij} \\ jX_{ij} \end{pmatrix}.$$

Use S_0 on the right for a particular solution. Its upper and lower entries determine two affine lines of possible values with directions E_a, E_b, respectively. Each mixed derivative with two positive indices occurs once in each kind of line; these directions are independent, so their intersection is unique. For total degree k the two pure derivatives now lie on one line each. Their sum is fixed by $k!w_k - \sum_{i=1}^{k-1} \binom{k}{i} X_{i,k-i}$, fixing both. Compatibility in each step follows from the regular angular integral. Induction through $2H$ proves the differential readout and its equivalence to the physical solution. The algorithm separates source initialization and algebraic recovery. Near a listed radius, a small value of $|j - \rho|$, or a large power of the group inverse, this coordinate realization can lose precision.

The discriminant quadratics have only nonnegative real roots in x: their discriminants are $[p(r+l) - l(r+p)]^2 + 2m^2[p(r+l) + l(r+p)] + m^4$. Thus the rational tangent matrix on the nonresonant base, formed with the endpoint selector above, has no additional pole in the open upper or lower half-plane. At an artificial real radius the local holomorphic physical germ across that point permits either sufficiently small semicircular detour. An arc containing no other obstructions can be deformed to such a semicircle. A mere bypass at a genuine critical trace radius need not select the physical integral on the far side. For floating integration one can solve $LX = GW$ in the orthogonal complement of its kernel on compatible physical input, since any two solutions have the same DX. The group inverse in the normal-jet formulas continues to be required. An orthogonal inverse used for tangent stepping changes the off-constraint extension of the matrix, so finite-precision drift must be checked against separately computed physical data.

In using the critical connection for the augmented system, the shifted physical curve $a = Nz + \epsilon$ has its singular real point at the correspondingly displaced radius. At fixed small real ϵ use the physical angular germs and arcs enclosing that moving point. Their two-arc weights are independent of ϵ. Differentiating the regular endpoint data thus gives the same connection for the finite normal jets. If the critical connection itself requires an order derivative at a resonance and $\rho = j$ is to be held fixed, take $ds/dh = 1/N$ along the slice, differentiating both preparation and readout; the arc weights depend on h alone. A derivative at fixed s instead uses the unreduced angular system of Theorem 10.5 or the intrinsic integral, since it leaves the augmented stratum. The exact Poisson examples below test normal-jet resonance; they do not test every doubly resonant arc.

Computational checks of the reduction. At rank five with $s = -5$, $h = 2$, $z = 2/7$, exact rational initialization of all 56 modes and exact differentiation of the reduced readout give $34402/2401$ before the physical multiplier $(1 - z^2)^{-25}$. This agrees with Haar trace orthogonality. Exact rank-four cases include $z = 499/1000, 501/1000$ on opposite sides of the critical radius $1/2$, with separate exact seeds. On the resonant slice $s = 1 - N$ the one-angle Fourier coefficients of the preparation are $z^{|j|}/(1 - z^2)$. They fix the missing order-ρ jet independently. Exact checks at ranks three and four reproduce the full permutation determinant at $\rho = 2, 3$, respectively. Dropping $(h+1)_H^2$ fails the checks where it differs from one.

For independent nonreal orders, the companion implementation integrates the compact system from angular data. At rank four the regular interval $[0.375, 0.38]$ with $s = -2.81 + 0.31i$, $h = 2.35 + 0.26i$ gave 2.6×10^{-8} scaled discrepancy from the directly integrated original moment at the right end. Separate regular integrations on either side of the rank-three trace caustic used their own initial data. At rank two, comparing the compact value with the midpoint of the separate Section 21 enclosure at $z = 0.57$, $h = 0.75 + 0.29i$, $s = 0.37 - 0.61i$ gave 2.8×10^{-10} at 512 angular nodes per coordinate. That enclosure bounds the reference by 7.2×10^{-10} absolutely. The compact ODE computations use floating arithmetic. At $N = 4$, $z = 0.82$, $s = -0.56 + 0.12i$, $h = 1.15 + 0.26i$, the nonzero singular-value condition number of the compact pencil is about 2.8×10^6; 36 nodes per angle and double-precision jet recovery give a scaled error exceeding 10^4. A smaller system alone does not control angular initialization error or amplification by repeated spatial differentiation.

Complex arc integration with one left-hand seed at each test crosses artificial radii $1/\sqrt{2}$ at rank two and $1/2$ at rank three. Both upper and lower arcs reproduce direct right-hand angular data with scaled moment discrepancies below 3.2×10^{-11} and 6.5×10^{-9}, respectively. The same uncombined prescription at the genuine rank-three

critical radius, for $h = -0.24 + 0.08i$, $s = -2.3 + 0.17i$, produced discrepancies greater than 3% on both arcs. The physical critical connection developed below uses the two boundary values. Its independent rank-four mode test crosses $z = 1/2$ between 0.434 and 0.566 at $s = -3.92 + 0.13i$, $h = -0.68 + 0.19i$. Comparing all 35 modes with independent angular data from an 80^4 grid, the maximum absolute component error divided by the largest reference component was 2.9×10^{-8} after the prescribed combination, 9.7×10^{-7} for the upper arc, 3.0×10^{-7} for the lower arc and 4.4×10^{-7} for the half sum. The right-hand angular quadrature is used only for checking. This particular comparison tests the propagated mode vector. Applying its high-derivative scalar readout requires a separate accuracy assessment.

Analytic continuation across an apparent singularity

Theorem 10.7 (analytic transport through noncritical radii). Let $w_i = e^{i\theta_i}$, $g = Nz - \sum w_i = g_1 + ig_2$, and let J be the real two-row derivative matrix of $\sum w_i$ in the angles. Write $G = JJ^{\mathsf{T}}$ and $D = \det G + |g|^2$. The following construction applies to all components of the displacement system, and separately to the original Vandermonde combination. It gives an analytic continuation rule at every interior radius z_0 with $a = Nz_0 \notin \mathcal{C}_N = \{|N - 2j| : 0 \le j \le N\}$, whether or not a selected elimination minor vanishes. For real z_0 it preserves the actual integral cycle.

Indeed $\det G = \sum_{i<j} \sin^2(\theta_i - \theta_j)$. Rounding each w_j to the nearer of $w_1, -w_1$ costs at most $\sqrt{2}|\sin(\theta_j - \theta_1)|$. Thus $\delta = \operatorname{dist}(a, \mathcal{C}_N) \le |g| + \sqrt{2(N-1)\det G}$ and $D \ge \mu := \delta^2/(2N-1)$. Evolve the angles in z by the permutation-equivariant periodic vector field

$$V = \frac{NJ^{\mathsf{T}} \operatorname{adj}(G) e_1}{D}.$$

On a real flow line $\dot g = N|g|^2/D$, so g acquires the scalar factor $\exp \int N\bar g/D\, dz$. The kernel $|g|^{2h}$ acquires $\exp \int 2hNg_1/D\, dz$. The flow Jacobian acquires $\exp \int \operatorname{div}_\theta V\, dz$. This is also valid in the pulled-back integral at negative orders: discard the initial null set $g = 0$, and dominate the remaining initial kernel as below. No reciprocal of g occurs in the multipliers. The local solution is consequently determined by the convergent Taylor expansions of these factors, of $w_i^{j_i}$ and of the preparation along the flow, all integrated against the single initial kernel. The same argument applies to the Haar Vandermonde as an extra trigonometric polynomial.

Here is one fully explicit, conservative size bound. Put

$$b = \min\{1/4, \mu/(256N^2), (1 - z_0)/12\}, \quad H = 1 + 100N^2/\mu, \qquad \epsilon = b/(8NH).$$

Complexify the angular coordinates and z in the polydisc of radius b about each initial real configuration. Use $D = \sum \sin^2(\theta_i - \theta_j) + g_1^2 + g_2^2$ there with analytic $g_1 = Nz - \sum \cos\theta_i$, $g_2 = -\sum \sin\theta_i$. Along straight segments the change in the sine sum is bounded by e^4N^2b. The two squares change by at most $58N^2b$, using $|g_1| \le 5N$, $|g_2| \le 3N$ and increments of at most $4Nb, 3Nb$. Hence $|D| \ge \mu/2$. Each entry of V has modulus $\le 4e^3N^2/\mu \le H$, and on half the polydisc the Cauchy derivative estimate gives a row-sum Jacobian bound $2NH/b$. Picard iteration for $|z - z_0| \le \epsilon$ preserves this half polydisc and has contraction factor at most $1/4$. The same contraction holds using the sup norm on analytic trajectories based at each real point. All factor estimates therefore hold on a fixed complex disc independent of the initial angles; by the strict inequalities one can slightly enlarge it when applying Cauchy's estimate. Each factor $1 - ze^{\pm i\theta}$ has real part at least $(1 - z_0)/2$ and modulus at most 3. Put

$$M_\nu = 3^{\max(\Re\nu, 0)}[(1 - z_0)/2]^{\min(\Re\nu, 0)} e^{\pi|\Im\nu|/2}, \qquad m_u(a) = \int |a - \sum w_i|^{2u} \prod_i d\theta_i/(2\pi), \quad u = \Re h.$$

The analytic component $W(z)$ of (10.7), evaluated at Nz, has sup norm on the disc bounded by

$$E = m_u(a) M_\nu^{2N} \exp\Big[b \sum |j_i| + \epsilon(20|h|N^2/\mu + 2NH/b)\Big].$$

For $|z - z_0| \le t\epsilon$ with $0 < t < 1$, truncation after degree l costs at most $Et^{l+1}/(1 - t)$. This is an analytic truncation bound for exact integrated coefficients. It does not bound the numerical error of their quadrature. A segment of real radii inside a compact regular interval can be covered by finitely many such steps, including the roots of any apparent minor. The step bound deteriorates near a critical trace value.

For $u \ge 0$ one can use $m_u(a) \le (a+N)^{2u}$. For $N \ge 3$, $a > 0$ and $-1 < u < 0$, one explicit bound is

$$m_u(a) \le \frac{2^{2u+1}\Gamma(1+u)}{\Gamma(-u)} \left[\frac{1}{-2u} + \frac{8^{N+1}}{\sqrt{a}\,[2u+(N+1)/2]} \right].$$

Indeed the radial source for the product of uniform angular measures is $J_0(a\rho)J_0(\rho)^N$. Use the positive Gaussian Mellin representation $r^{2u} = \Gamma(-u)^{-1}\int_0^\infty t^{-u-1}e^{-tr^2}dt$, invert the Gaussian on the plane and integrate the absolute radial bound first. The elementary inequality $|J_0(x)| \le \min(1, 8/\sqrt{x})$ follows for $x \ge 1$ by discarding two end arcs of length $x^{-1/2}$ in the cosine integral and applying the monotone first-derivative bound on each of the two remaining half-intervals. This proves the bound including at critical $a > 0$, with the finite absolute integral needed to interchange in the Gaussian proof. At $N = 2$, $0 < a < 2$, the independent angular sum has planar density $1/[\pi^2 r\sqrt{4-r^2}]$. For $b' = \min(a, 2-a)/2$, separation into the b' disk about a and its exterior gives $m_u(a) \le (b')^{2u} + (b')^{2u+2}/[\pi(1+u)(a-b')\sqrt{4-(a+b')^2}]$. In all cases the s, h of the readout remain independent.

The connection at a genuine critical trace radius

Theorem 10.8 (physical germs at an interior critical trace radius). Fix $N \ge 3$, $n+m = N$, $k = n-m \in (0, N)$, $z_* = k/N$, and $t = Nz - k$. For independent $s \in \mathbb{C}$ and $\Re h > -1$, put

$$\beta = 2h + (n^2+m^2+1)/2, \qquad \phi = \pi(Nk-1)/4, \qquad K(h) = 2^{2h+1}\Gamma(1+h)/\Gamma(-h),$$

and define the nonzero analytic factor on a real neighborhood of z_* by

$$A(z) = \frac{(1-z^2)^{N^2+2Ns}4^{nm}F_nF_m}{(2\pi)^{(N+1)/2}\sqrt{Nz}}\,(1-z)^{-2n(N+s)}(1+z)^{-2m(N+s)}.$$

For $h \notin \mathbb{Z}_{\ge 0}$ the first nonsmooth term of the physical scalar T_N is

$$K(h)A(z)\,2\Gamma(-\beta)|t|^\beta \cos(\phi - \operatorname{sgn}(t)\pi\beta/2). \tag{10.10}$$

Here and below terms differing by a smooth function may represent the same singular germ. At $\beta = l \in \mathbb{Z}_{\ge 0}$ replace the whole factor after $K(h)A(z)$ by

$$\frac{2(-1)^{l+1}}{l!}|t|^l \left[\cos(\phi - \operatorname{sgn}(t)\pi l/2)\log|t| + \frac{\pi}{2}\operatorname{sgn}(t)\sin(\phi - \operatorname{sgn}(t)\pi l/2)\right].$$

At integral $h \ge 0$ the direct integrand is a polynomial in $g, \bar{g}$ times an analytic preparation. All interior singular contributions vanish and the ordinary solution is real analytic. For nonintegral h the first germ is genuinely singular. At nonresonant β the two cosines cannot both vanish, since their two arguments differ by $\pi\beta$. At integral β, either a logarithm remains or the remaining expression is a nonzero multiple of $\operatorname{sgn}(t)t^l$. These distinctions apply at every allowed complex tilt; absolute positive preparation is needed only for the local integrability bound, not to compute the phases. The value at $t = 0$ is the ordinary moment. All derivatives of orders strictly below $\Re\beta$ match across the boundary. At odd N the origin is a regular trace displacement; at even N it is critical, with a full angular stationary circle, and its thresholds and centre analysis in Sections 1–5 are separate. The endpoint $z = 1$ also has a changing singular preparation and is covered only by the earlier circle results.

Construction and error order. Define the cutoff transform $L_b(v) = \int_1^\infty r^{-1-b}e^{ivr}dr$ initially at $\Re b > 0$; its value at zero is $1/b$. On a punctured real interval, modulo analytic functions of v, it equals $\Gamma(-b)(-iv)^b$, using the principal logarithm (or positive damping $-iv \mapsto \eta - iv$, $\eta \downarrow 0$). In fact for $b \notin \mathbb{Z}_{\ge 0}$ the entire subtraction is $-\sum_{j\ge 0}(iv)^j/[j!(j-b)]$. Start on $-1 < \Re b < 0$ with Abel damping for the full half-line, subtract the integral from zero to one and continue. The poles cancel at a nonnegative integer b; the finite part gives the logarithmic formula above. This explicit subtraction also gives an evaluation stable in principle at resonance by taking a joint finite part instead of two nearly cancelling poles.

Apply the all-orders radial stationary-phase expansion (3.1) inside (5.3) on the fixed tail $r \ge 1$. For any desired integer L retain sufficient orders in (3.1) so that the integrated error has L continuous z derivatives. More explicitly, on any compact interior interval bounded away from zero, an amplitude remainder $O(r^{-P_{nm}-1/2-j})$ after removing the extracted phase has the same bounds after a fixed number of z derivatives. This follows directly in the product Morse coordinates of Section 3 since the critical points are fixed and Nz is bounded

below; a derivative of the phase then costs at most one power of r. Thus a term with first omitted index j in a saddle class can be put into a C^L remainder whenever $L < 2\Re h + P_{nm} + 1/2 + j$. Equivalently one may take a common large truncation for all saddles. The integrated compact-frequency part, with origin subtraction in (5.3), is analytic in z; its differentiated power series follows from bounded angular sources. All tail frequencies other than the pair $t, -t$ stay away from zero locally and L_b is analytic there. Collecting those background pieces, the critical nonanalytic terms to arbitrary finite smoothness order are

$$K(h) \sum_{j \geq 0} \big[c_{mn,+,j}(z) L_{\beta+j}(t) + c_{nm,-,j}(z) L_{\beta+j}(-t) \big].$$

This sum is interpreted at each finite order. Section 3 gives the coefficients from angular Taylor derivatives and Gaussian integrals. At order zero they are $A(z)e^{i\phi}$ and $A(z)e^{-i\phi}$. The coefficient at negative frequency has the same complex preparation as that at positive frequency; one must not conjugate s. This proves the displayed formulas and provides the signed connection data on both sides. It does not assert convergence of the full stationary-phase series. Differences of sufficiently high order annihilate the unknown smooth background, which allows a direct numerical test of the connection from the original determinant.

There is a corresponding constructive crossing for every vector component in (10.7). Use the independent angular measure with insertion $\prod w_i^{j_i} D_z(w_i)^\nu$ instead of the Weyl determinant. Its circular source is the angular average of $e^{i\rho\Re(e^{-i\alpha} g)}$ against this measure. Joint stationary phase in these $N+1$ angles has the same two resonant frequencies and the power $b = 2h + (N+1)/2$, without the vanishing Vandermonde. The leading $+t$ coefficient before $K(h)$ is

$$\frac{(1-z)^{2n\nu}(1+z)^{2m\nu}}{(2\pi)^{(N+1)/2}\sqrt{Nz}}\; e^{i\pi(k-1)/4} \sum_{\substack{I \subset \{1,\dots,N\} \\ |I| = m}} (-1)^{\sum_{i \in I} j_i}.$$

For $-t$ reverse the displayed phase, keeping the same other factors. At the $+t$ stationary point the minus signs are exactly the m phases $w_i = -1$ and the n plus phases are $+1$. Reversal of Fourier direction describes the same configuration. A zero subset sum suppresses this order for the component. Higher terms and the C^L bound follow by the same finite Taylor rule, with $P = N/2$. The ordinary vector integrals at the critical value exist for all these exponents by the independent angular absolute bound above; for $\Re h \geq 0$ bounded support suffices. Their radial identity follows from the same Gaussian inversion first for negative orders, then by the convergent subtracted representation and holomorphy as in Section 5. This also proves continuity, including at the integrable negative orders arbitrarily close to -1 in rank three.

For an explicit finite-order connection choose a Taylor degree l and choose tail truncation as above with $L = l+1$. Subtract the finite critical $L_b(\pm t)$ combination, retaining its smooth coefficients and the cutoff convention, from each vector component. Differentiate the remaining radial formula at $z = z_*$ through order l. These common Taylor data consist of the origin-subtracted finite-frequency integrals, the noncritical tail transforms and the absolutely convergent remainder integrals after the stationary subtractions. Their degree-l Taylor polynomial plus the same critical terms on either side approximates the physical solution with absolute error $O(|z - z_*|^{l+1})$. On compact parameter sets away from poles this follows from the preceding dominated derivative estimates; across resonance use L_b itself, which is regular in b at every retained $\Re b > 0$. This constructs physical continuation to arbitrary prescribed algebraic order and selects the branch by its original angular preparation. Theorem 10.9 below proves convergence of a related local representation and gives an exact connection rule. The error constants here are supplied by stationary-phase derivative bounds, not certified numerical values. Finite one-sided jets alone cannot select the two branch coefficients when the incoming singular term vanishes on one side. No monodromy choice for the homogeneous rational ODE is presumed.

There is a useful simplification of the branch data at all orders. After shifting the resolved Fourier direction by π, the two resonant stationary pairs describe the same angular configurations and have the same preparation and angular Jacobian. The full real phase is negated. In the Morse coordinates of Section 3 the Gaussian operator at each additional integer order therefore changes by $(-1)^j$ under reversal: a homogeneous term of degree $2j$ relative to the first nonzero even term gives i^j times the same real differential operation on the amplitude in the forward phase, and $(-i)^j$ in the backward phase. This is an algebraic operation on a potentially complex amplitude. Thus $c_{mn,+,j} = e^{i\phi} i^j b_j(z,s)$ and $c_{nm,-,j} = e^{-i\phi}(-i)^j b_j(z,s)$ with common analytic b_j and $b_0 = A$.

For noninteger β the singular expansion consequently has the single two-sided multiplier

$$2K(h)|t|^{\beta}\cos(\phi-\operatorname{sgn}(t)\pi\beta/2)\sum_{j\geq 0}\Gamma(-\beta-j)b_j(z,s)t^j.$$

Its interpretation remains finite-order. For $t>0$ the two additional phase increments $\pi j/2$ cancel; for $t<0$ their sum supplies precisely $(-1)^j$. At integer β take the same finite parts term by term. In particular when a nonresonant cosine vanishes on one side all its nonsmooth terms disappear on that side, while the other side retains its leading cusp. For example at $N=4$, $k=2$, $h=-1/2$, one has $\beta=9/2$, $\phi=7\pi/4$: the side $t>0$ is smooth to every order and $t<0$ has a nonzero $|t|^{9/2}$ term throughout the tilt plane. Smooth one-sided Taylor matching alone would miss this physical branch.

The centre as a separate endpoint

Corollary to Theorem 10.8 (the central saddle). For odd $N\geq 3$ the trace value zero is regular. The angular flow at $z_0=0$ has the same positive denominator since the distance from zero to $\mathcal{C}_N$ is one. The independent-angle kernel is locally integrable there by the submersion theorem, and all $\Re h>-1$ give an even real-analytic physical scalar. Evenness follows from changing every original eigenvalue to its negative as z changes sign.

For $N=2m$ the physical scalar has a different leading singular germ. Put $\gamma=2h+m^2$ and $A_0=4^{m^2}F_m^2/(2\pi)^m$. Modulo smooth background, its first term as $z\to 0$ is

$$K(h)A_0\,2^{-1-\gamma}\frac{\Gamma(-\gamma/2)}{\Gamma(1+\gamma/2)}|Nz|^{\gamma}.$$

At $\gamma=2l\in 2\mathbb{Z}_{\geq 0}$ the factor following $K(h)A_0$ is replaced, modulo a smooth term, by

$$(-1)^{l+1}2^{-2l}|Nz|^{2l}\log|Nz|/(l!)^2.$$

Integral $h\geq 0$ has the ordinary analytic polynomial-kernel solution. These formulas give the genuine even-extension singularity for every other h in $\Re h>-1$, with the value at zero taken only on the actual centre moment domain of Section 1. At rank two $-1<\Re h<-1/2$ gives a divergent modulus as $z\downarrow 0$; at $h=-1/2$ the leading divergence is $-(2/\pi)\log(2z)$. At $\Re h=-1/2$, $\Im h\neq 0$ the nonzero term oscillates as a function of $\log z$. Its amplitude is independent of the tilt. For $N\geq 4$ every $\Re h>-1$ gives a finite centre value. The endpoint $z=1$, where the transformed preparation can be singular, remains subject to the distinct hypotheses of Section 17 and the circle-limit results.

For the proof use the directional stationary-phase expansion before resolving the source angle, as in the derivation of (3.2). In each unbalanced class the frequencies $n-m+Nz\cos\alpha$ stay away from zero for small $|z|$. After integration in frequency the corresponding cutoff transforms are smooth there. For the balanced class the leading term is ρ^{-m^2} times $e^{iNz\rho\cos\alpha}C_{mm}(e^{i\alpha};z)$, with $C_{mm}=A_0+O(z^2)$ uniformly in angle. Thus the coefficient required is the cutoff transform of $\rho^{-\gamma-1}J_0(Nz\rho)$. Modulo analytic even powers its coefficient follows from the Bessel Mellin integral in Section 5, initially for $-1/2<\Re\gamma<0$, then by continuation in γ after subtraction at frequency zero. More explicitly one can average $L_{\gamma}(Nz\cos\alpha)$ first: its homogeneous contribution is locally integrable in α for $\Re\gamma>-1$, which covers the entire parameter range here. Abel damping of the radial frequency justifies this order even at negative $\Re\gamma$; for $\Re\gamma<0$ the damped homogeneous factors admit the integrable majorant $C|Nz\cos\alpha|^{\Re\gamma}$. The marginal integer cases follow by taking finite parts, and the poles only at even nonnegative γ yield the logarithm displayed above. Terms of higher saddle order have degree at least $\gamma+1$ with the corresponding angular average and possibly a logarithm. The uniform directional remainder, differentiated after extraction of its phase, is integrable through every prescribed derivative once its truncation order is sufficiently high. This orders all subsequent terms at larger degree and proves the leading germ with an arbitrarily differentiable background after finite further subtractions.

The exact two-sided connection of the physical solution

Theorem 10.9 (physical continuation by two complex arcs). At an interior critical value $z_*=k/N$, put $b=2h+(N+1)/2$ and $\varphi=\pi(k-1)/4$ for the full angular-moment vector of Theorem 10.5. Start from its

physical germ at $z < z_*$ and analytically continue the ordinary equation around the critical value to a point $z > z_*$, once in the upper half-plane and once in the lower half-plane. Denote these two vectors by $W^{\uparrow}$ and $W^{\downarrow}$. Use paths in a sufficiently small punctured disk, or deformations of them that do not wind around other singularities. Choose a disk with no other pole of the rational matrix and with both endpoints regular. Define $\vartheta = \varphi + \pi b/2$. The exact physical continuation is

$$W_{\mathrm{phys}} = \frac{e^{i\vartheta} W^{\uparrow} + e^{-i\vartheta} W^{\downarrow}}{2\cos\vartheta}. \tag{10.11}$$

This rule holds whenever $\cos\vartheta \neq 0$, also at integral b, for all $s \in \mathbb{C}$, $\Re h > -1$. The readout and its preparation are evaluated at the outgoing radius after combining the vector. A single arc generally gives a different solution. In the reverse direction use the same weights with $\vartheta = \varphi - \pi b/2$ and count the upper path as having argument of t increasing from 0 to π.

At $\cos\vartheta = 0$, the two incoming parameter-specialized continuations agree at the outgoing point, say $W^{\uparrow} = W^{\downarrow} = W_0$. In the increasing-radius direction the physical result is then

$$W_{\mathrm{phys}} = W_0 - \frac{i}{2\pi}(\partial_h W^{\uparrow} - \partial_h W^{\downarrow}). \tag{10.12}$$

The parameter derivatives include the derivatives of the physical starting data; their initial angular kernel is $|g|^{2h} \log |g|^2$. Along an arc they obey the inhomogeneous system obtained by differentiating the ordinary equation, or can be computed by a Cauchy integral in h. At decreasing radius the displayed subtraction becomes addition. An error $e_{\pm}$ in either outgoing vector produces absolute error at most $(|e^{i\vartheta}|\|e_+\| + |e^{-i\vartheta}|\|e_-\|)/(2|\cos\vartheta|)$ away from the exceptional case. This bound measures cancellation in the connection. The errors within the two arc integrations and in their initial data require separate control.

Analytic local form. The finite-order stationary expansion by itself cannot exclude sectorially flat terms. We establish the stronger, convergent local representation for the specified integrals. It suffices initially to work on an open set of $-1 < \Re h < 0$ with $2h, b \notin \mathbb{Z}$. For each component use the angular integral defining its circular Fourier source. Rotate the eigenangles relative to the resolved Fourier angle and, where needed, translate by π, so the phase is

$$\sum_{i=1}^{N} \cos x_i + Nz\cos\alpha.$$

Its angular amplitude consists of trigonometric polynomials and the two analytic powers of $1 - ze^{\pm i\theta_i}$. It is holomorphic in a common complex angular strip and in z near the interior real z_*: shrink the strip so $|z|e^{|\Im\theta_i|} < 1$. This also applies to the Weyl amplitude, using the analytic trigonometric polynomial for its squared Vandermonde. Use the real-log branch on the real cycle, with these two analytic continuations for the two factors. Contributions before the fixed frequency cutoff in (5.3) are analytic near z_*. We now treat the whole frequency tail exactly.

Deform each of the $N+1$ circle contours inside that strip. The contours pass through $0, \pi$ on steepest descent arcs. Near a stationary angle x_* of sign $\epsilon = \cos x_*$ use the **exact** change $2\sin((x - x_*)/2) = e^{-i\epsilon\pi/4} v$ with v real. Then $\cos x = \epsilon + iv^2/2$. These short analytic arcs can be joined by curves with $\Im\cos x > 0$: away from the stationary points take a small deformation $x = u - id\sin u$, joining the local arcs as graphs with $\Im x$ of the opposite sign to $\sin(\Re x)$. Take the lengths and transverse widths small enough for the common strip. Periodicity and Cauchy's theorem preserve the angular integral at each frequency. On the part of the product contour outside fixed small balls in its real steepest coordinates at all its saddles, the sum of the imaginary parts of the phases is bounded below by a positive constant uniformly for real z near z_*, because every coefficient is positive. For complex z sufficiently close to z_* the same bound holds with a smaller constant. The frequency integral of this complement is therefore analytic in z, by exponential damping. Boundaries of the balls lie in this damped set and need no analytic partition of unity.

Write $d = N + 1$ just in this proof. On a fixed little ball about a saddle set $v = (2x)^{1/2}\omega$, $\omega \in S^{d-1}$. After extracting its constant real phase frequency $\Omega(z)$, the damping is $e^{-\rho x q(z,\omega)}$, where $q = 1 + (Nz - 1)\omega_d^2$ is positive and bounded away from zero on these real neighborhoods. The product angular Jacobian and the full amplitude are analytic in v, z. Average over ω and $-\omega$ before expanding, or equivalently add the two amplitudes: the resulting power series in x has a common positive convergence radius for all ω. Choose the ball strictly within that radius. For real z, change variables $U = xq$ and cut the U integral at a fixed $a_0 > 0$ smaller than every upper

endpoint. The discarded upper segment is analytic in z even for a critical $\Omega(z_*) = 0$, by its positive damping; for complex z continue its variable upper endpoint by parametrizing the segment. For the remaining integral the angular amplitude is analytic in U, z on $|U| < a_1$ with $a_1 > a_0$, after integration over ω; the factor $q^{-d/2}$ uses its analytic branch. The contribution of the ball to the Taylor-sensitive part of the radial integral now has precisely the form

$$\int_0^{a_0} U^{v-1} H(U,z) \int_1^\infty \rho^{-2h-1} e^{-(U-i\Omega(z))\rho}\, d\rho\, dU.$$

Here $v = d/2$ for the ordinary vector, and $v = P_{nm} + 1/2$ after stripping the first vanishing order of the squared Vandermonde in the scalar component. The coefficient H is analytic on this disk. Choose the ball so small that its amplitude series converges well beyond its boundary, and then choose a_0 with a further fixed margin so the U-series converges on $|U| < a_1$ for some $a_1 > a_0$ uniformly in z. At a nonresonant saddle frequency $-i\Omega(z_*) \neq 0$ the cutoff transform inside is analytic on a neighborhood of the segment from $-i\Omega(z_*)$ to $a_0 - i\Omega(z_*)$ on a consistent branch; it gives only analytic background. At a critical saddle the interchange for real z follows by absolute convergence, using $\Re(v + 2h) > 0$ and the positive real damping. Only $\Omega = t$ or $-t$ occurs there.

Set $w = -i\Omega$ and write $H = \sum H_j(z) U^j$. The inner cutoff transform equals $\Gamma(-2h)(U + w)^{2h}$ plus a function entire in $U + w$ for the chosen noninteger $2h$. The latter gives an analytic background. For $\alpha = v + j$, the former integral is evaluated by

$$\int_0^{a_0} U^{\alpha-1}(U + w)^{2h} dU = \frac{\Gamma(\alpha)\Gamma(-2h - \alpha)}{\Gamma(-2h)} w^{2h+\alpha} + \sum_{l \geq 0} \binom{2h}{l} w^l \frac{a_0^{2h+\alpha-l}}{2h + \alpha - l}.$$

To prove it, take $w > 0$, $\Re(2h+\alpha) < 0$, evaluate the full positive half-line by the beta integral and subtract its tail by the binomial expansion for $|w| < a_0$. Continue the resulting identity meromorphically in h, and analytically in w off the negative real cut; imaginary w is reached by continuity. Here take the initial open parameter set to exclude integers for each of the finitely many exponents $2h + v$ being used. Since $2h + v \notin \mathbb{Z}$, all denominators stay a positive distance from zero for fixed parameters. On $|w| < a_0/2$ the analytic-background series converges normally after summation in j, using $|H_j| \leq C a_1^{-j}$ with any slightly smaller $a_1 > a_0$. The singular-series coefficients are $H_j \Gamma(v + j)\Gamma(-2h - v - j)$: by gamma reflection their size apart from H_j is bounded by a fixed power of $1 + j$. The common analytic coefficient of each homogeneous branch therefore converges on a complex neighborhood of $t = 0$. This derivation controls both frequency cutoffs and proves convergence of the analytic background as well as of the singular-series coefficients.

Apply the paired-phase calculation above to the two convergent germs. The coefficients are unique off integral b and coincide with the stationary coefficients already computed; alternatively the two ball changes reverse their Gaussian phases and preserve their initial angular amplitude. Thus for the full vector there exist holomorphic vector germs $P(t), Q(t)$, possibly with individual zero components, such that on its real sides the physical solution is exactly

$$W(t) = P(t) + |t|^b\, 2\cos(\varphi - \operatorname{sgn}(t)\pi b/2) Q(t).$$

The background P is common to both sides by the convergent analytic-background calculation. The scalar Weyl combination has the analogous exponent and phase given earlier. Its two-semicircle weights agree with the vector weights: the change in $\varphi + \pi b/2$ is $\pi n(n-1)/2$, an integral multiple of π. Here φ refers to the vector and the shifted angle to the scalar.

From the negative side $(-t)^b$ continues along the upper and lower arcs to $e^{-i\pi b} t^b$ and $e^{i\pi b} t^b$, respectively. Substituting the two weights displayed in the theorem keeps P and produces exactly the positive-side multiplier on Q. This proves the formula first at nonintegral parameters with nonzero denominator. It holds along any corresponding deformation in the singularity-free punctured disk by analytic uniqueness for the ordinary equation. For general h multiply through by $2\cos\vartheta$ before continuing in h. The physical endpoint integrals are holomorphic for $\Re h > -1$, including their logarithmic derivatives by integrability with a surplus exponent. The two continued endpoint vectors are holomorphic there too: the matrix in (10.7) has polynomial dependence on h for a parameter-independent pivot; analytic dependence of an ordinary initial-value problem along each fixed regular path applies. Therefore the multiplied identity holds throughout the half-plane. At a zero of the denominator it forces equality of the two arc values, and differentiation in h gives the stated derivative rule. This upgrade supplies the physical transmission across every interior critical radius, although numerical stability still depends on the arc, the equation representation, the initial data and parameter proximity to the exceptional set.

Connecting the integral-defined mode vector and propagating it on regular panels

Proposition 10.10 (source-selected continuation of all physical modes). For this construction let $d = \binom{2K+N}{N}$ as in Theorem 10.5 and write $V_j(z)$ for a single entry of its physical vector $W(Nz; z)$, indexed by an ordered representative $j = (j_1, \dots, j_N)$. Put $a = Nz$, $S = \sum_i w_i$, $\nu = -N - s$, and

$$k_j(z; w) = |a - S|^{2h} \prod_i w_i^{j_i} D_z(w_i)^\nu.$$

Here the independent uniform angle measure is $dm = \prod_i d\theta_i/(2\pi)$. The two ends of any closed interior window $[z_-, z_+]$ can be joined by the following additive rule, independent of every pivot,

$$V_j(z_+) = V_j(z_-) + \int [k_j(z_+; w) - k_j(z_-; w)]\, dm(w).$$

This is a source-based connection on the integral-defined solution. It also supplies the critical value itself by taking one endpoint there. On its own it has no implication for homogeneous solutions of the local equation outside that preparation. The errors in a supplied left value and an enclosure of the increment add, with coefficient one on the incoming error. The same angular grid can be used at both sides, and an independent source evaluation at the right side is also permitted. The following bounds justify this rule for every auxiliary mode, including inverse powers, and give an algorithm that converges with an explicit error budget. Controlling only the physical determinant combination would leave this componentwise issue open.

On a compact interior interval the absolute angular preparation of each mode costs at most $H = \max((1 - z)^{2N\Re\nu}, (1+z)^{2N\Re\nu})$ times dm. For the *unweighted independent* unit angles and $a \geq a_* > 0$, Gaussian majorization of a ball and Fourier inversion give

$$m\{|S - a| < e\} \leq \frac{\exp(1)e^2}{2} \int_0^\infty \exp(-e^2t^2/4)|J_0(t)|^N |J_0(at)|\, t\, dt, \qquad 0 < e \leq 1.$$

Indeed the Fourier transform of each angle law is $J_0(|\xi|)$, and integration of the translated Gaussian over its Fourier angle gives the extra $J_0(at)$. The elementary bound $|J_0(t)| \leq \min(1, 4/\sqrt{t})$ follows by removing arcs of length $t^{-1/2}$ about the extrema of cosine and integrating by parts between them (for $t \geq 1$). From $t \geq 1$ the integrand without its Gaussian costs at most $4^{N+1}a_*^{-1/2}t^{(1-N)/2}$. For $N = 3$ the remaining integral on that half-line is at most $\log(1/e) + 2$, by splitting at $1/e$. For $N \geq 4$ its bound is $2/(N-3)$. The $0 \leq t \leq 1$ integral costs at most $1/2$. Thus the probability bound is $Ce^2(1 + |\log e|)$ at rank three and Ce^2 above it, uniformly through each positive critical trace radius. At rank two, the independent two-angle sum has plane density $1/(\pi^2|w|\sqrt{4 - |w|^2})$ on $0 < |w| < 2$: the relative angle gives the radial law and the common angular displacement is uniform. Compact interior radii stay away from $0, 2$, so the same local quadratic ball estimate follows there. For larger e use the bound one.

For $\sigma = \Re h > -1$ these estimates bound the entire contribution of $|S - a| < e$ by $C_{h,s,N}e^{2+2\sigma}(1 + |\log e|)$, with the logarithm dispensable except at rank three. When $\sigma < 0$ use the probability bound both at e and in $(-2\sigma)\int_0^e r^{2\sigma-1}m\{|S - a| < r\}\, dr$. This proves absolute existence and uniform integrability of each complex mode through interior crossings. Truncation makes its ordinary continuity there immediate. A fully specified elementary approximation replaces $|S - a|$ in the power by $\max(e, |S - a|)$. The truncation error is bounded by the preceding integral plus $He^{2\sigma}m\{|S - a| < e\}$. Put $R = N(1 + z)$ and $M_b = \max(e^b, R^b)$. In each angle the Lipschitz constant of the truncated complex integrand is bounded by

$$H\left[2|h|M_{2\sigma-1} + \left(K + \frac{2z|\nu|}{(1-z)^2}\right) M_{2\sigma}\right].$$

The single-angle mark moves at speed at most one. The other term differentiates its monomial and the log preparation. A product lattice of m_0 nodes per angle has error at most the displayed constant times $N\pi/m_0$, by partitioning the torus into nearest-node cubes. Choosing e first and then m_0 constructs arbitrary absolute component accuracy at fixed rank, with m_0^N node evaluations. The recipe uses ordinary real positive bases and preserves the physical solution on the two sides independently of a singular connection formula. Tighter polynomial bounds and coordinate changes are needed for useful costs in difficult inverse cases.

Physical propagation with reflection. On the physical curve simultaneous complex conjugation of all *angles* carries j to its sorted negative. Denote this permutation by R_0. It gives $R_0W = W$ and $\partial_{\bar{a}}W = R_0\partial_a W$ at real

a, by invariance of the angular integral. Neither exponent is conjugated. In the blocks of (10.6), with the natural splitting $D = (D_1, D_2)$, define

$$B = L_{11} + L_{12}R_0, \qquad G_1 = hI - A_{+,0}, \qquad E = D_1 + D_2R_0.$$

The lower block equation is the reflection of the upper one. This follows also by $j \mapsto -j$, $t \leftrightarrow u$ in the one-angle recurrences. Hence B has generic rank $d-1$: restricting the full two-dimensional kernel of (10.6) to $X_{\bar{a}} = R_0X_a$ leaves the line generated by $e(z)$. It is killed by E. Let P repeat one representative value on each reversal orbit and P^+ average over the orbit. Then $W = Pv$ and the evolution can be computed as

$$v' = P^+(C_0P + EB^+G_1P)v.$$

Here B^+ can be the singular-value inverse dropping the known null direction, or any fixed nonzero $(d-1)$-minor solve with the remaining free coordinate set to zero. The identity is asserted for the compatible physical states where G_1Pv lies in the range of B. Different extensions to incompatible initial states can behave differently. A fixed-minor construction may equivalently restrict the output to orbit representatives. In this chart ranks three and four evolve 19 and 110 entries respectively. The numerical driver uses singular values to record the conditioning of the retained solve. Rank-three panels use an adaptive eighth-order Runge–Kutta scheme; the short fourth-rank panels bound the available work and compare successive RK4 refinements. The source increment bridges a chosen window, so no ordinary integration step crosses a declared critical radius. Floating-point step refinement and sampled singular values give diagnostics, while the validated regular-panel test below bounds its whole interval.

A local transfer bound and a verified crossing. Fix a minor on $[b, b+t]$. Enclose its inverse throughout the interval and assemble an interval matrix for the reflected physical generator M. If $L \ge \sup \|M(z)\|_\infty$ and $E_0 \ge \sup \|M(z) - M(b)\|_\infty$, its fundamental matrix satisfies

$$\|\Phi(b+t,b)\|_\infty \le \exp(tL), \qquad \|\Phi(b+t,b) - I - tM(b)\|_\infty \le tE_0 + \exp(tL) - 1 - tL.$$

The ordered-integral series proves both estimates, since every term of degree m costs at most $(tL)^m/m!$. Noninvertibility or failure of the interval inverse returns an unresolved panel. The verified computation chose a minor by floating-point column and row QR at the midpoint or left endpoint, then proved invertibility by a ball inverse of the actual rational blocks on the complete real interval. Pivot selection is only a proposal. The arithmetic enclosure is what establishes the bound.

For reproducibility, the coupled test uses an inexpensive seed for $\sigma > 0$. With $x = |a - S|^2/R^2 \in [0,1]$, write $b_0 = 1$, $b_{j+1} = b_j(j-h)/(j+1)$. Truncate $R^{2h}\sum b_j(1-x)^j$ at degree k. For $0 < \gamma < \sigma$, $k+1 > \gamma$ and $2(k+1)(\sigma - \gamma) \ge |h|^2 - \gamma^2$, the component error is at most

$$HR^{2\sigma}|b_{k+1}|(k+1)/\gamma.$$

Indeed $|j-h| \le j - \gamma$ for $j \ge k+1$. The positive dominating recurrence $c_{j+1} = c_j(j-\gamma)/(j+1)$ sums to $(k+1)c_{k+1}/\gamma$ by telescoping $jc_j - (j+1)c_{j+1} = \gamma c_j$. Converting the polynomial to powers of x, each required moment is a diagonal coefficient in $\exp(ta+ua)\prod_i \langle w^{j_i} D_z^\nu \exp(-tw - u/w)\rangle$ multiplied by the two factorials. For $m \ge 0$ the one-angle Fourier moments of D_z^ν are $z^m(-\nu)_m\, {}_2F_1(m-\nu, -\nu; m+1; z^2)/m!$, from the two binomial series, and the negative-index moments are equal to them. Products of truncated bivariate series and balls for these scalar coefficients enclose every required mode. Positive weights and relative error play no role in this construction.

At rank three with independent $h = 2.0001 + 0.0002i$ and $s = -2.98 - 0.017i$, degree 14 and 192-bit balls, the component truncation errors at $z = .30, .38$ are below .000594, .000765. Starting with the left enclosure, the source increment crosses the critical radius 1/3. A regular ODE step of length .0000002 then gives $T_3(h, s; .3800002)$ in a rectangle centered at $35.03778 + 0.94840i$ with both radii below .05037 (rounded outward to cover the displayed center). The full 34×34 pivot tested on that short interval gives $L < 6404$, $E_0 < 14.31$ and $\exp(tL) < 1.001282$. A degree-15 direct endpoint enclosure overlaps it. Perturbing the normalization by ten percent gives disjoint rectangles. These are finite certified statements with deliberately conservative seed and flow bounds. Plain singular-value evolution has no associated certification of its long-step stability.

Independent endpoint and failure tests. With $N = 3$, $h = 2.25 + .31i$, $s = -1.28 - .45i$, the path $.27 \to .31$, source window $.31 \to .36$, and ordinary continuation to .39 gives a scaled discrepancy 9.54×10^{-10} against an

independently shifted original-Haar angle integration. Holding the components fixed across the window instead gives 1.73. Omitting the derivative of the disk preparation on the last panel gives .0915. The largest retained singular-value condition estimate on this run was about 1.93×10^3. For $h = -.08 + .17i$, $s = -2.65 + .21i$ the analogous $1/3$ crossing gives 1.76×10^{-5}; the independent reference itself changed by 3.57×10^{-5} in absolute value on refinement. At $h = 1$, $s = -3$, the rank-three exact moment $(1 - z^2)^{-9}(1 + 9z^2)$ checks the readout to 4×10^{-14} scaled. At rank four with $h = 2.13 - .24i$, $s = -3.35 + .19i$, short ordinary panels $.393 \to .394$ and $.569 \to .570$ joined across $1/2$ give 5.52×10^{-7} scaled discrepancy against the separate original-Haar integration. The reference changed by .0544 in absolute value, or about 1.8×10^{-5} on its own scale. The largest retained condition estimate was 4.22×10^6. The tests use $|\Delta|/\max(1, |\text{reference}|)$ for scaled discrepancies; they do not certify decimal places.

At rank two an unmodified uniform grid is a poor inverse-order seed. For $h = -.85 + .03i$, $s = -.7 + .1i$, evolving $.51 \to .55$ from 128 nodes per angle missed the midpoint of an independent certified singular cubature by .137 on that scale. A change of source coordinates repairs the computation. Write $w_{1,2} = e^{i(\phi \pm \theta)}$ with $0 \le \theta \le \pi/2$ and $0 \le \phi \le \pi$. The Haar-independent mode integral has factor $2/\pi^2$, factors $\cos((j + k)\phi)\cos((j - k)\theta)$, preparation $[D_z(e^{i(\phi+\theta)})D_z(e^{i(\phi-\theta)})]^\nu$ and power $|2z - 2\cos\theta e^{i\phi}|^{2h}$. These follow by the two label permutations and simultaneous reflection of both angles, without taking a real part of the complex-tilted amplitude. Split at $\theta_0 = \arccos z$. For each signed side length L map the two triangles by $(\theta - \theta_0, \phi) = (Lt, \pi ty)$ or $(Lty, \pi t)$, $0 \le t, y \le 1$. Extract t^{2h+1}. For the remaining smooth factor use interpolatory Gauss–Legendre product integration; the exact moments of $P_j(2t-1)$ with this complex weight obey $I_0 = 1/(2h+2)$ and $I_{j+1} = I_j(2h+1-j)/(2h+3+j)$ by the shifted Rodrigues formula. This gives a finite rule for *every* auxiliary starting mode. The resulting ODE agrees with the independently certified endpoint midpoint to 2.35×10^{-11} scaled at 56 nodes per chart coordinate. For the independent strip case $h = .75 + .0007i$, $s = .016 - .028i$, the 96-node raw-seed ODE discrepancy is 4.69×10^{-8} against the replayed rank-two enclosure. The cubature is certified; these last ODE comparisons are floating-point evidence. Extension of efficient singularity-resolving mode quadrature and long-interval validated integration to substantially higher ranks is a remaining cost and conditioning problem.

Numerical continuation along two complex arcs. To implement the connection at a genuine critical radius, the driver anchors a nonzero minor of B at its incoming point. It evaluates the same rational formula at complex z along $z = z_* - r\exp(\mp i\pi t)$, $0 \le t \le 1$. It multiplies the generator by dz/dt and uses the upper sign in the exponential for the upper path. It uses ordinary linear solves on this fixed minor. The preparation parameters and the two occurrences of the complexified physical coordinate Nz are held to their holomorphic definitions. A right-end source is used only to assess the result. The complex-arc calculations in the following comparisons use double precision.

At rank three the incoming and comparison mode quadratures condition on the first unit angle w. The trace target for the remaining pair has modulus $b = |3z - w|$ and argument $\psi = \arg(3z - w)$. Write the two remaining angles as $\psi + \phi \pm \theta$. On $b < 2$ their zero lies at $(\phi, \theta) = (0, \arccos(b/2))$; using the same two Duffy triangles on each real side of this point gives the t^{2h+1} rule derived above. Both signs of ϕ are retained because rotating the trace also rotates the preparation. At $b > 2$ the nearest point has $\theta = \phi = 0$ and the positive distance leaves an ordinary quadrature. The outside angle is split at $b = 2$ when that level occurs. At $N = 3$, $z_* = 1/3$, crossing radius .055, $s = -2.54 + .29i$ and $h = .65 + .19i$, the weighted two-arc answer agrees with a separate outgoing joint-mode quadrature to 1.52×10^{-12} in scaled maximum norm. The pure upper and lower paths give discrepancies 3.02×10^{-4} and 9.16×10^{-5}. The mixed scalar differs by 5.13×10^{-8} from direct integration in the original, untransformed Haar angles. With inverse $h = -.24 + .19i$ the corresponding mode discrepancies are 2.93×10^{-8}, .0466 and .0141, respectively. At the noncritical rank-three pencil singularity $z = .5$, independent $h = .81 - .23i$, $s = -2.41 + .32i$, both arcs of radius .01 agree with the outgoing physical state to 1.08×10^{-10} on its scale.

For the exceptional case $h_0 = 1/2$, $N = 3$, $z_* = 1/3$, radius .065 and the same nonreal s, the code evolves $Y_h' = MY_h + (\partial_h M)Y$ simultaneously with the original vector. The fixed-minor matrix is affine in h, so its h derivative is an exact first difference in the algebraic formula. The incoming parameter derivative was computed by a centered difference of the resolved angular integrals at two spacings with Richardson extrapolation. At the outgoing point the two zeroth-order arc states differ by 2.02×10^{-12} in absolute maximum norm. The parameter-derivative connection gives a scaled mode discrepancy 1.73×10^{-11}. Dropping the derivative correction gives 6.42×10^{-4}. Direct untransformed Haar quadrature gives scalar discrepancies 1.11×10^{-7} and 2.14×10^{-4} respectively.

The same construction avoids dividing by a nearly zero cosine. Let h_0 be a weight pole, fix all other parameters and write $d_h = h - h_0$, $\mathcal{A}(h) = W^{\uparrow}(h) - W^{\downarrow}(h)$. By the exceptional connection $\mathcal{A}(h_0) = 0$ on the physical incoming family. The ordinary complex fundamental theorem of calculus in h gives the exact increasing-radius formula

$$W_{\mathrm{phys}}(h) = \frac{W^{\uparrow}(h) + W^{\downarrow}(h)}{2} - \frac{i}{2}\, d_h \cot(\pi d_h) \int_0^1 \partial_h \mathcal{A}(h_0 + t d_h)\, dt.$$

The coefficient $d_h \cot(\pi d_h)$ tends to $1/\pi$. If the derivative in the integral is frozen at h_0, the error has norm at most $|d_h \cot(\pi d_h)|\, |d_h| \sup_{[h_0,h]} \|\partial_h^2 \mathcal{A}\|/4$. Holomorphic compact-parameter estimates for the arc equations give finite bounds on this derivative on compact admissible segments. Numerical quadrature in h or additional parameter jets give higher orders. This formula controls the connection weight; stability of propagation inside each arc is still a separate estimate. At $h - h_0 = 10^{-12}$ the direct combination in double precision has a scaled mode error of 0.101. The first regularized jet gives 1.79×10^{-11} against the independent outgoing mode quadrature with the same working precision.

Corollary 10.11 (arbitrary absolute accuracy along a fixed admissible path). Take fixed N, independent h, s with exact rational real and imaginary parts and $\Re h > -1$. Let the incoming and outgoing points be regular rational interior radii on opposite sides of a single positive critical radius. Choose two rational polygonal paths in the upper and lower half-planes with the winding prescribed by Theorem 10.9. Both paths and the short real connections to them must avoid all poles of the chosen rational chart. Such paths can be constructed locally: its nonzero pivot polynomial has finitely many roots, which can be isolated, or disks can be verified directly by polynomial bounds. An incoming real point on the boundary of a chart may first be transported to a regular point by Theorem 10.7. Given a positive rational absolute tolerance, the following algorithm terminates in exact or sufficiently increased ball precision. Its cost estimate depends on the entire chosen path and can be very large.

Use the unreduced physical matrix (10.7) to avoid parameter-dependent normal-jet dimensions. On each substep with centre p, complex increment v, and a verified polar-free disk $|z - p| \le r$ with $q = |v|/r < 1$, enclose M there by $K \ge \sup \|M\|_\infty$. Interval evaluation on a surrounding square suffices. Splitting the step eventually succeeds on each compact path: at a nonzero pivot its interval evaluation converges to its nonzero central value. Taylor coefficients A_j of $M(p + x)$ are obtained by rational series division. For the initial-identity fundamental matrix the coefficients are

$$F_0 = I, \qquad F_{j+1} = \frac{1}{j+1} \sum_{l=0}^{j} A_l F_{j-l}.$$

On the whole disk integration along radial segments gives $\|F\|_\infty \le e^{rK}$. Cauchy's estimate bounds the omitted terms above degree m by $e^{rK} q^{m+1}/(1-q)$ in the induced norm, using the matrix integral formula in that norm. In particular a target local tolerance e is met by choosing $m + 1 \ge [rK + \log(1/(e(1-q)))]/\log(1/q)$. Add the actual arithmetic error in computing the finite polynomial separately. For a product of steps, if the local approximants have errors e_i and true norms bounded by $b_i = e^{|v_i| K_i}$, the error is at most $\prod_i (b_i + e_i) - \prod_i b_i$, by telescoping. An incoming uncertainty is multiplied by at most $\prod_i b_i$ along each arc. These bounds allow the incoming angular error, the finite truncations, and then the arithmetic errors to be prescribed before combining the two arc endpoints. The complex coefficients of Theorem 10.9 are computed as balls to the required absolute tolerance. Multiplication by the analytic physical prefactor and scalar readout is included at the endpoint.

At a zero of the cosine use the triangular system for $(W, \partial_h W)$ with diagonal blocks M and lower left block $\partial_h M$, and combine by (10.12). The seed kernel for the derivative has the extra factor $\log |g|^2$. For any rational $0 < \eta < \Re h + 1$, the elementary bound $|\log x| \le x^{-\eta}/(e\eta)$ on $0 < x \le 1$ and the preceding small-ball bound give a computable origin budget. On the complement the cutoff kernel and its angular derivatives are bounded explicitly, so the same torus grid refinement terminates. Distances from poles, the cost of angular initialization and the exponential products prevent this existence and cost formula from implying a practical rank-uniform resource guarantee. Proposition 21.7 illustrates a useful independent inverse-order scalar benchmark.

A residual bound for a sequence of complex path panels

A posteriori transport estimate. Parameterize each smooth complex arc by a real parameter t, including dz/dt in its coefficient matrix $A(t)$. For the first-order equation $y' = Ay + f$, choose an approximate vector v_j and an invertible approximate fundamental matrix V_j on panel $[a_j, b_j]$. Their entries may be piecewise polynomials;

continuity of the selected bases across panels is unnecessary. Put

$$r_j = Av_j + f - v_j', \qquad E_j = V_j^{-1}(AV_j - V_j'), \qquad g_j = V_j^{-1} r_j.$$

Let a real constant matrix C_j and a nonnegative vector $\gamma_j(t)$ bound $\Re((E_j)_{ii}) \le (C_j)_{ii}$, $|(E_j)_{ik}| \le (C_j)_{ik}$ for $k \ne i$, and $|g_j(t)| \le \gamma_j(t)$ componentwise. Given componentwise starting bounds $d_j \ge |V_j(a_j)^{-1}(y(a_j) - v_j(a_j))|$, valid ending and next starting bounds are

$$e_j = e^{(b_j - a_j)C_j} d_j + \int_{a_j}^{b_j} e^{(b_j - t)C_j} \gamma_j(t)\, dt,$$
$$d_{j+1} = |V_{j+1}(a_{j+1})^{-1} V_j(b_j)| e_j + |V_{j+1}(a_{j+1})^{-1}(v_j(b_j) - v_{j+1}(a_{j+1}))|.$$

Adjacent endpoints refer to the same complex radius. The physical error for a given exact scalar readout row l at the final endpoint is bounded by $|lV_j(b_j)|e_j$, with a separate bound for any uncertainty in l or rounding of lv_j. Indeed $q = V_j^{-1}(y - v_j)$ satisfies $q' = E_j q + g_j$. Taking upper right derivatives of $|q_i|$ gives $D^+|q| \le C_j|q| + \gamma_j(t)$, including at zero components. Adding a multiple of the identity to C_j makes it entrywise nonnegative, proving comparison by the matrix exponential. The second line is the exact change of coordinates and approximate-vector jump followed by the triangle inequality. The same rule propagates a parameter derivative by applying it to the block differential system for the solution and that derivative. Absolute endpoint bounds from separate branches are multiplied by the moduli of their connection weights before addition.

These formulas permit a certificate with residual-sized growth even when $\|A\|$ is large. Matrix inverses in the proof need not be evaluated by interval Gaussian elimination throughout the arc. For example, choose a polynomial H_j approximating V_j^{-1}, and certify $|I - H_j V_j| \le K_j$ entrywise, $K_j \ge 0$, with $\rho(K_j) < 1$ (a weighted row-sum bound suffices). For $F = AV_j - V_j'$ one obtains

$$|V_j^{-1} F - H_j F| \le (I - K_j)^{-1} K_j\, |H_j F|.$$

This permits a signed bound on the diagonal real parts of E_j. The same inverse bound applies to residuals and endpoint transformations. For rational A and polynomial approximants one can first form a common-denominator numerator for F, then bound that polynomial on the panel; a positive lower bound for the modulus of its denominator is needed. The certificate depends on verified residual, inverse, source and jump enclosures. It need not be sharp if the inter-panel matrices have badly aligned bases.

The included two-component control checks this distinction in exact rational arithmetic. With $J_{12} = 1$ the sole nonzero entry, take $A(t) = 120(1-2t)J$, $f = (0, 10^{-3})^{\mathsf{T}}$, and the zero initial vector. On $[0, 1]$ the direct integral of $\|A\|_\infty$ is 60. Take two panels with $v_j = 0$ and $V_j = (I + [120t(1-t) + t/16]J)D_j$, $D_1 = I$, $D_2 = \mathrm{diag}(1/4, 2)$. The exact first-component endpoint error is 0.020000. The displayed bound gives 0.020125, including the transformed forcing, nonzero frame residual and final readout. Omitting the change of basis at the middle produces a false upper bound below 0.013. This manufactured example checks the error propagation and failure control. Applying it to a particular Haar arc requires enclosures for the actual matrices and physical seeds of that arc.

A certified polynomial generator for the compact state

Theorem 10.12 (rational tangent and validated path propagation). Use the four-mode tuple order of Theorem 10.6 (lexicographic nondecreasing tuples in $-1, 0, 1, 2$). Write $d = 20$ or 35, $H = 1$ or 2, and $g = h + H$. In (10.6) delete two rows of L and G, and two columns of L and D. With zero-based indices the deleted rows and columns are respectively $(13, 31), (0, 39)$ at rank three, and $(11, 62), (0, 69)$ at rank four. Denote the retained row and column sets by I, J. Define the real rational action

$$Y(z) L_{IJ}(z) = D_J(z), \qquad M(z) = C_0(z) + Y(z) G_I(z).$$

Here Y depends only on the geometry. For the angular solution, the two omitted displacement coordinates can be set to zero by a kernel shift wherever the minor is invertible: the deleted columns include one nonzero entry from each of the two disjoint kernel vectors. The shift leaves DX unchanged, by Theorem 10.5. Thus $W' = MW$ is an ordinary equation for the full compact state, including its dependence on the preparation. Values with complex z on a continuation path use the rational coefficients themselves.

The integer polynomials for this chart can be recovered with verifiable low degree. Up to a nonzero rational constant the common denominators for Y in the checked identities are

$$q_3 = z^2(9z^2-1)(3z^2-2)(2z^2-1)(4z^2-1)(3z^2-1)^2(z^2-1)^4,$$
$$q_4 = z^4(9z^2-1)(3z^2-2)(z^2+1)(4z^2-3)(4z^2-1)^2(2z^2-1)^2(3z^2-1)^2(z^2-1)^5.$$

Their degrees are 22 and 34. The constructed numerator matrices $B = q_N Y$ have degrees 25 and 35. To find a candidate q_N, solve the square rational system at positive integers $z \geq 2$, take a fixed seeded rational linear combination of the entries, and use univariate Euclidean rational reconstruction on these samples. Next interpolate $q_N Y$ entrywise. The scalar combination only proposes the denominator. Exact arithmetic verifies the full matrix identities $BL_{IJ} = q_N D_J$ at 38 and 50 distinct rational points, respectively. The degrees suffice: zL has degree at most two, while $z^6(1-z^2)$ clears the remaining geometric one-angle coefficients to polynomials of degree at most 14. This follows by substitution in the four angular rows, also checked symbolically before lifting. Multiplying the identity by $z^6(1-z^2)$ gives degree at most $\max(\deg B + 9, \deg q_N + 14)$, which is smaller than the corresponding count. Existence of a rational inverse of the square minor follows from any one successful nonsingular sample. These finite identities certify the geometry for arbitrary independent s, h in the physical domain. Poles of a chosen rational chart away from the real interval carry no new evidence of a physical singularity.

For exact rational real and imaginary components of the parameters, interpolate the polynomial $z^6(1-z^2)(q_N C_0 + BG_I)$ from the same identities and cancel any common scalar factor. The two parameter dependences of C_0 and G_I are affine, and D_J has no parameter dependence. Thus separate rational real and imaginary arithmetic suffices. The output $M = A/p$ at the reported parameters has $\deg p = 22, 34$, with numerator degrees at most $26, 36$ respectively. Once generated, this data avoids a new singular-pencil solve at every complex time step.

Enclosing both complete path matrices by a polynomial defect

Let $z = x + vt$ on a panel $0 \leq t \leq 1$. Translate the exact numerator and denominator to $B(t) = vA(x+vt)/p(x)$ and $q(t) = p(x+vt)/p(x)$, with $q(0) = 1$. An enclosure $\ell > 0$ for $\min_{[0,1]} |q|$ is found by subdividing the real t interval: at each midpoint take the absolute value of the constant coefficient minus the absolute sum of the higher translated terms with the subinterval half-length included in each power. Failure of a proposed partition or panel leads to refinement.

Two polynomial approximations. Let P, H be degree-m approximations to the initial-identity fundamental matrix and its inverse, both starting at I. With the induced infinity norm, put

$$d_P \geq \sup \|P' - BP/q\|, \qquad d_H \geq \sup \|H' + HB/q\|, \qquad p_* = \sum \|P_j\|, \quad h_* = \sum \|H_j\|.$$

If $\eta = d_H p_* + h_* d_P < 1$, then on the entire panel $\|P^{-1}\| \leq h_*/(1-\eta)$. Indeed $(HP)' = (H' + HB/q)P + H(P' - BP/q)$, whence $\|HP - I\| \leq \eta$. For the exact fundamental matrix $F = PV$ the transformed generator for V has norm at most $h_* d_P/(1-\eta)$. Therefore a verified final-panel error is

$$\|F(1) - P(1)\| \leq \|P(1)\| \left[\exp\left(\frac{h_* d_P}{1-\eta}\right) - 1\right].$$

Large entries of the untransformed generator affect the effort needed to form the approximations, rather than appearing directly in this exponential. Omitting the inverse defect or the test $\eta < 1$ would invalidate this argument.

One implementation encloses the exact Taylor coefficients using the recursion for $qP' = BP$ through degree $m-1$, with $H'q = -HB$ on the inverse side. At rank three, the coefficients of $HP - I$ up to m vanish exactly. This permits the alternative inverse test $\eta = \sum_{i+j>m} \|H_i\|\|P_j\|$ using the same endpoint error estimate. For the forward differential defect, only coefficients of degrees at least m remain. Their absolute sum divided by ℓ bounds d_P. In particular, if $b_j = \|B_j\|$, $f_i = \|P_i\|$ and out-of-range coefficients are zero, a convenient upper bound for their numerator is

$$\sum_j b_j \sum_{m-j \leq i \leq m} f_i + \sum_{j \geq 1} |q_j| \sum_{m-j+1 \leq i \leq m} i f_i.$$

At rank four a fixed-point implementation speeds up the dense recursions. With $S = 2^b$, approximate the real and imaginary parts of the normalized coefficients on the lattice $S^{-1}\mathbb{Z}$. Compute each forward or inverse numerator by exact Gaussian-integer matrix multiplication and addition; divide componentwise by $S(k+1)$, rounding down to the integer lattice before the next multiplication. Set $q_0 = 1$ exactly. In physical units, each order-k residual from the final division has induced norm at most $2dk/S$, $1 \le k \le m$. If the sums of the coefficient perturbations for B and $q_{j\ge1}$ are bounded by Δ_B and Δ_q, add

$$dm(m+1)/S + \Delta_B \sum_i f_i + \Delta_q \sum_i i f_i$$

to the high-degree numerator bound and divide the result by ℓ. The rounded input widths and the conversion to the integer lattice are included in Δ_B, Δ_q. The same calculation for H gives d_H. Thus the integer recursion needs no floating-arithmetic model. All remaining bounds use outward-rounded balls. Rejected panels bisect, and approved endpoint balls multiply in path order using a balanced product tree. This last step transports errors through the actual matrix products, including noncommutation. It also gives all columns of each branch matrix, so the incoming component radii and the final scalar functional can be combined after integration. The panel degree, working precision, requested local tolerance and all subdivisions are recorded.

Transporting local defects to the scalar

For a branch of m macro-panels, write $F_i = C_i + \Delta_i$. Here C_i is the represented midpoint of the verified panel matrix, and $|\Delta_i| \le D_i$ componentwise. Take D_i to be the sum of the real and imaginary radii, an upper bound for the complex modulus of each entry error. Write $C_{b:a} = C_b \cdots C_a$, with empty product I. The exact identity

$$F_{i:1} - C_{i:1} = \sum_{j=1}^{i} C_{i:j+1} \Delta_j F_{j-1:1}$$

follows by telescoping. A componentwise enclosure for the full matrix difference is obtained recursively by setting $E_0 = 0$ and

$$E_i = \sum_{j=1}^{i} |C_{i:j+1}| D_j \big(|C_{j-1:1}| + E_{j-1}\big).$$

Absolute values of subproducts are taken *after* their matrix multiplication. Signed cancellation among the known midpoint matrices is preserved. The products themselves require sufficient precision, as their computed intervals also enter these bounds.

There is a sharper completely verified estimate for a specified physical seed. Let w be the vector of enclosed polynomial centres, with a separate vector e of absolute analytic error bounds on $W_0 - w$. For each branch define $V_0 = |w| + e$ and

$$V_i = |C_{i:1} w| + |C_{i:1}| e + \sum_{j=1}^{i} |C_{i:j+1}| D_j V_{j-1}.$$

Induction gives $|F_{i:1} W_0| \le V_i$. Let l be the physical scalar row at the final radius, with any valid reduction by the continued right-end constraints. Telescoping now gives the goal-oriented bound

$$d_\pm = \sum_{j=1}^{m} |l C_{m:j+1}| D_j V_{j-1}, \qquad |l(F_{m:1} - C_{m:1}) W_0| \le d_\pm.$$

These are positive scalar majorants computed separately on the two paths. Form $r = \omega l C^+_{m:1} + (1-\omega) l C^-_{m:1}$, using the physical connection weight. If r_0 is any representative of r modulo the *incoming* exact constraints, an absolute error bound about $r_0 w$ is

$$|r_0| e + |\omega| d_+ + |1-\omega| d_-.$$

The substitutions by compatibility rows apply to the physical solution. They do not assert compatibility of arbitrary coordinate perturbations or of the midpoint matrices. Evaluation and rounding intervals are carried separately by ball arithmetic.

In the degree-42 rank-four run the componentwise midpoint-product bound reduces the upper-branch maximum entry radius from 2.33×10^{-5} to below 8.24×10^{-16} using the same local polynomials. Proposition 21.9 gives the tighter full-matrix and scalar budgets.

One can also certify the conditioning of the complete branch matrices themselves. Compute a dyadic midpoint approximate inverse K and enclose $d = \|I - FK\|_\infty$. When $d < 1$, $\|F^{-1} - K\|_\infty \le \|K\|_\infty d/(1-d)$ by the Neumann series. At rank four the two inverse residuals are below 1.653×10^{-23} and 1.895×10^{-23}. Taking upper and lower absolute row sums on the resulting full enclosures gives $1.72456 \times 10^{20} < \kappa_\infty(F_+) < 1.72458 \times 10^{20}$ and $3.31546 \times 10^{20} < \kappa_\infty(F_-) < 3.31548 \times 10^{20}$. Both inverse products enclose I; that consistency check alone would not establish invertibility. The same proof at rank three gives $1.84396 \times 10^7 < \kappa_\infty(F_+) < 1.84397 \times 10^7$ and $1.81794 \times 10^7 < \kappa_\infty(F_-) < 1.81795 \times 10^7$. These are condition numbers of the full maps, distinct from the norm of the physical scalar row.

A final replay uses the native polynomial centres from a fresh angular seed integration at the same left endpoint. The centre is

$$6634.51746712714261052377156484931830746 4 - 1591.32787090943961478867753614070136812 9\, i.$$

Its Euclidean radius, including display rounding, is below 1.881×10^{-16} and its relative radius below 2.757×10^{-20}. The unsigned analytic seed tail dominates the result. The separate branch defects, independent outgoing comparison and three strictly positive wrong-connection lower bounds survive the replay.

Singular germs at the first interior critical radius

Theorem 10.13 (a two-germ rank-three transfer). At the nonreal rank-three orders $h = 7/4 + i/4$ and $h = 3/2 + 10^{-8}i$, with $s = -2.86 + .21i$, take $z_* = 1/3$, $z_l = 13/50$, $z_r = 2/5$, and $x = (z - z_*)/(9/100)$. The full rational equation of Theorem 10.6 has a simple pole at $x = 0$. Its residue R satisfies

$$R^2 = bR, \qquad \operatorname{tr} R = b = 2h + 4.$$

These equalities are identities of the exact rational real and imaginary matrices at the indicated points. The additional two in b relative to the unraised trace order come from $g = h + 1$. Set $P = R/b$. There is a 19-dimensional analytic space, and a one-dimensional space with exponent b. Write their matrix series as $H_0(x)$ and $x^b H_b(x)$, normalized by $H_0(0) = I - P$ and $H_b(0) = P$. For $x_l < 0 < x_r$ the two transfers are

$$F^{\uparrow,\downarrow} = [H_0(x_r) + |x_r/x_l|^b e^{\mp i\pi b} H_b(x_r)][H_0(x_l) + H_b(x_l)]^{-1}.$$

Powers of a positive real number always use its real logarithm. The upper path moves the argument of x from π down to zero. The diagonal projection on the right of each initial coefficient is retained at every recurrence step. This explains why absorbing the incoming power on its one-dimensional subspace gives the stated inverse.

Proof and bounds. Clear denominators and write $xp(x)W' = B(x)W$, $p(0) = 1$, $B(0) = R$, with both polynomials determined exactly. For $\lambda = 0, b$ and $A_0 = I - P, P$ respectively, the coefficients satisfy

$$[(j+\lambda)I - R]A_j = \sum_{k=1}^{j} [B_k - (j-k+\lambda)p_k I]A_{j-k}.$$

Since b is nonreal, the inverse factor is $[I + R/(j+\lambda-b)]/(j+\lambda)$ for $j \ge 1$. This recursion together with the tail bound also proves convergence on the required disk. To prove a coefficient bound, multiply the equation by the first 13 coefficients of the formal reciprocal of p, obtaining $\widetilde{p}, \widetilde{B}$. For $n = m + 1 > |b|$ put

$$\chi_\lambda = \left(1 + \frac{\|R\|}{n - |b|}\right)\left(\frac{\sum_{k>0} \|\widetilde{B}_k\|}{n} + \left(1 + \frac{|\lambda|}{n}\right)\sum_{k>0} |\widetilde{p}_k|\right).$$

In these examples $\Re b > 0$. Therefore $|j + \lambda| \ge j$ and $|j + \lambda - b| \ge j - |b|$. If $\chi_\lambda < 1$, every later matrix coefficient has norm at most the maximum L of the last $D = \max(\deg \widetilde{p}, \deg \widetilde{B})$ computed norms. Induction uses only $j - k \ge 0$ and $|j - k + \lambda| \le j + |\lambda|$. At either endpoint the tail is bounded by $L|x|^{m+1}/(1 - |x|)$. The Taylor coefficients themselves may be computed with the shorter original polynomials. At the primary rank-three point

$D = 38$, $m = 240$, and both contraction bounds are below .865. The weighted sum in Theorem 10.9 acts as the identity on the regular germ. On the singular germ its phase factor simplifies to one for $k = 1$, because $\vartheta = \pi b/2$ and

$$\frac{e^{i\vartheta - i\pi b} + e^{-i\vartheta + i\pi b}}{2\cos\vartheta} = 1.$$

This is a useful cancellation before rounding as the cosine decreases. The separate full-state germs can still become ill-conditioned near an integral b. For an interval endpoint matrix L_0, a point inverse approximation K with $\eta = \|I - KL_0\| < 1$ gives $\|L_0^{-1} - K\| \le \eta\|K\|/(1-\eta)$. This checks the endpoint solve independently of pivot heuristics. The proof of the rank-three formula uses the rational residue, the coefficient bounds, and a verified inverse. No fit to values on the other side fixes its branch constants.

A double pole at rank four. The same generator at $N = 4$, $h = 7/4 + i/4$, $s = -193/50 + 21i/100$ has a double pole at $z_* = 1/2$. Let its first Laurent coefficients be $A/t^2 + B/t + C$, $t = z - z_*$. Exact rank computations give $\operatorname{rank} A = 2$, $A^2 = 0$ and $B \operatorname{im} A \subset \operatorname{im} A$. The range has a real rational basis. With P the corresponding orthogonal projector and $K = I - P$, put $W = (K + P/t)V$. Subtracting the derivative of this gauge from the transformed generator cancels its higher poles. In detail, $PA = A$, $AP = 0$ and $KBP = 0$. The only remaining residue is

$$R_4 = KBK + PBP + A + KCP + P.$$

The exact projector has $\|P\|_\infty = 36/25$. The realification of R_4 has rank ten and characteristic polynomial proportional to

$$x^{60}(4x^2 - 80x + 401)(2500x^2 + 18600x + 35037)(2500x^2 + 3600x + 1737) \\ \times (2500x^2 - 1400x + 637)(2500x^2 + 13600x + 18937).$$

The constant is fixed by monicity. Hence the zero eigenspace has complex dimension 30 and zero is semisimple. The physical nonintegral exponent from the trace connection is $2g + 5/2 = 10 + i/2$. The other indicial roots belong to the 35-coordinate extension. Inferring physical coefficients for all these roots from the scalar trace asymptotic would require extra matching information. The rank-four certificates below transport both complete matrices on paths disjoint from the pole. The rational shear is a separate exact explanation of the singularity at the tested parameters.

Conditioning the scalar on the physical angular data

At a regular real endpoint take the nonresonant chart of Theorem 10.6. Let $D = \binom{N+3}{3}$, let W be its D-component compact angular state at $g = h + H$, and include the full physical prefactor and the divisors $(h+1)_H^2$ in the scalar row l. The row is computable by the matrix recurrences of Theorem 10.6 acting on $W_0 = I_D$. The recovered matrices X_{ij} are fixed linear extensions of the mixed jets to arbitrary input columns. Only their action on the physical column is prescribed. An interval evaluation uses the rational group inverse from Theorem 10.6, including its invertibility check. The normal equations are solved through degree $2H$. An interval containing $j - \rho = 0$ is never divided into. Theorem 10.6 supplies an augmented construction for the full normal jet. For the scalar at ranks three and four, use the division-free row of Theorem 23.1.

Proposition 10.14 (physical compatibility and correlated error). One can compute a matrix C satisfying $CW = 0$. For each available displacement jet, apply a left null matrix of L to $GX_{ij} - \binom{iX_{ij}}{jX_{ij}}$. The two-row left null matrix is $C_* J^{-1}$ in the notation of Theorem 10.6. Include the differences of the alternative mixed-jet solutions after fitting their two free coefficients, and the analogous difference in the sum of the two pure jets. These differences vanish on W by their common angular integral. Reflection gives more relations: for the overlap of the mode window with its negative, $X_{ij}[t]W = X_{ji}[-t]W$. This is reflection of all angles at real displacement. Neither exponent is conjugated. Thus $(l - qC)W = lW$ for any row q. Dyadic coefficients chosen by floating-point least squares suffice: only the identity and the interval evaluation of the resulting row and its norm enter a certificate. The construction can be used a second time on the incoming row after complex transport. If F is the correct two-path transfer, the scalar is

$$[(l - q_+C_+)F - q_-C_-]W_-.$$

The outgoing annihilator applies after physical mixing. It also applies to either arc from exact physical input by analytic continuation of $C(z)W(z) = 0$ from the incoming germ: the rational two-coordinate construction of C

is single-valued off its poles. For the real-endpoint orthogonal extension the rational transpose formulas agree on the real line and supply that same type of holomorphic continuation. One may instead retain the original row on each arc. The incoming annihilator always applies to the physical initial state. Measuring the resulting row gives a bound on the effect of incoming component errors and avoids estimating it by a product of three unrelated matrix norms. The construction needs no declaration of the exact numerical rank of the assembled constraints.

Correlated angular error. Write $d\nu_s = \prod_i |1 - zw_i|^{2\nu}\, dm$, $\nu = -N - s$, and $d\mu = \prod_i |1 - zw_i|^{2\Re\nu}\, dm$, where dm is independent uniform angular measure. For a sorted mode tuple I let P_I be the symmetric average of $\prod_i w_i^{I_i}$ over permutations. The preparation and mark are symmetric, so this substitution preserves all compact entries. For l evaluated at an incoming real point put $P_l = \sum l_I P_I$. Its Gram matrix under μ is

$$K_{IJ} = \frac{1}{N!} \sum_{\pi \in S_N} \prod_{i=1}^{N} f_{I_i - J_{\pi(i)}}(z; \Re\nu), \qquad m = \mu(1) = f_0(z; \Re\nu)^N.$$

The f are the one-angle Fourier moments in Section 21. Expand the two permutation sums in $P_I \overline{P_J}$ and relabel the independently integrated variables to prove the formula. The Gram matrix is positive definite since distinct orbit sums are linearly independent and the real weight is positive. If p approximates x^g on $[0, 1]$ with supremum error e, put $R = N(1 + z)$ and $X = |Nz - \sum w_i|^2/R^2$. Then

$$\left| lW - R^{2g} \int P_l\, p(X)\, d\nu_s \right| \le R^{2\Re g} e \sqrt{m\, lKl^*}.$$

This is Cauchy–Schwarz under the positive majorant of the complex preparation. The polynomial integral is computed from all compact modes with the same coefficients, retaining its correlations. Minimizing the *bound* over representatives $l - qC$ can be much more effective than bounding components separately. If M is a set of constraint rows with invertible MKM^*, the Gram-minimal representative relative to that set is

$$l - lKM^*(MKM^*)^{-1}M.$$

The formula follows by completing the square. An interval solve verifies an invertible pivot for this version. A dyadic approximate minimizer is also valid with its own computed norm, even when the proposed Gram solve is poorly conditioned.

For reproducibility use $x = (1 + \cos\theta)/2$, $x^g = c_0 + \sum_{j \ge 1} c_j \cos(j\theta)$, $c_0 = \Gamma(g + 1/2)/[\sqrt{\pi}\,\Gamma(g + 1)]$, with the recurrence in Corollary 21.6. For $u = \Re g > 0$, choose $0 < \alpha < u$ and $m' = d + 1 > \alpha$ with $2m'(u - \alpha) \ge |g|^2 - \alpha^2$. For $j \ge m'$ this gives $|j - g| \le j - \alpha$ and $|j + 1 + g| \ge j + 1 + \alpha$. Telescoping yields the degree-d uniform error $|c_{m'}|(m' + \alpha)/(2\alpha)$. A second available estimate uses the Gauss Hermite interpolant in Theorem 21.5. With the positive comparator γ, let $G = H_\gamma - L_\gamma$ be its polynomial bracket, with either sign. The pointwise modulus of the remainder is at most $D_k(g, \gamma)|G(X)|$. Its integrated error is bounded by

$$R^{2u} D_k(g, \gamma) \sqrt{(lKl^*) \int G(X)^2\, d\mu}.$$

The second integral uses only the constant angular tuple at the real preparation and a polynomial of degree $4k - 2$. These estimates allow genuinely complex tilt. A scalar relative guarantee also requires a positive lower bound for its modulus.

Smaller transport charts on the physical family

The constraints above also reduce the transported state. A constant reduction works on every path used by the four-mode chart. Inside the angular window $\{-1, 0, 1, 2\}$, each sorted tuple t using only $\{-1, 0, 1\}$ has a reflected tuple $-t$, sorted after reversal. Changing all angles to their negatives leaves the preparation and the radial power unchanged, including for complex parameters. Thus $W_t = W_{-t}$ on the real angular germ. The identity continues along either complex path. Of the $\binom{N+2}{2}$ tuples in the overlap, exactly $\lfloor N/2 \rfloor + 1$ are fixed, with equal numbers of -1 and $+1$. Choosing a single representative for each nontrivial pair removes

$$r_0 = \tfrac{1}{2}\left[\binom{N+2}{2} - \lfloor N/2 \rfloor - 1\right]$$

coordinates. Let P repeat the paired entries and let S select the retained entries, so $SP = I$. For the coefficient matrix M of Theorem 10.6 the smaller equation is $v' = SMPv$. Indeed the physical vector satisfies $W = PSW$ at every point of the continued germ. Then $v = SW$ solves the smaller equation, and uniqueness from the physical initial value proves $W = Pv$ on the whole path. Both branch lifts and their physical mixture are recovered by this constant map. This result concerns the integral-defined solution; arbitrary incompatible columns of a fundamental matrix need not satisfy the angular identities. The dimensions at ranks three and four become 16 and 29. A chosen implementation can still propagate the full 20 or 35 states for a direct comparison. At normal-jet resonance the base reflection identity continues to hold; any added resonant jet coordinates still need their own initial data and evolution.

A variable rational chart gives a further reduction over regular intervals. Choose row indices J of C and dependent-mode indices D such that $A = C_{J,D}$ is square and invertible. If F is the complementary mode set, put $S_F W = W_F$ and let K have rows $K_F = I$, $K_D = -A^{-1}C_{J,F}$. The actual state satisfies $W = KW_F$. Its retained entries solve $v' = S_F MKv$. No derivative of the moving basis appears in this selected-row equation because $S_F K = I$ with S_F constant. The recovered full state and hence the scalar are correct for any exact physical initial state, by the same uniqueness argument. When this variable chart changes, initialize the next retained entries by $S_{F'}Kv$ with a corresponding interval error bound. A rational minor which has one verified nonzero value is nonzero on a Zariski-open parameter and radius set away from its denominators. An actual complex path requires an invertibility check on each panel where that minor is used.

At $h = 1.75 + .25i$, $s = -N + .14 + .21i$, the verified minors at $N = 3, z = .26$ and $N = 4, z = .44$ have sizes 8 and 14, giving charts for 12 and 21 coordinates respectively. For the selected dyadically row-scaled minors the determinant moduli exceed .0038407 and 9.2784×10^{-9}, with infinity-norm condition bounds below 80 and 1464. The inclusion matrices have infinity norms below 3.238 and 7.114. Direct outward interval tests also verify the minors on complex squares of half-widths 2^{-120} and 2^{-220} about those points. These deliberately conservative neighborhoods localize the certificate. They supply no coverage of an entire arc. Checks against independent angular data at 60 and 32 nodes per coordinate gave scaled component reconstruction discrepancies below 3.1×10^{-14} and 1.4×10^{-14}, and derivative discrepancies below 8.6×10^{-10} and 1.7×10^{-9} respectively. The derivatives in those comparisons came from independent centered differences. The dimension bounds follow from the exact identities and verified minors.

Parameter-uniform full transfer

Theorem 10.15 (full transfer matrices on an independent parameter polydisk).

Write the polynomial numerator in the canonical frame as $M_0(z) + (h - h_0)M_h(z) + (s - s_0)M_s(z)$, with common scalar denominator $p(z)$. Here $h_0 = 7/4 + i/4$, $s_0 = -N + 7/50 + 21i/100$. The affine dependence follows directly from the angular pencil. The geometric left action on the deleted-row chart is independent of both parameters. The remaining two blocks G, C are affine with real rational coefficients. The center and two independent imaginary contrasts therefore determine the radial generator exactly. The program also checks both real parts after reconstructing the contrasts. The verification of the geometric left action and its polynomial degree belongs to the prior edition. As a separate rational check the reconstructed generator equals the matrix assembled at the four radii $13/50, 39/100, 9/20, 14/25$ at both ranks, for $h = 137/100 + 13i/73$, $s = -N + 79/989 + 18i/61$. Dropping the preparation block changes an imaginary entry at every one of these tests.

Let $F_\pm$ denote the entire transfer matrices along the two broken lines through $1/3 \pm .07i$ from .26 to .40 for rank three, and through $.50 \pm .06i$ from .44 to .56 for rank four. Each leg has 32 equal panels. Use the recorded constant invertible dyadic complex frame V for each path, with no parameter dependence. In panel time $0 \le t \le 1$ write the balanced generator as $A(t) = B(t)/q(t)$, with $B = vV^{-1}M(z_j + vt)V$ and $q = p(z_j + vt)$. Split $A = A_0 + (h - h_0)A_h + (s - s_0)A_s$. The local polynomial factor of degree m is $P_j = \sum_{k=0}^{m} U_k$, where $U_0 = I$ and, writing ordinary ascending coefficients,

$$q_0(k+1)U_{k+1} = \sum_{a=0}^{k} B_a U_{k-a} - \sum_{a=1}^{k} q_a(k+1-a)U_{k+1-a}.$$

Take out-of-range coefficients to be zero. All denominators are independent of (h, s). This gives an explicitly specified parameter polynomial of degree at most m per factor, which can be applied directly to vectors. The canonical approximant is $VP_{64} \cdots P_1 V^{-1}$.

Uniform remainder. For $|h-h_0|\le 1,\ |s-s_0|\le 1/2$, both full matrices satisfy

$$\|F_\pm - VP_{64}\cdots P_1V^{-1}\|_\infty < 10^{-57}\quad (N=3,m=320),\qquad < 8.1\times 10^{-46}\quad (N=4,m=1280).$$

These are operator errors of the exact polynomial. At a concrete input any finite-precision evaluation contributes its own outward arithmetic ball. For rational complex parameters and dyadic frame these recurrences can alternatively be computed in exact rational complex arithmetic.

In each panel, the norm of each numerator polynomial on a disk is bounded by the sum of the norms of its recentered and scaled coefficients. The denominator modulus is bounded below by the modulus of its constant coefficient minus the sum of all other coefficient moduli. The script verifies this lower bound is strictly positive on the midpoint disk of radius one half covering the real segment and on the initial-point disk of radius two. This proves regularity along both polygonal paths for the entire polydisk. If u_j, a_j, b_j majorize the real-panel integrals of the three generator norms, put $L_j = u_j + a_j + b_j/2$. If D_j majorizes twice the norm of the complete generator on the complex-time disk, integration along rays gives a bound e^{D_j} for the local fundamental matrix on the disk. The Banach-space Cauchy inequality gives local endpoint error $e_j = e^{D_j}2^{-m}$. Expanding the difference of the ordered products with $\|F_j\| \le e^{L_j}$ gives

$$\|F-\widehat{F}\|_\infty \le \kappa_\infty(V)\, e^{\sum L_j}\,\mathrm{expm1}\Big(\sum e_j\Big).$$

All inputs to these inequalities, including inversion of the frame and row-sum norms, are enclosed in ball arithmetic. At rank three the two exponents $\sum L_j$ are below 77.488 and 77.984 and the condition numbers below 212.470 and 217.749. At rank four these bounds are 588.479 and 582.461, and 31622.704 and 30819.499. The largest complex-time constants are below 3.349 and 184.558 at ranks three and four, respectively. The receipts use the separate D_j, which is important in the rank-four degree-1280 bound. These estimates concern full radial transport. Initialization, scalar readout, physical path combination, and jet or connection resonances have separate budgets.

Endpoint stability in a smaller polydisk. Write C_j for the midpoint in the balanced frame of the previously certified center panel, and let ϵ_j bound its distance from the exact center panel. Let K_{ij} enclose $\|C_i\cdots C_{j+1}\|$, with $K_{ii}=1$. These contiguous products are evaluated before bounding their norms. In the Euclidean norm put $u_j \ge \int \lambda_{\max}((A_0+A_0^*)/2)$, $a_j \ge \int \|A_h\|_2$, $b_j \ge \int \|A_s\|_2$. The logarithmic-norm differential inequality gives the exact center evolution bound on every real subsegment. Applying the inhomogeneous variation formula between the two generators gives

$$\|F_j(h,s)-C_j\|_2 \le d_j = \epsilon_j + e^{u_j}\,\mathrm{expm1}(a_jH+b_jS),\quad |h-h_0|\le H,\ |s-s_0|\le S.$$

The integrand after factoring out e^{u_j} is bounded by $a(t)\exp(\int_0^t a)$ with $a(t)=\|(h-h_0)A_h+(s-s_0)A_s\|$. Inserting the rightmost perturbed-product prefixes into the ordered-product difference yields

$$G_{ii}=1,\qquad G_{ij}=K_{ij}+\sum_{r=j+1}^{i} K_{ir}d_rG_{r-1,j}.$$

Thus G_{ij} majorizes the true transfer on every contiguous subarc. To obtain an error for the truncated polynomial, compute $\widehat{G}$ from $d_j+\sqrt{d}\,e_j$, where $d=20,35$ is the dimension, converting the matrix infinity-norm Taylor tail to Euclidean norm. Telescoping gives canonical infinity-norm error at most

$$\sqrt{d}\,\|V\|_2\|V^{-1}\|_2\sum_{j=1}^{64} G_{64,j}\sqrt{d}\,e_j\,\widehat{G}_{j-1,0}.$$

The same canonical conversion gives amplification at most $\sqrt{d}\,\|V\|_2\|V^{-1}\|_2G_{64,0}$.

The finite Euclidean certificate for u_j, a_j, b_j divides each rational matrix coefficient by its scalar denominator through degree six at the real-panel midpoint. The polynomial residual divided by the denominator lower bound controls the tail on the segment. Five equal subdivisions bound the change from each new midpoint by summing Frobenius norms of its nonconstant recentered coefficients. For a Hermitian enclosure H, any dyadic proposal R and real b give $\lambda_{\max}(H)\le b+\|bI-H-RR^*\|_F$. Numerical eigensolvers and Cholesky provide proposals only.

The residual, interval radii and conversion $\|A\|_2^2 = \lambda_{\max}(A^*A)$ are bounded by ball arithmetic. All quantities needed to replay the final scalar recurrence without eigensolvers are encoded as outward scalar bounds after verification.

A prescribed finite precision on rational inputs. There is also a fixed-point realization without a posteriori success gates. For each local matrix factor, form $q/q_0, B/q_0$ in the *canonical* frame in exact Gaussian-rational arithmetic, clear a common integer denominator, apply the coefficient recurrence, then round each component of each new coefficient independently to the nearest multiple of 2^{-b}. Round only once per newly computed coefficient. The m-term panel sum is an exact dyadic matrix. Its factors can be multiplied using dyadic integer arithmetic. Thus no further rounding is required in forming the operator.

Indeed, conjugate the coefficient residuals into the balanced frame. Each additive update error Δ_k satisfies $\|\Delta_k\|_\infty \le \kappa_\infty(V) d\, 2^{-b} =: a$. Through degree m the resulting coefficient errors are the Taylor coefficients of the solution $E(0) = 0$ of

$$qE' = BE + q_0 \sum_{k=1}^{m} k\Delta_k t^{k-1}.$$

The radius-two denominator calculation gives $g_j = |q_0| / \inf_{|t|\le 2} |q(t)|$. On the circle of radius $r = 1 + 1/m$, variation along a ray bounds $\|E(t)\| \le e^{D_j} g_j a \sum_{k=1}^{m} r^k \le 3me^{D_j} g_j a$. Cauchy's estimate for the first $m+1$ coefficients therefore bounds the local additional numerical error by $3m(m+1)e^{D_j} g_j a$, in the same balanced norm used by the truncation proof. The ratio of this term to $e^{D_j} 2^{-m}$ is at most $3m(m+1) g_j \kappa_\infty(V) d\, 2^{m-b}$. For $b = m+60$, and $m = 320, 1280$ respectively, the largest verified ratios on the two ranks are below 1.410×10^{-9} and 8.365×10^{-6}. The denominator ratios are below 1.211 and 1.772. Replacing each local e_j in the product estimate by $e_j(1 + \text{ratio})$ still gives absolute errors below 10^{-57} and 8.1×10^{-46} on the outer polydisk, now including the stated rounding. The construction works in particular for all rational complex parameters in the polydisk. For a general computable point its input enclosure is separate. On inner polydisks, the bounded holomorphic exact transfer also gives a Cauchy parameter-rounding bound via the distance to the outer boundary. These finite precision claims are arithmetic existence and instruction-count guarantees. The four recorded full-matrix local test cases used the explicitly reported smaller degree and precision; large-degree full-matrix endpoint values were not materialized by the fixed-point script.

In each degree-m step only the last $\max(\deg q, \deg B)+1$ coefficients are needed if one keeps the running endpoint sum. Dense arithmetic requires $O(m(1 + \max(\deg q, \deg B))d^3)$ integer products per matrix panel, or $O(m(1 + \max(\deg q, \deg B))d^2)$ per single column. Integer numerators include the input parameter's own denominator, and extra bits can be required for accumulating exact products. The figure b is a fractional bit count for coefficient quantization. It is not a bound on the internal integer word length.

Applying the contiguous-subproduct calculation to the enlarged dyadic truncation errors allows smaller degrees. For a conservative rounding charge use the degree-$m-1$ error in the bound for the rounded degree-m method, since the proven rounding ratio is at most one and the complex disk radius is two. On the full outer polydisk the rounded canonical operator errors are then below 6.365×10^{-58} and 1.665×10^{-50} at degrees 236 and 640, with 296 and 700 fractional bits respectively. The exact-polynomial errors at these degrees are below 3.183×10^{-58} and 8.322×10^{-51}. The exact integral/denominator laws and the concrete integer coefficient rounding prescription make these bounds independent of finite sampling in parameter space.

Representative canonical gains from the signed-subproduct computation are as follows. Each entry is rounded upwards. The two radii refer to absolute complex disks in the independent parameters about the stated nonreal center.

Rank and path	Both radii .001	Both radii .01	Both radii 1/16	Order radius .37, tilt radius .01
3, upper	1535	2709	16867	546267
3, lower	1497	2000	7941	180871
4, upper	1.487e9	1.186e13	7.065e22	1.791e27
4, lower	4.871e8	1.607e12	4.889e21	8.942e25

The positive canonical conversion factors for Euclidean gains are below 330 and 337 in rank three and 43854 and 43301 in rank four, in upper/lower order. In rank four the integrated center logarithmic norm is below 58.210

(upper) and 55.160 (lower), while the earlier upper bound on the integrated matrix infinity norm in the same frame exceeds 336 on either branch. The upper-bound orders differ sharply without any change to the underlying full state or singularity geometry.

The fixed-point scheme also gives a uniform algorithm for arbitrary computable complex inputs, including points on the boundary. Enclose each real and imaginary component of the two parameter *displacements* by a rational interval of width 2^{-p}. From each interval choose the rational point of smallest modulus. This makes the chosen complex displacements no larger in modulus, and changes each by at most 2^{1-p}. The queried rational point is therefore still in the original closed polydisk.

To charge this perturbation, use the exact generator's holomorphy on the larger polydisk of radii $1.1, .6$. Its canonical transfer bound there is

$$M = \sqrt{d}\,\|V\|_2\|V^{-1}\|_2 \exp\left[\sum_j (u_j + 1.1a_j + .6b_j)\right].$$

This bound uses the *real-time* Euclidean laws, independent of parameter radius; no complex-time approximation from the smaller polydisk is used outside its domain. The Cauchy bound for each partial derivative is $10M$ on the original closed region. The input perturbation adds at most $40M2^{-p}$ to the canonical operator error. Taking $p = 260$ and 460, respectively, bounds this by 1.830×10^{-66} and 2.862×10^{-63} on both paths. Thus the conservative total bounds 6.366×10^{-58} at rank three and 1.666×10^{-50} at rank four include parameter snapping and coefficient quantization. Source-vector evaluation, connection and scalar extraction use their own bounds.

A regular physical connection throughout an exceptional-order disk

Theorem 10.16 (recovering the missing derivative on a disk). Take the paths of Theorem 10.15. Write $e = 3/2$ in rank three and $e = 2$ in rank four, and $u = h - e$. Let $W_+(u, s)$ and $W_-(u, s)$ be the two exit states, each initialized with the order-dependent full angular vector. Define

$$L(u, s) = e^{i\pi u}W_+(u, s) - e^{-i\pi u}W_-(u, s).$$

Then $L = 2i\sin(\pi u)W_{\mathrm{phys}}$, including at zero as a holomorphic identity. In particular the derivative of L at zero retains precisely the information in (10.12). For $|u| \le r < \rho < R$, suppose that the physical angular vector on $|u| \le R$ has norm at most M_W. Suppose also that each branch sample at $u_j = \rho e^{2\pi ij/m}$ has component error at most E. Form $\widehat{a}_k = m^{-1}\rho^{-k}\sum_j L(u_j, s)e^{-2\pi ijk/m}$ from the approximated samples. A single polynomial evaluates the connection at every order in the inner disk,

$$\widehat{W}(u, s) = \frac{\sum_{k=1}^{m-1}\widehat{a}_k u^{k-1}}{2\pi i\,\operatorname{sinc}_\pi(u)}, \qquad \operatorname{sinc}_\pi(u) = \frac{\sin(\pi u)}{\pi u}, \quad \operatorname{sinc}_\pi(0) = 1. \tag{10.13}$$

If r is small enough that $b_r = 2 - \sinh(\pi r)/(\pi r) > 0$, its uniform component error in exact postprocessing is at most

$$\frac{1}{2\pi b_r}\left\{\frac{2e^{\pi R}M_W}{R - r}\left[(r/R)^{m-1} + \frac{(\rho/R)^m}{1 - (\rho/R)^m}\right] + \frac{2e^{\pi\rho}E}{\rho - r}\right\}. \tag{10.14}$$

Proof. Substitute $h = e + u$ into (10.11) before taking a quotient. The phases at e are opposite pure imaginary numbers. Cancelling their common sign gives the displayed identity, first away from the cosine zero and then at it by holomorphy. The input and initial order derivative both depend on the complex preparation. No complex conjugation of a branch is used. The right-hand real-fibre angular integral supplies an especially economical majorant for the analytic *numerator* on the larger order disk. This use of the source requires only its mass bound. The samples themselves come from the two radius systems.

Write $L(u) = \sum_{k\ge1} a_k u^k$ and $M = 2e^{\pi R}M_W$. Cauchy's inequality gives $\|a_k\| \le MR^{-k}$. The exact discrete coefficient aliases $a_{k+lm}\rho^{lm}$ for $l \ge 1$. Sum the two geometric series after dividing the positive-degree terms by u symbolically. The omission of terms of index m and above costs $M(r/R)^{m-1}/(R - r)$, and the aliases contribute the second term in square brackets. Each input sample has numerator error at most $2e^{\pi\rho}E$. Its contributions to coefficients 1 through $m-1$, evaluated after the degree shift, sum to at most $2e^{\pi\rho}E/(\rho - r)$. The sine series gives $|\operatorname{sinc}_\pi u| \ge b_r$. There is no numerical division by an interval containing $u = 0$. The constant coefficient, whose

exact value is zero on the physical starting vector, is deliberately discarded. Differentiating L at zero restores the average and the full order-derivative difference in (10.12). Discarding the derivative of the preparation at this stage would change the transported state. The identity needs the prepared initial data; an arbitrary column of the fundamental matrix can have a nonzero constant jump.

For the two ranks here take $R = 1$, $\rho = 3/32$, $r = 1/16$ and $m = 56$. Thus the sampled points lie strictly inside the source rectangle of Proposition 21.11. The larger disk is used only to bound L through the real-fibre angular representation. In particular, if z_r is the outgoing real radius, $s_0 = -N + .14 + .21i$ and $|s - s_0| \le r$, one may take

$$M_W = [N(1 + z_r)]^{2(e+1+H)}(1 - z_r)^{-2N(.14+r)}.$$

Indeed all tagged phase factors have modulus one, the raised order has positive real part and the preparation exponent $-N - \Re s$ is negative throughout. This use of absolute values applies to the complex measure before angular integration. It imposes no positivity assumption on the tilt.

The rank-four exceptional divisor and its physical singular column

At the rank-four interior wall put $t = z - 1/2$, $g = h + 2$, $b = 2g + 5/2$ and $\phi = \pi/4$. Thus $\vartheta = \pi(h + 7/2)$, equivalent modulo 2π to $\pi(h + 3/2)$. The ordinary connection exceptions are precisely $h = m = 0, 1, \ldots$. The following argument exploits the angular preparation on this whole divisor.

Theorem 10.17 (physical transport at a rank-four exceptional order). At each such m, for every complex s, the 35 tagged angular components extend holomorphically throughout $|z| < 1$. Their values on the two crossing arcs agree at the exit. Their *total* incoming-continued order derivatives also agree at the exit. The physical connection at the exceptional order takes their common undifferentiated value. This statement concerns the angularly prepared state. The two order derivatives need not equal the derivative of the physical state on the exit side.

Indeed with $w_j = e^{i\theta_j}$, the source power is the polynomial $[(4z - \sum w_j)(4z - \sum w_j^{-1})]^{m+2}$; use the analytic binomial branches in each $(1 - zw_j)^{\nu}(1 - z/w_j)^{\nu}$, $\nu = -4 - s$. Compact domination gives holomorphy. Uniqueness on regular arcs identifies its tagged Fourier coefficients with the ordinary-system branches. The differentiated connection of Theorem 10.9 now implies the derivative difference is zero. Equivalently, the left nondifferentiable germ carries both a simple zero of $K(g) = 2^{2g+1}\Gamma(1 + g)/\Gamma(-g)$ and a simple zero of $\cos(\phi + \pi b/2)$. Its first order derivative is analytic through the wall. These derivatives include the logarithmic insertion in the initial data.

A uniform error bound on this divisor. Take $m = 2$, $r = 14/25$, $s_0 = -193/50 + 21i/100$, $|z| \le r$, $|s - s_0| \le 1/2$. Here the separate normal-jet exponent is $\rho = -8 - 4s$, with $\Re\rho \ge 5.44$; every readout divisor $j - \rho$, $1 \le j \le 4$, has modulus at least 1.44. The radius disk includes the complete polygonal paths $.44 \to .50 \pm .06i \to .56$. Approximate each half factor by $\sum_{j=0}^{160}(-\nu)_j(zw)^j/j!$, and multiply before constant-term extraction. Because $|\nu| < 1$, the half-factor coefficients have modulus at most one. Both exact and truncated half factors have modulus at most $(1 - r)^{-1}$. The uniform error of their product over the four angles is at most $8r^{161}/(1 - r)^8$. Multiplication by the bounded degree-eight mark gives an absolute error smaller than 3.761×10^{-31} on every component. For the original scalar use the normalized positive Haar eigenangle measure and the mark of degree four, with the factor $(1 - z^2)^{16+8s}$ taken on its branch at zero. Its modulus is at most $(1 - r^2)^{16+8(\Re s_0 - 1/2)} \exp(8(|\Im s_0| + 1/2) \arcsin r^2)$. This gives absolute scalar error smaller than 1.849×10^{-30}. These bounds are analytic truncation errors for all parameters in the specified disks. The rational-input routine additionally controls arithmetic ball radius below 10^{-40} or increases working precision. A complex disk bound can be stored as a square of the same coordinate radius, with the corresponding $\sqrt{2}$ change in enclosing-disk radius. The 25 actual arithmetic controls and independent integer source at both ends are recorded separately. This gives physical transport by finite Fourier factorization. It does not bound the fundamental solution for arbitrary data. Holding $h = 2$ removes an entire independent complex direction.

The sheared pencil. At the exact pair $(h, s) = (2, s_0)$ use the rational projector P onto the rank-two leading image specified by the chart, $K = I - P$, and $V = (K + tP)W$. Translating and multiplying the unshifted polynomial matrices gives $tp(t)V' = B(t)V$, $p(0) = 1$. The transformed numerator has no negative powers. For unnormalized numerator coefficients A_j and original denominator $t^2 d(t)$, the coefficient at index j is

$$[KA_{j+1}K + KA_{j+2}P + PA_jK + PA_{j+1}P + Pd_j]/d_0.$$

The same rational projector removes the double pole for all independent h, s. Before the shear the rational ODE is affine in them with a common denominator. Exact vanishing of the forbidden coefficients at three affinely independent pairs therefore proves their identical vanishing. For every h, s the residue R satisfies

$$R(R-(2h+13/2)I)\prod_{u\in\{4,5,7,8\}}(R-(2s+u)I)=0.$$

Each entry has total degree at most six. The supplied rational calculation checks zero on the 28 integer pairs (j,k), $j,k\ge 0, j+k\le 6$; this triangular lattice is unisolvent by successive divisibility on the lines $j=0,1,\dots$. The same calculation verifies the physical leading eigenvector identity on this lattice. Where all six roots are distinct, the residue is diagonalizable and their multiplicities are locally constant. The complement of these collision hyperplanes in $\mathbb{C}^2$ is connected, so the multiplicities follow globally from this one rational complex parameter point. On $|h-2|, |s-s_0|\le 1/16$, the imaginary parts of the four tilt roots stay at least 0.295 away from zero and those of their differences with $2h+13/2$ at least 0.17 away from zero; the latter exponent has real part between 10.375 and 10.625. The only integral differences among distinct roots on this polydisk are accordingly the six internal to the tilt group. Their explicit spectral-basis calculation at the center is followed below by a two-parameter identity.

At the center the residue has a semisimple zero of multiplicity 30, the simple physical exponent $21/2$, and four simple exponents $u/25+21i/50$, $u=-93,-68,-18,7$. These identities are checked over $\mathbb{Q}(i)$. A rational spectral basis also resolves the six integral differences among the four latter exponents. At a step j for a starting exponent λ, put

$$f_j=\sum_{k=1}^{j}\big(B_k-(j-k+\lambda)p_kI\big)v_{j-k}.$$

At a resonance $j+\lambda=\mu$, the projection of f_j onto the μ eigenspace vanishes exactly for all six ordered pairs even with every earlier free resonant coefficient set to zero. Thus each starting vector admits a pure Frobenius column. Past the last resonance all inverses are $O(1/j)$; the polynomial-coefficient recurrence has an exponential majorant on a sufficiently small disk after rescaling. This supplies actual convergent columns. It identifies no physical amplitude for the four tilt-dependent modes.

All six log obstructions vanish identically. Write $b=2h+13/2$ and consider the open domain

$$b\notin\mathbb{Z},\qquad 2s\notin\mathbb{Z},\qquad b-2s\notin\mathbb{Z}.$$

On this domain the entire sheared rank-four equation admits a fundamental matrix with 35 pure convergent Frobenius columns. This includes the above polydisk around the exceptional connection order $h=2$. The result concerns the local linear system and assigns no physical coefficients to its four tilt-dependent modes.

For a constructive proof set $L(x)=x(x-b)\prod_{u=4,5,7,8}(x-2s-u)$, $Q(x,y)=(L(x)-L(y))/(x-y)$. At a simple root a, the spectral projector is $Q(a,R)/L'(a)$, because $L(R)=0$. To start at one of the simple tilt roots λ, take the projection of the fixed column $e=(1,2,\dots,2^{34})^T$, generically nonzero as verified by an exact rational specialization for each root. Let $g=\lambda+j$. With the right hand side f_j in the preceding recurrence, an ordinary step gives $v_j=Q(g,R)f_j/L(g)$. At a structural resonance, the obstruction is $Q(g,R)f_j$. When it vanishes set

$$v_j=\partial_xQ(g,R)f_j/L'(g).$$

This solves $(gI-R)v_j=f_j$ with zero resonant component. It is the finite part of the resolvent on the complementary eigenspaces. In the formula $\partial_xQ(g,R)$ denotes the derivative in the first argument evaluated at $x=g$.

Each denominator introduced at one step, including the initial projection, has total degree at most two in h, s. Indeed, the four tilt roots differ by constants, so only the factors at zero and at b can vary after substituting $g=2s+u+j$ into L or L' at a structural root. A common denominator through order j is the product of these successive denominators. After clearing it, the initial numerator has total degree at most five. If the order-i numerator has degree at most $5+6i$, the terms in f_j, cleared to the order-$j-1$ denominator, have degree at most $5+6(j-k)+2(k-1)+1\le 6j$. Here the added one is the affine degree of the sheared numerator or of $j-k+\lambda$. The matrices $Q(g,R)$ and $\partial_xQ(g,R)$ have degree at most five and four. Thus every obstruction through the last

resonance $j = 4$ has a numerator of degree at most 29. Integral differences are resolved successively using the indicated zero free component.

The exact calculation tests all six projected obstructions on the 465 unisolvent integer pairs $h, s \geq 0$, $h + s \leq 29$. There are no denominator zeros in these eight steps on that lattice: the tilt roots are positive integers, $g > 0$, and b is a half-integer. The structural resonances are precisely the prescribed positive differences. These six vector polynomials are identically zero. On the dense open set where each starting projection of e spans its eigenline, the canonical compatibility operator annihilates the entire eigenline. It follows by rational identity on spectral projectors that the same holds on the whole stated domain, even at a zero of that particular projection. Other starting vectors then supply the corresponding eigenline. Every later Frobenius recurrence is invertible and converges on a sufficiently small disk by the polynomial recurrence majorant already given. The zero eigenspace and the physical b-line have no positive integral resonance under the displayed restrictions. This proves the assertion and excludes logarithms without imposing any branch coefficient on the physical solution. One exclusion is essential in the ordinary moment domain. If $b = l \in \mathbb{Z}$, then $l \geq 5$ and $g = h + 2$ is nonintegral. The tagged saddle coefficient is nonzero in a component with $q_I \neq 0$, since $K(g) \neq 0$, the preparation factor is nonzero, and $\cos(\pi/4 \mp \pi l/2) = \pm 1/\sqrt{2}$. The integer finite part from Theorem 10.8 therefore supplies a nonzero $|t|^l \log |t|$ term for the angularly prepared solution itself. A log-free fundamental system cannot cover this divisor. No analogous necessity is asserted here for the other two exclusions.

Angular selection. In the tagged component indexed by I, let $q_I = \sum_{l=1}^{4} (-1)^{I_l}$. There are three positive and one negative phases in each contributing saddle. In the unscaled coordinate $t = z - 1/2$ the leading plus and minus angular factors are $Ce^{\pm i\phi} q_I$, where

$$C = (2\pi)^{-5/2} 2^{-1/2} (1/2)^{6\nu} (3/2)^{2\nu}.$$

This follows from the tagged stationary-phase coefficient at the wall and the analytic two-sided source germs of Theorem 10.9. At s_0 the isolated physical exponent is above the real parts of all the remaining roots. Write $H(0) = q$ in the original, unsheared coordinate. Its analytic continuation is the analytic coefficient of the t^b Frobenius solution. Indeed $B(0)Kq = bKq$, and at degree one unshearing restores $Kv_0 + Pv_1 = q$, where here the series variable is t. Both vector identities were checked exactly in all coordinates by rational Gaussian elimination. The normalization at the nonlinear angular wall fixes the coefficient. Differentiating the right-hand singular germ, while the incoming first derivative has zero singular coefficient, now gives, on $t > 0$,

$$(\partial_h W)_{\text{phys,right}} - (\partial_h W)^{\uparrow} = (\partial_h W)_{\text{phys,right}} - (\partial_h W)^{\downarrow} = 2K'(4)\Gamma(-21/2) C \cos(\phi - 21\pi/4)(4t)^{21/2} H(t).$$

Here $K'(4) = -2^9(4!)^2$ and the cosine is -1. The two differentiated *arc* states agree, while this angular derivative on the right differs. The background derivative is the same on both sides by the holomorphic local source splitting near $g = 4$; the pole-free $b = 21/2$ coefficients of the two germs depend holomorphically on g. Principal positive-real powers are used on $t > 0$. Regular continuation extends the identity to the exit on the same interval.

Validation of the singular column. Put $t = rx$, with $r = 1/8192$, in the sheared equation. Diagonalize the residue to $J+E$, using a rounded and then validated dyadic basis, and multiply numerator and denominator by the first seven coefficients of their scalar reciprocal series. In the scaled basis the verified bounds are $\sum_{k>0} \|B_k\|_\infty < 6.252$, $\sum_{k>0} |p_k| < 2.591 \times 10^{-19}$, $\|E\|_\infty < 2.510 \times 10^{-9}$. The inverse of $(j + b)I - J$ has norm at most $1/j$. For $n = 97$, the recurrence tail is controlled by

$$\chi = \frac{\sum_{k>0} \|B_k\|_\infty / n + (1 + |b|/n) \sum_{k>0} |p_k|}{1 - \|E\|_\infty / n} < 0.06445.$$

Hence each later coefficient has norm at most the maximum of the preceding 42. Multiplying that maximum by $2^{-97}/(1 - 1/2)$ bounds the series tail at $t = 1/16384$ by 3.636×10^{-103} in the diagonalized, scaled coordinates. The finite recurrence and unshearing used 480-bit interval arithmetic. The maximum stored-before-serialization component radius of H was below 2.827×10^{-37}. A single majorant at $r = 1/16$ gave $\sum \|B_k\| > 10^6$; reaching the exit requires another chart or regular-panel propagation.

From the ray to the scalar. Continue the analytic column, after removing t^b from V, from $t = 1/16384$ to $3/50$ by the ordinary equation with denominator $tp(t)$ and numerator $B(t) - bp(t)I$. An initial 31-block geometric covering, subdivided to 130 accepted panels, used degree 46 Taylor polynomials, a 300-bit interval environment and the residual and denominator lower bounds of the full-system panel method. Each local error bound was

below 9.18×10^{-29}. At 760 bits the direct product had norm below 206 and, after unshearing, radius below 2.15×10^{-10}. Recentring before multiplication brought the last bound below 7.34×10^{-18}. In detail, write each accepted block as $A_j + D_j$, with midpoint A_j and entrywise radius bound R_j. Retain the midpoint trajectory y_j, the initial error, and each defect vector $R_j(|y_{j-1}| + E_{j-1})$; bound its transported contribution with the modulus of the corresponding midpoint suffix product. Summing these terms, with interval evaluation of the products, bounds the actual error E_j by telescoping. The panel files include the full 35 by 35 matrices. This propagation follows a single singular column selected by the angular integral.

At the exit the first component of the physical-minus-arc order-derivative shift is $(1.41702030589790309 + 1.68569227296868621i) \times 10^{-9}$ to within 6×10^{-27}. Applying the normal-jet row to the whole shift gives $(3.97729994 + 1.42547630i) \times 10^{-7}$ to within 6×10^{-16}. Since the undifferentiated states agree, derivatives of the readout row cancel from this scalar difference. At $t = 1/16384$ the same projected shift divided by the *original scalar* leading saddle (Theorem 10.8 with $\beta = 19/2$, $\phi = 7\pi/4$, $K'(2) = -128$) lies within 5×10^{-17} of $1.00132250615613635 + 0.00007500066062592 06i$. The ratio checks the absolute factor and the change in the leading exponent. At the far endpoint the ratio is about $4.32 + 0.54i$, so substituting that first saddle term alone misses the true exit correction.

The first independent angular Hermite calculation supplied the full ordinary right order derivative. A refinement to degree 199 and 1820 bits gave source disk error below 3.715×10^{-12} in 256 seconds. Subtracting the certified column shift gave both continued total order derivatives at the exit, maximum disk radius below 1.192×10^{-11} before the final report is rounded, resolving the first-component change above. The angular input at the entry was also enclosed separately. This recovers the physical exceptional derivative connection by the specified source and singular-column identity rather than propagating an arbitrary 70-component initial value by two 70-state ordinary solves. Dropping just one of the two order-derivative contributions in the raw compact scalar readout gives an absolute miss exceeding 2.57×10^{12}; the correctly paired difference is zero. The undifferentiated 35-component states at the entrance and exit overlap independently computed source enclosures. At the exit the compact scalar readout has disk radius below 6.44×10^{-20} and the direct Fourier–Weyl scalar below 2.614×10^{-30}. Both contain the independent integer-order result near $8195.24404760733169472 - 7940.96131066118309091i$. Deleting the preparation prefactor misses it by more than 11377.

Independent ordinary path integrations at a displaced tilt. With $h = 2$, $s = -3.85 + 0.22i$, each 35-state residual trajectory used 64 panels, degree at most 168 and 1100 bits. Runtimes were 289 and 296 seconds. An 800-term independent finite Fourier calculation enclosed the error of their common dyadic starting state by 1.985×10^{-71}. At parameter displacements bounded by 0.354 and 0.01415, the verified contiguous-product estimates give original-coordinate gains smaller than 1.446×10^{27} and 7.317×10^{25}. Charging that input error, the upper and lower vector endpoint errors are below 5.552×10^{-36} and 1.546×10^{-35}, respectively. All 35 scalar component comparisons with the independent exit integral pass. Their midpoint vectors differ by less than 9.414×10^{-67} in the maximum norm. Applying the physical readout gives disk radii below 9.118×10^{-25} and 2.538×10^{-24}, both about $7615.476370618516438730701352 47 - 7917.88798777955789205832320882i$. A separate determinant expansion at the exit has radius below 1.810×10^{-191}. These tests exercise ordinary path integration at an exceptional order; exact equality of the two branches and their total order derivatives uses the angular proof above.

11. The large-matrix limit on compact subsets of the disk

Theorem 11.1 (compact-interior limit). Use normalized Haar measure, real $0 \le z \le r < 1$, and the convention $S_N = -(1 - z^2)\Lambda_N'/\Lambda_N$. Set $d = 1 - z^2$. Write $D_N(\zeta; s, z) = \mathbb{E}[|\Lambda_N|^{2s} \exp(i \operatorname{Re}(\bar{\zeta} S_N))]$ and Φ_N for its circular average. For every compact set $K \subset \{(h, s) : \operatorname{Re} h > -1,\ s \in \mathbb{C}\}$,

$$T_N(h, s; z) \longrightarrow d^{-s^2} \Gamma(1 + h)\, {}_1F_1(-h; 1; -s^2 z^2)$$

uniformly on $[0, r] \times K$. This value is the equal-point special case of Simm–Wei, Theorem 1.2, after Kummer transformation and multiplication by d^{2h}. We prove the limit directly through the circular finite part. In the Gaussian-regularized planar integral, the same limit holds when $N \to \infty$, the source-disk radius $R \to \infty$, and the physical Gaussian coefficient $\varepsilon \downarrow 0$ at arbitrary relative rates. Constants depend on the compact sets; this gives no rate for $z \to 1$ and no certified numerical tolerance.

A compact-source limit with its Taylor coefficients

For $\lambda = e^{i\theta}$ put $f_z = d\lambda/(1-z\lambda)$, $L_z = \log|1-z\lambda|^2$. The Toeplitz symbol has logarithm $F = sL_z + i(\bar\zeta f_z + \zeta \bar f_z)/2$, of mean zero. For $k \geq 1$ its Fourier coefficients are

$$F_k = -sz^k/k + (i/2)\bar\zeta dz^{k-1}, \qquad F_{-k} = -sz^k/k + (i/2)\zeta dz^{k-1}.$$

The strong Szegő limit is $\exp(\sum_{k\geq 1} kF_kF_{-k})$. Summing the three geometric or logarithmic series gives

$$D_\infty(\zeta; s, z) = d^{-s^2} e^{-|\zeta|^2/4 - isz\,\mathrm{Re}\,\zeta}, \qquad \Phi_\infty(\rho; s, z) = d^{-s^2} e^{-\rho^2/4} J_0(sz\rho).$$

In particular, the shift in this Fourier convention is $-sz$. For real s the normalized tilted limit is a translated standard complex Gaussian. The displayed entire formula specifies the continuation to complex s.

Here convergence is locally uniform in independent complex source coordinates (replace $\zeta, \bar\zeta$ by independent parameters), s, and the complexified radial parameter z with $|z| < 1$ (use the analytic series for the logarithm and replace $\bar f_z$ by $d\lambda^{-1}/(1 - z\lambda^{-1})$). One justification uses the following elementary finite consequence of strong Szegő. For a real smooth log symbol v with zero mean,

$$D_N[e^v] \leq \exp\left(\sum_{k\geq 1} k|v_k|^2\right).$$

In fact D_{j+1}/D_j is the minimum squared weighted L^2 norm of a monic polynomial of degree j. Jensen's inequality and the circle average of $\log|P|$ show that this norm is at least one. Thus D_j increases to the strong Szegő limit. By Heine's formula $|D_N[e^F]| \leq D_N[e^{\mathrm{Re}\,F}]$. On compact complex parameter sets the real parts have uniformly bounded Fourier $H^{1/2}$ norm, by geometric coefficient decay. The analytic family is locally bounded; pointwise strong Szegő convergence and the normal-family theorem imply local uniform convergence and convergence of all finite source jets. In particular, with s complex and ζ a real planar frequency, the frequency-independent bound

$$|D_N(\zeta; s, z)| \leq \mathbb{E}|\Lambda_N(z)|^{2\,\mathrm{Re}\,s} \leq d^{-(\mathrm{Re}\,s)^2}$$

holds for every N.

Uniform large-source estimate for a compact set of tilts

Lemma 11.2 (large Fourier frequencies). Given any $m > 0$, a compact $S \subset \mathbb{C}$, and $r < 1$, there are n_0 and C such that for $N \geq n_0$,

$$\sup_{s\in S,\, 0\leq z\leq r,\, |u|=1} |D_N(\rho u; s, z)| \leq C(1+\rho)^{-m} \qquad (\rho \geq 0).$$

The quantifier on n_0 is essential. The claim does not give arbitrary inverse powers at one fixed finite rank.

Proof. First let $s = iy$, $|y| \leq B$. For $\rho \geq 1$, this is the characteristic function at frequency ρ of the real linear statistic generated by

$$g(\theta) = \mathrm{Re}(\bar u f_z(e^{i\theta})) + \rho^{-1} y L_z(\theta).$$

All its fixed-order smooth norms are bounded uniformly. The first summand is a constant plus a cosine reparametrized by the circle diffeomorphism $w = (\lambda - z)/(1 - z\lambda)$. On $0 \leq z \leq r$ this diffeomorphism and its inverse have bounded derivatives of each fixed order, and the first derivative has a positive uniform lower bound. Thus the unperturbed phase has exactly two uniformly nondegenerate stationary points, is uniformly nonstationary off fixed-size neighborhoods, and its derivative has a positive lower L^2 norm. These properties persist for g once ρ exceeds a constant depending on B, r (use uniform C^2 perturbation).

For the medium frequencies use Simm–Wei, Lemma 2.6, published equation (2.50), arXiv v2 (2.49). Its general real-phase hypothesis applies to the displayed g, with the same g used throughout each individual estimate. Its exponent is bounded above by

$$-\frac{c\rho^2}{1 + \rho/N + \rho^2/N^2}.$$

Indeed its numerator uses the square of the average of $(g')^2$, bounded away from zero. Its denominator constants are controlled by $\|g''\|_\infty^2$ and the $H^{1/2}$ seminorm squared of $(g')^2 - g'(0)g' - \int (g')^2/(2\pi)$, both uniformly bounded. For $1 \ll \rho \le N^8$ this gives $C\exp[-c\min(\rho^2, N^2)] \le C\exp[-c\rho^{1/4}]$.

For $\rho > N^8$ use the original Toeplitz determinant. Each Fourier entry $\widehat{e^{i\rho g}}(k)$ has modulus at most $C(1+|k|)\rho^{-1/2}$. A uniform partition into the above critical neighborhoods and their complement gives this estimate by one-dimensional van der Corput and integration by parts, with amplitude $e^{-ik\theta}$ of bounded variation $O(1+|k|)$. Hadamard's row inequality gives

$$|D_N| \le (CN^{3/2}\rho^{-1/2})^N \le (C/\sqrt{N})^N \rho^{-N/4}.$$

Hence any prescribed power p is available on the imaginary segment for sufficiently large N, uniformly in all parameters there. This is the high-frequency argument of Simm–Wei, Lemma 2.5, with its real phase explicitly checked after insertion of the imaginary tilt.

Finally choose B so large that S lies inside the union of the two half rectangles $0 \le \pm \operatorname{Re} s < B$, $|\operatorname{Im} s| < B$, a positive distance from their three outer sides and the endpoints of the common imaginary segment. The uniform bound on the other sides is $d^{-B^2} \le (1-r^2)^{-B^2}$. On the common vertical side we have $C_p(1+\rho)^{-p}$. In either half rectangle the harmonic measure of that side has a positive lower bound α on the indicated compact subset; it approaches one at interior points of that side. Apply the two-constants theorem to the subharmonic function $\log|D_N|$ in the tilt variable to obtain $C'(1+\rho)^{-\alpha p}$. Choosing $p > m/\alpha$ proves the lemma. This propagation uses analyticity in the tilt variable, not positivity of a complex tilted probability law.

Corollary 11.3 (convergence of tilted densities). For any fixed integer $j \ge 0$, choose $m > j+2$. The lemma and compact-frequency convergence imply $D_N \to D_\infty$ in $L^1(\mathbb{R}^2, (1+|\zeta|^j)\, d^2\zeta)$, uniformly on the same compact parameter sets, by splitting into a disk and its complement. Fourier inversion therefore gives uniform convergence on the plane of the tilted densities and of their partial derivatives through order j, for sufficiently large N. In real coordinates (x, y) the limiting density is

$$\frac{d^{-s^2}}{\pi} \exp[-(x+sz)^2 - y^2].$$

For complex s the square in this analytic formula has no conjugation. This convergence is a smoothness statement at every fixed derivative order with rank allowed to grow; it makes no assertion that the finite-rank density is infinitely differentiable.

Passing the large-rank limit through the circular finite part

Split at $\rho = 1$. Let $J \ge 1$ be an integer exceeding $\max_K \operatorname{Re} h$, $a_{j,N}$ the even Taylor coefficients of Φ_N, and $C(h) = 2^{2h+1}\Gamma(1+h)/\Gamma(-h)$. The circular finite-part expression is

$$C(h)\left[\sum_{j=0}^{J-1} \frac{a_{j,N}}{2j-2h} + \int_0^1 \rho^{-2h-1}\left(\Phi_N(\rho) - \sum_{j=0}^{J-1} a_{j,N}\rho^{2j}\right) d\rho + \int_1^\infty \rho^{-2h-1}\Phi_N(\rho)\, d\rho\right].$$

Removable integer values are interpreted after multiplying by $C(h)$. Compact complex-source convergence gives a uniform $O(\rho^{2J})$ Taylor remainder on $[0,1]$, with convergence of its normalized remainder, by Cauchy estimates on a larger disk. The lemma supplies uniform absolute domination of the tail on any compact set in the stated domain. More precisely, for any m with $m + 2\inf_K \operatorname{Re} h > 0$, the integral beyond $R \ge 1$ is bounded by $C_K R^{-m-2\operatorname{Re} h}$ for all sufficiently large N. Thus the ordinary sharply truncated circular finite part converges jointly as $N, R \to \infty$ and the limiting expression uses Φ_∞.

For $-1 < \operatorname{Re} h < 0$, the origin needs no subtraction and direct integration of the J_0 power series against the limiting Gaussian gives

$$C(h)\int_0^\infty \rho^{-2h-1} e^{-\rho^2/4} J_0(sz\rho)\, d\rho = \Gamma(1+h)\,{}_1F_1(-h; 1; -s^2z^2).$$

The absolute series is dominated at infinity by a Gaussian times $e^{|sz|\rho}$ and is integrable at zero. Multiplication by d^{-s^2} and analytic continuation of the already justified finite part complete the proof for all $\operatorname{Re} h > -1$. This starts from the determinant and uses a published characteristic-function **bound**, not a published value of the limiting moment.

The physical Gaussian regulator and all three limits

For the Gaussian regularization of the physical moment,

$$K_{h,\varepsilon}(\rho) = \frac{\Gamma(1+h)}{4\pi\varepsilon^{1+h}}\,{}_1F_1(1+h;1;-\rho^2/(4\varepsilon)).$$

The compact-parameter Kummer expansion along the negative real ray implies $|K_{h,\varepsilon}(\rho)| \le C_K\rho^{-2-2\operatorname{Re}h}$ for $\rho \ge 2$ and $0 < \varepsilon \le 1$. Indeed multiply the Kummer function by $x^{1+\operatorname{Re}h}$ with $x = \rho^2/(4\varepsilon) \ge 1$; the algebraic branch is bounded and the exponential branch decays. At nonnegative integer h the leading algebraic coefficient vanishes. The source tail lemma therefore controls the entire omitted planar annulus in absolute value by $C_K R^{-m-2\operatorname{Re}h}$, uniformly even before angular averaging. By the finite-rank Fourier identity the full integral is $\mathbb{E}[|\Lambda_N|^{2s}|S_N|^{2h}e^{-\varepsilon|S_N|^2}]$. Its distance from T_N is at most

$$\varepsilon\,\mathbb{E}[|\Lambda_N|^{2\operatorname{Re}s}|S_N|^{2\operatorname{Re}h+2}] \le C_K\varepsilon.$$

For the last inequality, the nonnegative powers in question are uniformly bounded by a finite sum of exponentials $C\sum_{v\in\{1,-1,i,-i\}}\exp(\operatorname{Re}(\bar v S_N))$. The real symbols $\operatorname{Re}s\,L_z + \operatorname{Re}(\bar v f_z)$ have zero mean and bounded $H^{1/2}$ norm, so the same finite strong-Szegő inequality applies. It follows that in the disk-truncated planar expression the difference from the limit is bounded by $|T_N - T_\infty| + C_K(\varepsilon + R^{-m-2\operatorname{Re}h})$ for $N \ge n_0(m,K)$, $R \ge 2$.

The bounds concern fixed-interior compacts and permit any relative rates for these three limits; they neither extend to microscopic depth nor assign an explicit convergence rate to $T_N - T_\infty$. The finite-rank endpoint obstruction at $\operatorname{Re}h = -1$ prevents a wider statement for the underlying absolute expectation.

Sources. N. Simm and F. Wei, *On moments of the derivative of CUE characteristic polynomials and the Riemann zeta function*, J. London Math. Soc. 113 (2026), e70487, §2.2, Lemmas 2.5 and 2.6; the prior equal-point value is a specialization of their Theorem 1.2. Published paper, open text. The other inputs are the classical strong Szegő theorem for smooth scalar Toeplitz symbols of winding zero, Bessel and Kummer identities, and the subharmonic two-constants theorem.

12. The first microscopic correction for mixed integer moments

Take integers $m \ge 1$ and $0 \le j \le m$. Set $P_{N,j,m}(z) = \mathbb{E}[|\Lambda_N'(z)|^{2j}|\Lambda_N(z)|^{2(m-j)}]$. Thus $T_N(j,m;z) = (1-z^2)^{2j}P_{N,j,m}(z)$. Set $z^2 = 1 - c/N$, with $c \ge 0$ fixed. The conclusions for P include $c = 0$ directly. The expression for T at the circle is understood by an interior limit. Use $I_d(c) = \int_0^1 t^d e^{-ct}\,dt$ for $d \ge 0$.

Theorem 12.1 (first variation of the confluent determinant). Uniformly on compact real depth intervals,

$$N^{-m^2-2j}P_{N,j,m}(z) = B_{j,m}(c) + N^{-1}L_{j,m}(c) + O(N^{-2}).$$

Here both coefficients are explicit finite sums. Put $\mu = (1^j, 0^{m-j})$. Sum over ordered pairs of partitions λ, ρ of j with at most m parts, padding them with zeros. Write $a_i = \lambda_i + m - i$, $b_k = \rho_k + m - k$. The weight is $W_{\lambda\rho} = K_{\lambda\mu}K_{\rho\mu}/(\prod_i a_i!\prod_k b_k!)$, where the K are Kostka numbers. For $j = 0$ use the empty partition of weight one before the factorials. Define $A_{ik} = I_{a_i+b_k}(c)$. The correction matrix V has entries, with $a = a_i, b = b_k, d = a + b$,

$$V_{ik} = (m - \tfrac12)e^{-c} + \tfrac12\mathbf{1}_{d=0} + bcI_d(c) - \tfrac{c^2}{2}I_{d+1}(c) - [\tbinom{a}{2} + \tbinom{b}{2}]I_{d-1}(c).$$

Omit the last term when its multiplier is zero. Then

$$B_{j,m} = \sum_{\lambda,\rho} W_{\lambda\rho}\det A, \qquad L_{j,m} = \sum_{\lambda,\rho} W_{\lambda\rho}\sum_{k=1}^{m}\det[A_1,\dots,A_{k-1},V_k,A_{k+1},\dots,A_m],$$

where the subscripts here denote columns. For $c > 0$ this gives the corresponding expansion of $N^{-m^2}T_N(j,m;z)$ on multiplying both coefficients by c^{2j}.

From the planar source to the finite matrix. At $h = j$ the removable integer value of the circular finite part is the (j,j) source jet of the same determinant. Before taking the jet, introduce independent copies of the spectral point in the polynomial symbol

$$G(\mathbf{a},\mathbf{b}) = D_N\left[\prod_{i=1}^{m}(1-a_iw)(1-b_iw^{-1})\right].$$

In this display $D_N[\cdot]$ means the Toeplitz determinant of its symbol. Differentiate once in each of the first j variables on both sides of the symbol, then set every spectral point to z. The result equals $P_{N,j,m}$. To check the operation on the original realization, the holomorphic mark in the planar jet is $S_N^j \Lambda_N^m = (-d)^j (\Lambda_N')^j \Lambda_N^{m-j}$, $d = 1 - z^2$; differentiating j distinct copies in G produces exactly the factor on the right without $(-d)^j$. The conjugate factors give the other power. Thus the jet of the planar readout and the differentiated polynomial determinant agree after the displayed normalization.

For distinct copies, $G = \det[K_{N,m}(a_i b_k)]/(\Delta(\mathbf{a})\Delta(\mathbf{b}))$ with $K_{N,m}(w) = \sum_{l=0}^{N+m-1} w^l$. Indeed, expanding the two finite dual Cauchy identities and using Haar orthogonality of Schur characters retains $\sum_{\lambda \subseteq (N^m)} s_\lambda(\mathbf{a}) s_\lambda(\mathbf{b})$. The alternant formula and Cauchy–Binet turn this sum into the stated determinant. Removal of coincident points follows since G is polynomial. This is a change of representation of the same integer derivatives, not a continuation in the number of copies.

Proof of the expansion. For the finite differentiation and coalescence we use Grover, Mezzadri and Simm, Theorem 2.9, applied to two copies of μ. Their exact confluent determinant has (a, b) entry

$$\sum_{l=0}^{N+m-1} l^{\underline{a}} l^{\underline{b}} (1 - c/N)^{l-b},$$

where falling factorials vanish when the index is too small. This follows by differentiating their finite geometric sum twice as prescribed in (2.44). Fix $t = l/N$. Removing N^{a+b}, the product of falling factorials is $t^d - N^{-1}[\binom{a}{2} + \binom{b}{2}]t^{d-1} + O(N^{-2})$ by finite polynomial expansion. The power of $1 - c/N$ is $e^{-ct}[1 + (bc - c^2 t/2)/N + O(N^{-2})]$. Both errors are uniform, including $l = 0$ and the finitely many terms with $l > N$. The endpoint correction for $N^{-1} \sum_{l=0}^{N+m-1} f(l/N)$ is $N^{-1}[(m - 1/2)f(1) + f(0)/2]$, by the trapezoid rule and the extra $m - 1$ upper endpoint terms. Thus the entry divided by N^{a+b+1} equals $A_{ik} + V_{ik}/N + O(N^{-2})$. The row and column powers give N^{2j+m^2} in each determinant. Column multilinearity gives the claimed first variation even when a matrix is singular. The finite sum and smooth functions on compact depth intervals preserve the uniform remainder. □

For $m = j = 1$ this reduces to

$$N^{-3}\mathbb{E}|\Lambda_N'(\sqrt{1 - c/N})|^2 = I_2(c) + \frac{e^{-c}/2 + cI_2(c) - c^2 I_3(c)/2}{N} + O(N^{-2}).$$

At $c = 0$ the exact answer is $1/3 + 1/(2N) + 1/(6N^2)$. For $m = 1, j = 0$ the leading coefficient is I_0 and at $c = 0$ the normalized answer is exactly $1 + 1/N$. For $c > 0$, both the leading argument c and the $-c^2 I_{d+1}(c)/2$ term in V_{ik} distinguish $z^2 = 1 - c/N$ from $z = 1 - c/N$ (and from $z = 1 - c/(2N)$, which matches the leading parameter $c = \tau$ of Grover, Mezzadri and Simm, Theorem 1.2, while changing $-c^2 I_{d+1}(c)/2$ to $-c^2 I_{d+1}(c)/4$).

The calculation starts with the removable integer value of the planar formula and uses the published confluent determinant to compute that jet. For noninteger powers, differentiation in a finite list of copies no longer represents the observable. The leading term is consistent with Theorem 1.2 in the same source.

13. The local projection for an integer tilt

At depth $c > 0$ the polynomial tilt also gives a finite-rank projection. Fix an integer $m \geq 0$ for the tilt and allow the **moment exponent** h to be complex. Set $z = \sqrt{1 - c/N}$ and $Z_N(m) = \mathbb{E}|\Lambda_N(z)|^{2m}$. Work initially at $N > c$. Let $\mathcal{F}$ be the isometry from $L^2[0, 1]$ into $L^2(\mathbb{R}, dt)$ with kernel $(2\pi)^{-1/2} e^{iut}$. In $L^2[0, 1]$ let $Q_{m,c}$ be the orthogonal projection onto the span of

$$u^l e^{cu/2}, \qquad l = 0, \ldots, m - 1.$$

An empty span gives the zero projection. Define the local determinantal point process $\Xi_{m,c}$ by the projection kernel $\mathcal{F}(1 - Q_{m,c})\mathcal{F}^*$. Put $f_c(t) = c/(c/2 - it)$. Define the random variable as an L^2 limit of compensated sums,

$$X_{m,c} = \lim_{L \to \infty} \left(\sum_{t \in \Xi_{m,c},\ |t| \leq L} f_c(t) - \frac{1}{2\pi} \int_{-L}^{L} f_c(t)\, dt \right).$$

The subtracted quantity tends to $c/2$. The tilt genuinely changes the distribution through $Q_{m,c}$.

Theorem 13.1 (microscopic projection formula). For $\Re h > 0$,

$$N^{-m^2} T_N(h, m; \sqrt{1 - c/N}) \longrightarrow B_{0,m}(c)\, \mathbb{E}|X_{m,c}|^{2h},$$

where $B_{0,0} = 1$ and $B_{0,m}$ for $m \geq 1$ is the finite-sum leading coefficient in Section 12. It also holds at $h = 0$ with the rightmost expectation defined as one. Convergence is locally uniform for positive c and $\Re h > 0$. The circular finite-part formula passes to this limit.

Proof from the finite determinant. Under the normalized positive tilt, the eigenangle density is the squared determinant of the functions $(1 - zw)^m w^k$, $0 \leq k < N$, divided by its Gram normalization, for $w = e^{i\theta}$. This is the Gram representation of the same Toeplitz determinant; dividing by its zero-source value removes the normalization. Orthonormalizing the functions gives the projection ensemble on $(1 - zw)^m \mathcal{P}_{N-1}$ in circle $L^2(d\theta/(2\pi))$. The phase one gains on replacing a positive weight by the analytic polynomial cancels in each correlation determinant. Inside $\mathcal{P}_{N+m-1}$ the subspace consists exactly of the polynomials whose first m jets (orders zero to $m - 1$) vanish at $q = 1/z$. Its orthogonal complement is spanned in the coefficient basis by the real vectors $k^l q^{k-l}$, $0 \leq k < N + m$.

In coordinates $t = N\theta$, with dt reference measure, the full polynomial projection has kernel

$$(2\pi N)^{-1} \sum_{k=0}^{N+m-1} e^{ik(t-u)/N}.$$

Its diagonal is the constant $b_N = (N + m)/(2\pi N)$. The complement is an orthogonal projection of rank m. Divide the lth vector by N^l and equip the coefficient vectors with N^{-1} times counting measure for the Gram comparison. Riemann sums give convergence of the finite Gram matrices to those of $u^l e^{cu/2}$. Those matrices are positive definite by polynomial linear independence. The Fourier sums for the complementary functions converge uniformly on bounded t intervals, yielding exactly the stated kernel, locally uniformly also in $c > 0$. On a finite interval, Hadamard's inequality bounds each correlation determinant by the product of the diagonal bounds. Its generating Fredholm series therefore converges termwise and is dominated by an exponential series. This proves local convergence of the processes against bounded test functions, also for cutoffs with endpoints of zero intensity measure.

The mark of a single point is $f_N(t) = (c/N)e^{it/N}/(1 - ze^{it/N})$. Its full-period integral is zero by its positive-mode Fourier series, and it tends locally uniformly to f_c. For $|t| \leq \pi N$, the identity $|1 - ze^{it/N}|^2 = (1 - z)^2 + 2z(1 - \cos(t/N))$ gives $|f_N(t)| \leq C/(1 + |t|)$ at large N, uniformly on compact positive depth intervals. Subtracting $b_N \int f_N$ from the full sum leaves S_N unchanged. For the part outside $[-L, L]$ the residual mean after this subtraction is at most $m \sup_{|t|>L} |f_N(t)|$. This follows by integrating $|f_N|$ against the diagonal of the complementary projection, of total mass m. Its centered variance is at most $b_N \int_{|t|>L} |f_N(t)|^2 dt = O(1/L)$. Indeed the variance formula for a projection subtracts a nonnegative squared Hilbert–Schmidt norm from the one-point second moment. The same estimates hold for the limiting kernel, with full intensity $1/(2\pi)$. Thus the limiting compensated sum exists in L^2, and cutting at L, taking the local limit, then sending L to infinity proves convergence in law of S_N to $X_{m,c}$. A common realization of all the finite ensembles is unnecessary.

For uniform integrability take any real linear projection $v(t)$ of $f_N(t)$ with fixed complex coefficient. For the finite projection P the exponential generating determinant equals $\det_{\operatorname{ran} P}(1 + P(e^v - 1)P)$. Its eigenvalues are positive. The inequality $\log(1 + a) \leq a$ yields

$$\log \mathbb{E}_m e^{\sum v - \mathbb{E}_m \sum v} \leq \int (e^v - 1 - v) P(t, t)\, dt \leq C \int |f_N(t)|^2\, dt.$$

Here $\mathbb{E}_m$ is the normalized tilted expectation. The means are bounded by $m \sup |f_N|$ since the homogeneous integral vanishes. These estimates for all four signed coordinate directions give uniform exponential moments in $|S_N|$ at any fixed exponential order. Thus $|S_N|^{2h}$ is uniformly integrable on compact subsets of $\Re h > 0$, and is continuous at zero with value zero. Normal families give the local uniform statement in h; for c use the same argument along every convergent positive depth sequence. The normalization limit now proves the stated formula.

For the planar assertion, the normalized circular determinant converges to $\mathbb{E}J_0(\rho|X_{m,c}|)$. The exponential moment bounds give convergence of the compact-frequency Taylor coefficients and uniform bounds for the origin remainder

after subtracting sufficiently many coefficients. At large frequency the absolute circular mean is at most one, so the integral of $\rho^{-2\Re h-1}$ beyond R vanishes uniformly when $\Re h$ stays positive. This proves passage through the same finite part, including its removable nonnegative integer parameters. No estimates of negative moments at microscopic depth enter this proof.

A check outside the integer family of the preceding section. For $m = 0$, $h = 1$ the untilted trace covariance $\mathbb{E}[\operatorname{Tr} U^k \overline{\operatorname{Tr} U^l}] = \delta_{kl} \min(k, N)$ also follows by inserting the Fourier series of f_z in the finite projection variance identity. It gives the exact value $1 - z^{2N}$. Hence

$$T_N(1, 0; \sqrt{1 - c/N}) = 1 - e^{-c} + \frac{c^2 e^{-c}}{2N} + O(N^{-2}).$$

For $m = 1, h = 1$ the limiting normalized second moment is $c^2 I_2(c)/I_0(c)$. The numerical controls compare these cases and $m = 2, h = 1$ with the direct projected covariance.

The untilted local logarithmic derivative of CUE characteristic polynomials is established literature. Chhaibi, Najnudel and Nikeghbali study the microscopic landscape and logarithmic derivatives in *Inventiones Mathematicae* 207 (2017). Here the projection argument specifies the tilted finite-dimensional complement, normalization, and the passage through the circular integral. This projection proof uses integer tilt and positive $\Re h$. The negative-moment extension is proved in Section 15; a first-order correction requires separate control.

14. Positive moments under the circular Jacobi change of measure

Theorem 14.1 (circular Jacobi representation). Fix $c > 0$, $a = c/2$, $s > -1/2$ real, and $z = z_N = \sqrt{1 - c/N}$ for $N > c$. Let $\mathcal{X}_s$ be the symmetric circular Jacobi local point process, in coordinates $t = N \arg \lambda \in \mathbb{R}$. This convention has limiting mean density $1/(2\pi)$ at zero tilt. For its points put

$$W = \prod_{t \in \mathcal{X}_s} (1 + a^2/t^2)^s, \qquad S = -a + \sum_{t \in \mathcal{X}_s} \frac{ca}{a^2 + t^2} + i \lim_{L \to \infty} \sum_{\substack{t \in \mathcal{X}_s \\ |t| \le L}} \frac{ct}{a^2 + t^2}. \tag{14.1}$$

The product is positive and finite almost surely. The real sum converges absolutely; the imaginary limit is symmetric and exists in L^2. With $g_s = G(1 + s)^2/G(1 + 2s)$, the fixed-depth limit is

$$\lim_{N \to \infty} N^{-s^2} T_N(h, s; z_N) = g_s e^{-sc/2} \mathbb{E}_{\mathcal{X}_s} \left[W \, |S|^{2h} \right], \qquad \operatorname{Re} h > 0. \tag{14.2}$$

Set the value at $S = 0$ equal to zero. At $h = 0$ the formula holds separately with the integrand W. In particular, for every real $k > 0$, including nonintegers,

$$B_k(c) = \lim_{N \to \infty} N^{-k^2 - 2k} \mathbb{E} |\Lambda'_N(z_N)|^{2k} = c^{-2k} g_k e^{-kc/2} \mathbb{E}_{\mathcal{X}_k} \left[W \, |S|^{2k} \right] > 0, \tag{14.3}$$

where (14.1) uses $s = k$. This is an expression in terms of the specified local process, with no fitted coefficients. The proof works at fixed positive c; uniform transition to another depth scale requires separate estimates.

Two inputs on the circular Jacobi ensemble. Under the circle probability tilt $|\Lambda_N(1)|^{2s}/Z_N(s)$ the eigenangles have the circular Jacobi orthogonal polynomial ensemble with weight $w_s(\theta) = |1 - e^{i\theta}|^{2s}$ and Vandermonde square. In coordinates $t = N\theta$, the local correlation functions away from zero converge to those of the confluent hypergeometric determinantal process $\mathcal{X}_s$. One explicit reference and normalization are Forrester and Shen, §§2.1–2.2, (2.2)–(2.7). Move the singular point from -1 to 1, take their parameters $p = s, q = 0$, and set their coordinate to $t/(2\pi)$. Thus a kernel relative to dt is $(2\pi)^{-1} K_\infty^{(s,0)}(t/(2\pi), u/(2\pi))$, up to the usual correlation-preserving gauge. At $s = 0$ this is the sine process. This local theorem supplies no estimate by itself at infinity or for an unbounded functional.

Here is a uniform finite-size majorant for the intensity $\rho_{N,s}$ relative to dt. For $0 < |t| \le \pi N$,

$$\rho_{N,s}(t) \asymp_s (|t|/(1 + |t|))^{2s}. \tag{14.4}$$

Indeed $\rho_{N,s}(t) = w_s(t/N)/(2\pi N \lambda_{N-1}(e^{it/N}))$, where λ_n is the degree-n Christoffel function for $w_s(\theta) d\theta/(2\pi)$. The mass of the arc of angular radius δ centered at θ is comparable to $\delta(d(\theta, 0) + \delta)^{2s}$, with d circular distance

in radians: compare the weight to its central value when $d > 2\delta$, and rescale the integrable power $|\theta|^{2s}$ otherwise. In particular the measure is doubling. On the circle the degree-n boundary scale in Varga's Christoffel estimate is comparable to $1/n$ (the exterior level curves are concentric circles). Applying Varga, Theorem 2.4, $p = 2$ and auxiliary weight parameter 0 gives $\lambda_n \asymp_s$ the mass of that arc. This proves (14.4), enlarging constants for bounded N. The limiting density obeys the same upper bound. Hadamard's inequality bounds each determinantal m-point density by the product of its one-point densities. On bounded sets (14.4) supplies an integrable majorant, also when $s < 0$. Thus the local correlation convergence gives convergence in law of the restricted point processes by their Laplace functionals. There is almost surely no point at the origin or at prescribed truncation endpoints.

Exact finite-size change of measure. With $\mathbb{E}_{N,s}$ the circle-tilted expectation, for every bounded test of the eigenangles the ratio of the unnormalized interior tilt to the circle tilt is

$$z^{Ns} W_N, \qquad W_N = \prod_t \left(1 + \frac{(1-z)^2}{z|1 - e^{it/N}|^2}\right)^s.$$

This is the identity $|1 - zw|^2 = z|1 - w|^2 + (1 - z)^2$. It applies in particular to the bounded Fourier-source integrand defining the planar Toeplitz determinant. Also, with $d = 1 - z^2 = c/N$,

$$S_N = -\frac{c}{2z} + \sum_t m_N(t), \qquad m_N(t) = \frac{d}{2z}\frac{1 + ze^{it/N}}{1 - ze^{it/N}}.$$

This is an identity for the original logarithmic-derivative mark. On bounded t-intervals $m_N(t) \to c/(a - it)$. For all large N and $|t| \le \pi N$ the real part is nonnegative and $\le C_c/(1 + t^2)$, and $|\operatorname{Im} m_N(t)| \le C_c|t|/(1 + t^2)$. These bounds follow from $|1 - ze^{it/N}|^2 = (1 - z)^2 + 4z \sin^2(t/(2N))$, $N(1 - z) \to a$ and $|\sin(t/(2N))| \ge |t|/(\pi N)$. The imaginary part is odd and the intensity is even.

Joint convergence and integrability. The modulus of the real logarithm of W_N per point is at most $C_s \log(1 + C_c/t^2)$. Above $|t| > L \ge 1$ its expected sum and the expected real-mark tail are $O_{s,c}(1/L)$ by (14.4). On $|t| < \epsilon$ the expected log contribution is bounded by $C \int_0^\epsilon t^{2s}(1 + |\log t|)dt = o(1)$. Both estimates hold for the limiting process as well. For the signed imaginary tail its mean is exactly zero by parity. For a Hermitian determinantal positive contraction K, the variance of a real linear statistic $\sum f$ is at most $\int f^2 K(t, t)dt$: the subtracted double integral equals $\operatorname{Tr}[(K^{1/2} f K^{1/2})^2] \ge 0$. Thus the imaginary tail has second moment $O_{s,c}(1/L)$ uniformly in N. Apply the same estimate on symmetric annuli to obtain the L^2 limit in (14.1). These truncation bounds, local convergence away from zero, and the continuous mapping theorem give $(W_N, S_N) \Rightarrow (W, S)$.

When $s > 0$ choose $p > 1$ with $2s(p - 1) < 1$. The determinantal product inequality $\mathbb{E}\prod(1 + g(t)) \le \exp(\int g\rho)$ for nonnegative g follows by expanding correlation functions and using Hadamard. With g the pth power of a single factor in W_N minus one, $g\rho$ is bounded by $C|t|^{-2s(p-1)}$ near zero and by $C|t|^{-2}$ at infinity. Hence $\sup_N \mathbb{E}_{N,s} W_N^p < \infty$. For $s \le 0$ one has $0 < W_N \le 1$.

All fixed real exponential moments of both components of S_N are bounded uniformly in large N. For a bounded real mark f, the finite-rank determinant identity and $\log(1 + u) \le u$ applied to $K^{1/2}(e^{\lambda f} - 1)K^{1/2}$ give

$$\log \mathbb{E} \exp\Big(\lambda \Big[\sum f - \mathbb{E}\sum f\Big]\Big) \le \int (e^{\lambda f} - 1 - \lambda f)\rho \le C_{\lambda, \|f\|_\infty} \int f^2 \rho.$$

The determinant argument is strictly positive because $I - K + K^{1/2} e^{\lambda f} K^{1/2} \ge \min(1, e^{-|\lambda| \|f\|_\infty}) I$. The bounds for the marks and (14.4) uniformly bound the right side, the mean real part, and the deterministic term; the mean imaginary part is zero. It follows by Hölder, using an exponent strictly between 1 and the available p, that $W_N |S_N|^{2h}$ is uniformly integrable, locally in $\Re h > 0$. The map $y \mapsto |y|^{2h}$ extended by zero is continuous there. Joint convergence now gives convergence of its weighted expectation. The remaining deterministic factors are $z^{Ns} \to e^{-sc/2}$ and $N^{-s^2} Z_N(s) \to g_s$, giving (14.2). Normal-family convergence is locally uniform in the complex h half-plane. At $h = 0$ use the weight bound on its own. On the diagonal $s = h = k$ one has $T_N = (c/N)^{2k} \mathbb{E}|\Lambda_N'(z_N)|^{2k}$ identically. This proves (14.3).

To verify strict positivity there, the limiting imaginary statistic has positive variance. For a Hermitian contraction the variance is at least $\frac{1}{2} \iint (f(t) - f(u))^2 |K(t, u)|^2 dtdu$ for real f (first truncate and then pass in L^2). Take $f(t) = ct/(a^2 + t^2)$. The limiting kernel is continuous off zero and has positive diagonal on some open interval away from zero by (14.4) and local convergence. On a subinterval f is strictly monotone and $|K(t, u)| > 0$ for sufficiently

close pairs. The double integral is positive. Therefore $\mathbb{P}(S \neq 0) > 0$ and the weight W is positive almost surely. The positive-moment argument above controls the large values of the mark. Section 15 treats its behavior near zero. Formula (14.2) also applies to the Fourier-source test, giving $N^{-s^2} D_N(s, z_N; \zeta) \to g_s e^{-sc/2} \mathbb{E}[W e^{i \operatorname{Re}(\bar{\zeta} S)}]$. Thus the limit of the marked source and its positive-order readouts use the same preparation; the uniform integrability argument is what licenses the unbounded moment readout.

Passage through the Mellin cutoff. Normalized by N^{-s^2}, the circular mean has uniformly bounded total variation by the positive-weight estimate at $h = 0$. For $\Re h > 0$ the weighted mean above radius R is therefore bounded by $CR^{-2\Re h}/(2\Re h)$. On a compact interval in frequency, the exponential moments just proved, combined with the L^p bound for W_N, give convergence of the compact-source jets and uniform control of the Taylor remainder. Subtract more terms than the largest $\Re h$ on the chosen compact parameter set, exactly as in the fixed-interior finite part. Both ends can now be passed under the integral, including the removable positive integer values. This identifies (14.2) using the same circular readout as the fixed-rank theorem.

15. Sharp microscopic moments at positive depth

Fix $c > 0$, $s \in \mathbb{R}$ and $z = z_N = \sqrt{1 - c/N}$. Write $Z_N = \mathbb{E}|\Lambda_N(z)|^{2s}$. Let $\mathbb{P}_{N,s,c}$ denote the probability obtained from Haar measure by multiplying by $|\Lambda_N(z)|^{2s}/Z_N$. All planar densities in this section are relative to $d\Re y\, d\Im y$.

Theorem 15.1 (sharp finite-depth moment domain). There are a positive finite mass $A_s(c)$ and a probability density $p_{s,c} \in C^\infty(\mathbb{C})$ such that, locally uniformly in h for $\Re h > -1$,

$$N^{-s^2} T_N(h, s; z_N) \;\longrightarrow A_s(c) \int_{\mathbb{C}} |y|^{2h} p_{s,c}(y)\, d^2 y. \tag{15.1}$$

Here $A_s(c) = \lim N^{-s^2} Z_N$. The finite-size mark law has a density p_N for all sufficiently large N. For every fixed derivative order j, $p_N \to p_{s,c}$ in the uniform norm through order j when N is sufficiently large for that order. Moreover, for some $b, B, r_0 > 0$,

$$b \le p_N(y) \le B \quad (|y| < r_0), \qquad b \le p_{s,c}(y) \le B \quad (|y| < r_0). \tag{15.2}$$

In particular the origin is a point of positive planar density. The ordinary limiting absolute moment exists exactly for $\Re h > -1$. The mass and Fourier transform are specified by the Fredholm formula (15.5) below. For real $s > -1/2$ the same unnormalized measure is the circular-Jacobi expectation in (14.2), now also for $-1 < \Re h \le 0$.

For every real $k > -1$ the diagonal derivative moment therefore satisfies

$$\lim_{N \to \infty} N^{-k^2 - 2k} \mathbb{E}|\Lambda_N'(z_N)|^{2k} = c^{-2k} A_k(c) \int_{\mathbb{C}} |y|^{2k} p_{k,c}(y)\, d^2 y \quad \in (0, \infty). \tag{15.3}$$

The equality uses $T_N(k, k; z_N) = (c/N)^{2k} \mathbb{E}|\Lambda_N'(z_N)|^{2k}$. This includes the interval $-1 < k \le -1/2$ where the circle measure with tilt k cannot serve as a probability. All statements use fixed positive depth. The estimates also allow sequences of positive depths tending to such a c.

Why the extra estimate is needed. Weak convergence and bounded positive moments alone allow a tiny amount of mass very near zero. For example, adding a mass e^{-n} at e^{-n^2} to a probability on $[1, 2]$, and multiplying its original mass by $1 - e^{-n}$, preserves the weak limit and the limits of all positive moments. Every fixed negative real moment then grows without bound. The determinant must rule out that possibility for the actual Haar preparation. The proof does so before taking the limit in the inverse moment.

Kernel localization for the actual interior tilt

Work with the probability density on the eigenangles proportional to the square of the circular Vandermonde times the weight product, with one-point weight $w(\theta) = |1 - z e^{i\theta}|^{2s}$, s real, and $z^2 = 1 - c/N$. Take c in a compact subset of $(0, \infty)$ and s in a fixed compact interval. All constants in this subsection may be chosen uniformly there, for all sufficiently large N. Let d be circle distance in radians. Since $|1 - z e^{i\theta}|^2 = (1 - z)^2 + 4z \sin^2(\theta/2)$, we have

$$|1 - z e^{i\theta}| \asymp N^{-1} + d(\theta, 0), \qquad \frac{w(\theta)}{w(\phi)} \le C(1 + N d(\theta, \phi))^{2|s|}.$$

Let H_N be the analytic trigonometric polynomials of degree below N with squared norm $\int |p|^2 w\, d\theta/(2\pi)$. Its orthogonal projection has reproducing kernel $B_N(\theta,\phi)$ relative to that weighted measure.

Choose $\eta \in C_c^\infty(\mathbb{R})$ equal to one on $[-1,1]$ and set $V_N(\alpha) = \sum_k \eta(k/N) e^{ik\alpha}$. Repeated finite summation by parts in k, applied also to $(ik)^j \eta(k/N)$, gives $|V_N^{(j)}(\alpha)| \le C_{L,j} N^{1+j}(1 + Nd(\alpha,0))^{-L}$ for $j = 0, 1$ and arbitrary fixed L. Convolution against $V_N^{(j)}$ reproduces $p^{(j)}$. Cauchy–Schwarz against w and the ratio bound give

$$|p^{(j)}(\theta)| \le C N^{j+1/2} w(\theta)^{-1/2} \|p\|_{H_N}, \qquad j = 0, 1.$$

For the reverse bound at $j = 0$, fix an integer $L > |s| + 1$, $M = \lfloor N/L \rfloor$, and use

$$p_\theta(\phi) = \left(M^{-1} \sum_{k=0}^{M-1} e^{ik(\phi-\theta)} \right)^L .$$

Its degree is less than N, its value at θ is one, and its modulus is at most $C_L(1+Nd(\theta,\phi))^{-L}$. Integration against w gives $\|p_\theta\|_{H_N}^2 \le C w(\theta)/N$.

Consequently the squared evaluation norm $B_N(\theta,\theta)$ is at least $bN/w(\theta)$. On $Nd(\theta,\phi) \le 1$ the above evaluation bounds give $|\partial_\phi B_N(\theta,\phi)| \le CN^2/w(\theta)$. For some $\delta, b_0 > 0$, integration of this last inequality yields

$$\left| \frac{\sqrt{w(\theta)w(\phi)}}{2\pi N} B_N(\theta,\phi) \right| \ge b_0 \quad \text{if } Nd(\theta,\phi) \le \delta.$$

The expression on the left is the probability projection kernel relative to microscopic Lebesgue measure dt, $t = N\theta$.

From the finite determinant to a planar density

The Toeplitz determinant at frequency ζ divided by the determinant at zero is precisely the characteristic function $\chi_N(\zeta)$ of the mark under $\mathbb{P}_{N,s,c}$. In the angular representation, the density is proportional to $|\Delta|^2 \prod w(\theta_j)$, by the finite determinant integration identity, with $w = |1 - ze^{i\theta}|^{2s}$. Its projection P onto the N weighted polynomials has kernel K_N relative to microscopic Lebesgue measure dt. For $|\zeta| = \rho$ let U be multiplication by $u(t) = e^{i\rho g(t)}$, where g is the directional component of one mark. Computing the ratio of the two Gram determinants in an orthonormal basis gives $\chi_N = \det(PUP|_{\operatorname{ran} P})$. All singular values of this compression are at most one. Write $C = PUP|_{\operatorname{ran} P}$. By $\log x \le x - 1$ on the squared singular values,

$$|\chi_N| \le \exp[-\tfrac{1}{2} \operatorname{Tr}(I - C^*C)], \qquad \operatorname{Tr}(I - C^*C) = \tfrac{1}{2} \iint |u(t) - u(v)|^2 |K_N(t,v)|^2 \, dt\, dv. \tag{15.4}$$

The trace identity uses $P^2 = P$ and symmetry in t, v. A zero singular value makes the inequality immediate. Thus damping of the finite determinant follows from phase differences on any measurable subset with sufficient kernel mass.

Directional oscillation and the far Fourier tail

Use the Fourier direction $e^{i\beta}$. In scaled eigenangle $t = N\theta$, a single summand of S_N projects to $g_\beta(t) = z\cos\beta + \cos(\psi(t) - \beta)$, where

$$\psi(t) = 2\arctan(A \tan(t/(2N))), \qquad A = (1+z)/(1-z), \qquad A/N = (1+z)^2/c.$$

Indeed $(1-z^2)e^{i\theta}/(1-ze^{i\theta}) = z + (e^{i\theta} - z)/(1 - ze^{i\theta})$ and the second term has argument ψ. Fix a compact depth interval in $(0,\infty)$, take N sufficiently large there, and write $0 < \eta \le 1$ for the one-point kernel coherence length in scaled angles. Choose a fixed $0 < d < 1/4$. Whenever $L \ge L_0$ and $2L \le dN$, uniformly on $L \le |t| \le 2L$,

$$\psi'(t) = \frac{A}{N} \frac{1 + \tan^2(t/(2N))}{1 + A^2 \tan^2(t/(2N))} \asymp L^{-2}, \qquad |\sin\psi(t)| \asymp L^{-1}, \qquad -\cos\psi(t) \asymp 1.$$

These follow by $A|\tan(t/(2N))| \asymp L$ and the tangent half-angle formulas, with L_0 chosen to make the last cosine negative. The sign of t can be chosen once so $\sin\psi(t)\cos\beta$ and $-\cos\psi(t)\sin\beta$ have the same sign (either sign

is permissible if one coefficient vanishes). On this whole signed interval $g'_\beta = -\psi' \sin(\psi - \beta)$ keeps one sign and has size comparable to $L^{-2}(|\sin\beta| + L^{-1}|\cos\beta|)$, hence its supremum and infimum are comparable. Set $L = \min(b\rho^{1/3}, dN/2)$ with $b > 0$ small. Uniformly in the direction, $\rho\eta \inf|g'_\beta| \geq 4\pi$, because $\rho L^{-3} \geq b^{-3}$. After increasing fixed lower thresholds on N, ρ, $L \geq \max(L_0, 2\eta)$.

For $L \leq |t| \leq 3L/2$ on this sign and u in the length-η interval outward from t, set $H = \rho|g_\beta(u_{\mathrm{end}}) - g_\beta(t)| \geq 4\pi$. The integral in u of $1 - \cos(\rho(g_\beta(u) - g_\beta(t)))$ is bounded below by $(H - \sin H)/(\rho \sup|g'_\beta|) \gtrsim \eta$. Integrating t gives a lower bound $\gtrsim L$ for the commutator energy whenever the projection kernel is bounded below at these separations. It yields

$$|\chi_N(\rho, \beta)| \leq \exp[-\kappa \min(\rho^{1/3}, N)].$$

One last estimate controls arbitrarily large frequencies. The normalization is $D_N[w] \geq 1$ by Jensen's inequality, since $w(\theta) = |1 - ze^{i\theta}|^{2s}$ with real s, and the mean of its logarithm on the circle vanishes. In an entry with $|k| < N$, change variables from θ to ψ throughout the circle (choose continuous lifts). The unimodular constant phase can be discarded. The amplitude $w(\theta(\psi))e^{-ik\theta(\psi)}d\theta/d\psi$ has supremum plus total variation $O(N^{2|s|+2})$. To see this, $\|w\|_\infty \leq CN^{2|s|}$ and its variation is twice its oscillation. The inverse Jacobian $d\theta/d\psi = (1 - z^2)/|1 + ze^{i\psi}|^2$ has supremum $A = O(N)$ and variation at most $2A$. The variation of $e^{-ik\theta}$ is $2\pi|k|$. These bounds survive reparametrization. On finitely many fixed-length arcs the phase $\cos(\psi - \beta)$ has either its second derivative bounded away from zero, or monotone first derivative bounded away from zero. The elementary first- and second-derivative oscillatory integral bounds for a bounded variation amplitude give $O(N^{2|s|+2}\rho^{-1/2})$ entrywise. Hadamard's determinant inequality gives

$$|\chi_N(\rho, \beta)| \leq (CN^{2|s|+5/2}\rho^{-1/2})^N.$$

For $M > 4(2|s|+5/2)$ this is at most $\rho^{-N/4}$ when $\rho \geq N^M$ and N is large. On $\rho \leq N^M$ the preceding exponential is bounded by $C_p(1+\rho)^{-p}$, as $\min(\rho^{1/3}, N) \geq \rho^{\min(1/3, 1/M)}$ for $\rho \geq 1$. Thus every prescribed inverse power holds uniformly when N is sufficiently large (depending on the prescribed power). The same reasoning works uniformly on compact sets of positive depths and real tilts if their kernel coherence constants are uniform.

The microscopic Fredholm determinant

Let $a = c/2 > 0$. Use independent complex source variables p, q in the log symbol $V = s \log|1 - ze^{i\theta}|^2 + i(pf_z + q\bar{f}_z)/2$, with $f_z = (1 - z^2)e^{i\theta}/(1 - ze^{i\theta})$. The physical Fourier plane is $p = \bar{\zeta}$, $q = \zeta$. **Theorem 15.2 (Fredholm formula).** Allow arbitrary complex s, p, q. Define the nonvanishing function of real t

$$B(t) = \exp\left[s\{\log(a + it) - \log(a - it)\} + \frac{ic}{2}\left(\frac{q}{a + it} - \frac{p}{a - it}\right)\right],$$

where the two logarithms are principal. For $v \geq 1$ set

$$b_+(v) = -\frac{1}{2\pi v^2}\int_{\mathbb{R}} B''(t)e^{-ivt}dt, \quad b_-(v) = -\frac{1}{2\pi v^2}\int_{\mathbb{R}} (B^{-1})''(t)e^{ivt}dt.$$

Let H_+, H_- have kernels $b_\pm(1 + x + y)$, respectively, on $L^2(0, \infty)$. Both are Hilbert–Schmidt. With $z^2 = 1 - c/N$, the source limit is

$$N^{-s^2} D_N[e^V] \longrightarrow c^{-s^2} \exp[-is(p + q)/2 - pq/4] \det(I - H_+H_-). \tag{15.5}$$

Convergence is locally uniform in complex (s, p, q), uniformly also on compact positive real depth intervals. This gives compact-source derivatives of all finite orders. A complex power of N or c in (15.5) uses the real logarithm.

Proof. Split $V = V_+ + V_-$ into strictly positive and strictly negative Fourier modes. In particular $V_+ = s \log(1 - ze^{i\theta}) + ipf_z/2$, and $V_- = s \log(1 - ze^{-i\theta}) + iq\bar{f}_z/2$. Every finite-$N$ symbol here admits its smooth zero-winding factorization, since $0 < z < 1$. In the Fourier convention $u_k = (2\pi)^{-1}\int u(\theta)e^{-ik\theta}d\theta$, the scalar Borodin–Okounkov identity gives

$$D_N[e^V] = E_N \det(I - X_N Y_N), \quad (X_N)_{jk} = (e^{V_- - V_+})_{N+j+k+1}, \quad (Y_N)_{jk} = (e^{V_+ - V_-})_{-N-j-k-1}, \quad j, k \geq 0.$$

Indeed the tail projection in the identity surrounds the product $H(b)H(\tilde{d})$, where $b = e^{V_- - V_+}$, $d = b^{-1}$; shifting the outer rows and columns by N gives these two Hankel factors. Direct summation of $\sum_{k \geq 1} kV_kV_{-k}$ gives

$E_N = (1-z^2)^{-s^2}\exp[-isz(p+q)/2 - pq/4]$. The identity is due to Borodin and Okounkov; the tail Hankel factorization is also given by Basor and Widom.

Set $b_N(t) = e^{V_-(t/N)-V_+(t/N)}$ on $|t| \le \pi N$. It converges locally smoothly to $B(t)$, since $N(1-ze^{\pm it/N}) \to a \mp it$ and the two $-\log N$ contributions cancel. The b_N and their inverses are uniformly bounded on this full interval for compact parameters: the difference of the two finite logarithms is purely imaginary of modulus at most π, and $|f_z| \le 1+z$. Also $|1-ze^{it/N}| \gtrsim (1+|t|)/N$ for positive depth in a compact interval. Differentiating each logarithm in t bounds its first two derivatives by $C_j(1+|t|)^{-j}$, $j=1,2$. For the source terms the derivatives satisfy the same bounds: explicitly $f_z' = i(1-z^2)e^{it/N}/[N(1-ze^{it/N})^2]$, and another derivative gives terms with denominators of orders two and three. Hence $|b_N''(t)| + |(b_N^{-1})''(t)| \le C(1+|t|)^{-2}$. Extended by zero as functions on the real line, these *second derivatives* converge in L^1 to B'' and $(B^{-1})''$ locally uniformly in the parameters.

For every $n \ge N$, twice integrating by parts on the full periodic interval gives exactly

$$N(e^{V_- - V_+})_n = -\frac{1}{2\pi(n/N)^2}\int_{-\pi N}^{\pi N} b_N''(t)e^{-i(n/N)t}dt.$$

The inverse factor at $-n$ has the same formula with the opposite Fourier sign. Thus the rescaled coefficients are $O((n/N)^{-2})$ and tend to $b_\pm(v)$ whenever $n/N \to v \ge 1$. Embed $\ell^2(\mathbb{N}_0)$ isometrically as normalized indicators of the mesh-$1/N$ cells on $\mathbb{R}_+$. The extended matrices have kernels equal to N times each matrix entry on its cell rectangle. They converge pointwise to the two asserted Hankel kernels and are bounded by $C(1+x+y)^{-2}$, square-integrable on the quadrant. Hilbert–Schmidt convergence gives trace-norm convergence of the product, and continuity of the Fredholm determinant proves (15.5). All estimates are uniform on the stated compact sets.

Exact controls. With zero source and $s=-m$, m any positive integer, $e^{V_- - V_+} = (1-ze^{i\theta})^m/(1-ze^{-i\theta})^m$ has no positive Fourier modes above m, so for $N \ge m$ the Fredholm factor is exactly one and $D_N = (1-z^2)^{-m^2}$. For $s=1$ the two limiting kernels both use $b_\pm(v) = ce^{-av}$. Their product has one nonzero eigenvalue e^{-c}. The resulting mass $(1-e^{-c})/c$ agrees with the direct finite identity $D_N = (1-z^{2(N+1)})/(1-z^2)$. Equality of the two sources in the overlapping real-tilt range follows from their derivation as limits of the same finite determinant.

Positive mass at every real tilt. Write $Z_N(s,c) = D_N(s,z;0)$. At frequency zero, put $b = e^{V_- - V_+}$ and $e = b^{-1}$ on the angle circle. With $q = |1-ze^{i\theta}| \asymp 1-z+|\theta|$ for $z \ge 1/2$, log-symbol first and second derivatives have sizes $O_s(q^{-1})$ and $O_s(q^{-2})$. The log difference is bounded and $\|b\|_\infty + \|e\|_\infty$ is bounded. Consequently $\|b''\|_1 + \|e''\|_1 \le C_s/(1-z)$ by integrating q^{-2}. Two integrations by parts bound the kth Fourier coefficient by $C_s/[(1-z)k^2]$ for $k \ne 0$. Summing $(k-N)|b_k|^2$ for $k > N$, and likewise for e_{-k}, bounds both tail Hilbert–Schmidt norms by $C_s/[N(1-z)]$. Their product has trace norm at most C_s/c^2 because $N(1-z) = c/(1+z)$. The prefactor at zero source is c^{-s^2}. For a fixed sufficiently large c' the Fredholm determinant differs from one by at most $\exp(C_s/(c')^2) - 1 < 1/2$ at all sufficiently large N. Thus $N^{-s^2}Z_N(s,c') \ge (c')^{-s^2}/2$. Propagate to the desired c along the compact interval with endpoints c, c'. For the *normalized* tilted probability let $I_{N,s,c}(\theta)$ be its one-point intensity relative to $d\theta/(2\pi)$, bounded by CN on that compact interval by the polynomial evaluation estimate above. The exact derivative and its expectation give

$$\partial_c \log w(\theta) = \frac{s}{2Nz^2}(P_z(\theta) - 1), \qquad P_z(\theta) = \frac{1-z^2}{|1-ze^{i\theta}|^2}, \qquad |\partial_c \log Z_N(s,c)| \le C.$$

Indeed P_z has mean one and the intensity has total mass N. Integrate and pass to the compact-source limit. This proves its strictly positive mass at c for all real s. One may therefore normalize the resulting limiting characteristic function. It is continuous at the origin by (15.5), so it is the transform of a probability measure by Lévy's continuity theorem. At real $s \le -1/2$ this construction uses the actual interior weight; the singular circle weight would fail to be integrable.

Exactly solvable negative integer tilts

For $s=-m$, an integer $m \ge 1$, and $N \ge m$, one has

$$Z_N(-m,c) = d^{-m^2}, \qquad \mathbb{E}_{-m}S_N = mz, \qquad \mathbb{E}_{-m}|S_N|^2 = 1 + m^2z^2,$$

where $\mathbb{E}_{-m}$ is the normalized interior expectation. For the mass, the positive Fourier coefficients of $b = (1-z\lambda)^m/(1-z\lambda^{-1})^m$ vanish above m, so the Fredholm correction at zero source is exactly one.

For the other identities let $n = N - m$, $b_z(\lambda) = (\lambda - z)/(1 - z\lambda)$ and $k_z(\lambda) = \sqrt{d}/(1 - z\lambda)$. Multiplication by $(1 - z\lambda)^{-m}$ realizes the tilted polynomial space as the span in unweighted circle norm of the n ordinary monomials of degrees 0 through $n - 1$ and the m functions $\lambda^n b_z^j k_z$, $0 \le j < m$. Orthogonality of the latter after removing λ^n follows by $|k_z|^2 d\theta = d \arg b_z$; the degrees below n are orthogonal by analyticity. Dimension and the common denominator prove equality. The new projection kernel gives exactly the tilted point process, up to a unit-modulus gauge. Its diagonal is $n + mP_z$. Integrating the analytic mark g by the Poisson formula gives the mean $mg(z) = mz$.

For the variance, denote the above projection by P, set $B = \lambda^n b_z^m$, and append the one further unit vector $v = Bk_z$. Multiplication by g maps the original space into the enlarged space, by the common denominator and the degree bound on the numerator. Hence $(I - P)gP$ has only the possible range $\mathbb{C}v$. Its Hilbert–Schmidt norm squared equals $\|PT_{\bar{g}}v\|^2$, where $T_{\bar{g}}$ is the analytic-space compression of multiplication by $\bar{g}$. The elementary backwards-shift formula is $T_{\bar{g}}f = d(f(\lambda) - f(z))/(\lambda - z)$, as is checked on the monomials. Since $B(z) = 0$,

$$T_{\bar{g}}v - zv = (B/b_z)k_z = \lambda^n b_z^{m-1} k_z,$$

the last of the old orthonormal vectors. Thus the defect has squared norm one, which is exactly $\mathbb{E}_{-m}|S_N - \mathbb{E}_{-m}S_N|^2$ by the determinantal variance identity.

This basis supplies a concrete microscopic kernel at negative integer tilt. In the gauge above, relative to dt in the coordinate $t = N\theta$, it is

$$K_{-m,c}(t,u) = \frac{1}{2\pi}\int_0^1 e^{iv(t-u)}dv + \frac{ce^{i(t-u)}}{2\pi(a - it)(a + iu)}\sum_{j=0}^{m-1}\left(\frac{a + it}{a - it}\frac{a - iu}{a + iu}\right)^j, \qquad a = c/2.$$

The finite geometric sum of the ordinary monomials gives the first term and the m displayed functions give the second on using $N(1 - z) \to a$. The finite projection kernels converge on compact sets of (t, u), so the formula also identifies local determinantal correlation functions. The exact mean and second moment limits for the logarithmic derivative are m and $1 + m^2$.

Passing the inverse moment through the limit

Let $F(s, c; \zeta)$ denote the right side of (15.5) on the physical Fourier plane and put $A_s(c) = F(s, c; 0)$. Positive mass and compact-source convergence imply convergence of χ_N to $\chi = F/A_s(c)$. For every fixed j, the two Fourier tail estimates above give an integrable uniform bound on $(1 + |\zeta|)^j|\chi_N(\zeta)|$ for all sufficiently large N. Fourier inversion and dominated convergence give uniform convergence of the densities and their derivatives through order j on the entire plane. In particular $\sup_{N \ge N_0}\|p_N\|_\infty \le B$ and, for $0 < r \le 1$ and $u > -1$,

$$\mathbb{P}_{N,s,c}(|S_N| \le r) \le \pi B r^2, \qquad \mathbb{E}_{N,s,c}[|S_N|^{2u};\ |S_N| \le r] \le \frac{\pi B}{1 + u}r^{2+2u}. \tag{15.6}$$

The same bounds hold for the limiting law. Exponential moments of both real components, of either sign, are uniformly bounded. Indeed their finite Laplace transforms are (15.5)'s finite determinants at fixed imaginary frequencies, divided by their positive masses. On any annulus bounded away from zero and infinity the moment integrand is bounded and continuous. Truncate to such an annulus, use (15.6) at its inner edge and the exponential bounds at its outer edge, then remove both cutoffs. These estimates are uniform on compact subsets of $\Re h > -1$, which proves (15.1). The same argument, using the compact uniform estimates and continuity in (15.5), permits varying real $s_N \to s$ and $c_N \to c > 0$. Equality with (14.2) on its generalized domain follows from equality of their Fourier transforms and absolute integrability of the resulting radial statistic.

The same limit follows from the circularly averaged determinant. Write $\bar{F}(\rho)$ for the angular mean of $F(s, c; \zeta)$. For $-1 < \Re h < 0$ the limiting moment in (15.1) is

$$\frac{2^{2h+1}\Gamma(1 + h)}{\Gamma(-h)}\int_0^\infty \rho^{-2h-1}\bar{F}(\rho)\,d\rho. \tag{15.7}$$

The finite-rank planar formula gives this integral with the finite source first. The mass bound controls zero frequency and the uniform inverse powers control infinity. At nonnegative real part, use the compact-source

Taylor subtractions in the fixed-interior proof. At nonnegative integers take their removable values. This recovers the same answer directly from the planar determinant.

For example, at $h = s = -1/2$ the gamma prefactor in (15.7) is one. With $\bar{F}_{-1/2,c}$ the angular average of (15.5) at this tilt, the first inverse derivative moment obeys

$$\lim_{N\to\infty} N^{3/4}\,\mathbb{E}\frac{1}{|\Lambda_N'(\sqrt{1-c/N})|} = c\int_0^\infty \bar{F}_{-1/2,c}(\rho)\,d\rho \quad \in (0,\infty). \tag{15.8}$$

This example sits at the endpoint of integrability of the *circle tilt*. The positive-depth determinant on the right remains well defined.

A bounded approach to a complex tilt. Suppose $c_N \to c > 0$, $s_N = u_N + iv_N \to s \in \mathbb{R}$, and $v_N^2 \log N$ stays bounded. The complex measure of the mark normalized by $N^{-s_N^2}$ has total variation dominated by $e^{v_N^2 \log N} N^{-u_N^2} Z_N(u_N, c_N)$ times the probability law for the real interior tilt u_N. The preceding estimates transfer tightness, exponential tail control and (15.6) to this dominating measure. By (15.5) the Fourier transforms on every fixed disk tend to $F(s, c; \zeta)$. Tightness, bounded total variation and Fourier uniqueness then give weak convergence to that measure. Truncation on annuli gives (15.1) along these complex sequences as well. For a fixed nonreal tilt the displayed factor grows with N, so this argument does not supply the same moment theorem there. At each nonnegative integer h, derivatives in the two complex source variables of (15.5) also supply the normalized moment limit at arbitrary fixed complex s.

Positive density at the origin

Proposition 15.3 (uniform lower density bound). Let $c > 0$, $a = c/2$ and $s \in \mathbb{R}$. Normalize the finite interior tilt $|\Lambda_N(z_N)|^{2s}$ to a probability, where $z_N^2 = 1 - c/N$. Write p_N and p for the corresponding mark densities at finite size and in the limit. There are $b, d > 0$ and $N_0(c, s)$ such that

$$p_N(y) \ge b, \qquad p(y) \ge b, \qquad |y| < d, \quad N \ge N_0(c, s). \tag{15.9}$$

This is a local statement in the ordinary complex plane. Its lower bound does not require a density formula for the limiting point process.

An exterior event. In the coordinates $t = N\theta$ used above, write

$$S_N = -a/z_N + \sum_t m_N(t), \qquad m_N(t) = \frac{c/N}{2z_N}\frac{1 + z_N e^{it/N}}{1 - z_N e^{it/N}}, \qquad m(t) = \frac{2a}{a - it}.$$

On fixed bounded intervals $m_N \to m$ in C^1, by the quotient formula and $N(1 - z_N) \to a$. The real parts are even, positive and bounded by $C_c/(1 + t^2)$; the imaginary parts are odd and bounded by $C_c|t|/(1 + t^2)$. The interior tilted projection kernel has intensity bounded above and below by positive constants in these coordinates, by the evaluation estimates above.

For fixed large L and N sufficiently large write $B = (-L, L)$, $k = \#B$, $E_N = \sum_{u\notin B} m_N(u)$, and

$$H_N = N^{-1}\sum_{u\notin B} \cot(u/(2N)), \qquad Q_N = N^{-2}\sum_{u\notin B} \cot^2(u/(2N)).$$

On $L \le |u| \le \pi N$, $|N^{-1}\cot(u/(2N))| \le 2/|u|$. For a real statistic of a projection process, $\operatorname{Var}\sum f \le \int f^2 \rho_N$. Symmetry gives zero mean for odd marks, so

$$\mathbb{E}\Re E_N + \operatorname{Var}(\Im E_N) + \operatorname{Var}(H_N) + \mathbb{E}Q_N \le C/L.$$

Also $d_1 L \le \mathbb{E}k \le d_2 L$ and $\operatorname{Var} k \le d_2 L$. Hence for any fixed threshold k_0 and $\epsilon > 0$, one can first choose L sufficiently large that, uniformly for all sufficiently large N, the following exterior event has probability at least $1/2$:

$$k_0 \le k \le 2d_2 L, \quad |E_N| \le \epsilon, \quad |H_N| \le 1, \quad Q_N \le 1. \tag{15.10}$$

The count k is determined by the exterior, since the full ensemble has exactly N points.

Conditional finite-dimensional density. Given the exterior configuration, label the k interior points uniformly at random. Their joint density in B^k is proportional to their squared circular Vandermonde, their k interior tilt factors, and the product over k inserted angles of the exterior interaction. Relative to insertion at zero, a single exterior interaction is

$$V(t) = \prod_{u \notin B} [\cos(t/(2N)) - \cot(u/(2N)) \sin(t/(2N))]^2.$$

The ratio in brackets is positive for $|t| < L$, $|u| \geq L$, apart from boundary points of null probability. The inequality $\log(1+x) \leq x$ gives $\log V(t) \leq C_L$ throughout B on (15.10). Indeed the constant term in the sum is $(N-k)(\cos(t/(2N)) - 1) \leq 0$, and the linear cotangent sum is at most $L|H_N|/2$ in modulus. For $|t| \leq L/2$ each bracket differs from 1 by at most $1/2 + O(L^2/N^2)$. Using $\log(1+x) \geq x - Cx^2$ there, the sum of squares of these deviations is at most $C_L(Q_N + N^{-3})$, while the absolute value of the linear sum is bounded by $C_L(1 + |H_N|)$. Thus $V(t) \geq e^{-C_L}$ on the half-interval. The tilt relative to its value at $t = 0$ is bounded above and below on B, with constants depending on c, s, L, by $|1 - ze^{it/N}|^2 = (1-z)^2 + 4z \sin^2(t/(2N))$. Multiply each circular Vandermonde difference by N. Its modulus is at most $2L$ on B and at least $2|t_i - t_j|/\pi$ for large N. These estimates bound the conditional normalizer above, after canceling common constants. For every fixed separation $e > 0$ they give a strictly positive uniform lower bound on the conditional joint density wherever $|t_i| < L/2$ and $|t_i - t_j| \geq e$ for all distinct i, j. There are finitely many possible k in (15.10). The resulting constant can be very small.

A regular arrangement giving zero. Choose an integer $J > 2a + 1$. Choose distinct positive numbers $v_j < 1$ with $\sum_{j=1}^{J} v_j = a$, for example small distinct centered perturbations of a/J. Set $t_j = a\sqrt{4/v_j - 1}$. Then $t_j > a$ and $m(t_j) + m(-t_j) = v_j$. The mark sum of these $2J$ distinct points is a. For the two independently variable coordinates of one pair, the map $(x, y) \mapsto m(x) + m(y)$ has nonsingular real Jacobian at $(t_1, -t_1)$. Indeed $\Re m'(t) = -4a^2 t/(a^2 + t^2)^2$ is odd and nonzero there, and $\Im m'(t) = 2a(a^2 - t^2)/(a^2 + t^2)^2$ is even and nonzero there. Consequently its image on a small neighborhood of this pair contains a fixed disk about its value. The disk persists upon shrinking it once for all sufficiently large N, by C^1 convergence; one proof restricts to a ball on which the derivative differs from its invertible center matrix by less than half its smallest singular value and applies the contraction mapping theorem. Take ϵ smaller than one eighth of this disk radius and $k_0 = 2J$ in (15.10).

Choose L large enough also to contain all core points in $(-L/4, L/4)$. For each permitted k, put the remaining $k - 2J$ points in distinct opposite pairs with positive coordinates between $L/3$ and $5L/12$. If the count is odd, put the last point close to $0.46L$. Distinct separated placements exist since $k \leq 2d_2 L$ and this interval has length proportional to L. Their total real mark is $O(k/L^2) = O(1/L)$ and their imaginary mark vanishes except for the optional last point, whose contribution is $O(1/L)$. This estimate is uniform for m_N as well. Increase L as necessary to make the combined error below ϵ, and then take N large enough for the core approximation and constant offset. Place all coordinates other than the selected pair into small disjoint intervals around their specified locations. Their total mark perturbation can be made smaller than ϵ for all sufficiently large N, uniformly over the finitely many k. The two selected coordinates may then range over their nonsingular neighborhood. That image covers a fixed disk about zero for the full statistic, uniformly in the exterior on (15.10) and in the inactive coordinates. All points in the boxes remain in $(-L/2, L/2)$ and stay a fixed positive distance apart.

Integrate the conditional density lower bound over the inactive boxes. On the active pair use the change of variables to the complex mark; the Jacobian determinant is bounded above uniformly there. For each Borel subset A of a fixed disk this gives $\Pr(S_N \in A \mid \text{exterior}) \geq b_0 \operatorname{area}(A)$ on (15.10), with $b_0 > 0$. Averaging proves (15.9) at finite size. The limiting inequality follows by weak convergence tested on nonnegative continuous functions supported on that disk and continuity of the limiting density.

In particular the limiting small-ball probability has exact leading term $\pi p(0) r^2$ and $p(0) > 0$. The ordinary moment at real $h = -1$ diverges logarithmically, and the absolute moment diverges for $\Re h \leq -1$, both in the limit and for all sufficiently large finite sizes. For the probability-normalized moment $M(h)$ one also has

$$\lim_{x \downarrow 0} x M(-1 + x) = \pi p(0) > 0. \tag{15.11}$$

More generally the local polar-coordinate expansion of the smooth density gives a meromorphic continuation of the limiting moment as a function of h, with possible simple poles at $h = -1 - j$ and residues $\pi \Delta^j p(0)/(4^j (j!)^2)$.

Indeed the circular mean at radius r has through order $2m$ the Taylor coefficients $\Delta^j p(0)/(4^j(j!)^2)$, and subtracting these powers in the radial integral continues it one finite strip at a time. The integral over $|y| \geq 1$ is entire since the positive moments of every order are finite. For the unnormalized tilted moment, all these residues are multiplied by the limiting normalized tilt mass $\lim N^{-s^2} T_N(0, s; z_N)$. Only the first pole is asserted to be present.

Corollary 15.4 (matrix-size-uniform small balls). Let $0 < c_- \leq c \leq c_+ < \infty$, with s in a fixed compact real interval. The upper-density proof gives constants $C, r_0 > 0$ and a cutoff rank independent of s, c such that $\mathbb{P}_{N,s,c}(|S_N| \leq r) \leq Cr^2$ for $0 < r < r_0$. One may include every integer $N > c_+$ in this upper bound. Only finitely many extra ranks occur. At those ranks $z = \sqrt{1 - c/N}$ varies on a compact subinterval of $(0, 1)$. For $N \geq 3$ use the integrable Fourier bound of Section 2, for $N = 2$ the local trace density and bounded weight after the disk change of variables in Section 4, and for $N = 1$ the mark stays a positive distance from zero. Normalizing masses have positive minima by continuity. Enlarging C and reducing r_0 over these finitely many ranks proves the assertion. For each fixed c, s the lower density in (15.2) gives a matching lower multiple of r^2 for sufficiently large N.

16. Finite-size expansions at positive microscopic depth

Expansion of the Fourier determinant

Theorem 16.1 (compact complex sources). Let $F(c, s; p, q)$ denote the limiting unnormalized Fourier source at fixed positive depth, with $p = \bar{\zeta}, q = \zeta$ on the physical plane. Keep p, q independent in holomorphic formulas. For every compact subset of $0 < c < \infty$, $s, p, q \in \mathbb{C}$, the first correction is

$$N^{-s^2} D_N = F + N^{-1}\mathcal{L}F + O(N^{-2}), \qquad \mathcal{L} = (cs + c^2/2)\partial_c + s^2(s + c/2) + isc(p + q)/4. \tag{16.1}$$

This includes finite derivatives in p, q by Cauchy estimates. In particular the mixed integer derivative, $(-4)^j \partial_p^j \partial_q^j$ at zero, gives the first correction for every $j \geq 0$ and every complex tilt s. The calculation also applies to tests with Fourier transforms supported in a fixed compact set.

Expansion of the finite Hankel factors. Use the exact logarithmic depth $a = -N \log z$ and $t = N\theta$. On the physical circle the logarithmic ratio and the positive mark have exact forms

$$\log \frac{1 - ze^{-it/N}}{1 - ze^{it/N}} = -it/N + \log \frac{a + it}{a - it} + \log \frac{\sinh((a + it)/(2N))}{(a + it)/(2N)} - \log \frac{\sinh((a - it)/(2N))}{(a - it)/(2N)},$$
$$f_z(e^{it/N}) = \sinh(a/N)\{\coth((a - it)/(2N)) - 1\}.$$

The logarithm of the rational quotient here is the difference of its two logarithms, continuous from $t = 0$. Write B_a for the limiting ratio symbol in the half-line determinant at depth $2a$ and $b_N = e^{V_- - V_+}$ for the finite symbol at t/N. Put $d_a = i(p - q)a/2$. Uniformly for $|t| \leq \pi N$,

$$b_N(t) = B_a(t)[1 + (d_a - ist)/N] + R_N(t), \qquad |R_N^{(j)}(t)| \leq C_j N^{-2}(1 + |t|)^{2-j} \quad (0 \leq j \leq 4).$$

Indeed $\log(\sinh w/w) = O(w^2)$ and $\coth w - 1/w = O(w)$ on the relevant bounded complex region away from the nonzero zeros of $\sinh w$. For derivatives continue into disks centered at t of radii $\delta(1 + |t|)$ for sufficiently small fixed δ on the depth compact. There $|a \pm it'| \gtrsim 1 + |t|$, both local logarithm branches have bounded difference, and $|(a \pm it')/(2N)|$ stays separated from nonzero zeros of sinh. The zeroth remainder bound and the derivative bounds follow by Taylor's formula for the exponential and Cauchy's estimates. The inverse symbol has the analogous expansion with both first-order signs reversed.

Write u_+, u_- for the limiting Fourier factors at depth $2a$. Four integrations by parts in the original periodic coefficient give, at $v = n/N \geq 1$,

$$N(b_N)_n = u_+(v) + N^{-1}[su'_+(v) + d_a u_+(v)] + O(N^{-2}v^{-4}),$$
$$N(b_N^{-1})_{-n} = u_-(v) + N^{-1}[su'_-(v) - d_a u_-(v)] + O(N^{-2}v^{-4}).$$

In this display the coefficient on the left uses the angle Fourier convention. The integral of the fourth remainder derivative on the finite interval is $O(N^{-2})$. Extending the two main fourth derivatives to the line costs $O(N^{-3})$,

since $B_a^{(j)} = O((1+|t|)^{-j})$, and $(tB_a)^{(j)} = O((1+|t|)^{1-j})$. The Fourier transform of $-itB_a$ at positive frequency is u'_+; one can use tempered distributions here since only $v \geq 1$ is needed. The negative-sign Fourier convention for the inverse gives the second formula. The factors and their first several frequency derivatives decrease as any specified inverse power on $v \geq 1$: integrate sufficiently high derivatives of $t^k B_a^{\pm 1}$, which are integrable. These estimates are uniform on parameter compacts.

Midpoint rule in the determinant. Write $h_0 = 1/N$ and let P project onto constants on the cells of width h_0 on the half-line. The sample $1 + (j+k+1)/N$ is the sum of the two cell midpoints plus one. For a kernel $u(1+x+y)$ as above, its midpoint sample differs from the doubly averaged kernel of PHP by $O(h_0^2(1+x+y)^{-3})$, by Taylor expansion with its bounded, decreasing second derivative. The Hilbert–Schmidt error is $O(h_0^2)$, and $\|(1-P)H\|_2 + \|H(1-P)\|_2 = O(h_0)$ by the one-cell Poincaré inequality. Apply these facts to $H_\pm + h_0(sH'_\pm \pm d_a H_\pm)$ with kernel derivative in the argument. In replacing these two continuum operators by their cell compressions the product's low-to-low trace-norm error is $O(h_0^2)$, since every missed middle high component supplies two $O(h_0)$ factors. Its high-to-high trace norm is also $O(h_0^2)$. The remaining off-diagonal blocks have trace norm $O(h_0)$. Their first Fredholm determinant variation at the low diagonal block vanishes by conjugation by $2P - I$; the quadratic error is $O(h_0^2)$ by the Fredholm series (first and second derivatives are bounded on bounded trace-norm balls). Thus rank loss from the cell projection entails no first-order endpoint term. The d_a terms cancel in the product. The $sH'_\pm$ terms differentiate its determinant with respect to a common shift of its two kernel arguments, even if that determinant vanishes.

For a real shift λ near zero, kernels $u_\pm^a(1+\lambda+x+y)$ have Fredholm product determinant equal to that at depth $2a(1+\lambda)$: $B_a(t)$ depends on t/a, so $u_\pm^a(v) = a u_\pm^1(av)$, and dilation on the half-line proves the assertion. Its first derivative, multiplied by s, is the required perturbation for complex as well as real s, by complex linearity. Depth derivatives can be taken directly in the integrable differentiated-symbol bounds. At the prescribed $z^2 = 1 - c/N$, $2a = c + c^2/(2N) + O(N^{-2})$. The exact prefactor is $c^{-s^2} \exp[-isz(p+q)/2 - pq/4]$. Expanding this and the depth shift gives $\mathcal{L}$ above. Working at $c = 0$ would invalidate the bounds on the logarithms.

The correction for noninteger and inverse moments

Theorem 16.2 (integer tilt and continuous order). Fix an integer s, a compact positive depth interval and a compact subset of $\Re h > -1$. Let $M(c, s; h, u)$ be the limiting unnormalized moment of $|S+u|^{2h}$ under the limiting measure, with u real, and abbreviate its value at $u = 0$ by M. For every $\epsilon > 0$ (in particular for $0 < \epsilon < 1$),

$$N^{-s^2} T_N(h, s; \sqrt{1 - c/N}) = M + \frac{1}{N}\left[(cs + c^2/2)\partial_c M + s^2(s + c/2)M + \frac{sc}{2}\partial_u M(c, s; h, 0)\right] + O_\epsilon(N^{-2+\epsilon}). \quad (16.2)$$

For $s = 0$ only $(c^2/2)\partial_c M$ remains. The two derivatives here are derivatives of the evaluated moment. In particular the translation derivative at a strongly negative exponent is not defined by integrating a pointwise derivative of the singular power. The proof uses the Fourier readout throughout. The integer condition applies to the tilt alone.

A finite-rank comparison in Fourier coordinates. Write $d = 1/N$, $a = -N \log z$, $b = 1 + s/N$, $p = \bar{\zeta}$, $q = \zeta$, $\rho = |\zeta|$. On $L^2(\mathbb{R}, dx)$ let L be convolution with

$$\ell(x) = a[p e^{-ax} \mathbf{1}_{x>0} + q e^{ax} \mathbf{1}_{x<0}].$$

Its real Fourier multiplier (on the physical plane) is the real component of the limiting mark at depth $2a$, since $\int_0^\infty e^{-ax} e^{itx} dx = (a - it)^{-1}$. It is self-adjoint, and its norm and its norm from L^2 to H^1 are $O(\rho)$ on the stated depth compacts. Let P be the projection onto step functions on the full mesh of width d, with cells $[kd, (k+1)d)$ and their normalized indicators as basis. Put

$$R = (ad/2)\coth(ad/2) = 1 + O(d^2), \qquad \alpha = (p+q)ad\,\frac{ad - 1 + e^{-ad}}{(ad)^2}.$$

In the cell basis the full lattice operator for the finite real mark $\Re(pf_z)$ is **exactly** $RPLP - R\alpha I$ on PL^2. The diagonal of PLP is α, obtained by integration over the two triangles of a cell. Its upper and lower off-diagonal coefficients are the respective exponential coefficients of ℓ times $d[\sinh(ad/2)/(ad/2)]^2$. Multiplication by R yields

the finite coefficients $p\sinh(ad)e^{-akd}$ at $k>0$, and their conjugates at negative k. Thus exponentiation, before compressing to the band of occupied modes, gives the actual finite angular phase.

Let Q_0 multiply by $\mathbf{1}_{[0,b]}$. Define $Q=Q_0+\sigma E$, where $\sigma=-\operatorname{sign} s$. For $s>0$, E projects onto the span of x^je^{ax} on $[0,b]$, $0\le j<s$, extended by zero. For $s=-m<0$, use $(x-b)^je^{-a(x-b)}$ on $[b,\infty)$, $0\le j<m$. For $s=0$ put $E=0$. Let E_P project onto the span of the cell averages of the same functions and $Q'=Q_0+\sigma E_P$. The finite tilted polynomial projection, after changing its unimodular gauge if needed, is exactly PQ' in the cell basis. For positive tilt, multiplication by $(1-zw)^s$ embeds the polynomial space into degrees below $N+s$. Its image vanishes to order s at $1/z$, so the missing coefficient vectors span k^jz^{-k} there. For $s=-m$ the image after multiplication by $(1-zw)^{-m}$ contains the first $N-m$ monomials; the next m independent tails, starting at $N-m$, span jth-degree polynomials in the tail index times z^k. This follows by expanding $(1-zw)^{-l}$ for $1\le l\le m$. Cell averages of polynomial times exponential give exactly these spans by an invertible triangular change of basis. All partition-function factors are restored after the probability comparison below.

The centered determinant. For either projection Q, the operator $A=QLQ+(I-Q)L(I-Q)$ is bounded and self-adjoint, and $B=L-A$ has bounded finite rank independent of N. For Q_0 the map from $[0,b]$ to its two exterior intervals is the sum of two separated exponential kernels. Replacing Q_0 by Q adds only boundedly many finite-rank terms. In particular B has a rank-one decomposition whose factors, split into the three intervals at $0,b$, have bounded H^1 norms, with a total coefficient bound $C\rho$. For clarity, the extra terms in $B=(I-Q)LQ+QL(I-Q)$ have range or corange generated by the selected normalized exponential-polynomial vectors, their images under L and the restrictions of these images. The $L^2\to H^1$ bound and bounded Gram inverses on compact a,b give the stated factor bounds.

On the occupied subspace use the determinant of $Qe^{-iA}e^{iL}Q$, extended by the identity on its complement. This is a contraction differing from the identity by a trace-class operator, since

$$e^{-iA}e^{iL}-I=i\int_0^1 e^{-itA}Be^{itL}\,dt.$$

In a finite occupied subspace it is exactly the centered determinant, with the deterministic mean phase removed. The same formula applies with RL in place of L.

Here are the comparison details that retain two powers of mesh size. The finite collection defining E can be chosen orthonormal with piecewise H^1 bounds. The orthogonal projections E,E_P have distance $O(d)$ by the one-cell Poincaré inequality. A unitary U rotates their ranges into one another inside their span, preserves Q_0, and is the identity off the at most $2|s|$ involved dimensions. In the $P,I-P$ splitting its off-diagonal blocks are $O(d)$ and its two diagonal blocks differ from the identity by $O(d^2)$. Indeed diagonalize the finite Gram matrix of the cell averages. Each unit principal vector then has the form $\cos\theta\,v+\sin\theta\,w$ with $v\in P$, $w\perp P$, $\sin\theta=O(d)$. The plane rotation has diagonal change $1-\cos\theta=O(d^2)$. Thus $UQU^*=Q'$ and Q' commutes with P. Put $L'=ULU^*$, $A'=UAU^*$ and $B'=UBU^*$. We have

$$\|(I-P)L'P\|+\|(I-P)A'P\|\le Cd\rho,\qquad \|P(L'-L)P\|_1\le Cd^2\rho.$$

The first inequality follows from Poincaré and piecewise smoothing for L,A before rotation. For the second, expand the diagonal block of ULU^*, using the $O(d^2)$ diagonal change, $O(d)$ off-diagonal change and $\|(I-P)LP\|=O(d\rho)$; all differences have bounded finite rank.

For each smooth rank-one factor v of B with bounded piecewise H^1 norm, $\|(I-P)e^{itL'}Uv\|+\|(I-P)e^{itA'}Uv\|\le Cd(1+\rho)$ for $|t|\le 2$. Before rotation this follows from $e^{itA}v=v+i\int_0^t Ae^{iuA}v\,du$ and the $L^2\to H^1$ bound on each piece (and likewise for L); unitarity controls the integral. Rotation costs $O(d)$ in norm. Duhamel after projecting the evolution consequently gives

$$\|Pe^{itL'}Uv-e^{itPL'P}PUv\|+\|Pe^{itA'}Uv-e^{itPA'P}PUv\|\le Cd^2\rho(1+\rho).$$

Indeed the forcing is $PL'(I-P)e^{iuL'}Uv$ or its A' counterpart. These bounds apply unchanged after the bounded rescaling $L\mapsto RL$.

Compress the interaction integral above to Q' and denote the resulting defect from identity by J. Its P-to-P block differs from the purely discrete centered defect using $PL'P$ by $O(d^2(1+\rho)^4)$ in trace norm: use the last estimates on each factor in the rank-one decomposition, then integrate. The double-high block of J has trace

norm $O(d^2(1+\rho)^3)$ and its mixed blocks have total trace norm $O(d(1+\rho)^2)$. Removing these mixed blocks changes the determinant only quadratically in their norm. In detail, at any contraction the first and second determinant variations in trace-class directions are bounded by the respective products of their trace norms. In finite dimension this follows by expanding the directions into rank-one singular vectors and using the bound one on every exterior-power minor of the contraction. For identity plus trace class, finite-dimensional orthogonal compressions and trace-norm approximation give the same estimates. The off-diagonal first variation vanishes under conjugation by $2P - I$; the line from the diagonal pinch to the full operator consists of contractions. It follows that the two centered determinants differ by $O(d^2(1+\rho)^K)$ for a fixed finite K. Replacing $PL'P$ by PLP costs $O(d^2\rho)$ in the centered comparison, by their trace-norm difference, Duhamel for the two unitaries, and the first variation bound. This argument needs no inverse for a compressed determinant.

Mean, dilation and the moment. The finite normalized mean of the directional statistic is

$$R[s\alpha + \sigma \operatorname{Tr}(E_P L)].$$

Here the Nb base cells contribute $Nb\alpha$ and subtraction of the scalar on the N occupied modes removes $N\alpha$. Replacing E_P by E in the trace costs $O(d^2\rho)$ by the same rotation block calculation. Also $R = 1 + O(d^2)$ and $R\alpha = (p+q)ad/2 + O(d^2\rho)$. Replacing RL by L in the continuum centered determinant costs $O(d^2(1+\rho)^K)$: differentiating its finite-rank interaction integral with respect to R differentiates two bounded unitary evolutions and the explicit factor RB. At $b = 1$, the limiting determinant with centered interaction and mean $\sigma \operatorname{Tr}(EL)$ is the normalized law of the continuum mark, since the finite determinants converge to it and the already established compact-source limit is unique. Dilation $x = bv$ gives the same continuum expression at depth $2ab$ when the occupied interval has length b. The preceding results therefore compare the finite normalized source directly to

$$e^{isad(p+q)/2}\,\chi(2ab, s; p, q)$$

with absolute error $O(d^2(1+\rho)^K)$ on the entire physical frequency plane. On every compact complex source set the same error is $O(d^2)$ and controls jets by Cauchy estimates. To justify the latter version of the comparison, L, A may be non-self-adjoint there, but their norms are bounded, evolution norms are bounded by exponentials of those fixed norms, and the trace norm of the interaction defect is bounded independently of N. Ordinary Fredholm derivative bounds on this fixed ball replace the contraction bound. Equivalently one may use the compact-source correction after dividing by its positive mass.

The finite characteristic function and the translated limiting one separately satisfy uniform inverse-power decay of arbitrary prescribed order by the microscopic Fourier damping theorem, with N sufficiently large for the prescribed order. Interpolating their bound for every fixed inverse power with the global comparison above gives, for every k and $0 < \epsilon < 1$,

$$|\chi_N - e^{isad(p+q)/2}\chi(2ab, s; p, q)| \le C_{k,\epsilon} d^{2-\epsilon}(1+\rho)^{-k}.$$

Restore the mass by the compact-source correction at $p = q = 0$. For the circular Mellin readout, the compact-source $O(d^2)$ estimate controls the origin after all required Taylor subtractions and the removable integer values; the displayed bound controls the infinite tail. This yields the moment at shifted depth $2ab = c + d(cs + c^2/2) + O(d^2)$ and real translation $sad = scd/2 + O(d^2)$.

For completeness, depth and translation derivatives of the limiting integrand also pass through this readout. In the representation on the fixed band $b = 1$, the convolution, the regular finite-rank perturbations and their defining factors have derivatives through every fixed order in a with norms polynomial in $1 + \rho$ on depth compacts. Their orthogonal projections are smooth there by the fixed positive Gram matrices. Differentiate the interaction integral and the unitary evolutions by Duhamel. The centered defect extended by the identity on the complement has trace-class derivatives with polynomial bounds; the exterior-power minor bound at a contraction gives polynomial bounds for the derivatives of its determinant. Pure translations multiply it by a unitary phase with the same property. Local finite-difference interpolation in a now gives rapid decay of each fixed derivative: approximate the jth derivative by a finite-difference formula of order one with steps $(1+\rho)^{-L}$, use arbitrarily rapid decay of the function on a slightly larger depth compact, and bound the error by the polynomial bound on its $(j+1)$st derivative times the step. Take L arbitrarily large. Near bounded frequencies Cauchy estimates allow source jets as before. Taylor expansion of the resulting twice differentiable shifted moment, together with the restored mass factor, gives the claimed coefficient.

A fixed pair of Hardy spaces

Theorem 16.3 (fixed-depth Fourier expansion at real tilt). Put $z_N = \sqrt{1 - c/N}$ and let $F_N(c, s; p) = N^{-s^2} D_N$ on the physical plane, where $p = \bar{\zeta}$. For each compact interval of positive depths, compact interval of real tilts, and fixed nonnegative integers r, k, there are coefficients F_j and a constant such that, for sufficiently large N,

$$\sup_p (1 + |p|)^k \left| F_N(c, s; p) - \sum_{j=0}^{r} N^{-j} F_j(c, s; p) \right| \le C N^{-r-1}. \tag{16.3}$$

Here $F_0 = F$ of (16.1). We give a prescription for every coefficient. No growth estimate uniform in the order r is needed.

Complementary determinant.

Use $w = e^{i\theta}$ and work on the full circle Fourier space. Let J_- and J_+ be the isometric injections of the modes $k < 0$ and $k \ge N$, respectively. For real s, put $D(w) = (1 - zw)^s$ (the branch continuous from $z = 0$) and $b = D/\overline{D}$. Let $W = (J_-, bJ_+)$ act from the direct sum of the two exterior half-lines, and $G = W^*W$. The occupied space $\mathcal{Q} = D \operatorname{span}(1, w, \dots, w^{N-1})$ gives the probability-tilted determinantal ensemble, up to a unitary multiplication gauge. It equals $H_{\ge 0} \cap bH_{<N}$. Indeed an element of the intersection divided by D belongs to $H_{\ge 0}$ by the bounded analytic multiplier $1/D$ and belongs to $H_{<N}$ by division by the bounded coanalytic multiplier $\overline{D}$ in the second description. The converse follows by multiplication. The two exterior ranges have trivial intersection: $f_- = bf_+$ gives $\overline{D} f_- = D f_+$ in two disjoint Fourier half-lines. The overlap $J_-^* b J_+$ is trace class for fixed N, z, by smoothness of b and rapid decay of its circle coefficients. Therefore $G - I$ is trace class, its kernel is zero, and G is boundedly invertible. The range of W is closed and equals $\mathcal{Q}^\perp$.

Write Q for the projection on $\mathcal{Q}$, $J = WG^{-1/2}$ and L for multiplication by $\Re(pf_z)$ with $p = \bar{\zeta}$ and $f_z = (1 - z^2)w/(1 - zw)$. The exterior reference generator and its propagation are

$$B = (J_-^* L J_-) \oplus (J_+^* L J_+), \qquad C = W^* e^{-iL} W, \qquad T = e^{iB} C.$$

In particular the off-diagonal symbols occurring in C are be^{-iL} and $\bar{b}e^{-iL}$. They have modulus one on the physical Fourier plane. The exact finite probability characteristic function is

$$\chi_N(p) = e^{-isz\Re p} \frac{\det T}{\det G}.$$

To verify the identity, put $A = JBJ^*$, extended by zero on $\mathcal{Q}$. The operator $L - A$ is trace class. Blocks touching the finite-dimensional range of Q have finite rank; the exterior compression differs from B by trace-class terms because $G^{-1/2} - I$ and $W^*LW - B$ are trace class. The latter difference has only off-diagonal blocks, from the two smooth symbols Lb and $L\bar{b}$. It follows by differentiating $e^{itL}e^{-itA}$ and using cyclicity of a trace-class product that $\det(e^{iL}e^{-iA}) = e^{i \operatorname{Tr}(L-A)}$. For any invertible $V = I+$ trace class, the complementary-minor identity gives $\det_Q(QVQ) = \det V \, \det_{I-Q}((I - Q)V^{-1}(I - Q))$, using determinants on the indicated subspaces. This follows by the finite-dimensional Jacobi identity and finite-rank approximation of $V - I$ on subspaces containing Q; it does not require the compressed minor to be invertible. Apply it to $V = e^{iL}e^{-iA}$. The occupied minor is the desired characteristic function. The complementary minor in the isometric coordinates J is $e^{iB}G^{-1/2}CG^{-1/2}$. It is identity plus trace class, and so is T. Fredholm multiplicativity and unitary conjugation of $G^{-1/2}$ give its determinant as $\det T / \det G$.

For the phase, $W^*LW - B$ has zero trace. Hence cyclicity applied to the trace-class differences yields

$$\operatorname{Tr}(L - A) = \operatorname{Tr}(QL) + \operatorname{Tr}\left[(G^{-1} - I)W^*LW\right] = \operatorname{Tr}\left[(I - J_-J_-^* - bJ_+J_+^*\bar{b})L\right].$$

The unweighted middle band contributes $N \int L \, d\theta/(2\pi) = 0$. For the remaining difference $J_+J_+^* - bJ_+J_+^*\bar{b}$, its diagonal relative to normalized angle measure is $(1/i)\partial_\theta b \bar{b}$: in its kernel take the diagonal limit of $e^{iN(\theta-\phi)}[1 - b(\theta)\overline{b(\phi)}]/[1 - e^{i(\theta-\phi)}]$. Smoothness removes the diagonal singularity; the possible diagonal distribution in the half-space projection is killed by its zero numerator. Equivalently this diagonal follows by Abel summation of the geometric kernel and integration. With $b = e^{i\kappa}$ we have $\kappa' = -2s \sum_{j \ge 1} z^j \cos(j\theta)$. Integrating against L gives $-sz\Re p$, proving the claim. The zero-source Borodin–Okounkov formula gives $\det G = (1 - z^2)^{s^2} Z_N$. Indeed

$\det G = \det(I - (J_-^* b J_+)^*(J_-^* b J_+))$ and the two Hankel factors have the Fourier coefficients of b at negative indices and b^{-1} at positive indices.

Restoring the mass gives the exact identity

$$F_N(c, s; p) = c^{-s^2} e^{-isz\Re p} \det T. \tag{16.4}$$

This is the source used below. The division by the Gram determinant has disappeared.

Disk change of coordinates. Put $d = 1/N$, $z = e^{-ad}$ and $\mu = (\lambda - z)/(1 - z\lambda)$. The unitary change on the full angular L^2 space, from λ to μ, is composition with $I_z(\mu) = (\mu + z)/(1 + z\mu)$ and multiplication by $(1 - z^2)^{1/2}/(1 + z\mu)$. Its modulus squared supplies the angular Jacobian. The multiplier and the forward and inverse substitutions are bounded analytic in the open disk for fixed $z < 1$. Both maps preserve the Hardy space H_+. Unitarity therefore preserves its orthogonal complement H_-. The finite complementary pair consequently becomes H_- and $W_d H_+$ on this one fixed circle, with

$$W_d(w) = w^{-s} I_z(w)^{N+s} = w^{-s} \left(\frac{1 - tP(w)}{1 + tP(w)} \right)^{N+s}, \quad P(w) = \frac{1 - w}{1 + w}, \quad t = \tanh(ad/2).$$

This expression denotes the boundary phase obtained from $\lambda^N (1 - z\lambda)^s/(1 - z/\lambda)^s$. On $w = e^{i\psi}$, $-\pi < \psi < \pi$, take the continuous argument for I_z from $I_z(1) = 1$. On the interior slit disk use separate principal logs of w and $I_z(w)$. The jumps cancel on $(-1, -z)$ for integer N. The diagonal observable is now multiplication by $z + \mu$. The factors in T contain opposite scalar phases from $z\Re p$, so this constant cancels exactly inside T. The physical one-particle generator is then $l(w) = \Re(pw)$ and $U_\tau = e^{i\tau l}$; neither depends on the mesh.

Estimates for the relative phase. For w in the slit disk the expansion in d of W_d at zero has coefficients

$$W_j(w) = w^{-s} e^{-aP(w)} Q_j(P(w); a, s), \qquad Q_0 = 1.$$

Here Q_j is a polynomial in P, obtained by multiplying formal series for the exponential of

$$-2(d^{-1} + s) \operatorname{arctanh}\big(\tanh(ad/2)P\big).$$

For example $Q_1 = -saP$ and $Q_2 = (saP)^2/2 + a^3(P - P^3)/12$. Derivatives of fixed order with respect to a give the same class of bounds. In the statements below one may also substitute $a(d, c) = -\log(1 - cd)/(2d)$ directly and expand at fixed c; it is smooth at zero with positive limit $c/2$.

Write Fourier coefficients as $[f]_n = \int f(e^{i\psi}) e^{-in\psi} d\psi/(2\pi)$. For N sufficiently large, every integer $J, L \geq 0$, and $E = W_d - \sum_{j=0}^{J} d^j W_j$, one has

$$|[E]_{-n}| \leq C d^{J+1} (1 + n)^{-L} \quad (n \geq 1), \qquad |[E]_m| \leq C d^{J+1} (1 + m)^{K_J} \quad (m \geq 0).$$

The coefficient distributions W_j are defined by approaching the unit circle radially from the slit disk. The opposite off-diagonal symbol at complex tilt is the continuation $\overline{W_{j,\bar{s}}}$ on the circle. The bounds are uniform on compact $a > 0$ and real s intervals.

Here are details of the contour estimates. On $1/4 \leq |w| < 1$ the modulus of w^{-s} is bounded; $\Re P > 0$ and $|I_z(w)| \leq 1$. When $d(1 + |P|)$ is smaller than a fixed constant, derivatives through order $J + 1$ in real d of the exponent above are bounded by fixed polynomials in $1 + |P|$, by the convergent Taylor series of arctanh and tanh. Its exponential has modulus at most one for all intervening sufficiently small real d and real s. Consequently the Taylor remainder is at most $C d^{J+1} (1 + |P|)^K$ there. When $d(1 + |P|)$ is larger than that constant, bound the exact phase in modulus by C and its Taylor coefficients by polynomials, increasing K to obtain the same estimate. This last estimate requires no differentiated expansion across the point $I_z = 0$.

On the two banks at $w = -x$, $1/4 \leq x < 1$, $P = (1 + x)/(1 - x) > 0$. For $x < z$ and N large the positive base satisfies $I_z(-x)^{N+s} \leq e^{-\kappa P}$ by $\log[(1 - y)/(1 + y)] \leq -2y$, $y = tP \in [0, 1)$. Where $d(1 + P)$ is small, all intervening derivatives of the exponential retain this bound, decreasing $\kappa > 0$ if necessary. On its complement $d(1 + P)$ is bounded below, and a fixed polynomial in P absorbs the required inverse powers of d. For $x \geq z$ the exact phase jump vanishes, while each coefficient jump is bounded by a polynomial in P times e^{-aP}. Thus the jump of E has modulus at most $C d^{J+1} (1 + P)^K e^{-\kappa P}$ on the entire truncated slit.

For $[E]_{-n}$ move the coefficient contour to $|w| = 1/4$ and include the accumulated slit jump. The inner contour gives $O(d^{J+1}4^{-n})$. The slit contribution is bounded by $Cd^{J+1}\int_{1/4}^{1} x^{n-1}(1+P)^K e^{-\kappa P}dx$, which is $O_L(d^{J+1}(1+n)^{-L})$ for every L since the exponential dominates every power of $1-x$. For $[E]_m$ move only to $r = 1-1/(m+2)$; $r^{-m-1} \le 4$ and $|P| \le C(1+m)$ on that circle. The slit integral from r to one obeys the same pointwise exponential bound with $x^{-m-1} \le 4$. These deformations also prove existence of the coefficient distributions at the boundary, by using a second concentric circle tending to one; for W_d itself the resulting values are its ordinary Fourier coefficients by dominated radial convergence for fixed sufficiently large N. For clarity, these radial approximants have Fourier coefficients of uniformly bounded polynomial growth for outer radii $R \ge 3/4$. For negative index $-n$ the partial jump integrates against $(x/R)^{n-1}dx/R$, with bounded jump. For nonnegative index m use the same inner circle $r = 1-1/(m+2)$ when $r < R$, and otherwise use $|P| \le C(1+m)$ directly. This proves distributional radial convergence and permits multiplication by a smooth propagator. No contour reaches the endpoint at zero, so no condition such as $s < 1$ is needed. For a real a derivative in the Taylor region, differentiate the convergent expansion of the exponent and keep the exponential at real a. This costs only a fixed polynomial in $1+|P|$. In the remaining circle region use the elementary derivative $\partial_a I_z = (\partial_a z)(1-w^2)/(1+zw)^2$, $|1+zw| \ge 1-z \gtrsim d$ and $|I_z| \le 1$ at real a: any fixed number of derivatives costs at most a fixed inverse power of d, absorbed by $(1+|P|)^K$ in that region. On the slit the differentiated exact powers have a positive exponent $N+s-k$ for fixed k, preserving exponential damping. The same estimates for the *static symbols* hold for complex s on compact sets by $|w^{-s}| \le C$, $|I_z^{N+s}| \le e^{\pi|\Im s|}|I_z|^{N+\Re s}$. In this analytic extension replace the conjugate static block by its coefficientwise holomorphic continuation from real s.

Multiplication by the physical propagator. For $|\tau| \le 1$, every prescribed number of angular derivatives of U_τ is bounded by a polynomial in $1+|p|$. Its Fourier coefficients therefore decrease to every fixed inverse power, at that polynomial cost. In $[EU_\tau]_{-n}$ sum the negative indices of E using rapid decay on both factors. For nonnegative indices m of E, the other coefficient index is $-n-m$; choose its decay order larger than $K_J + L + 2$. It follows that the negative coefficients of the product obey $Cd^{J+1}(1+|p|)^K(1+n)^{-L}$ to every fixed order L. Conjugation and $\tau \mapsto -\tau$ give the reverse off-diagonal block. For a Hankel matrix on two half-Hardy spaces, the absolute sum of the anti-diagonal trace norms is $\sum_{n\ge1} n|b_{-n}|$. We have thus obtained trace-norm expansions of the cross Gram blocks, the cross generator blocks and the cross propagators to every fixed order, with polynomial dependence on physical frequency. At compact independent complex sources use the same proof on compact sets, replacing unitarity of the propagator by its compact bound. In particular it applies to all fixed origin jets.

Determinant estimate over all frequencies. In the Cayley coordinate let $V_N(f,g) = f + W_d g$ on $H_- \oplus H_+$, $l(w) = \Re(pw)$, and B_l be its block diagonal compression. Equivalently,

$$T_N^{\mathrm{ext}} = e^{iB_l} V_N^* e^{-il} V_N.$$

This superscript distinguishes the exterior operator from the scalar moment $T_N(h,s;z)$. Write V_0 for the pair with boundary multiplier W_0 and T_0^{ext} for its operator. The diagonal of each uncentered matrix is the corresponding compression of e^{-il}. After multiplication by e^{iB_l} it differs from the identity by a trace-class operator. Indeed l has only first harmonics. Its difference from the block diagonal part on the full circle has rank at most two, and Duhamel's formula gives a trace-class difference of the propagators. The off-diagonal terms have the estimates just proved. For each fixed order the expansion of $T_N^{\mathrm{ext}} - T_0^{\mathrm{ext}}$ in trace norm has polynomial frequency costs. In particular its norm is $O(N^{-1}(1+|p|)^K)$.

At real tilt $G_N = V_N^* V_N$ satisfies $\|G_N\| \le 2$ and $\|G_N - I\|_1 \le C$ uniformly in N by the static Hankel bound. This also holds at the limit. Polar decomposition shows that $V_N^* e^{-il} V_N = G_N^{1/2} K_N G_N^{1/2}$ with $\|K_N\| \le 1$. Since $|\sqrt{t}-1| \le |t-1|$ on $t \ge 0$, each T_N^{ext} is within bounded trace norm C_0 of a contraction, uniformly over the entire frequency plane. The segment joining this actual operator to T_0^{ext} has the same property.

For an identity plus trace-class matrix T within trace norm C_0 of a contraction, its determinant variation of order b in directions E_i satisfies

$$|D^b \det(T)[E_1,\dots,E_b]| \le C_b e^{C_0} \prod_{i=1}^{b} \|E_i\|_1.$$

In finite dimension, singular-value comparison bounds every exterior-power norm of T by $\prod_i (1+s_i(K)) \le e^{\|K\|_1}$, where K is the perturbation of the contraction. Expand the directions into rank-one singular terms and use this bound on the complementary minors. Finite-dimensional compression, with identity on the omitted space,

converges in trace norm for $T - I$ and for the directions. The determinant and its derivatives converge by the Fredholm series. Apply Taylor's formula along the segment of actual operators, then substitute the finite trace-norm expansions in the derivatives at T_0^{ext}. The scalar phase in (16.4) also has a Taylor remainder of polynomial cost since its exponent is imaginary. For each $J \geq 1$ this proves the preliminary real-tilt estimate

$$F_N = \sum_{j=0}^{J-1} N^{-j} F_j + O\big(N^{-J}(1+|p|)^{K_J}\big). \tag{16.5}$$

Using the segment avoids applying a contraction estimate to a truncated polynomial outside a bounded set of frequencies.

Decay and explicit coefficients. The real characteristic functions F_N obey the arbitrarily high algebraic decay of Section 15 for sufficiently large N depending on the required power. To prove rapid decay of F_j, use (16.5) at the $j+1$ ranks $N, 2N, \dots, (j+1)N$ through order j, at the same c. Inverting their Vandermonde matrix gives F_j as N^j times a fixed linear combination of the sources with error $O(N^{-1}(1+|p|)^K)$. For a prescribed decay exponent choose N of order $(1+|p|)^A$ with A larger than K plus that exponent, raising N on bounded frequencies when necessary. The uniform source decay absorbs N^j. The remainder in (16.5) therefore has a second bound $C_b(1+|p|)^{-b}$ for arbitrary fixed b. Taking the geometric mean with powers $1-\eta, \eta$ gives $C_{k,\epsilon} N^{-J+\epsilon}(1+|p|)^{-k}$ for any prescribed $k, \epsilon > 0$, by choosing η small and b large. One surplus order proves (16.3).

Here are the first two insertions at fixed c. With $x = \Re p$, write $W_0 = w^{-s} e^{-cP/2}$. Substitution of $a = -\log(1-cd)/(2d)$ gives

$$\begin{aligned} b_1 &= -(c^2/4 + sc/2)P, & W_1 &= W_0 b_1, \\ b_2 &= -(5c^3/32 + sc^2/4)P - c^3P^3/96, & W_2 &= W_0(b_2 + b_1^2/2). \end{aligned} \tag{16.6}$$

Let E_j be the order-j coefficient of T_N^{ext} for $j \geq 1$. It is obtained by inserting W_j in the top-right block and its opposite-wall counterpart in the bottom-left block, followed by the centered diagonal propagation. Its diagonal is zero. Set $Q_0 = \det T_0^{\mathrm{ext}}$, $Q_1 = D\det(T_0^{\mathrm{ext}})[E_1]$, and

$$Q_2 = D\det(T_0^{\mathrm{ext}})[E_2] + \tfrac{1}{2} D^2 \det(T_0^{\mathrm{ext}})[E_1, E_1].$$

In these formulas the determinant derivatives are defined even at a zero of Q_0. Expanding the phase of (16.4) yields

$$F_2 = c^{-s^2} e^{-isx} \left[Q_2 + \frac{iscx}{2} Q_1 + \frac{c^2}{8}(isx - s^2x^2) Q_0 \right]. \tag{16.7}$$

Since $W_1 = (cs + c^2/2)\partial_c W_0$, the first determinant variation differentiates Q_0 in depth. Restoring the mass and phase gives $F_1 = \mathcal{L} F_0$ on the physical plane, independently reproducing (16.1). At order two the term P^3 and the second determinant variation both enter.

Independent complex tilts and the planar measure

Theorem 16.4 (expansion of the complex mark measure). Let c range in a compact subset of $(0, \infty)$ and s in any compact subset of $\mathbb{C}$. Form the unnormalized measure

$$\mu_{N,c,s}(E) = N^{-s^2} \mathbb{E}\left[|\Lambda_N(z_N)|^{2s} \, \mathbf{1}_{\{S_N(z_N) \in E\}} \right].$$

There are smooth rapidly decreasing densities $p_j(c, s; y)$, entire in s for each c, such that for every fixed $r, k \geq 0$,

$$\int_{\mathbb{C}} (1+|y|)^k \left| d\mu_{N,c,s}(y) - \sum_{j=0}^{r} N^{-j} p_j(c, s; y)\, d^2y \right| = O(N^{-r-1}). \tag{16.8}$$

The same expansion holds in any prescribed finite list of uniform density derivative norms with polynomial weights, for all ranks sufficiently large for that list. In particular, uniformly also for h in compact subsets of $\Re h > -1$,

$$\begin{aligned} N^{-s^2} T_N(h, s; z_N) &= \sum_{j=0}^{r} N^{-j} M_j(c, s; h) + O(N^{-r-1}), \\ M_j(c, s; h) &= \int_{\mathbb{C}} |y|^{2h} p_j(c, s; y)\, d^2y. \end{aligned} \tag{16.9}$$

The moment order and tilt are independent. At real tilt $p_0 = A_s(c)p_{s,c}$ in the notation of Theorem 15.1.

A bound for comparable ranks. Write $s = u + iv$. For each real frequency multi-index α, the finite Fourier transforms are entire functions of s and have the bound

$$|\partial_p^\alpha F_N(c, s; p)| \le N^{v^2} N^{-u^2} \mathbb{E}\big[|\Lambda_N|^{2u}(1 + |S_N|)^{|\alpha|}\big] \le C_\alpha N^{v^2}. \tag{16.10}$$

Here ∂_p^α denotes derivatives in the two real frequency coordinates. Section 15 gives bounded real-tilt moments of every fixed positive order on the indicated compacts. This estimate leaves the possibly growing variation on the original ensemble explicit.

Fix an integer J. Choose weights $w_{j\ell}$ for $0 \le j < J$, $1 \le \ell \le J$, by $\sum_\ell w_{j\ell}\ell^{-k} = \mathbf{1}_{j=k}$ for $0 \le k < J$. Put

$$X_{n,j} = n^j \sum_{\ell=1}^{J} w_{j\ell} F_{\ell n}(c, s; p), \qquad F_n = \sum_{j=0}^{J-1} n^{-j} X_{n,j}.$$

The last identity is exact because 1 is one of the interpolation nodes $1/\ell$. For $L \le n, m \le 2L$ form $Y = L^{-j}(X_{n,j} - X_{m,j})$. On the real tilt axis the same coefficient F_j is recovered at either rank. The improved bound following (16.5) thus gives $|Y| \le CL^{-J+\epsilon}(1 + |p|)^{-b}$ for every fixed b and $\epsilon > 0$. One may differentiate this estimate at the price of an arbitrarily small increase in ϵ. Indeed for derivative order l approximate by a finite-difference formula with Taylor remainder of order t^M on an $O_{l,M}(t)$ neighborhood. The first term costs Ct^{-l} times the bound for Y. The remainder costs Ct^M by (16.10) on the real axis since the factor L^{-j} cancels n^j, m^j. Take $t = L^{-\delta}(1+|p|)^{-1}$ with δl as small as desired. Choose M large enough to absorb the requested rank and frequency powers, increasing b for the undifferentiated estimate. Mixed derivatives follow by polarization of directional derivatives. All constants can depend on the fixed orders.

Holomorphic interpolation. Fix a desired tilt compact, let $v_0 = \max|\Im s|$, and take $H = \sqrt{J} > v_0$. On a rectangle with real base and top at height H, (16.10) bounds each $|\partial_p^\alpha Y|$ by CL^{H^2}. On the base we have the much smaller differentiated bound just obtained. For interior points in the desired compact, the harmonic measure of the union of the top and sides is at most $v_0/H + \delta$ for any fixed $\delta > 0$, by increasing the rectangle's width. For example on the rectangle of half-width B centered horizontally at u_0, a harmonic majorant of the indicator of its top and sides is

$$\frac{v}{H} + \frac{\cosh(\gamma(u - u_0))\cos(\gamma(v - H/2))}{\cosh(\gamma B)\cos(\gamma H/2)}, \qquad \gamma = \pi/(2H).$$

Apply the maximum principle for $\log|\partial_p^\alpha Y|$, using a limit at zeros. The bottom harmonic weight is bounded away from zero, so taking b large retains any fixed power k of frequency decay. The reflected rectangle handles negative heights. This proves for each $\epsilon > 0$

$$\sup_p (1 + |p|)^k |\partial_p^\alpha (X_{n,j} - X_{m,j})| \le CL^{j-q}, \qquad q = J - 2\sqrt{J}\, v_0 - \epsilon. \tag{16.11}$$

Only finitely wide rectangles are used. Constants on their widely separated real ends may depend on J.

If $j < q$, sum (16.11) over successive dyadic ranks and compare an arbitrary intervening rank to its adjacent dyadic rank. This gives a limit F_j with error $O(n^{j-q})$ in the stated seminorm. For $j \ge q$ the sum from a fixed base rank gives $O(1 + n^{j-q}(1 + \log n))$ for $X_{n,j}$ in the same seminorm. Choose the base rank sufficiently large: Proposition 2.1 gives any prescribed algebraic decay there for each of the finitely many differentiated finite sources by increasing that fixed rank. Its constants are finite on the fixed depth and tilt compact since the corresponding radii lie in $(0, 1)$. Local uniform convergence gives holomorphic limits. Constructions with different J agree by uniqueness on real tilts and the identity theorem on overlapping rectangles. Choosing J with $q > r + 2$ and substituting in the exact reconstruction gives the error $O(n^{-r-1})$ after order r in each desired Fourier seminorm. The unused coefficients with $r < j < q$ are bounded after taking their limits, and the rest cost $O(n^{-q}(1 + \log n))$.

Fourier inversion and integration by parts convert these estimates to the asserted uniform weighted density and derivative bounds. Indeed weights in y become Fourier derivatives, and derivatives in y become frequency multipliers. Choose enough frequency decay for the resulting integrals to converge absolutely, then choose more than two extra spatial weight powers for the integral in (16.8). The limiting coefficients are entire in the tilt by locally uniform Fourier inversion. Integrate the uniform density remainder on $|y| \le 1$ against $|y|^{2\Re h}$, using $\int_0^1 t^{2\Re h+1} dt < \infty$. Away from this disk use (16.8) with sufficient weight. This proves (16.9) with ordinary

integrals, jointly holomorphic in (h, s) on the indicated domain. For bounded physical frequencies the coefficient formulas (16.6)–(16.7) continue holomorphically too. Their contour bounds hold locally in complex s, and the opposite multiplier there is $\overline{W_{j,\bar{s}}}$. Uniqueness from the real axis identifies these explicit coefficients with the Fourier transforms of p_j.

First moment coefficient. Write $M(c, s; h, u) = \int |y + u|^{2h} p_0(c, s; y)\, d^2y$ for real translation u, and $M = M(c, s; h, 0)$. Then (16.2)'s coefficient holds for every complex s and $\Re h > -1$:

$$M_1 = (cs + c^2/2)\partial_c M + s^2(s + c/2)M + (sc/2)\partial_u M(c, s; h, 0). \tag{16.12}$$

Translation is defined by translating the density in this formula, which remains valid for singular inverse powers. For the depth derivative, (16.1) identifies $\partial_c F_0$ pointwise wherever $cs + c^2/2 \neq 0$. There it is a linear combination of the rapidly decreasing F_1, F_0, xF_0 divided by that nonzero scalar, so all needed uniform seminorms hold. At a point $s = -c/2$, apply Cauchy's integral formula in s on a small circle about that point, keeping the denominator nonzero on the contour for all nearby real depths. Differentiation of that contour formula extends the uniform estimates across the point. Thus both derivatives pass through Fourier inversion and the ordinary density integral, proving (16.12). At $s = 0$ only the depth derivative remains.

Corollary 16.5 (exceptional tilts and the Mellin poles). At each fixed $c > 0$ the limiting mass and the central value $p_0(c, s; 0)$ are entire functions of s, both strictly positive on the real axis by Theorem 15.1. Each zero set is discrete. Where the mass is nonzero, division by the actual finite mass for sufficiently large N and by its limit gives convergence of the mass-one complex measures in weighted variation. Where the central density is nonzero, its modulus is bounded below near zero and the absolute-moment domain of the limiting measure is exactly $\Re h > -1$. For the original finite matrix expectation at $N \geq 2$, $0 < z < 1$, the domain of absolute integrability already follows from Section 5, since taking the modulus replaces the tilt by $\Re s$.

The leading moment has a meromorphic continuation in h with possible simple poles at $-1 - j$, $j = 0, 1, \ldots$, and residues

$$\operatorname*{Res}_{h=-1-j} M_0(c, s; h) = \frac{\pi \Delta^j p_0(c, s; 0)}{4^j (j!)^2}. \tag{16.13}$$

Indeed, the circular average of a smooth planar density has Taylor coefficient $\Delta^j p_0(0)/(4^j(j!)^2)$ at r^{2j}, by angular averaging its Taylor polynomial. Subtract a finite number of terms on the unit disk, integrate $2\pi r^{2h+1+2j}$ there, and repeat to each desired half-plane. Rapid decay controls the outer integral. In particular the pole at -1 occurs whenever $p_0(c, s; 0) \neq 0$. The meromorphic values outside the domain of absolute integrability are separate from the underlying expectations.

At an exceptional complex tilt the density jets still give a criterion. If m is the least total degree of a nonzero Taylor term of $p_0(c, s; y)$ at zero, its absolute-moment threshold is $\Re h > -1 - m/2$. Taylor's bound proves sufficiency, and the leading homogeneous polynomial is bounded away from zero in modulus on an angular interval after restriction to the unit circle, proving necessity on that cone. If all jets vanish, every inverse power is locally integrable. The actual exceptional tilts and their orders of vanishing are undetermined here.

The residue formula also holds with M_j, p_j for each coefficient. More generally, on a prescribed compact set of h avoiding the possible poles, subtract sufficiently many circular Taylor terms from each finite density and from its expansion. The resulting Mellin functional is bounded by finitely many of the weighted density seminorms of Theorem 16.4. Indeed Taylor's remainder on the unit disk gains the required power of radius, each integrated subtraction is a bounded evaluation of a density jet times $1/(h + 1 + k)$, and the exterior is controlled by a polynomial weight. Thus (16.9) extends with its error order on that compact for these regularized integrals at sufficiently large rank. The residues themselves have the corresponding expansion by evaluating Laplacians at zero.

17. The unit-circle determinant and its mixed moment

Write $D_N(s, z; \zeta)$ for the Fourier-source Toeplitz determinant of $S_N(z) = -(1 - z^2)\Lambda_N'(z)/\Lambda_N(z)$, in the convention $e^{i \operatorname{Re}(\bar{\zeta} S_N)}$. The circle readout is obtained at fixed N by using $\zeta = \eta/(1 - z^2)$ before taking $z \uparrow 1$. The real and imaginary components of η have different roles in this limit.

Proposition 17.1 (circle determinant). For $\lambda = e^{i\theta} \neq 1$,

$$\frac{\lambda}{1-\lambda} = -\frac{1}{2} + \frac{i}{2}\cot(\theta/2).$$

Let $Z_N(s) = \mathbb{E}|\Lambda_N(1)|^{2s}$ and put $t = \operatorname{Im}\eta/2$. Taking the limit of each entry of the Toeplitz determinant gives

$$\mathcal{D}_N(s;\eta) := \lim_{z\uparrow 1} D_N(s,z;\eta/(1-z^2)) = e^{-iN\operatorname{Re}\eta/2} Z_N(s)\,\chi_{N,s}(t). \tag{17.1}$$

Here $\chi_{N,s}(t)$ is the Toeplitz determinant for the symbol $|1-e^{i\theta}|^{2s}e^{it\cot(\theta/2)}$, divided by its value at $t=0$. For $\operatorname{Re} s > -1/2$, entrywise dominated convergence is valid: the phase has modulus one, $|1-ze^{i\theta}|^2 = (1-z)^2 + z|1-e^{i\theta}|^2$, and negative real powers of the latter are locally integrable at zero in this range. Nonnegative real powers are bounded. For real s the normalized determinant is the characteristic function of $Y_N = \sum_j \cot(\theta_j/2)$ under the probability tilt $|\Lambda_N(1)|^{2s}/Z_N(s)$. For a complex tilt it denotes the corresponding normalized complex integral; the zero-source Selberg product below has no zeros in the indicated half-plane.

To evaluate (17.1) set $y = \cot(\theta/2)$, $\nu = N+s$, and $F_\nu(t) = \int_{\mathbb{R}} e^{ity}(1+y^2)^{-\nu}\,dy$. The Toeplitz basis $1,\lambda,\dots,\lambda^{N-1}$ becomes the rational basis $((y+i)/(y-i))^j$. Multiplying through its common denominator gives polynomials $(y+i)^j(y-i)^{N-1-j}$, a basis in degrees at most $N-1$ by independence of $1,\lambda,\dots,\lambda^{N-1}$. The squared denominator and the Cayley Jacobian change the weight to a constant times $(1+y^2)^{-\nu}dy$. The two basis changes cancel in the quotient, so

$$\chi_{N,s}(t) = \frac{\det[i^{-(j+k)}F_\nu^{(j+k)}(t)]_{j,k=0}^{N-1}}{\det[i^{-(j+k)}F_\nu^{(j+k)}(0)]_{j,k=0}^{N-1}}. \tag{17.2}$$

All required moments up to order $2N-2$ converge absolutely for $\operatorname{Re} s > -1/2$. This derivation is a change of basis in a single determinant. By Andréief, expanding (17.2) also identifies the joint law of the y_j at real s as proportional to $\Delta(y)^2\prod_j(1+y_j^2)^{-N-s}\,d^Ny$. This is the eigenvalue law of the Hua–Pickrell probability measure in the normalization specified below.

For $b = |t| > 0$, Laplace-transforming the weight and integrating the Gaussian gives

$$F_\nu(t) = \frac{2\sqrt{\pi}}{\Gamma(\nu)}(b/2)^{\nu-1/2}K_{\nu-1/2}(b) = \frac{2^{2-2\nu}\pi}{\Gamma(\nu)}e^{-b}U(1-\nu,2-2\nu,2b).$$

This provides the finite Kummer determinant in (17.2), with its normalization at zero imposed by continuity. More explicitly, for $t>0$ its numerator is proportional to e^{-Nt} times

$$\det\big[(-2)^{j+k}(1-\nu)_{j+k}U(1-\nu+j+k,2-2\nu+j+k,2t)\big]_{j,k=0}^{N-1}.$$

The constant is independent of t. Indeed, in the Hankel determinant for the derivatives of $e^{-t}f(t)$ the binomial change $d/dt \mapsto d/dt - 1$ acts by unit lower triangular matrices on both indices. Complex parameters at polynomial specializations are interpreted by continuity of the differentiated function. Reflection $y \mapsto -y$ gives evenness in t.

Theorem 17.2 (circle limit at large matrix size). Here take $s > -1/2$ real, and let X_s be the limiting normalized trace of the Hua–Pickrell ensemble. The established inputs used at this point are

$$Y_N/N \Rightarrow X_s, \qquad \sup_N \mathbb{E}_s|Y_N/N|^{2r} < \infty \quad (0 < r < s+1/2),$$

and the Selberg–Barnes evaluation

$$Z_N(s) = \frac{G(N+1+2s)G(N+1)G(1+s)^2}{G(N+1+s)^2G(1+2s)}, \qquad N^{-s^2}Z_N(s) \longrightarrow g_s = \frac{G(1+s)^2}{G(1+2s)}.$$

The trace convergence is Theorem 2.2 of Assiotis–Keating–Warren (Borodin–Olshanski and Qiu); their Theorem 2.4 gives the Barnes formula. Their Theorem 1.2 combined with Proposition 2.7 and Theorem 2.4 gives convergence, hence boundedness, of every positive moment in the stated range. The complex-s normalization in (17.1) follows from the real product by holomorphic continuation at fixed N. These are external limit and normalization inputs; they do not follow from entrywise convergence in (17.1).

Define $\tau_s(u) = \mathbb{E}e^{iuX_s/2}$. By evenness and weak convergence, (17.1) with η/N now gives

$$N^{-s^2}\mathcal{D}_N(s;\eta/N) \longrightarrow g_s e^{-i\operatorname{Re}\eta/2}\tau_s(|\operatorname{Im}\eta|). \tag{17.3}$$

The convergence of the characteristic functions is uniform on compact real arguments, hence locally uniform in η. In the corresponding standard Painlevé normalization $t\,d\log\chi_{N,s}(t/(2N))/dt$ obeys a finite-size σ-Painlevé V equation and $t\,d\log\tau_s(t)/dt$ a σ-Painlevé III′ equation on $t>0$, by Assiotis–Bedert–Gunes–Soor, Proposition 2.1 and Theorem 1.2. Their notation $\phi^{(s)}$ denotes our τ_s; their $\tau^{(s)}$ denotes its logarithmic derivative multiplied by t.

Uncentred derivative at the circle. For Haar-almost every matrix, $\Lambda_N(1)\neq 0$ and

$$\left|\frac{\Lambda_N'(1)}{\Lambda_N(1)}\right|^2 = \frac{N^2+Y_N^2}{4}.$$

Thus the circle moment has the finite-size identity

$$N^{-s^2-2h}\mathbb{E}\Big[|\Lambda_N(1)|^{2(s-h)}|\Lambda_N'(1)|^{2h}\Big] = 4^{-h}N^{-s^2}Z_N(s)\mathbb{E}_s\big[(1+(Y_N/N)^2)^h\big], \tag{17.4}$$

where the last expectation acts on the powered integrand. In particular,

$$\lim_{N\to\infty} N^{-s^2-2h}\mathbb{E}\Big[|\Lambda_N(1)|^{2(s-h)}|\Lambda_N'(1)|^{2h}\Big] = 4^{-h}g_s\mathbb{E}\big[(1+X_s^2)^h\big], \qquad \operatorname{Re}h < s+\tfrac12. \tag{17.5}$$

For $\operatorname{Re}h\le 0$, $(1+y^2)^h$ is bounded and continuous. Otherwise choose $\operatorname{Re}h < r < s+1/2$; the Hua–Pickrell moment bound at r gives uniform integrability of the powered integrand, so weak convergence suffices after truncation. The same higher moment, chosen above the largest real part on a compact subset, gives locally uniform convergence in h (holomorphy and the normal-family theorem). The 1+ is essential for the ordinary complex characteristic polynomial; the derivative of a characteristic polynomial made real on the circle has a different readout.

The finite-size upper threshold is sharp. For large $|y_1|$ with the other y_j in disjoint fixed bounded intervals, the density in (17.2) is comparable to $|y_1|^{-2s-2}$ and $|Y_N|$ to $|y_1|$. For the converse bound, $|y_j-y_k|^2 \le 2(1+y_j^2)(1+y_k^2)$ bounds the joint density by a constant times $\prod_j(1+y_j^2)^{-1-s}$. These bounds yield absolute existence exactly for $\operatorname{Re}h < s+1/2$.

The moment in (17.4) is evaluated at the circle. Its interior counterpart, before scaling in N, is $(1-z^2)^{-2h}T_N(h,s;z) = \mathbb{E}[|\Lambda_N(z)|^{2s}|\sum_j \lambda_j/(1-z\lambda_j)|^{2h}]$. An actual radial moment limit at fixed N can additionally be taken when $0\le\operatorname{Re}h < s+1/2$: bound $|\sum_j\lambda_j/(1-z\lambda_j)|^{2\operatorname{Re}h}$ by a fixed constant times $\sum_j|1-z\lambda_j|^{-2\operatorname{Re}h}$. Multiplication by $|\Lambda_N(z)|^{2s}$ gives integrable product majorants by the single-angle inequality used for (17.1), since the exponents on each term are $s-\operatorname{Re}h$ at one angle and s at all others; the Haar Vandermonde is bounded on the torus.

Theorem 17.3 (fixed-rank radial limit). For $N\ge 2$, $s>-1/2$ real and $-1<\sigma=\operatorname{Re}h<0$, the radial moment also converges. This needs a small-ball estimate uniform as $z\uparrow 1$. Let $\delta=1-z$, $F=\sum_j\lambda_j/(1-z\lambda_j)$, $w_j=(\lambda_j-z)/(1-z\lambda_j)$ and $u_j=1+w_j$. Fix $r_0=N/8$. On $|F|\le r_0$ we have

$$\sum_j u_j = N\delta+(1-z^2)F, \qquad \sum_j|u_j|^2 = 2N\delta+2(1-z^2)\operatorname{Re}F \asymp_N \delta, \qquad \left|\sum_j \operatorname{Im}u_j\right| \le 2r_0\delta.$$

The middle equality uses $|u|^2=2\operatorname{Re}u$ for $|u-1|=1$. All $|u_j|=O_N(\sqrt{\delta})$; at least one is bounded below by $c_N\sqrt{\delta}$. Since $\operatorname{Re}u_j=|u_j|^2/2$, that component has imaginary part of modulus at least $c_N'\sqrt{\delta}$ for small δ. The sum of the imaginary parts is only $O_N(\delta)$, so another component of opposite sign has imaginary part of modulus at least $c_N''\sqrt{\delta}$. Cover the small-ball event by the finitely many index pairs with these properties.

For each such pair j,k, write $w_j=e^{i\psi_j}$, $A_j=|1-z\lambda_j|$. Both $A_j,A_k\asymp_N\sqrt{\delta}$, since $A_j=(1-z^2)/|\delta+zu_j|$. Also $|\sin(\psi_j-\psi_k)|\gtrsim_N\sqrt{\delta}$: the cosines are close to -1 and the sines have opposite signs and the displayed lower

bounds. Keeping all other angles fixed, the Jacobian of the two remaining angles into the plane of F has absolute determinant

$$J_{jk} = \frac{|\sin(\psi_j - \psi_k)|}{A_j^2 A_k^2} \gtrsim_N \delta^{-3/2}.$$

Indeed $\partial_{\theta_j}(\lambda_j/(1-z\lambda_j)) = iw_j/A_j^2$. On this part of the event the map has at most two preimages at any output: the sum $w_j + w_k$ is prescribed, it is close to -2, and two ordered points on the unit circle with a given nonzero sum have at most two choices. The selected Vandermonde factor satisfies $|\lambda_j - \lambda_k|^2 = O_N(\delta)$ because both $|1-\lambda_j|$ and $|1-\lambda_k|$ are at most $O_N(\sqrt{\delta})$. Bound the other Vandermonde factors by constants. The two selected tilt factors are $O_{N,s}(\delta^{2s})$ together, and each of the other angle integrals of A_l^{2s} stays bounded for $s > -1/2$. By the area change of variables, followed by summing over the pairs,

$$\mathbb{E}\big[|\Lambda_N(z)|^{2s}\,\mathbf{1}_{\{|F|\le r\}}\big] \le C_{N,s}\delta^{5/2+2s}r^2, \qquad 0 < r \le r_0, \quad 0 < \delta < \delta_N. \tag{17.6}$$

Dyadically summing this estimate on the shells $2^{-m-1}r_0 < |F| \le 2^{-m}r_0$ bounds the entire weighted contribution of $|F|^{2\sigma}$ on $|F| \le r_0$ by $O_{N,s,\sigma}(\delta^{5/2+2s}r_0^{2+2\sigma})$, which tends to zero. Off this event $|F|^{2\sigma}$ is bounded; the tilt has the integrable majorant already used in (17.1). The limiting F has real part $-N/2$, and hence always lies outside this event. Dominated convergence proves the radial moment limit. At rank two the power of δ in (17.6) agrees with the exact density at zero: the density for $S_2 = (1-z^2)F$ at zero is $(1-z^2)^{2s+1/2}/(2\pi^2 z)$, so the density for F there is $(1-z^2)^{2s+5/2}/(2\pi^2 z)$.

In summary, the unscaled interior mixed moment tends to the circle mixed moment for all $-1 < \operatorname{Re} h < s + 1/2$ at fixed $N \ge 2$. The lower bound is necessary for an ordinary interior expectation because a noncolliding zero of F gives a positive planar density contribution when $0 < z < 1$. For example at $N = 2$, $s = 0$, $h = -1$, every ordinary interior expectation diverges while (17.4) on the circle is finite. At $N = 1$ one has $|\Lambda_1'| = 1$, so the radial limit holds for every $\operatorname{Re} h < s + 1/2$ by the one-angle majorant. The existence of circle values at arbitrarily negative exponents in (17.5) remains a separate statement.

Normalization controls. At $s = 0$, $U(1-N, 2-2N, 2t)$ is a polynomial of degree $N-1$. Its derivative Hankel determinant is constant and nonzero because the entries above derivative order $N-1$ vanish while the order $N-1$ antidiagonal is nonzero. Consequently $\chi_{N,0}(t) = e^{-N|t|}$ for every N, so Y_N/N is exactly standard Cauchy. In particular (17.4) then equals $4^{-h}\Gamma(1/2-h)/(\sqrt{\pi}\Gamma(1-h))$ for $\operatorname{Re} h < 1/2$, without an asymptotic error. For $s = h = 1$, one has $g_1 = 1$ and $\mathbb{E}X_1^2 = 1/3$ (Assiotis–Keating–Warren, eq. (6)). Formula (17.5) gives $1/3$, agreeing with $N^{-3}\sum_{j=1}^{N} j^2$ in the limit. These check respectively the factor of two in (17.3) and the additive 1 in (17.5).

Sources include Assiotis, Keating and Warren, *On the Joint Moments of the Characteristic Polynomials of Random Unitary Matrices*; Assiotis, Bedert, Gunes and Soor, *On a distinguished family of random variables and Painlevé equations*.

18. The transition to Gaussian moments at growing depth

Theorem 18.1 (simultaneous approach from the disk). Let $d = 1 - z^2$, $c = Nd$ and $z \uparrow 1$. For h on a compact subset of $\Re h > -1$ and s in a compact subset of $\mathbb{C}$, there are constants $C, \kappa, c_0 > 0$ such that, for z sufficiently close to one and $c \ge c_0$,

$$\left|d^{s^2}T_N(h,s;z) - \Gamma(1+h)\,{}_1F_1(-h;1;-s^2z^2)\right| \le C(1+d^{-(\Im s)^2})e^{-\kappa c}. \tag{18.1}$$

Consequently every real tilt admits the transition for every $c_N \to \infty$ with $z_N \uparrow 1$, including all microscopic inverse exponents in the ordinary domain. For arbitrary fixed complex tilt it suffices that $\log(1/d_N) = o(c_N)$. The finite-size comparison retains z_N in the Gaussian mean. For h a nonnegative integer the same comparison has error $O(e^{-\kappa c})$ for all complex tilts in a compact set without the logarithmic restriction. The form of the Gaussian moment is the known fixed-interior value; the growing-depth estimates establish the simultaneous limit.

Frequencies below a fixed multiple of depth. Use $b = \exp(V_- - V_+)$, $e = b^{-1}$ and the two shifted Hankel factors in the finite Borodin–Okounkov identity above. Write $\delta = 1 - z$. For $|\Im\theta| \le \delta/4$ both $1 - ze^{\pm i\theta}$ have positive real part and modulus comparable to $Q = \delta + |\Re\theta|$ on $|\Re\theta| \le \pi$. Their principal log difference is bounded there: the ratio of moduli stays bounded above and below and both arguments are bounded. The marks are

bounded since $d = O(\delta)$. Thus $|b|+|e| \le Ce^{C\rho}$ where $|p|+|q| \le 2\rho+2$ for the two independent source coordinates. The log derivatives are bounded in order one by $C(1+\rho)/(\delta+|\Re\theta|)$ and in order two by $C(1+\rho)/(\delta+|\Re\theta|)^2$. It follows that the integrals of $|b''|+|e''|$ over either shifted line are at most $C\delta^{-1}(1+\rho)^2e^{C\rho}$. Shifting the coefficient contour down for b_k and up for e_{-k}, and integrating twice by parts, bounds each by

$$C\delta^{-1}(1+\rho)^2e^{C\rho-k\delta/4}k^{-2}, \qquad k > N.$$

The square of either tail Hilbert–Schmidt norm sums $(k-N)$ times the squared coefficient. Hence the product trace norm is $O(e^{-ac})$ uniformly for $0 \le \rho \le \epsilon c$, for suitable $a, \epsilon > 0$, since $N\delta = c/(1+z)$. Using $|\det(I-A)-1| \le e^{\|A\|_1} - 1$,

$$d^{s^2} D_N(s, z; \zeta) = e^{-isz\Re\zeta - |\zeta|^2/4}\,[1 + O(e^{-ac})], \qquad |\zeta| \le \epsilon c.$$

On a fixed complexified source polydisk this is a holomorphic estimate, so the finitely many jets and Taylor remainders on a smaller polydisk satisfy the same error. At zero frequency the normalized real-tilt mass is $1 + O(e^{-ac})$.

The remaining frequencies. Put $u = \Re s$, $v = \Im s$ and take the *real* interior probability tilt u. In its projection determinant insert the phase $\phi(t) = \rho g_\beta(t) + v \log|1 - ze^{it/N}|^2$, $t = N\theta$. The polynomial evaluation proof above has constants independent of $c \ge 1$: the Lipschitz bound for $|1 - ze^{i\theta}|$ divided by its minimum $\delta \ge 1/(2N)$ gives the required two-sided weight ratio $C(1+N\operatorname{dist}(\theta,\phi))^{2|u|}$. Thus its scaled kernel is bounded below on separations at most $\eta > 0$, uniformly for the parameters here. The trace defect of the projection compression bounds the modulus of the characteristic determinant.

Fix a small numerical $d_0 > 0$. On $L \le |t| \le 2L$ with $L \ge Ac$, $2L \le d_0N$ and A a fixed sufficiently large number, the angle $\psi = 2\arctan[(1+z)\tan(t/(2N))/(1-z)]$ satisfies $\psi' \asymp c/L^2$, $|\sin\psi| \asymp c/L$ and $-\cos\psi \asymp 1$. Choose the sign of t as in the microscopic proof. The derivative of $g_\beta = z\cos\beta + \cos(\psi - \beta)$ has fixed sign and has size

$$\frac{c}{L^2}\left(|\sin\beta| + \frac{c}{L}|\cos\beta|\right).$$

The additional angle derivative of $v\log|1 - ze^{it/N}|^2$ is $O(|v|/L)$ on this shell. For $\epsilon c \le \rho \le Mc$ take $L = Ac$. Then $\rho|g'_\beta|$ is bounded below by a positive constant and its supremum is comparable to its infimum; for large c the added tilt derivative is smaller than half this infimum. For $\rho \ge Mc$, take

$$L = \min\{bc^{2/3}\rho^{1/3},\ d_0N/2\}.$$

Choose b fixed and M sufficiently large that $L \ge Ac$ (also choose z close enough to one to ensure $Ac \le d_0N/2$). The bound $\rho c^2/L^3 \ge b^{-3}$ again supplies a fixed lower bound and absorbs the tilt derivative. On either shell, integration of $1 - \cos(\phi(t') - \phi(t))$ over a one-sided interval of length η is bounded below by a fixed positive constant: substitute the monotone phase difference and use $H - \sin H$ with $H \ge H_0 > 0$ and a bounded derivative ratio. Integration in t therefore gives suppression e^{-a_1L}. Returning from the probability tilt to $d^{s^2}D_N$ costs at most Cd^{-v^2}, by the zero-frequency comparison for u.

For $\rho \ge N^M$ (increasing M if necessary) use the same Möbius change and entrywise oscillatory estimate as at fixed depth. Here $(1-z)^{-1} \le 2N$. The additional amplitude $e^{iv\log|1-ze^{i\theta}|^2}$ has total variation $O(1 + |v|\log N)$, so all amplitudes still have supremum and variation bounded by a fixed power of N for compact s. Hadamard's bound, divided by the real mass $Z_N(u,z) \ge 1$, is at most $\rho^{-N/4}$ for all sufficiently large N. For any fixed polynomial weight in ρ the integral of the resulting positive majorant from ϵc to infinity is $O(d^{-v^2}e^{-a_2c})$. Indeed integrate $e^{-a_1bc^{2/3}\rho^{1/3}}$ until the shell saturates; the saturation plateau contributes at most a polynomial in N times e^{-a_3N} up to N^M, and the final power tail is smaller. Constants and the lower rank threshold can depend on the polynomial weight.

Insert the two frequency estimates in the circular Mellin formula. At the origin subtract a common Taylor polynomial of degree exceeding the compact range of $2\Re h$; Cauchy's estimate on the compact-source difference controls its remainder and the removed jets by $O(e^{-ac})$. The simple integer denominators are canceled by $1/\Gamma(-h)$ as in the fixed-interior proof. From one to ϵc the Gaussian comparison error is integrable against every fixed power, and beyond ϵc use the preceding tail bound. This proves the estimate. The Gaussian Mellin integral gives the stated Kummer value by the computation above. The integer readouts require only the compact jets. Equivalently, for any fixed derivative order the real tilted planar densities converge uniformly through that order to the Gaussian with mean $-sz_N$ and variance $\mathbb{E}|G|^2 = 1$, with error $O(e^{-\kappa c})$. On sending N to infinity first at a sufficiently large fixed depth and then sending c to infinity, the same inequalities recover the large-depth asymptotics of the real microscopic coefficient.

Arbitrary rates at complex tilt

Theorem 18.2 (unrestricted growing depth). Fix compact sets $S \subset \mathbb{C}$ and $K \subset \{\Re h > -1\}$. There are $C, \kappa, c_0 > 0$ and $d_0 \in (0,1)$ such that, with $d = 1 - z^2 \le d_0$ and $c = Nd \ge c_0$,

$$\left| d^{s^2} T_N(h, s; z) - \Gamma(1+h)\, {}_1F_1(-h; 1; -s^2 z^2) \right| \le C e^{-\kappa c} \qquad (s \in S,\ h \in K). \tag{18.2}$$

The Gaussian expression is the known fixed-interior value. The estimate compares with this value at the actual z, for every relative growth rate of rank and depth. This is a statement about the unnormalized complex moment.

Uniform price of the real-tilt expansions. In the following comparisons keep c fixed when the rank n changes, put $z_n = (1 - c/n)^{1/2}$, and take $n \ge Bc$ for fixed sufficiently large B. Write

$$H_n = (c/n)^{s^2} D_n, \qquad Z_n^{\mathrm{G}}(p) = \exp(-i s z_n \Re p - |p|^2/4).$$

At real tilt the preliminary estimate (16.5) applies to $H_n - Z_n^{\mathrm{G}}$ with remainder $C_J(1 + c + |p|)^{A_J} n^{-J}$ for all $c \ge c_0$. Here A_J is finite; coefficients may depend on c. We justify the dependence on c, which is essential in this use of Section 16.

Put $b = 1/n$, $t(b) = (1 - \sqrt{1 - cb})/(1 + \sqrt{1 - cb}) = cb/(1 + \sqrt{1 - cb})^2$. On $0 \le cb \le 1/B$, this is a smooth function of cb with uniformly bounded derivatives in that variable. In $b(1 + c)(1 + |P|) \le \delta$ the power series for $-2(b^{-1} + s)\operatorname{arctanh}(t(b)P)$ and its first J real b derivatives have polynomial bounds in $1 + c + |P|$. The apparent singularity $t(b)/b$ is removable. For example the analytic expression for the exponent on a complex b-disk of radius proportional to $[(1+c)(1+|P|)]^{-1}$ is bounded by $C(1+c)(1+|P|)$; Cauchy on a smaller disk bounds these derivatives. Exponentiation is differentiated on the *real* b interval, where $|I_z(w)|^{1/b+s} \le 1$. Taylor's bound there has polynomial cost. On the complementary region $b^{-1} \le C(1 + c)(1 + |P|)$ absorbs the required inverse powers by increasing the polynomial degree. On the two banks of the slit the exact jump for $x < z$ retains $e^{-\gamma c P(-x)}$ because $t(b)/b \ge c/4$ and $1 + bs \ge 1/2$. The Taylor terms and their real remainders on the small-parameter region retain this exponential with smaller γ. For $x \ge z$ the exact jump vanishes and the Taylor terms retain it. On $|w| = 1/4$ all powers of P are bounded; on $|w| = 1 - 1/(m + 2)$ they are polynomial in $1 + m$. Thus the slit proof of (16.5) costs at most powers of $1 + c$ in every fixed mode estimate. In the zeroth-order static symbols themselves the inner contour is uniformly bounded and the bank jump is bounded by $Ce^{-\gamma c P}$. This gives $\|G_n - I\|_1 + \|G_0 - I\|_1 \le C$ independent of c (negative modes are bounded by $C_L(1 + k)^{-L}$). Consequently the determinant variation bound along the actual segment costs a constant C_J, uniformly in c. All remaining constructions are sums and products of a fixed number of polynomial bounds. The prefactor c^{-s^2} cancels under the growing-depth normalization, while the phase $e^{-isz_n \Re p}$ has polynomial Taylor costs at real tilt. The Gaussian source has the same property. This proves the preliminary bound.

The two source estimates in the proof of Theorem 18.1 give $|H_n| + |Z_n^{\mathrm{G}}| \le C_k(1 + |p|)^{-k}$ uniformly for real s in any fixed compact, $c \ge c_0$, $n \ge Bc$, for each fixed k (enlarge B, c_0 if needed). This follows from the Gaussian bound below ϵc, exponential shell suppression above it, and the power tail beyond n^M; on the saturation plateau the frequency is at most n^M. All frequency derivatives of fixed order are separately bounded in the uniform norm, by real positive absolute moments from Theorem 18.1. Constants may depend on the compact real interval.

Cancellation at comparable ranks. Work first with the source difference $E_n(p) = H_n - Z_n^{\mathrm{G}}$. Fix J and use the unique weights from Section 16, $\sum_{\ell=1}^{J} w_{j\ell} \ell^{-k} = \mathbf{1}_{j=k}$ for $0 \le j, k < J$. Write

$$X_{n,j} = n^j \sum_{\ell=1}^{J} w_{j\ell} E_{\ell n}, \qquad E_n = \sum_{j=0}^{J-1} n^{-j} X_{n,j}.$$

For $L \le m, n \le 2L$ and $L \ge Bc$, put $Y = L^{-j}(X_{n,j} - X_{m,j})$. The fixed-$c$ coefficients through order $J - 1$ cancel. Thus $|Y| \le C(1 + c + |p|)^A L^{-J}$ on the real tilt axis. Since Y is a bounded linear combination of actual sources it also has arbitrarily high uniform algebraic frequency decay. Taking a geometric mean gives $|Y| \le C(1 + c)^A L^{-J+\epsilon}(1 + |p|)^{-k}$ for any prescribed $\epsilon > 0$ and k. The same bound, with arbitrarily small additional rank loss, holds for each fixed frequency derivative. As in (16.10)–(16.11), apply finite differences of arbitrarily high order at step $L^{-\delta}(1 + |p|)^{-1}$. The undifferentiated bound pays the inverse step powers upon increasing k and taking δ small. The Taylor remainder is bounded by an arbitrarily high step power using the uniform higher-derivative bound just obtained. Fourier inversion and integration by parts now give this rank

error for the density of the signed difference with any chosen polynomial spatial weight. Integration against $|y|^{2h}$ is uniform on K, by a bounded density on the disk and a sufficiently high spatial weight outside. From this point use E_n and $X_{n,j}$ for the corresponding *scalar moment errors*, so that $E_n = (c/n)^{s^2} T_n - \Gamma(1+h)_1F_1(-h;1;-s^2 z_n^2)$. The real-axis bound on $L^{-j}(X_{n,j} - X_{m,j})$ is $C(1+c)^A L^{-J+\epsilon}$.

For complex $s = u + iv$ the absolute expectation gives $|(c/n)^{s^2} T_n(h, s; z_n)| \le (n/c)^{v^2} (c/n)^{u^2} T_n(\Re h, u; z_n) \le C(n/c)^{v^2}$ by Theorem 18.1 at real tilt. The Gaussian moment is bounded on the parameter compact. Take $v_0 = \max_S |\Im s|$ and a fixed J with $q = J - 2\sqrt{J}\, v_0 - \epsilon > 0$. For $0 \le v \le \sqrt{J}$ on the finite, wide tilt rectangle used for (16.11), the absolute bound for Y is $C_J L^J$. On the base it is the high-order bound above. The harmonic measure argument of (16.11), choosing the half-width sufficiently large and using the reflected rectangle on the lower half-plane, gives

$$|X_{n,j} - X_{m,j}| \le C(1+c)^A L^{j-q}.$$

All required constants are independent of n, m, L, c, with the indicated compact choices. In particular the finite depth price is polynomial; the maximum principle contributes no exponent growing with depth.

Anchor and telescoping. Put $n_0 = \lceil e^{\eta c} \rceil$ with fixed $\eta > 0$ sufficiently small depending on S, K. At ranks $r \le Jn_0$, $r \ge Bc$, Theorem 18.1 gives $|E_r| \le Ce^{-ac}$, because $((r/c)^{v_0^2} + 1)e^{-\kappa_0 c} \le Ce^{-ac}$ after reducing η. In particular $|X_{n_0,j}| \le Cn_0^j e^{-ac}$. For $N > n_0$, telescope $X_{n,j}$ at ranks $n_0, 2n_0, \dots, 2^M n_0 \le N$ and then at N. Dividing every increment by *the terminal* N^j gives the summed bound

$$C(1+c)^A \sum_{m=0}^{M} (2^m n_0/N)^j (2^m n_0)^{-q} \le C'(1+c)^A n_0^{-q}.$$

This argument requires only $q > 0$, also for the higher unused coefficients. The exact finite reconstruction of E_N and the anchor estimate give $C[e^{-ac} + (1+c)^A e^{-\eta q c}]$, bounded by $C'e^{-\kappa c}$. This proves (18.2), including independent noninteger inverse exponents. No probability normalization at a nonreal tilt is used.

Planar version. The same comparison holds before taking the Mellin integral. For every fixed finite list of derivative orders and polynomial spatial weights, the density of the d^{s^2}-scaled mark measure differs by $O(e^{-\kappa c})$ in the corresponding weighted uniform norms from

$$g_{s,z}(x+iy) = \pi^{-1} \exp\{-(x+sz)^2 - y^2\}.$$

It also differs by this order in every fixed polynomially weighted variation norm, with constants and the threshold rank allowed to depend on the norm. For real s this is the Gaussian with mean $-sz$. The expression is its analytic continuation in s as a complex planar density, with total absolute mass $e^{z^2(\Im s)^2}$.

To verify the stronger claim, carry the real-axis bound for the source derivatives of Y directly through the tilt rectangle. At nonreal tilt $u + iv$, a fixed frequency derivative of the finite source costs at most $C(n/c)^{v^2}$ by its real-tilt positive moments; the Gaussian derivatives obey a bounded version. In the interpolation of (16.11) the harmonic weight of the real base is uniformly positive, so an arbitrarily large power of frequency decay on that base retains any specified power after interpolation. It remains to verify the exponentially small anchor error in those same seminorms. The low-frequency complex comparison of Theorem 18.1 gives, at $\rho \le \epsilon c$, $Ce^{-ac}e^{-\rho^2/4 + |\Im s|\rho}$. Its two high-frequency bounds above ϵc give a bound by $C_k[(n/c)^{v^2} + 1]e^{-a'c}(1+\rho)^{-k}$: use part of each exponential shell bound to pay the fixed polynomial, and on the saturated plateau $\rho \le n^M$ the factor e^{-an} absorbs it. Beyond n^M split off half of the available power $\rho^{-n/4}$. Thus $n \le Jn_0$ gives fixed seminorms of the *values* with exponentially small errors by decreasing η. Differentiate by the same finite-difference formula, this time using step $e^{-\delta c}(1+\rho)^{-1}$. The inverse step cost is absorbed by choosing δ small and the input decay exponent large; in the Taylor remainder choose sufficiently high order to dominate $C(Jn_0/c)^{v_0^2}$. Now the same telescoping applies in each chosen seminorm. Fourier inversion gives the stated density and variation estimates. This recovers (18.2) directly by the uniform density error in the unit disk and the weighted variation error on its exterior.

19. The approach to the circle at shrinking depth

Theorem 19.1 (simultaneous circle limit). Let $c = N(1-z^2) \downarrow 0$ as $N \to \infty$, let $s > -1/2$ be real, and set $A = 1 + 4\max(-s, 0)$ and $\alpha = s + 1/2$. With the Hua–Pickrell variable X_s and Barnes mass g_s defined in the

circle section, one has

$$N^{-s^2}c^{-2h}T_N(h,s;z)\longrightarrow 4^{-h}g_s\,\mathbb{E}(1+X_s^2)^h,\qquad -\frac{\alpha}{2A+\alpha}<\Re h<s+\tfrac12. \tag{19.1}$$

The sufficient lower endpoint is weaker than the fixed-positive-depth result. In particular this theorem cannot be inferred by inserting $c=0$ in that result. We prove uniform integrability in the displayed range for arbitrary rates $c\downarrow 0$.

Change of preparation and large values. Write $Y=S_N/c$, $t=N\theta$, and let P° be the circle-tilted law at size N. Its intensity satisfies $I^\circ(t)\le C(|t|/(1+|t|))^{2s}$ as shown above. The interior weight relative to the circle tilt is $z^{Ns}W$, where $W=\prod(1+(1-z)^2/(z|1-e^{it/N}|^2))^s$. For $s\ge 0$, $\mathbb{E}^\circ W^p$ stays bounded for some $p>1$ and $\mathbb{E}^\circ W\to 1$. Indeed, for a one-point factor $b(t)$ of W, $b(t)\le(1+Cc^2/t^2)^s$ and Hadamard gives $\mathbb{E}^\circ W^p\le\exp[\int(b^p-1)I^\circ]$. The integrand is dominated at zero when $2s(p-1)<1$, dominated at infinity by C/t^2, and tends to zero. For $-1/2<s<0$ one has $0<W\le 1$ and $\mathbb{E}^\circ|\log W|\to 0$ by the integrable envelope $C\log(1+C/t^2)I^\circ$. Thus the probability change of measure tends to identity in total variation, $z^{Ns}\to 1$, and $N^{-s^2}Z_N(s,z)\to g_s$.

Set $n(t)=(1+ze^{it/N})/[2Nz(1-ze^{it/N})]$. Then

$$Y=-1/(2z)+\sum n(t),\qquad |n(t)|\le C/(c+|t|),\quad 0\le\Re n(t)\le Cc/(c^2+t^2),\quad |\Im n(t)|\le C|t|/(c^2+t^2).$$

On every fixed annulus $0<\epsilon\le|t|\le L$, $n(t)-i\cot(t/(2N))/(2N)$ tends uniformly to zero. Under P° the probability of a point with $|t|<\epsilon$ is $O(\epsilon^{2s+1})$. Beyond L, the expectation of the real tail is $O(c/L)$; the imaginary tail of each statistic has mean zero and variance $O(1/L)$ by the projection variance inequality. Local counts on the annulus are tight. Hence under the circle law $Y-(-1/2+i\sum\cot(t/(2N))/(2N))\to 0$ in probability. The total variation comparison and the known normalized trace limit yield $Y\Rightarrow(-1+iX_s)/2$ under the interior probability.

For clarity, control on the large values of Y survives the change of measure throughout the positive range. Put $a(t)=b(t)$ for $s\ge 0$ and $a(t)=1$ otherwise, and define $\nu(t)=a(t)I^\circ(t)$. On $|t|\le 1$, $\nu(t)\le C(c+|t|)^{2s}$ for $s\ge 0$ and $\nu(t)\le C|t|^{2s}$ for $s<0$. Beyond one it is bounded. The product-correlation inequality, also with one distinguished point, gives

$$\mathbb{E}^\circ\Big[We^{\#\{|t|\le 1\}}\sum f(t)\Big]\le C\int f(t)\nu(t)\,dt\quad(f\ge 0).$$

Indeed expand the nonnegative product with factors $a(t)e^{\mathbf{1}_{|t|\le 1}}\ge 1$, single out the chosen point with its own factor, bound each joint intensity by the product of the one-point intensities, and sum the exponential series. Its exponent is uniformly bounded by the preceding estimates. For $0<q<2s+1$, the qth power of $\sum_{|t|\le 1}|n(t)|$ is bounded by a constant times $e^{\#\{|t|\le 1\}}\sum_{|t|\le 1}|n(t)|^q$ (also valid for $q<1$ by subadditivity). The resulting integral is bounded uniformly: integrate separately $0<t<c$ and $c<t<1$ using the bounds on ν. On $|t|>1$ the bounded real and imaginary marks have uniformly bounded variances via $\int|n|^2I^\circ$; the mean of the real sum is bounded and the imaginary mean is zero. Their exponential moments are uniformly bounded by the determinant exponential estimate already proved, and Hölder with $\mathbb{E}^\circ W^p$ transfers every positive power of these exterior sums. This proves convergence of positive moments with $2\Re h<2s+1$.

A near-zero estimate for the shrinking-depth readout. On $|Y|\le 1/4$ the real mark sum must exceed $1/4$. The weighted one-point inequality bounds the chance of at least one point within $|t|<\sqrt{c}$ by $Cc^{s+1/2}$. If there is none, take a fixed integer $m>\alpha$ and expand the mth power of the remaining nonnegative real sum by grouping repeated indices. For $j\ge 1$,

$$\int_{|t|\ge\sqrt{c}}(\Re n(t))^j\nu(t)dt\le C_jc^{\min(j,\alpha)}(1+|\log c|).$$

This follows by integrating c^jt^{2s-2j} from $\sqrt{c}$ to one and c^jt^{-2j} beyond one. The preceding distinguished-point expansion applies to any fixed number of distinct points with the product of their tests, so a block partition $j_1+\cdots+j_k=m$ contributes at most $C_mc^{\sum_i\min(j_i,\alpha)}(1+|\log c|)^m$. That exponent is at least α since $m>\alpha$. Markov's inequality now gives $\mathbb{P}(|Y|\le 1/4)\le C_{\alpha'}c^{\alpha'}$ for every $0<\alpha'<\alpha$. This uses the probability normalization, already bounded above and below relative to P°.

A second bound, uniform in radius, is $\mathbb{P}(|Y| \le r) \le Cc^{-2A}r^2$. Here the origin layer of the angular weight needs care. For the phase shell it suffices to control the scaled projection kernel on $|t| \ge 1$ away from the angular origin. Let $x = N\,\mathrm{dist}(\theta, 0) \ge 1$, $y = N\,\mathrm{dist}(\phi, 0)$ and $D = N\,\mathrm{dist}(\phi, \theta)$. The angular weight is comparable to $N^{-2s}(c + x)^{2s}$ at θ, and to the same expression with y at ϕ. For an integer $m > |s|$, put $Q_\theta(\phi) = [(1 - e^{i\phi})/(1 - e^{i\theta})]^m$. Both

$$|Q_\theta(\phi)|^2 \frac{w(\phi)}{w(\theta)}, \qquad |Q_\theta(\phi)|^2 \frac{w(\theta)}{w(\phi)}$$

are bounded by $C(1+D)^{2m+2|s|}$: use $|Q| \le C(y/x)^m$, $x \ge 1$ and $|x-y| \le D$. The extra zero removes the singular weight or its reciprocal when $y \ll 1$. To obtain the upper evaluation and derivative bounds in the polynomial projection proof, reproduce $Q_\theta p$ using a smooth cutoff allowing degree $N + m$; at θ subtract $Q'_\theta(\theta)p(\theta)$ for the derivative, with $|Q'_\theta(\theta)| \le CN$. For the lower evaluation bound multiply the localized trial polynomial by Q_θ, leaving room for m more degrees. The two ratios above yield exactly the earlier kernel lower bound at microscopic separations on $|t| \ge 2$, uniformly even as $c \downarrow 0$.

For the characteristic function of Y, use frequency ρ/c in the phase-shell proof. On $L \le |t| \le 2L \le d_0 N$, $L \ge L_0$, the same directional choice gives $|(g_\beta/c)'| \asymp L^{-2}(|\sin\beta| + c|\cos\beta|/L)$. For $c^A\rho$ larger than a fixed constant take $L = \min(b(c^A\rho)^{1/3}, d_0N/2)$; then $\rho c/L^3$ is bounded below since $A \ge 1$. The commutator thus gives $\exp[-\kappa \min((c^A\rho)^{1/3}, N)]$. In the far Fourier estimate the inverse Jacobian costs $O(N/c)$ and the weight supremum and variation cost $O((N/c)^{2\max(-s,0)})$. The pure cosine now has frequency ρ/c. The resulting Hadamard bound is $[CN^{5/2+2\max(-s,0)}(c^A\rho)^{-1/2}]^N$. Jensen's lower bound $Z_N \ge 1$ justifies its normalization. Splitting in the variable $c^A\rho$ at a large fixed power of N gives a uniformly integrable two-dimensional Fourier bound in that rescaled variable. Fourier inversion gives the asserted $O(c^{-2A})$ density bound.

For $q = -2\Re h \in (0, 2)$ integrate the smaller of $Cc^{\alpha'}$ and $Cc^{-2A}r^2$ on $0 < r < 1/4$, with any $0 < \alpha' < \alpha$. The layer-cake formula gives $O(c^{\alpha'(1-q/2)-Aq})$ for the inverse-power contribution on this disk. It goes to zero for $\Re h > -\alpha/(2A+\alpha)$ on choosing α' close enough to α. The limiting variable has modulus at least $1/2$. Truncating at the two ends proves the stated complex moment limit, including purely imaginary h, with locally uniform convergence on the open strip. No uniform quadratic coefficient as $c \downarrow 0$ is asserted for Y.

The local density and the sharp strip

Theorem 19.2 (shrinking-depth density). Fix $s > -1/2$ real and write $Y = S_N/c$, $c = N(1 - z^2)$, $e_s = 2s + 5/2$. Write $p^Y_{N,s,z}$ for the density under the probability tilt $|\Lambda_N(z)|^{2s}/Z_N(s, z)$ with respect to $d\Re y\, d\Im y$. For every fixed compact D in the open half-plane $\Re y > -1/2$, there exist $C, N_0, c_0 > 0$ depending on s, D such that

$$\mathbb{P}_{N,s,z}(Y \in E) \le Cc^{e_s}\,|E|, \qquad E \subset D \text{ Borel}, \quad N \ge N_0, \quad 0 < c \le c_0. \tag{19.2}$$

Here $|E|$ denotes planar area. The normalized density has the following leading coefficient, uniformly in essential supremum on D along every sequence $N \to \infty$, $c \to 0$:

$$c^{-e_s} p^Y_{N,s,z}(y) \longrightarrow L_s(\Re y), \qquad L_s(x) = \frac{g_{s+2}}{2\pi^2 g_s}(1/2 + x)^{-2s-7/2}. \tag{19.3}$$

The half-plane is the side of the limiting vertical line reached by the rare configurations in this theorem. A disk about zero is a positive distance from that line. In particular any $r = r_N \downarrow 0$ in such a disk satisfies $\mathbb{P}(|Y| \le r) \sim \pi L_s(0) c^{e_s} r^2$. The depth and radius may shrink at unrelated rates.

The starting ensemble in this proof is the interior probability tilt. The limiting circle law identifies where typical values lie. It gives no estimate of the probability density on D. To recover that density, keep the two distinguished eigenangles, their mutual Vandermonde factor and the area Jacobian before integrating over the remaining angles. The two inserted angles also change the exponent of the circle weight for the remaining particles.

An envelope for tagged eigenangles. The period of $t = N\theta$ is $2\pi N$. Let $w(t) = |1 - ze^{it/N}|^{2s}$. For fixed k the interior probability factorial intensity is at most $C_{s,k} \prod \nu(t_j)$ by the circle-tilt product estimate of Section 19. Indeed single out all k points in the nonnegative product expansion with factors $\max(1, b(t))$ and use the determinant Hadamard bound. The denominator of the probability change is bounded below. On $|t| \le 1$ use

$\nu(t) \le C(c+|t|)^{2s}$ for $s \ge 0$ and $C|t|^{2s}$ for $s < 0$. Beyond one ν is bounded. Consequently, for a sufficiently large $L = L(s)$,

$$\int (1+|t|)^{-L} \nu(t) w(t)^{-1} dt \le C N^{2s}.$$

Indeed $w(t) \asymp N^{-2s}(c+|t|)^{2s}$ on $|t| \le \pi N$. At negative tilt the only additional local factor is $(1 + c/|t|)^{2|s|}$, uniformly integrable because $2|s| < 1$.

Take smooth even cutoffs $0 \le \chi, \eta \le 1$ with $\chi = 1$ on $|t| \le 2$ and zero on $|t| \ge 3$, and $\eta = 0$ on $|t| \le 1$ and one on $|t| \ge 2$. Use n as in Section 19. Set

$$K = 1 + \sum \chi + \sum \eta \Re n/c + \left| \sum \eta \Im n \right|, \qquad f_\pm = \chi + \eta \Re n/c \pm \eta \Im n.$$

Then $\mathbf{1}_{K \ge T} \le e^{1-T} \sum_\pm e^{\sum f_\pm}$. The $f_\pm$ have bounded sup norm and total variation in microscopic angle uniformly in N, c. To see this, write

$$a(t) = (1-z)^2 + 4z \sin^2(t/(2N)), \quad \Re n(t) = c/(2N^2 z a(t)), \quad \Im n(t) = \sin(t/N)/(N a(t)).$$

On $1 \le |t| \le \pi N$ the two terms $\Re n/c, \Im n$ have respective size $C/t^2, C/|t|$ and derivatives bounded by $C/|t|^3, C/t^2$. Symmetry kills the mean of the odd part. The intensity bound gives $|\mathbb{E} \sum f| + \int f^2 \rho_1 \le C$ for each $f = f_\pm$. The same bounds apply to its reduced k-fold Palm law for fixed k. Indeed the Palm kernel of a finite orthogonal projection at k distinct points is obtained by subtracting the projection onto the span of the k evaluation vectors, by the Schur complement of the correlation determinant. Its intensity decreases, and its signed mean changes by at most $k\|f\|_\infty$. Since $\mathbb{E}^! \exp \sum f \le \exp \int (e^f - 1)\rho_1^!$, and $e^f - 1 \le f + Cf^2$ for bounded real f, the Palm exponential expectations are bounded uniformly in the tagged positions, including $k = 0$.

With k labelled and ordered tags the joint factorial integral takes the form $\prod_{j \le k} w(t_j) |P(t_1, \dots, t_k)|^2 \, d^k t \, d\sigma(\text{rest})$, where P is the analytic Vandermonde polynomial in $e^{it_j/N}$ and each variable has degree at most $N-1$; $d\sigma$ includes the normalization and exterior weights. It vanishes when $t_1 = t_2$. For tags in $[-2, 2]$, the square of the derivative $\partial_{t_1} P$ is bounded uniformly in those tags by

$$B = C \int |P(x_1, \dots, x_k)|^2 \prod_j (1 + |x_j|)^{-L} \, d^k x.$$

Use the periodized smooth Fourier cutoff, equal to one on $|m| \le N$ in each unscaled index, differentiated in its first microscopic coordinate. Summation by parts gives rapid decay in period-distance with size $O(1)$ in dt normalization, as the frequency multiplier m/N is bounded. Cauchy–Schwarz and $|t_j| \le 2$ give the bound uniformly. By the vanishing diagonal $|P(t)|^2 \le |t_1 - t_2|^2 B$. Fubini, the k-point intensity bound and the Palm exponential estimate just proved imply

$$\int e^{\sum_{\text{rest}} f} B \, d\sigma \le C N^{2ks}.$$

Indeed $\prod_j w(x_j) \int e^{\sum_{\text{rest}} f} |P(x)|^2 d\sigma$ is precisely the k-point intensity times the Palm exponential. This argument avoids any division by a conditional exterior partition function.

Two angles forced by a small mark. Consider a target in a fixed compact set D in $\Re Y > -1/2$, for example $|Y| \le 1/8$. Then $1/(2z) + \Re Y$ lies between two positive constants for sufficiently small c, and $|\Im Y|$ is bounded. Positivity bounds $\sum \Re n$ above and below by positive constants. In particular every angle has $|t| \ge b\sqrt{c}$, by the formula for $a(t)$. On $T \le K < 2T$, $1 \le T \le \gamma c^{-1/3}$, the outer real sum is at most $2cT$ and there are at most $2T$ points in $[-2, 2]$. Some point consequently satisfies $b\sqrt{c} \le |t_1| \le C\sqrt{cT}$. On this range $|\Im n(t_1)| \ge b'/\sqrt{cT}$. The total imaginary mark of angles outside $[-2, 2]$ has modulus at most CT, by the definition of K and the bounded transition on $1 \le |t| \le 2$. Choose γ sufficiently small. Cancellation now forces an opposite-sign point with $|\Im n(t_2)| \ge b'/(C\sqrt{c}T^{3/2})$, so both tags lie between $b\sqrt{c}$ and $C\sqrt{c}T^{3/2}$ in absolute value. Choose γ smaller if necessary so the upper endpoint is below one. Order the tags by sign.

The derivative formulas on this window give $|(\Re n)'| \asymp c/|t|^3$ with sign opposite t and $(\Im n)' \asymp -1/t^2$. For example the exact numerator of the latter derivative times $N^2 a^2$ is $(1+z^2)\cos(t/N) - 2z$, comparable to $-t^2/N^2$ because $t^2 \ge b^2 c \gg c^2$. For the pair map to $n(t_1) + n(t_2)$ the two Jacobian terms add in modulus:

$$J \ge b' \frac{c}{t_1^2 t_2^2} (|t_1|^{-1} + |t_2|^{-1}) \ge b' c^{-3/2} T^{-15/2}.$$

The pair map has at most two ordered inverse images at any regular value, since each mark lies on a circle and its partner on a translate of the reflected circle. For prescribed positive and negative tags there is at most one. On the window $w(t_1)w(t_2) \le CN^{-4s}c^{2s}T^{6\max(s,0)}$, and $|t_1 - t_2|^2 \le CcT^3$. Apply area change for fixed exterior, using B to remove the tagged polynomial and the exponential weight to impose the dyad. The two tag factors e^f are bounded. The factorial integral bounds the probability of the event by its count, giving for all Borel E in D

$$\mathbb{P}(Y \in E,\ T \le K < 2T) \le Ce^{-T}T^{21/2+6\max(s,0)}c^{e_s}|E|.$$

For $K > \gamma c^{-1/3}$ use $\exp(-\gamma c^{-1/3})$ times the same two exponential weights. The coarse bound Cc^{-2A} for the planar density in Section 19 holds after multiplying the angular symbol by $e^{f_\pm}$. In the projection evaluation and derivative proof all weight ratios change by bounded constants. In the oscillatory far-tail estimate the amplitude's supremum and total variation change by bounded multiples of the previous sup-plus-variation estimate, since e^f has uniform bounded variation; total variation is invariant under the monotone circle reparametrization. Jensen gives the modified auxiliary normalization at least one, since the angular mean of f is nonnegative (its odd part integrates to zero). The normalization relative to the original probability is at most C by the $k = 0$ exponential estimate. These facts retain the two Fourier estimates and their integrated bound. Thus the contribution is $O_B(c^B)|E|$ for every fixed B. This proves the quadratic upper bound. It also bounds the tail $K > T_0$ in the rescaled density by $Ce^{-T_0/2} + o(1)$ for each large constant T_0.

The leading coefficient. Write $M = N - 2$ and use $\mathbb{P}^\circ_M(s+2)$ on the exterior angles. On selecting two ordered tags, the coefficient of their area element dt_+dt_- is

$$C_N = \frac{Z^\circ_M(s+2)}{(2\pi)^2N^2Z_N(s,z)}.$$

The two single weights and their squared mutual Vandermonde remain. The ratio of the exterior weights to the circle preparation with tilt $s+2$ is the product of the interior/circle power ratio at tilt s and the two insertion ratios

$$\prod_{j=1}^{M}\left[\cos(t/(2N)) - \cot(\theta_j/2)\sin(t/(2N))\right]^2 \qquad (t = t_+, t_-).$$

Take an exterior with $|N\theta_j| \ge b > 0$, $N^{-2}\sum \csc^2(\theta_j/2) \le H$ and $|N^{-1}\sum \cot(\theta_j/2)| \le H$. The real exterior mark is $O_H(c)$ and its imaginary mark is bounded by $C_{b,H}$. For the latter, compare $\Im n$ to $(2Nz)^{-1}\cot(\theta/2)$ using the factor $1/[1+(1-z)^2/(4z\sin^2(\theta/2))]$ and the gap and inverse-square bounds. The target $w_* = Y + 1/(2z) - \sum_{\mathrm{ext}} n$ has $A_* = \Re w_* = 1/2 + \Re Y + O_H(c)$ and bounded imaginary part. The single-mark circle has center $C_z = (1+z^2)/(2zc)$ and radius $R = 1/c$. Put $v = w_*/2 - C_z$. The two marks solving the pair equation are exactly

$$w_*/2 \ \pm\ i(v/|v|)\sqrt{R^2 - |v|^2}.$$

Since $C_z^2 - R^2 = 1/(4N^2z^2)$, the radicand is $A_*/c + O_{b,H}(1)$. The two inverse angles have distinct signs. Uniformly on D, writing $A_0 = 1/2 + \Re Y$, one has $t_\pm = \pm\sqrt{c/A_0}\,(1 + o(1))$ by the explicit real/imaginary marks. The tagged weight product is $N^{-4s}(c/A_0)^{2s}(1 + o(1))$, the mutual squared difference is $4c/(N^2A_0)(1 + o(1))$, and $J = 2A_0^{5/2}c^{-3/2}(1 + o(1))$. The insertion ratios converge to one uniformly on these exteriors: expand each logarithm, bounding the linear cotangent sum by H and the quadratic error by $O_H(t^2 + t^2/N)$. The exterior tilt ratio equals $z^{Ms}\prod(1 + (1-z)^2/(z|1 - e^{i\theta_j}|^2))^s = 1 + O_{H,s}(c)$. The Barnes formula and the Section 19 mass convergence give $C_N/N^{4s+2} \to g_{s+2}/(4\pi^2 g_s)$. Hence the two-tag contribution at every such exterior, after multiplying by c^{-e_s}, converges uniformly to the planar profile (19.3).

For the lower bound choose the allowed exteriors first with probability at least $1 - \epsilon$ under $\mathbb{P}^\circ_M(s+2)$. The circle intensity bound in the scale $N\theta$ is uniform since $M/N \to 1$. The probability of a point below b is $O(b^{2s+5})$, and the expected inverse-square sum and variance of the signed cotangent sum are bounded, using $s + 2 > 3/2$, reflection and the projection variance inequality. Take b small, H large. On these exteriors the two inverse tags are eventually the only pair within $|t| < b$, one on each side, so their factorial integral counts each configuration just once. Send $\epsilon \to 0$.

For the upper bound first discard $K > T_0$ with the rescaled density loss proved above. On $K \le T_0$ the pair is forced into $C_{T_0}\sqrt{c}$. Discard cases with a third point below b, where b is fixed small and then $c \to 0$. Use three-tag smoothing, retaining the factor $|t_+ - t_-|^2$ supplied by the first two tags. Pair area change costs $C_{T_0}c^{3/2}|E|$,

the first two weights and collision factor cost $C_{T_0}N^{-4s}c^{2s+1}$. The integrated polynomial envelope is CN^{6s}, and the third tagged weight integrates to $CN^{-2s}b^{1+2\min(s,0)}$ when $c<b$. Their total rescaled density cost is $C_{T_0}b^{1+2\min(s,0)}$. The remaining pair is unique. The exterior has gap b and has the two displayed bounds with some deterministic $H=H(T_0,b)$. On $|t|\le 2$ this follows from the gap and count. Outside, the inverse-square sum is controlled by $\sum \eta\Re n/c$ by the formula for a (away from zero these denominators are comparable); for the signed cotangent sum use the comparison for $\Im n$ above, where its error is controlled by that inverse-square sum and the gap. Its truncated exterior sum is bounded by K plus the bounded contribution from $1\le|t|\le 2$. Tagged area change therefore has the uniform asymptotic just calculated. Its indicator contributes at most one to the exterior probability. The preceding estimates bound the contribution for every Borel set by its profile integral with error at most a uniform constant times its area, and likewise bound it below on the allowed exteriors. Take $c\to 0$, then $b\downarrow 0$, then $T_0\to\infty$. All error bounds are multiples of $|E|$ uniformly for Borel $E\subset D$, proving the asserted essential-uniform density asymptotic.

Finite-rank coefficient. For fixed $N\ge 2$ use $Z_n^\circ(v)=\mathbb{E}|\Lambda_n(1)|^{2v}$, with $Z_0^\circ=1$. In (19.3) the same fixed-rank limit as $c\downarrow 0$ has coefficient

$$\frac{Z_{N-2}^\circ(s+2)}{2\pi^2N^{4s+4}Z_N^\circ(s)}(1/2+\Re y)^{-2s-7/2}.$$

Indeed, for fixed rank the count K used above is bounded by $1+C_sN$ deterministically, since all its truncated summands are uniformly bounded. The large-K step is empty for sufficiently small c. The polynomial estimates with two or three tags still apply at that rank (at $N=2$ there is no third tag), with constants allowed to depend on N. The exterior weight at rank $N-2$ has a bounded inverse-square integral because $s+2>3/2$, and its probability of an eigenangle in $(-b/N,b/N)$ tends to zero with b. For rank zero the exterior is empty. Finally $Z_N(s,z)\to Z_N^\circ(s)$ by dominated convergence in the fixed-dimensional Weyl integral: for negative s use $|1-ze^{i\theta}|^2\ge z|1-e^{i\theta}|^2$ and $2s>-1$; for nonnegative s the factors are bounded. Inserting this mass directly into C_N gives the coefficient above. All estimates for prescribed targets remain uniform on D. Combining the finitely many ranks below N_0 with (19.2) gives that upper bound for **all** $N\ge 2$ after adjusting C,c_0. At rank one the mark lies on a circle.

Theorem 19.3 (sharp simultaneous moment strip). For every fixed real $s>-1/2$ and every sequence $N\to\infty$, $c=N(1-z^2)\to 0$, the ordinary mixed moment obeys

$$N^{-s^2}c^{-2h}T_N(h,s;z)\longrightarrow 4^{-h}g_s\,\mathbb{E}(1+X_s^2)^h,\qquad -1<\Re h<s+\tfrac12. \tag{19.4}$$

The convergence is locally uniform in the complex order h on this strip. At the lower endpoint and below, the finite interior expectation fails absolute integrability for $N\ge 2$ and $0<z<1$. At the upper endpoint and above, the limiting circle absolute moment is infinite and the corresponding finite positive absolute moments tend to infinity.

For $q=-2\Re h\in(0,2)$, (19.2) gives

$$\mathbb{E}_{N,s,z}\big[|Y|^{-q};\ |Y|\le r\big]\le\frac{2\pi C}{2-q}c^{e_s}r^{2-q},\qquad 0<r\le r_0. \tag{19.5}$$

Section 19's positive moment estimates control the large values with a surplus exponent on each compact set of orders. Apply weak convergence on the intervening annulus and the positive mass limit $N^{-s^2}Z_N(s,z)\to g_s$. For locally uniform convergence, truncate both ends uniformly and use convergence on the bounded annulus uniformly over the compact parameter set, by continuity and a finite parameter net. Section 5 gives the lower-end divergence for each finite interior ensemble. We next prove sharpness at the upper end.

Sharpness at the upper end by insertion on the circle

Let $Z_n(a)=\mathbb{E}|\Lambda_n(1)|^{2a}$ and $Q_n^{(a)}$ denote the probability tilt on the circle. Fix $s>-1/2$. Begin with $n=N-1$ resident eigenangles under $Q_{N-1}^{(s+1)}$. Use $t=N\theta$ also for these residents, which changes the usual microscopic scale by a bounded factor. We claim that there is a constant K independent of $N\ge 2$ such that the event

$$\left|N^{-1}\sum_j\cot(\theta_j/2)\right|\le K,\qquad \sum_j[N\sin(\theta_j/2)]^{-2}\le K$$

has probability at least $1/2$. For the first condition use the uniform trace moment bound (Theorem 17.2) for the exponent $s+1$. For the second, the circle one-point density at this exponent is bounded above by $C\min(1,|t|^{2s+2})$. Since $N^{-1}|\csc(t/(2N))| \le C/|t|$ for $|t| \le \pi N$, its integral against the squared cosecant is at most $C(\int_0^1 t^{2s}dt + \int_1^\infty t^{-2}dt) < \infty$. Markov's inequality proves the claim. Every resident then obeys $|N\theta_j| \ge 2/\sqrt{K}$.

Insert a point at t/N, $x \le t \le 2x$, with $x > 0$ less than a fixed sufficiently small number depending on K. Dividing its Vandermonde interaction by the interaction at zero leaves the product over residents of

$$[\cos(t/(2N)) - \cot(\theta_j/2)\sin(t/(2N))]^2.$$

Write each bracket as $1+v_j$. On the event just specified, $\sup|v_j| \le Ct\sqrt{K}+Ct^2/N^2 < 1/2$, $|\sum v_j| \le C(tK+t^2/N)$ and $\sum v_j^2 \le C(t^2K + t^4/N^3)$. Thus the log of the product is bounded below by a constant independent of N, x on this event. Inserting a tag through the Weyl density has the prefactor

$$\frac{Z_{N-1}(s+1)}{2\pi N Z_N(s)}|1-e^{it/N}|^{2s}\,dt \asymp_s t^{2s}\,dt.$$

Here the combinatorial factor N cancels the change from $N!$ to $(N-1)!$. The ratio estimate also follows directly from $Z_m(a) \sim m^{a^2}g_a$, with both limiting constants positive. On the resident event the tag is unique in the prescribed window, so this distinguished-point integral is a lower bound for its probability. The normalized signed trace after tagging is bounded below by b/x for a fixed $b > 0$ because its resident part has modulus at most K. Consequently $Q_N^{(s)}(N^{-1}\sum\cot(\theta_j/2) \ge b/x) \ge b_s x^{2s+1}$. By weak convergence and the closed-set inequality this bound persists for X_s. Layer cake now gives $\mathbb{E}(1+X_s^2)^{q/2} = \infty$ for every $q \ge 2s+1$, including the logarithmic divergence lower bound at equality. Weak convergence for the shrinking-depth mark then forces $\mathbb{E}|S_N/c|^q \to \infty$ along each such sequence for real $q \ge 2s+1$, by bounded continuous truncations. This establishes sharpness of the open upper range as an absolute-moment statement.

Corollary 19.4 (a moment order tending to the inverse endpoint). Suppose $s > -1/2$ is fixed, $N \to \infty$, $c \to 0$ and $h = -1+\delta$ with $\delta \to 0$ complex and $\Re\delta > 0$. Write $L_s(x) = g_{s+2}(1/2+x)^{-2s-7/2}/(2\pi^2 g_s)$. For the probability-normalized mark,

$$\mathbb{E}_{N,s,z}|Y|^{-2+2\delta} = 4\mathbb{E}(1+X_s^2)^{-1} + o(1) + \frac{\pi L_s(0)c^{2s+5/2}}{\delta}\,[1+o(1)]. \tag{19.6}$$

In particular the two error terms refer separately to the ordinary circle contribution and to the growing or vanishing near-zero contribution. On the complement of a fixed disk of radius $r_0 < 1/4$, the integrands are bounded and converge uniformly to $|y|^{-2}$ as $\delta \to 0$. The limiting measure gives no mass to the boundary of this disk. Weak convergence thus gives the first term. For a uniform estimate even at tangential complex approaches to the pole, subtract the actual finite density at zero. The two Fourier tail bounds in the proof of (19.1) integrate also with one power of the rescaled frequency $c^A|\zeta|$, by choosing the rank large enough. Hence the continuous finite density satisfies $\|\nabla p^Y_{N,s,z}\|_\infty \le Cc^{-3A}$. On the fixed disk its supremum is $O(c^{e_s})$ by (19.2). Therefore

$$\int_{|y|<r_0} \frac{|p^Y_{N,s,z}(y) - p^Y_{N,s,z}(0)|}{|y|^2}\,d^2y \le C\int_0^{r_0} \min(c^{-3A}r, c^{e_s})\frac{dr}{r} = O\big(c^{e_s}(1+|\log c|)\big).$$

The constant-density contribution is $\pi p^Y_{N,s,z}(0) r_0^{2\delta}/\delta$. Equation (19.3) evaluates that continuous density at zero and $r_0^{2\delta} = 1 + O(|\delta|)$. These bounds prove (19.6) without an assumption on $|\delta|/\Re\delta$. For positive real δ, the ratio c^{e_s}/δ determines whether the circle value is recovered, receives a finite additional term, or is exceeded by a divergent contribution.

An exact untilted check. For $s = 0$, the finite circle variable $N^{-1}\sum_j \cot(\theta_j/2)$ already has the standard Cauchy law. Indeed for $t > 0$ the bounded analytic function $\exp[-t(1+w)/(1-w)]$ has boundary value $e^{-it\cot(\theta/2)}$ almost everywhere and constant coefficient e^{-t}. Its Toeplitz determinant of size N is triangular with determinant e^{-Nt}. Reflection supplies the other frequency sign. A beta integral for the standardized trace now gives

$$\lim \mathbb{E}_{N,0,z}|Y|^{2h} = \frac{4^{-h}\Gamma(1/2-h)}{\sqrt{\pi}\,\Gamma(1-h)}, \qquad -1 < \Re h < 1/2. \tag{19.7}$$

For example $h = -1/2$ gives $4/\pi$. The coefficient of the local density for the untilted ensemble uses $g_2/g_0 = 1/12$. At fixed rank the circle insertion mass factor in the same calculation is $Z^\circ_{N-2}(2)/N^4 = (1-N^{-2})/12$ for $N \ge 2$, directly by the product in Theorem 17.2.

A single near eigenangle above the positive threshold

Theorem 19.5 (upper critical and supercritical powers). Put $a = 2s+1 > 0$ and retain $c = N(1-z^2) \downarrow 0$, $N \to \infty$. Beyond the strip of finite circle moments a different normalization gives an explicit answer. For real $s > -1/2$ and complex $\Re h > s + 1/2$,

$$N^{-s^2} c^{-a} T_N(h, s; z) \;\longrightarrow\; \frac{g_{s+1}}{2\pi} \int_{\mathbb{R}} (1/4 + x^2)^{s-h} dx = \frac{g_{s+1} 2^{2h-2s-2}}{\sqrt{\pi}} \frac{\Gamma(h - s - 1/2)}{\Gamma(h-s)}. \tag{19.8}$$

At the real critical index $h = s + 1/2$, $N^{-s^2} c^{-a} T_N(h, s; z)/\log(1/c) \to g_{s+1}/\pi$. At any fixed nonreal point $\Re h = s + 1/2$ the same log-normalized complex expectation tends to zero. The absolute moment still grows at the real critical rate in the circle normalization. Theorem 19.6 determines the bounded terms on this line.

One-point insertion. Write $I_{s,c,N}(t)$ for the probability-normalized interior one-point density relative to dt, $t = N\theta$. Tag one eigenangle and use the circle tilt at exponent $s+1$ for the $N-1$ residents. If their angles are θ_j, put $u_j = N\theta_j$. The normalized Weyl formula gives

$$\frac{I_{s,c,N}(t)}{[N|1 - ze^{it/N}|]^{2s}} = \frac{Z_{N-1}(s+1)}{2\pi N^a Z_N(s,z)} \, z^{(N-1)s} \, \mathbb{E}^{\circ}_{N-1,s+1} \prod_j A(u_j) [\cos(t/(2N)) - \cot(\theta_j/2) \sin(t/(2N))]^2,$$

where $Z_{N-1}(s+1)$ is the circle mass and $A(u) = [1 + (1-z)^2/(z|1 - e^{iu/N}|^2)]^s$. The expectation tends to one jointly when $N \to \infty$, $c \to 0$, $t \to 0$, and stays bounded uniformly for $|t| \le 1$. To prove the upper bound apply $\mathbb{E} \prod R \le \exp[\int (R-1) I^{\circ}]$ to the nonnegative one-point factor R. For unbounded factors use truncation and monotone convergence of the finite product. The inequality follows from $\log\det(I + B) \le \mathrm{Tr} B$ on the occupied finite-dimensional space, with zero eigenvalues interpreted by a limit. The odd cotangent term integrates to zero against the even intensity. The resident intensity obeys $I^{\circ}(u) \le C \min(1, |u|^{2s+2})$ in the coordinate $u = N\theta$. Thus

$$\int |A - 1| I^{\circ} \, du = O_s(c^2 + c^{2s+3}), \qquad \int A(u) [N \sin(u/(2N))]^{-2} I^{\circ}(u) \, du \le C_s.$$

For $|u| \ge c$, use $|A - 1| \le C_s c^2/u^2$ and $A \le C_s$, with the intensity bound. For $|u| < c$ and $s \ge 0$, $A \le C_s (c/|u|)^{2s}$ while $s < 0$ gives $A \le 1$. These establish both estimates, using $2s > -1$. After symmetry the integral of $R - 1$ is consequently bounded above by $C_s(c^2 + c^{2s+3} + t^2)$. For the lower bound, with probability at least $1 - \epsilon$ both the signed trace $|N^{-1} \sum \cot(\theta_j/2)|$ and $H = \sum [N \sin(\theta_j/2)]^{-2}$ are bounded by some $K_{s,\epsilon}$. This follows from Theorem 17.2 and the same intensity integration with $A = 1$. On this event the sum of the absolute logarithms of the A-factors is at most $C_s c^2 H$. For the linear factors write each as $1 + d_j$. Then $\sup |d_j| \le C(t^2/N^2 + |t|\sqrt{K})$, $|\sum d_j| \le C(t^2/N + |t|K)$ and $\sum d_j^2 \le C(t^4/N^3 + t^2 K)$. Their product tends uniformly to one on this event by the logarithmic Taylor bound. Let $\epsilon \downarrow 0$. Finally $z^{(N-1)s} \to 1$ and the mass ratio tends to $g_{s+1}/(2\pi g_s)$ by the circle mass limit and the earlier change-of-tilt calculation. In particular

$$\frac{I_{s,c,N}(t)}{[N|1 - ze^{it/N}|]^{2s}} \;\longrightarrow\; \frac{g_{s+1}}{2\pi g_s} \quad (t \to 0), \qquad I_{s,c,N}(t) \le C_s (c + |t|)^{a-1} \quad (|t| \le 1).$$

The convergence here is simultaneous, and the last inequality is uniform in all sufficiently large ranks and small depths.

Separating the closest angle. Use $n(t)$ from the proof of (19.1) and retain the point of smallest $|t|$ in $|t| \le 1$, denoting its mark by V and setting $V = 0$ for an empty window. For $q > 0$ let

$$B_q(c) = 1 + c^{2a-q} + \int_c^1 t^{2a-q-1} dt.$$

The remaining marked sum $R = Y - V$ obeys

$$\mathbb{E}|R|^q + \mathbb{E} \sum_{\substack{|t| \le 1 \\ t \ne t_*}} |n(t)|^q \le C_{q,s} B_q(c).$$

Indeed, the exterior and the deterministic offset have bounded moments of every fixed order as already established. Inside, the qth power of the sum of absolute marks is bounded by $C_q e^{\#\{|t| \le 1\}}$ times their summed qth powers.

Every remaining point has a distinct nearer point u. The DPP joint intensities are bounded by products of $I_{s,c,N}$ by Hadamard. Expand the exponential of the local count as a positive product; with two distinguished locations the extra factor in the bound is at most $e^2 \exp((e-1)\int_{|u|\le 1} I_{s,c,N}(u)du)$, uniformly bounded. The required integral is therefore at most

$$C_q \int_0^1 (c+t)^{-q}(c+t)^{a-1} \int_0^t (c+u)^{a-1} du\, dt \le C_q B_q(c).$$

This holds at $a<1$ too by splitting at c. The analogous one-point estimate gives $\mathbb{E}|V|^q \le C(1+\int_0^1 (c+t)^{a-1-q}dt)$. For $q = 2\Re h \ge a$ define $L_q = c^{a-q}$ if $q > a$ and $L_a = \log(1/c)$. Then $B_q = o(L_q)$ while $\mathbb{E}|V|^q = O(L_q)$. For $0<\delta<\min(1,q)$ the difference of complex radial powers obeys

$$\big||v+b|^{2h} - |v|^{2h}\big| \le C_h |b|^\delta (|v|+|b|)^{q-\delta}.$$

This follows by separating $|b| \ge |v|/2$ and applying the radial derivative bound on the complementary segment. Hölder gives $\mathbb{E}|Y|^{2h} = \mathbb{E}|V|^{2h} + o(L_q)$. Restoring all marked one-point terms in $|t|\le 1$ costs at most CB_q, giving

$$\mathbb{E}|Y|^{2h} = \int_{|t|\le 1} |n(t)|^{2h} I_{s,c,N}(t)dt + o(L_q).$$

For $q > a$ put $t = cx$. At each fixed x, $cn(cx) \to (1/2 - ix)^{-1}$ and $N|1 - ze^{icx/N}|/c \to |1/2 - ix|$. The scaled absolute integrand is at most $C(1+|x|)^{a-1-q}$, which is integrable. The one-point insertion and dominated convergence, multiplied by the mass $N^{-s^2} Z_N(s,z) \to g_s$, yield the supercritical formula, including its complex phase through c^{2h}. For $q = a$ split the integral at Kc and at ϵ. The two outer portions are $O_K(1) + O_\epsilon(1)$ in absolute value. On $Kc \le |t| \le \epsilon$, increasing K and decreasing ϵ make $|n(t)||t|$ and $N|1 - ze^{it/N}|/|t|$ uniformly as close to one as desired in the joint limit. With the uniform near-zero one-point ratio, the integral on the positive half has leading integrand $g_{s+1}|t|^{-1-2i\Im h}/(2\pi g_s)$, up to arbitrarily small relative error measured against $dt/|t|$. At real h the two halves give the stated logarithmic coefficient. For fixed nonreal h the integral of $t^{-1-2i\Im h}$ from Kc to ϵ stays bounded, hence the log-normalized complex moment tends to zero. The unit-modulus factor $c^{2i\Im h}$ does not affect that last conclusion.

Special cases. For $s = 0$, $h = 1$ the exact Haar trace covariance yields $T_N(1,0;z) = 1 - z^{2N}$, giving the predicted $g_1 = 1$ coefficient. At rank one the exact scalar moment is $c^{2h}{}_2F_1(h-s, h-s; 1; 1-c)$. Its supercritical coefficient after division by c^{2s+1} is $\Gamma(2h-2s-1)/\Gamma(h-s)^2$, obtained also by the preceding one-point integral with its finite-rank normalization $Z_0(s+1) = 1$. At the critical rank-one index its ratio to c^{2s+1} is $2\mathrm{K}(1-c)/\pi$ in the elliptic parameter convention, with leading term $\log(16/c)/\pi$. These exact cases check both competing normalizations.

Matching the circle and pole terms at the critical exponent

Theorem 19.6 (finite part at the upper critical exponent). The logarithmic and oscillatory readouts have a common finite part. Let $s > -1/2$ be fixed and real, $a = 2s+1$, $h_* = a/2$, and write

$$B_N = \frac{N^{-s^2} Z_{N-1}(s+1)}{2\pi N^a}, \qquad B = \frac{g_{s+1}}{2\pi}, \qquad f_N(h) = N^{-s^2} c^{-2h} T_N(h,s;z).$$

Here $Z_{N-1}(s+1)$ is the circle mass. Fix $\delta = \min(1,a)/4$, $\eta = \delta/6$, and take the vertical strip $|2\Re h - a| < \eta$. The circle readout $f_\circ(h) = 4^{-h} g_s \mathbb{E}(1+X_s^2)^h$ extends meromorphically from below into this strip. Its sole pole there is h_*, simple with residue $-B$. Put $H(h) = f_\circ^{\mathrm{mer}}(h) - 2B/(a-2h)$, holomorphic on the entire strip. For all sequences $c \downarrow 0$, $N \to \infty$,

$$f_N(h) = H(h) + B_N \int_{-1}^1 (c^2/4 + t^2)^{s-h} dt + o(1). \tag{19.9}$$

locally uniformly in that strip, including the pole of the meromorphic summands below. In particular on compacts avoiding h_*,

$$f_N(h) = f_\circ^{\mathrm{mer}}(h) + B_N (c/2)^{a-2h} \frac{\sqrt{\pi}\,\Gamma(h-s-1/2)}{\Gamma(h-s)} + o(1). \tag{19.10}$$

At $h = h_* + ib$, $b \neq 0$ real, this identifies an explicit nonvanishing oscillatory term and the constant finite part. Its coefficient can here be replaced by B since the phase has modulus one. For example, take $c_n = 2\exp[-\pi n/|b|]$ and $\widetilde{c}_n = c_n \exp[-\pi/(2|b|)]$ at rank $N = n$. The two phases are opposite, so the ordinary complex moment in this normalization has distinct subsequential limits. At $h = h_*$ the additive-error formula is

$$f_N(h_*) = 2B_N \log(4/c) + H(h_*) + o(1). \tag{19.11}$$

The finite-rank coefficient matters in this centering for unrestricted depths. For example, at $s = 1$ the Barnes product gives $B_N = (1 + 1/N)^2(1 + 2/N)/(24\pi)$ and $B = 1/(24\pi)$. Replacing B_N by B at $c = e^{-N}$ changes the finite part by $1/(3\pi)$ in the limit.

To prove these formulas use the quantitative version of the insertion estimate. With $r = c + |t|$ small, set $K = r^{-1/2}$ in its lower-bound event. Both the first absolute moment of the normalized signed trace at tilt $s + 1$ and the mean squared-cosecant sum are uniformly bounded. Markov's inequality therefore gives exceptional probability $O(\sqrt{r})$. The product on its complement is bounded below by $1 - O(\sqrt{r})$ because its log deviations have bounds $C_s(c^2K + |t|K + t^2K + t^2/N)$. The upper estimate already proved is $1 + O(c^2 + c^{2s+3} + t^2)$. Including $z^{(N-1)s} = 1 + O_s(c)$ gives, for the unnormalized one-point intensity,

$$N^{-s^2} Z_N(s, z) I_{s,c,N}(t) = B_N[N|1 - ze^{it/N}|]^{2s}(1 + O_s(\sqrt{c + |t|})).$$

On $|t| \leq 1$ one also has $N|1 - ze^{it/N}| = \sqrt{c^2/4 + t^2}(1 + O(c + t^2))$ and $|n(t)| = (c^2/4 + t^2)^{-1/2}(1 + O(c + t^2))$. Use the identities for their squared moduli, with $N(1 - z) = c/(1 + z)$. Consequently the difference of the one-point integrand and $B_N(c^2/4 + t^2)^{s-h}$ is bounded near zero by $C(c + |t|)^{a-1-2\Re h+1/2}$, integrable uniformly on this strip.

For the many-point error, the nonclosest sum R above has bounded pth moment for $p = 3a/2 < 2a$ whereas the nearest mark V has bounded moments at every power below a. For $q = 2\Re h$ on a compact in the indicated strip, $q < p$ and $(q - \delta)p/(p - \delta) < a$. Thus the bound $C|R|^{\delta}(|V| + |R|)^{q-\delta}$ for the radial power difference has bounded expectation by Hölder, uniformly on each such compact. The summed powers of the other near angles are also uniformly bounded, since $q < 2a$. The masses $N^{-s^2} Z_N$ are bounded. Subtracting the model integral from f_N therefore gives a locally bounded family of holomorphic functions. For $2\Re h < a$, the ordinary shrinking-depth theorem and dominated convergence in the model integral give its limit $f_\circ(h) - 2B/(a - 2h)$. The identity theorem and the normal family theorem imply convergence on the full strip for every original sequence; limits agree between sequences by uniqueness. This defines H and establishes the meromorphic continuation and the first matched formula.

Finally write $d = c/2$. For $\Re h > h_*$ the integral over the entire real axis is $d^{a-2h}\sqrt{\pi}\Gamma(h - s - 1/2)/\Gamma(h - s)$. Subtract the two tails from one to infinity. There replacing $(d^2 + t^2)^{s-h}$ by $t^{2(s-h)}$ costs $O(d^2)$ uniformly on compact subsets of the strip: the difference decays as $Cd^2t^{2(s-\Re h)-2}$. The integral of this difference is holomorphic throughout the strip. Analytic continuation now gives the gamma term plus $2/(a - 2h)$ and this analytic error on either side, away from h_*. At $h = h_*$ the model integral is exactly $2\,\mathrm{arsinh}(2/c) = 2\log(4/c) + O(c^2)$. This supplies the stated additive constants for arbitrary rates.

The complex circle preparation and its Fourier source

Theorem 19.7. Let $u = \Re s > -1/2$ and $c = N(1 - z^2) \downarrow 0$, $N \to \infty$. The N^{-s^2}-scaled interior mass tends to g_s and the Fourier transforms of $Y = S_N/c$ and of $((\Re Y + 1/2)/c, \Im Y)$ have the locally uniform limits below for real frequencies. The underlying matrix preparation has unbounded variation at a fixed nonreal tilt. We recover cancellation using its polynomial kernel before taking absolute estimates.

Use the angular coordinate $t = N\theta$ in $I_N = (-\pi N, \pi N]$, circular distance d_N, and $u = \Re s > -1/2$. Divide the circle preparation by its nonvanishing Barnes mass $Z_N^\circ(s)$. Its factorial densities are determinants of the following kernel with respect to dt:

$$K_{N,s}(t, w) = \frac{|1 - e^{it/N}|^s |1 - e^{iw/N}|^s}{2\pi N} \sum_{j=0}^{N-1} \frac{\Phi_j(e^{it/N})\Phi_j(e^{-iw/N})}{b_j}, \quad b_j = \frac{\Gamma(j + 1)\Gamma(j + 1 + 2s)}{\Gamma(j + 1 + s)^2}.$$

The powers have real logarithms. The second polynomial has the same parameter s as the first. The circular Jacobi monic polynomial is

$$\Phi_j(\lambda) = \frac{j!}{(1+s)_j}[v^j](1-v)^{-s}(1-\lambda v)^{-s-1} = \frac{(1+2s)_j}{(1+s)_j}\,{}_2F_1(-j, 1+s; 1+2s; 1-\lambda).$$

For real parameters this is the circular Jacobi polynomial (the Askey biorthogonal polynomials specialized to equal parameters; see L. Vinet and A. Zhedanov, *An algebraic treatment of the Askey biorthogonal polynomials on the unit circle*, Forum Math. Sigma, 2021). Alternatively the orthogonality follows from the Fourier coefficients $(-1)^m\Gamma(1+2s)/[\Gamma(1+s+m)\Gamma(1+s-m)]$ by finite binomial summation. The squared monic norm is the consecutive circle determinant ratio Z°_{j+1}/Z°_j. Bilinear orthogonality, the kernel expression and determinant correlations then extend holomorphically from real s at each fixed size; every Gamma argument in b_j has positive real part.

Put $V_u(t) = (|t|/(1+|t|))^{2u}$. With constants locally uniform in s,

$$|K_{N,s}(t,w)| \le C\frac{\sqrt{V_u(t)V_u(w)}}{1+d_N(t,w)}, \qquad |\det[K_{N,s}(t_i,t_j)]_{i,j\le k}| \le C^k\prod_{i\le k}V_u(t_i).$$

Here and below estimates at the point $t=0$ are used in their almost-everywhere sense. For the proof first establish $|\Phi_j(e^{i\theta})| \le C[(j+1)^{-1} + |1-e^{i\theta}|]^{-u}$. For $j \ge 2$ apply Cauchy's coefficient estimate to the mth derivative of the generating function at radius $1-1/j$, with fixed $m > 2+2|u|$, dividing by the falling factorial of order m (handle bounded j separately). Each integral has prefactor $O(j^{-m})$ and factors $|1-v|^{-u-l}|1-e^{i\theta}v|^{-u-1-m+l}$ for $0 \le l \le m$. Imaginary powers cost only a compact-dependent constant. Write $D = |1-e^{i\theta}|$. When $jD \le 2$, the distances are comparable and integration gives $O(j^{2u})$ including the prefactor. Otherwise split into neighborhoods of the two pole angles of radius comparable to D and the complement. At the second pole the other factor costs CD^{-u-l}, and integrating the remaining factor costs Cj^{u+m-l} if its exponent exceeds one; the total is at most Cj^uD^{-u}. At the first pole, when its exponent exceeds one, the corresponding bound is $Cj^uD^{-u}(jD)^{l-m-1}$. An exponent below one costs $Cj^{-m}D^{-2u-m}$ after integration. At exponent one the extra $1+\log(jD)$ is absorbed by $(jD)^{-(m+u)}$. The complement costs $Cj^{-m}D^{-2u-m}$ by comparison to the integral of distance to the nearer pole to the power $-2u-1-m$. The prefactor $j!/(1+s)_j = O(j^{-u})$ gives the claimed bound.

Now $|b_j| \asymp 1$. The squared norm of either absolute feature vector of the bilinear sum is bounded by $CV_u(t)$: sum the polynomial bound first for $j+1 \le |1-e^{it/N}|^{-1}$ and then for larger j, using $2u > -1$. Cauchy–Schwarz in the exterior power gives the determinant estimate with no factorial loss. For $d_N(t,w) > 1$ the Christoffel–Darboux identity gives the difference of two products of degree-N polynomials (one uses the reversed polynomials $\Phi^*_N(z) = z^N\Phi_N(1/z)$), divided by $b_N(1-e^{i(t-w)/N})$. This follows by analytic continuation of the real-parameter identity. The bound on Φ_N and $N|1-e^{i(t-w)/N}| \asymp d_N(t,w)$ give the off-diagonal decay.

The limit at fixed nonzero t, w in this gauge is

$$K_s(t,w) = \frac{|tw|^s}{2\pi}\left(\frac{\Gamma(1+s)}{\Gamma(1+2s)}\right)^2\int_0^1 x^{2s}\,{}_1F_1(1+s;1+2s;ixt)\,{}_1F_1(1+s;1+2s;-ixw)\,dx. \tag{19.12}$$

Indeed for $j/N \to x > 0$ the terminating series in the polynomial formula converges to this confluent hypergeometric series: $|(-j)_l(1-e^{it/N})^l| \le C_t^l$ and the remaining ratio grows at most polynomially in l. The norm and gamma ratio use Stirling. Bounded j/N near zero costs $O(\epsilon^{1+2u})$ for locally bounded t, w away from zero. This proves the Riemann sum and local uniformity on parameter compacts.

Joint limit of the normalized Fourier source

Set $n(t) = (1+ze^{it/N})/[2Nz(1-ze^{it/N})]$, so $Y = -1/(2z) + \sum n$. Put

$$A(t) = \left(1 + \frac{(1-z)^2}{z|1-e^{it/N}|^2}\right)^s, \quad F(t) = A(t)\exp\{i(p_x\Re n(t) + p_y\Im n(t))\} - 1$$

for real p_x, p_y. The finite determinant giving the unnormalized Fourier transform of Y, after multiplication by N^{-s^2}, is the product of $N^{-s^2}Z^\circ_N(s)z^{Ns}e^{-ip_x/(2z)}$ and

$$\det{}_2(I+L_N)\exp\int_{I_N}F(t)K_{N,s}(t,t)\,dt, \qquad L_N(t,w) = \mathrm{phase}(F(t))\sqrt{|F(t)|}\,K_{N,s}(t,w)\sqrt{|F(w)|}.$$

The phase of zero is set to zero. This follows by finite-rank factorization and $\det(I+L) = e^{\mathrm{Tr}L}\det_2(I+L)$. The regularized determinant is continuous in Hilbert–Schmidt norm, e.g. by its convergent exterior-power construction or its standard regularized Fredholm determinant inequality. The complex circle preparation is integrated before absolute bounds are taken.

As $N \to \infty$ and $c \to 0$ freely, $A(t) \to 1$ and $n(t) \to i/t$ at fixed $t \neq 0$. The determinant tends to the same expression on the real line with K_s, $F_0(t) = e^{ip_y/t} - 1$, and symmetric principal value for the trace. The prefactor tends to $g_s e^{-ip_x/2}$. The convergence is locally uniform in s with $\Re s > -1/2$ and in the real frequencies. If $\mathcal{D}_s[F]$ denotes this regularized determinant times the exponential of its symmetrized trace at K_s, the two limiting Fourier transforms, in their respective coordinates, are

$$g_s e^{-ip_x/2}\mathcal{D}_s[e^{ip_y/t} - 1], \tag{19.13}$$

$$g_s\mathcal{D}_s[\exp(ip_B/(2t^2) + ip_y/t) - 1]. \tag{19.14}$$

The transform divided by g_s has value one at zero. At real tilt it is exactly the circle characteristic function including its displayed translation.

Here are bounds that give this limit without any relation between rank and depth. At $|t| < 1$, $|F(t)|V_u(t) \leq C[(c+|t|)^{2u} + |t|^{2u}]$; in particular its integral on $|t| < \epsilon$ is $O(\epsilon^{1+\min(0,2u)})$ uniformly for $c \leq 1$. At $|t| > 1$, write $j(t) = |F(t)|V_u(t) \leq C_p/|t|$. Then $|L_N(t,w)|^2 \leq Cj(t)j(w)(1 + d_N(t,w))^{-2}$. The portion with a variable below ϵ tends to zero uniformly by the local integrable bound and the bounded convolution tail. For a variable above $R > 4$ and the other of modulus at most one the circular distance is at least $R - 1$ (and grows at least as $|t| - 1$); this portion tends uniformly to zero. With both moduli above one use Cauchy–Schwarz and Young's convolution inequality on the circle: the L^2 norm of $j\mathbf{1}_{|t|>R}$ is $O_p(R^{-1/2})$, the other norm is bounded, and the periodic decay weight has bounded L^1 norm. Extending kernels by zero, local dominated convergence now proves Hilbert–Schmidt convergence on the line. The diagonal $K_{N,s}(t,t)$ is even. Pairing the trace at $t, -t$ replaces F by $Ae^{ip_x\Re n}\cos(p_y\Im n) - 1$, bounded by C_p/t^2 for $|t| > 1$. This gives convergence of the traces. Local compact bounds, or the same argument along arbitrary convergent parameter subsequences, give joint local uniformity, and analyticity in s follows from the finite transforms.

In particular $N^{-s^2}Z_N(s,z) \to g_s$ on the full half-plane, and $g_s \neq 0$ there by the Barnes product. The ordinary circle and interior normalizing masses are nonzero eventually on each compact. The total variation of the original matrix preparation scaled by N^{-s^2} is $N^{v^2}(g_u + o(1))$ for $s = u + iv$. For the preparation divided by its own complex mass the corresponding asymptotic is $N^{v^2}(g_u/|g_s| + o(1))$. This fixed-frequency argument supplies convergence of Fourier readouts at fixed frequencies, not weak convergence against every bounded continuous function for the projected complex measures.

Boundary layer. For $B = (\Re Y + 1/2)/c$, keep the real phase $p_B\Re n/c + p_y\Im n$. The deterministic shift $(1/2 - 1/(2z))/c = -1/[2Nz(1+z)]$ tends to zero. The same near-origin majorant applies by bounded modulus, while $\Re n/c \leq C/t^2$ outside one. Thus $F_0(t) = \exp(ip_B/(2t^2) + ip_y/t) - 1$ replaces the preceding phase in the regularized determinant with prefactor g_s. This proves unconditional complex source convergence also on the resolved transverse scale. At real tilt its probability interpretation is the joint circle-process statistic for $\frac{1}{2}\sum t^{-2}$ and the symmetric sum of $1/t$.

Ordinary integral powers. If k is a nonnegative integer and $u > k - 1/2$, all Fourier derivatives of total order at most $2k$ pass to this unscaled Y limit. One can use a fixed dominating weight for differentiating: take $\omega(t)V_u(t) = 1 + |t|^{\min(2u-2k,0)}$ on $|t| \leq 1$ and $\omega(t)V_u(t) = 1/|t|$ beyond one. Use the equivalent kernel $(F/\omega)(t)\sqrt{\omega(t)}K_{N,s}(t,w)\sqrt{\omega(w)}$. At $|t| < 1$, the normalized majorants for ℓ derivatives are bounded by $C[(c + |t|)^{2u-\ell} + |t|^{2u}]$ for $\ell \leq 2k$; at infinity they cost at most $C_p/|t|$. Consequently every differentiated kernel converges in Hilbert–Schmidt norm by the preceding truncation argument, while the differentiated symmetrized diagonal is $O_p(t^{-2})$ for first derivatives as well. The regularized determinant is an entire function of a Hilbert–Schmidt operator and its derivatives converge on convergent jets. Applying $(-\Delta_p)^k$ at the origin proves convergence of $N^{-s^2}c^{-2k}T_N(k,s;z)$ to the ordinary integer circle readout obtained by applying the same operator to the limit, locally uniformly in that half-plane. Equivalently it is the unique holomorphic extension of the corresponding real-tilt trace polynomial moment in that half-plane. At $k = 0$ the undifferentiated proof applies directly.

The scalar circle readout throughout the complex half-plane

Theorem 19.8 (ordinary circle integrals at independent complex parameters). Set $u = \Re s > -1/2$ and $X = \operatorname{Tr} H/N$, where H is the Cayley matrix with eigenvalues $\cot(\theta_j/2)$. Let $P_{N,s}$ be its complex circle preparation divided by $Z_N^\circ(s)$. Then

$$\mathcal{C}(s,h) = \lim_{N\to\infty} 4^{-h} \int (1+X^2)^h \, dP_{N,s}, \qquad \Re h < u + 1/2, \tag{19.15}$$

exists locally uniformly and is jointly holomorphic. Every finite-rank member is an ordinary absolutely existing integral. Its limit includes all negative orders on the circle. For real s the value is $4^{-h}\mathbb{E}(1+X_s^2)^h$. This theorem concerns the exact circle, where the complex mark has real part $-1/2$. The distinction from interior inverse moments is essential. The absolute-existence threshold on the circle is exact at each finite rank by the one-eigenvalue tail test in Section 17 with s replaced by u.

We prove the missing global frequency estimate for the trace. Write $\chi_N(\xi) = \int e^{i\xi X} dP_{N,s}$ in this subsection. The determinant in Section 17 uses the frequency ξ/N for the unscaled trace. We obtain

$$|\chi_N(\xi)| \le C \exp(-|\xi| + C\sqrt{|\xi|}), \qquad \xi \in \mathbb{R}. \tag{19.16}$$

All constants here may be chosen on compact subsets of $u > -1/2$. At $s = 0$ the exact characteristic function is $e^{-|\xi|}$. This estimate controls real frequencies of every size uniformly in rank.

A matrix gamma integral. Under the Cayley map the matrix density of H is proportional to $\det(I+H^2)^{-N-s}$ with respect to Lebesgue measure on Hermitian matrices. Factor it into $\det(I+iH)^{-N-s}\det(I-iH)^{-N-s}$, using the sum of the principal eigenvalue logarithms for each matrix factor. The matrix gamma integral represents each as the Fourier transform of $e^{-\operatorname{Tr} A}\det(A)^s \mathbf{1}_{A>0}$ up to a common normalization. Indeed the change $A \mapsto B^{-1/2}AB^{-1/2}$ for positive B gives the general Laplace integral from that at I, with Jacobian $\det(B)^{-N}$, and holomorphic extension gives $B = I \pm iH$. The two factors in matrix space are square integrable for $2u > -1$, as follows by diagonalizing the positive matrix. Fourier multiplication therefore gives their convolution with one reflected, using the bilinear pairing at the same complex exponent. The harmless Fourier constants cancel at zero. At shift $|\xi|I/N$, one positive integration matrix is the other plus this shift. Rescaling the remaining positive matrix by two gives

$$\chi_N(\xi) = e^{-|\xi|}\, \mathbb{E}^{\mathrm{L}}_{N,2s} \prod_{j=1}^{N} \left(1 + \frac{2|\xi|}{N x_j}\right)^s. \tag{19.17}$$

Here the Laguerre functional on $(0,\infty)^N$ is normalized to mass one with density proportional to $\Delta(x)^2 \prod x_j^{2s} e^{-x_j}$. Its Hankel determinant is nonzero by the gamma product. The prefactor and the two inside the product correspond to $X = \operatorname{Tr} H/N$.

Comparison of Laguerre factorial densities. Put $\alpha = 2s$, $a = \Re\alpha > -1$, and use L_j^α with squared bilinear norm $b_j(\alpha) = \Gamma(j+\alpha+1)/j!$. The generating function gives the triangular connection

$$L_k^\alpha(x) = \sum_{j=0}^{k} d_{k-j} L_j^a(x), \qquad \sum_{l\ge 0} d_l w^l = (1-w)^{-i\Im\alpha}.$$

The right side is bounded analytic in the disk and $|d_l| \le C/(1+l)$. Convolution by these coefficients is bounded on ℓ^2 by the disk Hardy norm. In normalized polynomial coordinates the matrix contains the additional factor $b_j(a)^{1/2}/b_k(\alpha)^{1/2}$, of size comparable to $[(1+j)/(1+k)]^{a/2}$. The resulting triangular map has bounded operator norm uniformly under finite truncation. To see this, split indices $1+j, 1+k$ into dyadic intervals. Within the same or adjacent intervals the map is an unweighted convolution block between two diagonal factors with bounded product of norms; summing these bands costs a constant. In the remaining region $1+k \ge 2(1+j)$ the absolute kernel is bounded by $C(1+k)^{-1-a/2}(1+j)^{a/2}$. The two Schur sums with test sequence $(1+j)^{-1/2}$ are bounded because $a > -1$. The phases of the norm roots cost no additional factor. This argument also gives local compact parameter control.

At any real $x > 0$, the complex Laguerre feature vector is that same bounded transform of the normalized real vector times a phase $x^{i\Im\alpha/2}$. The determinant is a bilinear Gram determinant. Bounding its exterior power by the squared norm of the wedge gives

$$|\rho^{\mathrm{L}}_{k,\alpha}(x_1,\dots,x_k)| \le C^k \rho^{\mathrm{L}}_{k,a}(x_1,\dots,x_k).$$

This retains the repulsion in the real ensemble. Each orthogonality and correlation identity follows for complex α by finite-size continuation of the Laguerre integral, whose weight and all polynomial moments are absolutely integrable on this half-plane.

Bounding the deformation in (19.17). Write $q = 2|\xi|$, $d = q/N$. For $u \le 0$ one has $|(1 + d/x)^s - 1| \le C \min(1, d/x)$. Expand the multiplicative expectation in factorial densities and apply the preceding comparison and the real Gram diagonal bound. Its modulus is bounded by $\exp(C\mathbb{E}_a \sum d/(d + x_j))$. For $S = \sum_j (d + x_j)^{-1}$, integration by parts against $x_j/(x_j + d)$ in the real Laguerre density gives

$$d\,\mathbb{E}_a S^2 + (a + d)\mathbb{E}_a S = N.$$

The factor x_j removes the endpoint term for $a > -1$. The symmetrized Vandermonde terms give $d(S^2 - \sum (d + x_j)^{-2})$, cancelling the diagonal derivative. Jensen yields $\mathbb{E}_a(dS) \le C_a(1 + \sqrt{q})$. This proves (19.16) in this case.

For $u > 0$ choose the integer $m = \lceil u \rceil$, so $\beta = a - m > -1$. For $b \ge 0$ one has $1 + C|(1+b)^s - 1| \le (1 + C'b)^m$. The factorial comparison now bounds the modulus of the product expectation by $\mathbb{E}_a \prod (1 + C'd/x_j)^m$. Set $C'q = q'$ and $d' = q'/N$. Changing the Laguerre weight to $\beta = a - m$ writes this last expression as the ratio of the Wronskians at $-d'$ and at zero of the m polynomials L^{β}_{N+j}, $0 \le j < m$. To verify the identity, insert m distinct characteristic-polynomial arguments into the Vandermonde, replace powers by monic orthogonal polynomials, and integrate the N original variables by Andréief. Dividing by the inserted Vandermonde and taking coincident arguments gives the Wronskian. All leading constants cancel in the ratio.

Take forward differences of degree j in column j, and extract the common derivative sign from each row i. The entries become $L^{\beta+i-j}_{N+j-i}(-q'/N)$, understood as zero for negative degree. For $N \ge m$ the absolute value of this entry is bounded by

$$C N^{\beta+i-j} (1 + q')^C e^{2\sqrt{q'}}.$$

Indeed, putting $b = \beta + i - j$ and $n = N + j - i$, its coefficient of $(q'/N)^l$ is $[\Gamma(n+b+1)/n!]\, n^{\underline{l}}/[\Gamma(1+b+l)l!]$. The reciprocal gamma function covers negative integral specializations. Here $(n/N)^l$ is bounded for $l \le n$ at fixed m, and $1/|\Gamma(1 + b + l)| \le C(1 + l)^C/l!$. The resulting positive series is bounded by the stated expression using $\sum x^l/(l!)^2 \le e^{2\sqrt{x}}$ and finitely many derivatives. Every determinant term has rank power $N^{m\beta}$. The denominator divided by this power tends to $\det[1/\Gamma(1 + \beta + i - j)]_{i,j=0}^{m-1} = \prod_{i<j}(j - i)/\prod_i \Gamma(1 + \beta + i) > 0$. The finitely many small ranks are controlled directly by their polynomial ratios. Thus the desired bound is $C \exp(C\sqrt{q})$. Around positive integral u take the larger of the adjacent integer choices, which still satisfies $m < 2u + 1$. Near $u = 0$ compact uniformity follows separately: for $0 < u \le u_0 < 1/4$ and $a = 2u$, use the diagonal factorial bound with $|(1+b)^s - 1| \le C \min(b, 1)(1+b)^{u_0}$. For $y = Nx < 1$ the real intensity in dy is at most Cy^a uniformly near $a = 0$, directly by the Laguerre polynomial series just used at $x = y/N$ and the sum over $0 \le j < N$ (each unweighted normalized feature is $O((1 + j)^{a/2})$). This part costs $C(1 + q)^{u_0}$. For $y \ge 1$ and $q > 1$, use dyadic sets $1 \le y \le q$: the resolvent inequality gives $\mathbb{E}_a \#\{y_j \le R\} \le C(1 + \sqrt{R})$, and the sum of $(q/y)^{u_0}$ on these sets costs $C\sqrt{q}$ since $u_0 < 1/2$. The region $y > \max(1, q)$ is bounded by the same resolvent. This completes the uniform proof of (19.16).

Inversion and the variation of the projected trace. We in fact get a stronger statement than (19.15). For every $0 < q < 2u + 1$ the complex trace has a density $p_{N,s}$ with

$$|p_{N,s}(x)| \le C_q(1 + |x|)^{-1-q}. \tag{19.18}$$

Its limit p_s is obtained by Fourier inversion from the circle transform of Theorem 19.7, evaluating the transform for $\Im Y$ at 2ξ to obtain the trace transform at ξ. The convergence is in total variation with any weight $(1 + |x|)^{q_0}$, $0 \le q_0 < 2u + 1$. In particular

$$\mathcal{C}(s, h) = 4^{-h} \int_{\mathbb{R}} (1 + x^2)^h p_s(x)\, dx.$$

The mass of p_s is one. Its possible complex zeros cause no division in this formula.

Here are the frequency estimates needed for inversion. Fix a noninteger q' with $q < q' < 2u + 1$ and $j_0 = \lfloor q' \rfloor$. The finite circle transform has a Taylor polynomial at zero through degree j_0 with bounded coefficients and uniform remainder $O(|\xi|^{q'})$ on the real axis. For details use the complex circle kernel from Theorem 19.7 with $f(t) = N^{-1} \cot(t/(2N))$ and $F = e^{i\xi f} - 1$. Set $\omega(t) = |t|^{-q'}$ on $|t| \le 1$ and $|t|^{-1}$ outside. Factor the perturbation as $M_{F/\omega}\sqrt{\omega} K_{N,s} \sqrt{\omega}$. The second factor is uniformly Hilbert–Schmidt by the local integrability of ωV_u and the

square integrable tail, as in the proof of (19.13). For the Taylor remainder on $|t| \le 1$ use $C|\xi f|^{q'} \le C|\xi|^{q'}\omega$; outside one use $C|\xi|^{j_0+1}|t|^{-j_0-1}$ for $|\xi| \le 1$. The coefficient multipliers divided by ω are bounded. The regularized determinant therefore has a bounded Taylor jet with the stated remainder, by analyticity and uniform bounds on Hilbert–Schmidt balls. The trace obeys the same bound: the outer remainder is integrable for $j_0 \ge 1$, and for $j_0 = 0$ evenness gives a cosine error $C\xi^2/t^2$. The coefficients are the actual moments by finite-dimensional integrability. Odd ones vanish by reflection.

The Wishart expression for $\xi > 0$ in (19.17) extends analytically to $\Re\xi > 0$ using the principal power of $1 + 2\xi/(Nx)$. In any sector $|\arg\xi| \le \theta_0 < \pi/2$ the same majorants hold with $|\xi|$ inside the product bounds and $e^{-\Re\xi}$ in front. Indeed the base has positive real part, its modulus is between 1 and $1 + 2|\xi|/(Nx)$, and its argument is bounded. The bound for a small perturbation follows by differentiating the scalar power on the intervening segment. Finite-size holomorphy under the positive matrix integral follows from the same integrable bounds on compact subsets. Denote this analytic right-half-plane branch by G_N. Let $P_N(w) = e^{-w^2}$ times the degree-j_0 Taylor polynomial on the real axis of $e^{w^2}\chi_N(w)$. It is even, with uniformly bounded polynomial coefficients. The difference $G_N - P_N$ is bounded on $|w| \le 1$ in the sector, and is $O(|w|^{q'})$ on the positive real ray. On the ray of angle θ, $0 < |\theta| < \theta_0$, it is $O(|w|^{q'(1-|\theta|/\theta_0)})$. For this last bound apply the maximum principle to the logarithm of the modulus in $\log w = x + iy$, with upper barrier $C + q'x(1 - |y|/\theta_0)$ in each half-strip $x < 0$. On a rectangle $-R < x < 0$ the missing left boundary costs $O(R)$ times its harmonic measure, which tends to zero at each interior point as $R \to \infty$ (by the sine series, exponentially in $R + x$). This gives the claimed constants uniformly in rank.

Choose $0 < \theta < \min(\pi/4, \theta_0(1 - q/q'))$. In the inverse cosine transform for $x > 0$ deform the two exponential integrals of $G_N - P_N$ onto the rays $\arg w = \pm\theta$ with the corresponding damping sign. The outer arcs vanish by $|G_N(w)| \le Ce^{-\Re w + C\sqrt{|w|}}$ and the Gaussian bound on P_N; the inner arcs vanish by boundedness. Each integral for $x \ge 1$ is bounded by $C\int_0^1 r^q e^{-xr\sin\theta}dr + Ce^{-bx}$. The inverse transform of P_N is a Gaussian times a polynomial with bounded coefficients. Evenness supplies $x < 0$ and (19.16) bounds the density near zero. This proves (19.18). Compact-frequency convergence and (19.16) give convergence of densities in uniform norm, and (19.18) gives the stated weighted variation convergence using an exponent strictly above q_0. The arguments on parameter compacts and finite-rank holomorphy now prove Theorem 19.8. In particular the circle trace projection has bounded variation even while the original matrix measure has growing variation.

The leading signed tail of the circle trace. In fact the projected density in (19.18) has an explicitly nonzero leading tail. With $b = 2s + 1$, on a sufficiently small neighborhood of every s with $\Re s > -1/2$ there exist $C, \delta > 0$ such that for $|x| \ge 1$ and all N,

$$p_{N,s}(x) = A_N(s)|x|^{-2s-2} + O(C|x|^{-2\Re s-2-\delta}), \qquad A_N(s) = \frac{2^{2s}\Gamma(1+s)^2}{\pi}\frac{\Gamma(N+b)}{N^b\Gamma(N)\Gamma(b)\Gamma(b+1)}.$$

Thus p_s has the same expansion with $A(s) = 2^{2s}\Gamma(1+s)^2/[\pi\Gamma(b)\Gamma(b+1)]$. This describes the complex phase as well as its absolute size. It implies sharpness even after the signed matrix measure has been projected to the real trace. For $\Re h \ge \Re s + 1/2$ the integrals on $R < |x| < LR$ have leading nonzero multiple of $R^{2h-2s-1}$ for some fixed $L > 1$, with a logarithm of L if the power vanishes. Thus even the symmetrically truncated improper circle integrals fail to converge there. Near the boundary the ordinary normalized circle readout has a meromorphic continuation in h with residue $-4^{-(s+1/2)}A(s) = -g_{s+1}/(2\pi g_s)$ at $h = s + 1/2$. Indeed subtract the leading tail on $|x| > 1$; the error gains a positive power and the integral of the leading power is $2A(s)4^{-h}/(2s+1-2h)$. This concerns the exact circle readout.

To prove the expansion, use (19.17) first for parameters with $b \notin \mathbb{Z}$. Put $q = 2\xi$, $y = Nx_j$, and use a fixed closed subsector of $|\arg q| < \pi/2$. The one-point density of the complex Laguerre ensemble in dy is $D_N y^{2s} + O(y^{2u+1})$ for $0 < y < 1$, where $D_N = \Gamma(N+b)/(N^b\Gamma(N)\Gamma(b)\Gamma(b+1))$. This follows directly from the Laguerre kernel: $L_j^{2s}(y/N)/L_j^{2s}(0) = 1 + O(y)$ by the terminating series, uniformly for $j < N$; the absolute sum of its squared endpoint values divided by $|b_j|$ is $O(N^{2u+1})$. The signed endpoint sum is evaluated by $\sum_{j<N}(1+2s)_j/j! = (2+2s)_{N-1}/(N-1)!$.

In the factorial expansion write $F(q,y) = (1+q/y)^s - 1$. Its integral in absolute value against the real Laguerre intensity is $O(|q|^\gamma)$ for any $0 < \gamma < \min(1, 2u+1)$. Split at $|q|$ and at one, using the local Cy^{2u} bound and $\int_{y>1} y^{-1}\rho_1(y)dy \le C$ by the resolvent estimate. All constants in what follows are uniform on small closed parameter neighborhoods. Put $b_R = 2u + 1$ at the center of such a neighborhood. Choose the greatest integer

$d < b_R$ and take $p^- < b_R$ close enough that $d < p^- \le d+1$, $p^- > u$. Shrink the neighborhood so that $p^- < \inf(2\Re s+1)$. Let T_d denote the binomial polynomial in q/y of degrees $1,\dots,d$. Then $\int |F - T_d|\rho_1 dy = O(|q|^{p^-})$: for $y<1$ use $C|q/y|^{p^-}$, and for $y>1$ use the Taylor bound $C|q/y|^{d+1}$. Also $\int |T_d|\rho_1 dy = O(|q|)$ for $d \ge 1$, and $T_0 = 0$. The factorial Gram comparison shows that replacing all F by T_d in terms with at least two tags costs $O(|q|^{p^-+\gamma})$. Indeed each product difference has one such error and at least one extra small factor; the exponential series bounds their sum. The remaining series made solely of T_d is analytic at zero, with uniformly bounded coefficients on a small disk by the same absolute factorial bound. Choose a noninteger $p^+ > \sup(2\Re s+1)$ smaller than $p^- + \gamma$ and $\inf(2\Re s+2)$; this is possible on a sufficiently small neighborhood. Retain that series through degree $J = \lfloor p^+ \rfloor$ with remainder $O(|q|^{p^+})$.

In the single-tag term, after subtracting $D_N y^{2s}\mathbf{1}_{(0,1)}(y)$ from its density, the same binomial expansion through J works with an $O(|q|^{p^+})$ remainder: the density error gains one power of y at zero, and the tail admits every inverse power of degree at least one. For the subtracted term the elementary beta integral gives for $|q|<1$

$$\int_0^1 y^{2s}[(1+q/y)^s - 1]dy = q^b \frac{\Gamma(1+s)\Gamma(-b)}{\Gamma(-s)} + \sum_{j\ge 1}\binom{s}{j}\frac{q^j}{b-j}.$$

One can first evaluate the unsubtracted integral over $(0,\infty)$ in $-1 < \Re s < -1/2$, remove its integral over $y>1$ by the convergent binomial series, and continue the resulting formula for the integral on $(0,1)$ before subtracting its constant. Positive q fixes the branch and analyticity gives the sector formula.

Multiplying by $e^{-q/2}$ now yields an analytic polynomial through degree J, the fractional term $D_N\Gamma(1+s)\Gamma(-b)q^b/\Gamma(-s)$, and $O(|q|^{p^+})$ (reduce p^+ also below $\inf(2\Re s+2)$ as above). Each odd coefficient below $\Re b$ vanishes by reflection and finite ordinary circle moments. If J includes an additional odd degree when $\Re b$ is an integer and $\Im b \ne 0$, shrink to a neighborhood with $J = \Re b$ at its center. The coefficient is holomorphic there and vanishes on the side $\Re b > J$, hence everywhere in that neighborhood. For noninteger $\Re b$ one can take p^+ below the next integer. Consequently there is a uniformly bounded even polynomial P_N such that $e^{-\xi^2}P_N(\xi)$ has precisely these integral-power terms. Subtract this function and the fractional term multiplied by $e^{-\xi^2}$. The inverse cosine transform of the remainder is $O(|x|^{-1-p^+})$ by the ray rotation used above. On the same rays the fractional term has leading cosine integral $\Gamma(b+1)\cos(\pi(b+1)/2)|x|^{-1-b}$; replacing $e^{-\xi^2}$ by 1 in this calculation costs $O(|x|^{-3-\Re b})$ by direct Laplace integration. After the factor $2^b/\pi$ and gamma reflection, the coefficient is exactly $A_N(s)$ above.

For real s with $b \in \mathbb{Z}$ take a small circle in parameter space around s, containing no other such point. All points on its boundary have the proved estimates, with a common positive surplus by compactness. For each $x \ge 1$, $x^{2s+2}p_{N,s}(x) - A_N(s)$ is holomorphic inside, by the previous Fourier bound. The maximum principle fills the circle with the same error; evenness treats $x<0$. This also covers the resonant integer values without interpreting a singular gamma coefficient in isolation. Passing to the limiting density at fixed x proves its expansion.

Cancellation after retaining the near eigenangles and the exterior sums

Theorem 19.9 (complex variation on the retained coordinates). Fix a compact subset of $\Re s > -1/2$. For all sufficiently large N and sufficiently small $c>0$, the complex law of all eigenangles in $[-2,2]$ in microscopic coordinates and the two exterior sums has the density bound (19.19) on the count sectors $k \le N/2$. The omitted high counts obey the absolute estimates below. The full transverse Fourier transform decreases faster than any prescribed inverse frequency power, with the rank cutoff allowed to depend on that power. We first prove the source bound, then its version with prescribed inner angles.

Use the preceding circle kernel $K = K_{N,s}$ as an idempotent on $L^2(I_N, dt)$. Write $s = u + iv$, and let P be the orthogonal projection onto its range. This is explicitly the circle projection at u conjugated by the unitary multiplier $|1-e^{it/N}|^{iv}$. Indeed its range consists of functions $|1-e^{it/N}|^s$ times polynomials in $e^{it/N}$ of degree below N. Consequently $B = K - P = PB(I-P)$. The constants below are locally uniform in s.

Dyadic square norm of the nonorthogonal part. If $E_R = \{R < |t| \le 2R\} \cap I_N$ for dyadic $R \ge 1$, then $\|B\mathbf{1}_{E_R}\|_2^2 \le C$, with the same bound for the central interval $|t| \le 1$. Subscript 2 is the Hilbert–Schmidt norm. To prove this, sharpen the polynomial bound at $ND \ge 2$, where $D = |1-\lambda|$, to

$$\Phi_N(\lambda) = \lambda^N(1-\lambda^{-1})^{-s} + O\big(D^{-u}/(ND)\big).$$

Subtract $(1-\lambda^{-1})^{-s}$ from the factor $(1-v)^{-s}$ of the generating function. Near $v=\lambda^{-1}$ the undifferentiated difference is at most $CD^{-u-1}|v-\lambda^{-1}|$ by the mean value integral along the line segment inside the disk. In the previous derivative-Cauchy proof this gains $(ND)^{-1}$ at that pole; terms differentiating this factor at least once already gain the same factor. The other pole already has that gain, and the smooth complementary part has $(ND)^{-m-u}$, taking $m+u>2$ also to absorb borderline logarithms. The explicitly subtracted coefficient is the leading term stated above.

For $|w| \asymp R \ge 2$ and $d = d_N(t,w) < R/2$, insert the leading polynomials in the two Christoffel–Darboux formulas for K_s and K_u. Their leading numerators before division by $2\pi N(1-e^{i(t-w)/N})$ are

$$a_s(t)/a_s(w) - e^{i(t-w)}a_s(w)/a_s(t), \qquad a_s(t) = e^{-is\arg(1-e^{it/N})}.$$

The monic norm factor $b_N^{-1} = 1+O_s(1/N)$ may be included in the remainder. Along this arc the circular argument function changes by $O(d/N)$ because it is linear between successive copies of zero. The gauge conjugating P changes by $O(d/R)$, by the derivative of $\log|1-e^{it/N}|$. Thus

$$|B(t,w)| \le C\min\{1, R^{-1}+(Rd)^{-1}\}.$$

For $d \ge R/2$ the earlier kernel bound for K and P applies. Its square integrates to $O(1/R)$ in t because $V_u(t)$ is bounded off $[-1,1]$ and integrable inside. The preceding minimum has the same square integral, splitting at $d = 1/R, 1, R/2$. Integration in w proves the assertion. For bounded dyads use the global kernel bound directly, which also gives $\int |K(t,w)|^2 dt \le CV_u(w)$.

Oscillatory transfer. Let U multiply by a unit phase with $|U(t)-1| \le C\min(1, H/|t|)$ for $|t| \ge 1$, $H \ge 2$. If $A(t)$ is the circle-to-interior weight ratio in the preceding proof, then

$$\Big|\det_P\big((P+B)AUP\big)\Big| \le CH^C \exp\big(-\gamma\|(I-P)UP\|_2^2\big).$$

Here constants may depend on the fixed constant in the phase bound. This finite determinant is exactly the circle-normalized expectation of the multiplicative symbol AU, since restricting KAU to its range gives it.

Choose L dyadic between H^2 and $2H^2$ and split $B = B_0 + B_1$ with $B_0 = B\mathbf{1}_{|t|\le L}(I-P)$. Its squared Hilbert–Schmidt norm is $O(1+\log L)$. The exterior perturbation $B_1UP = B\mathbf{1}_{|t|>L}(I-P)(U-1)P$ has bounded trace norm. For the identity part of $I-P$, each dyad $R \ge L$ costs $C(H/R)\sqrt{R}$ by the previous square norm and $\|\mathbf{1}_{E_R}P\|_2 \le C\sqrt{R}$. For the $-P$ part decompose the variable at $U-1$ into dyads S (the central interval counts as $S=1$). Each costs $C\min(1,H/S)\|\mathbf{1}_{E_R}P\mathbf{1}_{E_S}\|_2$. For comparable dyads this last norm is $O(\sqrt{R})$. For noncomparable dyads it is $O(\sqrt{\min(R,S)/\max(R,S)})$ by the off-diagonal bound and the integrability of V_u in the central interval. Summing $S < R/4$ costs $O(\sqrt{H/R})$, and summing $S > 4R$ costs $O(H/R)$. All dyadic $R \ge L$ therefore cost $O(1)$. If L exceeds the period there is no exterior perturbation. The perturbation $K(A-1)UP$ has trace norm at most $C\int |A-1|V_u$, by the two weighted Hilbert–Schmidt factors using the column estimate on K and the diagonal bound on P. This integral is bounded independently of the depth and rank by the local and far integrals already proved.

To retain the phase contraction put $V = (I_P + B_0B_0^*)^{-1/2}(P+B_0)$, a row isometry onto P. Its squared Hilbert–Schmidt distance from P is at most $C\|B_0\|_2^2$ by the scalar singular-value bounds. Factoring out $(I+B_0B_0^*)^{1/2}$ costs at most $\exp(\|B_0\|_2^2/2)$. The remaining compressed operator is $VUP+E$, with $\|E\|_1 \le C$. Since VUP is a contraction, the inequality $\log x \le x-1$, the trace-norm perturbation inequality for singular values, and $1-x \ge (1-x^2)/2$ on $[0,1]$ imply

$$\log|\det_P(VUP+E)| \le C - \tfrac12\|VU(I-P)\|_2^2.$$

The latter square norm is at least $\frac12\|PU(I-P)\|_2^2 - C\|B_0\|_2^2$. Unitarity makes $\|PU(I-P)\|_2 = \|(I-P)UP\|_2$. This proves the estimate. The case of a singular determinant follows by continuity.

Resolved Fourier frequencies. Take $U = e^{i\phi}$ with $\phi = \beta\Re n/c + \xi\Im n$, and put $r = |\beta|+|\xi|$, $H = 2+r$. For every fixed m there are C_m, N_m such that

$$\Big|N^{-s^2}\mathbb{E}\{|\Lambda_N(z)|^{2s}e^{i\beta(\Re Y+1/2)/c+i\xi\Im Y}\}\Big| \le C_m(1+r)^{-m}$$

for $N \ge N_m$ and all sufficiently small positive c. The convergence and estimates here concern the normalized readout, allowing the matrix preparation to have increasing total variation.

For the contraction, $\|(1-P)UP\|_2^2$ is half the integral of $|U(t)-U(w)|^2|P(t,w)|^2$. Write $T = \max(|\beta|^{1/3}, |\xi|^{1/2})$ and first take T large. On one sign of an angular shell with $|t| \asymp T$ and $T \le \epsilon N$, the two terms of the phase derivative add in modulus. Indeed with $a = (1-z)^2 + 4z\sin^2(\theta/2)$ the exact derivative in the original angle θ is

$$\phi'_\theta = \frac{-\beta \sin\theta/N^2 + \xi[(1+z^2)\cos\theta - 2z]/N}{a^2}.$$

For bounded small ϵ and $1 \ll |t| \le 3\epsilon N$, the second bracket is negative and comparable to $-t^2/N^2$, since $c \le 1$. Choose the sign of t to align the two terms, obtaining $|\phi'_t| \asymp |\beta|/|t|^3 + |\xi|/t^2$. On the indicated shell this is bounded above and below by positive constants. For $T > \epsilon N$ instead choose a fixed small angular shell $|t| \asymp \epsilon' N$, $0 < \epsilon' < \epsilon/4$, with the same choice of sign. There the displayed derivative is between constant multiples of $G = |\beta|/N^3 + |\xi|/N^2$, and G is bounded below. On either shell use separations $d = w - t \in [d_0, 2d_0]$ for a fixed small $d_0 > 0$. The real-projection kernel there is bounded below by a positive constant by the leading Christoffel–Darboux sine numerator and the $O(1/|t|)$ remainder on this separation interval. The integral in d of $|U(w)-U(t)|^2$ is bounded below: the phase is monotone, its image has length at least a positive constant times Gd_0, and the substitution has density between two constants times $1/G$ (use $G = 1$ on the first shell). Every interval of length at least a fixed positive number has its average of $1-\cos$ bounded below. Hence the contraction is at least $b\min(T, N)$ for T above a fixed cutoff. For $r \le N^M$ with fixed M, this exponential contraction absorbs every polynomial in r.

For $r > N^M$ use the original finite Toeplitz determinant. Choose a small $b > 0$ uniformly on a parameter compact. Cutting away $|\theta| \le r^{-b}$ from one angular entry costs $Cr^{-b\min(1,2u+1)}$, since for $u < 0$ the absolute weight is at most $C|\theta|^{2u}$. On the complement the supremum and total variation of $|1 - ze^{i\theta}|^{2s}$ cost $Cr^{b(1+2|u|)}$ by differentiating along the two monotone halves of its positive radial argument. The Fourier monomial multiplies the variation estimate by $C(1+N)$. In the formula for ϕ'_θ the numerator divided by $G' = \max(|\beta|/N^2, |\xi|/N)$ is a constant plus a sine and cosine with combined amplitude between two absolute positive constants. Its sublevel set of width $r^{-1/2}$ has angular length $O(r^{-1/4})$ by the elementary cosine sublevel bound, even at a double root. Outside this set $|\phi'_\theta| \ge b' r^{1/2}/N^2$ since a is bounded above. The derivative has a bounded number of monotonicity intervals (its derivative after clearing a^3 is a trigonometric polynomial of bounded degree). The first derivative test gives per entry a bound $CN^3 r^{-\delta}$ for some $\delta > 0$, choosing $b(1+2|u|) < 1/8$. Hadamard's determinant bound then gives $(CN^4 r^{-\delta})^N$ before the normalization, which costs at most a fixed power of N. Choosing M large relative to $1/\delta$ proves the asserted rapid decay for any prescribed m, at sufficiently large rank.

Exterior sums jointly with the interior eigenangles

Fix the central window $D = [-2, 2]$ in microscopic coordinates. Retain all its angles, and only the two sums $b = \sum_{t \notin D} \Re n(t)/c$, $j = \sum_{t \notin D} \Im n(t)$ outside. In the unnormalized measure scaled by N^{-s^2}, the ordered Janossy density of exactly k central angles at $t_1, \dots, t_k$ and the two exterior sums, integrated with $dt_1 \cdots dt_k/k!$ and $db\,dj$, satisfies, for $k \le N/2$ and sufficiently large N,

$$|J_k(t_1, \dots, t_k; b, j)| \le C^{k+1} e^{-|b|-|j|} \prod_{i \le k} (c + |t_i|)^{2u}. \tag{19.19}$$

For any two distinct tagged indices one may multiply this bound by $\min(1, |t_i - t_j|^2)$, with a larger C. Constants are locally uniform in s with $u > -1/2$. The Janossy density is a complex density, and $b \ge 0$.

The Fourier transform in b, j is the mixed coefficient in k rank-one insertions in the preceding compressed determinant. In its multiplicative symbol set the weight to zero on D and use AU outside. Inserting a tag at t adds the matrix $A(t)K(\cdot,t)P(t,\cdot)$ (outer product of column $K(\cdot,t)$ and row $P(t,\cdot)$). This follows directly by multilinearity of the finite determinant or by integrating the Weyl density with k specified angles held fixed. The prefactor $N^{-s^2} Z_N^\circ(s) z^{Ns}$ is uniformly bounded. We prove a rapid bound on its Fourier transform uniformly also for imaginary parts of both frequencies in $[-1, 1]$.

Write the corresponding positive multiplier as e^g with real g a linear combination, with coefficients bounded by one, of the two exterior per-angle marks. Extend g and the real phase by zero on D. Then $\|g\|_\infty \le C$,

$\int gP(t,t)dt = O(1)$ by evenness and the integrable even real mark, and $\int g^2P(t,t)dt \le C$. In the preceding dyadic argument use the main matrix

$$RUC_0, \qquad R = (P + B_0)e^{g/2}, \quad C_0 = e^{g/2}P.$$

The exterior remainder uses $e^gU - 1$ and satisfies the same $H/|t|$ estimate; $K(A-1)e^gUP$ remains bounded in trace norm. Removing the weight on D costs an additional bounded trace norm since $\int_D |A|V_u \le C$. The row and column Gram determinants each cost at most CH^C on factoring out their positive square roots. In fact the column trace excess is $\mathrm{Tr}P(e^g - 1)P = O(1)$ by the centering and square integral. For the row Gram add $\|B_0\|_2^2$, the cross terms bounded by $C\|B_0\|_2\|(e^g - 1)P\|_2$, and a final term $O(\|B_0\|_2^2)$. Both Gram matrices are bounded below by an absolute compact-dependent multiple of the identity of P, since e^g is bounded below and $(P + B_0)(P + B_0)^* \ge I_P$. The polar row and column isometries are at Hilbert–Schmidt distances $O(\sqrt{1 + \log H})$ and $O(1)$ from their starting row and column P. Indeed before polar normalization these estimates follow by the square integral of $e^{g/2} - 1$, and the extra distance is bounded by the initial distance to the isometry P by singular-value perturbation. The loss in the squared Hilbert–Schmidt defect of the resulting contraction is consequently controlled as before: if V, W are the row and column isometries, $\|VU(I - WW^*)\|_2 \ge \|PU(I-P)\|_2 - C\sqrt{1 + \log H}$. Its shell lower bound still holds as the high-frequency shells are outside D.

For a square matrix M the mixed coefficient in $\det(M + \sum_{j\le k} \epsilon_j a_j b_j^*)$ is bounded by $\|\bigwedge_{j\le k} a_j\| \, \|\bigwedge_{j\le k} b_j\|$ times the product of the largest $N - k$ singular values of M, by the complementary exterior power identity. No factorial occurs. The trace-norm perturbation inequality used above costs at most an extra k in its logarithmic bound when the smallest k singular values are dropped. Inverse Gram square roots on the tagged vectors have operator norm bounded uniformly, costing C^k. The two vector norms per tag supply $CV_u(t)$, multiplied by $|A(t)|$. On D, $|A(t)|V_u(t) \le C(c + |t|)^{2u}$ for either sign of u. To retain repulsion, strip the factors $|N(1 - e^{it/N})|^s$ from $K(\cdot, t)$ and $|N(1 - e^{it/N})|^{\bar s}$ from $P(\cdot, t)$. The remaining column in either case is a vector-valued trigonometric polynomial of degree at most $N - 1$ with norm $\le C(1 + |t|)^{-u}$ on the microscopic period. For the column P this follows from its explicit phase conjugation, with a constant unit-modulus factor possibly depending on N. The differentiated smooth bandlimited convolution reproducer, as in the two-tag proof above, bounds its derivative uniformly on D. Subtracting one column from the other on each wedge gives the stated squared separation. We obtain the exponential shell bound times $C^k \prod_i (c + |t_i|)^{2u}$, with the optional repulsion factor.

For ultrahigh frequencies use the original angular monomial basis. Its entries outside D have the previous first-derivative bound $CN^3r^{-\delta}$ with the same cutoffs, because e^g has bounded supremum and variation there (the two truncated single marks and their variations are bounded off D uniformly). Excluding D only introduces two additional endpoints. The mixed coefficient uses $N - k$ such singular values, each $\le CN^4r^{-\delta}$, and the original tagged vectors $N^{-1/2}(e^{ilt/N})_{0\le l<N}$ and their evaluation rows have norm and derivative norm at most one. The original angular weights on D cost at most $CN^{2|u|}(c + |t|)^{2u}$ per tag, with the $1/N$ from $d\theta = dt/N$ used in the normalization of the vectors. The overall N^{-s^2} costs only a power of N. For $k \le N/2$, taking $r > N^M$ with M sufficiently large relative to $1/\delta, |s|$ absorbs all these powers and yields arbitrary fixed rapid frequency decay at sufficiently large N. Thus the Fourier transform, throughout the fixed strip, is bounded by $C_m C^k (1 + r)^{-m} \prod_i (c + |t_i|)^{2u}$ including the optional repulsion. Finite-rank transforms of the exterior sums are entire, since exterior per-angle observables are bounded. Fourier inversion shifted to imaginary parts of signs chosen for b, j now gives the claimed exponential tails in both variables.

Finally, $k > N/2$ contributes $o(1)$ in total absolute readout for any fixed order strictly inside the ordinary real-tilt strip, uniformly in small depths. Indeed take absolute values in the matrix ensemble, costing $O(N^{v^2})$ times real-tilt probability. Its factorial intensity on D admits the product envelope of Section 19 with uniformly bounded integral, so $\Pr(k > N/2) \le C^{\lceil N/2 \rceil}/\lfloor N/2 \rfloor!$ by the factorial moment bound. Hölder with a surplus real-tilt absolute moment in Theorem 19.3 absorbs the singular or growing readout at a cost bounded uniformly in N, c, which proves the assertion. A bounded observable requires only the same probability estimate.

Independent complex tilt and order at all shrinking-depth rates

Theorem 19.10 (ordinary complex moments and the density near zero). Let $u = \Re s > -1/2$, $-1 < \sigma = \Re h < u + 1/2$, $Y = S_N/c$ and $c = N(1 - z^2)$. Then, locally uniformly in the two independent complex parameters,

$$\lim_{N\to\infty,\ c\downarrow 0} N^{-s^2} c^{-2h} T_N(h, s; z) = g_s \mathcal{C}(s, h) = 4^{-h} g_s \int_{\mathbb{R}} (1 + x^2)^h p_s(x)\, dx. \tag{19.20}$$

The relative rate is arbitrary. Use real logarithms for powers of positive numbers. The finite integrals and the displayed limiting integral exist absolutely at the stated parameters. Passing to the limit uses cancellations within the preparation. At $\Re h \le -1$ the original finite interior integral fails absolute existence for $N \ge 2$. At $\Re h \ge u + 1/2$ the exact-circle integral fails absolute existence, also after trace projection by the signed tail following (19.18). Both inequalities in (19.20) are sharp for this ordinary circle readout. Dividing by the tilted mass is legitimate for large ranks by Theorem 19.7. No division by the value of a moment or by a pointwise density is used.

Write $p^{Y}_{N,s,z}$ in the following formulas for the density of the **unnormalized** matrix weight $N^{-s^2}|\Lambda_N(z)|^{2s}$ pushed onto Y. For any fixed compact $D_0 \subset \{\Re y > -1/2\}$, one has along the same simultaneous limit, in $L^\infty(D_0)$,

$$c^{-(2s+5/2)} p^{Y}_{N,s,z}(y) \;\longrightarrow L^*_s(\Re y), \qquad L^*_s(x) = \frac{g_{s+2}}{2\pi^2}(1/2 + x)^{-2s-7/2}. \tag{19.21}$$

This convergence is also locally uniform in s. In particular the complex mass of $|Y| \le r_N$ is $\pi L^*_s(0) c^{2s+5/2} r_N^2 (1 + o(1))$ at any $r_N \downarrow 0$. The coefficient is nonzero for $u > -1/2$. Finite complex densities need not have a sign.

Variation at the two ends. Work first with at most $N/2$ central angles in (19.19). Take the absolute value of that joint density after integrating all other matrix coordinates. It defines a positive dominating measure on the retained angles and the two exterior sums. Its total mass is bounded by the exponential series over the number k of central angles. For $0 < d < 2u + 1$ its $|Y|^d$ integral is bounded. The exterior terms and constant offset have bounded moments by their exponential tails, and the local positive sum is bounded in the dth power by $C_d e^k \sum_i (c + |t_i|)^{-d}$. Single out the corresponding tag and integrate $(c + |t|)^{2u-d}$ on $[-2, 2]$. For more than $N/2$ tags use the real count bound and Hölder in Theorem 19.9, with a positive-order surplus still within $2u + 1$. Thus the total variation of the planar pushforward is bounded and its tail tends to zero uniformly, also with any strictly admissible positive power weight.

For small marks we use the collision factor in (19.19). With exterior variables b, j and a fixed count k, put $T_* = 1 + k + b + |j|$. This bounds the number of central angles, the exterior real contribution cb, and the exterior signed imaginary sum. On $Y \in D_0$, $1/(2z) + \Re Y$ is bounded above and below by positive constants. Positivity of the constituent real marks is an identity on configurations even for a complex integration weight. On a dyad $T \le T_* < 2T$ with $T \le \gamma c^{-1/3}$ the forcing argument in Theorem 19.2 therefore applies verbatim to the angles: two opposite tags satisfy

$$b_1 \sqrt{c} \le |t_\pm| \le C\sqrt{c}\, T^{3/2}, \qquad |J_{+-}|^{-1} \le C c^{3/2} T^{15/2}.$$

Here b_1, γ depend only on the target compact and the angular bounds. For fixed exterior and all other tags, pair area change has bounded multiplicity. The two powers in (19.19) cost $C c^{2u} T^{6\max(u,0)}$ and their squared separation costs CcT^3. Integrate the other tagged weights and sum over at most $k(k-1)$ choices against $C^{k+1}/k!$. The exponential bound in $b, |j|$ and the factorial in k allow an extra weight $e^{d_0 T_*}$ for fixed small $d_0 > 0$. The dyad therefore costs at most $C e^{-d_0 T} \operatorname{poly}(T) c^{2u+5/2} |E|$ for any Borel $E \subset D_0$. Above $T = \gamma c^{-1/3}$ one can instead hold all local angles fixed. The affine map $(b, j) \mapsto Y$ has area Jacobian c, so the cost is at most $C c^{-1} e^{-d_1 c^{-1/3}} |E|$. For this last estimate absorb the indicator into the spare exponential in $b, |j|, k$ before taking the supremum over the translated target. This proves the required estimate for the absolute joint measure on the retained coordinates.

For $k > N/2$ the original real-tilt proof of (19.2) gives a stronger high-count estimate. Its variable K dominates k, since its count cutoff equals one on $[-2, 2]$. On the moderate dyads the exponentially decreasing dyadic estimates start at $T > N/4$ and give $O(e^{-d_2 N} c^{2u+5/2})|E|$. Above the cutoff that proof gives $C c^{-2A} \exp[-\max(N/2, \gamma c^{-1/3})]|E|$, which is bounded by the same expression with a smaller d_2. The absolute complex matrix weight costs $O(N^{(\Im s)^2})$ and the high-count loss absorbs this factor. For compact parameter uniformity all the low-count estimates above are uniform in s on compacts. The real high-count bounds may alternatively be interpolated between two neighboring real tilts by Hölder on the positive, unnormalized integral: the exponent $2u + 5/2$ is affine and the Barnes normalization loses at most a fixed power of N, absorbed by the exponential. We have proved the upper bound $C c^{2u+5/2}|E|$ for planar variation on D_0.

The normalized matrix-space variation is of order $N^{(\Im s)^2}$. In contrast the estimates just proved give tight, uniformly bounded planar variation. The convergence of the Fourier transform in Theorem 19.7 identifies every subsequential weak limit of these complex measures by uniqueness. The limit is supported on $\Re y = -1/2$, with trace density $g_s p_s$ under $x \mapsto (-1 + ix)/2$. At a negative order, the variation contribution to the radial integral from $|Y| < r < 1/4$ is at most $2\pi C c^{2u+5/2} r^{2+2\sigma}/(2 + 2\sigma)$. At large modulus a surplus exponent in the preceding

positive bound permits truncation. Between these cutoffs the functions are bounded and continuous. This proves (19.20); normal-family uniqueness, or uniform cutoffs on compact parameter sets and subsequences, gives joint local uniformity. The limiting line has zero two-dimensional area, so this weak planar convergence has a different meaning from the weighted variation convergence of the scalar trace at the exact circle.

To identify the coefficient in (19.21), for any sequence of positive-area Borel sets $E_N \subset D_0$ apply Vitali's theorem to

$$\frac{c^{-2s-5/2}\int_{E_N} p^Y_{N,s,z}(y)\,d^2y - \int_{E_N} L^*_s(\Re y)\,d^2y}{|E_N|}.$$

The numerator is holomorphic in s at each finite rank. The variation bound makes the quotient locally bounded independently of the sets. It tends to zero at every real $s > -1/2$ by (19.3) and the mass conversion $N^{-s^2}Z_N(s,z) \to g_s$. Hence it tends to zero on complex compacts. If essential-supremum convergence failed, one could select positive-area sets on which a fixed rotated real part of the difference exceeded a fixed threshold, passing to a subsequence and choosing from four fixed rotations. This contradicts the preceding test. This use of analytic continuation relies on the complex joint variation estimate.

Approaching the inverse endpoint. For $h = -1 + \delta$, $\Re\delta > 0$, $\delta \to 0$, the unnormalized readout equals

$$g_s\mathcal{C}(s,-1) + o(1) + \pi L^*_s(0)c^{2s+5/2}\delta^{-1}[1 + o(1)].$$

Indeed the full resolved Fourier bound in the proof of Theorem 19.9 gives a continuous density with $\|\nabla p^Y\|_\infty \le Cc^{-2}$ by rescaling the transverse coordinate. On the fixed disk we also have $\|p^Y\|_\infty \le Cc^{2u+5/2}$. Subtract the actual central value and integrate the smaller of $Cc^{-2}r$ and $Cc^{2u+5/2}$ against dr/r, exactly as in Corollary 19.4. The error is $O(c^{2u+5/2}(1 + |\log c|))$. Off the disk weak convergence with bounded variation gives the first term. The two error terms allow unrelated approaches of c and δ, including tangential complex approaches.

Supercritical powers and matching at the complex upper endpoint

Theorem 19.11 (large orders and the complex critical finite part). Write $s = u + iv$, $u > -1/2$, $a = 2u + 1$, $a_s = 2s + 1$, and put $f_N(s,h) = N^{-s^2}c^{-2h}T_N(h,s;z)$. For $\Re h > u + 1/2$, at arbitrary relative rates $N \to \infty$ and $c \downarrow 0$,

$$N^{-s^2}c^{-a_s}T_N(h,s;z) \longrightarrow \frac{g_{s+1}2^{2h-2s-2}}{\sqrt{\pi}}\,\frac{\Gamma(h-s-1/2)}{\Gamma(h-s)}. \tag{19.22}$$

The powers of positive scalars use their real logarithms. The coefficient is nonzero, and the convergence is locally uniform in both independent complex parameters. The imaginary part of s enters the depth power as well as the gamma ratio.

There is also a corresponding finite part through the upper boundary. Write $h_*(s) = s + 1/2$, $B(s) = g_{s+1}/(2\pi)$ and $B_N(s) = N^{-s^2}Z^\circ_{N-1}(s+1)/(2\pi N^{2s+1})$. On the open tube

$$|2\Re h - a| < \min(1,a)/24$$

the ordinary circle limit $f_\circ(s,h) = g_s\mathcal{C}(s,h)$ continues meromorphically from $2\Re h < a$. Its sole polar hypersurface in the tube is $h = h_*(s)$, with h-residue $-B(s)$. Set $H(s,h) = f^{\mathrm{mer}}_\circ(s,h) - 2B(s)/(a_s - 2h)$. Then locally uniformly throughout the tube,

$$f_N(s,h) = H(s,h) + B_N(s)\int_{-1}^{1}(c^2/4 + t^2)^{s-h}dt + o(1). \tag{19.23}$$

In particular at $h = h_*(s)$ one has $f_N = 2B_N(s)\log(4/c) + H(s,h_*(s)) + o(1)$. Away from this hypersurface the equivalent matched formula is

$$f_N(s,h) = f^{\mathrm{mer}}_\circ(s,h) + B_N(s)(c/2)^{a_s-2h}\,\frac{\sqrt{\pi}\,\Gamma(h-s-1/2)}{\Gamma(h-s)} + o(1). \tag{19.24}$$

If $\Re h = u + 1/2$ and $b = \Im(h-s) \neq 0$, the second term has a nonvanishing coefficient and oscillates as $(c/2)^{-2ib}$; the coefficient B_N may here be replaced by B. For example the depths $2e^{-\pi N/|b|}$ and $2e^{-\pi N/|b| - \pi/(2|b|)}$ give opposite phases. At resonance the exact finite-rank coefficient of the logarithm is needed for additive error at

unrestricted rates. The case $s = 1$ of Theorem 19.6 already demonstrates the change of finite part that can otherwise occur.

Complex one-point coefficient. With $M = N - 1$, the unnormalized one-point intensity $J_N(t)$ (including N^{-s^2}) in $t = N\theta$ is exactly

$$\frac{J_N(t)}{[N|1 - ze^{it/N}|]^{2s}} = B_N(s) z^{Ms} \int \prod_{j=1}^{M} A(x_j) E_t(x_j)^2 \, dP_{M,s+1},$$

where $x_j = N\theta_j$, $A(x) = [1 + (1-z)^2/(z|1-e^{ix/N}|^2)]^s$ and $E_t(x) = \cos(t/(2N)) - \cot(x/(2N)) \sin(t/(2N))$. This is the Weyl insertion of Theorem 19.5, with positive bases for all powers. The integral is bounded uniformly for $|t|, c \le 1$ at sufficiently large rank and equals $1 + O_s(c^2 + |t|)$ as $(c,t) \to (0,0)$. For the proof use the complex circular Jacobi kernel at $s+1$ with $F = AE_t^2 - 1$. The coordinate scale N differs from M by a bounded dilation. On $|x| \le 1$ one has $\int |A-1| V_{u+1} \le C_s c^2$ and $\int |A|(1+|x|^{-2}) V_{u+1} \le C_s$. Split at $|x| = c$, using $|A| \le C(c/|x|)^{2\max(u,0)}$ below it, $|A-1| \le C_s c^2/x^2$ above it, and $2u > -1$. The difference $E_t^2 - 1$ costs $C(|t|/|x| + t^2/x^2 + t^2/N^2)$, giving a local integral of $|F|V_{u+1}$ bounded by $C_s(c^2 + |t|)$. Outside one, $|F|V_{u+1} \le C_s[(c^2+t^2)/x^2 + |t|/|x|]$. Pairing $x, -x$ against the even diagonal removes the odd linear cotangent term, leaving an integrable $O_s((c^2+t^2)/x^2 + t^2/N^2)$ trace integrand. The off-diagonal decay of the kernel and the square-integrable exterior majorant give $\|\sqrt{|F|} K \sqrt{|F|}\|_{\mathrm{HS}} = O_s(c^2 + |t|)$ by splitting both variables at one and applying the bounded L^1 norm of the squared distance kernel. The trace and regularized determinant prove the estimate. Finally $B_N(s) \to B(s)$ and $z^{Ms} = 1 + O_s(c)$. These bounds are uniform on compact parameter sets.

Nearest-angle subtraction in variation. Apply (19.19) with central window $[-1,1]$, which only changes the fixed shell threshold and constants. Put $K = \#\{|t| \le 1\}$. Let V be the mark $n(t)$ of the closest local point in modulus, set $V = 0$ if $K = 0$, and put $R = Y - V$. The exterior coordinates used in the Janossy estimate determine the exterior mark: its real component is cB_{out} and its imaginary component is J_{out}, apart from the bounded deterministic offset. For $K \le N/2$ use the positive majorant for the variation of the Janossy measures in the local coordinates and $B_{\mathrm{out}}, J_{\mathrm{out}}$. It is bounded by the product of an integrable exponential in the two exterior variables and $C^k/k! \prod_{j=1}^{k} (c + |t_j|)^{2u} dt_j$. For powers $l > 0$ this gives

$$\int |V|^l \le C \left[1 + \int_0^1 (c+t)^{a-1-l} dt\right], \qquad \int \left(|R|^l + \sum_{j \ne *} |n(t_j)|^l\right) \le C B_l(c),$$

where the sum runs over the remaining local points and $B_l(c) = 1 + c^{2a-l} + \int_c^1 t^{2a-l-1} dt$. Indeed $|n(t)| \le C/(c+|t|)$; each nonclosest point has a distinct nearer one. Single out that ordered pair, bound powers of the inner sum by an exponential of k times its summed powers, and sum the remaining Poisson series. This yields the two integrals of Theorem 19.5. The bounds also hold with a factor e^K inside because it only changes C^k. All positive moments of the exterior are bounded under this majorant.

For $K > N/2$, take variation first at real tilt u, incurring $O_s(N^{v^2})$. For this part the same positive estimates hold with the extra factor e^K. The interior real factorial intensities obey Hadamard's product bound with one-point intensity $O_s((c+|t|)^{2u})$ by Theorem 19.5. Inserting e^K and any further exponential of the count in the local sum only multiplies the factorial integral by a bounded exponential of its uniformly integrable one-point envelope. For the exterior moments use Cauchy–Schwarz between e^K and the real exterior moments of twice the required order. Both are uniformly bounded. Thus, after multiplying by $N^{v^2} e^{-N/2}$, these same bounds dominate the $K > N/2$ contribution. Their constants are independent of c. In particular one must subtract the nearest power before majorizing the matched critical readout: bounding the two divergent terms separately on this event could introduce $\log(1/c)$, which need not be dominated by $e^{N/2}$.

To prove the supercritical assertion set $q = 2\Re h > a$, $L_q = c^{a-q}$, $d = \min(1,q)$. The real-variable inequality $\big||v+r|^{2h} - |v|^{2h}\big| \le C_h |r|^d (|v| + |r|)^{q-d}$ and Hölder under either positive majorant show that the replacement by the sum of the local one-point powers costs $CL_q(B_q/L_q)^{d/q} = o(L_q)$. The high-count part contributes the extra factor $N^{v^2} e^{-N/2}$ to this same error bound. Thus, after multiplication by c^{2h-a_s}, only the one-point integral remains. Put $t = cy$ in it. The absolute rescaled integrand is bounded by $C(1+|y|)^{a-1-q}$, and its pointwise limit is $B(s)(1/4 + y^2)^{s-h}$ by the complex insertion estimate. Integrating gives the gamma formula.

For the tube use $d = \min(1, a)/4$ and $p = 3a/2$. Its stated width implies $q < p$, $q < 2a$ and $(q-d)p/(p-d) < a$. Hölder in the same radial inequality therefore bounds the integral of the power difference by a constant, since the pth moment of R and every moment of V below a are bounded. Restoring the nonclosest one-point terms costs $O(1)$ too. At high count the factors e^K permit exactly the same Hölder calculation in the exponentially reweighted real measure; the resulting $O_s(N^{v^2}e^{-N/2})$ is uniform in depth even for these additive errors.

On $|t| \le 1$ use $|n(t)| = (c^2/4+t^2)^{-1/2}(1+O(c+t^2))$ and $N|1-ze^{it/N}| = (c^2/4+t^2)^{1/2}(1+O(c+t^2))$ near zero as in Theorem 19.6. With the insertion estimate the error after subtracting $B_N(s)(c^2/4+t^2)^{s-h}$ is locally bounded by $C(c+|t|)^{a-q}$ and is uniformly integrable on the tube. Together these estimates give local boundedness of the difference between f_N and the displayed model integral throughout this connected open tube in (s, h). Its limit on the nonempty open subdomain $q < a$ is $f_\circ(s,h) - 2B(s)/(a_s - 2h)$ by the ordinary joint limit and dominated convergence. Finite-rank holomorphy, local normality and the identity theorem give convergence on the full tube and define H. The beta-integral evaluation and holomorphic continuation after subtracting the two tails of the integral at $|t| = 1$, as in Theorem 19.6, give the gamma term and the additive logarithmic formula.

The transverse distribution at the limiting line

Proposition 19.12 (transverse readout and its tail). Let $B_N = (\Re Y + 1/2)/c$ and $J_N = \Im Y$. The boundary-layer Fourier formula in Theorem 19.7 holds throughout $\Re s > -1/2$. For real $s > -1/2$ it gives the joint probability limit

$$(B_N, J_N) \implies (B, J) = \left(\tfrac{1}{2} \sum_{t \in \mathcal{X}_s} t^{-2}, \mathrm{PV} \sum_{t \in \mathcal{X}_s} t^{-1} \right). \tag{19.25}$$

Here both sums use the microscopic coordinate of Theorem 14.1 and the principal value uses symmetric cutoffs at infinity. In particular J has the law of $X_s/2$. There is almost surely a gap about zero by the locally integrable one-point bound. The far tail of the first sum has finite mean and the centered symmetric tails of the second have variance $O(1/L)$ outside $[-L, L]$, by the projection variance inequality and the bounded intensity there. This gives absolute convergence of the first and convergence in probability of the second, sufficient for the characteristic function; the principal value here denotes this limit. Determinant convergence at the origin gives continuity there, so Lévy's theorem identifies the pair. For fixed nonreal tilt the same limiting transform describes the two resolved coordinates and carries no assertion of a positive distribution.

Put $a = 2s + 1$ and let $D_s = g_{s+1}/(2\pi g_s)$. The transverse probability has the sharp upper tail

$$\mathbb{P}(B > R) \sim \frac{2D_s}{a}(2R)^{-a/2}. \tag{19.26}$$

Indeed the limiting kernel diagonal at zero is asymptotic to $D_s|t|^{a-1}$ by (19.12), since $D_s = \Gamma(1+s)^2/[2\pi(1+2s)\Gamma(1+2s)^2]$. Hadamard bounds the chance of a second point within distance d by $O(d^{2a})$. Thus for $V = 1/(2t_*^2)$ at the closest point of $|t| \le 1$, with $V = 0$ when there is none, $\Pr(V > R) \sim (2D_s/a)(2R)^{-a/2}$. The nonclosest positive sum has bounded pth moment for every $0 < p < a$: single out a point t and one nearer point, expand an exponential of the local count to bound the power of a sum, and use the real factorial bound. This gives at most $C \int_0^1 t^{a-1-2p} \int_0^t x^{a-1} dx\, dt < \infty$. The exterior sum has bounded exponential moments by the determinant inequality. Taking $a/2 < p < a$, sandwich the full tail between that of V at R and at $(1-\epsilon)R$ plus $O_\epsilon(R^{-p})$ and send ϵ to zero. This proves (19.26). A single closest eigenangle produces this positive transverse excursion at its natural depth scale; the rare finite-depth density at a fixed distance to the right, in Theorem 19.2, additionally requires cancellation in the imaginary component.

Variation on the resolved scale. For all complex s in the same half-plane, the joint (B_N, J_N) density of the N^{-s^2}-scaled measure converges to a smooth complex density of mass g_s, in variation weighted by $(1+|B|)^r(1+|J|)^d$ for $r, d \ge 0$ with $2r + d < 2u + 1$. In fact (19.19) bounds absolute variation of the low-count marginal. Each local contribution to B is at most $C(c+|t|)^{-2}$ and each to $|J|$ at most $C(c+|t|)^{-1}$. Their joint moment with a strict surplus costs at most a constant times the integral of $(c+|t|)^{2u-2r-d}$ over the window, by bounding the powers of local sums by a polynomial in $1+k$ times the largest summand to the corresponding power. The exterior has exponential tails. For the high counts the same positive moment estimate under the real interior tilt follows by the real factorial correlation envelope: the tagged near weights are bounded by $C(c+|t|)^{2u}$ for both signs of u by the one-point insertion in Theorem 19.5, and the positive normalized ensemble is an orthogonal polynomial projection. The real exterior b also has bounded positive exponential moments by the real one-point

bound and projection determinant inequality, and j has bounded two-sided exponential moments by reflection and the square integrable tail in Theorem 19.1. Hölder with a strict surplus suppresses the factor $N^{(\Im s)^2}$ at high counts. Pointwise convergence of the full Fourier source at fixed frequencies and the rapid bound of Theorem 19.9 give uniform convergence of densities with each fixed spatial derivative. Tight weighted variation supplies the assertion by integration over a compact set and its complement. The limiting density vanishes for $B < 0$ because $b + \sum_{|t|\le 2} \Re n/c \ge 0$ and the deterministic offset in B_N tends to zero.

There is an extension of (19.26) to the mass-one complex limiting density. Its mass in $B > R$ is asymptotic to $2D_s(2R)^{-(2s+1)/2}/(2s+1)$, where $D_s = g_{s+1}/(2\pi g_s)$. To justify local boundedness after multiplying by $(2R)^{s+1/2}$, first pass to the local limiting coordinates under (19.19), integrating away the high counts which disappear at fixed R. On any fixed excluded neighborhood of the origin the factors converge in their elementary angular marks. The upper variation on the removed neighborhood tends to zero at fixed R by the same count envelope. The resulting central weights in the bound are $|t|^{2u}$. The single closest point contributes a tail bounded by $CR^{-a_u/2}$, $a_u = 2u + 1$, and the nonclosest sum has a uniformly bounded pth moment for $a_u/2 < p < a_u$ by the two-distinguished-point integral above. These variation bounds hold for the complex projected marginal by domination and are locally uniform in s. For fixed R the limiting half-plane mass is holomorphic by finite-rank holomorphy and the locally uniform cutoff bounds. Vitali applied to the rescaled mass and (19.26) now proves the complex assertion. This is an asymptotic for a complex integral; a probability interpretation applies at real tilt.

Large values in the joint boundary layer

Write ν_s for the limiting, mass-g_s complex measure of (B, J) obtained from the resolved Fourier transform. For every continuous compactly supported F on $([0,\infty)\times\mathbb{R})\setminus\{(0,0)\}$,

$$R^{1+2s}\int F(B/R^2, J/R)\,d\nu_s \longrightarrow \frac{g_{s+1}}{2\pi}\int_{\mathbb{R}} |x|^{2s}F(1/(2x^2), 1/x)\,dx.$$

This identifies the parabolic relation satisfied by a single large boundary excursion, including its complex coefficient. The limit refers to the limiting boundary layer followed by $R\to\infty$.

To prove this, the central Janossy bound at zero depth has factor $C^k\prod|t_i|^{2u}/k!$. The exterior variables have exponentially decreasing density. These bounds carry to the limiting readout by first truncating the number of central points, the centered exterior statistics and the singular angular origin, then passing to the limit. Equivalently extract weak subsequences of the bounded Janossy measures on these truncations; their common readout is identified by the unique limiting Fourier transform. The total variation of a bounded test supported where either $B \ge \epsilon R^2$ or $|J| \ge \epsilon R$ is consequently $O_\epsilon(R^{-a})$, $a = 1 + 2u$. In fact, outside exponentially small exterior tails, reaching either threshold requires some central point of modulus below $C_\epsilon k/R$. Integrate its density $|t|^{2u}$ and sum $C^k k^{a+1}/k!$ times bounded angular integrals; the bound is locally uniform in s. For compactly supported F, the integral against ν_s is holomorphic in s by the density convergence on bounded sets, hence its product by R^{1+2s} is a locally bounded family.

For real s it remains to calculate the limit by a single angle. One may first restrict to $k \le k_0$; after multiplying by R^a, the error from $k > k_0$ is bounded by the tail of the factorial series above. Discard exterior values $|b| + |j| > R^{1/4}$ at exponentially small cost. For bounded k, the cost after multiplication by R^a of having one point below Ck/R and another below $R^{-1/2}$ is $O_{k_0}(R^{-a/2})$ by the same Janossy product bound (the squared collision factor can be omitted). On the rest, the second and later marks contribute $O_{k_0}(R^{-1/2})$ to J/R and $O_{k_0}(R^{-1})$ to B/R^2. Uniform continuity of F, extended by zero, permits their removal with vanishing scaled error. Replacing the resulting single-tag sum by the full one-point integral costs the same exceptional estimate. For real s the circle one-point intensity satisfies $I_s(t)/|t|^{2s} \to g_{s+1}/(2\pi g_s)$ by the circle insertion, or by the diagonal of K_s and the Barnes recursion. Substituting $x = Rt$ supplies the claimed formula. Its right side is holomorphic throughout the half-plane and the normal family theorem transfers the formula to every complex s there.

In particular one can take F supported in a small rectangle around any point $(y^2/2, y)$ with $1 < y < 2$ so that the right side is nonzero. For the projected J marginal one may instead take a smooth bump depending only on J/R, supported in a sufficiently narrow subinterval of $(1, 2)$: the same threshold proof applies, and the required holomorphy follows by the locally uniform absolute tail estimate in B. Its coefficient is nonzero. The marginal total variation on $[R, 2R]$ is then at least $c_s R^{-a}$ for large R. Disjoint dyads prove divergence of its ordinary absolute $2\Re h$ moment at and beyond $\Re h = u + 1/2$.

A simultaneous tail crossover for the transverse coordinate. Set $B_N = (\Re Y + 1/2)/c$, and use the unnormalized matrix functional $I_{N,s}(F) = N^{-s^2}\mathbb{E}[|\Lambda_N(z)|^{2s}F]$. Let $R = R_N \to \infty$, put $r = (2R)^{-1/2}$ and suppose $c^2R \to \lambda \in [0,\infty]$. With $a_s = 2s+1$ and $\Re s > -1/2$,

$$r^{-a_s} I_{N,s}(\mathbf{1}_{B_N>R}) \longrightarrow \frac{g_{s+1}}{2\pi} \int_{-\sqrt{1-\lambda/2}}^{\sqrt{1-\lambda/2}} (\lambda/2 + x^2)^s \, dx \quad (0 \le \lambda < 2).$$

The limit is zero for $2 \le \lambda \le \infty$. All limits are locally uniform in complex s. In particular at $c^2R \to 0$ the power law has the nonzero coefficient $g_{s+1}/[\pi(2s+1)]$ in units of r^{a_s}. The case $0 < \lambda < 2$ resolves the finite-depth cutoff because the largest single contribution to c^2B_N tends to two. A zero limit at higher thresholds specifies the scale proved here.

For real s first use the probability preparation normalized by $Z_N(s,z)$. In $D = [-2,2]$ choose the point of least absolute coordinate $t = N\theta$ and let V be its contribution $b(t) = \Re n(t)/c$, set to zero if the window is empty. This contribution is positive and decreases in $|t|$. The remainder $B_N - V$ has pth absolute moment bounded uniformly in N, c for every $0 < p < a = 2s+1$. Indeed $b(t) \le C/(c+|t|)^2$, and the real interior intensity is at most $C(c+|t|)^{a-1}$ on D by the one-angle insertion of Section 19. Every nonclosest point has a distinct nearer point, so the local moment costs at most

$$C \int_0^2 (c+t)^{a-1-2p} \int_0^t (c+y)^{a-1} dy\, dt \le C_p.$$

As in the proof of Theorem 19.5, the power of the local count costs at most a bounded exponential-count factor in this distinguished-particle estimate. Outside D, $b(t) \le C/t^2$, whose sum has bounded exponential moments. The offset $(1/2 - 1/(2z))/c$ is bounded. Choose $a/2 < p < a$. The discrepancy between $B_N > R$ and thresholds for V at $(1 \pm \epsilon)R$ costs $O_\epsilon(R^{-p})$. The probability for V is its one-point integral up to an $O(r^{2a})$ error when c^2R stays bounded: each exceeding tag has $|t| \le Cr$, and Hadamard's two-point bound controls double counting since on that interval the integrated intensity is $O(r^a)$ for $c \le Cr$. For $c^2R \to \infty$ a single tag cannot reach $(1-\epsilon)R$, as $c^2 b(0) = (1+z)^2/(2z) \to 2$. This proves the zero limit there.

For $t = rx$ and finite λ, $b(rx)/R \to (\lambda/2 + x^2)^{-1}$ away from the degenerate point $\lambda = x = 0$. The one-point insertion gives $I^{\mathrm{prob}}_{N,s}(rx) = [N|1 - ze^{irx/N}|]^{2s}[g_{s+1}/(2\pi g_s) + o(1)]$ for bounded x as $N \to \infty$, $c \to 0$, $r \to 0$. Divide the squared angular factor by r^2 to obtain $\lambda/2 + x^2$. At negative real tilt the possible origin singularity after scaling is dominated by $C|x|^{2s}$, integrable. At positive tilt the factors are bounded on the fixed x interval. Dominated convergence, then $\epsilon \downarrow 0$ in the two threshold comparisons, gives the integral, including zero at $\lambda = 2$. Restore the mass $N^{-s^2} Z_N(s,z) \to g_s$.

For complex $s = u + iv$, with $a = 2u+1$, a uniform bound $|I_{N,s}(\mathbf{1}_{B_N>R})| \le C_s R^{-a/2}$ suffices for holomorphic convergence in s. In the marked Janossy estimate sum $k \le N/2$ using its positive majorant. The same distinguished-point calculation bounds the absolute pth moment of the nonclosest sum, and the exponential exterior density bounds the remaining coordinate. If $c \le Cr$, a single tag exceeding $R/2$ has integrated majorant $O(r^a)$; if c/r exceeds a sufficiently large constant there is no such tag. These bounds apply also to the high-count part at a cost $O(N^{v^2}e^{-N/2})$: take matrix absolute values, then insert $\mathbf{1}_{\#D>N/2} \le e^{\#D - N/2}$ into each real distinguished-point or moment estimate above. Extra exponential count factors are harmless by the factorial expansion, and the jointly exponentially weighted exterior sum is bounded by the same determinant estimate on the nonnegative integrable function $\mathbf{1}_D + C\mathbf{1}_{D^c}/t^2$. In particular the rare-count error retains the essential r^a factor even for radii shrinking faster than any power of rank. Choose p with a little slack on each small parameter compact. The asserted complex bound follows. Each rescaled finite-rank integral is holomorphic in s, and its limit on the real interval has the displayed holomorphic expression, including the identically zero case. Vitali's theorem proves the full statement. On the exact limiting transverse distribution, the same $\lambda = 0$ complex tail follows by taking the fixed-threshold limit through intermediate ranks and then letting R increase, since the transverse marginal has a continuous density and the projected measures have uniform integrable tails.

A finite determinant approximation across the density transition

We retain the finite rank in the comparison. Set $x(t) = N^{-1}\cot(t/(2N))$, $\gamma = c/(1+z)^2$, $\tau = \gamma^2$, and, for $v \geq 0$, write

$$q_v(x) = \frac{x^2}{1+vx^2}, \qquad p_v(x) = \frac{x}{1+vx^2}, \qquad Q_v = \sum_j q_v(x_j), \quad P_v = \sum_j p_v(x_j).$$

The circle measure used below has weight $N^{-s^2}|\Lambda_N(1)|^{2s}$ and includes its Barnes mass. Let $d_v(Q,P)$ denote the planar density of its (Q_v, P_v) projection after multiplication by $\prod_j (1+vx_j^2)^s$. Exact substitution in each angular summand gives

$$B_N = AQ_\tau + b, \quad J_N = DP_\tau, \quad A = \frac{2}{(1+z)^4}, \quad b = -\frac{1}{2N(1+z)^2}, \quad D = \frac{2}{(1+z)^2}. \tag{19.27}$$

The actual unnormalized density in (B, J) is therefore $M d_\tau((B-b)/A, J/D)/(AD)$ with $M = ((1+z)/2)^{2Ns}$. Indeed $|1 - ze^{i\theta}|^2/|1-e^{i\theta}|^2 = ((1+z)/2)^2(1+\tau x^2)$. The planar density in the original Y coordinates has the additional Jacobian $1/c$. Retaining M, A, b, D exactly permits unrestricted relative rates. For instance $M = 1 - sc/2 + O_s(c^2 + c^2/N)$, whereas the translation b is of order $1/N$ even at the circle.

Theorem 19.13 (expansion of the exterior angular contribution). Fix a compact subset of $\Re s > -1/2$, a nonnegative integer l, and $m \geq 1$. There exist $C, N_0, \tau_0 > 0$ independent of N, τ, Q, P such that, for $N \geq N_0$ and $0 \leq \tau \leq \tau_0$, the following explicit Fourier determinant approximates d_τ and its spatial derivatives through order l, with absolute error at most $C\tau^m$ everywhere in the plane. Mark angles $|N\theta| \leq 2$ with $v = \tau$ and the other angles with $v = w$. Form the circle Toeplitz determinant for the symbol

$$|1 - e^{i\theta}|^{2s}(1+vx^2)^s \exp\{i\beta q_v(x) + i\xi p_v(x)\}.$$

Include N^{-s^2} in the determinant prefactor and denote the result by $H(\tau, w; \beta, \xi)$. Invert the two-dimensional Fourier transform, with the negative sign in inversion and factor $(2\pi)^{-2}$, of

$$\sum_{j=0}^{m-1} \frac{\tau^j}{j!}\, \partial_w^j H(\tau, 0; \beta, \xi). \tag{19.28}$$

For the first exterior correction the multiplier inserted into the source on one exterior angle is $sx^2 - i\beta x^4 - i\xi x^3$, summed over all such angles. Equivalently one differentiates the determinant by replacing each column in turn by its derivative. This formula involves no division by a determinant and applies at its zeros. The inner angles retain their exact finite-depth weights and marks in every term. This is an expansion of the exterior contribution with an exact treatment of the part which becomes singular. The order m is fixed before the rank cutoff is chosen.

Proof. We record the estimates needed to apply Theorem 19.9 to this piecewise symbol. Write $r = |\beta| + |\xi|$. For real $w \in [0, \tau_0]$ allow an additional complex increment $|w' - w| \leq \epsilon/(1+r)$ in the exterior symbol. There $|x| \leq C/(1+|t|)$, and $1 + w'x^2$ stays in the right half-plane. Relative to the real-w exterior symbol the multiplier is $1 + O((1+|t|)^{-2})$, uniformly, using bounded logarithmic derivatives and $r|w' - w| \leq \epsilon$. On each exterior half-interval its total variation is bounded uniformly: as a function of the bounded monotone variable x, its logarithm has bounded derivative. It equals one on the interior by definition. Fix the principal logarithm for this short complex displacement and the real logarithm at real parameters.

In the circle-kernel determinant of Theorem 19.9 the additional multiplier thus costs a bounded trace-norm perturbation, by the two weighted Hilbert–Schmidt factors there. The removal of the constant circle-to-interior scalar in (19.27) is harmless: the central weight ratio $(1+\tau x^2)^s$ obeys the same bound $\int_{|t|\leq 2} |(1+\tau x^2)^s - 1| V_{\Re s}(t)dt \leq C$. The real unit phase on either part still differs from one by at most $C\min(1, (1+r)/|t|)$ for $|t| > 2$. For the contraction estimate the shell at large frequency lies entirely outside this fixed window. The exterior phase is the real phase for the single parameter w, up to rescaling its two frequencies by factors bounded above and below and a constant on that shell. This follows from (19.27) with $\sqrt{w} = N(1-z_w)/(1+z_w)$, or directly by differentiating $\beta q_w + \xi p_w$. Its derivative on the shell of the chosen sign is comparable in modulus to $|\beta|/|t|^3 + |\xi|/t^2$. Thus the proof by integration of the projection defect on that shell gives the contraction $\exp[-b\min(N, \max(|\beta|^{1/3}, |\xi|^{1/2}))]$ up to the same polynomial in $1+r$. The argument only needs the phase on that shell to obtain its lower bound. The constants can be chosen also at $w = 0$ by the same derivative calculation. This gives decay of arbitrary fixed polynomial order for $r \leq N^K$ with K fixed.

For $r > N^K$ split each monomial Toeplitz entry into the central interval and the two exterior intervals. On each interval the real phase has a single constant parameter, so the angular first-derivative and sublevel estimates in Theorem 19.9 apply separately, with at most two extra endpoints. To check this uniformly, the ingredient at parameter v is the original angular symbol at $z_v = (1-\sqrt{v}/N)/(1+\sqrt{v}/N)$ times a scalar uniformly bounded with its reciprocal. The phase differs from the corresponding single-angle transverse phase by a constant and by bounded invertible frequency scalings. At $v = 0$ remove the origin along with the same r^{-b_0} central arc used in that proof, or pass to $v \downarrow 0$ by dominated convergence at fixed rank and frequencies. The complex exterior perturbation has uniformly bounded supremum and variation and so preserves the first-derivative estimate. The size of each entry is at most $CN^3 r^{-\delta}$ for a compact-dependent $\delta > 0$. Hadamard's determinant bound absorbs both the finite-rank normalization and every requested fixed inverse frequency power once K and then N_0 are large. Consequently $|H(\tau, w'; \beta, \xi)| \le C_L(1+r)^{-L}$ for every required L, uniformly on the indicated disk. Cauchy's formula on this disk gives the same estimate for any prescribed fixed w derivatives, with a cost of one frequency power per derivative. Taylor's integral remainder on the real segment $[0, \tau]$ and absolutely integrable Fourier inversion, including the factors for the spatial derivatives, give the assertion.

In particular a fixed exterior order suffices even when measuring errors in units of the *rare* density. On $1 \le Q \le L/c$ put $\nu_u = 2\Re s + 7/2$. On a compact set of tilts take $m > \sup \nu_u/2$. The remainder after multiplication by Q^{ν_u} is at most $C_L c^{2m - \sup \nu_u}$. This is a uniform absolute estimate in the natural density units, without dividing by a possibly vanishing complex value. Increasing m gives any prescribed fixed algebraic accuracy in these units. It still requires the singular interior determinant with its exact depth parameter. The circle-based correction below removes this dependence on the inner angles in the region where the two-tag expansion applies.

The finite-rank transport of the transverse density

Work with the unnormalized Haar functional scaled by N^{-s^2}, with $u = \Re s > -1/2$. The following change of coordinates keeps both rank effects and the regularization at an individual eigenangle. Set

$$x_i = N^{-1}\cot(\theta_i/2), \quad \tau = [c/(1+z)^2]^2, \quad Q_\lambda = \sum_i \frac{x_i^2}{1+\lambda x_i^2}, \quad P_\lambda = \sum_i \frac{x_i}{1+\lambda x_i^2}.$$

Use the unnormalized circle weight $dI^\circ = N^{-s^2}|\Lambda_N(1)|^{2s} dU$. Let $d_{\lambda,N}(q,p)$ be the density in $dq\,dp$ after multiplying this weight by $W_\lambda = \prod_i (1+\lambda x_i^2)^s$ and reading (Q_λ, P_λ). A suffix $[H]$ in a density denotes insertion of the symmetric statistic H before projection. All powers of positive numbers use their real logarithm. Put

$$m_z = ((1+z)/2)^{2Ns}, \quad a_z = 2/(1+z)^4, \quad b_z = 2/(1+z)^2, \qquad d_z = -1/[2N(1+z)^2].$$

Exactly, $B_N = a_z Q_\tau + d_z$, $J_N = b_z P_\tau$, and the interior weight is $m_z W_\tau dI^\circ$. In particular the original planar density at y is $m_z d_{\tau,N}(q,p)/(c a_z b_z)$ at $q = [(\Re y + 1/2)/c - d_z]/a_z$, $p = \Im y/b_z$. These identities follow by expressing $e^{i\theta} = (Nx+i)/(Nx-i)$ and using $|1 - z e^{i\theta}|^2/|1-e^{i\theta}|^2 = ((1+z)/2)^2(1+\tau x^2)$. They retain the exact scalar, shift and dilation at each rank.

Theorem 19.14 (finite-depth density transport). Fix a compact set of tilts in $\Re s > -1/2$ and $M < \infty$. Write $\nu_u = 2u + 7/2$. For each $0 < \eta < 1$ the result holds for $\lambda q \le 1 - \eta$ and sufficiently small λ as proved below. We first show there are $\epsilon > 0, C$ and a lower rank threshold such that for all ranks above it, $q \ge 0$, $|p| \le M$, $\lambda \ge 0$, $\lambda(1+q) \le \epsilon$,

$$d_{\lambda,N}(q,p) = d_{0,N}(q,p) + \lambda D_{1,N}(q,p) + r_{\lambda,N}(q,p), \qquad |r_{\lambda,N}(q,p)| \le C\lambda^2 (1+q)^{2-\nu_u}, \tag{19.29}$$

where at the circle

$$D_{1,N} = sq\, d_{0,N} + \partial_q d_{0,N}\big[\sum x_i^4\big] + \partial_p d_{0,N}\big[\sum x_i^3\big]. \tag{19.30}$$

The constants allow arbitrary relative rates for c and N. More generally the mth derivative in λ is $O_m((1+q)^{m-\nu_u})$ for any prescribed m and sufficiently large rank depending on m. The coefficients are finite-rank circle densities. They can be computed by inverse Fourier transformation after a Laplace factor $e^{-\delta q}$ with $\delta > 0$. Each power-sum insertion is a first derivative of a Toeplitz determinant under an additive perturbation of its multiplicative symbol by its product with the one-angle factor. This derivative is equivalently a one-tag integral of complementary minors. Laplace damping keeps the differentiated entries integrable at the circle for the stated tilts. The physical

change of density requires the exact factors in the preceding paragraph. A correction solely in c relative to the infinite-rank limit discards an independent finite-rank error.

Differentiating the preparation and the mark. Put $q_i = x_i^2/(1+\lambda x_i^2)$, $p_i = x_i/(1+\lambda x_i^2)$. Differentiating the pushforward weakly gives $\partial_\lambda W_\lambda = sQ_\lambda W_\lambda$, $\partial_\lambda Q_\lambda = -\sum q_i^2$, $\partial_\lambda P_\lambda = -\sum p_i q_i$. Integration by parts on the readout gives the two positive derivative signs above. Repeated differentiation produces sums of $\partial_q^k \partial_p^l d_{\lambda,N}[H]$ with $k+l \le m$. Here H is a product of sums of monomials q_i^a or $p_i q_i^a$ with $a \ge 1$, including factors after merging coincident indices. Give p_i degree one and q_i degree two. Each term has total degree $D = 2m + 2k + l$. This follows inductively from $q_i' = -q_i^2$, $p_i' = -p_i q_i$. On $Q_\lambda \le CR$, $R \ge 1$, $|p_i| \le \sqrt{q_i}$ and $|H| \le CR^{D/2}$, since the degree of every local sum is at least two. These differentiations can first be made under smooth compactly supported tests: in the support and for $\lambda Q_\lambda < \epsilon$, $\sum x_i^2 \le Q_\lambda/(1-\lambda Q_\lambda)$. Branches stay on positive bases. The estimates below identify continuous versions after any fixed number of differentiations at large rank.

Fourier estimates with insertions. We record two consequences of the proof of Theorem 19.9, including how its bounds behave for these new factors. There is an exact physical depth corresponding to $\sqrt{\lambda} = N(1-z')/(1+z')$, so $z' = (N-\sqrt{\lambda})/(N+\sqrt{\lambda})$. The two coordinate systems differ by bounded affine factors throughout this proof. The circle-to-interior multiplier in (19.19) and W_λ differ by a scalar to the power N, uniformly bounded above and away from zero on parameter compacts for small λ. The Fourier shell derivative and its lower bound are preserved after this affine change. The same estimates extend to $\lambda = 0$ by the explicit rational marks or finite-rank convergence with damping.

First, for $0 < \delta \le 1$, the joint Fourier transform for the multiplier $W_\lambda e^{-\delta Q_\lambda}$ with any one such insertion H is bounded by $C_L \delta^{-D/2}(1+|\xi|)^{-L}$ for any fixed L, at sufficiently large N. It admits the same bound after multiplying by ω^K, $|\omega| = 2$, where K is the number of angles in $D_0 = [-2,2]$ in $t = N\theta$. Here and below all specified insertions have fixed degree. For details, the two extra one-angle multipliers on D_0 cost bounded trace norm in the Fourier compression argument by $\int_{D_0}(1+|W_{\lambda,1}|)V_u(t)dt \le C$, where $W_{\lambda,1} = (1+\lambda x^2)^s$ and V_u is the circle envelope of Theorem 19.7. On the exterior the damping differs from one by $O((1+|t|)^{-2})$, also bounded in weighted trace norm. Thus the shell and polynomial prefactor of Theorem 19.9 are preserved. At ultrahigh frequencies the two jumps at the edge of D_0 and the damping have bounded variation, since q_i is monotone on each angular half. The original weighted angular amplitude away from the cut at the origin obeys the same variation estimates as in that theorem. For H, separate equal indices to leave finitely many distinguished angles. Dropping these fixed singular values leaves the preceding shell bound with a fixed constant. In the estimate for a distinguished angle of degree e integrate $|W_{\lambda,1}|V_u e^{-\delta q_i}$ times its factor. Its integral on $|t| \le 2$ is at most $C\delta^{-e/2}$ by $|p_i| \le \sqrt{q_i}$ and $q_i^{e/2} e^{-\delta q_i} \le C_e \delta^{-e/2}$. On the rest of the period all such factors decay at least as $C/(1+t^2)$, integrably. The Toeplitz basis at ultrahigh frequencies loses fixed rank powers per distinguished angle, absorbed by the same $N - O(1)$ small singular values. These arguments establish the asserted Fourier bound, in particular bounded derivatives of damped densities of every prescribed spatial order, with cost $C\delta^{-D/2}$. The choice $\delta = (1+q)^{-1}$ costs only a fixed factor when removing the damping locally, including for derivatives. By Cauchy coefficient extraction in ω, the restriction to $K > N/3$ gains a further factor $C2^{-N/3}$. The constants are uniform even though full matrix-space variation can grow with rank.

Second, on $K \le N/3$ fix all k central angles and use the exterior coordinates $b = \sum_{D_0^c} q_i$, $j = \sum_{D_0^c} p_i$. Allow also a fixed number of distinguished exterior angles, arising from the part of H carried by the exterior. The joint complex density has the same $C^{k+1} e^{-ab-a|j|}/k!$ bound times the central weights $(\sqrt{\lambda}+|t_i|)^{2u}$, for some fixed $a > 0$, as in (19.19). It also has that bound for each fixed derivative in either exterior coordinate, by using higher prescribed Fourier decay. The prescribed exterior angles are estimated before integrating them: each contributes its bounded integrable mark factor and its bounded correlation envelope. Excluding these fixed angles in the definition of the exterior sums changes the exponential bound by a constant since their marks are bounded; translating it back costs only that constant. In the cofactor proof the number of prescribed rows is at most $N/3 + O(1) \le N/2$. For two selected central tags t_+, t_-, the density also retains their squared separation. More precisely, strip the two weights $[N|1 - z' e^{it_i/N}|]^{2s}$, up to bounded constants, and divide by $(t_+ - t_-)^2$. The remaining factor and its fixed derivatives in these two angles have the same bound with those factors removed. To see this on the shell, use the two wedges of evaluation columns in Theorem 19.9. Each stripped vector has all fixed angular derivatives bounded on D_0 by the bandlimited reproducer used there. Replace one of the two corresponding columns by its difference quotient, the integral of its derivative on their joining segment. Derivatives of that quotient are again bounded. The same argument on the two original monomial wedges at ultrahigh frequency costs only rank powers already absorbed. The two real weights stripped here use the complex

exponent in the density, and their absolute size uses u. This reasoning differentiates tags only, never absolute values of the complex density.

Localized angular estimates. We prove for $q = R \ge R_0$, $|p| \le M$ and $\lambda R \le \epsilon$ that

$$|\partial_q^k \partial_p^l d_{\lambda,N}[H](R,p)| \le C_{k,l,H} R^{-\nu_u + D/2 - k - l/2}.$$

All estimates below work in a fixed small relative neighborhood of the real coordinate and for $|p| \le M+1$. The first Fourier estimate covers bounded q. For the low-count sector use the second estimate. Set $T_* = 1+K+b+|j|$ and split it into dyads $T \le T_* < 2T$. It depends on the exterior and on the count and remains fixed when moving the selected interior pair. For $T \le \gamma R^{1/3}$ the event forces an opposite pair obeying

$$C_0^{-1} R^{-1/2} \le |t_\pm| \le C_0 T^{3/2} R^{-1/2}.$$

Indeed $q_i \le (1+o(1))R$ implies $x_i^2 \le CR$ for every point, after choosing ϵ small. The exterior sum of squares is $O(T)$, so an interior $q_i \ge b_0 R/T$ is required. Its $|p_i| \ge b_1\sqrt{R/T}$ since $1+\lambda x_i^2$ is bounded. The other sign must supply at least a constant times this mark as $|p|+|j| \le M+2T$ and γ is small. At least one of its $O(T)$ terms has $|p_i| \ge b_2\sqrt{R}/T^{3/2}$. The formula for x gives the window. The same proof includes $\lambda = 0$.

Use scaled pair coordinates $h_i = x_i/\sqrt{R}$. The map to the tagged part of $(v,w) = (q/R, p/\sqrt{R})$ is exactly

$$(h_1,h_2) \longmapsto \left(\sum_{i=1}^{2} \frac{h_i^2}{1+\lambda R h_i^2}, \sum_{i=1}^{2} \frac{h_i}{1+\lambda R h_i^2} \right).$$

On the slightly enlarged opposite-sign window, $c_1 T^{-3/2} \le |h_i| \le C_1$. Its Jacobian determinant is $2(h_1-h_2)(1+\lambda R h_1 h_2)/[(1+\lambda R h_1^2)^2(1+\lambda R h_2^2)^2]$. By reducing ϵ it is bounded below in modulus by a negative fixed power of T. The inverse and all its prescribed derivatives in v, w cost at most a polynomial in T by implicit differentiation. The multiplicity is uniformly finite: for $\lambda > 0$ each mark lies on a circle in linearly scaled coordinates, so the two opposite-circle intersection equations give at most two ordered solutions away from a zero Jacobian; at zero depth the sum and sum of squares give two roots. Also $t = 2N \arctan(1/(N\sqrt{R}h))$ on both signs, so t and its fixed inverse-map derivatives cost $CR^{-1/2}\,\mathrm{poly}(T)$. The two angular differentials per $dv\,dw$ therefore cost $O(R^{-1}\,\mathrm{poly}(T))$, also after these derivatives.

One can make the selection of forced tags smooth. On each sign use a nonnegative bump in h, equal to one on the forced window and supported on a slightly enlarged window with all derivatives $O_m(\mathrm{poly}(T))$. If needed also include a bump in t supported on $|t| < 1$, equal to one on the forced window by the choice of γ. Divide the product of two such bumps by the product of their sums over the respective signs. Replace the reciprocal of each sum by a smooth bounded function agreeing with it at arguments ≥ 1. On the target these pair weights sum to one; outside it their smooth extension causes no boundary term. At fixed other angles the derivatives of a summation denominator involve only the moving pair. The dyadic restriction on T_* stays fixed. Change variables in the selected pair for every fixed exterior and all remaining tags, and differentiate the smooth coarea integrands. In (v,w), derivatives of the two selected weights cost at most $CR^{-2u}\,\mathrm{poly}(T)$ in total: $N|1-z'e^{it/N}|$ is comparable on each support to $R^{-1/2}$ times factors between inverse and positive powers of T, with scaled derivatives of its logarithm polynomially bounded. The squared separation with its derivatives contributes $CR^{-1}\,\mathrm{poly}(T)$. The inserted central polynomial and its derivatives cost $CR^{D/2}\,\mathrm{poly}(T)$ here, by the bounds on q_i, p_i and their pair derivatives and the local count. The exponential and factorial integrals of the remaining tags converge after any polynomial in T, leaving $O(R^{-2u-2+D/2})$ per $dv\,dw$. Return to $dq\,dp$: the area factor is $R^{-3/2}$ and each derivative brings the respective R^{-1} or $R^{-1/2}$. This gives the displayed bound.

For low counts with $T_* > \gamma R^{1/3}$, keep all central angles fixed and evaluate the exterior density at the translated target. Use a smooth cutoff between $T_* = \gamma R^{1/3}/2$ and $\gamma R^{1/3}$ for this and the preceding moderate sector, using $\sqrt{1+j^2}$ in T_* to make its j-dependence smooth. The moderate dyads use a partition depending only on these same external variables, unchanged on pair differentiation. Derivatives in the large sector act on the smooth cutoff and on the exterior density, which retains the exponential weight by Fourier inversion. At support $q = R$ all central factors are bounded by $CR^{D/2}$ since $b \ge 0$; the derivatives of the exterior density vanish for $b < 0$ as well. The remaining integrations, with the factorial in K, give $C(1+R)^C e^{-dR^{1/3}}$, absorbing all the required powers. Distinguished exterior factors have already been integrated with their integrable envelopes.

For $K > N/3$ and $R \le N^4$, the damped full Fourier estimate and Cauchy extraction in ω give $C(1+R)^{D/2}2^{-N/3}$, enough for every fixed list of powers. When $R > N^4$ all the dyads are moderate for sufficiently large rank,

because $K + b + |j| \le CN$ deterministically. Use the same smooth pair coarea at fixed remaining angles in the original Weyl integral, with the indicator of $K > N/3$. It is constant as the two selected angles move inside D_0. Absolute values on all coordinates cost at most $CN^{(\Im s)^2}$ relative to the real unnormalized tilt at u. The fixed two-tag polynomial bound in Theorem 19.2, derived with a bandlimited reproducer, applies also to any prescribed derivatives of the Vandermonde in the two tag coordinates: differentiate the smooth cutoff kernel the required number of times, divide its vanishing difference by $t_1 - t_2$ by the segment formula, and bound its squared modulus and the products of differentiated copies by the same integrable polynomial envelope. Its integral over the remaining variables with an extra $e^{\#D_0}$ stays $O(N^{4u})$ by the real reduced-Palm exponential and two-tag estimate there. The rank powers N^{4u} cancel those from the two physical weights, and the factor $e^{-N/3}$ absorbs $N^{(\Im s)^2}$ and all the powers of $T = O(N)$ arising from selectors, derivatives and central counts. Exterior inserted factors before differentiation are bounded here directly by their degree and the real bounds on the full coordinate sums. The physical factor relating W_λ to the real interior weight is bounded above and below for $0 \le \lambda \ll 1$. This proves the required bound also on the omitted ranks and at $\lambda = 0$, where one can use the circle two-tag envelope directly or take a damped limit. This completes the proof of the localized derivative inequality and hence the transport theorem, including its uniform Taylor remainder.

Corollary to Theorem 19.14 (moving overlap and the first coefficient). Write $\nu_s = 2s + 7/2$ and $A_s = 8^{\nu_s} g_{s+2}/(32\pi^2)$. For $N, R \to \infty$ at any relative rates, $|p| \le M$, and $0 \le \ell = \lambda R \le \epsilon$,

$$R^{\nu_s} d_{\ell/R,N}(R,p) = A_s \frac{\sqrt{1-\ell/2}}{1-\ell} + o(1), \qquad R^{\nu_s - 1} D_{1,N}(R,p) \longrightarrow \tfrac{3}{4} A_s.$$

The first error and both results are uniform on compact tilt sets and on this coordinate range. In particular, when $\tau R \to 0$ with $R \to \infty$,

$$d_{\tau,N}(R,p) - d_{0,N}(R,p) = \tfrac{3}{4} A_s \, \tau R^{1-\nu_s} (1 + o(1)).$$

This asymptotic for the **difference from the exact finite-rank circle density** remains valid when τR shrinks arbitrarily fast. A leading formula for the two densities separately cannot justify dividing their difference by τR.

Here are details of the coefficient. First $R^{\nu_s} d_{0,N}(R,p) \to A_s$ follows without a new two-angle constant computation. Set the physical depth equal to $1/R$ along the chosen ranks and evaluate (19.21) at $B_N = a_z R + d_z$, $J_N = b_z p$. Then $\Re Y + 1/2 \to 1/8$ and $a_z b_z \to 1/16$, while the transport bound $|d_{\tau,N} - d_{0,N}| \le C(\tau R) R^{-\nu_u}$ gives a negligible relative-scale error. This proves the circle-tail matching for arbitrary N, R. It also identifies the leading coefficient for nonreal s, with phase given by the real logarithm of R.

For fixed $0 \le \ell \le \epsilon$ compute the ratio of leading profiles at real s. Use the positive circle preparation of rank $N - 2$ at tilt $s + 2$ for the resident angles, exactly as in the proof of (19.3). For residents with microscopic gap at least $b > 0$, and bounded scaled inverse-square sum and signed cotangent sum, their contributions to $Q_{\ell/R}/R, P_{\ell/R}/\sqrt{R}$ tend to zero. In fact $|P_{\ell/R} - \sum x_i| \le (\ell/R) \sum |x_i|^3$, bounded using the gap and inverse-square sum. Their weight ratio $\prod (1 + \ell x_i^2/R)^s$ tends to one, as do the two squared insertion products of Theorem 19.2, uniformly on each such truncated resident set since $|t_\pm| = O(R^{-1/2})$. There are exactly two opposite tags, which on this set are unique and satisfy $h_+ = -h_- + o(1) = (2-\ell)^{-1/2} + o(1)$, by the explicit pair map and nonzero Jacobian. For clarity the solutions of the second coordinate at zero obey $(h_+ + h_-)(1 + \ell h_+ h_-) = 0$; $1 + \ell h_+ h_-$ is bounded away from zero by the smallness of ϵ. Resolution of the first coordinate gives the stated root. General bounded p changes these scaled coordinates by $o(1)$.

It remains to justify this two-tag replacement at the scale of the signed density. At real s the moderate-dyad bound above, with an exponential in the exterior variables and factorial control of the count, discards $T_* > T_0$ for a relative-scale cost $Ce^{-dT_0} + o(1)$. The high-count terms obey the same bound by the two branches already proved. At bounded T_* the opposite tags are confined to $|t| < C_{T_0}/\sqrt{R}$. A third tag below b costs at most $C_{T_0} b^{1+2\min(u,0)}$ after factoring the scale of the density, by singling it out in the central-tag bound, retaining the pair repulsion and integrating its single weight on $(-b, b)$ for $\sqrt{\lambda} < b$. With a gap b for the rest, the inverse-square and signed cotangent sums are then bounded in terms of T_0, b: apply the inverse formulas in the bounded central window, and outside compare $\sum x_i^2$ to $b_{\text{out}} = \sum q_i$ and $\sum x_i$ to $j_{\text{out}} = \sum p_i$, with error bounded by $C\lambda \sum_{\text{out}} x_i^2$. Conversely the rank-$(N-2)$ circle preparation at $s + 2$ gives the gap and bounded resident sums probability arbitrarily near one, by the real circle intensity and variance estimates used in (19.3). Fix the truncations first, apply pair area change, then remove them by these estimates as in the upper and lower bounds of that theorem.

Put $h=(2-\ell)^{-1/2}$. Relative to $\ell=0$, the two angular weights at the roots give ratio one because $(1+\ell h^2)/h^2=2$. The squared mutual separation gives ratio $1-\ell/2$ since $t_+-t_-\sim 4/(h\sqrt{R})$. The angular-to-$(q,p)$ inverse pair Jacobian at the roots is proportional, in its ℓ dependence, to $h^{-5}(1+\ell h^2)^4/(1-\ell h^2)$, including the two Cayley angular Jacobians. Its ratio to that at zero is $[(1-\ell)\sqrt{1-\ell/2}]^{-1}$. All resident normalizations cancel in the ratio. The preceding bounds hold along arbitrary convergent subsequences of ℓ in the indicated small interval. For complex s the established density bound makes $R^{\nu_s}d_{\ell/R,N}$ locally bounded in tilt. The densities are holomorphic there by the Fourier estimates. Convergence at real s and one-variable normal-family uniqueness give the same profile on the half-plane, locally uniformly in tilt. To differentiate at $\ell=0$, the localized second derivative estimate gives

$$R^{\nu_s-1}D_{1,N}(R,p)=R^{\nu_s}\frac{d_{h/R,N}(R,p)-d_{0,N}(R,p)}{h}+O(h),\quad 0<h<\epsilon,$$

uniformly in rank and R. Take the rank and radius limits first, then send h to zero. The derivative of the profile ratio is $3/4$. Together with the finite-rank Taylor theorem this proves the difference asymptotic. The same argument also identifies every fixed depth derivative in the overlap. The normalized functions $f_{N,R}(v)=R^{\nu_s}d_{v/R,N}(R,p)$ have bounded derivatives through any fixed order on $0\le v\le\epsilon$ by the localization theorem. For $m\ge 1$, $h^{-m}\Delta_h^m f_{N,R}(0)=f_{N,R}^{(m)}(0)+O_m(h)$ by the integral representation of repeated forward differences and the bound through order $m+1$. Thus $R^{\nu_s-m}\partial_\lambda^m d_{0,N}(R,p)$ tends to A_s times the mth derivative at zero of $\sqrt{1-v/2}/(1-v)$. This gives successive normalized coefficients $1,3/4,23/32$ in ordinary Taylor-power convention through order two. The large-R overlap concerns bounded physical imaginary readout. The small-q end reduces to Proposition 19.12 after the exact affine change, and at fixed $\Re Y+1/2>0$ one has $q\asymp 1/c$, $\tau q=O(c)$, recovering (19.21) with a controlled depth correction relative to the finite circle reference. The results in fact hold on each closed subinterval of $0\le\lambda R<1$, with constants depending on its right endpoint and with λ still sufficiently small. To check this extension, fix $0<\delta<1$ and take $\lambda R\le 1-\delta$. At every configuration contributing to the density, $\lambda q_i\le 1-\delta$, hence $x_i^2=q_i/(1-\lambda q_i)\le q_i/\delta$ and $|p_i|\ge\sqrt{\delta q_i}$. For any selected pair write $v_i=\lambda q_i$. Since $v_1+v_2\le 1-\delta$, one has

$$|\lambda x_1x_2|^2=\frac{v_1v_2}{1-v_1-v_2+v_1v_2}\le\left(\frac{1-\delta}{1+\delta}\right)^2.$$

The tagged Jacobian is therefore bounded below on the actual target by the same inverse power of T, with a constant depending on δ. Upon extending the smooth coarea selectors also multiply them by a smooth cutoff in v_1+v_2 equal to one below $1-3\delta/4$ and zero above $1-\delta/2$; its derivatives in the scaled coordinates are bounded on the required windows. These estimates replace each earlier appeal to smallness of λR in the forcing, inverse-map and unique-root arguments. The term τR must still tend to zero to have a two-term asymptotic with a strictly smaller remainder. At $\lambda R=1$ the two-tag Jacobian can vanish. Its critical neighborhood needs a separate analysis.

The two-angle density in the overlap and at fixed off-line distance

Let $F_{N,s,c}(B,J)$ denote the density relative to $dB\,dJ$ under the unnormalized preparation $N^{-s^2}|\Lambda_N(z)|^{2s}$. Put $M=N-2$, $v=s+2$, $G_{N,s}=Z_M^\circ(v)/N^{v^2}$, and

$$U_N=\frac{M(M+2v)}{4v^2-1},\qquad p_2=\frac{U_N}{4N^2},\qquad q_1=\frac{M^2+U_N}{8vN^2}.$$

Use the real logarithm of B in its complex powers.

Theorem 19.15 (matched two-angle expansion). Fix a compact subset of $\Re s>-1/2$, and $L,J_0<\infty$. There exist B_0,N_0,C uniform on this set such that at $N\ge N_0$, $B\ge B_0$, $|J|\le J_0$, $0<cB=\ell\le L$,

$$F_{N,s,c}(B,J)=\frac{G_{N,s}}{2\pi^2}B^{-2s-7/2}\left(1+\frac{D_{N,s}(J,\ell)}{B}+R_{N,s}(B,J,\ell)\right),\qquad |R_{N,s}(B,J,\ell)|\le CB^{-2},\tag{19.31}$$

where

$$\begin{aligned}D_{N,s}(J,\ell)=&(s-\tfrac14)q_1+(s+\tfrac{15}{8})J^2+(s-\tfrac18)p_2+\tfrac38\ell^2-\tfrac12 s\ell\\&+\frac{(2s+2)\ell}{N}-\frac{4s+15}{16N}-\frac{s}{2N^2}.\end{aligned}\tag{19.32}$$

The error in the parentheses is an absolute modulus bound. The asymptotic requires B large. It permits any size of $1/N$ relative to $1/B$, including fixed sufficiently large N. The rank-dependent prefactor has been kept before taking an asymptotic difference.

In particular, at $A = \Re Y + 1/2 > 0$ put $B = A/c$ and $J = \Im Y$. Changing area gives

$$p^{Y}_{N,s,z} = \frac{G_{N,s}}{2\pi^2}\, c^{2s+5/2} A^{-2s-7/2} \left[1 + \frac{c}{A} D_{N,s}(J,A) + R_{N,s}(A/c, J, A)\right], \qquad |R_{N,s}(A/c,J,A)| \le C(c/A)^2.$$

This holds throughout $B_0 c \le A \le L$, $|J| \le J_0$. The relative remainder tends to zero at the stated quadratic rate when $A/c \to \infty$. At fixed A the leading term reduces to (19.21). At $1 \ll B \ll 1/c$ the same two-tag coefficient has $\ell \to 0$ and gives a large-B, bounded-J asymptotic of the transverse density. To see the latter for the limiting density, take $N \to \infty$ and $c \to 0$ first at fixed $B \ge B_0$, using the uniform convergence of the densities in Proposition 19.12. Then $G_{N,s} \to g_{s+2}$, $p_2 \to 1/[4(4v^2-1)]$, and $q_1 \to v/[2(4v^2-1)]$. A single point at this transverse height typically has $|J|$ of order $\sqrt{B}$. Keeping J bounded requires the opposite tagged point and its squared mutual Vandermonde. Integrating this bounded-J expansion over the entire imaginary axis would lose that distinction.

From a conditional density to two Cayley coordinates. Use $r = B^{-1}$, $q = (2N)^{-1}\cot(\theta/2)$, $m = 1/(2N)$. The single-particle contributions to B, J and the constant shift of B are, respectively,

$$b(q) = D\frac{q^2+m^2}{1+\omega^2 q^2}, \qquad j(q) = E\frac{q}{1+\omega^2 q^2},$$
$$d_0 = -\frac{1}{2Nz(1+z)}, \quad D = \frac{2}{z(1+z)^2},\ E = \frac{4}{(1+z)^2},\ \omega = \frac{2c}{(1+z)^2}.$$

For residents at angles θ_i, write $P = \sum q_i$, $Q = \sum q_i^2$ and $b_e = \sum b(q_i)$, $j_e = \sum j(q_i)$. Weyl insertion of a positive and a negative angle gives prefactor $G_{N,s}/(2\pi)^2$ in front of the mass-one circle preparation at exponent v on the M residents. Given these residents the two retained coordinates $q_+ > 0 > q_-$ contribute the following factor to the density:

$$\left(\frac{1+z}{2}\right)^{4s} z^{Ms}\, \frac{(q_+ - q_-)^2}{|\partial(B,J)/\partial(q_+,q_-)|} \prod_{i=\pm} \frac{(1+\omega^2 q_i^2)^s}{(q_i^2+m^2)^{s+2}(1+m^2/q_i^2)^M}$$
$$\times \prod_{a=1}^{M} (1+\rho(q_a^2+m^2))^s (1 - x q_a + y q_a^2)^2, \qquad x = q_+^{-1} + q_-^{-1}, \quad y = (q_+ q_-)^{-1}, \quad \rho = \frac{c^2}{z(1+z)^2}.$$

Indeed $d\theta = |dq|/[N(q^2+m^2)]$, $N|1 - ze^{i\theta}| = (1+z)\sqrt{1+\omega^2 q^2}/[2\sqrt{q^2+m^2}]$, and the squared ratio of the Vandermonde between a tag and a resident to its value at zero angle is $(1-q_a/q_i)^2/(1+m^2/q_i^2)$. The ordered factorial insertion counts a configuration once when the two small angles consist of exactly one of each sign. The coarea determinant is for the resolved pair (B, J).

Uniform signed estimates for the expansion. We detail the truncations because raw complex matrix variation would lose uniformity. In angular coordinates $t = N\theta$, call $|t| \le 2$ the inner window and set $T = 1 + k + b_o + |j_o|$ for its count and the two exterior sums. At the original tilt, (19.19) bounds the density of these retained variables in sectors $k \le N/2$. It also gives a bound with the full squared Vandermonde of three specified inner tags. In each of the two exterior-power norms in that proof, strip the one-point factors, replace the first three columns by their successive divided differences, and extract the three differences. A divided difference of order two is an average of the bounded second derivative on the convex hull (with the simplex normalization); the differentiated band-limited reproducer there bounds each derivative up to order two. For the ultra-high-frequency proof use the same differences on the original normalized monomial columns, whose second derivatives have bounded norm. All other column estimates and the C^k factor survive. At real tilt the analogous bound after integration with a nonnegative exterior exponential also follows from the polynomial reproducer and the Palm exponential bound of Theorem 19.2, using second derivatives in the three tagged variables. Only three tags need be distinguished.

For $T > K\log(1/r)$ the original resolved density, restricted to this event, is $O(r^H)$ for any prescribed H on choosing K sufficiently large. For $k \le N/2$ integrate (19.19) over inner coordinates at the target: the exterior (b_o, j_o) have unit area Jacobian into (B, J), their exponential decay and the count factorial allow a spare $e^{\epsilon T}$.

For the high counts take real-tilt matrix absolute values at cost $O(N^{(\Im s)^2})$. On $k > N/2$ the indicator is at most $Ce^{-N/4-K\log(1/r)/4}\sum_{\pm} e^{2(k+b_o\pm j_o)}$ on the specified event. The resolved Fourier density with either exponential inserted is bounded uniformly in N, c. Here is a direct justification. In the proof of (19.19) use the full unitary phase for the two coordinates and insert $g(t) = 2\mathbf{1}_{|t|\le 2} + 2\mathbf{1}_{|t|>2}(b(t) \pm j(t))$, without a hole. This bounded, piecewise smooth amplitude has bounded variation. The even trace of g and its quadratic trace are bounded, by reflection and the exterior $1/t^2$ decay after removing the odd part. Row and column Gram comparison, the unchanged shell phase and the ultra-high-frequency angular estimate of Theorem 19.9 give integrable Fourier decay. This proves the asserted bound even when c is much smaller than any power of r. We use the same estimate for the circle ensemble with the observables at positive depth, by setting its weight multiplier A in that Fourier proof equal to one.

On the remaining event $T \le K\log(1/r)$, positivity of the individual real marks, $c \le Lr$, and the explicit formula for $b(t)$ give $|t| \ge d\sqrt{r}$ for every point. One point has $|t| \le C\sqrt{rT}$ because $b_o \le T \ll B$ and the other $k \le T$ nonnegative summands supply $B + O(T)$. Its imaginary contribution is of size at least $d/\sqrt{rT}$. The bounded target J and $|j_o| \le T$ force an opposite point with $|t| \le C\sqrt{r}\,T^{3/2}$. The two-tag area bound for (B, J) is $Cr^{5/2}T^{15/2}$ by the derivative argument in Theorem 19.2 applied to $(\Re n/c, \Im n)$. There is at most one inverse with the prescribed signs, since the two marks lie on the single-mark circle.

Let $u = \Re s$. Work on small parameter compacts and choose $\alpha < 1/2$ satisfying $\alpha(2u+5) > 2$ throughout; finitely many such compacts suffice. Discard configurations having a third $|t| < r^\alpha$. The two distinguished weights cost $Cr^{2u}\,\mathrm{poly}(T)$, their squared mutual separation costs $Cr\,\mathrm{poly}(T)$, and the other two squared separations cost $C(r^{4\alpha} + r^2\,\mathrm{poly}(T))$. The third tag weighs at most $C|t|^{2u}$ on its permitted range $|t| \ge d\sqrt{r}$, also for positive u, since $c \le Lr$. Apply the three-tag estimate and pair area change holding all other inner tags and the exterior sums fixed. Relative to $r^{2u+7/2}$ the density cost is $O(\mathrm{polylog}(1/r)r^{\alpha(2u+5)}) = O(r^2)$. At $k > N/2$ on the moderate event $N \le 2K\log(1/r)$ so the extra matrix variation costs only a logarithmic power. On this high-count sector hold all other angles fixed and use successive divided differences of the real antisymmetric three-tag polynomial. The squares of its mixed derivatives (total order three, at most two in each variable) are dominated by the integrated smooth reproducer of Theorem 19.2; integrate that envelope against the three-point reduced-Palm exponential bound. This preserves all three squared differences through the area change. An unconditional intensity bound alone would not justify substituting exterior-dependent roots. This proves the identical power estimate without requiring a density of the sums exterior to the large inner count. This also proves that with the stated error the inserted roots are the only two angles in $|t| < r^\alpha$.

For the remaining M residents use the circle preparation at $v = s + 2$. The mass-one complex Janossy density of the local resident coordinates, with external sums b_o, j_o at depth c, has envelope $C^{k+1}e^{-\epsilon(b_o+|j_o|)}\prod|t_i|^{2u+4}$ for $k \le M/2$ and $|t_i| \le 2$. This is (19.19) with circle multiplier $A = 1$ and rank M in the microscopic coordinate $N\theta$. The ratio M/N stays bounded above and below and does not affect the shell or ultrahigh-frequency estimates. We require the same bound with the following deformation on the *outer* residents:

$$\prod_{|t_i|>2}(1 - Xq_i + Y'q_i^2)^2(1 + R(q_i^2 + m^2))^s.$$

It holds on a fixed complex polydisk about $(0, 0, 0)$, as do the corresponding Cauchy derivative bounds on a smaller polydisk. In fact $|q| \le C/(1+|t|)$ there. The logarithm of the per-angle multiplier is $-2Xq+O((1+|t|)^{-2}+N^{-2})$, with bounded sup norm and absolute variation, on choosing a small polydisk. The odd part integrates to zero against the even real orthogonal-projection diagonal. In the row and column polar comparison in Theorem 19.9 the two halves of the log multiplier may be complex: their Gram bounds use its real part and the Hilbert–Schmidt comparison to P uses the squared modulus of the half-amplitude minus one. The two real phase coordinates and the shell contraction are unchanged. On the ultrahigh-frequency arcs its supremum and total variation are bounded. This proves the envelope after the complex exterior integration and gives the needed locally bounded holomorphic jets. In particular the coefficients of X, Y' at zero are the insertions of $-2P_o, 2Q_o$, for $P_o = \sum_{\mathrm{out}} q_i$, $Q_o = \sum_{\mathrm{out}} q_i^2$; these are signed densities in the retained variables. Cauchy's quadratic remainder applies when the arguments are subsequently evaluated as functions of those retained coordinates. This order of operations is justified also directly at finite rank by the uniformly convergent Taylor series on smaller closed polydisks and the tagged area change. It never requires the total variation of a conditional complex probability.

Define

$$H_0 = (1 + k)^2(1 + \max_{\mathrm{inner}} q_i^2) + 1 + b_o + j_o^2$$

for these residents, with the maximum set to zero if the inner window is empty. Its second moment under the above positive envelope is uniformly bounded because $\int_0^1 t^{2u+4-4}dt < \infty$. The same assertion with an extra exponential of a sufficiently small multiple of T holds. With high resident counts we use the real circle envelope: the factorial intensity is dominated by the product of its one-point envelopes and the outer sums have two-sided exponential moments. For the inner maximum and polynomial count take one distinguished particle and its reduced Palm law; the exponential of an additional count and the two outer sums is uniformly bounded on that law by the rank-one projection decrement and the bounded mean and squared trace estimate as in Theorem 19.2. Thus $\mathbb{E}[e^{\epsilon T}H_0^2]$ is bounded, allowing another $e^{\epsilon k}$ at the high counts to absorb $N^{(\Im s)^2}$. For the unconditioned outer deformation on these counts the same real estimates control its expansion: $Q_o \le C(1+b_o)$ and $|P_o| \le C(|j_o| + c^2(1+b_o))$ by the exact formulas for b, j and boundedness of each outer q. Taylor-expanding its logarithm with absolute quadratic remainder after summing the linear term therefore costs at most $Cr^2H_0^2$ in the calculation below. These are bounds for positive majorants after the necessary exterior integrations in the low-count sector.

The local calculation. Impose the resident gap $|t| \ge r^\alpha$ and the preceding moderate T cutoff. Adding or deleting two tags changes T by exactly two on this gap with the reconstructed pair inner. Discrepancies at the threshold have the preceding exponentially small estimate after adjusting K. On this set $rH_0 = o(1)$ uniformly. The two solutions have opposite signs and are the only roots in $|t| < r^\alpha$. For example the coarea circle construction in Theorem 19.2 gives this by $b_e = O(H_0)$, $|j_e| = O(\sqrt{H_0})$, or one may invert directly in the coordinates below. Write $q_\pm = w_0 \pm d$ with $d > 0$ and $w = (J - j_e)/2$. The equations are $B = d_0 + b_e + b(q_+) + b(q_-)$ and $J = j_e + j(q_+) + j(q_-)$. Expanding at $rd^2 = 1$ yields

$$w_0 = w + O(r\sqrt{H_0}), \qquad d^2 = B + V + O(rH_0^2), \quad V = -w^2 - b_e - d_0 - m^2 - \ell/N + \ell^2/4.$$

For clarity, the exact Cayley sum of the two imaginary parts is $2Ew_0[1+\omega^2(w_0^2-d^2)]/[(1+\omega^2q_+^2)(1+\omega^2q_-^2)]$ and has a bounded invertible coefficient near $rd^2 = 1$. In the real sum the term from $-\omega^2(q_+^4+q_-^4)/2$ is $-\ell^2/4 + O(rH_0^2)$, and $2D = 1 + \ell r/N + O(r^2/N^2)$. These expansions can equivalently be obtained by the implicit function theorem on $(\sqrt{r}\,w_0, rd^2)$ at $(0,1)$, uniformly for $rH_0 = o(1)$. This proves existence, uniqueness by the two-circle inverse, and the quoted remainders. Consequently $x = -2wr + O(r^2H_0^{3/2})$, $y = -r + O(r^2H_0)$.

The ratio of $(q_+ - q_-)^2$ to the pair Jacobian is

$$2d\,[1 + r(5\ell^2/4 - 3\ell/(2N)) + O(r^2H_0^2)].$$

Indeed $b'(q) = 2Dq(1-\omega^2m^2)/(1+\omega^2q^2)^2$ and $j'(q) = E(1-\omega^2q^2)/(1+\omega^2q^2)^2$. Their determinant has the common denominator $\prod_\pm(1+\omega^2q_\pm^2)^2$ and numerator $2DE(1-\omega^2m^2)(q_+-q_-)(1+\omega^2q_+q_-)$. The tagged denominator contributes $(d^2-w_0^2)^{-2s-4}$, times $1 - 2(s+2+M)m^2r + O(r^2H_0^2)$ including the finite resident chord factors. The tagged deformation contributes $1 + s\ell^2r/2 + O(r^2H_0^2)$. The two scalar preparation factors have product $1 - s\ell r/2 + O(r^2)$.

Finally the local resident product expands through order r into $1 + r(4wP_i - 2Q_i)$ for the inner resident sums; its remainder is $O(r^2H_0^2)$. Indeed the sum of $|xq_i| + |yq_i^2|$ is at most CrH_0 and the additional ρ term has size $O(r^2H_0)$. For the outer residents use the polydisk bound proved above, or the high-count real estimates. The combined linear coefficient then has insertions $4wP - 2Q$. In statements of integrated almost-everywhere density bounds the error $O(r^2H_0^2)$ here means its integral against the indicated positive envelope, also for the differentiated outer densities. Thus the unnormalized density divided by $G_{N,s}r^{2s+7/2}/(2\pi^2)$ is the fused-law integral of one plus r times

$$-(2s+7/2)V + (2s+4)w^2 + 4wP - 2Q - 2(s+N)m^2 + 5\ell^2/4 - 3\ell/(2N) + s\ell^2/2 - s\ell/2$$

with error $O(r^2)$. The T cutoff in these coefficient integrals can be removed using the spare exponential. Removing the gap for the constant term costs $O((r^\alpha)^{2u+5})$ by one distinguished point. Its cost in terms bounded in envelope by rH_0 is $O(r(r^\alpha)^{2u+3})$ by integrating the maximal q_i^2 at the closest point. Both are $O(r^2)$ because $\alpha(2u+5) > 2$ and $2u + 1 > 0$. Polynomial count or exterior factors are controlled as above, including at high counts by the spare exponential. This justifies taking the unrestricted coefficient integrals under the fused law.

In those coefficient integrals replace j_e with P and b_e with $Q/2 + Mm^2/2$ at cost $O(r)$ before multiplying by r. For the latter identity the one-point bound at v gives an error $O(c/N + c^2)$ using the bounded integral of q^4. For the former, first moments of both odd statistics vanish. For covariances of odd statistics use the finite determinantal trace identity with kernel $K_{M,v}$. Its off-diagonal decay in Theorem 19.7 and Young's inequality

bound the covariance by $C\|f\sqrt{V_{u+2}}\|_2\|g\sqrt{V_{u+2}}\|_2$; V_{u+2} is bounded everywhere. For $f=j-q$, the norm is $O(c/N+c)$ since $|j-q|\le C[(c/N)|q|+|q|\min(c^2q^2,1)]$ and $\int q^4V_{u+2}\le C$. The norms for q,j are bounded. Moreover $d_0=-1/(4N)+O(c/N^2)$, and $Nm^2/2-1/(4N)=-1/(8N)$. For the fused law the Cayley Ward identities used in Section 22 give $\mathbb{E}P^2=p_2$, $\mathbb{E}Q=q_1$, with the scale $2N$ retained at rank M. Inserting these values and using reflection gives precisely the coefficient displayed in the theorem. The proof makes all estimates before division by any limiting density; the explicit nonzero $G_{N,s}$ in its statement is the finite Barnes factor.

The same pair at imaginary heights of order the square root of the transverse height

Corollary to Theorem 19.15 (angular sector). There is a wider transition sector in which the two angles have different leading magnitudes. Write $J=\xi\sqrt{B}$. Fix $\kappa<\sqrt{2}$, $|\xi|\le\kappa$, $0\le\ell=cB\le L$ with $c>0$, and use $r=B^{-1}$. Uniformly with the ranks and tilt compacts of the preceding two-angle theorem one has

$$\frac{2\pi^2F_{N,s,c}(B,\xi\sqrt{B})}{G_{N,s}B^{-2s-7/2}}=H_s(\xi)+rK_{N,s}(\xi,\ell)+O(r^2),\qquad H_s(\xi)=\sqrt{1-\xi^2/4}\,(1-\xi^2/2)^{-2s-4}. \tag{19.33}$$

The coefficient $K_{N,s}$ can be evaluated by two derivatives of scalar algebraic functions. The formula below has no remaining high-dimensional integral. Define a linear functional $\mathcal{E}$ on polynomials in P,Q of weighted degree at most two (P has weight one, Q weight two) by replacing $1,P,P^2,Q$ by $1,0,p_2,q_1$. Put $a=\sqrt{r}$ for evaluation, and treat a as a Taylor variable at zero when computing the coefficient. Write

$$z_a=\sqrt{1-\ell a^2/N},\quad \Omega=4\ell^2a^2/(1+z_a)^4,\quad b_a(U)=\frac{2(U^2+a^2m^2)}{z_a(1+z_a)^2(1+\Omega U^2)},\quad j_a(U)=\frac{4U}{(1+z_a)^2(1+\Omega U^2)}.$$

Starting at $U_\pm(0)=\xi/2\pm\sqrt{1-\xi^2/4}$, solve the two analytic scalar equations

$$\sum_{i=\pm}b_a(U_i)=1-a^2\left[-\frac{1}{2Nz_a(1+z_a)}+\frac{Q+Mm^2}{2}\right],\qquad \sum_{i=\pm}j_a(U_i)=\xi-aP.$$

Denote their positive oriented Jacobian at zero, analytically continued, by $\Delta_a=b_a'(U_+)j_a'(U_-)-b_a'(U_-)j_a'(U_+)$. Set $A=1/U_++1/U_-$, $D=1/(U_+U_-)$. With all noninteger powers continued locally from positive bases at $a=0$, the coefficient is

$$K_{N,s}(\xi,\ell)=\mathcal{E}[a^2]\Bigg\{z_a^{Ms}\left(\frac{1+z_a}{2}\right)^{4s}\frac{(U_+-U_-)^2}{2\Delta_a}\prod_{i=\pm}\frac{(1+\Omega U_i^2)^s}{(U_i^2+a^2m^2)^{s+2}(1+a^2m^2/U_i^2)^M}$$
$$\times\left[1-2aAP+a^2\{2DQ+A^2(2P^2-Q)\}\right]\Bigg\}.$$

Here $[a^2]$ denotes the Taylor coefficient, one half the second derivative. Only a 2×2 real Jacobian at $a=0$ is needed to differentiate the implicit roots. The formula is even in ξ by reflection and holomorphic in s. At $\xi=0$ it gives $D_{N,s}(0,\ell)$ above. Also $H_s(\xi)=1+(s+15/8)\xi^2+O(\xi^4)$, which recovers the bounded-J coefficient including its J^2 term.

Proof. We give the changes needed in the two-angle estimates. On the moderate count and exterior event every inner $|q|\le C\sqrt{B}$, since all individual b are nonnegative and their saturating maximum is much larger than B at $cB\le L$. More explicitly invert $D(q^2+m^2)/(1+\omega^2q^2)\le B+O(1)$ using $B\omega^2=O(1/B)$. There $\sum_{\text{inner}}q^2=(2+o(1))B$ and $\sum_{\text{inner}}q=J+o(\sqrt{B})$ uniformly; the errors follow by the bounds on T, $\omega^2q^2=O(1/B)$ and Cauchy–Schwarz over the inner count. Write S_+,S_- for the sums of the positive and absolute negative q respectively. Then $S_++S_-\ge(\sum q^2)^{1/2}$, and $|S_+-S_-|\le(\kappa+o(1))\sqrt{B}$. Both signs consequently have a point of magnitude at least $d_\kappa\sqrt{B}/T$. The previous area and third-point bounds continue to hold with at most logarithmic losses in the moderate range. They remove the third-angle sector, and the large-T estimates were already uniform in the target. A third nearby angle costs $O(r^2)$ relative to the displayed normalization.

In the remaining fused resident integral set $U_\pm=aq_\pm$. The exact analytic root equations at the target use b_e,j_e in place of $(Q+Mm^2)/2,P$. For the Taylor argument freeze these two real numbers at their actual depth. At zero parameter the oriented Jacobian $U_+(0)-U_-(0)$ is uniformly positive and both $|U_i(0)|$ are bounded below

by a positive number depending on κ. On $|a'| \le d_\kappa/\sqrt{H_0}$ the scaled perturbations $a'^2 b_e, a' j_e$ stay in a fixed small neighborhood of zero. The analytic implicit-function theorem on the compact ξ interval supplies uniformly bounded roots, bounded away from zero, and a nonvanishing Jacobian for these auxiliary complex a'. The scalar factors involving an Mth power are bounded there because $Mm^2 \le 1$ and $M|1 - z_{a'}| \le C|a'|^2$. For the local resident interactions the sums $|a'| \sum |q_i|$ and $|a'|^2 \sum q_i^2$ are bounded on this disk by the definition of H_0. Use the preceding exterior holomorphic deformation there, with $X = a'A$, $Y' = a'^2 D$ and $R = O(a'^4)$. Its Cauchy bounds are independent of H_0. In high-count absolute estimates the possible linear cotangent contribution on the exterior is bounded by $|a' P_o|$, uniformly, since $|P_o| \le C(|j_o| + c^2(1 + b_o))$ and $T \le K \log(1/r)$ on the truncated region. Its absolute quadratic contribution costs $C|a'|^2(1 + b_o)$. Thus the scaled coarea integrand and its integrated outer density are bounded on this analytic disk by a constant times the same integrable envelope. The actual argument satisfies $a\sqrt{H_0} = o(1)$ on the resident gap. Cauchy's estimate through degree three leaves $O(a^4 H_0^2)$ under that envelope.

For the auxiliary expansion, simultaneous reflection of all resident angles and $a' \mapsto -a'$ leaves the scaled root equations and the pair weights unchanged. Indeed the frozen b_e is even, j_e is odd, and Xq_i is invariant under the combined operation. This is a symmetry of the equal-exponent complex measure and of the cutoffs. Both odd-degree contributions therefore integrate to zero, also at nonzero fixed ξ. In the coefficient of a'^2 the resident multiplicative factors give $2DQ + A^2(2P^2 - Q)$ together with the derivative of the linear term $-2a'AP$. The frozen marked variables enter polynomially through $b_e, j_e^2, j_e P$ and lower terms. The covariance and mean estimates of the preceding proof replace them by their circle expressions with $O(c + 1/N \cdot c) = O(r)$ error in this coefficient; the constant $Mm^2/2$ is kept. Removing the gap and large-T cutoffs costs $O(r^2)$ by the same moment estimates. The positive Jacobian permits its analytic extension in this calculation in place of the absolute real Jacobian. At zero parameter $(U_+U_-) = \xi^2/2 - 1$ and $U_+ - U_- = 2\sqrt{1 - \xi^2/4}$, giving $H_s(\xi)$ and the asserted derivative formula. As $|\xi| \to \sqrt{2}$, one root goes to zero in the scaled variable, which is the explicit obstruction to this uniform two-angle expansion at the one-angle front.

A second term for transverse tail integrals and the higher threshold bands

The following readout integrates over the full imaginary coordinate. This includes large imaginary excursions from a single nearby angle. Retaining a bounded imaginary coordinate selects different configurations. Write $I = I_{N,s}$ for the unnormalized functional of Proposition 19.12, $u = \Re s > -1/2$, $a_s = 2s + 1$, $a = 2u + 1$, $\ell = N(1 - z)$, and put

$$D_{N,m}(s) = \frac{N^{-(s+m)^2} Z^\circ_{N-m}(s + m)}{m!(2\pi)^m}.$$

It retains the exact rank dependence of the resident circle normalization. Its limit is $g_{s+m}/(m!(2\pi)^m)$. For $R > 0$ let $r = (2R)^{-1/2}$, $\lambda = c^2 R$, $v = 2\lambda z/(1 + z)^2$ and $d_0 = -1/[2Nz(1 + z)]$. The even integrals needed below are

$$F_s(v) = \int_{|x| < \sqrt{1-v}} (v + x^2)^s dx, \qquad G_s(v) = \int_{|x| < \sqrt{1-v}} x^2 (v + x^2)^s dx.$$

For $M = N - 1$, $\tau = s + 1$ write

$$U = \frac{M(M + 2\tau)}{N^2(4\tau^2 - 1)}, \qquad Q_0 = \frac{(M/N)^2 + U}{2\tau} + \frac{M}{N^2}.$$

Proposition 19.16 (transverse tail expansion and open threshold bands). Fix $0 < \epsilon < 2$ and a compact tilt set $K \subset \{s : \Re s > -1/2\}$. Uniformly for $s \in K$, $0 < \lambda \le 2 - \epsilon$, all sufficiently large ranks and sufficiently small r, there is $\delta > 0$ such that

$$\begin{aligned} \frac{I(\mathbf{1}_{B_N > R})}{D_{N,1}(s) r^{a_s} z^{Ns - a_s}} &= F_s(v)\left(1 + \frac{s\ell^2 Q_0}{4z}\right) + \frac{r^2}{z^2}\left(\frac{1}{8N^2} + \frac{U}{2} - \frac{Q_0}{4}\right) G_s(v) \\ &\quad + \frac{2r^2}{\sqrt{1 - v}}\left(\frac{Q_0}{8z^2} + d_0\right) + O_{K,\epsilon}(r^{2+\delta}). \end{aligned} \tag{19.34}$$

Powers use the real logarithm. The size of the coefficient is measured additively, including at its possible complex zeros. The exact scalar $z^{Ns - a_s} = 1 - sc/2 + a_s c/(2N) + O_K(c^2)$ exhibits a mixed term. At $R \asymp 1/c$ the r^2

correction and the linear c contribution have the same order. At $c \ll r$ the endpoint $v = 0$ is an ordinary integrable limit. The displayed expression recovers the entire one-angle tail of Proposition 19.12. The denominator $\sqrt{1-v}$ records the degeneration at the cutoff.

Targets requiring several angles. Fix $m \geq 2$ and take λ in a compact subinterval of $(2(m-1), 2m)$. Put $q_m = m(2s+m)$, $d = \ell/\sqrt{z}$, $M_z = (1+z)^2/(2z)$, and $\Delta(x) = \prod_{i<j}(x_i - x_j)$. Then

$$\frac{I(\mathbf{1}_{B_N > \lambda/c^2})}{D_{N,m}(s) z^{(N-m)s} \ell^{2ms} d^{m^2}} = \int_{\sum_{i=1}^m (1+x_i^2)^{-1} > \lambda/M_z} \Delta(x)^2 \prod_{i=1}^m (1+x_i^2)^s \, d^m x + O_{K,m,\lambda}(c^2).$$

The error is uniform on the specified subinterval. The denominator equals $D_{N,m}(s)(c/2)^{q_m}[1 - sc/2 + q_m c/(2N) + O_K(c^2)]$. This yields, in particular, the first nonzero order for real s strictly between the first and second cutoffs. The integral is strictly positive for real s and is an ordinary complex integral throughout the half-plane. These estimates make no uniform assertion at the threshold values $2m$.

A repulsion estimate with distinguished angles. For every fixed p the positive complex-Janossy majorant (19.19) can be multiplied by $C_p|\Delta(t_1, \dots, t_p)|^2$ for p chosen central tags. Indeed replace the successive distinguished columns in each of the two complementary wedges by their Newton divided differences in the real variable t. Their wedge gains one factor Δ on each side. After removing the scalar angular powers, derivatives through order $p-1$ of the remaining vector columns on $[-2, 2]$ have uniformly bounded Hilbert norms by the differentiated band-limited reproducer in the proof of (19.19). The real-node integral formula for divided differences bounds the resulting vectors, including as nodes coincide. In the ultra-high-frequency argument the angular monomial columns have this same property directly. The p-dependent constant costs no additional rank power.

The high-count sector also admits these distinguished factors for estimates involving the exterior positive sum b. Here take matrix absolute values with the factor $O_K(N^{(\Im s)^2})$ at real tilt u. Divide the range of b into unit intervals indexed by $j \geq 0$ and dominate their indicators by e^{b-j+1}. For each exact central count $k > N/2$ one may remove the exclusion of further central points when bounding its k-tag integral by a real factorial integral. To see its bound directly, pass to the circle at u, expand the remaining multiplicative deformation with symbol $A_u e^{b(t)\mathbf{1}_{|t|>2}} - 1$ in factorial densities, and apply the circle bilinear Gram bound, retaining the distinguished wedges. Here $b(t) = \Re n(t)/c \leq C/t^2$ outside the window, so the $L^1(V_u)$ cost of the deformation is bounded by Theorem 19.7. The same argument allows each central count an extra fixed exponential factor. This gives $C_p C^k e^{-j}/k!$ times the interior angular weights and selected repulsion. The factorial tail absorbs $N^{(\Im s)^2}$, including when another fixed exponential or polynomial in k is inserted. Keeping the small angular factors throughout is essential when c is extremely small compared with rank.

Replacing a tail event by its tagged events. Use scale $b_* = r$ for the first band and $b_* = c$ in band $m \geq 2$. The exponent of b_* from m near tags and their repulsion is $A_m = m(2u+m)$. With $b(t)$ as above, replace the full indicator by the sum over *unordered* local m-sets of the indicator that their sum of $b(t)$ exceeds R. The difference in integrated complex variation is $O(b_*^{A_m+2})$. We detail the estimate since an individual event has a larger mass. Restrict $1+k+b \leq L = 1+|\log b_*|^2$ initially. The bounds above lose $O(b_*^H)$ for every fixed H on its complement, even with the polynomial multiplicity of the tagged events. In the high-count sector the factorial and the e^{-j} estimate absorb the rank power while reserving an exponential of $k+j$. An event of either kind forces m tags within $Cb_*\sqrt{L}$. For the first band this follows from $b(t) \leq C/t^2$. In a higher band $c^2 b(t) \leq M_z$, and $m-1$ such tags leave a fixed positive gap in λ. Choose $h = b_*^\kappa$ with $2/(a+2m) < \kappa < 1$, locally uniformly in u. A further tag within h costs

$$Cb_*^{A_m} L^C h^{a+2m}.$$

For the m forced tags integrate their product weights and Vandermonde on their stated box. Their integrals cost at most $Cb_*^{A_m} L^C$ also for $u < 0$, using $|t|^{2u}$ if $c \ll r$. For a further tag within h the cross differences cost at most Ch^{2m} and its integral costs Ch^a; for $u \geq 0$ this uses $c \leq Cb_* \ll h$. This bound, including the count of all choices, gains a strict power beyond $A_m + 2$.

On the remaining configurations all outside local contributions to the normalized threshold cost at most $Cb_*^2 L/h^2 = o(1)$. Therefore the forced tags lie within Cb_* and are unique. For fixed exterior and other central angles, disagreement costs a strip of scaled width

$$Cb_*^2 \left(1 + b + \sum_{\text{other local}} |t|^{-2}\right).$$

In the first band the single-tag boundary in the variable $x = 2Nz\sin(t/(2N))/r$ is $|x| = \sqrt{1-v}$, separated from both zero and infinity. In higher bands use $x = 2\sqrt{z}\sin(t/(2N))/(1-z)$, for which $c^2 b(t) = M_z/(1+x^2)$. Each boundary is compact and regular uniformly on the specified thresholds: the only stationary point of the full sum is $x = 0$, and a coordinate escaping to infinity would put the sum at most $m-1$ in units of M_z. A finite coordinate cover and the one-dimensional change of variable in a coordinate with derivative bounded away from zero bound the volume of the strip by its width. The m tag integrals cost $Cb_*^{A_m}$ times this width. For the term $|y|^{-2}$ from another tag with $|y| > h$, retain its m cross-differences; these supply $C|y|^{2m}$. Its integral is bounded since $\int_0^2 y^{a+2m-3}dy < \infty$. The exterior cost has an exponential moment. These arguments work for the low-count Janossy majorant and for the real high-count bound just proved. This proves the estimate independently of the speed of approach to the circle.

We record a localization of this argument. In the first band the disagreement from an additional resident below $0 < \eta < 1$, $h < \eta$, costs $O(r^{a+2}\eta^{\min(a,1)})$ in addition to the strict-power error above. When the same resident supplies the factor $|y|^{-2}$ its integral is $O(\eta^a)$. When it is a different resident, keep both sets of cross differences with the forced tag and discard their mutual repulsion at bounded cost. The tail $k+b+|j| > L_1$ costs $Ce^{-dL_1}r^{a+2}$ in the low-count strip estimate (here j is the exterior imaginary sum). If the high counts also require this restriction, first bound them without the restriction by $Ce^{-dN}r^{a+2}$. For a power error independent of the relative rates one can impose the two signs of the exterior j by the following real weighted-factorial bound instead. Use the real interior orthogonal projection at u with the extra real weight $e^{\pm j_{\mathrm{out}}+b}$. Its mass divided by the original mass is uniformly bounded: in the Fredholm determinant bound $\det(I + P(e^g - 1)P) \le e^{\int (e^g-1)P(t,t)dt}$ the odd linear term cancels by reflection and the square is integrable. The multiplier is bounded above and below pointwise. The feature-space Gram matrix changes by bounded operator factors, preserving the real distinguished-wedge bounds. More explicitly the real interior correlation Gram determinants with p distinguished points obey the same product envelope with $|\Delta_p|^2$ by the preceding circle expansion at u even before this change of weight; multiplication by a bounded positive symbol and insertion of the inverse Gram matrix in the projection kernel costs at most C^k by the exterior-power inequality. Thus retaining the indicator $|j| > L_1$ in this sector costs a further exponential while preserving both the rank gain and all angular factors.

Factorial integration and its Taylor terms. After Weyl insertion of m designated particles the resident circle ensemble has tilt $s+m$ and rank $N-m$. With θ_j the resident angles, define

$$Q = N^{-2}\sum_j \csc^2(\theta_j/2), \quad L_0 = N^{-1}\sum_j \cot(\theta_j/2), \quad E_t(\theta) = \cos(t/(2N)) - \cot(\theta/2)\sin(t/(2N)).$$

The remaining integral after the exact scalar $z^{(N-m)s}$ is the expectation $\Phi_c(\boldsymbol{t})$ of $\prod_j A(N\theta_j)\prod_i E_{t_i}(\theta_j)^2$ in that mass-one circle preparation. This expression applies the Weyl insertion before taking absolute values. For $|t_i| \le Cb_*$ we have $\Phi_c(\boldsymbol{t}) = 1 + O(c^2 + b_*^2)$. For completeness it is holomorphic and bounded on a *fixed* small complex polydisc in the tag arguments, uniformly in rank and depth. In the determinant argument of (19.13) the absolute central integrand is bounded by $CV_{u+m}(y)[1 + |A(y)|(1+|y|^{-2m})]$, integrable with uniform integral by $2u > -1$ after splitting at $|y| = c$. Away from the origin the perturbation is $O(1/|y| + N^{-2})$, with an even symmetrized trace of order $O(1/y^2 + N^{-2})$; the off-diagonal squared kernel supplies the Hilbert–Schmidt bound as before. Joint reflection annihilates every first tag derivative at zero. The depth-only deviation from one is $O(c^2)$ by the factorial expansion and the integrable quadratic inverse weight at the shifted tilt. Taylor's formula proves the claim.

For $m = 1$ more is available. With the circle mean denoted by brackets, for $|t| \le Cr$, $c \le Cr$,

$$\Phi_c(t) = 1 + \frac{s\ell^2}{4z}\langle Q\rangle + t^2\left(\frac{\langle L_0^2\rangle}{2} - \frac{\langle Q\rangle}{4}\right) + O_K(r^{2+\delta_1})$$

for some $\delta_1 > 0$. At $c = 0$ the coefficient follows by differentiating the finite product. At positive depth expand the zero-tag symbol $A - 1$: its $L^1(V_{u+1})$ norm is $O(c^2)$, and its linearization in $\ell^2/(4zN^2)\csc^2$ has an integrated remainder $O(c^{2+\gamma})$ for $0 < \gamma < \min(1, 2u+1)$. Split $|y|$ at c and one, and for $c < |y| < 1$ use the quadratic Taylor remainder Cc^4/y^4. Higher factorial terms cost $O(c^4)$. To replace the quadratic tag coefficient by that at zero depth, on the fixed complex tag circle use $\int_{|y|<1}|A-1|(1+y^{-2})V_{u+1}dy = O(c^\gamma)$ by the same splitting. Outside one the difference in the two symbols is $O(c^2/y^2)$. Their symmetrized traces differ by $O(c^\gamma)$. The two Hilbert–Schmidt kernels in (19.13) differ by $O(c^{\gamma/2})$, using the square-root factorization inequality

$|\sqrt{|v|}\,\mathrm{phase}(v)-\sqrt{|w|}\,\mathrm{phase}(w)|\le C\sqrt{|v-w|}$ and the existing weighted convolution estimate. The regularized determinants on this bounded set therefore differ by $O(c^{\gamma/2})$. Cauchy's coefficient bound and uniform even Taylor expansion yield the assertion. By the two circle Ward identities in Section 22, or by integrating the divergences of $(1+x_j^2)\sum x_k$ and $x_j(1+x_j^2)$ in the Cayley density, $\langle L_0^2\rangle = U$ and $\langle Q\rangle = Q_0$. Absolute integrability is ensured by $\Re(s+1)>1/2$.

In the higher bands the tagged weights become $\ell^{2ms}\prod(1+x_i^2)^s$. The angular volume and the mutual squared Vandermonde become $d^{m^2}\Delta(x)^2(1+O_m(c^2/N^2))$ after the angular powers of N have been extracted into $D_{N,m}$. The chord ratio is uniformly regular also when coordinates coincide, by a divided difference of the smooth local inverse map. Inserting the bound on Φ_c in the compact tagged domain and using the strip estimate proves the several-angle formula.

In the first band use instead $x = 2Nz\sin(t/(2N))/r$. The identities are $b(t)/R = 1/(v+x^2)$, $N|1-ze^{it/N}| = rz^{-1/2}\sqrt{v+x^2}$, and the remaining Jacobian after r/z is $(1-r^2x^2/(4N^2z^2))^{-1/2}$. The expansion of the last factor gives $r^2x^2/(8N^2z^2)$. The preceding expansion of Φ_c gives every term of the proposed one-tag formula except the term divided by $\sqrt{1-v}$. We determine that term from the threshold disagreement.

Displacement of the threshold. Begin with real s. In the region where the closest tag is unique, choose the resident configuration first. With $W = d_0+\sum_{\mathrm{res}} b(t)$ the actual interval in x has endpoints $\pm\sqrt{(1-2r^2W)^{-1}-v}$, while the tagged-event interval has endpoints $\pm\sqrt{1-v}$. Fix a small $\theta>0$, set $\eta = r^\theta$ and discard for the displacement the cases with a resident below η or $1+k+b+|j| > |\log r|^2$; by the localized strip bounds this costs $O(r^{a+2+\delta_2})$ for some $\delta_2>0$. Exterior here means all variables except the forced tag, with the far marks and count as in (19.19); the count changes by one when that tag is removed. The same truncation may be used in the ordinary circle mean of $1+Q$: the single near weights are $O(|t|^{2u+2})$, so Q times the excluded small-gap indicator integrates to $O(\eta^a)$ by the one- and two-tag factorial bound. The positive far sum and count, and the two signs of the signed far sum, have uniform exponential moments by the real orthogonal projection argument above. The same Q-weighted bounds follow either by a surplus absolute moment of Q (any order $1+\nu<(a+2)/2$) and Hölder or by its distinguished-point integral.

On this restricted resident set one has $Q+|L_0|\le C(1+|\log r|)^C\eta^{-C}$ with a fixed finite power: the central count controls each inverse sine down to the gap, while outside the central window the inverse-square sum is bounded by Cb, and the signed cotangent sum differs from the signed imaginary mark times $2z$ by $O(c^2\sum_{|t|>2}|t|^{-3})$. The product of insertion ratios and depth weights differs from one by $O(r^\alpha)$ for some $\alpha>0$ if θ is small, by expanding their logarithms. Also $W = d_0+Q/(8z^2)+O(c^2\eta^{-2}Q)$ using the exact denominator $1+(1-z)^2\csc^2(\theta_j/2)/(4z)$. Endpoint expansion of the even scalar integrand costs $2r^2W/\sqrt{1-v}$ to first order, with error $O(r^4W^2)$ since $1-v$ stays bounded away from zero. Its leading endpoint value equals one. The pointwise product and Jacobian errors on the shell cost $O(r^{2+\alpha}(1+Q))$ upon reducing θ if necessary. Taking resident expectation and restoring the excluded contributions gives the last term with a power surplus at real tilt, locally uniform in s.

For complex s the strip estimate gives a bound $O_K(r^{a+2})$ for the displaced mass. Subtract the computed term and divide by $D_{N,1}r^{a_s+2}z^{Ns-a_s}$; the resulting holomorphic functions of s are locally bounded, and on real intervals they are $O(r^{\delta_2})$. This implies a locally uniform power gain throughout $\Re s>-1/2$. For a compact in that half-plane take a closed rectangle in the half-plane with its bottom edge on a real interval, containing the upper part of the compact away from its other three sides. Apply the two-constants maximum principle to the logarithm of the modulus: the bottom edge contributes $\delta_2\log r$ times its harmonic measure, which has a positive lower bound on that part of the compact. Treat the lower part by reflection of the rectangle. This argument uses ordinary finite-rank matrix holomorphy and the complex projected strip bound. Combining the two contributions proves the stated one-angle expansion.

The first cutoff on its inner scale. There is a distinct asymptotic when $R = M_z/c^2+\eta$ with η in a fixed compact subset of $\mathbb{R}$, including the threshold $c^2R=2$ itself. Continue to use $m=1$, $d=\ell/\sqrt{z}$, $M=N-1$, $\tau=s+1$ and $Q = N^{-2}\sum_{j\le M}\csc^2(\theta_j/2)$ on the resident circle. Write $x_+ = \max(0,x)$. There is $\delta>0$ locally uniform in s and uniform on such compact sets of η for which

$$\frac{I(\mathbf{1}_{B_N>M_z/c^2+\eta})}{D_{N,1}(s)z^{(N-1)s}\ell^{2s}dc} = \frac{2}{\sqrt{M_z}}\int\left(\frac{Q}{8z^2}+d_0-\eta\right)_+^{1/2} dP^\circ_{M,s+1}+O(c^\delta). \tag{19.35}$$

At $c^2R=2$ use $\eta = -1/[2N^2z(1+z)^2]$. In particular, if $\eta\to\eta_0$ while $N\to\infty$, $c\to 0$, the mass divided by c^{2s+2}

tends to

$$\frac{g_{s+1}}{2\pi}\,2^{-2s-1}\sqrt{2}\int(B-\eta_0)_+^{1/2}\,d(\nu_{s+1}/g_{s+1})(B,J).$$

For real tilt this signed-ensemble formula is a positive coefficient (the transverse distribution has an unbounded positive tail). For nonreal tilt it requires no assertion of nonvanishing of the last integral. This is a new angular scale $|t|\asymp c^2$ inside the usual one-tag scale $|t|\asymp c$. The remaining angles enter at leading order through the distribution of their transverse contribution.

Here are the estimates at the cutoff, where the regular-level argument for the preceding band would fail. Truncate $T=1+k+b+|j|$ at $1+|\log c|^2$ with an error smaller than any power as in the distinguished-angle proof. The event forces one angle within $Cc\sqrt{T}$. Choose $h=c^\kappa$ with $1/(a+2)<\kappa<1$. A second angle below h costs $Cc^aT^Ch^{a+2}$ by the two-tag repulsion estimate. This gains a strict power over c^{a+1}. On the complement the other angles contribute $O(Th^{-2})$ to B_N apart from its offset, so $c^2(|W|+1)=o(1)$, where $W=d_0+\sum_{\mathrm{res}}b(t)-\eta$. Introduce the exact coordinate

$$w=\frac{2N\sqrt{z}\sin(t/(2N))}{\ell c}.$$

The tag contributes $b(t)=(M_z/c^2)/(1+c^2w^2)$, and its admissible interval has length $2\sqrt{W_+}/\sqrt{M_z-c^2W}$. Consequently its angular integral is bounded by $Cc^{2u+2}(1+b+\sum_{\text{other local}}|t_i|^{-2})^{1/2}$ times the other weights. Indeed $|t|\le Cc^2\sqrt{1+|W|}=o(c)$ throughout the interval. Integrate the square-root bound by $1+\sqrt{b}+\sum|t_i|^{-1}$ with the distinguished repulsion factors for the tag and the contributing local points. The integral at zero is finite; a resident cut $|t_i|<\eta_1$, $h<\eta_1<1$, in this bound costs $O(\eta_1^{\min(a,1)})$ relative to c^{a+1}. If a second, distinct resident supplies the inverse power and the first the small-gap indicator, distinguish both and keep their two squared cross differences with the tag. The exponential tails of the count and exterior sums can be retained. The high-count real estimate in the preceding proof therefore applies without any condition on N relative to c. This yields a locally uniform bound for the normalized complex mass.

For real tilt restrict the residents to gap $\eta_1=c^\theta$ and to the logarithmic cutoff above, taking $\theta>0$ sufficiently small. The discarded normalized mass is $O(c^{\delta_1})$ by the preceding small-gap argument. The selected tag is unique and its conditional area element relative to $D_{N,1}z^{(N-1)s}\ell^{2s}dc$ is

$$(1+c^2w^2)^s(1-d^2c^2w^2/(4N^2))^{-1/2}\prod_j A(N\theta_j)E_{t(w)}(\theta_j)^2\,dw.$$

On this truncated set the integrand differs from one by $O(c^\alpha)$ with $\alpha>0$: $Q+|L_0|$ is bounded by a fixed power of η_1^{-1} times a logarithm, and $|t(w)|\le Cc^2\sqrt{1+|W|}$. Expand the logarithm of the insertion as in the displacement proof. Its integral is $2\sqrt{W_+}/\sqrt{M_z}$ up to $O(c^{\alpha'}(1+\sqrt{Q}))$, including expansion of the denominator, for a sufficiently small θ. Furthermore $|W-(d_0+Q/(8z^2)-\eta)|\le Cc^2\eta_1^{-2}Q$. The inequality $|x_+^{1/2}-y_+^{1/2}|\le|x-y|^{1/2}$ allows this replacement at cost $O(c\eta_1^{-1}(1+\sqrt{Q}))$ even when the threshold crosses zero. The circle estimates with the Q weight remove the truncations at a power cost. The degree-$1/2$ coefficient on the right is holomorphic in s at each finite rank by absolute integrability at $\Re(s+1)>1/2$. It is locally bounded uniformly in rank after the circle projection: apply (19.19) at $s+1$ with $A=1$, passing to depth zero at fixed rank, and integrate the positive envelope with the $\sqrt{1+Q}$ weight as in Proposition 19.12. The exterior part of Q is recovered from its positive resolved coordinate at zero depth. The high counts are bounded by the real factorial estimate with a surplus moment as above. The two-constants argument applied to the normalized difference transfers a positive power of c to every complex parameter compact.

Finally, $Q/8$ on these circle residents equals $(M/N)^2B_M^\circ+O(1/N)$, where B_M° is the rank-M zero-depth transverse readout (including the $-1/(4M)$ offset). The fixed-frequency Jacobi proof and the resolved uniform bounds in Proposition 19.12 persist at zero depth by the same $A=1$ argument. Weighted variation through any exponent $1/2<p<\Re(s+1)+1/2$ suffices to pass the displayed square-root integral to its limit. This and continuity of the positive-part square root in the threshold give the claimed complex or real coefficient.

Planar densities beyond the first degeneracy of the pair map

There is a further leading result when a bounded longitudinal mark is accompanied by a transverse readout proportional to $1/\lambda$. This concerns **planar density at bounded** p; integrating over all longitudinal marks to get a marginal tail would require uniform control on their growing range.

Proposition 19.17 (joint density with several distinguished angles). Fix $k \ge 2$ and a compact interval of $k-1 < \ell < k$. At $q = R$, $\lambda = \ell/R$, $|p| \le M$, as $N, R \to \infty$ at arbitrary rates, the unnormalized density satisfies

$$R^{ks+k^2/2+3/2}\, d_{\ell/R,N}(R,p) \longrightarrow \frac{g_{s+k}}{(2\pi)^k k!} \int_{\mathcal{M}_{k,\ell}} \frac{\prod_{i=1}^k (y_i^2+4\ell)^s\, \Delta(y)^2}{\sqrt{\det(DF\, DF^{\mathsf{T}})}}\, d\mathcal{H}^{k-2}(y). \tag{19.36}$$

Here $F = (\sum 4/(y_i^2+4\ell), \sum 2y_i/(y_i^2+4\ell))$ and $\mathcal{M}_{k,\ell} = F^{-1}(1,0)$. The branch uses positive real bases. The limit is locally uniform in $\Re s > -1/2$, in the indicated intervals and bounded p. The coefficient is positive at real tilt. It is a convergent complex coarea integral at general tilt, where its zero set has not been determined. At $1 < \ell < 2$ the coefficient is $A_s\sqrt{1-\ell/2}/|1-\ell|$, extending the two-angle profile across the excluded critical value. At $2 < \ell < 3$ three angles give the first nonvanishing real-tilt planar scale, with exponent $3s+6$.

To see why the indicated regularity and multiplicity hold, reparametrize a single tag by $e^{i\phi} = (1+i\sqrt{\lambda}x)/(1-i\sqrt{\lambda}x)$. Then $1-\cos\phi = 2\lambda q_i$ and $\sin\phi = 2\sqrt{\lambda}p_i$. Let $\delta > 0$ be less than the distance of the compact interval from the integers. The total $\sum(1-e^{i\phi_i}) = 2\ell - 2i\sqrt{\lambda}p$. For the localized low-count dyads used above, discard the exterior terms; their error is $O(T/\sqrt{R})$. Also discard central tags with $|1-e^{i\phi_i}| \le \delta/(CT)$, costing at most $2\delta/C$. Take $T \le \gamma R^{1/3}$ and C sufficiently large. The remaining tags number at least k, since each real contribution is at most two and $2\ell > 2(k-1) + 2\delta$. At least one pair among them has $|\sin(\phi_i - \phi_j)| \ge \delta/(C'T)$. Otherwise every remaining unit phase is within $O(\delta/(C'T))$ of either of two antipodal unit numbers. If m, n are the two counts, the total of the retained differences would be within $O(\delta/C')$ of $m+n-(m-n)e^{i\phi_0}$. The reverse triangle inequality would put $|m+n-2\ell|$ within a small fraction of δ of $|m-n|$. Both $m+n \pm |m-n|$ are even integers, a contradiction.

Choose these two regular tags and $k-2$ more retained tags smoothly. For instance sum over distinct ordered k-tuples the product of smooth cutoff factors for $|1-e^{i\phi_i}|$ and for the determinant of the selected pair, equal to one on the preceding windows and supported on windows enlarged by a factor two; normalize their sum as in the pair proof. Every retained tag has $|t| \le CT/\sqrt{R}$ by $t = 2N\arctan(\sqrt{\lambda}\cot(\phi/2)/N)$. On these windows the fixed derivative bounds for the selected pair in $q/R, p/\sqrt{R}$ follow by implicit differentiation: in the phase coordinates the two-column Jacobian is a fixed ℓ-dependent factor times $\sin(\phi_i - \phi_j)$, and the microscopic angular derivatives of the inverse are $O(R^{-1/2}\,\mathrm{poly}(T))$. This includes $t = 0$ at the point $\phi = \pi$, using a continuous local phase chart. The other $k-2$ central integrations each cost $CT/\sqrt{R}$. The tag weights are $O(R^{-ku}\,\mathrm{poly}(T))$ also at $t = 0$ because $\sqrt{\lambda} \asymp R^{-1/2}$.

Retain the full squared Vandermonde of these k tags in the joint bound (19.19). For fixed k the elementary column operations that replace the k stripped vectors successively by their divided differences factor out $\prod_{i<j}(t_j - t_i)$ in each wedge. Uniform bounded derivatives up to order $k-1$ control the difference quotients by their simplex-integral representation, including at coincidences. The same factor may be removed from the original two real Vandermonde copies in the high-count branch using the bandlimited multivariable reproducer. Indeed successive divisions by $t_i - t_j$ are smooth segment differences of the antisymmetric polynomial, and after each division all the other, as yet unremoved, coincidence zeros persist, first at distinct remaining nodes and then by continuity. Fixed derivatives needed after division have the same majorant from the reproducer and Cauchy–Schwarz. Use the k-tag factorial bound and reduced-Palm exponential in place of the two-tag bound as in Theorem 19.2. The squared Vandermonde now costs $O(R^{-k(k-1)/2}\,\mathrm{poly}(T))$. Together with the k angular differentials and the final area scaling $R^{-3/2}$ this proves the absolute bound $CR^{-ku-k^2/2-3/2}$ at the target. The high-count dichotomy and the suppression of $T > \gamma R^{1/3}$ work as before: for $R \le N^4$ each target exponent is fixed and the exponential in N absorbs every power, while for $R > N^4$ the count and exterior sums are deterministically $O(N)$ and every dyad is moderate.

For real tilt the two-sided localization used for the two-tag profile applies with these k selected tags. At bounded T, a further distinguished angle in $|t| < b$ costs $C_T b^{1+2\min(u,0)}$ after removing the target-scale power, with all k mutual separations retained. On the remaining configurations exactly k angles are in that shrinking window. Conversely, the rank-$(N-k)$ circle preparation at $s+k$ gives gap b and bounded resident inverse-square and signed cotangent sums with probability tending to one when the truncations are removed as before. For a good residence configuration each selected $t_i = y_i/\sqrt{R}$ lies in a bounded set in y: on the scaled level a single contribution tending to zero leaves at most $(k-1)/\ell < 1$ in the first coordinate. The limiting level is compact and regular by the noninteger phase argument. The maps for these k angles converge smoothly on this compact set even when some $y_i = 0$. This follows directly by using $2N\sqrt{R}\tan(t_i/(2N))$ with $t_i = y_i/\sqrt{R}$; it tends smoothly to y_i and yields the two rational components of F. Resident weights and all k insertion products tend to one

on these truncations. The area integral converges by a finite regular-coordinate cover with a smooth partition of unity on the compact level. Existence of a point with distinct y_i follows by choosing the phases symmetric about π in distinct opposite pairs (and one π if k is odd): continuously vary their angles from zero, keeping the offsets distinct, so the real deficit ranges from zero past $2(k-\ell) < 2$. This also gives positivity at real tilt.

Finally, the selected angular weights contribute $N^{-2ks}R^{-ks}\prod(y_i^2+4\ell)^s$ to leading order. The mutual angular Vandermonde is $N^{-k(k-1)}R^{-k(k-1)/2}\Delta(y)^2$. The k microscopic variables contribute $R^{-k/2}$ and the remaining coarea scaling is $R^{-3/2}$. The Weyl factor is $N^{-s^2}Z^{\circ}_{N-k}(s+k)/[(2\pi N)^k k!]$; the factorial counts the unordered cluster exactly once. The Barnes asymptotic cancels all the powers of rank and yields the displayed coefficient. For nonreal tilt the complex upper bound already obtained proves local boundedness after scaling. The finite density is holomorphic in s and the compact regular coarea integral is holomorphic with the stated complex powers. Normal-family uniqueness then gives the assertion, with uniformity on parameter compacts by taking arbitrary convergent subsequences. At $k=2$ evaluating the two symmetric roots gives the preceding square-root profile, taking the absolute value in the real Jacobian. Critical integer thresholds of the scaled real coordinate remain outside this result.

Exact rank-two diagnostic at the first critical value. At $N=2$ hold $p\neq 0$ and d fixed and put $q=\lambda^{-1}+d$. Set $x_*=(p^2+d)/(2p)$. As $\lambda\downarrow 0$,

$$\lambda^{-s-1}d_{\lambda,2}(\lambda^{-1}+d,p)=\frac{4^{2s+1}\,2^{-s^2-2s}}{2\pi^2|p|}(1+4x_*^2)^{-s-2}+O(\lambda).$$

The error is uniform on compact sets of (s,d,p) with $p\neq 0$ in the tilt domain. To see this, use the scaled Cayley variables x for the ordinary tag and $1/(\lambda y)$ for the nearly saturated tag. The two output coordinates are exactly

$$d=\frac{x^2}{1+\lambda x^2}-\frac{y^2}{1+\lambda y^2},\qquad p=\frac{x}{1+\lambda x^2}+\frac{y}{1+\lambda y^2}.$$

At $\lambda=0$ their inverse is $x=x_*$, $y=(p^2-d)/(2p)$, with absolute Jacobian $2|p|$. The implicit function theorem supplies the nearby branch with an $O(\lambda)$ error in its inverse and Jacobian. The two single marks lie on a circle and the displaced reflected circle has at most two intersections away from coincident circle centers; since $p\neq 0$ the only other ordered solution interchanges the tags. Its multiplicity cancels the 2! in Weyl integration. With $n=2$, the saturated angular differential is $2\lambda n\,dy/(n^2+\lambda^2y^2)$ and its tilted weight is $[4\lambda(1+\lambda y^2)/(n^2+\lambda^2y^2)]^s$. Both extend through $y=0$ after removing the displayed powers of λ. The resident angular differential and weight are $2n\,dx/(1+n^2x^2)$ and $[4(1+\lambda x^2)/(1+n^2x^2)]^s$. The squared mutual separation tends to $4/(1+n^2x^2)$. Including $n^{-s^2}/(2\pi)^2$ and the Jacobian gives the formula. This core has a different depth power from the regular two-angle surface. The calculation is a finite-rank control; the distribution of the remaining angles at growing rank requires additional estimates.

The single-angle front tested against a smooth imaginary coordinate

Proposition 19.18 (weak expansion at the one-angle front). There is a second expansion at the boundary of the preceding angular sector. Put $\sigma\in\{-1,1\}$, $a=B^{-1/2}$, $M=N-1$, $v=s+1$, $m=(2N)^{-1}$. In this subsection $p(x)$ is the mass-one circle density of $P=(2N)^{-1}\operatorname{Tr}H_M$ at exponent v, retaining the indicated N in the denominator. For $\varphi\in C_c^\infty(\mathbb{R})$ and any $0<\eta<\min(1,\Re s+1/2)$ one has

$$\begin{aligned}&\frac{(2B)^{s+3/2}}{Z^{\circ}_M(v)/(2\pi N^{v^2})}\int F_{N,s,c}(B,\sigma\sqrt{2B}+y)\varphi(y)\,dy\\&\quad=\int\varphi(y)\left[p(y)+\frac{\sigma}{2\sqrt{2B}}\left\{(\ell^2-\tfrac{1}{4N}-Mm^2)p'(y)-(2s+6)yp(y)\right\}\right]dy+O_\varphi(B^{-(1+\eta)/2}).\end{aligned}\tag{19.37}$$

The constant is uniform for N sufficiently large, $0<cB=\ell\le L$, and compact tilt subsets on which the strict restriction on η holds. This is an expansion against a fixed smooth test at fixed transverse height. It involves the finite-rank trace density on the natural J displacement of order one at the front. It does not provide a pointwise remainder there or a bound for tests whose support shrinks with B.

One-tag change of variables. Retain one angle of maximal $|q|$ and solve its real equation $b(q)=B-d_0-b_e$. At moderate T, at least one $|q|\ge d\sqrt{B/T}$, and every $|q|\le C\sqrt{B}$. The single real Jacobian in the original

microscopic angular variable has inverse $O(r^{3/2}\operatorname{poly}(T))$, where $r = B^{-1}$. To discard a second $|t| < r^{\alpha}$, integrate the real coordinate by this Jacobian, use the two-tag repulsion factor and integrate the imaginary target against $|\varphi|$. For the Janossy estimate one can solve the remaining imaginary equation for j_o, with unit Jacobian. On the real high-count part the polynomial reproducer of Theorem 19.2 bounds the two-tag squared Vandermonde, holding the remaining variables fixed; the test needs only its supremum for this bound. Relative to $r^{\Re s+3/2}$ the cost is $O(\operatorname{polylog}(1/r)r^{\alpha(2\Re s+3)})$. Large T has the arbitrarily small density bound already proved, integrated on the fixed support. Choose $\alpha < 1/2$ sufficiently close to $1/2$. Under the resident gap the remaining mark is $o(\sqrt{B})$, so only the root of sign σ can enter the test. It is unique.

The resident preparation after fusion is the circle law at v. Its local envelope is $|t|^{2\Re s+2}$ in the one-tag version of the preceding proof. With the same H_0 one has bounded envelope moments of order $1+\eta$. The outer holomorphic insertions are $(1-Xq)^2(1+R(q^2+m^2))^s$. The only first-order outer insertion is $-2XP_o$. The proof of the polydisk bounds, including the high-count exponential weighting, applies with $\Re v > 1/2$ and $2+2\eta < 2\Re s+3$. The remaining factor at the root is

$$z^{Ms}\left(\frac{1+z}{2}\right)^{2s}\frac{(1+\omega^2q^2)^s}{|b'(q)|(q^2+m^2)^{s+1}(1+m^2/q^2)^M}\prod_e(1-q_e/q)^2(1+\rho(q_e^2+m^2))^s.$$

Constants here are as in the preceding pair calculation. The single factor $|b'|^{-1}$ converts to conditional density in B. Relative to $(2B)^{-s-3/2}$ the first two orders of this factor are $1-\sigma\sqrt{2}aP+O(a^2H_0)$ in the integrated-envelope sense. The tagged imaginary displacement satisfies

$$j(q)-\sigma\sqrt{2B} = -\frac{\sigma a}{\sqrt{2}}(b_e+d_0+m^2/2+\ell^2/2)+O(a^3H_0^2).$$

Indeed the exact positive q^2 equals $(B-d_0-b_e-Dm^2)/[D-\omega^2(B-d_0-b_e)]$; expanding it in $rH_0 = o(1)$ in $j(q)$ gives this formula. Taylor expansion in the test uses its bounded first and second derivatives. The displacement is $O(aH_0)$ and its Taylor remainder is $O_\varphi(a^{1+\eta}H_0^{1+\eta})$, by bounding the smaller of the linear and quadratic errors. The root-expansion error $O(a^3H_0^2)$ obeys the same estimate since $a^2H_0 = o(1)$. The product of the linear insertion and the displacement costs at most $Ca\sqrt{H_0}\min(1,aH_0)^\eta$. Thus the first integrals, before replacing finite-depth resident marks, have terms $\varphi(j_e)$, $-\sigma\sqrt{2}aP\varphi(j_e)$, and $-\sigma a(b_e+d_0+m^2/2+\ell^2/2)\varphi'(j_e)/\sqrt{2}$. Removing the resident gap costs $O(r^{\alpha(2\Re s+3)})$ for the constant and $O(ar^{\alpha(2\Re s+1)})$ for the coefficient. Both are $O(a^{1+\eta})$ for the above choice of α. Large counts and exterior sums allow spare exponentials as before.

Replacing the resident mark inside a signed test. For clarity, the required comparisons use the circle preparation itself. On bounded parameter compacts and for any $2\eta < d < \min(2, 2\Re s+1)$, put $V = V_{\Re v}$. Then $\int(|q|^{2+d}+q^2)V\,dt \le C$. Write $f = j/E = q/(1+\omega^2q^2)$. For q large one can use $|f-q| \le Cc^{d/2}|q|^{1+d/2}$, and the stronger integrated estimate $\int|f-q|V\,dt = O(c^{1+d/2})$ follows from $\min(c^2q^2,1) \le C(c|q|)^{1+d/2}$. In the first inequality the exponent $d/2$ can alternatively be replaced by $1+d/2$ with the corresponding higher power of $|q|$. The finite determinant for $\exp(i\xi\sum f)$ differs from the one for $\exp(i\xi P)$ by at most $C(1+|\xi|)^Cc^{1+d/2}$. To verify this, interpolate linearly between the two multiplicative unit symbols. Their pointwise convex combination is a contraction and its difference from one off the central window is at most $C\min(1,|\xi|/|t|)$. The polar comparison in Theorem 19.9 without its negative contraction term bounds the product of the largest $M-j$ compressed singular values by $C_j(1+|\xi|)^C$ for $j = 0,1,2$: the same Hilbert–Schmidt and exterior trace estimates apply and the remaining compression is a contraction. Differentiate the determinant in the interpolation variable and use the single cofactor bound with the trace-norm estimate from $\int|e^{i\xi f}-e^{i\xi q}|V$. This proves the assertion for every real frequency. The E rescaling on the circle costs $O(c/N)$ times a frequency power by the uniform mass-one trace moments of order one.

For an insertion of Q, take a distinguished tag with weight q^2. Interpolating the other symbols costs the same power with the two-cofactor bound. At the distinguished tag the difference costs

$$\int q^2|e^{i\xi f}-e^{i\xi q}|V\,dt \le C(1+|\xi|)^Cc^{2d/3},$$

by $|f-q| \le Cc^2|q|^3$ and $\min(2,x) \le Cx^{d/3}$. Replacing b_e by $(Q+Mm^2)/2$ inside the test costs $O((1+|\xi|)^C(c/N+c^d))$ by a single tagged insertion using $\int(q^2+m^2)\min(c^2q^2,1)V\,dt = O(c^d)$. For a P insertion, subtract $\sum f$ at cost $O((1+|\xi|)^Cc^{1+d/2})$ and use the unweighted comparison on the Schwartz test $x\varphi(x)$. All polynomial frequency bounds integrate against the Fourier transform of the test. To justify frequency rescaling in the Q-weighted circle

term, denote its finite signed density by p_Q. Integration of the divergence of $(1+x_i^2)\varphi(\sum x_j/(2N))$ in the original Cayley variables $x_i = 2Nq_i$ gives the distributional identity

$$(p_Q + Mm^2 p)' = -2vyp(y).$$

It follows first at large real tilt by integration by parts and extends throughout $\Re v > 1/2$ by the integrability of second moments and holomorphy. The density p is even. The integrable solution is $p_Q + Mm^2 p = 2v\int_{|y|}^{\infty} xp(x)\,dx$. Theorem 19.8 therefore gives a bounded $d/2$ absolute moment for this signed density, so frequency rescaling costs $O((1+|\xi|)^C (c/N)^{d/2})$. Multiplying the weighted-comparison errors by a makes them $O(a^{1+\eta})$ since $c \le La^2$ and $d > 2\eta$. Thus the resident mark may be replaced by P in all three terms. Finally $d_0 + Nm^2/2 = -1/(8N) + O(c/N^2)$. Integrate the term with φ' by parts using the displayed Ward identity. This yields the claimed signed correction and its rank and depth dependence.

Matching of the two front coefficients. Theorem 19.8 gives the tail of the scalar trace density in the preceding formula as $p(y) \sim A_P|y|^{-2s-4}$. If $G_{\mathrm{one}} = Z^{\circ}_{N-1}(s+1)/N^{(s+1)^2}$ and $G_{\mathrm{pair}} = Z^{\circ}_{N-2}(s+2)/N^{(s+2)^2}$, its finite-rank coefficient is exactly $A_P = G_{\mathrm{pair}}/(2\pi G_{\mathrm{one}})$. Indeed the rescaling $P = MX_M/(2N)$ multiplies the trace coefficient $A_M(v)$ following (19.18) by $(M/(2N))^{2v+1}$. Its gamma expression equals this ratio by consecutive Barnes products. From the interior side $\sigma y < 0$, set $\xi = \sigma\sqrt{2} + y/\sqrt{B}$. The algebraic leading term of $H_s(\xi)$ near that boundary is $2^{-1/2}(\sqrt{2}|y|/\sqrt{B})^{-2s-4}$. Restoring the scale gives exactly $G_{\mathrm{pair}} 2^{-s-5/2} B^{-s-3/2}|y|^{-2s-4}/(2\pi^2)$ from either formula. This equality matches the leading coefficients in their sequential asymptotics. The sector remainder above is proved on closed subsectors and the front remainder against fixed smooth tests; their coefficient agreement alone does not give a pointwise error uniform at arbitrary moving y.

A joint weak limit at the first planar fold

Proposition 19.19 (the critical core as a locally finite measure). There is also a growing-rank result at the first integer threshold when the two resolved coordinates are tested together. Let μ°_{s+1} be the mass-one limiting circle law of (Q_0, P_0) at tilt $s+1$ in the coordinates above. Relative to the notation of Proposition 19.12 its two entries are $8B$ and $2J$. For every continuous compactly supported F on $\mathbb{R}^2$, along all simultaneous $N \to \infty$, $\lambda \downarrow 0$,

$$\lambda^{-s-1} I^{\circ}\big[W_\lambda F(Q_\lambda - \lambda^{-1}, P_\lambda)\big] \;\longrightarrow\; \frac{4^s g_{s+1}}{\pi} \int_{\mathbb{R}^2}\int_{\mathbb{R}} F(v - y^2, w + y)\,dy\,d\mu^{\circ}_{s+1}(v,w). \tag{19.38}$$

The convergence is locally uniform in $\Re s > -1/2$. The assertion is vague convergence on the two finite readout coordinates. The limiting measure can have infinite total mass. The inner integral is a bounded continuous function of (v,w): if the test has $|p| \le M$, only an interval of y of length at most $2M$ is used at any resident value. At real tilt the limiting measure is nonzero; for example choose a bounded box of positive resident probability and a positive bump on an enlarged box reached by a bounded interval of y. The weak result does not assert pointwise convergence inside this critical core.

Here are the localization estimates needed even to pass this bounded test at its exceptional mass scale. Take a small fixed $b_0 > 0$ and call a tag saturated if $|u_i| = |N\tan(\theta_i/2)| \le b_0\sqrt{\lambda}$. Its individual $q_i = 1/(u_i^2 + \lambda)$ is at least $1/[(1+b_0^2)\lambda]$, so there can be at most one on the support of the test for small λ. Use the complex Janossy majorant on the central interval and the exterior sums, and the same T_* as above. On a dyad $T \le T_* < 2T$ with $T \le \gamma/\sqrt{\lambda}$, in the absence of a saturated tag we have $q_i \le (1-\delta_0)/\lambda$ for all i, with fixed $\delta_0 > 0$. The total is $1/\lambda + O(1)$, the exterior has q sum at most $2T$, and there are at most $2T$ central tags. Singling out a maximum first, one must have two central tags with $q_i \ge d_0/(\lambda T)$. Thus $|t_i| \le C\sqrt{\lambda T}$. On these two intervals the integrals of the local weights are bounded by $C\lambda^{u+1/2}\,\mathrm{poly}(T)$ each, and the squared separation contributes $C\lambda T$. Summing the exponentially decreasing dyads gives $O(\lambda^{2u+2})$, which is $o(\lambda^{u+1})$. Larger T costs $O(e^{-d/\sqrt{\lambda}})$ by the exponential exterior bound and factorial central bound.

For clarity these last relative-scale estimates include the high central counts. For $K > N/3$ take absolute values at the matrix level at cost $O(N^{(\Im s)^2})$ in the real preparation. On the moderate dyads use the real two-tag smoothing estimate in Theorem 19.2 with its squared separation, reweighted by an exponential of the central count and the exterior sums. The count can be dominated by a smooth count equal to one on D_0; the difference between hard and smooth exterior cutoffs costs another bounded multiple of the count on $1 \le |t| \le 3$. The associated exponential moment of the signed exterior sum under a reduced real Palm projection is uniformly

bounded by reflection, the square-integrable tail, and the bounded finite-codimension Palm shift of the mean, as in that theorem. A separate exponential-count weight yields an additional e^{-dN}; on the large dyads one retains $e^{-dN-d'/\sqrt{\lambda}}$ with smaller fixed constants. This gives the asserted bounds without comparing λ and N.

On the saturated interval change its angle to $y = p_i = u_i/(u_i^2+\lambda)$. It is one-to-one there and $|dt_i/dy| \le C\lambda$. Its angular-weight majorant in the normalized microscopic coordinates is $C\lambda^u$ for either sign of u. Holding all other coordinates fixed, F restricts $y + P_{\mathrm{res}}$ to $[-M, M]$. Its available range thus has length at most $2M$, independently of P_{res}. The low-count Janossy majorant shows the saturated contribution is $O(\lambda^{u+1})$. On high counts the same change at fixed other angles and the real one-tag polynomial smoothing estimate (the undifferentiated reproducer bound of Theorem 19.2, without a separation factor) give $C\lambda^{u+1}N^{(\Im s)^2}e^{-dN}$. Indeed, after bounding the tag polynomial uniformly in its position, the remaining measure with $e^{K_{\mathrm{res}}}$ has integral $O(N^{2u})$, cancelling the N^{-2u} in its angular weight. This high-count estimate uses only the bounded length of the y interval and already disappears relative to the target scale.

In the low-count part one may truncate the resident central count, the exterior two sums, and exclude resident angles with $|t| < b$. The discarded cost after removing λ^{u+1} is arbitrarily small. The preceding tag change removes the saturated tag first, and the remaining product and exponential majorants bound these exceptional masses: a single resident tag in the smaller interval costs $Cb^{1+2\min(u,0)}$ if $\sqrt{\lambda} < b$. If a separate cutoff $|y| \le L$ is desired, the complement requires $|P_{\mathrm{res}}| > L - M$. For any $0 < \alpha < 2u+1$, the majorant for its αth moment is uniform. On $|t| \le 2$ use $|p_i| \le C/(\sqrt{\lambda}+|t|)$ and single out a resident point against $(\sqrt{\lambda}+|t|)^{2u-\alpha}$, with an exponential of the remaining count bounding the power of the sum. The integral is finite uniformly for exactly this strict inequality. The exterior uses its exponential bound. This argument permits u arbitrarily close to $-1/2$; the surplus is chosen locally on tilt compacts.

For real tilt, integrate the single tag directly against the rank-$(N-1)$ circle preparation at $s+1$ for the residents. On the preceding good sets $|y|$, the resident inverse-square sum and signed cotangent sum are bounded. There $t_i = 2\lambda y + O(\lambda^2)$, $dt_i/dy = 2\lambda(1+O(\lambda))$, and $q_i = 1/\lambda - y^2 + O(\lambda)$. Its combined circle and deformation weight is $N^{-2s}(4\lambda)^s(1+O(\lambda))$. The single resident-insertion product tends uniformly to one by its two-term logarithm estimate; the resident deformation W_λ also tends to one. The resident vector tends on these sets to its unregularized (Q_0, P_0) with errors bounded by $C\lambda$ by the gap and inverse-square bounds. The surviving Weyl factor is $N^{-s^2}Z^\circ_{N-1}(s+1)/(2\pi N)$, with no factorial for the single distinguished point. Combining it with the angle and weight factors gives $\lambda^{s+1}4^s g_{s+1}/\pi$ to leading order. In more detail one may first restrict in the resident circle law to gap, inverse-square and signed-sum bounds and $|y| \le L$. Larger such bounds and smaller gaps exhaust its probability uniformly by the real circle one-point and trace estimates at tilt $s+1 > 1/2$. Conversely the preceding Janossy cutoffs imply these resident bounds, so removal of the restrictions on the original integral loses arbitrarily little after rescaling. Bounded uniform continuity of F and the bounded available y length allow the full resident circle expectation. The microscopic scale N instead of $N-1$ in the two resident marks gives linear factors tending to one. Proposition 19.12 and its circle Fourier proof identify this real limit.

At complex tilt the preceding variation bounds make the rescaled tests locally bounded. The right-hand side is holomorphic in s: the resident mass is nonzero and its circle projected laws converge in bounded, tight variation when tested against bounded continuous functions, locally on parameter compacts, by the circle Fourier and weighted estimates. The inner test is bounded and continuous as observed above. Normal-family uniqueness from the real interval completes the complex result. This readout retains the saturated angle's imaginary contribution as a real integration coordinate. It explains how the limiting critical measure depends on the full resident joint law rather than just a circle mass.

Quantitative joins for the ordinary derivative moment

Use the same Haar preparation and radial convention as in Sections 11, 16 and 19. Put $d = 1-z^2$, $c = Nd$, $p = s^2 + 2h$, and

$$F_N(c;h,s) = N^{-p}\mathbb{E}\left[|\Lambda_N'(z)|^{2h}|\Lambda_N(z)|^{2(s-h)}\right], \qquad z = \sqrt{1-c/N}.$$

At $c = 0$ use the exact-circle expectation. All powers of positive numbers use the real logarithm. Write

$$F(c;h,s) = c^{-2h}M_0(c,s;h) \quad (c>0), \qquad F(0;h,s) = g_s\mathcal{C}(s,h), \qquad \mathcal{G}_z = \Gamma(1+h)\,{}_1F_1(-h;1;-s^2z^2).$$

These constants have the normalizations in (16.9), (19.15) and (19.20). The derivative diagonal is $s = h$.

Theorem (quantitative depth joins). Let K be a compact subset of

$$\Re s > -1/2, \qquad -1 < \Re h < \Re s + 1/2.$$

There are $b \in (0, 1/2]$, $A, C, \kappa, \eta, \beta > 0$ and a lower rank threshold, depending on K, with the following properties. Constants in the bounds are uniform on K. Set $L(x) = \log(e + x)$ for $x \geq 0$.

$$\begin{aligned} |F_N(c) - F(c)| &\leq CL(N)^{-\eta}, && 0 \leq c \leq b, \\ |F(c) - F(0)| &\leq Cc^{\beta}, && 0 < c \leq b, \\ |c^p(F_N(c) - F(c))| &\leq C(1+c)^A/N, && b/2 \leq c \leq N/B, \end{aligned}$$

where $B > 1$ may be chosen depending on the same compact. Furthermore, for every fixed integer $m \geq 1$ there is a constant C_m and a rank threshold such that

$$\begin{aligned} |c^p F_N(c) - \mathcal{G}_z| &\leq Ce^{-\kappa c}, && c \geq c_0, \quad d \leq d_0, \\ |c^p F_N(c) - \mathcal{G}_z| &\leq C_m N^{-m}, && d \geq d_0/2, \\ |c^p F(c) - \mathcal{G}_1| &\leq Ce^{-\kappa c}, && c \geq c_0. \end{aligned}$$

Here $c_0 \geq 1$, $d_0 \in (0, 1)$ are the constants of the growing-depth estimate (18.2), decreased in d_0 or increased in c_0 as needed. In particular there is a single approximation on $b/2 \leq c \leq N$,

$$|c^p\{F_N(c) - F(c)\} - \mathcal{G}_z + \mathcal{G}_1| \leq \frac{C(1+\log N)^A}{N}. \tag{19.Q1}$$

The two approximations have the common depth interval $[b/2, b]$. Their difference there is $O_K(N^{-1})$ in either normalization. The small-depth bound also implies $|F_N(c) - F(0)| \leq C[L(N)^{-\eta} + c^{\beta}]$ with arbitrary relative rates.

The bounds are additive. The constants inherited from the projected variation, complex kernel and growing-depth estimates are used as compact-uniform constants. This theorem does not provide numerical values for all of those constants.

Proof of the overlaps. The small-depth comparison is proved below. On fixed positive-depth compacts (16.9) gives the third bound directly. For depths $c \geq c_0$ use the comparable-rank estimate in the proof of Theorem 18.2. At fixed c, write $E_n = c^p F_n(c) - \mathcal{G}_{\sqrt{1-c/n}}$. For a fixed interpolation order J let

$$X_{n,j} = n^j \sum_{l=1}^{J} w_{jl} E_{ln}, \qquad E_n = \sum_{j=0}^{J-1} n^{-j} X_{n,j}.$$

Here w_{jl} are the inverse Vandermonde weights of that proof. Choose J large enough that the comparable-rank estimate holds with a fixed noninteger $q > 2$, uniformly on K:

$$|X_{n,j} - X_{m,j}| \leq C(1+c)^A D^{j-q} \quad (D \leq m, n \leq 2D,\ D \geq Bc). \tag{19.Q2}$$

This is the polynomial-in-depth estimate before the exponential anchor in Section 18. Its real-tilt bound uses rapid decay of the Fourier source and weighted inversion. Extension to the stated complex compact loses at most $2\sqrt{J}\max_K |\Im s|$ and a fixed slack in the exponent J.

Instead anchor at $n_0 = \lceil Bc \rceil$. The ranks ln_0 have bounded ln_0/c and obey (18.2), hence $|X_{n_0,j}| \leq Cn_0^j$. For $j \geq 1$ the anchor contributes at most Cn_0/N after division by N^j. Along successive doubled ranks up to N, the increments from (19.Q2) contribute at most

$$C(1+c)^A N^{-j} \begin{cases} n_0^{j-q}, & j < q, \\ N^{j-q}, & j > q. \end{cases}$$

The last increment to N has the same bound. Each expression is $O((1+c)^A/N)$. For $j = 0$ sum forward from N to infinity. The fixed-depth limit (16.9) identifies $X_{\infty,0} = c^p F(c) - \mathcal{G}_1$, with error at most $C(1+c)^A N^{-q}$. This

proves (19.Q1) with the provisional right side $C(1+c)^A/N$ for $c \le N/B$, increasing $A \ge 1$ if necessary. The same bound without the radius correction follows from

$$|\mathcal{G}_z - \mathcal{G}_1| \le \frac{c}{N} \sup_{0\le x\le 1} |s^2 h\Gamma(1+h)_1F_1(1-h;2;-s^2x)|.$$

The large-c limiting Gaussian bound follows by fixing such c in (18.2) and using (16.9) as $N \to \infty$. On $c \ge c_0$, $d \le d_0$, the corrected comparison is therefore also bounded by $2Ce^{-\kappa c}$. On the explicit band $[D_* \log N, 2D_* \log N]$, $D_* = \max(1, 1/\kappa)$, both estimates apply for sufficiently large N. The moment at the actual radius agrees with either approximation there to $O_K((1+\log N)^A/N)$ in the c^p normalization. Use the rank estimate below this band and the exponential bound above it. On $d \ge d_0/2$ the compact-interior estimate below and the limiting Gaussian bound finish (19.Q1). In the fixed band $d_0/2 \le d \le d_0$ both finite-rank estimates compare to exactly $\mathcal{G}_z$.

Compact-interior rate. Fix $r < 1$ and $1 < R < 1/r$, interpreting the upper limit as infinity when $r = 0$. The logarithm of the symbol in Theorem 11.1 has analytic positive and negative Fourier parts on the annulus with radii R^{-1}, R. On the respective contours their sup norms are $O_{K,r,R}(1+\rho)$, where ρ is the planar frequency length. In the Borodin–Okounkov identity (cf. Section 15), Cauchy's coefficient bound on the two Hankel factors gives

$$\|Q_N H(b) H(\widetilde{a}) Q_N\|_1 \le C \exp(C_1\rho) R^{-2N},$$

where $b = \exp(V_- - V_+)$, $a = b^{-1}$, and $V_\pm$ are the two Fourier parts. Indeed each projected squared Hilbert–Schmidt norm sums $jR^{-2(N+j)}$ with the multiplicity j counted from the rank cutoff. Choose $\theta > 0$ with $C_1\theta \le \log R$. The exact determinant identity and $|\det(I+H) - 1| \le \|H\|_1 e^{\|H\|_1}$ give exponential error up to $\rho = \theta N$, times the Gaussian factor bounded by $Ce^{-\rho^2/4 + C\rho}$. The same Cauchy bound on a fixed complex disk in the radial source variable gives exponential error for the Taylor jets at zero. The real-frequency tail estimates in the proof of Theorem 11.1 give every fixed inverse frequency power uniformly for large rank on this radius compact. The exponentially bounded core and arbitrary-power outer tail also give the needed derivative seminorms: use finite differences of any fixed order with step $N^{-a}(1+\rho)^{-1}$ for some fixed $a > 1$, increasing the input decay and differentiation order. Higher source derivatives for the Taylor remainder are bounded by a fixed polynomial in N, from $|S_N| \le N(1+r)$ and bounded tilted mass on this radius compact. Taking a sufficiently high Taylor order pays this polynomial. Invert the two-dimensional Fourier transform and integrate by parts to get arbitrarily high fixed powers of N^{-1} in weighted density sup norms. Integration against $|y|^{2h}$ is then bounded on the unit disk by $\Re h > -1$ and outside it by a sufficiently large weight. This proves the stated compact-interior rate, including the factor d^{s^2}, which is bounded on this compact. It also treats integer orders without a meromorphic division.

Scale-limiting checks. The normalizations in the statement compare all overlap formulas for the same Haar observable. Relative bounds require an independent positive lower bound for the modulus of that observable. On the small side the inverse-order margin controls the discard at the origin and the circle order margin controls the large-mark tail, as proved below. Neither bound requires a pointwise density at the one-angle front.

A quantitative scalar comparison down to the circle

Theorem (quantitative circle and small positive depths). For a compact set

$$K \Subset \{(h,s) :\ \Re s > -1/2,\ -1 < \Re h < \Re s + 1/2\},$$

there are $N_0, C > 0$, a depth $0 < c_0 \le 1/2$, and explicit positive exponents β, η specified below, such that for $N \ge N_0$, $0 \le c \le c_0$, and $(h,s) \in K$,

$$|F_N(c;h,s) - F(c;h,s)| \le C(\log N)^{-\eta}, \qquad |F_N(c;h,s) - F_N(0;h,s)| \le Cc^\beta.$$

Here $F(c;h,s) = c^{-2h} M_0(c,s;h)$ for $c > 0$, and $F(0;h,s) = g_s\mathcal{C}(s,h)$. In particular the two approximations agree with error at most Cc^β, and

$$|F_N(c;h,s) - g_s\mathcal{C}(s,h)| \le C(c^\beta + (\log N)^{-\eta}).$$

No coupling between c and N is required. The bounds are additive. The constants inherit the compact-set comparison constants of Theorems 19.7–19.10. The rate exponents are specified here, while no numerical evaluation of all those constants is asserted.

Proof. Work on finitely many product patches covering K. For each patch fix a compact set of orders and an enlarged real-tilt interval $[u_-, u_+]$ on which both strict moment margins persist, together with an imaginary tilt bound M strictly larger than the patch bound. The real parts of the patch's tilts lie strictly inside this interval. All estimates in this proof are uniform for the orders in the patch and the tilts in the enlarged rectangle. Set

$$\delta = \min(1, 1 + 2u_-) > 0, \quad U = \max(0, u_+), \quad H = \sup|\Re h|, \quad D = 8 + 2H.$$

Let q satisfy $\max(0, \sup 2\Re h) < q < 1 + 2u_-$, and put

$$b = \min(1, 2 + 2\inf \Re h, q - \max(0, \sup 2\Re h)) > 0.$$

Suprema and infima over the orders refer to the enlarged patch. Write $u = \Re s$ and $V_u(t) = (|t|/(1 + |t|))^{2u}$.

Let $\nu_{N,c}$ be the unnormalized complex pushforward in Theorem 19.10 onto $Y = -\Lambda_N'(z)/(N\Lambda_N(z))$. Thus $F_N(c; h, s) = \int |y|^{2h} d\nu_{N,c}(y)$, and $\nu_{N,0}$ is the circle pushforward on the line $\Re y = -1/2$. Use the bounds in the proofs of Theorems 19.8 and 19.10. Uniformly for all sufficiently large ranks and all $0 \le c \le c_0$, these give bounded total variation and $\int (1 + |y|)^q |d\nu_{N,c}| \le C$. On $|y| \le 1/4$ for $c > 0$ they give the pointwise variation density bound $Cc^{2u+5/2}$. At $c = 0$ the disc does not meet the supporting line. Hence removing $|y| < B^{-1}$ and $|y| > B$, for $B \ge 4$, costs at most CB^{-b} in the ordinary moment.

Rate for the local circle kernel. Let $K_{N,s}$ and K_s be the kernels of Theorem 19.7. For $1 \le R \le N/2$ and $|t|, |w| \le R$, at nonzero coordinates,

$$|K_{N,s}(t, w) - K_s(t, w)| \le C|tw|^u (1 + R)^4 N^{-\delta/2}. \tag{*}$$

For details put $a = 1 + s,\ A = 1 + 2s,\ v = 1 - e^{it/N}$. Euler's beta integral at denominator parameter $A + 1$, followed by $1 + (v/A)\partial_v$, gives

$${}_2F_1(-j, a; A; v) = \int_0^1 \left[(1 - vx)^j - \frac{jvx}{A}(1 - vx)^{j-1}\right] \frac{x^{a-1}(1 - x)^{a-1}}{\mathrm{B}(a, a)}\, dx.$$

For $j = 0$ the second term is zero. The beta density has compact-uniform total variation and A stays away from zero. Since $1 - vx$ is a chord of the unit disk,

$$|1 - vx| \le 1, \qquad |1 - vx - e^{itx/N}| \le C(t/N)^2.$$

The difference of powers therefore costs at most $Cj(t/N)^2$. Putting $x_j = (j+1)/N$, this also compares $(1-vx)^{j-1}$ for $j \ge 1$ with $e^{ix_j tx}$, at the extra cost $C|t|/N$. The prefactor $-jv$ differs from $ix_j t$ by $C(|t| + t^2)/N$. Thus the integral differs by at most $C(1 + R)^3/N$ from

$$\Psi_s(x_j t) = \int_0^1 e^{ix_j tx} \left(1 + \frac{ix_j tx}{A}\right) \frac{x^{a-1}(1 - x)^{a-1}}{\mathrm{B}(a, a)}\, dx = {}_1F_1(a; A; ix_j t).$$

Both Ψ_s and its first derivative in their real argument are bounded by $C(1 + R)$ on this interval. In the product of the two polynomial features, the gamma prefactors and b_j^{-1} are their leading constants times $(j + 1)^{2s}(1 + O((j + 1)^{-1}))$, with bounded adjustment at small j. After the outside factor N^{-2s} and Riemann normalization the error uses

$$\frac{1}{N} \sum_{j<N} \frac{((j + 1)/N)^{2u}}{j + 1} \le CN^{-\delta/2}.$$

For the integral of $x^{2s}\Psi_s(xt)\Psi_s(-xw)$, the first Riemann cell costs $C(1+R)^2 N^{-1-2u}$. Bound the remaining error by N^{-1} times the integral of the absolute derivative on $[1/N, 1]$. The term from differentiating x^{2s} has the same exponent $\delta/2$ with room for a logarithm, and differentiating the two confluent factors costs at most $C(1 + R)^3$. Finally replacing $N|1-e^{it/N}|$ by $|t|$ costs a relative $O(R^2/N^2)$. This proves (*), including the parameter-uniform bound claimed.

Uniform Fourier comparison. Use the regularized determinant representation in Theorem 19.7. Write $F^p_{N,c}(t) = A_{N,c}(t)e^{ip\cdot n_{N,c}(t)} - 1$, where the dot denotes the Euclidean pairing of a real two-vector with a complex number in its two real coordinates. At $c = 0$ set $A_{N,0} = 1$ and take the exact circle mark. The limiting functions at all $0 \le c \le c_0$ are

$$A_{\infty,c}(t) = (1 + c^2/(4t^2))^s, \qquad n_{\infty,c}(t) = (c/2 - it)^{-1}.$$

This representation of the limiting characteristic function has prefactor $g_s e^{-cs/2} e^{-ip_x/2}$. In fact at $|t| \le R \le N/2$, put $D_N = N(1 - ze^{it/N})$, $D_0 = c/2 - it$. The bounds $|D_N| \asymp |D_0| \asymp c + |t|$ and $|D_N - D_0| \le C(c+|t|)^2/N$ show that $n_{N,c} - n_{\infty,c} = O(N^{-1})$ uniformly. With $w = N|1 - e^{it/N}|$, the finite factor is $(1+\xi^2/w^2)^s$, $\xi = c/((1+z)\sqrt{z})$. Hence

$$|A_{N,c} - A_{\infty,c}| \le C(N^{-1} + R^2/N^2)(1 + c^2/t^2)^u.$$

For $|p| \le P$, $P \ge 1$, the diagonal weights $j_F = |F| V_u$ for either preparation are locally integrable with $\int_{|t|<1} j_F \le C$; beyond one they are bounded by $C(1+P)/|t|$. The corresponding difference weight on $|t| \le R$ obeys

$$\int_{|t| \le R} |F^p_{N,c} - F^p_{\infty,c}| V_u(t)\, dt \le C(1+P)(1+R)^3/N.$$

In the regularized determinant kernel use the two multipliers $\sqrt{|F|}$ and $F/\sqrt{|F|}$ (both zero at zero); changes of each are bounded by a constant times $\sqrt{|F - G|}$. The Hilbert–Schmidt norms of the full operators are $O(1+P)$, by the convolution estimate for j_F used in Theorem 19.7. Cutting either variable to $|t| \le R$ costs $C(1+P)R^{-1/4}$ in this norm: with both variables off $[-1,1]$, the L^2 norm of the outer weight is at most $C(1+P)R^{-1/2}$, and the squared kernel is bounded by the convolution with $(1+d_N)^{-2}$. The part with one variable inside $[-1,1]$ has the stronger circular-distance bound used there. The same estimates hold on the limiting line. On the cut kernel use (*) and $|t|^u \le (1+R)^U \sqrt{V_u(t)}$; the difference of the multipliers uses the last integral bound and the inequality for square roots. The sum of these local errors is at most $C(1+P)^2(1+R)^L N^{-\delta/2}$ in Hilbert–Schmidt norm for $L = 8 + 2U$. The corresponding symmetrized traces have this same local bound, and their tails are bounded by $C(1+P)^2/R$: pair t with $-t$, and apply the cosine bound from Theorem 19.7. The respective prefactors differ by $O((1+P)/N)$ from the Barnes-product estimate and the expansions of z^{Ns} and z^{-1}.

Put $R = N^{\delta/[4(L+1)]}$ and $\gamma = \delta/[16(L+1)]$. The Hilbert–Schmidt inequality for $\det_2$, and the trace and prefactor bounds, give

$$|\widehat{\nu}_{N,c}(p) - \phi_{\infty,c}(p)| \le C \exp(C(1+P)^2) N^{-\gamma} \quad (|p| \le P). \tag{**}$$

One can also use (**) as a comparison between two ranks via the same limiting regularized determinant. All these estimates include $c = 0$. The limiting local kernel is derived from the equal-tilt circle preparation, so the comparison has preserved its complex cancellation before taking absolute bounds.

Return to the scalar observable. Choose a smooth radial cutoff identically one on $[1/B, B]$ and supported in $[1/(2B), 2B]$. Its product ψ with $|y|^{2h}$ has $W^{4,1}(\mathbb{R}^2)$ norm at most CB^D: each derivative of order $j \le 4$ costs at most a constant times $|y|^{2\Re h - j}$ on the support, with the same bound for derivatives falling on the cutoff. Its Fourier transform is bounded by $CB^D(1+|p|)^{-4}$. For two ranks at the same c, using (**) and the uniformly bounded variations, the difference between their scalar moments is bounded by

$$C\big[B^{-b} + B^D/P^2 + B^D P^2 e^{C(1+P)^2}(N^{-\gamma} + N'^{-\gamma})\big].$$

Here B^{-b} records the inverse-mark and large-mark errors, and the other terms record observations on the intervening annulus. Let $N' \to \infty$ at fixed c, using Theorem 16.4 for $c > 0$ and Theorem 19.8 at zero. The bound is uniform as a function of c, so this step establishes a simultaneous bound as claimed for the resulting coefficient. Take $P = (\gamma \log N/(8C))^{1/2}$ and $B = P^{1/(2D)}$ for large enough ranks. The exponential term then decays with a positive power of N^{-1}, while the first term is $O((\log N)^{-b/(4D)})$. This proves the first estimate with $\eta = b/(4D)$.

Power comparison in the depth. For real s, couple the marks at c and at the circle on the same circle ensemble with its positive mass-one preparation. The interior preparation reweights this ensemble by $z^{Ns}\prod_j A_{N,c}(t_j)$. The factorial Gram bound in Theorem 19.7 gives

$$\mathbb{E}_s \left| \prod_j A_{N,c}(t_j) - 1 \right| \le \exp\left(C \int |A_{N,c}(t) - 1| V_u(t)\, dt \right) - 1 \le C c^{\delta/2}.$$

For the last inequality split at $|t| = \sqrt{c}$, using $(c+|t|)^{2u} + |t|^{2u}$ inside and Cc^2/t^2 times V_u outside. The deterministic change $z^{Ns} - 1$ costs $O(c)$. For the mark comparison the exact formula for n yields

$$|n_{N,c}(t) - n_{N,0}(t)| \le Cc/t^2 \quad (0 < |t| \le \pi N).$$

For example, use $n_{N,c} = e^{it/N}/[N(1 - ze^{it/N})] + 1/(2Nz)$, the product of denominators in the difference, and $cN^{-2} \le \pi^2 c/t^2$. The deterministic offset costs $O(c/N)$. Truncate the mark difference by one and use $\min(1, \sum_j a_j) \le \sum_j \min(1, a_j)$ for $a_j \ge 0$. Integrating the one-point bound with a split at $|t| = c^{1/4}$ gives $Cc^{\delta/4}$. Thus every bounded Lipschitz test has its two readouts differing by at most $Cc^{\delta/4}(\|\psi\|_\infty + \operatorname{Lip}\psi)$. The annular test above has bounded Lipschitz norm at most CB^D, and the cutoff costs CB^{-b}. Taking $B = c^{-\delta/(8D)}$ gives the claimed power with real-tilt exponent $\delta b/(8D)$.

For complex s, apply the two-constants principle to $F_N(c; h, s) - F_N(0; h, s)$ on the upper or lower rectangle based on $[u_-, u_+]$, height M. Holomorphy follows from the ordinary integrals on the enlarged parameter patch. The uniform bound on the three nonreal edges follows from the same weighted variation and small-mark bounds above. On the real edge the power estimate has just been proved. With $W = u_+ - u_-$, the harmonic measure of that edge dominates

$$\sin(\pi(\Re s - u_-)/W)\,\frac{\sinh(\pi(M - |\Im s|)/W)}{\sinh(\pi M/W)}.$$

Indeed this expression is harmonic inside the corresponding rectangle, zero on the other three sides, and bounded by one on the real side. Its infimum $\omega_* > 0$ on the original patch gives $\beta = \delta b\omega_*/(8D)$. Use the minimum of the exponents over the finite cover. Passing to the respective fixed-depth and circle limits in this comparison gives $|F(c; h, s) - F(0; h, s)| \le Cc^\beta$. All three estimates follow. □

Proposition (a linear depth bound for positive real powers). For real $0 \le h \le s$, $N \ge 1$, and $0 \le c < N$,

$$(1 - c/N)^{Ns-h} F_N(0; h, s) \le F_N(c; h, s) \le F_N(0; h, s). \tag{QP.1}$$

For $0 \le c \le 1/2$ and (h, s) in a compact subset of this wedge, the difference is at most Cc uniformly in N. In the limit the same inequalities hold with lower factor e^{-sc}:

$$e^{-sc} F(0; h, s) \le F(c; h, s) \le F(0; h, s). \tag{QP.2}$$

In particular the linear depth bound applies to the positive real noninteger derivative diagonal.

Proof. Fix the matrix and write $P(w) = \Lambda_N'(w)$, $Q(w) = \Lambda_N(w)$. The nonnegative function $|P(w)|^{2h}|Q(w)|^{2(s-h)}$ is subharmonic since its logarithm is a nonnegative combination of subharmonic logarithms and the exponential is increasing and convex. Its circular mean is nondecreasing in the radius. This gives the upper bound after using Haar invariance under the common rotation of all eigenvalues. For the lower bound apply the same argument to the reciprocal polynomials $w^{N-1}P(1/w)$ and $w^N Q(1/w)$. By changing the sign of the integration angle their mean at radius $1/z$ is $z^{-2(Ns-h)}$ times the original mean at radius z. Comparing with radius one gives the lower bound after Haar averaging and the common normalization. Zero exponents are interpreted as the absent factor, so this proof includes the edges of the wedge. For $c \le 1/2$ one has

$$1 - (1 - c/N)^{Ns-h} \le (Ns - h)\big|\log(1 - c/N)\big| \le 2sc.$$

The circle values are uniformly bounded on each such compact by Theorem 19.8 and the Barnes mass estimate, with bounded ranks finite by direct positive integrability. Fixed-depth convergence and the circle limit give (QP.2). □

Quantitative return through the upper moment threshold

Put $t = h - s - 1/2$ and use the upper-threshold strip from Theorem 19.11,

$$u = \Re s > -1/2, \qquad |\Re t| < w(s) := \min(1, 2u + 1)/48.$$

Let $B_N(s)$, $B(s)$, and $H(s, h)$ have their meanings in that theorem, and retain the integral before splitting off its pole:

$$I(c, t) = \int_{-1}^{1} (c^2/4 + x^2)^{-1/2-t}\,dx.$$

On each compact in the strip there are $b, C, \eta, \beta > 0$ and a rank threshold such that for $0 < c \le b$

$$\big|[F_N(c) - B_N I(c, t)] - [F(c) - BI(c, t)]\big| \le C[\log(e + N)]^{-\eta},$$
$$|F(c) - BI(c, t) - H(s, h)| \le Cc^\beta.$$

In particular the matched formula for the finite-rank moment has additive error at most $C([\log(e+N)]^{-\eta}+c^{\beta})$, with no restriction between the rates of the two limits. The constants here depend on the inherited bounds for the subtracted scalar. The integral form covers the regime of bounded $2t\log c$, including the resonant point. At $t=0$ the leading integral is $2\,\mathrm{arsinh}(2/c)=2\log(4/c)+O(c^2)$. The exact-circle ordinary domain is given by Theorem 19.8.

Proof. Theorem 19.11 gives local boundedness of $R_N(c)=F_N(c)-B_NI(c,t)$ on the strip, uniformly for sufficiently large rank and sufficiently small depth. The arbitrary-relative-rate statement gives one product range on each compact, by the sequential form of the limit. At each fixed $c>0$, (16.9) and the Barnes expansion $B_N=B+O(N^{-1})$ give the locally uniform rank limit $R(c)=F(c)-BI(c,t)$. In particular $R(c)$ is bounded on the same compact. The regular part H is locally holomorphic by Theorem 19.11.

On a compact strictly to the subcritical side, $I(c,t)$ is bounded and $I(0,t)=-1/t$. Its difference from $I(c,t)$ is $O(c^{\beta_0})$ for any $0<\beta_0<\min(2,\inf(-2\Re t))$. To see this, separate $|x|\le c$, where both integrals are $O(c^{-2\Re t})$, from $c<|x|\le 1$, where one differentiation in the positive added square bounds the difference by $Cc^2|x|^{-3-2\Re t}$. The logarithm at a power boundary is absorbed by the strict slack. Use the two small-depth estimates in the preceding theorem, together with $F(0)=H+BI(0,t)$. This gives the desired rank and depth bounds for R_N-R and $R-H$ on that subcritical compact.

For propagation fix s and take disks in the variable t. On any compact target in the strip there is a common $r>0$ so small that one can join a subcritical starting center at $\Re t=-w(s)/2$ to each target by a finite chain, keeping the $4r$-disks in a slightly larger compact within the strip. Take the starting imaginary part to be that of the target. The number of centers is bounded in terms of the compact and the step size r. The entire starting r-disk lies on the subcritical side with strict margin uniformly in s. If a holomorphic difference is bounded by M on a $4r$-disk and by ϵ on its concentric r-disk, the three-circle inequality gives $M^{1/2}\epsilon^{1/2}$ on the $2r$-disk. It therefore gives the same bound on the next r-disk at distance at most r. Apply this to each difference using the uniform bound on the enlarged compact. A chain of length j costs the exponent 2^{-j}. This proves both inequalities, with the smaller exponent from a common bound on chain length. It is essential to propagate the renormalized difference. Already at resonance $(B_N-B)\log c$ can be macroscopic when the two scales vary independently.

Supercritical normalization. Put $w=2h-2s-1$. On every compact with $\Re s>-1/2$ and $\Re w>0$, the same argument gives, for sufficiently small $c>0$ and sufficiently large N,

$$|c^w(F_N(c)-F(c))|\le C[\log(e+N)]^{-\eta},$$
$$|c^wF(c)-L(s,w)|\le Cc^{\beta},\qquad L(s,w)=B(s)2^w\sqrt{\pi}\,\frac{\Gamma(w/2)}{\Gamma((1+w)/2)}.$$

Here the constants and the positive exponents can change with the compact. For the endpoint bound in this normalization one in fact has $|c^wF_N(c)-L(s,w)|\le C(N^{-1}+c^a)^{\theta}$ for some $a,\theta>0$. To prove these claims, begin on a small disk with $\Re w\ge a>0$ inside the preceding strip. After extending the model integral to the whole line, the beta integral gives

$$c^wI(c,w/2)=2^w\sqrt{\pi}\,\frac{\Gamma(w/2)}{\Gamma((1+w)/2)}+O(c^a).$$

The removed tails are bounded before multiplication by c^w. The bounded residual and $B_N-B=O(N^{-1})$ give the last finite-rank estimate there with $\theta=1$. For the rank comparison, use the bound for R_N-R and the bounded product $c^wI(c,w/2)$ on that disk. On larger compacts of the half-plane the two holomorphic differences are bounded by the supercritical assertion of Theorem 19.11 and its fixed-depth rank limit. Propagate along overlapping disks within $\Re w>0$, using the same three-circle argument. This gives the asserted rank and depth bounds. The rate uses the supercritical normalization and does not imply boundedness of the unrenormalized circle integral in this half-plane.

The bounded transition variable and a finite-rank obstruction. Let $w=2t$, $D_*=c/2$ and $\lambda=w\log(1/D_*)$. With $J(w)=\sqrt{\pi}\,\Gamma(w/2)/\Gamma((1+w)/2)-2/w$, continued at $w=0$ by $J(0)=2\log 2$, one has

$$I(c,w/2)=2\log(1/D_*)\frac{e^{\lambda}-1}{\lambda}+e^{\lambda}J(w)+O(c^2).$$

The error is uniform on the stated strip compacts. Indeed, for $\Re w>0$ subtract the two tails of the whole-line beta integral. They equal $2/w+O(c^2)$, since the difference of integrands is bounded by $Cc^2|x|^{-3-\Re w}$ for $|x|\ge 1$. The

absolutely converging difference continues holomorphically through the strip, which gives the claimed formula. The displayed quotient has value one at zero. For $s = 1$ the Barnes product in Theorem 19.11 gives exactly

$$\frac{B_N(1)}{B(1)} = \frac{N(N+1)^2(N+2)}{N^4} = 1 + 4/N + 5/N^2 + 2/N^3.$$

At $w = 0, c = e^{-N^2}$, replacing B_N by B in the matched formula introduces an additive error asymptotic to $8B(1)N$. Thus the retained coefficient is essential for the arbitrary-rate statement.

A quantitative supercritical one-angle law

Let K be compact in $\Re s > -1/2$, $2\Re h > 2\Re s + 1$. For $(h, s) \in K$ put $a = 2\Re s + 1$, $a_s = 2s + 1$, $q = 2\Re h$, and $d = \min(1, q)$. Set

$$\vartheta_K = \frac{1}{2} \min(1, \inf_K a, \inf_K (q - a)) \inf_K \frac{d}{q} > 0.$$

Then for all sufficiently large N and all sufficiently small $c > 0$, with no constraint between them,

$$\left| c^{2h-a_s} F_N(c; h, s) - \frac{g_{s+1} 2^{2h-2s-2}}{\sqrt{\pi}} \frac{\Gamma(h - s - 1/2)}{\Gamma(h - s)} \right| \le C_K(c^{\vartheta_K} + N^{-1}).$$

This quantifies (19.22) on compacts strictly on its supercritical side. The threshold itself is covered in its additive matched normalization by the preceding result.

Proof. Use the nearest-angle subtraction and two positive majorants from Theorem 19.11. Write $L_q = c^{a-q}$ and

$$B_q(c) = 1 + c^{2a-q} + \int_c^1 t^{2a-q-1}\, dt.$$

In the raw moment the replacement of the scalar power by the sum of the local one-point powers costs at most $C_K L_q (B_q/L_q)^{d/q}$ after increasing C_K so that it also bounds the high-count factor $N^{(\Im s)^2} e^{-N/2}$. This uses Hölder on the same retained preparation, which preserves the dependence between the closest mark and the residual. The nonclosest one-point powers cost at most $C_K B_q$, which is bounded by a constant times the same error for small depth. After rescaling to the statement's normalization, the residual is bounded by $C_K(B_q/L_q)^{d/q}$. The integral satisfies

$$c^{q-a} \int_c^1 t^{2a-q-1}\, dt \le |\log c| \max(c^a, c^{q-a}).$$

This follows by bounding t^{2a-q} on $[c, 1]$, and remains uniform when $q = 2a$. The factor $|\log c|$ is absorbed by half of the strict exponent. Hence the residual is $O_K(c^{\vartheta_K})$.

The one-point insertion estimate of Theorem 19.11 and its local mark and weight expansions show that the unscaled one-point integrand for $|t| \le 1$ is

$$B_N(s)(c^2/4 + t^2)^{s-h} + O_K\big((c + |t|)^{a-q}\big).$$

Use the estimates near zero and enlarge the constant on the rest of the fixed interval. Upon rescaling $t = cy$ and multiplying by c^{2h-a_s}, the error is bounded by a constant times

$$c \int_0^{1/c} (1 + y)^{a-q}\, dy \le C_K c^{\min(1, \inf_K (q-a))/2}.$$

The model integral outside $|y| \le 1/c$ has absolute mass $O_K(c^{\inf_K (q-a)})$. The entire model integral converges absolutely on K and gives

$$B_N(s) \int_{\mathbb{R}} (1/4 + y^2)^{s-h}\, dy = B_N(s) 2^{2h-2s-1} \sqrt{\pi} \frac{\Gamma(h - s - 1/2)}{\Gamma(h - s)}.$$

The Barnes ratio gives $B_N = B + O_K(N^{-1})$, and replacing B_N here has that error in the supercritical normalization. Combining the bounds proves the assertion. □

For an exact check separate from the one-point calculation, take $s = 0, h = 1$. Haar trace orthogonality gives $\mathbb{E}\,\mathrm{Tr}(U^j)\overline{\mathrm{Tr}(U^k)} = \mathbf{1}_{j=k}\min(j, N)$ for positive j, k. Expanding the logarithmic derivative and summing the resulting geometric series gives $T_N(1, 0; z) = 1 - z^{2N}$. Therefore

$$cF_N(c; 1, 0) = \frac{1 - (1 - c/N)^N}{c}.$$

Bernoulli's inequality and the quadratic Taylor bound for $(1 - x)^N$ on $0 \le x \le 1$ give $0 \le 1 - cF_N(c; 1, 0) \le (N - 1)c/(2N)$. The gamma coefficient above equals one in this normalization.

Error budget for evaluating the microscopic coefficient

Fix $c > 0$, a compact set of tilt parameters, and a compact set of orders with $\Re h > -1$. Denote the limiting complex Fourier source from (15.5) by $D_\infty(c, s; \zeta)$, and its circular average at radius ρ by $\Phi_\infty(\rho)$. In the following formula a_j are the even Taylor coefficients of the latter at the origin. The normalized scalar coefficient is

$$\begin{aligned} F(c; h, s) &= c^{-2h}\frac{2^{2h+1}\Gamma(1 + h)}{\Gamma(-h)}\,\mathcal{I}(h), \\ \mathcal{I}(h) &= \sum_{j=0}^{J-1}\frac{a_j}{2j - 2h} + \int_0^1 \rho^{-2h-1}\left(\Phi_\infty(\rho) - \sum_{j<J} a_j\rho^{2j}\right)d\rho \\ &\quad + \int_1^\infty \rho^{-2h-1}\Phi_\infty(\rho)\,d\rho. \end{aligned}$$

where $J > \max \Re h$. All integer terms are interpreted by removing the apparent poles in the products with $1/\Gamma(-h)$.

Here is an explicit finite-frequency approximation and its separate remaining input for certification of the full integral. Fix a frequency disk of radius R, or a larger compact independent complex source polydisk for the Taylor subtraction. For $v \ge 1$ compute the Hankel kernels in (15.5) with $m \ge 3$ derivatives of $B^{\pm 1}$, using the equivalent integration-by-parts formula

$$b_\pm(v) = \frac{1}{2\pi(\pm iv)^m}\int_{\mathbb{R}}(B^{\pm 1})^{(m)}(t)e^{\mp ivt}\,dt.$$

The corresponding frequency-sign convention is the one in (15.5). The explicit rational derivatives of the logarithmic exponent and the chain rule give, on this source compact,

$$|(B^{\pm 1})^{(j)}(t)| \le D_j(1 + |t|)^{-j}, \qquad j = m, m + 1.$$

One can compute D_j by bounding each derivative in the exponent using $|c/2 \pm it| \ge 2^{-1/2}\min(c/2, 1)(1 + |t|)$, taking the bounded log-argument difference, and using the polynomial derivative recurrence for the exponential. Thus cutting the integral at $|t| = T$ costs at most $D_m(1 + T)^{1-m}v^{-m}/[\pi(m - 1)]$. Differentiating in v under this same integral for $m \ge 3$ gives a computable bound $|b_\pm(v)|, |b'_\pm(v)| \le C_m v^{-m}$ from the integrability of $|t|(1 + |t|)^{-m}$ (together with the preceding bound on $|b_\pm|$).

Truncate the half-line operators to $[0, L]$, and use the piecewise constant kernel sampled on a square mesh of width at most ℓ. The omitted Hankel part is controlled in Hilbert–Schmidt norm by

$$C_m\left(\int_L^\infty 2u(1 + u)^{-2m}\,du\right)^{1/2}.$$

The retained sampling cost is at most $2L\ell\sup_{v\ge 1}|b'_\pm(v)|$. The error from the t truncation in each matrix entry is bounded in Hilbert–Schmidt norm by the computed pointwise bound $O((1 + T)^{1-m})$ times at most L. Riemann integration with interval derivative or oscillatory estimates on the compact t interval supplies the remaining entrywise error. If $\widetilde{H}_\pm$ are the resulting finite operators, then

$$\|H_+H_- - \widetilde{H}_+\widetilde{H}_-\|_1 \le \|H_+ - \widetilde{H}_+\|_2\|H_-\|_2 + \|\widetilde{H}_+\|_2\|H_- - \widetilde{H}_-\|_2.$$

The Fredholm determinant perturbation inequality multiplies this trace-norm error by at most $\exp(1+\|H_+H_-\|_1+\|\widetilde{H}_+\widetilde{H}_-\|_1)$. The finite approximating determinant and the prefactor in (15.5) can then be enclosed by standard interval arithmetic. The resulting finite-frequency estimates apply also on the independent complex source polydisk. Cauchy bounds there control the origin jets and the Taylor remainder, so the integrable origin singularity is treated with its actual radial powers, including at integer orders. These estimates account for every truncation within the Fredholm calculation on a fixed frequency disk.

The remaining numerical allowance for a full certificate is a *computed* bound $B_m(c,S)$ on

$$\sup_{s\in S,\ \rho\ge 1,\ |\zeta|=\rho} (1+\rho)^m |D_\infty(c,s;\zeta)|$$

for some $m+2\inf \Re h>0$, or a direct certified bound on the corresponding weighted radial tail. Theorem 16.4 proves finiteness for each prescribed m, and its proof identifies the real-tilt damping and complex-tilt interpolation that need to be quantified for this allowance. Given $B_m(c,S)$, the contribution omitted by the radial cutoff $R\ge 1$ is bounded by

$$\left| c^{-2h}\frac{2^{2h+1}\Gamma(1+h)}{\Gamma(-h)}\right| \frac{B_m(c,S)}{m+2\Re h}\,R^{-m-2\Re h}.$$

Finite-frequency enclosure and this tail bound give a complete tolerance whenever the numerical constants have been supplied. For nonnegative integer h, only the corresponding origin jet is needed. The qualitative existence of the high-frequency seminorm is enough for the asymptotic comparison, while numerical certification of a noninteger scalar requires its priced value.

A computable tail at real tilt. For a real tilt s the static mass is bounded by c^{-s^2} by the finite strong Szegő inequality used in Section 11. The damping argument of Section 15 supplies a computable tail, as follows. All constants below can be chosen on a compact interval of positive depths and a compact interval of real tilts. Use the normalized real tilted ensemble and $w(\theta)=|1-ze^{i\theta}|^{2s}$, and let $d(\theta,\phi)$ be circle distance. For N sufficiently large that $z\ge 1/2$,

$$\max(w(\theta)/w(\phi), w(\phi)/w(\theta)) \le (1+2Nd(\theta,\phi)/c)^{2|s|}.$$

This follows from $1-z\ge c/(2N)$ and the Lipschitz bound for $|1-ze^{i\theta}|$. One can produce explicit upper evaluation norms for a polynomial p in the weighted space of degree less than N by convolution with $V_N(\theta)=\sum_k \eta(k/N)e^{ik\theta}$, where $\eta=1$ on $[-1,1]$, is supported on $[-2,2]$, and can be chosen as a piecewise polynomial with finitely many prescribed bounded derivatives. For each needed integer r, repeated differences of $(ix)^j\eta(x)$, $j=0,1$, bound

$$|V_N^{(j)}(\theta)| \le C_{j,r}N^{j+1}(1+Nd(\theta,0))^{-r}.$$

Indeed differences of order r cost at most $N^{-r}\sup|((ix)^j\eta(x))^{(r)}|$, and at most $4N+r+1$ terms are summed. Summation by parts divides by $|1-e^{i\theta}|^r$, for which $2d(\theta,0)/\pi$ is a lower bound. Combine this with the undifferenced sum. The kernel evaluation constants are then computable by integrating the product of this squared envelope and the weight ratio. For a lower evaluation bound at θ, the test polynomial in Section 15, with $L>|s|+1$ an integer and $M=\lfloor N/L\rfloor \ge N/(2L)$, satisfies

$$\left|\frac{1}{M}\sum_{j=0}^{M-1} e^{ij(\phi-\theta)}\right|^L \le \min\left(1, \frac{2}{M|1-e^{i(\phi-\theta)}|}\right)^L.$$

Its squared norm is bounded above by a computable multiple of $w(\theta)/N$ using the same weight ratio. The reciprocal bounds the diagonal of the reproducing kernel from below. The derivative evaluation estimate and the weight ratio on $Nd(\theta,\phi)\le 1$ then bound the change in that kernel from its diagonal. Thus find $0<e\le 1$ and $k_0>0$, explicitly from these constants, such that the probability projection kernel in the coordinate $t=N\theta$ has modulus at least k_0 whenever $|t-t'|\le e$. This is the kernel used in (15.4), with respect to dt.

For every fixed sufficiently large frequency radius ρ, put

$$\mathcal{L}=(\rho e c^2/(1024\pi))^{1/3}.$$

Increase the lower frequency threshold so that $\mathcal{L}\ge\max(2c,2e)$. Send the rank to infinity at this fixed frequency, so $2\mathcal{L}\le N/4$. In the favorable sign of t from Section 15, on the shell $\mathcal{L}\le|t|\le 2\mathcal{L}$,

$$\inf|g'_\beta(t)| \ge c^2/(256\mathcal{L}^3), \qquad \sup|g'_\beta(t)|/\inf|g'_\beta(t)| \le 5000.$$

For example $A/N = (1+z)^2/c \in [9/(4c), 4/c]$, and $x \le \tan x \le 2x$ for $0 \le x \le 1/8$, imply $9|t|/(8c) \le A|\tan(t/(2N))| \le 4|t|/c$. The formulas for ψ', $\sin\psi$, and $\cos\psi$ then give $c/(8t^2) \le \psi' \le 7c/t^2$, $c/(4|t|) \le |\sin\psi| \le 16c/(9|t|)$, and $1/2 \le |\cos\psi| \le 1$, with $\cos\psi < 0$. The favorable sign makes the two terms in $|g'_\beta|$ add. These inequalities give the displayed lower and ratio bounds.

Integrate (15.4) over the favorable shell of length $\mathcal{L}/2$ and a one-sided interval of length e from each point. The phase travel is at least 4π. The change of variable from displacement to phase and $H - \sin H \ge H/2$ for $H \ge 4\pi$ give a lower bound $e/(2\cdot 5000)$ on the one-sided integral of $1-\cos$ of the phase difference. It follows, after passing to the fixed-frequency limit, that

$$|D_\infty(c,s;\rho e^{i\beta})| \le c^{-s^2}\exp\{-k_0^2 e\mathcal{L}/(8\cdot 5000)\}.$$

Below the threshold simply use c^{-s^2}. This supplies a computable B_m at every real tilt by taking the maximum of a known polynomial times a known stretched exponential. It proves an enclosure procedure for the CUE coefficient on the positive real noninteger derivative diagonal. The extension of this numerical tail certification to independent nonreal tilts needs the additional interpolation allowances described above (supplied in the following subsections of Section 19).

An effective complex-tilt Fourier tail on a strip

Write $\mathcal{D}_N(c,s;\zeta) = N^{-s^2}D_N[e^V]$ for the finite Fourier source of (15.5), using $p = \bar\zeta, q = \zeta$, and $\mathcal{D}_\infty$ for its limit, with prefactor $c^{-s^2}\exp[-is(p+q)/2 - pq/4]$. Fix $0 < c_- \le c \le c_+$, $|\Re s| \le U$, and $|\Im s| \le v_0 < 1/2$. There are computable positive C_*, b, ρ_0 such that

$$|\mathcal{D}_\infty(c,s;\zeta)| \le C_*(2+|\zeta|)^4\exp(-b|\zeta|^{1/3}), \qquad |\zeta| \ge \rho_0. \tag{19.M1}$$

A computable bound on the lower annulus is given below. In particular the microscopic scalar integral has a computable tail allowance for every $\Re h > -1$ on this strip. This fixed-depth assertion uses the ordinary domain of Theorem 16.4, without needing the upper-order restriction for the circle limit.

Priced rank comparison on the real axis. Choose $v_0 < \lambda < 1/2$ and choose $B \ge U+1$ such that $2\sqrt{2}\exp[-\pi(B-U)/2] \le \lambda - v_0$. Here and below the axis comparison is made for all real $u \in [-B, B]$. Set

$$A = \max(1, c_-^{-B^2}), \quad \kappa = c_-/4, \quad N_* \ge \max(2c_+, 2B, 2).$$

All rank lower bounds may be rounded up. In the Cayley coordinate of Theorem 16.3 take $a = c/2$, $z = \sqrt{1-c/N}$, $\tau = (1-z)/(1+z)$, and let

$$P(w) = \frac{1-w}{1+w}, \quad W_N(w) = w^{-u}\left(\frac{1-\tau P(w)}{1+\tau P(w)}\right)^{N+u}, \qquad W_0(w) = w^{-u}e^{-aP(w)}.$$

Use separate principal logs in the slit disk. Put $D = 1 + 4c_+ + 4c_+^2 + 2Bc_+$. For $E = W_N - W_0$, on circles $1/2 \le |w| < 1$, including the two bank values, one has

$$|E(w)| \le \frac{2^B D}{N}(1+|P(w)|)^2. \tag{19.M2}$$

Indeed $N\tau = c/(1+z)^2 \in [c/4, c]$, $|2N\tau - a| \le 2c_+^2/N$, and for $|y| \le 1/2$, $|\log(1-y) - \log(1+y) + 2y| \le |y|^3$. For $y = \tau P$ this gives a log-exponent difference at most

$$N^{-1}[(2c_+^2 + 2Bc_+)|P| + c_+^2|P|^2].$$

Both exponential exponents have nonpositive real part. The bound $|e^x - e^y| \le |x-y|e^{\max(\Re x, \Re y)}$ gives (19.M2) in this region. For $|\tau P| > 1/2$, the modulus difference is at most 2 before multiplication by w^{-u}, and $2 \le 4c_+|P|/N$.

On the slit $w = -x$, $1/2 \le x < z$, $P = (1+x)/(1-x) > 0$; both exponents are bounded above by $-\kappa P$. This follows from $N + u \ge N/2$ and $\log[(1-y)/(1+y)] \le -2y$ for $0 \le y < 1$. The preceding proof therefore gives (19.M2) with the extra factor $e^{-\kappa P}$ on each bank. For $x \ge z$, the bank jump of W_N is zero, owing to the integer

N and the opposite phases of w and $I_z(w)$. Here $P \geq 1/\tau$ and the jump of W_0 is bounded by $2^{B+1}e^{-aP}$. The full jump of E is consequently no larger than $2^{B+1}D(1+P)^2e^{-\kappa P}/N$.

Let $\rho = |p| = |\zeta|$, $R = 2+\rho$, and $U_p(w) = \exp[-i(pw+\bar{p}/w)/2]$. On $|w| = r = 1-1/R$ and on the slit with $x \geq r$, $|U_p| \leq e^2$ because $\rho(r^{-1}-r)/2 \leq 2$. Also $|P| \leq 2R$ on the inner contour. Move the negative-index coefficient contour of EU_p to $|w| = r$, including its bank jump. The trace norm of a Hankel block is bounded by the sum of the absolute anti-diagonal entries weighted by their multiplicities. Using $\sum_{n\geq 1} nr^n = r/(1-r)^2$ on the contour and $\sum_{n\geq 1} nx^{n-1} = (1-x)^{-2}$ on the slit gives

$$\sum_{n\geq 1} n|[EU_p]_{-n}| \leq \frac{D2^Be^2}{N}\left((1+2R)^2R^2 + \frac{1}{2\pi}\int_3^\infty (1+t)^2e^{-\kappa t}dt\right). \tag{19.M3}$$

In the last term use $dP/dx = 2/(1-x)^2$. The analytic contour manipulation can first be made at outer radius less than one and then passed to the boundary by bounded convergence, since W_N, W_0, U_p are bounded near the circle on each slit side for fixed p and N. Conjugation with $p \mapsto -p$ gives the opposite off-diagonal block estimate. The diagonal blocks of the exterior operators are identical. Setting the inner radius to $1/2$ in the static calculation bounds each Gram off-diagonal block by

$$S = 2^B(2+\kappa^{-1}),$$

using the individual static bank bounds and dropping their exponential at the lower endpoint in the resulting elementary integral. Both exterior operators in (16.4) are within trace norm $5S$ of a contraction. Indeed $\|G\| \leq 2$ and $\|G-I\|_1 \leq 2S$; the trace-norm distance replacing $G^{1/2}KG^{1/2}$ by K, for a contraction K from the polar decomposition, is at most $(1+\sqrt{2})2S$. The reference unitary factor in (16.4) preserves this bound. The segment between the two operators has the same property by convexity. The first determinant variation bound of Theorem 16.3 is e^{5S} times trace norm: in its proof, a rank-one direction uses the complementary exterior power, and summing singular terms gives constant one. Passing from finite compressions preserves that constant. Therefore (19.M3), the scalar phase of (16.4) and the finite strong Szegő mass bound imply

$$|\mathcal{D}_N(c,u;\zeta) - \mathcal{D}_\infty(c,u;\zeta)| \leq CR^4/N, \quad C = A\left[Bc_+ + 2D2^Be^{2+5S}\left(9 + \frac{1}{2\pi}\int_0^\infty (1+t)^2e^{-\kappa t}dt\right)\right]. \tag{19.M4}$$

The elementary integral equals $\kappa^{-1} + 2\kappa^{-2} + 2\kappa^{-3}$. For the scalar phase use $1 - z \leq c_+/N$; the real-tilt limiting source is bounded by A.

Coherence and shell damping with finite thresholds. Here are explicit constants for the real-axis shell, also at finite ranks satisfying its geometry. Take integers $j_0, L > B+1$ and a compactly supported C^{j_0} function η that is one on $[-1,1]$ and zero outside $[-2,2]$. One choice for $1 \leq |x| \leq 2$ is the normalized integral $\int_{|x|-1}^1 [y(1-y)]^{j_0}\,dy$. For $j = 0, 1$, let

$$C_j = (j_0+6)\pi^{j_0}\max\left(\|x^j\eta\|_\infty, \|(x^j\eta)^{(j_0)}\|_\infty\right), \quad W = \max(1, 2/c_-)^{2B}, \qquad U_j = C_j\sqrt{\frac{W}{\pi(2j_0-2B-1)}}.$$

The polynomial suprema can be replaced by any computed upper bounds. For the convolution $V_N(\theta) = \sum_k \eta(k/N)e^{ik\theta}$,

$$|V_N^{(j)}(\theta)| \leq C_jN^{j+1}(1+Nd(\theta,0))^{-j_0}.$$

To see this use the undifferenced sum and then differences of order j_0, divided by $|1-e^{i\theta}|^{j_0}$. There are at most $(j_0+6)N$ terms and each difference is at most $N^{-j_0}\|(x^j\eta)^{(j_0)}\|_\infty$; combine the bounds using $|1-e^{i\theta}| \geq 2d(\theta,0)/\pi$. Convolving reproduces every polynomial of degree less than N. Cauchy–Schwarz and $w(\theta)/w(\phi) \leq W(1+Nd(\theta,\phi))^{2B}$ give the evaluation and first derivative norms $U_jN^{j+1/2}/\sqrt{w(\theta)}$ relative to normalized angular measure.

Increase N_* to at least $2L$. Test evaluation at θ on the L-th power of the Fejér geometric average of length $\lfloor N/L \rfloor$, centered at θ. Its modulus is bounded by $\min(1, 2\pi L/(Nd(\theta,\phi)))^L$ and its value is one at θ. Its squared norm is at most $C_Lw(\theta)/N$, where

$$C_L = \frac{W(1+2\pi L)^{2L}}{\pi(2L-2B-1)}, \qquad W_1 = (1+2/c_-)^B.$$

Indeed $\min(1, A/x) \le (1+A)/(1+x)$. Thus the reproducing kernel diagonal is at least $N/(C_L w(\theta))$. The first derivative evaluation bound gives a change of at most $U_0 U_1 N^2 W_1 d(\theta,\phi)/w(\theta)$ for $Nd(\theta,\phi) \le 1$. It follows that the normalized probability projection kernel in microscopic Lebesgue measure has modulus at least k_0 at distances at most ϵ, with

$$\epsilon = \min(1, (2C_L U_0 U_1 W_1)^{-1}), \qquad k_0 = (4\pi C_L W_1)^{-1}.$$

Define

$$d_0 = (\epsilon c_-^2/(1024\pi))^{1/3}, \quad \rho_0 = \max(1, (\max(2c_+, 2\epsilon)/d_0)^3), \quad a_0 = k_0^2 \epsilon d_0/(8 \cdot 5000).$$

For $\rho \ge \rho_0$ and $N \ge \max(N_*, 8d_0\rho^{1/3})$, the shell argument of (15.4) gives

$$|\mathcal{D}_N(c, u; \zeta)| \le A e^{-a_0 \rho^{1/3}}. \tag{19.M5}$$

In detail let $\mathcal{L} = d_0 \rho^{1/3}$. The phase travels at least 4π in an outward interval of length ϵ on the sign-selected shell $[\mathcal{L}, 2\mathcal{L}]$. The lower bound on $|g'_\beta|$ is $c^2/(256\mathcal{L}^3)$, and the ratio of upper and lower bounds is at most 5000, as in the real-tilt tail argument in Section 19. Its hypotheses $z \ge 1/2$, $\mathcal{L} \ge \max(2c, 2\epsilon)$ and $2\mathcal{L} \le N/4$ now all hold at this finite rank. Integrating the commutator first over the offset and then over a shell of length $\mathcal{L}/2$ yields (19.M5).

Comparable ranks and the complex anchor. For the two rectangles with base $[-B, B]$ and opposite heights 1 and -1, the harmonic measure of the three nonreal edges at the desired targets is at most λ. This follows from the harmonic majorant in Section 16, since its second term is at most $2\sqrt{2}\exp[-\pi(B-U)/2]$. The finite-rank modulus on the whole rectangle satisfies

$$|\mathcal{D}_N(c, u+iv; \zeta)| \le A N^{v^2}$$

by the real strong Szegő bound. Put $\sigma = 1 - 2\lambda > 0$ and $M = \max(2C, 4A)$. For comparable ranks $n, m \in [Q, 2Q]$, $Q \ge N_*$, the difference is at most $2CR^4/Q$ on the base by (19.M4), and at most $4AQ$ on the other edges. The two-constants theorem gives a bound $MR^4 Q^{-\sigma}$ on the target compact. Summing at ranks $Q, 2Q, 4Q, \dots$ therefore gives

$$|\mathcal{D}_Q - \mathcal{D}_\infty| \le \frac{M}{1 - 2^{-\sigma}} R^4 Q^{-\sigma}. \tag{19.M6}$$

The limit is (15.5), taken at each fixed frequency before using any frequency-dependent choice of the starting rank. This step prices the cancellation of the raw variation growth by taking the difference at comparable ranks before interpolation.

Take $T = \max(1, N_*, 8d_0)$ and, above ρ_0, choose $Q = \lceil TR \exp(a_0 \rho^{1/3}) \rceil$. This rank satisfies the shell hypotheses. Apply the same two-constants theorem to the single finite determinant, with base (19.M5) and raw upper bound AQ on the other edges. Then

$$|\mathcal{D}_Q| \le A(2TR)^\lambda e^{-\sigma a_0 \rho^{1/3}}.$$

Equation (19.M6) now proves (19.M1) with

$$b = \sigma a_0, \qquad C_* = A(2T)^\lambda + M/(1 - 2^{-\sigma}).$$

For $1 \le \rho \le \rho_0$, use $Q = N_*$ in (19.M6) and the bound $A N_*^{v_0^2}$ for the anchor.

Use as a Mellin tail. For $m \ge 0$, the high-frequency part of B_m is bounded by

$$81\, 2^m C_* \left(\frac{3(m+4)}{eb} \right)^{3(m+4)}.$$

This maximizes $\rho^{m+4} e^{-b\rho^{1/3}}$, and uses $2 + \rho \le 3\rho$, $1 + \rho \le 2\rho$. Add the lower-annulus allowance, namely $(1+\rho_0)^m [A N_*^{v_0^2} + M(2+\rho_0)^4 N_*^{-\sigma}/(1 - 2^{-\sigma})]$. These formulas give a computable B_m for every fixed m. Alternatively one can integrate (19.M1) directly after the substitution $t = b\rho^{1/3}$. Use the Mellin prefactor $\left| c^{-2h} 2^{2h+1} \Gamma(1+h)/\Gamma(-h) \right|$ and the allowance $B_m R^{-m-2\Re h}/(m + 2\Re h)$ for a cutoff $R \ge 1$ with $m + 2\Re h > 0$. For a nonnegative integer order the origin jet removes the tail. This proof yields computability and gives a way to price its conservatism. The constants of the first-order finite-rank comparison and of the explicit coherence bound can require a cutoff far above a feasible Fredholm quadrature.

Effective Fourier tails on arbitrary tilt compacts

The restriction on $|\Im s|$ in the preceding first-order proof can be removed by a priced higher-order comparison. Fix $|\Re s| \le U$, $|\Im s| \le v_0$, and choose an integer $J > \max(1, 4v_0^2)$. Set $H = \sqrt{J}$, choose $v_0/H < \lambda < 1/2$, and choose $B \ge U+1$ with $2\sqrt{2}\exp[-\pi(B-U)/(2H)] \le \lambda - v_0/H$. Use the real-axis constants of the preceding proof on $[-B, B]$, including $C_*, A, N_*, \kappa, d_0, \rho_0, a_0$ where applicable. We show how to compute a real-axis polynomial bound

$$\left| \mathcal{D}_N(c,u;\zeta) - \sum_{j=0}^{J-1} N^{-j} d_j(c,u;\zeta) \right| \le P_J(2+|\zeta|)N^{-J}. \tag{19.M9}$$

The coefficients d_j do not depend on rank. Their numerical evaluation is unnecessary for the tail proof.

Priced contour remainder. In the exterior Cayley coordinate put $d = 1/N$, $z(d) = \sqrt{1-cd}$ and $\tau(d) = cd/(1+z(d))^2$. At a fixed slit-disk point w with $|w| \ge 1/2$, analytically continue d in a centered disk of radius

$$r_w = \frac{\delta}{(1+|P(w)|)^2}, \qquad \delta = \min(1, 1/(2c_+), 1/D).$$

Here $D = 1 + 4c_+ + 4c_+^2 + 2Bc_+$ as above. For $|cd| \le 1/2$, $|z-1| \le c|d|$, $|\tau| \le c|d|$, and $|\tau - cd/4| \le c^2|d|^2$, from the square-root identity and the difference of $(1+z)^{-2}$ and $1/4$. In particular $|\tau P| \le 1/2$ on the auxiliary disk. Expanding the logarithm about zero gives

$$\left| (d^{-1}+u)\log\frac{1-\tau P}{1+\tau P} + \frac{c}{2}P \right| \le D|d|(1+|P|)^2 \le 1.$$

For the cubic tail use $|\log[(1-y)/(1+y)] + 2y| \le |y|^3$ and bound $|(d^{-1}+u)\tau^3 P^3|$ by $(1+B|d|)c^2|d||P|^2/2$, which is covered by D since $B|d| \le B/D \le 1/(2c_+)$. The term containing $B|d|$ costs at most $Bc_+^2\delta/2 \le Bc_+/4$ in the coefficient before $|d||P|^2$, by $\delta \le 1/(2c_+)$. All logarithms in the auxiliary disk start at zero for the ratio and match the chosen branch on its real portion near zero. The continued $W(d,w)$ therefore has bound $2^B e e^{-(c/2)\Re P}$. Cauchy's formula bounds its coefficient of order j by this bound times r_w^{-j}, and its remainder to order $J-1$ by twice this bound times $(d/r_w)^J$ if $0 \le d \le r_w/2$.

For real $d > r_w/2$ at an admitted integer rank, use the bound 2^B on the exact exponential and the coefficient bounds just obtained. The sum is at most $2^{J+2}2^B e(d/r_w)^J$. On the slit $w = -x$, $1/2 \le x < z$, this estimate retains the factor $e^{-\kappa P}$ because the exact exponential and all the coefficients share that bound. For $x \ge z$ the exact jump vanishes, and $\tau P \ge 1$ implies $d/r_w \ge 1$, so the same estimate holds for the jump, with the factor $e^{-\kappa P}$ and an extra factor two for the banks. Consequently the contour argument (19.M3) gives effective trace-norm bounds for the exterior operator coefficients and remainder, all on the physical plane. For $R = 2+\rho$ define the polynomials

$$Q_j(R) = 2^{B+1}e^3\delta^{-j}\left[(1+2R)^{2j}R^2 + \frac{1}{2\pi}\int_0^\infty (1+t)^{2j}e^{-\kappa t}dt\right].$$

Their integral coefficients are finite factorial sums. The two-block coefficient norm is at most $Q_j(R)$, and the two-block remainder norm at most $2^{J+2}Q_J(R)d^J$. Diagonals are independent of rank. Also $\|T_N - T_0\|_1 \le 8Q_1(R)d$ by the same argument at order one.

From operator to scalar. Let S be the Gram bound already computed and put $K(R) = 8Q_1(R) + \sum_{j=1}^{J-1} Q_j(R)$. The first through J-th normalized Taylor forms of the determinant at the actual segment between T_N and T_0 have norm at most e^{5S}. For a rank-one direction in each factor, the mixed derivative is the pairing with the complementary exterior power, as follows from the finite matrix determinant lemma and continuity, including at singular matrices. Expansion into rank-one singular terms gives the bound e^{5S} on the mixed derivative itself, since the segment is within trace norm $5S$ of a contraction. Division by the Taylor factorial only improves the bound. Finite-rank compression and trace-norm convergence give the Fredholm statement. Taylor-expand along the actual segment, then substitute the trace-norm coefficient polynomial into the finite Taylor forms at T_0. The substitution error in the l-th form is bounded by $e^{5S}lK(R)^{l-1}2^{J+2}Q_J(R)d^J$ for $d \le 1$. Drop monomials of degree at least J, using $d^k \le d^J$ and summing the products of coefficient bounds. Thus the

determinant coefficients have absolute sum at most

$$D_0(R) = e^{5S} \sum_{l=0}^{J-1} K(R)^l$$

and its remainder is bounded by $D_1(R)d^J$, where

$$D_1(R) = e^{5S} \left[(8Q_1(R))^J + \sum_{l=1}^{J-1} \left(lK(R)^{l-1} 2^{J+2} Q_J(R) + K(R)^l \right) \right].$$

This calculation uses only the contraction estimate at the actual segment, not at a polynomial approximant.

The scalar phase of (16.4) is $e^{-iuz(d)\Re p}$. On the auxiliary complex d disk of radius δ_ϕ/R with $\delta_\phi = \min(1, 1/(2c_+), 1/\max(1, Bc_+))$, its modulus is at most e, by $|z-1| \le c|d|$. Put $P_0(R) = e\sum_{j=0}^{J-1}(R/\delta_\phi)^j$. The sum bounds its coefficients and the same small-disk and fallback argument bounds its remainder by $P_1(R)d^J = 2^{J+2}e(R/\delta_\phi)^J d^J$. Using the phase modulus one for real d, a valid polynomial in (19.M9) is

$$P_J(R) = A\left[D_1(R) + D_0(R)(P_1(R) + P_0(R))\right].$$

Indeed multiply the two expansions and charge the discarded higher-degree monomials by $D_0(R)P_0(R)d^J$.

Complex interpolation and output allowance. Use the rational Richardson weights $w_1, \dots, w_J$ with $\sum_l w_l l^{-j} = \mathbf{1}_{j=0}$ for $0 \le j < J$. Put $W_* = \sum_l |w_l|$ and $X_n = \sum_l w_l \mathcal{D}_{ln}$. At comparable $n, m \in [Q, 2Q]$ the difference on the real base is bounded by $2W_* P_J(R) Q^{-J}$ by (19.M9). On the three other edges of the rectangle of height H (or its reflection), the bound is $2W_* A(2JQ)^J$, since $H^2 = J$. Set $\sigma = 1 - 2\lambda > 0$ and $M_J(R) = 2W_*[P_J(R) + A(2J)^J + 1]$. The two-constants theorem and the dyadic sum give

$$|X_Q - \mathcal{D}_\infty| \le \frac{M_J(R)}{1 - 2^{-J\sigma}} Q^{-J\sigma}.$$

The limiting identity at fixed frequency is (15.5) and $\sum_l w_l = 1$. On $\rho \ge \rho_0$, use the anchor $Q = \lceil TR \exp(a_0 \rho^{1/3}/J) \rceil$, $T = \max(1, N_*, 8d_0)$. Every rank in the anchor satisfies the hypotheses of the real shell estimate. Interpolate the anchor using the base bound $W_* A e^{-a_0 \rho^{1/3}}$ and the other-edge bound $W_* A (JQ)^J$. The result and the dyadic error prove

$$|\mathcal{D}_\infty| \le e^{-\sigma a_0 \rho^{1/3}} \left[W_* A (2JTR)^J + \frac{M_J(R)}{1 - 2^{-J\sigma}} \right].$$

On the lower annulus take $Q = N_*$, using raw variation for the anchor and the same dyadic error. Since the polynomial envelope has computable positive coefficients, maximize its monomials times the stretched exponential exactly as in the first-order proof. This yields computable Fourier seminorms and hence a computable omitted radial tail for all compact complex tilts at fixed positive-depth compacts and $\Re h > -1$. It gives effective bounds with potentially large constants. The directly exercised nonreal controls use narrower complex domains and the zeroth or first source jet.

A direct polynomial boundary bound at complex tilt

The exterior determinant of (16.4) supplies a different way to pay the complex-tilt interpolation. It avoids finite-rank variation and keeps the large-frequency phase cancellation inside the limiting determinant. Fix $0 < c_- \le c \le c_+$, $s = u + iv$, $|u| \le U_*$, $|v| \le V_*$, and a physical frequency $p = \bar{q}$, $\rho = |p|$. Use the limiting circle symbol

$$W_s(w) = w^{-s} \exp[-(c/2)(1-w)/(1+w)],$$
$$l(w) = (pw + q/w)/2, \qquad \mathcal{U} = \exp(-il).$$

Here $\arg w \in (-\pi, \pi)$. On the direct sum of the negative and nonnegative Hardy spaces, write

$$C_s = \begin{pmatrix} P_- \mathcal{U} P_- & P_- \mathcal{U} W_s P_+ \\ P_+ \mathcal{U} W_s^{-1} P_- & P_+ \mathcal{U} P_+ \end{pmatrix}, \qquad B_l = P_- l P_- \oplus P_+ l P_+.$$

By (16.4) and compact-source convergence, for real s the limiting source is $c^{-s^2}e^{-is\Re p}\det(e^{iB_l}C_s)$. The coefficient bounds below show that its Fredholm determinant is holomorphic for independently complex s. Hence the identity continues to all s by (15.5).

Here are explicit tail estimates for the off-diagonal blocks. Set

$$n_0=\lceil 2(U_*+1)\rceil,\quad \beta=\min(\log 2,\sqrt{c_-}),\quad A=1+2^{U_*},\quad K=e^{\pi V_*}.$$

For $n\ge n_0$, the negative coefficient of $\mathcal{U}W_s$, and the positive coefficient of $\mathcal{U}W_s^{-1}$, have modulus at most

$$Ke^{5\rho/4}\big(2^{U_*-n}+e^{-\sqrt{c_-n}}\big)\le AKe^{5\rho/4}e^{-\beta\sqrt{n}}. \tag{19.P1}$$

Indeed deform the negative coefficient contour from the unit circle to the circle of radius $1/2$ with the two banks of the slit $(-1,-1/2)$. One can first deform at any radius in $(1/2,1)$ and use dominated convergence on the outer circle. The factor $\exp[-(c/2)(1-w)/(1+w)]$ has modulus at most one inside the disk. The $\mathcal{U}$ factor has modulus at most $e^{5\rho/4}$ on the deformation. On a bank with $w=-x$, the coefficient integrand is bounded by $Ke^{5\rho/4}x^{n-1-u}e^{-(c/2)(1+x)/(1-x)}$. Use $n-1-u\ge n/2$ and $(n/2)(1-x)+(c/2)/(1-x)\ge\sqrt{cn}$. The bank length and the contour normalization cost at most one. Reciprocity $W_s(w^{-1})=W_s(w)^{-1}$ on the circle proves the opposite bound by swapping p,q. The corresponding two cross blocks of $\mathcal{U}$ alone satisfy the same allowance by the circles of radii $1/2,2$. Each Hankel antidiagonal for frequency $n\ge1$ has trace norm n times the modulus of its coefficient. In particular all cross blocks are trace class, locally holomorphic in s. The centered diagonal is identity plus trace class: multiplication by l couples the two half-lines by two rank-one maps, so the off-diagonal-free evolution differs by a trace-class Duhamel integral. This also verifies the Fredholm determinant identity and its analytic continuation used above.

Let $\alpha=\beta/2$. Choose an integer $M_0\ge n_0$ with $M_0\ge(2/\alpha)^2$ and

$$2\int_{\sqrt{M_0}}^{\infty}x^3e^{-\alpha x}\,dx\le1.$$

Use

$$T_0=5/4+\log(AK),\qquad M=\left\lceil M_0+4T_0^2(1+\rho)^2/\beta^2\right\rceil.$$

The trace norm of each cross block with either its columns or its rows beyond the first M modes of its half-line is at most one. For by (19.P1) each retained tail coefficient is bounded by $e^{-\alpha\sqrt{n}}$, and $ne^{-\alpha\sqrt{n}}$ is decreasing beyond M_0. The integral criterion bounds its sum over $n>M$.

To compare complex and real tilt, let $D(w)=e^{v\arg w}$, $E=P_+DP_+$ on the positive half-line, and set $Q=I\oplus E$. Then $W_s=W_uD$, and $\|E\|,\|E^{-1}\|\le K$ by positivity. Set $J=\sinh(\pi V_*)/\pi$. The Fourier coefficients of D are $(-1)^n\sinh(\pi v)/[\pi(v-in)]$, with the continuous value at $v=0$. For either crossed orientation the jump Hankel with at least one side restricted to its first $m\ge1$ modes has trace norm at most $J(\log m+2)$. Indeed the denominator has the integral representation $(n\pm iv)^{-1}=\int_0^1 t^{n\pm iv-1}\,dt$ for $n\ge1$. The resulting rank-one integral has its norm bounded by

$$J\int_0^1(1-t^{2m})^{1/2}(1-t^2)^{-1}\,dt.$$

Splitting at $1-1/m$, use $1/(1-t)$ below the split, and $\sqrt{m}/\sqrt{1-t}$ above, to get the bound. For the positive Toeplitz block between indices $<M$ and indices $\ge2M$, both orientations have trace norm bounded by $3J$. In the same rank-one integral there is an extra factor t^M. Its norm is at most $\sqrt{2M}J\int_0^1 t^M(1-t)^{-1/2}\,dt\le\sqrt{2\pi}J$.

Writing A_s^{ij} for the four blocks of C_s, the top-right difference before right multiplication by E^{-1} is

$$A_s^{12}-A_u^{12}E=P_-\mathcal{U}W_uP_-DP_+.$$

On input modes $<2M$ use the truncated jump bound just obtained. On the remaining input modes use $A_s^{12}-A_u^{12}E$ directly. The tail of A_s^{12} and the contribution with A_u^{12} on columns $\ge M$ cost at most $1+K$ by (19.P1), while the product with columns $<M$ costs at most $3J$ by the separated Toeplitz bound. Thus this block of $QC_sQ^{-1}-C_u$ has trace bound $K[J(\log(2M)+5)+K+1]$. For the bottom-left difference use $EA_s^{21}-A_u^{21}=-P_+DP_-W_s^{-1}\mathcal{U}P_-$, truncate the output modes at $2M$, and then split EA_s^{21} at its intermediate index M. This costs at most $KJ(\log(2M)+5)+K+1$, since $\|W_s^{-1}\|_\infty\le K$. The bottom-right difference is

the commutator of P_+DP_+ with $P_+\mathcal{U}P_+$, multiplied on the right by E^{-1}. By commutation on the full circle its two terms each involve one crossed block of D and one of $\mathcal{U}$. Restrict the shared negative modes to their first M modes and use the trace bound for the complementary tail of $\mathcal{U}$. The cost is at most $2K[J(\log M+2)+K]$. The top-left block is unchanged. Hence a single bound is

$$\|QC_sQ^{-1}-C_u\|_1 \le 4KJ(\log(2M)+5)+5K^2+2. \tag{19.P2}$$

The centering phase contributes an exact factor. On the positive half-line put $B_+=P_+lP_+$. Then

$$\det(Ee^{iB_+}E^{-1}e^{-iB_+}) = e^{-v\Re p}. \tag{19.P3}$$

For a proof replace D by $D_r=(1+rw)^{-iv}(1+rw^{-1})^{iv}$, $0<r<1$. The Toeplitz compression of the product is the product of the coanalytic and analytic compressions, in this order. They are the exponentials of the Toeplitz logarithms $G_-=T(iv\log(1+rw^{-1}))$ and $G_+=T(-iv\log(1+rw))$. Each logarithm has trace class commutator with B_+, since commutation with the unilateral shift or its adjoint changes only one row or column. If $[X,Y]$ is trace class, the determinant of $e^Xe^Ye^{-X}e^{-Y}$ equals $\exp(\mathrm{tr}[X,Y])$. This follows by differentiating the determinant along $e^Xe^{tY}e^{-X}e^{-tY}$ and integrating the trace of the conjugated difference. Apply it to each factor of the product $e^{G_-}e^{G_+}$, using similarity invariance and multiplicativity. Only the first positive and negative Fourier coefficients of $G_\pm$ enter the trace. Since $[S^*,S]$ is the first-coordinate projection, $\mathrm{tr}([G_-+G_+,iB_+])=-rv\Re p$. Let $r\uparrow 1$. The compressions and their inverses converge strongly by dominated convergence and the common positive lower bound. The row and column commutators with B_+ converge in trace norm because the Fourier coefficients converge in ℓ^2. The Duhamel formula then gives trace-norm convergence of the multiplicative commutators minus identity, proving (19.P3).

At real tilt, Section 16 represents C_u as $W^*\mathcal{U}W$ with $G=W^*W$ and $\|G\|\le 2$. Polar decomposition shows that $e^{iB_l}C_u$ is within trace norm $(1+\sqrt{2})\|G-I\|_1$ of a contraction. This uses $\|G^{1/2}-I\|_1\le\|G-I\|_1$. An explicit upper bound for $\|G-I\|_1$ is

$$G_* = 2\sum_{n<n_0} n + 2A\sum_{n\ge n_0} ne^{-\beta\sqrt{n}}.$$

Use (19.P1) at zero frequency and real tilt. Each infinite sum here admits an elementary bound by a finite prefix and the integral used for M_0.

For $U_*<1$ a better bound follows by extending the contour all the way to the origin when $\rho=0$ and $n\ge 1$. Its inner circle integral tends to zero because $n>u$. The jump factor at real u has modulus at most two. Summing nx^{n-1} before substituting $y=(1+x)/(1-x)$ gives

$$\begin{aligned}\|G-I\|_1 &\le \frac{1}{\pi}\int_1^\infty \left(\frac{y+1}{y-1}\right)^{U_*} e^{-a_-y}\,dy \\ &\le \frac{e^{-a_-}}{\pi}\left[a_-^{-1}+2^{U_*}\Gamma(1-U_*)a_-^{U_*-1}\right], \qquad a_-=c_-/2.\end{aligned}$$

The last step uses subadditivity of the U_*-th power for $0\le U_*<1$.

The matrix $e^{iB_l}QC_sQ^{-1}$ now differs from a contraction by at most the sum of (19.P2) and $(1+\sqrt{2})G_*$, in trace norm. A trace-norm perturbation by amount L of a contraction has determinant modulus at most e^L when the perturbed matrix is identity plus trace class. Indeed finite-dimensional compression bounds the product of singular values by $\prod_j(1+s_j(K))$, where $s_j(K)$ are the singular values of the perturbation. Then pass to the limit in trace norm for the perturbed matrix minus identity. In this estimate the missing phase in (16.4) is exactly restored by (19.P3):

$$\det(e^{iB_l}C_s) = e^{-v\Re p}\det(e^{iB_l}QC_sQ^{-1}).$$

Taking the modulus in (16.4) cancels this exponential against $|e^{-is\Re p}|$. Consequently

$$|D_\infty(c,s;\zeta)| \le |c^{-s^2}|\exp\Big[(1+\sqrt{2})G_*+5K^2+2+4KJ(\log(2M)+5)\Big]. \tag{19.P4}$$

In particular this is a computable bound $A_0(1+\rho)^P$ with $P=8KJ$, using $M\le(M_0+1+4T_0^2/\beta^2)(1+\rho)^2$. No finite-rank absolute variation enters (19.P4).

For $2\Re h > P$ the polynomial envelope already suffices for absolute Mellin tails. With $R \ge 1$, the error after the final normalization is bounded by

$$\left| c^{-2h} \frac{2^{2h+1}\Gamma(1+h)}{\Gamma(-h)} \right| \frac{2^P A_0}{2\Re h - P} R^{P-2\Re h}. \tag{19.P5}$$

This can be a much smaller error budget near a positive integer order or at small nonreal tilt. The denominator inequality is strict; it does not cover inverse orders.

Combine (19.P4) with the priced real-tilt bound in the preceding section. On a complex rectangle extended from a prescribed compact, let $\theta > 0$ be any explicitly verified lower bound on bottom harmonic measure at its targets. Such a bound follows from the cosine–hyperbolic cosine majorant following (16.11), with a sufficiently wide rectangle and a top above the target. The subharmonic maximum principle applied to $\log|D_\infty|$ then gives, beyond the real-tail threshold,

$$|D_\infty(c, s; \zeta)| \le A_1(1+\rho)^P e^{-\theta\, a_0 \rho^{1/3}}$$

for a computable A_1 bounding the two prefactors. Below threshold use (19.P4). The reflected rectangle gives the negative imaginary part. Bounding $(1+\rho)^{m+P} \le (1+\rho^{1/3})^{3(m+P)}$ and maximizing the elementary right side after multiplication by the stretched exponential gives a numerical B_m for every $m \ge 0$. The radial allowance is that of the preceding Mellin error budget. This route gives compact-uniform computability for the fixed positive-depth domain $\Re h > -1$, with arbitrary compact complex tilt. The estimate optimizes a positive envelope of the Fourier integral, and its cutoff can greatly exceed a practical scalar computation.

An explicit finite-frequency source enclosure

Here is an independent, contracting enclosure of the source $D_\infty(c, s; p, q)$ in (15.5). It is valid at independent complex sources, including complex neighborhoods used in quadrature. Fix $a = c/2 > 0$ and put $\delta = r_0 = a/2$. Let $\ell = \log B$ in the convention of (15.5), and set $S \ge |s|$, $P \ge |p| + |q|$. For $|\Im t| \le \delta$, write $r(t) = (r_0^2 + (\Re t)^2)^{1/2}$. On that band

$$|\exp(\pm\ell(t))| \le E := \exp\{|\Re s| \log 3 + |\Im s|\pi + aP/r_0\}.$$

Indeed the two logarithm arguments have positive real parts, the ratio of their moduli is between $1/3$ and 3, and their argument difference has modulus at most π. Each denominator has modulus at least $r(t)$. Direct differentiation yields

$$\begin{aligned} |\ell'(t)| &\le A_1/r(t), & A_1 &= 2S + aP/r_0, \\ |\ell''(t)| &\le A_2/r(t)^2, & A_2 &= 2S + 2aP/r_0, \\ |\ell'''(t)| &\le A_3/r(t)^3, & A_3 &= 4S + 6aP/r_0. \end{aligned}$$

Thus $|(\exp(\pm\ell))'''| \le K/r(t)^3$, where $K = E(A_1^3 + 3A_1A_2 + A_3)$.

Perform a third integration by parts in (15.5) and translate each line to $t = x \mp i\delta$, respectively. The vertical integrals vanish at infinity by the displayed cubic bound, and the two effective kernel formulas are

$$b_\pm(v) = \frac{e^{-\delta v}}{2\pi(\pm iv)^3} \int_{\mathbb{R}} (\exp(\pm\ell))'''(x \mp i\delta)\, e^{\mp ivx}\, dx, \qquad v \ge 1.$$

Cutting the line at $|x| = T$ costs at most $e^{-\delta v}K/(2\pi v^3 T^2)$. The remaining integral has a holomorphic integrand in a neighborhood of the line. It can be enclosed by interval quadrature at finite T. The implementation uses the Arb complex integrator with the analytic flag forwarded to both principal logarithms. Its certified line-integral ball is propagated through the finite determinant.

Since $\int_{\mathbb{R}} (r_0^2 + x^2)^{-3/2} dx = 2/r_0^2$ and $\int_{\mathbb{R}} |x|(r_0^2 + x^2)^{-3/2} dx = 2/r_0$, one has

$$|b_\pm(v)| \le Je^{-\delta v}, \qquad |b'_\pm(v)| \le J'e^{-\delta v}, \quad J = K/(\pi r_0^2), \quad J' = (\delta+3)J + K/(\pi r_0).$$

Truncate the Hankel square to $[0, L]^2$, then use a midpoint sample on every square cell of side $\Delta = L/n$. The Hilbert–Schmidt truncation allowance per factor is $Je^{-\delta}\sqrt{2}e^{-\delta L}/(2\delta)$. For the cell error the segment of arguments from $v = 1 + x + y$ to the cell sample has length at most Δ. Its derivative bound is $J'e^{-\delta v}e^{\delta\Delta}$. The resulting

allowance is $J'\Delta e^{\delta\Delta-\delta}/(2\delta)$. Finally the squared Hilbert–Schmidt line-truncation allowance is at most the sum over cells of Δ^2 times the squared line-truncation allowance at the corresponding sample.

Let ε be the sum of these three allowances. In the orthonormal cell basis, the finite matrix has entries Δ times the cut-line integrals for its sampled kernels. Let x_+ and x_- be upper Hilbert–Schmidt norm bounds for the *actual* finite matrices obtained from their entry balls. Then the trace-norm error of the Hankel product is at most $\varepsilon(x_+ + x_- + \varepsilon)$. The exact and finite products have respective trace norms bounded by $(x_+ + \varepsilon)(x_- + \varepsilon)$ and x_+x_-. The standard Fredholm determinant perturbation bound multiplies the trace-norm error by at most the exponential of one plus the sum of these two trace-norm bounds. Multiply by the modulus of the explicit prefactor in (15.5), then add this allowance outward to the ball for the finite determinant times that prefactor. All rounding in the cut-line integration and the determinant is included in the finite ball. The construction works without inverting the Hankel product or assuming the limiting determinant is nonzero.

For fixed bounded source parameters, $L, T \to \infty$ and $\Delta \to 0$ drive all three Hilbert–Schmidt allowances to zero. The actual finite-matrix norms remain bounded because the exact Hankel norms are finite and the Hilbert–Schmidt errors tend to zero. For each fixed triple of geometric parameters the line integrals and finite determinant can be evaluated to arbitrarily small rounding error using subdivision and increased precision. A direct interval line partition suffices: the integrand is uniformly continuous on the compact line and the interval extensions of the elementary expressions converge to point values. These facts also provide a deterministic fallback if the adaptive integrator's resource limit is reached. The resulting finite-frequency certificate prices every error term in this representation. Its global analytic constants are conservative and its linear cell refinement can be expensive, especially at small depth and high frequency.

A Laplace formula and numerical certificates for origin jets

Put $a = c/2 > 0$, $v = 1 + x + y$, and $R_\nu(z) = \sum_{j\ge0} z^j/(j!\Gamma(\nu+j))$. The Hankel symbol in Theorem 15.2 admits a Laplace representation without a real-line Fourier integral. In the range $0 < \Re s < 1$, writing $X = v + t$, it is

$$\begin{aligned} b_+(v;p,q) &= e^{-av}\int_0^\infty e^{-ct}t^{-s}R_{1-s}(iaq\,t)\big[cX^{s-1}R_s(-iapX) - X^{s-2}R_{s-1}(-iapX)\big]\,dt,\\ b_-(v;p,q) &= b_+(v;q,p). \end{aligned} \tag{19.V1}$$

In particular, both coefficients are holomorphic in the two independent source variables. The exchange of p, q in the second identity is without complex conjugation of s. All real positive powers use the real logarithm.

Here are the exact jets and a numerical enclosure procedure. Choose a positive integer $d > \Re s > 0$ and use $A_{jk}(v)$ for the coefficient of p^jq^k in $b_+(v;p,q)$. For $j, k \ge 0$,

$$A_{jk}(v) = \frac{e^{-av}(-ia)^j(ia)^k}{j!k!}\sum_{\ell=0}^{d}\binom{d}{\ell}\frac{(-1)^\ell c^{d-\ell}v^{d+j+k-1-\ell}}{\Gamma(s+j-\ell)}U(d-s+k, d+j+k-\ell, cv), \tag{19.V2}$$

where U is Tricomi's function and the reciprocal gamma is interpreted by its entire extension. This includes $s = 1$ with $d = 2$. For a proof, factor $(a+it)^d$ from the symbol $B(t)$ in (15.5). The remaining two factors have exponents $d - s$ and s in the denominators of the respective one-sided Laplace transforms. Explicitly,

$$(a-it)^{-s}e^{-iap/(a-it)} = \int_0^\infty e^{itx}e^{-ax}x^{s-1}R_s(-iapx)\,dx.$$

This follows by termwise integration, initially on a bounded source polydisk and then by analytic continuation. The series is absolutely integrable there by the gamma recurrence or the exponential power series of $e^{|ap|/a}$ after termwise integration. The corresponding factor with $a + it$ uses e^{-itx} and $d - s, iaq$. The reciprocal Fourier transform of their product on $v > 0$ is the convolution integral with $X = v + t$. Multiplication by $a + it$ is the operator $a - \partial_v$ on this Fourier transform, hence $c - \partial_v$ after removing e^{-av}. The product with $(a+it)^d$ is initially interpreted in tempered distributions. The density on $v \ge 1$ is smooth and integration by parts of the original symbol gives the ordinary expression of Theorem 15.2, so this restriction is legitimate. Applying the derivative recurrence

$$\frac{d}{dX}\big[X^{\nu-1}R_\nu(zX)\big] = X^{\nu-2}R_{\nu-1}(zX)$$

gives (19.V1) when $d = 1$. Taking coefficients for any admitted d and substituting $t = vu$ into the Laplace integral defining U gives (19.V2). Interchanging p, q follows from $B^{-1}(-t;p,q) = B(t;q,p)$.

Compact numerical enclosure of a finite list of jets. For $J \ge 0$ fix a source radius $r > 0$ and replace b_+ by the polynomial with $0 \le j, k \le J$ from (19.V2); do the same for b_-. For the coefficients within that rectangle this replacement of the operators changes no Taylor coefficient of their Fredholm product or determinant. This follows because the coefficients have nonnegative bidegrees, and the Fredholm determinant is a locally analytic function of a trace class operator. The polynomial kernels are interpreted on the full quadrant before any spatial cutoff.

The following explicit majorants price the spatial truncation and polynomial Nyström approximation. For each j, k, ℓ define

$$q_0 = d - \Re s + k > 0, \quad \alpha = \Re s + j - 1 - \ell,$$
$$C_{jk\ell} = \frac{a^{j+k}\binom{d}{\ell} c^{d-\ell} e^{\pi|\Im s|/2}}{j!k!\,|\Gamma(d-s+k)|\,|\Gamma(s+j-\ell)|}.$$

A pole of a gamma factor in the denominator gives a zero bound for that term. For $\Re v \ge D > 0, |v| \le V$ the respective absolute kernel integral before the factor e^{-av} is bounded by $C_{jk\ell}$ times

$$\begin{cases} D^\alpha I(q_0), & \alpha \le 0, \\ 2^{\max(\alpha-1,0)}[V^\alpha I(q_0) + I(q_0+\alpha)], & \alpha > 0, \end{cases} \qquad I(q) = \Gamma(q)c^{-q}. \tag{19.V3}$$

Indeed the complex power of $v + t$ costs at most $e^{\pi|\Im s|/2}\,|v+t|^\alpha$, and $(V+t)^\alpha \le 2^{\max(\alpha-1,0)}(V^\alpha + t^\alpha)$. For real $v \ge 1$ use $D = v$, $V = v$, and bound each positive v^α by v^P for an integer $P \ge \max(0, \alpha)$. Summing with r^{j+k}, this gives an explicit majorant $Ce^{-av}v^P$ for either polynomial kernel. The part of the quadrant outside $[0, L]^2$ is contained in $x + y \ge L$, so its squared Hilbert–Schmidt cost is bounded by

$$C^2 e^{-c} \int_L^\infty t(1+t)^{2P} e^{-ct}\, dt. \tag{19.V4}$$

This is a finite sum of elementary incomplete gamma terms.

Divide $[0, L]$ into panels and choose the n Gauss–Legendre nodes and positive weights on every panel. Tensor interpolate the kernels at the nodes, within each panel rectangle. For a product of Bernstein ellipses of common parameter $\lambda > 1$, chosen so $\Re(1 + x + y) > 0$, (19.V3) bounds the polynomial kernel uniformly by M via the sum with r^{j+k} and the factor e^{-aD}. The L^2 error of each tensor interpolant is bounded by

$$(\text{area})^{1/2} 16 M \lambda^{-n} (1 - \lambda^{-1})^{-2}. \tag{19.V5}$$

In fact the double Chebyshev coefficients have absolute bounds $4M\lambda^{-i-j}$, by the two Laurent coefficient integrals on the annuli of the elliptic parametrizations. The double tail with either index at least n gives at most $8M\lambda^{-n}(1-\lambda^{-1})^{-2}$ in the supremum norm. Interpolate that tail. Its interpolant has L^2 norm equal to the positively weighted discrete norm of its nodal values because its degree is at most $n-1$ in each variable, and Gaussian quadrature is exact through degree $2n-1$. The triangle inequality gives (19.V5). Use the sum of squared panel costs followed by a square root. The same Gaussian identity makes the interpolated operator exactly the matrix with entries $\sqrt{w_i w_j}\, b(1 + x_i + x_j)$ in its orthonormal Lagrange basis. Thus matrix arithmetic controls the polynomial operator, including its finite-rank determinant.

The triangle inequality bounds the exact-polynomial and interpolated operator Hilbert–Schmidt difference by δ, the sum of the two preceding costs. Compute the weighted sum of the finite matrices' Hilbert–Schmidt norms to get a common bound L_0 on the polydisk. The product trace-norm error is at most $\delta(2L_0 + \delta)$. The Fredholm determinant error is at most this number multiplied by $\exp[1 + L_0^2 + (L_0 + \delta)^2]$. The prefactor in (15.5) has bound $|c^{-s^2}| \exp(|s|r + r^2/4)$. Two Cauchy integrations convert the entire source error into an error for the (j, k) jet by dividing by r^{j+k}. For a fixed finite list, increasing L, refining n, and increasing ball precision gives arbitrary absolute contraction. For example the successive panels can have bounded width and an ellipse extending at most $1/4$ beyond either end in real part; the omitted-region bound decreases exponentially.

For the finite matrix determinant, write its matrix inside the determinant as $M_0(I - T)$, where M_0 is the value at zero source. When its inverse is certified, compute $\det(M_0)\exp(-\sum_{l=1}^{2J} \operatorname{tr}(T^l)/l)$ through bidegree (J, J). Every term with $l > 2J$ vanishes in the truncated series because T has zero constant term. If the inverse test does not

certify, the determinant polynomial can instead be evaluated with finite polynomial arithmetic without dividing by M_0. The reported runs certified the inverse in this test. The numerical scripts use ball enclosures of Legendre nodes and Tricomi entries, and keep the separate analytic allowance even when the arithmetic error is smaller.

Finally let D_{jk} denote the enclosed coefficient of $p^j q^k$ in (15.5). The limiting moments for the nonnegative integral order are $F(c; j, s) = (-4)^j (j!)^2 c^{-2j} D_{jj}$. This follows from Theorems 15.2 and 16.4 and the two-source exponential with factors $i/2$. The same source data give a direct inequality for the positive fractional order $h = 1/2$ at real tilt. Write $M_j = F(c; j, s)$ for the resulting positive-measure moments of $X = |S/c|^2$. Hölder and Cauchy–Schwarz give

$$M_1^{3/2} M_2^{-1/2} \ \le F(c; 1/2, s) \ \le (M_0 M_1)^{1/2}. \tag{19.V6}$$

These inequalities use $M_1 \le M_{1/2}^{2/3} M_2^{1/3}$ and $M_{1/2}^2 \le M_0 M_1$; combine the outward endpoints of the certified moments when forming the bracket. This finite-jet bracket has positive width in general even with arbitrarily small jet error. It does not price an oscillatory Mellin tail.

Certified return of the microscopic Mellin readout

Write $D(p, q) = \mathcal{D}_\infty(c, s; p, q)$ using the independent source extension of (15.5), and let $\Phi(\rho)$ denote its average on $p = \rho e^{-i\beta}, q = \rho e^{i\beta}$ against $d\beta/(2\pi)$. If $a_j = [p^j q^j] D(p, q)$, and $J > \Re h$, the radial formula from Section 19 can be implemented with an independent origin cutoff $0 < d < 1$:

$$F(c; h, s) = \frac{c^{-2h} 2^{2h+1} \Gamma(1+h)}{\Gamma(-h)} \left\{ \sum_{j<J} \frac{a_j d^{2j-2h}}{2j-2h} + \int_d^R \rho^{-2h-1} \Phi(\rho)\, d\rho + E_0 + E_\infty \right\}.$$

This follows by adding back the polynomial on $[d, 1]$. For a nonnegative integer $h = j$ the removable limit is $c^{-2j}(-4)^j (j!)^2 a_j$, also obtained by Taylor expansion of the radial characteristic function. For nonintegral h, including $-1 < \Re h < 0$, the expression is the ordinary moment on the fixed-depth domain of Theorem 16.4.

Here are explicit bounds to complete the shifted-line determinant enclosure. Set $a = c/2$, let $0 < \xi < a$ be the line shift, and put $b = a - \xi$. Use $S \ge |s|$, $P \ge |p| + |q|$. On either shifted line the logarithmic exponent of $B^{\pm 1}$ has real part at most

$$E = S\{\log((a+\xi)/b) + \pi\} + aP/b.$$

Its first and second derivatives have moduli bounded by $(2S + aP/b)/\sqrt{b^2 + x^2}$ and $(2S + 2aP/b)/(b^2 + x^2)$, respectively. This uses the two denominators $|a \pm it| \ge \sqrt{b^2 + x^2}$. With

$$L = \frac{e^E}{2b}\{(2S + aP/b)^2 + 2S + 2aP/b\}, \qquad T = \left(\frac{Le^{-\xi}}{2\xi}\right)^2,$$

contour displacement in the B'' formula bounds $|b_\pm(v)| \le L v^{-2} e^{-\xi v}$. The horizontal edges tend to zero by the derivative envelope. The Hankel product trace norm is at most T, by integrating $e^{-2\xi(1+x+y)}$ over the quadrant. If $G = c^{-s^2} e^{-is(p+q)/2 - pq/4}$, the exact comparison is

$$|D - G| \le |G| T e^T.$$

The same construction gives $|D| \le |G| e^T$. In particular let M be the latter upper bound on the independent polydisk of radius 2. Cauchy's estimate gives $|a_j| \le M 4^{-j}$ and

$$|E_0| \le \frac{M d^{2J - 2\Re h}}{4^J (1 - d^2/4)(2J - 2\Re h)}.$$

With $n > j$, the two-dimensional discrete Fourier coefficient at the n-th roots of unity on each unit source circle differs from a_j by at most

$$M 4^{-j} \big[(1 - 2^{-n})^{-2} - 1\big].$$

Indeed the extra Taylor indices are $j + kn, j + \ell n$ for $k, \ell \ge 0$, with at least one nonzero. Bound the source sample errors separately.

The tail E_∞ is priced by Section 19 (effective complex-tilt tail). For the finite annulus use a rectangular (ρ, β) mesh and evaluate the Hankel source at each cell center by the shifted-line algorithm. Integrate the radial

power exactly on each cell. If M_R is the polydisk bound at radius $R+1$, Cauchy's estimate on unit circles about the physical points bounds the derivatives in ρ, β by $2M_R, 2RM_R$, respectively. A cell with radial width ℓ and angular width ω therefore costs $M_R(\ell + R\omega)$ times the integral of the absolute radial weight and $1/(2\pi)$ times the angular width. All cell, sample, jet and outer-tail allowances are multiplied by the modulus of the Mellin prefactor. Ball arithmetic encloses the finite sum. The origin cutoff can tend to zero and the outer cutoff to infinity independently. At each chosen pair of cutoffs the number of jets and source samples, the line and operator truncations, the mesh sizes, and the precision can then be chosen to meet any finite residual budget. This establishes a contracting enclosure with explicit allocation for each component. The general mesh may use very large cutoffs, even at depth one.

An alternative return at large fixed depth. For $0 < \Re h < 1$ it is enough to correct the complex Gaussian coefficient

$$F_G = c^{-s^2-2h}\Gamma(1+h)\,{}_1F_1(-h;1;-s^2)$$

by the Mellin integral of $D - G$ with $J = 1$. Its formula is the same absolute-moment integral for the complex Gaussian in Section 18. Price the constant coefficient and origin remainder by the polydisk bound for $D - G$ above. On the physical plane, $|G| \le c^{-\Re(s^2)}e^{(\Im s)^2}$, throughout the finite annulus. Bound Te^T there using $P = 2R$; this encloses the entire middle integral without sampling. At large c, choosing $\xi = c/4$ and $R \ll c$ makes the Hankel discrepancy exponentially small in depth.

There is a simpler tail bound in this positive-order case. Denote the constant multiplying $R^4Q^{-\sigma}$ in the comparable-rank telescope by E_*, with $R = 2 + \rho$ there. For any integer $D_* \ge 4/\sigma$, choose $Q = \lceil T_*(2+\rho)^{D_*}\rceil$ with $T_* \ge \max(N_*, 1, E_*^{1/\sigma})$. On the target tilt rectangle the unnormalized finite-source bound from the real Szegő estimate gives

$$|\mathcal{D}_\infty| \le A(2T_*)^{v_0^2}(2+\rho)^{D_*v_0^2} + 1.$$

The dyadic error was already bounded before this rank was chosen. For $\alpha = D_*v_0^2 < 2\Re h$, the weighted integral above a cutoff $R \ge 1$ is at most

$$\frac{A(2T_*)^{v_0^2}3^\alpha R^{\alpha-2\Re h}}{2\Re h - \alpha} + \frac{R^{-2\Re h}}{2\Re h}.$$

This allowance and the elementary Gaussian tail close the complete comparison. At the exact $c = 2^{128}$, $h = 1/2 + i/8$, $s = (1+i)/16$, cutoffs 2^{65} and 2^{100} gave relative bounds below $1.228\cdot10^{-18}$ and $7.408\cdot10^{-29}$, respectively. The analytic tail dominates both observed budgets. The very large positive depth is part of this control. The proof prices the exact microscopic coefficient at that depth, before any depth limit.

Stable Mellin return near an integer at finite depth. For h near 1, retain $J = 2$ and use the exact factor

$$\frac{\Gamma(-h)^{-1}}{2-2h} = -\frac{h}{2}\Gamma(2-h)^{-1}.$$

All other terms carry $(-h)(1-h)\Gamma(2-h)^{-1}$. Enclose the pole term by the certified a_1 jet. For the other terms use the origin Cauchy estimate at $d = 1$, bound a_0 by M, and bound the entire tail above one by the positive-order polynomial allowance. The small distance to the integer prices the latter terms without discarding them. At $c = 256$, $s = 3/4 + i/16$, $h = 1 + i\,2^{-4096}$, the Gaussian approximation to a_1 gives two complete absolute radii below $3.261 \cdot 10^{-31}$ and $4.943 \cdot 10^{-56}$ using shifts $c/8, c/4$. The refined relative bound is below $4.594 \cdot 10^{-50}$. The independent integer control $s = h = 1$ agrees with the Schur coefficient $\int_0^1 t^2e^{-ct}dt$ within the certified jet error. The separate inverse-order example uses the removable $h = 0$ term.

An executed inverse-order certificate near zero order

The following control uses $c = 256$, $s = i/8$ and $h = (-1+i)2^{-1500000}$. Its order is deliberately close to zero. The high-frequency enclosure on the full real plane is otherwise too conservative for a practicable radial computation with this proof. The exact order has negative real part and nonzero imaginary part, independent of the nonreal tilt. We separate the zeroth source jet and bound both integrals in the radial representation directly.

Write $a_0 = \mathcal{D}_\infty(c, s; 0)$ in this subsection and put

$$Q(c,h) = (2/c)^{2h}\Gamma(1+h)/\Gamma(1-h).$$

The radial formula of Section 19, using $\Gamma(1-h) = -h\Gamma(-h)$, gives

$$F(c;h,s) = Q(c,h)\left[a_0 - 2h\left(\int_0^1 \rho^{-2h-1}(\Phi_\infty(\rho) - a_0)d\rho + \int_1^\infty \rho^{-2h-1}\Phi_\infty(\rho)d\rho\right)\right]. \tag{19.M7}$$

This also follows by subtracting the zeroth jet in the absolutely convergent integral for the chosen inverse order.

For a bound on the origin remainder let $|p|, |q| \le R_0$ and $0 < d < a = c/2$. In the second-derivative formulas for $b_\pm(v)$ shift the contours to $\mp id + \mathbb{R}$. The shifts do not cross logarithmic cuts or poles; second derivatives decay quadratically along the two joining segments as their real part tends to infinity. Put

$$g = a - d, \qquad M = |s|(\log[(a+d)/g] + \pi) + cR_0/g, \qquad L_1 = 2|s| + cR_0/g, \quad L_2 = 2|s| + 2cR_0/g.$$

On either shifted line the logarithm of the exponential factor has modulus at most M. Its first two derivative moduli are at most $L_1/(g^2+x^2)^{1/2}$ and $L_2/(g^2+x^2)$. These follow by the triangle inequality on the two logarithmic derivatives and the two source denominators $a \pm it$. The logarithmic difference has real part bounded by $\log((a+d)/g)$ in modulus and imaginary part bounded by π. Hence

$$|b_\pm(v)| \le Ke^{-dv}v^{-2}, \quad K = \frac{e^M(L_1^2 + L_2)}{2g}, \quad \|H_+H_-\|_1 \le (Ke^{-d}/(2d))^2 =: J(R_0, d). \tag{19.M8}$$

For the integral giving K, use $\int_{\mathbb{R}}(g^2+x^2)^{-1}dx = \pi/g$, and for the Hilbert–Schmidt bound integrate $e^{-2d(1+x+y)}$ over the quadrant. These bounds are valid for independent complex p, q.

At $R_0 = 2, d = 64$, (15.5) is bounded on the complex radial circle $|r| = 2$, with $p = re^{-i\beta}, q = re^{i\beta}$, by

$$D_2 = c^{-\Re(s^2)}\exp(2|s| + 1 + J(2,64)).$$

The circular average in β is even and entire as a function of r. Cauchy's coefficient inequality gives $|\Phi_\infty(\rho) - a_0| \le D_2\rho^2/3$ for $0 \le \rho \le 1$. The two integrals in (19.M7) are therefore bounded by $D_2/[3(2-2\Re h)]$ and $B_2/(2+2\Re h)$ respectively. Here B_2 is the computable constant from the preceding tail theorem, with $v_0 = 1/8$, $U = 0$, $B = 2$, $\lambda = 3/8$, and $j_0 = L = 4$. For the first two polynomial derivative suprema in the coherence proof, bound the derivatives of $\eta(y+1)$ by the coefficient one norm on $0 \le y \le 1$ and use the product rule for $x\eta(x)$. This gives $\log_{10} B_2 < 1224.514$ by outward interval arithmetic.

For the center take $Q(c,h)c^{-s^2}$. The difference between the zeroth jet and c^{-s^2} is bounded by $c^{-\Re(s^2)}(e^{J(0,d)} - 1)$ from (19.M8) and the Fredholm determinant series. The certificate sums this determinant approximation error times $|Q|$, both radial allowances times $2|hQ|$, and the arithmetic radius for the center. It does not require angular or radial quadrature on this order window since the two entire residual integrals are charged. For the requested absolute tolerances 10^{-7} and 10^{-12}, the run using $d = 2, 64$ and $96, 180$ bits respectively gave absolute radii below $4.244 \cdot 10^{-9}$ and $3.804 \cdot 10^{-53}$. The second run has relative radius below $3.489 \cdot 10^{-53}$. The first enclosure is limited by the determinant estimate and the second by finite arithmetic. The two charged radial integrals have allowances below $1.823 \cdot 10^{-451545}$ and $4.685 \cdot 10^{-450321}$ after their prefactors. This is a near-integer control and the smallness of these last allowances depends on the exact choice of h.

An independent finite-rank comparison. At $N = 512$, $z^2 = 1/2$, the zero-order finite normalizing factor in the Borodin–Okounkov identity is exactly c^{-s^2}. Estimate the finite Hankel factors by angle-contour shifts of size $d_f = -\log(z)/2$, using the analytic annulus about $|w| = 1$. Both principal logs in the static factor have arguments bounded by $\pi/2$ there. Since $s = i/8$, the factor moduli are at most $e^{\pi/8}$. Each Hankel factor has Hilbert–Schmidt norm at most

$$e^{\pi/8 - (N+1)d_f}/(1 - e^{-2d_f})$$

by summing squared geometric series. The error in the zero-order finite moment from c^{-s^2} is less than $1.703 \cdot 10^{-76}$ using the product norm and the determinant series.

For the finite order perturbation, set $Y = |S_N|/c \le 4$. Use the transformed Haar weight bound in the direct evaluator of Section 21 at real tilt zero. With its constant C_*, the weighted pair density is bounded by $2/(\pi^2|v|)$. Its integral on a disk of radius cr about any center is at most $12cr/\pi$: the disk near zero is contained in the disk

of radius $3cr$ about zero, and otherwise the distance on the disk from zero is at least cr. Conditioning on the remaining angles gives $\Pr(Y \le r) \le C_{\mathrm{sb}} r$, where $C_{\mathrm{sb}} = 12cC_*/\pi$. For $q = |h| \le 1/8$,

$$|Y^{2h} - 1| \le 2q |\log Y| \max(Y^{-2q}, Y^{2q}).$$

On $Y \le 1$ the right side is at most $8qY^{-1/2}$ and the dyadic expectation of $Y^{-1/2}$ on that range is bounded by $\sqrt{2}C_{\mathrm{sb}}/(1-2^{-1/2})$. On $1 \le Y \le 4$, use $2q(\log 4)4^{1/4}$. Since the modulus of the purely imaginary tilt factor is one under Haar measure, the normalized variation multiplier is $N^{1/64}$. The resulting finite order-change allowance is below $2.581 \cdot 10^{-173264}$. The finite-rank disk and the limiting disk give a verified discrepancy less than $4.207 \cdot 10^{-53}$ for the same order, tilt and depth. The calculations use different domains for the determinant estimates and different ways to bound the order perturbation. Exact input and output dyadics and the separate arithmetic and analytic terms are in the inverse-order replay.

Effective high-frequency decay in a nonreal tilt strip

Write $D_N(c, s; p)$ for the Fourier source of (16.4) with $z = (1 - c/N)^{1/2}$ and $p = \bar{\zeta}$, and write D_∞ for its limit (15.5). These sources include the tilt mass. In particular, the probability characteristic function at real s is divided by the value at zero, whereas D_N retains the factor N^{-s^2}. Fix $[c_-, c_+] \Subset (0, \infty)$. For every compact S in $|\Im s| < 1/2$, and every real $m \ge 0$, the estimate

$$|D_\infty(c, s; p)| \le B_m (1 + |p|)^{-m}$$

holds with a computable B_m that will be specified below. In particular no ordinary circle-domain restriction on $\Re s$ is needed at positive depth. The bound is a numerical majorant and its constants can be very large.

An effective real-tilt comparison of ranks. Fix $|s| \le U$ on the real axis. In (16.4), use the static boundary phase

$$W_N(w) = w^{-s} \left(\frac{1 - t_N P(w)}{1 + t_N P(w)} \right)^{N+s}, \qquad P(w) = \frac{1-w}{1+w}, \qquad t_N = \frac{c}{N(1 + \sqrt{1 - c/N})^2},$$

and $W_0(w) = w^{-s} e^{-cP(w)/2}$. The boundary and slit branches are those in Section 16. Put $k = c_-/4$ and $C_\Delta = 12c_+^2 + 2Uc_+ + 2$. At $N \ge 4c_+ + 2U + 4$, the difference $E = W_N - W_0$ satisfies

$$|E(w)| \le \frac{4^U C_\Delta}{N} (1 + |P|)^2 \quad (1/4 \le |w| < 1)$$

on the slit annulus. Its jump across $w = -x$, $1/4 \le x < 1$, has the same bound multiplied by $2e^{-kP}$. Indeed $t_N \le c_+/N$ and $|(N+s)t_N - c/4| \le (c_+^2 + Uc_+)/N$. If $t_N|P| \le 1/2$, then $|\operatorname{arctanh}(t_N P) - t_N P| \le 2|t_N P|^3$. The difference of the exponents is at most $(4c_+^2 + 2Uc_+)(1 + |P|)^2/N$. The exponential is 1-Lipschitz between two points in the closed left half-plane. On the slit with $x < z$, the two exponents are at most $-kP$, since $(N+s)t_N \ge c/8$. If $t_N|P| > 1/2$, bound the exponentials separately and use $1 < 4c_+^2|P|^2/N^2$. Where $x \ge z$ the exact jump vanishes and the limiting jump is bounded by $2x^{-s}e^{-cP/2}$; here $t_N P \ge 1$. These estimates give both assertions with the displayed common constant.

Define the finite, explicitly integrable constants

$$A_- = 4^U C_\Delta \left[\frac{64}{9} \left(\frac{4}{9} + \frac{1}{3} \right) + \frac{1}{\pi} \int_{1/4}^1 \frac{(1 + P(-x))^2 e^{-kP(-x)}}{(1-x)^2} (2 - x)\, dx \right],$$

$$A_+ = 4^U C_\Delta \left[16e + \frac{e}{\pi} \int_{1/4}^1 (1 + P(-x))^2 e^{-kP(-x)}\, dx \right],$$

$$A_0 = 4^U \left(\frac{4}{9} + \frac{1}{2\pi k} \right).$$

For the first slit integral, $y = (1+x)/(1-x)$ converts it into an exponentially converging integral of a rational function of y beginning at $5/3$; replacing $2 - x$ by 2 gives a finite polynomial integral. The same substitution and $dx \le dy$ work for the second integral. These replacements can also define $A_\pm$. Deform the coefficient contour

for $[E]_{-j}$ to radius $1/4$, with a slit term on $1/4 < x < 1$. The inner contour costs $4^U C_\Delta (64/9) 4^{-j}/N$; summing with $j+1$ weights gives the first term of A_-. The slit uses $\sum_{j\ge1}(j+1)x^{j-1} = (2-x)/(1-x)^2$. For $[E]_j$, $j \ge 0$, use radius $r = 1 - 1/(j+2)$. Here $r^{-j-1} \le e$ and $1 + |P| \le 2(j+2) \le 4(j+1)$. The slit contribution uses $x^{-j-1} \le e$ on $[r,1]$. It follows that $\sum_{j\ge1}(j+1)|[E]_{-j}| \le A_-/N$ and $|[E]_j| \le A_+(j+1)^2/N$. The same negative contour with W_N or W_0, and weight j, gives A_0: the jump of either phase is at most $2 \cdot 4^U e^{-kP}$ and $\int_{1/4}^1 (1-x)^{-2} e^{-kP}\,dx \le 1/(2k)$.

Let $U_p = e^{-i\Re(pw)}$ on the unit circle. From the fifth derivative and Cauchy–Schwarz,

$$\sum_{j\in\mathbb{Z}} (1+|j|)^4 |[U_p]_j| \le 1 + 1664(1+|p|)^5.$$

In detail, $|U_p| = 1$, the first five derivatives of its exponent are bounded by $|p|$, and the fifth complete Bell number is 52. For $j \ne 0$ use $(1+|j|)^4 \le 16|j|^4$ and $(\sum_{j\ne0}|j|^{-2})^{1/2} < 2$. The weighted negative coefficient sum of EU_p is therefore bounded by $1665(A_- + A_+)(1+|p|)^5/N$. For the negative coefficients of E use $n \le (j+1)(1+|j-n|)$ in the convolution. For the nonnegative coefficients use $\sum_{n=1}^k n(k-n+1)^2 \le (k+1)^4$.

The half-Hardy exterior operators of Section 16 have only two off-diagonal residual blocks in their difference, with the above Hankel bound for each. Each operator is within trace distance $2(1+\sqrt{2})A_0$ of a contraction: write the uncentered matrix $G^{1/2}KG^{1/2}$ with $\|K\| \le 1$ and $\|G\| \le 2$, and use $\|G^{1/2} - I\|_1 \le \|G - I\|_1 \le 2A_0$. This also holds at $N = \infty$ since the boundary phase is unimodular. The segment of the two operators remains within this trace distance of a contraction. The complementary-minor derivative estimate in Section 16 bounds the absolute determinant difference by the trace norm of the difference times $e^{2(1+\sqrt{2})A_0}$. For the scalar phase of (16.4) use $|e^{-isz\Re p} - e^{-is\Re p}| \le Uc_+|p|/N$. With $B_0 = \max(1, c_-^{-U^2})$ and

$$C_1 = B_0 e^{2(1+\sqrt{2})A_0}[3330(A_- + A_+) + Uc_+]$$

we consequently have $|D_N(c,s;p) - D_\infty(c,s;p)| \le C_1(1+|p|)^5/N$ for real $|s| \le U$. Only real tilts are used for the contraction estimate.

Interpolation and explicit rank choice. Put $v_0 = \sup_S |\Im s| < 1/2$, choose any $v_0 < \eta < 1/2$, and take $b > 0$ with $\sqrt{2}/\cosh(\pi b/2) \le \eta - v_0$. Set $U = \sup_S |\Re s| + b$ and use the real estimates above on this wider interval. At $s = u + iv$ with $|u| \le U$, $|v| \le 1$, the finite absolute source estimate is $|D_N(c,s;p)| \le B_0 N^{v^2}$ by the real static mass bound from strong Szegő. Interpolate in the half-rectangle of height 1 and width $2b$ centered horizontally at each target, using its reflection for negative v. The harmonic measure of its top and vertical sides is bounded at the target by η, by the harmonic majorant

$$y + \frac{\sqrt{2}\cosh(\pi x/2)\cos(\pi(y-1/2)/2)}{\cosh(\pi b/2)}$$

in centered coordinates. Apply this to $D_{2N} - D_N$. The real-axis bound is $2C_1(1+|p|)^5/N$, the remaining bound $4B_0N$. With $q = 1 - 2\eta > 0$ and $C_2 = \max(2C_1, 4B_0)$, dyadic telescoping gives

$$|D_\infty - D_N| \le \frac{C_2}{1-2^{-q}}(1+|p|)^5 N^{-q}.$$

This uses convergence (15.5) at each fixed p. The finite-rank absolute bound is used only before taking the limit, while the real exterior difference controls the error that telescopes.

Use any explicit real-tilt constants e, k_0 supplied by the kernel construction in the previous subsection. A fully specified choice is given below. Set $d = (ec_-^2/(1024\pi))^{1/3}$, $k_1 = k_0^2 ed/(8 \cdot 5000)$, and $\rho_0 = \max(1, (\max(2c_+, 2e)/d)^3)$. By (15.4) and the directional shell argument on $[d\rho^{1/3}, 2d\rho^{1/3}]$ (with the favorable sign), the real-axis bound is $B_0 e^{-k_1\rho^{1/3}}$ for $\rho \ge \rho_0$ and $N \ge 8d\rho^{1/3}$. Interpolate D_N itself on the same rectangles to get $B_0 N^\eta e^{-k_1(1-\eta)\rho^{1/3}}$ at the targets. Below ρ_0 use $B_0 N^\eta$. For fixed ρ, now take $N = \lceil Q(1+\rho)^A \rceil$, with Q greater than the fixed rank threshold and $8d+1$ and with $A = \max(1, (m+5)/q)$. The telescoped error weighted by $(1+\rho)^m$ is at most $C_2 Q^{-q}/(1-2^{-q})$. With $M = m + \eta A$ and $a_1 = k_1(1-\eta)$, one can take

$$B_m = \frac{C_2 Q^{-q}}{1-2^{-q}} + B_0(Q+1)^\eta \left[(1+\rho_0)^M + 2^M \left(\frac{3M}{e^1 a_1}\right)^{3M}\right].$$

Here $0^0 = 1$. The second term uses the maximum of $x^{3M}\exp(-a_1 x)$ on the nonnegative half-line. In the Mellin budget of the preceding subsection, multiply $B_m R^{-m-2\Re h}/(m+2\Re h)$ by $|c^{-2h}2^{2h+1}\Gamma(1+h)/\Gamma(-h)|$. If the prefactor is nonzero, choose $R \ge 1$ by solving the resulting power inequality for the allotted tail tolerance. At nonnegative integer orders the moment is given by the corresponding removable origin term. Compact order sets are handled with a bound on the prefactor and $\inf \Re h > -1$, taking $m + 2\inf \Re h > 0$.

An explicit coherence length for the real shell. Take integers $r, L > U+1$ and $N \ge \max(r+1, 2L, 4c_+ + 2U + 4)$. Construct the smooth-symbol substitute η_0 by convolving $\mathbf{1}_{[-3/2,3/2]}$ with r copies of $r\mathbf{1}_{[-1/(2r),1/(2r)]}$. Its weak derivatives through order r are bounded by $(2r)^j$ for differentiation order j; it equals one on $[-1,1]$ and is supported on $[-2,2]$. Let

$$D_0 = (2r)^r, \qquad D_1 = 2(2r)^r + r(2r)^{r-1}, \qquad U_j = 5\cdot 2^r \max(2^j, D_j(\pi/2)^r), \quad j = 0, 1.$$

Finite differences of the sampling coefficients of $(ix)^j\eta_0(x)$, followed by r circle summations by parts, give $|V_N^{(j)}(\theta)| \le U_j N^{1+j}(1 + Nd(\theta,0))^{-r}$. Indeed at most $5N$ indices occur, each r-th difference costs $D_j N^{-r}$, and $|1 - e^{i\theta}| \ge 2d(\theta,0)/\pi$. Combine this with the undifferenced bound. Set $W = \max(1, 2/c_-)^{2U}$ and $a_j = U_j\sqrt{W/[\pi(2r-2U-1)]}$. Weighted Cauchy–Schwarz with the weight ratio of Section 15 gives $|p^{(j)}(\theta)| \le a_j N^{j+1/2} w(\theta)^{-1/2}\|p\|$. For a reverse evaluation bound, the test polynomial of Section 15 with $M = \lfloor N/L \rfloor$ gives $\|p_\theta\|^2 \le Jw(\theta)/N$, with $A = 2\pi L$ and

$$J = \frac{W}{\pi}\left[\frac{(1+A)^{2U+1} - 1}{2U+1} + \frac{A^{2U+1}(1+1/A)^{2U}}{2L - 2U - 1}\right].$$

This follows by bounding its modulus by $\min(1, A/(Nd(\theta,\phi)))^L$ and integrating the two power bounds. An admissible choice of coherence constants is

$$e = \min\left(1, \frac{1}{2Ja_0a_1(1+2/c_-)^U}\right), \qquad k_0 = \frac{1}{4\pi J(1+2/c_-)^U}.$$

In fact, the nearby derivative of the reproducing kernel is at most $a_0a_1(1+2/c_-)^U N^2/w(\theta)$, from the norm bounds for zeroth and first evaluation. Move by at most e/N from the diagonal lower bound $N/[Jw(\theta)]$ and convert the result to the projection kernel relative to microscopic Lebesgue measure. This gives k_0.

An inverse complex control close to the integer anchor

The priced high-frequency bound yields a certified scalar control with nonreal s and noninteger h, independent of each other. The order in this construction is deliberately very close to zero. At

$$c = 1, \qquad s = i/8, \qquad h = (-1+i)10^{-1200},$$

the absolute disk was refined from radius less than $2.042\cdot 10^{-9}$ to radius less than $3.131\cdot 10^{-12}$, with certified relative radius less than $3.1271\cdot 10^{-12}$. The last midpoint, rounded for display, is $1.00105145406674519905 + 0.0004499133158298262643i$. Exact dyadic disks and all error terms are in the executable record. This control uses scalar variation from $h = 0$, so it establishes a complete certificate at this exact input. The general radial quadrature required for an order bounded away from the nonnegative integers is a different computational task.

Order variation. Abbreviate the limiting circular source by Φ and put $a_0 = \Phi(0)$. Use the first origin subtraction in the radial Mellin formula. At $c = 1$ it reads

$$F(1;h,s) = G(h)a_0 - 2hG(h)\left(\int_0^1 \rho^{-2h-1}(\Phi(\rho) - a_0)\,d\rho + \int_1^\infty \rho^{-2h-1}\Phi(\rho)\,d\rho\right), \qquad G(h) = 2^{2h}\frac{\Gamma(1+h)}{\Gamma(1-h)}.$$

For $|h| \le 1/4$ the convergent log-gamma series with Euler's constant less than 1 and $\zeta(n) < 2$ for integers $n \ge 2$ gives $|\log G(h)| \le 5|h|$. Thus $|G(h)| < 7/2$ and $|G(h) - 1| \le 18|h|$. Let M bound the holomorphic radial source on $|\rho| \le 1/8$, using the substitution $p = \rho e^{-i\beta}$, $q = \rho e^{i\beta}$ in (15.5). If $a = 1/2$, $v = 1/8$, and $\sigma = 1/8$, a direct bound is

$$D_2 = e^{\pi v + 2\sigma}\left((2v + 8v^2)\pi/a + 4\sigma/a^2 + \sigma^2\pi/a^3\right),$$
$$M = \exp\left(v\sigma + \sigma^2/4 + D_2^2/(24\pi^2)\right).$$

To see this, write $X = \log B$, $R = (a^2 + t^2)^{1/2}$. Then $|B^{\pm 1}| \le e^{\pi v + 2\sigma}$, $|X'| \le 2v/R + \sigma/R^2$ and $|X''| \le 2v/R^2 + 2\sigma/R^3$. Integration of the bound for $|(B^{\pm 1})''|$ gives D_2. The two Hankel Hilbert–Schmidt norms are bounded by $D_2/(2\pi\sqrt{6})$ and the source prefactor is bounded by $e^{v\sigma+\sigma^2/4}$. This proves the estimate. Evenness of the angular average and Cauchy's formula now give $|\Phi(\rho) - a_0| \le M\rho^2/(3\delta^2)$ on $0 \le \rho \le \delta = 1/16$. For $\delta \le \rho \le 1$ use $|\Phi - a_0| \le M + B_2$, and for $\rho \ge 1$ use $B_2\rho^{-2}$. On $|h| \le 1/4$ the corresponding integral bounds are $8M/9$, $8(M + B_2)$, and $2B_2/3$. Consequently

$$|F(1; h, i/8) - a_0| \le |h|(81M + 61B_2).$$

The numerical evaluation of the explicit B_2 from Section 19 (complex-frequency tail) can use $v_0 = 1/8$, $\eta = 1/4$, $b = 5/2$, $U = 5/2$, $r = L = 4$, $Q = 16$. The code rounds the elementary logarithms outwards, giving $\log B_2 < 2540.46$, $\log M < 0.364$, and an order variation less than $e^{-217.49}$. This term is included in every output disk.

Static Fredholm calculation on the cut. Set $a = 1/2$ and $C_s = \sin(\pi s)/\pi$. At zero source the two Hankel kernels agree since $B^{-1}(t) = B(-t)$. For $s = i/8$ the positive-frequency coefficient is

$$b_s(v) = C_s \int_0^\infty \exp\left(s \log \frac{1+y}{y}\right) e^{-(a+y)v}\, dy, \qquad v > 0.$$

Move the positive-frequency Fourier contour downwards around the cut $t = -i(a + y)$. On the right and left banks of this cut the denominator logarithm has imaginary parts $-\pi$ and π, respectively, so the jump produces $2i \sin(\pi s)$. One may first work on a finite contour with a cutoff in the distributional Fourier integral. Integration by parts with the two derivatives in (15.5) identifies the same transform for $v > 0$. Equivalently, pair with a smooth frequency test supported strictly in $v > 0$ before deforming: its inverse Fourier factor decays rapidly horizontally and exponentially downwards, and the small circle around the branch point costs $O(\epsilon)$ since $\Re s = 0$. This justifies the cut expression with no boundary term at infinity.

For $k_\lambda(x) = e^{-\lambda x}$ on $\mathbb{R}_+$ the Hankel operator is the continuous sum of rank-one kernels $C_s e^{-(a+y)}((1 + y)/y)^s k_{a+y}(x) k_{a+y}(x')$ against dy. Thus $a_0 = \det(I - H^2)$, because the scalar Szegő prefactor is one here. The Laguerre functions $\ell_j(x) = e^{-x/2} L_j(x)$ form an orthonormal basis in the Lebesgue norm and their Laplace coefficients are $\langle \ell_j, k_{a+y} \rangle = y^j/(1 + y)^{j+1}$. If P_r projects to the first r basis vectors, the squared tail fraction of k_{a+y} is $(y/(1 + y))^{2r}$ by geometric summation. Subtracting the two rank-one operators before integrating gives

$$\|H - P_r H P_r\|_1 \le 2|C_s| e^{-a} \int_0^\infty e^{-y} (y/(1+y))^r\, dy \le \frac{2|C_s| e^{-a}}{1-\alpha} e^{\alpha - 2\sqrt{\alpha r}}, \qquad 0 < \alpha < 1.$$

The last bound follows from $\log(y/(1 + y)) \le -1/(1 + y)$ and $\alpha(1 + y) + r/(1 + y) \ge 2\sqrt{\alpha r}$. The calculation uses $\alpha = 0.9$.

Change variables to $x = \log y$ in the compressed integral and include only $-33 \le x \le 4$. Before compression, the trace norm of the omitted portion is at most $|C_s| e^{-a}(e^{-33} + e^{-e^4})$ since $2\lambda \ge 1$. On a complex disk of radius one about any real x, the rank-one analytic integrand in x has trace norm at most $|C_s| e^{-a} e^{2|\Im s|}/(e \cos 1)$. Indeed $\Re(e^x) \ge \cos(1)|e^x|$, the continued logarithm in the phase has imaginary part bounded by two, and the norm of the rank-one kernel with complex exponent λ is $1/(2\Re\lambda) \le 1$. Compression to P_r preserves the trace-norm bound. On each length-one panel apply first Fejér quadrature of order j. Its nodes are $\cos\theta_k$ with $\theta_k = \pi(k + 1/2)/j$, $0 \le k < j$. Its unscaled weights are

$$\frac{2}{j}\left[1 - 2 \sum_{\ell=1}^{\lfloor (j-1)/2 \rfloor} \frac{\cos(2\ell\theta_k)}{4\ell^2 - 1}\right].$$

The weights are positive by the telescoping sum of the absolute nonconstant coefficients, and this is exact to polynomial degree $j - 1$ by discrete cosine orthogonality. Apply Cauchy's formula to bound the Taylor remainder on each panel from its radius-one disk. Summed over the 37 panels, the resulting quadrature trace error is at most $4 \cdot 37 \cdot 2^{-j} |C_s| e^{-a} e^{2|\Im s|}/(e \cos 1)$.

The three trace errors above sum to an allowance E_H for the compressed numerical Hankel operator $\widetilde{H}$ before roundoff. A direct integral using $|b_s(v)| \le |C_s| e^{-av}/v$ gives $\|H\|_2^2 \le |C_s|^2 e^{-1}/4$, since $u/(1 + u)^2 \le 1/4$ for $u = v - 1$. For $B_H = |C_s| e^{-a}/2$ the product trace error is at most $(2B_H + E_H)E_H$. The Fredholm determinant perturbation bound multiplies this by at most $\exp(1 + B_H^2 + (B_H + E_H)^2)$. Validated finite arithmetic encloses the

determinant of $I-\widetilde{H}^2$ and the reported disk includes that arithmetic radius and the h-variation allowance. Both determinant disks result from the same analytic protocol, with $(r,j)=(112,32)$ and $(192,46)$. The Laguerre projection error dominates the last disk. For fixed static s the cutoff, projection, quadrature, and arithmetic errors all decrease under refinement. The order variation is a fixed separate allowance for the chosen noninteger input.

An independent broad check evaluates the trace $\operatorname{tr} H^2$ directly by double midpoint quadrature in $\log y$ and bounds all higher determinant terms by $\|H^2\|_1^2\exp(\|H^2\|_1)/2$. Its last disk has radius less than $7.635\cdot10^{-5}$ and contains the sharper reported disk. The independent route shares the cut identity and uses neither a Laguerre basis nor a determinant computation.

A short tilt rectangle and analytic bridge at depth one

All transforms here retain the factor N^{-s^2}, with no division by the tilt mass. Put $s_*=1/2+i/20$ and $h_*=1/2+i/8$. A useful positive-order tail bound is obtained by choosing an analytic comparison rank independently at each frequency. That rank will not be used for numerical matrix computations.

For $c=1$, choose a rectangle in s of height $H=1/4$, real half-width $W=3/4$, centered horizontally at $1/2$, with bottom on the real axis. The harmonic measure of the upper and vertical sides at s_* is bounded by

$$\frac{1}{20H}+2\sqrt{2}e^{-\pi W/(2H)}<\lambda:=\frac{113}{500}.$$

This is the harmonic majorant of Section 16 with height H: $\Im s/H$ plus $\sqrt{2}\cosh(\pi(\Re s-1/2)/(2H))\cos(\pi(\Im s-H/2)/(2H))/\cosh(\pi W/(2H))$. In (19.M4) take $B=5/4$, $c_-=c_+=1$, and $A=1$. This gives

$$\sup_{u\in[-1/4,\,5/4]}|D_n(u;\zeta)-D_\infty(u;\zeta)|\le\frac{C}{n}(2+\rho)^4,\qquad \rho=|\zeta|,$$

with $C<1.381\cdot10^{35}$ as evaluated by `analytic_bridge.py`. In particular the bottom-edge bound for D_n-D_m, $n,m\in[N,2N]$, is $a_N=2C(2+\rho)^4/N$. On the other edges the finite-rank absolute estimate is at most $b_N=2(2N)^{H^2}$, using the real strong Szegő mass bound $A_u(1)\le1$ also at finite rank.

Choose $N\ge4$ such that $a_N\le b_N$. The two-constants theorem gives the comparable-rank bound

$$|D_n(s_*;\zeta)-D_m(s_*;\zeta)|\le(2C)^{1-\lambda}2^{(1+H^2)\lambda}(2+\rho)^{4(1-\lambda)}N^{-q},\quad q=1-\lambda(1+H^2)=0.759875.$$

The hypothesis $a_N\le b_N$ is retained at all larger ranks. A dyadic telescope at this fixed ζ, followed by the limiting identity (15.5), gives the same bound for D_N-D_∞ divided by $1-2^{-q}$. Define

$$L=\frac{(2C)^{1-\lambda}2^{(1+H^2)\lambda}}{1-2^{-q}},\quad k=\frac{4(1-\lambda)}{q},\quad B_\delta=\max\left(4,\left(\frac{C}{2^{H^2}}\right)^{1/(1+H^2)},\left(\frac{L}{\delta}\right)^{1/q}\right).$$

The pointwise choice $N=\lceil B_\delta(2+\rho)^k\rceil$ satisfies $a_N\le b_N$ since $k\ge4/(1+H^2)$. It also makes the error to the now defined limit at most δ. The finite-rank mass bound at s_* is $N^{(\Im s_*)^2}$; it follows that

$$|D_\infty(1,s_*;\zeta)|\le(1+B_\delta)^{1/400}(2+\rho)^\gamma+\delta,\qquad\gamma=k/400<0.010186.\tag{19.D1}$$

The cancellation used here is that of the dyadic rank difference. Applying finite-rank absolute variation to the limiting mark directly would leave an unbounded power of rank.

On $\rho\ge R$, use $2+\rho\le(2+R)\rho/R$ and then integrate (19.D1). At h_*, the modulus of the Mellin prefactor is

$$\left|2^{2h_*+1}\Gamma(1+h_*)/\Gamma(-h_*)\right|=17/16.$$

Indeed $1+h_*=\overline{(-h_*)}+2$ and the gamma recurrence gives $4|(-h_*)(1-h_*)|=17/16$. Thus an absolute allowance for the omitted scalar tail is

$$\frac{17}{16R}\left(\frac{(1+B_\delta)^{1/400}(2+R)^\gamma}{1-\gamma}+\delta\right).\tag{19.D2}$$

Using $\delta = 1/256$, the Arb replay gives the following upper bounds, rounded upward:

R	4	5	6	8	12	16
tail bound	0.344855	0.276317	0.230576	0.173325	0.115945	0.087181

The same proof applies on any rectangle and target compact for which $q > 0$, using the corresponding real-side rank constants, the mass factor from (19.M4), and replacing γ by $4(1-\lambda)\sup|\Im s|^2/q$. For scalar tails it requires $2\Re h > \gamma$. Consequently the bound and its cutoff accounting persist on a small positive-depth and independent order–tilt neighborhood of the executed tuple. For inverse orders (19.D1) alone does not give an integrable upper bound.

A fixed bridge for integrating before absolute values. Let $M \geq R$ and choose a single integer $N = \lceil B_\delta(2+M)^k \rceil$. The same estimate proves $\sup_{\rho \leq M} |D_N - D_\infty| \leq \delta$. Writing

$$K_{R,M}(y) = \int_R^M \rho^{-2h-1} J_0(\rho|y|)\, d\rho$$

and using angular averaging with Haar mark measure μ_N from Theorem 16.4 yields

$$\left| \int_R^M \rho^{-2h-1} \Phi_\infty(\rho)\, d\rho - \int K_{R,M}(y)\, d\mu_N(y) \right| \leq \delta \int_R^M \rho^{-2\Re h-1}\, d\rho.$$

This finite band uses Fubini with an explicitly bounded finite measure. In the second term, absolute domination by the matched real preparation now costs $N^{(\Im s)^2}$, with N fixed on the band. Beyond M use (19.D2) or its parameter-uniform version. A spatial estimate such as an inverse moment bound for $K_{R,M}$ would need to hold uniformly at that chosen rank. No such estimate is implicit in (19.D2).

A small-strip source bound from the positive shifted Gram

This bound is useful in complex-frequency ellipse quadrature of the retained integral. The static comparison retains the unnormalized mark law. At $c = 1$, set $s = u + iv = 1/2 + i/20$, $K = e^{\pi/20}$, $J = \sinh(\pi/20)/\pi$, $g = 127/500$, $\epsilon = 10^{-4}$, $C_0 = (\log 4)/2 + 3 + \sqrt{2\pi/3}$. Use Cartesian complex sources α, β so that $l(w) = \alpha\cos\varphi + \beta\sin\varphi$, $w = e^{i\varphi}$, and let $\rho = \|(\Re\alpha, \Re\beta)\|_2$, $b = \|(\Im\alpha, \Im\beta)\|_2$. For $0 \leq b \leq 1/2$ use $M = \lceil 400 + 3\rho \rceil$; for $1/2 < b \leq 1$ use $M = \lceil 484 + 3\rho \rceil$. Then the continued source obeys

$$|D_\infty(1, s; \alpha, \beta)| \leq \exp\left\{ \frac{b}{2} + \frac{b^2}{4} + \frac{e^b}{1-g} \left[2Ke^b J\{\log(2M) + C_0\} + 4K^2\epsilon \right] \right\}. \tag{19.D3}$$

At $b = 0$ this also provides an independently priced physical polynomial envelope of exponent less than 0.157495. At $R = 64$ its scalar tail budget is 0.135096, larger than (19.D2). The strip bound above is useful for a different part of the error ledger, where (19.D2) is only a physical-plane estimate.

Crossed operators. Use the exterior representation of (16.4) and (19.P1)–(19.P4), with independent $p = \alpha - i\beta$, $q = \alpha + i\beta$. Let $W_s(w) = w^{-s} e^{-(1-w)/(2(1+w))}$ and $\mathcal{U}(w) = e^{-il(w)}$. The two cross blocks of C_s are $P_- \mathcal{U} W_s P_+$ and $P_+ \mathcal{U} W_s^{-1} P_-$; the diagonal blocks are those of $\mathcal{U}$. Write $D(w) = e^{v \arg w}$, $E = P_+ D P_+$, and $\mathcal{Q} = I \oplus E$. The matrices C_t below use the same $\mathcal{U}$, with t denoting tilt. Thus $W_s = W_u D$ and $\|E\|, \|E^{-1}\| \leq K$.

For $x \in [1/2, 1)$, the factor $\mathcal{U}(-x)$ has modulus at most $\exp[3\rho(1-x)/2 + 5b/4]$; on $|w| = 1/2$ it is at most $\exp(3\rho/4 + 5b/4)$. These inequalities follow by separately bounding the real and imaginary Laurent coefficients of l; one uses $x^{-1} - x \leq 3(1-x)$ on the slit. For $n \geq 3\rho + 3$, deform the negative coefficient contour to $|w| = 1/2$ and its slit as in (19.P1). The bank phase is bounded using $x^{n-3/2} \exp[3\rho(1-x)/2] \leq e^{-n(1-x)/2}$. Since $1/(2(1-x))$ is a lower bound for the real exponent from W_s on the slit, one obtains

$$|[\mathcal{U} W_s]_{-n}| \leq K e^{5b/4} \left[\sqrt{2}\, e^{-n(\log 2 - 1/4)} + e^{-\sqrt{n}} \right].$$

The reciprocal cross block has the same bound by changing w to $1/w$. The cross blocks of $\mathcal{U}$ satisfy the same bound by the 1/2 and 2 contour estimates, without a slit. The real-tilt cross blocks obey the same bounds with

$K = 1$. Each block with either its rows or its columns beyond M has trace norm below ϵ: its antidiagonals have rank at most n, and

$$\sum_{n>M} n e^{-\sqrt{n}} \le 2e^{-\sqrt{M}}(M^{3/2} + 3M + 6\sqrt{M} + 6).$$

The geometric sum for the other term is elementary. The stated values of M make the bounds valid even at the maximum b in each case. For the physical case the constants are reproduced in `tilt_budget.py`.

The jump Hankels of D on either side, clipped to their first $m \ge 10$ modes on one side, have trace norm at most

$$J \int_0^1 \frac{(1-t^{2m})^{1/2}}{1-t^2}\, dt \le J\big[\tfrac{1}{2}\log(2m) + \tfrac{3}{2}\big].$$

For the inequality split at $1-1/m$, integrate $(1-t^2)^{-1}$ below it, and use $(1-t^{2m})^{1/2} \le \sqrt{2m(1-t)}$ above it. For the same integral representation, the Toeplitz block between indices below M and those at least $4M$ has trace norm at most $\sqrt{2\pi/3}\, J$ in both orientations. The separation contributes t^{3M}, and the integrand is bounded by $t^{3M}\sqrt{2M}/\sqrt{1-t}$.

For the top-right block of $\mathcal{Q}C_s\mathcal{Q}^{-1} - C_u$, first evaluate the difference before right multiplication by E^{-1}. On the first $4M$ columns use

$$A_s^{12} - A_u^{12}E = P_-\mathcal{U}W_u P_- D P_+.$$

On the remaining columns write the same difference as $(A_s^{12} - A_u^{12}) - A_u^{12}(E - I)$. Split A_u^{12} at intermediate column M: the large columns cost at most $\epsilon(K-1)$, and the small columns cost at most $e^b\sqrt{2\pi/3}\, J$ by the separated Toeplitz bound. The remaining difference costs at most 2ϵ. The bottom-left block uses $EA_s^{21} - A_u^{21} = -P_+ D P_- \mathcal{U} W_s^{-1} P_-$ on the first $4M$ rows. In the far rows use $(A_s^{21} - A_u^{21}) + (E-I)A_s^{21}$ and the analogous intermediate row split; the operator $\mathcal{U}W_s^{-1}$ has norm at most Ke^b. The bottom-right commutator consists of two products, each of a crossed block of $D - I$ and one of $\mathcal{U}$, followed by E^{-1}. Clip the shared modes to M, where the jump Hankel bound applies, and bound the rest by $2K(K-1)\epsilon$. Summing all these bounds gives

$$E_{\mathrm{def}} := \|\mathcal{Q}C_s\mathcal{Q}^{-1} - C_u\|_1 \le 2Ke^b J\{\log(2M) + C_0\} + 4K^2\epsilon.$$

Positive Gram and determinant. At the real tilt $u = 1/2$, use the exterior isometric column pair $W = (J_-, W_u J_+)$ and let $G = W^*W$. Under the Cayley transform to $t = (1/2)\tan(\varphi/2)$, Hardy positive modes correspond to positive frequencies. The unimodular multiplier becomes $e^{it}[(1/2 - it)/(1/2 + it)]^{1/2}$, with the original upper half-plane slit convention. Its negative cross coefficient is obtained by moving the Fourier line to the cut $t = iy,\ y \ge 1/2$. The crossed matrix is the positive Hankel operator on the half-line with kernel

$$\frac{1}{\pi}\int_{1/2}^{\infty} e^{-(1+\xi+\eta)y}\left(\frac{y+1/2}{y-1/2}\right)^{1/2} dy.$$

One can justify the Fourier line by first adding a smooth Abel factor or integrating by parts in the nonzero frequency; the nondecaying constant term after factoring e^{it} has no negative-frequency coefficient. The branch jump has magnitude $2((y+1/2)/(y-1/2))^{1/2}$, is locally integrable, and yields the displayed exponential with the indicated sign. For the norm only its modulus is needed. The trace bound is its positive rank-one integral with $\|e^{-y\xi}\|_2^2 = 1/(2y)$. After $y = 1/2 + x^2$ and $\sqrt{1+x^2} \le 1 + x^2/2$ the bound is at most

$$\frac{e^{-1/2}}{4\sqrt{\pi}} + \frac{3\sqrt{2}}{8}\operatorname{erfc}(1/\sqrt{2}) < g.$$

Consequently $G \ge (1-g)I$.

Write $l = l_{\mathrm{r}} + i l_{\mathrm{i}}$ with the two real-valued functions on the circle and put $G_b = W^* e^{l_{\mathrm{i}}} W$. Then $G_b \ge e^{-b}(1-g)I$, and $G_b^{-1/2} C_u G_b^{-1/2}$ is a contraction by writing $e^{l_{\mathrm{i}}/2} W G_b^{-1/2}$ as an isometry. The bounded reference B_l is the two diagonal Hardy compressions of l. Its parts $B_{\mathrm{r}}, B_{\mathrm{i}}$ have a rank-two commutator with trace zero: the blocks are linear combinations of the unilateral shift and its adjoint, with opposite trace contributions from the two half-lines. Also $G_b - e^{B_{\mathrm{i}}}$ is trace class by the crossed coefficient bounds and diagonal Duhamel comparison. The

same holds for $\log G_b - B_{\mathrm{i}}$ by the resolvent integral of the logarithm and the positive lower bounds. Fredholm multiplicativity then gives

$$|\det(e^{iB_l}\mathcal{Q}C_s\mathcal{Q}^{-1})| = \det(e^{-B_{\mathrm{i}}}G_b)|\det(e^{iB_{\mathrm{r}}}G_b^{-1/2}\mathcal{Q}C_s\mathcal{Q}^{-1}G_b^{-1/2})|.$$

Indeed replacing e^{iB_l} by $e^{iB_{\mathrm{r}}}e^{-B_{\mathrm{i}}}$ has determinant-one quotient by the trace-zero commutator formula. Next factor $e^{-B_{\mathrm{i}}}G_b$ from the expression in the determinant. The symmetric $G_b^{-1/2}$ placement follows by conjugating the remaining determinant by $G_b^{1/2}$: the extra multiplicative commutator has determinant one since $\mathrm{tr}[\log G_b, B_{\mathrm{r}}] = 0$. The bounded-operator exponential commutator identities follow by differentiation in a scalar parameter, with the trace-class commutators making all trace differences cyclic.

The last determinant is within trace-norm argument error $e^b E_{\mathrm{def}}/(1-g)$ of a contraction. For an operator $I+$ trace class within trace distance d of a contraction, the determinant has modulus at most e^d, by singular-value comparison and finite compression; this is the estimate already used in (19.P4). The exact Toeplitz commutator phase of (19.P3) extends to independent p, q by holomorphic continuation and gives a factor $e^{-v\alpha}$. This cancels the modulus change from the imaginary part of tilt in $e^{-is\alpha}$; the remaining factor $e^{u\Im\alpha}$ multiplies $\det(e^{-B_{\mathrm{i}}}G_b)$ to recover the positive real-tilt mass with imaginary source. By the strong Szegő bound on the positive finite-rank symbol, followed by the compact source limit, that mass is at most $\exp(|u|b + b^2/4)$ at $c = 1$. For example this follows directly from the quadratic prefactor in (15.5), before passing to the limit; the finite positive-symbol Hankel product contributes a contraction determinant of modulus at most one. This proves (19.D3).

A direct limiting-projection bound for the radial tail

Fix $c = 1$, $u = 1/2$, $s = u + iv$, $|v| \le 1/20$, and $h = 1/2 + i/8$. Write $D = D_\infty(1, s; \zeta)$ with the exterior representation (16.4), $\rho = |\zeta|$, and let $\Phi(\rho)$ be its normalized circular average. The following bound concerns the original complex pushforward. The total variation of the finite ensemble before pushforward is not a uniform upper bound for it.

Trace deficit in the limiting Cayley coordinate. Use the Hardy projections P_-, P_+ on the circle and the real boundary phase $W = W_u$ of (19.P1). Write

$$V = (J_-, M_W J_+), \qquad G = V^*V, \qquad Q = I - VG^{-1}V^*, \qquad R_0 = I - VV^* = P_+ - M_W P_+ M_{\bar{W}}.$$

Here J_-, J_+ are the isometries from the two Hardy components to the full circle space. This is the limiting exterior Gram construction of Theorem 16.3. The exact static mass $m = \det G$ is in $(.94, 1]$, by the real source-zero enclosure in the moment certification controls of this edition. For example the enclosure in `jet_half_reference.json` gives $m = 0.9423646306369\ldots$ to less than $3 \cdot 10^{-9}$ in absolute modulus. If $C = J_-^* M_W J_+$, then $G - I = \left(\begin{smallmatrix} 0 & C \\ C^* & 0 \end{smallmatrix}\right)$ and $m = \det(I - C^*C)$. In particular G is invertible and

$$\|G - I\| \le \gamma, \qquad \|G - I\|_2 \le \sqrt{2}\gamma, \qquad \gamma = \sqrt{-\log(47/50)}.$$

This uses $-\log\det(I - C^*C) \ge \|C\|_2^2$. The norm $\|\cdot\|_2$ is the Hilbert–Schmidt norm. The isometry $VG^{-1/2}$ gives $\|Q - R_0\|_2 = \|G - I\|_2$.

With $U = M_{\mathcal{U}}$ the unitary multiplication in (19.P1), the unitary-centered real exterior compression A_u is a contraction and is the identity plus a trace-class operator. Its deficit satisfies

$$\mathrm{tr}(I - A_u^* A_u) = \tfrac{1}{2}\|[Q, U]\|_2^2 \ge \tfrac{1}{2}\left(\|[R_0, U]\|_2 - 2\sqrt{2}\gamma\right)_+^2. \tag{19.DT1}$$

The first equality follows from the two off-diagonal blocks of U relative to Q. Their squared norms are $\mathrm{tr}(I - A_u^* A_u)$ and $\mathrm{tr}(I - A_u A_u^*)$; the traces are equal because $A_u - I$ is trace class. The inequality follows by applying the triangle inequality to the commutators.

Set $t = \frac{1}{2}\tan(\theta/2)$ and $\vartheta(t) = 2\arctan(2t)$. Thus $W = e^{i(t - u\vartheta(t))}$ and $\mathcal{U}(t) = \exp[-i\rho\cos(\vartheta(t) - \beta)]$ for the appropriate Fourier direction β. The Hardy commutator kernel yields the exact expression

$$\|[R_0, U]\|_2^2 = \frac{1}{(2\pi)^2}\iint_{\mathbb{R}^2} \frac{|\mathcal{U}(t) - \mathcal{U}(t')|^2 |W(t) - W(t')|^2}{|t - t'|^2}\, dt\, dt'. \tag{19.DT2}$$

Indeed the Hardy projection kernel has denominator $1 - w\bar{w}'$. The multiplier difference removes its diagonal singularity, and the Cayley change gives $d\theta\, d\theta'/|w - w'|^2 = dt\, dt'/|t - t'|^2$. The commutator formula can first be applied to the bounded smooth symbol $\mathcal{U}$; multiplication by W and $\bar{W}$ is then unitary on the circle.

Choose the sign of t so that the real and imaginary components of the derivative of $\cos(\vartheta(t) - \beta)$ add in modulus. For $x = |t| \geq 2$ their nonnegative sizes on this sign are

$$\frac{16x}{(1+4x^2)^2}|\cos\beta|, \qquad \frac{4(4x^2-1)}{(1+4x^2)^2}|\sin\beta|.$$

They are decreasing and are at least $\frac{4}{5}x^{-3}|\cos\beta|$ and $\frac{4}{5}x^{-2}|\sin\beta|$, respectively. Put

$$x_0 = (2\rho/5)^{1/3}, \qquad L = \max\{x_0,\ (2\rho|\sin\beta|/5)^{1/2}\}, \qquad C_0 = 3/(4\pi^2).$$

For $x \in [4, L-2]$ and signed offsets $|\tau| \leq 2$, the Fourier phase has monotone derivative of magnitude at least 2. The first derivative integral estimate, from integration by parts and monotonicity of the inverse derivative, gives

$$\int_{-2}^{2} |\mathcal{U}(t) - \mathcal{U}(t+\tau)|^2\, d\tau \geq 6.$$

On the same intervals the derivative of the W phase in t lies between $15/17$ and 1. Hence

$$\frac{|W(t) - W(t+\tau)|^2}{\tau^2} \geq \sin^2(15/17) > 1/2.$$

Integrating this rectangle in (19.DT2) proves $\|[R_0, U]\|_2^2 \geq C_0(L-6)_+$. This improvement uses the actual limiting Hardy projection, without requiring a lower kernel coherence length for a finite weighted polynomial space.

Transferring the real deficit to nonreal tilt. In (19.P2) put $K = e^{\pi/20}$, $J = \sinh(\pi/20)/\pi$. The complex–real trace norm estimate there sharpens to

$$\Delta \leq 4KJ(\log(2M) + 5) + \epsilon(5K^2 + 2), \qquad \epsilon = 1/100, \qquad M = 8192 + \lceil 3\rho + 3 \rceil. \tag{19.DT3}$$

For this refinement, on the slit and inner contour of (19.P1) use $|\mathcal{U}(w)| \leq \exp[(3/2)\rho(1 - |w|)]$ for $|w| \geq 1/2$. Combining it with the negative-frequency coefficient on the slit, $x^{n-1-u} \leq \exp[-(n-1-u)(1-x)]$, leaves the exponent $-\frac{n}{2}(1-x)$ whenever $n \geq 3\rho+3$. The old slit factor $\exp[-(1+x)/(2(1-x))]$ then gives $\exp[-\sqrt{n}]$ as before. The inner-circle term is bounded by $2^u \exp[-n(\log 2 - 1/4)]$, and the unitary cross block alone has the same circle estimate. Thus each high coefficient, inclusive of the reflected counterpart, is bounded by $(1+\sqrt{2})Ke^{-(2/5)\sqrt{n}}$. The sums $\sum_{n>M} n|b_n|$ for every cross block are less than ϵ: the elementary integral with lower boundary 8192 is less than $2.16 \cdot 10^{-9}$. In the block proof of (19.P2) the terms $5K^2 + 2$ come solely from these high-mode tails, which now cost $\epsilon(5K^2 + 2)$. The low-mode jump and separated Toeplitz estimates are unchanged.

Apply the same complex Toeplitz similarity as in (19.P3), then divide the exterior compression on both sides by $G^{1/2}$. This restores the factor $\det G = m$ and changes the upper bound on the trace-norm perturbation from A_u to $\Delta/(1-\gamma)$. The exponential trace from (19.P3) cancels the modulus of the complex centering phase exactly. For a contraction A with (A-I) trace class and trace-class perturbation E,

$$|\det(A+E)| \leq \exp\left(\|E\|_1 - \tfrac{1}{2}\operatorname{tr}(I - A^*A)\right).$$

Indeed in finite dimension use the product of singular values, $log x \leq x - 1$, the trace-norm triangle inequality, and $1 - x \geq (1-x^2)/2$ for $0 \leq x \leq 1$. Finite coordinate compressions pass to the Fredholm determinant and its deficit in trace norm. Therefore the phase-centered complex comparison retains the real deficit from (19.DT1):

$$|D| \leq \exp\left(\frac{\Delta}{1-\gamma} - \tfrac{1}{4}\left(\sqrt{C_0(L-6)_+} - 2\sqrt{2}\gamma\right)_+^2\right). \tag{19.DT4}$$

The omitted factor $m \leq 1$ only reduces this bound.

For $\rho \ge 8196$ one has $M \le 4\rho$. Use $(\sqrt{a}-b)_+^2 \ge (7/8)a - 7b^2$ for $a, b \ge 0$ and set

$$d = \frac{4KJ}{1-\gamma}, \qquad k = \frac{7}{32}C_0, \qquad \sigma = (2/5)^{1/3},$$
$$H = \exp\left[d(\log 8 + 5) + \frac{\epsilon(5K^2+2)}{1-\gamma} + 14\gamma^2 + 6k\right].$$

Thus $|D| \le H\rho^d e^{-kL}$. A further angular integration is explicit. On the set $|\sin\beta| \le 2/x_0$, whose normalized angular measure is at most $2/x_0$, use $L \ge x_0$. On each quarter circle of the complementary set, $\sin\beta \ge 2\beta/\pi$ after reflection, and $\beta \ge 2/x_0$. Integrating $e^{-k\sqrt{(2/\pi)x_0^3\beta}}$ from this point to infinity gives

$$|\Phi(\rho)| \le H\rho^d e^{-kx_0} \min\left\{1,\ \frac{2}{x_0}\left(1 + \frac{1}{kx_0} + \frac{1}{k^2x_0^2}\right)\right\}. \tag{19.DT5}$$

In the integral, substituting $y = \sqrt{(2/\pi)x_0^3\beta}$ reduces the bound to the elementary integral of ye^{-ky}, with lower endpoint at least x_0.

At the stated h, the absolute Mellin prefactor is exactly $4|h|^2 = 17/16$: use $\Gamma(1+h) = h\Gamma(h)$, $\Gamma(-h) = \Gamma(1-h)/(-h)$, and $1 - h = \bar{h}$. Let $x_R = \sigma R^{1/3}$, $\kappa = k\sigma$ and

$$A_R = \frac{2}{\sigma}\left(1 + \frac{1}{kx_R} + \frac{1}{k^2x_R^2}\right).$$

Integration of the two envelopes of (19.DT5) from $R \ge 8196$ to infinity then gives

$$|\mathcal{E}_R| \le \frac{3(17/16)H}{\kappa} e^{-\kappa R^{1/3}} \min\{R^{d-4/3},\ A_R R^{d-5/3}\}. \tag{19.DT6}$$

Use $y = \rho^{1/3}$ and bound the residual, decreasing power at $y = R^{1/3}$. The rigorous numerical ledger `shell_receipts.json` gives $d < .313$, $H < 27.061$, $\kappa > .0122479$. The angular bound is less than $2.133 \cdot 10^{-12}$ at $R = 5 \cdot 10^8$ and less than $6.52 \cdot 10^{-14}$ at $R = 10^9$. The improvement over the prior sufficient cutoff exceeding 10^{35} does not make direct retained integration to these cutoffs feasible.

Integration in the mark plane and its limitation. Let p_s be the signed planar density from Theorem 16.4 with Fourier source D, and $r = |z|$ in the mark plane. The exact tail equals the integral against $p_s(z)\,d^2z$ of $K_R(r) = \int_R^\infty \rho^{-2h-1}J_0(\rho r)\,d\rho$, with the same Mellin prefactor. Fubini follows from the integrability of p_s and $\Re h > 0$. For $x = Rr > 0$, integrate by parts using $(xJ_1(x))' = xJ_0(x)$, or use $|J_0| \le 1$ directly. This gives

$$|K_R(r)| \le R^{-1}\min\{1, B(Rr)^{-3/2}\}, \qquad B = \tfrac{6}{5}\left(1 + \frac{|2h+2|}{5/2}\right) < 2.645.$$

For completeness, $|J_1(x)| \le (6/5)x^{-1/2}$ on $x \ge 1$: $f = \sqrt{x}J_1(x)$ obeys $f'' + (1 - 3/(4x^2))f = 0$, so $f^2 + f'^2/(1 - 3/(4x^2))$ decreases. At 1, the alternating series for J_0, J_1 give $0.440 < J_1(1) < .441$ and $0 < f'(1) = J_0(1) - J_1(1)/2 < .546$, which bound the initial energy by $(6/5)^2$. The Bessel integration by parts on $[x,\infty)$ therefore bounds the endpoint by $(6/5)x^{-5/2}$ and the integral part by $(6/5)|2h+2|x^{-5/2}/(5/2)$. The estimate includes $r = 0$ using the elementary integral.

With $P_\infty \ge \|p_s\|_\infty$, $P_2 \ge \|p_s\|_2$ and any $\delta \ge 1/R$, the three regions $r \le 1/R$, $1/R < r \le \delta$, and $r > \delta$ cost

$$\frac{17}{16}\left\{\pi P_\infty R^{-3} + BR^{-5/2}\left(4\pi P_\infty\sqrt{\delta} + \sqrt{2\pi}P_2/\sqrt{\delta}\right)\right\}. \tag{19.DT7}$$

Use the pointwise density bound on the first two and Cauchy–Schwarz on the last. Fourier inversion and Parseval supply computable prices for these signed-density bounds from (19.DT4). For $\rho < 8196$ bound by $\exp(\Delta/(1-\gamma))$, and for the rest use $H\rho^d e^{-\kappa\rho^{1/3}}$. The ledger gives $P_\infty < 1.529 \cdot 10^{17}$, $P_2 < 2.592 \cdot 10^9$. Consequently (19.DT7), with δ chosen by balancing the two costs, is still above $5.5 \cdot 10^9$ at $R = 1024$. Integrating the Bessel tail first does give cancellation, but its price using these separate signed-density norms is worse than (19.DT6). A practical approach needs to retain additional cancellation in the mark integral or use a scalar representation that does not resolve this frequency annulus.

There is also an exact L^2 check, independent of a pointwise Bessel majorant. In the transform convention of (15.5), the radial Fourier transform of K_R is $2\pi\,\mathbf{1}_{\{\rho\ge R\}}\rho^{-2h-2}$, first by truncation at a second finite radius and then by Parseval. Thus

$$\|K_R\|_2^2 = \frac{2\pi}{4\Re h+2}\,R^{-4\Re h-2}.$$

The best estimate available from a standalone L^2 norm of the density and Cauchy–Schwarz is consequently $(17/16)\sqrt{\pi/2}\,P_2R^{-2}$ at this input. The constant is sharp over the complex L^2 unit ball by choosing the test density proportional to $\overline{K_R}$. With the present priced P_2 this allowance still exceeds $3.29\cdot10^3$ at $R=1024$. It is a further diagnostic for the need to retain more information than just an absolute signed-density norm.

A depth-one bound retaining real projection leakage

Here $c=1$, $s=\frac12+iv$, $|v|\le 1/20$. Denote by P the limiting occupied orthogonal projection at the real tilt $u=1/2$. The following argument compares the exterior determinant at complex tilt to the real exterior compression, retaining its singular-value deficits. It gives an independent angular-average allowance at the fixed depth.

Explicit coherence of the real projection. In the original coordinate $t\in\mathbb{R}$, put $a=1/2$ and

$$w(t)=\frac{a+it}{a-it},\qquad g(t)=e^{it}\left(\frac{a-it}{a+it}\right)^{1/2}.$$

The unitary Cayley change from the circle to the line preserves the positive and negative Hardy subspaces. This follows from the analytic substitution $w(t)$ and Jacobian factor proportional to $(a-it)^{-1}$ on the positive subspace, and unitarity on its orthogonal complement. The limit of the exterior pair from Section 16 is therefore $W=(J_-,gJ_+)$, with J_-,J_+ inclusions from the negative and positive half-axes of the unitary Fourier transform, respectively. Its Gram is $G=I+X$ and $P=I-WG^{-1}W^*$.

In the half-line Fourier variables the cross block of X has, up to a constant sign, the Hankel kernel

$$H(\xi,\eta)=\int_0^\infty e^{-(a+y)(\xi+\eta)}\,d\nu(y),\qquad d\nu(y)=\pi^{-1}e^{-(a+y)}\sqrt{\frac{1+y}{y}}\,dy.$$

Indeed the negative Fourier coefficient with frequency $b>0$ of $((a-it)/(a+it))^{1/2}$ is computed on the upper cut $t=i(a+y)$. The jump magnitude of the square root is $2\sqrt{(1+y)/y}$, and the factor e^{it} shifts b to $1+\xi+\eta$. To justify the deformation, first multiply the branch symbol by $R^2/(R-it)^2$, with its pole in the lower half-plane. On the upper cut the additional factor is $R^2/(R+a+y)^2\le1$. The Fourier transforms converge in tempered distributions as $R\to\infty$, and the resulting cut integrals converge locally uniformly at $b>0$ by the displayed exponential. The opposite cross block is the adjoint. Since $2(a+y)\ge1$ and $\sqrt{(1+y)/y}\le1+y^{-1/2}$,

$$\|H\|\le\operatorname{Tr}|H|\le\nu((0,\infty))\le M:=\pi^{-1}e^{-1/2}(1+\sqrt{\pi})<.536,\qquad \|G^{-1}\|\le(1-M)^{-1}.$$

Consequently $P-P_0=W(X-X^2G^{-1})W^*$ for $P_0=I-WW^*$. The kernel of P_0 away from the diagonal has modulus

$$\frac{|1-g(t)\overline{g(t')}|}{2\pi|t-t'|}.$$

For the correction, the Fourier evaluation vectors for each half-line have normalization $(2\pi)^{-1/2}$. Integration against $e^{-(a+y)\xi}$ has modulus at most $(2\pi)^{-1/2}|t|^{-1}$. The kernel contribution of the two cross blocks multiplied by W is therefore bounded by $M/(\pi|tt'|)$. Also $\|XW^*\delta_t\|\le M/(\sqrt{\pi}|t|)$, using the same integration bound and $\|e^{-(a+y)\cdot}\|_2=(2(a+y))^{-1/2}\le1$. These distributional evaluations can be made with a decaying factor $e^{-\epsilon\xi}$ and then passed to the limit by the displayed integrable bounds. The second Gram correction costs at most $M^2/(\pi(1-M)|tt'|)$. In total

$$|P(t,t')-P_0(t,t')|\le\frac{M}{\pi(1-M)|tt'|}.$$

On a same-sign interval with $|t|,|t'|\ge4$ and $0<|t-t'|\le2$, the argument derivative of g is $1-(1/2)/(1/4+t^2)$, between $1-(1/2)/(16+1/4)$ and 1. Use $\sin x/x\ge\sin1$ for $0<x\le1$ in the base kernel bound. Subtracting the correction proves

$$|P(t,t')|\ge\frac{(1-(1/2)/(16+1/4))\sin1}{2\pi}-\frac{M}{16\pi(1-M)}>\frac{1}{10}.\tag{D.1}$$

Preserving leakage at nonreal tilt. Let $\mathcal{U} = e^{-il}$ with $l = (pw + q/w)/2$ as in (19.P2) and set $J = WG^{-1/2}$. The exterior compression $K_0 = J^*\mathcal{U}J$ is a contraction. The unitary reference operator $e^{iB_l}K_0$ differs from I by trace class, since this holds for $e^{iB_l}C_u$ and $G^{-1/2} - I$ is trace class. In particular K_0 is Fredholm of index zero. Its two trace deficits agree, because its nonzero singular values are the same in the two orientations, and the nullities agree by index zero. These two deficits are the squared Hilbert–Schmidt leakage norms for the occupied and exterior complements. Hence

$$\tfrac{1}{2}\operatorname{Tr}(I - K_0^*K_0) = \tfrac{1}{4}\iint |\mathcal{U}(t) - \mathcal{U}(t')|^2 |P(t,t')|^2\, dt\, dt'.$$

The identity follows first on bounded intervals from the integral kernel, then on the full line by the Hilbert–Schmidt norm and exhaustion. For any trace class perturbation A of $e^{iB_l}K_0$ with distance $\mathcal{E}$ in trace norm, finite-dimensional compression and the singular-value triangle inequality give

$$|\det A| \le \exp\bigl[\mathcal{E} - \tfrac{1}{2}\operatorname{Tr}(I - K_0^*K_0)\bigr].$$

Indeed in each compression use $\log x \le x - 1$, the triangle inequality for the sum of singular values, and $1 - x \ge (1 - x^2)/2$ for the compressed contraction. Both the Fredholm determinant and the squared-contraction deficit converge under compression with identity on the omitted space, by trace-norm convergence of the operators minus identity. For the conjugated complex exterior determinant, $\mathcal{E}$ may be taken as the defect in (19.P2) plus $(1 + \sqrt{2})2M$. The centering phase cancels exactly by (19.P3).

Write $\rho = |p|$ and let β denote its real-plane angle, with the sign of t selected so the two directional phase derivatives add. At $x = |t| \ge 4$, the modulus of that derivative is

$$\rho\frac{|\cos\beta|x + |\sin\beta|(x^2 - 1/4)}{(x^2 + 1/4)^2} \;\ge\; .95\rho\bigl(|\cos\beta|x^{-3} + |\sin\beta|x^{-2}\bigr).$$

Both summands in the fraction decrease with x. Set

$$L_\beta = \max\{(\rho/8)^{1/3}, (\rho|\sin\beta|/8)^{1/2}\}.$$

Here the first term uses $|\cos\beta| + x|\sin\beta| \ge 1$ at $x \ge 4$, so each of its two component alternatives guarantees the same minimum slope throughout its admitted interval. If $L_\beta > 20$, restrict the leakage integral to $16 \le x \le L_\beta - 4$, t' an outward offset $y \in [0,4]$, and the transposed region. Define $S(y) = (\sin(y/2)/(\pi y))^2$, with $S(0) = (4\pi^2)^{-1}$. The argument derivative of g, and the correction before (D.1), show that $\bigl||P(t,t')| - \sqrt{S(y)}\,\bigr| \le q_0$ with

$$q_0 = \frac{(1/2)/(256 + 1/4)}{2\pi} + \frac{M}{256\pi(1 - M)}.$$

Consequently $|P|^2 \ge S - q_0/\pi$. The phase derivative on the offset interval is monotone and has modulus at least 7.6. Integration by parts against the decreasing $S(y)$ gives

$$\left|\int_0^4 S(y)e^{i(l(t') - l(t))}dy\right| \le \frac{3S(0)}{7.6}.$$

Indeed the endpoint absolute sum is at most $[S(0) + S(4)]/7.6$. The term from S' costs at most $[S(0) - S(4)]/7.6$ and the one from the reciprocal derivative costs at most $S(0)/7.6$ by monotonicity. Finally $\int_0^4 S(y)dy \ge (4 - 4^3/36 + 4^5/2880)/(4\pi^2)$ from $\sin x \ge x - x^3/6$ on $[0,2]$. Subtract $3S(0)/7.6 + 8q_0/\pi$ from this last quantity. The result exceeds $1/20$. The leakage integral therefore gives

$$\tfrac{1}{2}\operatorname{Tr}(I - K_0^*K_0) \ge \gamma\max(0, L_\beta - 20), \qquad \gamma = 1/20. \tag{D.2}$$

A smaller exterior defect. The trace-norm comparison in (19.P2) can use any $0 < \tau \le 1$ in place of its cross-block tail tolerance one. The coefficient estimate at inner contour $r = 1 - 1/R$, $R = 2 + \rho$, gives

$$|[\mathcal{U}W_s]_{-n}| \le C_0(r^n + e^{-\sqrt{n}}) \quad (n \ge 3), \qquad C_0 = 2^{1/2}Ke^2, \quad K = e^{\pi/20}.$$

Indeed $|\mathcal{U}| \le e^2$ on the contour and both banks, and the remaining slit estimate is as in (19.P1). The same envelope holds for the opposite cross orientation and for $\mathcal{U}$ alone. Here $n-1-\Re s \ge n/2$ for $n \ge 3$, as required in the slit bound. Take an integer $M_0 \ge 4$ with

$$2C_0 \int_{\sqrt{M_0}}^{\infty} x^3 e^{-x}\, dx \le \tau/2$$

and $M_\rho = \lceil M_0 + 2R\log(4C_0R^2/\tau)\rceil$. Then the weighted slit sum for $n > M_\rho$ is at most $\tau/2$ by monotonicity and the integral estimate. For the contour sum use $\sum_{n>M_\rho} nr^n \le R^2(2+M_\rho/R)e^{-M_\rho/R} \le 2R^2 e^{-M_\rho/(2R)}$. These give the cross-block tail tolerance τ. The same block proof as (19.P2), keeping the factors of τ in each of its three tail terms, now bounds the defect there by

$$4KJ(\log(2M_\rho)+5) + \tau(5K^2+2), \qquad J = \sinh(\pi/20)/\pi. \tag{D.3}$$

Execution of the angular tail allowance. For an arbitrary $\epsilon > 0$, use

$$C_\epsilon = M_0 + 1 + 2\log(4C_0/\tau) + 4/(\mathrm{e}\epsilon), \quad M_\rho \le C_\epsilon(2+\rho)^{1+\epsilon}, \quad p_* = 4KJ(1+\epsilon).$$

This follows from $\log R \le R^\epsilon/(\mathrm{e}\epsilon)$. Set

$$A_* = \exp\{(1+\sqrt{2})2M + 4KJ(\log(2C_\epsilon)+5) + \tau(5K^2+2)\}, \quad L_0 = (\rho/8)^{1/3}.$$

For $\rho \ge 8\sqrt{2}$, one has both $L_\beta \ge L_0$ and $L_\beta \ge (\rho|\sin\beta|/8)^{1/2}$. Use their maximum in the exponential and use $\sin\beta \ge 2\beta/\pi$ in the first quadrant. In the angular estimate write $x = 2\beta/\pi$, and split the upper integral at $x = 8L_0^2/\rho$; after the split extend to infinity and use $u = (\rho x/8)^{1/2}$. This proves

$$|\Phi_\infty(\rho)| \le A_*(2+\rho)^{p_*} \min\left(1, e^{\gamma(20-L_0)}, \frac{8e^{\gamma(20-L_0)}}{\rho}(L_0^2 + 2L_0/\gamma + 2/\gamma^2)\right). \tag{D.4}$$

For $\Re h = 1/2$ and $B \ge 8\sqrt{2}$, let D_B denote the minimum in (D.4) at B. Since all three entries of that minimum are decreasing, the tail budget before multiplying the Mellin prefactor is $A_*(1+2/B)^{p_*} D_B B^{p_*-1}/(1-p_*)$ when $p_* < 1$.

At high frequency one can use a linear mode budget. For $|w| \ge 1/2$, $|\mathcal{U}(w)| \le \exp[\frac{3}{2}\rho(1-|w|)]$. In the coefficient contour with inner radius $1/2$, if $n \ge 3\rho+3$ the bank factor $x^{n-1-1/2}$ pays the added radial exponential and retains $e^{-n(1-x)/2}$. On the circle the factor 2^{-n} retains $e^{-n(\log 2 - 1/4)}$. The cross-block coefficient and the two reflected bounds are therefore at most $(1+\sqrt{2})Ke^{-(2/5)\sqrt{n}}$. For the same tolerance $\tau = 1/128$, one may choose $M_\rho = 8192 + \lceil 3\rho + 3\rceil$. The integral bound for the weighted coefficient sum is then $2(1+\sqrt{2})K\int_{\sqrt{8192}}^{\infty} x^3 e^{-(2/5)x} dx < \tau$. When $\rho \ge 8196$, $M_\rho \le 4\rho$. In (D.3) this yields the envelope $H\rho^p$ with

$$p = 4KJ, \qquad H = \exp\{(1+\sqrt{2})2M + p(\log 8 + 5) + \tau(5K^2+2) + 20\gamma\}.$$

Use $L_0 = \rho^{1/3}/2$, $\kappa = \gamma/2$ and bound the angular multiplier after extracting $e^{-\kappa\rho^{1/3}}$ by $A_B\rho^{-1/3}$, where

$$A_B = 8\left(\tfrac{1}{4} + \frac{1}{\gamma B^{1/3}} + \frac{2}{\gamma^2 B^{2/3}}\right).$$

At $B \ge 8196$ this gives the improved pre-prefactor tail bound

$$\frac{3}{\kappa} H A_B B^{p-5/3} e^{-\kappa B^{1/3}}. \tag{D.5}$$

Indeed substituting $t = \rho^{1/3}$ reduces the integral to $3\int_{B^{1/3}}^{\infty} t^{3p-5} e^{-\kappa t} dt$, and $3p - 5 < 0$. Both (D.4) and (D.5) may be applied and the smaller budget retained. This is an independent estimate for the weighted angular tail. It leaves the cost of evaluating the retained annulus as a separate issue.

Keyhole quadrature for the Fourier source

Use the notation $a = c/2$ of (15.5). Substitute $u = it$ and put

$$Q(u; p, q) = \exp\left(s\{\log(a+u) - \log(a-u)\} + ia\{q/(a+u) - p/(a-u)\}\right).$$

Choose $0 < \delta < a$. Let Γ run from infinity on the ray $u = a + x - i\delta$ $(x \geq 0)$ to its finite endpoint, then around the left semicircle of radius δ centered at a, then outward on the ray $u = a + x + i\delta$. On the lower and upper rays use $\log(a-u) = \log(x \mp i\delta) \pm i\pi$, respectively. Then

$$b_+(v; p, q) = \frac{1}{2\pi i} \int_\Gamma Q(u; p, q) e^{-uv}\, du \qquad (v \geq 1), \qquad b_-(v; p, q) = b_+(v; q, p). \tag{K1}$$

To prove the deformation, start with the twice differentiated symbol in (15.5). On the imaginary axis $u = it$, $B''(t) = -Q''(u)$. For fixed sources and tilt, $Q''(u) = O((1+|u|)^{-2})$ on the large closing arcs in the right half-plane on either side of the slit. One may first truncate both heights and right endpoints at a common large T, use horizontal closing segments at heights $\pm T$ and vertical segments at real part T, and pass $T \to \infty$. The horizontal $O(T^{-1})$ integral estimate uses $|e^{-uv}| \leq 1$; the vertical segments have exponential decay. No singularity is crossed away from the ray $[a, \infty)$. The twice differentiable contour integral has a prefactor v^{-2}; two integrations by parts on Γ cancel it. At the two joins the endpoint terms telescope, and at infinity the terms vanish exponentially. This proves (K1) with the sign fixed by the upward orientation of the original line. The interchange for the second kernel follows from the identity $B^{-1}(-t; p, q) = B(t; q, p)$.

An operator norm error budget. Put $f_u(x) = e^{-ux}$, $x \geq 0$, and let $f_u \otimes f_u$ denote the bilinear rank-one kernel $e^{-u(x+y)}$. It has Hilbert–Schmidt norm $(2\Re u)^{-1}$. The two Hankel operators of (15.5) are therefore contour integrals of $Q(u; p, q)e^{-u}(f_u \otimes f_u)/(2\pi i)$ and its source-swapped version. Truncating the rays at $x = X > 0$ costs in Hilbert–Schmidt norm at most

$$\frac{e^{-a-X}}{2\pi(a+X)} \left(1 + \frac{2a+\delta}{X}\right)^{|\Re s|} \exp\left(3\pi|\Im s| + \frac{a(|p|+|q|)}{X}\right). \tag{K2}$$

Here $|a-u| \geq x$, $1 \leq |a+u|/|a-u| \leq 1 + (2a+\delta)/x$, and $\Re u = a + x$. The constant covers both rays.

For each truncated contour use the real ray parameter x or the normalized semicircle parameter $t \in [0, 1]$, with $u = a + \delta e^{-i\pi(t+1/2)}$ on the semicircle. Use panels of width w, with analytic Bernstein ellipse parameter 2. The ellipse lies within the real extension $w/8$ of the panel and imaginary height $3w/8$. If $m > 0$ bounds $\Re u$ below there, $m_\pm > 0$ bound $|a \pm u|$ below, $M_\pm$ bound them above, and V bounds $|du/dt|$ (or $|du/dx|$), then a common Hilbert–Schmidt integrand bound for both factors is

$$\begin{aligned} M_{\mathrm{ell}} = \frac{Ve^{-m}}{4\pi m} &\max\{(M_+/m_-)^{\Re s}, (m_+/M_-)^{\Re s}\} \\ &\times \exp\left(3\pi|\Im s| + a \max\left\{\frac{|p|}{m_-} + \frac{|q|}{m_+}, \frac{|q|}{m_-} + \frac{|p|}{m_+}\right\}\right). \end{aligned}$$

These quantities are computed by elementary triangle inequalities. On a ray panel use the larger of its extended real left endpoint and $\delta - 3w/8$ for m_-. On the semicircle use $\delta e^{-3\pi w/8}$ for m_- and $m = a - \delta e^{3\pi w/8}$. In this run $\delta = a/2$, the semicircle panels have width $1/4$, and the ray panels grow geometrically from $a/2$. The logs are analytic in a neighborhood of every ellipse by the strict denominator and real-part margins. The Gauss–Legendre error for a panel with n nodes is at most

$$8wM_{\mathrm{ell}} 2^{-2n}/(1 - 1/2). \tag{K3}$$

Indeed, the Hilbert–Schmidt-valued Chebyshev coefficient of order $k > 0$ has norm at most $2M_{\mathrm{ell}}2^{-k}$ by Cauchy's formula. Truncate after degree $2n-1$, bound the remaining geometric sum on the panel, and use the exactness and positive weights of the Gauss rule. Formula (K3) allows a factor two of slack.

The quadrature is a finite-rank sum $\widehat{H}_\pm = \sum_j d_j^\pm f_{u_j} \otimes f_{u_j}$. Without further compression, the determinant of its product reduces to $\det(I - D_+ G D_- G)$, where $D_\pm = \mathrm{diag}(d_j^\pm)$ and $G_{jk} = (u_j + u_k)^{-1}$. This is the finite-rank

$\det(I-AB)=\det(I-BA)$ identity. For the faster calculation let Π_k be projection onto the first k normalized Laguerre functions $\sqrt{2b}\,e^{-bx}L_j(2bx)$, for a chosen $b>0$. Integration of the Laguerre polynomial gives

$$\left\langle f_u,\sqrt{2b}\,e^{-bx}L_j(2bx)\right\rangle=\frac{\sqrt{2b}}{u+b}\left(\frac{u-b}{u+b}\right)^j.$$

There is no conjugation on u, since the Laguerre functions are real. Completeness and summation of this geometric series show that the Hilbert–Schmidt cost of compressing each factor is at most

$$\sum_j\frac{|d_j^{\pm}|}{\Re u_j}\left|\frac{u_j-b}{u_j+b}\right|^k. \tag{K4}$$

This uses the sum of the two rank-one perturbations obtained by projecting first the left and then the right argument. The finite Laguerre matrix entries are Hankel and use the same coefficient with index equal to the sum of the two Laguerre indices.

Let $n_\pm$ bound the Hilbert–Schmidt norm of the two finite-rank operators, and let $\epsilon_\pm$ be the corresponding summed errors from (K2)–(K4). The trace norm of the Hankel product error is at most $\epsilon_+n_-+\epsilon_-n_++\epsilon_+\epsilon_-$. A standard Fredholm perturbation bound propagates this to the determinant even at a zero. For improved quantitative propagation, when the numerical finite section certifies invertibility of $K=I-\widetilde{H}_+\widetilde{H}_-$, use multiplicativity of the Fredholm determinant. If ν bounds the norm of $(I-\widetilde{H}_+\widetilde{H}_-)^{-1}$ on the half-line and η bounds product error in trace norm, the sharper allowance is

$$|\det K|\big(e^{\nu\eta}-1\big).$$

Here $\nu\le 1+\|K^{-1}(I-K)\|_{\mathrm F}$ in the orthonormal Laguerre coordinates. All finite nodes, weights, source values, matrix operations and the final prefactor from (15.5) use ball arithmetic. The determinant is evaluated without assuming that the limiting source is nonzero.

Outer quadrature. The source is symmetric in p,q by $\det(I-H_+H_-)=\det(I-H_-H_+)$. For a real ρ, angular averaging uses the full periodic trapezoid rule, pairing reflected nodes. If the shift strip of half-width σ has source bound M, the aliasing charge is $2M/(e^{N\sigma}-1)$ for N equally spaced nodes. This follows by the Laurent coefficient estimate on the two circular contours. With Cartesian frequency $\alpha=\rho\cos\theta$, $\beta=\pm\rho\sin\theta$, the imaginary Euclidean shift on $\Im\theta=\pm\sigma$ is $\rho\sinh\sigma$ and the real Euclidean norm is $\rho\cosh\sigma$. Thus any bound for complex Cartesian shift of size $1/2$ applies with $\sigma=\operatorname{arsinh}(1/(2\rho))$.

On a retained radial panel $[x,y]$, use Gauss–Legendre with ellipse parameter 2 and $3(y-x)/8\le 1/2$, $x-(y-x)/8>0$. If M_D bounds the source on the radial ellipse and $d=x-(y-x)/8$, then $M_Dd^{-2\Re h-1}e^{\pi|\Im h|}$ bounds the radial integrand there for $2\Re h+1\ge 0$. The quadrature allowance has the same form as (K3); the weighted sum of nodewise angular aliasing, source and numerical errors is added separately. The final Mellin prefactor multiplies all allowances.

For $[0,1]$, set $\Xi(\rho)=(\Phi(\rho)-a_0)/\rho^2$; it has a removable origin since Φ is even and analytic. On the boundary of the parameter-two ellipse of $[0,1]$, $|\rho|\ge 1/8$, hence $\|\Xi\|_\infty\le 64(M_D+|a_0|)$. Interpolate at the n shifted Chebyshev roots and integrate its polynomial against ρ^{1-2h} exactly. Each monomial ρ^k gives the factor $1/(k+2-2h)$. A Chebyshev coefficient of order $k\ge n$ aliases to a signed polynomial of norm at most one at those roots. Hence the interpolation error is at most $4\|\Xi\|_\infty 2^{-n}/(1-1/2)$; integrate its absolute weight using $1/(2-2\Re h)$. The mass a_0 comes from an independently validated origin jet, and its separate finite-part term is $-a_0/(2h)$. All costs include the error in this jet, its use at each node, and the certified angular and numerical source errors.

Validated angular integration before absolute values at depth one

The analytic comparison rank also allows use of the actual Bessel tail kernel. At the same exact target $c=1$, $s=1/2+i/20$, $h=1/2+i/8$, the absolute Mellin allowances proved here are below $0.221172, 0.164811, 0.140756, 0.104487$ at $R=4,5,6,8$, respectively. Thus the finite-band angular integration beats the direction-uniform estimate (19.D2) at these cutoffs. It alone does not reach a high-accuracy tail.

For $x\ge 0$, write

$$Q_h(x)=\int_1^\infty v^{-2h-1}J_0(vx)\,dv.$$

The absolute bound $|Q_h| \le (2\Re h)^{-1} = 1$ holds globally. The hard-cutoff Laplace–Mellin identity in (15.7) gives

$$Q_h(x) = 2^{-2h-1}\frac{\Gamma(-h)}{\Gamma(1+h)}x^{2h} - \sum_{j=0}^{\infty}\frac{(-x^2/4)^j}{(j!)^2(2j-2h)}. \tag{19.D4}$$

For a direct justification, first use the Bessel Mellin identity in the absolute convergence strip $-1/4 < \Re h < 0$, then subtract the constant on $(0,1)$ and continue to $0 < \Re h < 1$. Equivalently in this latter strip, integrate the series of $J_0(vx) - 1$ on $(0,1)$ and restore the explicit $1/(2h)$ constant from $\int_1^\infty v^{-2h-1}dv$. All powers in this equation use the real logarithm. For $x > 0$, the representation $Q_h(x) = x^{2h}\int_x^\infty t^{-2h-1}J_0(t)dt$ also gives

$$xQ_h'(x) = 2hQ_h(x) - J_0(x), \qquad |Q_h'(x)| \le (|2h|+1)/x.$$

Certified shape bound. For each of the four R, the following polynomial $P_R(X) = a_R + b_R X + d_R X^2$ majorizes $|Q_h(R\sqrt{X})|$ on $X \ge 0$:

R	a_R	b_R	d_R	lower verified panel margin
4	1.02	−2.25	1.50	0.0860
5	1.02	−2.46	1.61	0.0667
6	1.02	−2.73	2.04	0.0690
8	1.02	−2.46	1.62	0.0625

The coefficients are exact decimals. On $0 \le r = \sqrt{X} \le 1/40$ or $r \ge 5/4$, the polynomial is above one by its explicit coefficients and monotonicity at the upper endpoint. On the intervening interval the replay `bessel_bridge.py` uses 2450 rational panels of length $1/2000$ in r. At each midpoint r_0, evaluate (19.D4) through order 63 with outward complex arithmetic. For the series from order 64 onward, use its first absolute term divided by $1 - q_0$, where $q_0 = (Rr_0)^2/[4(65)^2]$, using also $|2j-2h| \ge 128 - 2\Re h$. The change of $Q_h(Rr)$ from its midpoint is at most $(|2h|+1)/(4000r_{\text{left}})$. Evaluate the polynomial on the full closed panel and subtract these absolute allowances to obtain the positive reported margins. This validates the shape bound without assumptions about the sign or decay of the actual complex mark density.

Matched real moments at the bridge rank. Use the single integer $N = 10^{60}$ and $M = 1024$ for the analytic interval of physical frequencies up to M. No determinant at this rank needs to be evaluated. Equation (19.D1)'s preceding comparable-rank proof gives the uniform discrepancy $\delta_M = L(2+M)^{4(1-\lambda)}N^{-q}$ between the original complex finite and limiting transforms there. The matching real measure $\mu_{N,1,1/2}$ retains its mass. Define $m_{j,N} = \int |y|^{2j}\, d\mu_{N,1,1/2}(y)$. Strong Szegő with imaginary source of norm 3 bounds the real positive exponential moment uniformly in direction by $\exp(3/2 + 9/4)$. Angular averaging and the term $3^6r^6/2304$ of $I_0(3r)$ give $m_{3,N} \le M_3 = 2304e^{15/4}/729$. The same holds for its limit and $m_{2,N}, m_{2,\infty} \le M_2 = M_3^{2/3}$ since their masses are at most one. To transfer the validated origin jets of the limiting real measure to rank N use $t = 1/1000$. The uniform real-axis source error at radii $0, t, 2t$ is at most $e = C(2+2t)^4/N$ by (19.M4). Angular cosine Taylor expansion gives $\Phi_N(r) = m_{0,N} - m_{1,N}r^2/4 + m_{2,N}r^4/64 + \text{rem}$ with $|\text{rem}| \le M_3 r^6/2304$, for either rank. From $\Phi_N(t) - \Phi_N(0)$ and $\Phi_N(2t) - 4\Phi_N(t) + 3\Phi_N(0)$, explicit allowances for the three finite-to-limit moment comparisons are

$$e, \qquad 8e/t^2 + 2M_2t^2/16 + 2M_3t^4/576, \qquad \frac{16}{3t^4}\{10e + 136M_3t^6/2304\}.$$

These are added to the respective exact dyadic discs of the real depth-one control `jet_half_tight.json`. Only these matched real preparatory moments enter the polynomial majorant. The original complex observable stays independent of the real comparison tilt.

Final budget. Angular integration on $[R, M]$ before absolute values is justified with μ_N by the fixed-rank comparison following (19.D2). For that fixed measure, absolute domination by $\mu_{N,1,1/2}$ costs $N^{1/400}$. Consequently, with $\mathfrak{b}(M)$ the limiting residual allowance (19.D2) beyond M, the complete limiting tail allowance is

$$\mathfrak{b}(M) + \frac{17}{16}\left(\frac{N^{1/400}}{R}\sum_{j=0}^{2}P_{R,j}m_{j,N} + \frac{N^{1/400}m_{0,N}}{M} + \delta_M\left(\frac{1}{R} - \frac{1}{M}\right)\right) \tag{19.D5}$$

using upper interval bounds for the right side. The first term within parentheses bounds the integrated finite mark tail beyond R. The second bounds restoring the part beyond M in that finite measure, and the last is the error of the finite-band bridge. For $R = 4$, for instance, the contributions in `bessel_bridge.json` are dominated by the first, from the global quadratic shape majorant. The direct numerical shortfall relative to 10^{-12} is therefore in a positive majorant of a sign-changing spatial kernel, after angular integration. Further progress to that tolerance requires cancellation in the pairing with the real or complex mark law beyond what the three matched moments can certify.

Retaining an explicit complex part of the Bessel tail. A smaller disk follows by subtracting a complex polynomial in $X = |y|^2$ from $Q_h(R|y|)$ before taking an absolute bound. Use $P_R(X) = a + bX + dX^2$ to majorize $\left|Q_h(R\sqrt{X}) - q_R(X)\right|$; the exact decimals for P_R and for q_R in ascending degree are

R	a	b	d	$q_{R,0}$	$q_{R,1}$	$q_{R,2}$
4	.54	−1.42	1.22	$.445 - .137i$	$-1.647 + .373i$	$1.155 - .232i$
5	.59	−1.49	1.18	$.395 - .127i$	$-1.407 + .384i$	$1.101 - .249i$
8	.590	−1.458	.954	$.385 - .102i$	$-.966 + .268i$	$.622 - .172i$.

The validation on $.001 \le r \le 2$ uses the midpoint and tail series of (19.D4), through degree 95 in x^2, with the same radial Lipschitz bound plus the derivative of q_R. On $0 \le r \le .001$ compare to $Q_h(0) = 1/(2h)$: the direct series and $\Re h = 1/2$ bound the change by $\left|2^{-2h-1}\Gamma(-h)/\Gamma(1+h)\right| Rr + w/[(2 - 2\Re h)(1 - w/4)]$, $w = R^2r^2/4$.

For $r \ge 2$ the bound $|Q_h(Rr)| \le 3(Rr)^{-3/2} < .14$ is enough. Indeed $f(x) = \sqrt{x}J_1(x)$ satisfies $f'' + q(x)f = 0$, $q(x) = 1 - 3/(4x^2)$; the derivative of $(f'^2 + qf^2)/q$ is $-q'f'^2/q^2 \le 0$ on $x \ge 2$. The explicit data $J_0(2), J_1(2)$ and $f'(2) = \sqrt{2}J_0(2) - J_1(2)/(2\sqrt{2})$ give $\sqrt{x}|J_1(x)| \le C$, where the replay verifies $C(1+|2h+2|/(2\Re h+3/2)) < 3$. Integration by parts with $(xJ_1(x))' = xJ_0(x)$ gives the claimed bound. For $X \ge 4$ a check of the coefficients in $X - 4$ gives $P_R - .14 > 0$ and $(P_R - .14)^2 - |q_R|^2 \ge 0$ on this ray. These three regions verify the majorant globally.

Use now the analytic comparison rank $N = 10^{100}$, still at $M = 1024$. For the new shift use the normalized *complex* finite moments, retaining their exact tilt. Their limiting source jets are the exact dyadic disks of the depth-one complex integer-moment control `jet_complex_reference.json`. For the finite-to-limit comparison, at $t = 10^{-5}$ perform the same real radial finite differences as above, now using the complex rank error from (19.D1) on $0, t, 2t$. The finite complex Taylor remainder is bounded by $C_{\mathrm{fin}}r^6$, $C_{\mathrm{fin}} = N^{1/400}M_3/2304$. For the limiting complex transform, (19.D3) on the complex radial disk of radius 1/2 gives modulus below 1000. The angular average is even in the radial argument, so Cauchy's coefficient estimate gives a remainder $C_{\mathrm{lim}}r^6$ with $C_{\mathrm{lim}} = 128000$ on $0 \le r \le 2t$. The triangle bound on the second moments needed for the first difference formula is $1024 \cdot 1000 + N^{1/400}M_3^{2/3}$, by the fourth coefficient Cauchy bound and the matched real moment. The complex moment errors and dyadic centers are then propagated into

$$\frac{2^{2h+1}\Gamma(1+h)}{\Gamma(-h)} R^{-2h} \sum_{j=0}^{2} q_{R,j} m_{j,N}^{(s)}.$$

Add the limiting residual tail, the finite bandwidth mismatch, and the shape allowance as in (19.D5), now with P_R majorizing the residual rather than the full Bessel kernel. The script `centred_bessel.py` returns tail centers approximately $-.036491674 + .026083087i$ and $-.031887332 + .021860469i$ for $R = 4, 5$, with respective radii below .163024 and .136794. At $R = 8$ it returns a center near $-.021682373 + .015559189i$ and radius below .076273. The same three-region validation was executed with the displayed $R = 8$ polynomials. The use of complex signed jets keeps this calculated low-degree piece inside the scalar rather than in its error allowance. The remaining shape majorant still dominates the radius.

Hybrid tail budget, compact scope and nearby order

At the primary depth-one tuple one can combine the normalized Gram comparison of Section 19 (shifted-source Gram comparison) with the real-tilt angular trace deficit (D.2). Indeed for physical sources $b = 0$, factoring the positive static Gram as in the proof of (19.D3) compares the determinant to the same contraction $e^{iB_l}K_0$ as in (D.2). The static determinant is positive and at most one. The trace displacement is at most $E_{\mathrm{def}}/(1 - g)$. Use

the contraction deficit in the determinant bound before including that displacement rather than discarding it as in (19.D3). The angular result (D.4) then applies with $L_0 = (\rho/8)^{1/3}$, $\gamma = 1/20$,

$$p = \frac{2KJ}{1-g}, \qquad A = \exp\{p[\log(402) + C_0] + 4K^2\epsilon/(1-g)\}.$$

Here $2M \le 402(2+\rho)$, as $M = \lceil 400 + 3\rho \rceil$. For $R > 8 \cdot 20^3$, let $L = (R/8)^{1/3}$. The angular factor bounds the weighted integrand by

$$2A(1+2/R)^p \left(1 + \frac{2}{\gamma L} + \frac{2}{(\gamma L)^2}\right) R^{p-7/3} \exp[\,\gamma(20 - (\rho/8)^{1/3})\,], \qquad \rho \ge R.$$

To obtain this, use the last entry in (D.4), bound its two decreasing rational factors at R, and use $p - 7/3 < 0$. The remaining integral in ρ is exactly $24e^{\gamma(20-L)}(L^2/\gamma + 2L/\gamma^2 + 2/\gamma^3)$. With the Mellin prefactor 17/16, the Arb replay gives allowances below $1.468 \cdot 10^{-11}$ at $R = 3 \cdot 10^7$ and $6.170 \cdot 10^{-13}$ at $R = 6 \cdot 10^7$. This prices a high-accuracy tail in isolation, leaving the cost of that retained annulus open.

Parameter-uniform comparison. The short-rectangle argument of Section 19 (finite-rank comparison) can be priced uniformly on

$$\frac{99}{100} \le c \le \frac{101}{100}, \quad |\Re s - 1/2| \le \frac{1}{100}, \quad |\Im s| \le \frac{3}{50}, \quad |\Re h - 1/2| \le \frac{1}{100}, \quad \frac{11}{100} \le \Im h \le \frac{7}{50}.$$

Use the same rectangle and its reflection, $\lambda = 7/25$, and $A_0 = \max(1, c_-^{-(5/4)^2})$. The harmonic measure majorant is bounded by $\frac{3}{50H} + 2\sqrt{2}e^{-\pi(W-1/100)/(2H)} < \lambda$. In the short-rectangle proof use the real rank bound C from (19.M4) on this depth interval. Replace the nonreal-edge bound by $A_0 b_N$; equivalently insert A_0^λ in the numerator defining L and replace the rank threshold $C/2^{H^2}$ by $C/(A_0 2^{H^2})$, before taking its power. Then (19.D1) holds with the anchor term multiplied by A_0 and exponent $k(3/50)^2 < .01476$. For real-order lower bound u_0, the tail is bounded by

$$P_* R^{-2u_0} \left\{ \frac{A_0(1+B_\delta)^{(3/50)^2}(R+2)^{k(3/50)^2}}{2u_0 - k(3/50)^2} + \frac{\delta}{2u_0} \right\},$$

where P_* bounds the normalized Mellin prefactor. Validated evaluation yields a uniform allowance below .36370 at $R = 8$ for the displayed compact. At the distinct tuple $c = 101/100, h = 51/100 + 7i/50, s = 49/100 + 3i/50$, the same allowance is below .18710. This calculation tests the tail and does not involve retained-integral quadrature.

A certified nearby independent order. At fixed $c = 1, s = s_*$ set $h' = 1/2 + 63i/500$, and let $K(h)$ be the normalized Mellin prefactor. Divide the scalar by $K(h)$ before comparing the two orders. In the finite part at origin the change of the constant term is at most $|a_0|\,|(2h')^{-1} - (2h)^{-1}|$. In the two integrals use $|\rho^{-2(h'-h)} - 1| \le 2|h' - h|\,|\log\rho|$. For $0 < \rho \le 1/8$ enclose $\Phi - a_0$ by the two validated nonconstant jets and the order-six Cauchy remainder on $|\rho| = 1/2$ from (19.D3). For $1/8 \le \rho \le 1$ use (19.D1) and $|a_0|$; above 1 use (19.D1) with $2 + \rho \le 3\rho$. The three resulting $\rho^{-2}|\log\rho|$ integrals are elementary. Multiplying the returned variation budget by $|K(h')|$ and propagating the disk by $K(h')/K(h)$ gives the nearby-order enclosure at this fixed preparation. The bound uses ordinary holomorphic order variation and is independent of the numerical determinant samples for the original disk.

Independent finite-Haar source check. At $c = 1$, $s = 1/2 + i/20$ and any of the registered finite ranks n, let $z = \sqrt{1 - 1/n}$. Use the original-circle finite Toeplitz matrix, with $d = 1/n$, from the symbol

$$a(\theta) = \exp\left\{ s[\log(1 - ze^{i\theta}) + \log(1 - ze^{-i\theta})] + \tfrac{i}{2}\left[p\,\frac{de^{i\theta}}{1 - ze^{i\theta}} + q\,\frac{de^{-i\theta}}{1 - ze^{-i\theta}} \right] \right\}, \quad q = \bar{p}.$$

The eigenangle density formula gives the finite unnormalized source $n^{-s^2}\det[\widehat{a}(j-k)]_{j,k=0}^{n-1}$. This exact finite-rank representation is independent of the limiting contour-Hankel and exterior-propagator computations. It also preserves the multiplier n^{-s^2} before taking the determinant limit.

Let $\delta = -\frac{1}{2}\log z > 0$, $Q = ze^{\delta} < 1$ and $\rho = |p| = |q|$. Both logarithms are analytic in $|\Im\theta| \le \delta$, since their arguments have positive real part there. On the strip

$$|a(\theta)| \le A := \exp\left[-2|\Re s|\log(1-Q) + \pi|\Im s| + \frac{\rho d e^{\delta}}{1-Q}\right].$$

Indeed each logarithm argument has modulus between $1-Q$ and $1+Q$, with argument bounded by $\pi/2$. Shifting the Fourier contour gives $|\widehat{a}(k)| \le Ae^{-\delta|k|}$. If $L \ge 2n$ grid points are used, their normalized discrete Fourier coefficient at index $|k| < n$ differs from $\widehat{a}(k)$ by at most

$$\frac{2Ae^{-\delta(L-n+1)}}{1-e^{-\delta L}},$$

by absolute convergence of the alias sum. The check computes this allowance in Arb, propagates the whole coefficient balls through the finite matrix determinant, and saves exact dyadic component radii. The finite-rank source checks and a separate floating finite-rank Mellin sequence are separate deliverables. The latter shows the observed convergence across ranks at fixed numerical cutoff. It supplies a diagnostic comparison of the limiting scalar calculation because neither the finite-rank scalar discrepancy nor the floating scalar tail is charged there.

Pricing a frequency window on one comparison rank

Write $h = 1/2 + i/8$, $s = 1/2 + i/20$, $c = 1$, and $\kappa = 2^{2h+1}\Gamma(1+h)/\Gamma(-h)$. Thus $|\kappa| = 17/16$. On each positive annulus the scalar readout is $\kappa \int \rho^{-2h-1}\Phi(\rho)\,d\rho$, with angular average $\Phi = (2\pi)^{-1}\int D_{\infty}(\rho e^{i\theta})\,d\theta$. The origin subtraction occurs only in the integral through one. The unnormalized finite complex measure includes N^{-s^2}. All powers of a positive number use its real logarithm.

A finite-rank quadrature estimate. At $N = 10^{100}$, let δ_b be the dyadic telescope bound on the physical disk of radius b preceding (19.D1). The check $2C(2+b)^4/N \le 2(2N)^{1/16}$ permits the short rectangle used there. At this rank the modulus of the complex preparation is bounded by $N^{1/400}$ times the positive real-tilt preparation. For any Cartesian imaginary translation of norm t the finite source has modulus at most

$$A(t) = N^{1/400}\exp(t/2 + t^2/4).$$

Indeed the real plane wave has modulus one, and the exponential moment of its imaginary part under the matched real tilt obeys Lemma 5.9, with $z = \sqrt{1-1/N}$, $|u| = 1/2$, and $c = 1$. This also bounds the angular average on a complex radial ellipse.

Let $[a,b] \subset (0,\infty)$, $w = b-a$, and let (r_j, v_j) denote the n-node Gauss–Legendre rule on this interval. The v_j are positive. Use l equispaced angles and set $V = \sum_j v_j r_j^{-2}$. For the exact limiting source at the sampled points, the discrepancy of the two-dimensional rule is at most the sum of the following three charges:

$$\begin{aligned} E_{\text{bridge}} &= |\kappa|\delta_b(1/a - 1/b + V),\\ E_{\text{angle}} &= 2|\kappa|VA(b\sinh\sigma)/(e^{l\sigma}-1),\\ E_{\text{radial}} &= 4|\kappa|wA(t)e^{\pi/8}x^{-2}q^{-2n}/(1-q^{-1}). \end{aligned}$$

Here $\sigma > 0$, $q > 1$, $x = (a+b)/2 - w(q+q^{-1})/4 > 0$, and $t = w(q-q^{-1})/4$.

To prove the bound, replace the integrated limiting source and the sampled limiting source by the same finite-rank source at their real arguments. The changes cost E_{bridge} by the physical comparison and positivity of the weights. On $|\Im\theta| \le \sigma$ the imaginary Cartesian translation is at most $b\sinh\sigma$; the geometric sum of omitted Fourier aliases yields E_{angle}. On the radial Bernstein ellipse the analytic weight has modulus at most $e^{\pi/8}x^{-2}$ because $|\arg\rho| < \pi/2$. The Chebyshev tail after degree $2n-1$ is at most $2A(t)e^{\pi/8}x^{-2}q^{-2n}/(1-q^{-1})$. The Gauss rule is exact on that polynomial, and both positive integration operators have mass w. This proves the last charge. A real taper $0 \le \chi \le 1$ does not increase the bridge or angle prices. For a polynomial taper the radial price is multiplied by a bound for $|\chi|$ on its chosen ellipse. Every source approximation and its determinant perturbation enter with the absolute weights actually used. The proof needs complex arguments only at the comparison rank.

With the same dyadic midpoints, the seven old positive annuli now cost less than $2.90 \cdot 10^{-8}$ together. The following origin estimate reduces the complete retained price through eight to less than $3.27 \cdot 10^{-8}$. The positive annulus computation replays in verification_window/bridge_quad.py.

The removable origin quotient at a fixed comparison rank. The finite-rank strip estimate also prices the existing origin nodes. Let Φ_N, Φ be the finite and limiting circular averages at the specified tuple and $N = 10^{100}$. Put $\Delta = \Phi - \Phi_N$ and let δ be the physical comparison error through radius one from the dyadic telescope preceding (19.D1). Write $A(b) = N^{1/400}\exp(b/2 + b^2/4)$ for the finite-rank envelope. On the complex radial circle of radius $1/2$, the even analytic function Δ is bounded by M, the sum of (19.D3) evaluated with both real and imaginary size $1/2$, and $A(1/2)$. The geometric sum of its even Cauchy coefficients gives $|\Delta(r) - \Delta(0)| \le (16M/3)r^2$ for $0 \le r \le 1/4$. On $[0,1]$ the physical comparison also gives $|\Delta(r) - \Delta(0)| \le 2\delta$. At $e = 2^{-81}$ the change in the subtracted continuous integral, before multiplying by $17/16$, costs at most

$$(16M/3)e + 2\delta(e^{-1} - 1).$$

Indeed its absolute radial weight is r^{-2}. The finite-part mass $-\Phi(0)/(2h)$ stays in the limiting formula on both sides.

For the finite integral apply the original Chebyshev rule to the entire quotient $\Xi_N(r) = (\Phi_N(r) - \Phi_N(0))/r^2$. For the Bernstein ellipse of $[0,1]$ with parameter $t > 1$, put $d = (t + t^{-1} - 2)/4$ and $b = (t - t^{-1})/4$. Its boundary has $|r| \ge d$ and $|\Im r| \le b$ by the ellipse parametrization. Its quotient is bounded by $(A(b) + A(0))/d^2$. With n roots the Chebyshev coefficients and their signed aliases give an interpolation error at most four times this bound times $t^{-n}/(1 - t^{-1})$. Integration against r^{1-2h} has absolute weight one at this input. At the retained nodes let w_j be the complex interpolatory weights before dividing by r_j^2. The change back from finite to limiting samples in the discrete subtracted rule costs at most $2\delta\sum_j |w_j|/r_j^2$. The finite angular alias at each node with n_a angles and strip $\sigma > 0$ costs at most $2A(r_j \sinh\sigma)/(e^{n_a\sigma} - 1)$, multiplied by $|w_j|/r_j^2$. Each price receives the Mellin modulus $17/16$. These comparisons use a physical-frequency discrepancy only on real arguments. Large complex shifts are applied to the finite positive majorant at its single specified rank.

At the inherited $n = 29$, $n_a = 38$ nodes, $t = 30$ gives a radial allowance below $1.219 \cdot 10^{-36}$ and nodewise choice of the angular strip gives less than $7.431 \cdot 10^{-39}$ in total. The continuous bridge costs less than $6.376 \cdot 10^{-22}$ and the discrete bridge less than $2.510 \cdot 10^{-43}$. Retaining the source, arithmetic and origin-jet charges at their upper endpoints therefore gives the same origin midpoint with radius below $3.6920 \cdot 10^{-9}$. The exact calculations are in `verification_window/audit_origin.json`.

Two signed readouts of the first transition. Put $p = 2^{2h+1}\Gamma(1 + h)/\Gamma(-h)$ at the registered tuple, and write $H_{a,b}(v) = p\int_a^b v(\rho)\rho^{-2h-1}\Phi_\infty(\rho)\,d\rho$. On $[8,9]$ let $t = \rho - 8$, $u(t) = 10t^3 - 15t^4 + 6t^5$, and $w = 1 - u$. The multiplier equal to one below 8, equal to w on the panel and zero above 9 is C^2, since $u'(t) = 30t^2(1 - t)^2$. Its computed new part is $H_{8,9}(w)$. If T_B denotes the full signed tail above B, the changed complement is exactly $H_{8,9}(u) + T_9$. Both window integrands have zero contact with the origin finite part. In particular, the polynomial moment center belonging to T_8 is replaced in its entirety by the center belonging to T_9.

Here are details of the quadrature for the two polynomial weights. At real nodes $0 \le w, u \le 1$, so the finite-rank bridge and angular aliasing charges for weight one are valid for either. For the radial Gauss charge let $E > 1$ be the ellipse parameter after mapping the panel to $[-1,1]$, and put $v_E = 1/2 + (E + E^{-1})/4$. On this ellipse $|t| \le v_E$. An upper bound for either weight is

$$1 + 10v_E^3 + 15v_E^4 + 6v_E^5.$$

Multiply the finite-rank ellipse bound by this factor before minimizing over E. This prices growth of the polynomial across the integration contour. At each real radial node the periodic angular sum uses reflected pairs by $\det(I - AB) = \det(I - BA)$ as in the keyhole quadrature of Section 19. Each input is a keyhole/Laguerre source disk. The quadrature sums its errors with absolute weights. The retained complex node midpoints receive their signed weights. The same construction applies to a panel $[a,b]$ upon setting $t = (\rho - a)/(b - a)$.

With six radial nodes and forty equispaced angular directions, 126 distinct source calls took 39.61 seconds on three workers. The accepted weighted charges were as follows. Each decimal in the last two columns is rounded

upward.

	w	u
finite source and projection	$9.411\,10^{-9}$	$3.863\,10^{-8}$
radial ellipse ($E = 13$)	$1.058\,10^{-8}$	$1.058\,10^{-8}$
angular strip ($\sigma = 13/20$)	$1.147\,10^{-7}$	$1.147\,10^{-7}$
finite-rank transfer	$3.964\,10^{-47}$	$3.964\,10^{-47}$
ball arithmetic	$9.929\,10^{-41}$	$4.478\,10^{-40}$
disk radius	$1.347\,10^{-7}$	$1.639\,10^{-7}$

The signed center for the falling weight is $0.001962907441708613-0.000661177777619242i$ and for the rising weight it is $0.001662341268017736 - 0.000582175370352909i$ (rounded here). Simple omission of the rising term costs at most 0.014762, using $\int_0^1 u(t)\,dt = 1/2$, $\rho^{-2} \le 1/64$, and the finite-rank variation plus (19.D1) on real physical frequencies. Its signed calculation instead bounds its modulus by 0.001762 and its uncertainty by $1.639\,10^{-7}$. The two individually computed disk radii sum to less than $2.985\,10^{-7}$. Using the common nodes and $u + w = 1$ before summing the errors gives a single radius below $1.627\,10^{-7}$. The discrepancy of the two exact dyadic centers added together from the independently accumulated unit-weight center is below $3.877\,10^{-57}$, within the arithmetic allowance of $1.095\,10^{-39}$. The node disks and all three reductions are in `window_89_taper.json` and `smooth_partition_89.json`.

Measured cost of extending the sources. The pilot at direction $\pi/2$, frequency 9, with 52 Laguerre coordinates, 41 contour nodes per subpanel, and scale 0.8, gave a source radius greater than 19. Changing to 85 coordinates, 49 nodes and scale one gave a radius below $1.10\,10^{-4}$. This comparison determines the source precision before pricing the full residual. On the physical axis $\zeta = 8, 10$, the new pilot midpoints differed from the inherited higher-order keyhole results by less than $1.68\,10^{-18}$ and $1.54\,10^{-18}$, respectively. Both pairs of outward disks intersect. These are controls of the same determinant implementation under different discretizations.

The first four fresh unit panels used the following signed sources. The last column is the complete Mellin error on the indicated panel. The times are elapsed seconds of the individual run; some runs overlapped in wall time.

$[a, b]$	n_{rad}	n_{ang}	calls/time (s)	radius below
$[8, 9]$	6	44	138/30.78	$2.5130\,10^{-7}$
$[9, 10]$	6	48	150/36.73	$4.6564\,10^{-7}$
$[10, 11]$	5	48	125/40.87	$1.2522\,10^{-7}$
$[11, 12]$	5	48	125/52.55	$5.8825\,10^{-7}$

A limiting-strip angular majorant on these deliberately sparse grids alone charged more than 0.6255 on $[8, 9]$ and 0.5268 on $[9, 10]$. Transferring the whole quadrature discrepancy across the finite-rank physical band reduced those angular terms to $7.710\,10^{-9}$ and $7.193\,10^{-9}$. The source sums, exact dyadics, ellipse and strip choices, and alternative estimates are in `new_bands_12.json` and its four raw receipts.

The angular contour mean on a wider band. For a real vector ξ with imaginary displacement η, taking the modulus of the finite Haar integrand gives a positive real-tilt symbol. Its Szegő quadratic form, obtained from the Fourier coefficients in Section 11, gives at the comparison rank Q and radius $z = \sqrt{1 - 1/Q}$ the estimate

$$|D_Q(s; \xi + i\eta)| \le Q^{1/400} \exp\bigl(|\eta|^2/4 + z\eta_1/2\bigr).$$

The sign of η_1 follows the convention that the real-tilt Gaussian shift is $-z/2$. Both signs have the same angular mean. At $\theta \pm i\sigma$ the displacement is of fixed length $d = r \sinh \sigma$ and its direction makes one complete rotation. Hence the *mean* modulus along either translated circle is bounded by $A = Q^{1/400} e^{d^2/4} I_0(zd/2) \le Q^{1/400} e^{d^2/4} I_0(d/2)$. Cauchy's formula on these circles gives the same Fourier coefficient bounds $Ae^{-|m|\sigma}$ as a supremum estimate. Summing over the nonzero multiples of n_{ang} prices the aliasing by $2A/(e^{n_{\mathrm{ang}}\sigma} - 1)$. Each real Gauss node admits its own σ; use its measured radius and positive Gauss weight in the sum, along with the absolute value of any taper at that node. The finite-to-limit bridge is once again used on the real quadrature and the real integral. This argument requires directional exponential moments solely at the fixed finite rank.

For $[12, 16]$, 196 source calls on a 7 by 54 grid took 154.87 seconds on six workers. Its signed value is near $-0.002306692609378653 + 0.001058733175489664i$. The maximum-radius strip estimate charged $2.987\,10^{-5}$ in

angular error. The mean-contour calculation reduces it to $1.221\,10^{-6}$ and gives complete radius below $1.649\,10^{-6}$, including $3.898\,10^{-7}$ for radial quadrature and $3.868\,10^{-8}$ for the validated determinants. At the first smooth grid the same mean-contour estimate gives a sharp $[8,9]$ radius below $5.684\,10^{-8}$. Exact refinements are in `window_1216_mean.json` and `window_89_mean.json`. For every new wide-panel computation the program can replace an unusable pointwise determinant disk by the disk centered at zero of radius $Q^{1/400}+\sup_{|\xi|\le b}|D_Q-D_\infty|$ from (19.D1). Every sample through 16 retained its determinant disk.

Two fresh floating evaluations use different source constructions on these same signed panels. A 72-coordinate Hardy compression agrees with the four unit-panel keyhole centers to within $1.63\,10^{-12}$ in modulus and with the $[12,16]$ center to within $1.04\,10^{-13}$. The 96-dimensional finite Haar determinant gives $-0.002321049 + 0.001065471i$ on $[12,16]$ at its exact depth-one radius, a deviation of $1.59\,10^{-5}$ from that limiting center. Both comparisons are diagnostics. The files `window_exterior72.jsonl` and `window_finite96.jsonl` record radii, grids and timings. The physical source grids, pilots, weighted reductions and ellipse prices can be repeated with `replay_frequency.py`.

The last physical panel $[16,20]$ used six radial and 64 angular nodes. All 198 distinct source calls returned usable determinant disks in 476.74 elapsed seconds on four workers. Its signed center is $-0.000535879476527531 + 0.000320250687768481i$ (rounded). The mean-contour angular charge is below $2.345\,10^{-6}$, the radial charge below $3.864\,10^{-6}$ and the determinant charge below $2.039\,10^{-7}$. Transfer and final arithmetic cost less than $3.2\,10^{-46}$ together. The complete panel radius is below $6.413\,10^{-6}$. The independent exterior truncation differs from this center by less than $1.034\,10^{-11}$. The two finite Haar rank diagnostics $96, 192$ give real parts -0.0004974362 and -0.0005165395, respectively. The file `window_1620_mean.json` records the exact wide-panel disk.

An infinitely differentiable transition with priced leakage. There is also a smooth split on the remaining half-line $[8,\infty)$ that can use each measured sharp window. Let T have any symmetric probability density of class C^∞ supported in $[-\epsilon,\epsilon]$, for instance a normalized $\exp(-1/(1-(t/\epsilon)^2))$ on $|t|<\epsilon$. At $B-\epsilon\ge 8$, set $\chi(\rho)=\Pr\{B+T\ge\rho\}$ and $d(\rho)=\chi(\rho)-\mathbf{1}_{\rho\le B}$. Fubini gives $\int d=0$, $\int|d|=\mathbb{E}|T|\le\epsilon$, and $\int|\rho-B||d(\rho)|\,d\rho=\mathbb{E}(T^2)/2\le\epsilon^2/2$. For $a=B-\epsilon$ the difference between the two signed windows costs at most

$$L_\epsilon=|\kappa|\left[\frac{\epsilon^2N^{1/400}}{2}\left(\frac{|2h+1|}{a^3}+\frac{\sqrt{2\exp(3/4)}}{a^2}\right)+\frac{\delta_{B+\epsilon}\,\epsilon}{a^2}\right].$$

Indeed, for a real mark projection X the matched real measure has mass at most one and $\int X^2\le\int(\exp X+\exp(-X))\le 2\exp(3/4)$. Cauchy–Schwarz bounds the first moment. This prices the derivative of $\rho^{-2h-1}\Phi_N(\rho)$ at all real points of the transition. Subtract its value at B and apply the mean-zero identity. Only the rank discrepancy on this short real interval remains.

If H is the measured sharp window and T_B its priced complement, write the smooth window and remainder as $H+D$ and T_B-D. The leakage variable D is identical in these two expressions. Independent treatment costs at most $2L_\epsilon$; keeping the shared variable in the sum cancels it exactly. At $B=9$ one edge costs less than 0.000429 for $\epsilon=1/8$ and 0.00002618 for $\epsilon=1/32$. The latter width puts the independently charged pair below 0.000053, well under the measured first-window contribution. The complete calculation for three transition widths is in verification_window/smooth_edge.json.

A changed Bessel residual and a spatial check on the signed window

Throughout this calculation $(c,h,s)=(1,1/2+i/8,1/2+i/20)$. Write $A_h=2^{2h+1}\Gamma(1+h)/\Gamma(-h)$, with $|A_h|=17/16$, and use the unnormalized circular average in (15.5). Let $I_{ab}=A_h\int_a^b\rho^{-2h-1}\Phi_\infty(\rho)\,d\rho$ and let $T_b=I_{b,\infty}$. Both terms are added to the already regularized origin integral. Thus the constant Taylor subtraction, and its finite part at the origin, are paid exactly once.

Polynomial comparison at a single analytic rank. Put $X=|y|^2$ and use Q_h from (19.D4). For a tail take $K(r)=Q_h(br)$, $v=b^{-2h}$. For a finite window take

$$v=1/a-1/b,\qquad K(r)=\{a^{-2h}Q_h(ar)-b^{-2h}Q_h(br)\}/v.$$

In each case $vK(r)$ is exactly the mark kernel obtained by angular averaging $J_0(r\rho)$ before integrating in ρ. Suppose the polynomials p,q satisfy $p(X)\ge|K(\sqrt{X})-q(X)|$ on $X\ge 0$. The signed polynomial contribution is

$A_h v \sum q_j m_{j,N}^{(s)}$. The remainder in the finite preparation costs at most

$$|A_h v|\, N^{1/400} \sum_j p_j m_{j,N}^{(1/2)}.$$

On Haar configurations the absolute density at this rank equals $N^{1/400}$ times the matched unnormalized real density. Pushing forward gives the required variation inequality for the mark. All powers here and in the numerical evaluation use the positive-base logarithm. At $N = 10^{71}$ put $M = 131072$ and $e(L) = L_0(2+L)^{4(1-113/500)}N^{-q_0}$, with the telescope constant L_0 and exponent q_0 from (19.D1). For the window add $|A_h|e(b)(1/a - 1/b)$. For the tail add

$$|A_h|e(M)(1/b - 1/M) + |A_h|N^{1/400}m_{0,N}^{(1/2)}/M + \mathfrak{b}(M),$$

where $\mathfrak{b}$ is (19.D2) at $\delta = 1/256$. These follow by first transferring only the finite physical band. In the tail case one then restores the portion above M separately on each side. The replay checks the comparable-rank hypothesis at the largest frequency used. Each new cutoff has its own global shape proof. In particular the polynomial priced at cutoff 8 is removed in its entirety upon using the newly computed window and the residual at b.

Moment transfers. The complex disk at radial radius $1/2$ in (19.D3) has supremum below 1000. Evenness and Cauchy's bound give a sixth-order remainder constant 128000 at radii below $1/10$. For the finite transform the real Taylor remainder of cosine and angular averaging give the constant $N^{1/400}M_3/2304$, with $M_3 = 2304e^{15/4}/729$. Call the sum C_6. Choose $t = (e(1/10)/C_6)^{1/6}$ and verify $2t < 1/10$. The errors on the first two nonconstant complex moments can be bounded respectively by

$$\frac{32e(2t) + 80C_6t^6}{3t^2}, \qquad \frac{16}{3t^4}\{10e(2t) + 68C_6t^6\}.$$

For the first bound use the stencil with coefficients $(-15, 16, -1)$ at $(0, t, 2t)$, which eliminates the fourth Taylor coefficient. For the second use $(3, -4, 1)$, which eliminates the quadratic coefficient. The zero moment costs $e(2t)$. Add the inherited exact limiting moment disk radii, using the higher-precision source jets for orders zero and one. The real moments through order two use the existing real difference proof.

A cubic positive majorant can also use the inherited real third moment in `real_order_control.json`. At $t_0 = 10^{-4}$ use the stencil $(-10, 15, -6, 1)$ at $(0, t_0, 2t_0, 3t_0)$. It annihilates the zeroth, quadratic and quartic terms. The multiplier on the sixth-order moment is $-360t_0^6/2304$. The real bound on $\int I_0(4r)$ is e^6 by the same strong Szegő estimate used in (19.D5), so $M_4 = 4^4(4!)^2e^6/4^8$ bounds the real fourth radial moment at either rank. Taylor's theorem on the real line and averaging the cosine bound the eighth order remainder by $M_4\rho^8/[4^4(4!)^2]$. If C is the real constant from (19.M4), the real third-moment transfer therefore costs at most

$$\frac{2304}{360}\left\{\frac{32C(2+3t_0)^4}{Nt_0^6} + \frac{2 \cdot 8112M_4t_0^2}{147456}\right\}.$$

Every signed polynomial in this construction has degree at most two.

Global shape checks. For example at $b = 9$ the tail proof uses

$$p(X) = .571 - 1.457X + .959X^2 + .002X^3, \quad q(X) = (.390 - .126i) + (-1.049 + .354i)X + (.676 - .244i)X^2.$$

For the normalized window on $[8, 9]$ the corresponding polynomials are

$$p(X) = .764 - 1.189X + .696X^2, \quad q(X) = (.212 - .120i) + (-.532 + .269i)X + (.367 - .188i)X^2.$$

On $0 \le r \le 1/20000$ use the (19.D4) series relative to its value at zero. For the window one may instead use $|1 - J_0(\rho r)| \le (br)^2/4$. From that endpoint through $r = 2$ use adaptive outward panels, the terms of (19.D4) through degree 95 in x^2, and its geometric remainder. The derivative bound for a tail is $(1 + |2h|)/r$. On $br < 1$ the differentiated series also gives

$$b|2hC_h| + b^2r/[2(1 - (br)^2/16)], \qquad C_h = A_h^{-1}.$$

For a window $|K'| \le \log(b/a)/v$ by $|J_0'| \le 1$. The error at a panel midpoint is expanded by the supremum of this derivative plus that of $q(r^2)$ times the panel half-width. Finally on $X \ge 4$ the inherited energy bound gives $|Q_h(b\sqrt{X})| \le 3/(2b)^{3/2}$. For the normalized finite window one can always use $|K| \le 1$. For either bound H, verify that $p - H$ and $(p-H)^2 - |q|^2$ have nonnegative shifted coefficients in $X - 4$, with positive constant. This covers the entire half-line. The floating optimization supplies candidate coefficients only. `mark_shapes.py` performs the enclosure from the rational coefficients with 160-bit ball arithmetic.

Cutoff b	Cubic tail radius	Mark-only $[8, b]$ radius	Complete spatial check
9	.052403	.011104	.063507
10	.046349	.019084	.065433
12	.038729	.028235	.066964
16	.028736	.037167	
20	.023053		

Entries are rounded upwards. The complete spatial checks use the repriced integral through 8, and their new finite-window components use mark moments independently of the new annulus determinant calls. Their exact dyadic disks overlap the corresponding frequency-side window disks in each of the three comparisons. Enlarging the window improves the tail estimate while making its separate mark-only enclosure wider. This explains the use of frequency-side signed windows in the sharper combined calculation.

A smooth window with a priced complement. For $8 \le \rho \le 9$ put $t = \rho - 8$ and $\chi = 1 - 10t^3 + 15t^4 - 6t^5$, and let I_χ denote the corresponding weighted Mellin integral. It extends the constant retained weight on the left to zero on the right with two continuous derivatives. The exact residual after adding I_χ to the retained readout is $T_9 + I_{89} - I_\chi$. Since $0 \le 1 - \chi \le 1$ and $\int_8^9 (1-\chi) = 1/2$, using (19.D1) at the fixed rank 10^{48} on this band gives

$$|I_{89} - I_\chi| \le \frac{17}{16 \cdot 128}\{(10^{48})^{1/400} + e_{48}(9)\} < .010942598,$$

where e_{48} is the preceding band discrepancy at that rank. With the directly computed quintic window the resulting full radius is below .063345385. Evaluating the signed complementary weight by subtraction of the same quintic from the sharp window allows exact symbolic cancellation on recombination. The full radius with this cubic residual is then below .052402816 at $b = 9$. The disk for the complementary weight plus tail has its own outward receipt in `mark_comparison.json`. These bounds concern the displayed input and the cutoffs whose coefficients were checked. Tightening finite arithmetic with the same spatial envelopes leaves the positive shape allowance in the budget.

Independent check of the positive Bessel envelopes. The spatial inequality using measured real-tilt Bessel moments was also verified at $R = 16, 20$ by a second evaluation of the tail kernel. In (19.D4) the identity $(-h)_j/(1-h)_j = (-h)/(j-h)$ gives

$$Q_h(x) = C_h x^{2h} + \frac{1}{2h}\,{}_1F_2(-h; 1, 1-h; -x^2/4).$$

`mark_crosscheck.py` calls the ball hypergeometric function and encloses the first derivatives at panel midpoints using $r\,\partial_r Q_h(Rr) = 2hQ_h(Rr) - J_0(Rr)$ and $J_0' = -J_1$. It prices the quadratic Taylor error for both sides and checks the origin and exterior separately. The two full half-line bounds passed with 229 and 212 finite panels, respectively. This independently checks the spatial approximation step. The moment and determinant inputs remain shared with the first calculation. The same independent check of the joint signed-shell and positive Bessel envelopes at $R = 16, 20$ took 1237 and 1006 panels. For a shell $[a, b]$ it evaluates $a^{-2h}Q_h(ar) - b^{-2h}Q_h(br)$ from two hypergeometric values. The independently evaluated derivatives enclose the midpoint Taylor error for the complete spatial residual. The inputs and verification receipts are in `mark_joint_check.json`.

The independent checks use frozen candidate files and their SHA-256 digests in `mark_crosscheck_inputs/`. The checkers verify each digest before reading its coefficients. The final expanded envelopes, with real controls through 16, used the separately frozen constant slack 0.000006 and coefficient slack 0.0000001 on r^2. The independent check certified the entire half-line at $R = 16, 20$ using 6544 and 4518 finite panels. In the latter case it includes the signed shell $[16, 20]$. See `mark_joint_final_check.json`.

Signed control from the measured frequency windows. Fix the benchmark throughout. Write $\kappa = 2^{2h+1}\Gamma(1+h)/\Gamma(-h)$, $Q = Q_h$ from (19.D4), and $T = \kappa R^{-2h}$. For any measured band $I = [a, b]$, let

$$A_I = \frac{a^{-2h} - b^{-2h}}{2h}, \quad B_I(r) = \frac{1}{A_I}\int_a^b \rho^{-2h-1} J_0(\rho r)\, d\rho, \qquad D_I = \kappa \int_a^b \rho^{-2h-1}\Phi_\infty(\rho)\, d\rho.$$

Here $A_I \neq 0$, since $a < b$ and $\Re h > 0$. At a fixed comparison rank, $\int B_I(|y|)\, d\mu_{N,s} = D_{I,N}/(\kappa A_I)$, where the right side uses the same finite-rank circular source. This equality uses the actual unnormalized complex preparation. It converts any computed signed band into an observable against which the residual Bessel kernel may be approximated.

Choose a complex polynomial $q(X)$, complex numbers b_I, and a real polynomial $P(X)$ satisfying the global inequality

$$\left| Q(Rr) - q(r^2) - \sum_I b_I B_I(r) \right| \le P(r^2), \qquad r \ge 0. \tag{W1}$$

The coefficients are exact decimals in the indicated fit files. Let $m_{j,N}^{(s)}$ and $m_{j,N}^{(1/2)}$ denote the corresponding complex and positive radial moments. An approximation to the limiting tail is

$$T\sum_j q_j \widehat{m}_j + T\sum_I \frac{b_I \widehat{D}_I}{\kappa A_I}. \tag{W2}$$

Here e_j bounds $|\widehat{m}_j - m_{j,N}^{(s)}|$, and ϵ_I bounds $|\widehat{D}_I - D_I|$. Put $N = 10^{56}$, $M = 65536$, $V = N^{1/400}$, $p = 4(387/500)$. Use the comparable-rank constants K, ν preceding (19.D1), so $\delta(u) = K(2+u)^p N^{-\nu}$ holds on $[0, M]$. A complete radius for (W2), in addition to outward rounding, is

$$\begin{aligned} |T|\left[V\sum_j P_j m_{j,N}^{(1/2)} + \sum_j |q_j| e_j\right] + \sum_I \frac{|Tb_I|}{|A_I|}\left[\frac{\epsilon_I}{|\kappa|} + \delta(b)(a^{-1} - b^{-1})\right] \\ + |\kappa|\left[\frac{K(1+2/R)^p M^{p-1}}{(p-1)N^\nu} + \frac{V m_{0,N}^{(1/2)}}{M}\right] + \mathfrak{b}(M). \end{aligned} \tag{W3}$$

In the sum over I, a, b refer to that interval. The first term uses (W1) against the finite-rank positive majorant of the complex variation. The second line follows by transferring the limiting tail on $[R, M]$, extending the resulting finite integral to infinity, and restoring the limiting contribution above M by (19.D2). In particular, the first charge on the second line integrates $\delta(\rho)\rho^{-2}$ using $2 + \rho \le (1 + 2/R)\rho$; each observed band is transferred over its own support. No comparison rank tends to infinity inside a finite-rank variation bound.

The matched real moments use the finite differences of (19.D5). For the complex moments of degrees zero and one, use the limiting dyadic jets of verification_microscopic/jet_complex_precision.json and $t = 10^{-3}$. Writing m_2^+ for an upper bound on the limiting complex second-moment modulus and M_3 for the positive sixth mark moment bound in the integrated Bessel proof, the additional errors at degrees zero and one may be taken to be

$$\delta(t), \qquad \frac{8\delta(t)}{t^2} + \frac{(m_2^+ + V m_{2,N}^{(1/2)})t^2}{16} + 4\big(128000 + VM_3/2304\big)t^4.$$

Indeed, subtract the angular source at zero from its value at t, retain its coefficient $-m_1 t^2/4$, and use the finite cosine and limiting Cauchy remainders already proved following (19.D5). All envelopes in the first signed-control sequence use a quadratic positive comparator and a signed polynomial of degree at most one.

Global check of the signed residual. On $0 < r \le 9/2$, expand each B_I using the entire J_0 series and expand Q by (19.D4). The term proportional to r^{2h} is evaluated with the real logarithm. In the Taylor series for the entire part, the coefficient of $(-r^2/4)^j/(j!)^2$, before subtracting q, is exactly

$$-\frac{1}{2j-2h}\left[R^{2j} + \sum_I b_I \frac{b^{2j-2h} - a^{2j-2h}}{A_I}\right].$$

Use $n = 250$ terms. With $w = [(9/2)\max(R, \max b)]^2/4$, the absolute discarded series is bounded by

$$\frac{w^n}{(n!)^2(1 - w/(n+1)^2)} \left(\frac{1}{2n - 2\Re h} + \sum_I |b_I| \frac{a^{-1} - b^{-1}}{|A_I|} \right).$$

At zero use the limiting value $1/(2h)$; on $[0, 10^{-7}]$ bound the fractional power and the first omitted analytic term by a geometric series. On each subsequent subinterval $[l, u]$, enclose the absolute residual at both endpoints. The interpolation allowance for the difference of a scalar majorant and a complex norm is bounded by $(u - l)^2/8$ times the sum of the bounds on the second derivatives of the majorant and the complex residual. This follows by linear interpolation of the two functions and convexity of the norm. For $Q(Rr)$ use

$$|\partial_r^2 Q(Rr)| \le \frac{|2h - 1|(|2h| + 1)}{l^2} + \frac{R}{l},$$

from (19.D4)'s differentiated identity. For B_I use $b^2(a^{-1} - b^{-1})/(2|A_I|)$, since the second derivative of J_0 on the real axis is bounded by $1/2$ via its angular integral. For $r \ge 9/2$ use $|Q(Rr)| \le 3/(Rr)^{3/2}$ from the Bessel energy bound, $|B_I| \le (a^{-1} - b^{-1})/|A_I|$, and compare polynomial coefficients about $X = (9/2)^2$. These estimates certify (W1) on the entire half-line. The pilot optimization has no role in the validity of the inequalities.

At $R = 12$ the seven inherited signed windows give a tail radius below .026625. Repeating (W1) with the four new unit bands through 12 brings this below .019562; the shape and propagated band errors in that calculation are below .019159 and .000337, respectively. The comparison holds at the same cutoff. The new signed integrals enter the center of the residual as well as the retained integral. Charging their errors separately in (W3) and in the retained part is valid by the triangle inequality even when the same enclosure occurs twice. The dyadic proofs are in verification_window/signed_tails.json and verification_window/signed_full12_tail.json.

Using positive and complex frequency data together. A second sequence replaces the right side of (W1) by

$$P(r^2) + \sum_{k \in \mathcal{K}} d_k J_0(kr), \qquad d_k \in \mathbb{R}. \tag{W4}$$

It suffices to certify the original modulus inequality with this entire expression. At the comparison rank, its real expectation is $\sum_j P_j m_{j,N}^{(1/2)} + \sum_k d_k \Phi_{N,1/2}(k)$. The positive tilt in this formula controls the variation. The D_I in (W2) continue to come from the independent complex tilt. Thus each term in (W4) uses a different measured quantity from the signed correction in (W2). If φ_k is a real source center with $|\Phi_{N,1/2}(k) - \varphi_k| \le e_k^+$, the additional entries inside the real shape expectation in (W3) are $\sum_k d_k \varphi_k + \sum_k |d_k| e_k^+$. These entries may bring the total expectation well below the value for a polynomial comparator. The errors e_k^+ include the limiting real keyhole calculation, its angular quadrature and its discrepancy from the chosen rank. The comparison remains a finite-rank inequality throughout.

For the global validation of (W4), add $\sum_k |d_k| k^2/2$ to the second-derivative allowance and evaluate the real Bessel terms at the same endpoints as the complex residual. On the upper ray use $|J_0(x)| \le (5/4)x^{-1/2}$ for $x \ge 2$. Indeed $f = \sqrt{x} J_0(x)$ satisfies $f'' + (1 + 1/(4x^2))f = 0$, so $f'^2 + (1 + 1/(4x^2))f^2$ decreases on the positive real ray. The data at 2 certify the required constant. This also sharpens the upper-ray band bound by the factor $\min(1, 5/(4\sqrt{ar}))$. The joint proofs check $r \le 5$ by panels and compare polynomial coefficients beyond 5. At $R = 16$, using the eleven unit complex bands, the complex band $[12, 16]$, and real probes $k = 2, 4, 6, 8, 10$, the complementary tail has radius below .001594.

For the finer joint calculation we also price (W3) at the fixed ranks $10^{56}, \ldots, 10^{65}$ and band endpoints listed in the receipt, checking the comparable-rank hypothesis on the entire band at each choice. The matched real transfer costs $C(2 + k)^4/N$, so its price scales by the ratio of the old and new ranks. The limiting source and its angular quadrature have the same allowances at every rank. A denser set of real measurements at the integer frequencies from 2 through 16 allows (W4) to control more of the sign changes in the spatial residual. Only the best available input disk at each of these physical frequencies is used. The final computation checks candidate shapes over the whole half-line and selects the smallest successful total radius from its finite list of rank choices. The files verification_window/joint_refined_tails.json and verification_window/SIGNED_CONTROLS.md give the exact coefficients by reference, dyadic tail disks, rank comparisons and replay instructions.

For $R = 8, 12, 16, 20$, respectively, the final complementary radii are bounded by .001105353, .000717446, .000536257, and .000288927. All four use the same real probe frequencies. Each complex signed band is confined to the retained interval of its own test. At $R = 20$, the selected rank is 10^{62} with $M = 2^{21}$. The real shape expectation contributes less than .000253382; the earlier complex band and real probe uncertainties contribute less than .000030987 and .000002400. These are charges for the complementary tail alone. The full coefficient requires the finite part and all retained bands, whose disks are assembled in the verification section.

Pricing the complement with measured real-tilt Bessel moments. For the original complex input write $u = 1/2$, $s = u + i/20$ and $h = 1/2 + i/8$. Take one comparison rank $n = 10^{56}$ and bandwidth $M = 65536$. Denote the complex and matched positive finite mark measures by $\mu_{n,s}$ and $\mu_{n,u}$, retaining each mass. On this fixed preparation $|d\mu_{n,s}| \le n^{1/400} d\mu_{n,u}$ after pushforward. For real $k \ge 0$ the signed functional on the positive measure satisfies

$$B_{k,n} := \int J_0(k|y|)\, d\mu_{n,u}(y) = \Phi_n(1, u; k).$$

The angular average gives this identity directly and ensures that $B_{k,n}$ is real. Its error from $\Phi_\infty(1, u; k)$ is bounded by $C(2+k)^4/n$ by (19.M4). To compute the latter, run (K1)–(K4) at real tilt on equally spaced angular nodes. At radial frequency k, a shift by $i\sigma$ in the angular variable has imaginary Cartesian norm $b = k \sinh \sigma$. The finite positive-weight bound $e^{b/2+b^2/4}$ holds at u without a power of rank, and passes to the limiting source by compact-frequency convergence. Consequently the angular alias costs at most $2e^{b/2+b^2/4}/(e^{n_a\sigma} - 1)$. Take the real parts of the node values, add their weighted determinant and arithmetic errors, and retain the separate finite-rank comparison. Reflection across the real axis preserves the source by swapping its two Hankels. At real tilt reversing both real Cartesian coordinates conjugates the source, so its real part also has the corresponding half-turn symmetry. These facts justify the angular reductions in the receipts.

Choose a constant $q \in \mathbb{C}$ and real coefficients satisfying the global majorant

$$|Q_h(Rr) - q| \le V(r) := p_0 + p_1 r^2 + p_2 r^4 + \sum_k b_k J_0(kr) \qquad (r \ge 0).$$

Despite the signs of individual b_k and $B_{k,n}$, their linear combination in the expectation of V is retained before taking an upper bound. Put $T_R = \kappa R^{-2h}$, $\kappa = 2^{2h+1}\Gamma(1+h)/\Gamma(-h)$. The tail disk center is $T_R q$ times the midpoint of the limiting complex mass. Its principal radius charge is

$$|T_R| n^{1/400} \left(\sum_{j=0}^{2} p_j m_{j,n} + \sum_k b_k B_{k,n} \right)$$

evaluated outward using the signed coefficients. The positive moments $m_{j,n}$ follow the finite comparison below (19.D4). The complex mass error includes both the certified origin jet and the complex rank discrepancy at zero. Beyond M add (19.D2) for the limiting source and $|\kappa| n^{1/400} m_{0,n}/M$ for the finite tail. On $[R, M]$ the remaining comparison is at most

$$\frac{|\kappa| L (1 + 2/R)^P M^{P-1}}{(P-1) n^{q_*}}, \qquad P = 4(1 - 113/500), \qquad q_* = 0.759875.$$

This follows by integrating the pointwise discrepancy $L(2+\rho)^P n^{-q_*}$ against ρ^{-2}, with the comparable-rank condition checked at M. The resulting disk encloses the complement of the actual signed frequency integral beyond R.

The coefficient search supplies decimal rationals. The following checks establish each accepted majorant. At $r = 0$ use (19.D4) through $r = 10^{-8}$ and $|J_0(x) - 1| \le x^2/4$, by angular averaging. For $10^{-8} \le r \le 5$ evaluate Q_h at dyadically subdivided panel endpoints using (19.D4) and its absolute geometric series remainder. The fractional-power term uses the real logarithm. Between endpoints the curvature bound for $Q_h(Rr)$ is $|2h-1|(|2h|+1)/r^2 + R/r$, by differentiating $r(d/dr)Q_h(Rr) = 2hQ_h(Rr) - J_0(Rr)$. The curvature bound for $J_0(kr)$ is $k^2/2$ by its angular representation. Subtract the combined curvature bounds of the complex residual and real majorant, multiplied by the squared panel width divided by eight, from the smaller endpoint margin. Positive margins certify the entire panel by linear interpolation and the triangle inequality.

For $r \ge 5$ use $|Q_h(Rr)| \le 3/(Rr)^{3/2}$ from (19.D4)'s energy estimate and $|J_0(x)| \le (5/4)/\sqrt{x}$ at $x \ge 2$. Indeed $f = \sqrt{x}J_0(x)$ obeys $f'' + (1 + 1/(4x^2))f = 0$; $f'^2 + (1 + 1/(4x^2))f^2$ decreases and its value at 2 is strictly below $(5/4)^2$. The polynomial in r^2 exceeds the sum of the exterior allowances and $|q|$ at 5 and is nondecreasing thereafter. The script `verification_window/audit_real_shape.py` executes all three checks with outward arithmetic. `verification_window/audit_real_samples.py` records the independent real-tilt source calls and angular allowances. The enclosed coefficient itself retains $s = 1/2 + i/20$ throughout.

Direct check of the real half-order scalar. At the positive control $h = s = 1/2$, $c = 1$, the observable is the integral of $r = |y|$ against the unnormalized positive limiting measure. Apply the same real-source measurements directly in that measure. For each sign $\epsilon = \pm 1$, construct a separate real V_ϵ in the preceding polynomial and Bessel span with $V_\epsilon(r) \ge \epsilon r$. On $[0, 5]$ the endpoint interpolation check uses curvature $2|p_1| + 300|p_2| + \sum |b_k|k^2/2$. Beyond 5 expand the polynomial $p_0 + p_1 r^2 + p_2 r^4 - \epsilon r$ in $r - 5$. Its constant coefficient exceeds $\sum |b_k|(5/4)/\sqrt{5k}$ and its remaining coefficients are nonnegative. Integrating both inequalities with certified real limiting moments and real source disks gives

$$0.51021861831884 < F(1; 1/2, 1/2) < 0.51454890188939.$$

The five-frequency certificate is `verification_window/audit_real_half.json`. It is contained in the earlier Stieltjes–Gauss interval.

Adding frequencies through 16 gives all integer frequencies $k = 2, 3, \dots, 16$. The additional 175 real-source evaluations took 323.72 seconds over the eleven radii on five workers. The exact receipts are `verification_window/audit_real_samples_expanded.json`. For the $R = 20$ majorant the 384-bit replay gives a positive-shape expectation charge below 0.001511720 and a real-probe uncertainty below $2.2830 \cdot 10^{-6}$. The finite-band bridge costs at most $1.8484 \cdot 10^{-5}$, while the finite and limiting tails beyond M cost at most $2.1090 \cdot 10^{-5}$ and $2.3134 \cdot 10^{-5}$. Including the signed complex-mass correction and arithmetic gives a tail radius below 0.001576709. A constant slack of 0.00004 in the pilot shape alone failed at a tested point near $r = 3.203$, with a deficit exceeding 0.000211 in one panel. Adding $0.0001r^4$ to the constant and $10^{-7}r^2$ slacks prices this failure against the measured fourth moment. The global verification passes.

The following table isolates the effect of actually moving the cutoff with the same family of fifteen real-probe tests. The first line has no new signed frequency window. All subsequent lines add their signed frequency bands and pay for the complement anew.

R	complement radius upper	complete radius upper
8	.008674160	.008674192
9	.006543357	.006543641
10	.004980280	.004981030
12	.002727949	.002729412
16	.002560424	.002563535
20	.001576709	.001586233

These rows use the individual sharp $[8, 9]$ source receipt and the mean-contour charges on $[12, 16]$ and $[16, 20]$. Their exact dyadic sums and rational modulus checks are in `verification_window/audit_real_expanded_combined.json`. At the real diagonal the same fifteen tests separately give

$$.51373591197996 < F(1; 1/2, 1/2) < .51432978179489.$$

The latter interval follows from `verification_window/audit_real_expanded_half.json`.

A higher-order transfer of the four positive moments. For the real tilt $s = 1/2$ and $c = 1$, write m_j for the radial moment of degree $2j$ in the mark. The comparison rank is $N = 10^{56}$. For either the finite or the limiting positive preparation, the strong Szegő exponential-moment bound of Section 19 gives $\int I_0(U|y|)\, d\mu(y) \le e^{U/2+U^2/4}$, $U > 0$. At finite rank this follows by averaging the directional exponential bounds. In the limit, apply weak convergence first to the truncation of the nonnegative continuous function $I_0(U|y|)$ and then let its truncation height increase. Take $n = 12$, $t = 1/10$, and $U = 7$. Since every coefficient of I_0 is nonnegative,

$$\frac{m_{n+1}}{4^{n+1}((n+1)!)^2} \le e^{U/2+U^2/4} U^{-2n-2}.$$

Taylor expansion of the angular cosine through degree $2n+1$, with the usual absolute remainder, now bounds the remainder in the source series after degree $2n$ by $e^{U/2+U^2/4}(\rho/U)^{2n+2}$. Here one uses $\mathbb{E}_\theta \cos^{2n+2}\theta = (2n+2)!/[4^{n+1}((n+1)!)^2]$.

Let w_{jk} denote the coefficient of X^j in the k-th Lagrange polynomial for the distinct nodes $0^2, 1^2, \dots, n^2$. Thus $\sum_k w_{jk} k^{2l} = \mathbf{1}_{j=l}$ for $0 \le l \le n$. Apply this identity to the finite and limiting sources at $\rho = kt$. The real-frequency bound (19.M4) gives

$$|m_{j,N} - m_{j,\infty}| \le \frac{4^j (j!)^2}{t^{2j}} \sum_{k=0}^{n} |w_{jk}| \left[\frac{C(2+kt)^4}{N} + 2e^{U/2+U^2/4}(kt/U)^{2n+2} \right].$$

At $j = 0$ one may also use $16C/N$ directly. The four transfer allowances are below $2.209 \cdot 10^{-20}$, $4.448 \cdot 10^{-17}$, $5.239 \cdot 10^{-14}$, and $5.166 \cdot 10^{-11}$. Intersect the inherited limiting real-jet enclosures in degrees zero through two, use the degree-three enclosure from the real half-order control, and add the corresponding allowances. The rational weights, outward finite-moment endpoints, and exact input references replay in verification_window/refined_real_moments.py.

A lower bound on the error charged by seven fixed signed tests. At the comparison rank $N = 10^{56}$, let $B_j(X)$ be the annular kernel $J_0(\rho\sqrt{X})$ integrated against ρ^{-2h-1} over $[j, j+1]$, divided by the integral of the scalar weight on that band. Suppose the centering function is any complex linear combination of $1, X, X^2, B_1, \dots, B_7$. Suppose that a real cubic P majorizes the absolute residual on $[0, \infty)$ and is then integrated against the four matched real moments at this rank. The resulting shape charge, including $(17/16)N^{1/400}/R$, exceeds $.0211162, .0203567, .0181725, .0095718$ at $R = 9, 12, 16, 32$, respectively. For every $R \ge 64$ it exceeds $.13648/R$. These are lower bounds for the error allowance of this particular procedure. Enlarging the signed span to the first fifteen or nineteen unit bands still forces shape charges above $.00749459$ at $R = 16$ or $.00544109$ at $R = 20$, respectively. With those enlarged spans held fixed, the corresponding lower bounds are $.05505/R$ for $R \ge 64$ and $.04710/R$ for $R \ge 128$. The argument gives no such bound for a span growing without limit or a different measure of the residual.

To prove the bounds, choose eleven distinct squared radii $x_0 = 0, x_1, \dots, x_{10} > 0$. Set $v_0 = 1$ and solve $\sum_{j=0}^{10} v_j f(x_j) = 0$ for the ten centering functions f. This is a complex linear system. Ball arithmetic verifies that its matrix is invertible. In the normalized band integrals the power series of J_0 can be integrated termwise. Truncating just before index n (150 or 300 in the replay) costs at most

$$\frac{w^n}{(n!)^2} \frac{j^{-1} - (j+1)^{-1}}{(1 - w/(n+1)^2)\,|\int_j^{j+1} \rho^{-2h-1}\, d\rho|}, \qquad w = x(j+1)^2/4,$$

at a witness point x, with $w < (n+1)^2$. Let $b_j \ge |v_j|$ be numerical upper bounds. Choose a dyadic $u > 0$ such that $m'_k = m_{k,N} - u\sum_j b_j x_j^k$ satisfy $m'_0, m'_1 > 0$, $m'_0 m'_2 > (m'_1)^2$ and $m'_1 m'_3 > (m'_2)^2$. For $m_{3,N}$ use the third divided difference of the source at $0, t, 2t, 3t$, $t = 1/250$, as in the cubic majorant, achieving $.31 < m_{3,N} < .35$. The two positive definite Hankel matrices built from the m'_k define a positive two-node quadrature. Indeed, in the inner product $\langle x^i, x^j \rangle = m'_{i+j}$, $0 \le i, j \le 1$, define A by $\langle Ax^i, x^j \rangle = m'_{i+j+1}$. Then $A > 0$, $A1 = x$, and its spectral measure at 1 has the required four moments. Adjoining atoms of mass ub_j at x_j thus exactly reproduces the real moments priced by P. This gives

$$\sum_{k=0}^{3} P_k m_{k,N} \;\ge u \left| \sum_j v_j Q_h(R\sqrt{x_j}) \right|.$$

For the all-R conclusion the positive nodes are $.01, .08, .2, .5, 1, 2, 4, 6, 9, 12$, and $u > .19184$. On these nodes the Bessel bound $3(R\sqrt{x_j})^{-3/2}$ shows that the nonzero-node terms together are smaller than $|Q_h(0)|/2$ for every $R \ge 64$. At the individual cutoffs, the Bessel series (19.D4) evaluates the witness directly. For the fifteen-band case take squared radii $x_j = (2j/15)^2$, $0 \le j \le 18$, and solve the analogous eighteen-by-eighteen system. For nineteen bands take $x_j = (5j/44)^2$, $0 \le j \le 22$. The same two Hankel tests certify the remainders in the four-moment problems. The exact inputs, dyadic bounds and replay are in verification_window/fixed_feature_floor.json and its companion script.

A check with all fifteen unit bands through sixteen. The same obstruction can be tested after allowing more signed data. In an idealized shape bound grant the four exact limiting real moments and all fifteen signed unit-band tests on $[1, 16]$. Allow a complex quadratic and arbitrary complex multiples of these band tests as the centering function. At $R = 16$ the resulting absolute cubic-majorant allowance, even with unit variation cost, exceeds $3.7770 \cdot 10^{-5}$ in scalar units. This lower bound addresses the specified information and comparison rule. A signed constraint on the positive majorant itself changes the test.

Here is an independent witness. For $j = 0, \dots, 18$ set $r_j = j/18$ and $X_j = r_j^2$. The functions $1, X, X^2$ and the fifteen band kernels give eighteen linear equations $\sum v_j f(X_j) = 0$. Set $v_0 = 1$ and solve the remaining square system with interval arithmetic. Normalize by $L = \sum |v_j|$. Every X_j lies in $[0, 1]$. Subtracting the atomic masses $|v_j|/(100L)$ leaves each of the four real moments between its old value minus $1/100$ and its old value. The two strict Hankel determinant tests above hold on these whole enclosures. A positive measure can therefore realize the residual moments. For any admissible majorant P the scalar charge is at least

$$\frac{17}{16R} \frac{|\sum v_j Q_h(Rr_j)|}{100L}.$$

verification_window/dictionary_floor.py evaluates (19.D4) with 300 terms, an explicit geometric remainder, and 820-bit arithmetic. It checks the solve and gives the displayed lower bound even for a procedure granted the exact limiting moments. The test does not posit that the auxiliary atomic measure is an actual CUE mark law.

Testing a majorant with measured Bessel averages. For the five positive probes $k = 2, 4, 6, 8, 10$, consider an algorithm which prices a globally nonnegative majorant from separate intervals for $m_0, \dots, m_3$ and $\int J_0(kr)\, d\mu_{N,1/2}$. At $R = 20$ allow the centering function to use $1, X, X^2$ and all nineteen signed unit bands through twenty. An interval-information test gives a shape cost greater than $2.77 \cdot 10^{-6}$, even at unit variation cost.

Specifically, take $r_j = j/22$, $0 \le j \le 22$, use the preceding complex linear solve, and allocate the masses $|v_j|/(1000 \sum_i |v_i|)$ at these marks. The target record in this test uses the coordinate midpoints of the supplied enclosures. Subtract the moments of the allocated atoms, including the five real J_0 tests. For the residual record, the nine radii $32, 41, 48, 69, 88, 119, 128, 182, 185$ divided by 80 support a positive measure. The nine-by-nine real interval solve has all weights above $2.15 \cdot 10^{-5}$. The resulting measure matches the midpoint record exactly. Pairing the global inequality against it proves the claimed worst-case lower bound for any rule that uses only these separate intervals. This particular test concerns the information supplied to the rule; finer or additional probes change it. verification_window/measured_floor.py records both the proposal search and the outward certification. For the displayed test its option is `--midpoints`.

There is also a test for the actual finite moment record at $N = 10^{56}$ with these five positive probes. Use the tighter four finite moments above, take the smaller certified positive-source disk at each selected frequency, and allocate $|v_j|/(10^4 \sum_i |v_i|)$ at the same marks. The interval inverse for the residual real weights, applied to all admissible right-hand sides, yields weights strictly above $1.25 \cdot 10^{-7}$. The resulting shape charge exceeds $2.7795 \cdot 10^{-7}$ even with unit variation cost. The exact radii for that real solve and its replay are in verification_window/five_probe_floor.json. The final fifteen-probe calculation uses a larger comparison class.

Positive integer diagonal and an independent finite-size check

Let $k \ge 1$ be an integer and put $p_k = k^2 + 2k$. The observable at $h = s = k$ is the derivative product with k differentiated copies on each side. Expanding the product of characteristic polynomials at independent spectral points by the finite dual Cauchy identity and using Haar orthogonality gives the parent polynomial

$$\sum_{\lambda \subseteq (N^k)} s_\lambda(x_1, \dots, x_k) s_\lambda(y_1, \dots, y_k).$$

The signs $(-1)^{|\lambda|}$ from the two characteristic-polynomial products cancel. Taking one derivative in every x_i and y_j before coalescing gives $\mathbb{E}|\Lambda_N'(z)|^{2k}$. The same derivatives of the alternant form of this polynomial give the confluent determinant in Section 12. In particular, specializing the Grover–Mezzadri–Simm lists to $\mu = \nu = (1^k)$ identifies the same finite polynomial, with U^* in place of U making no difference to Haar expectation. Their path $z = 1 - a/N$ has manuscript depth $c_N = 2a - a^2/N$. The compact-depth uniformity of Section 12 and

continuity of $B_{k,k}$ imply that the Grover–Mezzadri–Simm coefficient for $a \geq 0$ is exactly $B_{k,k}(2a)$. At $a > 0$ this is $F(2a; k, k)$ by the positive-depth theorem. At $a = 0$ it is $g_k \mathcal{C}(k, k)$ by exact-circle convergence. This proves coefficient identities from the common finite observable.

The independent finite computation can bypass differentiation of the confluent kernel. For $k = 1$ it uses $N^{-3} \sum_{j=1}^{N} j^2 z^{2j-2}$. For $k = 2$, write $s_{(a,b)}(x, y) = \sum_{j=0}^{a-b} x^{a-j} y^{b+j}$, where $0 \leq b \leq a \leq N$. The mixed derivative on the diagonal is $D_{a,b} z^{a+b-2}$ for $a + b \geq 2$, with

$$D_{a,b} = (a - b + 1)ab + \frac{(a - b)(a - b + 1)(a - b - 1)}{6}.$$

Haar orthogonality therefore gives $N^{-8} \sum_{a+b \geq 2} D_{a,b}^2 (z^2)^{a+b-2}$ for $F_N(c; 2, 2)$. At the circle the limiting coefficients are $1/3$ and $61/10080$. The reproducibility record checks the finite Schur sums against the confluent kernel with exact rational arithmetic. It encloses each $I_j(c) = \int_0^1 t^j e^{-ct}\, dt$ between adjacent rational Taylor partial sums, taken after the alternating terms decrease monotonically.

At $N = 128$ and $a = 13/10$ the actual depth is $33111/12800$. The absolute leading-coefficient discrepancies for $k = 1, 2$ are respectively about $4.94387 \cdot 10^{-4}$ and $1.80879 \cdot 10^{-5}$. Including the first correction of Section 12 changes these to $1.71634 \cdot 10^{-6}$ and $3.89022 \cdot 10^{-7}$. The depth conversion alone changes the leading coefficients by about $4.59818 \cdot 10^{-4}$ and $4.08931 \cdot 10^{-6}$ on that input. At $N = 512$, $c = 32$, $z^2 = 15/16$ the absolute discrepancies in the Gaussian normalization $c^{p_k} F_N$ from $\mathcal{G}(k, k; z)$ are $4.86066 \cdot 10^{-12}$ and $2.02892 \cdot 10^{-7}$. The differences between the actual-radius Gaussian and its evaluation at one are respectively $1/16$ and $47/16$ here. This check distinguishes the exponentially small Gaussian error from the finite-radius shift.

Quantitative check on the integer depth overlaps. The determinant representation also gives the following bounds with explicit constants for every fixed k. Write $x = 1 - d = z^2$ and $c = Nd$. For $N \geq k$, $0 < d \leq 1/2$, there are explicit constants A_k and B_k such that

$$\left| c^{p_k} \left(F_N(c; k, k) - B_{k,k}(c) \right) \right| \leq A_k d, \qquad \left| c^{p_k} F_N(c; k, k) - \mathcal{G}(k, k; z) \right| \leq B_k e^{-c/2}.$$

To prove this, use row and column normalization by d powers in the confluent determinant of Section 12. The resulting entry indexed by a, b, with $p = a + b$, is

$$H_{a,b} = d \sum_{l=0}^{N+k-1} d^p \, l^{\underline{a}} \, l^{\underline{b}} \, x^{l-b}.$$

Terms with $l < \max(a, b)$ are zero. In the remaining terms let $t = ld$ and $q_l = d^p l^{\underline{a}} l^{\underline{b}}$. Replacing each factor by its positive part leaves the product unchanged at integer l. Telescoping this product gives $0 \leq q_l \leq t^p$ and $t^p - q_l \leq D_{a,b} d\, t^{p-1}$, where $D_{a,b} = \binom{a}{2} + \binom{b}{2}$ in this paragraph. Omit that term when its coefficient is zero. The elementary inequalities

$$0 \leq \frac{-\log(1 - d) - d}{d} \leq d, \qquad x^{-b} \leq 2^b, \qquad |x^{-b} - 1| \leq b 2^{b+1} d$$

then bound the difference between the summand without d and $t^p e^{-t}$ by

$$d e^{-t} \left(D_{a,b} t^{p-1} + b 2^{b+1} t^p + 2^b t^{p+1} \right).$$

For $f_r(t) = t^r e^{-t}$ on $[0, \infty)$, the integral is $r!$, the supremum is at most $r!$, and the total variation is at most $2r!$. Thus $d \sum_{l \geq 0} f_r(ld) \leq 2r!$. Comparing the first N terms with the integral and adding the last k terms gives

$$\left| H_{a,b} - \int_0^c t^p e^{-t}\, dt \right| \leq d \left(2D_{a,b}(p - 1)! + (b 2^{b+2} + 2 + k) p! + 2^{b+1} (p + 1)! \right).$$

Each of the two entries in this comparison is bounded by $2^{b+1} p!$. Appending the infinite tail to $H_{a,b}$ costs at most $2^{b+p+2} p! e^{-c/2}$: split e^{-ld} into two equal factors and apply the same Riemann bound at mesh $d/2$. The full infinite entry obeys the same $2^{b+1} p!$ bound. On fixed z the infinite matrix gives precisely the compact-interior limit in this normalization, $\mathcal{G}(k, k; z)$. This identifies the infinite determinant as a function of the actual radius.

For explicit A_k, B_k, take the maximum of each displayed entry constant for $0 \le a, b \le 2k-1$ and multiply it by $k!kU_k^{k-1}$ and the sum of the nonnegative Kostka/factorial weights in Section 12, where $U_k = \max_{a,b} 2^{b+1}(a+b)!$. This follows by telescoping the products in the Leibniz formula. Passing $N \to \infty$ at fixed c in the Gaussian bound gives $|c^{p_k} B_{k,k}(c) - \mathcal{G}(k,k;1)| \le B_k e^{-c/2}$.

For clarity, at $0 \le c \le H$ and $N \ge \max(k, 2H)$ the same argument works directly at mesh $1/N$, with $t = l/N$ and $t^p e^{-ct}$. The compact entry bound is 2^{p+b+1} and the entry error is at most N^{-1} times

$$p + H + k2^p + 2\left[D_{a,b}2^{p-1} + 2^{p+b+1}(bH + H^2)\right].$$

Here $p + H$ bounds the derivative on $0 \le t \le 1$, $k2^p$ prices the extra points, and the bracket bounds the falling-factorial and power errors on $0 \le t \le 2$. The term $D_{a,b}2^{p-1}$ is zero for $p = 0$. This gives an explicitly bounded $O_k(N^{-1})$ remainder on $[0, 2]$ and an overlap on $[1, 2]$ with the d-mesh bound. The derivative of each limiting entry has magnitude at most one for $c \ge 0$, so the finite-rank conversion from $c_N = 2a - a^2/N$ to $2a$ has a separate computable $O_k(a^2/N)$ charge. These proofs and checks are specific to the integer diagonal.

Consequences of the depth profile for the zeta comparison

Let $L = \log(T/(2\pi))$ and evaluate at $\sigma_T = 1/2 + a/L$ with fixed $a \ge 0$. The radial matching $z = 1 - a/N$ has $c = 2a - a^2/N$. For positive real k, the usual CUE comparison leads to the conjectural asymptotic

$$\frac{1}{T}\int_T^{2T} |\zeta'(\sigma_T + it)|^{2k}\, dt \;\sim\; a_{\mathrm{arith}}(k) L^{k^2+2k} \begin{cases} F(2a;k,k), & a > 0, \\ g_k \mathcal{C}(k,k), & a = 0. \end{cases}$$

Here the universal factors are CUE theorems. They are positive on this diagonal: at zero this follows from the positive circle law, and at positive depth it follows from the positive mass and nondegenerate limiting mark in Section 15. The candidate arithmetic factor in the usual moment conjecture is

$$a_{\mathrm{arith}}(k) = \prod_{\mathfrak{p}\ \mathrm{prime}} (1 - \mathfrak{p}^{-1})^{k^2} \sum_{m=0}^{\infty} \frac{((k)_m/m!)^2}{\mathfrak{p}^m}.$$

On the positive integer diagonal it specializes to the arithmetic factor used by Grover, Mezzadri and Simm. Transferring this coefficient and the local law to the indicated zeta averages requires a number-theoretic comparison for the joint characteristic polynomial and derivative observables at the moving shift. The CUE proof supplies neither that comparison nor a uniform integrability estimate on zeta.

With independent orders the candidate corresponding observable is $|\zeta'|^{2h}|\zeta|^{2(s-h)}$, with log power $s^2 + 2h$ and universal factor $F(2a; h, s)$ under the corresponding arithmetic comparison. Inverse powers require separate integrability at zeros. For complex parameters the universal factor can vanish, so an additive leading-coefficient statement is the appropriate form unless a nonzero coefficient is justified. The iterated off-line limit studied by Najnudel and Wei takes the long-height average at fixed $\sigma > 1/2$ before $\sigma \downarrow 1/2$. That order of limits does not supply the simultaneous microscopic shift or the critical-line transfer used here.

On a compact interval of positive real diagonal orders, the additive depth-join bounds also give relative asymptotics in the corresponding normalizations. On bounded depths the profile is continuous and strictly positive, so it has a positive minimum on the compact. At large depth the corrected approximation differs from the actual-radius Gaussian moment by an exponentially small quantity. That Gaussian moment has a positive minimum on the same order interval and $0 \le z \le 1$ by its positive Gaussian integral and continuity. Increasing the rank threshold puts the finite-rank moments above half the respective positive minima. The relative statement follows by these lower bounds.

20. Determinant derivatives and a finite-rank error bound

The planar moment formula admits a complementary certified approximation in terms of the integer derivatives of its determinant. This section gives explicit mathematical error bounds. Their size is material, especially near a divergent-moment boundary. The bundled exact-rational jet implementation reaches rank eight at selected inputs. Its cost and the bound itself still limit useful precision at generic noninteger values.

Theorem 20.1 (finite-rank truncation with absolute error control). Set $B = N(1+z)$, $Y = |S_N|^2/B^2 \in [0,1]$, and $W = |\Lambda_N|^{2s}$ for real $0 \le z < 1$. Let $c_j = (-h)_j/j!$. Define

$$U_j = \mathbb{E}[W(1-Y)^j] = \sum_{l=0}^{j} (-1)^l \binom{j}{l} B^{-2l} T_N(l, s; z).$$

Each $T_N(l, s; z)$ is a mixed derivative at zero of the finite Toeplitz determinant. In the ordinary moment domain,

$$T_N(h, s; z) = B^{2h} \sum_{j \ge 0} c_j U_j.$$

At nonnegative integer h the series terminates. For other h this assertion and its tail bounds follow below; it also follows by integrating the binomial series once absolute integrability of its terms is established. The singular point $Y = 0$ has measure zero. Positive bases use real logarithms.

A bounded planar density for $N \ge 3$ with an explicit constant. Let $s_0 = \Re s$,

$$W_* = \max\{(1-z)^{2Ns_0}, (1+z)^{2Ns_0}\}, \qquad C_* = W_* \frac{(1-z^2)^{N^2}}{(1-z)^{2N^2}}.$$

After $w_j = (\lambda_j - z)/(1 - z\lambda_j)$ the tilted absolute eigenangle density is bounded by $C_* |\Delta(w)|^2/N!$ against product normalized angles. Indeed the smooth joint density after changing variables has the untilted factor $(1-z^2)^{N^2} \prod_j |1+zw_j|^{-2N}$, and $|W| \le W_*$. Write $S_N = Nz + \sum w_j$. For any three unit vectors two have circular angular separation at most $2\pi/3$, by ordering the three angles. Cover their triples with the three choices of this pair. For the chosen pair i, k, dividing its squared Vandermonde factor by the Jacobian of their sum gives

$$\frac{|w_i - w_k|^2}{|\sin(\phi_i - \phi_k)|} = 2|\tan((\phi_i - \phi_k)/2)| \le 2\sqrt{3}.$$

The remaining pair factors are at most four each. Almost every value of the sum has at most two ordered preimages for the selected pair with the others fixed. The sets with zero Jacobian have angular measure zero. The area formula, summation over the three choices, and integration of all other normalized angles thus bound the planar density of the absolute weighted pushforward by

$$M_N = \frac{12\sqrt{3}\, C_*\, 4^{N(N-1)/2-1}}{N!(2\pi)^2}.$$

Consequently $|U_j| \le \pi M_N B^2/(j+1)$ by integration on the supporting disk about zero. This density argument is a fixed-rank a priori estimate for the error; the numbers in the series itself are determinant derivatives.

Rank two away from the centre. Relative to the untilted transformed Haar pair the absolute weight is at most C_*. The sum of two eigenvalues under this reference law has planar density $\sqrt{4 - |u|^2}/(2\pi^2|u|)$ on the disk. For $|S_2| \le z$, we have $|S_2 - 2z| \ge z$ and density at most $M = C_*/(\pi^2 z)$. For $|S_2| > z$, $1 - Y \le 1 - b$ where $b = z^2/B^2$. Since $(j+1)(1-b)^j \le 1/b$ (bound it by its geometric partial sum), we get $|U_j| \le (\pi M B^2 + W_*/b)/(j+1)$. The bound deteriorates at $z = 0$, where the centre gamma formula supplies the correct threshold $\Re h > -1/2$. For rank one use the separate certified hypergeometric series.

Computable absolute error. For $N \ge 2$ in the bounded/local-density cases above write $|U_j| \le A/(j+1)$ and let $u = \Re h > -1$. Put $\gamma = (1+u)/2 > 0$. Choose a nonnegative integer J with $J > u$ and $(\Im h)^2 \le 2\gamma(J-u) + \gamma^2$. Then for $j \ge J$, $|j - h| \le j - u + \gamma$. Thus $|c_{j+1}| \le (1 - \gamma/(j+1))|c_j|$. The positive multipliers and telescoping differences give

$$\left| T_N - B^{2h} \sum_{j=0}^{J-1} c_j U_j \right| \le B^{2u} A \sum_{j \ge J} \frac{|c_j|}{j+1} \le B^{2u} A\, |c_J|/\gamma.$$

This tends to zero since $|c_J| = O_h(J^{-u-1})$; the same decay follows directly from the product bound above with exponent γ. Thresholds must be tested before summation. From an approximation v and disk bound e, a valid relative bound is $e/(|v| - e)$ whenever $|v| > e$.

Each finite set of determinant derivatives can in principle be enclosed by interval quadrature of the symbol coefficients on $[0, 2\pi]$ and ball-polynomial operations. For example, enclose the continuous Fourier integrands on each subinterval and multiply their interval ranges by the subinterval lengths. For $z < 1$ all denominators stay away from zero, and mesh refinement and increased precision give shrinking enclosures. Multivariate Taylor truncation at bidegree (J, J) suffices, including all cross terms in the determinant. The alternating binomial sum can lose many digits. No practical 10^{-10} runtime throughout the full parameter box of the original accuracy target follows from a convergent series with these constants. This construction supplies an independent absolute error mechanism even when the moment is close to a complex zero.

21. Certified values for independent parameters

Integer orders at every rank

Proposition 21.1 (finite coefficient extraction). For $N \geq 1$, $0 \leq z < 1$, $j \in \mathbb{Z}_{\geq 0}$ and $s \in \mathbb{C}$, the moment $T_N(j, s; z)$ is an exact finite combination of Gauss functions and determinants. All coefficients below can be enclosed by complex ball arithmetic. Use $[\lambda^k]$ for the Fourier coefficient on the circle and put

$$U_k(u, v) = [\lambda^k](1 - z\lambda)^u(1 - z/\lambda)^v = z^k \frac{(-u)_k}{k!}\, {}_2F_1(k - u, -v; k + 1; z^2) \quad (k \geq 0), \qquad U_{-k}(u, v) = U_k(v, u).$$

This follows by expanding both binomials, absolutely for $z < 1$. In the finite Toeplitz determinant insert $e^{af+b\bar{f}}$, $f = d\lambda/(1 - z\lambda)$. The coefficient of $a^u b^v$ in its *entry* of index k, where u, v now denote integers from zero to j, equals

$$[G_{uv}]_k = \frac{d^{u+v}}{u!v!} U_{k-u+v}(s - u, s - v).$$

Every term discarded by entry truncation exceeds j in one of the two powers and cannot contribute to the (j, j) coefficient of the determinant. Write $P(a, b) = \det(\sum_{u,v=0}^{j} G_{uv} a^u b^v)$ and $m = Nj + 1$. Its degree is at most $m - 1$ in each variable. If $\omega = e^{2\pi i/m}$, discrete orthogonality gives

$$T_N(j, s; z) = \frac{(j!)^2}{m^2} \sum_{k,l=0}^{m-1} \omega^{-j(k+l)} P(\omega^k, \omega^l). \tag{21.1}$$

This uses at most m^2 determinants of size N, with $(j + 1)^2(2N - 1)$ symbol entries before symmetries. The basic construction avoids division by the mass. For $j = 1$ and a provably invertible $G = G_{00}$, the first mixed determinant derivative is

$$\det G\, [\mathrm{Tr}(G^{-1}G_{11}) + \mathrm{Tr}(G^{-1}G_{10})\, \mathrm{Tr}(G^{-1}G_{01}) - \mathrm{Tr}(G^{-1}G_{10}G^{-1}G_{01})].$$

The implementation uses this alternative and otherwise has the finite sum available. Rounding error and cancellation enter through the returned ball. For a rectangular complex enclosure with midpoint v, take e to be the sum of its two coordinate radii and L a lower bound on the modulus on the rectangle. The reported relative radius is at most e/L when $L > 0$. This convention uses the internally retained midpoint before display rounding. Exact decimal strings or rational inputs specify points. An inconclusive enclosure, a divergence guard, and exhaustion of a resource cap are separate outcomes.

Validated quadrature for two independent exponents at rank two

Proposition 21.2 (validated singular quadrature). For $N = 2$, $0 < z < 1$, $\Re h > -1$ and complex s, the following quadrature encloses $T_2(h, s; z)$. The inputs to the implementation are exact rationals, including each component of the exponents. A successful return gives an absolute complex enclosure. A subdivision or precision failure is reported separately. There is a lower bound on the true modulus on the closed parameter region specified below.

Reduction of the Haar integral. Set $d = 1 - z^2$, $\gamma_0 = \arccos z$, $\tau = s - h$. Write the eigenvalues as $e^{i(\phi+\gamma)}, e^{i(\phi-\gamma)}$ and $r = \cos\gamma$. The rank-two Weyl density gives an independent uniform common phase and relative-angle density $(2/\pi)\sin^2\gamma$ on $[0, \pi]$. This follows also by the linear pushforward on the angular torus and

the factor $|e^{i(\phi+\gamma)} - e^{i(\phi-\gamma)}|^2/2 = 2\sin^2\gamma$. Reflection in the common phase, and replacing r by $-r$ while shifting ϕ by π, reduce the domain to $0 \le \gamma \le \pi/2$, $0 \le \phi \le \pi$, with density $(4/\pi^2)\sin^2\gamma$. Define

$$X_0 = (r-z)^2 + 2rz(1-\cos\phi), \quad D_\pm = (1-z)^2 + 4z\sin^2((\phi \pm \gamma)/2), \quad W = D_+ D_-.$$

Then $|\Lambda_2'|^2 = 4X_0$ and $|\Lambda_2|^2 = W$. The moment integrand apart from the density is $(4d^2)^h X_0^h W^\tau$. Positive real bases use the real logarithm. The unique zero of X_0 on the reduced rectangle is $(\gamma_0, 0)$.

On each side of γ_0, take $\alpha = -\gamma_0$ or $\pi/2 - \gamma_0$. Use two triangular charts $\gamma = \gamma_0 + \alpha t u$, $\phi = \pi t v$ with $(u, v) = (1, y)$ or $(y, 1)$ and $0 \le t, y \le 1$. Their Jacobian is $\pi|\alpha|t$. With $\operatorname{sinc}(x) = \sin(x)/x$ extended by one at zero,

$$A = X_0/t^2 = [\alpha u \sin(\gamma_0 + \alpha t u/2)\operatorname{sinc}(\alpha t u/2)]^2 + z\cos\gamma[\pi v \operatorname{sinc}(\phi/2)]^2.$$

The right side extends analytically over $t = 0$. It is strictly positive on each real square. Indeed the radial term vanishes only when $u = 0$, in which case $v = 1$ and $\cos\gamma = z > 0$; the endpoint with $\cos\gamma = 0$ has nonzero radial term. Thus, with $\nu = 2h + 1$ and $C = (4/\pi)(4d^2)^h$,

$$T_2 = C \sum_{\alpha,\,\text{chart}} |\alpha| \int_0^1 \int_0^1 t^\nu f(t, y)\, dy\, dt, \qquad f = \sin^2\gamma\, A^h D_-^\tau D_+^\tau.$$

All of the real integral's singular behavior is in t^ν; absolute integrability is exactly $\Re\nu > -1$, since the factors at the original zero are nonzero and $\Re h$ controls the local singular power. The three analytic bases are enclosed separately on complex boxes. The implementation accepts a box only when all three real-part lower bounds are strictly positive. Their principal logarithms then define single-valued holomorphic powers throughout that box. At real interior quadrature nodes the equivalent formula $W = [(1+z^2)\cos\phi - 2zr]^2 + d^2\sin^2\phi$ is used with its positive real logarithm. This avoids assigning a principal logarithm to a product on a complex region where a sum of logarithms would have a different branch.

Local remainder and the singular weights. On a dyadic panel $[a, b] \times [l, r']$, interpolate in t at the n first-kind Chebyshev roots, and integrate in y with $m = \lfloor (n+1)/2 \rfloor$ Gauss–Legendre nodes. Let M bound $|f|$ when t varies over the filled Bernstein ellipse of parameter 3 and y stays real, and let K bound $|f|$ with the coordinates exchanged. For each coordinate the bounding rectangle of the ellipse has semiaxes $5/3$ and $4/3$ times the interval's half-width. The two independent interval evaluations yield M, K by outward rounding.

For a function bounded by M on such an ellipse, its Chebyshev coefficients at index $j \ge 1$ have modulus at most $2M3^{-j}$, by the Laurent expansion on the annulus. The degree-$n-1$ truncation therefore has error at most $3M3^{-n}$. The interpolation operator at the n roots has norm at most $2n$ by its discrete cosine formula. An m-point positive Gauss rule on a normalized unit interval integrates degree $2m-1$ exactly, so its error is at most twice the corresponding Chebyshev tail $3K3^{-2m}$. First apply the y rule pointwise for real t. Its normalized weighted sum is itself bounded by M on the t ellipse, since the Gauss weights are positive and sum to one after division by the interval length. Interpolate that sum and integrate the resulting polynomial exactly against t^ν. The local error is bounded by

$$(r' - l)\int_a^b t^{\Re\nu} dt\, \left[3(1+2n)M3^{-n} + 6K3^{-2m}\right].$$

This order of estimation avoids assuming positivity of the complex-weight quadrature.

In the coordinate $x = (t-a)/(b-a)$ the moments of the monomials x^j against $(a + (b-a)x)^\nu dx$ are

$$\frac{b^\nu}{\nu + j + 1} \quad (a = 0), \qquad \frac{b^\nu}{j+1}\, {}_2F_1(-\nu, 1; j+2; 1 - a/b) \quad (a > 0).$$

The second identity follows from Euler's integral after $x \mapsto 1 - x$; $0 < 1 - a/b < 1$ and the base of the power is positive. Shifted Chebyshev polynomial coefficients and the discrete cosine transform convert these into exact interpolation weights, evaluated by ball arithmetic. If every accepted panel has bracket at most η, the total analytic error is at most

$$|C|\pi\eta/(\Re\nu + 1),$$

since the four absolute chart weights sum to π. The implementation adds this radius to each rectangular component and includes all interval arithmetic errors in the returned ball. If the sum of the two component radii

is e and the enclosure's modulus has lower bound $L > 0$, the midpoint has absolute error at most e and relative error at most e/L. At a zero only an absolute claim follows. Each accepted panel uses nm real nodes, and cap exhaustion returns a resource failure.

Proposition 21.3 (a region separated from zeros). On

$$\tfrac{1}{2} \le z \le \tfrac{9}{10}, \qquad \tfrac{1}{2} \le \Re h \le 1, \qquad |\Im h| \le 10^{-3}, \qquad |\Re s| \le \tfrac{1}{10}, \qquad |\Im s| \le \tfrac{1}{16},$$

one has $\Re T_2 > 1/50$. Put $X = |S_2|^2$. Each summand of S_2 is $z + (\lambda - z)/(1 - z\lambda)$, giving $X \le 16$, and $10^{-4} \le W \le 16$. Hence $1/3 \le W^{\Re s} \le 3$. On $X \ge e^{-100}$ the absolute phase of $X^h W^s$ is at most $0.1 + \log(10^4)/16 < 0.68$, and its cosine exceeds $3/4$. Also $X^{\Re h} \ge X/4$ throughout $0 \le X \le 16$. On the discarded set $X < e^{-100}$ the absolute integrand is at most $3e^{-50}$. Finally $\mathbb{E}X = 1 - z^4$: in the expansion $S_2 = d\sum_{k\ge1} z^{k-1}\operatorname{Tr}(U^k)$ the rank-two Weyl density gives $\mathbb{E}[\operatorname{Tr}(U^k)\overline{\operatorname{Tr}(U^l)}] = \delta_{kl}\min(k,2)$, by integrating its constant and cosine terms. Thus

$$\Re T_2 \ge (1 - z^4 - e^{-100})/16 - 3e^{-50} > 1/50.$$

The analytic error at panel tolerance η on this strip is at most 3η, because $4d^2 \le 9/4$ and $\Re\nu + 1 \ge 3$. For example $e \le 2 \times 10^{-12}$ then certifies relative error below 10^{-10} by the independent modulus bound. Attainment is checked from the actual final ball.

The analytic panel tolerance 10^{-13} at order $n = 52$ is feasible under unrestricted subdivision uniformly on this compact strip. In fact on the real charts $A \le 5\pi^2/4 < 13$ and $W^{\Re(s-h)} \le 10^{4.4}$, so $|f| < 3.4 \times 10^5$. The three real bases have a common positive minimum by compactness and strict positivity. As both box widths and input rounding radii vanish, the complex interval enclosures approach their real point values uniformly by continuity of the operations on these nonsingular compact sets. Thus $M, K < 4 \times 10^5$ can be achieved on all sufficiently small panels at adequate precision, and the displayed bracket is less than 10^{-13}. This existence argument gives no practical bound on the required panel count or working precision. The timings, capped runs and returned enclosures are separate computational evidence.

A separate interval computation supplies a concrete uniform analytic bound on the same strip. Divide $[1/2, 9/10]$ into 32 closed intervals of length $1/80$. On each interval use ball inputs for the whole z interval and both full complex-exponent rectangles. At $n = 52$, 320-bit working precision and the stricter local tolerance 5×10^{-14}, the unchanged ellipse test certifies all four charts in all 32 boxes. The maxima across boxes are 3,554 accepted panels, 7,104 visited rectangles and 14 dyadic bisections along the longest refinement path. Consequently the certified template for any one box uses at most $3{,}554 \cdot 52 \cdot 26 = 4{,}805{,}008$ function nodes if its full mesh is used. The uniform remainder before node roundoff is at most 1.5×10^{-13} in modulus. This template check performs no nodal integration for the parameter rectangles; individual returned balls supply their own floating-point and relative-error certificates. The companion script reproduces the covering trees starting from their exact dyadic coordinates.

Theorem 21.4 (certified relative accuracy on a closed parameter region). On the closed zero-free strip above, the routine `evaluate_strip` takes exact rational components and returns a certified relative error at most 10^{-10}. With unrestricted working precision it terminates for every such point. The proof gives a uniform bound of 7,104 tested rectangles, 3,554 accepted panels and 4,805,008 function nodes per integration pass. The routine reports its final precision, pass count and panel and node counts. Timings for the replayed examples are recorded separately.

The routine first determines which of the 32 exact spectral subintervals contains the input. It reproduces the certified ellipse tree for the whole complex parameter box with tolerance 5×10^{-14}. In each integration pass a parent rectangle may pass the pointwise ellipse test at 10^{-13} and replace all its descendants. Otherwise the recursion stops at a certified template leaf. Every possible mesh is therefore a pruning of a single verified finite tree. Analytic enclosure does not depend on a point run reproducing the box run's interval arithmetic decisions.

The outer arithmetic and all singular quadrature weights use the current working precision. The first pass may restrict node arithmetic to 112 bits for speed; on every later pass the node precision equals the outer precision. After forming the rectangle for the answer, let e denote its outward-rounded sum of component radii. Use the smaller of $50e$ and e/L when a positive computed modulus bound L is also available. Return only when the chosen upper bound is at most 10^{-10}. Otherwise double the precision. The optional bit cap terminates the search with a resource status if the requested accuracy has not been certified; a final capped pass may first retry at the full allowed node precision.

To verify termination, there are only finitely many possible panels for each input, and all quadrature nodes are in their interiors. Their real analytic bases are strictly positive. The central weight moments have denominators with positive real parts, and each off-centre hypergeometric argument lies in $[0,1)$. In fact $1-a/b \le 1/2$ on noncentral dyadic panels. The ball evaluations of these quantities and of the finite arithmetic expressions at the nodes contract to their exact values as the precision increases. For sufficiently large precision every admissible pruning therefore has arbitrarily small nodal and weight errors, even if an earlier pass suffered cancellation. The remaining analytic allowance is at most 3×10^{-13} per component. The fixed relative padding of the two outward-rounded Arb radii is immaterial at this margin (their magnitude mantissas have 30 bits, as specified in the FLINT magnitude bounds). In particular $e < 2 \times 10^{-12}$ eventually. The modulus bound $1/50$ proves the stopping criterion. This argument supplies no universal numerical upper bound on the precision or running time. It proves termination and certified relative accuracy on the stated strip; general calls elsewhere retain their separate success and failure statuses.

The isolated replay certified both spectral endpoints with relative radii below 4.34×10^{-13} and 1.07×10^{-13}. At $z = 0.55$, $h = 0.75 + 0.0007i$, $s = 0.016 - 0.028i$, starting at 64 bits triggered the actual refinement path through 128 to 256 bits, returning relative radius below 4.23×10^{-13}. The same input capped at 64 bits returned a precision failure. At $z = 1/2, h = 1, s = 0$ the output contains the exact value $15/16$. Three outside-strip rational inputs were rejected by exact comparisons.

Certified scalar connection by polynomial interpolation

Theorem 21.5 (a determinant enclosure on both sides of a critical radius). Write $R = N(1+z)$, $X = |S_N|^2/R^2 \in [0,1]$, $d\mu_s = |\Lambda_N|^{2s} dU$ for $0 \le z < 1$, and let $u = \Re s$. Regard μ_s also as a measure of X. The following algorithm computes an absolute-error enclosure at an individual physical radius, including each interior critical radius. It uses one-variable series to obtain all the required finite moments. It supplies an independent value on either side of a connection. It is distinct from propagation of an entire differential-system basis. In the proved density-bound branch take $N \ge 3$, $\Re h > -1$. The positive-order bracket below also applies at $N = 2$.

Choose $k \ge 2$ and a nonintegral real $-1 < \gamma \le \Re h$. Let H_h be the degree-$2k-1$ Hermite interpolant of x^h (value and first derivative) at the k shifted Gauss–Legendre nodes a_j on $[0,1]$, with normalized quadrature weights w_j. Let $Q_k(f) = \sum w_j f(a_j)$. Put

$$D_k(h,\gamma) = \left| \frac{(-h)_{2k}}{(-\gamma)_{2k}} \right|, \qquad V_k = R^{2h} \int H_h(X)\, d\mu_s.$$

On a rank-N Haar preparation, a global density upper bound for X under μ_u is

$$C_X = \pi R^2 \frac{3\sqrt{3}\, 16^{N-2}}{\pi^2 N(N-1)} (1-z^2)^{N^2+2Nu} \max\left((1-z)^{-2N(N+u)}, (1+z)^{-2N(N+u)}\right).$$

Consequently

$$|T_N(h,s;z) - V_k| \le R^{2\Re h} D_k(h,\gamma) C_X \left| \frac{1}{\gamma+1} - Q_k(x^\gamma) \right|. \tag{21.5}$$

To obtain C_X, use the disk transformation from Section 10. Among any three named angles at least one of their three pairs has circular separation at most $2\pi/3$. Resolve that pair into the plane. Its squared Vandermonde divided by the area Jacobian is at most $2\sqrt{3}$, with at most two ordered preimages. Bound only the tags' cross chords by 16^{N-2} and integrate the resident Vandermonde exactly, giving $(N-2)!/N!$. The displayed tilt multiplier is its actual supremum bound in these transformed coordinates. Finally the map from planar displacement to its squared modulus divided by R^2 has radial area factor πR^2. This refines the explicit majorant in Theorem 20.1.

Here is a second enclosure when $0 < \gamma \le \Re h$. Let L_γ interpolate x^γ at both endpoints with multiplicity one and at any distinct $k-1$ interior nodes with multiplicity two. It has the same degree bound as H_γ. Then

$$|T_N(h,s;z) - V_k| \le R^{2\Re h} D_k(h,\gamma) \left| \int (H_\gamma - L_\gamma)(X)\, d\mu_u \right|. \tag{21.6}$$

The last integral requires only the same finite list of integer moments for the *real* tilt. Its sign is fixed before integration. This enclosure is useful when a global sup norm for the prepared planar density is large.

Proof. At $0 < x \le 1$ the Hermite remainder is the product of the repeated-node factors times the divided difference with x appended. Its simplex formula integrates the derivative of order $2k$ at convex combinations of the nodes. The derivative modulus of y^h is bounded by $D_k(h,\gamma)$ times the absolute derivative of y^γ. The latter derivative has fixed sign; the Gauss product $\prod(x-a_j)^2$ is nonnegative. Thus $|x^h - H_h(x)| \le D_k|x^\gamma - H_\gamma(x)|$. Coincident nodes follow by continuity. The closed-node product $x(x-1)\prod(x-b_j)^2$ has the opposite sign. For $0 < \gamma$ moving the left endpoint from 0 to a positive $\epsilon < x$ and sending it to zero proves the bracket also for $\gamma < 2k$. Integration gives (21.6) since $|d\mu_s| \le d\mu_u$ after projection. Integration with the constant density majorant instead gives (21.5), by exactness of Gauss–Legendre quadrature for H_γ. For $\gamma < 0$ Gaussian quadrature underestimates $\int x^\gamma dx$ by the same sign argument. Test convergence first on bounded continuous functions below x^γ and exhaust its integral, using positivity of the weights. For $\gamma > 0$ ordinary uniform polynomial approximation suffices. The Pochhammer ratio is bounded as $k \to \infty$ for fixed h,γ by the gamma-ratio estimate since $\gamma \le \Re h$. Thus (21.5) tends to zero, including for inverse orders at a critical radius. Direct polynomial evaluation gives the terminating integer case. The decision to divide by a computed lower bound for $|T_N|$ is made only after including analytic truncation and arithmetic radii.

Computing the complete moment list. Put $\nu = -N - s$ and

$$f_j(z) = z^{|j|}\frac{(-\nu)_{|j|}}{|j|!}\,{}_2F_1(|j|-\nu,-\nu;|j|+1;z^2).$$

These are the circle Fourier coefficients of D_z^ν, obtained by multiplying its two convergent binomial series. Use series order $2d+1$ for a requested highest integer moment d. For the ray angle ϕ set

$$b_{j,0} = e^{ij\phi}f_j, \qquad b_{j,l+1} = \frac{b_{j-1,l} + b_{j+1,l}}{2R(l+1)}, \qquad B_j(v) = \sum_{l=0}^{2d} b_{j,l}v^l.$$

This is the angular Taylor series for $e^{v\Re(e^{i\phi}w)/R}D_z(w)^\nu$ after rephasing. Start with $|j| \le N-1+2d$ and shrink the retained band by one at each step. In the determinant the phases $e^{ij\phi}$ cancel between row and column. Let

$$D(v,\phi) = e^{-Nzv\cos\phi/R}\det[B_{i-j}(v)]_{i,j=0}^{N-1} \pmod{v^{2d+1}}.$$

Then, for $0 \le j \le d$,

$$\int X^j\,d\mu_s = (1-z^2)^{N^2+2Ns}4^j(j!)^2\frac{1}{d+1}\sum_{b=0}^{d}[v^{2j}]D(v,\pi b/(d+1)). \tag{21.7}$$

Indeed the coefficient before the angular average is the $2j$th directional moment divided by $(2j)!$. Its harmonics are even and have order at most $2j$, so the rays integrate it exactly. The average of $\cos^{2j}\phi$ is $4^{-j}\binom{2j}{j}$. Reflection halves the number of distinct determinant calculations in the Haar scalar case, also for complex tilt since simultaneous angle reflection leaves the preparation unchanged. To compute a component of the independent-angle vector, replace the determinant by a product of its requested one-angle entries, undo their phases, retain all rays, and omit the physical scalar prefactor. This last identity computes polynomial seeds; inverse-mode tails use the separate small-ball bound in Section 10.

The verification code uses a subset expansion of the truncated determinant. For each subset of selected columns it accumulates all permutation prefixes with their signs. This requires $O(N2^N)$ products of truncated one-variable series per ray and only scalar multiplications and additions. It remains valid if one or more prepared minor constants vanish. Interpolant coefficients, Fourier modes, finite averages and analytic remainders are computed with outward-rounded real and complex balls. For a double interpolation node a, form the product of the factors at the *other* nodes, with their multiplicities, normalized to one at a and denoted P_a. Its contribution is $a^hP_a(x)[1 + (h/a - P_a'(a))(x-a)]$. Single nodes use a^hP_a; at $a = 0$, $\gamma > 0$ gives zero. Exact rational interior nodes near the Lobatto nodes are sufficient for (21.6), so a rounded suggested node is first interpreted as its exact dyadic rational. Cancellation in the polynomial coefficients and determinant jets can require substantially more precision than the requested final answer. A nonfinite ball is a rejected computation.

A uniform approximation budget on a parameter box

Corollary 21.6 (a zero-free box and an explicit degree). For every integer $3 \le N \le 8$, throughout

$$0 \le z \le \tfrac{1}{2}, \quad \tfrac{5}{2} \le \Re h \le 3, \quad |\Im h| \le \tfrac{1}{8}, \quad |\Re s| \le \tfrac{1}{16}, \quad |\Im s| \le \tfrac{1}{32},$$

one has $\Re T_N > 1/6$. A single degree bound 8192 gives a relative *analytic truncation* error less than 4.74×10^{-12} for the integrated shifted Chebyshev expansion of x^h. The statement specifies an upper budget for exact polynomial integration, including all interior critical radii in the box. The full determinant at that degree was not evaluated in this work.

To prove the lower bound, note $|S_N| \le 12$ and $|\log|\Lambda_N|| \le 8\log 2$. On $|S_N| \ge 1/2$ the phase of the mixed power has absolute value bounded above by $\frac{1}{4}\log 12 + \frac{1}{2}\log 2 < \pi/3$. The absolute tilt weight lies between $1/2$ and 2 everywhere. Directly $\mathbb{E}|S_N|^2 = 1 - z^{2N}$: expand the logarithmic derivative in positive trace powers and use the Haar covariance $\mathbb{E}[\operatorname{Tr} U^j \overline{\operatorname{Tr} U^k}] = \delta_{jk}\min(j,N)$ for positive j,k. To see the latter, rotation kills the unequal orders. In the equal-order covariance subtract from N the number of indices in the Fourier projection $0,\dots,N-1$ remaining in that projection after a shift by j; this is $(N-j)_+$. Jensen's inequality gives the real power lower bound $(1-z^{2N})^{\Re h}$. Removing $|S_N| < 1/2$ first and allowing the worst sign there leaves a uniform lower bound $[(1-2^{-6})^3 - 1/32]/4 - 2/32 > 1/6$.

Write $x = (1+\cos\theta)/2$ and $x^h = c_0 + \sum_{j\ge1} c_j \cos j\theta$. Integrating the cosine coefficient of $\cos^{2h}(\theta/2)$ gives $c_1/c_0 = 2h/(h+1)$ and $c_{j+1}/c_j = (h-j)/(h+j+1)$ for $j \ge 1$, using the product identity when a coefficient vanishes. For example, the recurrence follows by integrating the derivative of $\cos^{2h+1}(\theta/2)\sin((j+1/2)\theta)$ over $0 \le \theta \le \pi$. Let $l = 5/2, u = 3, v = 1/8$, and take $U_1 = 2\sqrt{u^2+v^2}/(l+1)$. Successively multiply U_j by $\sqrt{\max(|j-l|,|j-u|)^2+v^2}/(j+l+1)$ to obtain U_{j+1}. Since $|c_0| \le 1$, these give uniform coefficient bounds. For $j \ge m = 8193$ the ratio is at most $(j-\alpha)/(j+1+\alpha)$, $\alpha = 12/5$, by squaring the numerator bound. The tail is bounded by $U_m(m+\alpha)/(2\alpha)$ by telescoping. Multiply by $2\cdot12^6$ to include the preparation and physical scaling. The companion real-ball product bounds the resulting absolute error by 7.96×10^{-13}; dividing the computed bound by the sharper lower bound 0.16815090179443359375 above gives relative truncation error below 4.734×10^{-12}. A validated calculation of that finite polynomial could use (21.7) with increased precision until its separate rounding budget is met. At selected points the smaller Hermite grids below already attain ten relative decimal digits.

An independent inverse-moment certificate at an interior trace critical value

Proposition 21.7 (a critical inverse-moment benchmark). Take $N = 3$, $s = -3$, $h = -1/2$, and $a = 3z$, $0 < a < 3$. The Möbius preparation is Haar in the translated coordinates. Put $U(a) = \mathbb{E}|a - \operatorname{Tr} V|^{-1}$ there. In the paper's normalization,

$$T_3(-1/2,-3;z) = (1-z^2)^{-9}U(a).$$

This calculation supplies scalar benchmarks for comparison with continued solutions. It uses the ordinary moment and includes the critical point $a = 1$.

By the planar Fourier transform of $|x|^{-1}$ and Andréief's identity,

$$U(a) = \int_0^\infty J_0(ar)\Phi(r)\,dr, \qquad \Phi(r) = \det[J_{i-j}(r)]_{i,j=1}^3.$$

Equivalently insert $e^{-\epsilon r}$ to transform the kernel $1/\sqrt{\epsilon^2+|x|^2}$, then pass by monotone convergence on the Haar side. The bounds below give absolute integrability on the Bessel side. Write $A = J_0(r)$, $B = J_1(r)$, $C = J_2(r)$. The determinant is $A^3 + 2AB^2 + 2B^2C - AC^2$. The recurrence $C = 2B/r - A$ gives the cancellation-preserving form

$$\Phi(r) = \frac{4}{r}(B^3 + A^2B) - \frac{4}{r^2}AB^2.$$

On $[0,R]$ use even integer R and n-point Gauss–Legendre panels of length two. The integrand is a characteristic function supported in frequencies $[-a-3, a+3]$, since it multiplies the characteristic functions of $a\cos t$ and $\Re\operatorname{Tr} V$. Every real derivative of order j has modulus at most $(a+3)^j$. Taylor approximation about the midpoint to degree $2n-1$, quadrature exactness and positivity of the weights bound the composite error by $2R(a+3)^{2n}/(2n)!$. The implementation uses the unmodified determinant on this segment.

For the tail, define $A_{\nu,0} = 1$ and

$$A_{\nu,j+1} = A_{\nu,j}\frac{4\nu^2 - (2j+1)^2}{8(j+1)}.$$

For $\nu = 0, 1$, $b > 0$, and $L \geq 1$, represent $r^{1/2} J_\nu(br)$ by

$$P_{\nu,b}(r) = \sqrt{\frac{2}{\pi b}} \Re \left[e^{i(br - \pi\nu/2 - \pi/4)} \sum_{j=0}^{L-1} \frac{i^j A_{\nu,j}}{(br)^j} \right],$$

$$|r^{1/2} J_\nu(br) - P_{\nu,b}(r)| \leq E_{\nu,b} r^{-L}, \qquad E_{\nu,b} = \sqrt{\frac{2}{\pi b}} \frac{|A_{\nu,L}|}{b^L}.$$

For this error inequality, set $t = 1 + v/w$ in the positive-real $K_\nu(w)$ Laplace representation (NIST DLMF 10.32.8). The resulting gamma integral in v analytically continues through $\Re w > 0$ to $w = -ix$ for $x > 0$, with dominated boundary limits. The continuation identity for K_ν and $H_\nu^{(1)}$ (DLMF 10.27.8) leaves the bracket of the normalized Hankel function as the gamma expectation of $(1 + iv/(2x))^{\nu - 1/2}$, with unit-scale gamma shape $\nu + 1/2$. Taylor's integral remainder on the segment from 0 to $iv/(2x)$ is at most $|\binom{\nu-1/2}{L}|(v/(2x))^L$, since $|1 + iy| \geq 1$ and $\nu - 1/2 - L < 0$. Integration gives exactly the displayed first-omitted-coefficient bound.

For each factor i take $B_i = \sqrt{2/(\pi b_i)} \sum_{j<L} |A_{\nu_i,j}|/(b_i R)^j + E_i R^{-L}$. A tail monomial $m r^{-p} \prod_{i=1}^4 r^{1/2} J_{\nu_i}(b_i r)$, $p = 3$ or 4, has integrated replacement error at most

$$\frac{|m| R^{1-p-L}}{p + L - 1} \sum_i E_i \prod_{j \neq i} B_j.$$

Integrate the full finite product of all four P_i. Each term requires $\int_R^\infty r^{-j} e^{i\omega r} dr = R^{1-j} E_j(-i\omega R)$ for $j > 1$, by a one-sided Laplace limit. When the exact rational frequency is zero the value is $R^{1-j}/(j-1)$. This handles the critical radius without dividing by a vanishing frequency.

At $R = 96, L = 10, n = 24$ with 180-bit ball arithmetic the script gave the following *outward enlarged* enclosures. The last column uses the actual returned ball before decimal printing.

a	z	Enclosure of $T_3(-1/2, -3; z)$	Radius divided by lower absolute bound
3/4	1/4	$2.49186292689550745657 \pm 6.1 \times 10^{-21}$	$< 8.55 \times 10^{-22}$
1	1/3	$3.35198304971839748186 \pm 5.1 \times 10^{-21}$	$< 1.79 \times 10^{-22}$
161/100	161/300	$15.03282355696433846004 \pm 2.8 \times 10^{-21}$	$< 1.77 \times 10^{-22}$

The test rejects omission of the full tail at every point. The certificate checks the physical scalar at three specified parameters. The floating-point semicircle integrations at this half order have their own numerical error. Proposition 21.8 certifies two-arc propagation at quarter order. Reproduce with `python checks/inverse_rank3_balls.py` using the version of python-flint in the package requirements. The decimal record is in `records/inverse_rank3_balls.txt`.

NIST DLMF, §10.32, integral 8 · NIST DLMF, §10.27, connection formula 8

Independent incoming data at quarter order. For $h = -1/4$, $s = -3$ the planar Fourier identity for the Riesz kernel replaces the integrand by $K r^{-1/2} J_0(ar) \Phi(r)$, $K = \sqrt{2}\,\Gamma(3/4)/\Gamma(1/4)$. The possible singularity of the matrix trace has an integrable planar kernel, including at $a = 1$ by the bounded rank-three planar density. The Fourier formula can also be justified by Gaussian tempering and the approximate identity, or directly by the Abelian Riesz convolution of Section 10. The function $F(r) = J_0(ar)\Phi(r)$ has an entire extension with $|F(r)| \leq \exp(M|\Im r|)$, $M = 3 + a$, as follows from its representation as a characteristic function.

On $[0, 2]$, put $r = u^2$, so that $r^{-1/2} dr = 2du$. The degree-$(n-1)$ Taylor approximation to $F(r)$ at zero has error at most $(2M)^n/n!$. Its composition with u^2 has degree at most $2n - 2$. The error for n Gauss points on the transformed interval is therefore at most $4\sqrt{2}(2M)^n/n!$. On any remaining panel $[m - 1, m + 1]$, put $d = \min(8, m - 1)$, $m = 3, 5, \ldots, R - 1$. On the disk $|r - m| \leq d$, take the square root positive on the real axis. There $|r^{-1/2} F(r)| \leq (m - d)^{-1/2} e^{Md}$. Taylor expansion to degree $2n - 1$ followed by Gauss exactness bounds the panel error by $4(m - d)^{-1/2} e^{Md} d^{1-2n}/(d - 1)$. In the tail calculation add $1/2$ to every power of r in the denominator, both in the finite exponential integrals and the integrated remainder. The zero-frequency formula applies also to noninteger powers $j > 1$.

The script `checks/quarter_rank3_balls.py` used $R = 144$, $L = 20$, $n = 85$, and 260-bit arithmetic. It certified six independently seeded, **unscaled** translated moments $U(a)$ for $a = 0.59, 0.65, 0.72, 0.79, 1, 1.21$, with relative radii below 3.06×10^{-35} in every case. At $a = 1.21$, the returned decimal enclosure is

$$U(1.21) = 0.92432821007217452035205408957710377700 \ \pm 6.55 \times 10^{-39}.$$

The quarter-order transcript gives each source enclosure and its two truncation bounds. The physical paper moment at any of these points is $(1-a^2/9)^{-9}U(a)$. The relative radii reported here concern the Fourier readouts. Certifying transfer of the incoming data around either arc additionally requires control of its differential system.

A certified critical crossing at rank three

Proposition 21.8 (validated two-arc propagation at inverse order). In the translated-trace family of Theorem 10.2, take $N = 3$, $s = -3$, $h = -1/4$, $a = 3z$ and $x = a^2$. Four independent scalar enclosures of $H_h(x)$ at $a = 0.59, 0.65, 0.72, 0.79$ determine all four Euler derivatives of orders 0 through 3 at $a = 0.79$. Propagating that state along two polygonal paths through $1 \pm 0.21i$ to $a = 1.21$ and applying Theorem 10.9 gives

$$T_3(-1/4, -3; 121/300) = 4.56870010441547136650724\ldots.$$

The unshortened computed real and imaginary intervals each have radius below 6.77×10^{-32}. The corresponding unscaled result overlaps a fifth, independently enclosed Bessel integral at the outgoing radius; the absolute difference of the two enclosures is bounded by 1.98×10^{-32}.

Here are the equations and truncation bounds for this certificate. Set $V = (H, \theta H, \theta^2 H, \theta^3 H)^t$ with $\theta = x\partial_x$. The coefficients $(c_0, \ldots, c_4)$ of the Euler equation from (10.2), after clearing the denominator, are

$$\left(49a^4/16, \quad 21a^4, \quad 22a^4 - 66a^2 + 144, \quad -48a^4 + 272a^2 - 288, \quad 16(a^2-1)(a^2-9)\right).$$

Thus $pV' = QV$, where $p = ac_4$, the first three rows of Q have $2c_4$ on the superdiagonal and the last row is $-2(c_0, c_1, c_2, c_3)$. On each panel $a = u + vt$, let p_j, q_j be the polynomial coefficients of $p(u + vt), vQ(u + vt)$ in t. The fundamental matrix $F(t) = \sum A_j t^j$, $A_0 = I$, is computed by

$$p_0(k+1)A_{k+1} = \sum_{j=0}^{\min(4,k)} q_j A_{k-j} - \sum_{j=1}^{\min(5,k)} p_j(k-j+1)A_{k-j+1}.$$

On $|t| \le 2$, an upper bound for the connection norm in the t coordinate is

$$M = \frac{\sum_{j=0}^{4} 2^j \|q_j\|_\infty}{16 \prod_{b=0,\pm1,\pm3}(|u-b| - 2|v|)}.$$

All factors in the denominator are checked positive. Integrating along each disc radius gives $\sup_{|t|=2} \|F(t)\|_\infty \le e^{2M}$; Cauchy's inequality bounds each entry of the tail at $t = 1$ past degree 128 by $e^{2M}2^{-128}$. All coefficients, products, solves and interval inflations are outward rounded. For each of the three consecutive segments joining the four incoming nodes use four panels; for each of the four complex path legs use sixteen panels. The largest panel tail is below 6.68×10^{-39}. The zeroth rows of the four backward transfers from 0.79 give the shooting matrix, whose certified infinity-norm condition number is less than 3574.47. Its interval inverse exists. The physical mixing weights are $(1 - i)/2, (1 + i)/2$ for the upper and lower paths respectively. The real prefactor taking H to T_3 is $(1 - (121/300)^2)^{-9}$. A single path misses the outgoing Bessel result by more than 0.0069; averaging the two paths with equal weights misses by more than 0.0048. These exclusions concern the unscaled scalar. This proves a crossing at one fractional inverse order and one special tilt.

Enclosing every reduced incoming mode

Write $a = Nz$, $R = N(1 + z)$, $D_z(w) = |1 - zw|^2$, $\nu = -N - s$, $G = h + \lfloor (N-1)^2/4 \rfloor$, and $dm = \prod d\theta_i/(2\pi)$, with $w_i = e^{i\theta_i}$. The $\binom{N+3}{3}$ entries needed by Theorem 10.6 are

$$W_m = \int |a - \textstyle\sum w_i|^{2G} \prod_i w_i^{m_i} D_z(w_i)^\nu \, dm, \qquad -1 \le m_1 \le \cdots \le m_N \le 2.$$

They carry neither the Haar prefactor nor the squared Vandermonde. Two algorithms give enclosures for all these integrals. The first works for arbitrary s and $\Re G > 0$. The second handles arbitrary complex tilt, $0 < z < 1$, and nonintegral G with $\Re G > 0$. Integral nonnegative orders use finite jets. The two methods have different analytical remainders.

A common Hermite error for all modes. Use the open-node polynomial H_G and the two comparator polynomials H_γ, L_γ of Theorem 21.5, with $0 < \gamma \le \Re G$ nonintegral and degree $d = 2k - 1$. For $X = |a - \sum w_i|^2/R^2$, replace X^G by $H_G(X)$. The pointwise divided-difference bound in that theorem gives the following disk radius, valid for each m:

$$R^{2\Re G} \max((1-z)^{2N\Re\nu}, (1+z)^{2N\Re\nu}) \left|\frac{(-G)_{2k}}{(-\gamma)_{2k}}\right| \left|\int (H_\gamma - L_\gamma)(X)\, dm\right|.$$

The final measure is the independent uniform angular product. Its moments are especially inexpensive. If $B(t) = \sum_{j\ge 0} t^j/(j!)^2$, then

$$\int X^j\, dm = (j!)^2 [t^j] B(a^2 t/R^2) B(t/R^2)^N.$$

Rotation of all unit angles permits one to randomize the angle of the fixed vector a. Expanding the two multinomials then gives the identity, including the zero moment. The sign of $H_\gamma - L_\gamma$ is fixed on $[0,1]$. These facts avoid any positivity assumption on the requested tilt.

For the polynomial centres calculate the one-angle Fourier coefficients f_j of D_z^ν by the hypergeometric expression preceding (21.7). On the $d+1$ rays $\phi_b = \pi b/(d+1)$, the lth coefficient for mode m in its directional exponential, with the phases consistent with (21.7), is

$$\sum_{j=0}^{l} \frac{f_{m+l-2j} e^{i(l-2j)\phi_b}}{(2R)^l j!(l-j)!}.$$

For each m, l one discrete Fourier transform of length $d+1$ evaluates all rays, folding indices j modulo $d+1$ before transformation. At a ray multiply the relevant N series and the translation $\exp(-av\cos\phi_b/R)$. Coefficient v^{2j} averaged over the rays and multiplied by $4^j(j!)^2$ gives the exact X^j moment with the inserted angular modes. Indeed the surviving Fourier frequencies are even and their absolute values do not exceed $2j$. All sorted tuples reuse the same four initial series and their common products. The Hermite integration is a finite outward-rounded calculation augmented by the displayed disk radius.

An independent Bessel integral for a complete incoming state. Put $\Phi_m(r) = \int J_0(r|a - \sum w_i|) \prod_i w_i^{m_i} D_z(w_i)^\nu dm$ and $K(G) = 2^{2G+1}\Gamma(1+G)/\Gamma(-G)$. Use the radial inversion of Section 5 with a fixed split at $r_0 = 2$. The tagged integrals have the same inversion since their compact angular factors give finite measures. The expansion at zero is

$$\Phi_m(r) = \sum_{j\ge 0} \frac{(-r^2/4)^j}{(j!)^2} \int |a - \sum w_i|^{2j} \prod_i w_i^{m_i} D_z(w_i)^\nu dm.$$

Multiply each coefficient by $r_0^{2j-2G}/(2j-2G)$ and add the ordinary integral of $r^{-1-2G}\Phi_m(r)$ on $[r_0, \infty)$. Multiplication by $K(G)$ gives W_m. This subtraction and the elementary Fourier formula may first be taken in their distributional Riesz domain, then continued in G by the subtractions. On the positive nonreal half-plane used here all the displayed operations at the upper endpoint converge absolutely. With the first $d+1$ origin coefficients retained, their tail before $K(G)$ is bounded by

$$\max((1-z)^{2N\Re\nu}, (1+z)^{2N\Re\nu}) \frac{r_0^{-2\Re G}(Rr_0/2)^{2d+2}}{(d+1)!^2(2d+2-2\Re G)[1-(Rr_0/(2d+4))^2]},$$

whenever $d + 1 > \Re G$ and the bracket is positive. This follows by a geometric majorant starting with the first omitted coefficient.

For $r \ge r_0$ truncate each preparation to its Fourier modes $|k| \le M$. The exact truncated source is

$$\sum_{|l_i - m_i| \le M} J_{\sum l_i}(ar) \prod_i f_{l_i - m_i} J_{l_i}(r).$$

For proof, resolve the uniform angular direction in the defining J_0, expand each directional exponential, and integrate its angular frequency. The phases $i^{\sum l_i}$ from the particles cancel the phase from the fixed translation. Multiply Laurent polynomials in a formal angle and contract against the last Bessel vector to compute all tuples. Let $S_M = |f_0| + 2\sum_{j=1}^{M} |f_j|$. The two binomial series for D_z^ν give $|f_j| \le z^{|j|}/(1-z^2)$ for $|\nu| \le 1$, since $|(-\nu)_l/l!| \le 1$. With $B_M = 2z^{M+1}/[(1-z)(1-z^2)]$, the contribution of omitted angular coefficients to the integral is at most $NB_M(S_M + B_M)^{N-1} r_0^{-2\Re G}/(2\Re G)$.

For general ν a Laurent Cauchy bound replaces B_M. Choose $z < q_0 < 1$ and apply it on the two circles of radii q_0 and $1/q_0$. On either circle the two analytic factors have moduli bounded in product by

$$C(q_0) = \prod_{v = zq_0,\, z/q_0} \max((1-v)^{\Re\nu}, (1+v)^{\Re\nu}) e^{|\Im\nu| \arcsin v}.$$

Indeed $1 - ze^{i\theta}$ at complex radius lies in a disk about 1 of the corresponding radius v. Thus $|f_l| \le C(q_0) q_0^{|l|}$, and $B_M \le 2C(q_0) q_0^{M+1}/(1-q_0)$. Taking the smallest among several verified bounds costs no cancellation. Near $z = 1$ the required angular bandwidth can be large.

On a compact radial panel of half-width b and midpoint p, choose $b < d_0 < p$. On the complex disk of radius d_0 the truncated angular source is bounded by $S_M^N \exp(Rd_0)$, by its angular integral. The positive-real branch of r^{-1-2G} extends to this disk. For q Gauss nodes the error is at most

$$4bS_M^N (p - d_0)^{-1-2\Re G} e^{\pi|\Im(1+2G)|/2 + Rd_0} (b/d_0)^{2q}/(1 - b/d_0).$$

Cauchy's coefficient estimate and positivity and polynomial exactness of Gauss quadrature prove this bound. The implementation subdivides panels if their analytic budget is inadequate.

For a simple bound beyond a cutoff T use $|J_l(x)| \le 4/\sqrt{x}$ for $x \ge 16$, $|l| \le x/2$. Indeed, in the circle representation with phase $l\theta - x\cos\theta$, discard the arcs where the absolute phase derivative is below $\sqrt{x}$. Their total length is at most $4/[\sqrt{1-(3/4)^2}\sqrt{x}]$, since there $|\sin\theta| \le 3/4$. On the complement split at the extrema of the derivative. There are at most six monotone nonstationary pieces, each of integral modulus at most $2/\sqrt{x}$ by integration by parts. Division by 2π gives the claim. For $T, aT \ge 16$, $T \ge 2(M + \max|m_i|)$ and $aT \ge 2N(M + \max|m_i|)$ this gives the truncated-source tail bound

$$\frac{4^{N+1} S_M^N}{\sqrt{a}\,[2\Re G + (N+1)/2] T^{2\Re G + (N+1)/2}}.$$

Integrating the oscillatory tail. There is a sharper alternative. Retain a smaller Fourier cutoff $B < M$ on the tail only. Writing $D_{B,M} = 2\sum_{j=B+1}^{M} |f_j|$, removal costs at most

$$ND_{B,M} S_M^{N-1} 4^N \big/ \big[(2\Re G + N/2) T^{2\Re G + N/2}\big].$$

Here the last offset Bessel is bounded by one. Only $T \ge 16$ and $T \ge 2(M + \max|m_i|)$ are required. For each remaining order l, $b \in \{1, a\}$, retain J terms in the two signed Hankel expansions of $r^{1/2} J_l(br)$ as in Proposition 21.7. For $u = |l|$ and $A_{u,j}$ as in that proposition the uniform replacement error is $E_{l,b} r^{-J}$, with

$$E_{l,b} = \sqrt{\frac{2}{\pi b}} \frac{|A_{u,J}|}{b^J} \left(1 - \frac{(u - 1/2 - J)_+}{2bT}\right)^{-(u+1/2+J)}.$$

The parenthesis must be positive. To prove the bound for large orders, use the same gamma integral as in Proposition 21.7. Taylor's integral remainder now includes $|1 + itv/(2br)|^{u-1/2-J}$, $0 \le t \le 1$. Bound it by $\exp[(u - 1/2 - J)_+ v/(2bT)]$ and integrate against the unit-scale gamma density of shape $u + 1/2 + J$. The sign of a negative integral order is included by using $e^{-i\pi l/2}$ in its phase. Bound either exact or truncated scaled factor by the sum of its absolute retained coefficients at T and $E_{l,b} T^{-J}$, denoted below by $M_{l,b}$. For each multi-index, replacement of the $N+1$ factors costs at most $r^{-J} \sum_i E_i \prod_{j \ne i} M_j$. Sum with the absolute angular Fourier coefficients and integrate the resulting power; the denominator is $(2\Re G + (N+1)/2 + J) T^{2\Re G + (N+1)/2 + J}$. The computation performs these sums by polynomial convolution and keeps the dependence on each *actual* integer order, including the final order $\sum l_i$.

For every product of retained terms keep the signs of all $N+1$ phases. A term of total extra order j and frequency $\omega = \sum_{i=1}^{N} \epsilon_i + a\epsilon_0$ has integral $T^{-v} E_{1+v}(-i\omega T)$, $v = 2G + (N+1)/2 + j$, by continuation from positive Laplace tempering. At $\omega = 0$ its integral is T^{-v}/v. Because $\Re v > 0$ there is ordinary absolute convergence even at zero frequency. Multiplication by the complex $K(G)$ and addition of absolute errors using $|K(G)|$ completes the formula. Returning the two finite upper-end error contributions separately distinguishes truncation of preparation frequencies from truncation of the signed expansions. The original parameter branch throughout is the positive-real branch of the modulus power. This algorithm never interprets the complex preparation as a probability measure.

Incoming order jets at exceptional connection parameters

For $0 < z < 1$, independent $s \in \mathbb{C}$, and $\Re G > 0$, the incoming compact state is holomorphic in G. Indeed $x^{2G} \log x$ is bounded on $0 \le x \le R$ locally in this half-plane, with its value at zero set to zero. Thus $\partial_h W_m$ is obtained by insertion of $\log |a - \sum w_i|^2$ at fixed preparation. A zero of the cosine in the connection formula can require this extra datum even when all entries of W have ordinary absolutely convergent definitions.

Away from the nonnegative integers, differentiate the subtracted radial formula above. The prefactor contributes $K'/K = 2\log 2 + \psi(1+G) + \psi(-G)$. Every retained origin coefficient after integration acquires $2/(2j-2G) - 2\log r_0$. In the integrand on $[r_0, T]$ the multiplier is $-2\log r$. For a panel centered at p with a Cauchy circle of radius $d_0 < p$, its previous quadrature bound can be multiplied by $2(\max(|\log(p-d_0)|, |\log(p+d_0)|) + \pi/2)$. For the real tail, a power majorant $C x_0^{-q}/q$ on $[x_0, \infty)$ with $x_0 \ge 1$ and $q > 0$ acquires $2(\log x_0 + 1/q)$. This rule applies separately to the Fourier error with $x_0 = r_0, q = 2\Re G$ and the Bessel truncation with $x_0 = T, q = 2\Re G + (N+1)/2$. The origin error acquires at most $2\log r_0 + 2/(2d + 2 - 2\Re G)$. Combining errors includes $|K'/K|$ times the full undifferentiated error. These are absolute estimates, so complex signs never enter the budgets.

An independent Hermite computation interpolates $x^G(\log R^2 + \log x)$ at the ordinary interior nodes, $x = |a - \sum w_i|^2/R^2$. For $A = G(G-1)\cdots(G-2k+1)$, choose noninteger $0 < \gamma < \Re G$ and $\delta = \Re G - \gamma$. The pointwise Hermite divided-difference majorant uses the ratio

$$\frac{|A' + A\log R^2| + |A|/(e\delta)}{|\gamma(\gamma-1)\cdots(\gamma-2k+1)|}.$$

Indeed, the $2k$th derivative is $x^{G-2k}[A' + A(\log R^2 + \log x)]$, and $x^{\delta}|\log x| \le 1/(e\delta)$. Multiply by the previous common comparison error and the real preparation and normalization bounds. This supplies a separate angular-polynomial verification using neither the Mellin prefactor nor its derivative.

For $N = 3$, $z = 13/50$, $h = 3/2$ and $s = -143/50 + 21i/100$, all twenty coordinates of both arrays were enclosed using $M = 40$, $T = 434$, 46 Gauss nodes and 240-bit arithmetic. The common absolute analytic disk radii were below $4.946\,10^{-15}$ for W and $7.925\,10^{-14}$ for $\partial_h W$. The rounded finite-centre balls are recorded separately in `records/n3_exceptional.json`. With $k = 32$ and 640 bits the independent Hermite derivative calculation gave a common disk below $1.351\,10^{-7}$; all twenty comparisons overlapped, and a factor-two fault on the first component was excluded. These checks concern the incoming data. A differentiated path transfer and a differentiated scalar readout are separately necessary to use l'Hôpital's rule at an exceptional connection.

Certified full-state crossings

Proposition 21.9 (independent complex parameters on both sides of a critical radius). Take $h = 7/4 + i/4$, $s = -N + 7/50 + 21i/100$. At rank three continue from .26 to .4 through the two polygonal paths with vertices $1/3 \pm .07i$. At rank four continue from .44 to .56 through $1/2 \pm .06i$. Both branches of the 20- and 35-state systems, the initial angular data, the physical two-path mixture and the outgoing scalar admit rigorous absolute enclosures. These are pointwise theorems at ordinary exponents. The numerical evaluations of the bounds form part of the proof.

The angular source is the normalized Haar eigenangle law before its change of variables. The four-mode state retains the angular integrals at raised order. It removes the Vandermonde, which re-enters through the finite differential readout. At an interior critical radius the incoming analytic germ retains both complex boundary values, while either one by itself lacks the real-cycle prescription. The phase in Theorem 10.9 restores this information. At an apparent singularity one continues the holomorphic physical germ of Theorem 10.7 or changes

chart at an invertible overlap. The present polygonal paths have positive denominator bounds throughout and wind around only the designated critical radius. This follows also by inspection of the exact factors in Theorem 10.12. Farther apparent poles of this chart need their own checks.

For each branch compute $F_{\pm}$ using the polynomial defects in Theorem 10.12. With $k = 1, 2$, respectively, form

$$\omega = \frac{\exp(i\vartheta)}{2\cos\vartheta}, \qquad \vartheta = \pi\left(h + \frac{N+k}{4}\right), \qquad F = \omega F_{+} + (1-\omega)F_{-}.$$

Shifting h by an integer has no effect on the weights. If each independently integrated incoming component belongs to a complex disk of radius e about an enclosed quadrature centre v_j, and r is a compact scalar row, choose q using Proposition 10.14 and put $a = rF - qC_l$. The midpoint of av has absolute error at most $\operatorname{rad}(av) + e\sum_j |a_j|$, including the input arithmetic, the two complete path matrices and the final row arithmetic. For the independent determinant witness the physical preparation at the right endpoint is evaluated directly by Theorem 21.5. Input, path and readout never borrow that witness to choose the branch.

At rank three the common Hermite source bound was 1.217×10^{-11} per mode. The direct 14-panel transfers on each branch and compatibility at the two endpoints give absolute error below 3.261×10^{-10}. Independent Fourier–Bessel integration with the signed tail reduces the component input radius to 1.396×10^{-20}. The two-germ solution of Theorem 10.13 overlaps all 800 complex entries of the two path calculations. Intersect the real and imaginary intervals of the corresponding entries. With the signed seed and the intersections, the propagated moment has midpoint

$$25.573398470105632060 + 0.6168335785627311 05i.$$

The error about the full stored centre is below 3.636×10^{-19}; rounding the two printed coordinates gives a disk of radius 1.2×10^{-18}. The absolute row sums are below 889 at the outgoing endpoint, 152 after using the outgoing relations and 26.05 after transporting and using the incoming relations. The independently evaluated determinant disk has radius below 5.866×10^{-8}. Each wrong branch selection has a strictly positive lower discrepancy even against that wider witness: above 8.20×10^{-6} for the upper path alone, 1.63×10^{-6} for the lower alone, and 4.14×10^{-6} for equal weights. Removing the preparation from the differentiation changes the all-zero input derivative by more than 64.65; dropping the scalar prefactor changes the outgoing result by more than 19.60.

At rank four the input errors from Hermite and signed Bessel integration are below 5.24×10^{-12} and 4.975×10^{-23}. The upper and lower transfer norms are below 922453 and 257543. The right-end canonical row has absolute sum above 9.44×10^{10}, and its compatible representative has sum below 7.72×10^{9}. The transported row has sum above 7.44×10^{11} before using the left constraints and below 3.782×10^{6} after them. Thus the source error at the latter row is below 1.882×10^{-16}. A first complete calculation obtained absolute radius .02960, relative error below 4.34×10^{-6}, and the largest of the 35 state-component radii was below 2.131×10^{-11}. The held-out endpoint determinant gave $6634.51746780297 - 1591.32786780648i$ with absolute radius below 8.769×10^{-6}. This point also detects omission of the preparation derivative by more than 10017 in the all-zero incoming mode and omission of the normalizing prefactor by more than 6802 in the outgoing moment.

At rank four, propagating local errors only in the directions that can reach this scalar improves the first enclosure. The degree-42 adjoint calculation at 224 bits, with 660-bit subproducts, has absolute radius below 7.402×10^{-9} and relative radius below 1.085×10^{-12}. Its upper-only, lower-only and equal-mixture discrepancies from the true scalar exceed 9.45×10^{-7}, 1.965×10^{-7} and 4.827×10^{-7}, respectively. These three exclusions use a common physical input in the signed branch difference. The independently evaluated determinant has a wider disk here. It checks the outgoing value but cannot by itself distinguish the three exclusions at this resolution.

At degree 60 and 304 bits, each path uses 70 accepted Taylor steps on 64 initial panels. The largest accepted local tails are below 1.73×10^{-48} and 1.09×10^{-48}. A balanced product gives an absolute scalar radius below 2.309×10^{-13}, including the signed input. Transporting midpoint-product defects at 660 bits bounds every matrix entry with coordinate radii below 1.460×10^{-38} and 4.046×10^{-39} on the two paths. Independent interval inverse checks give infinity-norm condition numbers between 1.72×10^{20} and 1.73×10^{20} for the upper matrix and between 3.31×10^{20} and 3.32×10^{20} for the lower. These are condition numbers of a general transfer and its inverse. Physical forward error is governed by the particular source and scalar row. The adjoint calculation gives

$$T_4(7/4 + i/4, -193/50 + 21i/100; .56) = 6634.51746712714261052377 \\ - 1591.32787090943961478868i.$$

The absolute error about this printed centre is below 1.882×10^{-16}, and the relative error is below 2.757×10^{-20}. The signed angular truncation contributes less than 1.881×10^{-16} in the scalar direction; the two path defects together contribute less than 4.368×10^{-31}. Substituting approximate inverses from binary64 to estimate conditioning understated it by factors greater than ten on both paths. The conditioned physical scalar excludes upper-only, lower-only and equal weights by more than 9.629×10^{-7}, 2.0017×10^{-7} and 4.9176×10^{-7}. Large-matrix conditioning and the physical weight errors are distinct measurements.

For a dense degree-m Taylor panel with d coordinates and degree-q rational coefficients, forming the two recursions requires $O(md^3 \min(m, q+1))$ scalar operations with classical dense products. The forward coefficients can be discarded after recording the endpoint and residual norms; the implementation retains $O(md^2)$ entries on a panel. A balanced product of L panels needs $L-1$ matrix products. The explicitly stored suffix algorithm for transporting directional defects uses $O(L^2 d^3)$ arithmetic in this implementation and $O(Ld^2)$ intermediate storage. These counts refer to fixed-precision arithmetic after the panel list has been accepted. They do not bound the number of subdivisions or the bits needed over a parameter domain. On the recorded machine the main rank-three branch jobs took about 18 and 22 seconds. The improved rank-four adjoint postprocess from saved panels took about 84 seconds with the reintegrated source; the signed rank-four input was independently rebuilt in about 453 seconds. Parallel cold reconstruction of the panels is a separate cost, and the package includes them for a shorter replay.

Approaching and attaining an exceptional connection order

Keep the rank-three endpoints, paths and tilt of Proposition 21.9. At $h = 3/2 + 10^{-8} i$ the two coefficient moduli in (10.11) sum to more than 3.1830×10^{7}. The coefficient of the regular germ and the combined coefficient of the singular germ in Theorem 10.13 both remain bounded. The validated 512-bit germ calculation through degree 270 has $\chi_\lambda < .738$ and the verified incoming inverse approximation has norm below 30947. The joint row is applied to the same incoming vector. It encloses the outgoing scalar at $17.0010444015 - 5.7082465203i$ with absolute radius 1.966×10^{-7}, including rounding of this printed centre. The other determinant enclosure overlaps it, and each single branch and equal-weight rule is excluded even against that witness by more than 9.21×10^{-6}. The raw calculation identifies the conditioning of the weights separately from the accuracy of the final physical combination. At this non-dyadic imaginary order an early implementation chose the wrong initial projector by comparing two rounded complex balls for exact equality. The resulting singular incoming matrix failed its inverse test. Passing each projector explicitly with its exponent repairs this fault.

At $h = 3/2$ exactly, $\cos \vartheta = 0$. Propagate the 40-dimensional order jet by

$$\frac{d}{dz}\begin{pmatrix} W \\ W_h \end{pmatrix} = \begin{pmatrix} M & 0 \\ M_h & M \end{pmatrix}\begin{pmatrix} W \\ W_h \end{pmatrix}.$$

The denominator in the geometric chart is order-independent; the numerator of M is affine in h for fixed tilt. Thus the difference quotient of the two exact generators at the nonreal test orders gives the exact derivative, including at $h = 3/2$. Verify a common scalar denominator before this operation. The two finite-dimensional fundamental matrices have blocks $F_\pm, 0; D_\pm, F_\pm$, where $D_\pm = \partial_h F_\pm$. Apply (10.12) as

$$W_{\mathrm{phys}} = \left[\tfrac{1}{2}(F_+ + F_-) - \tfrac{i}{2\pi}(D_+ - D_-)\right] W_l - \tfrac{i}{2\pi}(F_+ - F_-)\, \partial_h W_l.$$

The average represents the common undifferentiated value on physical input. The starting derivative is computed independently by angular Hermite interpolation and by the differentiated Bessel integral. A compatibility row $C_l W_l = 0$ can reduce the first scalar functional. A relation for $C_l \partial_h W_l$ would also contain $(\partial_h C_l) W_l$, so the code uses the original second functional.

At 248-bit working precision and degree 39, each of the two paths used sixteen certified panels. Every component of the jump of the undifferentiated input contains zero. The two input contributions to scalar uncertainty are below 1.466×10^{-13} and 7.637×10^{-16}; the path and arithmetic contribution is below 3.014×10^{-16}. The result is

$$T_3(3/2, -2.86 + .21i; .4) = 17.0010443095541343 - 5.7082467510233774i \quad (\text{absolute error } < 1.478 \times 10^{-13}).$$

An independent outgoing determinant calculation encloses the result. Omitting the order correction gives an interval separated from the correct one by more than 9.586×10^{-6}. This verifies the exceptional phase connection

at one point; a resonance of the *normal-jet readout* $j = \rho$ is a separate condition in Theorem 10.6. The augmented coordinates retain the missing normal derivatives. Theorem 23.1 proves that the physical determinant at these ranks annihilates them even when the phase weights are exceptional.

What failed in the rank-four example

At $N = 4$, $z = 41/50$, $h = 1.15 + .26i$ and $s = -.56 + .12i$, the archived calculation evaluates a single point. It takes no integration step and applies no critical connection coefficient. The nearest reduced-chart exception is $\sqrt{2/3}$, an apparent radius at a distance below .00351. The sampled nonzero pencil condition number was 2.79×10^6, the sampled group-inverse norm 1.57×10^6, and the 36-node angular input contained entries larger than 5.50×10^{13}. On that same binary input the high-precision continuation of the original orthogonal row gave $96117.92 - 112423.05i$, whereas the archived floating arithmetic gave $95565.54 - 108420.88i$. Fixing its binary polar parameters exactly, the absolute arithmetic discrepancy was 4040.108 to the shown precision. Changing those input parameters to their intended exact decimals altered the frozen-input calculation by less than 6.1×10^{-10}. Using the validated physical scalar reference below, the error of the frozen 36-node input under the exact decimal row exceeded 147909. This last lower bound treats the returned angular floats as exact data. It tests the input actually given to the readout; it does not separate quadrature truncation from rounding inside that angular grid.

One numerical repair changes the angular integration variables before computing the full modes. With $d = 1 - z^2$, $w = (z - \lambda)/(1 - z\lambda)$, and $u(\lambda) = d\lambda/(1 - z\lambda)$, the identical integral for a tuple I is

$$d^{N(2\nu+1)} \int \left| \sum_i u(\lambda_i) \right|^{2g} \prod_i w(\lambda_i)^{I_i} |1 - z\lambda_i|^{-2(\nu+1)} \, dm(\lambda).$$

Indeed $1 - zw = d/(1 - z\lambda)$, the angular Jacobian is $d/|1 - z\lambda|^2$, and $Nz - \sum w_i = \sum u(\lambda_i)$. This removes a sharply peaked original preparation in the example. With 128 nodes per angle, an independently bounded row and its physical constraints, the scalar becomes $1.79719209 - .18879007i$. Using the archived double arithmetic with exactly the same remapped state gives $282.967 + 77.497i$. These are angular-grid comparisons. They exhibit losses in both incoming data and differential readout; refining only one of them leaves a substantial error.

For a point certificate use the correlated polynomial estimate. At this radius $m > 4.25 \times 10^{14}$. Treating modes separately with the original row gives $m\|l\|_1 > 1.13 \times 10^{12}$; after subtracting verified constraints the computed Gram quantity $\sqrt{m\, l K l^*}$ is below 2094. At 1300 bits a degree-120 Chebyshev polynomial integrated through all 35 raised angular components gives

$$T_4(1.15 + .26i, -.56 + .12i; .82) = 1.79719226249907 - .18879073058537i \quad \text{with absolute error below } 7.912 \times 10^{-5}.$$

The bound includes both the polynomial remainder and rounding. An independent determinant calculation directly at the unraised physical order, using Theorem 21.5 with $k = 46$ and 800 bits, gave midpoint $1.79717691197062 - .18878691329514i$ with absolute radius below 5.060×10^{-5}. Both disks contain the same scalar, and the distance between the reported centers is below 1.59×10^{-5}. The separate squared-gap bound with $k = 42$ is below .000201. This recovers the scalar in the original failed case and measures the accuracy attained by its full compact readout.

Reusing scalar data over a continuous complex parameter set

Proposition 21.10 (an endpoint evaluator on a four-real-dimensional set). Take $(N, z) = (3, .4)$ or $(4, .56)$ and $s_0 = -N + .14 + .21i$. For

$$1.5 \le \Re h \le 2, \qquad |\Im h| \le .4, \qquad |s - s_0| \le .035$$

a stored degree-11 polynomial in s with 48 node contributions in h gives an approximation to the ordinary moment. Its exact-arithmetic absolute errors are below .001474 and .13651, respectively. The stronger relative conclusions below use a verified lower bound on the modulus throughout the entire set. This independent endpoint evaluator does not propagate vectors for every parameter in the set.

Construction. Write $R = N(1 + z)$, $X = |S_N|^2/R^2$, $t = (s - s_0)/\rho$ and $\rho = .07$. Let x_i be the 24 open Legendre nodes rescaled to $[0, 1]$. The interpolation functional takes the values $(R^2 x_i)^h$ and derivatives $h(R^2 x_i)^h/x_i$.

Integrate the Hermite cardinal polynomials multiplying these 48 values against the original tilted Haar measure by (21.7), at each of $s_j = s_0 + \rho\exp(2\pi ij/12)$. The normalized discrete Fourier transform of each column gives twelve coefficient rows. Their evaluation by Horner's rule uses 48 exponentials and at most $12\cdot 48$ scalar multiply-adds for a new query. Store the complex intervals for the coefficients and the node enclosures. No further angular or path integration enters the query.

Uniform analytic error. Put $L = 2N\max\{-\log(1-z), \log(1+z)\}$. Then $|\log|\Lambda_N|^2| \le L$. For Hermite interpolation at the sample tilts take $\gamma = 3/2$, the positive preparation at $u_0 = \Re s_0$, and the bound

$$D = \prod_{j=0}^{47} \frac{\sqrt{\max(|1.5-j|, |2-j|)^2 + .4^2}}{|j-\gamma|}.$$

Theorem 21.5 bounds each sampling error by $R^4 De^{L\rho}$ times the absolute integral of $H_\gamma - L_\gamma$ at the real preparation. A modulus-e error in each sample gives an error at most $e\sum_{j=0}^{11}|t|^j \le 2e$ in its Fourier interpolant. For the tilt interpolation of the exact moment, differentiate twelve times under the finite Haar integral, and use $|S_N|^{2\Re h} \le 1 + |S_N|^4$. The integral of $1 + |S_N|^4$ at u_0 equals $m_0 + R^4 m_2$ for the normalized jets $m_j = \mathbb{E}[X^j|\Lambda_N|^{2u_0}]$. The complex divided-difference formula is the integral of the twelfth derivative on the simplex of convex combinations of the nodes and the query; its volume is $1/12!$. Since these combinations stay within ρ of s_0, the additional error is bounded by

$$(m_0 + R^4 m_2)e^{L\rho}\frac{L^{12}}{12!}[\rho^{12} + .035^{12}].$$

The last bracket bounds the modulus of the nodal polynomial. Both contributions are absolute and include variation of complex preparation. The independent endpoint determinants enter only the subsequent tests.

Uniform relative accuracy of the scalar patch. Write x_i for its positive Hermite nodes, $u_i = R^2 x_i$, $\ell_i = \log u_i$, and $t = (s - s_0)/\rho$. With the raw Fourier weights in the distributed tables, the approximant is

$$P(h,t) = \sum_{m=0}^{11} t^m A_m(h), \qquad A_m(h) = \sum_i W_{mi} v_i(h), \qquad v(h) = \big((u_i^h)_i, (hu_i^h/x_i)_i\big).$$

The powers use real logarithms. Let E_N be the analytic absolute-error bound for this patch. Consider one closed rectangular cell in the h-plane with centre b, half-diagonal d, maximum $H = \max|h|$, and end points p, q of its real projection. Put $U_i = \max(e^{p\ell_i}, e^{q\ell_i})$ and define

$$D = \big((U_i|\ell_i|)_i, (U_i(1 + H|\ell_i|)/x_i)_i\big).$$

The derivative of each node function is bounded by its entry of D throughout the cell. Integration along the straight segment from b to h, followed by the reverse triangle inequality, gives the physical lower bound

$$|T_N(h,s;z)| \;\ge\; |A_0(b)| - \sum_{m=1}^{11} 2^{-m}|A_m(b)| - d\sum_i D_i \sum_{m=0}^{11} 2^{-m}|W_{mi}| - E_N \quad (|t| \le 1/2).$$

This uses the full tilt disk, including its boundary, on every cell. The centre dot products retain the cancellations within each raw Fourier coefficient. The cell diameter is used only for the remaining variation in h.

The computation used a 32×48 rectangular partition of $[3/2, 2] + i[-2/5, 2/5]$ at 192 bits. It records all 1,536 lower bounds per rank, the exact grid prescription and the SHA-256 of each raw table. The minimum at rank three ($z = 2/5$) exceeds 15.67606646. The minimum at rank four ($z = 14/25$) exceeds 3238.03237472. On each whole box with $|s - (-N + 0.14 + 0.21i)| \le 0.035$, the analytic absolute errors are below 0.001473559636 and 0.136505053, respectively. Consequently $|P - T_N|/|T_N| < 9.400060 \times 10^{-5}$ and 4.215680×10^{-5}, respectively. To return a floating-point midpoint, add a pointwise enclosure of its distance from P. For example, after checking that this extra disk radius is at most 10^{-8}, the relative bounds for the returned midpoints are 9.400124×10^{-5} and 4.215680×10^{-5}. The coverage concerns the Hermite scalar evaluator at these two fixed radii. Its nonvanishing and error bounds have not been transferred to the path-propagation calculation.

A uniform full-state source with correct integer values

Proposition 21.11 (uniform preparation on the incoming fibres). In rank three put $z_l = .26$, in rank four $z_l = .44$. Let $11/8 \le \Re h \le 17/8$, $|\Im h| \le 3/8$, and let s run independently in the closed disk of radius $1/8$ about $s_0 = -N + .14 + .21i$. There is a single finite Fourier–Mellin quadrature on each fibre, with parameter-dependent coefficients and the same nodes throughout the region. Its uniform absolute component errors are below 1.945×10^{-41} and 3.382×10^{-75}, respectively, in exact arithmetic. It prepares all 20 or 35 coordinates before either branch is transported.

Proof and arithmetic specification. Use the independent product angular integral in the compact representation. A tag has modulus one. Put $G = h + H$, $H = \lfloor (N-1)^2/4 \rfloor$, $R_l = N(1+z_l)$, $\nu = -N - s$. Keep the central Bessel jets, finite-frequency Gaussian quadrature, Fourier cutoff and signed Hankel tail of Proposition 21.9. Two operations require uniform estimates. First replace its Mellin coefficient and every apparently singular central term by the following exact expressions:

$$K(G) = -2^{2G+1}\Gamma(1+G)^2 \sin(\pi G)/\pi, \qquad \frac{K(G)}{2j-2G} = 2^{2G}\Gamma(1+G)^2(-1)^j \operatorname{sinc}_\pi(G-j).$$

The gamma reflection formula (NIST DLMF 5.5.3) proves the identities, with the value at $G = j$ taken by continuity. At integral G the finite- and large-frequency contributions vanish and the central polynomial extracts exactly the corresponding angular moment. For all orders the other factors in the central coefficient are $2^{-2G}(-R_l^2)^j/(j!)^2$ with monomial X^j, $X = |Nz_l - \sum w_j|^2/R_l^2$. This fixes its sign and scale.

Second, write $g_- = 11/8 + H$, $g_+ = 17/8 + H$, $v = |.14 + .21i| + 1/8 < 1$. With $P_k = (v)_k/k!$, the Fourier coefficient of index $k \ge 0$ has the nonnegative envelope

$$f_k = z_l^k \left(\sum_{j=0}^{M+3} P_{j+k} P_j z_l^{2j} + \frac{z_l^{2(M+4)}}{1 - z_l^2} \right).$$

Use $|(-\nu)_k/k!| \le P_k \le 1$ on the product of the two binomial series. Either sign of the Fourier index has the same envelope. The discarded absolute Fourier mass above index M is at most $\delta = 2z_l^{M+1}/[(1-z_l)(1-z_l^2)]$. Write $w = f_0 + 2\sum_{k=1}^{M} f_k$. An upper bound for $|K|$ multiplies the five errors below. It is $2^{2g_+ + 1} \max_{x = g_-, g_+} \Gamma(1+x)^2 \cosh(3\pi/8)/\pi$, by the gamma integral and log convexity.

1. The central tail after degree d is bounded by the preparation mass times $2^{-2g_-} R_l^{2d+2}/[(d+1)!^2(2d+2-2g_+)(1-(R_l/(d+2))^2)]$. The Fourier tail from frequency 2 upward is at most $N\delta(w+\delta)^{N-1}2^{-2g_-}/(2g_-)$.
2. On each radial panel with midpoint x and half-length a, choose D by the receipt, with $a < D < x$. The integrand has modulus at most $w^N e^{3\pi/8 + R_l D} \max_{g = g_-, g_+} (x-D)^{-1-2g}$ on the circle of radius D. Taylor approximation through degree $2q-1$ and exactness and positive weights of the q-node Gauss rule give error at most this bound times $4a(a/D)^{2q}/(1-a/D)$. Add the actual accepted panels.
3. Past T, discard the retained Fourier indices above B at cost at most $N(2\sum_{k>B}^{M} f_k) w^{N-1} 4^N/[(2g_- + N/2)T^{2g_- + N/2}]$. Here $T \ge 2(M+2)$ and $T \ge 16$. The N particle Bessel factors have the envelope $4/\sqrt{t}$ of Section 21, and the terminal offset Bessel function has modulus at most one. On the surviving modes the exact J-term signed Hankel integration and the error of the gamma-integral remainder in Proposition 21.9 apply. Replace every Fourier coefficient in the product error by f_k, retain each actual integer Bessel order, and replace $\Re G$ by g_- in the positive radial tail integral. This is an upper bound by positivity of the error convolution. Both signs of each oscillation are retained in the evaluated centre.

N	M, B, J	T	q, d	radial panels	central / Fourier / Gauss / discarded large-frequency modes / Hankel error, after multiplication by the kernel bound
3	106, 60, 15	530	66, 64	73	3.62×10^{-107} / 1.16×10^{-60} / 5.62×10^{-61} / 3.62×10^{-49} / 1.945×10^{-41}
4	250, 143, 31	2754	110, 96	350	1.80×10^{-155} / 8.45×10^{-86} / 1.35×10^{-98} / 3.382×10^{-75} / 7.57×10^{-88}

The stated totals use the unrounded sums. Thus the source certificate requires 4,818 or 38,500 finite-frequency evaluations in addition to the central and signed-tail contractions. These are potentially expensive at rank four. The smaller quadrature with 44 or 59 panels, respectively, has errors below 4.086×10^{-30} and 1.579×10^{-35}. A table of Hermite cardinal functions below gives a separate, faster, lower-accuracy enclosure.

Two parameter-uniform endpoint constructions

Write $H = \lfloor (N-1)^2/4 \rfloor$, $G = h + H$, $a = Nz$, $R = N(1+z)$, $Y = |a - \sum_j w_j|$, $X = Y^2/R^2$ and $D_j = |1 - zw_j|^2$. The incoming angular entries are integrals of $Y^{2G} \prod_j w_j^{m_j} D_j^{-N-s}$ against uniform product measure. The following fast table is a second uniform source whose analytical error is independent of the Fourier–Mellin calculation. It simultaneously retains all 20 or 35 tagged coordinates.

Tagged cardinal interpolation. On the closed rectangle $1.375 \le \Re h \le 2.125$, $|\Im h| \le .375$ and the independent closed disk $|s - s_0| \le 1/16$, $s_0 = -N + .14 + .21i$, the two tables at $(N, z) = (3, .26), (4, .44)$ have respective uniform absolute component errors below 5.017×10^{-6} and 2.318×10^{-6} in exact evaluation. Both include exact and near-exceptional orders. To use a floating-point midpoint, add its verified interval arithmetic radius.

For proof, choose k open Legendre nodes x_i and their double-node Hermite cardinal polynomials of degree $2k-1$. At $s_j = s_0 + \rho \exp(2\pi i j/M)$, $\rho = 1/8$, $M = 16$, integrate all $2k$ cardinal polynomials times the particular angular tag under the complex preparation. The coefficient of each monomial X^l is obtained by the finite exponential directional jets of Section 21 and the exact $2k$-ray angular projection. Multiply the resulting matrix of tagged monomial moments by the cardinal coefficient matrix. The normalized length-M discrete Fourier transform of each entry gives its polynomial coefficients in $t = (s - s_0)/\rho$. Contract the evaluated cardinal weights against $((R^2 x_i)^G)_i$ and $(G(R^2 x_i)^G / x_i)_i$. This rules out a hidden Haar prefactor in the source.

Let g_-, g_+ denote the extrema of $\Re G$, $v = .375$ and $\gamma = H + 1.25$. The Hermite estimate of Section 21 applies to each tilt sample and each mode, with derivative-product majorant

$$D = \prod_{j=0}^{2k-1} \frac{\sqrt{\max(|g_- - j|, |g_+ - j|)^2 + v^2}}{|\gamma - j|}.$$

Put $M_0 = \max_{\sigma = -N - \Re s_0 \pm \rho,\ b = 1 \pm z} b^{2N\sigma}$. A uniform budget is $R^{2g_+} M_0 D \big|\mathbb{E}_0(H_\gamma - L_\gamma)(X)\big| / (1 - |t|)$, using the constant sign of the comparator gap and the Fourier interpolation bound. Here $\mathbb{E}_0$ is the uniform product

expectation. The independent error from interpolating *exact* angular moments in s is bounded by

$$M_0 \min\{R^{2g_+}, 1 + R^{2p}\mathbb{E}_0 X^p\} \frac{L^M(\rho^M + 16^{-M})}{M!}, \qquad L = 2N \max\{-\log(1-z), \log(1+z)\}, \quad p = \lceil g_+ \rceil.$$

Indeed the Mth tilt derivative inserts $(-\sum \log D_j)^M$; its bound holds on the convex hull of all nodes and the query. The complex divided-difference integral has simplex volume $1/M!$. We used $k = 36, 45$ and $750, 950$ bits, respectively. The tables took 70 and 321 seconds in their recorded builds. At each rank the four held-out parameter tests include the two real-order boundaries of the rectangle, nonreal orders and exact tilt-disk boundary points. All component enclosures overlap direct integrations on different grids. At $h = 2$ the independent integration is an exact finite polynomial with rounding enclosure.

A polynomial chart for the physical scalar row. At a regular real endpoint of Theorem 10.6 let $l(h, s)$ be its canonical normalized row. In particular this is an operation on the transported W. Let $d_j = \prod_{v=1}^{j}(v - \rho_0)$, $\rho_0 = h + H + N(1 - N - s)$. At $N = 3, 4$, the row

$$J(h, s) = (h + 1)_H^2 d_{2H}(1 - z^2)^{-N^2 - 2Ns} l(h, s)$$

is polynomial of bidegree at most $(4H, 4H + N(N - 2))$. For the proof, L in (10.6) is independent of h, s and so are its chosen group inverse, kernel projector and coordinate maps. Its right-hand side G_0 and projection B are affine. Inductively a normal jet or a mixed jet of total order j multiplied by d_j has total degree at most $2j$. For the normal recursion, its order-k term is linear in G_0. Multiplying an order-$j - 1 - k$ numerator by d_{j-1}/d_{j-1-k} introduces k scalar factors. The final numerator multiplier is $((j - \rho_0)I + B)/j$. The mixed recursion uses one affine displacement and one factor $j - \rho_0$, or the just established normal jet. The positive and negative mode lifts through ranks three and four require at most $N - 2$ elementary steps for a single determinant entry. Each step raises its degree in s by at most one. A product in the Weyl determinant has N entries. Bringing the readout of jets of varying order to the common denominator d_{2H} preserves the stated bidegree. These operations involve no inverse of a parameter-dependent pencil.

Consequently a tensor roots-of-unity transform of sizes $(4H + 1) \times (4H + N(N - 2) + 1)$ recovers every coefficient without degree truncation. The implementation uses normalized variables $(h - (1.75 + .125i))/.75$ and $(s - s_0)/.25$ and forms the cleared jets at each node. Only the endpoint group inverse and displacement projection matrices require matrix inverses. Every sampled operation and the Fourier transform are enclosed by ball arithmetic. On any target parameter polydisk sum the row one-norms of the coefficient bounds times the corresponding maximum parameter powers. Divide by a positive lower bound for $|(h+1)_H^2 d_{2H}|$, using $|j - \rho_0(h_c, s_c)| - r_h - Nr_s$ for each normal divisor, then multiply by the modulus bound for $(1 - z^2)^{N^2+2Ns}$. This operation explicitly tests for normal-jet exceptions. A vanishing connection cosine affects none of these calculations.

On $|h - (1.75 + .25i)|, |s - s_0| \le 1/16$ the outgoing row one-norm is below 1534.40 (rank three, .4) and 2.994×10^{11} (rank four, .56). On disks of the same radii centred at the respective exceptional orders 3/2 and 2 the bounds are 2444.50 and 2.154×10^{11}. Direct rectangular interval evaluation of all intermediates at rank four gave a 2.657×10^{35} upper bound around the main centre. The finite polynomial representation keeps cancellations in its coefficients before taking moduli. Independent original-jet interval calculations agree coefficient-by-component in the *values* of the row at the comparison points. The degree proof and outward transform establish the continuum claim; agreement at finitely many points only checks the implementation.

The rank-four integer order jet. At $N = 4$, $h = 2$, $G = m = 4$, $s = -3.86 + .21i$, the order derivative of each incoming mode is the tagged integral of $Y^{2m} \log(Y^2)$. At the zero set its continuous value is zero. For an independent representation, write $W_G = K(G)I(G)$ in the regularized Hankel formula, with $K(G) = -2^{2G+1}\Gamma(1 + G)^2 \sin(\pi G)/\pi$. In the central power series for I omit the term $b_m r_0^{2m-2G}/(2m - 2G)$ and call the remainder I_{reg}. It is holomorphic near m by the central series and the radial decay at infinity. Then

$$W_m' = (-1)^{m+1} 2^{2m+1} (m!)^2 I_{\mathrm{reg}}(m) + 2\,(\log 2 + \psi(m + 1) - \log r_0)\, W_m.$$

Indeed $K(G)/(G - m)$ has the displayed finite value at m and logarithmic derivative $2 \log 2 + 2\psi(m + 1)$. Differentiating the isolated power of r_0 supplies the remaining $-2 \log r_0$. This identity has neither a singular order quotient nor a differencing step. At $z = .44$ we took $r_0 = 2$, 38 central terms beyond the zeroth, $T = 170$, finite Fourier cutoff 70, signed-tail cutoff 24 and asymptotic order 5. The 26 adaptively split panels used 52-point Gauss rules at 256 bits. Bounds after multiplication by $|K'(m)|$ were 1.590×10^{-32} (central series), 2.749×10^{-22}

(finite Fourier), 4.456×10^{-26} (panels), 2.532×10^{-25} (high tail modes), and 5.994×10^{-26} (signed asymptotic remainder). Their sum is below 2.752×10^{-22} per mode. Serialized polynomial centres have arithmetic radius below 5.3×10^{-60}. The same 35 order derivatives were enclosed independently by the direct differentiated Hermite integral on 84 nodes and by that integral at .56 on 55 nodes. Absolute common analytic radii are below 1.147×10^{-11} and 1.214×10^{-9}, respectively. At .44 the largest distance between independent polynomial centres was below 1.341×10^{-12}. Replacing one vector by twice that vector fails the enclosure comparison. These calculations independently initialize and check an order jet; they do not on their own transport it.

At each of the four real endpoints we independently compared the raised full source followed by the physical normal-jet row with the original Haar determinant. For the boundary tilt $s = s_0 + 3/80 + i/20$, and both $h = 2$ and $h = 1.75 + .25i$, all eight float-ball pairs overlapped. Removing $(1 - z^2)^{N^2+2Ns}$ gave disjoint enclosures in all eight cases. Integer tests used exact polynomial degree and ball rounding. At rank four, .56 and the nonreal order, the 28-node full-source error budget was 1775, while the determinant error was below .000399. This records a conditioning failure of the coarse local contraction as well as a normalization check; it cannot serve as a precision claim for path transport.

Uniform absolute error for the physical crossing

Theorem 21.12 (full crossings on four closed parameter polydisks). Set $h_* = 7/4 + i/4$, $s_* = -N + 7/50 + 21i/100$, $r = 1/16$. At each rank use either $|h - h_*| \le r$ or $|h - e| \le r$, independently of $|s - s_*| \le r$. The endpoints and arcs are those of Theorem 10.15. For the unnormalized mixed moment T_N of Section 1, the computable family below has uniform absolute scalar error less than 1.031×10^{-25} on each of the four sets. The larger transport polydisk in Theorem 10.15 is a domain for the two full matrices. Angular initialization, connection and scalar projection in this theorem use the smaller sets.

Rank and order centre	bound on each branch error	connected vector error per component	physical row one-norm	final absolute scalar error
3, h_*	6.569×10^{-37}	1.603×10^{-36}	1534.40	1.001×10^{-25}
3, 3/2	7.943×10^{-35}	1.094×10^{-33}	2444.50	1.001×10^{-25}
4, h_*	1.001×10^{-39}	2.441×10^{-39}	2.994×10^{11}	1.008×10^{-25}
4, 2	1.009×10^{-39}	1.388×10^{-38}	2.154×10^{11}	1.030×10^{-25}

At an exceptional centre the branch bound holds on the sampling circle as well as on the target disk. Each vector error is added to the returned coordinate arithmetic ball. The scalar error is about the full-precision returned midpoint, including final arithmetic. For an enclosure of the *set of possible answers* on an input cell one must further enclose the variation of the approximant itself. The table quantifies the uniform approximation error for each input, not the diameter of that set. The constant-enclosure construction below gives an example of the second type. The full-grid worst-case query is expensive. The proof uses uniform estimates on continuous regions; individual test inputs validate parts of its implementation.

Proof. Let K bound the canonical infinity norm of either full transfer on the relevant set, using the signed contiguous-product estimate of Theorem 10.15. Its upper bounds in the order of the table are 16867, 2042702, 7.0651×10^{22} and 1.1941×10^{33}. For the Cauchy circles we used the slightly larger radii $|h - h_*| \le 9/20$, $|s - s_*| \le 1/16$, since $|e - h_*| + 3/32 < 9/20$. Let ϵ be the absolute per-component source error in Proposition 21.11. Evaluate its finite rule to rounding radius $\le \epsilon$ and retain its dyadic midpoint. Uniformly its input norm is at most $M_l + 2\epsilon$, where M_l is the elementary angular bound in Theorem 10.16 with the incoming radius and the largest real order in the sampled set.

Write τ for the polynomial transfer truncation error at degrees 320 and 640, evaluated by the signed-product error law. Compute the polynomial action to absolute rounding radius at most 10^{-39}. The result for each path differs from the exact angularly initialized outgoing branch by at most

$$E = 2K\epsilon + \tau(M_l + 2\epsilon) + 10^{-39}.$$

This is an error budget for both paths separately. On the ordinary disk the sum of the two weight moduli is bounded by $\cosh(5\pi/16)/\sinh(3\pi/16)$, using the imaginary part of the order. On the exceptional disk apply

(10.14). At ranks three and four its numerator alias-and-tail terms are below 5.704×10^{-52} and 4.501×10^{-48}. This avoids the unbounded conditioning of the raw quotient. For the scalar, multiply by the verified row one-norm, and evaluate the entire Fourier postprocessing and final dot product in balls. Accept the full-precision midpoint when the latter arithmetic disk has radius at most 10^{-25}. All the analytic inequalities used for these bounds are replayed from outward scalar receipts.

The normal-jet indices $j = 1, \dots, 2H$ obey $\Re(\rho_0) - j \geq 2.83$ on the four target disks. Indeed $\rho_0 = h + H + N(1 - N - s)$, so taking the least allowed real order and largest allowed real tilt suffices. Also $h + 1$ and, where used, $h + 2$ stay away from zero. Thus the row in this theorem uses the ordinary jet chart, including at the phase exception. For physical parameters at a normal-jet pole the present certificate supplies no augmented readout. Both critical crossings occur inside the ordinary moment domain.

Precision and alternative evaluation. All coefficient contractions are finite. Scalar denominators of the panel recurrences have verified nonzero lower bounds independent of the parameters. For computable point inputs the displayed finite operations can be refined to any of the stated arithmetic allowances. The analytic source terms at integer order are evaluated with the entire sinc form. Sampling only nonzero offsets in (10.13) and restoring the known numerator zero prevents an interval division at the centre. Ball output for an argument given with uncertainty must include that input uncertainty. Fixed precision for *all* internal operations on arbitrary input representations is a separate question. The finite-precision matrix recurrence in Theorem 10.15 gives a uniform rounding guarantee for rational inputs.

The point driver can reduce the cost of the matrix action by propagating a single vector in a verified frame, with an independent a posteriori residual. Within each panel form its Taylor polynomial P from an exact centre of the current state. The coefficients of $qP' - BP$ below its truncation degree vanish in exact arithmetic. The sum of the modulus bounds for its remaining coefficients divided by the verified lower bound for $|q|$ bounds the defect on the real panel. Write this bound as d_j in unit panel time and write a_j for the arithmetic error when resetting the endpoint to its dyadic midpoint. Then

$$\|V\|_\infty \exp\left(\int \|V^{-1}AV\|_\infty\right) \left(a_{\mathrm{init}} + \sum_j (d_j + a_j)\right) + a_{\mathrm{exit}}$$

bounds the canonical path error on the specified input by variation of constants. This bound charges frame conversion, midpoint rounding and all panel defects. A successful residual test can replace the polynomial-action term in E. If the degree or precision budget is inadequate the driver can use the fixed-degree polynomial. The two conforming computations have different costs. In the smaller-source regular-disk alternative the uniform scalar errors are below 6.165×10^{-22} at rank three on the main disk and 3.807×10^{-13} at rank four there. At rank four on $|h - h_*|, |s - s_*| \leq .01$, the 59-panel incoming rule and degree-480 path model give 8.394×10^{-11}. The corresponding rank-four input rules require 7,760 and 4,248 radial nodes per query. The exceptional-order driver caches the finite-frequency Bessel values once for all 56 orders at a fixed tilt and precision. Changing the tilt or precision selects a separate table. The radial Mellin powers, central contraction, signed tail and two path integrations retain their order dependence. A held-out, 20-component recalculation checks the cache at two orders and changes the tilt as a negative control.

Interpretation. These constructions keep the complex-prepared state throughout each arc. Holding only the outgoing scalar or a finite collection of sampled parameter values would lose the order derivative of the jump. The large-disk majorant for the phase-weighted numerator is recovered directly from the original angular preparation; the angular measure supplies its bound even where independent branch norms are large. The outgoing value is obtained only after transport, phase combination and the physical endpoint projection. All accuracy statements in the table are absolute and apply at zeros as well.

A low-cost certificate using the full transports at a single parameter pair

There is also a direct local result that stores a constant midpoint for each of the two matrices, for each of the continued states, and for the scalar. Put $h_* = 7/4 + i/4$, $s_* = -N + 7/50 + 21i/100$. Both differences $h - h_*$ and $s - s_*$ range independently over the closed disk of the radius in the table. The two triangular detours have incoming, critical and outgoing radii $(.26, 1/3, .4)$ or $(.44, .5, .56)$, with imaginary displacements $\pm.07$ and $\pm.06$ at the critical abscissa.

N	parameter radius	upper/lower matrix errors in ℓ^∞ operator norm	upper/lower state component errors	connected state component error	scalar absolute error
3	10^{-18}	1.228×10^{-13} / 5.285×10^{-14}	1.185×10^{-11} / 5.242×10^{-12}	7.431×10^{-12}	6.607×10^{-9}
4	10^{-35}	5.190×10^{-24} / 1.936×10^{-24}	1.058×10^{-16} / 3.796×10^{-17}	6.664×10^{-17}	2.717×10^{-9}

The scalar midpoints are about $25.573398470105632060 + 0.616833578562731105i$ and $6634.5174671271426123 - 1591.3278709094396118i$. All enclosures include centre arithmetic and pointwise integration error. Replaying the perturbation budget with the cached centre matrices and certified gain tables takes seconds. The short rank-four radius records the cost of bounding each path and then applying the canonical scalar row. It is not an intrinsic parameter singularity.

Proof. In the fixed frame of an arc, take its stored outward bounds C_{ij} on consecutive products of the *midpoint* local matrices, and the local norm errors e_j at the base point. For perturbation radii both equal to r, let a_j bound the integral of the base logarithmic norm, and b_j, c_j the integrals of the operator norms of the two parameter generators over panel j. Duhamel's formula on a full panel gives the local difference bound $v_j = \exp(a_j)\,\mathrm{expm1}((b_j + c_j)r)$. The base-flow bound up to the perturbation point, combined with its forward suffix, contributes the same integral a_j. Define

$$G_{ij}(x) = C_{ij} + \sum_{k=j+1}^{i} C_{ik}\, x_k G_{k-1,j}(x), \qquad G_{ii} = 1.$$

A telescoping product proves this bound for changes of the local midpoint matrices by errors x_j. Comparing the true parameter flow to the true centre flow, its change in canonical infinity norm is at most

$$D_F = \chi \sum_{j=1}^{L} G_{Lj}(e)\, v_j\, G_{j-1,0}(e + v),$$

where χ converts the fixed frame and Euclidean norm back to the canonical infinity norm. Keeping the actual centre products on the left avoids counting their prior rounding as a parameter defect. Add the centre point matrix radius to get the first matrix enclosures in the table.

For the incoming angular entries set $g = \Re G_*$, $R = N(1+z)$, $A = R^{2(g+r)}$, $L_0 = 2N\max(-\log(1-z), \log(1+z))$ and $V = \max_{b=1\pm z,\ p=-N-\Re s_*\pm r} b^{2Np}$. Integrating the parameter derivatives along the straight segment bounds the change of every incoming mode by

$$D_W = rV\big[\max\{1/(e(g-r)), 2A\log R\} + AL_0\big].$$

The two terms in the maximum bound $Y^{2\Re G}|\log Y^2|$ for $Y \le 1$ and $1 \le Y \le R$. The right-hand side also dominates the differentiated integral at $Y = 0$ by continuity. Thus each branch state changes by $D_{X,\pm} = D_{F,\pm}\|W_*\|_\infty + (\|F_{*,\pm}\|_\infty + D_{F,\pm})D_W$. For the connection weight $w = e^{i\pi\omega}/(2\cos\pi\omega)$ the base point has $\Im\omega = 1/4$. Its derivative is $i\pi/(2\cos^2\pi\omega)$, giving $D_w = \pi r/[2\sinh^2(\pi(1/4 - r))]$. The resulting physical-state change is bounded by

$$D_X = (|w_*| + D_w)D_{X,+} + (|1 - w_*| + D_w)D_{X,-} + D_w\|X_{*,+} - X_{*,-}\|_\infty.$$

The canonical scalar row is holomorphic throughout the outer disk of radius $1/16$ in each parameter. For a fixed direction inside the unit polydisk, restrict it to the complex line through the centre. The vector-valued Cauchy coefficient estimate with the certified outer row one-norm M gives $D_l = M \cdot 16r/(1 - 16r)$. The physical scalar therefore changes by at most $\|l_*\|_1 D_X + D_l(\|X_*\|_\infty + D_X)$. Adding the enclosed centre disk from the full-transport certificate proves the table. This budget uses both actual arc continuations and the physical row. It makes no appeal to the separate uniform approximation of the scalar.

For the one-branch and equal-weight controls, replace the true physical state by X_+, X_- or $(X_+ + X_-)/2$ in this final variation bound. Subtract this and the physical change from the centre discrepancy. For ranks three and

four, respectively, the uniform lower bounds for the upper-only, lower-only and equal-weight discrepancies are $(8.288, 1.715, 4.227) \times 10^{-6}$ and $(9.554, 1.956, 4.857) \times 10^{-7}$. Omitting the physical preparation factor produces absolute discrepancies exceeding 19.60 and 6802.34. Independent scalar determinant disks at a simultaneous boundary point of each polydisk check the resulting crossing disks; the proof of the continuum statement uses the product and derivative bounds above.

Evaluation in an orthonormal basis for a negative integer tilt

Severe cancellation can already occur when constructing a Toeplitz entry matrix at $t = 0$. An independent tilt can be retained while removing a soluble integer part of its real component. Let $0 \le m \le N$ be integral, $b_z(\lambda) = (\lambda - z)/(1 - z\lambda)$, and define

$$u_j(\lambda) = \begin{cases} \sqrt{d}\, b_z(\lambda)^j/(1 - z\lambda), & 0 \le j < m, \\ b_z(\lambda)^m \lambda^{j-m}, & m \le j < N. \end{cases}$$

These are the repeated-node Takenaka–Malmquist functions. A change of angular variable to $b_z(\lambda)$ gives orthonormality within the first block. Within the second block $|b_z| = 1$ gives orthonormality. In a cross-block inner product, the constant Fourier coefficient of $b_z^{m-j}\lambda^{k-m}/(1 - z/\lambda)$ vanishes: the factor $\lambda/(\lambda - z)$ cancels one of the $m - j$ interior zeros at z, and the remaining analytic disk function has zero constant term. This proves orthogonality in Haar angle. Multiplication by $(1 - z\lambda)^m$ gives N polynomials of degree at most $N - 1$. For $j < m$ the first m polynomials are $\sqrt{d}(\lambda - z)^j(1 - z\lambda)^{m-1-j}$. Their coefficient determinant in absolute value is $d^{m^2/2}$: shift to $\lambda - z$, read the triangular diagonal $\sqrt{d}\, d^{m-1-j}$, and multiply. The remaining polynomials $(\lambda - z)^m\lambda^{j-m}$ have unit successive leading coefficients. Hence the Fourier determinant in this basis is exactly

$$D_N(te^{i\phi}) = d^{-m^2} \det\left[\int u_j(\lambda)\overline{u_k(\lambda)}|1 - z\lambda|^{2(s+m)} e^{it\Re(e^{-i\phi} f_z(\lambda))}\, \frac{d\theta}{2\pi}\right].$$

In particular $D_N(0) = d^{-m^2}$ at $s = -m$. At general complex tilt the residual power uses $s + m$ with the real logarithm of the positive base. This identity conditions the positive reference preparation; it does not bound the condition number at zeros of its complex Fourier transform.

For the fast source evaluation, under $w = b_z(\lambda)$ and a common half-density factor $\sqrt{d}/(1 + zw)$, the two blocks are w^j and $\sqrt{d}\, w^m\lambda(w)^{j-m}/(1 + zw)$. Each matrix entry is an angular Fourier series of a smooth one-body amplitude multiplied coefficientwise by $i^k J_k(t)$ before Fourier synthesis in ϕ. After taking the determinant, the kth harmonic of the translation phase contributes $i^k J_k(Nzt)$. The implementation also integrates the original eigenangle at selected Fourier sources as a check on the sign, Jacobian, and preparation. At positive order with substantial imaginary part the lattice formula can subtract large terms. The practical evaluator then uses the finite-part integral with Taylor coefficients from Cauchy sampling. It varies the Cauchy radius, angular grid and radial cutoff. At an exactly critical radius it uses the exponents $D_{lm} + 1/2 + 2h$ and $D_{lm} + 3/2 + 2h$ for the first two powers in smooth-cutoff extrapolation with $|l - m| = Nz$. For even N with NzR negligible at the computed cutoff R, it uses the centre exponents $N^2/4 + 2h$ and $N^2/4 + 1 + 2h$ as an empirical approximation. The change of scale follows from the translation Bessel factor. Neither extrapolation replaces the absolute tail theorem.

The evaluator compares the maximum radial and discretization changes, a cancellation indicator and the requested tolerance. Its estimates are diagnostics. Its relative flag requires an estimated absolute error smaller than the computed modulus; an absolute-only result or an unresolved status is returned otherwise. A finite grid cannot establish the original parameter-uniform relative-accuracy target.

Resolving the two slow waves at a detuned rank-three wall

Suppose $N = 3$ and z is near $1/3$. For $l + m = 3$, $|l - m| = 1$, and $\epsilon = -(l - m)$ the two radial phases have frequencies $\omega = l - m + \epsilon 3z$. Determinant values well inside the computed radial interval can fail to reveal a tail at wavelength $2\pi/|1 - 3z|$. The correction used here computes the coefficients of these two waves from the prepared integral. The remaining frequencies stay separated from zero in a compact neighborhood of $1/3$.

Here are explicit finite Gaussian formulas for the coefficients. Put $a = 3z$, let $\sigma = (\epsilon, +1, \dots, +1, -1, \dots, -1)$ with l pluses and m minuses after the first sign. Put $R_0 = e^{-i\epsilon\pi/4}/\sqrt{a}$, $R_j = e^{-i\sigma_j\pi/4}$ for $j > 0$, and $x_j^* = 0$ or π

according as $\sigma_j = +1$ or -1. For the formal variable v and four independent standard real Gaussians X_j use

$$x_j = x_j^* + 2\arcsin(vR_jX_j/2), \qquad L(v) = \prod_{j=0}^{3}(1 - v^2R_j^2X_j^2/4)^{-1/2}.$$

Set $A(x) = \prod_{1\le i<j\le 3} 4\sin^2((x_i - x_j)/2)\prod_{j=1}^{3}[(1+ze^{i(x_0+x_j)})(1+ze^{-i(x_0+x_j)})]^{-3-s}$ using the analytic logarithms from the real saddle. Then the coefficient of $e^{i\omega t}t^{-3-b}$, $b \ge 0$, is

$$\frac{d^{9+6s}}{3!(2\pi)^2}\binom{3}{l}\left(\prod_{j=0}^{3}R_j\right)\mathbb{E}\,[v^{2+2b}]\{A(x)L(v)\}.$$

The coefficient operator acts **inside** the expectation. No unbounded Gaussian is substituted into a common disk of analyticity. To prove the formula, first localize the analytic stationary phase at each of the four angles as in the physical connection proof. The indicated Morse coordinates make the quadratic exponent $-\sum X_j^2/2$ after setting $v = t^{-1/2}$. Their Jacobians are $v^4(\prod R_j)L(v)$. The coincident pair forces the additional degree two. Gaussian integration of each finite Taylor polynomial gives the stated coefficient, with the stationary-phase remainder uniform for z in a compact neighborhood of $1/3$ and s in a compact set. A coefficient of total degree k is integrated exactly by a product Hermite rule of one-dimensional order at least $\lfloor k/2\rfloor + 1$. Only the coefficient itself is obtained by numerical Cauchy sampling in this implementation. At $b = 0$ the formula reproduces the leading coefficient of the radial stationary-phase theorem.

For each retained term $ce^{i\omega t}t^{-d_0}$ the sharp lattice tail after K reduces to the ordinary convergent sum $c\Delta^{-d_0}\sum_{k>K} e^{i\omega\Delta k}k^{-1-2h-d_0}$. At zero detuning this is a Hurwitz zeta value. At small nonzero detuning the implementation uses the exponential integral for the continuous tail and eight Euler–Maclaurin corrections. The fraction removed by the smooth cutoff below K is restored explicitly. The resulting computation has numerical error estimates. The rigorous coefficient formula and the existence of the next asymptotic order do not supply an evaluated bound for its remainder at the computed cutoff.

Executed tests. The practical interface returns estimated errors. At $N = 7, z = 0.08, h = -0.85 + 0.5i, s = 1 + 0.4i$ it gives $0.226234307190806 - 1.5046463498756 94i$. At $N = 8, z = 0.01, h = -0.95 + 3i, s = 3i$ it gives $0.0124708753102262 - 0.0057754123781122i$. Separate lattice sums using the untransformed Haar-angle quadrature at every sampled frequency and a different lattice spacing differ by 4.85×10^{-16} and 9.04×10^{-17} in absolute value. These computations share the sampled Mellin identity. The critical-rank-five example $(z, h, s) = (0.6, -0.75+0.2i, -0.2+0.1i)$ and critical-rank-six example $(1/3, -0.8-0.4i, -0.7+0.1i)$ reach estimated relative errors 7.59×10^{-11} and 1.29×10^{-12}. Independent point evaluations on the three rank-seven walls provide scalar tests without transporting a common state between the walls.

At $N = 3, z = 1/3 + 10^{-5}, h = -0.95 + 0.6i, s = 0.2 + 0.4i$ the uncorrected lattice sum changes by 1.11×10^{-5} between terminal windows at radial cutoff 768. With four source-derived slow-wave terms the change is 2.33×10^{-12}. The adaptive scalar $-0.696335597022387 - 1.097344055571075i$ has estimated relative error 9.77×10^{-12}. A five-term sum with different spacing and cutoff changes the answer by 2.55×10^{-13} in absolute value. At the exact wall, the $h = -1/2, s = -3$ comparison with the independently enclosed translated trace has relative midpoint discrepancy below 1.6×10^{-15}. For $N = 8, z = 0.9, h = -0.9 + 0.5i, s = 1 + 0.5i$, the radial cap 768 leaves a relative estimate 5.86×10^{-10}. Raising it to 1536 gives $2.89298938995958 + 5.07229024884647i$ with estimated relative error 2.77×10^{-13} in 67.2 seconds.

At $N = 8, z = 0.9, s = -3, t = 0$, the relative discrepancy from the known mass d^{-9} was 8.46×10^{-11} in the monomial basis and 1.06×10^{-15} in the changed basis. Dropping the basis prefactor produces a relative discrepancy above 0.9999996. The practical upper-corner run at $N = 5, z = 0.9, h = 3+3i, s = 3$ first returned an unresolved binary64 estimate 1.92×10^{-9} relative. The repair computes the Mellin integral on the first panels with a 64-bit significand and numerically integrates the prepared determinant twice, with different bases and quadratures. It returns $-22.32418966361237 + 37.89957762364567i$ with estimated absolute error 6.77×10^{-10} and relative error 1.54×10^{-11} in 30.2 seconds. An independently coded whole-range original-eigenangle calculation at 384 directions gave a relative midpoint discrepancy 4.61×10^{-11}. A whole-range original-eigenangle check with a separate radial partition ($r_0 = 2.22$, $R = 325$), 2762 source evaluations and a 64-bit significand through $t = 7$ reduced the relative midpoint discrepancy to 5.29×10^{-13} in 76.3 seconds. A 128-direction attempt had visible angular aliasing and gave an incorrect answer. Numerical comparisons leave the true error unknown. A separate

Arb calculation at $N = 8, z = 0.05, h = -0.9+0.6i, s = 0.2+0.5i$, with $\Delta = 2/[8(1+0.05)]$, enclosed the absolute sharp lattice tail after 4032 samples by 3.350×10^{-14}. This last bound concerns frequencies above 960 and does not enclose the finite sum.

Certified scalar sampling at nonzero critical radii

Proposition 21.15 (finite angular reconstruction and alias control). The lattice formula in Section 5 admits a finite ball computation on each admissible query for which the following strict cutoffs and tail bounds succeed. The test concerns the ordinary scalar at a physical radius. Its input includes the full complex order and tilt. No ODE connection data are needed for this readout.

Under the same change of variables as in Theorem 9.5, set $P = (1-z^2)^{N^2+2Ns}$, $B = N+s$, and $w(v) = (1+zv)^{-B}(1+z/v)^{-B}$. In the following implementation $\Re B \geq 0$, $0 < z < 1$. The Laurent coefficients are even under index reversal. For $j \geq 0$,

$$w_j = (-z)^j (B)_j \, {}_2F_1(B+j, B; j+1; z^2)/j!.$$

Fix $t > 0$ with $ze^t < 1$. At radii $e^{\pm t}$ one can bound $|w|$ by M_t, the product over $v = ze^{\pm t}$ of $\max\{(1-v)^{-\Re B}, (1+v)^{-\Re B}\} \exp(|\Im B| \arcsin v)$. Truncating the Laurent series at L costs $\epsilon = 2M_t e^{-t(L+1)}/(1-e^{-t})$ on the real circle. For real frequencies the induced pointwise error in the unshifted angular expectation is at most $|P| N \epsilon ((1-z)^{-2\Re B} + \epsilon)^{N-1}$ by telescoping the original product under Haar probability.

Rotate all angles to the real Fourier direction. The remaining angular variable ϕ enters this preparation and the separate translation $e^{iNzr\cos\phi}$. The unshifted directional determinant, including P, is analytic for $|\Im\phi| \leq t$ and bounded by $|P| M_t^N$ there at real r. From Q equispaced angles retain harmonics $|k| \leq q = Q/2 - 1$ and contract them against $i^k J_k(Nzr)$. The sum of aliasing and discarded-harmonic errors is at most $4|P| M_t^N e^{-t(q+1)}/(1-e^{-t})$: the omitted Fourier coefficients are summed once for the truncation and at most once for aliasing. The Laurent approximation error on the samples can enter each retained coefficient once, so multiply its preceding bound by $2q+1$. Denote the sum of the two bounds by e. The same estimate at complex radial frequency acquires the factor $e^{N(1+z)|\Im r|}$ by the integral representations of the two waves. Matrix indices in the rotated grid contribute the exact Fourier sums $\sum_l w_l i^{d-l} J_{d-l}(r) e^{-il\phi}$ up to the choice of angular orientation. Transposition shows that the determinant is even in ϕ, also at nonreal tilt. All numerical Bessel values, transforms and determinants in this construction are enclosed with ball arithmetic.

For a Cauchy radius $H > 0$ sample the even function Φ at $He^{i\pi l/m}$, $0 \leq l < m$. The recovered coefficient a_j, $j < m$, has error bounded by

$$H^{-2j}\left[e\exp(N(1+z)H) + \frac{M(N(1+z)H/2)^{2(j+m)}}{((j+m)!)^2\{1-(N(1+z)H/(2(j+m+1)))^2\}}\right],$$

where $M = (1-z^2)^{-(\Re s)^2}$ from Section 5, and the displayed denominator must be positive. This follows by summing the aliased Taylor coefficients and the real-space bound on the Taylor moments. Weight each of these errors by $|\zeta(1+2h-2j)\Delta^{2j}|$ and use the Section 5 bound for the unused image series. For the retained real samples the total input error is at most $e\sum_{k=1}^{K} k^{-1-2\Re h}$. For $r > K\Delta$, replace the strip bound for the weight by $|P| M_\tau^N$ in the deformed integral of Theorem 9.5. Integration of the decreasing power on the lattice gives the remaining sample error before the common prefactor:

$$|P| M_\tau^N \sum_{l+m=N} b_{lm} \Delta^{-D_{lm}} \frac{K^{-D_{lm}-2\Re h}}{D_{lm}+2\Re h}.$$

Finally multiply these analytic budgets by $|C(h)\Delta^{-2h}|$ and add the finite arithmetic radii. This test needs no fitted coefficient, variance interpretation for the complex tilt, or numerical extrapolation of the tail. The constants grow rapidly as z approaches one. The practical binary64 evaluator may be much faster there and carries its own empirical error status.

Executed values. The following are ceilings on relative error after reparsing the printed, outward-rounded coordinate rectangles. The high-precision internal radii in the solver receipts are usually tighter. The same steps were executed at every listed input, with $\Delta = 1/4$, 18 image coefficients, 72 Cauchy nodes on the radius-four circle, and 220-bit arithmetic. Digits in this table are rounded for reading.

N	z	h	s	Samples	Physical scalar, rounded	Portable relative bound
4	$1/4$	$2.5+0.4i$	$0.4-0.7i$	2300	$2.8717717+0.9169790i$	2.62×10^{-15}
5	$1/5$	$2.5+0.4i$	$0.4-0.7i$	1600	$2.9230262+1.0908928i$	1.32×10^{-16}
6	$1/3$	$2.5+0.4i$	$0.4-0.7i$	3200	$2.8727589+0.5804793i$	3.42×10^{-16}
7	$1/7$	$0.53+0.4i$	$-0.6+0.8i$	2400	$0.8256101+0.0011443i$	1.05×10^{-17}
8	$1/4$	$0.53+0.4i$	$-0.6+0.8i$	3200	$0.8225213-0.0548429i$	3.26×10^{-15}
7	$1/7$	$2.5+0.4i$	$-0.6+0.8i$	1000	$2.9826016+1.1606328i$	1.72×10^{-18}
7	$3/7$	$2.5+0.4i$	$-0.6+0.8i$	3840	$3.0402769-0.6706910i$	1.08×10^{-13}
7	$1/7$	$-0.95+3i$	$-0.6+0.8i$	8192	$0.0130988-0.0063332i$	2.75×10^{-14}
8	$1/4$	$-0.95+3i$	$-0.6+0.8i$	9600	$0.0143737-0.0076177i$	2.90×10^{-11}

Across the nine inputs, the recorded wall times ranged from 24.4 to 449.2 seconds. The two values at ranks seven and eight with $h=-0.95+3i$ use 8,192 and 9,600 finite radial samples. At rank seven, $h=2.5+0.4i$ and $s=-0.6+0.8i$ are held fixed while the physical scalar is evaluated at each of the first two walls. The two evaluations have independent initial data at the Fourier origin; no full-state transmission across intervening radii is claimed.

Continuous intervals containing a critical radius

Theorem 21.16 (uniform scalar accuracy on two critical-radius intervals). Let $N=7$ and $1/8\le z\le 1/6$, or let $N=8$ and $6/25\le z\le 13/50$. At every point of either region allow independent parameters

$$0.45\le \Re h\le 0.65,\quad |\Im h|\le 0.025,\quad |\Re s|\le 0.5,\quad |\Im s|\le 0.08.$$

The ordinary unnormalised moment is bounded away from zero throughout each region. On these regions one can evaluate it to relative error below 10^{-10} by the scalar lattice sum. The same step $\Delta=1/4$, $J=28$ image coefficients and $m=96$ complex radial samples on $H=4$ suffice throughout. The respective numbers of positive real radial samples are $K=2048$ and $K=6000$. The rank-seven interval contains $z=1/7$ and the rank-eight interval contains $z=1/4$. This is a scalar reconstruction at any queried radius in the interval. It imposes no connection condition on the full differential state.

Separation from zero. Write r for the upper endpoint, $D=N(1+r)$, $a_0=0.45$, $a_1=0.65$, $b=0.025$, $t_s=0.08$, $\epsilon=10^{-5}$, and $M=(1-r^2)^{-1/4}$. The positive majorant for the tilted mass is at most M. Pointwise $|\Lambda|^{2\Re s}\ge(1-r)^N$ since its two endpoint competitors are bounded below by $(1-r)^N$ and $(1+r)^{-N}$. Since $|S|\le D$, the positive marked mass is at least

$$M_0=(1-r)^N(1-r^2)^2D^{2a_0-2}.$$

Indeed, $|S|^{2\Re h}\ge D^{2a_0-2}|S|^2$ and $\mathbb{E}|S|^2\ge(1-z^2)^2$. For the latter identity expand $S=(1-z^2)\sum_{k\ge1}z^{k-1}\operatorname{Tr}U^k$. Central rotation kills the unequal powers and the first surviving squared coefficient has $\mathbb{E}|\operatorname{Tr}U|^2=1$.

On $|S|\ge\epsilon$ the absolute value of the phase angle of the integrand is at most

$$\Theta=2b\log(1/\epsilon)+2t_sN[-\log(1-r)]<\pi/2.$$

This uses $D < 1/\epsilon$ and the real logarithms in both powers. The omitted set contributes at most $M\epsilon^{2a_0}$ in absolute value. Consequently

$$|T_N| \ge \Re T_N \ge L = M_0 \cos\Theta - (1+\cos\Theta) M \epsilon^{2a_0}.$$

The outward calculation gives $L > 0.01856191$ at rank seven and $L > 0.00347424$ at rank eight. This argument controls cancellation for the whole rectangle.

Budget. The absolute multiplier of the image, source and tail budgets is at most

$$C_* = 2^{2a_1+1} \cosh(\pi b) \Delta^{-2a_1}/\pi.$$

Reflection expresses its gamma ratio through $\Gamma(1+h)^2 \sin(\pi h)$. Use $|\Gamma(1+h)| \le \Gamma(1+\Re h) \le 1$ by the integral bound and log-convexity on $[1,2]$. The angular algorithm can achieve $e < 10^{-47}$ for every input in the region with $Q \le 384, L_{\mathrm{Laurent}} \le 132$ or $Q \le 512, L_{\mathrm{Laurent}} \le 204$, respectively. For its choice $t = -0.6 \log z$, the two geometric arguments are $z^{0.4}$ and $z^{1.6}$; replace each by its value at r and replace e^{-t} by $r^{0.6}$. Use $\Re(N+s) \le N + 1/2$, $|\Im s| \le 0.08$ and $|P| \le 1$. Driving both monotone cutoff inequalities with these bounds and the worst permitted Q gives the two finite resource bounds.

The Cauchy coefficient budgets use the preceding proposition with upper values M, D and $e = 10^{-47}$. For $j = 0$ the zeta weight is at most $\zeta(1+2a_0)$; for $j = 1$ the bound 3 suffices. To see the second bound, put $w = 2h - 1$. Euler–Maclaurin summation through B_2 bounds the modulus by $1/2 + 1/|w-1| + |w|/12 + |w(w+1)|/[12(1+\Re w)]$. Here $-0.1 \le \Re w \le 0.3$ and $|\Im w| \le 0.05$. For $j \ge 2$ the zeta functional equation gives the bound

$$2(2\pi)^{2a_1-2j} \cosh(\pi b) \Gamma(2j-2a_0) \zeta(2j-2a_1).$$

The gamma factor is increasing on the positive interval used here, and zeta is decreasing on its real interval above one. The image tail uses these same majorants at $j = J$ and geometric ratio x^2, $x = \Delta D/(2\pi)$. The integral majorant for the lattice tail uses the common contour deformation 0.4, $\Re h \ge a_0$ and the worst preparation at r. The finite real-sample errors contribute at most $C_* e \zeta(1+2a_0)$.

At ranks seven and eight the analytic tail terms including C_* are bounded above by 1.772×10^{-14} and 3.196×10^{-16} for the positive real samples. The corresponding analytic image tails are below 5.532×10^{-30} and 7.842×10^{-25}; the Cauchy data errors are below 2.583×10^{-32} and 5.444×10^{-29}. These bounds come from outward arithmetic on rational rectangle endpoints, with no sampling of the parameter region. For the finite expression the point wrapper sums its two interval radii and charges 100 decimal units in the last printed place of each nonzero component of the 46-significant-digit midpoint. Adding a symmetric analytic error ball preserves that midpoint. A per-call allowance of 10^{-14} for finite arithmetic including this readout, together with two component allowances for the analytic errors, gives absolute budgets below 4.543×10^{-14} and 1.064×10^{-14}. Using L less twice this error as a lower bound for the whole accepted enclosure gives relative budgets below 2.448×10^{-12} and 3.063×10^{-12}. A retry replaces every sampled determinant by the Newton trace recursion. For the $N \times N$ sampled matrix A, form $c_0 = 1$ and $k c_k = -\sum_{j=1}^{k} c_{k-j} \operatorname{Tr}(A^j)$; then $\det A = (-1)^N c_N$. Its only divisors are fixed positive integers, so it remains valid at singular matrices. The matrices and the finite number of special-function values at an admitted exact point have enclosures that contract with precision. Polynomial operations on these entries preserve contraction. The finitely many allowable angular and Laurent cutoffs provide the same contraction conclusion even when a refinement changes which cutoff passes its bound. This justifies the retry also at a zero determinant. The decimal allowance is below 10^{-40} since $|T_N| \le M D^{2a_1} < 30$ on the regions and the analytic error is below 10^{-13}. The full-lattice formula therefore supports increasing precision when required. A fixed upper precision cap can return a resource failure. The region theorem concerns an error bound valid at each input and does not supply the range of all outputs. □

At the first wall of each interval the full regional rule was executed with $h = 0.583 + 0.017i$, $s = -0.371 + 0.063i$. At rank seven the result is $0.895500107457771626 + 0.000376987974038229i$ to the shown decimals; the stored midpoint has relative error below 4.900×10^{-18}. At rank eight the corresponding value is $0.903746321588541742 - 0.002416639772739996i$, with stored-midpoint relative error below 8.709×10^{-22}. The runs took 43.28 and 291.69 seconds at 220 bits. Separate direct radial quadrature differs from the stored midpoints by 2.63×10^{-15} and 6.41×10^{-16}, respectively. These are two executed inputs inside a region covered by the analytic theorem.

A uniform inverse-order sampler on both sides of the first wall

Theorem 21.17 (uniform absolute error for inverse orders). Take $-0.95 \le a = \Re h \le -0.8$, $|\Im h| \le 3$, and independently $|s| \le 3$. At rank seven take $0.13 \le z \le 0.155$ and at rank eight take $0.235 \le z \le 0.265$. These

closed intervals contain $1/7$ and $1/4$ respectively. The sampled Mellin algorithm with $\Delta = 1/4$, $K = 3200$ real samples, $J = 18$ image terms, and $m = 72$ Cauchy samples at radius $H = 4$ gives the physical scalar with a uniform **absolute** error below 7.270×10^{-14} and 1.739×10^{-12} respectively, including a 10^{-14} finite-arithmetic and export allowance. The algorithm raises precision until it verifies this allowance at the query. The analytic bound applies to the whole indicated region. The implementation accepts exact rational query components. No uniform precision, relative bound, or enclosure of all output values is asserted.

Proof. We refine the contour bound for the retained scalar preparation. Put $d = 1 - z^2$, $B = N + s$, and $S = 3$. Rotate into the real frequency direction and use the deformed angle $v = x - i\tau \sin x$. On the half circle about $x_* = 0$ or π, write $u = x - x_*$. The modulus of the derivative of the logarithm of $(1+ze^{i(v+\phi)})^{-B}(1+ze^{-i(v+\phi)})^{-B}$ is bounded by

$$L = 2(N+S)\sqrt{1+\tau^2}\,\frac{z_+e^{\tau}}{1-z_+e^{\tau}}, \qquad \beta = 4\tau/\pi^2,$$

where z_+ is the upper radius and $z_+e^{\tau} < 1$. Integrate the derivative on the arc from x_* to x. The preparation modulus at the deformed point is at most its value at the real saddle times $e^{L|u|}$. For $0 < \eta < 1$, $r \ge R = K\Delta$, complete the square to obtain

$$e^{-\beta r u^2 + L|u|} \le e^{L^2/(4\eta\beta R)} e^{-(1-\eta)\beta r u^2}.$$

At the two real saddles, l and $k = N - l$ angles see the opposite factors $|1+ze^{i\phi}|$ and $|1-ze^{i\phi}|$. Pair $p_0 = \min(l,k)$ of them and use $|1 - z^2e^{2i\phi}| \ge d$. With $j = |l-k|$, the product at the saddles, including the physical prefactor, is bounded by

$$B_{lk}(z,b) = d^{N^2-2Np_0}(1-z)^{-2Nj}\exp[b\{(2N-2p_0)\log d - 2j\log(1-z)\}], \qquad b = \Re s.$$

Here $N + b > 0$. This step retains the opposite real saddle weights before taking the supremum in the direction. For the balanced rank-eight saddle, for example, the expression reduces to d^{Nb}.

Let $D_{lk} = (l^2 + k^2)/2$ and use the constants b_{lk} of the Gaussian Vandermonde contour bound with same-half factor $1 + \tau^2\cosh^2\tau$ and opposite-half factor $4\cosh^2\tau$. Integrating the weakened Gaussian gives each term the extra factor

$$B_{lk}(z,b)(1-\eta)^{-D_{lk}}\exp\left(\frac{NL^2}{4\eta\beta R}\right).$$

Sum b_{lk} times this factor times $\Delta^{-D_{lk}}K^{-D_{lk}-2a}/(D_{lk}+2a)$ to bound the sharp sampled tail before the common Mellin multiplier. The exponent is positive throughout the domain. Use radius endpoints for each monotone logarithm in B_{lk} and $|b| \le S$. The calculation uses $(\tau,\eta) = (0.45, 0.18)$ and $(0.4, 0.35)$ respectively. A finite search for these constants affects efficiency only.

For completeness, all other parameter suprema can be taken with real arithmetic. Divide the order rectangle into six real strips of width $1/40$ and twelve $|\Im h|$ strips of width $1/4$. In a tile with endpoints a_0, a_1, t_0, t_1 write $x = 1 + a$, $y = -a$ and $M = 8$. Since $0 < x < y$, the beta integral and gamma recurrence give

$$\left|\frac{\Gamma(x+it)}{\Gamma(y+it)}\right| \le \frac{\Gamma(M+1+a_1)}{\Gamma(M-a_1)}\prod_{u=0}^{M-1}\left(\frac{(u-a_0)^2+t_0^2}{(u+1+a_0)^2+t_0^2}\right)^{1/2}.$$

Indeed the shifted beta integral bounds the ratio by $\Gamma(M+x)/\Gamma(M+y)$, and each remaining ratio of moduli decreases as $|t|$ grows. For $C_\Delta = C(h)\Delta^{-2h}$ multiply by $2(2/\Delta)^{2a_1}$. Bound $|\cos\pi h|$ by $\cosh(\pi t_1)$. For the image index j, zeta reflection yields

$$|\zeta(1+2h-2j)| \le 2(2\pi)^{2a_1-2j}\cosh(\pi t_1)\Gamma(2j-2a_0)\zeta(2j-2a_1).$$

The gamma arguments are at least 1.6, where gamma is increasing. For example its logarithmic derivative is increasing and is already positive at $3/2$. The same endpoints bound the image-tail ratio from the sampled Mellin formula. The mass is at most $(1-z_+^2)^{-9}$ and the support radius at most $N(1+z_+)$. For the angular symbol use $t = -0.6\log z$; the deformations $ze^t = z^{0.4}$ and $ze^{-t} = z^{1.6}$ are increasing. The same geometric alias and Laurent bounds as in the pointwise sampler prove a source tolerance 10^{-47} with the angular caps in the table. Multiply the real-node source error by K^{-2a_0} since k^{-1-2a} is increasing here. Bound the Cauchy alias and source errors termwise as in the finite reconstruction. All maxima in the proof are analytic bounds on tiles or fixed-radius intervals. The outward-rounded budgets below use 160-bit arithmetic.

Rank	Upper grids Q, L	Finite real-node source error	Cauchy source and alias	Image tail	Infinite sample tail
7	384, 132	4.09×10^{-41}	8.70×10^{-32}	9.97×10^{-17}	6.260×10^{-14}
8	768, 224	4.09×10^{-41}	4.00×10^{-18}	5.344×10^{-13}	1.195×10^{-12}

The per-query computation encloses the finite sum by complex ball arithmetic and directly bounds its distance from the exported decimal midpoint. Its acceptance threshold is 10^{-14}. The first calculation uses a pivoted determinant. If the gate fails, the code doubles precision and switches to a signed subset expansion using only ring operations, including at singular sampled matrices. Every special function in these finite expressions is evaluated at a regular point: the nonnegative hypergeometric denominator is a positive integer, the hypergeometric argument has modulus below one, and the gamma and zeta factors have no poles in this order rectangle. Arbitrary-precision convergent evaluation of the finite expressions thus makes the finite arithmetic radius tend to zero. The angular caps have strict slack, and the finite sample sizes do not depend on a spectral gap in the trace or a lower bound on the final scalar. The sum of absolute analytic errors is added as a single disk radius, so there is no need to charge it twice through a coordinate rectangle. This proves the claim.

Executed endpoints. The rank-seven cold run used $z = 0.155$, $h = -0.95 + 3i$, $s = -1.8 + 2.4i$, grids $384, 120$, 220 bits and 109.4 seconds. It enclosed the moment about $0.01929874034869803 - 0.01333887261556654i$. The rank-eight cold run used $z = 0.265$, $h = -0.8 - 3i$, $s = 1.8 - 2.4i$, grids $512, 208$, 220 bits and 177.0 seconds. It enclosed the moment about $-0.002414819133345478 + 0.0040132304255094 57i$. Peak process memory was below 30 MiB for each. The finite-sum and decimal-export radii were below 9.09×10^{-54} and 1.04×10^{-44}. Independent binary64 lattice implementations gave absolute midpoint differences below 1.19×10^{-16} and 1.57×10^{-16}. Those comparisons have no role in the certified budgets.

Charging the regional analytic majorants gives point relative bounds 2.673×10^{-12} and 3.692×10^{-10}. At the second input the regional budget therefore misses the requested relative precision. To repair the readout, retain the executed finite sum, its recorded arithmetic/export radius, and its 3200 nodes. Recompute all four analytic budgets at each exact input. In the paired tail use its exact b, z and $|N + s|$ in the Lipschitz constant. In the Cauchy and image bounds use the actual gamma, zeta, cosine and positive-mass estimates. Outward arithmetic gives absolute radii below 7.109×10^{-17} and 2.546×10^{-13}, and point relative bounds below 3.030×10^{-15} and 5.435×10^{-11}. This repair recomputed error bounds on the stored midpoint; no second finite-sum run is claimed. The improved relative values are pointwise. A separately forced nonfinite pivot and a deliberately raised pivot exception were both recovered, at an actual rank-seven source node, by the division-free fallback. A rank-deficient three-by-three control returned an exact zero determinant.

A uniform absolute truncation bound for the upper-radius inverse strip

Theorem 21.18. For each $4 \le N \le 8$, take the product domain

$$.82 \le z \le .90, \qquad -.95 \le \Re h < 0, \qquad |\Im h| \le 3, \qquad |s| \le 3.$$

At every input the finite formula specified below, in exact arithmetic, differs from the ordinary $T_N(h, s; z)$ by less than 1.260×10^{-16} in absolute value. This uniform bound covers the errors from the Fourier tail, preparation, direction, Cauchy extraction and Mellin image. The formula evaluates a different complex number at each input. Finite-precision costs are charged separately in Proposition 21.19. The faster estimator uses different cutoffs.

Proof. In Theorem 5.3 use $\Delta = .32, t = .027, K = 44000, b = 144, p = 60$. Across the five integer ranks $g_* \ge .4$ (compare the two nearest signed radii) and $D \le 15.2$. Subdivide $[0, .4]$ into 32 equal intervals and add $[.4, 15.2]$. Use $z = .9$ in the upper bounds on E, η, and replace M by $.19^{-9}$, $N(N + \Re s)$ by 88, and $N|\Im s|$ by 24. The variation is below 2.900×10^{24}. Reflection of gamma gives $|C_\Delta| \le 2\Gamma(.05)^2 \cosh(3\pi)/\pi =: C_0$ since $|\Gamma(1 + h)| \le \Gamma(1 + \Re h) \le \Gamma(.05)$ and $(2/\Delta)^{2\Re h} \le 1$. Euler's product gives

$$\frac{\Gamma(x)}{|\Gamma(x + iy)|} = \prod_{j \ge 0} \sqrt{1 + y^2/(x + j)^2} \le \sqrt{1 + 60^2}\sqrt{\sinh(6\pi)/(6\pi)}$$

for $x = 2 + 2\Re h \ge .1$ and $|y| \le 6$. All 33 terms of (5.8) are evaluated with directed balls. Their common bound after all factors is 1.259×10^{-16}, including the interval containing $X = 0$. The filter's final index is 52580.

For the real source use (5.9) with $v = .09, Q = P = 8192, L = 3072$. Put $z = .9$ in E_v, η_v, in the Möbius modulus, and in the lower and upper bounds g_0, g_1. Valid common bounds are $W \le 10^6$, $d^{1+2u} \le .19^{-5}$ and $\max(g_0^{-1-u}, g_1^{-1-u}) \le \max(g_0^{-4}, g_1^2)$. Thus the total real-projection error, including the bound $C_0(52580)^{1.9}$ on the sum of absolute weights, is below 2.384×10^{-33}.

For clarity, the image calculation in both the uniform and pointwise versions is as follows. Write $\Phi(r) = \sum a_j r^{2j}$. Evaluate at the m points $H\exp(i\pi l/m)$ and extract $H^{2j}a_j$ with the normalized discrete transform. The wraparound at index j costs at most

$$E_j = M\frac{(HD/2)^{2(m+j)}}{((m+j)!)^2[1-(HD/(2(m+j+1)))^2]},$$

from $|a_j| \le M(D/2)^{2j}/(j!)^2$. For these complex nodes, let $v = .09$, $b_0 = H/2$, and prepare modes through L on a P-point grid as in Proposition 5.4. A one-entry error bound is

$$e_A = \frac{2We^{b_0^2}b_0^{L+1}}{(L+1)!(1-b_0/(L+2))} + (2L+1)e^H\frac{2C_ve^{-v(P-L)}}{1-e^{-vP}}.$$

Indeed each exact Fourier coefficient is bounded by W on the real preparation circle. The complex Bessel series bounds $|J_j(r)| \le e^{b_0^2}b_0^{|j|}/|j|!$ on $|r| = H$. For the retained modes use $|J_j(r)| \le e^H$. On real directions the exact entry matrix has norm at most We^H, and the translation costs at most e^{HNz}. The true source, with its original real eigenangles, has direction-strip bound $Me^{HD\cosh 2}$ for $|\Im\phi| \le 2$. Its Q-point trapezoidal error and the propagated entry error therefore sum to

$$e_\Phi = 2Me^{HD\cosh 2}/(e^{2Q}-1) + N^2e_A(We^H + Ne_A)^{N-1}e^{HNz}.$$

Finite image error before the exterior factor is bounded by $\sum_{j<J}|\zeta(1+2h-2j)|(\Delta/H)^{2j}(e_\Phi + E_j)$; Proposition 5.2 bounds the remaining image.

For the uniform box use $J = 144, m = 432, H = 12, Q = 1024, L = 336, P = 8192$ for these complex nodes. For $j \ge 1$ the zeta functional equation gives $|\zeta(1+2h-2j)| \le 4(2\pi)^{-2j}\cosh(3\pi)(2j+1)!$, using $2j - 2\Re h \ge 2$. At $j = 0$ the zeta factor grows near $h = 0$. The *combined* bound $|C_\Delta\zeta(1+2h)| \le 55C_0$ holds including the limiting value. To see this apply the second Euler–Maclaurin formula to $v_0 = 1+2h$, isolating $1/(v_0-1)$: the rest has modulus at most $1/2 + 7/12 + 7\cdot 8/(12\cdot .1)$ since $|B_2(\{x\})| \le 1/6$. The sine from gamma reflection satisfies $|\sin(\pi h)/(2h)| \le (\pi/2)\cosh(3\pi)$, by integrating the cosine along the segment from zero. The constant-term pole therefore causes no loss in this bound. For the exterior image use the ratio of Proposition 5.2 at $\Re h = -.95$, replace the numerator gamma by $(2J+1)!$ and bound the real zeta by two. The finite complex-coefficient contribution here is below 1.92×10^{-150}. The exterior-image majorant also requires the prepared mass M. The corrected numerical budgets for the same formula follow below. The portable computation of these inequalities is in the uniform terminal receipt. Only scalar inequalities for the whole box are evaluated in that receipt; the 52580-node formula has smaller parameter-specific executions below.

A lower bound for the modulus with independent imaginary parts

Corollary 21.18A. In the domain of Theorem 21.18 put $a = \Re h$, $D_* = 15.2$, $a' = -.975$, and $A_* = 2.476 \times 10^{13}$. Write

$$\ell(a) = \max\left(\log D_*, \frac{\log(8A_*D_*^{-2a})}{2(a-a')}\right).$$

Throughout the connected subregion

$$2\ell(a)|\Im h| + 16\log(10)|\Im s| \le 1$$

the real part of the physical moment exceeds .0019759. Consequently the uniform finite formula has relative truncation error below 6.378×10^{-14}. A computation of that formula with, for example, absolute arithmetic error at most 10^{-13} meets 10^{-10} relative throughout the subregion. The modulus floor holds for every allowed real tilt, also when the order and tilt vary independently. For orientation $\ell(-.95) < 762$, $\ell(-.75) < 83$ and $\ell(-.53) < 41$. The full complex tilt disk in Theorem 21.18 requires an absolute criterion, as the zero in Theorem 21.20 shows.

Proof. At the more singular **real** order a' use the deformed preparation from Theorem 5.3 with $t = .006$, real tilt $u = \Re s$, and the **continuous** Mellin formula. Multiplying the radial integrand by $e^{-\varepsilon r}$ permits Fubini on the deformed contour. The exact radial integral is $\Gamma(-2a')(\varepsilon - iG)^{2a'}$ with the right-half-plane branch. The gap proof gives $|G| \ge g_* t/\sqrt{1+t^2}$ by Cauchy–Schwarz, and $|\varepsilon - iG| \ge |G|$ since $Y \ge 0$. Thus dominated convergence and gamma duplication give

$$0 \le T_N(a', u; z) \le \frac{\Gamma(1+a')\Gamma(1/2-a')}{\sqrt{\pi}}\, V \left(\frac{g_* t}{\sqrt{1+t^2}}\right)^{2a'} < A_*.$$

On the original real Fourier side removal of the Abel factor is justified by absolute convergence at these ranks. For the upper bound use $g_* \ge .4$, $z \le .9$, $N \le 8$, $M \le .19^{-9}$, $N(N+u) \le 88$ and $\Im u = 0$. Outward evaluation before rounding gives 2.47510×10^{13} as a strict upper bound. The deformation here estimates a positive physical expectation even though the integrand on the deformed contour need not be positive.

Put $L = \log|\Lambda_N|$. On the real ensemble, $2|L| \le 16 \log 10$ and the real positive mass is $\mathbb{E}e^{2uL} \ge 1$ by rotation, the logarithmic circle mean and Jensen. Hence $T_N(a, u; z) \ge D_*^{2a}$. With $|S| < e^{-\ell}$, the contribution to this positive moment is at most $e^{-2(a-a')\ell} A_* \le D_*^{2a}/8$. On the complement $|\log|S|| \le \ell$. There the phase of the complex integrand differs from zero by at most one radian under the hypothesis. Taking real parts on both pieces proves

$$\Re T_N(h, s; z) \ge D_*^{2a}\big[\cos 1 - (1+\cos 1)/8\big].$$

The lower endpoint $a = -.95$ gives the stated floor. This argument gives an a priori relative-error criterion in a genuinely complex region. The sharper pointwise checks below can succeed far outside it.

Three end-to-end runs test independent imaginary parts inside this relative region. At ranks 4, 6 and 8 respectively take $(z, h, s) = (.86, -.53 + .005i, .8 - .005i)$, $(.89, -.25 + .01i, 2 + .008i)$ and $(.9, -.95 + .0005i, -1 + .005i)$. The corresponding relative bounds were 1.283×10^{-14}, 4.295×10^{-16} and 1.177×10^{-15}, rounded up. These runs used 7929, 10908 and 12360 frequency indices and took 20.9, 85.6 and 168.6 seconds including all preparation on the recorded machine. A separate annular computation at each input returned an estimate that covered the discrepancy plus the full reference error disk.

Correction to the original common inverse-order formula. The original common formula of Theorem 21.18 still has absolute exact-arithmetic error below $1.260 \cdot 10^{-16}$ with its original 52,580 frequencies. The previously quoted exterior Mellin-image component $1.200 \cdot 10^{-20}$ did not include $M = (1 - .9^2)^{-9}$ in the common-cutoff verification script. The independent-input image implementation included M. The corrected bounds below apply to the original formula itself.

For $a = \Re h \in [-.95, 0)$, the beta integral and gamma recurrence give

$$\left|\frac{\Gamma(1+h)}{\Gamma(-h)}\right| = |h| \left|\frac{\Gamma(1+a+i\Im h)}{\Gamma(1-a+i\Im h)}\right| \le |h| \frac{\Gamma(1+a)}{\Gamma(1-a)} \le 4\Gamma(.05)e^2.$$

The numerator bound follows from log-convexity on $[.05, 1]$; the denominator is at least e^{-2} by its integral on $[1, 2]$. At $a = 0$ the ratio comparison is an equality by conjugation and continuity. Since $(2/\Delta)^{2a} \le 1$, we can replace the former common exterior-factor bound C_0 by $C_1 = 8\Gamma(.05)e^2$ in the terminal, real-source and exterior-image budgets. The low-image estimate with combined zeta-pole treatment retains C_0. Multiply the former exterior-image estimate by MC_1/C_0. Evaluating these changes at 192 bits, including a new execution of the inherited inequalities, gives $2.862259 \cdot 10^{-17}$ for the missing-image tail, $9.689569 \cdot 10^{-20}$ for the radial cutoff, $1.835 \cdot 10^{-36}$ for the real-source error and $1.918 \cdot 10^{-150}$ for the finite complex image. The aggregate is less than $2.871949 \cdot 10^{-17}$. This check concerns exact-arithmetic truncation over the inverse-order slab. It changes none of the input-specific finite-arithmetic certificates.

A finite-arithmetic enclosure of the physical sampler

Proposition 21.19 (absolute readout at an accepted query). A query in Theorem 21.18 can instead select its two angular orders, terminal and filter by a floating-point search. With the selected integers and exact rational input, reevaluate (5.8), (5.9) and the complex image estimates in ball arithmetic. Suppose the dyadic stage below accepts and emits centres p_k with absolute errors e_k relative to the finite angular formula. Put

$w_k = k^{-1-2h}\Pr(L_* > k)$ and denote the absolute complex-image error, with prefactor, by E_I. A disk around the emitted physical midpoint has radius

$$E = |C_\Delta| \sum_k |w_k|(e_k + \epsilon_\Phi) + E_I + E_{\text{terminal}} + E_{\text{readout}}.$$

Here E_{readout} includes ball arithmetic and copying the final decimal midpoint. If the decimal midpoint has modulus $m > E$, the relative bound is $E/(m-E)$. A disk containing zero gives only absolute accuracy. Gates on range, resource use and arithmetic can decline an input. This algorithm has no a priori success or timing guarantee on the entire parameter box.

Finite implementation and error proof. The arbitrary-precision stage prepares roots of unity, Möbius coefficients, complex powers and Bessel seeds on the exact rational mesh. Choose $U = 2^{-104}$. Copy to a signed dyadic pair only after checking that each real component is within $2U$ of the stored value. In the fast stage split each real mantissa at 52 bits. The dropped low-times-low term and the floor of the scaled cross term each cost less than U. Thus one complex product costs less than $8U$ in component one-norm. Additions of these integers are exact in the checked range; sums are checked before export. The binary header and implementation require little-endian signed 128-bit intermediates and a long-double significand of at least 64 bits on the tested GNU/IEEE platform.

For a requested maximum order l, compute the modes $i^j J_j(x)$ for the source and translation separately. At $x \le 2(l+1)$ use the normalized transform of the sampled exponential on a power-of-two grid $M_0 \ge 3.5(l+1)+105$. Contour shifting by one gives $|J_j(x)| \le e^{|x|\sinh 1-|j|}$. Summing both omitted alias tails gives less than 10^{-32}. The phase at the start of each chunk is raised by binary powering then advanced locally. The number of effective phase factors, counting error multiplicities under squaring, is k. With the input root bound, one product error and unit exact phase modulus, accumulated error is at most $32(k+1)U$. A normalized butterfly averages two inputs with a unit exact twiddle, priced root and product errors and a dyadic half shift. Its error increases by at most $64U$ per stage at these bounded moduli. The startup, levels and alias are included in $[32(k+1)+64(1+\log_2 M_0)]U+10^{-32}$.

For $x > 2(l+1)$ use enclosed $J_0(x), J_1(x)$ and $J_{j+1} = (2j/x)J_j - J_{j-1}$. The two-stage integer quotient computes $\lfloor (2j/x)/U \rfloor$ without forming an oversized numerator. The metric $a^2+b^2-2(j/x)ab$ is preserved by one exact transfer at fixed j/x and is between one half and three halves of a^2+b^2. Between consecutive indices its growth factor is at most $1+(1/x)/(1-j/x)$, whose product is below e. The coefficient rounding, $|J_j| \le 1$, and split product cost at most $5U$ additive error per step (bootstrap using the resulting bound). Seeds and all local errors together cost less than $64(l+1)U$ per emitted component.

For a direction grid of size Q, let w be the sum of the stored one-norms of a single row's coefficients and e_w the Bessel error above. Propagating products and butterfly additions through each level gives the common per-entry error

$$(2L+1)16U + 2we_w + 32QU + (1+\log_2 Q)8U(w+1).$$

The first two terms price preparation and waves; local multiplication errors sum over the $Q-1$ internal butterfly nodes, while a twiddle perturbation per level multiplies at most the row's input one-norm. The projected translation has the bound $Q(e_t+48U)+(1+\log_2 Q)12UQ$ by the same argument, with e_t from its own Bessel grid. The final Nyquist mode is omitted and reflection pairs directions without conjugating the tilt.

Apply pivoted elimination to each entry matrix after scaling by a power of two. The long-double quotient is only a proposed dyadic multiplier: bound its actual pivot residual $r = \max|a-mb|_1$ and check $|m|_1 \le 4.1$. Summing the roundoff of the local row updates and the pivot-column residual along each permuted row gives componentwise backward error $e_b = 2^j(N+1)(r+16U)$ at dyadic scale 2^j. In detail, the exact product of the implicit lower and computed upper factors reconstructs each entry through the telescoping update history for that entry; each update contributes one local residual. Subsequent multipliers do not multiply these residuals in this backward reconstruction. A zero pivot in a zero column costs no division. The final product of diagonal entries has the independently accumulated forward product bound. For a matrix with maximum stored entry one-norm m_0, an entrywise error e changes the determinant by at most $N\sqrt{N}e[\sqrt{N}(m_0+e)]^{N-1}$ by multilinearity and Hadamard. Apply this once to backward elimination and once to the common angular-row finite error. Charge both translation errors and their product in the final weighted direction average.

The positive long-double error calculations use small integer powers, upper rational square roots and exact bit counts. Under the stated arithmetic and size caps fewer than 2^{18} accumulated rounding steps per reported positive sum cost less than 2×10^{-14} relative. The factor-two margins in the determinant and direction bounds dominate

this effect. The reader additionally inflates each exported radius by $1 + 10^{-11}$ and charges $10^{-18}(|p_k| + 10^{-21})$ for exporting the centre. The final combination, filter probabilities, image and contour error are respectively evaluated with ball arithmetic and exact integer polynomial coefficients. At the hard rank-eight input even the value-dependent decimal export term contributes about 1.45×10^{-16} to the moment error. Fourteen instrumented check runs include the two Bessel switches, and three retained samples have separate original-Haar enclosures. These check the implementation of the inequalities. The five-term budget, all sample counts and the numerical outcomes are retained in the per-query records.

Reusing certified Fourier data across complex orders

For each exact preparation (N, z, s), the Fourier samples $\Phi(k\Delta)$ and the coefficients a_j in $\Phi(t) = \sum a_j t^{2j}$ are independent of h. Their enclosed values can be stored once. At the 144 nodes $t = H\exp(\pi i l/144)$ the verified angular determinant supplies the discrete coefficient A_j of $H^{2j}a_j$, $0 \le j < 72$. If e_Φ is the angular-source error and $M = (1 - z^2)^{-(\Re s)^2}$, the additional scaled coefficient error is bounded by

$$\epsilon_j = e_\Phi + M\frac{v^{2(144+j)}}{((144 + j)!)^2[1 - (v/(145 + j))^2]}, \qquad v = HN(1 + z)/2.$$

This follows by expanding the Bessel function in the physical source and summing the aliased tail of the angular discrete transform. The cache records separate complex arithmetic balls and these systematic radii. Every new order contracts the origin coefficients with

$$w_j = C_\Delta \zeta(1 + 2h - 2j)(\Delta/H)^{2j}.$$

The sum of $|w_j|\epsilon_j$, the independent bound on the image beyond $j = 71$, and the rounded complex readout all enter the image budget. The same order reweights each finite Fourier row, propagates its error and recomputes the filtered tail. If the stored filter misses the relative target, a numerical search may choose a different cutoff distribution on the available rows. The program rechecks that candidate's complete sum and tail with ball arithmetic before adopting the smaller absolute budget.

At $h = 0$ the answer is a_0 itself. Close to zero use $Z(w) = \zeta(w) - 1/(w - 1)$ and form the removable product as

$$w_0 = -(2/\Delta)^{2h}\frac{\Gamma(1 + h)}{\Gamma(1 - h)}[1 + 2hZ(1 + 2h)].$$

This permits a certified evaluation even at $h = -10^{-300}$. At each of the six exact preparations the zero-order mass was independently checked by the original-angle Toeplitz determinant with Fourier entries

$$f_k = z^{|k|}\frac{(-s)_{|k|}}{|k|!}{}_2F_1(|k| - s, -s; 1 + |k|; z^2).$$

The expression follows by multiplying the two convergent binomial series for $(1 - ze^{i\theta})^s(1 - ze^{-i\theta})^s$. The largest upper bound on the discrepancy between the independently evaluated ball and the printed cached mass was 5.09×10^{-48}.

Each cache binds its exact preparation, verified anchor, Fourier row files and coefficient implementation by SHA-256. A query uses the verified bytes loaded into memory. Altered coefficients, mismatched preparations, nonfinite midpoints and nonfinite or negative error budgets are rejected. These repeated-order results certify the individual readouts. Their common source, the ordinary inverse-order strip and the exact zero-order mass define the scope of reuse.

The six executed preparations are the rank-four through rank-eight anchor cases and the separate rank-eight $s = 3i$ preparation. There were 36 fixed-source order requests, including six exact masses and six evaluations at $h = -10^{-300}$. Using the original filters, 28 relative certificates met 10^{-10}. Retuning the filters with the same rows raised this to 32; all four repaired cases were at ranks five and six. The six caches took 1.14–3.97 seconds each to construct from the preserved source metadata, exclusive of the original Fourier rows. The median warm query took .403 seconds and the slowest, including retuning, took 2.18 seconds. Four rank-eight $s = 3i$ readouts still required absolute-only status at the original row count. Two concern the localized zero. The first-stage and refined receipts record the full budgets separately.

At the $s = 3i$ preparation the implementation then computed an additional 3,034 guarded Fourier rows, indices 13,967 through 17,000. This cost 39.71 seconds including setup, with 35.26 seconds in the four-worker kernel. With these extra rows $h = -.95 + 3i$ has midpoint $.0004954134843805956442 - .0000021068127639342773i$, absolute error below 1.459×10^{-14} and relative error below 2.944×10^{-11}. At $h = -.91 - 2.7i$ the relative bound is below 1.701×10^{-13}. Both replayed through the public cache loader; the two zero-neighborhood probes each have absolute error below 1.617×10^{-16}. These are 34 relative successes and two absolute-only outputs among the same 36 requests. Substituting the smaller physical center error into the preceding shifted Rouché calculation reduces the single-zero disk around h_{c} to radius 1.5×10^{-13} at $s = 3i$.

Frequency-guarded annular sampling for outer-radius inverse orders

Put $B = N(1 + z)$, $C_h = 2^{1+2h}\Gamma(1 + h)/\Gamma(-h)$ and $\Phi(t) = \mathbb{E}[|\Lambda_N|^{2s} J_0(t|S_N|)]$. All powers with positive base use the real logarithm. For the inverse orders considered here the inherited sampling identity on any fine lattice $\Delta B < 2\pi$ reads

$$T_N = C_h \left[\Delta \sum_{k \geq 1} (k\Delta)^{-1-2h} \Phi(k\Delta) - \Delta^{-2h} \sum_{j \geq 0} \zeta(1 + 2h - 2j) a_j \Delta^{2j} \right], \qquad \Phi(t) = \sum_{j \geq 0} a_j t^{2j}.$$

The second sum restores the origin contribution. Its coefficients depend on both the tilt and the physical eigenangle preparation. Computing the entire first sum on one fine lattice costs most of the running time for the large inverse-order examples.

Annular alias estimate. Let $N \geq 4$, $0 < z < 1$, $-1 < \Re h < 0$, and $s \in \mathbb{C}$. Take an integer $d \geq p \geq 2$. Set $a_0 = 2/5$ and let $W(x)$ be one for $x \leq a_0$, zero for $x \geq 1$, with the beta survival polynomial $1 - I_{(x-a_0)/(1-a_0)}(d+1, d+1)$ between them. Write $g_R(t) = t^{-1-2h}[W(t/(2R)) - W(t/R)]$ for $t > 0$, and zero otherwise. Set

$$\Omega = \{-N, -N + 2, \dots, N\} + \{-Nz, Nz\}.$$

For $\tau > 0$ with $a = ze^{2\tau} < 1$, put $D_0 = 1 - z^2$, $\kappa = 1/\tau + \frac{1}{2}\tau \cosh \tau$, and

$$M = \frac{D_0^{N^2 + 2N\Re s}}{N!} (1 + \tau^2)^{(N+1)/2} (4 \cosh^2 \tau)^{N(N-1)/2} \big[e^{2|\Im s| \arcsin a} \max_{\pm} (1 \pm a)^{-2(N + \Re s)} \big]^N.$$

For any offset $0 \leq \alpha < 1$ and spacing $\delta > 0$ for which the following distances are positive,

$$\left| \delta \sum_{k \in \mathbb{Z}} g_R((k + \alpha)\delta) \Phi((k + \alpha)\delta) - \int_0^\infty g_R(t) \Phi(t)\, dt \right| \leq M(1 + \kappa^2)^{p/2} \|g_R^{(p)}\|_1 \max_{\omega \in \Omega} \sum_{j \neq 0} |2\pi j/\delta - \omega|^{-p}.$$

The same expression for the original fine lattice and the new coarse lattice, added and multiplied by $|C_h|$, bounds the change in an exact-source annulus. The norm is $R^{-p-2\Re h} \|g_1^{(p)}\|_1$. A finite majorant for the right side is provided below. The identity separates an error from reciprocal-lattice aliasing from errors in individual angular determinants.

Proof. In the transformed Weyl integral put relative phase angles $x_1, \dots, x_N$ and the common direction y. The real Fourier phase before deformation is $\sum_j \cos x_j + Nz \cos y$; the one-body factors have arguments $x_j \pm y$ up to a consistent orientation. Replace each real angular coordinate u by $u - i\tau \sin u$. The analytic factors $1 + ze^{\pm i(x_j \pm y)}$ stay in the disk $|w - 1| \leq a$, and their analytic logarithms are the continuations from the positive real-base preparation. The deformed angular amplitude, including normalized integration, has variation at most M. Indeed each pair of factors is bounded by $e^{2|\Im s| \arcsin a} \max_{\pm}(1 \pm a)^{-2(N + \Re s)}$. The change of variables supplies $D_0^{N^2 + 2N\Re s}/N!$ in absolute value. Each squared sine-difference factor in the Vandermonde is bounded by $4 \cosh^2 \tau$, and each contour derivative by $\sqrt{1 + \tau^2}$.

Write the complex phase as $v + iD$ after deformation. With $\sigma(u) = \operatorname{sign}(\cos u)$ (either convention at zero), the frequency $\omega = \sum_j \sigma(x_j) + Nz\sigma(y)$ belongs to Ω. The imaginary part $\sin u \sinh(\tau \sin u)$ is at least $\tau \sin^2 u$, and

$$|\cos u \cosh(\tau \sin u) - \sigma(u)| \leq (1 + \tfrac{1}{2}\tau^2 \cosh \tau) \sin^2 u.$$

Consequently $|v-\omega| \le \kappa D$, giving $|D+i(b-v)| \ge |b-\omega|/\sqrt{1+\kappa^2}$ for every real b. At $b = 2\pi j/\delta$, integrate $g_R(t)e^{-[D+i(b-v)]t}$ by parts p times. The norm of the resulting numerator is at most $\|g_R^{(p)}\|_1$. Shifted Poisson summation supplies a phase of modulus one per alias. One must collect the reciprocal sum **before** maximizing over the physical angular configuration. Integration against the deformed amplitude then gives the bound as stated. Finite differentiability of the joins suffices because W is flat through derivative d there and $p \ge 2$ makes the alias sum convergent.

For completeness, the exact fine-lattice terminal beyond $W(t/R)$ is bounded by the same argument applied to $g_R(t) = t^{-1-2h}(1-W(t/R))$, now summing **all** j, including $j = 0$. This requires $0 \notin \Omega$ and no exact aliased frequency. All ranks and radii in the outer rectangle below satisfy the first condition. For the infinite tail one may apply Poisson summation at each deformed angular point with $D > 0$, a full-measure set. The undifferentiated average is absolutely integrable and summable at infinity since the deformed torus integral of e^{-Dt} is $O_{N,z,\tau}(t^{-(N+1)/2})$ by the product bound from $D \ge \tau \sum_j \sin^2 x_j + Nz\tau \sin^2 y$. The pth derivative of the tail weight is integrable since $p + 2\Re h > 0$. These estimates justify interchange and the stated tail bound.

To compute the constants, derivatives of order $r \ge 1$ of the transition satisfy

$$D_r = (2d+1)^{\underline{r}} \binom{r-1}{\lfloor (r-1)/2 \rfloor} (1-a_0)^{-r}.$$

Here D_r is an **upper bound** on their magnitude. This follows by differentiating the Bernstein polynomial with coefficients one through index d and zero thereafter. A forward difference of order r at the step has magnitude at most the indicated binomial. Thus the dimensionless compact window has derivative bound $(1+2^{-r})D_r$; its magnitude is at most one. Leibniz's formula on $[a_0, 2]$ gives the displayed L^1 bound, taking maxima of the elementary powers at the two endpoints. The terminal window uses D_r on $[a_0, 1]$ and the remaining integral $|(1+2h)_p|/(p+2\Re h)$. For $L = 2\pi/\delta$, $J > \max|\omega|/L$, the omitted reciprocal tail after $|j| \le J$ is at most $2L^{-p}(J-|\omega|/L)^{1-p}/(p-1)$. These formulas use no fitted asymptotic amplitudes. The sample calculation with $N = 8, z = .9, h = -.9 + .5i, s = 1 + .5i, \tau = .040, R = 96, \delta = \pi/3, d = 16, p = 3$ gives an alias majorant around 10^{198} including $|C_h|$. Near $z = .9$ the global amplitude supremum is too large to certify the practical schedules. The proof establishes the frequency and scale dependence, not ten-digit certification of those schedules.

Implementation and evidence. We retain the fine image series and first smoothly cut-off sum. For each successive annulus we choose a coarse δ maximizing the usable spacing subject to a minimum distance from Ω to the nonzero reciprocal lattice. The search uses $\delta = \pi k/j$ with small integers; ω values two units apart can share the same folded frequency. If its threshold has no admissible candidate the code uses its finest candidate and tests the independent refinement. Preparation uses a common resolved preconditioned Fourier basis. The angular determinant for direction $-\phi$ equals that for ϕ by reflecting every original angle. This argument involves no conjugation of s. The implementation only factors half the directional matrices and contracts the translation by its Fourier coefficients when pointwise multiplication would alias. The angular order grows with radial frequency until it reaches the profile cap. The reported absolute estimate is the maximum of six times the successive profile difference, eight times the last shell magnitude, six times each image-tail indicator, and the two condition-weighted roundoff indicators. Profiles change the initial spacing, window, coarse offset, frequency guard and angular resolution. A last shell by itself misses errors from earlier annuli.

The executable domain is $4 \le N \le 8$, $.82 \le z \le .90$, $-.95 \le \Re h < 0$, $|\Im h| \le 3$, $|s| \le 3$. Eighteen stress cases took 1.30 to 10.46 seconds each. Each reached its estimated relative target on this set. At rank eight, $.9, -.9+.5i, 1+.5i$ gave $2.892989389959591 + 5.072290248846464i$ in 4.12 seconds; a fresh inherited run took 79.96 seconds under the same single-BLAS-thread convention. The two independent continuum results differed from the new value by less than 7.2×10^{-14} in absolute value. At rank four, $.9, -.95 + 3i, .4 + .7i$ gave $-1.551639045505191 + 2.334704455923828i$ in 2.88 seconds, 3.4×10^{-14} from the independent comparison. The predecessor stopped with estimated relative error 2.57×10^{-9} after 10.00 seconds at this point. At rank six, $.88, -.8 - .6i, -1.2 + .7i$, the independent discrepancy was 4.7×10^{-15}. These observations are measured comparisons in absolute units. They use ordinary inverse moments with independent complex tilts. No inference from a finite test set gives a uniform relative guarantee.

Two deliberately resonant shell grids at the rank-eight point, with $\delta = 2\pi/[N(1-z)]$ and distinct offsets, miss the independent result by 9.81 and 8.19. A different, smooth but premature coarse schedule has a final shell only 6.43×10^{-15} while its scalar error is 3.03×10^{-7}. Dropping preparation changes the rank-eight source at $t = .7$ by 3.21, whereas direct original-angle evaluation and the accelerated source agree there to 2.0×10^{-14}.

The source observable, complex preparation, absolute direction and reciprocal-lattice separation are all needed for this readout. A rigorous fast evaluator would additionally require useful *localized* amplitude estimates for the annuli and validated arithmetic for the contracted source.

Thirty additional rim cases use six distinct radii, $\Re h \in \{-.950, -.948, -.946\}$, $|\Im h| \in \{2.978, 2.989, 3\}$ and $|s|$ within 4×10^{-15} of 3 with varying phase. A withheld schedule changes the initial lattice, coarse offsets, taper and angular resolution after the adaptive scalar has returned. The largest relative discrepancy was 7.55×10^{-13} and the largest discrepancy divided by the estimated absolute error was .0981. This is a same-representation stability test. A separate comparison of nine original-eigenangle continuum evaluations, covering all five ranks and two small rank-eight values, found a maximum discrepancy 1.37×10^{-12} in relative units and .081 as a fraction of the estimated absolute error. All thirty practical calls returned estimated relative success; no accuracy claim on an untested part of the rectangle follows.

Near $h = 0$, direct separate evaluation of $1/\Gamma(-h)$ and $\zeta(1 + 2h)$ loses their cancellation. The implementation forms the analytic combination

$$C_h \Delta^{-2h} \zeta(1 + 2h) = -(2/\Delta)^{2h} \frac{\Gamma(1 + h)}{\Gamma(1 - h)} [2h\zeta(1 + 2h)].$$

The right side extends with value -1. Precision in its bracket is chosen according to $|h|$ before conversion to binary64. At $N = 8, z = .9, s = 1 + .5i$, the smallest negative binary64 order gave a value 6.8×10^{-15} from the independently computed original-angle mass at $h = 0$. This checks the removable limit at machine scale.

Reusing a preparation over complex order. Once (N, z, s) and a radial profile are fixed, let t_ℓ range over its retained nodes, A_ℓ be its window and quadrature weight times $\Phi(t_\ell)/t_\ell$, and $b_j = a_j \Delta^{2j}$ its retained origin coefficients. Then the profile readout is explicitly

$$C_h \left[\sum_\ell A_\ell e^{-2h \log t_\ell} - \Delta^{-2h} \sum_{j<J} b_j \zeta(1 + 2h - 2j) \right].$$

All expensive source values are independent of h, including for complex s. This is direct evaluation of each finite quadrature; it introduces no interpolation in the order. Two implementations at $N = 8, z = .9, s = 3i$ scanned 396 orders each in .13 and .17 seconds *after* preparation (3.28 and 15.96 seconds, respectively). They are two resolution profiles of the same representation.

The scan led to the probe $h = -.4133064928254429 + 1.723195275895845i$. The adaptive scalar was $3.41395 \times 10^{-14} + 1.21832 \times 10^{-14} i$, with estimated absolute error 1.69×10^{-15} and estimated relative error .049. It returned absolute-only status. Two independent continuous-quadrature profiles gave absolute differences 1.49×10^{-17} and 2.40×10^{-17}. At this scale the original-angle comparison explicitly restores the contribution below $t_0 = e^{-32}$ as $C_h \Phi(0) t_0^{-2h}/(-2h)$. For this imaginary tilt the omitted residual is at most

$$|C_h| B^2 t_0^{2-2\Re h}/[4(2 - 2\Re h)] < 1.32 \times 10^{-38},$$

by $|J_0(t|S|) - 1| \le t^2 B^2/4$. The remainder bound concerns the origin correction only. The full continuum comparison is numerical. On circles in order space of radii $.01, 10^{-4}, 10^{-6}$ around the probe, both profiles had a numerical winding of one at 96 increments. The following theorem supplies different certified data and controls entire circles, allowing a count of the zeros of the physical moment.

A near-zero-order approximation from the tilted mass

Corollary 21.19A (small order disks at ranks four through eight). Let $.8 \le z \le .9$ and $|s| \le .01$. In order of increasing rank, take $|h| \le (116, 86, 68, 55, 46) \times 10^{-12}$. On each independent product of disks the following approximation returns relative error less than 9.8×10^{-11}:

$$T_N(h, s; z) \simeq e^{2hb} M_s(z), \qquad b = \log(dN) + (N - 1)\log(z)/2, \qquad M_s = \mathbb{E} e^{2sL}.$$

This is a near-zero-order result. The negative real orders have nonzero extent, but the disk widths do not cover deep inverse orders.

Here are the estimates behind the very narrow disks. Set $m = N - 1$, $Y = \log|S| - b$, $W = e^{2sL}$, $S_* = .01$, $z_- = .8$, $z_+ = .9$, $d_0 = 1 - z_+^2$, $D = N(1 + z_+)$, $q = 1/(4m)$, $\omega = -m \log z_-/2$, $\ell_2 = \sqrt{-\log d_0/2}$, and $\theta = -2S_* N \log(1 - z_+)$. Conditional on an eigenvalue configuration modulo global rotation, write the monic-up-to-phase derivative as $\Lambda_N'(t) = C \prod_{j=1}^m (t - \rho_j)$ with $|C| = N$. The closed unit disk contains the roots ρ_j by Gauss–Lucas. Jensen's circle identity gives the conditional mean of $\log|\Lambda_N'(ze^{it})|$ as $\log N + \sum_j \log\max(z, |\rho_j|)$. Its distance from $\log N + m \log z/2$ is at most ω. The centered variable for each root has Fourier coefficients from $\log|1 - \beta e^{it}|$, $|\beta| \le 1$, giving squared L^2 norm at most $\sum_{k\ge1}(2k^2)^{-1} = \pi^2/12$, including the limiting unit case. Therefore the centered full derivative has norm at most $m\pi/\sqrt{12}$. The logarithm L has mean zero by rotation, and the finite strong-Szegő bound in §16 gives $\mathbb{E}e^{2tL} \le d^{-t^2}$ for every real t. Its quadratic coefficient gives $\|L\|_2 \le \ell_2$. From $\log|S| = \log d + \log|\Lambda_N'| - L$, Cauchy–Schwarz and $|W - 1| \le 2S_*|L|e^{\theta}$,

$$|\mathbb{E}WY| \le B_1 = \omega + 2S_* e^{\theta} \ell_2 \left(\ell_2 + \sqrt{\omega^2 + m^2\pi^2/12} \right).$$

For a quadratic Taylor remainder we need an inverse integrability margin. For $0 < p < 1$, the maximum of the circle average $\mathbb{E}_t|1 - \beta e^{it}|^{-p}$ over $|\beta| \le 1$ is at one by its nonnegative binomial series. At $p = 1/2$ the chord bound $2\sin(t/2) \ge 2t/\pi$ on $0 \le t \le \pi$ gives mean at most $\sqrt{2} < 2$. Conditional Hölder applied to the m roots, each with exponent $2qm = 1/2$, shows

$$\mathbb{E}|\Lambda_N'|^{-2q} \le 2(Nz_-^m)^{-2q}.$$

Since $|S| \le D$, Cauchy–Schwarz and the real mass bound give

$$\mathbb{E}\,|W|\,|S|^q \le D^q d_0^{-S_*^2}, \qquad \mathbb{E}\,|W|\,|S|^{-q} \le (d_0 N z_-^m)^{-q}\sqrt{2}\, d_0^{-(2S_*+q)^2/2}.$$

The latter uses $|S|^{-q} = d^{-q}|\Lambda_N'|^{-q}e^{qL}$. Put $b_* = \max(|\log d_0 N|, |\log[N(1 - z_-^2)]|) + \omega$. If $|h| \le \eta$ and $2\eta \le q/2$, then $Y^2 e^{2\eta|Y|} \le 16q^{-2}e^{q|Y|}$. Thus for B_2 equal to the sum of the two preceding upper bounds multiplied by $16q^{-2}e^{qb_*}$, Taylor's formula yields

$$|T - e^{2hb}M_s| \le e^{2\eta b_*}(2\eta B_1 + 2\eta^2 B_2).$$

Finally $\Re M_s \ge \cos(\theta)\mathbb{E}e^{2\Re(s)L} \ge \cos(\theta)$ by Jensen. Subtract the absolute error from $e^{-2\eta b_*}\cos\theta$ to obtain a lower bound for the physical modulus. The Toeplitz formula for M_s uses coefficients

$$c_k = z^k(-s)_k\, {}_2F_1(k - s, -s; k + 1; z^2)/k!, \quad k \ge 0, \qquad M_s = \det[c_{|i-j|}].$$

A Newton-trace determinant and an adaptive midpoint-copy test allocate 10^{-15} for finite arithmetic. All constants and the resulting relative bounds in the stated boxes were evaluated outward. Fifteen sample calculations cover both radial endpoints and an interior radius at every rank. A separate 60,000-matrix Haar QR experiment checked the weighted first logarithmic response, which the near-one scalar values alone could hide. At all five ranks dropping d shifted the measured response outside the proven bound by more than five empirical standard errors. Only the analytic and ball-arithmetic arguments give the certificates.

Zeros within the requested box

At rank one take $z = 0.9$, $s = 0$, $h = 1/2 + it$, and $x = z^2$. The finite rank-one formula factors into a nonzero power times

$$G(t) = (1 - x)^h\, {}_2F_1(h, h; 1; x).$$

Euler's transformation and $\bar{h} = 1 - h$ imply $G(t) = \overline{G(t)}$. It is real analytic in real t. Outward-rounded evaluations at the ends of $[3/4, 1]$, $[7/4, 2]$, $[11/4, 3]$ gave opposite signs in each interval. Sign-certified bisection reduced each width to 2^{-90}. Thus the requested box contains at least three distinct zeros on this single line, at heights approximately 0.853815, 1.890027 and 2.948675 (the exact brackets are in the receipt). The same three zeros occur at fixed $h = 1/2$ and $s = -it$, because $h - s$ is unchanged and the remaining prefactor is nonzero. The first bracket's left endpoint has $|T_1| < 10^{-28}$. This gives a source-based obstruction to a universal relative-error criterion. For an absolute disk (v, e) a sufficient relative bound is $e/(|v| - e)$ if $|v| > e$. A disk meeting zero can report absolute accuracy; existence of a zero needs an independent argument such as the sign change here. The practical estimator uses the analogous numerical ratio with its error explicitly labelled as an estimate.

Theorem 21.20 (a simple rank-eight zero inside the evaluator specification). Fix $N = 8$, $z = .9$ and

$$h_* = -.4133064928254429 + 1.723195275895845i.$$

At $s_0 = 3i$ the genuine Haar moment $T_8(h, s_0; .9)$ has precisely one zero, counted with multiplicity, in $|h - h_*| < 10^{-10}$. For every complex s with $|s - s_0| \le 5 \times 10^{-13}$ there is precisely one zero in $|h - h_*| < 10^{-4}$. It is simple and varies holomorphically on the open tilt disk. In particular this applies to interior points of the target $|s| \le 3$. This theorem uses absolute enclosures, including at the points where a relative error test fails.

Proof. Set $F(h) = T_8(h, s_0; .9)$ and $R = .06$. We first prove an analytic majorant $|F| \le 3041$ on $|h - h_*| \le R$. For $p = .95$, $|S|^{2\Re h} \le 1 + |S|^{-p}$ throughout the disk. In the original Weyl integral write the last variable as $w = (\lambda - z)/(1 - z\lambda)$, so $S = A + w$ given the other eigenangles. The transformed uniform one-angle density is at most $(1 + z)/(1 - z) = 19$ times the uniform density in w. After rotating A, $|A + e^{i\theta}| \ge |\sin\theta|$; using $\sin\theta \ge 2\theta/\pi$ on $[0, \pi/2]$ bounds its averaged inverse pth power by $1/(1 - p)$. The remaining interaction with the last eigenvalue is $|P_{N-1}(\lambda)|^2$, P_{N-1} being the monic characteristic polynomial of the other $N - 1$ eigenvalues. The Weyl normalization leaves $1/N$ times their rank-$(N - 1)$ expectation. Cauchy–Schwarz gives $\|P_{N-1}\|_\infty^2 \le N \sum_{j=0}^{N-1} |e_j|^2$ for the elementary symmetric coefficients. Each has squared Haar norm one by the alternant formula: multiplying an elementary symmetric polynomial by the Weyl alternant yields a single alternant with distinct integer powers, whose squared torus norm is $(N - 1)!$. Therefore $\mathbb{E}\|P_{N-1}\|_\infty^2 \le N^2$ and

$$\mathbb{E}|S|^{2\Re h} \le 1 + N\frac{1 + z}{(1 - z)(1 - p)} = 3041.$$

This also supplies an integrable dominating function on a neighborhood of the order disk in the original variables. The tilt factor has modulus one at s_0, and is bounded on compact tilt sets since $z < 1$, so the physical moment is jointly holomorphic there.

Put $d = 5 \times 10^{-6}$, $q = d/R$ and $u = (h - h_*)/d$. Applying the validated full-source scalar algorithm to the four exact decimal orders $h_* + di^k$, $0 \le k < 4$, gives four absolute radii each below 5.006×10^{-14}. The same 13,966 order-independent prepared Fourier samples can be reused. For each of the four orders the computation forms its own enclosed origin series, finite weighted sum and filtered tail. Define $B_j = \frac{1}{4}\sum_{k=0}^{3} F(h_* + di^k) i^{-jk}$. If $F(h_* + du) = \sum c_j u^j$, then $B_j = \sum_{m \ge 0} c_{j+4m}$ and $|c_j| \le 3041 q^j$. The scalar comparison function is the nonzero linear polynomial $B_1 u$. An additional certified evaluation at h_* bounds $|F(h_*)| < 8.631 \times 10^{-14}$. For $|u| = v$, $qv < 1$, the difference from this comparison function is at most

$$|F(h_*)| + |B_2|v^2 + |B_3|v^3 + 3041\frac{q^4}{1 - q^4}\sum_{j=1}^{3}(qv)^j + 3041\frac{(qv)^4}{1 - qv}.$$

Here using the physical center value removes the constant-term alias. If the tilt moves by at most b, add $3041(e^{37b} - 1)$, since $|\log|\Lambda_8(.9)|^2| \le 16 \log 10 < 37$. This controls the entire boundary in both parameters. The values in the table are conservative outward decimal bounds from 256-bit ball arithmetic.

Order radius dv	Tilt radius b	Lower bound on $\lvert B_1\rvert v$	Upper bound on all other terms
10^{-10}	0	1.1261×10^{-13}	8.631×10^{-14}
10^{-4}	5×10^{-13}	1.1261×10^{-7}	8.037×10^{-8}

Rouché's theorem gives both zero counts, hence simplicity. Uniqueness and the analytic implicit function theorem give a holomorphic zero on the open tilt disk. The input hashes, five physical enclosures, coefficient balls, boundary margins and a replay are in the zero-count receipt. This proves existence and localization of a physical zero without requiring a single point computation to output zero.

Separating the probe from the zero. Reoptimizing the averaging of the terminal cutoff uses exactly the same 13,966 source rows. With minimum omitted index 11,746, thirty uniform boxes of width 75, contour depth .02570289889383231 and 256 spectral panels, the rechecked terminal budget at h_* is below 4.186×10^{-15}. The full absolute radius is below 4.348×10^{-15}, giving $|F(h_*)| > 3.1907 \times 10^{-14}$. The pole-free order probe therefore has a nonzero value even though a nearby physical zero prevents uniform relative evaluation.

A smaller disk centered at

$$h_{\mathrm{c}} = -.4133064928142612470 + 1.7231952758656547310i$$

contains that zero with radius 5×10^{-12} at $s = 3i$. For this check set $u_c = (h_{\mathrm{c}} - h_*)/d$ and $v = |u_c| + 5 \times 10^{-12}/d$. Use the same Taylor and alias bounds at v, replace the constant term by $|F(h_*) + B_1 u_c|$ using the retuned ball, and compare to $B_1(u - u_c)$. The latter has boundary modulus greater than 5.6306×10^{-15}, and the full remainder is below 4.3481×10^{-15}. The disk excludes h_* since their centers differ by more than 3.2194×10^{-11}. The filter optimization selects parameters in floating point; the reused image enclosure, terminal replacement and Rouché inequalities all carry rigorous bounds.

The 17,000-row calculation in §21 sharpens this same disk to **radius** 1.5×10^{-13} **about** h_{c}. In the preceding shifted comparison use the new absolute enclosure of $F(h_*)$ and the smaller boundary radius. The linear lower bound is 1.68919×10^{-16} and the remaining terms total less than 1.62275×10^{-16}. The strictly positive margin exceeds 6.644×10^{-18}. At the nearby decimal order h_* the new modulus lower bound exceeds 3.60936×10^{-14}. The calculation at the centre of the zero disk remains a zero-containing absolute enclosure.

A common exterior approximation through positive orders

Theorem 21.21 (absolute truncation on the full exterior order box). Fix $4 \le N \le 8$, $.82 \le z \le .9$, $-.95 \le \Re h \le 3$, $|\Im h| \le 3$ and $|s| \le 3$. For the ordinary unnormalized Haar moment the exact-arithmetic finite formula below has absolute error below 1.077×10^{-17} at every input. It uses 8,202 as the last filter index at $\Delta = .32$, $Q = P = 4096, L = 2040$ on the real radial lattice and $J = 240, m = 528, H = 12, Q_c = 1024, L_c = 336, P_c = 8192$ for the complex Cauchy image of Theorem 21.18. At integer orders take the removable products in the Mellin image. The bound concerns the value at each specified input. Floating-point conditioning and the magnitude of that particular moment govern the additional work required for a relative certificate.

Proof. The last-index and filtered-tail parameters are those of Corollary 5.7A. Its common tail contribution is below 1.073×10^{-17}. Put $a = \Re h, d_* = .19, D_* = 15.2, M = d_*^{-9}$ and $v = .09$. Reflection and log-convexity on $[.05, 4]$ give

$$|C_\Delta| \le C_* = 2(2/\Delta)^6 \Gamma(.05)^2 \cosh(3\pi)/\pi.$$

The rotated mass of Proposition 5.5 is bounded by $M[1 - 4(.9)^2 \sinh^2(v)/d_*^2]^{-121/4}$. For the one-body error use the geometric estimate in (5.9) with v, (P, L) as specified and the common cap of Theorem 21.18. Write ϵ for that absolute one-entry error. In Proposition 5.6 the positive Gram floor is at least 10^{-6}. The determinant error is therefore at most $M[(1 + 8 \cdot 10^6 \epsilon)^8 - 1]$. Add the direction error of Proposition 5.5 and multiply by $C_* \, 8202^{1.9}$, bounding the sum of the moduli of all radial weights. The real-projection error is below 3.627×10^{-20}.

For $j = 0, \dots, 4$, write $v_j = 1 + 2h - 2j$. Euler–Maclaurin with six Bernoulli terms gives

$$\left| \zeta(v_j) - \frac{1}{v_j - 1} \right| \le H_0 = 1 + \sum_{k=1}^{6} \frac{4 \, 32^{2k-1}}{(2\pi)^{2k}} + \frac{4 \, 32^{12}}{(2\pi)^{12}}.$$

Indeed $\Re v_j \ge -8.9$, the shifted factors through $v_j + 11$ have modulus below 32 and the integrated remainder has a denominator $\Re v_j + 11 > 1$. The Bernoulli Fourier bound is $\sup |B_{2k}(\{x\})|/(2k)! \le 4/(2\pi)^{2k}$. The quotient $|\sin(\pi h)/(h - j)| \le \pi \cosh(3\pi)$ follows by integrating the derivative along the segment from j to h. Hence the combined low-index multiplier has modulus at most $C_*(H_0 + \pi/2)$. For $j \ge 5$ the zeta functional equation gives the multiplier bound $4C_*(2\pi)^{6-2j} \cosh(3\pi)(2j + 1)!$ before $(\Delta/H)^{2j}$. The real parts of the reflected zeta arguments are at least four, and log-convexity bounds the remaining gamma by its indicated factorial. These are applications of the Euler–Maclaurin and reflection formulas for zeta, NIST DLMF §§25.2(iii), 25.4.

Apply the E_j and e_Φ bounds of Theorem 21.18 at the displayed Cauchy dimensions. The weighted sum is below 2.495×10^{-138}. With $x = \Delta D_*/(2\pi)$ and q the ratio bound of Proposition 5.2 evaluated at $a = -.95$, the exterior image including the mass factor is bounded by

$$\frac{4C_*(2\pi)^6 \cosh(3\pi) M (2J + 1)!}{(J!)^2 (1 - q)} (x/2)^{2J} < 7.882 \times 10^{-26}.$$

Combining the outward bounds before rounding gives 1.076182×10^{-17}. The five continuous-domain rank computations are in the signed-sector region receipt; the rest is reproduced by the scalar script for the full box. This proof does not require computing the common finite formula on a mesh of inputs.

Removable products in computation. If $h = j + v$ is close to a nonnegative integer j, write $Z(v) = \zeta(1 + 2v) - 1/(2v)$. The multiplier of $H^{2j}a_j$ in the image equals

$$-(2/\Delta)^{2h}\Gamma(1 + h)\,\frac{\prod_{\ell=0}^{j-1}(\ell - h)}{\Gamma(1 - v)}[1 + 2vZ(v)](\Delta/H)^{2j}.$$

This follows by gamma recurrence. Subtract j from the supplied rational real part before forming the complex ball for v. At $h = m$ exactly the answer is $(-4)^m(m!)^2a_m$. Each use of these identities keeps its scaled Cauchy-coefficient error. No limiting division by a pole enters the implementation.

Proposition 21.22 (a positive-order route at critical radii). For $a = \Re h > 0$ the discarded part of the unfiltered lattice after K contributes at most $|C_\Delta|d^{-(\Re s)^2}/(2aK^{2a})$. This holds even when Nz is a critical trace radius. It follows from $|J_0(r|S|)| \le 1$, the prepared mass bound and the integral test. For the executed critical cases the implementation selects K using this inequality and retains the angle, image and arithmetic budgets. Small positive a can make this an expensive method. At $a \le 0$ this proof provides no tail estimate. The signed exterior proof uses separation from the signed saddles; these two arguments have different domains.

Corollary 21.23 (a common folded rule for new preparations). Throughout the full parameter domain of Theorem 21.21, a single two-rate formula uses 5,342 distinct positive frequencies and has absolute exact-arithmetic error below 4.434×10^{-15}. On the smaller domain $|\Re s| \le 1$ within the same tilt disk, another formula uses 4,310 frequencies and has error below 3.243×10^{-15}. At the integer orders the combined Mellin coefficients have their removable values. The angular and Cauchy dimensions are those of Theorem 21.21.

Proof. Use Corollary 5.11. For the full disk set $\Delta = .27$. Use switch $(K, b, p) = (6, 17, 33)$ and terminal $(5800, 65, 68)$; for the alternating aliases use height .0026203584904072527. For the narrower tilt region take $\Delta = .32$, switch $(4, 17, 26)$, terminal $(4822, 53, 65)$ and alternating-alias height .0026103999350085005. For the ordinary terminal both formulas use the clipped profile of Corollary 5.7A. To perform the inequalities for continuous z at fixed N, enclose each signed value $Nz + 2j - N$ by its two endpoint values at $z = .82, .9$. Split its absolute image if necessary at zero. The distance between a frequency band and these intervals gives a common lower bound for the saddle distance on that band. Use $D \le 1.9N$, the maximum allowed $|u|$ in the signed-mass bound of Lemma 5.9, and $M \le .19^{-u_{\max}^2}$. The region script partitions the spectrum at uniform nodes and at additional endpoints and midpoints around the odd reciprocal frequency. Floating-point nodes here specify exact rational boundaries. Each intervening closed band enters an outward inequality. The positive increments of the running maximum in Theorem 5.10 retain its probability bound at the band's lower edge. Bound the gamma factors by the two real-order endpoints as in Corollary 5.7A. All five rank enclosures are recorded.

At $\Delta = .27$ the resulting allowances for the signed switch, the signed terminal and the ordinary terminal are below $3.187 \times 10^{-15}, 1.246 \times 10^{-15}, 2.041 \times 10^{-18}$. The supports of the two cutoff transitions are disjoint. The retained weights are consequently bounded by two, so twice the real-source multiplier in the proof of Theorem 21.21 suffices, with the new value of Δ and terminal length. Re-evaluate the regularized image and its exterior tail at that same spacing. The real-source charge is below 3.015×10^{-19}; the image and the readout's mathematical truncations give the stated total before rounding the separate contributions. At $\Delta = .32$ the first signed bound is below 3.232×10^{-15}. Applying the same calculation gives the second total. At both spacings the determinant, source and image are evaluated at the query itself. The regional bound does not enclose the range of all output values in a single disk.

The common 5,342-site rule was also run cold at $N = 4, z = .873, h = -.93 + .8i, s = -.6 + 1.1i$, with the fixed prescribed source and image dimensions throughout. Four workers took 36.78 seconds, including 18.20 seconds for the native samples and 15.58 seconds for the image. Its centre begins $.20447209840006950145 - .47763454677500595477i$ and the absolute radius about the full saved centre is below 8.792×10^{-18}. This is a complete finite-arithmetic execution at one input. The input-specific alternatives in §22 use fewer frequencies where the signed inequalities allow them.

Uniform scalar bounds on connected critical intervals

Theorem 21.24 (the full order range on critical intervals). For the radii and filters below, take independently $-.95 \le \Re h \le 3$. At ranks five through eight take $|\Im h| \le 3$, $|s| \le 3$. At rank four take $|\Im h| \le 1$, $|\Re s|, |\Im s| \le 1$. The specified exact-arithmetic finite formula has the complete absolute error in the last column

at every input. All powers and normalizations are those of Section 1. A separate finite-arithmetic and modulus check is necessary for any returned relative certificate.

The core and complementary spectral estimates follow from Propositions 5.14–5.16 and Corollary 5.17, with their endpoint inequalities checked outwards. In these cases the additional core envelope, including $a = -1/2$, is at most .32, below the already paid inverse factor. The shared deep endpoint is carried identically; every nonshared comparison is a strict interval inequality. No conclusion is drawn from mere overlap of two interval balls.

For the following table use the **full-order** common finite source and image of Theorem 21.21: real $Q = P = 4096, L = 2040$, complex image $J = 240, m = 528, H = 12, Q_c = 1024, L_c = 336, P_c = 8192$. These image dimensions replace the earlier inverse-only common formula. The spectral filter has $\Delta = .32, b = 32, p = 48$ in every row. The number of sampled frequencies is $K + 1488$.

Rank	Connected radius interval	K	Uniform spectral allowance	Uniform complete exact-arithmetic allowance
4	$[.45, .55]$	90000	$5.762615 \cdot 10^{-11}$	$5.762615 \cdot 10^{-11}$
5	$[.195, .605]$	50000	$2.335983 \cdot 10^{-16}$	$2.347878 \cdot 10^{-16}$
6	$[.330, .670]$	32000	$3.333675 \cdot 10^{-21}$	$5.286122 \cdot 10^{-19}$
7	$[.14, .72]$	24000	$1.112554 \cdot 10^{-19}$	$4.239628 \cdot 10^{-19}$
8	$[.245, .755]$	24000	$3.609217 \cdot 10^{-18}$	$3.921924 \cdot 10^{-18}$

At ranks 5–8 the parameter domain is the **full original independent order and tilt domain** $-.95 \le \Re h \le 3$, $|\Im h| \le 3$, $|s| \le 3$. At rank four it is $-.95 \le \Re h \le 3$, $|\Im h| \le 1$, $|\Re s|, |\Im s| \le 1$. The rank-five and rank-six intervals contain two critical radii; the rank-seven and rank-eight intervals contain three.

Proof of the finite-source join. The common real-source error proof of Theorem 21.21 uses $z \le .9$, $N \le 8$, $|s| \le 3$, $D \le 15.2$, the stated complex-order box and the number L_* of weighted frequencies. Its lower-radius restriction was used only in the separately replaced terminal gap estimate. Its real-projection allowance can therefore be replaced by

$$3.627 \cdot 10^{-20} \left(\frac{L_*}{8202} \right)^{1.9}.$$

This follows by replacing $8202^{1.9}$ in its bound for the sum of absolute radial weights by $L_*^{1.9}$; every filter weight is still between zero and one. The common exterior-image bound $7.882 \cdot 10^{-26}$ and finite complex image bound $2.495 \cdot 10^{-138}$ are unchanged. Adding these terms to the new spectral allowances gives the final column. The actual unrounded additions and gamma comparisons are recorded in `critical/core/regions-full-order.json`. This proof uses the existing source and image theorems with their declared normalizations; it does not replace them by agreement of a numerical parameter grid. □

These are error bounds for the same physical scalar at **every input** in each stated continuum. The exact finite formula was not computed at every input. Input-specific finite arithmetic, branch-removable implementation and the lower-modulus gate remain necessary for a returned relative certificate. No uniform positive lower modulus is asserted, and a complex zero remains an absolute-output case. Nor does the table prove transport of an entire reduced differential state through the several walls.

Joining the centre-adjacent interval to the outer construction

This section is a new continuation of the signed-sector and critical-core estimates. The source, preparation and scalar readout are unchanged. It supplies a single connected domain of **exact-arithmetic absolute approximation**. It does not promise that every query will pass a fixed finite-arithmetic resource cap or a relative-error test.

Source and retained readout.

The source is the unnormalized Haar measure prepared by $|\Lambda_N(z)|^{2s}$, whose variation is the real-tilt measure at $\Re s$. The retained readout is the Fourier–Bessel function $\Phi(r) = \mathbb{E}[|\Lambda_N(z)|^{2s} J_0(r|S_N|)]$ and its physical, regularized Mellin contraction. Both the signed-gap estimate of Proposition 5.7 and the localized resonant-core estimates bound the discrepancy of **the same finite fine-lattice formula** from this readout. The first loses control when a signed frequency meets zero. The second keeps the sign population and its same-sign Vandermonde factors at that zero. Thus they can be selected by radius without a missing connection coefficient or an assumption of differential-state transport. There is no deletion of an angular population.

At small positive radius the inherited menu of clipped contours can fail the condition $f/T < 1$ even though the moment exists. This is a chart limitation. Reducing the clipping coefficient supplies admissible core charts, while a wider cutoff convolution suppresses the small but nonzero signed frequencies in the complement. The distinction between a chart failure and divergence changes the implemented method selection.

Theorem 21.25 (connected scalar approximation on the full complex box).

Let $4 \le N \le 8$, $.02 \le z \le .9$ and

$$-.95 \le \Re h \le 3, \qquad |\Im h| \le 3, \qquad |s| \le 3.$$

There is a specified piecewise finite scalar formula for the ordinary unnormalized moment $T_N(h, s; z)$ with the following uniform absolute errors. For $.02 \le z \le .82$ it uses the dense convolution filter $\Pr(K+U_1+\cdots+U_{48} > k)$, with independent uniform $U_j \in \{0, \dots, b-1\}$, on the lattice $\Delta = .32$. On $.82 < z \le .9$ use the common exterior formula of Theorem 21.21. The change at .82 is a choice of numerical representation of the same physical scalar. It is not an asserted equality of the two finite approximants.

Rank	Interior K	Width b	Last index	Interior absolute error	Joined absolute error on $[.02, .9]$
4	300000	320	315312	$7.954 \cdot 10^{-11}$	$7.954 \cdot 10^{-11}$
5	50000	32	51488	$5.650 \cdot 10^{-13}$	$5.650 \cdot 10^{-13}$
6	32000	320	47312	$2.897 \cdot 10^{-13}$	$2.897 \cdot 10^{-13}$
7	24000	32	25488	$3.895 \cdot 10^{-13}$	$3.895 \cdot 10^{-13}$
8	24000	320	39312	$1.575 \cdot 10^{-18}$	$1.077 \cdot 10^{-17}$

All bounds are strict. The finite angular dimensions are those of the full-order Theorem 21.21: real-source $Q = P = 4096, L = 2040$ and complex image $J = 240, m = 528, H = 12, Q_c = 1024, L_c = 336, P_c = 8192$. At nonnegative integer orders the Mellin products have their removable values. The parameter coordinates vary independently, subject to the displayed disk for the tilt. These are errors at each input, not one enclosure of the range of all moments in the region.

Proof. For a closed radius cell $I = [z_-, z_+]$ put $D = N(1 + z_+)$. The clipped signed-sector proof remains valid with

$$A_0 = N z_- \sqrt{1 - r^2}, \qquad A_1 = N z_+ \min(1, \sqrt{1 - l^2} \cosh v_0)$$

in each direction strip $\sigma \in [l, r]$, and $N z_- l^2$ in the positive lower bound for the direction damping. Use z_+ in the upper prices, $\alpha = (1 - z_+)/\sqrt{z_+}$ in the common clipping profile, and $M \le (1 - z_+^2)^{-9}$. The deformed source lies between these enclosing signed translates for every $z \in I$. In the square-root phase price use $1 + 1/z_-$ as an upper bound. The full complex order prefactor is bounded by

$$\frac{2\cosh(3\pi)}{\pi} \max_{a \in \{-.95, 3\}} \frac{\Gamma(1+a)^2 (2/\Delta)^{2a}}{K^{2+2a}}.$$

This is the reflection/beta-integral bound used in Corollary 5.7A, followed by log-convexity in a. The surrogate exponents $\Re s = |\Im s| = 3$ in this bound are simultaneous majorants, not a replacement physical preparation. This gives a continuous signed-gap bound on I whenever its strictly positive denominator checks pass.

Alternatively pass the whole radius ball I to the localized core bound, retaining the complete order/tilt majorants of Proposition 5.16. For its extension to all real orders, let $a_0 = -.95$, $a_1 = -.5$ and put

$$\begin{aligned} C_d &= \max_{a\in\{a_0,a_1\}} 2(2/\Delta)^{2a}\frac{\Gamma(1+a)}{\Gamma(-a)},\\ C_a &= \frac{2\cosh(3\pi)}{\pi}\max_{a\in\{a_1,3\}}\Gamma(1+a)^2(2/\Delta)^{2a}K^{-2(a-a_0)},\\ f(a) &= \Gamma(1+a)^2(2/\Delta)^{2a}K^{-2-2a},\\ H_K &= \max\left(1,\frac{C_a}{C_d},\frac{\max(f(a_0),f(3))}{\max(f(a_0),f(a_1))}\right). \end{aligned}$$

Multiplying the inverse-strip bound by H_K is sufficient. Indeed, the factor $K^{-2(a-a_0)}$ stays correlated with the core gamma prefactor; the remaining reciprocal tail denominator decreases as a increases. Both added endpoint maxima follow from log-convexity. This proves the comparison without interpreting interval overlap as an inequality. The actual receipts evaluate H_K outward; it is close to one for these parameters.

The implementation starts with cells of width .01 and bisects only when needed, at most twice. In each accepted cell it keeps a fully evaluated core or gap allowance. Changing the selected proof does not change the filter. The selected cells are closed and adjacent; the exact rational endpoint check gives an unbroken cover of $[.02, .82]$. The five final receipts have respectively 82, 93, 80, 88 and 80 cells. At every core use the positivity, preparation-zero, other-population gap and damping-rate tests are strict interval tests. At every gap use the phase-distance test is strictly positive over the entire cell. All four real parameter coordinates remain enclosed throughout; no finite parameter sample supplies the assertion.

The finite-source inequalities of Propositions 5.4–5.6 are uniform for all real frequency. In particular, increasing the last index does not presume an unresolved product quadrature for the translation: its Bessel coefficients are contracted exactly. If $L_* = K + 48(b-1)$, the full-order source charge is at most

$$E_{\text{source}} = 3.627\cdot 10^{-20}(L_*/8202)^{1.9}.$$

The complex-image charges are less than $7.882\cdot 10^{-26} + 2.495\cdot 10^{-138}$, with the preparation mass included as in the corrected image proof. These estimates use only $z \le .9$, $D \le 15.2$ and the indicated length. The earlier lower exterior radius was needed for its spectral gap, which has just been replaced. Add these costs to the maximum selected spectral allowance. The arithmetic calculations were run at 192 bits and replayed at 256 bits, including all cells, the rational tiling and the final conservative decimal inequalities. This gives the interior column. The exterior theorem gives $1.077\cdot 10^{-17}$; taking the maximum of the two valid errors gives the joined column. No extra boundary weight is needed because the formula is evaluated pointwise on one branch or the other. □

Execution scope and practical companion.

The preceding computation executes the **bound construction**, not all of the finite moments on a continuum. The rank-four common formula is intentionally conservative and long. A useful practical algorithm should select a much shorter input-dependent filter and then check its own source, image, arithmetic and readout errors. A proof that a finite formula has a uniform absolute error is not an unconditional finite-arithmetic relative guarantee.

The new `terminal_hybrid.py` implements the complementary pointwise selection. It exposes `design(N,z,s, h,delta,cap,goal)` and `bound(N,z,h,s,delta,operation)`. The operation includes the actual filter, chart, population if any, and direction/spectral panel counts. Every proposed schedule is evaluated in outward arithmetic. Warm orders must call `bound` again; an incoming inverse-order allowance is not reused for a different order. The complete sampler must also reprice folded aliases and all other budgets. The native integration and its cold/warm receipts are recorded in the practical verification section; a terminal-design receipt alone is not an end-to-end certificate.

The design menu tests the signed-gap representation away from an exact wall and low-clipping core charts as well as the inherited charts. It rejects invalid contours rather than changing branches. If no candidate meets the target before the resource cap, it returns the best finite allowance with `goal_met=false`, or raises an explicit resource exception when none is valid. The full query's absolute/relative status remains the final decision.

Failed branches retained.

The first common width-32 attempt up to .9 had a rank-five upper bound of $1.394\cdot10^{-4}$. At small positive radius, coarse width-32 sector filters at even ranks also gave enormous bounds, despite the physical expectations being finite. These attempts are preserved. The first defect was repaired by joining to the already proved exterior formula, the second by retaining low clipping charts and using a wider exact filter. Increasing precision alone would not repair either structural loss. The working cutoffs have a proved recovery identity and explicit cost; they are not fitted to observed moment values.

Files `hybrid*-connected*.json` preserve each proposed bound, including failures. `hybrid-connected-verified.json` names the five final input receipts and hashes, replays every selected cell, and records the final scope. Its higher-precision replay is an arithmetic re-evaluation of the same mathematical inequalities, not an independent proof of them. Independent source and whole-moment comparisons remain separately identified.

A shorter common formula across the rank-four wall

Corollary 21.26 (a stride-three formula with independent parameters). At rank four, take $z \in [.45, .55]$, $-.95 \le \Re h \le 3$, $|\Im h| \le 1$, and independently $|\Re s|, |\Im s| \le 1$. The exact-arithmetic formula of Proposition 5.18 with $\Delta = .32$, stride $q = 3$, first filter $(K, b, p) = (16, 80, 48)$ and terminal filter $(90000, 80, 48)$ uses 33,801 distinct positive frequencies. With the full-order source and image dimensions of Theorem 21.21 its absolute error is less than $5.762616 \cdot 10^{-11}$ at every input of this connected region.

Proof. The reciprocal-support gap is positive throughout this interval: $2\pi/3 - .32 \cdot 4(1 + .55) > 0$. The 40 closed radius-cell core bounds give the same spectral allowance as Theorem 21.24, with the wider filter only improving its complementary bound. The two folded allowances are below $1.7170 \cdot 10^{-24}$ and $8.4982 \cdot 10^{-24}$. The beta bound of Proposition 5.18 is valid for every $\Re h > -1$. Its real-order endpoint at three is strictly smaller than the deep endpoint at both $K = 16$ and $K = 90000$; the respective ratios are below $5.656 \cdot 10^{-5}$ and $1.339 \cdot 10^{-34}$. The extra core envelope of Corollary 5.17 is at most .32, below the paid factor 1.16085035. These are outward comparisons of distinct endpoints, not comparisons by interval overlap.

The last index is 93,792, and the sparse weights can have modulus three. Accordingly the finite real-source charge is $3 \cdot 3.627 \cdot 10^{-20}(93792/8202)^{1.9}$, below $1.116 \cdot 10^{-17}$. Add the full-order image charges of Theorem 21.21 and the two aliases. The unrounded total is below $5.762615741 \cdot 10^{-11}$, proving the claim. The exact rational masks and the common first and last indices give the stated sample count. `uniform-sparse-full-order.json` records the promotion and finite-source join. □

The common **radial schedule** was actually run cold at $z = .55, h = -.95 + i, s = 1 + i$, using input-specific adaptive angular dimensions. It returned absolute radius below $2.587\cdot10^{-12}$ and relative radius below $7.730\cdot10^{-12}$. Several positive and inverse orders were then contracted from those same source rows. This execution is not a claim that the larger fixed angular dimensions in the uniform theorem were used at every input. Its code and receipt distinguish the common radial schedule, the adaptive source and the theoretical uniform fixed-grid formula.

An integrated scalar evaluator with explicit evidence status

The executable continuation is `work/haar_critical/evaluator.py`. It keeps the inherited upper-radius evaluator and the rank-two and special rank-three branches. The new general rank-four through rank-eight branch evaluates a scalar directly from the prepared Haar source. It does not initialize or propagate a complete reduced differential state. The physical solution is selected by the exact Haar source and its Mellin identity; there is no unspecified connection coefficient at a critical radius in this representation.

The error contract. Let $\widehat{\Phi}_k$ be the computed source at $k\Delta$, with separate absolute errors $e_{k,\mathrm{fp}}$ and $e_{k,\mathrm{ang}}$, both expressed in physical units. If w_k is the literal rational filter weight, the computed scalar is

$$\widehat{T} = C_\Delta \sum_k w_k k^{-1-2h} \widehat{\Phi}_k - \widehat{I}_\Delta(h).$$

The returned allowance is

$$E = |C_\Delta| \sum_k |w_k| k^{-1-2\Re h}(e_{k,\mathrm{fp}} + e_{k,\mathrm{ang}}) + E_{\mathrm{image}} + E_{\mathrm{terminal}} + \mathcal{A}_q(F_1) + \mathcal{A}_q(F_2) + E_{\mathrm{readout}}.$$

The core, signed-gap and folded terminal allowances already contain the Mellin multiplier. They are not multiplied by it twice. The finite image has its own coefficient, truncation, alias and arithmetic bounds. Likewise, the source angular allowance is for the physical determinant. The literal dyadic basis recovery of Proposition 5.8 applies to its computed arithmetic residual; it does not multiply the physical analytic source error again.

Every accepted input uses exact rational strings for $z, \Re h, \Im h, \Re s, \Im s$. Positive moduli use their real logarithms. The complex preparation is never normalized to a probability. At nonnegative integer order, the enclosed Taylor coefficient gives the result directly. Near such an order the deflated products of Theorem 21.21 avoid a numerical division by a pole. Warm noninteger queries recompute every order-dependent multiplier and error term.

Construction and reuse. The planner selects a finite convolution filter, admissible contour and resonant population, or a valid signed-gap bound. Its floating proposals are followed by outward checks. The alternative `terminal_hybrid.py` adds low-clipping contours and wider exact convolution filters; each saved operation records its representation, panels and parameters. A terminal goal is an allocation, not a certificate. A best finite bound that misses that allocation may still give a valid absolute result; its final modulus test decides whether the requested relative tolerance is met.

For each eligible integer stride, the reciprocal-support separation and the two folded costs are checked. Dense stride one is a fallback. The source is computed at the actual retained frequencies, with angular resolution selected from the prepared-symbol inequalities. The framed native determinant uses 104-bit fixed point and exports integer centres with their exact dyadic divisors; Arb handles 192/256-bit source, special-function and final contractions. These are the executed arithmetic settings, not a rank-uniform claim that this precision always suffices. A fresh Cauchy image, code hashes and source-row hashes complete the preparation. Every replay checks these hashes, the expected frequency sequence, the angular denominators and the absence of an omitted nonzero weight.

The cache binds (N, z, s), its numerical source and image, and the implementation that enclosed them. It does not bind the query order h. Its terminal filter stays fixed for warm orders, while the entire error budget is recomputed. Preparations from a different radius or tilt cannot be substituted. The original critical engine remains unchanged so its sealed receipts are replayable; the new gap/core engine has a separate seal. A partial interrupted source is not treated as a finished preparation. A mismatched cache returns an invalid- preparation outcome, rather than a numerical value with a certificate.

If a valid nonzero disk misses the relative tolerance, the selector can propose a smaller absolute allocation from its modulus lower bound and construct a separate order-adapted child preparation. This matters when a warm positive order amplifies the folded-alias allowance of an inverse-order guard. The new filter uses the actual query order; it is justified by the same identity and the $\Re h > -1$ tail and beta bounds. A new source and code seal prevents it from changing the meaning of an earlier cache. The final disk must again pass every error and modulus check. If the refinement is impossible within the cap, the already valid absolute disk is retained with the failed-refinement status.

Method selection. For $N = 1$, the exact hypergeometric identity avoids the historical crash. At $N = 2, z = 0$ the gamma formula is used only in the ordinary domain $\Re h > -1/2$; outside it the answer is divergent. At positive rank-two radius the inherited validated Duffy branch is retained, with its specified domain and resource tests. Rank three uses the new conditional source estimator on the tested critical interval $[.25, .4]$, or the inherited certified $s = -3$ slice when applicable. An explicit `rank3-wide` option attempts $0 < z \le .9$ with further bounded refinements; it is an estimated extension, not a uniform theorem. Other low-rank and centre branches retain their predecessor status. At ranks four through eight below .82 the planner selects the new critical/gap construction; above it the earned exterior construction remains available. Theorem 21.25 proves a connected ideal-formula domain, while the actual adaptive query checks its own formula and can report a resource limit.

The rank-three estimator jointly refines the singular pair, spectator and regular-source grids, and compares a second exact partition. It monitors its absolute summation size and the proven omitted central contribution. Its eightfold refinement/roundoff allowance is an empirical estimator; it is never reported as an interval proof for

the complete quadrature. The low-rank tests below include a failure at the required tolerance and a concrete false-convergence example that justifies retaining the regular channel.

Statuses and accuracy. For an enclosed centre v and absolute radius E, relative accuracy is reported only when an outward lower bound for $|v| - E$ is positive and $E/(|v| - E) \le 10^{-10}$. Otherwise a valid disk is reported as absolute-only, with a separate zero-possible flag. A zero-containing disk does not prove that its centre is a zero; the inherited zero-count theorem has a separate argument. These distinctions are implemented as follows.

Status family	Meaning
`DIVERGENT`	The ordinary expectation is outside its integrability domain; no continued gamma value is substituted.
`CERTIFIED_RELATIVE`	All source, spectral, image, arithmetic and readout costs are enclosed and the relative gate passes.
`CERTIFIED_ABSOLUTE_ONLY`	The disk is valid; relative accuracy is insufficient or zero cannot be excluded.
`ESTIMATED_RELATIVE` / `ESTIMATED_ABSOLUTE_ONLY`	A numerical estimate is supplied with its refinement and comparison evidence, not a rigorous remainder certificate.
`UNRESOLVED_RESOURCE_LIMIT` / inherited `RESOURCE_LIMITED`	No requested complete certificate or accepted estimate was earned within the explicit limits.
`UNTESTED` / `INVALID_PREPARATION`	A method-range gate or source-integrity check prevents a supported readout.

The original target asks for an error estimate, so the estimated outcomes remain useful. They are not relabelled as failures merely because a stronger certificate is unavailable. Conversely, neither a source match nor a stable numerical value turns an estimate into a certificate. Cold time includes preparation; warm time includes source integrity and the new order contraction. The accompanying receipts record both, rather than counting a cached preparation as free for a first query.

Connected finite-rank coverage, physical arithmetic and zero geometry

The following arguments extend this section. Lettered identifiers retain stable links to the integrated constructions; their correspondence is given at the beginning of the paper. Earlier bounds remain valid on their stated domains. A limitation described at an intermediate stage is superseded only by a later explicitly proved result, as summarized in the current coverage table.

Rank-three critical-radius theorem and scope (R1)

The ultimate target remains the ordinary unnormalized Haar expectation

$$T_N(h, s; z) = \mathbb{E}_{U(N)}\big[|S_N(z)|^{2h}|\Lambda_N(z)|^{2s}\big], \tag{R1.1}$$

$$\Lambda_N(z) = \det(I - zU), \qquad S_N(z) = -(1 - z^2)\Lambda_N'(z)/\Lambda_N(z), \tag{R1.2}$$

on $1 \le N \le 8$, $0 \le z \le .9$, $-.95 \le \operatorname{Re} h \le 3$, $|\operatorname{Im} h| \le 3$, $|s| \le 3$, with relative error below 10^{-10} where ordinary integrability and a nonzero modulus permit. The present construction addresses $N = 3$ on a connected interval through $z = 1/3$. It does not replace that broader objective or identify meromorphic continuation with expectation.

The source materials are the supplied HaarCritical manuscript, restart, results and coverage records, verification archive, executable evaluator, and preserved HaarSpectral source. The active method is Shadow_Research_1, development edition 1, including the Reflective Mathematics Research Handbook, Combined Protocol 0.2-dev.1, and Boundary–Property Key 3.4-dev.1. Older copies are retained as provenance.

The following inherited results retain exactly their previous scope.

- Theorem 21.25 gives connected *exact-arithmetic absolute* approximation for ranks 4–8, $.02 \le z \le .9$, and the full complex box. Its joined strict absolute bounds by rank are respectively $7.954\,10^{-11}$, $5.650\,10^{-13}$, $2.897\,10^{-13}$, $3.895\,10^{-13}$ and $1.077\,10^{-17}$. This is not a universal relative-error or runtime assertion.
- Proposition 3.3 fixes the rank-three resonant r^{-6} coefficient. Its previous $O_{\mathcal{K}}(r^{-8})$ did not provide a usable constant. The exact symbolic calculation and the independent $s = -3$ specialization were replayed before constructing the new bound.
- Proposition 4.3 is an exact conditional-source partition. Lemmas 4.4–4.5 and Corollary 4.6 control integrability and a central omission. That omission allowance never certified the remaining quadrature.
- The known false-convergence example is decisive: conditional refinement with an eight-node regular grid changed the value by about $1.57\,10^{-14}$, while joint refinement changed it by $9.8101\,10^{-4}$.
- The inherited hard input $z = 1/4$, $h = -.95 + 2.7\mathrm{i}$, $s = 2.4 + 1.8\mathrm{i}$ returned a relative estimate $1.1683\,10^{-10}$ and a resource-limit status. Its last change was only $4.48\,10^{-15}$; the deciding empirical allowance was a binary64 summation floor. Increasing resolution alone did not repair that arithmetic limitation.

The new result has three distinct levels. Theorems below are analytic statements with explicit finite majorants. Parameter-wide numerical constants come from executed outward ball inequalities. Individual scalar certificates add the actual finite arithmetic, image and readout bounds. Agreement of estimated conditional values is a separate diagnostic, not a substitute for these inequalities.

Uniform connected-region inequalities (R6)

The following constants were executed at 256-bit outward precision. They refer to complete parameter ranges, not sampling of a parameter grid:

$$z \in [1/4, 2/5], \quad -.95 \le \operatorname{Re} h \le 3, \quad |\operatorname{Im} h| \le 3, \quad |s| \le 3.$$

Use

$$L = 112, \qquad M = 20, \qquad R = 2048, \qquad \Delta = 1/2, \qquad K = 4096.$$

The preparation coefficient majorant uses $|(3+s)_n| \le (6)_n$ and $z \le 2/5$. In the direction bounds use $a \ge 3/4$; in the absolute physical prefactor use $(1-(2/5)^2)^{-9}$. All sums in (R4.6) are positive, so these substitutions are valid simultaneous majorants.

Quantity	Strict uniform upper bound
$F_{112,20}(2048)$	$3.859134\,10^{-18}$
Asymptotic source error at $r = 2048$	$9.200891\,10^{-25}$
Physical preparation difference δ	$4.222438\,10^{-29}$
Moment asymptotic remainder E_{Bessel}	$9.060497\,10^{-19}$
Full-moment preparation difference	$2.941324\,10^{-25}$
Weighted finite-prefix preparation difference	$1.742995\,10^{-17}$
Weighted complete-image preparation difference	$1.221596\,10^{-18}$
Complete preparation return E_{return}	$1.865154\,10^{-17}$
Tail plus return	$\mathbf{1.955759\,10^{-17}}$

For completeness, the order majorants use the beta integral for $u \le -1/2$ and reflection above it. On $[-.95, -.5]$, $|\Gamma(1+h)/\Gamma(-h)| \le \Gamma(1+u)/\Gamma(-u)$. The logarithm of the real ratio has nonnegative second derivative because $\psi_1(1+u) \ge \psi_1(-u)$. Above $-.5$,

$$|C(h)| \le \frac{2\cosh(3\pi)}{\pi}\Gamma(1+u)^2 2^{2u}.$$

After multiplication by the cutoff power, log convexity reduces the majorant to four endpoints. This proves the common tail price. The comparison moment is bounded uniformly by its inverse endpoint allowance plus 4.2^6, splitting the mark support at one.

For the complete image return, poles are removed before maximization. Writing $\mathcal{R}(w) = (w-1)\zeta(w)$, which is entire,

$$C_\Delta \zeta(1+2h-2j) = -\frac{4^{2h}\Gamma(1+h)^2}{\pi}\frac{\sin \pi h}{h-j}\,\mathcal{R}(1+2h-2j) \quad (\Delta = 1/2).$$

The quotient is bounded by $\pi e^{3\pi}$ through its cosine-integral representation, including the removable points. Explicit Euler–Maclaurin formulas bound $\mathcal{R}$ on whole complex rectangles; a periodic Bernoulli bound controls their remainders. Gamma endpoint bounds and the positive reflected-zeta tail complete the price. Detailed finite sums, rectangles and chosen truncations are recorded in route_a/UNIFORM_RETURN.md and uniform-return.json.

These estimates certify the mathematical tail operation. They do not silently include finite original-source sampling, the approximation of the original image, or finite arithmetic. Those charges follow separately.

A common finite formula for the complete box

Theorem R6.1 (Connected exact-arithmetic scalar approximation)**.** *For $N = 3$, $1/4 \le z \le 2/5$, $-.95 \le \operatorname{Re} h \le 3$, $|\operatorname{Im} h| \le 3$, $|s| \le 3$, there is a specified common finite scalar formula $\mathcal{F}$ for the ordinary moment such that*

$$|T_3(h,s;z) - \mathcal{F}(h,s,z)| < 1.955759\,10^{-17}.$$

The parameters vary independently subject to the stated tilt disk. This is an absolute approximation at each input, not one enclosure of the range of all moments.

Proof. Use $\Delta = 1/2$, $K = 4096$ and the $L = 112$, $M = 20$ tail above. For every retained real sample, use the original one-body preparation DFT with $P = 4096$ and modes $|\ell| \le 2040$. Form the untranslated Toeplitz determinants on $Q = 4096$ direction nodes, project onto signed direction modes $|k| \le 2047$, and contract the exact translation coefficients. Neither Nyquist mode is retained. This specifies the signed projection; a poorly resolved fully translated pointwise product would be a different formula.

For the original image, retain $J = 72$ coefficients, sampled on a complex half-circle of radius $H = 3$ with $m = 144$ nodes. Its angular source uses $Q_i = 256$, $L_i = 88$, $P_i = 4096$. The finite formula consists of this finite physical prefix, this finite original image with weighted zeta products regularized, and the finite special-function tail contraction in equation (R7.1).

At the uniform strip $t = .4$ and $z_* = .4$, the original one-body Cauchy bound is below 8783.065, the preparation mass is at most $.84^{-9}$, and the real-tilt Gram matrix is at least $.6^6 I$. Fourier truncation, DFT aliases and the signed-direction strip inequality give a real-source error below $1.518205\,10^{-346}$ per sample. Its weighted contribution is below $6.267046\,10^{-335}$. The image's complex-radius mode, preparation, direction and Taylor-alias bounds give scaled coefficient error below $7.188986\,10^{-111}$. Entire-zeta bounds for the first four weights and reflected-zeta bounds for the others give finite image error below $5.764889\,10^{-76}$. The omitted image terms cost below $2.010364\,10^{-56}$. All strip lower bounds and geometric ratios are positive and explicitly tested. Adding these three bounds to Theorem R5.1, using unrounded outward constants, gives

$$1.955758598295016781\,10^{-17} < 1.955759\,10^{-17}.$$

The complete formulas for these elementary majorants are in route_a/UNIFORM_FORMULA.md; uniform_formula.py executes them, and an independent 384-bit replay confirms the inequality. □

The common large source grids in this theorem were not executed. The inequalities defining their approximation error were executed. The adaptive scalar certificates below execute smaller, separately priced grids with finite arithmetic. Thus the theorem and the actual certificates provide distinct forms of coverage, and neither implies uniform relative accuracy, nonvanishing or a common runtime bound.

Centre-to-critical theorem and scope (C1)

The original objective remains

$$T_N(h,s;z) = \mathbb{E}_{U(N)}\big[|S_N(z)|^{2h}|\Lambda_N(z)|^{2s}\big], \tag{C1.1}$$

$$\Lambda_N(z) = \det(I - zU), \qquad S_N(z) = -(1-z^2)\Lambda_N'(z)/\Lambda_N(z), \tag{C1.2}$$

for $1 \le N \le 8$, $0 \le z \le .9$, and the independent parameter set

$$\mathcal{B} = \{(h,s) \in \mathbb{C}^2 : -.95 \le \operatorname{Re} h \le 3,\ |\operatorname{Im} h| \le 3,\ |s| \le 3\}. \tag{C1.3}$$

The numerical target is relative error below 10^{-10} wherever the ordinary expectation exists and a nonzero modulus permits that guarantee. Complex powers of positive real quantities use their real logarithms. The present work addresses rank three. It neither replaces the overall programme nor identifies a meromorphic continuation with an ordinary moment.

The active protocol is Shadow_Research_1, development edition 1, with Combined Protocol 0.2-dev.1 and Boundary–Property Key 3.4-dev.1 [7]. Its concrete role is to keep the Haar realization, complex preparation, exact source transformations, discarded information and final readout in one argument. It supplies no mathematical premise by itself.

What was already available

Direct inspection of the complete HaarCritical source corrects a potential overstatement in a centre-only restart summary. The following results are inherited, not new claims of this continuation [5, 6].

- HaarCritical Proposition 10.2D covers the full order rectangle and every $0 \le z \le .9$ on $s = -3$. Its certified absolute error $< 3.02\,10^{-17}$ applies to $I_h(3z) = (1-z^2)^9 T_3(h,-3;z)$, including adaptive finite arithmetic. The physical moment retains the factor $(1-z^2)^{-9}$ and final readout allowance. At small radii that construction already expands only the three trace Bessels and keeps the translated angular factor exact.
- Theorem 10.2F already proves uniform relative error $< 5.24\,10^{-11}$ on $0 \le z \le 10^{-6}$ for the complete set (C1.3), with $|T_3| > .00087054$ throughout that set. This remains a stronger nonvanishing and relative assertion on its tiny interval.
- The completed critical-radius continuation gives a common exact-arithmetic absolute formula with error $< 1.955759\,10^{-17}$ on $[1/4, 2/5] \times \mathcal{B}$, and fifteen separately executed pointwise certificates. Its common large source grids were not executed.
- Theorem 21.25 preserves connected exact-arithmetic absolute approximation at ranks 4–8 for $.02 \le z \le .9$. The exact resonant rank-three coefficient, conditional partition, central-cutoff theorem, and fixed-interior, microscopic and circle results retain their original hypotheses and evidence grades.

The inherited identity

$$D_3(r) = \frac{4J_1(r)(J_0(r)^2 + J_1(r)^2)}{r} - \frac{4J_0(r)J_1(r)^2}{r^2}$$

also appears in the original source. The present work uses and reprices it; it does not claim a new recurrence or the first ordinary centre result. The newly connected generic-tilt gap is

$$10^{-6} < z < 1/4.$$

The new construction extends the retained-direction method to all finite Laurent preparation modes and to an effective sampled Mellin/Abel readout.

Theorem C1.1 (Connected absolute coverage)**.** *There is a specified common finite exact-arithmetic formula $\mathcal{F}_{\mathrm{c}}(h,s,z)$ such that*

$$|T_3(h,s;z) - \mathcal{F}_{\mathrm{c}}(h,s,z)| < 6.365495\,10^{-22} \quad (0 \le z \le .3,\ (h,s) \in \mathcal{B}).$$

Together with the inherited interior formula, it defines a piecewise finite formula $\mathcal{F}_{\mathrm{joined}}$ satisfying

$$|T_3 - \mathcal{F}_{\mathrm{joined}}| < 1.955759\,10^{-17} \quad (0 \le z \le .4,\ (h,s) \in \mathcal{B}).$$

Both constructions refer to the same ordinary Haar moment on their nonempty overlap $[.25, .3]$.

The constructive proof is given below, ending in Section C7. Executed outward inequalities validate its constants. It is distinct from the pointwise finite-arithmetic certificates, which price their actual grids, precision and modulus. Neither theorem asserts a common practical runtime, nonvanishing on the enlarged box, or uniform relative accuracy there.

A common formula on the complete centre box (C7)

The design proving Theorem C1.1 is

$$\Delta = \tfrac{1}{2}, \quad K = 4096, \quad R = 2048, \quad L = 88, \quad M = 20, \quad B = 48, \quad Q = 4096, \quad \rho = \tfrac{1}{10}. \tag{C7.1}$$

These are the tail preparation, Bessel order, Abel order and direction parameters. They are distinct from the original finite-source and image grids described next. Every parameter-wide price is an inequality on a continuum, rather than an interpolation of tested values.

Uniform order and preparation prices

Let $u_0 = -.95$, $u_1 = 3$, $V = 3$ and

$$G(u) = \Gamma(1+u)^2(2/\Delta)^{2u}, \qquad C_* = \frac{2\cosh(\pi V)}{\pi}\max\{G(u_0), G(u_1)\}.$$

The gamma reflection formula and $|\Gamma(1+h)| \le \Gamma(1+\operatorname{Re} h)$ show $|C_\Delta(h)| \le C_*$. Logarithmic convexity proves that the maximum occurs at the displayed endpoints after majorization. The same argument applied to $G(u)\sum_{k\le K} k^{-1-2u}$ gives an endpoint price for the weighted prefix. At u_0 use $(K+1)^{1.9}/1.9$; at u_1 use $\zeta(7)$. Executed outward values are

$$C_* < 5.816231\,10^{8}, \quad |C_\Delta| \sum_{k\le K} k^{-1-2u} < 4.127934\,10^{11}, \quad I_{\mathrm{diff}} < 2.499348\,10^{10}.$$

The last bound uses the inherited entire Euler–Maclaurin rectangles and the reflected tail (C6.7). It is uniform across exact and near-integer orders, rather than a product of separately singular factors.

At $Z = .3, L = 88$, formula (C3.4) gives $\delta < 1.453778\,10^{-33}$. Its three return contributions are

$$E_{\mathrm{full}} < 5.286878\,10^{-30}, \quad E_{\mathrm{prefix}} < 6.001096\,10^{-22}, \quad E_{\mathrm{image\,return}} < 3.633494\,10^{-23}.$$

They sum, before display rounding, to less than $6.364445\,10^{-22}$. The finite prefix is the dominant uniform charge.

Uniform Bessel, Abel and direction prices

Use (C4.8) with $Z = .3$, and let

$$P_{j\ell} = \prod_{t=0}^{\ell-1} \sqrt{(8.5+j+t)^2 + 36}.$$

Since $.6 + j \le \operatorname{Re} p_j \le 8.5 + j$ and $|\operatorname{Im} p_j| \le 6$, $|(p_j)_\ell| \le P_{j\ell}$. Thus

$$\overline{E}_{\mathrm{Abel}} = C_*\Delta^{-3/2}K^{.4-B}\sum_{m,j}\frac{A_{mj,\rho}P_{jB}}{(B+j-.4)c_m^B} \tag{C7.2}$$

bounds the weighted Abel error. For the strip, the finite-difference integral gives

$$K^j|\mathcal{D}^\ell f_{p_j}(K_+)| \le P_{j\ell}(K/K_+)^j K_+^{-.6-\ell} \le P_{j\ell}K_+^{-.6-\ell}.$$

Consequently (C5.5) is majorized by

$$\overline{M}_m = e^{bK_+}\sum_{\substack{j<M\\ \ell<B}} A_{mj,\rho}P_{j\ell}K_+^{-.6-\ell}e^{b\ell}\widehat{c}_m^{-\ell-1}.$$

All j sums start at the exact Vandermonde threshold. The largest translation $a = .9$ gives both the growth bound and the smallest gaps. Conditions (C5.3) hold at $\rho = .1$.

The uniform source price from (C4.7) is $F < 4.172923\,10^{-35}$. Combining this with (C6.5), the endpoint order bounds, (C7.2) and the strip estimate gives the three new tail charges in Table 18. The initial common choice $B = 32$ had a valid but weaker total about $8.9792423\,10^{-17}$, dominated by its Abel allowance. Increasing the Abel order to 48 resolved that identified component. The eigen-Bessel order stayed at 20.

Original finite source and image

The common real-source formula uses a $P = 4096$-point preparation DFT, modes $|\ell| \le L_r = 2040$, and a $Q_r = 4096$-point direction grid. It projects the *untranslated* determinant onto signed direction modes $|k| \le 2047$, excludes both Nyquist modes, and then contracts exact translation Bessels. This is the inherited signed-direction contract; an unresolved pointwise translated product cannot replace it.

For completeness, its explicit source price can be summarized by the same endpoint constants used in the critical-radius proof. Put $z_* = .4$, $d_* = 1 - z_*^2$, $t = .4$,

$$E_* = \frac{2z_*(\cosh t - 1)}{(1-z_*)^2}, \quad g_- = (1-z_*)^2(1-E_*), \quad g_+ = (1+z_*e^t)(1+z_*e^{-t}),$$

$$\eta_* = \arctan \frac{2z_* \sinh t}{(1-z_*^2)(1-E_*)}, \quad C = d_*^{-5} \max(g_-^{-4}, g_+^2) e^{3\eta_*} \left(\frac{e^t - z_*}{1 - z_* e^t} \right)^2 .$$

Here $g_- > 0$ and $C < 8783.065$. Let

$$M_* = d_*^{-9}, \quad m_* = (1-z_*)^6, \quad V_* = M_* \left[\frac{d_*^2}{(1-z_*^2e^{-2t})(1-z_*^2e^{2t})} \right]^9 .$$

The signed-direction error is $4V_* e^{-tQ_r/2}/(1-e^{-t})$, and the entry error is

$$\epsilon_r = \frac{2C}{1-e^{-t}} \left[e^{-(L_r+1)t} + (2L_r+1)e^{-(P-L_r)t} \right].$$

The determinant perturbation price adds $M_*[(1 + 3\epsilon_r/m_*)^3 - 1]$. Multiplying their sum by the weighted prefix yields the stated finite real-source allowance.

Every radius-dependent bound here is controlled by the upper radius .4: $g_{\min} = 1 + z^2 - 2z\cosh t$ decreases and remains positive, the corresponding maximum and strip-argument bounds increase, the Möbius ratio increases, and the Gram floor decreases. None requires a positive lower radius. This is the reason the old finite-source price extends to zero, rather than an extrapolation of its previous theorem's stated interval.

The original image uses

$$J = 72, \quad m_{\mathrm{circ}} = 144, \quad H = 3, \quad Q_i = 256, \quad L_i = 88, \quad P_i = 4096.$$

It samples the original source at bounded complex radii, extracts the scaled coefficients $H^{2j}\alpha_j$ by a DFT, and prices the Cauchy alias, angular source and omitted image tail. Its mode and alias bounds, with $b_i = H/2$, are

$$E_{\mathrm{mode}} = \frac{2We^{b_i^2} b_i^{L_i+1}}{(L_i+1)![1 - b_i/(L_i+2)]}, \quad E_{\mathrm{alias}} = \frac{2Ce^{-t(P_i-L_i)}}{1-e^{-tP_i}}, \quad W = \max((1-z_*)^{-6}, (1+z_*)^6).$$

With $\epsilon_i = E_{\mathrm{mode}} + (2L_i+1)E_{\mathrm{alias}}e^H$ and $D_* = 3(1+z_*)$, the bounded-circle source error is

$$\frac{2M_* e^{HD_* \cosh 2}}{e^{2Q_i} - 1} + 9\epsilon_i (We^H + 3\epsilon_i)^2 e^{3Hz_*}.$$

The coefficient alias adds $M_* v^{2m_{\mathrm{circ}}}/[(m_{\mathrm{circ}}!)^2(1 - (v/(m_{\mathrm{circ}}+1))^2)]$, where $v = HD_*/2$. Deflated finite image weights and the reflected geometric tail then give the two image rows of Table 18. These mass, support, coefficient and alias bounds also increase with the upper radius and extend to $z = 0$ unchanged.

Proof of Theorem C1.1. Use the finite formula (C6.8) with design (C7.1) and the original grids just specified. Theorems C4.4 and C6.1, Lemma C5.2, and the inherited original-source/image contracts give the seven independent exact-arithmetic charges in Table 18. Outward computations at 256 bits, independently replayed at 384 and 512 bits, give the unrounded sum $6.3654942549856648\ldots\ 10^{-22}$, below the claimed bound. This proves the centre formula on the entire continuum. Both it and the inherited interior formula return to (C2.1) on $[.25, .3]$. Choose the centre formula through .3 and the interior formula above .3; the maximum of the two proved absolute allowances is $1.955759\,10^{-17}$. □

The common large grids have **not** been executed. The theorem is about a finite exact-arithmetic expression with executed outward error inequalities. It does not add unexecuted finite-arithmetic performance to that claim. The uniform runner now refuses $K \neq 4096$, because the reused original finite-prefix allowance is already weighted for that cutoff.

Table 18: Uniform exact-arithmetic prices on $0 \le z \le .3$, for the full independent box. The total is formed from unrounded outward values.

Component	Strict upper bound
Original finite real source	$6.267046 \times 10^{-335}$
Original finite image	5.764889×10^{-76}
Original omitted image	2.010364×10^{-56}
Three-Bessel remainder	9.756969×10^{-26}
Abel remainder	7.393385×10^{-27}
Tail direction quadrature	3.303519×10^{-85}
Complete preparation return	6.364445×10^{-22}
Total	6.365495×10^{-22}

Implemented finite arithmetic and exact centre specialization (C8)

The positive-radius physical preparation delegates to the sealed finite_source.py and its rank-three native kernel. The complex tilt, original image, untranslated signed-direction convention and 104-fraction-bit dyadic arithmetic remain unchanged. The inherited contracts price input enclosures, preparation aliases, Bessel evaluation, fixed-point residuals and determinant perturbations. Those analytical and software contracts are explicit dependencies; this construction does not claim proof-assistant verification or a new proof of every low-level native arithmetic lemma.

At $z = 0$ the new source adapter uses the exact determinant polynomial $D_3(r)$ in Arb. At $r = k\Delta$, let v_k be its outward ball, $S = 2^{104}$, and $m_k = \lfloor \mathrm{mid}(Sv_k) \rfloor$. Each sample is accepted only after checking

$$|v_k - m_k/S| < 2^{-103}.$$

The inherited five-field row format records this exact dyadic allowance. Its last normalization field is 1; it does not claim that a one-node source quadrature was used. The angular-source error is exactly zero. All 4096 samples passed the encoding gate. A separate 384-bit recurrence audit checked every sample; its largest encoded-centre gap was below $4.929\,10^{-32}$.

For the centre image, put $t = r^2$ and

$$A(t) = \sum_{j\ge0} \frac{(-1)^j t^j}{4^j (j!)^2}, \quad B(t) = \sum_{j\ge0} \frac{(-1)^j t^j}{2\,4^j j!(j+1)!}, \quad C(t) = \sum_{j\ge0} \frac{(-1)^j t^j}{4\,4^j j!(j+2)!}.$$

Then $J_0 = A$, $J_1 = rB$, $J_2 = r^2 C$, and

$$D_3(r) = A^3 + 2tAB^2 + 2t^2 B^2 C - t^2 AC^2.$$

Exact rational products produce the first 72 coefficients. The systematic source and Cauchy-alias errors of these coefficients are zero. Their finite ball arithmetic and the omitted image tail remain priced by the unchanged image contraction.

An independent Schur-character calculation checks every coefficient:

$$\mathbb{E}|\operatorname{Tr} U|^{2j} = \sum_{\substack{\lambda \vdash j \\ \ell(\lambda)\le 3}} (f^\lambda)^2, \qquad f^\lambda = \frac{j!(\lambda_1-\lambda_2+1)(\lambda_1-\lambda_3+2)(\lambda_2-\lambda_3+1)}{(\lambda_1+2)!(\lambda_2+1)!\lambda_3!}.$$

Trailing zero rows are allowed. The first eight exact moments are $1, 1, 2, 6, 23, 103, 513, 2761$. All 72 rational coefficient comparisons passed, and exact integer contractions enclose $1, 1, 2, 6$.

The new tail coefficients, forward differences, DFT, special functions and final readout use outward Arb/Acb arithmetic, ordinarily at 512 bits in the pointwise matrix. Finite differences can suffer cancellation, but their balls retain it. All error components are required to be finite; the returned decimal midpoint's gap is charged. Increasing asymptotic order cannot repair a budget dominated by source arithmetic.

The public interface rank3_centre.py checks the full original parameter box and dispatches to the centre formula for $z \le .3$ and the inherited interior formula for $.3 < z \le .4$. Explicit method selection supports overlap checks. It verifies reviewed source hashes, the transitive dependency set, exact requested radius and tilt against a reused cache, the original image identity, data seals and consecutive rows. Fifty final interface controls passed, and an actual call through the public entry point returned CERTIFIED_RELATIVE.

The native positive-radius header still requires both rational steps Δ and $3z\Delta$ to have positive numerator and denominator below 2^{31}. Thus $z = 10^{-9}$ is supported at $\Delta = 1/2$, while a requested radius with denominator 10^{15} is explicitly refused. The input is never silently rounded. The exact centre branch bypasses the native positive-frequency header. Files are written to new destinations, and sealed inherited receipts are preserved.

Upper-radius rank-three theorem and scope (U1)

The original goal remains the Haar expectation

$$T_N(h,s;z) = \mathbb{E}_{U(N)}\left[|S_N(z)|^{2h}|\Lambda_N(z)|^{2s}\right], \tag{U1.1}$$

$$\Lambda_N(z) = \det(I - zU), \qquad S_N(z) = -(1-z^2)\frac{\Lambda_N'(z)}{\Lambda_N(z)}, \tag{U1.2}$$

for $1 \le N \le 8$, $0 \le z \le .9$, $-.95 \le \Re h \le 3$, $|\Im h| \le 3$, and $|s| \le 3$, with independently varying order and tilt. Powers of positive moduli use the real logarithm. The desired practical relative accuracy is below 10^{-10} wherever the ordinary expectation exists and a positive lower modulus justifies a relative claim.

This construction completes the rank-three *radius gap* in the connected exact-arithmetic absolute construction. It also supplies complete executed pointwise certificates at the upper endpoint. The larger programme, and uniformly practical relative readouts throughout its complex parameter space, remain separate obligations.

Theorem U1.1 (Connected rank-three absolute approximation)**.** *Throughout the original independent complex box there is a piecewise finite exact-arithmetic formula $\mathcal{F}$ on $0 \le z \le .9$ with*

$$|T_3(h,s;z) - \mathcal{F}(h,s;z)| < 1.955759\,10^{-17}.$$

Its new upper component is valid on $3/8 \le z \le .9$ and has error below $3.501607\,10^{-19}$. All adjacent representations have positive-width overlaps. This theorem does not include the unexecuted finite arithmetic of the common grids.

The upper-cell bounds and their complete finite formula are derived below. Their positive convolutions were executed in 192-bit Arb; the composition was executed at 256 bits and independently replayed at 384 bits. The centre component retains its established $6.365495\,10^{-22}$ allowance on $[0,.3]$, and the critical component retains its established $1.955759\,10^{-17}$ allowance on $[.25,.4]$. They are inherited results, not new claims of this investigation.

Preserved frontier and evidence levels

The 17 new centre certificates and 15 preceding critical certificates remain unchanged. The inherited coverage also includes Theorem 10.2F's full-box relative bound $5.24\,10^{-11}$ and nonvanishing for $0 \le z \le 10^{-6}$; Proposition 10.2D's $s = -3$ all-radius construction; and Theorem 21.25's connected exact-arithmetic absolute construction for ranks 4–8 on $[.02,.9]$. The physical conversion on the special slice is $T_3 = d^{-9}I_h(3z)$, $d = 1 - z^2$.

Five evidence categories are kept distinct throughout: analytic statements proved on continua; executed outward inequalities; actual finite-arithmetic scalar certificates; estimated comparisons; and unexecuted or resource-limited formulas. A common-grid theorem is never substituted for the arithmetic allowance of an input's actual source cache. The new ledger assesses immutable raw candidate receipts after review; their original files are not relabeled.

The complete connected upper-radius finite formula (U8)

Scope, result, and evidence level

Let

$$N = 3, \qquad 3/8 \le z \le 9/10, \qquad -.95 \le \Re h \le 3, \quad |\Im h| \le 3, \quad |s| \le 3.$$

There is a piecewise finite exact-arithmetic formula $\mathcal{F}_u$, with the cells and resources below, for which

$$\boxed{|T_3(h,s;z) - \mathcal{F}_u(h,s,z)| < 3.501607\,10^{-19}.}$$

The cells have positive-width overlaps. Joining this construction to the inherited centre and critical constructions gives a finite exact-arithmetic formula on the entire original rank-three interval $[0,.9]$, with bound $1.955759\,10^{-17}$. The old bound remains the maximum after the join.

The positive coefficient convolutions defining the new Bessel remainder were executed in 192-bit Arb arithmetic. Their radius rescaling, the complete preparation return, the finite Abel remainder, and the original source/image inequalities were composed in 256-bit Arb arithmetic. The full common source grids and their finite arithmetic have **not** been executed by this theorem. Pointwise executable certificates use their actual parameters and separate finite-arithmetic contracts. This theorem asserts neither uniform relative accuracy nor uniform nonvanishing nor a common practical runtime.

The producing receipt is `uniform-upper-cells-256.json`. Each base receipt is referenced by hash in it. Inherited sources were not modified.

1. Physical source and finite formula

Write $a = 3z$, $d = 1 - z^2$, $p = 3 + s$. The exact transformed Haar source is

$$T_3 = \mathbb{E}_{\mathrm{CUE}_3}|a + \operatorname{Tr} V|^{2h} d^{9+6s} \prod_{j=1}^{3} (1 + zw_j)^{-p}(1 + z/w_j)^{-p}.$$

Every complex power has the inherited physical analytic branch. Both factors have the same complex exponent; none is conjugated or probability-normalized. The ordinary absolute-moment domain is $\Re h > -1$, proved for the present radius range in `../bounds/UPPER_SOURCE_IMAGE_PROOF.md`.

For each cell use the inherited physical signed-direction finite source $\widetilde{\Phi}$, with $P = Q = 8192$, one-body degree $L_r = 4090$, and exact translation contraction after the untranslated direction projection. Use the original physical Mellin image with

$$J = 72, \quad m = 144, \quad H = 3, \quad Q_i = 256, \quad L_i = 88, \quad P_i = 8192.$$

The associated strip is $t = 1/20$. All these source/image resources are the ones priced in `../bounds/source_image_bounds.py`, at uniform upper radius $Z = .9$. Their finite-prefix weight is repriced at the cell's actual K.

Put $\Delta = 1/2$, $R = K\Delta$, and

$$C_\Delta(h) = 2(2/\Delta)^{2h}\Gamma(1 + h)/\Gamma(-h).$$

Prepare the degree-L Laurent source using exactly the coefficients

$$b_n = (-1)^n (p)_n z^n/n!, \qquad w_k = \sum_{n=0}^{L-|k|} b_{n+|k|} b_n, \quad |k| \le L.$$

The inherited all-population coefficient construction then gives

$$A(r) = r^{-2} \sum_{m_0=0}^{3} \sum_{j<M} (R/r)^j [c^+_{m_0 j} e^{i\omega_{m_0} r} + c^-_{m_0 j} e^{-i\omega_{m_0} r}], \qquad \omega_{m_0} = 3z + 2m_0 - 3.$$

All determinant permutations and eigenangle sign placements are retained before aggregation. The exact low-degree Vandermonde zeros remain in force. The upper-radius formula uses the original finite prefix and image, and replaces the remaining sampled tail by the finite $B = 64$ Abel contraction of A described in `../FOUR_ABEL_PROOF.md`:

$$\mathcal{F}_u = C_\Delta \sum_{k=1}^{K} k^{-1-2h}\widetilde{\Phi}(k\Delta) - \sum_{j=0}^{71}[C_\Delta\zeta(1+2h-2j)]\widetilde{a}_j\Delta^{2j} + C_\Delta\,\mathfrak{A}_{64}[A].$$

This is a finite formula. The gamma-zeta products in brackets are evaluated by their entire regularization, including exact nonnegative integer orders. The finite differences in $\mathfrak{A}_{64}$ act on the combined degree polynomial. They do not rely on subtracting separately evaluated infinite polylogarithm and long prefix values.

2. Correlated disk majorants for preparation

The decisive useful correlation is between $u = \Re s$, the determinant power d^{9+6u}, and every Pochhammer factor. For $|s| \le 3$,

$$|n+3+s|^2 \le (n+3)^2 + 2(n+3)u + 9.$$

Divide $[-3,3]$ into 96 closed bands $[u_\ell, u_r]$. On a radius cell $[z_-, Z]$, define a nonnegative sequence by

$$\beta_0 = 1, \qquad \beta_{n+1} = \frac{Z\beta_n}{n+1}\sqrt{(n+3)^2 + 2(n+3)u_r + 9}.$$

It majorizes the actual $|b_n|$ for every tilt in that band. A bound for all ratios starting after β_{L+1} is

$$q_L = Z\max\left\{1, \sqrt{1 + \frac{4+2u_r}{L+2} + \frac{13+4u_r}{(L+2)^2}}\right\}.$$

Indeed the square of the ratio at denominator index t is $Z^2[1+(4+2u_r)/t+(13+4u_r)/t^2]$. The second coefficient is positive. If the first is nonnegative the expression decreases. If it is negative, there is at most one critical point on the positive axis and it is a minimum. The maximum over $t \ge L+2$ is therefore at the endpoint or its limiting value 1. All executed ratios are strictly below 1. Hence

$$e_L = \beta_{L+1}/(1-q_L), \qquad B_\ell = \sum_{n=0}^{256}\beta_n + \beta_{257}/(1-q_{256})$$

bound the omitted one-sided preparation and its complete coefficient norm. For $D_- = 1-Z^2$, $D_+ = 1-z_-^2$, set

$$q_\ell^* = \max(D_-^{3+2u_\ell}, D_+^{3+2u_\ell}), \quad Q_\ell^* = \max(D_-^{9+6u_\ell}, D_+^{9+6u_\ell}).$$

Since $d \in (0,1)$, the lower band endpoint majorizes the actual exponent. Then

$$\overline{w}_k = \max_\ell q_\ell^* \sum_{n=0}^{L-|k|}\beta_{n+|k|}\beta_n$$

has the necessary correlated product domination

$$d^{9+6u}|w_{k_1}w_{k_2}w_{k_3}| \le \overline{w}_{k_1}\overline{w}_{k_2}\overline{w}_{k_3}.$$

The six-factor telescoping identity also gives the physical preparation density error

$$\delta_L = \max_{\ell} 6Q_\ell^* B_\ell^5 e_L.$$

These operations are implemented in `disk_majorant.py`; the coefficient convolution is performed as a positive Arb polynomial product. This changes only the bounding function, never the complex physical coefficients.

The complete preparation return used in the theorem is

$$E_{\mathrm{prep}} = \delta_L(M_*^{\mathrm{tr}} + W_K + W_{\mathrm{image}}).$$

Here M_*^{tr} is the inherited translated unprepared CUE trace moment bound, and W_K, W_{image} are the inherited full-order prefix and regularized image weights from `centre_investigation/centre_bounds/centre_bounds.py`. The ordinary moment, finite prefix, and image are all present. The sharper heterogeneous return in `../bounds/RELATIVE_PREPARATION_RETURN.md` is available for practical resource selection but is not needed for the displayed theorem.

3. Effective four-Bessel remainder

The new one-factor estimate is the Nicholson/Green theorem proved and independently audited in `../bounds/NICHOLSON_GREEN_REMAINDER.md`. For integer n, $x > |n|$, and $M \geq 1$, the inherited outgoing expansion obeys

$$|J_n(x) - J_{n,M}(x)| \leq \sqrt{\frac{2}{\pi x}}\, 2|A_M(n)| x^{-M}(1 - n^2/x^2)^{-1/2}.$$

The exact Green kernel estimate removes the previous exponential $\exp(|n^2 - 1/4|/x)$. Both strict gates $R > L + 2$ and $aR > 3L$ are checked before the bound is used.

For the four factors use arguments r, r, r, ar. Positive convolution of the retained polynomial parts, their terms of total degree at least M, and the exact product telescope for factor remainders gives

$$|\Phi_L(r) - A(r)| \leq F r^{-2}(R/r)^M, \qquad r \geq R.$$

`nicholson_remainder.py` uses the inherited positive product functional and all six determinant permutations. Reflection symmetry permits the inherited four positive offset patterns with multiplicities $1, 2, 1, 2$; it does not discard or approximate a sign population. The coefficient weights are the $\overline{w}_k$ above, and the normalizing determinant power has already been included in them. The implementation sets the artificial bounding exponent to zero; that choice is confined to the majorant.

Let $u = \Re h$. Monotone integral comparison of the sampled remainder yields

$$E_{\mathrm{Bessel}} \leq |2^{2h+1}\Gamma(1+h)/\Gamma(-h)| \frac{F R^{-2u-2}}{M + 2u + 2}.$$

The inherited gamma-ratio and log-convexity endpoint inequalities in `investigation/route_a/uniform_remainder.py` bound this expression over the whole order rectangle. Its old cell-specific trace-comparison fields are discarded: preparation return is priced instead by the translation-uniform centre theorem. The tail factor itself has no old radius dependence.

4. Rigorous radius widening and cutoff rescaling

It is unnecessary to repeat a large positive convolution merely to increase the cutoff or to give neighboring cells a positive overlap. Suppose a base receipt has lower radius z_0, upper radius Z, cutoff R_0, and positive remainder constant F_0. Choose a new lower radius $0 < \ell \leq z_0$, keeping the same L, M, Z, and set

$$\gamma = z_0/\ell, \qquad \eta = (1 - \ell^2)/(1 - z_0^2), \qquad \tau = (R_0/R)\gamma \leq 1.$$

Then valid widened bounds are

$$\boxed{F \le F_0 \eta^{27} \sqrt{\gamma}\, \tau^M, \qquad \delta_L \le \delta_{L,0} \eta^{27}.}$$

Proof. For each tilt band the one-angle determinant factor has exponent at most 9. Expanding the allowed upper value of d therefore grows its majorant by at most η^9. Three weights contribute at most η^{27}. The four-Bessel square-root prefactor grows by at most $\sqrt{\gamma}$. Each inverse argument of an eigenangle factor decreases by $R_0/R \le \tau$; each inverse direction argument decreases by at most τ. All omitted polynomial terms have total degree at least M. Every product remainder contains a degree-M term and otherwise nonnegative degrees. Its Nicholson denominator only improves because every argument has increased. Therefore the entire positive remainder functional decreases by at least τ^M before the two prefactors are restored. The preparation coefficient tails and norms depend only on the unchanged upper radius; the full determinant factor has exponent at most 27 and grows by at most η^{27}. This proves both statements.

The actual finite coefficients for the new formula are evaluated at its new R. The theorem does not reuse old coefficients with a changed meaning of $(R/r)^j$. The gate $\tau \le 1$ is checked outward and was deliberately not relaxed when initial widened designs failed it.

5. Uniform finite Abel error

For all new cells, every physical phase is nonzero and has absolute value less than π. A common phase gap is

$$g = \min(3z_- - 1,\, 3(1 - Z)) > 0, \qquad c = 2\sin(\Delta g/2) > 0.$$

The strict condition $\Delta(3 + 3Z) < \pi$ ensures $|1 - e^{\pm i\omega_m \Delta}| \ge c$ for every population. This does not make a small-detuning assumption: the inherited critical construction handles the zero-detuning radius, and the first new cell overlaps it strictly above that radius.

Here is an explicit coarse bound for the sum of all retained coefficient moduli. Put

$$W = \sum_{\ell} q_\ell^* B_\ell^2, \quad P_M(n, x) = \sum_{j=0}^{M-1} \frac{\prod_{v=1}^{j} [4n^2 + (2v-1)^2]}{8^j\, j!\, x^j}.$$

The sum of the maximum over bands is at most the sum of their norms, so $\sum_k \overline{w}_k \le W$. The inequality $|4n^2 - (2v-1)^2| \le 4n^2 + (2v-1)^2$, followed by the triangle inequality over all 16 outgoing signs and all six determinant permutations, proves

$$Q_c := \sum_{m,\pm,j<M} |c_{mj}^{\pm}| \le \frac{24 W^3}{\pi^2 \sqrt{3 z_-}} P_M(L+2, R)^3 P_M(3L, 3z_- R).$$

This bound need not use the exact Vandermonde zeros; those cancellations remain in the actual formula.

In the Abel theorem, $p_0 = 3 + 2h$, $\Re p_0 \ge 1.1$, and $|p_0 + j + t| \le \sqrt{(M + 8 + t)^2 + 36}$ for $j < M$. If C_* is the proved uniform bound for $|C_\Delta(h)|$, then the weighted Abel remainder is at most

$$\boxed{E_{\mathrm{Abel}} \le \frac{C_* Q_c K^{-.1-B}}{\Delta^2 (B + .1) c^B} \prod_{t=0}^{B-1} \sqrt{(M + 8 + t)^2 + 36}.}$$

This includes every coefficient, order, and tilt in each cell; no sampled coefficient fitting or numerical agreement is used as proof. The bound is evaluated outward in `uniform_cells.py` with $B = 64$.

6. Executed composition and overlap

All numbers below are rounded strictly upward. Each row includes the original source and image prices at its own K. The omitted original image is less than $1.819873\,10^{-31}$ in every row; original real-source and finite image contributions are still smaller.

Cell	L	M	K	Bessel	Preparation	Total
$[3/8, .5]$	168	20	8192	$9.213\,10^{-22}$	$6.248\,10^{-22}$	$1.546029\,10^{-21}$
$[.49, .6]$	240	24	8704	$6.161\,10^{-21}$	$3.935\,10^{-22}$	$6.554063\,10^{-21}$
$[.59, .7]$	360	28	16896	$5.954\,10^{-23}$	$4.489\,10^{-21}$	$4.547774\,10^{-21}$
$[.69, .8]$	624	32	33280	$1.557\,10^{-20}$	$4.752\,10^{-21}$	$2.031373\,10^{-20}$
$[.79, .9]$	1480	32	262144	$7.569\,10^{-22}$	$3.495\,10^{-19}$	$3.501607\,10^{-19}$

Here $R = K/2$ and $B = 64$. The respective Abel allowances are below $1.095\,10^{-25}$, $5.910\,10^{-52}$, $6.228\,10^{-78}$, $1.560\,10^{-75}$ and $1.132\,10^{-117}$.

The first cell overlaps the inherited interior formula on $[3/8, .4]$. Successive new overlaps are $[.49, .5]$, $[.59, .6]$, $[.69, .7]$, and $[.79, .8]$. On each overlap both independently priced analytic formulas approximate the identical physical moment, so their difference is at most the sum of their displayed absolute errors. This proves compatibility of the piecewise formula. It is not presented as independent finite-arithmetic execution of either common grid. Pointwise overlap certificates must price their actual arithmetic and identify shared prefix/image dependencies.

One deterministic convention is to use the inherited centre formula up to .3, the inherited interior formula through .4, and then the new cells successively, switching at $.5, .6, .7, .8$. Every switch lies in a proved overlap. All original rank-three radii through .9 are covered.

7. Reproduction, limitations, and useful failures

The five base remainder receipts are:

- `disk-cell-.4-.5-base.json` (L168,M20,R2048),
- `disk-cell-.5-.6-base.json` (L240,M24,R4096),
- `disk-cell-.6-.7-base.json` (L360,M28,R8192),
- `disk-cell-.7-.8-base.json` (L624,M32,R16384),
- `disk-08-09-L1480-M32-R16384-nicholson.json`.

Each is reproduced with `disk_majorant.py --nicholson` and the recorded cell, precision, degree, order, and cutoff. To recompose without overwriting the sealed receipt, run:

```
python3 upper_radius_investigation/tail/uniform_cells.py \
  --bits 384 --output upper_radius_investigation/tail/uniform-upper-cells-replay.json
```

The last base remainder itself has $F > 10^8$ at $R_0 = 16384$. This is a valid but inadequate estimate, preserved in the receipt. Raising the cutoff via the proved degree-32 contraction repairs it; no cancellation between large positive error terms is assumed. The full-box common upper resources are conservative. For example the independently complex point $z = .9, s = 2.4 + 1.8i, h = -.95 + 3i$, with L1280,M64,R32768, has an executed four-Bessel tail allowance below $1.914\,10^{-28}$. That component result is separately recorded in `point-nine-corner-L1280-M64-R32768.json`; it is not a complete scalar certificate.

The early exact singleton-radius comparison failure is retained in `disk-weight-diagnostics-failed.json`; the corrected code compares exact rationals before converting to Arb. Invalid widened designs that did not increase every Bessel argument were rejected. These failures concern representation or guards and make no negative statement about the Haar moment.

Practical costs still grow toward the upper endpoint. Preparation degree, coefficient contraction and finite-source arithmetic must be selected by their actual dominant contribution. No pointwise result may borrow the common theorem's unused arithmetic allowance, and no disk containing zero may be called a relative certificate.

The connected finite-formula theorem (O6)

Use the following common exact-arithmetic resources:

$$\Delta = 8/25, \quad K = 512, \quad b = 32, \quad p = 64, \quad k_* = K + p(b-1) = 2496, \quad t = 7/10,$$
$$P = 512, \quad L = 128, \quad Q = 256, \quad t_0 = 1,$$
$$J = 72, \quad m = 144, \quad H = 3, \quad P_i = 512, \quad L_i = 88, \quad Q_i = 256.$$

The exterior uses 256 equal bands in $[0, D]$. All strip, support, ratio, and positive-denominator gates are checked outward. In particular, $g = 7/8$ at rank five and $g = 33/40$ at rank seven.

Let $\widehat{\Phi}_N$ and $\widehat{a}_j$ denote the finite original-source approximations just specified. Define

$$\mathcal{F}_N = C_\Delta(h) \left\{ \sum_{k=1}^{2496} \rho_k k^{-1-2h} \widehat{\Phi}_N(k\Delta) - \sum_{j=0}^{71} \zeta(1+2h-2j) \widehat{a}_j \Delta^{2j} \right\}. \tag{O6.1}$$

At integer orders each complete gamma–zeta product is deflated before evaluation. The last prefix weight is zero, so including the stated last index only enlarges the error majorant.

Theorem O6.1 (Connected central absolute construction)**.** *Uniformly on* (O2.2)*,*

$$|T_5 - \mathcal{F}_5| < 3.274022395828 \times 10^{-28}, \qquad |T_7 - \mathcal{F}_7| < 2.783363232819 \times 10^{-21}. \tag{O6.2}$$

These are exact-arithmetic absolute errors of finite formulas at each input, not enclosures of the range of all moments on the box.

Proof. Add Proposition O5.2, with Lemma O5.3, to $W_{k_*} E_\Phi$, the finite image allowance, and (O4.9). All terms concern the same physical source, same filter, and same sampling step. The outward executions at 256 and 384 bits give the following strict convenient upper bounds:

N	E_{ext}	$E_{\text{real}} + E_{\text{image}}$	E_{total}
5	$3.274022395827\,10^{-28}$	$6.982895\,10^{-42}$	$3.274022395828\,10^{-28}$
7	$2.783363232818807\,10^{-21}$	$1.141004\,10^{-40}$	$2.783363232819\,10^{-21}$

The receipts retain more digits and exact source hashes. No finite preparation return is needed because the original preparation was never replaced. This proves (O6.2) on a connected radius interval, without interpolation between sampled parameter values. □

Corollary O6.2 (Join to the inherited interior construction)**.** *Combining Theorem O6.1 with inherited Haar-Critical Theorem 21.25 gives a piecewise exact-arithmetic absolute construction on* $0 \le z \le 0.9$*, throughout the original independent complex box, with respective uniform errors*

$$N = 5: \quad 5.650 \times 10^{-13}, \qquad N = 7: \quad 3.895 \times 10^{-13}.$$

The old and new domains overlap on $[0.02, 0.025]$.

Proof. Use (O6.1) below any selected switch in the overlap and the inherited piecewise formula above it. Both return the same physical scalar with their separately proved absolute errors; taking their maximum gives the displayed inherited full-radius bounds. Equality of the two finite approximants is neither asserted nor needed. □

The new source/image inequalities and their two precision replays are executed outward inequalities. The common grids of the theorem are specified exact-arithmetic formulas and have not themselves all been executed. Actual scalar certificates use the resources and finite arithmetic recorded in their individual receipts. A lower bound for the enclosed modulus is needed before an absolute disk can be reported as a relative certificate. Neither theorem asserts uniform nonvanishing or uniform runtime.

Implemented scalar readout and arithmetic contract (O9)

The entry point is odd_rank_investigation/odd.py. It accepts exact decimal or rational strings for z, the real and imaginary parts of h, and the independent parts of s. Its certified domain is $N \in \{5, 7\}$, $0 \le z \le 1/40$, and the original complex box. The source cache is fixed at 2496 consecutive lattice indices with $\Delta = 8/25$ and the exact filter $K = 512, b = 32, p = 64$. The last weight is zero; every preceding nonzero weight is retained. There is no decimated or frozen sparse prefix.

At positive radius the source adapter calls the unchanged HaarSpectral physical-source planner, witness and native kernel. Source bands use their actual preparation and direction dimensions, with target angular allowance 10^{-30} and preparation DFT ceiling 4096. The original complex Mellin image comes from the inherited coefficient and deflated readout engines. The small-radius physical restoration factor is proved to be one; the source is neither conjugated nor probability-normalized.

At the centre the source is exactly $\det[J_{j-k}(r)]_{j,k=0}^{N-1}$. Arb evaluates the determinant and checks its conversion to a 104-bit dyadic centre, with allowance 2^{-103} per sample. Its Taylor image coefficients are exact rationals from the inherited subset determinant. This avoids passing a fictitious positive translation frequency through the native header. The requested tilt remains in metadata, while the mathematical source is correctly tilt-independent.

Engine	Executed precision or arithmetic
Positive-radius native source	104-bit fixed point, explicit residual
Native preparation witness	192-bit Arb/Acb
Inherited image evaluation	256-bit Arb/Acb
Final contraction and printed centre	384-bit Arb/Acb; 85 decimal digits
Centre determinant and rational image	384-bit evaluation before checked encoding
Filter CDF and symbolic identities	Exact integer/rational arithmetic
Uniform inequalities	Separate 256- and 384-bit outward executions

The final disk adds five individually nonnegative quantities: native finite arithmetic, finite angular/source approximation, the complete Mellin image, the actual filtered terminal price, and ball accumulation plus decimal export. At exact orders $h = 0, 1, 2, 3$, the code extracts the corresponding image coefficient directly. At a nearby order it deflates the gamma–zeta product using the exact rational offset before interval multiplication. No error allowance from an unexecuted common grid is borrowed.

For centre c and total absolute allowance E, the relative gate uses $m_{\mathrm{low}} \le |c| - E$. Only when $m_{\mathrm{low}} > 0$ and $E/m_{\mathrm{low}} < 10^{-10}$ does the result receive a relative certificate. Otherwise a valid absolute disk remains an absolute result. A requested input outside the exact native rational header is refused without rounding its physical radius.

Raw executions retain their original `CANDIDATE` status. The separate certification ledger checks each physical input, its producing code and source bytes, all error components, the terminal resources and the lower-modulus test. The public interface requires a final mathematical and source audit manifest. Certified reuse of an existing cache requires its preparation hash to be an approved executed cache; a newly generated source can be used in the same verified execution. Hashes are checked before and after the readout. Internal consistency of a self-rehashed cache is not accepted as evidence that the reviewed source engine produced its rows.

The unified finite scalar and its error contract (E8)

Let $\widehat{\Phi}_k$ and $\widehat{\mathcal{I}}$ be the finite original-source prefix and complete truncated image just described. For $N = 6, 8$ take $\widehat{\mathcal{T}} = 0$ and price the original sharp terminal by (E3.8). For $N = 4$, let $\widehat{\mathcal{T}}$ be the finite retained-population tail obtained from (E5.8) and (E6.1), using the same $R = K\Delta$ as its coefficient construction. The finite formula is

$$\mathcal{F}_N = C_\Delta(h) \left[\sum_{k=1}^{K} k^{-1-2h} \widehat{\Phi}_k + \widehat{\mathcal{T}} \right] - \widehat{\mathcal{I}}. \tag{E8.1}$$

The formula at exact integer orders uses its removable coefficient value.

Theorem E8.1 (Composition on the original source)**.** *Under the hypotheses of the preceding results, the error of* (E8.1) *is bounded by the sum of its finite-source and image allowances and the following rank-specific analytic*

terminal:

$$\begin{aligned} N=6,8: &\quad E_{\mathrm{terminal}} \textit{ from } (\mathrm{E3.8}),\\ N=4: &\quad E_{\mathrm{return}}+E_{\mathrm{prod}}+|C_\Delta|\big(E_{\mathrm{Abel}}+E_{\mathrm{angular}}+E_{\mathrm{EM}}+E_{\mathcal{H},\mathrm{total}}\big). \end{aligned} \tag{E8.2}$$

Here the balanced allowances carry every actual coefficient and scale from (E4.6)*. Finite ball arithmetic and decimal export are additional allowances for an executed scalar.*

Proof. For ranks six and eight, split the exact sampled identity (E7.2) at K and apply the complete-source bound. For rank four, first replace only the terminal preparation using the exact three-term subtraction leading to (E7.3). Apply Proposition E4.2 to its finite source. Then split the complete retained population sum into its balanced and unbalanced terms and apply their independently priced readouts. The finite prefix and image throughout remain those of the original physical preparation. The triangle inequality yields exactly (E8.2). Each interface has the same radius, order, tilt, source normalization, and sharp cutoff; no missing population or unpriced return is hidden in the join. □

The common exact-arithmetic designs use $\Delta = 8/25$ and

$$(P_r, L_r, Q_r) = (512, 128, 256), \qquad (J_i, m_i, H, P_i, L_i, Q_i) = (72, 144, 3, 512, 88, 256).$$

For ranks six and eight $K = 4096$. Their executed outward allowances for the source and image, in increasing rank order, are below

$$7.434849058969 \times 10^{-41}, \qquad 1.108875178151 \times 10^{-39}.$$

Combining them with the terminal gives the uniform exact-arithmetic conclusions

$$|T_6 - \mathcal{F}_6| < 7.960261698533 \times 10^{-15}, \qquad |T_8 - \mathcal{F}_8| < 4.472333707961 \times 10^{-29} \quad \text{on } \mathcal{B}_6, \mathcal{B}_8. \tag{E8.3}$$

At rank four the retained design is $(L, M, K, B, Q, \rho, P, J) = (24, 16, 2048, 32, 1024, 1/10, 16, 160)$; its parameter-wide coefficient and readout majorants follow below. The pointwise formulas above do not borrow an unexecuted arithmetic allowance from a uniform theorem.

A complete parameter-wide rank-four bound

This subsection supplies the continuum majorants for the fixed rank-four design. Set $d_Z = 1 - Z^2$, and let $w_k^+ = |w_k(Z, 3)|$ be the absolute finite Laurent weights at the real preparation exponent $p = 7$. For every $z \le Z$ and $|s| \le 3$,

$$|(4+s)_j| \le (7)_j, \qquad |w_k(z,s)| \le w_k^+, \qquad |d^{16+8s}| \le d_Z^{-8}.$$

The first inequality follows factor by factor; at $p = 7$ all summands of each w_k have the same sign, so their absolute sum is its exact positive convolution. For $\rho \ge 0$ define positive polynomials

$$\begin{aligned} P_o^+(X;\rho) &= \sum_{j=0}^{M-1} \sum_{k=-L}^{L} w_k^+ e^{|k|\rho} |A_j(k+o)| R^{-j} X^j,\\ \beta_{mj}(\rho) &= \frac{d_Z^{-8}}{(2\pi)^2} \binom{4}{m} [X^j] \operatorname{per}[P_{c-r_0}^+(X;\rho)]_{r_0,c=0}^3. \end{aligned} \tag{E8.4}$$

Here the permanent is a finite sum over all 24 permutations with positive sign. Taking absolute values of the complete coefficient identity, and using $|\sum k_r| \le \sum |k_r|$, proves

$$\sum_n |c_{mjn}| e^{|n|\rho} \le \beta_{mj}(\rho). \tag{E8.5}$$

The binomial coefficient counts every sign placement in a norm bound; it does not assert equality of the individual signed placements. Apply the proved Vandermonde zeros before this majorant is used in the readout.

Let $\mathfrak{M}_K$ be the Euler-product rectangle-cover bound for $\sup_h |C_\Delta(h)| K^{-2\Re h}$ from (E3.9), and put

$$S = \mathfrak{M}_K \Delta^{-2} K^{-2}, \qquad X_* = 4ZR = 65.536, \qquad Q_{j,v} = \prod_{\ell=0}^{v-1} \sqrt{(9+j+\ell)^2 + 36}, \quad Q_{j,0} = 1. \tag{E8.6}$$

For $q_j = 3 + 2h + j$ its real part lies in $[1.1 + j, 9 + j]$ and its imaginary part has modulus at most six. Thus $|(q_j)_v| \le Q_{j,v}$ and $\Re q_j + v - 1 \ge j + v + 0.1$. The scale S carries the exact common power of K: the coefficient contains R^{-j} and the sampled readout contains K^j, so no degree-dependent cutoff factor is omitted.

Let F^+ be (E4.8) evaluated with the positive weights w_k^+ and physical prefactor d_Z^{-8}. This is exactly the implemented real-$s = 3$ positive product bound multiplied by d_Z^{-48}. The uniform product allowance is

$$E^*_{\mathrm{prod}} = SF^+/(M + 0.1). \tag{E8.7}$$

To state the remaining allowances compactly, set

$$b = 4Z\Delta \sinh \rho, \quad c_m = 2 \sin \frac{\Delta(|2m - 4| - 4Z)}{2}, \quad c^*_m = 2e^{-b/2} \sin \frac{\Delta(|2m - 4| - 4Z \cosh \rho)}{2}.$$

For $m \ne 2$ both lower bounds are positive on the stated design. Applying (E8.5) to (E6.5) gives

$$\begin{aligned} E^*_{\mathrm{Abel}} &= S \sum_{m \ne 2} \sum_{j=v_m}^{M-1} \frac{\beta_{mj}(0) Q_{j,B}}{(Kc_m)^B (j + B + 0.1)}, \\ E^*_{\mathrm{angular}} &= \frac{2Se^{b(K+1)}}{K(e^{Q\rho} - 1)} \sum_{m \ne 2} \sum_{j=v_m}^{M-1} \beta_{mj}(\rho) \sum_{\ell=0}^{B-1} \frac{Q_{j,\ell} e^{b\ell}}{K^\ell (c^*_m)^{\ell+1}}. \end{aligned} \tag{E8.8}$$

The finite differences are bounded at $K + 1$ by the derivative integral; replacing that endpoint by K is in the upper direction because all relevant real powers are positive. The independent phase at $K + 1$ is included in the strip factor $e^{b(K+1)}$.

The balanced Euler–Maclaurin and incomplete-integral allowances are

$$\begin{aligned} E^*_{\mathrm{EM}} &= S \sum_{j=2}^{M-1} \beta_{2j}(0) \frac{2\zeta(2P)}{(2\pi K)^{2P}} \sum_{v=0}^{2P} \binom{2P}{v} \frac{Q_{j,v} X_*^{2P-v}}{j + v + 0.1}, \\ E^*_{\mathcal{H}} &= S \sum_{j=2}^{M-1} \beta_{2j}(0) \max_{0 \le n \le 4L} \frac{(X_*/2)^{n+2J}}{J!(n + J)! \, [n + 2J + 1 - (9 + j)] \left[1 - \dfrac{(X_*/2)^2}{(J + 1)(n + J + 1)}\right]}. \end{aligned} \tag{E8.9}$$

All denominators here are strictly positive. These bounds depend only on the coefficient one-norm, so combining positive and negative modes cannot leave an unpriced factor of two. Neither expression divides by z or uses a nonzero balanced frequency.

The finite log series used in the pole deflation also admits a uniform allowance. Write $\rho_e = 1/2$, $r_e = 1/4$, and

$$e_G = \frac{\zeta(2) r_e^J}{(J + 1)(1 - r_e)}, \qquad A_G = \max(1, X_*/2)^{47/2} (3/4)^{-23} \exp\left\{\frac{\gamma}{2} + \frac{2\zeta(2) r_e^3}{3(1 - r_e^2)}\right\}. \tag{E8.10}$$

Whenever the local branch is used, its integer pole satisfies $3 \le q_0 = n + 1 + 2\ell \le 24$ and $|\varepsilon| < 1/2$. In $\alpha_\ell F(\varepsilon)$ combine the two powers of $x/2$ *before* taking absolute values. Their combined exponent lies in $[1.5, 23.5]$. There are at most 23 finite denominator factors in (E5.4), each of modulus at least $3/4$; the odd Euler series for the gamma ratio gives the exponential in A_G. Consequently $|\alpha_\ell F(\varepsilon)| \le A_G$ uniformly even as x decreases to zero. The derivative of the paired expression with respect to G is $-\alpha_\ell e^{\varepsilon G}$, including its value at $\varepsilon = 0$. Integration along the segment from exact to truncated G proves the additional allowance

$$E^*_G = S \left(\sum_{j=2}^{M-1} \beta_{2j}(0) \right) A_G e_G e^{e_G/2}. \tag{E8.11}$$

At $x = 0$ the exact branch applies. In an executed scalar this uncertainty is already included in its Acb value ball; (E8.11) prices it separately only for the literal common finite-formula theorem.

Finally the positive one-body geometric remainder gives

$$\delta^* = 8 d_Z^{-8} (1 - Z)^{-49} \binom{L + 7}{6} \frac{Z^{L+1}}{1 - Z(L + 8)/(L + 2)}. \tag{E8.12}$$

Use this in (E7.3) with the full-box moment majorant (E2.8), the full-box weighted finite prefix, and the *complete* deflated image weight. The latter two use the inherited entire gamma–zeta bounds in HaarCritical Propositions 5.4–5.6 and the completed upper-radius return, evaluated with the present K and support $D = 4(1 + Z)$. Equivalently, they are finite positive bounds for (E7.3) and (E7.4); the image weight uses 16 retained terms and its explicit functional-equation tail. Call the resulting quantity E^*_{return}.

Theorem E8.2 (Connected rank-four central construction)**.** *For every parameter in $\mathcal{B}_4$, the stated common finite formula, with its removable integer-order definition, satisfies*

$$|T_4 - \mathcal{F}_4| < 4.857160954239 \times 10^{-22}. \tag{E8.13}$$

Proof. The composition theorem bounds its error by $E^*_{\mathrm{return}} + E^*_{\mathrm{prod}} + E^*_{\mathrm{Abel}} + E^*_{\mathrm{angular}} + E^*_{\mathrm{EM}} + E^*_{\mathcal{H}} + E^*_G$ and the finite original-source/image allowance. Every summand has just been derived from a parameter-wide positive inequality. Evaluating these explicit finite inequalities with outward arithmetic at both 256 and 384 bits gives, in the same order, upper bounds

$$4.857160954239 \times 10^{-22}, \quad 1.646661 \times 10^{-36}, \quad 5.389090 \times 10^{-60}, \quad 1.371411 \times 10^{-49},$$
$$4.697607 \times 10^{-74}, \quad 7.521605 \times 10^{-90}, \quad 1.502563 \times 10^{-62}, \quad 1.068473 \times 10^{-42}.$$

The outward sum, retained at full precision in the two receipts, is $4.857160954238615183651336174694 \times 10^{-22}$ from above and is strictly smaller than the displayed bound. The rounded individual figures above are explanatory; the conclusion uses the full outward sum. This establishes a connected exact-arithmetic absolute theorem, not a finite-arithmetic evaluation at every point in the box. □

For an actual exported complex centre c, add the numerical source error, angular error, complete image error, all applicable terms of (E8.2), and the final ball/export radius to obtain E. Only if $\ell = |c| - E > 0$ can the receipt report the relative bound E/ℓ. A disk containing zero is an absolute enclosure. Successful parameter samples imply neither uniform nonvanishing nor uniform relative accuracy. Positive-radius native rows use 104-bit fixed point, their preparation witnesses 192-bit Arb/Acb, the inherited image 256-bit, and the principal final contractions 384-bit; these precisions are separate. Increasing final readout precision does not upgrade a cached source.

Both the new central constructions and inherited Theorem 21.25 approximate the identical ordinary Haar moment on the positive-width overlap $[.02, .025]$. Selection between them therefore gives connected mathematical coverage. The prescribed common grids are finite exact-arithmetic formulas; only their outward error inequalities, and the separately identified actual pointwise computations, have been executed. The numerical overlap tests retain separate error prices and identify their shared native source/image engine; independent original-circle checks challenge that common dependency.

Connected theorems and the positive-width join (E9)

Theorem E9.1 (Central and joined even-rank coverage)**.** *For each $N \in \{4, 6, 8\}$ and every parameter in $\mathcal{B}_N$, the finite formula of Section E8, with the prescribed uniform resources, satisfies the central bounds in the table immediately below ($4.857160954239 \times 10^{-22}$ at $N = 4$, $7.960261698533 \times 10^{-15}$ at $N = 6$, and $4.472333707961 \times 10^{-29}$ at $N = 8$). Selecting that formula on $[0, .025]$ and the inherited Theorem 21.25 construction on $(.025, .9]$ gives the joined bounds in the same table (7.954×10^{-11} at $N = 4$, 2.897×10^{-13} at $N = 6$, and 1.077×10^{-17} at $N = 8$) throughout the complete independent complex order and tilt box.*

Proof. For rank four use Theorem E8.2. For ranks six and eight combine the full-source tail bound of Section E3 and Corollary E3.2 with the finite source and image bounds of Section E7. The outward sums at 256 and 384 bits give the strict numerical constants stated. Both central and inherited constructions return to the same original Haar moment on $[.02, .025]$. Taking the larger bound on each joined radius interval proves the claim. No interpolation between numerical samples or assumption of nonvanishing enters this proof. □

For ranks six/eight the common mathematical resource contract is $\Delta = 8/25$, $K = 4096$, original preparation DFT size 512, retained preparation degree 128, direction size 256 and analytic strip width 1. The image uses 72 coefficients, 144 half-circle samples at complex radius 3, preparation DFT size 512, preparation degree 88 and

direction size 256. For rank four the common prefix ends at $K = 2048$, with Laurent degree 24, eigen-Bessel order 16, Abel order 32, tail direction size 1024, Euler–Maclaurin order 16 and incomplete-integral series cutoff 160. The complete common-grid formulas are specified and bounded in exact arithmetic. Actual source caches use their own adaptive resources and must price the resulting finite arithmetic independently.

Rank-four uniform component	Absolute allowance
Complete preparation return	$4.857161\,10^{-22}$
Bessel product remainder	$1.646661\,10^{-36}$
Unbalanced Abel remainder	$5.389090\,10^{-60}$
Unbalanced angular quadrature	$1.371411\,10^{-49}$
Balanced Euler–Maclaurin	$4.697607\,10^{-74}$
Incomplete Bessel integral series	$7.521605\,10^{-90}$
Finite balanced-pole deflation	$1.502563\,10^{-62}$
Finite original source and image	$1.068473\,10^{-42}$
Complete total	$4.857160954239\,10^{-22}$

Each allowance is rounded upward for presentation. The preparation return dominates the uniform rank-four bound.

Rank	Full-source terminal	Finite source and image	Complete total
6	$7.960262\,10^{-15}$	$7.434850\,10^{-41}$	$7.960261698533\,10^{-15}$
8	$4.472334\,10^{-29}$	$1.108876\,10^{-39}$	$4.472333707961\,10^{-29}$

These are parameter-wide exact-arithmetic allowances. Actual finite-source arithmetic is charged separately in pointwise runs.

Executable evaluator and finite-arithmetic contract (E10)

The reviewed public entry point is even_rank_investigation/even.py. It accepts exact rational physical inputs, covers $N = 4, 6, 8$ and $0 \le z \le 1/40$, and returns a complex disk, a full component budget, source provenance, and a recomputed modulus classification. Existing source caches require reviewed generation provenance for a certified result. A fresh cache may be generated during the verified run. Explicit candidate mode never issues a certified status. Receipts are created exclusively and are kept outside the source-cache directory.

For a final centre c and absolute error E, the modulus floor and relative bound are

$$\ell = |c|_{\mathrm{lower}} - E, \qquad \varepsilon_{\mathrm{rel}} = E/\ell \quad (\ell > 0).$$

The status is CERTIFIED_RELATIVE only if this recomputed upper bound is strictly below 10^{-10}. Otherwise the valid result is CERTIFIED_ABSOLUTE; a disk containing zero cannot earn a relative claim. An unsupported source or input is refused rather than assigned an estimated certificate.

The positive-radius native source uses the unchanged 104-bit fixed-point engine, 192-bit preparation witnesses and 256-bit image generation. Actual scalar contractions and new rank-four coefficients use 384-bit Arb/Acb in the main matrix. At the centre the determinant is generated with Arb and checked before dyadic encoding, and image coefficients are exact rational data. The displayed final precision does not increase the precision of an existing cache. Source, angular and image errors remain separate from the final ball radius. Positive-source compilation disables fast-math and floating contraction.

The original untranslated signed-direction projection is retained, followed by its exact translation Bessel contraction. A trapezoid applied after translation would require a different alias bound and is not substituted. The native positive-frequency rational header remains signed-32-bit; unsupported exact numerators or denominators are explicitly refused. No physical radius is rounded.

Actual resources and practical cost

The 21 principal caches are the seven preparations at each of three ranks. The five principal radii are $0, 10^{-6}, .01, .02, .025$, all with $s = 2.4 + 1.8\mathrm{i}$. Two more preparations at .02 use $s = -2.4 + 1.8\mathrm{i}$ and $s = 3\mathrm{i}$. Rank four stores 2048 consecutive source rows; ranks six and eight store 4096. Positive sources use the actual Fourier

bands and angular allowances recorded in each prepare.json, not the larger unexecuted common grids of the uniform theorem.

The rank-four main matrix uses $L = 24$ at positive radius. Building its reusable population coefficients usually took roughly 13 seconds in this environment; one very small-radius build took about 133 seconds because of coefficient dynamic range. Reusing the coefficients makes scalar contractions much cheaper. The public interface selects $8 \le L \le 24$ using the proved complete preparation return at the requested input, and recomputes every resulting budget. At $z = 0$ or exact nonnegative integer order it uses the corresponding simplified route. Resource selection is driven by priced error, not matching refinements.

Finite readout and heterogeneous arithmetic (A3)

An admitted inherited route supplies the original-source identity with a priced remainder

$$T_N = C_\Delta(h) \sum_{k \in \mathcal{F}} w_k \Phi(k\Delta) - I + Q + R, \qquad C_\Delta(h) = 2^{1+2h} \Delta^{-2h} \frac{\Gamma(1+h)}{\Gamma(-h)}. \tag{A3.1}$$

Here $w_k = \theta_k k^{-1-2h}$ with exact finite filter or lattice weights, I is the full Mellin image, Q is an evaluated terminal contribution if present, and R includes all explicit analytic residuals of that route. A dense filter has $0 \le \theta_k \le 1$. Sparse lattice rules can have larger weights and separate folded-alias terms; their actual weights and errors cannot be replaced by the dense formula. At exact nonnegative integer orders, the original coefficient identity is used. Near integers, the removable products are deflated before ball multiplication.

Theorem A3.1 (Mixed physical-source precision)**.** *Fix one admitted physical input and one route* (A3.1)*. For each retained index, let a numerical centre v_k satisfy the physical sample bound*

$$|\Phi(k\Delta) - v_k| \le e_k + a_k,$$

where e_k is arithmetic error and a_k is the separately priced source approximation. The rows may come from different precision, angular grids or exact frames, provided that every row returns to this same $\Phi(k\Delta)$. If the executed contraction, image and terminal produce centre c with rounding allowance E_{readout}, then

$$|T_N - c| \le |C_\Delta(h)| \sum_{k \in \mathcal{F}} |w_k| e_k + |C_\Delta(h)| \sum_{k \in \mathcal{F}} |w_k| a_k \tag{A3.2}$$

$$+ E_{\mathrm{image}} + E_{\mathrm{terminal}} + E_{\mathrm{preparation}} + E_{\mathrm{other}} + E_{\mathrm{readout}}. \tag{A3.3}$$

Every method-specific term in R is retained in E_{other}.

Proof. Insert the exact source values into the finite sum and subtract the numerical sum. The triangle inequality gives the two weighted sums. Apply the original route theorem to its unchanged weights, image and terminal, and add the executed rounding radius. There is no infinite integration of a constant source-error bound and no independence assumption. Different finite source approximants are permitted because each encloses the same original sample. □

Lemma A3.2 (Minimal prefix for an inherited suffix budget)**.** *Let $b_k \ge |C_\Delta(h) w_k| e_k$ be outward nonnegative bounds, and fix $B > 0$, $0 < \rho < 1$. Choose the least J such that*

$$\sum_{k > J} b_k \le (1 - \rho) B.$$

If the regenerated rows $1 \le k \le J$ have an actually executed weighted error at most $B - \sum_{k>J} b_k$, the complete source arithmetic is at most B.

Proof. Add the two nonnegative sums. Monotonicity proves minimality among initial prefixes for this inherited suffix requirement. It makes no global runtime optimality claim and predicts no unexecuted fine-source bound. □

For the implemented selector $\rho = 1/2$. It reports a refusal or a full-source regeneration obligation if the required prefix exceeds the resource cap. The suffix keeps its original 104-bit contract. Increasing readout precision does not relabel any old source row. For inverse orders, $k^{-1-2\Re h}$ may grow; early-row dominance is measured, never presumed.

Proposition A3.3 (Adaptive acceptance and relative certification)**.** *Suppose each proposed route and resource set has checked hypotheses and returns a complete disk $D(c, E)$. Choosing any one such disk after examining previous computations preserves containment of T_N. If an outward lower bound $\ell \le |c| - E$ is positive, then*

$$|T_N| \ge \ell, \qquad \frac{|T_N - c|}{|T_N|} \le \frac{E}{\ell}.$$

Thus the strict executed test $E/\ell < \tau$ earns the requested relative certificate. Otherwise the disk is absolute only, or is refined.

Proof. Each disk already contains the same deterministic physical quantity, so selection does not affect its validity. The reverse triangle inequality gives the modulus bound. Division by the positive lower bound proves the last inequality. No sampled parameter values prove nonvanishing elsewhere. □

The implementation serializes every error upwards, sums the resulting exact rationals, and applies the relative test to the serialized bound. It preserves the best earlier disk if a later calculation deteriorates or exhausts its resource budget. These details matter near a tight tolerance boundary.

HP2: an effective original-source arithmetic contract (A4)

The new engine uses GMP integer arithmetic with dyadic scale 2^{-B}, where $104 \le B \le 512$ and B is a multiple of eight. Its default upgraded source precision is 192 bits. Fourier grids, source preparation, image coefficients and final readout retain separate precision records. HP1 remains a preserved prototype; HP2 replaces its rounded determinant elimination by the exact construction below.

Exact Gaussian-integer determinants

Theorem A4.1 (Fraction-free determinant and quantization)**.** *Let A be a Gaussian-integer matrix. Fraction-free Bareiss elimination with recorded nonzero row pivots computes* $\det A$ *exactly, with updates*

$$A_{kl} \longleftarrow \frac{pA_{kl} - A_{kj}A_{jl}}{p_{\text{previous}}}.$$

The first previous pivot is one. Every division has zero Gaussian-integer remainder; a row swap changes the determinant sign. If a remaining pivot column is identically zero, the determinant is zero. For a stored matrix $A/2^B$, componentwise quantization of the exact determinant back to scale 2^{-B} has complex 1-norm error less than $2 \cdot 2^{-B}$.

Proof. The bordered-minor identity gives each numerator as the previous pivot times the next bordered minor. This identity is valid over the Gaussian integers; induction after each row permutation proves the fraction-free formula. The code verifies both integer remainders in $\Re(x\overline{y})/|y|^2$ and $\Im(x\overline{y})/|y|^2$ before accepting a Gaussian quotient. The final diagonal entry, with the permutation sign, is the determinant. For the dyadic matrix, divide that exact integer determinant by 2^{BN}. Truncating each real component to a multiple of 2^{-B} loses less than one unit per component. The charged allowance is the conservative $4 \cdot 2^{-B}$. □

Exact elimination removes rounding amplification inside the determinant of the stored matrix. It does not remove uncertainty in the original Gram entries. If each entry has absolute error at most ϵ and each stored entry has complex 1-norm at most M, telescoping the columns and applying Hadamard gives

$$|\det(A + E) - \det A| \le N\sqrt{N}\,\epsilon\,[\sqrt{N}(M + \epsilon)]^{N-1}. \tag{A4.1}$$

The source contract retains this full sensitivity bound. Independent exact subset-expansion determinants test the native fraction-free algorithm on 120 matrices across ranks three through eight, including row swaps, singular matrices and small pivots.

Input, waves, FFT and physical export

Put $u = 2^{-B}$. A rounded dyadic real product loses less than u; a complex product loses less than $4u$ in complex 1-norm. Constants are produced by Arb/Acb at $\max(256, B + 128)$ bits. Each encoded real component verifies

$$|2^B x - q| < 2.$$

The test is an executed enclosure; failure aborts generation. The finite arithmetic has no integer overflow, and the native guards bound source length, transform sizes, rank and physical-frame entries.

For a Bessel order l and $x \le 2(l+1)$ the engine uses a plane-wave transform on an M-point power-of-two grid. The omitted-alias estimate is

$$\frac{2\exp(x\sinh 1 + l - M)}{1 - e^{-M}} < u,$$

checked outwards. The historical fixed 10^{-32} alias floor is not reused. A conservative power-and-FFT rounding allowance is

$$e_{\text{wave}} = [32(k+1) + 64(1 + \log_2 M)]u + u.$$

For the guarded $k \le 10^6$, $B \ge 104$, accumulated root perturbations satisfy $(1+4u)^k < 1 + 5ku$. Propagate the input errors, dyadic products and normalized butterflies in complex modulus, where an exact unit phase is isometric. Convert to complex 1-norm once at the output by $|v|_1 \le \sqrt{2}|v|$; binary powering contributes less than $32(k+1)u$, the normalized transform less than $64(1+\log_2 M)u$, and the last u is the independently verified alias.

For clarity, the required norm addendum supplies a direct bound also covering independent worker starts. Unfold binary powering into a multiplication tree. At global index k there are k encoded phase leaves, each within $3u$ in modulus, and at most k rounded products, each with modulus error below $4u$. Thus the initial transform error is

$$E_0 \le [(1+3u)(1+4u)]^k - 1 < 9ku.$$

In a normalized butterfly the encoded root contributes at most $3u(1+E)/2$, the rounded product $2u$, and halving less than $2u$. Consequently a stage with $E < 1$ obeys

$$E' \le (1 + 3u/2)E + 11u/2 < E + 7u.$$

There are $q = \log_2 M \le 16$ stages, so $E_q < (9k + 7q)u < 1$ uniformly under the guards. Converting to complex 1-norm once, and allowing less than $2u$ for the converted analytic alias, gives $(14k + 10q + 2)u$. The stored allowance is $(32k + 64q + 97)u$, larger by $(18k + 54q + 95)u > 0$. The preserved original proof record is read together with arithmetic/ARITHMETIC_NORM_ADDENDUM.md; no code, constant or receipt is changed by this clarification.

When $x > 2(l+1)$, the outward J_0, J_1 seeds feed upward recurrence. The oscillator quadratic form

$$E_j(v, w) = v^2 + w^2 - 2(j/x)vw$$

has eigenvalues between $1/2$ and $3/2$. The sum of successive metric drifts is bounded by the corresponding increments $(1/x)/(1 - j/x)$, so their product is at most e. Propagating seed and local rounding errors gives the conservative $64(l+1)u$ bound. The resulting bootstrap $|J_j| < 1 + 64(l+1)u < 2$ justifies the product estimates. The branch guard excludes unstable upward recurrence near the transition.

For a retained coefficient row with complex 1-norm sum W_j, eigenangle index L, and $f = \log_2 Q$, use

$$\epsilon_j = (2L+1)16u + 2W_j e_{\text{wave}} + 32Qu + (f+1)8u(W_j + 1).$$

These terms price input coefficient error, coefficient-wave multiplication, wave transport and the unnormalized direction FFT. Apply (A4.1) with the maximum entry bound and add exact-determinant quantization. The translation bound is

$$e_{\text{tr,total}} = Q(e_{\text{tr}} + 48u) + (f+1)12uQ.$$

For each direction, with computed determinant $\widehat{d}$, translation $\widehat{t}$ and respective errors e_d, e_t, charge

$$e_d(|\widehat{t}|_1 + e_t) + |\widehat{d}|_1 e_t + 16u.$$

All reflection multiplicities are retained before averaging. Restore the physical frame exactly and price the finite Mellin contraction by Theorem A3.1.

The native diagnostic bound is a nonnegative expression evaluated in guarded floating arithmetic. The expanded dependency path has fewer than 10^8 positive operations. Integer-to-double conversion loses less than 2^{-52} relatively; the subsequent long-double path has at least 64 significand bits and remains normal under the stated guards. The total positive-expression inflation is less than

$$(1 - 10^8\, 2^{-52})^{-1} < 1.0000001.$$

The native code multiplies the diagnostic by four and adds u. The reader further enlarges its 12-digit decimal export by the exact factor $1+10^{-10}$ and another u. This makes the exported bound conservative despite rounded diagnostic formatting. The bound does not treat a displayed floating number as an exact upper bound.

The signed 32-bit frequency header is still a resource limitation. Unsupported exact rational frequencies are refused, never silently rounded. The general finite-source theorem applies to ranks three through eight, but this release admits the new HP2 *scalar* composition only for ranks four through eight; the inherited complete rank-three routes remain available.

A new connected interior/exterior overlap (A5)

Theorem A5.1 (Positive-width overlap)**.** *For $4 \le N \le 8$, $4/5 \le z \le 21/25$, and the full independent complex parameter box, the original moment has the finite filtered source/image approximation specified below with exact-arithmetic absolute error less than $3.296 \cdot 10^{-19}$.*

Use $\Delta = 8/25$. The exact rational filter is $1 - F(k)$, where F is the CDF of $8000 + U_1 + \cdots + U_{65}$, with independent uniform integers $U_j \in \{0, \dots, 52\}$. This probability notation describes filter coefficients only; it does not renormalize the complex Haar preparation. The last retained index is 11380. Take

$$Q = P = 4096, \quad L = 2040; \qquad J = 240,\ m = 528,\ H = 12,\ Q_c = 1024,\ L_c = 336,\ P_c = 8192.$$

The contour parameters are the exact decimal numbers

$$T = 0.11600374579299436, \qquad \lambda = 0.6538735309035306.$$

Proof. Apply the original signed-sector contour of HaarCritical Proposition 5.7 and its continuous-radius regional theorem to $[z_-, z_+] = [4/5, 21/25]$. For each direction panel with $\sin\phi \in [l, r]$, retain the documented bounds

$$A_0 = N z_- \sqrt{1 - r^2}, \qquad A_1 = N z_+ \sqrt{1 - l^2}\cosh\nu,$$

with its clipping at $N z_+$, and positive damping $N z_- l^2$. Every population, both spectral signs, preparation-zero exclusion and positive phase-distance gate is included. The inherited gamma-prefactor bound uses reflection, the beta integral and real-part log-convexity over the full order rectangle. The surrogate $3 + 3i$ occurs solely in a majorant for the tilt disk; it is never substituted for the physical tilt.

Executed regional inequalities at 256 and 384 bits give, with the largest value at rank eight,

$$E_{\text{terminal}} < 2.619695290702 \cdot 10^{-19}.$$

The real-source estimate inherited from Propositions 5.5–5.6 is uniform for *every real frequency*. Shifting the preparation angle in the untranslated signed direction gives a truncation bound $4V(t)e^{-Qt/2}/(1 - e^{-t})$, independent of the radial sample. The one-body preparation and determinant sensitivity estimates also use only the unit modulus of the real plane wave. Translation is contracted through its retained Bessel coefficients. Thus the common source grids remain valid when the cutoff is enlarged. Their full-box allowance is

$$E_{\text{source}} \le 3.627 \cdot 10^{-20}(11380/8202)^{1.9}.$$

This factor follows from the finite Mellin weight sum; it is not an extrapolation of a finite-frequency experiment. The original image theorem on $z \le 0.9$ gives

$$E_{\text{image}} < 7.882 \cdot 10^{-26} + 2.495 \cdot 10^{-138}.$$

The outward sum is below $3.295421566121 \cdot 10^{-19}$, proving the statement. For exact integer orders use the deflated products or direct coefficient identity. The ordinary domain is unchanged. □

The common grids define an exact-arithmetic theorem, not executed arithmetic on a continuum. Actual pointwise runs use their own priced resources. The new dense exact-source composition is valid in the overlap even where the inherited exterior executable retains its guard $z \geq 0.82$. That old guard is not modified. An independently priced pair at $N = 4, z = 0.81$ is discussed below. Its two numerical routes share source/image dependencies, so their agreement is an overlap check, not an independent verification of those shared engines.

An exact characteristic-moment route and a physical zero (A6)

Original-Haar Toeplitz identity

Theorem A6.1 (Exact $h = 0$ representation)**.** *For every $N \geq 1$, real $0 \leq z < 1$ and complex s, define*

$$c_k(s, z) = \frac{z^k(-s)_k}{k!}\, {}_2F_1(k - s, -s; k + 1; z^2), \qquad k \geq 0.$$

Then the ordinary original-Haar moment is

$$T_N(0, s; z) = \det[c_{|j-k|}(s, z)]_{j,k=0}^{N-1}.$$

It is entire in s. At $z = 0$ it equals one.

Proof. Expand both factors of $(1 - zw)^s(1 - z/w)^s$ on $|w| = 1$. Their binomial series converge absolutely and uniformly on compact s sets because $z < 1$. The coefficient of w^k is

$$\sum_{j \geq 0} \frac{(-s)_{j+k}(-s)_j}{(j + k)!j!} z^{2j+k},$$

which factors into the displayed hypergeometric series. The coefficient of w^{-k} equals this same coefficient, without complex conjugation. The normalized Haar Weyl integral and the determinant integration identity give the Toeplitz determinant. The sum of the two principal logarithms is $\log|1 - zw|^2$, a real logarithm, so this is exactly the original independent complex tilt. The logarithm of $|\Lambda_N(z)|^2$ is bounded for fixed $z < 1$, proving entire dependence on s by dominated differentiation. At $z = 0$ the Toeplitz matrix is the identity. □

The implementation uses outward Acb coefficient and determinant evaluation. It has no separate source truncation, Mellin image, preparation return or terminal. Its complete disk is the exported arithmetic radius. The general identity is proved above; the public interface in this release retains ranks three through eight and the original box. It is a distinct original-source fallback, not a change to the physical input.

A unique simple zero in the original tilt box

Let $f(s) = T_8(0, s; 9/10)$. Define s_0 by the following two finite decimal strings, interpreted as exact rationals. The line breaks below concatenate; no digits are omitted.

```
Re(s0) = 0.555315001669983057767719447793343940643436666110944
         640310748114120165446735891689938322536781453387557
Im(s0) = 2.799258042473298134858169474008631799350654702245 56
         144242654557470751657200888008129885523719904729 38
```

Authority for the centre: the unbroken exact strings in arithmetic/zero_probe/near-zero-certificate.json. Displaying a short approximation to s_0 does not define the following 10^{-50} disk.

Theorem A6.2 (A physical simple zero)**.** *There is exactly one zero, counting multiplicity, of f in $|s - s_0| < 10^{-50}$. This zero is simple and the disk lies strictly within $|s| < 3$. The rational centre s_0 itself is not the zero.*

Proof. Set $\rho = 1/10$, $\varepsilon = 10^{-12}$, $r = 10^{-50}$. The exact rational squared-norm test places the small disk inside the tilt box. On the halo $|s - s_0| \leq \rho$ its real part is positive. Since $|\Lambda_8(9/10)| \leq (19/10)^8$, Haar mass one gives

$$|f(s)| \leq M = (19/10)^{16(\Re s_0 + \rho)} < 837.034.$$

Let the exact secant be $q = [f(s_0 + \varepsilon) - f(s_0)]/\varepsilon$. Cauchy's coefficient estimates on the halo give

$$|f'(s_0) - q| \le D = \frac{M\varepsilon}{\rho^2(1 - \varepsilon/\rho)},$$

and, on $|w| = r$,

$$|f(s_0 + w) - f(s_0) - f'(s_0)w| \le \frac{M(r/\rho)^2}{1 - r/\rho}.$$

Hence

$$|f(s_0 + w) - qw| \le |f(s_0)| + Dr + \frac{M(r/\rho)^2}{1 - r/\rho}.$$

Outward evaluation of the exact endpoints and all elementary bounds gives

$$\begin{aligned} |q| &> 0.0054957804957159511, \\ D &< 8.370331603736 \cdot 10^{-8}, \\ |f'(s_0)| &> 0.0054956967923999137, \\ |f(s_0)| + Dr + M(r/\rho)^2/(1 - r/\rho) &< 8.370331603736 \cdot 10^{-58}, \\ |q|r &> 5.4957804957159511 \cdot 10^{-53}. \end{aligned}$$

The strict Rouché inequality compares $f(s_0+w)$ with qw. The latter has one zero, counting multiplicity. Therefore f has precisely one, and that zero is simple. An outward 640-bit evaluation at the exact rational centre also gives

$$|f(s_0)| > 1.4233567593610471642 \cdot 10^{-104},$$

with disk radius below $3.960 \cdot 10^{-185}$, so the centre is not itself zero. □

A separate original-Haar calculation verifies the theorem without using the hypergeometric coefficients, Mellin engine or native source. It forms outward Toeplitz coefficients by a 4096-point angular transform with an explicit analytic strip/alias bound, then repeats the same secant/Cauchy/Rouché argument. A further 8192-point, 768-bit computation at s_0 gives an absolute radius below $6.882 \cdot 10^{-178}$ and relative bound below $4.835 \cdot 10^{-74}$. These checks are independent in source representation, though they share the Arb/Acb arithmetic library.

Corollary A6.3 (Nonvanishing and local noninteger orders)**.** *Uniform nonvanishing on the original independent complex parameter box is false. Moreover, at fixed $N = 8, z = 9/10$, the simple zero extends locally to a holomorphic zero curve $s = s(h)$ through $h = 0$.*

Proof. The first statement follows from Theorem A6.2. For the second, ordinary integrability on compact subdomains of $\Re h > -1$, with bounded preparation at this fixed radius, gives joint holomorphy in (h, s) near the point. Logarithmic factors from differentiation are controlled by slightly stronger locally integrable powers. The derivative with respect to s is nonzero at the simple zero, so the holomorphic implicit function theorem applies. □

This last statement is qualitative: no effective h-neighborhood or noninteger zero enclosure is claimed. Computing such a neighborhood is a specific next mathematical task.

Near-zero arithmetic and representation selection (A8)

At the exact rational s_0 of Theorem A6.2, the inherited 256-bit image gives centre zero with absolute radius below $1.369 \cdot 10^{-67}$. The true value at that rational point is nonzero but has modulus only about $1.42336 \cdot 10^{-104}$. Consequently this image disk contains zero and cannot support relative certification. Displaying more digits from the old image would not change that fact.

The direct original-Haar Toeplitz fallback recomputes the coefficient source. At 256 bits it also returns a zero-containing disk, with radius below $6.273 \cdot 10^{-70}$. At 512 bits an actual public adaptive run obtains

$$E < 1.332 \cdot 10^{-146}, \qquad E/\ell < 9.358 \cdot 10^{-43}.$$

A capped 256-bit run deliberately retains an absolute-only answer. The independent 8192-point original-source readout separately resolves the same small nonzero rational-centre value. The exact zero theorem concerns the nearby disk, not a mistaken claim that the rational centre equals the zero.

This is a real physical conditioning challenge. It also demonstrates why the original objective correctly conditions relative accuracy on a positive modulus test. At a true zero, relative error is not an appropriate scalar criterion; a valid absolute disk remains the meaningful output.

Dispatch, exact inputs and complete output contracts (A9)

The public entry is unified_investigation/unified.py. Inputs are exact rational strings or finite decimal strings; binary floating-point and Boolean physical inputs are refused. The rank, radius, order rectangle and independent tilt disk are checked with rational arithmetic. Decimal strings such as `0.025` mean exactly 1/40.

Family	Rank and radius	Principal readout
Rank-three centre	$N = 3$, $[0, .3]$	Retained translation
Rank-three critical	$N = 3$, $[.25, .4]$	Four-Bessel tail
Rank-three upper	$N = 3$, $[.4, .9]$	Effective finite Abel readout
Odd central	$N = 5, 7$, $[0, .025]$	Original-source contour
Even central	$N = 4, 6, 8$, $[0, .025]$	Balanced or absolute contour
Interior filtered	$N = 4, \ldots, 8$	Actual-order sparse or dense source
Upper filtered	$N = 4, \ldots, 8$	Exterior signed-source filter
Positive mass	$N = 4, \ldots, 8$, $\Re h \geq 2$	Positive-order tail
Characteristic exact	$h = 0$, all admitted radii	Original-Haar Toeplitz

The exact executable guards and default choices are in dispatch/routes.py. The inherited exterior executable starts at 0.82; the new dense composition supports the proved $[0.80, 0.84]$ overlap. The default central branches join interior coverage on a positive-width overlap. A branch's source length, spacing, exact filter, frame, preparation and image must match its terminal contract. Two routes need not have identical finite approximants simply because they approximate the same Haar moment.

A successful result records the exact physical input, outward complex disk, all error components, actual generating precisions, route and proof reference, source and code identities, resource history, and the strict lower-modulus test. The classifications are:

`CERTIFIED_RELATIVE` Complete reviewed disk with positive lower modulus and strict requested relative tolerance.

`CERTIFIED_ABSOLUTE` Complete reviewed disk, with relative or requested tolerance explicitly unmet if applicable.

`CANDIDATE_*` An exploratory calculation without final review and origin authorization. Numerically small printed bounds do not promote it.

`REFUSED`**/resource limit** Unsupported exact input, missing proved composition, incomplete arithmetic, unapproved reused source, or insufficient resources. This is not a claim of ordinary-moment divergence.

The final review requires an explicit runtime implementation closure, proof closure and executed audit gates. Reused data need a reviewed generation origin separate from their current hash. Fresh generation occurs inside an empty round directory and is bound before and after execution. Recursive data snapshots include integer image files, mixed-source subdirectories and every actual JSON/data source used. A source cache cannot certify itself by replacing its own digest. External tail coefficient files have the same origin requirement; supplying a nonexistent external tail is refused rather than silently creating an untracked artifact.

HP1 remains a candidate prototype. Reviewed upgraded calls use HP2 `exact` or `mixed-exact`. The predecessor exterior branch is not silently entered through an option. A conflicting dependency-root environment override is refused. The review is a reproducibility and mathematical authority boundary, not a security claim against an adversary who can rewrite every source and every retained review record.

Local noninteger zero theorem (Z1)

For U Haar distributed on $U(N)$, define

$$\Lambda_N(z) = \det(I - zU), \qquad S_N(z) = -(1-z^2)\frac{\Lambda_N'(z)}{\Lambda_N(z)}, \qquad T_N(h,s;z) = \mathbb{E}\big[|S_N(z)|^{2h}|\Lambda_N(z)|^{2s}\big]. \tag{Z1.1}$$

The radius is real. Complex powers of positive quantities use the real logarithm: $x^{2h} = \exp(2h\log x)$ for $x > 0$. The order h and tilt s vary independently. Values on the probability-zero mark set are handled through the ordinary integrability conditions, never through an assumed bounded logarithm or an unidentified analytic continuation. Throughout, $\mathbb{D}(c,E) = \{w \in \mathbb{C} : |w-c| \le E\}$ denotes a closed complex enclosure disk; root-counting boundaries are specified separately.

The continuing target is all $1 \le N \le 8$, $0 \le z \le 0.9$, $-0.95 \le \operatorname{Re} h \le 3$, $|\operatorname{Im} h| \le 3$, and $|s| \le 3$, with relative error below 10^{-10} wherever the ordinary moment exists and a positive modulus bound permits relative certification. This construction advances the local zero and modulus problem. It does not replace the global evaluator programme.

The preceding unified investigation established connected exact-arithmetic absolute constructions for ranks three through eight. Their largest inherited connected bounds are preserved in Table 19. They are not universal finite-arithmetic relative certificates. In particular, the proved rank-eight complex zero disproves uniform nonvanishing on the original parameter box.

Table 19: Inherited connected exact-arithmetic absolute approximation bounds on $0 \le z \le 0.9$. No new claim of practical uniform relative coverage is made by reproducing this ledger.

Rank	Absolute bound	Rank	Absolute bound
3	1.955759×10^{-17}	6	2.897×10^{-13}
4	7.954×10^{-11}	7	3.895×10^{-13}
5	5.650×10^{-13}	8	1.077×10^{-17}

Hereafter set $F(h,s,z) = T_8(h,s;z)$ and

$$z_0 = \frac{9}{10}, \qquad H = \frac{1}{100}, \qquad \rho = \frac{3}{500}, \qquad \delta = \frac{1}{50000000}. \tag{Z1.2}$$

The exact rational complex number s_0 is the complete finite-decimal input in the inherited file unified_investigation/arithmetic/zero_probe/near-zero-certificate.json. Its complete digits are printed in Appendix Z14. A shortened decimal is never substituted into a theorem or physical source. The inherited zero s_* obeys $|s_* - s_0| < 10^{-50}$ at $h = 0, z = z_0$; the rational centre itself is not asserted to be the zero.

Theorem Z1.1 (Connected noninteger zero and modulus geometry)**.** *For every complex $|h| \le H$ and real $z_0 - \delta \le z \le z_0$, the ordinary moment $F(h,\cdot,z)$ has exactly one zero, counted with multiplicity, in $|s - s_0| < \rho$. This zero is simple and defines a single branch $\alpha(h,z)$. The branch is holomorphic in h for $|h| < H$, with continuous extension to the closed disk, and is C^1 in the real radius, with endpoint derivatives read inward on the stated physical interval.*

On the full product domain there is an exact factorization

$$F(h,s,z) = (s - \alpha(h,z))G(h,s,z), \qquad |G(h,s,z)| > \frac{1}{400}. \tag{Z1.3}$$

Consequently, a complete physical residual enclosure $F(h,a,z) \in \mathbb{D}(c,E)$ at an admitted exact tilt a gives

$$|a - \alpha(h,z)| \le 400(|c| + E). \tag{Z1.4}$$

If $\alpha(h,z) \in \mathbb{D}(a,r)$, then on the same physical (h,z) fibre,

$$|F(h,s,z)| \ge \frac{1}{400}\max\{0, |s-a| - r\}. \tag{Z1.5}$$

The theorem is proved by the analytic constructions and the explicit outward inequalities in Sections Z3–Z8; it is not inferred from interpolation between the executed pointwise tests.

The interval has genuine, though small, width 2×10^{-8}. Its endpoint is the original target $z = 0.9$. Nothing in this theorem silently extends the physical target to radii above 0.9. The h disk contains real and imaginary noninteger orders of both signs, and the tilt remains an independent complex variable throughout the containing product domain.

Physical scalar samples and arithmetic contracts (Z6)

The inherited finite-source and Mellin formulas are used within their proved domains. A source sample $\Phi(k\Delta)$ depends on N, z, s, Δ, not on the order used to choose a finite scalar filter. Changing h therefore reuses the same physical source only when the image, weights and terminal allowance are repriced for that h. Nearby values of s or z require fresh physical preparations and images; relabelling the original cache would be incorrect.

The decisive baseline replay reproduces the original h=0 zero enclosure and a difficult $N = 8, z = 0.9, h = 3 + 3i, s = 2.4 + 1.8i$ scalar certificate. The latter has complete error below 2.007×10^{-14} and relative error below 4.606×10^{-16} under the unchanged inherited review. A fresh source at $h = 10^{-4}, s = s_0$ initially had terminal-dominated complete error about 9.469×10^{-15}. The resource repair targets that component.

The stronger exact finite filter has

$$K = 2316, \quad b = 30, \quad p = 39, \quad K + p(b-1) = 3447. \tag{Z6.1}$$

Its transition law is the integer coefficient sequence of $(1 + x + \cdots + x^{b-1})^p / b^p$, shifted by K. The resource proposal is not an error estimate: the actual terminal theorem is evaluated outward at every physical input. The central source extends an existing 1812-row source by 1635 consecutive rows with their own angular band. Every old byte and its return allowance is preserved. The full nearby sources at $s_0 \pm 10^{-5}$ and at the real tilt v_0 are independently generated with the unchanged native witness, frame, kernel and image producer.

Proposition Z6.1 (Finite source composition)**.** *Suppose an admitted finite scalar formula has weights w_k, prefactor C, and physical source samples Φ_k. If $|\Phi_k - v_k| \le a_k + e_k$, where a_k is source-approximation error and e_k is arithmetic error, then the source contribution to the scalar error is at most*

$$|C| \sum_k |w_k| a_k + |C| \sum_k |w_k| e_k. \tag{Z6.2}$$

The full scalar disk must additionally include the actual image, terminal, aliases where applicable, and read-out/export errors.

Proof. Subtract the two finite sums, use the samplewise physical bounds, and apply the triangle inequality. Add the separately proved returns of the complete scalar identity. No infinite integration of a constant source error occurs, and no independence or cancellation assumption is needed. □

Every scalar sample in the Cauchy construction carries the complete set

$$E = E_{\text{finite arithmetic}} + E_{\text{prepared/direction}} + E_{\text{image}} + E_{\text{filtered terminal}} + E_{\text{readout}}. \tag{Z6.3}$$

The new composition preserves native generating precision: 104-bit fixed point samples are not advertised as higher precision merely because the final Arb contraction uses 384 or 512 bits. The previous HP2 repair remains available where needed. The present small-order source is adequate after the stronger terminal filter is installed and fully repriced.

Exact physical inputs, origin records, old and new snapshots, sample indices, angular bands, frame factors, image identity and producer hashes are checked. A self-rehashed modified cache is not a reviewed generation origin. New candidate calculations retain their labels until the distinct continuation review admits their source and composition proof. The old sealed review and receipts are not edited.

Measured Cauchy jets with complete coefficient returns (Z7)

Take $r = 1/100$, $R = 1/50$, $M = 6$, and $Q = 64$ nodes. At each of the three exact tilts s_0, $s_0 + \epsilon$, $s_0 - \epsilon$, where $\epsilon = 10^{-5}$, let $f(h) = F(h, s, z_0)$. For $\omega_j = e^{2\pi ij/Q}$, the exact discrete Cauchy coefficient is

$$A_n = \frac{1}{Qr^n} \sum_{j=0}^{Q-1} f(r\omega_j)\omega_j^{-n}, \qquad 0 \le n < Q. \tag{Z7.1}$$

If $f(h) = \sum_{m\ge 0} a_m h^m$, absolute convergence and the finite root-of-unity sum give the exact alias identity

$$A_n = a_n + \sum_{q\ge 1} a_{n+qQ} r^{qQ}, \qquad |A_n - a_n| \le MR^{-n} \frac{(r/R)^Q}{1 - (r/R)^Q}. \tag{Z7.2}$$

This folded coefficient alias is retained even when the numerical nodes agree to many printed digits.

The physical evaluator accepts exact rational or finite-decimal inputs. If its actual node h_j differs from $r\omega_j$ by at most d_j, Cauchy's derivative bound along the joining segment prices the displacement by

$$\frac{Md_j}{R - r - d_j}. \tag{Z7.3}$$

The nodes have executed displacement below 10^{-95}. Their complete scalar errors and (Z7.3) are propagated with factor $1/(Qr^n)$. Acb encloses transcendental phases and finite contraction. Its exact exported centre displacement is included. Thus each stored disk encloses the actual Taylor coefficient of the ordinary physical moment.

The three sets of 64 nodes are extended to degree $D = 60$ without regenerating or silently changing their source values. The constant term is replaced by the independently evaluated exact h=0 Toeplitz formula after checking it against the original Cauchy disk. On $|h| \le H$, the omitted analytic tail is

$$\tau(h) = \frac{6(|h|/R)^{D+1}}{1 - |h|/R}. \tag{Z7.4}$$

An independent reconstruction checks all coefficient radii, including the degree-60 extension, at higher precision. Agreement of scalar samples is not the source of their error bounds; the complete contracts in Section Z6 are.

Tilt stencils, Rouché inequality, and the derivative cone (Z8)

Define the exact analytic stencil functions

$$\begin{aligned} A(h) &= F(h, s_0, z_0), \\ B_\epsilon(h) &= \frac{F(h, s_0 + \epsilon, z_0) - F(h, s_0 - \epsilon, z_0)}{2\epsilon}, \\ C_\epsilon(h) &= \frac{F(h, s_0 + \epsilon, z_0) - 2F(h, s_0, z_0) + F(h, s_0 - \epsilon, z_0)}{2\epsilon^2}. \end{aligned} \tag{Z8.1}$$

Taylor's theorem on the real tilt segment, using (Z5.11), gives

$$|B_\epsilon - F_s(h, s_0, z_0)| \le \frac{138\epsilon^2}{6}, \qquad |C_\epsilon - F_{ss}(h, s_0, z_0)/2| \le \frac{673\epsilon^2}{24}. \tag{Z8.2}$$

The denominator 24 in the second bound matters: C_ϵ approximates $F_{ss}/2$. The h-tail returns of these three quantities are τ, τ/ϵ, and $2\tau/\epsilon^2$, respectively.

Write $w = s - s_0$. The quadratic model, with its coefficient/stencil returns understood, satisfies

$$F(h, s, z) = A(h) + B(h)w + C(h)w^2 + R_F, \qquad |R_F| \le \frac{138|w|^3}{6} + 196|z - z_0|, \tag{Z8.3}$$

$$F_s(h, s, z) = B(h) + 2C(h)w + R_s, \qquad |R_s| \le \frac{138|w|^2}{2} + 4464|z - z_0|. \tag{Z8.4}$$

The complex tilt Taylor remainder is an integral along its straight segment. The real-radius return follows from Proposition Z4.2 and the actual connected derivative bounds. No parameter derivative of a truncated source formula is substituted for either remainder.

Choose the freely specified exact rational comparison coefficient

$$q = -0.00509705027622045760618345746163 - 0.00205515978420007602261962966788\,i. \tag{Z8.5}$$

This coefficient is not an assertion that a rounded value equals F_s. The complete disk coefficients and all returns yield uniform outward bounds

$$A_{\max} < 1.767367 \times 10^{-5}, \quad B_{\mathrm{diff}} < 4.711484 \times 10^{-5}, \quad C_{\max} < 0.02362729, \tag{Z8.6}$$

for $|A|$, $|B-q|$, and $|C|$ on $|h| \le H$. Exact rational outward endpoints, rather than these explanatory decimals, are recorded in uniform-geometry.json.

Proof of Theorem Z1.1. On the tilt boundary $|w| = \rho$, compare F with qw. The perturbation is bounded by

$$P = A_{\max} + 196\delta + B_{\mathrm{diff}}\rho + C_{\max}\rho^2 + \frac{138\rho^3}{6}. \tag{Z8.7}$$

The actual outward execution gives

$$P < 2.769494 \times 10^{-5}, \qquad |q|\rho > 3.297468 \times 10^{-5}, \qquad |q|\rho - P > 5.279750 \times 10^{-6}. \tag{Z8.8}$$

Rouché's theorem gives precisely one zero counted with multiplicity for every admitted pair (h, z). The same data control the derivative throughout the entire tilt disk:

$$|F_s - q| \le \eta := B_{\mathrm{diff}} + 2C_{\max}\rho + \frac{138\rho^2}{2} + 4464\delta. \tag{Z8.9}$$

The executed bounds are

$$\eta < 0.002903923, \qquad |q| - \eta > 0.002591858 > \frac{1}{400}. \tag{Z8.10}$$

Hence the zero is simple. Local holomorphic implicit-function branches in h and C^1 branches in the real radius agree on their overlaps by uniqueness in the common disk. They form the asserted connected branch. The inherited zero lies on this branch because its 10^{-50} disk lies inside the present tilt disk.

For any admitted s, convexity keeps the segment joining α and s inside the disk. The exact identity

$$G(h, s, z) = \int_0^1 F_s(h, \alpha + t(s-\alpha), z)\,\mathrm{d}t \tag{Z8.11}$$

places G in the same complex disk $\mathbb{D}(q, \eta)$. This gives $|G| \ge |q| - \eta > 1/400$ and also $|G| \le |q| + \eta$. Equations (Z1.4) and (Z1.5) follow by the factorization and the triangle inequality. □

Remark Z8.1 (Why a common complex disk is required). A positive pointwise lower bound for $|F_s|$ alone would not bound the modulus of the integral in (Z8.11): its phase could change along the segment. The common complex derivative cone is the additional information that makes the factor and modulus readout valid. Independent reconstruction checks both strict inequalities; a proposed false floor $1/200$ is rejected.

Certified parameter derivatives at the zero branch (Z10)

The local implicit identities are

$$\alpha_h = -\frac{F_h}{F_s}, \qquad \alpha_z = -\frac{F_z}{F_s}. \tag{Z10.1}$$

This section supplies derivative enclosures with actual analytic returns.

Differentiated Cauchy jets and remainders

If a stored coefficient is $a_n \in \mathbb{D}(c_n, e_n)$, its derivative contribution is nc_nh^{n-1} with radius $ne_n|h|^{n-1}$. Differentiating the analytic Cauchy majorant gives, for $x = |h|/R < 1$,

$$\tau_1(h) = \frac{6}{R}\frac{x^D((D+1) - Dx)}{(1-x)^2}. \tag{Z10.2}$$

At h=0 the first derivative is exactly the a1 coefficient, and this tail is zero. The coefficient itself still contains its sample, alias, displacement and arithmetic error.

For a specified $|h| < H$, write $g = H - |h| > 0$. The exact stencil errors in (Z8.2) are analytic functions of h, uniformly bounded on $|h| \le H$. Cauchy's inequality bounds their h derivatives by their bounds divided by g. The same argument applies to the cubic tilt and real-radius returns. Therefore, in addition to differentiated coefficient uncertainty, the h-derivative readout prices

$$\begin{aligned} E_{h,\text{tail}} &= \tau_1(1 + |w|/\epsilon + 2|w|^2/\epsilon^2), \\ E_{h,\text{stencil}} &= (138\epsilon^2|w|/6 + 673\epsilon^2|w|^2/24)/g, \\ E_{h,\text{tilt}} &= 138|w|^3/(6g), \qquad E_{h,\text{radius}} = 196|z - z_0|/g. \end{aligned} \tag{Z10.3}$$

These differentiate actual analytic error functions, not bare numerical values. This readout refuses $|h| = H$, where its particular Cauchy distance vanishes; it does not infer a physical derivative singularity there.

For F_s, the h-tail and stencil allowances are

$$\frac{\tau}{\epsilon} + \frac{4\tau|w|}{\epsilon^2}, \qquad \frac{138\epsilon^2}{6} + \frac{673\epsilon^2|w|}{12}, \tag{Z10.4}$$

and the remaining returns are $138|w|^2/2 + 4464|z - z_0|$. On an actual root disk $\mathbb{D}(a, r)$, put $W = |a - s_0| + r$ in all majorants. The midpoint derivative polynomials are evaluated at $a - s_0$ and their exact linear or quadratic variation across the disk is added separately. Thus the derivative disks enclose the derivatives at every point in the root disk, not merely at its rounded centre.

For disks $F_h \in \mathbb{D}(n, e_n)$, $F_s \in \mathbb{D}(d, e_d)$, set $L = \max(1/400, |d| - e_d)$. The common cone proves $|F_s| \ge L$. When $d \ne 0$,

$$\left|-\frac{F_h}{F_s} + \frac{n}{d}\right| \le \frac{e_n}{L} + \frac{|n|e_d}{|d|L}. \tag{Z10.5}$$

Acb evaluation and exact centre export of $-n/d$ add their own component.

Precise anchor slopes and noninteger derivative evidence

At h=0, the original-Haar Toeplitz coefficients are

$$c_k(z) = \frac{(-s)_k}{k!}z^k {}_2F_1(k - s, -s; k + 1; z^2), \qquad k \ge 0, \tag{Z10.6}$$

with $c_{-k} = c_k$ for this symmetric original symbol. Hypergeometric differentiation and determinant multilinearity give F_z and F_{zz} by column replacements, avoiding inversion of a nearly singular matrix. Indeed Weyl's eigenangle formula, with its squared Vandermonde expanded and the resulting one-angle factors integrated, gives exactly $F(0, s, z) = \det[c_{j-k}(z)]_{j,k=0}^{7}$. Differentiating this finite determinant replaces one column for the first derivative. The second derivative replaces one column twice and adds twice the terms with two distinct differentiated columns. The complex preparation remains unchanged. An independent original-circle trapezoid calculation differentiates the weight e^{sL} as sL_ze^{sL} and $((sL_z)^2 + sL_{zz})e^{sL}$. With 4096 nodes and strip width 1/20, explicit analytic alias bounds enclose its coefficients. It shares neither the hypergeometric coefficients nor the radial Mellin source.

At the exact rational anchor the original-source derivatives have centres

$$\begin{aligned} F_z &\simeq -0.0156216722408102851 - 0.0691064861824699146\,i, \\ F_{zz} &\simeq -0.7325973165111925651 + 0.6388209608971487015\,i. \end{aligned}$$

The independent angular derivative radii are below 6.064×10^{-77} and 5.585×10^{-75}. These are h=0 derivative checks, not an extension of second-radius regularity to noninteger order.

To obtain the h slope at the true zero, use the central a1 disk and the independently evaluated F_s disk. For $r_* = 10^{-50}$ the larger halo gives

$$|F_{hs}| \le \frac{6}{R(1/10 - r_*)}, \qquad |F_{ss}| \le \frac{12}{(1/10 - r_*)^2}. \tag{Z10.7}$$

Multiplication by r_* prices the displacement from s_0 to s_*. The resulting true-zero derivatives are

$$\begin{aligned} \alpha_h(0, z_0) &\in \mathbb{D}(0.29885174381756456413 - 0.10224962556310426142\,i, 3.186 \times 10^{-15}), \\ \alpha_z(0, z_0) &\in \mathbb{D}(-7.338505878066439982506 - 10.599205638170013784001\,i, 5.16 \times 10^{-15}). \end{aligned} \tag{Z10.8}$$

The displayed-centre rounding displacements are included in the stated radii. The underlying receipts retain still more precise exact rational centres and their complete outward budgets. These slope centres do not replace the exact physical tilt input.

All eight actual noninteger root records have separately priced F_h, F_s and α_h disks; the derivative table below reports them. The uniform physical bound and cone also give

$$|\alpha_z| \le 196/(1/400) = 78400. \tag{Z10.9}$$

This is effective but broad. No fine pointwise noninteger z slope is claimed. The h-slope disks near the h-domain boundary and inward radius endpoint are also broad because the Cauchy and radius-return components dominate. More final arithmetic precision would not remove that analytic limitation.

h	z	Centre for α_h	Disk radius upper
$0.002 + 0.003i$	0.9	$0.295334729 - 0.106036633i$	6.12556×10^{-3}
$0.002 + 0.003i$	0.89999998	$0.295334627 - 0.106037095i$	1.26633×10^{-1}
$0.002 + 0.003i$	0.89999999	$0.295334678 - 0.106036864i$	6.58780×10^{-2}
$0.008 + 0.005i$	0.9	$0.286731771 - 0.107212659i$	2.43590×10^{-1}
$-0.001i$	0.9	$0.299052989 - 0.100814351i$	4.09946×10^{-4}
$0.001i$	0.9	$0.298635200 - 0.103682481i$	4.11947×10^{-4}
-0.001	0.9	$0.300293529 - 0.102459730i$	4.15371×10^{-4}
0.001	0.9	$0.297425258 - 0.102041941i$	4.06618×10^{-4}

Table 20: Physical branch h-derivative disks, including all differentiated Cauchy, stencil, tilt and radius returns and display rounding. The wider disks near the h boundary and at inward radii reflect effective analytic bounds, not an observed singularity.

The independent derivative audit reconstructs all components at 768 bits and separately checks the anchor F_s by a 1024-bit secant with an analytic remainder. All eight branch derivative disks and the true-zero anchor slope pass this audit. It is distinct from final source-admission authority.

Supporting sparse heterogeneous-precision composition (Z11)

The main result uses the dense physical source. A separate supporting result closes a restricted sparse composition gap without changing the sealed evaluator. Its admitted domain is the inherited exterior two-rate inverse construction: $N = 4, \dots, 8$, $0.82 \le z \le 0.9$, $-0.95 \le \operatorname{Re} h < 0$, $|\operatorname{Im} h| \le 3$, $|s| \le 3$, subject to each query's terminal and folded-alias inequalities. No arbitrary sparse stencil or positive-real-order extension is asserted.

Let $A(k)$ and $B(k)$ be the exact rational CDFs of the switch and terminal filters. Their finite transition laws are shifted coefficients of $(1 + x + \cdots + x^{b-1})^p / b^p$. The retained weight is exactly

$$\theta(k) = 1 - A(k) + 2\mathbf{1}_{k \text{ even}}(A(k) - B(k)) = 1 - B(k) + (-1)^k (A(k) - B(k)). \tag{Z11.1}$$

The factor two compensates the sampling rate. The second identity exposes a dense terminal rule and two signed tail returns. The complete ordinary terminal, switch odd alias, and terminal odd alias therefore remain present. The implementation checks the inherited nonoverlapping-filter conditions, $0 \le \theta(k) \le 2$, and zero weight for every omitted positive index. Physical index k, native row j, and stride r obey $k = rj$ and are never identified without that map.

Theorem Z11.1 (Restricted sparse heterogeneous source return)**.** *Fix one admitted source, its exact filters and complete inherited image/terminal identity. For each retained k, let $|\Phi(k\Delta) - v_k| \le e_k + a_k$ in physical source units. Put*

$$w_k = \theta(k)k^{-1-2h}, \qquad C = 2^{1+2h}\Delta^{-2h}\frac{\Gamma(1+h)}{\Gamma(-h)}.$$

A complete scalar enclosure is obtained with radius

$$|C|\sum_k |w_k|e_k + |C|\sum_k |w_k|a_k + E_{\text{image}} + E_{\text{terminal}} + E_{\text{switch odd alias}} + E_{\text{terminal odd alias}} + E_{\text{readout}}. \tag{Z11.2}$$

Different retained rows may have different arithmetic precision and angular grids if each has a proved return to the same physical source sample.

Proof. The exact identity (Z11.1) supplies the same finite weights and the same three terminal/alias returns before and after replacement. Apply Proposition Z6.1 to the finite changed sample sum, then retain the unchanged image and terminal identities. A higher-precision subset changes only its sample values and their actual error bounds. It does not change the unchanged suffix's precision or remove a folded alias. □

Old sparse coordinates return to physical units with the exact factor divisor$^N 2^{2\sum_j e_j}$ from their native frame. Their rounding allowance is retained. New HP2 rows use the reviewed exact Gaussian-integer determinant engine and its modulus-to-one-norm addendum. The actual old image contractor is preserved; an algebraically equivalent new image midpoint is not silently substituted. Source snapshots and generating identities bind each retained physical index.

The executed challenge uses $N = 4, z = 0.9, s = 12/5 + 9i/5$, with 40 freshly generated 192-bit HP2 samples replacing a prefix of an unchanged 2672-sample sparse source. At $h = -10^{-8}$ the complete error decreases from $5.711589309269262 \times 10^{-24}$ to $5.908617957319812 \times 10^{-25}$, crossing the requested 10^{-24} absolute target. The source term decreases from $5.622893791775091 \times 10^{-24}$ to $5.021663719256126 \times 10^{-25}$; the fine term is below 1.015×10^{-54}. Both aliases remain priced.

At $h = -0.001$ and $h = -0.001 \pm 0.001i$, the source improvement factor exceeds 11.12. At $h = -0.95 + 3i$, the same early 40 rows yield only a factor 1.014. This adverse result is retained: early-prefix dominance must be measured, not assumed for deep inverse orders. An independent integer sliding convolution verifies 5078 filter-index identities. Dropping the stride-two factor changes the deep-order scalar by more than 38.3008; all four wrong-weight controls exceed twice the correct complete radius. A rank-mismatched HP2 source is rejected. All 40 replaced rows independently overlap their inherited physical-source enclosures, but their error bounds come from their own arithmetic contracts, not that overlap.

Exact anchor and physical parameter definitions (Z14)

The following text reproduces the complete exact finite-decimal centre. Line wrapping is typographical only; concatenating each decimal's digit blocks gives the exact input. The authoritative source remains the inherited JSON receipt and its bound hash.

Real part:

```
0.555315001669983057767719447793343940643436661109446403107481141201654467358916899383225
36781453387557
```

Imaginary part:

```
2.799258042473298134858169474008631799350654702245561442426545574707516572008880081298855
2371990472938
```

All source tilts in the stencil are formed by exact rational addition of $\pm 1/100000$ to this real part, not by editing a short printed decimal. The positive transport measure uses the full exact real part with zero imaginary part. The physical radius endpoints are exactly 9/10 and 44999999/50000000. Every root and off-branch result binds its own exact rational h, s, z and original preparation.

Real-radius extension of the zero theorem (T1)

For Haar-distributed $U \in U(N)$, the physical moment is

$$\Lambda_N(z) = \det(I - zU), \qquad S_N(z) = -(1-z^2)\frac{\Lambda_N'(z)}{\Lambda_N(z)}, \tag{T1.1}$$

$$T_N(h, s; z) = \mathbb{E}\big[|S_N(z)|^{2h}|\Lambda_N(z)|^{2s}\big]. \tag{T1.2}$$

Positive real moduli use their real logarithms in the complex powers. The ultimate target remains $1 \le N \le 8$, $0 \le z \le 0.9$, $-0.95 \le \operatorname{Re} h \le 3$, $|\operatorname{Im} h| \le 3$, and independent $|s| \le 3$. Relative error below 10^{-10} is sought wherever the ordinary expectation exists and a positive modulus bound permits it. The existence of complex zeros prevents any assertion of uniform nonvanishing on this box.

Here $F(h, s, z) = T_8(h, s; z)$. The inherited exact tilt centre s_0 is the full rational pair in near-zero-certificate.json; the displayed approximation

$$s_0 \simeq 0.55531500166998305777 + 2.79925804247329813486\,i$$

is for orientation only. Every implementation reads the full rational pair. The inherited $h = 0, z = 0.9$ theorem locates a unique simple zero within 10^{-50} of this centre. The centre itself is not asserted to be a zero.

The previous noninteger investigation proved one unique simple zero for each $|h| \le .01$, $z \in [.89999998, .9]$ in the tilt disk of radius .006, with $F = (s - \alpha)G$ and $|G| > 1/400$. Its uniform bounds were $|F_z| < 196$, $|F_{zs}| < 4464$, and $|\alpha_z| \le 78400$. It also supplied a real-radius absolute-integrand halo bounded by 6 on $|h| \le .02$, $|s - s_0| \le .1$, and $.899 \le z \le .9$. The successful Hölder-11/4 receipt, rather than the earlier unsuccessful exponent-2 estimate, is the dependency used here.

Theorem T1.1 (Wider physical continuation)**.** *On*

$$|h| \le \frac{1}{100}, \qquad \frac{8999}{10000} \le z \le \frac{9}{10}, \qquad |s - s_0| \le \frac{3}{500},$$

the original rank-eight ordinary moment has exactly one zero $\alpha(h, z)$ in the tilt disk, counted with multiplicity. This zero is simple. The branch is holomorphic in h, real analytic in z, and satisfies

$$F(h, s, z) = (s - \alpha(h, z))G(h, s, z), \qquad |G| > \frac{1}{380}.$$

On the full stated physical parameter region,

$$|F_z| < \frac{32}{25}, \qquad |\alpha_z| < 286.$$

The new branch agrees with the inherited branch on their entire overlap.

This theorem combines analytic proofs with executed outward inequalities and admitted physical coefficient disks. Its constants do not arise from interpolation of successful root samples. The exact certificate closure and the distinction between proof and execution are recorded in the executed results in Section T7 and the reproduction ledger in the editable source bundle.

Connected interpolation with the complete physical return (T4)

Set $z_c = .89995$, $\ell_z = .00005$, $t = (z - z_c)/\ell_z$, and $t_j = -1 + j/6$, $0 \le j \le 12$. The thirteen exact physical radii are $z_j = 8999/10000 + j/120000$. Let

$$\Omega(t) = \prod_{j=0}^{12}(t - t_j), \qquad L_j(t) = \frac{\Omega(t)}{(t - t_j)\Omega'(t_j)}.$$

The circle $|\xi| = 8$ is inside the radius halo of Theorem T3.3, and paired nodes give

$$|\Omega(\xi)| \ge D_\Omega = 8\prod_{k=1}^{6}(64 - (k/6)^2).$$

The actual contour interpolation identity gives, for $|t| < 8$,

$$E_0(t) = \frac{2048 \cdot 8\,|\Omega(t)|}{D_\Omega(8-|t|)}, \tag{T4.1}$$

$$E_1(t) = \frac{2048 \cdot 8}{D_\Omega \ell_z}\left(\frac{|\Omega'(t)|}{8-|t|} + \frac{|\Omega(t)|}{(8-|t|)^2}\right). \tag{T4.2}$$

These bound respectively the interpolation remainder and its physical radius derivative. Equation (T4.2) differentiates the actual analytic remainder; it is not a derivative inferred from matching numerical samples.

At every radius the three tilts $s_0, s_0 \pm \varepsilon_s$ use $\varepsilon_s = 10^{-5}$. Each h jet has 64 physical circle samples of radius .01, degree 60, and the inherited analytic halo of radius .02. Its coefficient disks include actual scalar errors, aliasing, node displacement, and arithmetic. The constant coefficient is replaced by the independent exact $h = 0$ Toeplitz return only after an enclosure overlap check. The unrepresented h tail is

$$\tau(h) = 6\frac{(|h|/.02)^{61}}{1-|h|/.02}.$$

The common analytic remainder after radius interpolation of the exact h Taylor polynomials is bounded by

$$e = E_0 + \sum_j |L_j|\tau, \qquad e_z = E_1 + \ell_z^{-1}\sum_j |L_j'|\tau.$$

Actual finite coefficient errors remain separately weighted by $|L_j|$ or $|L_j'|/\ell_z$.

Lemma T4.1 (Common tilt remainder)**.** *If one analytic function is bounded by E on $|s - s_0| \le r$, its centered first difference at step ε_s is bounded by $E/(r-\varepsilon_s)$; its centered half-second difference is bounded by $E/(r-\varepsilon_s)^2$.*

Proof. The first difference is the average of the first derivative along the real segment. The half-second difference is a weighted average of half the second derivative. Cauchy's inequalities bound the derivatives by $E/(r-\varepsilon_s)$ and $2E/(r-\varepsilon_s)^2$ respectively. □

The radius and h remainders are common analytic functions on the full tilt halo $r = .1$. Lemma T4.1 is therefore applicable. Applying a separate absolute error at each stencil point would instead introduce ε_s^{-1} and ε_s^{-2} and discard this information. The independently rounded physical coefficient errors do not share this analytic correlation and retain their actual stencil weights.

On the physical interval the inherited bounds are $|F_{sss}| < 138$ and $|F_{ssss}| < 673$. The first and half-second stencil returns are therefore $138\varepsilon_s^2/6$ and $673\varepsilon_s^2/24$. The executable obtains uniform bounds A_*, B_*, C_* for

$$|F(h, s_0, z)|, \quad |F_s(h, s_0, z) - q|, \quad |F_{ss}(h, s_0, z)/2|,$$

where q is the exact rational complex reference retained from the inherited geometry. Radius polynomials use exact rational cardinal coefficients and outward interval cells. A distinct implementation uses Newton divided differences and a finer partition. The two implementations share the physical sample evidence; neither is described as an independent physical source.

Zero geometry and differentiated continuation (T5)

With $\rho = .006$, Rouché's theorem applies when

$$A_* + B_*\rho + C_*\rho^2 + B_3\rho^3/6 < |q|\rho. \tag{T5.1}$$

It gives one zero counted with multiplicity, hence a simple zero. The common derivative cone has radius

$$\eta_s = B_* + 2C_*\rho + B_3\rho^2/2.$$

If $\eta_s < |q|$, integration on the segment from the zero to s proves $F = (s-\alpha)G$ with $|G| \ge |q| - \eta_s$. A pointwise nonzero derivative would not suffice for this integrated lower bound.

A thin complex-radius tube

To control the differentiated tilt remainder without a huge global Cauchy constant, use the upper and lower half disks centered at .89995 with radius $R = .0004$. Original-Haar logarithmic tilt estimates on their real diameter $[.89955, .90035]$ give

$$A_3 < 138.037703, \qquad A_4 < 677.058489.$$

The selected Hölder resource is $a = 6$, with tilt-log shifts 13/20 and 31/40. These real radii above .9 are auxiliary proof points, not an extension of the public target. The flow formula agrees there with the real physical moment. On the curved boundaries, tilt Cauchy bounds give $B_k = k!2048/(.094)^k$.

For $\tau = \zeta - .89995$ in the upper half disk, harmonic measure of the arc is

$$\omega(\tau) = \frac{2}{\pi} \arg \frac{R + \tau}{R - \tau}.$$

The subharmonic maximum principle gives $|\partial_s^k F| \le A_k^{1-\omega} B_k^{\omega}$. The lower half uses the same scalar function at fixed h,s with the corresponding lower-half harmonic function; no physical tilt is conjugated. On

$$\operatorname{Re} \zeta \in [.899895, .900005], \qquad |\operatorname{Im} \zeta| \le .000005,$$

the maximum is $\omega_* = (2/\pi) \arctan(80/3139) < .016221268$. Outward composition proves

$$|F_{sss}| < 167, \qquad |F_{ssss}| < 847.$$

The complex-radius interval model verifies (T5.1) and a common factor floor 1/500 on this rectangle. Unique local branches therefore glue to a holomorphic zero branch there. This alone yields $|\alpha_z| \le .006/.000005 = 1200$ on the physical interval.

Sharper actual physical radius derivatives

Differentiate the actual interpolation formula and its h polynomial return. Let A_z, B_z, C_z bound the radius derivatives of the three tilt coefficients. In addition to the actual physical coefficient errors and e_z, the stencil-to-derivative returns are priced by Cauchy on the thin radius tube:

$$\frac{167\varepsilon_s^2}{6\varepsilon_z}, \qquad \frac{847\varepsilon_s^2}{24\varepsilon_z}, \qquad \varepsilon_z = .000005.$$

The differentiated cubic tilt remainder is at most $167|s - s_0|^3/(6\varepsilon_z)$. Consequently

$$|F_z| \le A_z + B_z\rho + C_z\rho^2 + \frac{167\rho^3}{6\varepsilon_z}. \tag{T5.2}$$

This is a bound for the original physical moment.

At a zero, a stronger radius bound follows by beginning with $r = \rho$ and repeatedly applying the outward update

$$r \;\leftarrow\; \min\left(r, \frac{A_*}{|q| - B_* - C_* r - 138r^2/6}\right)$$

when the denominator is positive. The zero's own tilt Taylor equation justifies each update. On the resulting root disk,

$$|F_s(h, \alpha, z)| \ge |q| - B_* - 2C_* r - 138r^2/2.$$

Use r in (T5.2) and divide by this lower bound. The executed results and independent repetitions are recorded below; they prove $|F_z| < 32/25$ and $|\alpha_z| < 286$. Thus Theorem T1.1 includes effective physical derivative control, rather than only a wider existence region.

Sharper derivatives at a genuine noninteger zero (T6)

Endpoint transport without an unintegrable second derivative

The second method fixes the original Haar ensemble and separates a small mark region from its complement. Write $X_j = |S(z_j)|$ and use the unnormalized reference measure $\mathrm{d}\mu = |\Lambda(z_0)|^{2v_0}\mathrm{dHaar}$, where $v_0 = \operatorname{Re} s_0$. Executed positive moments bound its mass M and $\int X_0^{-q}\mathrm{d}\mu$, $\mathbb{E}[X_1^{-q}|\Lambda(z_1)|^{2v_0}]$, with $q = 1.9$. These are actual new endpoint data, not silently reused old-radius bounds.

For $t = |z_1 - z_0|$, let L bound $|S_z|$, split at $X_0 = 2Lt$, and set $R_c = 3Lt$. On the outer region, $X(z) \geq X_0/2$, so a Taylor remainder can be bounded there by the available inverse q moment. On the inner region, subtract the same reference power R_c^{2h} at both endpoints before taking absolute values. The estimate

$$|x^{2h} - R_c^{2h}| \leq \frac{2|h|}{e(q-2|h|)} R_c^{q-2|h|} x^{-q}, \quad 0 < x \leq R_c,$$

retains a factor of $|h|$. It follows by integrating the complex power in logarithmic radius and maximizing the resulting exponential-log function. The preparation, mark, and cross terms are retained explicitly. The complete six-term bound is in `ENDPOINT_RADIUS_DIFFERENCE.md` and its independently reimplemented 1024-bit audit. Its leading behavior is $O(t^{q-2|h|})$ for the difference remainder.

For the forward endpoints $z_1 > z_0$ used below, set $t = z_1 - z_0$. For $J(h, s, z) = F(h, s, z) - F(0, s, z)$, the centered construction removes the order-zero contribution exactly. If R_J is its proved endpoint remainder,

$$F_z(h, a, z_0) = \frac{F(h, a, z_1) - F(h, a, z_0)}{t} - \frac{F(0, a, z_1) - F(0, a, z_0)}{t} + F_z(0, a, z_0) + \mathcal{D}(0, R_J/t). \tag{T6.1}$$

Here a is the exact candidate tilt. The h=0 terms use that same tilt and the independent original-Haar Toeplitz formula. Both physical scalar disk radii, divided by the exact t, are added to (T6.1).

Exact short rational step and root displacement

At $z_0 = 8999/10000$ we execute both $t = 10^{-9}$ and the smaller exact step

$$z_1 = \frac{260979100}{290009001}, \qquad t = \frac{1}{2900090010000}.$$

The Bézout identity $10000 \cdot 260979100 - 8999 \cdot 290009001 = 1$ proves the difference. The native frequency for $dt = 8/25$ is $8z_1 dt = 668106496/290009001$, which fits the inherited signed-32 header. This changes the deliberately selected finite-difference resource; it does not round a requested physical input. Both endpoints are freshly prepared.

At the same exact candidate, centered physical tilt differences and warm order differences enclose F_s and F_h. Their respective analytic returns are $138\varepsilon_s^2/6$ and

$$\frac{6\varepsilon_h^2}{r_h^3[1 - (\varepsilon_h/r_h)^2]}, \qquad r_h = .02 - |h|.$$

The actual scalar errors divided by the step are separately retained. The chosen step minimizes the complete demonstrated error, not just the difference between printed derivative values.

If a physical disk $\mathcal{D}(f, E)$ is returned at candidate a, the factor theorem gives $|a - \alpha| \leq 380(|f| + E)$. Candidate-to-zero derivative changes are bounded using $|F_{ss}| < 33$, $|F_{hs}| \leq 6/(r_h r_s)$, and $|F_{zs}| \leq 2048/(.0004 r_s)$, with the complete positive tilt margin r_s. The tiny root disk makes the last, coarse mixed-derivative bound usable. For disks $\mathcal{D}(n, E_n)$ and $\mathcal{D}(d, E_d)$ at the true zero, $L = |d| - E_d > 0$ gives the quotient error

$$\left| -\frac{F_p}{F_s} + \frac{n}{d} \right| \leq \frac{E_n}{L} + \frac{|n|E_d}{|d|L}, \qquad p = h, z,$$

plus the explicit finite quotient/export allowance.

A sharper local modulus cone

The executed actual-root F_s disk implies a common derivative cone on $|s-\alpha| \le 10^{-5}$, using $|F_{ss}| < 33$. The resulting local factor floor is $1/200$. If the saved root disk is $\mathcal{D}(a, r_\alpha)$, an exact query b may use

$$|F(h,b,z)| \ge \frac{1}{200}(|b-a| - r_\alpha)$$

when $|b-a|+r_\alpha \le 10^{-5}$ and the lower distance is positive. This stronger bound belongs to the executed physical fiber; it is not promoted to a uniform constant on the whole parameter neighborhood.

Explicit centred endpoint budget (T11)

This appendix states the complete endpoint allowance used for the physical noninteger radius slopes. It is a first-difference theorem; it does not assume an absolutely integrable second-radius derivative of the moment. All expectations below use the same original Haar matrix.

Fix $N = 8$, two real radii $.899 \le z_0 < z_1 \le .9$, and $t = z_1 - z_0 > 0$. Put $v_0 = \operatorname{Re} s_0$, $q = 19/10$, and suppose $|h| \le H \le .01$ and $|s - s_0| \le \rho \le .006$. Define $X_j = |S_N(z_j)|$ and $L_j = \log|\Lambda_N(z_j)|^2$. Let rigorous positive ordinary-moment bounds satisfy

$$M_0 \ge \mathbb{E}e^{v_0 L_0}, \qquad A_0 \ge \mathbb{E}[X_0^{-q} e^{v_0 L_0}], \qquad A_1 \ge \mathbb{E}[X_1^{-q} e^{v_0 L_1}]. \tag{T11.1}$$

These bounds refer to the unnormalized measure $\mathrm{d}\mu = e^{v_0 L_0}\mathrm{dHaar}$. The endpoint-1 preparation is returned to that same measure explicitly below. The executed bounds are read from complete physical scalar disks at their exact respective radii.

Set $z_- = z_0$, $z_+ = z_1$ and define

$$\begin{aligned}
D &= N(1+z_+), & L &= \frac{N(1+z_+^2)}{1-z_+^2}, \\
L_2 &= \frac{2N}{1-z_+} + \frac{4Nz_+}{(1-z_+)^2} + \frac{2N(1-z_-^2)}{(1-z_+)^3}, \\
B_1 &= \frac{2N}{1-z_+}, & B_2 &= \frac{2N}{(1-z_+)^2}, & L_{\max} &= 2N\log\frac{1}{1-z_+}, \\
s_* &= |s_0| + \rho, & v_* &= |v_0| + \rho, \\
k &= 2H, & p &= 1+k, & a &= 2+k, \\
b &= 2Lt, & R_c &= 3Lt, & \kappa &= \frac{1}{2}, \\
C &= D^{4H}, & P &= \exp(\rho L_{\max} + v_* B_1 t), & A_{1,\mu} &= e^{|v_0|B_1 t} A_1, \\
A_p &= M_0^{1-p/q} A_0^{p/q}.
\end{aligned}$$

Require $R_c < 1$. Here $p < q < 2$ automatically on the stated order disk. The physical pointwise inequalities are $|S| \le D$, $|S_z| \le L$, $|S_{zz}| \le L_2$ and $|\partial_z \log|\Lambda|^2| \le B_1$, $|\partial_z^2 \log|\Lambda|^2| \le B_2$. The bound on S_{zz} is a smooth pointwise statement, not an assertion that an inverse-moment second derivative is integrable.

Define

$$\begin{aligned}
K_2 &= 2H(1+2H)L^2, \\
K_1 &= 2HL_2 + 4Hs_*B_1L, \\
K_0 &= s_*B_2 + s_*^2 B_1^2.
\end{aligned}$$

For any exact r with $k < r \le q$, put

$$\begin{aligned}
J_{\mathrm{out}} &= 2H\left[D^{2H}\log(D)M_0 + \frac{\kappa^{-r}M_0^{1-r/q}A_0^{r/q}}{e(r-k)}\right], \\
J_{\mathrm{in}} &= 2Hb^{q-k}\left[\log\frac{1}{b} + \frac{1}{e(q-k)}\right]A_0.
\end{aligned}$$

The executed actual-root cases select $r = 4/5$ from a finite exact rational grid of individually valid bounds. No optimality claim is needed.

Proposition T11.1 (Six-term centred endpoint return)**.** *Let $J(h,s,z) = F(h,s,z) - F(0,s,z)$. Under the preceding hypotheses,*

$$|J(h,s,z_1) - J(h,s,z_0) - tJ_z(h,s,z_0)| \le R_J, \qquad R_J = R_1 + R_2 + R_3 + R_4 + R_5 + R_6,$$

where the six nonnegative, explicitly computable terms are

$$R_1 = \frac{t^2 PC}{2} K_2 \kappa^{-a} b^{q-a} A_0, \qquad R_2 = \frac{t^2 PC}{2} K_1 \kappa^{-p} A_p, \tag{T11.2}$$

$$R_3 = \frac{t^2 P}{2} K_0 J_{\mathrm{out}}, \qquad R_4 = P \frac{2H}{e(q-k)} R_c^{q-k} (A_0 + A_{1,\mu}), \tag{T11.3}$$

$$R_5 = Pt\, 2HL\, b^{q-p} A_0, \qquad R_6 = \frac{t^2 P}{2} K_0 J_{\mathrm{in}}. \tag{T11.4}$$

All six terms vanish at $H = 0$. Reversing endpoints requires changing the reference measure and endpoint-positive returns together; one does not reuse this forward formula with an unsigned secant.

Proof. Split the original Haar source into $E = \{X_0 \le b\}$ and its complement. On E^c, every intermediate mark is at least κX_0. For $g_h(x) = |x|^{2h}$, the real gradient and Hessian satisfy

$$\|Dg_h(x)\| \le 2HC|x|^{-p}, \qquad \|D^2 g_h(x)\| \le 2H(1+2H)C|x|^{-a}.$$

Write the integrand relative to μ as $\psi(z) g_h(S(z))$, where $\psi(z) = \exp(s \log|\Lambda(z)|^2 - v_0 L_0)$. Its smooth preparation obeys $|\psi| \le P$, $|\psi'| \le P s_* B_1$, and $|\psi''| \le P K_0$. Taylor's theorem only on E^c gives R_1, R_2, R_3. In R_1, use $X_0^{-a} \le b^{q-a} X_0^{-q}$ there; Hölder in the same finite measure gives A_p in R_2. For R_3, the centred mark is $g_h - 1$. Splitting its modulus at $X = 1$ and using $\log(1/X) X^{-k} \le X^{-r}/[e(r-k)]$ gives J_{out}. The exponent $a > 2$ is never integrated without its outer cutoff.

On E, both endpoint marks are at most $R_c < 1$. For $0 < x \le R_c$,

$$|x^{2h} - R_c^{2h}| \le \frac{2H}{e(q-k)} R_c^{q-k} x^{-q}.$$

Indeed, the logarithmic integral is bounded by $2Hx^{-k}\log(R_c/x)$, and $ye^{-(q-k)y} \le 1/[e(q-k)]$. Subtract the same R_c^{2h} at both endpoints before taking absolute values. For $\widetilde{g}_j = g_h(S(z_j)) - 1$ the exact identity

$$\psi_1 \widetilde{g}_1 - \psi_0 \widetilde{g}_0 - t(\psi_0' \widetilde{g}_0 + \psi_0 g_0') = \psi_1(\widetilde{g}_1 - \widetilde{g}_0) - t\psi_0 g_0' + (\psi_1 - \psi_0 - t\psi_0')\widetilde{g}_0$$

gives R_4, R_5, R_6. Returning X_1^{-q} to μ supplies $A_{1,\mu}$ in R_4. The inequality $X_0^{-p} \le b^{q-p} X_0^{-q}$ on E supplies R_5. Writing $\log(1/X_0) = \log(1/b) + \log(b/X_0)$ gives J_{in} in R_6. Only the smooth preparation is Taylor expanded on this inner set.

The inherited first-radius differentiation and its uniform integrability permit identification of the integrated first derivative. Combining the fixed source split proves the claim. The result neither integrates a raw second-radius moment derivative nor estimates an uncontrolled numerical difference by agreement. □

For actual scalar disks at the two endpoints, the full candidate F_z readout is

$$\frac{F(h,s,z_1) - F(h,s,z_0)}{t} - \frac{F(0,s,z_1) - F(0,s,z_0)}{t} + F_z(0,s,z_0) + \mathcal{D}(0, R_J/t).$$

Both noninteger scalar error radii are divided by the exact t and retained. The order-zero correction is evaluated at the same exact tilt and receives its complete ball error; finite evaluation and exported-centre error are also added. For the Farey endpoint, the executed analytic allowance is $R_J/t < 9.914734 \times 10^{-9}$, while the two physical scalar returns total less than 1.794425×10^{-8}. The final receipt additionally prices movement from the rational candidate to the true zero.

A global radius interpolant on exact physical inputs (M4)

Set $z = z_c + \ell t$, with $z_c = .8995$, $\ell = .0005$. The ideal degree-40 Lobatto nodes are $-\cos(j\pi/40)$, $0 \le j \le 40$. Their selected nearby physical nodes are exact rationals on the mesh $1/(640000000)$. Each actual radius is passed unchanged to the physical source engine. This is a choice of interpolation resources, not silent rounding of a requested input.

If $z_j = k/(640000000)$, the native frequency is

$$8z_j\frac{8}{25} = \frac{k}{250000000},$$

before reduction; all numerator and denominator headers fit signed 32-bit integers. The normalized node displacement is at most $1/640000$ and is also checked individually by outward trigonometric evaluation. Write

$$\Omega(t) = \prod_{j=0}^{40}(t - t_j), \qquad L_j(t) = \prod_{k\neq j}\frac{t - t_k}{t_j - t_k}.$$

Every coefficient is rational. Evaluation never divides by $t - t_j$.

Lemma M4.1 (Radius contour and its differentiated remainder)**.** *For the unchanged actual nodes, the physical moment minus its exact radius interpolant has uniform error*

$$E_0 < 4.433222928 \times 10^{-9},$$

and the physical first radius derivative error is

$$E_1 < 7.416966943 \times 10^{-4}.$$

Convenient independently checked allowances are $E_0 < 1/200000000$ and $E_1 < 3/4000$.

Proof. Use the Bernstein ellipse with parameter $\varrho = 52/25$, semiaxes

$$a = \frac{3329}{2600}, \qquad b = \frac{2079}{2600}.$$

Its maximum distance from the real segment is b; its minimum contour distance is $g = a - 1$. Hence its physical distance from $[.899, .9]$ is at most

$$\ell b = \frac{2079}{5200000} < \frac{1}{2500},$$

with positive margin $1/5200000$. It lies in the inherited analytic source domain, with the same majorant 2048.

For ideal Lobatto nodes, writing $t = (w + w^{-1})/2$ gives

$$\Omega_0(t) = 2^{-41}(w - w^{-1})(w^{40} - w^{-40}).$$

If the actual maximum node displacement is bounded by $\delta < g$, then on the ellipse

$$|\Omega(t)| \ge \mathcal{D} = 2^{-41}(\varrho - \varrho^{-1})(\varrho^{40} - \varrho^{-40})(1 - \delta/g)^{41} > 0.$$

The ellipse length is at most $2\pi a$. The exact contour identity and its derivative therefore give, for every physical t,

$$E_0(t) \le \frac{2048a|\Omega(t)|}{\mathcal{D}g}, \tag{M4.1}$$

$$E_1(t) \le \frac{2048a}{\mathcal{D}\ell}\left(\frac{|\Omega'(t)|}{g} + \frac{|\Omega(t)|}{g^2}\right). \tag{M4.2}$$

For stable global evaluation retain the cancellation

$$\Omega_0 = 2^{-40}(T_{41} - T_{39}), \quad \|\Omega_0\|_\infty \le 2^{-39}, \quad \|\Omega_0'\|_\infty \le 40\,2^{-38}.$$

The last inequality follows from $|\sin(40\theta)| \le 40|\sin\theta|$; separately bounding the two Chebyshev derivatives would overpay. Convert $\Omega - \Omega_0 = \sum d_k T_k$ with exact rational arithmetic. Then

$$\|\Omega\|_\infty \le 2^{-39} + \sum|d_k|, \qquad \|\Omega'\|_\infty \le 40\,2^{-38} + \sum k^2|d_k|.$$

Substitution produces the displayed outward bounds. Local interval bounds may be intersected with these global allowances. No differentiated uncontrolled numerical formula or original-space F_{zz} integral is used. □

The complete noninteger parameter readout (M5)

Let c be the full exact rational midpoint of the independently checked $h = 0, z = .8995$ zero, read from its point certificate. Prepare the five exact tilts $c + k\epsilon$, $k = -2, -1, 0, 1, 2$, with $\epsilon = 1/200$. At each of the 41×5 preparations, 48 exact rational order nodes near the circle $|h| = .01$ provide degree-44 Cauchy coefficient disks. Node displacement, Fourier aliases, the actual physical scalar budget, and coefficient contraction are separately included. The constant is replaced by the exact original-Haar $h = 0$ Toeplitz value only after the two disks are checked to overlap.

For the exact omitted h tail, put $x = |h|/.02 \le 1/2$ and $D = 44$. Then

$$\tau = 6\frac{x^{D+1}}{1-x}, \tag{M5.1}$$

$$\tau_h = \frac{6}{.02}x^D\left(\frac{D+1}{1-x} + \frac{x}{(1-x)^2}\right). \tag{M5.2}$$

At a fixed physical radius, let $\mathrm{Leb} = \sum_j |L_j(t)|$ and $\mathrm{Leb}_z = \sum_j |L_j'(t)|/\ell$. Replacing the true radius-node functions by their exact h Taylor polynomials leaves one analytic error function of tilt satisfying

$$E = E_0 + \mathrm{Leb}\,\tau, \quad E_z = E_1 + \mathrm{Leb}_z\,\tau, \quad E_h = E_0/.01 + \mathrm{Leb}\,\tau_h. \tag{M5.3}$$

The h derivative of the radius remainder is justified by the full h halo. It does not differentiate independently rounded physical data.

For $w = s - c$, define

$$\Omega_s(w) = w(w^2 - \epsilon^2)(w^2 - 4\epsilon^2).$$

The complex Hermite–Genocchi identity represents the exact quartic tilt remainder as Ω_s times the fifth divided difference. Its simplex volume is $1/5!$; differentiating its last node repeats that node. The convex hull of the five nodes and all admitted query tilts stays in $|s - s_0| \le .025$. Consequently

$$|R| \le 4106|\Omega_s|/120, \tag{M5.4}$$

$$|R_s| \le 4106|\Omega_s'|/120 + 24405|\Omega_s|/720, \tag{M5.5}$$

$$|R_z| \le 12140|\Omega_s|/(120/50000), \tag{M5.6}$$

$$|R_h| \le 14632|\Omega_s|/(120 \cdot .01). \tag{M5.7}$$

The radius and h inequalities follow by applying Cauchy's theorem to the actual analytic remainder. In particular, on $|w| \le .013$ the new radius-differentiated tilt remainder is below .003433, compared with the inherited quadratic model's 1.2024 allowance.

The common error in (M5.3) must not be replaced by unrelated noise at the five tilt nodes. Its halo about c has radius $R_s = .09$; $|c - s_0| + .09 < .1$ is checked. Set $r = |w|$ and

$$D_s = R_s(R_s^2 - \epsilon^2)(R_s^2 - 4\epsilon^2).$$

The contour identity for that error gives

$$K_0 = 1 + \frac{R_s|\Omega_s(w)|}{D_s(R_s - r)}, \tag{M5.8}$$

$$K_1 = \frac{1}{R_s - r} + \frac{R_s}{D_s}\left(\frac{|\Omega_s'(w)|}{R_s - r} + \frac{|\Omega_s(w)|}{(R_s - r)^2}\right). \tag{M5.9}$$

Its value, tilt derivative, radius derivative, and order derivative returns are respectively EK_0, EK_1, E_zK_0, and E_hK_0.

If e_{jkn} is the actual error of the coefficient scaled by $(.01)^n$, the independent finite value error is

$$E_{\mathrm{fin}} = \sum_{j,k,n} |L_j(t)I_k(w)|e_{jkn}\left|\frac{h}{.01}\right|^n.$$

The derivative errors replace I_k by I'_k, L_j by L'_j/ℓ, or the order power by $n|h/.01|^{n-1}/.01$, as appropriate. Thus no independent rounding errors acquire a fictitious common analytic correlation. The implementation conservatively uses $|h/.01|^n \le 1$ (and the analogous derivative bound) in these independent arithmetic sums even for point queries. All final contractions and serialized disk centres retain their own outward arithmetic allowances.

Moving charts, uniqueness, and connected branch identity (M6)

The eleven exact anchors are $z_j = .899 + j/10000$, $0 \le j \le 10$. Their tilt centres c_j come from separately proved h=0 point zeros. Define

$$I_j = [z_j - 3/40000, z_j + 3/40000] \cap [.899, .9], \qquad \mathcal{C}_j = \{|h| \le .01,\ z \in I_j,\ |s - c_j| \le .006\}.$$

All disks lie within the common global query disk $|s - c| \le .013$. Their radius intervals overlap with positive width.

For each chart, translate the full polynomial exactly before interval evaluation. Expand in $\xi = (s-c_j)/\rho$, $\rho = .006$, and $h/.01$. The radius cells are complete rational intervals. Affine polynomial shifts retain coefficient cancellation before taking norms; summing order powers then covers the entire complex order disk.

Theorem M6.1 (Effective chart and gluing criterion)**.** *Let $q_j \neq 0$ be an exact complex reference. Suppose the complete polynomial, analytic, and finite error bounds on a chart establish*

$$\sup_{|s-c_j|=\rho} |F(h,s,z) - q_j(s-c_j)| < |q_j|\rho, \qquad \sup_{|s-c_j|\le\rho} |F_s(h,s,z) - q_j| \le \eta_j < |q_j|.$$

Then each admitted (h,z) has exactly one simple zero $\alpha_j(h,z)$ in the disk. On the whole disk,

$$F(h,s,z) = (s - \alpha_j(h,z))G_j(h,s,z), \qquad |G_j| \ge \gamma_j := |q_j| - \eta_j > 0.$$

If adjacent charts have a positive radius overlap and an earned bound $A_j \ge \sup|F(h,c_j,z)|$ there, the strict inequality

$$A_j/\gamma_j + |c_j - c_k| < \rho_k$$

proves identity of their zeros throughout the full order/radius overlap.

Proof. Rouché's theorem counts one zero with multiplicity; hence it is simple. The convex tilt disk contains the segment from its zero to each query, so

$$G_j = \int_0^1 F_s(h, \alpha_j + t(s-\alpha_j), z)\,\mathrm{d}t \in D(q_j, \eta_j).$$

The common cone, not merely pointwise derivative nonvanishing, proves the factor floor. It gives $|c_j - \alpha_j| \le A_j/\gamma_j$. The strict inclusion puts this same physical zero in chart k's uniqueness disk. Its zero must therefore be identical. This statement holds for every point of the full overlap, not just sampled roots. The local implicit branches glue to one branch, holomorphic in h and real analytic in z. □

The same inclusion test joins a positive-width part of the atlas to the inherited $[.8999, .9]$ branch. Analytic identity identifies the branches on their entire common connected radius interval. At $h = 0, z = .899$, the separately proved point zero lies in chart zero's uniqueness disk. A further strict tiny-disk inclusion identifies it with the inherited original-Haar endpoint proof. These are exact branch identities; root proximity alone would be insufficient.

Actual-zero derivatives and usable modulus bounds (M7)

An admitted physical scalar disk $F(h,a,z) \in D(v,E)$ in a chart gives

$$\alpha(h,z) \in D\left(a, \frac{|v|+E}{\gamma}\right),$$

provided that returned disk stays within a proved uniqueness chart. Its finite scalar budget is separate from the larger parameter-model error. For a query s in an admitted chart, a certified root disk $D(a, r)$ gives

$$|F(h, s, z)| \geq \gamma \max\{0, |s - a| - r\}.$$

This supplies a useful target absolute accuracy to the resource selector. A zero lower bound does not prove that the query is a zero; it merely provides no positive relative denominator.

The complete parameter model also encloses F_s, F_h, F_z at the rational candidate. To return them to the actual root, add respectively

$$B_{ss}r, \qquad 8000r, \qquad \frac{204800000}{3}r.$$

Here B_{ss} is the outward second-tilt derivative bound. The other two numbers follow from the actual joint Cauchy halos: $6/(.01 \cdot .075) = 8000$ and $2048/(.0004 \cdot .075) = 204800000/3$. Every candidate-to-root segment is checked to stay in $|s - s_0| < .025$. Only a positive lower modulus for the returned F_s disk permits

$$\alpha_h = -F_h/F_s, \qquad \alpha_z = -F_z/F_s.$$

The implementation prices numerator and denominator uncertainty, finite division, and serialization. These are derivatives at the true zero, not values at an unpriced approximate root.

On a fixed fiber, a sharper common cone follows from

$$|F_s - c_s| \leq E_s + B_{ss}(r + 10^{-5}).$$

If this is smaller than $|c_s| - 1/200$, it earns a local factor $1/200$. The complete derivative neighborhood must satisfy $|a - s_0| + r + 10^{-5} < .025$, and the query must satisfy $|s - a| + r \leq 10^{-5}$. This local improvement is enabled only when its actual inequality passes.

The structural limitation of the current transport (M8)

At $z = 3/4$, the configuration with one $w_j = +1$ and seven $w_j = -1$ has $S = 0$ and $M = \mathrm{diag}(0, 8)$. This is more than a loose estimate of an invertible matrix. If a real C^1 angular flow preserved that mark zero, differentiation would require

$$8 + i \sum_j w_j \theta_j' = 0.$$

At that configuration the second term is purely imaginary, while the real part of the first is 8, a contradiction. Thus changing a matrix regularization alone cannot produce a globally C^1, zero-preserving angular transport through this critical source configuration.

This is an obstruction to a specified transport class, not to the ordinary Haar moment or its continuation. The colliding configuration also has Vandermonde vanishing, which may permit an integral-level local or conditional construction. Away from the critical population a positive matrix floor can still be obtained; its deterioration must be priced together with the preparation, Jacobian, and complex-flow estimates before enlarging the current analytic halo. No new radius coverage near .75 is claimed here.

Public evaluator and arithmetic contracts (M10)

The public implementation is `atlas_evaluator.py`. Its methods load the canonical immutable atlas review, the inherited radius review, the complete chart inequalities, and independent physical-source admission. The exact-input domain is checked before source execution. A user radius unsupported by the native signed32 frequency header is refused; it is not rounded to the nearest precomputed interpolation node.

`scalar` Recompose an admitted physical scalar disk from all actual error components. Its lower-modulus test determines relative versus absolute classification.

`root` Combine an admitted physical scalar residual with the connected uniqueness theorem and factor bound. A small residual alone is not a root proof.

`derivatives` Evaluate complete parameter derivative disks, return them from the rational candidate to the true zero, and divide only after proving a positive lower bound for $|F_s|$.

`modulus` Return a geometric lower bound on a matching physical fibre. The optional local factor $1/200$ requires its actual common derivative-cone inequality.

`model` Return the complete absolute parameter model, with its differentiated remainders. It is a geometry tool, not automatically a high-accuracy physical scalar readout.

`locate` Use the model only to propose tilts, then generate fresh physical sources and certify residuals. Every accepted root comes from the original source and the full connected theorem.

Fresh source generation retains the unchanged native arithmetic and analytic contracts. It has a new explicit origin record. Within the generating process, the live execution can support subsequent root, derivative, and modulus calls. Across restarts, existing files require admission into a new immutable review. Copying a cache and recomputing its internal hash is not an admission procedure.

The exact $h = 0$ path uses the inherited integer-image formula and its two-component budget. It is not forced into the noninteger source-budget schema. The current generic fresh preparation path may compute an unused prefix at $h = 0$; eliminating that work is an implementation improvement, not a missing mathematical justification.

Error-directed refinement

For a physical disk $D(c, E)$, the ordinary relative certificate requires $\underline{|c|} - E > 0$ and

$$\frac{E}{\underline{|c|} - E} < 10^{-10}.$$

The atlas provides an additional independent lower bound from distance to the true zero. It can select a sufficient absolute tolerance before source generation. It cannot create a positive relative denominator at the zero. The executed image-only repairs retain the failed attempts, identical physical rows, unchanged exact inputs and the individually priced image replacement. Once source arithmetic dominates, increasing the terminal order or the image degree is not the justified next action.

Effective physical derivatives and finite parameter errors (J3)

For $L = \log Y$, $t > 0$, integer $k \geq 1$,

$$|L|^k e^{vL} \leq \left(\frac{k}{et}\right)^k (e^{(v+t)L} + e^{(v-t)L}).$$

Combining the two sign-specific moment bounds gives

$$|\partial_s^k F| \leq \left(\frac{k}{et}\right)^k \max\{M_+(v+t) + M_+(v-t), M_-(v+t) + M_-(v-t)\}.$$

Rational Hölder and log-shift choices are independently verified, not assumed globally optimal. On $|s - s_0| \leq .065$, $|h| \leq .1$, one obtains $|F_{ss}| < 237$, $|\partial_s^9 F| < 41815201$ and $|\partial_s^{10} F| < 301434929$. The analogous ninth derivative bound on $|h| \leq .2$ is 949999546.

For the radius derivative, combine the actual real-diameter bound A_k with the complex-halo Cauchy bound $B_k = k!M/(.1 - .065)^k$. The harmonic measure of the curved boundary of the half-disk of radius $\eta = .0004$ at distance at most $e < \eta$ is bounded by

$$\omega(e) = \frac{2}{\pi} \arctan \frac{2\eta e}{\eta^2 - e^2}.$$

The two-constants theorem gives $A_k^{1-\omega} B_k^{\omega}$; division by e prices its physical radius derivative. At $e = 10^{-5}$ the ninth-tilt thin-disk bound is 122375355. This prices the derivative of the remainder, rather than differentiating an unpriced finite formula.

Deterministic order-circle error contraction

At each exact radius/tilt preparation, $K = 96$ fresh physical samples on the circle $r = .1$ supply a degree-$D = 60$ polynomial in $x = h/r$. Rational sample coordinates differ from ideal nodes by less than 10^{-120}; the halo $R = .2$, $M = 228$ prices that displacement. The full physical source, angular, image, terminal and finite-readout errors enter the sample disks. Folded Cauchy aliases are explicitly bounded. The constant is replaced by an independent original-Haar Toeplitz enclosure only after overlap. For $F(h) = \sum a_n h^n$, exact circular sampling gives the folded coefficient $\widetilde{b}_n = \sum_{\ell \geq 0} a_{n+\ell K} r^{n+\ell K}$. Writing $q = r/R = 1/2$, its analytic alias obeys

$$|\widetilde{b}_n - a_n r^n| \leq \frac{M q^{n+K}}{1 - q^K}.$$

Thus the value alias for the retained nonconstant modes is bounded by $M q^K (1 - q^K)^{-1} \sum_{n=1}^{D} (|h|/R)^n$; differentiating that finite positive sum prices its h derivative. If the node displacement is at most δ, Cauchy on the source disk gives the separate allowance $M\delta/(R - r - \delta)$. The exact constant, aliases, node displacement, finite DFT arithmetic and serialization are all retained by the executed coefficient packet.

Lemma J3.1 (Correlated deterministic sample return)**.** *If the ideal node errors satisfy $|\epsilon_j| \leq e_j$ and $E_{\mathrm{rms}}^2 = K^{-1} \sum e_j^2$, then, for $|h| \leq r$ and $D < K$,*

$$|\Delta P_D(h)| \leq E_{\mathrm{rms}} \left(\sum_{n=1}^{D} |h/r|^{2n} \right)^{1/2},$$

$$|\partial_h \Delta P_D(h)| \leq \frac{E_{\mathrm{rms}}}{r} \left(\sum_{n=1}^{D} n^2 |h/r|^{2n-2} \right)^{1/2}.$$

The exact constant error, analytic aliases and finite contraction are separate.

Proof. Write the sample error as $K^{-1} \sum_j \epsilon_j \sum_{n=1}^{D} (h/r)^n e^{-2\pi i j n/K}$. Cauchy–Schwarz and exact discrete orthogonality give the first bound. Differentiate the finite kernel to obtain the second. No probabilistic independence is assumed. The retained sample correlation changes a worst-case D amplification into $\sqrt{D}$ at the circle boundary. The omitted Taylor tails are

$$\tau = 228/2^{60}, \qquad \tau_h = 141360/2^{60}.$$

□

Complete common and finite returns

Use the inherited forty-one exact rational radius nodes, degree forty, with cardinal polynomials $L_j(t)$, $t = (z - .8995)/.0005$. Use nine exact tilt nodes $c_0 + k/100$, $-4 \leq k \leq 4$, with cardinals $I_k(w)$, $w = s - c_0$. The finite tensor is

$$P(h, s, z) = \sum_{j,k} L_j(t) I_k(w) Q_{jk}(h).$$

The unchanged Bernstein ellipse parameter $52/25$ and the new source halo give $E_0 < 8.866446 \times 10^{-9}$, $E_1 < .001483394$. The h derivative requires the larger halo: $E_{0,h} < 8.658639 \times 10^{-7}$. On a complete radius panel, set

$$E = E_0 + \sum |L_j| \tau, \quad E_h = E_{0,h} + \sum |L_j| \tau_h, \quad E_z = E_1 + \sum |\partial_z L_j| \tau.$$

The underlying common error functions remain analytic in tilt on $|w| \leq .09$, with these uniform bounds.

Let $\Omega_9(w) = w \prod_{k=1}^{4} (w^2 - k^2/10000)$. Hermite–Genocchi gives the physical tilt remainders

$$R_0 \leq \frac{M_9 |\Omega_9|}{9!}, \quad R_s \leq \frac{M_9 |\Omega_9'|}{9!} + \frac{M_{10} |\Omega_9|}{10!},$$

with $R_h \leq M_{9,h} |\Omega_9|/9!$ and $R_z \leq M_{9,z} |\Omega_9|/9!$ using the priced derivative bounds. Explicit conservative choices are

$$M_{9,h} = \frac{949999546}{.2 - .1}, \qquad M_{9,z} = \frac{122375355}{10^{-5}}.$$

The simplex weight for the moving interpolation point supplies the 10!. For analytic tilt-circle radius $R_c = .09$, query radius $q < R_c$, put $D_s = R_c \prod_{k=1}^{4}(R_c^2 - k^2/10000)$. The common contour multipliers are

$$K_0 = 1 + \frac{R_c|\Omega_9|}{D_s(R_c - q)}, \quad K_1 = \frac{1}{R_c - q} + \frac{R_c}{D_s}\left(\frac{|\Omega_9'|}{R_c - q} + \frac{|\Omega_9|}{(R_c - q)^2}\right).$$

For actual finite-plus-alias packets $e_{jk}, e_{h,jk}$ retain every weight:

$$e_0 = \sum |L_j I_k| e_{jk}, \quad e_s = \sum |L_j I_k'| e_{jk}, \quad e_z = \sum |\partial_z L_j I_k| e_{jk}, \quad e_h = \sum |L_j I_k| e_{h,jk}.$$

The final value/h/z allowances are $K_0(E, E_h, E_z) + (R_0, R_h, R_z) + (e_0, e_h, e_z)$; the tilt allowance is $K_1 E + R_s + e_s$. The h tail is returned once. Separately priced finite packets do not inherit the common analytic correlation. Outward polynomial arithmetic prices all conversions, contractions and serialization.

A validated moving predictor and connected zero theorem (J4)

The stored exact rational predictor is

$$c(h, z) = c_0 + \sum_{n=1}^{8} b_n (h/.1)^n + (z - .8995) \sum_{n=0}^{3} a_n (h/.1)^n.$$

Its complete rational coefficients are stored in `analysis/predictor-joint-8x3.json`; those exact values are authoritative. They are chosen from physical data but are not asserted to equal exact branch Taylor coefficients. Nearby-radius divided differences only select rational coefficients; no unpriced finite-difference derivative enters the proof. Their full residual is validated using the new, complete parameter model. The degree-six additive proposal remains preserved as a successful but less accurate candidate. The old small-circle data are not extrapolated as a certificate.

Set $u = s - c(h, z)$ and $f(h, u, z) = F(h, c(h, z) + u, z)$. The exact identities

$$f_h = F_h + F_s c_h, \qquad f_z = F_z + F_s c_z, \qquad f_u = F_s$$

retain all mixed terms generated by polynomial substitution. In particular, writing $x = h/.1$, $b(x) = \sum b_n x^n$, $a(x) = \sum a_n x^n$, one has $c_h = [b'(x) + (z - .8995)a'(x)]/.1$ and $c_z = a(x)$. The target moving disks satisfy $|c - c_0| + .006 < .055$ and $|c - s_0| + .006 < .065$, with $|s| < 3$. Cauchy remainders use the original F-coordinate halos; no composed predictor halo on $|h| = .2$ is silently assumed.

Theorem J4.1 (Residual-coordinate zero and modulus criterion)**.** *On a complete parameter cell let* $\widetilde{P}(h, \rho v, z) = \sum_{k=0}^{8} B_k(h, z) v^k$, $\rho = .006$, *and* $A = B_1/\rho$. *Suppose* $|A| \geq a > 0$, $|B_k| \leq b_k$, *and the complete value/tilt return errors are* $\varepsilon_0, \varepsilon_s$. *If*

$$a\rho > b_0 + \sum_{k=2}^{8} b_k + \varepsilon_0, \qquad \gamma = a - \sum_{k=2}^{8} \frac{k b_k}{\rho} - \varepsilon_s > 0,$$

then every fiber has exactly one simple zero β *in* $|u| < \rho$. *For* $\alpha = c + \beta$,

$$|\beta| \leq \frac{b_0 + \varepsilon_0}{\gamma}, \qquad F(h, s, z) = (s - \alpha(h, z))G(h, s, z), \quad |G| \geq \gamma.$$

Proof. The first strict inequality is Rouché comparison with the linear function $A(h, z)u$ on the entire residual boundary. The second gives a common disk for f_u about the same fiber's $A(h, z)$ which excludes zero. It proves simplicity. Integrate f_u on the segment from β to u; that segment stays in the convex residual disk, and the integral stays in the same common derivative disk. This proves the factor and root-displacement bounds. Pointwise nonvanishing of F_s alone would not suffice. □

The reference slope is allowed to vary with h and z. Its lower bound is obtained from a fixed reference modulus minus the full polynomial variation, not by discarding that variation. The implemented substitution is exact polynomial algebra before taking norms. The independent checker instead composes the physical tilt cardinal derivatives directly and uses a global Chebyshev/cosine interval representation in the real-radius variable.

Every overlapping radius cell uses the same exact predictor and the same physical uniqueness disk at a common fiber, so branch identity on overlaps is exact. The local implicit-function theorem then glues a holomorphic h branch and a real-analytic physical-radius branch. To identify it with the inherited atlas, strictly include the exact original $h = 0, z = .9$ root disk in the new uniqueness disk. On the connected inherited domain, equality is closed by continuity and open by local simple-root uniqueness; it is therefore global on that overlap.

Physical zero readout and derivative return

A finite parameter root only proposes a tilt a. A complete physical scalar disk $F(h, a, z) \in \mathbb{D}(v, E)$ gives

$$\alpha(h, z) \in \mathbb{D}\left(a, \frac{|v| + E}{\gamma}\right),$$

provided the point and returned disk remain in the admitted tube. At the actual root, derivative disks are returned from the candidate point using $B_{ss} = 237$, $B_{hs} = 228/(.1 \cdot .035)$, and $B_{zs} = 4096/(.0004 \cdot .035)$ times the root radius. Division by a proved positive tilt-derivative modulus gives $\alpha_h = -F_h/F_s$ and $\alpha_z = -F_z/F_s$. The polynomial residual derivatives also give $\alpha_h = c_h - \widetilde{F}_h/F_s$ and $\alpha_z = c_z - \widetilde{F}_z/F_s$, with the complete chain-rule errors.

For a proved disk $\alpha \in \mathbb{D}(a, r)$, queries in the admitted tube satisfy

$$|F(h, s, z)| \geq \gamma \max\{0, |s - a| - r\}.$$

This selects an absolute accuracy target for near-zero evaluation. The actual physical scalar still carries every analytic and arithmetic error. Its relative certificate requires a strictly positive lower modulus and an outward error ratio below the requested tolerance.

Physical branch slopes with priced difference remainders (J5)

The parameter model supplies derivatives everywhere in the connected tube. At the difficult new boundary $h = -.1, z = .899$, a separate calculation uses actual physical scalar differences to obtain much sharper pointwise slopes. It retains the same exact rational tilt as the corrected physical zero query. The full proof and raw disks are in `physical/PHYSICAL_ROOT_DERIVATIVES_HM010.md` and `physical/REFINED_PHYSICAL_ROOT_RETURN.md`.

For the tilt derivative, use the complete scalar disks at offsets $0, d_1, d_2$, where $d_1 = 10^{-7}$ and $d_2 = 10^{-8}$; the two offset queries use the independently admitted image-degree-80 return. The quadratic derivative formula is

$$L_s f = -\left(d_1^{-1} + d_2^{-1}\right) f(0) + \frac{d_2 f(d_1)}{d_1(d_2 - d_1)} + \frac{d_1 f(d_2)}{d_2(d_1 - d_2)}.$$

An executed physical third-logarithmic-derivative bound $B_3 < 1000$ gives $|L_s f - f'(0)| \leq B_3 d_1 d_2/6$. This follows from the integral divided-difference remainder for the repeated-node derivative, not from agreement of nearby numerical values.

For either the order or radius variable, use

$$L_\delta f = \frac{f(-2\delta) - 8f(-\delta) + 8f(\delta) - f(2\delta)}{12\delta}.$$

It reproduces the derivative through polynomial degree four. If $|f| \leq M$ on a holomorphic disk of radius R and $q = \delta/R < 1/2$, the complete odd Taylor tail has the positive bound

$$|L_\delta f - f'(0)| \leq \frac{M}{6\delta}\left\{\frac{(2q)^5}{1 - 4q^2} - \frac{8q^5}{1 - q^2}\right\} = \frac{4Mq^5}{\delta(1 - q^2)(1 - 4q^2)}.$$

The last expression is used by the independent checker to avoid subtraction. For order, $(\delta, R, M) = (10^{-6}, .1, 228)$; the four contractions reuse the same h-independent full source with all five components repriced. The negative stencil orders are covered by the larger $|h| \leq .2$ halo, not by the zero theorem's smaller disk. For radius, $(\delta, R, M) = (10^{-8}, .0004, 4096)$; four new complete preparations use the exact requested radii. Their frequency headers are supported without rounding. The argument uses the proved transported holomorphic extension. It assumes no absolutely integrable original-space noninteger second-radius derivative.

All scalar disk radii are multiplied by the absolute exact stencil weights. The five physical error components, analytic Taylor tail, finite contraction and serialization are retained separately. The candidates are then returned to the true zero. The first return used raw Cauchy product bounds. A new first-tilt logarithmic bound, combined with the larger order halo and the proved thin-radius two-constants theorem, improves these to

$$|F_{hs}| < 8142, \qquad |F_{zs}| < 4473031.$$

This refinement requires no new physical source and retains the previous receipt. The derivative and quotient results below include these true-zero returns. Their independent check reconstructs all eleven scalar inputs and the exact stencil moments.

A separate connected modulus chart through tiny orders (J6)

At the exact rational midpoint tilt c_0 and real radius .8995, define $f(h) = F(h, c_0, .8995)$. The original-Haar Toeplitz route encloses $f(0)$; two separately priced symmetric differences, formed from the four physical queries at $\pm 10^{-12}, \pm 10^{-20}$ sharing one admitted source, control the first derivative. The original-source disk $R = .2$, $M = 228$ prices the derivative remainder. On $|h| \le 10^{-9}$, the complete common derivative cone has modulus floor greater than .00170964900336, hence greater than 1/600. A separate strict Rouché count proves exactly one simple zero β in that h disk and

$$f(h) = (h - \beta)H(h), \qquad |H(h)| > 1/600.$$

The refined zero disk is centred approximately at $-5.04385072727 \times 10^{-110} + 1.30603233439 \times 10^{-109} i$, with radius below 5.919×10^{-121}. It excludes zero. The rational tilt c_0 therefore must not be silently identified with an exact h=0 zero. For its certified disk $\beta \in \mathbb{D}(b, r_\beta)$,

$$|f(h)| \ge \frac{1}{600} \max\{0, |h - b| - r_\beta\}.$$

This is a continuum modulus theorem, not a fit to the four sample values. It supplies geometric relative bounds below 4.365×10^{-12} for all four executed tiny-order queries. The smallest moments have modulus about 1.721×10^{-23}. The exact full inputs and much longer outward enclosures remain authoritative in the accompanying receipts.

Public evaluator, provenance, and exact inputs (J8)

The executable `joint_atlas_evaluator.py` supplies physical scalar replay, zero return, parameter-model evaluation, branch derivatives, lower-modulus bounds, resource requests, and fresh validated location. It accepts exact decimal strings or rational strings, checks the proved order/radius domain and the original tilt disk, and uses a canonical review. Caller-supplied review dictionaries are compared with that authority; they cannot silently change a modulus factor or uniqueness radius.

The public model requires separate admission of every physical source and every h-polynomial. Consistent internal hashes alone do not admit a cache. Read-only inherited sources are tied to the previous canonical admission; fresh sources are bound to the inspected generating code, physical input, complete row range, frame, source/image identity and arithmetic contracts. The exact native signed-32-bit frequency header remains a resource restriction. Unsupported rational radii are refused before generation, without rounding the physical input.

The h=0 route is the original-Haar Toeplitz–hypergeometric formula, with its own exact-input interval evaluation. It is not passed off as a noninteger native-source execution. Fresh noninteger location uses the parameter model only to propose a tilt; each accepted root is returned from a newly executed physical scalar residual. A fresh live execution has explicit in-process origin authority. Reusing its exported receipts after restart requires independent admission into a new immutable review.

Objective, authority, and mathematical scope (N1)

The object remains the ordinary Haar expectation

$$T_N(h, s; z) = \mathbb{E}_{U(N)}\big[|S_N(z)|^{2h} |\Lambda_N(z)|^{2s}\big], \qquad \Lambda_N(z) = \det(I - zU), \quad S_N(z) = -(1 - z^2)\frac{\Lambda_N'(z)}{\Lambda_N(z)}. \tag{N1.1}$$

Complex powers of positive real magnitudes use their real logarithms. The ordinary integral, rather than an analytically continued divergent integral, is the target. The original programme is $1 \le N \le 8$, $0 \le z \le 0.9$, $-0.95 \le \Re h \le 3$, $|\Im h| \le 3$, and independently varying $|s| \le 3$. Relative error below 10^{-10} is requested where a positive lower modulus permits it. The rank-two centre threshold $\Re h > -1/2$ is unchanged.

The inherited connected constructions for ranks three through eight are preserved. They are finite exact-arithmetic absolute approximations on connected regions, not universal finite-arithmetic relative certificates. The prior joint atlas proves a simple-zero branch for $|h| \le 0.1$ and $0.899 \le z \le 0.9$, with a positive factor bound $1/291$; its active review is the immutable starting authority [14]. No old receipt is overwritten or promoted by changing its label.

The research method is `Shadow_Research_1`: its active development edition, Reflective Mathematics Research Handbook, Combined Protocol 0.2-dev.1, Boundary–Property Key 3.4-dev.1, Source Lift/Source Down, reflective mapping, and relevant verification modules. Here these methods are used concretely: identify the physical source, retain the complex preparation through every transformation, locate the limiting readout allowance, and price the return to the scalar. They supply no mathematical axioms. The new workspace is `near_zero_reconstruction_investigation/`; inherited trees are read-only.

The retained physical source and complete finite readout (N2)

Write $d = 1 - z^2$. The inherited exact Möbius transformation gives

$$S_N = Nz + \operatorname{Tr} V, \qquad A_{N,z,s}(w) = d^{N^2+2Ns} \prod_{j=1}^{N} (1 + zw_j)^{-(N+s)} (1 + z/w_j)^{-(N+s)}. \tag{N2.1}$$

The reference measure is normalized CUE(N) and retains the squared Vandermonde. The two exponents in each pair are identical complex numbers. Conjugating one tilt exponent or normalizing A as a probability would change (N1.1). For each fixed preparation, every original or regenerated row encloses its corresponding physical radial-source sample associated with (N2.1). A changed tilt or radius requires its own preparation or an independently priced exact transport.

For an admitted noninteger order, the inherited filtered Mellin construction has the finite form

$$T_N = C(h, \Delta) \sum_{k=1}^{L} v_k k^{-1-2h} \Phi_k - I(h) + R, \qquad C(h, \Delta) = 2^{1+2h} \Delta^{-2h} \frac{\Gamma(1+h)}{\Gamma(-h)}. \tag{N2.2}$$

The full image I, analytic terminal R, physical frame conversion, Fourier conventions, and folded aliases belong to one construction. For the decisive calculations $\Delta = 8/25$, $K = 2316$, $b = 30$, $p = 39$, and $L = K + p(b-1) = 3447$. The weights v_k are exact rationals from the finite filter; its complete distribution is reconstructed independently with integer convolution. The final weight may vanish, but the source support is still checked against the whole admitted schedule. The terminal uses the inherited complete signed-population construction, not a single selected saddle.

The formula does not license integration of a constant Fourier-source error to infinity against an inverse Mellin weight. Preparation and source approximation are already returned through the finite prefix, original-space comparison, and image contracts. We retain those contracts unchanged and improve the finite arithmetic which had dominated them.

Theorem N2.1 (Mixed physical rows)**.** *Suppose the physical parameters, sample indices, grid, and normalization of* (N2.2) *are fixed. For each used row choose any generated value x_k satisfying*

$$|\Phi_k - x_k| \le e_k + a_k,$$

where e_k is its arithmetic allowance in physical units and a_k is its source/angular approximation allowance. Different precisions or different finite angular approximations may be selected, provided every row encloses that

same physical sample. Then the arithmetic and angular contributions to the scalar disk are bounded by

$$E_{\mathrm{src}} = |C| \sum_{k=1}^{L} |v_k| k^{-1-2\Re h} e_k, \tag{N2.3}$$

$$E_{\mathrm{ang}} = |C| \sum_{k=1}^{L} |v_k| k^{-1-2\Re h} a_k. \tag{N2.4}$$

After adding the actual image, terminal, and readout allowances, the resulting disk encloses the original Haar moment.

Proof. Subtract the finite exact source sum from the finite computed sum, apply the triangle inequality to each complex weight, and add the proved image and terminal returns. No independence of row errors is assumed. The complex signs remain in the midpoint contraction; positive majorants are used only for its allowance. All terms are finite. □

This is an application of the inherited mixed-source theorem, not a new source engine. The frozen HP2 implementation rounds certified complex matrix entries to Gaussian integers and computes the finite determinant with exact integer Bareiss elimination. Uncertainty in the matrix entries, Fourier preparation, and frame conversion remains explicitly bounded. Exact determinant accumulation does not make the source error zero. The arithmetic norm addendum is essential: multiplication by a unit complex phase is a modulus isometry, not a rectangular ℓ^1 isometry. The validated contract proves the modulus bound before its final rectangular conversion [15, 16].

At nonnegative integer $h = m$ the implementation uses the separately admitted coefficient identity

$$T_N(m, s; z) = (-1)^m 4^m (m!)^2 a_m, \qquad \Phi(r) = \sum_{j \geq 0} a_j r^{2j}. \tag{N2.5}$$

Any internal coefficient scaling is explicitly undone. No singular gamma–zeta interval factors are multiplied. The $m = 0$ value is additionally checked against the exact original-Haar Toeplitz representation.

A reusable error-directed resource theorem (N4)

Theorem N4.1 (Modulus to the standard relative disk)**.** *Suppose a physical complex scalar T has a proved lower modulus $|T| \geq L > 0$. Let $0 < \tau < 1$. If a complete computation supplies $|T - c| \leq E$ and*

$$E < \frac{\tau L}{1 + 2\tau}, \tag{N4.1}$$

then $|c| - E > 0$ and $E/(|c| - E) < \tau$.

Proof. The reverse triangle inequality gives $|c| \geq L - E$, whence $|c| - E \geq L - 2E > L/(1 + 2\tau) > 0$. Substitute (N4.1). The non-strict variant is proved identically. □

The factor $1 + 2\tau$ ensures the ordinary midpoint-disk denominator. A different report using the independently proved lower bound L directly needs only $E < \tau L$, but that statement must not be silently substituted for the midpoint test. This distinction matters to proof composition even when $\tau = 10^{-10}$ makes its numerical effect tiny.

If an admitted zero chart gives $T = (s - \alpha)G$, $|G| \geq g > 0$, and $\alpha \in D(a, r)$, then

$$L_{\mathrm{geom}} = g \max\{0, |s - a| - r\}$$

is available. A previous complete scalar gives $L_{\mathrm{old}} = \max\{0, |c_{\mathrm{old}}| - E_{\mathrm{old}}\}$. The maximum of valid lower bounds remains valid without any independence assumption. At an actual zero no positive L exists.

Proposition N4.2 (An effective prefix allocation)**.** *Set* $q_k = |C||v_k|k^{-1-2\Re h}$*. Choose exact* $0 < \eta, \theta < 1$ *and let* B *be a complete upper bound for all contributions other than source arithmetic. Put*

$$A = \frac{\eta\tau L}{1+2\tau} - B.$$

If $A > 0$*, the smallest prefix length* p *with*

$$\sum_{k>p} q_k e_k^{\mathrm{coarse}} < \theta A$$

is computable by ordered sums of nonnegative outward bounds. Generate the fine rows and check

$$\sum_{k\le p} q_k e_k^{\mathrm{fine}} < A - \sum_{k>p} q_k e_k^{\mathrm{coarse}}.$$

If both inequalities hold with all other contracts admitted, the complete disk passes the target in Theorem N4.1.

Proof. The suffix sum decreases monotonically with p. The two inequalities give $E_{\mathrm{src}} < A$, hence total error below $\eta\tau L/(1+2\tau) < \tau L/(1+2\tau)$. Apply Theorems N2.1 and N4.1. □

If $A \le 0$, source regeneration alone cannot meet that selected complete budget; the limiting image or other term must change. This is a diagnosis of the plan, not a claim that the Haar moment is impossible to certify. When valid prospective fine bounds exist and replacement costs are equal, sorting nonnegative benefits $q_k(e_k^{\mathrm{coarse}} - e_k^{\mathrm{fine}})$ gives a cardinality-optimal subset. Unequal costs instead give a knapsack problem; a benefit/cost heuristic is not a proof of optimality. The implemented prefix rule makes no global optimality claim.

The policy is executable in `independent/precision_policy.py`. A conditional proposal remains a proposal until genuine generation and the fine-prefix inequality are checked. In particular, multiplying a coarse error by a nominal precision ratio does not establish a fine error. The executed primary repair meets its sufficient allocation; the closer query requires image refinement as well. An explicit 1,000-row cap returns an informative resource-limited result rather than an unsupported certificate. Exact integer orders use (N2.5) instead of the noninteger weight policy.

Independent verification and arithmetic admission (N5)

The independent scalar reconstruction does not import the producer's mixed-source contraction or scalar adapter. It reconstructs the exact filter by sliding integer convolution, evaluates its own complex weighted sum and positive error sums at 1024 bits, and uses an independently expressed logarithmic-gamma multiplier. All 3,447 primary source rows are read; all 1,909 regenerated rows agree with their coarse counterparts within the sum of their physical allowances. Agreement is a challenge, not the source of those allowances.

The physical checks include Acb finite projections at indices 1, 40, 160, 400, and 1909. Their independent evaluation uses 512 to 2048 bits as needed. An original-Haar eigenangle integral at the first sample does not use the Möbius/native source coordinates. Its fine-source gap is approximately $4.06109\cdot10^{-58}$ inside the independently priced $3.02560 \cdot 10^{-46}$ allowance. This is a selected-sample independent challenge, not an independent rebuild of every Haar integral. The image and terminal are re-executed using their reviewed inherited analytic engines; that shared dependency is disclosed.

Every admitted cache binds the exact physical input, native precision, generating implementation, generation-start record, source plans, row integers, image parameters, physical normalization, and complete readout. Internally consistent self-rehashed files are insufficient. Public certification requires an independently admitted generating origin and the canonical predecessor review. The new release retains the producing candidate receipts unchanged and places certification in a separate ledger.

Adversarial tests reject changed precision labels, an incorrect source grid, an incorrect physical multiplier, conjugated tilt, tiny exact radius/tilt substitutions, zeroed arithmetic allowances, source/image mismatches, and false relative claims for zero-containing disks. The final inequality is recomputed after exact rational serialization. Exact $h = 0, 1$ and $h = -10^{-12}, 1 \pm 10^{-12}$ are executed using the correct integer or deflated near-integer path.

A real implementation failure was also preserved: the first public planning wrapper encountered a same-named module from another inherited path. Its hash guard refused the operation; no certificate was issued. The next version loads the exact reviewed policy filename under a unique module name. Later versions similarly bind the scalar producer by its confined path. Failed files remain in the history rather than being silently rewritten.

An exact order factor in the terminal majorant

There is a further reusable improvement in the independent batch check. For fixed admitted $N, z, s, \Delta, K, b, p, T, \lambda$ and fixed direction and spectral panels, the nonregional inherited terminal majorant factors as

$$E_{\mathrm{terminal}}(h) \le A(h)B, \qquad A(h) = |C(h,\Delta)|\Gamma(2+2\Re h)\left|\frac{1}{\Gamma(2+2h)}\right| K^{-2-2\Re h}. \tag{N5.1}$$

Here $B \ge 0$ is independent of h. It retains every signed sector, source-preparation factor, contour clipping condition, distance estimate, and filter bound. This factorization is of a positive allowance; it makes no claim that the omitted physical complex source has a common phase.

Lemma N5.1 (Reusable terminal geometry)**.** *Under the unchanged upper-radius terminal hypotheses, suppose a noninteger anchor h_0 has actual outward bound $U_0 \ge A(h_0)B$ and a separately computed positive lower endpoint $0 < a_0 \le A(h_0)$. Then*

$$B \le U_0/a_0, \qquad E_{\mathrm{terminal}}(h) \le \overline{A(h)}\,\overline{U_0/a_0}$$

for every admitted order, with outward arithmetic.

Proof. The signed-sector radial integration puts all order dependence in the factor $A(h)$. The remaining supremum and positively weighted angular-panel sum are independent of h; their minimum is B. Positivity permits division at the anchor, and then multiplication by $A(h)$. An anchor with $A(h_0) = 0$ is refused. □

The independent order-circle check uses $h_0 = 7/50$ and reconstructs the full geometry once per physical preparation. Every source contraction, source allowance, image, and final readout is still checked at each actual order. The warmed check for a 128-node preparation fell from approximately 13.91 seconds to 2.175 seconds in the measured implementation. The prior partial literal replays are retained, and the final full-grid check uses this proved positive-factor return. Changing radius, tilt, contour, filter, or panel scheme requires its own B and hypothesis checks.

Refreshed source data and a wider connected zero atlas (N7)

New data, unchanged preparations

The atlas refresh evaluates a 128-node order circle of radius $r = 7/50$ on each of the 369 reviewed physical preparations. These are 47,232 fresh order-dependent complete scalar readouts of 369 preparations, not 47,232 newly generated native sources. The physical Fourier source depends on N, z, s; every changed h still requires its actual finite weights, image, terminal, and readout return. All preparations retain their admitted original generating origins.

The full fresh grid completed without a failed task. Its independent check reconstructs all 47,232 complete physical readouts. A separate independent check reconstructs all $369 \cdot 111 = 40,959$ coefficients in the degree-110 sampled order jets, their exact original-Haar constant terms, and their deterministic error packets. The selected finite model uses only the degree justified by its actual budget. Retaining a higher available degree does not require using it.

Lemma N7.1 (Correlated sampled-circle return)**.** *Let F be holomorphic on a neighborhood of $|h| \le R$ and bounded there by M. Let $K = 128$, $r = 7/50 < R$, and $D < K$. Suppose the actual sampled values on the K equally spaced circle nodes have complete errors e_j, including the displacement of the exact rational implemented nodes from their ideal circle locations. The sampled coefficient of degree n has alias allowance*

$$\frac{M}{R^n}\frac{(r/R)^K}{1-(r/R)^K}.$$

For derivative order $q = 0, 1$, the combined finite sample-error contribution on $|h| \le H < R$, after separately replacing the constant term, is bounded by

$$\left(\frac{1}{K}\sum_{j=0}^{K-1} e_j^2\right)^{1/2} \left(\sum_{n=\max(1,q)}^{D} \frac{(n)_q^2 H^{2(n-q)}}{r^{2n}}\right)^{1/2}. \tag{N7.1}$$

The additional value and first-derivative Taylor-tail allowances are

$$M\frac{(H/R)^{D+1}}{1-H/R}, \qquad \frac{M}{R}\left\{\frac{(D+1)(H/R)^D}{1-H/R} + \frac{(H/R)^{D+1}}{(1-H/R)^2}\right\}.$$

Proof. Cauchy's coefficient estimate and the exact finite Fourier alias identity give the geometric alias sum. For the finite error, express the entire polynomial error as the discrete inner product of the error vector with its degree-D Fourier kernel. Discrete Parseval is exact because $D < K$; Cauchy–Schwarz gives (N7.1). The omitted constant has its own independently admitted original-Haar disk. Summing the Cauchy coefficient bounds, and their differentiated series, gives the tails. No random-error or statistical-independence assumption occurs. □

Using $H > r$ is legitimate only with the amplified sample error in (N7.1). The first $H = .16$, $D = 50$, $R = .25$ continuation attempt failed a strict Rouché inequality at the endpoints: its finite sample return was about $1.52 \cdot 10^{-5}$. Independent arithmetic confirmed the failure. Increasing the polynomial degree made that term worse. The failed receipts remain part of the evidence.

The repair uses different analytic halos for different tasks. A larger ordinary-source order halo improves the alias and Taylor tail while a smaller degree reduces physical sample amplification. The already proved $R = .25$ halo is retained for the derivative and radius-return resources; it is not replaced by an unnecessarily large global constant. The following larger tail halos follow from Lemma N6.1 with the same tilt halo .15 and were independently executed at 1024 bits:

R	.30	.35	.40	.50	.60	.70
M	2974	10224	35883	483296	7929460	194726168

The larger values are harmless when outweighed by the sharper ratio $(H/R)^{D+1}$. This is a proved reorganization of the same physical readout, not an assumption that its old coefficients remain accurate outside the old order circle. The final selected degree and halo are recorded with the connected theorem below.

An exact weighted radius-interpolation bound

The 41 exact rational radius nodes, normalized to $[-1, 1]$, are $t_0 < \cdots < t_{40}$. Let

$$L_j(x) = \prod_{k \ne j} \frac{x - t_k}{t_j - t_k}$$

be their exact cardinal polynomials.

Lemma N7.2 (Fixed-sign weighted return)**.** *For fixed nonnegative weights w_j, on each node interval $[t_i, t_{i+1}]$,*

$$\sum_{j=0}^{40} w_j |L_j(x)| = \sum_{j=0}^{40} \sigma_{ij} w_j L_j(x), \qquad \sigma_{ij} = (-1)^{j-i-\mathbf{1}_{j>i}}. \tag{N7.2}$$

Consequently the complete positive interpolation allowance can be bounded as one real polynomial on each sign interval before taking its supremum.

Proof. Each cardinal has no zero in the open node interval. Counting its negative numerator and denominator factors gives the displayed constant sign. The endpoint identity follows by continuity. The left-hand side is already a positive triangle-inequality majorant, so combining the signed polynomial coefficients on the right does not presume cancellation among the unknown physical errors. □

The producer uses nonnegative Bernstein basis functions on four exact subpanels of every node interval. The maximum upper endpoint of the Bernstein coefficients bounds the entire continuum. The independent audit instead converts each local polynomial to a Chebyshev expansion and uses $\bar{b}_0 + \sum_{n\ge1} |b_n|$ on $[-1, 1]$. Every value and order-derivative error vector receives its own bound. Radius derivative errors retain their separately proved cardinal-derivative bounds.

For the actual nodes, the producing unweighted bound is below 3.310545142, compared with the previous independently bounded sum of cardinal norms, approximately 43.92095. No sampled maximum or assumed ideal-node formula is used. Weighted bounds retain all actual per-source errors and can be sharper still. This improvement is independent of the Haar application and applies to a finite interpolation return with known real nodes and nonnegative error weights.

Predictor, physical return, and zero theorem

The new predictor has the exact rational form

$$c(h, z) = c_0 + \sum_{n=1}^{16} b_n (h/H_*)^n + (z - z_c) \sum_{n=0}^{6} a_n (h/H_*)^n, \quad H_* = 3/20, \quad z_c = 1799/2000. \tag{N7.3}$$

It is degree 16 in order, with an order-degree-six radius-slope polynomial, and is linear in radius. It is not a degree-six radius polynomial. Its coefficients are selected from the finite implicit model and then frozen as exact rationals. They are proposals for a useful coordinate, not assertions about exact zero locations.

Set $u = s - c(h, z)$ and $\widetilde{F}(h, u, z) = F(h, c(h, z) + u, z)$. The finite physical polynomial is composed with this exact coordinate. Its return includes all physical circle errors, Fourier contraction, aliases, order tails, radius interpolation, tilt interpolation, and arithmetic. Common analytic remainders are bounded as functions on their whole tilt circle; they are not charged as independent errors at every stencil point. Actual query tubes are checked against both the analytic halo and the original $|s| \le 3$ box.

Theorem N7.3 (Effective residual-coordinate criterion)**.** *Suppose $\widetilde{F}$ is holomorphic on a neighborhood of each closed residual tilt disk. Suppose on every admitted order/radius cell and $|u| \le \rho$ a complete physical return proves*

$$|\widetilde{F}(h, u, z) - A(h, z)u| < |A(h, z)|\rho \quad (|u| = \rho), \qquad |A(h, z)| \ge a_* > 0.$$

Suppose further that one complex reference q on the entire chart obeys

$$|\partial_u \widetilde{F} - q| \le b < |q|.$$

Then each fiber has exactly one simple zero $\beta(h, z)$ in the residual disk. It has the factorization

$$\widetilde{F}(h, u, z) = (u - \beta(h, z))\widetilde{G}(h, u, z), \qquad |\widetilde{G}(h, u, z)| \ge |q| - b.$$

In particular $|\beta| \le \sup |\widetilde{F}(h, 0, z)|/(|q| - b)$. If the Rouché comparison has a uniform boundary allowance $|\widetilde{F} - Au| \le B < a_*\rho$, then the independent bound $|\beta| \le B/a_* < \rho$ also holds. The smaller of these two bounds may be used.

Proof. Rouché's theorem compares with the nonzero linear function Au and counts one zero including multiplicity. Hence it is simple. The segment from β to u lies in the convex residual disk, and

$$\widetilde{G} = \int_0^1 \partial_u \widetilde{F}(h, \beta + t(u - \beta), z)\, dt.$$

The integral remains in the same complex disk $D(q, b)$; the lower modulus follows. Set $u = 0$ for the final claim. Pointwise nonvanishing without a common cone would not prove this integrated factor bound. For the additional radius, the maximum-modulus principle bounds $|\widetilde{F} - Au|$ by B throughout the disk. At the zero, $|A\beta| \le B$, and division by the proved a_* gives $|\beta| \le B/a_*$. This is a priced Rouché enclosure, not a truncation of an oversized radius by fiat. □

Theorem N7.4 (Executed connected continuation)**.** *For the original rank-eight Haar moment, the admitted inner construction proves a single connected simple-zero branch on*

$$|h| \le 4/25, \qquad 899/1000 \le z \le 9/10,$$

in the moving residual disk $|s - c(h,z)| \le .006$*. The original target tilt restriction is preserved throughout the tube. On every admitted chart,*

$$F(h,s,z) = (s - \alpha(h,z))G(h,s,z), \qquad |G| > 1/563.$$

The executed physical return, strict inequalities, separate independent continuum check, source/jet admission, and branch glue are bound to the final review. The selected finite order degree is 28*, with tail halo radius* 3/5 *and majorant* 7929460*.*

Proof. The exact-rational inequalities are the executed instance of Theorem N7.3, with the component returns just proved and the independently admitted physical samples and jets. The radius panels cover $[.899, .9]$ with positive-width overlaps. They use the same exact predictor, order domain, and residual disk, so at every common parameter their uniqueness region is identical. Their zeros therefore coincide. The derivative cone gives local implicit continuity in real radius and holomorphy in order; the overlapping charts define one branch.

At $h = 0, z = .9$, strict containment of the exact original zero-certificate disk inside the new uniqueness tube is separately executed. This identifies the new and inherited branches at that anchor. On their connected common parameter domain, the set of equality is closed by continuity and open by local implicit uniqueness at a simple zero. It is nonempty and hence the whole intersection. Thus the larger branch is the continuation of the inherited physical branch, not a collection of unconnected numerical roots. □

For this inner $H = .16$ construction the independent 1024-bit checker reconstructs 128 overlapping radius cells and proves the following conservative summaries. The producer uses 64 overlapping cells and a different real-polynomial bound; its slightly stronger numbers are not substituted for the independent lower margins.

Quantity	Independently proved bound
Minimum Rouché slack	$> 1.02155 \cdot 10^{-5}$
Common derivative-cone floor	> 0.00177669328
Convenient exact modulus factor	$1/563$
Uniform predictor-to-root distance	< 0.001651285
Maximum query tilt radius about c_0	< 0.102504545
Full moving tube	$\lvert s\rvert < 2.963$
Anchor zero-disk containment slack	> 0.00599675
Uniform $\lvert\alpha_h\rvert$	< 1.535
Uniform $\lvert\alpha_z\rvert$	< 1251

An adaptive uniqueness disk extends the theorem to .17

Keeping the inherited residual radius .006 imposed a further geometric cost. At $H = .17$, degree 25 and tail halo $R = .7$, sharper physical tilt bounds still left a small negative Rouché margin. This was not evidence of a lost zero or failed ordinary expectation. The new coordinate permits a larger uniqueness disk if the entire return is repriced.

We therefore increase the residual radius to $9/1250 = .0072$. The actual moving query radius about c_0 is below .115455445, and adding the proved $|c_0 - s_0|$ displacement keeps it below the new physical tilt radius .122. The common analytic tilt contour .14 and source halo .15 are unchanged. The order tail uses $R = .7$, $M = 194726168$, degree 25; the derivative halo remains .25. Every component is re-executed.

Theorem N7.5 (Executed outer continuation)**.** *The same original rank-eight simple-zero branch extends over*

$$|h| \le 17/100, \qquad .899 \le z \le .9, \qquad |s - c(h,z)| \le 9/1250.$$

There is exactly one simple zero in each residual disk, and

$$F(h,s,z) = (s - \alpha(h,z))G_{\mathrm{out}}(h,s,z), \qquad |G_{\mathrm{out}}| > 1/1442.$$

The zero satisfies $|\alpha - c| < .007048994$, strictly inside the uniqueness disk. The entire tube lies in $|s| < 3$. Its branch agrees with Theorem N7.4 throughout the inner domain.

Proof. The independent 1024-bit reconstruction over 128 overlapping real-radius cells gives minimum Rouché slack greater than $3.153417 \cdot 10^{-7}$ and common-cone floor greater than $.000693732259 > 1/1442$. The original physical sources, complete jets, larger-tail halo, derivative bounds, and all returns are independently admitted. Apply Theorem N7.3 on each cell.

The centre/cone bound alone would give an unusable radius of approximately .0185864. The separately proved B/a_* bound instead gives .007048994; it is checked from the complete per-cell Rouché decomposition. Thus the smaller root disk is rigorously earned, not clipped. The new charts use the same exact predictor as the inner charts, and $.006 < .0072$ gives strict nested uniqueness disks. Every inner root is therefore the unique outer root on the common domain. The exact original anchor containment is also rechecked. Overlap of the radius cells gives connectedness as in Theorem N7.4. The full moving tube has a positive original tilt-box margin greater than .0248262. □

This outer theorem keeps the stronger inner factor and all prior certificates intact. The outer uniform derivative magnitudes are finite but broad: $|\alpha_h| < 5.974$ and $|\alpha_z| < 19170$. They establish effective control, not accurate pointwise slopes. Two freshly generated physical preparations at the outer order boundary give actual zero disks at $h = -.17, z = .899$ and $h = .102 + .136i, z = .9$. Their respective radii are below $3.258880 \cdot 10^{-8}$ and $2.681447 \cdot 10^{-12}$.

The .18 probes remain insufficient. Their finite source extrapolation and tilt/radius return exceed the usable Rouché margin, and a tested common cone also fails. This is a failure of the present quantitative construction, not a proof that the physical branch stops. No .2 zero theorem is claimed.

Derivative and modulus information

The chain rule is retained exactly:

$$\widetilde{F}_h = F_h + F_s c_h, \qquad \widetilde{F}_z = F_z + F_s c_z,$$

and $\alpha_h = c_h - \widetilde{F}_h/F_s$, $\alpha_z = c_z - \widetilde{F}_z/F_s$ at the zero. The full derivative allowances, rather than derivatives of an unpriced finite formula, are recorded. Larger-domain uniform derivative bounds may be substantially weaker than the inherited small-domain ones; widening the order disk does not imply an improvement of every derivative constant.

Choose one of the two theorems, including its full order, radius, and residual-tilt domain. Write its factor as g_*: 1/563 for the inner theorem or 1/1442 for the outer theorem. For a separately certified physical zero disk $\alpha \in D(a, r_0)$, the selected factor bound yields

$$|F(h, s, z)| \geq g_* \max\{0, |s - a| - r_0\}$$

within that theorem's admitted tube. Order membership alone does not permit the inner factor at a tilt outside the inner residual disk. The scalar resource theorem then converts a positive separation into a sufficient error target. At the zero itself relative certification is unavailable. The complete scalar computation remains necessary even when a geometric lower modulus is known.

The exact boundary queries and their fresh physical returns are recorded in the execution ledger. A finite-polynomial root proposal is only a query location. A certified scalar disk at such a location, together with the proved common factor, gives the actual root-radius bound $(|F_{\text{midpoint}}| + E_{\text{scalar}})/g_*$ after containment of the query and returned root disk in the selected uniqueness tube is checked. This is how the new physical zero challenges are admitted.

The worst inner negative-real boundary root was refined by a new exact query proposed from its actual physical residual and a model slope. The slope only selected the next query; a fresh preparation and complete physical return certified the result. At $h = -.16, z = .899$, the refined root radius is below $1.072654 \cdot 10^{-15}$. At $h = -.096 + .128i, z = .899$, it is below $5.749255 \cdot 10^{-17}$; the scalar disk at the latter query contains zero and correctly remains absolute-only.

At the exact initial negative-real root midpoint plus 10^{-6}, a new native 104-bit source and image-80 give absolute allowance below $5.097463 \cdot 10^{-20}$ and relative allowance below $1.726325 \cdot 10^{-11}$. Independently priced zero geometry supplies a lower modulus greater than $1.769286973 \cdot 10^{-9}$ using the initial root disk, and greater than $1.774783164 \cdot 10^{-9}$ using the refined disk. Both sufficient resource targets admit keeping the native source. This is an executed connection from the new zero geometry through the resource theorem to a complete physical relative certificate.

The moving predictor and enlarged complex-order domain (Q1)

All expectations in this construction use normalized Haar measure on $U(8)$. The object is

$$F(h,s,z) = \mathbb{E}\left[|S_8(z)|^{2h}|\Lambda_8(z)|^{2s}\right], \qquad S_8(z) = -(1-z^2)\frac{\Lambda_8'(z)}{\Lambda_8(z)}, \quad \Lambda_8(z) = \det(I - zU).$$

For a positive real number x, x^h means $\exp(h \log x)$ with the real logarithm. The null mark-zero set is handled by ordinary integrability. The original programme covers ranks 1–8, radii through 0.9, and independently complex parameters $-0.95 \le \Re h \le 3$, $|\Im h| \le 3$, $|s| \le 3$. This investigation concerns a local rank-eight zero branch. It does not replace the full evaluator objective or establish uniform relative accuracy near a zero.

The released predecessor proves connected zero theorems on $|h| \le 0.16$ with residual tilt radius 0.006 and factor 1/563, and on $|h| \le 0.17$ with radius 0.0072 and factor 1/1442, throughout $0.899 \le z \le 0.9$. Both use the same exact rational predictor

$$c(h,z) = c_0 + \sum_{n=1}^{16} b_n (h/0.15)^n + (z - 0.8995) \sum_{n=0}^{6} a_n (h/0.15)^n. \tag{Q1.1}$$

The full coefficients and c_0 are read from the immutable `predictor-fresh-16x6.json`. Printed decimal zero centres are never substituted for those exact inputs. The predictor is a coordinate, not an assertion that $F(h, c(h,z), z) = 0$.

The supplied protocol, *Shadow_Research_1*, is used to keep the original ensemble, preparation, finite source and scalar return together. Its role is methodological. Every new conclusion below requires an ordinary mathematical proof and its stated arithmetic dependencies.

Recovery and the failed construction

The five predecessor archives were recovered by their released SHA256 identities. An isolated execution checked the closed arithmetic, inner and outer authorities, replayed six physical scalar certificates and the zero/modulus interfaces, and reconstructed four complete physical order circles. All eighteen release replays passed. Independent fresh 1024-bit calculations also reproduced the 0.16 and 0.17 continuum inequalities.

The inherited $H = 0.18$ failure is an inequality failure, not evidence for a multiple zero. Its representative old degree-28 construction had Rouché slack about $-1.0585\,10^{-4}$ and a negative cone margin. The value return was about $1.1382\,10^{-4}$; about 76.5% came from the finite order-circle return. Further inspection showed that the dominant node error was the *filtered terminal remainder*, rather than native rounding. This distinction determines the repair: a terminal omitted from every node is one holomorphic function of h for that preparation. It need not be priced as unrelated noise at the 128 order nodes.

Exact finite-decimal coefficients of the common predictor

The predictor used by the outer and stronger inner theorems is exactly

$$c(h,z) = c_0 + \sum_{n=1}^{16} b_n (h/(3/20))^n + (z - 1799/2000) \sum_{n=0}^{6} a_n (h/(3/20))^n.$$

Every decimal in the following table is finite and exact. A line wrap inside a decimal does not insert a digit or change its value. These are coordinate coefficients, not a claim that the predictor is the zero. The source JSON is included unchanged in the editable bundle.

	Exact real part	Exact imaginary part
c_0	0.55898413253659880470577052489541847272618029988593202148999532599799943650745663144797326068202627212241450477	2.80455438586448267386285812682268189098608502916782460003924893007783288281793428411600862890603510461631174320
b_1	0.04454076819202721907233000549209753644791842396175993915974530528401034979115341146693638181210446230095584489 2	-0.01540781397261992228891040613475013278753223370307119308001008274213020121721025938339904779115467084220709367
b_2	-0.01622975536972829269766205910202857768156764645252830550039976825029734348854854063241195982841038895390128172 7	0.00251781926351641378953691285023639386825941574306313511854167596393781427809793670458396285040126712658130721 4
b_3	0.00779433029441852016774569309501498892301580451738267847759251008827494125600131963334048278159928188445483018 32	-0.00193472234598849751177273392132935560753451371236688016388891875535632521685099696144594681180004911826152326 38
b_4	-0.00355560205259329024964713178894666393105313941052426036620869659306148367789013298236387154932488277914934813 8	0.00082307363670277222506379021847549773601274898453129137192108222520332883226861786909979178123337405964955239768
b_5	0.00175667357547593652291879685012429648187263175910625233209394383512178506276846300209132649169709107059338048 13	-0.00031429194501023415560101928646213896024769102445420790413880252831623925326769369725270605569937978156464117754
b_6	-0.00091729486875489400463816590223082862900144334194851867709708997336479535093924697130393744478506964301164252373	0.00011868267227080034814305238194160101296218706142608210045478677161365061998775680743254347336691019452040868713
b_7	0.00049626046481087815897734556140836276658555652723592339432942620515185214350873942047319425019696750641051811264 9	-0.00003991979173692129706469383662947239852292170554954493445706243149827361123775531208380646299158189421495529903 3
b_8	-0.00027578099909027157409873344106261842624856064748673063358123459770651431827166003896790786623046451349608466214	0.00000849445624143084326749624099289412852173181556001579280155979141559295685826235503583833469350023927768271627 02
b_9	0.00015639457971306093386157969838521932264257173542062881059961759197997955373857181453130931703405135106034933984	0.00000299303352660298303279224151890196315420431949873901274482182113605645528925383493617001778110630038500155516 99
b_{10}	-0.00009007298349715131961180464909024367648810920428175227012897038514184344969294523516636221896385942606158608824 1	-0.00000625579462708408837573171696246613547032398239202026123531323798884320010485236705238342548778649324188698121 1
b_{11}	0.00005250550577839638459941883121420170544940247989390032114310339516445726295484623125586034269061071809910358403 7	0.00000631831823327784384647070698357645486191097497223128191937098124857184955450261112215085259270639419512458066 19
b_{12}	-0.00003089919044652003035769035945352565628138052397317468226819698019493776271523155306361471165994596688557097055 4	-0.00000531465620383382946727724497544723221029022718617436383601121723983726148397211556438686216214834949553761004 18
b_{13}	0.00001832173811293428499057367502816191997688715497799081213028727685605831808281055069877490348909438966479188652 8	0.00000411673187737151319554672814150454034033699233027819994385115068662964487191381720647481670260775002993750262525 01
b_{14}	-0.00001092915466570209055490550955957381700611619555001718356915414065304176165557160522026292791589068363832013840 8	-0.00000304587833539749953461341512564574659525889413096791349092551033742121098838993234758009101379153665375473191 39
b_{15}	0.00000655022922940309967184693905972766149054132153017653201544203395780212129529856535523428540640577086068388708 21	0.00000218990130274358237176522237154750593589165454755904227603064564711544963701851667247177449949264481209457147 57
b_{16}	-0.00000394019542005146931857003210941026230982880618230725168904379714296576704344828183989939514483337384775207367572	-0.00000154434815572599568726304271002377167542773240038131471812727510148093005805322548728680776611522665208332743 64
a_0	-7.33802721482600890157860039370514101830365716421627862721342657672596581075595456302959026733259949419330103 78	-10.58619350598865150208120653703796731614270127701068240532578114666052324835700130864295005504091368481228649 6

	Exact real part	Exact imaginary part
a_1	0.57573484200509460463743762457835555139930094011095798233981214503502577397059531969654404702446607402858621428	0.14237623956358651808058495882326384087660149232494510377203362943361851567415747073679367125159397059739576525
a_2	0.19063937559652175669410897798312319463331927372701790000721991149289272086310404841658892678512440684328398616	-0.33717936400218184384139069379062417569141709058947815048518154167990875067699055125859591506232145490162158686
a_3	-0.07792556139860060214333002918851446492387896123642205716966071555637003910339998645816098215198056563828224824	0.19889018082086270196237426506169249441842883739180572818890720668867853066702668279774096924155498610417912294
a_4	0.05021731282333063770937605212598561537177501620935179999310442272388579223968195626695336986635557765054370004	-0.11272423086091886283654241768988903554818772770562290552406483856075685031428533698666821490832273547772321207
a_5	-0.03475917540041421702830551971463181307150170334094277012794887660531091660177071032732806576829480344809177787	0.06785293630845626444298955706281329085593131317042798854863746186785756699764742345544818664056346120518837564
a_6	0.02366892599405891748373283863120992770390456783516914965133466175724446133917767924805109960190942434857873393	-0.04130970657884383650052959390650551254641546909985594812994274287195705006045832314831249997006741872711925172

Returning the terminal as one analytic function (Q3)

Fix a physical preparation $(8, z, s)$ and its admitted spacing Δ and finite filter v_k. Filters may differ between prepared nodes. The exact sampling identity has the form

$$F(h) = C_\Delta(h) \sum_{k\geq 1} \Phi(k\Delta) k^{-1-2h} - I(h), \quad C_\Delta(h) = 2^{1+2h}\Delta^{-2h}\frac{\Gamma(1+h)}{\Gamma(-h)}.$$

Here I is the complete regularized Mellin image. Define

$$G(h) = C_\Delta(h) \sum_{k} v_k \Phi(k\Delta) k^{-1-2h} - I(h), \quad R(h) = F(h) - G(h).$$

The actual numerical centres approximate G. Every error except the filtered-terminal allowance remains an error of this finite readout.

Lemma Q3.1 (Terminal holomorphy)**.** *For each admitted rank-eight preparation, R is holomorphic on a neighborhood of every disk $|h| \leq R_t < 1$, and $R(0) = 0$.*

Proof. The inherited complete determinant decay makes the omitted-source series absolutely and locally uniformly convergent for $\Re h > -1$. Its terms are holomorphic, $\Gamma(1+h)$ has no poles there and reciprocal gamma is entire. At zero, $C_\Delta(0) = 0$, while the series converges. Thus the independently enclosed physical constant coefficient is unchanged. □

The complete signed-population terminal bound factors as

$$|R(h)| \leq B\,\mathcal{A}(h), \qquad \mathcal{A}(h) = |C_\Delta(h)|\Gamma(2+2\Re h)|\,\mathrm{rgamma}(2+2h)|K^{-2-2\Re h}.$$

The fixed B contains the actual source, population, determinant and filter geometry. It is recovered from the admitted nonzero anchor $h = 0.14$ using the proved factorization and a positive lower endpoint for $\mathcal{A}(0.14)$. This inference uses the generating terminal theorem, not an arbitrary upper bound on an unknown error. Gamma duplication gives a stable form, with $u = \Re h$,

$$\mathcal{A}(h) = \sqrt{\pi}K^{-2}(\Delta K)^{-2u}\Gamma(2+2u)|\,\mathrm{rgamma}(-h)\,\mathrm{rgamma}(h+3/2)|.$$

Complete outward arc covers of $|h| = R$ give $M_R \geq \sup|R(h)|$ by maximum modulus. The independent audit also uses the unreduced gamma expression and a different arc cover.

Theorem Q3.2 (Coherent finite terminal projection)**.** *Let $r = 0.14$, $L = 128$, $1 \le D < L$, and $r, H < R_t < 1$. Let $\mathcal{P}_D R$ retain the positive degrees 1 through D of the exact L-node circular discrete Cauchy projection. With $t = H/R_t$ and $a = (r/R_t)^L$,*

$$\|\mathcal{P}_D R\|_H \le M_H + M_{R_t}\frac{t^{D+1}}{1-t} + M_{R_t}\frac{a}{1-a}\sum_{n=1}^{D} t^n. \tag{Q3.1}$$

For $\delta > 0$ with $H + \delta < R_t$,

$$\begin{aligned}\|(\mathcal{P}_D R)'\|_H \le{}& M_{H+\delta}/\delta \\ &+ \frac{M_{R_t}}{R_t}\left(\frac{(D+1)t^D}{1-t} + \frac{t^{D+1}}{(1-t)^2} + \frac{a}{1-a}\sum_{n=1}^{D} n t^{n-1}\right).\end{aligned} \tag{Q3.2}$$

Proof. Write $R(h) = \sum_{n\ge1} b_n h^n$ with $|b_n| \le M_{R_t}/R_t^n$. A discrete coefficient is $b_n + \sum_{\ell\ge1} b_{n+\ell L} r^{\ell L}$. The difference from R is its Taylor tail plus retained aliases. Summing these geometric bounds proves (Q3.1). Differentiate the geometric sums and bound R' by Cauchy's formula to obtain (Q3.2). □

For an exact executed order node q_j at distance d_j from its ideal circle node, add the terminal transport $M_{R_t} d_j/(R_t - r - d_j)$ to the retained physical-F node return. Let ϵ_j include this and all nonterminal arithmetic, image, angular/preparation and readout errors. Deterministic Parseval gives

$$E_{\mathrm{node},q} \le \left(L^{-1}\sum_j \epsilon_j^2\right)^{1/2}\left(\sum_{n=\max(1,q)}^{D} ((n)_q H^{n-q}/r^n)^2\right)^{1/2}, \quad q = 0, 1.$$

There is no statistical-independence assumption. Coefficient contraction rounding, exact-constant error, the physical-F aliases and its common analytic tail all remain in the full model.

For the former worst preparation, the old node RMS was $3.6882606199\,10^{-15}$; its nonterminal RMS is below $1.7272353679\,10^{-19}$. At $H = 0.2, D = 25, R_t = 0.4$, the repaired value packet is about $2.53\,10^{-14}$ rather than the old amplified $3.85\,10^{-11}$. These are component bounds. The downstream tilt and radius interpolation are still mandatory.

Because the filters differ across preparations, this construction does *not* assert joint tilt analyticity for a family of finite G's. It repairs each physical node's return separately and retains the common analytic bounds of the original F.

A continuum zero theorem from phase-aware finite enclosures (Q4)

Let $P(h, u, z)$ be the finite tensor after substituting $s = c(h, z) + u$, and write

$$P(h, u, z) = \sum_{k=0}^{8} P_k(h, z)(u/\rho)^k.$$

All coefficient centres are inherited; only their rigorously justified returns are changed. The finite tensor uses degree 25 in order, degree eight in tilt and the original 41 real-radius nodes for the outer construction.

On each complete normalized order arc, use a midpoint x_j on the unit circle and chord allowance $\delta = 2\sin(\pi/(2K_a))$. A polynomial enclosure retains its complex value at x_j and bounds only its variation by $\delta\sum_n n|a_n|$. Radius polynomials are translated into the local panel coordinate before absolute values are taken. This keeps complex phase in the finite expression without deleting any remainder.

Put $A = P_1/\rho$ and choose the same fixed unit rotation ζ throughout a chart. The outward calculations prove, on all boundary arcs, all real panel radii and all $|u| \le \rho$,

$$\begin{aligned}&\Re(\zeta A) \ge a_j > 0, \quad |F(h, c+u, z) - Au| \le B_j, \\ &B_j/a_j \le q < \rho, \qquad \Re(\zeta F_s(h, c+u, z)) \ge g > 0.\end{aligned} \tag{Q4.1}$$

Here j labels a complete order arc, and $q = \max_j B_j/a_j$ may then be maximized over the real-radius panels. Taking this ratio before maximization retains the strongest proved correlation: a separate maximum of B_j divided by a separate minimum of a_j would be a different, looser sufficient test. The value error in B_j includes the complete finite-node, tilt, common analytic, radius, coefficient and arithmetic returns. The derivative error in g has its separately priced differentiated return.

Theorem Q4.1 (Boundary-to-disk zero geometry)**.** *Suppose $(h,u) \mapsto F(h, c(h,z)+u, z)$ is jointly holomorphic on a neighborhood of the closed polydisk $|h| \le H$, $|u| \le \rho$ for each admitted real z, and* (Q4.1) *holds on the complete order boundary for every admitted real z. Then for every $|h| \le H$ there is exactly one zero $\alpha(h,z)$ in $|s - c(h,z)| < \rho$. It is simple. Throughout the residual disk,*

$$F(h,s,z) = (s - \alpha(h,z))\mathcal{G}(h,s,z), \qquad |\mathcal{G}(h,s,z)| \ge g.$$

The zero is enclosed by $|\alpha - c| \le q < \rho$, using the maximum of the executed arcwise ratios in (Q4.1)*.*

Proof. The harmonic minimum principle first extends the positive real part of ζA to the whole order disk, so A has no zero there. For fixed residual u, apply maximum modulus to $(F - Au)/A$. It gives $|F - Au|/|A| \le q < \rho$ on the tilt boundary at every interior order. Rouché's theorem in u then counts one zero with multiplicity. Apply the harmonic minimum principle to $\Re(\zeta F_s(h, c(h,z)+u, z))$ for each fixed u to extend its common cone to the full order disk. Along the straight residual segment from the zero to the query,

$$\mathcal{G} = \int_0^1 F_s(h, \alpha + t(s-\alpha), z)\, dt.$$

The disk is convex and the same rotated real part is at least g along the entire segment. Hence $|\mathcal{G}| \ge g$. This last step requires a common cone; pointwise nonvanishing alone would not suffice. At the zero the same quotient bound gives $|\alpha - c| \le q$, proving the stated enclosure. □

Every real-radius panel is a complete interval with strictly positive overlap with its neighbor. The predictor and residual disk are the same on overlaps, so uniqueness proves branch identity there. On the shared $|h| \le 0.17$ domain, the new outer residual disk contains the inherited 0.0072 uniqueness disk strictly. Thus its zero is the inherited branch. For the separately proved $H = 0.18, \rho = 0.006$ inner result, the containment is reversed; its zero lies in the inherited larger uniqueness disk. Both arguments concern identical physical moments at identical parameters.

Physical root disks, modulus bounds and relative readout (Q5)

A finite polynomial root is used only to propose an exact rational tilt. For a freshly admitted physical scalar disk $F(h, s_*, z) \in D(m, E)$, the geometric factor gives

$$|s_* - \alpha(h,z)| \le (|m| + E)/g.$$

The public interface checks that the query and returned disk remain in the admitted moving tube. It binds the actual source generation, prepared tilt, radius, finite filter, image resources and complete scalar budget.

If $\alpha \in D(a,r)$, then on the admitted tube

$$|F(h,s,z)| \ge g \max\{0, |s-a| - r\} =: L.$$

For a separate complete scalar disk $D(c,E)$, a conventional relative certificate requires $\underline{|c|} - E > 0$ and $E/(\underline{|c|} - E) < \tau$. Geometry can direct its resource target: $E < \tau L/(1+2\tau)$ is sufficient for that midpoint test, while $E < \tau L$ suffices only for a relative estimate using the independently proved geometric denominator directly. Neither inequality claims a relative certificate until its actual physical source, image, terminal and finite-arithmetic budget has been executed.

At an exact zero, only an absolute enclosure is meaningful. A wide disk containing zero neither proves a zero nor justifies a positive relative denominator. The executable adversarial tests retain these distinctions.

Contracting rank-two enclosures throughout the ordinary domain

Theorem (rank-two pointwise certification). Let $0 \le z < 1$ be real, and let $h, s \in \mathbb{C}$. Suppose that $\Re h > -1$ for $z > 0$, or $\Re h > -1/2$ for $z = 0$. For exact rational z and exact rational components of h and s, and for every positive rational ε, the procedure below gives a complex disk of radius at most ε containing $T_2(h, s; z)$ after finitely many operations, absent a user resource cap. Repeated absolute refinement also gives relative accuracy at any prescribed positive tolerance at every input where $T_2 \neq 0$. At the centre one uses

$$T_2(h, s; 0) = \frac{4^h \Gamma(h + 1/2)}{\sqrt{\pi}\,\Gamma(h + 2)}.$$

In $0 < z \le 1/2$ the angular partition uses only $O(1 + |\log z|)$ charts before dyadic subdivision. The absolute and relative certification assertions are pointwise. They do not give a uniform bound on cost or imply that a point has zero moment if its disk contains zero.

Proof. Use Proposition 21.2 and put $q = \pi/2 - \gamma$, $a = \arcsin z$, $\tau = s - h$, and $d = 1 - z^2$. The reduced Haar rectangle is $(q, \phi) \in [0, \pi/2] \times [0, \pi]$. Its density is $(4/\pi^2)\cos^2 q$, and the integrand apart from the density is $(4d^2)^h X_0^h D_-^\tau D_+^\tau$ with

$$X_0 = (\sin q - z)^2 + 4z \sin q \sin^2(\phi/2), \qquad D_\pm = (1 - z)^2 + 4z \sin^2((\phi \pm (\pi/2 - q))/2).$$

Each $D_\pm$ is strictly positive on the real rectangle. The only zero of X_0 there is $(a, 0)$. Near that point X_0 is comparable to $(q - a)^2 + \phi^2$ at fixed $z > 0$, since $\cos a > 0$ and $z > 0$. Since the other factors have positive real modulus there, this also proves the sharp ordinary domain at positive radius. At $z = 0$ the moment is the beta integral against the semicircle law of $\cos\gamma$, so it has the sharper domain stated in the theorem.

For $z \le 1/2$ take a central rectangle $0 \le q \le 2a$. For $z > 1/2$ take the whole q interval as central. In either case split at $q = a$. On each wing set $q = a + \alpha t u$, $\phi = \pi t v$ with $(u, v) = (1, y)$ or $(y, 1)$, where $(t, y) \in [0, 1]^2$ and α is the signed width of the wing. The Jacobian is $\pi|\alpha|t$. The analytic factor $A = X_0/(a^2 t^2)$ has the following expression using $\operatorname{sinc}(x) = \sin(x)/x$ continued by one at zero:

$$\begin{aligned} A = {} & \left[\frac{\alpha}{a} u \cos(a + \alpha t u/2) \operatorname{sinc}(\alpha t u/2)\right]^2 \\ & + \left(1 + \frac{\alpha}{a} t u\right) \operatorname{sinc}(q) \operatorname{sinc}(a) \left[\pi v \operatorname{sinc}(\phi/2)\right]^2. \end{aligned}$$

Both terms are nonnegative on the real square. The first is strictly positive if $u > 0$, including at the endpoint $q = \pi/2$, because $a + \alpha t u/2$ is the midpoint of a and q and lies strictly below $\pi/2$. If $u = 0$, then $v = 1$, $q = a$, and the second term is positive. The resulting chart has $\nu = 2h + 1$, prefactor $C = (4/\pi)|\alpha|(4d^2 a^2)^h$ and integrand $t^\nu f(t, y)$ with $f = \cos^2 q\, A^h D_-^\tau D_+^\tau$.

For $0 < z \le 1/2$, let m be the least power of two, at least two, for which $mz \ge 1/4$. Add exterior rectangles whose q intervals are $[L, 2L]$ for $L = 2a, 4a, \ldots, (m/2)a$, and $[ma, \pi/2]$ as the last interval. Indeed $ma \le \pi/3$, since $a/z \le \pi/3$ and either $m = 2$ or $mz < 1/2$. This choice uses only rational comparisons on the input radius. For one such rectangle $q = L + wt$, $\phi = \pi y$, where w is its width. Use $A = X_0/L^2$, $\nu = 0$, and $C = (4/\pi)w(4d^2 L^2)^h$, so the same integrand rule applies. In each exterior rectangle $\sin q/L - z/L \ge 2/\pi - 1/2 > 0$, by $\sin q \ge 2q/\pi$ and $L \ge 2a \ge 2z$. This scaling avoids requiring that the quadrature resolve a narrow peak inside a single fixed-width angular annulus as z decreases.

In all charts the three bases A, D_-, D_+ are analytic and strictly positive on their real squares. Cover each square by bisections of the longer side. On a candidate panel, test the two rectangles enclosing the filled Bernstein ellipses of parameter 3, one complex coordinate at a time with the other coordinate real. Use complex interval evaluation to require positive lower bounds for the real parts of all three bases and obtain a modulus upper bound for f. Evaluating the log of each base separately specifies the branch throughout the corresponding rectangle. Real-path integrations remain ordinary Haar integrals.

For each fixed admissible input this search eventually gives a finite mesh at adequate working precision. Indeed the bases have positive minima on each compact real square. The exact formulas for the interval extensions, including the entire sinc, contract to their point values as panel sizes and the rounding radii of input constants tend to zero. Therefore all panels on sufficiently fine longest-side bisection levels pass at some common finite precision. Increase the maximum bisection depth and working precision until the search succeeds, then retain

that mesh and its modulus upper bounds. Denote the upper bounds for the two ellipses by M_j, K_j on panel j. In each chart let M, K be their respective maxima.

Use the quadrature of Proposition 21.2 on the retained panels. Interpolate in t at n Chebyshev roots with exact integration against t^ν, and integrate in y with an $m_n = \lfloor (n+1)/2 \rfloor$ point Gauss–Legendre rule. The Chebyshev truncation estimate and the interpolation norm give $3(1+2n)M_j 3^{-n}$ in the first coordinate. Positivity and polynomial exactness of the Gauss weights give $6K_j 3^{-2m_n}$ in the second. On a panel $[l,r]\times[b,e]$, the combined bracket is multiplied by $(e-b)\int_l^r t^{\Re\nu}\,dt$. These panel measures sum to $1/(\Re\nu+1)$ for each complete square. In particular the exact quadrature error is bounded by

$$E_{\mathrm{an}}(n) = \sum_{\text{charts}} \frac{|C|}{\Re\nu+1}\left(3(1+2n)M3^{-n} + 6K3^{-2m_n}\right).$$

One can choose n by an integer search so that a rounded upper bound is strictly below $\varepsilon/2$. This is an analytic refinement, including the integration at the singular point. It leaves no independent unpriced angular, source, image or terminal truncation error because the formula integrates the original finite Haar rectangle in full.

For clarity, the exact one-dimensional moments on a weighted panel $[l,r]$ in local coordinate $x=(t-l)/(r-l)$ are

$$\int_0^1 x^j (l+(r-l)x)^\nu\,dx = \begin{cases} r^\nu/(\nu+j+1), & l=0,\\ r^\nu\, {}_2F_1(-\nu,1;j+2;1-l/r)/(j+1), & l>0.\end{cases}$$

The second identity follows by $y=1-x$ in Euler's integral. Its argument is strictly less than one. After choosing the finite mesh and order, all nodes lie in real panel interiors, all bases at them are positive, and the moment denominators in the first case have positive real parts. Ball enclosures of the nodes, moments and finite arithmetic contract with increasing precision. Thus one obtains the quadrature midpoint m_0 and a bound E_{ar} below $\varepsilon/2$ for the Euclidean rounding error, for example by summing the two coordinate radii of the quadrature ball. The resulting error bound is $E = E_{\mathrm{an}} + E_{\mathrm{ar}}$. At the centre the gamma evaluation alone contracts. Relative refinement uses $E/(\underline{|m_0|} - E)$ when the denominator is strictly positive. For fixed nonzero T_2 this tends to zero as the absolute tolerance tends to zero. This establishes all assertions. □

Quantitative return to the ordinary centre. Fix $0<p<1/2$ and suppose $\Re h \ge -p$, $|h|\le H$, $|s-h|\le J$. Uniformly for $0<z\le 1/4$,

$$|T_2(h,s;z) - T_2(h,s;0)| \le C_{p,H,J} z^{1-2p},$$

with an explicit constant as specified below. This estimate supplies a quantitative connection on each compact subset of the ordinary centre domain. For $-1<\Re h\le -1/2$ the positive-radius rule still applies and there is no ordinary centre value in that range.

Proof. Use the unreduced variables $x=\cos\gamma\in[-1,1]$ and a uniform independent $\phi\in[0,2\pi]$ as in Proposition 8.3. The x density is bounded by $2/\pi$. Put $D_z = |x - ze^{i\phi}|$ and $D_0 = |x|$. On $|x|\le 2z$ substitute $x = z\xi$. For $u = \Re h \ge -p$ and $r\le 3$ one has $r^{2u} \le r^{-2p} + 3^{2H}$. Since $z^{2u}\le z^{-2p}$, the contribution of this region to $\mathbb{E}|D_z^{2h} - D_0^{2h}|$ is at most $C_I z^{1-2p}$, where

$$C_I = \pi^{-2}\left[J_p + \frac{4\pi\,2^{1-2p}}{1-2p} + 16\pi\,3^{2H}\right], \qquad J_p = 2\pi\,2^{2p} + \frac{2\pi}{\sqrt{2}}\frac{2\pi\,2^{2-2p}}{2-2p}.$$

Indeed J_p bounds the integral of $|\xi - e^{i\phi}|^{-2p}$ on $[-2,2]\times[0,2\pi]$. On $|\xi|\le 1/2$ the modulus is at least $1/2$. For $|\xi|\ge 1/2$, shift ϕ by π if $\xi<0$ and choose the angle θ in $[-\pi,\pi]$. Then $|\xi - e^{i\phi}|^2 \ge (|\xi|-1)^2 + 2\theta^2/\pi^2$. Scale the angular variable by $\sqrt{2}/\pi$ and enclose the translated rectangle in a disk of radius two, once per sign of ξ. The stated integrals then follow by radial integration.

For $|x|>2z$, along translation by $te^{i\phi}$ with $0\le t\le z$ the modulus lies in $[|x|/2, 3|x|/2]$. Differentiate the power along this segment. Its derivative modulus is at most $2H[(|x|/2)^{-2p-1} + (3/2)^{2H}]$. Integrating in x gives the upper bound $C_O z^{1-2p}$ with $C_O = (8H/\pi)[p^{-1} + (3/2)^{2H}]$. Set $C_0 = C_I + C_O$. The same bounds give $\mathbb{E}|D_z^{2h}| \le 4/[\pi(1-2p)] + C_0$.

Finally $T_2 = 4^h \mathbb{E}[D_z^{2h} d^{2h} W^{s-h}]$ with $W = |\Lambda_2|^2$ and $(1-z)^4 \le W \le (1+z)^4$. For $0<z\le 1/4$, $|2h\log d + (s-h)\log W| \le Az$, where $A = 8H/15 + 16J/3$. Hence $|d^{2h}W^{s-h} - 1| \le Ae^{A/4}z$. The triangle inequality now proves the estimate with

$$C_{p,H,J} = 4^H\left[C_0 + Ae^{A/4}\left(\frac{4}{\pi(1-2p)} + C_0\right)\right].$$

□

Analytic complexity as the radius decreases. For $0 < z \le 1/2$ and (h, s) in a compact subset K of $\{(h, s) : \Re h > -1\}$, the number of rectangle panels required for the ellipse test can be bounded by $C_K(1+|\log z|)$. In the central charts, $\alpha/a = \pm 1$, $a \in (0, \pi/6]$, and the displayed formula for A extends to $a = 0$. Its argument for strict positivity still holds at $a = 0$: if $u > 0$ the radial square is u^2, and if $u = 0$ the angular square is positive. In the exterior charts the ratios z/L and w/L are bounded by $1/2$ and 2π, respectively, and A has the uniform positive lower bound $(2/\pi - 1/2)^2$ on the real squares. The use of $(q/L)\operatorname{sinc} q$ for $\sin q/L$ gives uniformly bounded analytic derivatives in t, y on a fixed complex neighborhood of each square. In both kinds of charts $D_\pm \ge 1/4$ on the real square, and derivative bounds for those factors are also uniform. Compactness and the positive minima thus give a uniform sufficient panel depth and uniform M, K bounds. At adequate precision the rectangle tests can verify such a cover.

Set $q_K = \max(0, -1 - 2\inf_K \Re h)$. Each prefactor has modulus bounded by $C_K a^{1+2\Re h}$ for the central charts or by $C_K L^{1+2\Re h}$ for an exterior chart. Using $z \le a \le (\pi/3)z$ and $L \ge 2a$, the error estimate therefore gives, after increasing C_K,

$$E_{\mathrm{an}}(n) \le C_K(1 + |\log z|)(1 + z^{-q_K})2^{-n}.$$

Here the factor $1 + n$ has been absorbed by replacing 3^{-n} with a constant times 2^{-n}. In particular the degree needed for an absolute target ε is $O_K(1+|\log z|+\log^+(1/\varepsilon))$. The order estimate refers to the analytic quadrature. It makes no assertion about the required working precision near the ordinary boundary or near a zero of the complex moment.

Executed checks. For the exact inputs $z = 9/10$, $h = -19/20 + 3i/10$, and $s = 2/5 - i/2$, increasing the analytic degree from 36 to 40 and the precision from 128 to 256 bits reduced the certified disk radius from less than 7.246×10^{-10} to less than 9.311×10^{-12}. The final modulus test gives relative error less than 5.623×10^{-13}. An independent harmonic-polynomial calculation with directed MPFI endpoints at $z = 10^{-10}$, $h = -0.82 + 1.5i$, $s = 0.3 - 0.4i$ gives a midpoint within 5.69×10^{-30} of the scaled cubature midpoint, which has a certified radius less than 9.540×10^{-12}. The rank-two cubature also returned disks containing the exact polynomials $(1 - z^2)^2(1 + 4z^2)$ at $h = s = 1$ and $1 - z^4$ at $h = 1, s = 0$. These are individual computed certificates; the termination and error statements above are proved independently of them.

A contracting absolute enclosure from the original Haar integral

The finite source, image and terminal representations can have different error floors. There is a direct fallback with arbitrary absolute refinement throughout the ordinary finite-size domain. It uses Weyl integration and an explicit small-mark bound, and has a high cost in rank and near the ordinary inverse threshold. It supplies an existence and termination theorem, with the faster certified routes retained for practical evaluation.

Theorem (direct evaluator and its ordinary domain). Take $0 \le z \le 0.9$. For $N = 1$, every complex h, s is admitted. At $N = 2, z = 0$ require $\Re h > -1/2$. For $N = 2, z > 0$ and $N \ge 3$ require $\Re h > -1$. At each exact admitted parameter tuple, a finite algorithm constructs a rigorous absolute enclosure of T_N at every prescribed positive absolute tolerance. At nonzero values the algorithm with successive absolute tolerances terminates with relative radius at most 10^{-10}. These statements are pointwise in the parameters. At a certified zero arbitrary absolute tolerances are available. Exact zero recognition requires separate evidence.

Small-mark estimate. Transform each eigenvalue by $\mu_j = (\lambda_j - z)/(1 - z\lambda_j)$. The mark becomes $D = Nz + \sum_j \mu_j$. With respect to independent uniform angles of the μ_j, the complex Haar weight is exactly

$$W(\mu) = \frac{d^{N^2+2Ns}}{N!} |\Delta(\mu)|^2 \prod_{j=1}^{N} |1 + z\mu_j|^{-2(N+s)}.$$

Indeed the angular Jacobian is $d/|1 + z\mu_j|^2$, each pair distance is multiplied by $d/(|1 + z\mu_i||1 + z\mu_j|)$, and each $|1 - z\lambda_j|$ equals $d/|1 + z\mu_j|$. For $N \ge 2$ bound every Vandermonde pair except the first by 4 in squared modulus. With $u = \Re s$, this gives

$$|W| \le C_*|\mu_1 - \mu_2|^2, \qquad C_* = \frac{d^{N^2+2Nu}}{N!} 4^{N(N-1)/2-1} \max\{(1 - z)^{-2(N+u)}, (1 + z)^{-2(N+u)}\}^N.$$

The weighted pushforward of $\mu_1 + \mu_2$ has planar density $\mathbf{1}_{0<|v|<2}\sqrt{4-|v|^2}/(\pi^2|v|)$. To check the formula, the conditional direction is uniform by rotation, the radial variable is $2|\cos(\theta/2)|$ for uniform angle difference θ, and the retained squared pair distance is $4-|v|^2$. Thus the square-root singularity at the aligned endpoint cancels.

At $N = 2, z = 0$ the bound on the mass of $|D| \le r$ is $4C_*r/\pi$. At $N = 2, z > 0$ and $r \le z$ the same mass is at most $2C_*r^2/(\pi z)$, since the pair sum then has modulus at least z. For $N \ge 3$, condition on the angles after the third and integrate the third angle against the pair density. For any center a and point ω, the integral of $|v|^{-1}$ on $B(a-\omega, r)$ is at most $18\pi r^2/(r+|a-\omega|)$. If the distance of the center from zero is at most $2r$, the disk is in $B(0, 3r)$ and the integral is at most $6\pi r$. Otherwise $|v|$ is at least half the distance of the center, giving the bound.

For $0 < \epsilon < 1$, the inequality $(r+x)^{-1} \le r^{-\epsilon}x^{-1+\epsilon}$ and a circle arc bound give $\mathbb{E}|a-\mu_3|^{-1+\epsilon} \le 2+1/\epsilon$ uniformly in a. In fact, for $t \le 1/2$ the arc of points at distance at most t from a has uniform probability at most t: choose one such point and use the chord bound $2t$ relative to that point. Integration of the distribution function of $|a-\mu_3|$ gives the stated estimate. Consequently the small-ball mass is at most

$$C_* \frac{36}{\pi}(2+1/\epsilon)r^{2-\epsilon}.$$

Choose $\epsilon < 2+2\Re h$. These computations require the rank case in the ordinary domain to which they are applied. The divergence boundaries are the original centre and interior boundaries in Sections 1 and 4. At rank one $|D| \ge 1 - z$ directly.

Absolute enclosure and the full refinement. Write the resulting small-ball inequality as $C_1 r^a$. For $H = \Re h < 0$, a dyadic decomposition of $|D| \le R$ bounds the absolute integral discarded there by

$$C_1 \frac{2^{-2H}R^{a+2H}}{1-2^{-(a+2H)}}.$$

For $H \ge 0$ the simpler bound $C_1 R^{a+2H}$ suffices. Both decrease to zero for the chosen parameters. Take a continuous cutoff in $Q = |D|^2$ equal to zero through r^2, linear on $[r^2, 4r^2]$, and one from $4r^2$ onward. For positive bases compute the power using $\max(Q, r^2)^h$. The error from this substitution and cutoff is bounded by the preceding formula with $R = 2r$. At fixed $r > 0$, all remaining factors are continuous elementary functions on the compact angular box and their bases are bounded away from zero. Interval evaluation followed by multiplication by cell volume encloses the integral on each cell. The implementation sums outward interval endpoints as exact dyadics before the final ball conversion. The sum of widths tends to zero: for fixed r each elementary operation, including the clipping operations, has a uniformly continuous interval extension on its input enclosure, and working precision can increase as the angular mesh shrinks. One can equivalently use a finite bound on the derivatives of the smooth factors and the explicit Lipschitz norm of the cutoff. Thus first choose r so that the discarded integral fits its budget, then refine mesh and arithmetic until the remaining budget is met. There is no separate source, Mellin image or terminal truncation in this direct representation. Its cutoff, angular and arithmetic errors are all refined. This terminates at every requested absolute tolerance.

If the output disk is $D(m, E)$, a validated $\ell \le |m|$ with $\ell > E$ returns the relative bound $E/(\ell - E)$. For a fixed nonzero value, as the absolute radius is driven to zero the modulus lower bound can be refined to the true modulus, so this rule eventually certifies the target. In contrast, a disk containing zero establishes only the additive bound. To evaluate very close to a zero, the local atlas and the adaptive source and image routes in Section 21 remain useful because the direct fallback can require very fine angular meshes. A bounded resource request can exhaust either method without deciding divergence or exact vanishing.

22. Verification and limits of the results

The scripts distinguish a numerical comparison from an enclosure with a proved error bound. The rank-two determinant derivation is checked at integer, noninteger and resonant exponents. The interior large-size checks evaluate a finite Toeplitz determinant and its radial integral against the limiting Kummer expression. The depth scripts compare the $1/N$ correction with the exact confluent determinant and compare the microscopic projection covariance with an independently evaluated finite moment. At $N = 384$, $m = 2, j = 1, c = 1.3$, the first-order corrected normalized value differs from the exact formula by approximately 9.17×10^{-7}; halving the mesh $1/N$

divides the error by approximately four. These samples test the derivations. The estimates in the text supply their proofs.

At the centre, rank three has a separate difference equation tested against exact trace moments. The executable interval evaluator includes exact rational input conventions, outward-rounded complex arithmetic and a separate relative-error status. Rank one covers independent h, s. The rank-two centre requires $\Re h > -1/2$. Its interior diagonal branch covers $0 < z < 1$, $s = h$, $\Re h > -1$, including the logarithmic resonances. At $N = 2, z = 0.9, h = s = 0.6 + 0.2i$ the exact-endpoint export certifies relative radius below 6.5×10^{-36}. An independent high-precision Haar integral lies inside. A second high-precision test checks a logarithmic resonance. At $N = 2, z = 0.12, h = 0.6 + 0.2i, s = 0.1 - 0.2i$ a separate two-angle method certifies a relative error below 8.053×10^{-14} against independently evaluated quadratures. The same pair at $z = 0.9$ exceeds its default degree budget. The $s = h + 1$ method for $\operatorname{Im} h \neq 0$ succeeds there on its own slice. These Haar-side checks give independent references for the determinant route. A general finite-degree determinant method supplies further enclosures; the size of its truncation bound depends strongly on the parameters. Its code and receipt record successful points and cases where the enclosure is broad.

The additional controls for the inverse-moment theorem exercise its different steps. Finite Toeplitz entries were compared in the original and transformed angles; two regularized inverse moments and two smoothed densities at each of ranks 4 and 10 were checked by independent direct Haar matrix sampling. At $N = 2$, $s = -1$, $h = -1/4$ and $c = 0.75$, two finite-angle quadratures give approximately 1.040163 for the probability-normalized inverse moment. Exact mass, mean and variance tests cover several negative integer tilts. Direct finite determinants and the limiting Fredholm quadrature provide a separate comparison at $s = -0.8$ and at genuinely complex sources. A finite construction checks the two-angle Jacobian and exterior interaction used for the lower bound. The package's replay reports parameters, refinement differences and sampling errors. The probability bounds and the sharp threshold follow from the analytic estimates.

Scope of the inherited checks. The integer correction and compact-interior or fixed-depth estimates were tested in their respective regimes. The extension to independent noninteger microscopic exponents uses the whole-plane estimates of Section 16. Sections 18 and 19 supply separate simultaneous estimates. Sections 20–21 give the domains and accuracy of the numerical enclosures. A divergent expectation requires a domain status, and a zero requires an absolute-error criterion.

Earlier finite-size and fixed-depth checks

We reconciled the 24-page predecessor, its two editable sources, the finite-size reconstruction, verification receipt and companion archive. All 52 entries in its checksum manifest matched. The 20 continuation check programs and four foundational programs ran again. In one foundation control at $N = 2, z = 0, h = 1/2$, truncation of the Mellin integral at $R = 512$ gives 0.8488275774 against $8/(3\pi) = 0.8488263632\ldots$. The explicit bound $\Phi(R)/R < 2.43 \times 10^{-6}$ covers the omitted tail, while numerical quadrature carries its own error.

Six further programs exercise the new asymptotics and equations. The source test compares finite Toeplitz determinants to an independently discretized Fredholm determinant. Nine fractional-moment cases cover real inverse and complex orders at tilts $-1, 0, 1$. An adversarial test omits the predicted translation and retains a first-order discrepancy. Direct finite sources, exact second moments, circle comparisons and Haar sampling test the scale transitions. Their finite grids and sampling uncertainties are recorded. They give no certification of an asymptotic rate. The exact rank-two modular minor, rational polynomial identities, 11 exact rank-three trace polynomials and two exact symmetric-power row relations are separate algebraic checks. Independent angular grids gave scaled residuals 6.75×10^{-13} and 3.11×10^{-15} for the rank-three radial equation on opposite sides of its singular point $z = 1/3$.

A seventh program exercises the enclosures of Section 21. At $N = 2$, $z = 0.9$, $h = 0.6 + 0.2i$, $s = 0.1 - 0.2i$ it gives

$$T_2 = 0.27444094092833382 + 0.00204013902317259i \quad \text{with absolute error below } 3.92 \times 10^{-14}. \tag{22.1}$$

The proof of the bound combines the analytic panel remainder with rigorous ball arithmetic. The relative radius for the full precision midpoint is below 1.427×10^{-13}. The calculation used 2,327 accepted panels and 2,908,750 node pairs at Chebyshev order 50. Independent Haar integration at angular grid sizes 4096, 8192, 16384 and 32768 gave decreasing differences, ending at 8.06×10^{-15} inside the enclosure. At $z = 0.4, h = -3/4, s = -2$ the

same code gave a relative radius below 9.42×10^{-14}. An independently certified diagonal computation overlaps after the exact change of normalization in Section 10.

N	z	Order j	Tilt s	Upper bound for relative radius, integer-jet method
8	0.9	1	$0.1 - 0.2i$	2.28×10^{-43}
5	0.9	2	$0.1 - 0.2i$	1.67×10^{-42}
32	0.9	1	-1	5.00×10^{-43}

Two more runnable checks verify the whole closed region of Proposition 21.3 and the adaptive algorithm of Theorem 21.4. Interval evaluation on 32 closed spectral subintervals covers the full complex parameter ranges of the proposition. The largest tree used 7,104 rectangle tests. A point with $z = 0.55$, $h = 0.75 + 0.0007i$, $s = 0.016 - 0.028i$ required successive passes at 64, 128 and 256 bits, giving a relative error bound below 4.23×10^{-13}. A deliberate cap at 64 bits returned a failure status. Both ends of the spectral interval and the exact value 15/16 at $z = 1/2, h = 1, s = 0$ were checked.

The last entry of the integer-jet table equals $(1+z^2)/(1-z^2)$, an exact check. Other controls use the untilted second moment at four ranks and an independent rank-two angular integral. The tests also exercise zero-containing enclosures, inadmissible exponents, excluded locations and resource exhaustion. All reported comparisons use the normalization of Section 1.

Checks on the expansion at fixed depth

The exact occupied-space determinant and (16.4) were evaluated by independent angular and half-line calculations. At four real-tilt test points the discrepancy was below 2×10^{-14}. Removing the scalar charge gave discrepancies as high as 0.64. An independent first-order comparison using the two exterior frequency windows included the phases of both orientations. A separate radial quadrature at two noninteger real tilts and three continuous orders (including inverse and nonreal powers) gave final rank-doubling error ratios between 0.240 and 0.278 after the first correction. Direct complex angular readouts at $h = -0.32 + 0.16i$, $c = 5$ and three nonreal tilts, including $s = 0.44 + 0.91i$, retained the imaginary components and satisfied the conjugation check. The largest observed change on quadrature refinement at rank 24 was 1.22×10^{-5}.

The Cayley multiplier was independently checked at positive and negative Fourier modes and at $s = 0.43, -0.85, 1.37$. Through the cubic term at ranks 12 to 96 the last doubling ratios ranged from 0.06077 to 0.06470, compared with 1/16 for the leading omitted power. Exact symbolic Laurent coefficients at tilts one and two test the P^3 insertion. At the two nonreal tilts below, the original Toeplitz determinant at zero source and an independent slit-integral Hankel determinant agreed within 2.4×10^{-13} at the tested ranks from 16 to 256. The entries are the ratios of the absolute errors at ranks 256 and 128 after subtracting the first three predicted terms.

Depth and tilt	Full second coefficient	Omit the cubic symbol term	Omit the second determinant variation
$c = 1.7$, $s = 0.42 + 0.93i$	0.12533	0.25969	0.25072
$c = 2.4$, $s = -0.72 + 1.05i$	0.12484	0.25112	0.24683

A separate calculation at independent nonzero source coordinates $p = 0.65 - 0.22i$, $q = -0.18 + 0.46i$, $c = 1.65$, $s = 0.4 + 0.95i$ tested the phase as well as the two mixed blocks. The full and omitted-cubic doubling ratios were 0.12544 and 0.26020.

Both omissions leave an error at order N^{-2}. The full coefficient gives behavior consistent with the next power N^{-3}. These are floating-point comparisons and exact algebraic controls on the specified examples. The uniform estimates in Theorems 16.3 and 16.4 come from the proof.

Checks for the two moving-depth limits

At rank two the two orderings of the eigenangles giving $Y = 0$ are $\theta_\pm = \pm \arccos z$. Direct angular area change gives the exact central density

$$p^Y_{2,s,z}(0) = \frac{2(1-z^2)^{2s+5/2}}{\pi^2 z Z_2(s,z)}.$$

Indeed Y is the average of the two terms $\lambda/(1-z\lambda)$. At the indicated angles write $b = \sqrt{1-z^2}$. The mutual squared Vandermonde is $4b^2$, the tilted product is b^{4s}, and the absolute Jacobian in the unscaled eigenangles is $z/(2b^3)$. Inserting the two orderings and Weyl's factor $1/[2!(2\pi)^2 Z_2]$ gives the formula. A direct integration of the probability of a disk, using mean angle and half-gap, recovered this coefficient at four tilts from -0.44 to 1.7. Two angular mass calculations agreed within 1.1×10^{-14}.

At rank three a separate integral conditions on one eigenangle and selects the nearest positive and negative solutions of the pair equation. At $c = 1/6400$ the ratios to the fixed-rank central density asymptote were 1.000035, 1.008181 and 1.000077 at $s = 0, -0.29, 0.65$, respectively. Removing the squared mutual Vandermonde at that depth enlarged the computed density by approximately 7200. Three deterministic exterior configurations at ranks 12, 23 and 45 also test (19.3) away from the origin. Independent root solving in the original angles and finite differences verified the pair Jacobian with relative discrepancy below 2.1×10^{-10} at the tested points. Those comparisons condition on the specified exterior. The integral over all exterior configurations is justified by the proof of Theorem 19.2.

At zero tilt independent Haar samples at $(N, c) = (6, 0.03), (12, 0.012), (24, 0.005)$ tested $h = -3/4$ against the exact Cauchy circle value 1.5737874654. The difference between the capped interior observable and its same-matrix circle value averaged 0.01226, 0.00625 and 0.00274 respectively. Sampling used a cap of eight for the interior observable. Equation (19.5) controls the singular uncapped observable analytically.

For growing depth, exact extrapolation and tilt-one mass identities test the rank comparison in Theorem 18.2. At rank 24, $s = 0.45 + 0.88i$, $h = -0.32 + 0.16i$, the observed errors relative to the moving Gaussian value at depths $4, 6, 9, 12$ were $0.1389, 0.0517, 0.00345, 0.000124$. On a slowly growing depth sequence at the three moderate ranks tested the errors increased from 0.0497 to 0.0850. The uniform asymptotic upper bound supplies no assertion of monotone errors at these ranks. The determinant comparisons and their refinements are numerical diagnostics. The rigorous finite-rank enclosures have the separate domains in Section 21.

The one-angle calculations at the upper threshold have independent controls. Direct two-angle Haar quadrature at rank two and $c = 2 \times 10^{-7}$ agreed with the predicted finite-rank supercritical coefficients within 9×10^{-8} for the tested complex orders. At critical real order, the observed logarithmic slopes were 0.34767849 and 0.28231424 for tilts -0.21 and 0.35, against the finite-rank values 0.34767860 and 0.28231406. The rank-one hypergeometric formula and the exact all-rank untilted second moment supply algebraically distinct checks. The computations keep the rank fixed in the angular quadratures. Passage to unbounded rank follows from the uniform insertion estimates.

At $s = 0$, direct rank-two angular quadrature for $h = 1/2 + 0.31i$ and $1/2 + 0.78i$ at $c = 10^{-8}$ gave absolute discrepancies below 1.7×10^{-9} after both terms of (19.10) were included. Suppressing its oscillatory term gave discrepancies exceeding 0.32 at both orders. The exact Barnes product at $s = 1$ also tests the nonvanishing change of centering in (19.11) for $c = e^{-N}$.

Independent checks of complex tilt at shrinking depth

At $h = 0$, (19.20) gives the Barnes mass g_s. At zero tilt the circle trace has characteristic function $e^{-|\xi|}$ at every rank by (19.17), so its mass-one density is $1/[\pi(1+x^2)]$. Integration gives $\mathcal{C}(0,h) = 4^{-h}\Gamma(1/2-h)/[\sqrt{\pi}\,\Gamma(1-h)]$ for $\Re h < 1/2$. At integer orders one and two there is another check. If $P = \sum \cot(\theta_j/2)$ and $Q = \sum \cot^2(\theta_j/2)$, integration by parts against the circle Cayley density with vector fields $(1+x_j^2)P$ and $x_j(1+x_j^2)$ gives respectively $2s\mathbb{E}_s P^2 = N + \mathbb{E}_s Q$ and $2s\mathbb{E}_s Q = N^2 + \mathbb{E}_s P^2$. Here $\mathbb{E}_s$ denotes the mass-one circle functional. The integrations may first be done for sufficiently large real s and extended to $\Re s > 1/2$ using finite-rank absolute integrability. For the fourth power, principal-corner consistency makes $\mathbb{E}_s P^4$ a polynomial of degree at most four in rank, whose coefficients can be obtained from the four finite-rank beta determinants and the zero constant term. The

independent integer-order derivation in the accompanying notes gives

$$g_s\mathcal{C}(s,1)=g_s\frac{s^2}{4s^2-1},\qquad g_s\mathcal{C}(s,2)=g_s\frac{8s^4-16s^2-3}{8(4s^2-1)(4s^2-9)}$$

on $\Re s>1/2$ and $\Re s>3/2$, respectively. For $h=s=1$ the first result is $1/3$.

Eleven additional verification programs accompany this edition. Independent angular and positive-matrix gamma determinants for the trace transform differed by less than 2×10^{-43} at five nonreal test points of ranks one to four. Dropping $e^{-|\xi|}$ changed the results by more than 0.58 in each test. Direct angular integration with prescribed interior angles agreed with the cofactor transform to within 3×10^{-16} at the tested ranks. The linear and quadratic integer-order checks use independent rotation identities and Cauchy determinants. Rank-two angular integrals also test noninteger inverse orders, and ranks three, six and twelve test the first integer order along logarithmic and polynomial depth sequences. A separate paired Haar simulation at $s=0.82i$, $h=-0.81+0.19i$ uses a radius cutoff of 0.17 in the inverse power and reports the sampling error of the paired difference. This simulation tests the truncated readout. The near-zero area estimate for the uncapped integral is proved in Theorem 19.10.

Two genuinely nonreal tilts test the transverse cutoff at $c^2R=0.32,1.4,2,2.45$. Critical-order quadrature uses both $h=s+1/2$ and $h=s+1/2+0.37i$, with a deliberate omission of the oscillatory term. Scripts, parameters, refinements and measured discrepancies are in the verification records. These comparisons check formulas and normalizations. The existing interval enclosures and their domains are given separately in Section 21.

Checks on the density transition and radius equations

All 59 programs in the complex-tilt edition were rerun. The exact input Markdown, archived manuscript, published-input citations and original separate research note were reconciled with the release manifest. New comparisons evaluate the two-angle map directly, with both signs, its real absolute Jacobian and a finite number of resident variables. At ranks two and three the direct angular integrals test the correction (19.32) for nonreal tilts and more than one depth sequence, including the term proportional to the squared imaginary mark. A separate angular-sector calculation checks (19.33) away from its symmetry axis. Omitting the coefficient or dropping the angular factor gives a different asymptotic discrepancy. The source-derivative tests compare direct angular integrals with Fourier determinants at ranks two, five and ten, and omit the mark derivative as a negative control. Exact rank-two inverse formulas test the transport and its moving-overlap coefficient.

Independent finite-rank angular quadratures test the one-angle tail correction, the next open threshold band and the inner scale at its first cutoff. The three-angle planar check instead keeps the imaginary coordinate fixed and compares an angular coarea with a separate level-surface integral. It includes upper-side checks of the absolute two-angle Jacobian. Every numerical comparison uses finite parameters. The uniform constants in (19.29)–(19.36) come from the density, coarea and remainder arguments.

The displacement checks use all 35 rank-three monomials, direct integration and deliberately reversed derivative signs. The ranks of the two elimination matrices in (10.6) are checked by exact modular pivots. This finite calculation certifies nonzero rational minors. Angular quadrature of the resulting differential equations is an independent floating-point comparison. These controls and their parameters are reproduced in the companion scripts and transcripts. The validated relative-error claims for evaluating the original moment continue to have exactly the scope of Section 21.

A symbolic control exercises the four quotient operators used for generic-rank elimination at several mode cutoffs, including larger cutoffs than the directly integrated ranks. At rank three with $z=2/5$, $s=-1.28-0.45i$ and $h=2.25+0.31i$, the largest scaled discrepancy across 35 physical derivatives at 88 nodes per angle was 2.09×10^{-9}. Dropping the displacement from the physical derivative gave 1.14. At the one-angle front we also integrated the exact rank-two planar density against a nonsymmetric smooth test for real and genuinely nonreal tilts. The tests distinguish the signed first-order correction for the two front directions.

Numerical checks on transmission and certified scalar values

The reference edition was recovered both as the named Markdown file and from its 193-entry verified release archive. Their manuscript bytes agree. We reran all 70 previous verification programs, including the modular rank, angular-derivative and filtration checks behind Theorem 10.5. Their transcripts and the unchanged separate

research note are included with this edition. The published fixed-interior limit and the imported determinants retain the attributions given where those results enter the paper.

The reduced system was checked by exact rational arithmetic on both sides of critical radii at ranks three and four, with an additional rank-five integer-moment test. A second exact test supplied the independent normal components at the resonances $\rho = 2, 3$ at ranks three and four. Source angular integrals and right-endpoint integrals for the floating-point comparisons were computed independently of the outgoing ordinary equation. Resolving signs matters even for the original scalar equation. At rank three, with $s = -3$ and $h = -1/2$, an order-derivative connection in the independently constructed fourth-order scalar equation was within 1.93×10^{-7} of a fresh Bessel determinant quadrature; either single arc missed by about 0.407. The analytic beta-integral model also tests the exact derivative rule independently of both matrix implementations.

For the reflected full-vector system, take $N = 3$, $s = -2.54 + 0.29i$, $h = 0.65 + 0.19i$. Continue round the upper and lower arcs of radius .055 about $z = 1/3$. With 34-node incoming and 46-node independent outgoing conditional integrations, the scaled discrepancy of the physical combination over all 19 retained components was below 1.6×10^{-12}. The upper arc alone gave 3.02×10^{-4} and the lower alone 9.16×10^{-5}. At the exceptional $h = 1/2$ the arcs themselves agreed within 2.1×10^{-12}, yet using just their common value gave a scaled discrepancy of 6.42×10^{-4}. Adding the order derivative reduced it below 1.8×10^{-11}. Sampling and ODE tolerance in these comparisons yield numerical discrepancies. Proposition 10.10 gives the separate certified full-vector example, including its much larger radius.

The following are outward upper bounds for a different computation, the original physical scalar integral evaluated at the radius shown. In the first two rows h is separated from all integers. The real parameter components in these runs were input as exact rational numbers.

N	z	h	s	Hermite grid k	Relative error bound
3	1/3	$2.65 + .30i$	$.18i$	90	2.80×10^{-11}
4	1/2	$2.9 + .08i$	$.2i$	95	2.01×10^{-11}
3	1/3	$2.99999 + .00002i$	$.4i$	30	7.98×10^{-13}
4	1/2	same	$.4i$	30	1.70×10^{-11}
5	1/5	same	$.4i$	30	1.25×10^{-11}
8	1/4	$2.99999999 + .00000002i$	$.4i$	22	5.95×10^{-12}
8	1/4	$2.85 + .09i$	$.4i$	14	.00133

At $N = 3, z = 1/3$, $s = -3 + .18i$, $h = -.15 + .3i$, a grid of 18 gives absolute error below .282 and relative error below .117. Changing the order to $-.85 + .3i$ gives absolute error below 48.45; its enclosure contains zero and supplies no relative claim. Independent integer-jet enclosures overlap the one-variable determinant answers through order two at ranks $2, 3, 4, 8$. A perturbation of the angular averaging factor was detected. A 100-bit evaluation at $k = 27$ produced a nonfinite enclosure and was rejected. The accurate rank-three and rank-four calculations used 1370 and 1648 bits respectively, taking about 43 and 91 seconds in the recorded runs. Corollary 21.6 bounds the analytic tail uniformly on its closed box; those two computations use Theorem 21.5 and much smaller grids.

Proposition 21.7 gives an independent scalar enclosure on the inverse-order slice $N = 3$, $s = -3$, $h = -1/2$, at radii $1/4, 1/3, 161/300$. The largest relative radius of the three full-precision balls was below 8.55×10^{-22}. Omitting the Bessel tail gives a disjoint interval at every point.

For Proposition 21.8 four independent left-hand Bessel enclosures were used as data in an interval shooting problem. The 76-panel validated calculation gave the physical value $4.56870010441547136650724\ldots$ at $z = 121/300$. The interval calculation proves that either single arc gives the wrong scalar. The companion test also reconstructs the source balls from their convergent integrals.

Verification of the full-state propagation

The named higher-rank radius source comprised 129 pages. Its editable text matched the companion archive byte for byte. All 250 entries of the predecessor manifest were checked and all 92 mathematical verification programs were rerun, including the inverse-order four-state crossing, rank-two controls, integer-moment tests, and the rank-four floating-point failure. The earlier special crossing uses $h = -1/4$, $s = -3$. The present 20- and 35-state runs use distinct parameters and distinct initial integrals.

The new exact checks are the degree-bounded generator identities, the rank-three residue identity, the rank-four Laurent identities and shear, and the coefficient constructions. The interval checks are the separate incoming source enclosures, the nonvanishing denominators on the complex paths, the polynomial defects and inverse bounds, the physical phase combination, the end-condition checks, and the continuous lower-modulus cover for the separate scalar evaluator. The raw files contain rectangular real and imaginary enclosures as well as scalar disk budgets. A disk about an unshortened centre may be narrower than the radius obtained by circumscribing its displayed componentwise rectangle. The standalone verification records give the exact rational parameters, the component order, precision, truncation, branch signs and endpoint definitions.

The following comparisons have a different evidential status. Angular grids and centered differences compare independent implementations of the physical reduction. They have no certified integration remainder. The floating-point minimization of a representative scalar row only proposes dyadic coefficients. Its eventual error bound uses exact annihilation on the physical solution and interval norms of the proposed row. Overlap between independent enclosures checks consistency; each construction supplies its own inclusion proof. The derivatives of the preparation and the Weyl normalization enter both the physical definition and the error analysis. Removing them makes the specified control intervals disjoint. The raw source, scripts and preserved research note accompany this edition.

Two restricted extensions are reproducible from the new material. At rank three the order-jet calculation propagates 40 coordinates and evaluates the derivative connection at a zero of the cosine. At the two regular outgoing radii the scalar table has a verified lower modulus across each continuous parameter set. These have distinct sources of accuracy: a full path proof at the chosen points, and direct original-Haar integration for the continuous sets. The new parameter disks and rank-four exceptional calculation are given in Theorems 10.15–10.17 and 21.12. Consecutive critical crossings with a shared uniform budget and full-path validation of smaller moving charts remain open.

For a fresh input, the distributed driver constructs its rational equation and both full branch matrices. It compares the scalar disk against the requested absolute budget and, if requested, a relative budget using a positive lower modulus. On a failed budget it refines the angular input and tests it with the already enclosed path matrices before increasing the path precision. At $N = 3$, $h = .8 + .33i$, $s = -1.1 - .4i$ the original 32-node seed gave radius .0003222, exceeding the requested .0001. Increasing the source to 58 nodes while retaining the 208-bit, degree-34 path matrices gave $1.08379441771 + .46006981499i$ with absolute radius below 1.224×10^{-5}, including rounding of the printed centre. The separate determinant disk overlaps it, and each of the two single paths and equal weighting is excluded against that witness by at least .0001724. This example uses a preparation outside the small-tilt neighborhood of Proposition 21.10.

Verification of the parameter-uniform crossings

The complete preceding manuscript and 560 archived checksum entries were recovered, and all 92 predecessor mathematical verification programs were rerun. We replayed the preceding pointwise source, branch-combination, adjoint, exceptional-order and scalar parameter-set checks. The new uniformity comes from finite polynomial and contour remainder bounds, signed product inequalities, and uniform source and endpoint constructions. Tested points include independent nonreal inputs on the parameter boundary, the rank-three half-integer exception, and the rank-four integer exception. The separate research note and supplied project correspondence are retained with the sources. A cold execution of the full 56-order, two-arc computation at rank four was not used to obtain the uniform estimates. The quadrature rules, mathematical error bounds, actual pointwise runs, and independent determinant and angular comparisons have separate receipts.

A direct, inexpensive check uses each central transfer unchanged over a very small disk and rigorously bounds its perturbation. The table after Theorem 21.12 reports the largest permissible budgets chosen for that test. The disk radii reflect interval overestimation in that constant approximation. Across both disks omitting either path,

setting the weights equal, or dropping the physical normalization gives separated enclosures. At an exact rank-four exception dropping the *paired* derivative correction preserves the value by the special polynomial identity in Theorem 10.17, whereas dropping just one term fails. Actual local Schwarz or Frobenius columns alone do not determine the physical normalization.

At rank four a constant-frame infinity-norm estimate of input amplification at an off-centre integer order exceeded 10^{169}. Enclosing the Euclidean logarithmic norm, and retaining signed interval products before bounding them, lowered the bound below 1.446×10^{27} there. Both vector detours were also recomputed from the same dyadic incoming centre using residuals. The independent angular input and output certify each branch separately. This example measures the price of treating every local perturbation as if it had the worst possible direction. It gives no estimate for the conditioning of repeated crossings at much larger rank.

At the rank-three exception we also used a short contour with only four orders $3/2+i^j/65536$, $j = 0, 1, 2, 3$, keeping $s = -2.86 + .21i$. Each signed Hankel source was evaluated and each 20-vector was integrated independently on both full paths. The largest charged sample-component error was below 4.054×10^{-23}. Applying the same coefficient shift, now with the four-sample alias bound, gives

$$T_3(3/2, -2.86 + .21i; .4) = 17.0010443095541343 - 5.7082467510233774i \quad \text{(absolute error below } 1.395 \times 10^{-11}\text{)}.$$

The inherited 40-state derivative result is contained in this enclosure. Omitting the derivative is excluded by more than 9.5869×10^{-6}. At $3/2 + 10^{-8}i$ the same four samples also overlap the previously recorded independent determinant witness. At the nearby nonreal order $3/2 + (1+i)/2^{26}$ the same samples give $17.001044780330144 - 5.708246541625590i$ with absolute error below 1.396×10^{-11}. This short-contour run checks the derivative construction with actual propagated physical states. The synthetic 56-node branch check, whose derivative contribution was deliberately large, separately tests the orientation and the implemented coefficient recovery.

For both main disks a simultaneous boundary point is $h = 29/16 + i/4$, $s = -N + .14 + .2725i$. An independent rank-three polynomial matrix product, at degree 80 and 140 fractional bits per panel, was applied to a unit column. All 20 entries overlapped an independent residual integration. At rank four a 700-fractional-bit integer computation propagated a unit vector along each 64-panel path. The canonical endpoint errors were below 6.354×10^{-42} and 4.009×10^{-43}. The independent interval column comparisons resolved the coordinates to 1.704×10^{-13} and 1.505×10^{-14}. A unit-column test does not by itself initialize the physical solution; both these checks and complete angularly initialized runs are reported.

The fresh rank-four boundary test gives a direct illustration of interval wrapping. A first ordinary product gave a disk radius above 2×10^{19}. Recentring the degree-42 panels and retaining their signed suffix matrices, including the correlated incoming error and the outgoing direction, gave an absolute scalar disk below .000470 about $6921.11657693 - 3443.99666536i$. This coarse run still could not separate every alternative connection rule. The stored failure of that control is part of the verification record. The subsequent high-precision full-path and directional receipts isolate the source and transport contributions. The preceding historical working edition's first rank-four floating failure occurred at a different radius and remains separately documented.

Using all 35 signed Hankel input coordinates and the higher-degree level-three branch matrices at this boundary gives the scalar $6921.116577911213553 - 3443.996667507268870i$ to within 3.52×10^{-13}. Its source term alone is below 1.136×10^{-14}. For the upper-only, lower-only and equal-weights alternatives the respective same-input discrepancy lower bounds exceed 6.765×10^{-7}, 1.406×10^{-7} and 3.709×10^{-7}. The independent scalar determinant has a wider uncertainty here and separates only the first wrong rule by itself. The full reference values, ordered panel matrices, precision and controls are retained.

On the same boundary data a final directional contraction of all 128 level-three panels reduces the disk to 1.136×10^{-14} about the stored high-precision centre. The propagated defect contributes below 6.066×10^{-31} in the physical scalar direction; the signed source supplies almost the entire remaining uncertainty. The three incorrect-branch tests now separate even after all directional uncertainties are charged.

At the same boundary in rank three a cold evaluation of the order-dependent uniform source and both full 20-state trajectories, with 800-bit working arithmetic, gave $27.925959968513768935659848062 48 - 2.127113554503328174719631910 20i$ with absolute error below 1.001×10^{-25} about the displayed centre. The separately integrated scalar determinant agreed with this disk. This executed query includes angular initialization, transport, physical mixing and the final scalar projection. Its comparison witness is substantially wider.

Accuracy against the finite-rank evaluation objective

For $N = 1, \dots, 8$, the historical specification requested relative accuracy 10^{-10} with an error estimate on $0 \le z \le 0.9$, $-0.95 \le \Re h \le 3$, $|\Im h| \le 3$, $|s| \le 3$. The comparison here uses T_N as defined in Section 1. A rigorous radius is a stronger result than a refinement estimate. The status at $N = 2, z = 0, \Re h \le -1/2$ is divergent. A relative error is undefined at a zero.

The complete predecessor release contained 2,791 checksummed members. All entries were verified against their actual bytes. Its 35-component rank-four and 56-component rank-five receipt checks were replayed. The three rank-four reference runs using 12, 16 and 56 order pairs retain their unexecuted status. The order-disk and tilt-disk statements at rank five keep their separate fixed parameters. The current high-rank lattice results reconstruct the scalar at a queried real radius. The two independently evaluated rank-seven walls do not connect full reduced states. Earlier fixed-depth and circle estimates are preserved with their stated hypotheses. The exact cubic-symbol and finite-rank complex-circle checks were repeated in this edition; they test those coefficients and normalizations. They do not furnish a fresh proof of the arbitrary-order or simultaneous-limit estimates.

The original fitted-tail executable and its two detailed comparison maps were absent. Its roughly 3,300 and 1,850 reference-point counts remain producer reports. The saved successor algorithms are available. Fourteen inherited low-rank tests were run before interpreting the changes. The general low-rank comparison matrix records 27 comparisons, including one out-of-box diagonal control. Ten returned certified relative accuracy, fifteen estimated relative accuracy, one a certified absolute-only result, and one a divergent status. Three adaptive two-angle Arb evaluations separately attained relative bounds below 1.667×10^{-11}. The $N = 1, z = 0.7$ programme example works in the shipped rank-one branch. The interval checks in Section 8 cover arbitrarily small positive input radii on the specified rank-two order strip.

The general finite-rank suite contains 32 core runs and seven stress runs before individual repairs or refinements. It includes a separately enclosed complex mass, the rank-four physical transfer where applicable, independent original-angle Fourier calculations, and independently calculated integer mass and diagonal benchmarks at ranks three through eight. Resource caps remain part of each reported status. A histogram of passes cannot certify a parameter continuum. The centre and $z = 10^{-32}$ inverse cases at ranks three and four exceeded the requested estimated tolerance in the fast core suite. The centre, tilt-transfer and response branches now enclose all four, including every tilt on the rank-four disk of Theorem 9.5 at the indicated fixed order. The signed-wave repair at rank three targets the slow detuning frequency at $z = 1/3 + 10^{-5}$; neglecting it gave a substantial change between cutoffs. At the original corner $(N, z, h, s) = (5, 0.9, 3 + 3i, 3)$ the first binary64 run returned an estimated relative error 1.92×10^{-9}. Computing the sensitive small-frequency part at wider precision returned approximately $-22.32418966361 + 37.89957762365i$ with estimated relative error 1.54×10^{-11}. The direct five-angle Weyl grid in the verification package sums over ordered subsets of distinct nodes using symmetry; all repeated-node terms vanish. Changing the common grid rotation tests angular aliasing. This is an independent numerical comparison. The separate whole-range original-angle calculation agrees with the repaired result to 5.29×10^{-13} relative. On a 160-node Weyl grid at a quarter-step shift the five-angle sum gives $-22.3241896635986 + 37.8995776236368i$. Its successive grid differences have no claimed rigorous rate.

The source-level controls at $N = 7, 8$ include the original single-eigenangle Fourier integral with an independently bounded trapezoidal rule at zero, three nonzero real frequencies, and $r = 1.5 + 0.75i$. At all ten inputs the original and transformed enclosures intersect; all eight nonzero inputs exclude the result obtained by dropping translation. The radial samples and their tails are bounded separately in Proposition 21.15. The table above and accompanying receipts record each full radial calculation, enclosure and independent comparison.

At the two inverse-region endpoints an independent calculation used the untransformed one-angle Weyl symbol and continuous radial Gauss integration. At cutoffs 12, 24, 40 and 64 it successively approached the enclosed values. The fine-rule absolute discrepancies at cutoff 64 were below 1.84×10^{-16} at both ranks. A coarser rank-eight rule gave a relative discrepancy near 4.46×10^{-10} even when the last two cutoffs agreed. Radial refinement alone would have concealed this quadrature error.

The limiting obstacle at the upper-radius, inverse-order corner is quantitative. Angular Fourier decay slows as the preparation poles move toward the integration circle, the inverse Mellin weight decays slowly, and a crude absolute contour estimate retains little of the balanced-saddle cancellation. The new calculations make each of those errors separately measurable. A finite-rank implementation with verified accuracy and practical cost throughout the original nonzero, integrable box remains open.

A continuous-frequency check in the original Haar angle

For the upper-disk inverse tests we computed a second readout that uses neither lattice images nor a numerical fit to the oscillatory tail. Put $p(u) = (1-z^2)u/(1-zu)$, $w = (u-z)/(1-zu)$ and $W_s(u) = \exp(s \log|1-zu|^2)$. Since $p = z + w$ and $|w| = 1$ on the original unit circle, write

$$A_{d,l} = \int_0^{2\pi} W_s(e^{i\theta}) e^{id\theta} w(e^{i\theta})^l \, \frac{d\theta}{2\pi}.$$

The symmetry $A_{-d,-l} = A_{d,l}$ holds for complex s by reflection. A complex conjugation in that identity would change the preparation. The Jacobi–Anger expansion inside the original Toeplitz matrix and the Haar determinant identity give exactly

$$\Phi(t) = \int_0^{2\pi} e^{itNz\cos\phi} \det\left[\sum_{l\in\mathbb{Z}} i^{|l|} J_{|l|}(t) A_{a-b,l} e^{-il\phi}\right]_{a,b=0}^{N-1} \frac{d\phi}{2\pi}.$$

At fixed t, absolute convergence follows from the factorial tail of $J_l(t)$ and $|A_{d,l}| \le \sup W_{\Re s}$. The angular mean against the translation factor can be evaluated by contraction with $i^{|k|}J_{|k|}(tNz)$. Each $A_{d,l}$ is integrated directly in the original Haar angle. This keeps the original monomial determinant basis. Both this calculation and the sampled radial calculation use the same physical Fourier identity and the same circle map. Their coefficient grids, high-frequency angular recovery and integrations in t are distinct.

For $-1 < \Re h < 0$ at the interior ranks and radii below, the integral used is $C(h)\int_0^\infty t^{-2h-1}\Phi(t)\,dt$, $C(h) = 2^{2h+1}\Gamma(1+h)/\Gamma(-h)$, with the ordinary real logarithm for $t > 0$. The numerical integration uses panels in $\log t$ below one, Gauss panels above one, and a smooth switch to the equally spaced continuum trapezoid. We taper the far endpoint by $1 - I_{(t/R-.55)/.45}(16,16)$, extending the beta distribution function by zero and one. The receipt varies R, the two mesh spacings, the original-angle sampling, the direction grid, and the retained Fourier orders. These refinements are numerical checks on the full moments. The separately enclosed low-frequency integral below has a rigorous error bound.

N	z	h	s	Independent numerical T_N
4	.90	$-.95+3i$	$.4+.7i$	$-1.55163904550522+2.33470445592381i$
5	.80	$-.6+1.2i$	$-.3+1.1i$	$.141023113445109-.198127687976893i$
5	.90	$-.8+.65i$	$.45-.85i$	$-1.41980236495513-1.41201982740931i$
6	.88	$-.8-.6i$	$-1.2+.7i$	$1.10253480676482+.0858933098728393i$
7	.85	$-.85+1.5i$	$.8-.6i$	$-.635283753247656-2.07498224948329i$
8	.90	$-.9+.5i$	$1+.5i$	$2.89298938995958+5.07229024884645i$

The rank-eight refined midpoint differs from the earlier sampled-radial calculation by 2.1×10^{-14} or less. At fixed cutoff $|l| \le 256$, the reported radial changes beyond $R = 576$ are below 2×10^{-15}, yet the error against the refined transform is 1.44×10^{-10} in absolute value. Doubling the number of directions alone leaves that discrepancy. Increasing the Fourier cutoff from 256 to 400 at the original 1024 directions recovers agreement to 2.5×10^{-14}. Direct untransformed Haar symbols at $t = 270, 290$ detect the truncation: the two coarse-source discrepancies are 9.26×10^{-14} and 1.55×10^{-13}, while the refined discrepancies are below 5×10^{-18}. Omitting the translation phase in the rank-eight integral gives $-.0790072339702-.0253989115508i$. Numerical agreement after radial refinement is thus insufficient as an error estimator. The rank-eight implementation used 28.8 seconds for the 400-mode, 2048-direction reference calculation and 35.6 seconds for the 512-mode repeat in the recorded environment.

Original-symbol enclosure. Here is a direct ball enclosure of $\Phi(t)$ for real $t \ge 0$. It also supplies nodes for a rigorously enclosed piece of the integrated readout. For an eigenangle strip width $0 < \alpha < -\log z$, set $a_\pm = ze^{\pm\alpha}$, $b = \Re s$, $D = N(1+z)$ and $U = (1+z)^{2Nb}$ if $b \ge 0$, $U = (1-z)^{2Nb}$ otherwise. Set $H = (1+a_+)(1+a_-)$ if $b \ge 0$, $H = (1-a_+)(1-a_-)$ otherwise. A single original Toeplitz entry on that strip is bounded in modulus by

$$H^b \exp\left\{|\Im s|(\arcsin a_+ + \arcsin a_-) + (N-1)\alpha + \frac{t(1-z^2)}{2}\left(\frac{e^\alpha}{1-a_+} + \frac{e^{-\alpha}}{1-a_-}\right)\right\} = E.$$

Indeed the analytic preparation is the product of the two powers of $1 - zu$ and $1 - z/u$ with the disk logarithms. The argument of either factor has modulus at most the indicated arcsine. The analytic phase is $\{e^{-i\phi}p(u) + e^{i\phi}p(1/u)\}/2$. For real eigenangles and $|\Im\phi| \le \beta$, the original Weyl average of the determinant has modulus bounded by $Ue^{tD\sinh\beta}$, since the modulus of the full mark is at most D and Haar mass is one. Cauchy's Fourier estimate gives a trapezoidal error at most $2E/(e^{M\alpha} - 1)$ per entry. Add it before taking each determinant in ball arithmetic. The error of the final Q-point direction rule is at most $2Ue^{tD\sinh\beta}/(e^{Q\beta} - 1)$ for the exact determinant; reflection halves the number of evaluations. The implementation includes rounding in all these operations. At the rank-four test $t = 4.3$ and the rank-six and rank-eight tests $t = 17.2$, the executed intrinsic disk radii were below 2.81×10^{-38}, 2.22×10^{-32} and 2.02×10^{-22} respectively.

Integral on the first frequency interval. Interpolate Φ at the $m + 1$ Chebyshev–Lobatto points of $[0, 1]$ using the preceding certified nodes. The Bernstein ellipse of parameter $\rho > 1$ has imaginary part of modulus at most $(\rho - \rho^{-1})/4$ there. The Haar source is entire and bounded on the ellipse by $V = Ue^{D(\rho-\rho^{-1})/4}$. The tail of the Chebyshev coefficients starting at $m + 1$ is at most $2V\rho^{-m}/(\rho - 1)$ by Laurent extraction on the ellipse. Interpolation aliases every omitted mode into a retained mode of sup norm one, so the uniform error is at most twice that tail. Integrating against $C(h)t^{-2h-1}$ costs at most $|C(h)|/(-2\Re h)$. Compute the interpolant integral by integrating each shifted Chebyshev polynomial exactly as a polynomial in t: each monomial t^j contributes $(j - 2h)^{-1}$. All remaining arithmetic is outward-rounded. At the rank-eight upper-edge test, $m = 72$, $\rho = 4$, and 85 decimal digits give the first-band contribution

$$(1.17021109205336280124820541431830 \pm 4.24\times10^{-33}) + i(1.14956670187932927485187057575422 \pm 4.04\times10^{-33}).$$

This rectangle includes rounding of the decimal centres shown here. The intrinsic joint radius at the full stored centre is below 2.207×10^{-33}. An ordinary continuum quadrature and the independent angular expansion give a midpoint differing by 1.34×10^{-14}. This certificate covers $0 \le t \le 1$ only. Independent radial and angular resolution controls remain necessary for $t > 1$.

The Fourier expansion follows NIST DLMF §10.12. The enclosure scripts, run parameters, profiles and individual cutoffs accompany this edition in the original-angle reference package.

The same 72nd-degree computation encloses the first-band contributions at the rank-four and rank-six inputs in the table. The midpoints round to $.018190480186157716 + .0135234147097746 29i$ and $-.702681137160862 - 1.3148616139618923i$. Before rounding these displayed centres the absolute radii are below 8.62×10^{-41} and 3.56×10^{-26}, respectively. The separate binary64 quadratures differ by 1.87×10^{-17} and 1.51×10^{-14}. Full-centre decimals are in the associated enclosures.

Against the fresh annular lattice evaluator we independently repeated the continuum calculation at nine common inputs, including the two smallest moduli in the rim screen. Across these tests the largest relative discrepancy was 1.362×10^{-12} at $N = 8$, $z = .9$, $h = -.95 - 2.989i$, $s = .03779964798115093 - 2.999761854983239i$, where $|T_N| \simeq 5.13 \times 10^{-4}$. The largest absolute discrepancy, 6.113×10^{-12}, occurred at the different test $N = 6$, $z = .891$, $|T_N| \simeq 26$. Every discrepancy was below 0.081 times the corresponding reported absolute estimate. These nine ratios compare two finite computations and supply no uniform guarantee over unsampled inputs.

Full upper-radius executions and the status of the evaluator

The full filtered source was evaluated from newly prepared angles for each of the following inputs. All radii refer to disks around the full stored decimal midpoint. The displayed upper bounds include the finite angular calculation, terminal, Mellin image and final rounding. Each of the five separated scalars meets the original relative target with over three digits of margin.

N	z	h	s	Last sample index	Absolute radius below	Relative error below
4	.90	$-.95 + 3i$	$.4 + .7i$	20381	4.944×10^{-14}	1.764×10^{-14}
5	.90	$-.8 + .65i$	$.45 - .85i$	15795	4.935×10^{-14}	2.465×10^{-14}
6	.88	$-.8 - .6i$	$-1.2 + .7i$	9740	4.908×10^{-14}	4.438×10^{-14}
7	.85	$-.85 + 1.5i$	$.8 - .6i$	7405	4.953×10^{-14}	2.283×10^{-14}
8	.90	$-.9 + .5i$	$1 + .5i$	13764	1.187×10^{-13}	2.032×10^{-14}

For the last row the centre starts $2.89298938995958150 + 5.07229024884649687i$. At the full centre the dyadic, angular, image and exterior charges were respectively below 6.903×10^{-14}, 5.173×10^{-18}, 1.135×10^{-16} and 4.948×10^{-14}. The final-centre export cost was below 5.74×10^{-47}. The radial sum of the absolute weighted sample contributions was about 145.37. The certified source used $Q = 4096, L = 1152, P = 4096$; the image used $J = 72, m = 144, H = 3$. The revised four-worker spectral run took 139.1 seconds under concurrent workload, 142.3 seconds including source reconstruction and finite readout, plus the separately timed 3.21-second image. The process high-water marks for this run were 64 MiB for the driver and 109 MiB for the largest child, separately measured. The faster estimated scalar took 4.12 seconds. An independent continuum calculation, using the original eigenangle and no filtered terminal, reproduced the value to the digits discussed above. Critical-radius results remain in §§10, 21 and 23–25, with full transport and scalar evaluation distinguished there.

At $N = 8, z = .9, s = 3i$ the full source was also run through index 13966. With the retuned terminal the scalar at the decimal order h_* in Theorem 21.20 has absolute error below 4.348×10^{-15} and lower modulus above 3.1907×10^{-14}. Extending to 17000 rows reduces the absolute error below 1.617×10^{-16} and the relative bound to .00448, still above the relative target. The narrower interval certifies that this test input and the nearby zero are distinct. The continuum check agrees with the small centre in absolute units. This is why the evaluator's absolute-only status is needed for some nonzero as well as zero-containing outputs.

The warm certified readout uses the six complete signed preparations listed in §21. It automatically extends the $s = 3i$ rank-eight source to index 17000 where needed. Uncached radii and tilts can request a fresh certified run or the fast empirical estimate. The common entry point dispatches among the spectral sampler, the fast annular estimates, rank-three formulas, the near-zero-order tilted-mass disks and the predecessor's finite-rank methods. For $N = 2, z = 0, \Re h \le -1/2$ it returns divergence for the ordinary moment. A resource limit or a loose estimate is reported even if the printed midpoint appears stable. Dispatch regressions check the rank-two divergence boundary, independent complex exponents, corners, cancellation and explicit resource guards. A separate fresh historical-input matrix exercises all eight ranks, small positive radii and six critical-radius examples, including $N = 7, z = 1/7$ and $N = 8, z = 1/4$. The rank-five corner $z = .9, h = 3 + 3i, s = 3$ kept estimated status. Its discrepancy from the stored independent original-symbol comparison was below 1.40×10^{-11} in absolute units against a reported 6.77×10^{-10} absolute estimate. The programme's historical missing executables retain their status in the preceding verification history. No high-rank full-state or moving-depth limit argument is needed in these scalar tests. The new finite-rank checks do not establish the inherited all-orders or simultaneous-limit claims independently.

An independent signed-coefficient calculation at high frequency

The one-body source of Proposition 5.4 admits a direct coefficient calculation which avoids sampling that preparation on its near-pole circle. Write $a = 1 + s + e$, $b = 1 + s - e$ and $k = l - e$. On $|w| = 1$ the Laurent symbol factors as $d^{1+2s} w^e (1 + zw)^{-a} (1 + z/w)^{-b}$. For $k \ge 0$ this gives

$$\widehat{f}_{e,l} = d^{1+2s} (-z)^k \frac{(a)_k}{k!} \, {}_2F_1(k + a, b; k + 1; z^2).$$

For $k < 0$ replace k by $-k$ and interchange a, b. Both binomial series converge absolutely on this circle. Multiplying the logarithmic derivative of the Laurent symbol by $(w + z)(1 + zw)$ gives the signed-order recurrence

$$z(j - s)\widehat{f}_{e,j+1} + [j(1 + z^2) - ed]\widehat{f}_{e,j} + z(j + s)\widehat{f}_{e,j-1} = 0.$$

The reference uses two independently enclosed Gauss seeds per block of 24 modes. It evaluates the remaining modes with complex balls, restarting with the Gauss expression whenever a divisor contains zero. For the unscaled Gauss series the ratio of successive absolute terms from index i onward is bounded by $z^2(1 + |a - 1|/(k + i + 1))(1 + |b - 1|/(i + 1))$. Once this is below one the geometric remainder gives the seed radius.

A uniform signed tail. On either signed side use the oriented (a, b) above, set $x = z^2$, and suppose $k \ge K \ge 0$, $q = z(1 + |a - 1|/(K + 1)) < 1$. Successive outer prefactors $p_k = d^{1+2s}(-z)^k (a)_k / k!$ are bounded by $q|p_k|$. A direct bound on the Gauss amplitude is $(1 - zq)^{-|b|}$. To reduce its dependence on the negative real part of b, choose an integer $m \ge 0$ such that $a_0 = a - m$ has $\Re(1 - a_0) > 0$ and $K + \Re a_0 > 0$. Put $v = 1 - a_0$, $t_j = K + a_0 + j$, $b_j = -\Re b - j$, $p_j = \max(0, \lceil b_j \rceil)$ and

$$U_j = \frac{\Gamma(\Re t_j)\Gamma(\Re v)}{|\Gamma(t_j)\Gamma(v)|} d^{b_j} \sum_{i=0}^{p_j} \binom{p_j}{i} (x/d)^i \frac{(\Re v)_i}{(K + 1 + j)_i}.$$

Then the unscaled Gauss factor at all $k \ge K$ is at most

$$H_K = \sum_{j=0}^{m} \binom{m}{j} \frac{|(b)_j| x^j}{(K+1)_j} U_j.$$

The corresponding signed tail of the prepared source is at most $|p_K| H_K/(1-q)$.

Proof. The elementary terminating Vandermonde identity (or induction in m on power-series coefficients) gives

$${}_2F_1(A+m, b; C; x) = \sum_{j=0}^{m} \binom{m}{j} \frac{(b)_j x^j}{(C)_j} {}_2F_1(A+j, b+j; C+j; x).$$

Use $A = k + a_0$, $C = k+1$ and Euler's beta integral on each right-hand factor. Both beta endpoint exponents have real part greater than -1. The variation of the normalized beta weight equals $\Gamma(\Re(k+a_0+j))\Gamma(\Re v)/|\Gamma(k+a_0+j)\Gamma(v)|$, which decreases as the integer k increases by the gamma functional equation. The other factor in absolute value is $(d + x(1-T))^{b_j}$ for $0 \le T \le 1$. It is bounded by $d^{b_j}(1 + x(1-T)/d)^{p_j}$. Integrating the binomial polynomial against the normalized positive beta law gives the displayed moments with denominator $(k+1+j)_i \ge (K+1+j)_i$. This proves the uniform amplitude bound; summing outer prefactors yields the tail. □

Direction integration without production direction coefficients. Use the two signed bounds at the first omitted l, retain $|l| \le L$, and obtain finite wave coefficients from the DFT of $\exp(ir\cos\theta)$ on an m-point grid. For each of these modes the alias is at most $2e^{|r|\sinh 1-(m-L)}/(1-e^{-m})$. Price this times the largest row coefficient one-norm and the discarded tails by the Gram perturbation bound. Denote the resulting determinant error by E. The finite determinant itself is a trigonometric polynomial of degree at most $B = NL$, with supremum at most $M + E$. To integrate its product with the untruncated pointwise translation, choose $Q > 2B$ and sample their product directly. By discrete aliasing and Cauchy–Schwarz on the at most $2B+1$ coefficients of this polynomial, the remaining absolute error is at most

$$E + 2\sqrt{2B+1}(M+E)\frac{e^{Nz|r|\sinh 1-(Q-B)}}{1-e^{-Q}}.$$

Here each reciprocal translation alias is separated from the support by at least $Q - B$. Thus this reference uses the same exact Haar change of variables as the production method, but independently computes all signed preparation modes, charges their unsampled tails by Euler beta estimates, and integrates the translation on a grid large enough for the full determinant polynomial.

At source indices $1199, 2291, 2049$ of the recorded rank-four, framed rank-six and historical hard rank-eight preparations respectively, the physical frequencies are $383.68, 733.12, 655.68$. The reference used $L = 704, 1024, 1152$ and $Q = 8192, 16384, 32768$. The differences from the corresponding native sample midpoints were below $8.09 \times 10^{-26}, 1.74 \times 10^{-23}, 3.22 \times 10^{-29}$. The independent reference errors including ball rounding were below $2.76 \times 10^{-34}, 4.89 \times 10^{-33}, 2.53 \times 10^{-33}$, all inside the respective native tolerances after accounting for the midpoint difference. The individual computations took 1.55, 3.16 and 6.32 seconds on this run. The scripts also checked 72 separate signed Gauss coefficients against the preparation DFT and 24 recurrence residuals. These checks resolve the preparation, reflection and translation errors at the tested frequencies. The radial tail and the rest of the moment sum have separate obligations.

A second run extended this check to ranks five and seven, the rank-eight near-zero preparation $(z, s) = (.89999, 3i)$, the exact critical radius $z = .75$ at rank eight, and the strongly negative rank-eight tilt $-2.88 - .84i$. Frequencies range from 415.68 through 889.92. All five independent source enclosures intersect their retained native enclosures. The largest midpoint difference here, 2.074×10^{-22}, occurs with the strongly negative tilt and is within its recorded native source bound. The reference takes 1.00–4.80 seconds per additional sample. The near-zero test here concerns a high-frequency Fourier sample of that preparation; zero detection applies to the final order-dependent sum.

Positive-order continuous-frequency checks. At $(N, z, h, s) = (5, .9, 3 + 3i, 3)$, two cold replays of the predecessor's continuous Mellin calculation used respectively 4704 and 7431 source calls. Independently varied radial grids and original-eigenangle versus Möbius-angle compact integrals gave midpoint distances 2.402×10^{-12} and 1.632×10^{-11} from the new discrete-frequency certificate, and 1.397×10^{-11} between groups. Their empirical

roundoff indicators were 8.197×10^{-11} and 2.367×10^{-10}. The second group's last two cutoff values coincide to the printed precision, illustrating why a radial cutoff change alone is inadequate. The calculations took 15.74 and 16.78 seconds. For $(4, .5, 2.85 + .65i, .47 - .63i)$ at a critical radius, the corresponding midpoint distances were below 2.16×10^{-16} after 3.94 and 6.46 seconds. Both continuous groups share the predecessor's binary64 high-frequency source implementation with separately selected angular and radial grids. The high-accuracy finite-part calculation uses extended-mantissa arithmetic and a continuous radial quadrature independent of the certified lattice. Transferring the lattice certificate to the particular continuous output decimals by the triangle inequality gives relative bounds below 1.197×10^{-11} at the corner and 7.191×10^{-14} at the rank-four wall. This does not certify the continuous algorithm's own roundoff indicator.

Cold preparations, repeat orders and failure controls

Every value in this subsection is the unnormalized T_N. A certificate consists of a complex midpoint and a radius E bounding the absolute error. A relative guarantee uses $E/(|v| - E)$ only for $|v| > E$. Values, outward-rounded bounds, rational input strings, source dimensions, subdivisions and timings are recorded together. A run at a decimal near a zero can exclude zero and still fail the requested relative tolerance.

Five held-out preparations used $h = -.93 + .8i$ and $\Delta = .32$. The following sparse runs used two kernel workers. Cold time includes compilation, heuristic design, outward rechecks, preparation, kernel evaluation, Cauchy image and readout. The repeat column is an order contraction from the resulting cache, including the integrity check. These are wall times on a shared host.

N	z	s	Distinct samples	Cold / repeat (s)	Absolute radius below
4	.873	$-.6 + 1.1i$	1,450	5.30 / .140	$1.461\,10^{-14}$
5	.891	$.85 - .65i$	1,502	8.77 / .159	$1.473\,10^{-14}$
6	.888	$-.85 + .875i$	1,402	12.33 / .159	$1.757\,10^{-14}$
7	.867	$.65 + .95i$	1,242	20.66 / .160	$1.744\,10^{-14}$
8	.899	$.8 + .7i$	1,462	24.62 / .260	$1.643\,10^{-14}$

At the last input, four workers took 14.87 seconds cold versus 127.50 seconds in a fresh, four-worker run of the predecessor dyadic sampler. Repeat contraction took .204 seconds in the new run. New design, angular-source construction, native kernel and image accounted for .57, .58, 9.13 and 2.98 seconds respectively. The largest measured driver and individual child peaks were 87,304 and 117,308 KiB; these are separate maxima. The ratio is an observed speedup of about 8.6 on that input. Implementations share the scalar Mellin identity and the dyadic Bessel kernel. Separate physical-eigenangle continuous-frequency checks for all five inputs test both the prepared symbol and the integrated readout. They have empirical discretization errors.

For the historical rank-eight input $z = .9, h = -.9 + .5i, s = 1 + .5i$, the two-rate disk has absolute radius below 5.166×10^{-14} and overlaps the predecessor's 1.187×10^{-13} disk. Its 1,445 evaluations use a different set of radial weights. The initial alternating-tail allowance on a fresh rank-eight case falls from more than 10^8 without signed concentration to below 7.75×10^{-15} when the prepared mass is retained. Removing the factor two on the even grid changed the moment by about .032; dropping the switch changed it by about .070. Replaying the older unguarded frequency choice produced errors of 9.81 and 8.19 with final-shell magnitudes near 2×10^{-8}. Refining the wrong grid can hide its error. The new rule validates the specific two-rate construction. The other annular profiles from the preceding edition retain their estimated status.

Negative tilt and an independent check. At $N = 6, z = .899, h = -.95 - 3i, s = -2.88 + .84i$, a scaled monomial calculation gave absolute radius 10.542. Its bound correctly warned of lost precision. Keeping the literal triangular preparation gave the ordinary moment near $796.9944818800625 - 2529.559262903428i$. The two-rate calculation with $\Delta = .27$ succeeded after the .32 terminal alias budget failed. At $N = 8, z = .8993, h = -.94 + 2.87i, s = -2.88 - .84i$ the corresponding result was

$$1838.30298713345216 + 2543.22063717707471i, \qquad E < 4.197 \times 10^{-13}$$

where E refers to the full stored midpoint. The physical-angle check uses QR on the original eigenvalue grid, independent of the literal dyadic frame in the certified sampler. Its two profiles differed from the stored midpoint

by less than 5.4×10^{-11} in the rank-eight case. An unconditioned rank-six check had disagreed by 3.64×10^{-7}; the orthogonalized physical-angle rule reduced that discrepancy to approximately 5×10^{-11}. Real-weight Gram condition numbers were about 1.94×10^{6} and 3.06×10^{6} at the two ranks. The independent numerical rules have their own error and need not fall within a much narrower certified disk.

Readout near cancellation. At $N = 8, z = .89999, h = -.4133064928254429 + 1.723195275895845i, s = 3i$, the first sparse disk resolved a nonzero moment of modulus approximately 2.94×10^{-7}. Its radius 2.299×10^{-13} justified only an absolute answer at the requested tolerance. The adaptive rule took a lower bound for that modulus, targeted one eighth of its requested absolute budget at the terminal, rebuilt the source, and used $J = 108, m = 216, L_c = 100$ for the image. The complete 39.11-second run gave an absolute radius below 3.300×10^{-19} and relative radius below 1.121×10^{-12}. At $z = .9$ and the sharper order centre $-.4133064928142612470 + 1.7231952758656547310i$, the dense computation returned a disk of radius below 5.436×10^{-15} containing zero. The proof that a simple root exists uses Theorem 21.20. That numerical disk alone does not prove its centre is an exact zero.

Positive orders and first critical radii. The original corner $N = 5, z = .9, h = 3 + 3i, s = 3$ activates cancellation between the lattice and its image. The initial export of the finite dyadic centres in floating-point decimals gave a valid absolute radius 2.636×10^{-6}. Exporting the integer centres exactly gave $E < 5.100 \times 10^{-10}$ and a relative bound below 1.160×10^{-11}. Positive-order point certificates also passed at $N = 4, z = 1/2$, $N = 6, z = 2/3$ and $N = 8, z = 3/4$ using Proposition 21.22. The corresponding inverse-order wall executions use Proposition 5.12. At ranks five through eight they take $h = -.9 + .5i, s = 1 + .5i$; at rank four they take $h = -.55 + .9i, s = -2.8 + .6i$. Their relative radii are below $5.280 \times 10^{-12}, 8.370 \times 10^{-12}, 2.704 \times 10^{-14}, 3.284 \times 10^{-16}, 1.080 \times 10^{-16}$ in increasing rank order. The witness records include both neighboring radii at rank six. These are independent scalar computations at each radius. A branch of the entire reduced differential state has different information and different continuation requirements.

Across 68 repeat-order checks of the dense caches, 61 returned relative certificates and seven returned absolute-only certificates. Exact Pieri expansions supplied independent rational checks at $N = 5, z = .9, s = 3, h = 0, 3$. Near the positive integer three a displacement as small as $10^{-120}i$ exercised the deflated image product. A modified witness row was rejected, a one-sample resource cap returned no value, and the divergent rank-two centre $z = 0, \Re h = -1/2$ was classified as divergent. Rank one at $z = .7$ and a small-radius rank-three case passed through the inherited selector. These counts do not represent uniform runtime tests of the original box.

The change of resonant population in Corollary 5.13 also covered consecutive walls. The rank-six and rank-eight executions there test the two- and three-agreeing-sign cores at physical noninteger orders. That edition left open how much of the original inverse-order and tilt box admits practical bounds throughout these connected radial intervals; Theorems 21.24–21.25 and Corollary 21.26 and the new computations below address this question without asserting uniform relative accuracy. At small rank the algebraic tail from the central population becomes less integrable as the order approaches $-.95$. Quantifying that loss before enlarging a radial interval would address a current gap in the evaluator. The four asymptotic regimes and the open identification of the displayed rank-three elliptic expression retain their predecessor qualifications.

Executed connected queries and reusable preparations

The fourteen fresh stress preparations below span all five ranks, exact or adjacent critical radii, multiple critical intervals, and independent complex parameters at the order and tilt boundaries. Every row has $\Re h = -.95$. All fourteen complete finite-arithmetic runs pass the 10^{-10} relative gate. The errors in the table are outward-rounded allowances about the full saved midpoints, not estimates of the actual errors. Independent references are discussed separately. Rounding the displayed midpoint would need an additional display error, so the precise centres are retained in the machine-readable files.

N	z	$\Im h$	s	Retained source rows	Cold / warm seconds	Relative allowance
4	.45	-2.8	$2.4 + 1.8i$	24563	16.88 / 0.881	$1.875 \cdot 10^{-12}$
4	.49	.33	$-2.7 + .9i$	17333	12.23 / 0.587	$6.379 \cdot 10^{-14}$
4	.51	-.7	$.9 - 1.1i$	24789	16.79 / 0.881	$3.978 \cdot 10^{-12}$
4	1/2	3	$0 + 3i$	35851	22.97 / 1.074	$1.303 \cdot 10^{-11}$

N	z	$\Im h$	s	Retained source rows	Cold / warm seconds	Relative allowance
4	.05	.5	$-.5+.6i$	18614	7.35 / 0.665	$4.724\cdot10^{-11}$
5	.195	3	$-1.8+2.4i$	2651	4.24 / 0.095	$5.459\cdot10^{-12}$
5	.605	-3	$0-3i$	4205	10.27 / 0.146	$1.526\cdot10^{-12}$
6	.33	3	$.8-2.8i$	1850	5.55 / 0.072	$1.893\cdot10^{-13}$
6	.5	.25	$1.5+2.5i$	2959	7.54 / 0.110	$4.215\cdot10^{-15}$
7	.42	2.7	$2.4-1.8i$	3288	9.22 / 0.086	$1.601\cdot10^{-15}$
7	.72	-2.7	$2.4+1.8i$	7988	48.85 / 0.189	$1.494\cdot10^{-15}$
8	.245	3	$-1.8-2.4i$	3288	7.65 / 0.088	$1.265\cdot10^{-13}$
8	.505	-3	$1.8+2.4i$	3288	12.41 / 0.114	$4.598\cdot10^{-12}$
8	.755	.66	$-2.88+.84i$	7988	42.12 / 0.185	$3.832\cdot10^{-18}$

Twelve rows were completed by the initial sequential driver. Its subsequent rank-eight middle query left an interrupted, unsealed source. The middle and right rank-eight queries were then executed from fresh inputs, in new folders; their completed receipts supply the last two rows. The unfinished attempt is preserved with no certificate. Most matrix rows used one native worker; the last two used two. Times include the actual source preparation, not only a warm contraction, and are observed on a shared host.

Exact first walls and additional populations. Separate dense cold runs at $z=1-2/N$, $h=-.95+.77i, s=-.7+1.13i$, for $N=4,\dots,8$, returned absolute allowances respectively below $9.988\cdot10^{-12}$, $1.765\cdot10^{-14}$, $6.451\cdot10^{-16}$, $4.114\cdot10^{-14}$ and $7.791\cdot10^{-19}$. Their warm queries include another inverse order and order one. At the additional walls $(N,z)=(5,1/5),(7,1/7)$ with $h=-.95+2.4i, s=.85-1.25i$, fresh sources took 5.39 and 6.55 seconds and gave relative allowances below $2.409\cdot10^{-12}$ and $2.332\cdot10^{-17}$. These executions use the actual resonant population at each radius. There is no claim that a complete differential state was carried between the separate preparations.

A measured sampling-rate reduction. At the rank-four first-wall input $h=-.95+.77i, s=-.7+1.13i$, the dense new rule used 33,488 source rows and took 16.30 seconds cold with two workers. The separated stride-three version used 12,000 rows, took 7.70 seconds to prepare and .410 seconds to contract, and returned absolute allowance $1.009\cdot10^{-11}$ and relative allowance $7.917\cdot10^{-12}$. This is an observed reduction on one matched preparation; the runs were not isolated machine benchmarks. At the common rank-four schedule of Corollary 21.26, 33,801 source rows were actually computed at $z=.55, h=-.95+i, s=1+i$. The independent source and arithmetic gates, rather than the uniform ideal-formula theorem alone, give its returned relative allowance below $7.730\cdot10^{-12}$.

Repairing the small-radius chart. At $N=5, z=.02, h=-.95+2.7i, s=-1.8+2.4i$, the initial critical-only planner reported that no admissible contour existed in its menu. This was not an ordinary moment divergence. The checked gap/core planner selects a signed-gap terminal with $K=300, b=24, p=48$ and a source genuinely computed on the resulting retained set. Its complete cold run took 3.18 seconds and returned

$$T_5 = 0.015281182770775441824215484399470789 5 - 0.016813843383523198622115285022399218 3\,i$$

with absolute allowance below $1.044\cdot10^{-14}$ and relative allowance below $4.595\cdot10^{-13}$ about the full stored midpoint. An independent original-Haar calculation differs by $1.07\cdot10^{-16}$ and carries its own numerical error. The new rank-four endpoint $z=.02, h=-.95+3i, s=1.8-2.4i$ takes 9.76 seconds through the public evaluator, using 8,491 source rows, and gives relative allowance below $3.811\cdot10^{-13}$. The small rank-six query $z=.03, h=-.95-2.7i, s=1.8-2.4i$ also passes, with relative allowance below $2.502\cdot10^{-11}$.

Adjacent numerical representations and warm orders. The public selector was run at rank five on both sides of its .82 switch: $z=.819, .821$, $h=-.95+2.1i, s=-.8+1.9i$. The complete relative allowances are below $1.739\cdot10^{-13}$ and $1.599\cdot10^{-13}$, with observed total costs 23.14 and 6.89 seconds. These are different physical radii; their unequal values are not a continuity-error test. The connected theorem supplies the rigorous overlap of the two domains. At $N=5, z=.4, h=-.95-1.7i, s=-1.2+2.6i$, both a critical-core and a signed-gap preparation give certified values; their distinct filters agree to far better than their absolute radii. The gap route uses 784 rows. An independent warm query $h=.37+1.4i$ passes the relative gate on the stored core preparation.

The order $h = 3 + 10^{-80}i$ exercises the deflated Mellin product and gives a relative allowance below $9.496 \cdot 10^{-48}$ on the gap preparation.

An order-dependent guard failure and its repair. Reusing the rank-four small-radius inverse-order cache at $h = 3 + 3i$ initially gave a valid absolute radius $2.217 \cdot 10^{-8}$, and therefore only absolute status. The dominant error was its switch alias, not a divergent expectation, a tail at the critical point or the image correction. A fresh guard designed for this actual positive complex order, with its own checked terminal and separate code seal, uses 1,029 source rows and takes 3.55 seconds. It returns absolute allowance below $3.927 \cdot 10^{-16}$ and relative allowance below $2.149 \cdot 10^{-16}$. The public selector now attempts this refinement when a nonzero absolute disk misses the relative target. All error terms are recomputed; the inverse-order guard is not silently relabelled as valid for the new order. The earlier absolute-only receipt is retained.

Regressions and zeros. A cold replay of the original hard input $N = 8, z = .9, h = -.9 + .5i, s = 1 + .5i$ through the integrated selector returns absolute allowance below $5.166 \cdot 10^{-14}$ and relative allowance below $8.846 \cdot 10^{-15}$, taking 19.97 seconds total. The inherited near-zero source at $z = .9, s = 3i$ was reused, with its hashes checked, at the specified zero-disc centre. Recontracting it returns a zero-containing disk of radius $5.436 \cdot 10^{-15}$ and no relative guarantee. This is a warm replay, not a fresh proof of the zero theorem. Rank one at $z = .7$ and genuinely complex parameters passes its exact hypergeometric route. The rank-two centre at $h = -.95 + .8i$ is returned as divergent. A positive small radius $z = 10^{-4}$ at rank two instead returns the inherited numerical estimate, explicitly marked estimated. These outcomes keep an ordinary expectation distinct from a meromorphic formula or a zero-containing answer.

The receipts record component budgets, the exact input strings, source and code hashes, precision, time and resident-memory observations. Parent and child process peaks are separate observations, not a measured aggregate parallel-memory bound. `execution-ledger.json` collects the fresh point records; it does not itself re-execute them. The scripts and complete source rows remain in the package.

Independent and adversarial verification of the critical continuation

The new certificate engine and the checking calculations share the physical Haar observable and the Weyl–Andreief identity. Their reference preparation, radial quadrature and scalar contraction are separately implemented. This is useful independence of representations and code, not an assertion that they have no common mathematical premise.

The recovered missing-mass correction was replayed at 192 bits. The old inverse formula's repaired exact-arithmetic allowance is less than $2.871948101 \cdot 10^{-17}$, with the preparation mass included in the uniform image tail. A complete cold rank-six source at its second wall was also rebuilt; it reproduced the inherited midpoint and relative allowance $5.228498525 \cdot 10^{-14}$. These receipts are current executions, whereas other inherited receipts remain producer reports unless individually marked. Neither replay audits the microscopic or circle-limit proofs.

The checker verified the Mehta constants by independent Gaussian Hankel determinants at ranks zero through eight, compared finite-rank integer moments using original-angle bivariate Toeplitz determinants, and checked the first two signed-saddle coefficients against exact Bessel expansions. The additional rank-three coefficient calculation is stated separately. Each is tested at its actual scope; an integer check does not certify a noninteger tail.

Fresh independent complex-boundary references

All three rows below use $\Re h = -.95$ and $|s| = 3$. Each continuous-integral reference was run from newly prepared original-Haar angles. The native radius includes its source, alias, terminal, image, arithmetic and readout allowances. The independent reference has an estimated, not certified, combined error.

Input (N, z, h, s)	Native absolute radius	Independent midpoint gap	Independent cost
$(4, .5, -.95 + 3i, 3i)$	$5.178 \cdot 10^{-13}$	$7.10 \cdot 10^{-14}$ after two saddle terms at $R = 3072$	64.70 s
$(5, .195, -.95 + 3i, -1.8 + 2.4i)$	$1.635 \cdot 10^{-13}$	$1.14 \cdot 10^{-15}$ at $R = 1152$	12.61 s

Input (N, z, h, s)	Native absolute radius	Independent midpoint gap	Independent cost
$(8, .505, -.95 - 3i, 1.8 + 2.4i)$	$9.061 \cdot 10^{-13}$	$2.68 \cdot 10^{-15}$ at $R = 1152$	14.94 s

The rank-four comparison provides a useful tail control. At $R = 1536$ its raw reference differs by $1.91 \cdot 10^{-9}$; subtracting only the leading resonant tail leaves $1.26 \cdot 10^{-10}$, and using both explicit terms leaves $4.97 \cdot 10^{-12}$. At $R = 3072$, the corresponding gaps are $1.61 \cdot 10^{-10}$, $5.10 \cdot 10^{-12}$ and $7.10 \cdot 10^{-14}$. Thus radial refinement alone or omission of the next algebraic term does not establish the desired accuracy. The successful comparison supports the native disk but supplies no missing numerical remainder theorem for the reference.

After replacing the pointwise terminal selector by the checked core/gap union, a fresh rank-five endpoint query at $z = .02, h = -.95 + 2.7i, s = -1.8 + 2.4i$ has native radius below $1.044 \cdot 10^{-14}$. Its independently prepared original-Haar reference at $R = 1152$ differs by $1.06 \cdot 10^{-16}$ and took 6.04 s. This tests the repaired low-radius choice at a new preparation; it is not inferred from the interval-bound computation.

The repaired positive-order case $N = 4, z = .02, h = 3 + 3i, s = 1.8 - 2.4i$ was also compared with two continuous-Mellin calculations using raw original-Haar and transformed sources. Their final midpoint gaps are $1.85 \cdot 10^{-16}$ and $3.80 \cdot 10^{-16}$, against the native absolute allowance $3.927 \cdot 10^{-16}$. The comparisons took 7.11 s together. They share the physical definition and Mellin identity but use different quadrature and source arithmetic from the certified lattice. Their own empirical roundoff indicator is $8.39 \cdot 10^{-14}$, and their inputs are converted to binary64; therefore their close agreement is a numerical corroboration, not an independent certificate at the native radius.

The original-angle implementations separately compare their prepared source to a direct original-symbol angular integral at five frequencies from .7 to 120. The maximum observed source gaps were respectively $1.43 \cdot 10^{-16}$, $9.43 \cdot 10^{-16}$ and $1.46 \cdot 10^{-15}$. This is a finite source comparison, not a uniform alias bound. Peak process storage was about 50–54 MiB. Reported times are observed wall times under concurrent workspace activity, not controlled machine-independent benchmarks.

At the opt-in rank-three input $z = .1, h = -.95 + .8i, s = -.6 + .9i$, a fresh original-Haar $R = 768$ reference took 3.71 s and differs from the adaptive source result by $3.6 \cdot 10^{-15}$, compared with the source estimate $2.36 \cdot 10^{-12}$. At the generic exact wall, a two-term asymptotic reference initially differed by $1.37 \cdot 10^{-11}$, exceeding the source estimate $4.34 \cdot 10^{-12}$. The explicit r^{-6} coefficient derived above reduces that discrepancy to $8.36 \cdot 10^{-14}$; at the large-imaginary-order wall it reduces $4.52 \cdot 10^{-12}$ to $1.49 \cdot 10^{-14}$. The insufficient earlier reference is preserved. These are improved numerical comparisons, not retrospective certification of the source estimator.

Controls that change the actual calculation

For the sparse rank-four critical preparation at $z = .5, h = -.95 + .77i, s = -.7 + 1.13i$, the certified absolute allowance is $1.009 \cdot 10^{-11}$. The following controls reuse the same physical source rows and change the stated contraction only:

Deliberate change	Midpoint displacement
Omit all far-stride rows	$2.701 \cdot 10^{-7}$
Replace the stride factor three by one	$1.957 \cdot 10^{-6}$
Multiply the source normalization by an extra $1 - z^2$	.318946

All controls are returned with an explicit noncertificate status. Their inherited allowance is not valid for the altered formula. The displacements exceed the correct disk by large margins and distinguish the required normalization and folded-lattice recovery from plausible-looking incomplete contractions.

At the same radius, stride three has a positive reciprocal-support gap and its guard filter has a proved alias allowance below $2.18 \cdot 10^{-35}$. Stride four fails the separation test and is rejected before a certificate is returned. A disposable copied cache with modified parameter bytes is rejected by the integrity gate; the saved cache itself is not changed. Synthetic readout tests return absolute-only status for a zero-containing disk and for inadequate

relative precision, and reject nonfinite or negative error components. Synthetic gate tests are not physical Haar evaluations.

An independent logarithm control at $s = 3i$ replaces the real $\log|\Lambda|^2$ by $\log|\Lambda|^2 + 2\pi i$. It multiplies the preparation by $e^{-6\pi}$, changing the displayed moment by more than .0397. This is a changed observable, not another permissible branch of the ordinary expectation. The physical calculation always uses real logarithms of positive moduli.

The rank-three source implementation retains its own particularly useful failed control: fixing the regular-source angular grid at eight nodes while refining the other two quadratures gives successive values differing by only $1.58\cdot10^{-14}$, despite an error about $9.81\cdot10^{-4}$. This directly motivates joint refinement and the alternate-partition check; an apparent radial convergence test alone is inadequate.

What the checks do not establish

The finite comparisons do not prove coverage of the full parameter box. The connected-region claims instead depend on their complete closed-cell interval cover and analytic order/tilt majorants. The uniform finite formula still needs input-specific finite-arithmetic and nonzero-modulus gates. No scalar result is full-state multiwall transport. No rigorous numerical constant for the full paired stationary-phase remainder has been obtained, and the general rank-three adaptive method remains estimated. Near zeros, a small absolute allowance does not imply a relative guarantee.

The checker also inspected the new connected terminal selector and its join to the earlier pointwise engine. The two terminal methods bound the same omitted fine-grid scalar sum, and the complete term is recomputed at each warm order. The implementation and seals are separate from the frozen earlier sparse code. For a regional gap cell, upper-radius preparation/support factors and lower-radius direction damping are both retained. The real-source and direction approximations are uniform in real frequency: their exact Bessel contraction uses coefficients of modulus at most one even at high frequency. Consequently extending the last index changes the finite-source bound by the explicitly priced sum of absolute weights, rather than silently requiring a new angular frequency theorem. The join to the exterior interval at .82 is a piecewise family of scalar formulas with the maximum of the two bounds; it is not one unchanged filter or a differential connection carrying hidden state.

Reproduction scripts are `final_controls.py`, `fresh_references.py`, `fresh_lowrank_reference.py`, `final_comparison.py`, `rank3_saddle_cubic.py`, `fresh_small_reference.py` and `rank3_third_correction.py`. The machine-readable receipts retain exact inputs, implementation hashes, source dependency hashes, numerical status and actual costs. `positive_repair_reference.py` records the additional positive-order comparison. Nine public-interface smoke checks also passed, including all three sealed engines, the positive-order child, two physical-preparation transplant rejections, a resource cap, divergence and the zero-containing case. These are warm replays and status checks, not fresh source integrations.

`final_comparison.py` recomputes differences from receipts; it does not represent itself as rerunning their source calculations.

The release was also tested from a fresh staged folder containing only the selected runtime sources, with dependency roots checked explicitly. From a different current directory, it rebuilt the $N = 5, z = .02$ complex inverse query in 3.95 s, then evaluated a different positive complex order in .534 s. The source was newly generated. This verifies the recorded executable paths and statuses, not the entire selector or a uniform cost bound. A separate read-only accounting audit replayed all 423 radius cells at 256 bits, including the population labels at all eleven positive critical radii; it found no accounting mismatch.

Rank-three source evaluation: executed scope and failure controls

The rank-three implementation is a scalar source quadrature. It does not continue a full differential state. The identity and the conditional integrability statements preceding it are proved. The numerical stopping rule estimates the error; it does not enclose the full cubature remainder.

`adaptive_rank3.py` is the frozen critical-interval routine. It attempts $1/4 \le z \le 2/5$, successively refines the conditional pair and outer-angle rules **and** the separate regular-source grid, and changes the exact partition from $K = 4$ to $K = 5$ before accepting. A conservative absolute-sum term monitors binary64 cancellation.

This term is part of an estimator, not a rounding certificate. Eight of the nine recorded input cases, counting the separately recorded generic critical input, met its estimated relative target. The lower-end complex corner returned `UNRESOLVED_RESOURCE_LIMIT` honestly.

Radius	Order h	Tilt s	Status	Estimated relative error	Total seconds
0.30	$-.95 + .3i$	$.4 + .6i$	estimated relative	4.147×10^{-11}	6.02
0.36	$-.95 + .3i$	$.4 + .6i$	estimated relative	3.874×10^{-11}	18.68
0.25	$-.95 + 2.7i$	$2.4 + 1.8i$	resource limit	1.1683×10^{-10}	15.04
0.40	$-.95 - 1.9i$	$-2.4 + 1.8i$	estimated relative	3.184×10^{-11}	45.49
$1/3 - 10^{-6}$	$-.95 + .3i$	$.4 + .6i$	estimated relative	1.120×10^{-12}	23.83
$1/3 + 10^{-6}$	$-.95 + .3i$	$.4 + .6i$	estimated relative	1.120×10^{-12}	93.54
$1/3$	$-.95 + .3i$	$3i$	estimated relative	1.022×10^{-12}	41.60
$1/3$	$-.95 + 3i$	$2 + .5i$	estimated relative	7.313×10^{-11}	81.31
$1/3$	$-.95 + .3i$	$.4 + .6i$	estimated relative	1.120×10^{-12}	45.20

These times include all adaptive levels and the alternate partition. They are measured on this run, not guaranteed costs. The region between the tested points is an implemented attempt domain, not a uniform accuracy theorem.

A separate opt-in routine, `adaptive_rank3_v2.py`, attempts $0 < z \le .9$, adds the next fixed resolution $(n, n_{\text{outer}}, n_{\text{regular}}) = (96, 192, 384)$, and retains the same acceptance and failure rules. The original critical-interval code is unchanged. Its fresh input

$$z = .1, \quad h = -.95 + .8i, \quad s = -.6 + .9i$$

returned

$$-.025065752072060084 - .843599137431552i$$

with estimated absolute error 2.353×10^{-12} and relative error 2.788×10^{-12}, in 4.24 seconds. A separately implemented original-Haar source integral with continuous inverse-Mellin integration returned $-.02506575207206052 - .84359913743154 85i$ in 3.70 seconds, a difference of 3.58×10^{-15}. This is an independent numerical comparison, not a second certificate: it shares the Haar–Toeplitz source identity and has its own numerical tail treatment.

The fixed exploratory family $h = -.95 + .3i, s = .4 + .6i$ was also computed at $z = 0, .1, .5, .7, .9$. The first four have joint refinements and alternate partitions agreeing to about 10^{-13} or better. At $z = .9$, the initially coarse values differed by 5.9×10^{-7}, so declaring convergence there would have been wrong. Further rules with $n = 80, 96$, together with the alternate $K = 5$ partition, gave

$$7.624572310693978 + 1.3057575294618602i.$$

The last primary difference was 2.7945×10^{-11}, and the alternate partition difference was 6.824×10^{-14}. The full recorded exploratory sequence cost 124.51 seconds and peaked at 70,588 KiB resident memory. This point is numerical evidence only; the complete wider adaptive v2 route was executed at the fresh $z = .1$ input, not re-executed at every wider exploratory point.

The controls expose why a single stable refinement path is insufficient. Holding the regular-source grid at only eight angles while refining the conditional rules changed the answer by 1.57×10^{-14}, although its discrepancy from the resolved source value was 9.8101×10^{-4}. Omitting the regular partition channel changed that value by 0.01076; omitting the preparation normalization changed it by 11.41; replacing the nonreal tilt by its real part

changed it by 0.1475. These are intentional corruptions, not alternative valid formulas. Their receipts preserve both corrupted outputs and the comparison values.

Normalization and integer checks use $h = 0, s = 0$, a separately computed complex-tilt mass, and exact polynomial trace moments on the $s = -3$ slice. Observed absolute differences were between 1.2×10^{-14} and 3.8×10^{-13}. The original-source off-critical references at $z = .30, .36$ agree at approximately 4×10^{-15} and 1.2×10^{-12}. At the generic exact critical input, the two-term corrected source reference at cutoff 3072 differs by about 1.4×10^{-11}, greater than the conditional estimator; its higher-tail remainder is not enclosed, so it neither certifies nor disproves that estimator. The critical corner reference differs by about 4.5×10^{-12}. The derived r^{-6} correction in Proposition 3.3 subsequently reduces these exact-wall gaps to approximately 8.36×10^{-14} and 1.49×10^{-14} respectively. The insufficient two-term references are preserved. A uniform validated remainder for these comparisons remains an explicit obligation.

The preserved rank-two Duffy evaluator was independently rerun at $h = -.95 + 3i, s = 2 + .5i$, $z = .3, .5, .9$. Its reported certified relative radii are approximately 1.667×10^{-11}, with respective cold times 2.60, 2.55 and 21.04 seconds. A separate $z = .5, h = -.95 + .3i, s = .4 + .6i$ run also passed. These are replays of an inherited certified method, rather than a new rank-two theorem.

The strongest next step for rank three is a validated joint quadrature remainder that preserves the pair repulsion and the regular partition channel. The exact endpoint and cutoff bounds now control the central chart, but they do not yet bound every quadrature and finite-arithmetic error. The v2 range remains opt-in, and no rank-three whole-box accuracy claim is made.

Coverage ledger and the next mathematical obligation

The original specification seeks 10^{-10} relative accuracy with an error estimate on $1 \le N \le 8$, $0 \le z \le .9$, $-.95 \le \Re h \le 3$, $|\Im h| \le 3$, $|s| \le 3$, wherever the ordinary expectation exists and relative accuracy is meaningful. The whole specification is not yet met. The following ledger separates the mathematical domains from the evidence of actual evaluation. A pointwise certificate can be stronger than a general error estimate without proving uniform cost or universal success.

Part of the target	Mathematical and computational status in this edition
$N = 1$, original box	Exact hypergeometric representation; a fresh genuinely complex regression run succeeds. This does not constitute a grid test of every input.
$N = 2, z = 0$	Ordinary domain is $\Re h > -1/2$. Inputs at or below the boundary are explicitly divergent; finite meromorphic values do not change this.
$N = 2, 0 < z \le .9$	Inherited validated and estimated branches retained. Four deep-inverse complex cases were replayed, including .9; a 10^{-4} radius case is estimated. The precise continuous certified strip of Theorem 21.4 is unchanged.
$N = 3$, critical radius and adjacent interval	Exact source partition, conditional thresholds and uniform central-cutoff theorem proved. Eight of nine critical-interval cases accepted the numerical estimate; one boundary case remains resource-limited at the target. Generic quadrature is not certified.
$N = 3$, wider positive radii	Opt-in source estimator on $(0, .9]$, with executed wider probes and a fresh independent .1 case. This is an attempt range, not a uniform accuracy theorem. The inherited certified $s = -3$ slice and elliptic results are retained.

Part of the target	Mathematical and computational status in this edition
$4 \le N \le 8$, $.02 \le z \le .9$, full complex box	Theorem 21.25 gives a proved connected finite-formula absolute approximation with all interval inequalities executed. Adaptive finite-arithmetic certificates were executed at walls, between walls, near the lower endpoint and across the representation switch. No uniform runtime or nonzero-modulus bound is asserted.
$4 \le N \le 8$, $0 \le z < .02$	Inherited centre and small-radius formulas remain. Their established proofs and tested points are not replaced by the positive-radius core. The new connected theorem has no claim here; further dense coverage is open.
Positive warm orders	Full-order ideal-formula bounds and removable image products are proved. New positive and near-integer runs pass; a guard that failed the target was repaired by an actual order-adapted preparation. Other cached orders can still require refinement.
Complex zeros and near-zero values	Valid absolute disks and zero-possible flags; a fresh warm replay preserves the known zero-containing case. Relative accuracy is withheld when its denominator or tolerance gate fails.
Finite arithmetic and resources	Pointwise complete error budgets and explicit failures. The longest uniform rank-four formula was not run in full; its proved truncation allowance is distinct from the executed shorter adaptive queries.

The four asymptotic regimes have not been lost in the finite-rank continuation:

Regime	Preserved result and present verification status
Fixed rank in the disk	Determinant/Mellin foundation, low-rank equations and thresholds, full-state connection results and the new scalar constructions. The current work directly audits the sampling, mass, core, source and image dependencies it uses.
Large rank at fixed interior radius	The stated Simm–Wei limiting value, compact-interior proofs and joint-limit qualifications are preserved. They are not dependencies of the new finite-rank certificates and have not received a new independent audit here.
Positive microscopic depth	Existing moment domains, complex-tilt expansion and its hypotheses are retained, including the distinctions between ordinary moments and continuation. Finite-rank tests do not independently prove their all-order remainder estimates.
Growing and shrinking depth; circle	Existing complex preparation, shrinking-depth readout and density-transition results retain their scope and attribution. Their uniformity and boundary-layer obligations remain separate from the fixed-size numerical work.

The identification of Grover's particular displayed rank-three elliptic expression is still open. The paper's own rank-three elliptic formulas, parameter slices and derivative normalization are preserved; no equivalence is claimed

without the actual external expression and definitions. The separate research note remains unchanged for restoration of complete provenance before publication.

Why the next step is lower-rank error control. The present source method already crosses the physical critical radii without needing a larger transported differential state. The most direct remaining improvements are (i) a usable remainder bound for the paired saddle expansion, retaining the detuning $\omega = Nz+2m-N$ instead of dividing by it, and (ii) validated joint quadrature for the rank-three partition. Proposition 3.3 supplies a concrete additional coefficient, and Corollary 4.6 supplies a useful uniform near-centre component. Neither alone bounds the rest of the quadrature or its arithmetic. These are precise missing estimates. Further repeated-wall full-state transport is a separate worthwhile objective when the full state is required, but the current evidence does not make it a prerequisite for improving the scalar evaluator target.

Remaining mathematical and numerical questions

At fixed positive depth the real-tilt threshold is sharp. For fixed $s = u + iv$ with $v \neq 0$, the total variation on the original unitary ensemble after complex mass scaling is

$$|N^{-s^2}|\, Z_N(u, z_N) \sim N^{v^2} A_u(c).$$

Theorem 16.4 proves weighted variation convergence after taking the planar mark at fixed positive depth. Its constants depend on compact depth and tilt ranges and on the order of the expansion. Thus the cancellation on the mark plane resolves the fixed-depth issue even for independent complex exponents. The zero sets in Corollary 16.5 have not been located explicitly.

Theorems 18.2 and 19.10 give the two moving-depth limits for independent complex parameters in their stated domains. Proposition 19.12 resolves the leading transverse scale and its rare excursions. Theorems 19.14–19.15 give a uniform first correction on the transverse-to-off-line overlap for bounded longitudinal coordinate. The compact interior of the sector $|J|/\sqrt{B} < \sqrt{2}$ has its own two-term expansion. A pointwise approximation uniform through its one-angle front and a pointwise planar resolution around $\lambda Q = 1$ remain open. Proposition 19.19 identifies the locally finite limiting measure in the latter window. Proposition 19.16 treats the first cutoff for the marginal tail. Its other threshold boundaries and the transition between adjacent planar bands in Proposition 19.17 require further analysis. The arguments give locally uniform constants on parameter compacts; effective numerical constants for the asymptotic comparison and estimates uniform at unbounded imaginary parameters remain to be developed.

Proposition 10.4 constructs planar equations for independently noninteger (h, s) at any rank. Theorem 10.5 supplies ordinary equations on regular intervals for every rank $N \geq 2$. Theorem 10.6 reduces the state dimension and Theorem 10.9 specifies the exact physical connection at every interior critical trace radius. The full 20- and 35-coordinate path matrices now have rigorous error bounds for the crossings of Proposition 21.9. Rank-uniform precision and cost bounds for long or multiple crossings remain open. Theorem 10.17 resolves the selected rank-four singular column and its scalar projection at the stated exceptional parameters. Section 23 resolves the normal-jet scalar projection at ranks three and four via Theorem 23.1's shortcut and at every rank $N \geq 3$ off (10.9) via Theorem 23.1A, and gives an independent physical calculation at intersecting divisors. Section 24 develops one-pair variable-order rank-four transport across the wall $z = 1/2$, and Section 25 executes noninteger rank-five two-wall transport on $s = -5$ and $|s+5| \leq 1/16$; additional indicial collisions in sheared full-state charts, excluded radii in (10.9), and efficient arbitrary-tilt or general-rank multiwall transport remain open. Large group-inverse powers, a near-resonant readout and loss of compatible digits can dominate the reduction. The bounds of Theorem 21.5 and the individual certificates in this edition give independent scalar checkpoints. They leave open a practical uniform inverse-order evaluator over the wider target. At rank two the adaptive evaluator attains the stated relative accuracy throughout the exact-rational points of the closed region of Theorem 21.4. Additional branches provide pointwise certificates. For the wider target $1 \leq N \leq 8$, $0 \leq z \leq 0.9$, $-0.95 \leq \Re h \leq 3$, $|\Im h| \leq 3$, $|s| \leq 3$, divergent cases require exclusion, and relative error is undefined at a complex zero. Uniform resource bounds and broad independent higher-rank reference values for admissible noninteger inputs remain to be established.

Executed scalar evidence, independent checks and preserved failures

The following arguments extend this section. Lettered identifiers retain stable links to the integrated constructions; their correspondence is given at the beginning of the paper. Earlier bounds remain valid on their stated domains. A limitation described at an intermediate stage is superseded only by a later explicitly proved result, as summarized in the current coverage table.

Implemented arithmetic and full scalar certificates (R7)

The finite physical-source samples use the preserved HaarSpectral 104-fraction-bit dyadic FFT and Toeplitz determinant engine. A separate copy changes only its admissible rank floor from four to three; the associated planner has the corresponding gate change. The Schur mass, Fourier alias, matrix perturbation, fixed-point residual and determinant inequalities have no rank-four singularity. The independent audit checked this extension and the image formulas. The inherited low-level arithmetic proof remains an explicit dependency; this construction does not claim a formal proof-assistant verification of the compiler or special-function library.

Source preparation encloses constants before fixed-point encoding and checks the fixed-point range. The source row is returned as exact integer coordinates, with a separately priced error. The original image is computed from the original preparation using Cauchy coefficients, alias bounds, the image tail and 256-bit ball arithmetic. The special-function tail contraction and final accumulation use 512-bit Arb/Acb arithmetic. All complex powers retain the physical branches.

For each term of (R4.4), the remaining lattice sum is

$$\sum_{k>K} e^{\mathrm{i}\theta k} k^{-v} = \mathrm{Li}_v(e^{\mathrm{i}\theta}) - \sum_{k=1}^{K} e^{\mathrm{i}\theta k} k^{-v}, \qquad v = 3 + 2h + j, \quad \theta = \pm\omega_m \Delta. \tag{R7.1}$$

Here $\operatorname{Re} v > 1$. At exact $\theta = 0$, use the Hurwitz zeta $\zeta(v, K+1)$. Exact rational frequency labels distinguish zero from small detuning. Every nonzero phase is evaluated independently as $e^{\mathrm{i}k\theta}$, so repeated rectangular interval multiplication cannot accumulate spurious geometric wrapping.

The returned full-precision midpoint m has a disk radius

$$E = E_{\text{finite arithmetic}} + E_{\text{angular}} + E_{\text{original image}} + E_{\text{Bessel}} + E_{\text{return}} + E_{\text{ball/readout}}. \tag{R7.2}$$

Each summand is nonnegative and enclosed upwards. If a lower bound for $|m|$ exceeds E, the true-relative error is bounded by

$$\frac{E}{|m|_{\text{lower}} - E}.$$

Otherwise the certificate remains absolute and the relative gate is withheld. The relative target is accepted only when this upper bound is less than 10^{-10}.

Executed input matrix

All fifteen prescribed cases passed the relative target after the documented repairs. The following table fixes each exact input; decimal strings denote exact rationals.

Case	Radius z	Order h	Tilt s
1	$1/3$	$-0.95 + 0.3\mathrm{i}$	$0.4 + 0.6\mathrm{i}$
2	$1/4$	$-0.95 + 2.7\mathrm{i}$	$2.4 + 1.8\mathrm{i}$
3	$1/3$	$-0.95 + 3\mathrm{i}$	$2 + 0.5\mathrm{i}$
4	$2/5$	$-0.95 - 3\mathrm{i}$	$2.4 + 1.8\mathrm{i}$
5	$3/10$	$-0.95 + 0.3\mathrm{i}$	$0.4 + 0.6\mathrm{i}$
6	$9/25$	$-0.95 + 0.3\mathrm{i}$	$0.4 + 0.6\mathrm{i}$
7	$1/3 - 1/(3\,10^9)$	$-0.95 + 0.3\mathrm{i}$	$0.4 + 0.6\mathrm{i}$
8	$1/3 + 1/(3\,10^9)$	$-0.95 + 0.3\mathrm{i}$	$0.4 + 0.6\mathrm{i}$
9	$2/5$	$3 + 3\mathrm{i}$	$2.4 + 1.8\mathrm{i}$

Case	Radius z	Order h	Tilt s
10	1/3	$-1\,10^{-12}$	$0.4 + 0.6\mathrm{i}$
11	1/3	0	0
12	1/3	1	0
13	1/3	$1.000000000001 + 1\,10^{-12}\mathrm{i}$	0
14	1/3	$-0.95 + 3\mathrm{i}$	-3
15	1/4	$-0.95 - 2.7\mathrm{i}$	$2.4 - 1.8\mathrm{i}$

The displayed values below are abbreviated. Error radii apply to the full 65-digit midpoints in the JSON receipts, not to these shortened display strings. All entries use $L = 112$, $M = 20$, $K = 4096$, $\Delta = 1/2$ and 512-bit tail contraction; each physical preparation has its own adaptive source bound.

Case	Abbreviated complex midpoint	Absolute radius	Relative bound
1	-0.7690722236640170 $-3.794284951347295\mathrm{i}$	$1.2981\,10^{-22}$	$3.3530\,10^{-23}$
2	-0.01868045347713328 $-0.01765844202391289\mathrm{i}$	$5.2607\,10^{-23}$	$2.0466\,10^{-21}$
3	-0.04993281040251982 $+0.08486780942465820\mathrm{i}$	$1.2701\,10^{-22}$	$1.2899\,10^{-21}$
4	0.5995313231884475 $+0.4057691698148900\mathrm{i}$	$8.1388\,10^{-22}$	$1.1243\,10^{-21}$
5	-0.9860417954122983 $-4.032404669813578\mathrm{i}$	$3.3427\,10^{-22}$	$8.0522\,10^{-23}$
6	0.1266635537699704 $-3.257314291332038\mathrm{i}$	$1.4761\,10^{-22}$	$4.5280\,10^{-23}$
7	-0.7690722336819848 $-3.794284940875960\mathrm{i}$	$1.2981\,10^{-22}$	$3.3530\,10^{-23}$
8	-0.7690722136460490 $-3.794284961818631\mathrm{i}$	$1.2981\,10^{-22}$	$3.3530\,10^{-23}$
9	1.710517048711870 $-9.297471984315920\mathrm{i}$	$4.7038\,10^{-17}$	$4.9757\,10^{-18}$
10	0.9751811187992102 $+0.05520116056816010\mathrm{i}$	$4.9734\,10^{-37}$	$5.0918\,10^{-37}$
11	1.000000000000000 $+0\mathrm{i}$	$2.1977\,10^{-47}$	$2.1977\,10^{-47}$
12	0.9986282578875171 $+0\mathrm{i}$	$3.5171\,10^{-46}$	$3.5219\,10^{-46}$
13	0.9986282578879326 $+4.154978956180977\,10^{-13}\mathrm{i}$	$4.4989\,10^{-36}$	$4.5050\,10^{-36}$
14	-0.03351324061200308 $+0.06772864303568537\mathrm{i}$	$3.4145\,10^{-23}$	$4.5185\,10^{-22}$
15	-0.01868045347713328 $+0.01765844202391289\mathrm{i}$	$5.2607\,10^{-23}$	$2.0466\,10^{-21}$

The 15 raw receipts are preserved unchanged. Fourteen were generated during review with a candidate status; the append-only certification ledger binds their subsequent successful mathematical audit, source hashes and acceptance gates. The repaired exact-one-order receipt was generated by the final certified wrapper. This distinction prevents rewriting execution history. Recorded contraction times ranged from 4.61 to 85.01 seconds; most noninteger matrix cases ran with two concurrent workers. These observations are not a performance guarantee.

Representative complete error budget

At $z = 1/3$, $h = -.95 + .3\mathrm{i}$, $s = .4 + .6\mathrm{i}$, the complete budget is:

Component	Upward rounded upper bound
Finite physical-source arithmetic	$1.298013\,10^{-22}$
Physical-source angular approximation	$6.861105\,10^{-27}$
Original image, including its arithmetic	$3.285670\,10^{-49}$
Effective Bessel product remainder	$4.992014\,10^{-33}$
Original-space preparation return	$1.713014\,10^{-40}$
Tail balls and midpoint readout	$1.512888\,10^{-65}$
Total	$1.298082\,10^{-22}$
Relative upper bound	$3.352966\,10^{-23}$

The finite-source arithmetic dominates this point. The rigorous tail and preparation-return bounds are already much smaller; adding further asymptotic terms alone would not improve the dominant allowance.

Independent checks, failures, and repairs (R8)

The finite Laurent source was evaluated independently by its direct finite Fourier/Bessel determinant, using 256-bit Acb Bessel calls. Four checks covered the critical generic tilt, the quarter-radius corner, the upper radius endpoint and the exact $s = -3$ slice. All differences lie inside the proved remainder. On $s = -3$, the resonant r^{-4} and r^{-6} coefficients enclose respectively $4\mathcal{P}_s/\pi^2$ and $-3\mathcal{P}_s/\pi^2$, as required by inherited Proposition 3.3.

The finite original-source engine was also checked against the independent identity

$$\Phi(r) = d^{-9} J_0(ar)[J_0(r)^3 + 2J_0(r)J_1(r)^2 + 2J_1(r)^2 J_2(r) - J_0(r)J_2(r)^2] \quad (s = -3).$$

Forty retained lattice samples lay inside the finite-source enclosures. Independent original-angle Toeplitz/hypergeometric mass checks validate the complex preparation at $h = 0$. The elementary identities $T_3(0, 0; z) = 1$ and $T_3(1, 0; z) = 1 - z^6$ test normalization and integer-order cancellation. The latter was independently obtained from the mixed coefficient of an original-Haar Toeplitz determinant.

Extended-precision conditional calculations provide a different numerical readout. They use actual 64-significand-bit long double arithmetic, corrected quadrature nodes and weights, stable local geometry, and compensated accumulation. The hard quarter input now meets its estimated target; the left, critical and right checks also meet their estimated targets. Their entire moments remain *estimated*, because their complementary conditional quadrature has no complete rigorous remainder. The whole-source certificates do not depend on their agreement.

Independent comparison	Absolute midpoint discrepancy
left.json	$1.29362\,10^{-16}$
critical.json	$1.95838\,10^{-17}$
right.json	$2.05957\,10^{-16}$
hard_quarter_final.json	$2.50955\,10^{-17}$
hybrid_hard_quarter_alternate.json	$1.06256\,10^{-18}$
zero_order.json	0
one_order.json	$7.27024\,10^{-50}$
CONJUGATE_PREPARATION	$1.10351\,10^{-26}$

All eight checks passed their appropriate combined allowances. The five conditional comparisons use estimated conditional allowances; the exact Haar identities and conjugacy use rigorous disks. Independent comparisons support the implementation but do not replace the analytic proof of the remainder.

The following failures remain preserved rather than overwritten:

1. The first Bessel coefficient aggregation multiplied a chosen sign placement by a binomial multiplicity after permutation reduction. An independent exact-source comparison caught it. All eight placements are now explicitly summed. Superseded coefficients are labelled in the route-A records.

2. Direct large-shift Lerch evaluation produced unusably wide balls. A subsequent repeated phase recurrence also produced a very large valid enclosure through interval wrapping. The successful implementation uses (R7.1), higher precision and independent phases.

3. The exact $h = 1$ test initially refused a valid result because a nonnegative absolute-value interval containing zero was stored by Arb as a symmetric ball. Testing that representation for a nonnegative lower endpoint was too strict. Taking its rigorous absolute upper endpoint repaired the guard; the rerun encloses the exact value 728/729.

4. An exact near-critical radius with a denominator exceeding the inherited signed 32-bit header failed before source evaluation. The failure is retained. The executed neighboring tests use exact radii $1/3 \pm 1/3000000000$, whose frequency steps fit the ABI. Requested parameters are never silently rounded.

5. A regular-channel prototype generated a nonfinite ball by applying a generic power operation to an interval straddling zero. Direct interval multiplication and explicit finiteness checks repaired it. Its failed receipt and large-error coarse-grid control remain separate.

6. Higher precision did not cure false convergence: with the regular grid frozen at eight nodes, conditional 48- versus 64-point results agreed to $6.65064\,10^{-16}$ while retaining a bias of $9.810125\,10^{-4}$ against joint refinement.

7. An independent expensive conditional test at the largest imaginary order was stopped during refinement after the useful completed checks. Its partial record is labelled unfinished; the corresponding whole-source input was independently enclosed by the new route.

Executed principal results and complete error budgets (C9)

The final hash-bound ledger assesses all seventeen principal new executions as CERTIFIED_RELATIVE. Their raw candidate labels remain unchanged; promotion records the producing versions and recomputed complete budgets. This count excludes the superseded first centre attempt, the separate interior-overlap calculation, audit-only controls and the final wrapper check. All fifteen inherited scalar certificates also remain intact.

Table 36 lists the principal inputs. The finite physical prefix has $K = 4096$, $\Delta = 1/2$; new tail calculations use $M = 20$, $B = 32$, $\rho = .1$ and 512 bits, with the actual displayed L, Q. The uniform theorem's different Abel order $B = 48$ is not substituted for any of these pointwise prices. The largest relative bound among the seventeen is below $9.11982\,10^{-19}$, well inside the requested target.

Table 36: Seventeen executed principal inputs. The error bounds apply to the complete decimal midpoints in the bound receipts. $\epsilon = 10^{-30}$.

Case	z	h	s	L/Q	E_{abs}	E_{rel}
C01	0	0	$2.4 + 1.8\mathrm{i}$	$0/1^*$	$= 0$	$= 0$
C02	0	1	$2.4 + 1.8\mathrm{i}$	$0/1^*$	$< 7.0169 \times 10^{-77}$	$< 7.0169 \times 10^{-77}$
C03	0	2	$2.4 + 1.8\mathrm{i}$	$0/1^*$	$< 2.1486 \times 10^{-76}$	$< 1.0743 \times 10^{-76}$
C04	0	3	$2.4 + 1.8\mathrm{i}$	$0/1^*$	$< 1.2484 \times 10^{-75}$	$< 2.0806 \times 10^{-76}$
C05	0	$-0.95 + .3\mathrm{i}$	$2.4 + 1.8\mathrm{i}$	$0/1^*$	$< 1.7063 \times 10^{-25}$	$< 6.5507 \times 10^{-26}$
C06	0	$-0.95 + 3\mathrm{i}$	$2.4 + 1.8\mathrm{i}$	$0/1^*$	$< 2.0268 \times 10^{-26}$	$< 3.0133 \times 10^{-25}$
C07	0	$3 + 3\mathrm{i}$	$2.4 + 1.8\mathrm{i}$	$0/1^*$	$< 5.7181 \times 10^{-24}$	$< 2.2197 \times 10^{-24}$
C08	0	$1 + \epsilon + \epsilon\mathrm{i}$	$2.4 + 1.8\mathrm{i}$	$0/1^*$	$< 1.7784 \times 10^{-50}$	$< 1.7784 \times 10^{-50}$
C09	10^{-9}	$-0.95 + .3\mathrm{i}$	$.4 + .6\mathrm{i}$	4/512	$< 4.0823 \times 10^{-23}$	$< 1.5672 \times 10^{-23}$
C10	.01	$-0.95 + .3\mathrm{i}$	$.4 + .6\mathrm{i}$	88/4096	$< 4.3216 \times 10^{-23}$	$< 1.6583 \times 10^{-23}$
C11	.01	$1 + \epsilon + \epsilon\mathrm{i}$	$.4 + .6\mathrm{i}$	24/1024	$< 1.2429 \times 10^{-45}$	$< 1.2430 \times 10^{-45}$
C12	.1	$-0.95 - 3\mathrm{i}$	$2.4 + 1.8\mathrm{i}$	44/2048	$< 7.8222 \times 10^{-24}$	$< 3.1643 \times 10^{-22}$
C13	.1	$3 + 3\mathrm{i}$	$2.4 + 1.8\mathrm{i}$	44/2048	$< 2.6963 \times 10^{-18}$	$< 9.1199 \times 10^{-19}$
C14	.2	$-0.95 + 3\mathrm{i}$	$-2.4 + 1.8\mathrm{i}$	64/2048	$< 8.2360 \times 10^{-24}$	$< 1.6565 \times 10^{-22}$
C15	.25	$-0.95 + 2.7\mathrm{i}$	$2.4 + 1.8\mathrm{i}$	80/4096	$< 5.2607 \times 10^{-23}$	$< 2.0466 \times 10^{-21}$
C16	.275	$-0.95 + 2.7\mathrm{i}$	$2.4 + 1.8\mathrm{i}$	80/4096	$< 3.2671 \times 10^{-22}$	$< 4.5723 \times 10^{-21}$
C17	.3	$-0.95 + 3\mathrm{i}$	$2.4 + 1.8\mathrm{i}$	88/4096	$< 1.7168 \times 10^{-22}$	$< 3.1049 \times 10^{-21}$

*At the exact centre the noninteger tail has a constant direction and uses one evaluation; at exact integer orders the weighted tail is zero. The raw receipts retain the requested direction parameter $Q = 64$. The zero-order error is exactly zero, rather than a strict positive bound.

The table bounds refer to the complete decimal midpoints in the sealed receipts. The following selected midpoints are copied at their full reported precision; their error disks include that serialization.

C06: zero-deep-imag.

$$\begin{aligned} m = {} & 0.010328744582411719599415300035407563058968556661427218742034455500 \\ & - 0.066462538812887509109345520158830627235304745759056486817238793165\,\mathrm{i}, \\ E < {} & 2.026735 \times 10^{-26}. \end{aligned}$$

C09: tiny-generic.

$$\begin{aligned} m = {} & 0.364185594949334580692063659168215199675678324051298263418264046 53 \\ & - 2.579204597891425767934696497321662958837798620909813946238270686 2\,\mathrm{i}, \\ E < {} & 4.082221 \times 10^{-23}. \end{aligned}$$

C12: tenth-corner.

$$\begin{aligned} m = {} & -0.024263667093972721426215936733618672003296001008691860416736498325 \\ & + 0.004728155352175254068947217712377965055958696283754340759635640250 8\,\mathrm{i}, \\ E < {} & 7.822166 \times 10^{-24}. \end{aligned}$$

C17: three-tenths-corner.

$$\begin{aligned} m = {} & -0.043923858124744365297999942892765163441705548625098024685293621629 \\ & - 0.033582173815381436435079881814151685540176311417210253544384981778\,\mathrm{i}, \\ E < {} & 1.716705 \times 10^{-22}. \end{aligned}$$

C13: tenth-positive.

$$\begin{aligned} m = {} & -0.965282121699428481049665813576461120454893075894656572999546098 40 \\ & - 2.794432396424964789985835012396712380495428529977700917626771633 4\,\mathrm{i}, \\ E < {} & 2.696233 \times 10^{-18}. \end{aligned}$$

Table 37: Representative complete budgets, with every displayed component rounded upwards. C11 is the near-integer input with independent complex tilt.

Component	C09	C17	C13	C11
Finite source arithmetic	4.0821×10^{-23}	1.7167×10^{-22}	2.6951×10^{-18}	9.0285×10^{-55}
Finite source angles	8.4120×10^{-65}	6.8654×10^{-28}	1.1573×10^{-21}	9.2076×10^{-89}
Original image	9.8295×10^{-50}	2.4150×10^{-46}	3.1633×10^{-41}	1.6462×10^{-49}
Three-Bessel remainder	8.2434×10^{-55}	6.2485×10^{-38}	1.5464×10^{-73}	6.9985×10^{-97}
Complete preparation return	3.4398×10^{-37}	1.9386×10^{-30}	1.2498×10^{-29}	1.2427×10^{-45}
Abel remainder	4.5509×10^{-73}	1.8276×10^{-38}	1.9390×10^{-80}	1.4469×10^{-110}
Tail direction rule	2.0180×10^{-27}	1.8503×10^{-101}	3.5633×10^{-87}	5.0516×10^{-89}
Ball and decimal readout	5.6262×10^{-65}	8.7356×10^{-67}	5.3787×10^{-65}	2.2244×10^{-66}
Total	4.0823×10^{-23}	1.7168×10^{-22}	2.6963×10^{-18}	1.2429×10^{-45}

Table 37 shows all eight charges for four representative inputs. The finite-source arithmetic dominates C09, C12, C13, C14 and C17. The original angular-source price is about 66% of C16's total. The complete preparation return dominates the deliberately near-integer independent-tilt input C11. For C09 the direction rule costs about $2.018\,10^{-27}$, much less than its $4.082\,10^{-23}$ source arithmetic charge. These observations identify the actual next precision resource; none warrants increasing the Bessel order by itself.

Overlap at the boundary and inside the common interval

At $z = 1/4$, $h = -.95 + 2.7\mathrm{i}$, $s = 2.4 + 1.8\mathrm{i}$, the new centre readout was applied to the preserved hard-quarter source and compared with its inherited certified interior result. At $z = 11/40$ the old interior evaluator was executed afresh with $L = 112, M = 20$ on the same new sealed source as C16. The tail representations were priced separately:

Radius	Midpoint distance below	Sum of radii greater than
1/4	$7.698359\,10^{-48}$	$1.05213916\,10^{-22}$
11/40	3.11107410^{-44}	$6.5340955\,10^{-22}$

The old quarter receipt is bound to the unchanged inherited promotion ledger. These comparisons use a shared physical prefix and image; they independently challenge the two tail constructions, not the shared prefix. The source's separate checks and arithmetic contracts remain necessary. The continuum overlap follows from the proofs, rather than from these two points.

Independent checks, failures, and repairs (C10)

An independently certified centre route

The inherited outer/rigor/allradius.py was executed independently at the exact centre for three complex orders. It uses exact origin coefficients, certified analytic Gauss quadrature on the compact interval, and a continuous exponential-integral tail. These differ from the new sampled lattice, forward differences and image regularization. The actual adaptive precision was 592 bits, starting from a request for 512. Both procedures supplied their own rigorous disks:

h	Midpoint distance below	Combined allowance
$-.95 + 3\mathrm{i}$	$8.408\,10^{-28}$	$5.3258959\ldots\,10^{-26}$
$-.95 + .3\mathrm{i}$	$4.273\,10^{-26}$	$4.4774777\ldots\,10^{-25}$
$3 + 3\mathrm{i}$	$5.111\,10^{-25}$	$1.6491267\ldots\,10^{-23}$

Every pair is compatible. The final receipt records actual adaptive precision and hashes of all four inherited continuous-Mellin modules. An earlier receipt stated the requested initial precision; its reporting version is preserved.

Original-source and implementation challenges

Before the extension, all 848 files in the preceding package and all fifteen inherited receipt hashes were verified. Four decisive inherited calculations were replayed, including the hard quarter case and exact integer controls. The new finite-source construction was challenged by:

- ten outward direct finite-Bessel determinant comparisons, including $z = 0, 10^{-6}, .1, .25, .3$ and two cutoffs per preparation;
- five weighted Fourier-coefficient comparisons against parameter-wide positive majorants;
- all 4096 exact-centre source samples checked through a separate Bessel recurrence, and 72 exact image coefficients checked by partition enumeration and character orthogonality;
- six independent scalar Abel/polylog comparisons at 768 bits, both frequency signs, $p = 1.6 \pm 6\mathrm{i}$, $9.5 \pm 6\mathrm{i}$, and a higher order $20.6 + 6\mathrm{i}$;
- literal Fourier-sum checks of the DFT sign at six nodes, and 328 direct complex-strip denominator checks over all populations;
- the two independently priced interior overlaps and three independently certified continuous-Mellin centre comparisons above.

The inequalities prove continuous scope; the finite checks challenge implementation and normalization. They are not substituted for proofs.

At $z = .01$, $s = .4 + .6\mathrm{i}$, an original-eigenangle Toeplitz calculation checks the physical mass at $h = 0$. Its coefficients are

$$c_k = (-z)^k \binom{s}{k} {}_2F_1(k-s, -s; k+1; z^2), \qquad k = 0, 1, 2.$$

The determinant agrees with the original image enclosure of radius less than $4.531\,10^{-49}$. Its value begins

$$.99997999804785984312811856827 3 + .00004800144005517714169473191 0\mathrm{i}.$$

An intentionally incorrect construction that freezes the preparation at the centre returns 1. Its distance outside the true enclosure exceeds $5.2002\,10^{-5}$. This adversarial control detects lost physical preparation information even when a numerical rule might appear stable.

A separate original-angle estimate

An independent numerical diagnostic starts directly from the Weyl eigenangle integral at $z = 0$. Removing common rotation and exchanging the remaining angles gives

$$T_3(h, s; 0) = \frac{1}{3(2\pi)^2} \int_{-\pi \le \psi \le \theta \le \pi} |1 + e^{\mathrm{i}\theta} + e^{\mathrm{i}\psi}|^{2h} 8(1-\cos\theta)(1-\cos\psi)(1-\cos(\theta-\psi))\, d\theta\, d\psi.$$

Its sole interior zero is $p = (2\pi/3, -2\pi/3)$, with trace-map Jacobian magnitude $\sqrt{3}/2$ and Vandermonde value 27. For each triangle from p to a boundary edge, write $x = p + \rho d(t)$, $0 \le \rho, t \le 1$. With $\zeta = (-1 + \mathrm{i}\sqrt{3})/2$,

$$q(\rho, t) = \frac{\zeta\ \mathrm{expm1}(\mathrm{i}\rho d_1) + \bar{\zeta}\ \mathrm{expm1}(\mathrm{i}\rho d_2)}{\rho}$$

has limiting squared modulus $Q_0(t) = d_1^2 + d_2^2 - d_1 d_2 > 0$. Let $G(\rho, t) = |q(\rho, t)|^{2h} V(p + \rho d(t))$, so $G(0, t) = 27 Q_0(t)^h$. For $\lambda = 2h + 2$,

$$\int_0^1 \rho^{2h+1} G(\rho, t)\, d\rho = \frac{G(0,t)}{\lambda} + \int_0^\infty e^{-\lambda u} [G(e^{-u}, t) - G(0, t)]\, du.$$

The subtracted integrand gains an extra e^{-u}, preserving the complex-order phase and the trace-zero cancellation.

The executed estimator uses Gaussian rules in t and a finite logarithmic interval in u. It is **not a certificate**: its remaining quadrature and cutoff errors are unproved. Arb-generated nodes are converted to the actual long-double format, which has 64 significand bits here, rather than IEEE binary128. Corrected integer normalization discrepancies are about $2\,10^{-16}$ or less. Deep inverse estimates agree with the independently certified centre values to the expected numerical precision. The positive complex case remains an estimate with a few 10^{-15} discrepancy; its agreement does not determine a rigorous error bar.

Preserved failures and precise repairs

1. The first new centre calculation used a generic direction-strip price for an exactly constant integrand. Its valid but loose allowance was about $6.9\,10^{-9}$. Exact specialization to one angular value removed that unnecessary quadrature charge without changing the midpoint. The initial receipt is preserved and excluded from the seventeen successful principal cases.

2. A 384-bit polylog comparison initially could not resolve a small Abel remainder because cancellation in the reference left a wide ball. At 768 bits the reference resolved all six checks. The Abel theorem never depended on observed agreement.

3. The first parameter-wide Abel order 32 produced the weaker uniform bound recorded in Section C7. Raising that specific order to 48 repaired the identified uniform component. Actual pointwise order-32 certificates retain their own budgets.

4. The original-angle diagnostic first used binary64 Gaussian nodes and weights; high-order normalization exposed errors up to roughly 10^{-9}. Arb-generated nodes repaired that diagnostic. Its remaining errors are still estimated.

5. Two audit helpers initially compared intervals using overly strict output conventions: one ignored a separate serialization radius in an image comparison; another demanded equality by overlap of a component sum and its larger upward-rounded total. The repaired audits use the actual priced midpoint and a conservatively recomputed outer radius. Failed helpers and logs remain; no numerical budget was reduced.

6. Review found two reusable-helper domain issues. The scalar Abel helper now requires $\operatorname{Re} p > 1$, matching its actual absolute-convergence scope. The uniform runner refuses $K \neq 4096$ rather than reusing an already weighted prefix charge for a different cutoff. Prior versions remain hash-bound to their successful target-box executions. Neither guard changes those calculations.

The older failed sign aggregation, interval phase wrapping, rational-header refusal and false-convergence example remain preserved. In particular, holding the regular conditional grid fixed at eight nodes allowed conditional refinement agreement near $6.65\,10^{-16}$ while leaving a bias near $9.81\,10^{-4}$. This continuation does not convert the conditional complement into a rigorous quadrature. Its full certificates use the separately priced source route.

Executed scalar results and complete budgets (U3)

The scalar routine retains seven error components:

$$E = E_{\text{native}} + E_{\text{angular}} + E_{\text{image}} + E_{\text{Bessel}} + E_{\text{Abel}} + E_{\text{prep}} + E_{\text{ball/readout}}.$$

Every analytic allowance is evaluated at the actual input and resources. The final complex decimal centre m is returned with its absolute disk. If $\ell = |m|_{\text{lower}} - E > 0$, the reported relative bound is E/ℓ. If the disk contains zero, the result remains absolute. No parameter sample is used to infer a global nonvanishing theorem.

Noninteger principal executions

All displayed error figures are rounded upward from the outward receipts. Centres are shortened for readability; the full decimal centre and absolute disk are retained in each JSON receipt. Here $\epsilon = 10^{-30}$.

z	h	s	Complex centre	Absolute error below	Relative error below
0.4	$3+3\mathrm{i}$	$2.4+1.8\mathrm{i}$	1.710517049 $-9.297471984\mathrm{i}$	$4.703732\,10^{-17}$	$4.975646\,10^{-18}$
0.5	$-0.95+3\mathrm{i}$	$2.4+1.8\mathrm{i}$	-0.5966703454 $-0.4964748081\mathrm{i}$	$5.365036\,10^{-21}$	$6.911831\,10^{-21}$
0.5	$-0.95-3\mathrm{i}$	$2.4+1.8\mathrm{i}$	0.05138232432 $+2.276825704\mathrm{i}$	$5.365036\,10^{-21}$	$2.355767\,10^{-21}$
0.5	$3+3\mathrm{i}$	$2.4+1.8\mathrm{i}$	-1.035668357 $-10.26169015\mathrm{i}$	$1.110811\,10^{-16}$	$1.077012\,10^{-17}$
0.5	$1+\epsilon(1+\mathrm{i})$	$2.4+1.8\mathrm{i}$	-3.653533208 $+2.556404313\mathrm{i}$	$4.137976\,10^{-28}$	$9.27986\,10^{-29}$
0.7	$-0.95+3\mathrm{i}$	$2.4+1.8\mathrm{i}$	-10.73555937 $+4.003414460\mathrm{i}$	$5.216247\,10^{-19}$	$4.552601\,10^{-20}$
0.7	$3-3\mathrm{i}$	$2.4+1.8\mathrm{i}$	0.2987277661 $-4.272830910\mathrm{i}$	$9.629532\,10^{-16}$	$2.248178\,10^{-16}$
0.9	$-0.95+3\mathrm{i}$	$2.4+1.8\mathrm{i}$	-282.0355075 $-380.6979483\mathrm{i}$	$1.141784\,10^{-16}$	$2.409904\,10^{-19}$
0.9	$-0.95-3\mathrm{i}$	$2.4+1.8\mathrm{i}$	402.7443729 $-175.1513274\mathrm{i}$	$1.141784\,10^{-16}$	$2.599794\,10^{-19}$
0.9	$3+3\mathrm{i}$	$2.4+1.8\mathrm{i}$	-0.03608000570 $-0.04059280123\mathrm{i}$	$5.406782\,10^{-15}$	$9.955465\,10^{-14}$
0.9	$1+\epsilon(1+\mathrm{i})$	$2.4+1.8\mathrm{i}$	0.7321455411 $-4.257109937\mathrm{i}$	$7.969946\,10^{-33}$	$1.845062\,10^{-33}$
0.9	$-0.95+3\mathrm{i}$	$-2.4+1.8\mathrm{i}$	125.4725953 $-332.8698944\mathrm{i}$	$1.588399\,10^{-16}$	$4.465146\,10^{-19}$
0.9	$3+3\mathrm{i}$	$-2.4+1.8\mathrm{i}$	747963.3709 $-1859280.818\mathrm{i}$	$1.467457\,10^{-13}$	$7.322313\,10^{-20}$
0.9	$-0.95+3\mathrm{i}$	-3	106380.3017 $-75054.36270\mathrm{i}$	$7.93894\,10^{-16}$	$6.097876\,10^{-21}$

z	h	s	Complex centre	Absolute error below	Relative error below
0.9	$3+3\mathrm{i}$	-3	236016519.8 $+1.769237442e+9\mathrm{i}$	$7.112954\,10^{-11}$	$3.985049\,10^{-20}$

Actual noninteger resources

Preparation	L	M	R	K	Cold tail cache seconds
two-fifths	112	16	2048	4096	17.90
half	144	20	2048	4096	34.79
seven	336	28	8192	16384	198.31
nine	1280	32	49152	98304	1818.72
nine-negative	960	24	32768	65536	521.60
nine-special	0	16	2048	4096	0.00

All principal tail contractions use Abel order 32 and 768-bit readout arithmetic. Reusable coefficient balls were constructed at 384 bits. The radius listed is the actual contraction radius; a cache may have been constructed at a smaller radius and rescaled by its proved contract.

Endpoint error components

Component	Positive tilt, inverse order	Positive tilt, $h=3+3\mathrm{i}$	Negative tilt, inverse order
Native arithmetic	$1.141044\,10^{-16}$	$5.406765\,10^{-15}$	$1.588312\,10^{-16}$
Angular source	$4.181914\,10^{-20}$	$1.702654\,10^{-20}$	$7.624779\,10^{-21}$
Mellin image	$7.4737\,10^{-43}$	$5.398685\,10^{-39}$	$2.817073\,10^{-33}$
Four-Bessel remainder	$3.21615\,10^{-20}$	$1.004942\,10^{-50}$	$9.978091\,10^{-22}$
Finite Abel remainder	$1.216774\,10^{-95}$	$2.59813\,10^{-121}$	$1.388142\,10^{-97}$
Complete preparation return	$1.056506\,10^{-26}$	$3.809529\,10^{-26}$	$2.541242\,10^{-25}$
Ball and decimal readout	$3.17142\,10^{-63}$	$7.400251\,10^{-63}$	$3.936496\,10^{-63}$
Total	$1.141784\,10^{-16}$	$5.406782\,10^{-15}$	$1.588399\,10^{-16}$

Independently checked exact integers

z	h	s	Absolute allowance below	Relative allowance below
0.5	0	$2.4+1.8\mathrm{i}$	$2.762287\,10^{-48}$	$1.012926\,10^{-48}$
0.5	1	$2.4+1.8\mathrm{i}$	$5.339595\,10^{-48}$	$1.197463\,10^{-48}$
0.5	2	$2.4+1.8\mathrm{i}$	$6.234408\,10^{-48}$	$8.294048\,10^{-49}$
0.5	3	$2.4+1.8\mathrm{i}$	$2.064219\,10^{-47}$	$1.574203\,10^{-48}$
0.9	0	$2.4+1.8\mathrm{i}$	$4.36394\,10^{-47}$	$9.20665\,10^{-49}$
0.9	1	$2.4+1.8\mathrm{i}$	$4.926123\,10^{-48}$	$1.14041\,10^{-48}$
0.9	2	$2.4+1.8\mathrm{i}$	$4.856637\,10^{-49}$	$1.238845\,10^{-48}$
0.9	3	$2.4+1.8\mathrm{i}$	$4.256223\,10^{-50}$	$1.237891\,10^{-48}$
0.9	0	$-2.4+1.8\mathrm{i}$	$4.111283\,10^{-45}$	$3.081123\,10^{-48}$
0.9	1	$-2.4+1.8\mathrm{i}$	$4.354059\,10^{-44}$	$3.860706\,10^{-48}$
0.9	2	$-2.4+1.8\mathrm{i}$	$3.6542\,10^{-43}$	$3.590417\,10^{-48}$
0.9	3	$-2.4+1.8\mathrm{i}$	$3.030281\,10^{-43}$	$3.103999\,10^{-49}$
0.9	0	-3	$1.601285\,10^{-42}$	$5.167148\,10^{-49}$
0.9	1	-3	$2.672536\,10^{-41}$	$1.040283\,10^{-48}$
0.9	2	-3	$4.783949\,10^{-40}$	$1.831135\,10^{-48}$
0.9	3	-3	$4.113627\,10^{-39}$	$1.323529\,10^{-48}$
0.7	0	$2.4+1.8\mathrm{i}$	$3.544835\,10^{-48}$	$3.240862\,10^{-49}$
0.7	1	$2.4+1.8\mathrm{i}$	$4.436944\,10^{-48}$	$5.542574\,10^{-49}$
0.7	2	$2.4+1.8\mathrm{i}$	$6.710043\,10^{-48}$	$1.142975\,10^{-48}$
0.7	3	$2.4+1.8\mathrm{i}$	$3.756444\,10^{-48}$	$8.722699\,10^{-49}$

An additional complete execution at $z=.9$, $h=-.95+3\mathrm{i}$, $s=2.4+1.8\mathrm{i}$ uses $L=1120$, $M=20$, $K=98304$ and $R=49152$. It returns absolute error below $2.331516\,10^{-10}$ and relative error below $4.921012\,10^{-13}$. Its signed coefficient cache took 505.87 seconds, compared with 1818.72 seconds for the higher-order principal cache. Both use the same already priced physical prefix and image. The smaller design, the principal certificate and

the unexecuted common formula have separate complete budgets. This additional repeated-input execution is outside the 35 principal cases and is retained as an audited practical resource repair.

Costs and conditioning

Nine sealed preparations contain 204800 executed native samples and about 16.9 MB of data. The positive generic $z = .9$ source used $K = 98304$ and took about 166 seconds with two workers under shared load. The independent negative generic tilt used $K = 65536$ and took about 109 seconds. Their exact physical restoration factors are respectively 256 and 262144. The inherited 104-bit fixed-point kernel passed every executed guard. It was not replaced merely because a conservative asymptotic bound worsened.

The endpoint positive-order example has modulus near .054 and its native allowance is about $5.407\,10^{-15}$. It therefore provides a useful smaller complex readout challenge. Coefficient preparation is a substantial cold-run cost; source and tail caches are reusable across orders at fixed radius and tilt. Warm contraction still prices every rounding operation and every source row. The report's timings describe actual executions, not a uniform runtime guarantee.

Overlap, independent checks, failures and repairs (U4)

The continuous overlap proof follows from both representations enclosing the same original Haar moment. The new cells overlap on $[.49, .5]$, $[.59, .6]$, $[.69, .7]$, and $[.79, .8]$; the first overlaps the old interior on $[3/8, .4]$. The common grids on these overlaps are not presented as executed finite-arithmetic certificates.

At $z = .4$, $h = 3 + 3\mathrm{i}$, $s = 2.4 + 1.8\mathrm{i}$, the inherited polylog-tail and new Abel-tail computations differ by less than $3.990\,10^{-55}$, inside a combined allowance below $9.408\,10^{-17}$. Their original finite-prefix and image engine is a shared dependency. This is an independently priced tail overlap, not independent verification of that shared source.

At $z = .9$, $h = -.95 + 3\mathrm{i}$, $s = -3$, the new sampled construction and the inherited continuous-Mellin calculation differ by less than $2.771\,10^{-19}$, inside their combined allowance. The latter uses origin coefficients, certified compact-interval quadrature and a continuous exponential-integral tail. It does not share the new sampled prefix, finite Abel lattice contraction or image correction.

For $\Re h > 0$, a further direct physical-source tail bound is

$$\left| C_\Delta \sum_{k>K} k^{-1-2h} \Phi(k\Delta) \right| \le |C_\Delta| d^{-(\Re s)^2} \frac{K^{-2\Re h}}{2\Re h}.$$

It uses the inherited physical mass inequality and no Laurent preparation or Bessel expansion. At the generic positive-tilt endpoint with $h = 3 + 3\mathrm{i}$ and $K = 98304$, this allowance is below $1.515403\,10^{-19}$. The resulting separately priced disk agrees with the full expansion readout. Its prefix and image are shared dependencies; its terminal-tail estimate is independent.

Additional independent and adversarial evidence includes:

- Original-eigenvalue-circle source integration at a complex radial frequency and original-circle hypergeometric Toeplitz mass checks for every prepared physical input; native first samples were also independently enclosed.
- Twenty exact-integer moment checks using a bivariate Toeplitz jet of the original eigenvalue circle, with a coefficientwise analytic quadrature allowance. They do not use the Mobius preparation coefficients.
- 119 outgoing Bessel expansion checks, 51 exact-Green checks, signed orders and near-turning arguments, and explicit unsupported-input refusals. The difficult $n = -3000$ case required 3072 bits after a lower-precision interval was too wide; it was never accepted at the inadequate precision.
- 36 separately priced Abel/polylog comparisons, including inverse, positive complex and 10^{-30} near-integer orders; wrong finite-difference signs are rejected.
- 15 direct finite-source product checks that sum Fourier triples, all determinant permutations and exact Bessel values without the encoded polynomial aggregation.

- A deliberate omission of the upper-radius physical frame factor is rejected by source gaps exceeding 46.94 and 838.72.
- Printed complex-ball cache strings initially caused a parser refusal. An audited two-component reader preserves both Arb radii and checks physical input, resource metadata, complete populations, frequencies and source seals. The failed reader and its refused executions remain preserved.
- Unsupported exact rational native headers are refused before source rows are created. The physical radius is never silently rounded.

The inherited incorrect sign aggregation, interval phase wrapping, frozen-grid false convergence and earlier failed controls remain preserved with their receipts. The new construction changes the inadequate estimates and computational representation; it makes no negative claim about the underlying moment when a numerical design fails.

Executed moments and complete error budgets (O10)

The main matrix uses five radii, 0, 10^{-6}, .01, .02 and .025, and independent boundary tilts. It includes $h = -.95 \pm 3\mathrm{i}$, real inverse order, positive complex orders through $3 \pm 3\mathrm{i}$, and the exact near-integer $h = 1 + \epsilon + \mathrm{i}\epsilon$, $\epsilon = 10^{-30}$. The certificate ledger contains 42 principal noninteger and 40 principal integer readouts plus the extra rank-five inherited-input comparison. Every entry passed its own relative-modulus gate.

Selected complex moments

The following values are rounded for display. The tiny error allowances refer to the full 85-digit centres in the JSON receipts; they are not enclosures around these shortened printed numbers. Tilts are $A = 2.4 + 1.8\mathrm{i}$, $B = -2.4 + 1.8\mathrm{i}$, $C = 3\mathrm{i}$, and $D = -1.8 + 2.4\mathrm{i}$.

N, z	h, s	Displayed moment	Absolute allowance
$5, 0$	$-0.95 + 3\mathrm{i}, A$	$0.010892030274983853 - 0.0065011755931016212\mathrm{i}$	$< 1.295228\,10^{-27}$
$7, 0$	$-0.95 + 3\mathrm{i}, A$	$0.012451369654496100 - 0.0057325454281773869\mathrm{i}$	$< 1.295282\,10^{-27}$
$5, 0.02$	$-0.95 + 3\mathrm{i}, A$	$0.010838745974716608 - 0.0062868240361459995\mathrm{i}$	$< 6.860686\,10^{-25}$
$7, 0.02$	$-0.95 + 3\mathrm{i}, A$	$0.012346242338786224 - 0.0056327650534098988\mathrm{i}$	$< 3.679143\,10^{-24}$
$5, 0.025$	$-0.95 + 3\mathrm{i}, A$	$0.010809439822169636 - 0.0061686130904771150\mathrm{i}$	$< 7.255509\,10^{-25}$
$7, 0.025$	$-0.95 + 3\mathrm{i}, A$	$0.012287093742244257 - 0.0055770727851638908\mathrm{i}$	$< 4.770791\,10^{-23}$
$7, 0.025$	$3 - 3\mathrm{i}, A$	$-1.1806895554849764 + 1.5259534990297683\mathrm{i}$	$< 5.696985\,10^{-15}$
$7, 0.02$	$1 + \epsilon + \epsilon\mathrm{i}, A$	$1.0019997820813352 + 0.0069231245794157956\mathrm{i}$	$< 3.794276\,10^{-49}$
$5, 0.02$	$-0.95 + 2.7\mathrm{i}, D$	$0.015281182770775442 - 0.016813843383523199\mathrm{i}$	$< 7.141503\,10^{-25}$

Component budgets at difficult inputs

All values below are rounded upward. The first two columns use $h = -.95 + 3\mathrm{i}$, $s = A$; the third uses $h = 3 - 3\mathrm{i}$, $s = A$.

Component	$N = 7, z = .02$	$N = 7, z = .025$	$N = 7, z = .025$, positive order
Native finite arithmetic	$< 3.398137\,10^{-24}$	$< 3.863966\,10^{-24}$	$< 5.696985\,10^{-15}$
Finite angular source	$< 4.620731\,10^{-33}$	$< 1.970199\,10^{-30}$	$< 5.600164\,10^{-31}$
Complete Mellin image	$< 1.160972\,10^{-50}$	$< 5.079959\,10^{-51}$	$< 2.947500\,10^{-40}$
Physical filtered terminal	$< 2.810054\,10^{-25}$	$< 4.384394\,10^{-23}$	$< 5.882660\,10^{-38}$
Ball arithmetic and export	$< 5.396441\,10^{-88}$	$< 4.537934\,10^{-87}$	$< 3.665281\,10^{-85}$
Complete certified disk	$< 3.679143\,10^{-24}$	$< 4.770791\,10^{-23}$	$< 5.696985\,10^{-15}$
Certified relative bound	$< 2.711138\,10^{-22}$	$< 3.535603\,10^{-21}$	$< 2.952733\,10^{-15}$

The fourteen source preparations took 0.78 to 3.81 seconds each in this recorded environment. Their combined generation time was 38.28 seconds; the 82 raw scalar readouts totalled 2.34 seconds. These timings describe this run, not a uniform resource theorem.

Complete principal and auxiliary ledger

The full table contains actual executed certificates, not interpolated coverage. Exact inputs and all full-precision disks are in the ledger. The source prefix is already available in these timings and resources.

N	z	h	s	Absolute bound	Relative bound
5	0	$-0.95+3\mathrm{i}$	A	$<1.295228\,10^{-27}$	$<1.021095\,10^{-25}$
5	0	$-0.95-3\mathrm{i}$	A	$<1.295228\,10^{-27}$	$<1.021095\,10^{-25}$
5	0	-0.95	A	$<6.566363\,10^{-26}$	$<3.396989\,10^{-27}$
5	0	$-0.31+0.67\mathrm{i}$	A	$<7.818546\,10^{-30}$	$<9.836401\,10^{-30}$
5	0	$3+3\mathrm{i}$	A	$<8.320869\,10^{-23}$	$<4.411027\,10^{-23}$
5	0	$1+\epsilon+\epsilon\mathrm{i}$	A	$<6.345288\,10^{-50}$	$<6.345288\,10^{-50}$
5	10^{-6}	$-0.95+3\mathrm{i}$	A	$<4.423120\,10^{-25}$	$<3.486973\,10^{-23}$
5	10^{-6}	$3-3\mathrm{i}$	A	$<2.009901\,10^{-16}$	$<1.065481\,10^{-16}$
5	0.01	$-0.95+3\mathrm{i}$	A	$<6.038576\,10^{-25}$	$<4.775288\,10^{-23}$
5	0.01	$-0.31+0.67\mathrm{i}$	A	$<4.997860\,10^{-25}$	$<6.290444\,10^{-25}$
5	0.01	$3+3\mathrm{i}$	A	$<2.160651\,10^{-16}$	$<1.147513\,10^{-16}$
5	0.02	$-0.95+3\mathrm{i}$	A	$<6.860686\,10^{-25}$	$<5.475378\,10^{-23}$
5	0.02	$-0.95-3\mathrm{i}$	A	$<6.860686\,10^{-25}$	$<5.349579\,10^{-23}$
5	0.02	$3+3\mathrm{i}$	A	$<2.350953\,10^{-16}$	$<1.255485\,10^{-16}$
5	0.02	$1+\epsilon+\epsilon\mathrm{i}$	A	$<3.685827\,10^{-48}$	$<3.678383\,10^{-48}$
5	0.025	$-0.95+3\mathrm{i}$	A	$<7.255509\,10^{-25}$	$<5.829726\,10^{-23}$
5	0.025	$3-3\mathrm{i}$	A	$<2.451284\,10^{-16}$	$<1.272340\,10^{-16}$
5	0.02	$-0.95+3\mathrm{i}$	B	$<6.502049\,10^{-25}$	$<5.043898\,10^{-23}$
5	0.02	$3+3\mathrm{i}$	B	$<2.251809\,10^{-16}$	$<1.176712\,10^{-16}$
5	0.02	$-0.95+3\mathrm{i}$	C	$<6.569561\,10^{-25}$	$<5.164169\,10^{-23}$
5	0.02	$3+3\mathrm{i}$	C	$<2.221264\,10^{-16}$	$<1.195013\,10^{-16}$
5	0	0	A	0	0
5	0	1	A	$<5.393127\,10^{-116}$	$<5.393127\,10^{-116}$
5	0	2	A	$<1.657594\,10^{-115}$	$<8.287967\,10^{-116}$
5	0	3	A	$<1.008028\,10^{-113}$	$<1.680047\,10^{-114}$
5	0.02	0	A	$<1.069739\,10^{-69}$	$<1.068661\,10^{-69}$
5	0.02	1	A	$<2.535438\,10^{-69}$	$<2.530318\,10^{-69}$
5	0.02	2	A	$<3.581492\,10^{-69}$	$<1.785310\,10^{-69}$
5	0.02	3	A	$<1.635837\,10^{-68}$	$<2.715335\,10^{-69}$
5	0.025	0	A	$<6.968559\,10^{-70}$	$<6.957588\,10^{-70}$
5	0.025	1	A	$<2.483240\,10^{-69}$	$<2.475396\,10^{-69}$
5	0.025	2	A	$<3.527360\,10^{-69}$	$<1.755296\,10^{-69}$
5	0.025	3	A	$<4.444176\,10^{-69}$	$<7.359855\,10^{-70}$
5	0.02	0	B	$<9.788182\,10^{-70}$	$<9.778319\,10^{-70}$
5	0.02	1	B	$<3.027917\,10^{-69}$	$<3.021802\,10^{-69}$
5	0.02	2	B	$<4.894080\,10^{-69}$	$<2.439611\,10^{-69}$
5	0.02	3	B	$<1.510075\,10^{-68}$	$<2.506582\,10^{-69}$
5	0.02	0	C	$<6.535787\,10^{-70}$	$<6.559363\,10^{-70}$
5	0.02	1	C	$<2.696317\,10^{-69}$	$<2.715820\,10^{-69}$
5	0.02	2	C	$<1.921928\,10^{-69}$	$<9.714181\,10^{-70}$
5	0.02	3	C	$<3.152788\,10^{-69}$	$<5.331072\,10^{-70}$
7	0	$-0.95+3\mathrm{i}$	A	$<1.295282\,10^{-27}$	$<9.449355\,10^{-26}$
7	0	$-0.95-3\mathrm{i}$	A	$<1.295282\,10^{-27}$	$<9.449355\,10^{-26}$
7	0	-0.95	A	$<6.566363\,10^{-26}$	$<3.373016\,10^{-27}$
7	0	$-0.31+0.67\mathrm{i}$	A	$<7.818546\,10^{-30}$	$<9.852655\,10^{-30}$
7	0	$3+3\mathrm{i}$	A	$<8.320869\,10^{-23}$	$<4.410635\,10^{-23}$
7	0	$1+\epsilon+\epsilon\mathrm{i}$	A	$<3.992854\,10^{-49}$	$<3.992854\,10^{-49}$
7	10^{-6}	$-0.95+3\mathrm{i}$	A	$<1.814520\,10^{-24}$	$<1.323731\,10^{-22}$
7	10^{-6}	$3-3\mathrm{i}$	A	$<4.312468\,10^{-15}$	$<2.285906\,10^{-15}$
7	0.01	$-0.95+3\mathrm{i}$	A	$<2.579523\,10^{-24}$	$<1.886544\,10^{-22}$
7	0.01	$-0.31+0.67\mathrm{i}$	A	$<7.643594\,10^{-24}$	$<9.636104\,10^{-24}$
7	0.01	$3+3\mathrm{i}$	A	$<4.777696\,10^{-15}$	$<2.536513\,10^{-15}$
7	0.02	$-0.95+3\mathrm{i}$	A	$<3.679143\,10^{-24}$	$<2.711138\,10^{-22}$

Continued on next page

N	z	h	s	Absolute bound	Relative bound
7	0.02	$-0.95-3\mathrm{i}$	A	$<3.679143\,10^{-24}$	$<2.655063\,10^{-22}$
7	0.02	$3+3\mathrm{i}$	A	$<5.373574\,10^{-15}$	$<2.866320\,10^{-15}$
7	0.02	$1+\epsilon+\epsilon\mathrm{i}$	A	$<3.794276\,10^{-49}$	$<3.786613\,10^{-49}$
7	0.025	$-0.95+3\mathrm{i}$	A	$<4.770791\,10^{-23}$	$<3.535603\,10^{-21}$
7	0.025	$3-3\mathrm{i}$	A	$<5.696985\,10^{-15}$	$<2.952733\,10^{-15}$
7	0.02	$-0.95+3\mathrm{i}$	B	$<2.890004\,10^{-24}$	$<2.085671\,10^{-22}$
7	0.02	$3+3\mathrm{i}$	B	$<5.051276\,10^{-15}$	$<2.639299\,10^{-15}$
7	0.02	$-0.95+3\mathrm{i}$	C	$<3.073369\,10^{-24}$	$<2.241711\,10^{-22}$
7	0.02	$3+3\mathrm{i}$	C	$<4.921112\,10^{-15}$	$<2.646380\,10^{-15}$
7	0	0	A	0	0
7	0	1	A	$<5.393127\,10^{-116}$	$<5.393127\,10^{-116}$
7	0	2	A	$<1.657594\,10^{-115}$	$<8.287967\,10^{-116}$
7	0	3	A	$<1.008028\,10^{-113}$	$<1.680047\,10^{-114}$
7	0.02	0	A	$<7.980909\,10^{-68}$	$<7.972867\,10^{-68}$
7	0.02	1	A	$<8.244636\,10^{-68}$	$<8.227985\,10^{-68}$
7	0.02	2	A	$<3.631175\,10^{-67}$	$<1.810076\,10^{-67}$
7	0.02	3	A	$<3.898203\,10^{-67}$	$<6.470649\,10^{-68}$
7	0.025	0	A	$<9.566949\,10^{-68}$	$<9.551888\,10^{-68}$
7	0.025	1	A	$<1.374376\,10^{-67}$	$<1.370035\,10^{-67}$
7	0.025	2	A	$<2.055805\,10^{-67}$	$<1.023016\,10^{-67}$
7	0.025	3	A	$<3.497084\,10^{-67}$	$<5.791406\,10^{-68}$
7	0.02	0	B	$<7.968595\,10^{-68}$	$<7.960565\,10^{-68}$
7	0.02	1	B	$<2.779797\,10^{-67}$	$<2.774183\,10^{-67}$
7	0.02	2	B	$<2.916430\,10^{-67}$	$<1.453788\,10^{-67}$
7	0.02	3	B	$<3.953450\,10^{-67}$	$<6.562354\,10^{-68}$
7	0.02	0	C	$<5.133752\,10^{-68}$	$<5.152270\,10^{-68}$
7	0.02	1	C	$<2.558225\,10^{-67}$	$<2.576730\,10^{-67}$
7	0.02	2	C	$<1.737393\,10^{-67}$	$<8.781467\,10^{-68}$
7	0.02	3	C	$<3.191200\,10^{-67}$	$<5.396023\,10^{-68}$
5	0.02	$-0.95+2.7\mathrm{i}$	D	$<7.141503\,10^{-25}$	$<3.143202\,10^{-23}$

Fresh-source public execution after the review

The fixed 83-entry ledger was left unchanged during final release checks. A separately generated, previously unreviewed physical input was evaluated through the completed public interface:

$$N=5,\qquad z=3/200,\qquad h=3+3\mathrm{i},\qquad s=3\mathrm{i}.$$

Its full-precision disk has absolute allowance below $2.172555\,10^{-16}$ and relative allowance below $1.161291\,10^{-16}$. The displayed value, rounded independently of that fine enclosure, is $-1.14010138062270336-1.48327388616199771\mathrm{i}$. This is an additional public certificate, stored separately from the 83-entry matrix. The same post-review checks confirmed approved-cache reuse, explicit candidate status, and refusal of fabricated or unreviewed existing sources. The complete receipt and producing data are retained under tail/postseal-execution/.

Independent checks, failures and repairs (O11)

Original-source and integer checks

Fifteen physical preparations were independently checked: fourteen in the main matrix and the additional rank-five preparation matching the inherited boundary case. The independent source integrals are formed directly on the original λ circle. They use neither the transformed preparation coefficients nor the native source kernel. Hypergeometric Toeplitz mass, a complex radial-source value and the first native source sample are compared with separately bounded angular quadrature. All fifteen checks passed. Discarding the imaginary part of s was rejected at all thirteen positive-radius preparations. The two centre preparations correctly lose tilt dependence because $\Lambda_N(0)=1$.

For positive-radius integer orders, define on the original circle

$$g(\lambda) = (1 - z\lambda)(1 - z/\lambda), \qquad q_+(\lambda) = \frac{(1 - z^2)\lambda}{1 - z\lambda}, \quad q_-(\lambda) = \frac{(1 - z^2)/\lambda}{1 - z/\lambda}.$$

The independent generating function is the Toeplitz determinant of $g^s \exp(tq_+ + uq_-)$. Extracting $(m!)^2[t^m u^m]$ gives the original integer moment. A row-subset determinant recurrence retains all permutation signs without an explicit factorial enumeration. For a strip of width $v = 1$, define

$$\ell = 1 + z^2 - 2z\cosh v, \qquad u_g = (1 + ze^v)(1 + ze^{-v}), \qquad Q_0 = \frac{(1 - z^2)e^v}{1 - ze^v},$$
$$W = \max(\ell^{\Re s}, u_g^{\Re s}) \exp\left(|\Im s| \arctan \frac{2z \sinh v}{\ell} \right).$$

All pole and positivity gates hold. The coefficientwise trapezoid allowance and real-circle entry bound are

$$E_{ab} = \frac{2We^{(N-1)v}}{e^{Pv} - 1} \frac{Q_0^{a+b}}{a!b!}, \qquad B_{ab} = \max((1 - z)^{2\Re s}, (1 + z)^{2\Re s}) \frac{(1 + z)^{a+b}}{a!b!}.$$

Positive polynomial telescoping bounds the moment error by

$$N!N(m!)^2[t^m u^m]E(B + E)^{N-1}.$$

At $P = 256$ and 384 bits all thirty-two positive-radius integer controls passed. The largest exported independent disk radius is below $4.777\,10^{-90}$ and the largest angular allowance below $2.856\,10^{-98}$. The eight centre controls separately return $T_N(m, s; 0) = m!$ for $m = 0, 1, 2, 3$. These are checks of the actual original preparation and mark, not comparisons between two settings of the same Mellin image engine.

Independent algebra and scalar checks

The exact filter agrees with a separately implemented bounded-composition inclusion–exclusion formula at all 2498 tested indices. Three scalar reconstructions use reflected gamma factors and reversed summation order; their independently accounted budgets agree. The auxiliary population algorithm verifies 1920 forced zeros by rational arithmetic, retaining each individual Fourier mode. Forty gamma-quotient checks include exact and very near integer orders. Eight explicit regular-zero configurations verify both nonzero squared Vandermonde and a rank-two trace differential.

The centre comparisons use the inherited continuous Mellin integral and the new sampled readout with independent terminal pricing. They share the CUE Bessel determinant identity and rational Taylor generator. The old/new positive-radius comparisons share the native source and image engines; agreement of those readouts alone is therefore not an independent source verification. The original-circle source and integer checks supply that separate challenge. Each comparison records its shared dependencies.

Controls that deliberately failed

Unbudgeted conversion of certified source centres to IEEE double precision was rejected in all three scalar controls: discrepancies of order $4\,10^{-18}$ to 10^{-17} exceed the corresponding declared fine enclosures. This directly detects false precision even when printed digits appear stable. Incorrect cutoff endpoints and inappropriate population aggregation are also retained as adversarial controls.

The first domain guards compared Arb balls with exact boundary values and incorrectly refused $\Re h = -.95$ or $|s| = 3$. Membership is now decided in exact rational arithmetic before ball conversion. An independent mass audit originally required a strict inequality when both exact discrepancy and allowance were zero; its zero-equality case was repaired and the earlier failure record retained. The public-interface audit also identified overstated centre precision on a reused cache and insufficient proof of origin for a self-rehashed cache. The generating metadata and approved cache provenance gates repair these issues without changing the mathematical core. Earlier source versions and refusal receipts remain available; none is relabelled as a successful certificate.

Executed scalar results and complete budgets (E11)

The fixed ledger contains 123 reviewed pointwise disks, 41 at each rank: 21 noninteger inputs and 20 integer controls per rank. The noninteger matrix includes $h = -.95$, $-.95 \pm 3\mathrm{i}$ at all five principal radii, positive $3 \pm 3\mathrm{i}$, a moderate complex order, an exact rational displacement of 10^{-30} near one, and independent negative-real and purely imaginary boundary tilts. The integer controls are $h = 0, 1, 2, 3$ at each principal radius. All 123 pass the relative target with a positive modulus floor.

Raw candidate receipts remain unchanged. A separate ledger reprices all cases, checks the declared physical matrix, producing sources, coefficient-cache origins, every required audit status, and before/after source and code hashes. The public interface and ledger builder have independent adversarial reviews. These provenance checks bind the mathematical and arithmetic evidence; hashes alone are not presented as a proof of a numerical claim.

Rank	Certificates	Absolute error at worst-relative case	Largest relative allowance
4	41	$5.839258\,10^{-17}$	$3.258735\,10^{-17}$
6	41	$6.858326\,10^{-17}$	$5.002076\,10^{-15}$
8	41	$2.997576\,10^{-14}$	$1.604451\,10^{-14}$

The worst relative case is the positive order $3 + 3i$ at ranks four/eight and the inverse order $-.95 + 3i$ at rank six; all occur at $z = .025, s = 2.4 + 1.8i$.

Rank-four hard-input component	Actual absolute allowance
Native finite-source arithmetic	$8.966043\,10^{-25}$
Original angular source	$3.268760\,10^{-37}$
Complete Mellin image	$1.126710\,10^{-50}$
Unbalanced Abel remainder	$1.130220\,10^{-68}$
Tail angular quadrature	$1.912150\,10^{-53}$
Balanced Euler–Maclaurin	$9.138015\,10^{-79}$
Balanced integral series	$2.001248\,10^{-93}$
Bessel product remainder	$1.781914\,10^{-38}$
Complete preparation return	$1.913142\,10^{-29}$
Ball arithmetic and decimal export	$4.296615\,10^{-87}$
Final disk	$8.966234\,10^{-25}$

Actual input: $z = 1/40$, $h = -19/20 + 3i$, $s = 12/5 + 9i/5$. The same physical source and complete image are used in every component.

The full precision centres and component budgets reside in the JSON ledger. The displayed representative disks below include an explicit allowance for rounding their centres; the main ledger retains the original centres.

$$\begin{aligned} c_4 &= 0.01696368920360287288335969724858 5 \\ &\quad - 0.00181493861281206765028575176416 74\,i, \\ |T_4 - c_4| &< 8.966235\,10^{-25}. \end{aligned}$$

$$\begin{aligned} c_6 &= 0.01251715293409937967492207791588 6 \\ &\quad - 0.00559564680418071939029197232322 83\,i, \\ |T_6 - c_6| &< 6.858327\,10^{-17}. \end{aligned}$$

$$\begin{aligned} c_8 &= 0.01231348644086250620037192450763 1 \\ &\quad - 0.00558793856940983795607484034173 74\,i, \\ |T_8 - c_8| &< 1.387014\,10^{-23}. \end{aligned}$$

Independent source, component and overlap checks

Every principal source passed direct original-circle mass, complex-source and first-native-sample comparisons. The original-circle construction uses the original derivative mark and tilt, not the transformed tail preparation. There are 48 original-circle integer comparisons, 12 exact centre factorial controls, and 12 exact rational Möbius witnesses. At positive radius, 18 tests reject loss of the imaginary tilt. An independent-eigenangle surrogate omitting the CUE Vandermonde is rejected at all three ranks.

The rank-four population audit enumerates all 24 determinant permutations and 16 sign placements with Gaussian-rational arithmetic. It checks 360 exact coefficients and 207 forced zeros, and rejects the selected-placement multiplicity shortcut. A separate finite angular DFT and exact retained Bessel contraction check the finite preparation at several radii and against the actual last native sample. The density, Mellin-integral and uniform-majorant audits include exact recurrence identities, independent Acb integration with explicit exterior bounds, near-pole checks, 160 positive-permanent identities, 1120 coefficient inequalities and all 21 noninteger rank-four budget comparisons.

The six complete inherited/new overlap comparisons use exactly $z = 1/50, 1/40$, $h = -19/20 + 3\mathrm{i}$ and $s = 12/5 + 9\mathrm{i}/5$. They compare independently priced, informative error disks and reject an intentional factor-of-two error. Both methods share the unchanged native source, angular planner and Mellin-image engines. Their agreement therefore validates the alternative complete tail/readout compositions, but is not an independent validation of that shared prefix. The original-circle audits provide the independent source challenge.

An additional 21 scalar executions cover each rank at $h = -1/2, 1/2, 3\mathrm{i}$ and near $0, 1, 2, 3$. They remain raw candidates outside the fixed 123-point ledger. The near-integer comparisons are supported by a density/support continuity inequality, not matching digits alone. The joined audit contains 37 checks.

Public execution after the final review

The real reviewed interface was exercised after sealing the fixed ledger. Reusing the approved rank-four cache at $z = 10^{-6}$ and $h = -.95{+}3i$ selects $L = 8$ by the proved preparation return and produces a relative certificate below $3.756423\,10^{-23}$. A separate centre integer execution encloses the exact value $T_4(2, s; 0) = 2$. Explicit candidate mode remains a candidate. Eight refusal tests include a copied cache with altered data and recomputed internal hashes: the reviewed-origin gate correctly rejects it.

A genuinely fresh source was then generated at $N = 4$, $z = 3/200$, $h = 3 + 3i$, $s = 3i$. The interface selected $L = 22$ and returned an absolute allowance below $5.307583\,10^{-17}$ and a relative allowance below $2.970388\,10^{-17}$. The complete execution took about 19.3 seconds in the recorded environment. A separate direct original-circle source audit passed for that fresh cache, including rejection of lost imaginary tilt. These public executions are recorded separately from the immutable 123-point ledger.

Failed controls, repairs and remaining limitations (E12)

The decisive frozen-prefix failure

At $N = 4, z = 0, h = -.95$, contraction of the same finite prefix at 384 and 512 bits agrees to within $9.61\,10^{-99}$. Nevertheless, omitting the complete tail changes the scalar by more than $3.8003401\,10^{-5}$. The complete balanced polynomial alone contributes more than $3.8003322\,10^{-5}$, while the complete scalar error is below $1.179401\,10^{-25}$. This executed control decisively separates arithmetic stability from correctness of the physical readout.

The zero-frequency balanced phase also remains zero at directions with $\cos\phi = 0$ at positive radius. Six exact controls reject the proposed positive odd-rank gap for that population. Absolute summability or the explicit balanced kernel is essential; changing precision cannot create the missing frequency gap.

Preserved failed attempts and repairs

The first independent scalar-composition audit used a large-shift Acb Lerch reference whose ball radius was enormous. Its noninteger overlap labels were vacuous and have been explicitly withdrawn, with the original receipt preserved. The replacement uses polylogarithm minus a finite prefix, requires an informative reference radius, and rejects a factor-two error. It does not use the withdrawn comparisons as evidence.

An initial original-integer audit omitted the cached image coefficient's ball radius from its comparison. The repaired audit includes that radius; the prior source and failure record remain preserved. An interval endpoint guard in an early contour component audit was likewise corrected without changing the underlying contour theorem. A preflight certificate builder initially recorded audit hashes without requiring each audit's successful status and producer binding; the final builder checks both, as well as global before/after source snapshots. The public scalar assessor also requires the integer route to agree with the exact input order. No such preflight was promoted as a final certificate.

Earlier inherited adversarial controls for wrong sign aggregation, rectangular phase wrapping, fixed-grid false convergence, missing complex preparation, inadequate native arithmetic, unsupported rational headers and gamma–zeta cancellation remain in their original packages and the new provenance record.

What is still open

The connected theorem supplies absolute approximations throughout the box; it does not prove a uniform positive modulus. Successful samples cannot rule out complex zeros. The finite-arithmetic certificates apply to recorded inputs and resources, and the public central interface may require more resources or return only an absolute disk at a different input. No broad performance guarantee is inferred from this finite matrix.

The rank-eight positive-order examples are dominated by finite-source arithmetic, despite the much smaller analytic central theorem. Increasing the tail expansion cannot repair that arithmetic limitation. The rank-six uniform central bound is dominated by the absolute contour tail; input-specific pricing is substantially sharper. The new public interface is central only. Full-radius operation still requires dispatch to the inherited interior constructions, whose larger common resources and arithmetic conditioning are not eliminated by the mathematical join.

Ranks one and two retain their distinct ordinary-moment domains. In particular, the rank-two centre requires $\Re h > -1/2$; an analytically continued value outside that domain is not an ordinary expectation. The fixed-interior, microscopic, shrinking-depth and circle regimes remain part of the ultimate programme and have not been re-proved or narrowed here.

Executed source-arithmetic diagnosis and repair (A7)

The primary challenge is the exact input

$$N = 8, \quad z = 9/10, \quad h = 3 + 3i, \quad s = 12/5 + (9/5)i, \qquad \Delta = 8/25.$$

The inherited dense source has 1608 rows and exact filter parameters $(K, b, p) = (1268, 21, 17)$. Its source arithmetic, not its tail, prevents the requested relative accuracy. The following are outward-rounded summaries of complete executed budgets; the exact decimal/rational disks and their code identities are retained in the receipt ledger.

Contribution	Inherited	HP2 rows 1–40	HP2 plus image 108
Source arithmetic	$1.075 \cdot 10^{-7}$	$8.018 \cdot 10^{-18}$	$8.018 \cdot 10^{-18}$
Image	$1.329 \cdot 10^{-10}$	$1.329 \cdot 10^{-10}$	$5.969 \cdot 10^{-20}$
Terminal	$8.986 \cdot 10^{-15}$	$8.986 \cdot 10^{-15}$	$8.986 \cdot 10^{-15}$
Complete absolute	$1.076 \cdot 10^{-7}$	$1.329 \cdot 10^{-10}$	$8.994 \cdot 10^{-15}$
Complete relative	$2.470 \cdot 10^{-9}$	$3.049 \cdot 10^{-12}$	$2.064 \cdot 10^{-16}$

Each displayed number is an upper summary, not the raw interval format. The unlisted angular/readout components are present in every complete sum. In the first two columns the image is unchanged. The third regenerates actual coefficients at $J = 108, m = 216, L = 100$; changing a final precision flag alone would not reduce the omitted image tail. The source and terminal are unchanged in that image comparison.

The full complex value is near

$$10.34746127989640009394 + 42.326332141504486055 94i.$$

This display is for orientation; use the receipt's exact centre with its stated radius. The original absolute disk remains valid even though its relative target fails. The new calculation resolves that failure without relabeling the old source or altering the physical moment.

Why these rows dominate

For $m \geq 0$ integer and real $t \neq 0$, gamma recurrence and conjugation give

$$|C_\Delta(m+it)| = 2^{1+2m}\Delta^{-2m}|t|\prod_{j=1}^{m}(j^2+t^2).$$

At $m = t = 3$, $\Delta = 8/25$, this is exactly 836849212.646484375. Twenty-eight outward checks verify the identity in its implemented use. The finite source is therefore contracted with a very large factor before cancellation against the image. The measured prefix–image cancellation ratios are approximately $8.72 \cdot 10^8$ at $z = 0.025$ and $9.22 \cdot 10^9$ at $z = 0.9$. These ratios diagnose conditioning; they are not used as error estimates.

At $N = 8, z = 1/40$ with the same h, s, the old source arithmetic costs about $2.998 \cdot 10^{-14}$, of which more than 99.45 percent comes from the first row. Replacing rows 1–40 gives a complete absolute error below $5.678 \cdot 10^{-28}$ and relative error below $3.039 \cdot 10^{-28}$, including source, image, angular and central contour terminal allowances. Its untouched suffix costs less than $5.619 \cdot 10^{-28}$. Extending the replacement to row 64 reduces the suffix bound to about $5.669 \cdot 10^{-30}$, but further resources should be selected only when the requested tolerance requires them.

At the upper input, 128-bit HP2 for the first forty rows already gives relative error below $3.050 \cdot 10^{-12}$ with the old image. The 192-bit first-forty source takes about 7.93 seconds on this run; the 128-bit version takes about 6.95 seconds. These are observed timings on a shared host, not uniform performance guarantees. The public default is 192 bits, with adaptive row count and image resources; no global optimum over bit counts is claimed.

Actual adaptive public runs

With a requested relative target 10^{-14}, the public selector starts from the reviewed inherited cache, observes source arithmetic dominance, and selects twelve replacement rows from the actual inherited suffix sum. It then sees image dominance and regenerates the Mellin image. The complete three-stage calculation reaches

$$E < 2.007 \cdot 10^{-14}, \qquad E/\ell < 4.606 \cdot 10^{-16}.$$

The remaining source suffix costs about $1.109 \cdot 10^{-14}$; there is no reason to regenerate forty rows merely because that was the benchmark. At the default 10^{-10} relative target, only three selected rows suffice: the final public run obtains $E < 1.507 \cdot 10^{-10}$ and relative error below $3.458 \cdot 10^{-12}$ in about 5.29 seconds using the reviewed warm coarse source. The tighter twelve-row run takes about 8.76 seconds. At the central input, a requested relative target 10^{-26} selects 47 rows and obtains $E < 1.113 \cdot 10^{-28}$ and relative error below $5.955 \cdot 10^{-29}$. The actual selected rows, source precision and image precision are disclosed.

A resource selector is permitted to stop before exhausting the available mathematical precision. Its target is the user's tolerance, with a defensible disk. If a later proposal worsens the bound, the earlier valid disk is kept. If the source arithmetic dominates, increasing asymptotic order is not a remedy. If the terminal dominates after the arithmetic repair, the next obligation is a new terminal/filter budget.

Connected validation and independent checks (A10)

The frozen backend matrix contains 75 actual complete scalar runs, promoted through separate reviewed certificates without changing their raw bytes. Seventy-four meet the original relative target; one is the deliberately preserved inherited rank-eight failure that motivates the repair. The tested ranks are all of three through eight. Cases include the exact centre, 10^{-6}, the 0.02 join, 0.025, critical radii, upper boundaries through 0.9, both signs of imaginary order, independent complex boundary tilts, exact integer orders, and near-integer orders. These are pointwise tests across the connected mathematical regions; they do not certify every parameter between tested points. After sealing the 193-source, 47-proof, 55-audit review, eight further public executions give six relative certificates, one deliberate absolute-only near-zero result and one deliberate exact-header refusal. There are therefore 82 complete reviewed scalar executions in these two sets, including 80 relative and two absolute-only results, plus the refusal. These are execution counts, not counts of distinct physical parameter values.

Final public case	Absolute bound	Relative bound	Outcome
Upper, default target	$1.507 \cdot 10^{-10}$	$3.458 \cdot 10^{-12}$	Relative
Upper, 10^{-14} target	$2.007 \cdot 10^{-14}$	$4.606 \cdot 10^{-16}$	Relative
Central, 10^{-26} target	$1.113 \cdot 10^{-28}$	$5.955 \cdot 10^{-29}$	Relative
Near zero, adaptive	$1.332 \cdot 10^{-146}$	$9.358 \cdot 10^{-43}$	Relative
Near zero, 256-bit cap	$6.273 \cdot 10^{-70}$	–	Absolute
Wide exact radius, $h = 0$	$4.534 \cdot 10^{-95}$	$4.527 \cdot 10^{-95}$	Relative
Wide exact radius, noninteger	–	–	Refused
Fresh rank-five centre	$1.296 \cdot 10^{-27}$	$1.022 \cdot 10^{-25}$	Relative

The wide radius is the exact decimal 0.025000000000000000000000000001. The direct characteristic source evaluates it; the native noninteger frequency header refuses it without rounding. The fresh rank-five centre uses $h = -0.95 + 3i, s = 0$. Final public receipts are indexed in receipts/final-index.json. The six later image-substitution and conditioning-repair candidates remain additional clearly classified audit evidence; they are not silently included in this certificate count.

The 24 exact centre controls use $h = 0, 1, 2, 3$ at each rank. Their values are $j!$ for $j \le N$, derived independently from the original CUE trace moments; the calculation uses exact rational Taylor coefficients. Other source checks include sixteen original-Haar comparisons across ranks, radii and critical points, plus targeted positive, negative and purely imaginary tilt cases. Independent Acb transforms check all forty HP2 upper rows against their physical arithmetic allowances. The reference avoids the native FFT and native determinant centres, while preserving the identical finite signed projection being checked. Its own insufficient-precision attempts remain in the failure history.

At $N = 4, z = 0.81, h = -0.95 + 3i, s = 2.4 + 1.8i$, the new dense outer and inherited interior constructions give respectively

$$E_{\text{outer}} < 1.537 \cdot 10^{-15}, \quad E_{\text{inner}} < 1.475 \cdot 10^{-16}, \quad |c_{\text{outer}} - c_{\text{inner}}| < 3.594 \cdot 10^{-26}.$$

Their complete disks overlap by a wide margin. This checks the actual join; shared source and image dependencies are recorded. Full HP2 generation at this point takes approximately 187 seconds, versus about 12 seconds for the inherited source, illustrating why selective repair is preferable when its mathematical hypotheses are available.

Preserved failures and repairs

The inherited sign aggregation, Vandermonde, phase wrapping, complex tilt, normalization, false-convergence, rational-header and near-integer controls remain unchanged. The new investigation adds the following concrete tests.

1. A fully consistent rehash of forged rank-four tail coefficients changes the scalar by more than $3.80034 \cdot 10^{-5}$ while two claimed small disks have summed radii below $2.359 \cdot 10^{-25}$. This demonstrates why structural hash consistency alone cannot confer mathematical origin. The public gate now rejects such an external tail without reviewed generation provenance.

2. Near a strict tolerance boundary, a pre-serialization comparison could pass while the outward displayed relative bound fails. Classification is now performed on the serialized exact upper bound itself.

3. The backend must identify a successful refined source rather than the original parent directory. It must also reproduce the exact old image centre consumed by that producer before replacing it. Sparse and dense inherited image contractors are algebraically related but have different finite centres. Dispatch v2 preserves v1 bytes and records an unchanged-branch bridge for the 75 earlier runs.

4. Increasing the image to $J = 108$ with $H = 3$ at $N = 3, z = 0.025, h = 3 - 3i, s = 2.4 + 1.8i$ worsens its arithmetic radius to about 0.28436, despite an unchanged printed centre. The systematic coefficient error is tiny; high-degree weights amplify finite coefficient noise. Keeping $J = 108, m = 216$ and changing the actual Cauchy radius to $H = 6$ reduces that image allowance below $2.694 \cdot 10^{-41}$, restoring a complete error below $1.131 \cdot 10^{-18}$. This explicit failure rules out indiscriminate image term growth as a universal policy.

5. Actual near-zero capped and adaptive runs verify absolute/relative classification. Injected scheduling timeouts additionally check that an earlier complete disk is preserved with its actual source/readout precision.

The audit does not treat matching printed digits, matching shared tails or a successful hash test as an independent error estimate. Every improvement is charged through an analytic or finite-arithmetic contract.

Executed zeros, off-branch moduli, and the public readout (Z9)

The uniform theorem proves existence and uniqueness independently of numerical root iteration. A quadratic predictor and subsequent physical-residual Newton steps propose exact rational tilts. Each accepted location is enclosed only after evaluating the complete original physical scalar at that tilt and applying (Z1.4). A wide scalar disk containing zero is not a zero-existence test. All executed candidates preserve their exact physical radius and independent tilt preparation.

The eight pointwise cases include positive and negative real h, positive and negative imaginary h, a mixed complex order at three physical radii, and a mixed order near the h-domain boundary. The following table records their actual locations and root radii. The continuation theorem, rather than interpolation of this table, covers the intervening parameters.

h	z	Displayed zero centre	Disk radius upper
0.001	0.9	$0.55561313865447250693 2 + 2.79915589675250441025 7732\,i$	3.50724×10^{-19}
-0.001	0.9	$0.55501543057135309892 9200 + 2.79936039709155034780 5004\,i$	3.53509×10^{-19}
$0.001i$	0.9	$0.55541796779471775287 9611 + 2.79955678747372101706 0120\,i$	3.52241×10^{-19}
$-0.001i$	0.9	$0.55521346963149648479 5122 + 2.79895908858147856264 2655\,i$	3.52017×10^{-19}
$0.002 + 0.003i$	0.9	$0.55622168613083456196 1398 + 2.79994101796024225771 0362\,i$	3.80231×10^{-17}
$0.008 + 0.005i$	0.9	$0.55818101812751857240 2888 + 2.79988293002790988881 5284\,i$	9.67600×10^{-18}
$0.002 + 0.003i$	0.89999999	$0.55622175946605782892 6554 + 2.79994112381755412966 4909\,i$	3.71789×10^{-17}
$0.002 + 0.003i$	0.89999998	$0.55622183280128099726 2864 + 2.79994122967486336026 3680\,i$	3.63593×10^{-17}

Table 41: Eight executed noninteger zero enclosures. The tilt entry is the real part followed by the imaginary part. Every displayed-centre rounding displacement is included in the stated radius. Exact rational centres and complete physical residual budgets are in the verification package.

Off-branch points use the same (h, z) fibre and the actual enclosing root disk. For an exact tilt s, an outward lower bound for $|s - a| - r$, divided by 400, gives a parameter-wide geometric modulus allowance. It does not assume nonvanishing outside the proved local tilt domain. The next two tables record the four executed off-branch checks and a complete scalar error budget.

h	z	Real tilt offset	E upper	Relative upper	Class
0.001	0.9	1.0×10^{-8}	8.65121×10^{-22}	1.57149×10^{-11}	Relative
0.001	0.9	1.0×10^{-12}	8.65121×10^{-22}	1.57149×10^{-7}	Absolute
$0.008 + 0.005i$	0.9	1.0×10^{-6}	7.95980×10^{-21}	1.43422×10^{-12}	Relative
$0.002 + 0.003i$	0.89999998	1.0×10^{-6}	3.11021×10^{-21}	5.65255×10^{-13}	Relative

Table 42: Fresh physical-source evaluations at exact offsets from the certified rational zero centres. The final row is at the inward endpoint. An absolute classification means that the requested 10^{-10} relative target was not earned; it does not discard the valid nonzero lower-modulus test.

The new public zero_evaluator.py keeps exact rational or decimal-string inputs, checks domain membership, binds the distinct continuation review, uses the approved generation origin or a fresh admitted execution, and returns a complex disk with a complete physical error budget. It does not claim global zero classification. The finite filter is repriced for the actual order, and the original gamma–zeta integer deflation and physical normalization contracts are retained.

The final public admission and modulus interface passed 24 adversarial checks, including changed physical fibres, forged zero disks, omitted image budgets, unreviewed receipt copies and strict relative-target serialization. A separate fresh public call at $h = 0.0005 + 0.0002i$, $z = .9$, generated two new physical sources and returned a unique-zero disk of radius below 7.817×10^{-17}. In the same verified execution it certified the full annulus,

Error component	Outward upper bound
Finite physical-source arithmetic	1.185487×10^{-22}
Prepared/angular source	2.933851×10^{-26}
Complete Mellin image	7.465420×10^{-22}
Filtered terminal remainder	3.638031×10^{-28}
Finite readout and serialization	5.293977×10^{-58}
Total complete disk radius	8.651204×10^{-22}

Table 43: Complete scalar error budget for $h = .001$, $z = .9$, at real tilt offset 10^{-8} from its certified zero centre. Source and image arithmetic dominate the already negligible terminal error.

centred at that exact rational disk centre, with inner radius 10^{-8} and outer radius 10^{-4}. Its modulus lower bound exceeds $2.49999998 \times 10^{-11}$. This ninth noninteger zero enclosure is separate from the eight-fibre matrix and the 229 historical scalar admissions.

The factor geometry also provides information lost by a coarse local Taylor readout. At $h = .001$ and real tilt offset 10^{-8} from its certified rational zero centre, the complete quadratic Taylor disk has error about 7.2071×10^{-10} and contains zero. The root-location and factor theorem nevertheless give a positive modulus lower bound above $2.4999999 \times 10^{-11}$. The fresh physical scalar error is below 8.65121×10^{-22}, so even that geometric denominator earns a relative bound below 3.461×10^{-11}. The sharper direct scalar denominator gives the value in Table 42. No lower bound is inferred from sampled nonzero values.

For a final scalar enclosure $\mathbb{D}(c, E)$, relative certification uses

$$\ell = \underline{|c|} - E > 0, \qquad \frac{E}{\ell} < 10^{-10}. \tag{Z9.1}$$

A geometric lower bound from (Z1.5) can supplement the modulus information on the same physical fibre. It cannot turn a zero into a relative certificate. At a proved zero, or when the completed enclosure has no positive modulus denominator, the correct output is absolute. Exact outward serialization must preserve this classification.

The two inward demonstration radii are 89999999/100000000 and 44999999/50000000. Their exact reduced native frequencies fit the inherited signed-32-bit headers. An initial warning based on an unreduced rational product was corrected before it became a claim of obstruction. Other unsupported exact headers retain a clear refusal; the radius is never silently rounded.

Verification, failures, and evidence classifications (Z12)

The verification chain distinguishes six kinds of evidence:

1. Analytic identities and theorems, including source transformations, holomorphy, transport, Cauchy aliases, and the implication from a common derivative cone to a modulus factor.

2. Executed outward inequalities, including $M < 6$, the local derivative constants, the strict Rouché slack, and the rational floor 1/400.

3. Complete finite-arithmetic scalar, zero and derivative disks, admitted only with their exact physical inputs, source generation and composed error contracts.

4. Numerical proposals such as a filter search or Newton predictor, which select candidates but prove no error estimate or zero existence.

5. Reproductions using a shared source/readout engine, which test provenance and arithmetic composition without being an independent original-source derivation.

6. Independent constructions, including original-Haar angular versus hypergeometric h=0 derivatives and the direct reconstruction of analytic bounds, aliases, geometry and derivative components.

The independent analytic audit checks the exact common-rotation degree, Hölder and Schur exponents, Riesz coefficient, Jacobians, moving-mark regularity, and the differentiated preparation term. The transport audit reconstructs the selected 384-bit bounds and checks the exact second-moment series symbolically. The Cauchy audits reconstruct all phases, node displacements, scalar-error sums and folded aliases, including the degree-60 extension. The geometry audit independently executes the uniform comparison at 768 bits without calling its producer. The derivative audit independently rebuilds all eight root slope disks and the true-zero anchor.

There is also an independent challenge at an actually executed noninteger zero preparation, rather than only at the h=0 anchor. For the $h = 0.001$ root source, an Acb reconstruction of the finite projection checks physical rows 1, 8 and 40 using its own DFT, Bessel and determinant contraction. Separately, an original-Haar eigenvalue-circle calculation checks the first physical source sample with 4096 eigenangle nodes, 256 direction nodes, and explicit strip errors. Its discrepancy from the native physical centre is less than 8.183×10^{-30}, while the complete comparison allowance is below 2.812×10^{-22}. The actual directed gap-versus-allowance comparison passes. The independent circle's own analytic error is below 8.731×10^{-82}. These checks use neither the native witness nor the fixed-point determinant arithmetic. They are independent sample checks with their own priced errors, not a second complete scalar zero proof.

The failure information is mathematically useful and is preserved:

- A pointwise supremum of the transformed preparation is too large for useful h continuation; original-Haar rotation and a correlated Schur mass replace it without changing the source.
- A crude radius majorant is valid but ineffective. Anchored inverse transport and the exact second mark moment reduce the local first-radius bound to below 196. This is a bound repair, not evidence of a physical singularity in the old representation.
- The first terminal filter is insufficient for accurate small-order coefficients. Appending physical rows and repricing a stronger finite filter repairs the terminal component. Raising readout precision alone would not do so.
- The $a = 2$ halo does not justify $M = 6$. The actual proof uses the independently audited $a = 11/4$ receipt.
- A nonzero derivative modulus alone does not justify the modulus factor. The fixed complex derivative cone is retained before integrating along the tilt segment.
- A Newton sequence, a scalar disk containing zero, or matching printed values does not certify a root. The uniform zero theorem and a complete physical residual do.
- The sparse prefix improvement can be negligible at deep inverse order. Both that adverse resource result and the stride-two adversarial control remain part of the verification package.

Inherited adversarial controls remain dependencies of the broader programme: incorrect saddle aggregation, omitted Vandermonde zeros, complex-tilt conjugation, native-to-physical normalization errors, interval phase wrapping, frozen-grid false convergence, missing balanced terminals, inadequate source precision, unsupported exact headers, near-integer gamma–zeta cancellation, unreviewed caches, and zero-containing relative disks. This construction does not relabel every inherited control as a newly executed test. Its new checks address the continuation, derivative, source-lineage, sparse-alias, and modulus-return operations actually introduced here.

The new public layer has a distinct admission record for source origins, code, proof files, independent audit verdicts and exact receipts. Rehashing data alone grants no authority. Candidate files are preserved unchanged even when a separate final record admits their completed composition. The final coverage ledger must state which layer has been earned.

Executed results and complete error budgets (T7)

Connected outward inequalities

The 512-bit producer and an independent 768-bit Newton-polynomial audit prove the same simple rational contracts. The following decimals are rounded outward from the producer receipts.

Quantity	Physical real region	Auxiliary complex tube
Rouché slack	$> 1.959893 \times 10^{-6}$	$> 5.192040 \times 10^{-7}$
Factor lower bound	$> 2.653973 \times 10^{-3}$	$> 2.129473 \times 10^{-3}$
$\lvert F_z \rvert$	$< 1.275507 \times 10^{0}$	—
$\lvert \alpha_z \rvert$	$< 2.858754 \times 10^{2}$	—

The physical grid contains thirteen exact radius nodes. Thirty-six new physical preparations supply 2304 new h-circle readouts; three inherited anchor jets are reused. Each jet retains degree 60. The complete interval inequalities include every radius between the nodes and every complex order in the stated disk.

Eight new executed noninteger zero fibers

The table gives actual portable root disks: rounding each printed centre has been added to its disk radius. The full rational candidates and unrounded enclosures remain in the release JSON files. Every row is a unique simple zero of the original physical moment by the connected theorem and its independently admitted residual.

h	z	$\operatorname{Re} a$	$\operatorname{Im} a$	Disk radius less than
$0.002 + 0.003i$	0.8999	0.55695503347640616173	2.80099945913778864224	1.203×10^{-18}
0.008	0.89995	0.55802644361686478508	2.79897605992190127569	2.559×10^{-18}
-0.008	0.89995	0.55324551305158778006	2.80061335690264496590	2.719×10^{-18}
$0.008i$	0.89995	0.55654590438147357257	2.80216935535972145289	2.645×10^{-18}
$-0.008i$	0.89995	0.55490972739119057605	2.79739313295508264962	6.229×10^{-18}
$0.008 + 0.005i$	0.8999	0.55891212677623809414	2.80094005893410851641	3.013×10^{-18}
$-0.008 - 0.005i$	0.8999	0.55311267049219684036	2.79958890041651371794	1.603×10^{-17}
$0.004 - 0.002i$	0.899915	0.55692129081055156352	2.79916505572496116140	1.480×10^{-18}

The last radius, 179983/200000 = .899915, is not one of the interpolation nodes. The fresh public v2 run reused one exact admitted scalar and generated three further physical sources. Its four validated root radii were respectively below 7.969×10^{-8}, 5.621×10^{-12}, 3.986×10^{-16} and 1.475×10^{-18}. It met the requested 10^{-16} root-radius target. The previous fixed-reference proposal used four new sources but reached only 5.990×10^{-14}; that valid but goal-limited execution is preserved. All eight inherited primary noninteger root disks and the inherited $h = 0$ anchor were replayed under their unchanged authority. The branch identity on the full old overlap follows from uniqueness for the same physical moment, not proximity of numerical candidates.

Derivatives at the actual mixed-order zero

At $h = .002 + .003i$ and $z = .8999$, the following disks enclose derivatives at the true zero, including candidate-to-zero displacement. Printed-centre rounding is again included.

Quantity	Real centre	Imaginary centre	Radius less than
F_h	0.00172143752467	0.00008698698642	4.464×10^{-12}
F_s	−0.00507332481323	−0.00212052862380	2.625×10^{-13}
F_z	−0.01476309467983	−0.06924220785007	2.793×10^{-8}
α_h	0.29494928250431	−0.10613580433375	8.260×10^{-10}
α_z	−7.33342501582255	−10.58309336975877	5.079×10^{-6}

The short rational secant has candidate F_z error below 2.786×10^{-8}: the endpoint analytic return contributes less than 9.915×10^{-9} and the physical-scalar errors divided by the exact step contribute less than 1.795×10^{-8}. The separately priced 10^{-9} step has error below 1.648×10^{-5}. Their disks overlap; the smaller error is earned by the complete shorter-step budget, not that agreement. The actual-root derivative cone gives $\lvert G_{\mathrm{loc}} \rvert > 0.005168660409775 > 1/200$ for $\lvert s - \alpha \rvert \le 10^{-5}$ on this fiber. The uniform whole-neighborhood factor remains 1/380.

An executed near-zero resource repair

Keep the exact same physical input $h = .002 + .003i$, $z = .8999$, and $s = a + 10^{-9}$, where a is the full rational mixed-root candidate. The original image degree $J = 72$ misses the relative target. Increasing only the image degree to $J = 80$ gives:

Error component	$J = 72$	$J = 80$
Finite source arithmetic	$< 4.26777 \times 10^{-22}$	$< 4.26777 \times 10^{-22}$
Preparation and direction	$< 9.66409 \times 10^{-26}$	$< 9.66409 \times 10^{-26}$
Mellin image	$< 2.66687 \times 10^{-21}$	$< 3.78365 \times 10^{-23}$
Filtered terminal	$< 1.24887 \times 10^{-27}$	$< 1.24887 \times 10^{-27}$
Final readout and export	$< 4.55441 \times 10^{-59}$	$< 4.55441 \times 10^{-59}$
Complete absolute disk radius	$< 3.093740 \times 10^{-21}$	$< 4.647104 \times 10^{-22}$
Certified relative bound	$< 5.626352 \times 10^{-10}$	$< 8.451339 \times 10^{-11}$

The physical rows, angular/frame data, and terminal filter are byte-identical in this repair. The finite-source precision, cutoff, and asymptotic resources are unchanged. The 1/200 local geometry supplies a lower modulus close to 5×10^{-12} and a sufficient absolute target close to 5×10^{-22}. The refined complete error is below that target; the actual scalar modulus test gives relative error below 8.452×10^{-11}. At a 10^{-8} offset, the original image already certifies relative error below 5.627×10^{-11}.

Receipt scope and independent challenges

The final source snapshot admits 89 source-origin records and 2436 physical scalar receipts (2405 relative and 31 absolute classifications at their recorded targets). These counts include warm h readouts, derivative endpoints and trial residuals; they are not counts of distinct root fibers. The release supplies zero-free annuli on every new fiber, exact-fiber resource decisions, and a valid absolute image of each uncertain root-location disk. A disk containing the actual zero never receives a positive relative denominator. Separate Acb finite-source and original-Haar source checks challenge the physical samples; they are distinct from agreement of two tail formulas. The complete moment budget remains physical throughout. Estimates used only as proposals, interrupted source folders, the outside-domain .899 noninteger candidate, and the earlier failed iteration target retain their original classifications. No candidate receipt is overwritten or promoted by its filename.

Implementation, admission, and adversarial checks (T8)

The new workspace is separate from every inherited source tree. The native physical engine, image theorem, terminal filter, and prior certification ledgers remain sealed. The radius adapter relocates outputs and uses the reviewed 3447-row filter, repriced at each actual h. It validates exact reduced rational frequencies, the physical preparation, frame, image, source origin, and before/after engine hashes.

The public `radius_evaluator_v3.py` admits existing receipts only through the distinct source-review manifest. A newly admitted source must be generated by the reviewed implementation. A fresh process may also reuse an already admitted exact sample, which is reported as reuse. Arbitrarily copied or self-rehashed caches do not acquire authority. Scalar certificates are canonically reconstructed from their physical budget; root and modulus certificates are reconstructed from their admitted scalar and exact fiber. No supplied status flag substitutes for that reconstruction. The first public version admitted an optional review dictionary without canonically reloading its authority; version two repairs that bypass by reloading and validating the current reviewed manifest at each admission boundary. The earlier interface and the rejection controls are preserved as separate evidence.

A fresh public continuation with a fixed reference slope remained valid but converged slowly: after four physical steps its root disk had radius about 5.99×10^{-14}, above the requested 10^{-16}. Version two uses an interpolated slope only to propose the next exact tilt. Every accepted root disk still requires its fresh or admitted physical scalar enclosure and the proved factor floor. A faster proposal is not itself a stronger certificate; fresh execution outcomes are reported only from their saved receipts. At the new exact off-grid input $h = .004 - .002i$, $z = .899915$, a fresh version-two run used one reusable exact scalar and three newly generated source preparations. Four iterations reduced the certified root radius to less than 1.47444×10^{-18}, meeting the requested 10^{-16} target. This success belongs to that executed input, not to a uniform iteration-count guarantee.

Fresh-process CLI reproduction then exposed a distinct precision-dependent false refusal in version two: the admitted image-refined scalar was rejected at the caller's default 53-bit context, and also at 128 or 256 bits, because a recomputed interval upper bound became needlessly wider than its valid saved bound. Version three sets the reviewed admission precision to 768 bits immediately before constructing and executing `Admission.scalar`. It subsequently recomposes the scalar at the same explicit 512-bit readout precision. This repairs the admission

boundary without changing physical samples, enlarging error budgets, relaxing inequalities, or claiming higher source precision. The earlier valid certificates and the refusal control retain their original review hashes. A fresh-process version-three model and locate replay met the same root goal using four exact admitted scalar readouts and no additional source generation; this is explicitly recorded as reuse of the physical evidence produced earlier. Independent fresh-process scalar and root calls passed, and caller contexts of 53, 128, 256, 512, and 1024 bits produced identical admitted outputs. The absolute-only and relative-refinement controls also passed.

Independent source checks reconstruct finite projections with Acb Fourier/Bessel/determinant arithmetic and separately use the original Haar circle source with explicit strip bounds. The interpolation audit uses a Newton representation rather than the producer's monomial contraction. Endpoint and final-root derivative audits independently reconstruct the mathematical bounds. Shared dependencies are declared: the two interpolation implementations use the same admitted physical jets, and the two endpoint slopes share the base physical source and endpoint theorem.

The inherited failure controls remain preserved. New checks reject omitted state-dependent Jacobian terms, false critical-value inversion, unearned tilt majorants, wrong physical fibers, altered root disks, copied unreviewed receipts, unsupported rational headers, and relative claims at a zero. An image replay initially rejected a dictionary equality solely because measured runtime differed; the repair compares every mathematical field while treating elapsed seconds as metadata. That event is retained separately from a mathematical or arithmetic failure.

Executed connected theorem and numerical evidence (M9)

Theorem M9.1 (Admitted moving-centre atlas)**.** *For every complex $|h| \le 1/100$ and every real $z \in [899/1000, 9/10]$, the eleven charts defined above give one connected simple-zero branch $\alpha(h,z)$. Each chart contains exactly one zero. The branch is holomorphic in h and real analytic in z, agrees with the inherited branch on its whole overlap, and at $h = 0, z = .899$ equals the independently certified original-Haar point zero.*

For every admitted chart and every tilt in its disk, $F(h,s,z) = (s - \alpha(h,z))G_j(h,s,z)$ with $|G_j| > \frac{1}{209}$.

Proof. The complete executed inequalities below give a minimum Rouché slack greater than 7.046036×10^{-6} and a common derivative-cone floor greater than 4.803514×10^{-3}. The independently reconstructed parameter model includes the original-source, finite arithmetic, h-tail, radius-contour, tilt-interpolation and differentiated remainder budgets. All ten adjacent radius overlaps have width $1/20000$. Their strict zero-containment witnesses have slack at least 1.932969×10^{-5}. The common-cone and gluing propositions therefore apply on the whole parameter continuum. The separate endpoint inclusion identifies the continued endpoint with the original-Haar point certificate. Independent physical-source, h-jet, geometry, and public-interface admission closes the finite-arithmetic dependencies.

□

All displayed inequality endpoints below are rounded in the conservative direction. Exact rational endpoints and full disk centres are retained in the JSON receipts.

Chart	Physical radius interval	Rouché slack $>$	Factor floor $>$	$\lvert\alpha_z\rvert <$
0	$[0.899000, 0.899075]$	7.046036×10^{-6}	4.803514×10^{-3}	1.570800×10^{1}
1	$[0.899025, 0.899175]$	7.212946×10^{-6}	4.837934×10^{-3}	1.544888×10^{1}
2	$[0.899125, 0.899275]$	7.381051×10^{-6}	4.872004×10^{-3}	1.524054×10^{1}
3	$[0.899225, 0.899375]$	7.548048×10^{-6}	4.905767×10^{-3}	1.507401×10^{1}
4	$[0.899325, 0.899475]$	7.714325×10^{-6}	4.939313×10^{-3}	1.493596×10^{1}
5	$[0.899425, 0.899575]$	7.880279×10^{-6}	4.972754×10^{-3}	1.481493×10^{1}
6	$[0.899525, 0.899675]$	8.044146×10^{-6}	5.005372×10^{-3}	1.476306×10^{1}
7	$[0.899625, 0.899775]$	8.207666×10^{-6}	5.037881×10^{-3}	1.472597×10^{1}
8	$[0.899725, 0.899875]$	8.370403×10^{-6}	5.070162×10^{-3}	1.471544×10^{1}
9	$[0.899825, 0.899975]$	8.531846×10^{-6}	5.102105×10^{-3}	1.474260×10^{1}
10	$[0.899925, 0.900000]$	8.708027×10^{-6}	5.133842×10^{-3}	1.482021×10^{1}

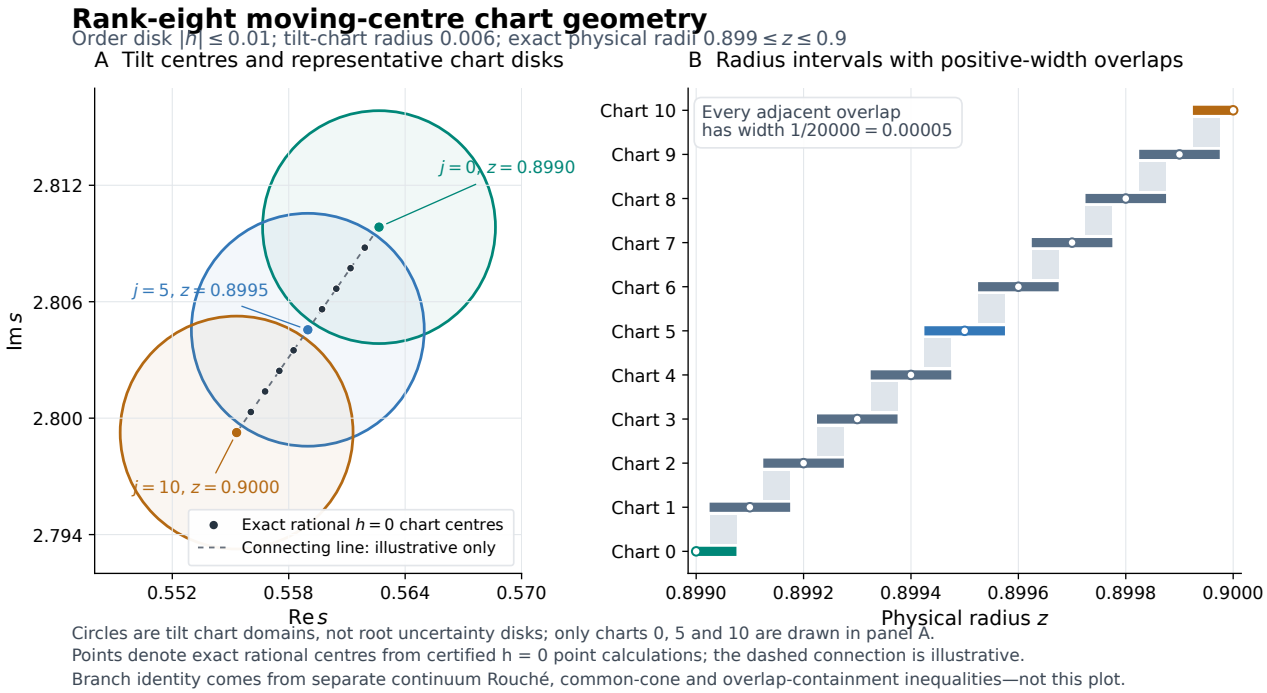

Figure 1: Exact chart geometry. The circles are chart domains, not root uncertainty disks. The dashed line through point centres is illustrative; the branch identity is proved by the complete continuum inequalities and strict containment witnesses.

Complete parameter-model error budget

The following maxima range over every complete chart panel and the full order and tilt disks. They are different from the much tighter physical scalar errors in the point certificates.

Component	Executed maximum $<$
Radius interpolation value	5.000001×10^{-9}
Radius interpolation derivative	7.500001×10^{-4}
Order tail after radius interpolation	1.342686×10^{-12}
Tilt value remainder	1.600143×10^{-8}
Radius derivative of tilt interpolation remainder	2.365530×10^{-3}
Independent finite value arithmetic	3.845990×10^{-12}
Independent finite tilt-derivative arithmetic	9.945610×10^{-10}
Independent finite radius-derivative arithmetic	3.801197×10^{-6}
Independent finite order-derivative arithmetic	1.864250×10^{-9}
Complete returned value uncertainty	2.100594×10^{-8}
Complete returned tilt-derivative uncertainty	5.419998×10^{-6}
Complete returned radius-derivative uncertainty	3.120729×10^{-3}
Complete returned order-derivative uncertainty	6.208525×10^{-6}

Executed physical zero disks

The following decimal-centred disks include the rounding of the printed centres. A rational midpoint is a representation of the enclosure, not an assertion that the midpoint itself is an exact zero.

(h, z)	Decimal centre of the zero disk	Radius $<$
$(0.003 + 0.004i, 0.899275)$	0.56193717674089319335 $+2.80779312901512520395\,i$	3.333505×10^{-17}
$(0.002 + 0.003i, 0.89975)$	0.55805503657470717477 $+2.80258662714117100669\,i$	9.794816×10^{-19}
$(0.004 - 0.002i, 0.899025)$	0.56343687841212059078 $+2.80858982959023791052\,i$	7.641445×10^{-19}
$(0.008 + 0.005i, 0.8995)$	0.56183644824365806210 $+2.80516591442949138353\,i$	1.623098×10^{-18}
$(0 - 0.008i, 0.899)$	0.56187416445245310794 $+2.80747771038568543258\,i$	1.379195×10^{-18}
$(0 + 0.008i, 0.899)$	0.56352472744971943476 $+2.81219555057223031085\,i$	1.387034×10^{-18}
$(-0.008 + 0i, 0.899)$	0.56024528241791917242 $+2.81067781671730014269\,i$	1.424775×10^{-18}
$(-0.008 - 0.005i, 0.89935)$	0.55716205103303279478 $+2.80542771635825898639\,i$	1.706992×10^{-18}
$(-0.01 + 0i, 0.899)$	0.55962796076867170196 $+2.81088881858668430086\,i$	1.789402×10^{-18}
$(0.008 + 0i, 0.899)$	0.56496787561704521346 $+2.80902601901065490519\,i$	1.340177×10^{-18}
$(0.002 + 0.003i, 0.899)$	0.56355475874738265341 $+2.81051365570181491010\,i$	6.185977×10^{-19}

Actual-zero branch derivatives

These derivative disks include the candidate-to-true-zero return. Their uniform availability over the atlas is the new feature; the inherited specialized physical secant method can remain more accurate at its particular fiber. For the first two pairs of rows, $z = .899$. For $h = .008 + .005i$, $z = .8995$; for $h = .002 + .003i$, $z = .89975$.

Fiber and quantity	Decimal centre	Radius $<$
$h = 0.008 + 0i$, α_h	$0.28383675 - 0.10140015i$	1.271633×10^{-4}
$h = 0.008 + 0i$, α_z	$-7.30620333 - 10.56653271i$	1.744544×10^{-1}
$h = -0.01 + 0i$, α_h	$0.31024959 - 0.10577534i$	1.863857×10^{-4}
$h = -0.01 + 0i$, α_z	$-7.37537521 - 10.58463835i$	1.971202×10^{-1}
$h = 0.008 + 0.005i$, α_h	$0.28468269 - 0.10767756i$	1.271833×10^{-5}
$h = 0.008 + 0.005i$, α_z	$-7.31058567 - 10.55934145i$	1.400042×10^{-1}
$h = 0.002 + 0.003i$, α_h	$0.29435754 - 0.10627456i$	1.168000×10^{-4}
$h = 0.002 + 0.003i$, α_z	$-7.33328315 - 10.57914919i$	1.428286×10^{-1}

Near-zero relative failures and image-only repairs

Each row compares the same exact physical input before and after changing only the Mellin-image degree from 72 to 80. The native source rows, angular preparation and terminal resources are unchanged. The failed estimates remain preserved; they are valid absolute enclosures but do not meet the requested relative target.

Fiber	Image degree	Absolute error $<$	Relative error $<$	Target met
$h = 0.008 + 0.005i$	72	7.751187×10^{-21}	1.401164×10^{-10}	no
$h = 0.008 + 0.005i$	80	1.179611×10^{-21}	2.132354×10^{-11}	yes
$h = 0.008 + 0i$	72	6.392846×10^{-21}	1.155428×10^{-10}	no
$h = 0.008 + 0i$	80	1.008688×10^{-21}	1.823077×10^{-11}	yes

The stronger local common cone earns the factor $1/200$ only on the actual certified fibers where its inequality passes. At real tilt offset 10^{-8} it yields a positive lower modulus close to 5×10^{-11}, with the exact root uncertainty

subtracted. Queries closer to the zero retain their actual failed-target or absolute classification; no modulus is inferred from printed zero digits.

Evidence counts and interpretation

The active physical admission contains 268 source-origin records and 9956 scalar receipts. Of these, 9913 meet their recorded relative target and 43 retain absolute classification. They include order-circle samples, trial residuals, integer controls, and derivative calculations. They are not that many distinct zeros, nor a grid proof of the continuum theorem.

The selected release contains 11 zero fibers: 9 new physical candidate sequences, the separately admitted inherited endpoint residual, and 1 fresh public continuation. Inherited-branch regression is recorded separately with exact inputs and provenance. The fresh public calculation generated two full physical sources at an off-grid radius and met its requested root-radius goal; the shifted-tilt modulus request is a geometric resource target, not a claimed additional scalar execution.

Independent checks and limits of independence (M11)

The geometry producer uses exact cardinal polynomials with interval coefficient contractions. The independent geometry reader reconstructs the radius polynomial in a Chebyshev basis and bounds it on trigonometric panels. The h-jet audit reconstructs the discrete Fourier contractions from every admitted physical node and separately reassembles the $h = 0$ Toeplitz constant. The logarithmic higher-tilt majorants and expanded-ellipse bounds have independent 1024-bit evaluations.

Original-Haar challenges at selected preparations do not merely replay the transformed prefix. They compare independent original-angular and finite Acb source calculations with the native source contract. The endpoint point zero is independently linked through strict containment in its original Haar uniqueness disk. These checks share Arb special functions and inherited analytic identities where stated; they are not independent proofs of the entire foundational HaarCritical programme.

Successful numerical agreement is never the remainder estimate. In particular, the atlas continuum follows from interval-wide inequalities and analytic remainders, not interpolation of root values. The same-source agreement of two terminal calculations does not independently verify their common prefix.

Executed connected theorem and physical results (J7)

All displayed numerical centres and table bounds are rounded for readability. The full exact input strings and outward rational enclosures in the named receipts are authoritative. No shortened display value is substituted into a proof.

Continuum inequalities and joins

The producing 768-bit calculation uses 64 radius cells with positive-width overlaps. Its independently implemented 1024-bit counterpart uses a Chebyshev/cosine representation and direct cardinal composition. Both bound every complex order in the entire disk, rather than a grid of orders.

Quantity	Producing calculation	Independent calculation
Rouché slack	2.153306×10^{-5}	2.153358×10^{-5}
Common derivative-cone floor	3.439274×10^{-3}	3.439437×10^{-3}
Residual zero radius	4.638981×10^{-5}	4.645843×10^{-5}
$\lvert\beta_h\rvert$	3.163494×10^{-3}	3.181503×10^{-3}
$\lvert\beta_z\rvert$	1.216736×10^{0}	8.953984×10^{-1}
$\lvert\alpha_h\rvert$	5.877499×10^{-1}	5.877679×10^{-1}
$\lvert\alpha_z\rvert$	1.472833×10^{1}	1.440699×10^{1}

The portable theorem uses $|G| > 1/291$, $|\alpha - c| < 4.647 \times 10^{-5}$, $|\alpha_h| < .588$, and $|\alpha_z| < 15$. There are 63 positive-width joins. At every shared fiber, adjacent cells use exactly the same rational predictor and uniqueness disk. The inherited anchor disk is contained with slack greater than .0059967; the open/closed simple-branch

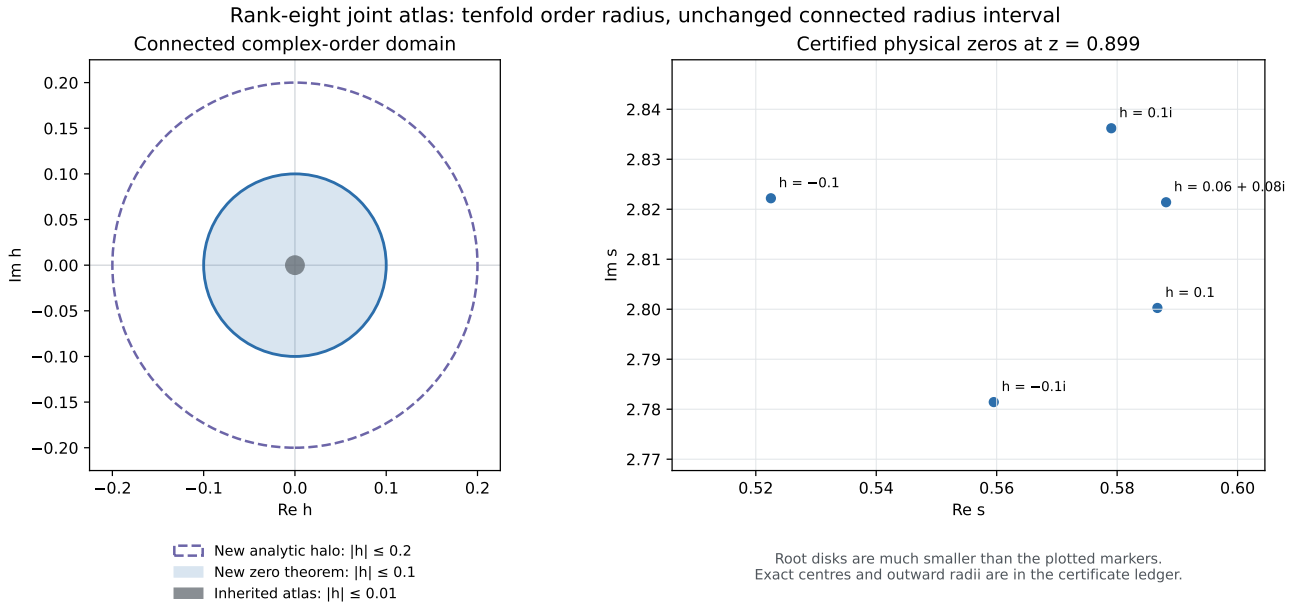

Figure 2: The earned order disk and selected physical zero fibers. The same theorem holds at every real radius in $[.899, .9]$; the plotted points do not supply the continuum proof.

argument identifies the entire old atlas. The complete moving tube has $|s| < 2.915$, leaving more than .085 to the original tilt boundary.

Physical preparation and arithmetic

The exact grid has 41 radius nodes and nine tilt nodes. It uses 123 canonically admitted predecessor preparations and 246 fresh preparations, followed by 96 new physical order readouts per preparation: 35,424 readouts in total. The h-independent preparation is reused only with its original physical input, frame, image and complete source contract. Each changed order receives a freshly repriced readout.

The acquisition took 2857.62 seconds with four source processes; the corrected immutable plan validation took 2.33 seconds. Native rows retain their original 104-bit fixed-point contract and 192-bit contraction contract. Final proof/readout arithmetic uses 768 bits, and the independent coefficient and continuum checks use 1024 bits. Increasing the final ball precision is never represented as regenerating a native source.

All 369 order polynomials, including 22,509 coefficients, were independently reconstructed. The largest complete h-polynomial allowances were 1.385797×10^{-14} in value, 4.913755×10^{-12} in the first derivative, and 2.273574×10^{-9} in the second derivative. The final source admission contains 399 origins and 35,471 physical scalar receipts, including the fresh public executions. Source, coefficient, continuum and public-interface gates remain distinct.

Executed physical zero returns

Nine prescribed physical fibers required 18 fresh full preparations. At each fiber the initial nominal polynomial zero was excluded by the actual physical scalar disk; a further physical correction reached the admitted source/image floor. One additional public input was then executed from the reviewed interface, using two more fresh preparations. The h=0 anchor uses the distinct original-Haar Toeplitz route.

Exact order h	Radius z (display)	Radius of the stored-centre zero disk
$0.06 + 0.08i$	0.899	1.986114×10^{-17}
$-0.1i$	0.899	2.480197×10^{-17}
$0.1i$	0.899	2.616131×10^{-17}
-0.1	0.899	3.320737×10^{-17}
0.1	0.899	1.567573×10^{-17}
$0.08 + 0.06i$	0.899146446875	1.794968×10^{-17}
$0.06 - 0.08i$	0.8995	1.965116×10^{-17}
0.05	0.899853553125	1.027423×10^{-17}
$-0.05 - 0.05i$	0.9	2.134181×10^{-17}
$0.04 + 0.03i$	0.8995	1.064075×10^{-17}
0	0.9	$4.141968 \times 10^{-102}$

Each radius applies to the full exact rational centre in its JSON certificate. The table does not replace those centres by shortened printed decimals. All these roots belong to the same connected physical branch.

Actual boundary derivatives

The physical stencil calculation at $h = -.1, z = .899$ gives

$$\alpha_h \approx .558204310793596963 - .155407044680054817i,$$
$$\alpha_z \approx -7.600345409961137351 - 10.919479309907619470i.$$

The respective rigorous disk radii are below 2.272424×10^{-9} and 1.056508×10^{-7}. The returned tilt derivative satisfies $|F_s| > .00420437438$. The final connected factor and root disk resolve the original conditional true-zero premise; none of the candidate receipts is edited.

Allowance	F_s	F_h	F_z
Weighted physical disks	1.537427×10^{-11}	1.711695×10^{-13}	1.711695×10^{-11}
Analytic difference remainder	1.666667×10^{-13}	9.120000×10^{-17}	1.600000×10^{-11}
Return to actual zero	1.081807×10^{-14}	3.716487×10^{-13}	2.041754×10^{-10}
Complete derivative disk radius	1.555176×10^{-11}	5.429094×10^{-13}	2.372924×10^{-10}

The complete records also include the smaller contraction and serialization terms. The original physical derivative radius in α_z was 3.233466×10^{-6}; the first-tilt/thin-radius return improved it by about a factor of thirty without another native preparation. It also proves $|\alpha_h| > .5794336886$, so the old .376 upper bound is false on the enlarged order disk.

A successful relative repair and a precise remaining obstruction

For the difficult fiber $h = -.1, z = .899$, let a denote the exact returned zero-disk midpoint. Four actual scalar readouts compare the same physical moments before and after image refinement.

Tilt	Image degree	Absolute allowance	Relative allowance	Classification
$a + 10^{-7}$	72	1.141131×10^{-19}	2.714150×10^{-10}	Absolute
$a + 10^{-7}$	80	2.514511×10^{-20}	5.980701×10^{-11}	Relative
$a + 10^{-8}$	72	1.141130×10^{-19}	2.714150×10^{-9}	Absolute
$a + 10^{-8}$	80	2.514510×10^{-20}	5.980698×10^{-10}	Absolute

The image-only repair preserves every physical row and the source, direction and terminal returns. At displacement 10^{-7} it meets the original 10^{-10} target. At displacement 10^{-8} it still gives an informative absolute disk but does not meet that relative target. The budget records the source-regeneration obligation precisely.

Independent and adversarial challenges

The inherited eleven-chart theorem and selected public root/derivative/modulus certificates were replayed. Three new preparations received independent Acb finite-projection checks at indices 1, 8 and 40, together with original-Haar source checks. The h=0 constants and original zero anchor were checked through the separate Toeplitz representation. These checks have different source dependencies from the main transformed finite-source calculation.

The complete geometry checks share the physical input samples and analytic halo contracts; they independently implement the algebra, interval norms and continuum inequalities. The physical derivative stencils share the inherited source kernel, while their error budgets and analytic remainders are independently reconstructed. This disclosed dependence prevents their agreement from being treated as independent proof of a shared source engine.

Executed adversaries include omitted chain-rule terms, incorrect moving-coordinate algebra, treating a predictor as a zero, out-of-domain orders and radii, a square substituted for a complex disk, unsupported exact frequency headers, altered review factors, copied/self-rehashed receipts, wrong root fibers, insufficient source precision, and relative claims for zero-containing disks. All nine initial nominal zero proposals were explicitly refuted by their physical residuals. Near-integer controls and the separate order-direction modulus theorem challenge removable gamma–zeta cancellation.

Preserved failures and repairs

Extrapolating the old radius-.01 order circle to $|h| = .1$ was rejected: full-degree sample-noise amplification reached about 5.8×10^{27} to 9.25×10^{27}. Even a lower-degree balance could not price the required small residual. New samples on the actual radius-.1 circle, together with the enlarged original-source halo, repaired that mathematical conditioning failure.

The additive degree-six predictor passed a fixed-radius test but gave a residual zero radius about thirteen times larger than the selected mixed degree-eight/degree-three predictor. Its successful but weaker receipt is retained. No failed predictor was silently relabelled as a full theorem.

The old plan display field h_degree=44 was corrected through a new immutable v2 descriptor and an exact task-identity bridge; all actual new computations already used degree 60. An independent checker API mismatch was repaired in a new version, preserving the failed version. The final h-jet checker also resolves historical absolute provenance through a confined relative path, preserving receipt bytes for recovery under a different workspace. These implementation repairs change no physical input or mathematical allowance.

Reproducing and repairing the inherited obstruction (N3)

Exact input and the failed target

Let $a_{-0.1,.899}$ denote the full rational midpoint stored in the released zero certificate. It is a midpoint of a certified disk, not an asserted exact zero. The primary input is

$$N = 8, \qquad h = -1/10, \qquad z = 899/1000, \qquad s = a_{-0.1,.899} + 10^{-8}.$$

The producer reads those rational coordinates from the certificate; no printed decimal approximation is resubstituted. The inherited degree-80 image calculation is a valid absolute disk with allowance approximately $2.514509593340728 \cdot 10^{-20}$ and relative allowance $5.980698379110736 \cdot 10^{-10}$. It fails the requested relative target.

An independent 1024-bit reconstruction reproduces the complete budget and the necessary-row estimates: at least 1,320 optimally selected rows must change under ideal replacement and perfect other components; retaining the image-80 allowance raises that necessary count to 1,535. These are constraints on the specified additive certificate. They are not lower bounds on unknown true floating-point error, and they do not rule out a different mathematically justified representation or error proof.

Actual 192-bit reconstruction

The proposed first 1,909 rows were genuinely regenerated at 192-bit native precision with a 320-bit input witness. The untouched suffix remains at 104 bits. The original image-80 construction is reused with the exact same

preparation. Source generation took approximately 278.27 seconds in this environment; this timing is a resource observation, not a complexity bound. The complete readout was then re-executed and independently audited.

The new midpoint is approximately

$$c = -3.9727542289306877 \cdot 10^{-11} - 1.3762227441357429 \cdot 10^{-11} i.$$

Its full rational coordinates are retained in the receipt. The exact serialized component sum is slightly below the upward-rounded allowance in the following table.

Component	Upward rounded allowance
Fine 192-bit prefix arithmetic	$1.486804007 \cdot 10^{-46}$
Coarse 104-bit suffix arithmetic	$1.399459513 \cdot 10^{-21}$
Preparation and direction approximation	$6.673940731 \cdot 10^{-25}$
Degree-80 Mellin image	$1.298682501 \cdot 10^{-21}$
Filtered analytic terminal	$9.715940311 \cdot 10^{-26}$
Final ball contraction and serialization	$4.233402921 \cdot 10^{-111}$
Complete disk allowance	$2.698906567 \cdot 10^{-21}$
Relative allowance	$6.419281979 \cdot 10^{-11}$

The rational lower modulus exceeds $4.2043745316 \cdot 10^{-11}$. Thus the complete executed disk, after outward serialization, satisfies the requested strict 10^{-10} relative inequality. Further increasing the fine prefix precision would have almost no effect on this particular budget: the coarse suffix and image now dominate.

A harder query and a successful keep-source case

At $s = a_{-0.1,.899} + 10^{-9}$, a fresh physical preparation was generated at the exact changed tilt. Reusing the old tilt's source would be invalid. The executed selector chose 2,664 rows for 128-bit regeneration; the suffix remains 104-bit. The actual degree-88 image has allowance approximately $1.892931641 \cdot 10^{-23}$. The complete disk has allowance below $1.584404827 \cdot 10^{-22}$ and relative allowance below $3.768467485 \cdot 10^{-11}$. Its midpoint is approximately

$$-3.9727541565888393 \cdot 10^{-12} - 1.3762225896464028 \cdot 10^{-12} i.$$

With the same fine source, the exact degree-80 prefix image yields a relative allowance of $3.420707829 \cdot 10^{-10}$ and misses the target. The fresh 104-bit source with degree-88 image gives $5.676311901 \cdot 10^{-9}$ and also fails. Both are retained as valid absolute results. The successful repair therefore exercises the source and image parts of the budget jointly, rather than hiding one error with an unrelated precision increase.

At $h = .04 + .03i$, $z = .8995$, and the corresponding released zero midpoint plus 10^{-8}, a fresh native 104-bit source with image-80 already gives relative allowance below $8.893728720 \cdot 10^{-11}$. No HP2 regeneration is warranted by that budget. Reusing the admitted primary preparation at different orders also produces new complete readouts, including $h = 3 + 3i$, $h = -.95 + 3i$, positive, imaginary, and mixed orders. Each such order has newly priced weights, image, and terminal. A deliberately cancelling order yields a zero-containing disk and is correctly classified as absolute-only; that disk is not a proof of a zero at the chosen input.

Executable interface and reproducible evidence (N8)

The new public arithmetic interface is `near_zero_evaluator_v4.py`. It accepts exact rational or decimal strings, verifies the canonical predecessor and new source admission, reconstructs the scalar independently, and returns a complex disk with the complete budget. Saved integer receipts require the admitted coefficient path. Fresh-order execution uses an admitted mixed source with the same physical N, z, s; unsupported fresh integer execution is explicitly refused rather than passed through a singular formula.

The principal commands, run from the recovered common project root, are:

```
python near_zero_reconstruction_investigation/near_zero_evaluator_v4.py \
  --output NEW.json scalar EXACT_ADMITTED_RAW_RECEIPT.json
```

```
python near_zero_reconstruction_investigation/near_zero_evaluator_v4.py \
  --output NEW.json evaluate EXACT_ADMITTED_ORIGIN.json \
  --h -0.099999999 0.000000002 --raw-output NEW_RAW.json

python near_zero_reconstruction_investigation/near_zero_evaluator_v4.py \
  --output NEW_PLAN.json plan EXACT_ADMITTED_RAW_RECEIPT.json \
  --max-rows 1000
```

Output files must be new. The source-generation scripts preserve their start records and all original metadata. A newly executed readout is independently checked before return; its exact raw hash must be admitted in a reviewed child record before later saved-receipt replay. A plan is not relabelled as a certificate. The complete source-repair and atlas commands, actual final review paths, and expected classifications are in the restart record and package README.

The final arithmetic gate binds 35 complete scalar receipts from 17 physical-source origins: 19 relative certificates and 16 absolute results. The earlier 22-receipt batch (18 relative and four absolute) remains unchanged as an explicitly identified component. These counts include preserved failure and cancellation iterations and are not counts of distinct mathematical fibers. The final ledger separately records 12 certified zero disks on ten distinct new fibers, including two physical Newton refinements of already certified fibers. The refreshed-circle gate records 47,232 further complete scalar executions. The ledger distinguishes source generation, order readout, root certification, and connected geometry so that these counts cannot be conflated.

The public geometry interfaces are `wider_atlas_evaluator_v3.py` for the stronger inner theorem and `outer_atlas_evaluator_v2.py` for the larger order disk. They accept `tube`, `root`, `modulus`, and `coverage` commands. For example, a complete outer uniform tube is replayed by

```
python near_zero_reconstruction_investigation/outer_atlas_evaluator_v2.py \
  --output NEW_TUBE.json tube --h -0.17 0 --z 0.899
```

Use exact decimal strings for negative command-line components; the Python APIs also accept exact fraction strings. Binary floating inputs are refused. A `root` command requires an admitted physical scalar receipt, and a `modulus` query remains restricted to the selected theorem's order, radius, and moving tilt tube.

Verification package and clean recovery

The package is an overlay containing the new source engines' adapters, unchanged raw generation evidence, actual complete readouts, exact polynomial predictors, mathematical source, failed attempts, and independent checks. Inherited mathematics and engines are kept by reference and SHA-256 rather than duplicated as project trees. Recovery requires the four pinned predecessor archives: noninteger continuation, wider-radius transport, moving-centre atlas, and joint order–radius atlas. The recovery utility refuses a wrong archive digest, unsafe member path, duplicate overwrite, or changed member manifest.

The final recovery check extracts into a fresh directory and runs with Python isolation. It verifies active authorities, replays decisive physical arithmetic and zero/modulus certificates, and records the paths of all imported project modules. Imports and actual project-file reads from the working investigation outside that recovered tree are rejected. The replay includes six complete scalar readouts, two physical root/tube/modulus groups, and four complete 128-node order circles (512 independently reconstructed readouts). This selected portability matrix is not relabelled as a new execution of all 47,232 nodes. The final recovery receipt is published alongside the package. It is not a substitute for the earlier physical-generation audit, but it closes a different obligation: that the released evidence and code are sufficient to run without hidden working files.

The first actual clean recovery caught a portability defect after all three source/geometry authorities had passed: the reconstruction auditor treated one inherited absolute cache reference as a current path. It correctly refused the foreign directory. The failed archive and receipt are preserved. The versioned repair selects the directory from its already independently admitted relative generating origin and requires equality with the predecessor's interpretation of the historical field. All physical-input, preparation, snapshot, row and scalar checks remain. All 35 complete scalar receipts were independently re-executed under the new auditor, with exactly unchanged admitted values and classifications. The new public interface and child reviews retain the original mathematical

authorities; the change supplies portable source identity, not a new numerical estimate. Final recovery uses the new versioned recovery utility.

The calculations use Python 3.12, python-flint/Arb/Acb, the inherited compiler flags without fast-math or contraction, and the other pinned dependencies described by the package. The exact source and review digests are authoritative. Human-readable tables round only for display; the certificates contain outward exact rational endpoints. Their classification is recomputed after serialization.

Executed continuum inequalities (Q7)

The final outer construction uses $H = 1/5$, residual radius $3/250$, order degree 25, 16 overlapping real-radius panels and 256 complete order boundary arcs per panel. The producing arithmetic uses 768 bits. A separately written 1024-bit audit reconstructs the nonterminal errors of all 47,232 physical scalar nodes, uses an unreduced gamma factor and a different terminal arc cover, independently evaluates the panel majorant and physical returns, and recomputes the complete geometry. The inherited finite tensor and physical source data are shared dependencies and are explicitly identified as such.

Uniform strict quantity	Producing calculation	Independent audit
Rouché slack $>$	$3.1053\,10^{-6}$	$2.8911\,10^{-6}$
Common derivative cone $>$	$7.8839\,10^{-4}$	$7.7813\,10^{-4}$
Linear comparison floor $>$	$1.4107\,10^{-3}$	$1.4107\,10^{-3}$
Complete moving tilt modulus $<$	2.973522	2.973522

The exact saved endpoints, rather than the rounded displays, establish $g = 1/1300$. The independent maximum of the correlated arcwise quotient B_j/a_j is less than 0.009998909456, so the public root radius $1/100$ is valid and strictly inside the uniqueness radius $3/250$. The whole tilt tube remains inside the original $|s| \le 3$ region.

The independent global component maxima are shown below. They may occur on different cells; the strict inequalities above use their correlated cellwise composition, not an incompatible mixture of these maxima.

Physical value-return component	Uniform upper display
Finite-node return after coherent terminal repair	$2.691679\,10^{-6}$
Tilt interpolation return	$5.103611\,10^{-6}$
Common order/radius analytic return	$1.171463\,10^{-8}$
Complete value return, maximized after composition	$7.572758\,10^{-6}$
Complete tilt-derivative return	$4.029779\,10^{-4}$

The stronger inner theorem

The independent inner calculation covers 20 overlapping real-radius panels and 384 complete order arcs using a direct rectangular Acb Horner enclosure, distinct from the producing phase enclosure. It gives slack greater than $6.2580\,10^{-6}$ and cone greater than 0.00167877. The producing 16-panel, 256-arc calculation gives slack greater than $5.4727\,10^{-6}$ and cone greater than 0.00161146. Thus on $|h| \le 0.18$ the factor $1/625$ and root radius 0.004537 are valid in the 0.006 uniqueness tube. This stronger inner result does not require the coherent terminal repair. It remains separately available; the frozen outer public interface uses its conservative uniform factor $1/1300$.

Corollary Q7.1 (Connected outer and inner rank-eight zero branches)**.** *Combining Theorems Q2.1, Q3.2, and Q4.1 with the executed producing and independent 1024-bit continuum inequalities above yields one unique holomorphic simple zero branch $s = \alpha(h,z)$ of $F(h,s,z) = T_8(h,s;z)$ throughout $0.899 \le z \le 0.9$ in the moving predictor tube around $c(h,z)$ of* (Q1.1)*:*

(i) On the outer domain $|h| \le 0.20$, $F(h,s,z)$ has a unique simple zero in $|s - c(h,z)| < 0.012$, lying inside $|s - c(h,z)| \le 0.01$, with factorization $F(h,s,z) = (s - \alpha(h,z))G(h,s,z)$ satisfying $|G| > 1/1300$ and $|s| < 2.973522 < 3$ throughout the tube.

(ii) On the inner domain $|h| \le 0.18$, the same branch satisfies the sharper enclosure $|\alpha(h,z) - c(h,z)| \le 0.004537$ inside the uniqueness tube $|s - c(h,z)| < 0.006$, with $|G| > 1/625$.

Why correlated quotient bounds matter

A deliberately looser aggregation fails even for the successful outer construction. The global minimum linear floor times 0.012 is about $1.69289\,10^{-5}$, while the sum of the separately maximized centre and nonlinear bounds is about $1.72610\,10^{-5}$. That premature separation would fail. If the centre and nonlinear bounds are first added on the same arc, their global maximum is instead about $1.42321\,10^{-5}$ and this coarser correlated comparison also passes. The execution retains the sharper arcwise quotients B_j/a_j for its canonical root envelope. The normalized maximum-modulus argument in Theorem Q4.1 does not assume that maxima at different parameter cells occur together.

Fresh physical challenges and scalar certificates (Q8)

The physical execution matrix includes $h = \pm 0.2$, $h = \pm 0.2i$ and $h = \pm(0.12 + 0.16i)$ at several exact rational radii in the target interval. Each new tilt receives its own genuinely generated preparation, 3447 native source rows, Mellin image and complete scalar readout. The preserved 128-node order-circle data are reused for the continuum construction; they are not relabeled as fresh physical executions.

The six initial polynomial-root proposals were tested against the actual physical moment. Their absolute scalar errors range from approximately $6.67\,10^{-21}$ to $6.80\,10^{-20}$. Most residuals are between $2\,10^{-14}$ and $3\,10^{-12}$. At $h = -0.2, z = 0.899$, however, the polynomial proposal has physical residual about $1.03\,10^{-9}$. It is preserved as evidence that a polynomial root is not a physical zero.

One correction based on the actual physical residual and a nominal derivative generated a new exact rational query. A fresh preparation at that query reduced the physical residual to about $4.1232\,10^{-14}$, with complete absolute error below $5.9071\,10^{-20}$. The derivative was used to choose a query only. The physical residual and the admitted factor prove the resulting root disk; no unpriced Newton theorem is assumed.

Two further preparations give useful relative certificates:

Order and real radius	Exact tilt construction	Relative error upper display
$h = -0.2$, $z = 0.899$	Corrected rational centre $+10^{-6}$	$3.444064\,10^{-11}$
$h = 0.12 + 0.16i$, $z = 0.89925$	Released rational candidate $+10^{-6}$	$2.148789\,10^{-12}$

The additions are in the real tilt direction. Full rational centres are stored in the actual requests and receipts. These are evaluations at nonzero points near certified zeros, not relative claims at the zeros. The first physical value is approximately $-1.70453228\,10^{-9} + 1.90447193\,10^{-10}i$.

Representative physical zero enclosures are given below. These displayed centres are rounded to sixteen decimal places, and the displayed disk radii are enlarged to include that rounding. The canonical records retain the full exact rational centres and smaller exact outward radii.

(h, z)	Displayed zero-disk centre	Disk radius
$(-0.2, 0.899)$	$0.4152287696623658 + 2.8435398763933760i$	$5.36018\,10^{-11}$
$(0.2, 0.9)$	$0.5979819936227767 + 2.7802624999279990i$	$2.73073\,10^{-11}$
$(0.12 + 0.16i, 0.89925)$	$0.6087105455112848 + 2.8238009836427883i$	$6.61328\,10^{-11}$

A final fresh query directly challenges the formerly blocked order $h = -0.18$ at $z = 0.899$. Its physical midpoint is approximately $-1.86480836\,10^{-11} + 7.33556997\,10^{-11}i$, with complete absolute allowance below $5.776469\,10^{-20}$. Its relative allowance is about $7.631857\,10^{-10}$, so it correctly remains absolute-only at the requested tolerance. It nevertheless produces a rigorous physical root disk through the proved factor. No claim that every near-zero scalar already meets the relative target is made.

In total, ten new noninteger preparations and readouts and six associated $h = 0$ checks were executed. The admitted noninteger scalars comprise three relative and seven absolute certificates; the six $h = 0$ controls are relative certificates. Root disks and modulus statements are separate outputs and are not counted as additional source evaluations.

The source admissions separately verify the generating code, exact preparation, source snapshots, all-row scalar contraction, angular allowances, image, terminal and final outward composition. Six exact $h = 0$ checks at the new tilts use the original-Haar hypergeometric Toeplitz representation and agree with the generated image masses within their complete allowances. An additional original-eigenvalue-circle check at source row 1 differs from the native physical source by about $1.0303\,10^{-29}$, inside the $6.8862\,10^{-23}$ allowance. Independent Acb finite projections at rows 1 and 400 also pass. These selected source checks supplement the complete arithmetic contracts; they are not a claim that every row was independently integrated in original coordinates.

Verification, interface and reproducibility (Q9)

The public `correlated_atlas_evaluator.py` provides exact-input coverage, zero-tube, physical-root, modulus and scalar-classification operations. It checks the canonical inherited outer authority and the new independent review before returning a certificate. A root refinement is accepted only from a separately admitted physical scalar with matching rank, order, tilt, radius, origin and complete budget.

The interface refuses binary floating inputs, unsupported parameter domains, unadmitted candidate scalars, changed dependencies, missing continuum panels, a diagnostic probe presented as a theorem, wrong-fiber root reuse, and unsupported relative claims. Exact rationals are preserved; the original native signed-frequency restriction remains a source-engine contract and is not bypassed by rounding a requested physical radius.

The independent tests also challenge omitted direction averaging, conjugated tilt, altered physical normalization, relabeled precision and zeroed arithmetic allowances. Failed configurations and early diagnostic probes are retained with their original status. The successful continuum result is not inferred by interpolating a finite collection of roots.

Resource record

On the available execution host, the final producing model and physical return reconstruction took about 24 seconds, followed by about 194 seconds for all 4096 outer parameter cells. The independent full geometry took about 285 seconds, with a separately executed 369-packet physical-return audit. These timings are observations, not complexity or performance guarantees. Six initial fresh physical preparations and readouts completed in about 131 seconds with parallel workers.

The numerical runtime was Python 3.12.14, python-flint 0.9.0 and NumPy 2.3.5; native sources used g++ 14.2.0 with the inherited arithmetic flags. The trusted computational base is Arb/Acb, their underlying libraries, the sealed native arithmetic contracts and the cited analytic proofs. This package is an executed interval verification record, not a formal proof-assistant development.

Exact restart and limits

The compact verification distribution is an overlay. It preserves the five prerequisite archive hashes and all new code, mathematical notes, producing and independent receipts, source origins, failures and review bindings. The restart document gives a clean recovery order, public smoke tests and full continuum reproduction commands. Historical absolute workspace paths in old audit records are provenance; portable launchers bind only the recovered filesystem location without changing mathematical inputs or sealed source bytes.

No theorem is claimed beyond $|h| \le 0.2$ or beyond the radius interval $[0.899, 0.9]$. No sharp new global bound for α_h or α_z over that full domain is released. The stronger inner modulus factor is not silently substituted into the outer public dispatcher. Very close to the branch, a physical query may still require the inherited high-precision source selector or image refinement; the present two off-zero queries already meet their targets with their executed resources.

The most direct continuation is to make the correlated terminal and parameter-return machinery reusable in a resource-adaptive physical evaluator, with locally admitted order/radius charts and tighter branch derivative information. Broader order or radius continuation then requires new strict inequalities, not extrapolation of this certificate. Practical low-rank completion, broader exact frequency support and remaining high-precision scalar compositions remain separate parts of the original programme and were not diverted into during this investigation.

Checks of the quantitative continuation

The principal positive integer comparisons are in Section 19 (positive integer diagonal). Separate finite hypergeometric sums and confluent integral evaluations test the local kernel comparison at independent complex tilt; for $s = -.35 + .5i$, $t = 1.2, w = -.8$, the kernel discrepancy falls from about .0474 at $N = 16$ to .00305 at $N = 256$. The exact mark comparison was also evaluated down to depths 10^{-8} and angular coordinates 10^{-9}. These are numerical consistency checks on the proof ingredients. A noninteger scalar control at $z = 0, h = s = 1/2$ uses a radial Bessel Toeplitz integral for $\mathbb{E}|\operatorname{Tr} U|$. At ranks $4, 6, 8, 12$ its discrepancies from $\Gamma(3/2)$ are about $-8.77 \cdot 10^{-4}, -1.34 \cdot 10^{-5}, -1.36 \cdot 10^{-7}, -4.98 \cdot 10^{-12}$. A separate source-tail bound and floating quadrature diagnostics are recorded, including the tight-tolerance roundoff warning. The floating integration is a check, with the tail bound quoted separately.

The dispatcher returned certified relative enclosures on three different routes. At $N = 2, z = .9, h = -.95+.3i, s = .4 - .5i$ the relative radius is below $5.624 \cdot 10^{-13}$, and the full absolute disk has radius below $9.311 \cdot 10^{-12}$. At $N = 3, z = 1/3, h = s = 1$ the exact finite polynomial route gives relative radius below $3.141 \cdot 10^{-38}$. The near-zero test uses the exact nonzero rational centre s_0 of Theorem A6.2, $N = 8, z = .9, h = 0$. A second calculation sums the original Toeplitz coefficient series through term 1600 with geometric tails before taking the determinant. Its outward disk contains the hypergeometric determinant enclosure and has relative radius below $2.376 \cdot 10^{-44}$. This checks nonzero relative certification even when the modulus is of order 10^{-104}. The full suite and scripts are in the source package. The rank-three check is for an integer order at the critical radius. The direct angular dispatcher was checked separately at $N = 3, z = 0, h = 1, s = 0$, where Haar orthogonality gives the exact result 1. The two requested absolute tolerances 2 and $1/2$ gave certified radii below 1.719 and .426, both containing that value. The general angular fallback can be expensive; the executed high-accuracy cases use the specialized routes above.

All new proofs are based on the stated hypotheses of the inherited asymptotic theorems. Within the quantitative continuation alone, numerical certification of the leading microscopic coefficient at nonreal tilt still needs a priced high-frequency seminorm or a direct radial tail bound (supplied in the microscopic-certification continuation summarized immediately below). The real-tilt construction supplies a computable tail and an enclosure procedure. The additional estimates here do not claim a replay of every inherited verification archive.

Verification of the microscopic certificates

At $c = 1, h = s = 1/2$, the Laplace jets and inequality (19.V6) gave approximate outward brackets $[.36682, .55032]$ and $[.38049, .55026]$. Their exact dyadic half-widths are below .092 and .085, respectively. This positive-measure bracket has an intrinsic shape width after the jet errors have been removed. Separately, at $c = 1, h = s = 1$ the jet calculation contains the Schur coefficient $2 - 5/e$. The finite arithmetic midpoint agrees with it to the displayed 18 digits.

At $c = 1, s = 1/2+i/20, h = 1+i2^{-10^{15}}$, two validated first jets and the inverse-gamma identity yield relative disks below $5.797 \cdot 10^{-5}$ and $6.865 \cdot 10^{-8}$. The order is deliberately close to an integer. The separately validated inverse-order example at $c = 1, s = i/8, h = (-1+i)10^{-1200}$ reaches $3.1271 \cdot 10^{-12}$ relative accuracy. Its independent trace computation is coarser than the final Laguerre certificate and contains it. Another inverse control at $c = 256$ uses a separately bounded finite-rank comparison. The large-depth control of Section 19 (certified Mellin return) exercises complex order well away from the integer anchors.

The shifted-line operator code also certifies independent nonreal source evaluations at $c = 64$ through two refinements. A separate mass check agrees with the $s = 1$ exact formula $(1 - e^{-c})/c$. The same direct source code at $c = 1, s = 1/2$ with 64 cells gives a Hilbert–Schmidt cell allowance larger than 37. The complete determinant radius then exceeds 10^{1234}. The Laplace jet calculation replaces this discretization for the executed depth-one fractional bracket.

For the genuinely fractional tuple $c = 1, h = 1/2 + i/8, s = 1/2 + i/20$, the general direction-uniform Mellin bound with $m = 2$ at frequency cutoff 64 costs more than 10^{2316} in absolute error. With that specific bound, a tail budget of 10^{-12} would require the sufficient cutoff R to exceed 10^{777}. The exterior-compression estimate of Section 19 (exterior polynomial bound) substantially reduces this particular positive-order budget. At cutoff 64 it gives an allowance of about $10^{5.783}$, and its sufficient cutoff for the same tail target is about $10^{35.3563}$. The direct depth-one quadrature still has no feasible budget from these bounds. The effective theorem, the executed

near-integer and large-depth results, and the remaining practical depth-one problem have different scopes. The receipts preserve the finite arithmetic, analytic errors and exact dyadic enclosures separately.

Executed nonzero disks at the depth-one target

The table combines the exact dyadic output of the finite part, retained annulus, and indicated Bessel tail at $c = 1, h = 1/2 + i/8, s = 1/2 + i/20$. Midpoints are rounded for display. The last line includes the signed polynomial part of the tail at its center. Each entry bounds the same limiting Haar scalar.

R	requested absolute	disk center	radius upper	modulus lower
4	.28	$.495455414 - .083269166i$	.279181	.223223
6	.16	$.493158137 - .083056360i$	.152012	.348092
8	.085	$.481506185 - .070438803i$	.083342	.403289

At $R = 8$, the retained-integral allowance is below .007070 and the centered-tail radius below .076273. The retained error contains the origin finite part and jet, angular aliasing, radial panels, source trace-norm error and ball arithmetic. The source evaluations used the retained radial frequencies near the origin and geometrically spaced keyhole quadrature panels, then projected to a Laguerre basis with the individual displacement quantified by (K4). For the last line each angular aliasing charge was tightened using its exact radial node and the best proved strip among Cartesian imaginary shifts $1/2, 11/20, \dots, 1$. This uses the same node values and compares exact outward error terms, leaving source and radial charges intact. The exact $R = 4$ disk was also recombined using rational arithmetic, and its modulus bound checked by rational squares. Applying the order variation in Section 19 (depth-one budget extensions) to the $R = 8$ disk at the independent nearby order $h' = 1/2 + 63i/500$ adds less than .050663 and produces a radius below .134096 and modulus above .352995.

The independent floating exterior computation through cutoff 64 gives about $0.50808 - 0.08754i$. The direct finite-Haar scalar calculation at ranks 32 and 64 and the same finite cutoff gives about $0.51668 - 0.08656i$ and $0.51232 - 0.08707i$. First Richardson combination gives about $0.50797 - 0.08758i$. These are diagnostic checks on the complex scalar. Finite-rank source values also have separately validated Arb errors at a list of frequencies, without a finite-rank-to-limit scalar allowance on these diagnostics. At $p = 3/4 + i/4, q = \bar{p}, v = 1$, the keyhole and the inherited shifted-line kernel enclosures overlap on the same limiting Hankel kernel. The independently validated integer control contains the Schur value $2 - 5/e$.

For the deliberately tighter relative target 10^{-10}, the current angular trace-deficit bound reaches an absolute tail allowance below 10^{-12} at $R = 6 \cdot 10^7$. The validated retained integral ends at $R = 8$. Its last panel uses several hundred certified source calls, and the simple trace perturbation constants already require increasing the keyhole quadrature order and projection size across these last panels. The actual $R = 8$ shortfall is the integrated shape allowance, even after the low-degree signed contribution is removed. A separate L^2-only Bessel transfer is also too large with its available signed density norm. No relative 10^{-10} certificate follows from these budgets.

Improved real-diagonal control. At $c = 1$, $h = s = 1/2$, let $X = |S|^2$ under the unnormalized positive limiting preparation and let m_j for $0 \le j \le 3$ denote its ordinary integer moments. For an independent computation of these moments, extract the coefficient of $p^j q^k$ of each projected keyhole Hankel matrix. Its quadrature weight at node u_ℓ is $d_\ell(0,0)\gamma_\ell^j \beta_\ell^k/(j!k!)$, where the full source weight is $d_\ell(0,0)e^{\gamma_\ell p + \beta_\ell q}$. The factor error remains bounded on the bidisk of radius $r = 1/4$ by (K2)–(K4), applying (K4) to the absolute multipliers $\exp(r(|\gamma_\ell| + |\beta_\ell|))$. To price the determinant there, bound the approximate factor's Hilbert–Schmidt norm by its certified zero-source norm plus

$$\sum_\ell \frac{|d_\ell(0,0)|}{2\Re u_\ell}\left(e^{r(|\gamma_\ell|+|\beta_\ell|)} - 1\right),$$

using the contraction of orthonormal projection. The Fredholm determinant perturbation inequality and the exact prefactor bound the source error uniformly on the bidisk. Cauchy's inequality gives the diagonal coefficient error by dividing that allowance by r^{2j}. The moment conversion remains $(-4)^j (j!)^2$. The finite determinant polynomial coefficients are obtained by factoring out its invertible constant matrix and expanding $-\sum_{n=1}^{6} \operatorname{tr}(T^n)/n$ for the remaining matrix $I - T$, whose T has zero constant term. In bidegrees at most $(3,3)$ all further terms vanish. Exponentiating this finite formal series and including the prefactor gives the certified moments recorded in `real_order_control.json`.

Let x_1, x_2 be the roots of the monic quadratic orthogonal to $1, x$ for the positive measure with moments m_j. Solve the two moment equations for weights w_1, w_2. The enclosures verify $0 < x_1 < x_2$ and $w_1, w_2 > 0$. Division by the orthogonal quadratic proves the weights integrate every cubic exactly. For $f(x) = \sqrt{x}$, its cubic Hermite interpolant with double knots x_1, x_2 lies above f on $[0, \infty)$. For $x > 0$, the Hermite remainder is $f^{(4)}(\xi)(x - x_1)^2(x - x_2)^2/4!$ with negative fourth derivative. The inequality at zero follows by continuity. Thus

$$\frac{m_1^{3/2}}{m_2^{1/2}} \le F(1; 1/2, 1/2) \le w_1\sqrt{x_1} + w_2\sqrt{x_2},$$

where the lower bound is the earlier Hölder inequality. Ball evaluation of these expressions gives the outward bracket [0.38050322141498, 0.52417857090888], tightening the earlier real upper endpoint 0.5502551135.

Signed windows at depth one

Theorem 22.W1 (Verified signed-window disk)**.** *Use normalized Haar measure, $z = \sqrt{1 - 1/N}$, $c = 1$, $h = 1/2 + i/8$ and $s = 1/2 + i/20$. For the limit of $N^{-s^2-2h}\mathbb{E}[|\Lambda_N'(z)|^{2h}|\Lambda_N(z)|^{2(s-h)}]$, a closed disk centered at*

$$0.507915310133050 - 0.087481791197421i$$

has sufficient radius 0.000263562331*. The exact dyadic center has certified radius less than* 0.000263562330130*, a lower bound $|F| >$ 0.515130486974, and relative error less than* 0.000511641879*. These bounds are for the displayed parameters.*

Proof. Let H_j be the limiting complex Mellin integral on the jth retained positive band, including κ, and let H_0 denote the origin finite part through one. Initially the cutoff-eight tail had already integrated the polynomial

$$q_8(X) = (.385 - .102i) + (-.966 + .268i)X + (.622 - .172i)X^2$$

against the signed complex jets. The new assembly replaces the entire old tail, including this center. For a window end R, start from $H_0 + \sum_{j:\, b_j \le R} H_j + T_R$. Equations (W1)–(W4) give a disk for the omitted T_R after returning the signed projections of the new residual. The matched real Bessel observations constrain the positive envelope. The costs of the finite comparison, both tails beyond M, the signed jets, and outward arithmetic remain in the calculation. At $R = 20$ the selected rank is 10^{62} and $M = 2^{21}$.

Write $u_j = R^{-2h}\beta_j/A_j$ for the coefficient of H_j in the tail center, with $A_j = \int_{a_j}^{b_j} \rho^{-2h-1}d\rho$. The exact coefficient of a shared band in the full scalar is $1 + u_j$. More explicitly, suppose the recorded tail center used the band midpoint d_j, and that the sharper disk for the same band is $D(m_j, e_j)$. The replacement shifts the full center by $u_j(m_j - d_j)$ beyond the sum of m_j and the old tail center. It charges $|1 + u_j|e_j$ for that band. The old separate charge for the uncertainty of d_j is removed, since the linear representation is evaluated afresh. This argument is an identity between functionals of the same exact H_j and uses no statistical independence. The code evaluates each multiplier by a rational enclosure. If its dyadic midpoint is v_j and its radius ϵ_j, the new charge is $(|1 + v_j| + \epsilon_j)e_j + \epsilon_j|m_j - d_j|$. The original rounding of the tail center stays in the budget.

The table gives exact-arithmetic refinements. Centers are displayed to nine decimal places. The last two columns are bounds for the exact dyadic centers. The same fifteen positive tilt observations, at the integer frequencies 2 through 16, are available in each row; the signed complex windows extend through the indicated cutoff. Each row has its own verified spatial envelope and comparison budget.

R	$\Re m$	$\Im m$	E below	$E/(\lvert m\rvert - E)$ below
8	.508186108	−.087691440	.001105365	.002148045
12	.508061845	−.087616020	.000718418	.001395412
16	.507936920	−.087505846	.000524944	.001019517
20	.507915310	−.087481791	.000263563	.000511642

At twenty the dominant shape charge is below 0.000253381236. The cost of the positive probe errors is below 0.000002399037. The main finite comparison costs less than 0.000000728337, and the finite and limiting past-M charges are below 0.000000682210 and 0.000000748812. The combined errors of the shared bands are below 0.000005619009. The origin contributes less than $3.6920 \cdot 10^{-9}$; the signed-jet, control-transfer and final arithmetic

allowances complete the ledger. The separate treatment of the band disks independently encloses the scalar with radius below 0.000298255365. The final calculation is in verification_window/shared_disks.json; the table can be regenerated with verification_window/shared_disks.py. Integer square-root bounds certify the lower modulus and the relative estimates. Rounding both displayed center coordinates to fifteen places costs less than 10^{-15} in absolute radius. This proves the statement. □

Attribution of the reduction and remaining accuracy. The published radius was 0.083341725692 to twelve decimal places. The total reduction exceeds 0.08307816. Against the improved cutoff-eight calculation in the table, extending and using the windows through twenty saves 0.00084180 of absolute radius (over 76%). These comparisons distinguish the new positive probes and quadrature estimates from the gain produced by measuring a larger signed band. The first full-width smooth transition and its independently priced complement are given in the finite-rank quadrature proof in Section 19.

At the current center the 10^{-10} relative test requires an absolute radius of about $5.154 \cdot 10^{-11}$. The spatial charge alone is about $4.9 \cdot 10^{6}$ times that price. Even a zero-cost spatial residual would leave retained-source and comparison charges above the target. Equations (W1)–(W4) reduce the problem to a weighted approximation against the actual mark law. In particular, a new localized bound on the matched mass near zero, with a priced pairing against the complex preparation on its complement, could be tested directly in this ledger. The lower-bound examples in Section 19 specify which finite collections of tests they cover. The observed contractions give no rate of contraction when the depth, order, tilt or number of bands changes.

A second calculation of the scalar. The finite-Haar Toeplitz calculation at ranks 24, 48 and 96, with $r_{\max} = 64$, 8192 Fourier points, 36 angles and a 14-node radial rule on each panel, returns respectively $.51960124 - .08621520i$, $.51376709 - .08689914i$ and $.51087649 - .08723256i$. The combination $2F_{96} - F_{48}$ is $.50798588 - .08756599i$, at distance less than .00010987 from the last center. This is a diagnostic: its quadrature, omitted tail and extrapolation do not furnish an error bound. The independent spatial checks and the two positive controls below address other steps of the proof.

For the final candidates at $R = 16, 20$, a second implementation replaced the truncated kernel series by the hypergeometric formula and propagated first derivatives from panel midpoints. It certified the entire radial half-line with 6544 and 4518 interior panels, respectively, and separate origin and exterior checks. It used the frozen coefficients and constant slack 0.000006 of the accepted shapes. An independent 510-bit check reconstructed all thirteen complex band multipliers at $R = 20$, including their signs and the correction for the changed $[8, 9]$ midpoint. Its rational corner tests enclose each charged modulus. See verification_window/mark_joint_final_check.json and verification_window/audit_shared.json.

Independent depth-one normalization and positivity checks. For $h = s = 1$, the finite Schur formula of Section 19, positive integer diagonal gives the normalized scalar $N^{-3} \sum_{j=1}^{N} j^2 (1 - 1/N)^{j-1}$ at $c = 1$. Since $(j-1)\log(1-1/N) + j/N = O(1/N)$ uniformly for $1 \le j \le N$, its Riemann limit is $\int_0^1 t^2 e^{-t}\, dt = 2 - 5/e$, by two integrations by parts. The alternating Taylor sums for the integral and, independently, for $2 - 5/e$, through consecutive degrees 63 and 64, enclose this number between consecutive multiples of 2^{-120}. The enclosure lies inside the inherited integer Fredholm disk.

A separate spatial check on $h = s = 1/2$ improves the real interval. Under the positive unnormalized preparation put $X = |S|^2$, and let m_j be the certified moments of X up to degree three. Take $a = 253/500$ and $b = 271/200$. The cubic P interpolating $\sqrt{x}$ and its derivative at a^2, b^2 satisfies, for $t \ge 0$,

$$P(t^2) - t = \frac{(t-a)^2 (t-b)^2 [t^2 + 2(a+b)t + a^2 + 3ab + b^2]}{2ab(a+b)^3} \ge 0.$$

Expansion verifies the identity and gives rational coefficients P_j. The upper bound is therefore $\sum_{j=0}^{3} P_j m_j$, with the endpoint of each certified interval chosen according to the sign of P_j. The lower bound $\sqrt{m_1^3/m_2}$ follows by Hölder. Exact rational arithmetic and a downward integer square root yield

$$0.38050322365532 < F(1; 1/2, 1/2) < 0.51985705002601.$$

Fixed rational knots avoid the interval loss incurred by returning both quadrature nodes and weights from uncertain moments. The input moments are inherited from verification_depthone/real_order_control.json.

The new readout and the independent Schur calculation replay together with verification_window/positive_controls.py.

23. Scalar recovery through intersecting resonances

The normal readout fails algebraically when a derivative in a displacement transverse to the physical radius is undetermined. A zero of a connection weight denominator occurs in the order parameter and can hide the derivative of a branch difference. We first determine which missing data the Haar moment actually measures. Then we propagate the source-selected solution through the intersections and give independently checkable absolute errors.

The determinant annihilates the free normal derivatives

Theorem 23.1 (the physical scalar through every normal-jet resonance at ranks three and four). Use the four-mode displacement pencil of Theorem 10.6, including its two extreme-row selectors. Let $N = 3$ or 4, $H = \lfloor (N-1)^2/4 \rfloor$, $D = 2H$, $g = h + H$, and $\rho = g + N(1 - N - s)$. At every regular physical endpoint $0 < z < 1$ of that theorem, and for every $\Re h > -1$, $s \in \mathbb{C}$, there is a scalar row

$$\ell_{N,z}(h,s) = \frac{(1-z^2)^{N^2+2Ns}}{(h+1)_H^2}\, Q_{N,z}(h,s)$$

on the $\binom{N+3}{3}$ raised angular components. Here Q is polynomial in (h,s) of bidegree at most $(D, D + N(N-2))$, with rational coefficients in z. It recovers the original unnormalized T_N. It is regular through every $\rho = 1, \dots, D$, with no normal differential, parameter derivative or additional initial coordinate in the scalar readout. Off the divisors it agrees entrywise with the canonical extreme-row scalar extension in Theorem 10.6. The coefficients give the same branch readout at a regular exit reached by continuation of the physical angular germ.

Construction. Retain the group inverse S_0, the two columns E_a, E_b and the matrix G of Theorem 10.6. The moment of order g is the input $W = X_{00}$. At degree k solve the differentiated displacement equations using their particular solution

$$\begin{pmatrix} U_{i+1} \\ V_i \end{pmatrix} = S_0 \left(G X_{ij} - \begin{pmatrix} i X_{ij} \\ j X_{ij} \end{pmatrix} \right), \qquad i + j = k - 1.$$

For $0 < i < k$, retain the upper line U_i and add E_a times the first coefficient of $V_i - U_i$ in the two extreme rows of (E_a, E_b). This value defines $X_{i,k-i}$. Set $X_{k,0} = U_k$, $X_{0,k} = V_0$. Apply the signed polynomial determinant of Theorem 10.6 through degree D. This is an algorithm for QW even when the individual derivatives so constructed differ from the angular derivatives. In particular it needs no inverse of $kI - B$.

Proof. Place arbitrary scalar corrections $u_k E_a, v_k E_b$ into the two pure derivatives at each degree. The actual angular derivatives satisfy this recursion for one choice of the corrections, by the displacement equations and independence of E_a, E_b. The same observation applies columnwise to the earlier nonresonant linear extension. Linearity reduces the claim to annihilation of a single correction, inserted in degree r on either side with zero initial state. The degree bound follows because each subsequent particular solution introduces at most one affine factor G, and all selectors and group inverses are parameter independent. Each single-mode lift in the determinant costs at most $N - 2$ powers of s at these ranks.

The following finite polynomial calculation proves annihilation over the function field, avoiding a sampling assumption in the radius. Number the four mode slots by $t = 0, 1, 2, 3$ (actual frequency $t - 1$). Set $V = \mathbb{C}^4$, $e(x)_t = x^{t-1}$, $x = z$ or $1/z$. Write F_q^x for the span of symmetric tensors with at least $N - q$ factors $e(x)$ and set $F_{-1}^x = 0$. Both diagonal shifts preserve the line $\mathbb{C}e(x)$ and both cross shifts annihilate it. Consequently the stacked L preserves $(F_q^x)^2$. At a regular point S_0 is a polynomial in L, by inverting the identity function on the nonzero primary factors of its minimal polynomial and taking zero on the semisimple zero factor. It preserves the same filtration. Each additive summand of G changes at most one tensor factor, so it increases q by at most one. A mixed-row correction can add a column in F_0^z even for a disturbance that started in $F_0^{1/z}$. Thus the invariant error subspace at degree $k \geq r$ is the **sum** $F_{k-r}^z + F_{k-r}^{1/z}$.

The general-rank cancellation. Put

$$V_N = \sum_{j=0}^{N-1} \lceil j/3 \rceil.$$

At any rank, every free normal coefficient inserted at degree $r > D - V_N$ is invisible to the physical scalar. Consequently one needs the ordinary normal inverses only through $\max(0, D - V_N)$ to handle a resonance above that threshold. At ranks five, six and eight the resulting free ranges are respectively $\rho = 4, \dots, 8,\ 6, \dots, 12$, and $13, \dots, 24$, at every regular endpoint for every $\Re h > -1$ and every tilt on the indicated divisors. These are algebraic scalar-recovery statements on the physical state. Certified propagation at those ranks requires separate estimates.

Write $p_{ij,t}$ for the determinant coefficient of the sorted tuple t multiplying the (i, j) derivative before its sign. Perturb the four basic mode values to $e(x) + \sum_{b=1}^{3} y_b \delta_b$ and set the frequencies $(t_{\mathrm{freq}}, u_{\mathrm{freq}}) = (\xi/\tau, \eta/\tau)$, with generic nonzero ξ, η. Every reconstructed Toeplitz entry is polynomial in nonnegative powers of τ, with coefficients linear in the basic modes. The mode sequence at $(\tau, y) = (0, 0)$ is x^j, so the Toeplitz matrix there has rank one and its determinant vanishes to total perturbation degree at least $N - 1$. The four-mode recurrence gives the stronger bound V_N as follows.

Let $A = z + z^{-1}$, $q = \eta/\xi$, and $Ef_j = f_{j+1}$. The two outer-mode reductions, solved forward and backward from the same four basic values, are the single identity

$$(E^2 - AE + 1)(E^2 - q) f_{j-2} = -\frac{\tau}{\xi} \left[j(f_{j+1} - Af_j + f_{j-1}) + (1 + \nu)(f_{j+1} - f_{j-1}) \right].$$

Work in the function field where the four characteristic roots $x, x^{-1}, \sqrt{q}, -\sqrt{q}$ are distinct. Substitute $\tau = \delta T$, $y_b = \delta v_b$ with independent indeterminates. At order m in δ, the coefficient sequence is a sum of terms $a^j p(j)$ at the four roots a. At the initial root x the degree of p is at most m. At x^{-1} it is at most $m - 1$, and at either frequency root it is at most $2m - 2$, with the latter three roots absent for $m = 0$. Indeed at either geometric root the difference $f_{j+1} - Af_j + f_{j-1}$ lowers the polynomial degree by one, compensating multiplication by j. At the frequency roots the right side can raise degree by one. Inversion of the constant-coefficient recurrence on a root times a polynomial raises its degree by one, since that root is simple. The homogeneous additions at each positive order have degree zero. The first forcing is supported at x, and the remaining three roots can first enter at order one. This proves the bounds by induction in both directions of the mode sequence.

In the matrix (f_{i-j}), expand each root term into left columns $i^a \lambda^i$ and right rows $(-j)^b \lambda^{-j}$. The connecting coefficient is zero between different roots. Its minimum order in δ at equal roots is bounded below by $a + b$, $1 + a + b$, and $1 + \lceil (a + b)/2 \rceil$ in the three respective root classes. Truncate to any fixed order in δ, so both rectangular confluent matrices are finite. Apply Cauchy–Binet on the left and the right. A nonzero term selects equal numbers of left and right indices at each root, with distinct nonnegative degree indices on each side. If the counts are u, v, w, l in the root order above, each permutation product in the central minor has order at least

$$u(u - 1) + v^2 + \tfrac{1}{2} w(w + 1) + \tfrac{1}{2} l(l + 1).$$

For example the w-block contributes at least $w + \frac{1}{2}(\sum a + \sum b) \geq w(w + 1)/2$. Minimize this bound subject to $u + v + w + l = N$. The increasing marginal costs have multiset union consisting of zero once and every positive integer three times. Taking the least N marginal costs gives V_N. Thus no monomial in (τ, y) of total degree below V_N occurs. This is a rational coefficient identity, so the generic use of distinct auxiliary frequency roots has imposed no restriction on the parameters of the original problem.

The coefficient of $\tau^{D-k} y^\alpha$ in that determinant, for $k = i + j$, separates into the distinct Laurent monomials $\xi^{i-H} \eta^{j-H}$. Its coefficient on each such monomial is $p_{ij} Y_\alpha$, where

$$Y_\alpha(t; x) = x^{\sum t_m - N - \sum_{b=1}^{3} b\alpha_b + q} \prod_{b=1}^{3} \binom{n_b(t)}{\alpha_b}, \qquad q = |\alpha|.$$

Here $n_b(t)$ counts slots equal to b. These tensors are the coefficients of y^α in $(e(x) + \sum y_b \delta_b)^{\otimes N}$. Those with degrees at most q span F_q^x. Therefore p_{ij} kills F_q^x if $D - k + q < V_N$. This applies on both lines, including their sum. For an injection in degree r, take $q = k - r$ to prove the claim. At rank three this already disposes of

every positive degree. At rank four it proves annihilation for $r \ge 2$ and for the part of a first-order disturbance in $F_{k-2}^{z} + F_{k-2}^{1/z}$. Every new extreme-row correction after degree one belongs to this discarded part, even when it falls on the opposite line.

For an independent finite verification, the nonzero pairs (i, j) at rank three are $(1,0), (1,1), (2,0)$. At rank four they are $(1,0), (1,1), (1,2), (1,3), (2,0), (2,1), (2,2), (3,0), (3,1), (4,0)$. Evaluating the displayed contraction for $q < k - 1$ gives respectively 2 and 54 exact zero coefficients per line in $\mathbb{Q}(z, s)$.

It remains to follow the top graded component of the two first-order insertions. We give the recurrence explicitly so that the cancellations can be checked independently. Write a one-mode shift A in the basis $(e(x), \delta_1, \delta_2, \delta_3)$ as T. If A preserves the line, its lift on grade q acts on Y_α by

$$(N - q)T_{00}Y_\alpha + \sum_{b,c=1}^{3} \mathbf{1}_{\alpha_c > 0}(\alpha_b + 1 - \delta_{bc})T_{bc}\, Y_{\alpha - e_c + e_b}.$$

The grade-increasing part of $-A$ on Y_α is $-\sum_b (\alpha_b + 1)T_{b0}Y_{\alpha+e_b}$. Both identities follow by differentiating the generating tensor in y. Form L_q by applying the first rule to the four shift blocks of L. Form G_q by applying the second rule to the two constant one-mode blocks of G. The scalar order term in G and the subtracted i, j terms preserve grade and drop out. For $1 \le q < N$ the stacked L_q is invertible. Indeed the two semisimple zero dimensions of L already occur on grade zero (the x-line in its matching block) and on grade N (the opposite eigenline projects nontrivially to the Nth symmetric power of the quotient). The induced inverse on the intermediate grades is therefore L_q^{-1}.

Start with coefficient 1 at $(1, 0)$ for $x = z$, or $(0, 1)$ for $x = 1/z$. At derivative degree q, the surviving tensor has grade $q - 1$. Apply $L_q^{-1}G_q$ to its column at each occupied (i, j) to reach tensor grade q and derivative degree $q + 1$. The upper half supplies $(i + 1, j)$. The lower half supplies $(0, j + 1)$ only if $i = 0$, because a mixed jet uses its upper predecessor. Contract with the signed $(-1)^k p_{ij} Y_\alpha$ at total degree k. Exact fraction-free elimination in the displayed bases gives the following entries, with $K = (s + 3)^3(z^2 - 1)^3/z$.

Rank and first insertion	Degree 1	Degree 2	Degree 3	Degree 4
Three, upper or lower	0	0		
Four, upper	K	$-3K$	$3K$	$-K$
Four, lower	0	0	0	0

For rank four the three stacked solves have sizes $6, 12, 20$. The identities in the table are over $\mathbb{Q}(z, s)$, so they hold at every regular specialization of the original formula, including specializations where an intermediate symbolic pivot changes. The row annihilates the two remaining insertions. At rank three a separate calculation on $e(x)^{\otimes 3}$ and its first derivative verifies the same result. These identities prove the assertion. The kernel-free scalar row extends holomorphically in the order throughout the ordinary domain and is entire in the tilt. They confer no such determination of the complete normal jet. □

Theorem 23.1A (universal polynomial scalar readout through all normal-jet resonances). Fix any rank $N \ge 3$ and any regular interior radius $0 < z < 1$ outside the finite algebraic exceptional set (10.9) of Theorem 10.6. Set

$$H = \left\lfloor \frac{(N-1)^2}{4} \right\rfloor, \qquad H_+ = \left\lfloor \frac{(N-2)^2}{4} \right\rfloor, \qquad D = 2H, \qquad d = \binom{N+3}{3},$$

and $g = h + H$, $\nu = -N - s$, $\rho = g + N(1 + \nu) = h + H + N(1 - N - s)$. On the complement of the normal-jet resonance hyperplanes $\rho \in \{1, \dots, D\}$, let

$$\ell_{N,z}(h, s) = \frac{(1 - z^2)^{N^2 + 2Ns}}{(h + 1)_H^2}\, Q_{N,z}(h, s)$$

be the canonical extreme-row scalar readout row of Theorem 10.6, formed by applying the normal-jet and mixed-derivative recurrences to $W_0 = I_d$ using the two extreme-mode rows $(-1, \dots, -1)$ and $(2, \dots, 2)$ of (E_a, E_b) as selector π_E and contracting with the cleared determinant polynomial $(tu)^H \det(F_{i-j})_{i,j=0}^{N-1} = \sum_{0 \le i+j \le D} t^i u^j p_{i,j}(z, s) \cdot V$. Then:

(i) *Entrywise removable resonances and global polynomiality.* Every apparent pole of $Q_{N,z}(h,s)$ along $\rho = r$ ($r = 1, \dots, D$) has identically zero residue on every coordinate of $\mathbb{C}^d$ (not merely on physically compatible states). Hence

$$Q_{N,z}(h,s) \in \mathbb{Q}(z)[h,s]^{1\times d}$$

is globally polynomial in (h,s), with

$$\deg_h Q_{N,z} \le D, \qquad \deg_s Q_{N,z} \le D + H + H_+, \qquad \deg_{(h,s)} Q_{N,z} \le D + H + H_+.$$

(ii) *All-rank recovery without supplementary normal coordinates.* For every $\Re h > -1$ and every $s \in \mathbb{C}$—including on every normal-jet resonance $\rho \in \{1, \dots, D\}$ and at every transverse intersection of $\rho = r$ with a connection-weight divisor $\cos\vartheta(h) = 0$—the unnormalized physical Haar moment satisfies

$$T_N(h,s;z) = \frac{(1-z^2)^{N^2+2Ns}}{(h+1)_H^2}\, Q_{N,z}(h,s)\, W_g(Nz;z),$$

with no supplementary normal-jet coordinates, no division by $k-\rho$, and no modification of the two-arc connection weights of Theorem 10.9.

(iii) *Division-free evaluation and contrast with Theorem 23.1's shortcut.* For any fixed regular z off (10.9) and fixed $s \in \mathbb{C}$, $Q_{N,z}(h,s)$ is recovered identically at every (possibly resonant) $h \in \mathbb{C}$ by degree-D univariate Lagrange interpolation in h from any $D+1$ nonresonant canonical evaluations (or by exact polynomial division of $d_D(\rho)Q_{N,z}(h,s)$ by $d_D(\rho) = \prod_{m=1}^{D}(m-\rho)$). The zero-injection shortcut of Theorem 23.1 agrees with $Q_{N,z}$ at $N = 3, 4$ because $D - V_3 = 0$ and $D - V_4 = 1$ leave at most the single boundary degree $r = D - V_N$, where only the h-independent top tensor grade survives the perturbation cutoff V_N; for $N \ge 5$, $D - V_N \ge 3 > 1$, so lower h-dependent grades enter for $1 \le r < D - V_N$ and the zero-injection shortcut does not replace the canonical construction even on physical states.

Proof. Fix $N \ge 3$ and a regular radius $0 < z < 1$ off (10.9). Then L, its rank-two spectral projector Π onto $\ker L = \operatorname{span}((E_a,0)^{\mathsf{T}}, (0,E_b)^{\mathsf{T}})$, its group inverse S_0 ($LS_0 = S_0L = I - \Pi$, $S_0\Pi = \Pi S_0 = 0$), and the extreme-row selector $\pi_E : \mathbb{C}^d \to \mathbb{C}^2$ (inverting the 2×2 submatrix of (E_a, E_b) on rows $(-1, \dots, -1)$ and $(2, \dots, 2)$, whose determinant $z^{-3N} - z^{3N}$ is nonzero on $0 < z < 1$) lie in $\mathbb{Q}(z)$ and are completely independent of (h,s). The matrices G, $B = R\Pi G$, and $B_m = (-1)^m R S_0^{m+1} G$ of Theorem 10.6 are affine (degree one) in (h,s) over $\mathbb{Q}(z)$, with $\operatorname{im} B \subseteq \operatorname{span}(E_a, E_b)$, $BE_a = \rho E_a$, $BE_b = \rho E_b$, and $B^2 = \rho B$.

Step 1: Denominators, parallel disjointness, and degree bounds of the cleared numerator. Put $d_k(\rho) = \prod_{m=1}^{k}(m-\rho)$ with $d_0 = 1$. Define the canonical matrices $w_k, X_{i,j} \in \mathbb{Q}(z,h,s)^{d\times d}$ recursively from $w_0 = X_{0,0} = I_d$ by

$$w_k = \left(\frac{1}{k}I + \frac{1}{k(k-\rho)}B\right)\sum_{m=0}^{k-1} B_m w_{k-1-m}, \qquad \binom{U_{i+1}}{V_i} = S_0\left(GX_{i,j} - \binom{iX_{i,j}}{jX_{i,j}}\right),$$

taking $X_{i,k-i} = U_i + \alpha_i E_a$ for $0 < i < k$ with $(\alpha_i, -\beta_i) = \pi_E(V_i - U_i)$, and $X_{k,0} = U_k + c_k E_a$, $X_{0,k} = V_0 + d_k E_b$ with $(c_k, d_k) = \pi_E\Big(k! w_k - U_k - V_0 - \sum_{i=1}^{k-1}\binom{k}{i} X_{i,k-i}\Big)$. We verify by induction on $k = 0, \dots, D$ that $d_k(\rho)w_k$ and $d_k(\rho)X_{i,k-i}$ lie in $\mathbb{Q}(z)[h,s]^{d\times d}$ and have $\deg_h$, $\deg_s$, and total degree $\deg_{(h,s)}$ each at most $2k$. The base $k = 0$ is immediate. For $k \ge 1$,

$$d_k(\rho)w_k = \frac{1}{k}\big[(k-\rho)I + B\big]\sum_{m=0}^{k-1} B_m \frac{d_{k-1}(\rho)}{d_{k-1-m}(\rho)}\big(d_{k-1-m}(\rho)w_{k-1-m}\big).$$

In the mth summand, the four factors have $(\deg_h, \deg_s, \deg_{(h,s)})$ bounded respectively by $(1,1,1)$, $(1,1,1)$, (m,m,m), and $(2(k-1-m), 2(k-1-m), 2(k-1-m))$, summing to $2k - m \le 2k$. Likewise $d_{k-1}(\rho)\binom{U_{i+1}}{V_i}$ has each degree at most $1 + 2(k-1) = 2k-1$, so multiplying by $k-\rho$ gives $d_k(\rho)U_i$ and $d_k(\rho)V_i$ of each degree at most $2k$; since π_E, E_a, E_b are independent of (h,s), $d_k(\rho)X_{i,k-i}$ has each degree at most $2k$.

For the determinant clearing coefficients $p_{i,j}(z,s)$, each upward step in (10.4) reducing $m > 2$ multiplies by coefficients of degree at most 1 in $\nu = -N - s$, so by induction on $m \ge 3$ the reduced polynomials in $t^{m-2}F_m = \sum_{r=-1}^{2} R_{m,r}F_r$ satisfy $\deg_\nu R_{m,r} \le m-2$; symmetrically, for $m \le -2$, $\deg_\nu R_{m,r} \le -1-m$. In each permutation

$\sigma \in S_N$ of $\det(F_{i-j})$, the positive and negative mode excesses satisfy $e_+(\sigma) = \sum_{i-\sigma(i)>2}(i-\sigma(i)-2) \le H_+$ and $e_-(\sigma) = \sum_{i-\sigma(i)<-1}(-1-(i-\sigma(i))) \le H$, so $\deg_h p_{i,j} = 0$ and $\deg_s p_{i,j} \le H + H_+$. Multiplying $Q_{N,z} = \sum_{i+j\le D}(-1)^{i+j}p_{i,j}X_{i,j}$ by $d_D(\rho)$ yields the polynomial vector $N_{N,z}(h,s) = d_D(\rho)Q_{N,z}(h,s) \in \mathbb{Q}(z)[h,s]^{1\times d}$, in which every summand $p_{i,j}\frac{d_D(\rho)}{d_k(\rho)}(d_k(\rho)X_{i,j})$ ($k = i+j \le D$) satisfies $\deg_h \le (D-k)+2k \le 2D$, $\deg_s \le (H+H_+)+(D+k) \le 2D+H+H_+$, and $\deg_{(h,s)} \le 2D+H+H_+$. Because $\rho(h,s) = h + H + N(1-N-s)$ is a single linear functional, the D normal-jet hyperplanes $L_r(h,s) = r - \rho(h,s) = 0$ ($r = 1,\dots,D$) are strictly parallel and pairwise disjoint ($L_{r_1} - L_{r_2} = r_1 - r_2 \ne 0$); hence $Q_{N,z}$ has at most a simple pole along each $\rho = r$ and no higher-order normal-jet self-intersections.

Step 2: Coordinatewise residue recursion on an arbitrary column. Fix $r \in \{1,\dots,D\}$, fix $s \in \mathbb{C}$, vary $h(\rho) = \rho - H - N(1+\nu)$ near $\rho = r$, and take an arbitrary constant column $W_0 \in \mathbb{C}^d$ (not assumed to satisfy $BW_0 = 0$). Write $\widetilde{w}_k = \mathrm{Res}_{\rho=r}(w_k W_0)$ and $\widetilde{X}_{i,j} = \mathrm{Res}_{\rho=r}(X_{i,j}W_0)$. For $k < r$, $d_k(r) \ne 0$, so $\widetilde{w}_k = 0$ and $\widetilde{X}_{i,k-i} = 0$. At $k = r$, $\sum_{m=0}^{r-1} B_m w_{r-1-m} W_0$ is holomorphic at $\rho = r$, so

$$\widetilde{w}_r = -\frac{1}{r}B\Big|_{\rho=r}\sum_{m=0}^{r-1}B_m\Big|_{\rho=r}w_{r-1-m}\Big|_{\rho=r}W_0 = \alpha E_a + \beta E_b \in \mathrm{im}(B|_{\rho=r}) \subseteq \mathrm{span}(E_a, E_b)$$

for scalars α, β depending on (W_0, z, s). Because U_iW_0 and V_iW_0 at degree r depend only on degree $r-1$, both are holomorphic at $\rho = r$; hence $\widetilde{X}_{i,r-i} = 0$ for $0 < i < r$, while applying π_E to $\mathrm{Res}_{\rho=r}(r! w_r W_0)$ gives $\widetilde{X}_{r,0} = r!\alpha E_a$ and $\widetilde{X}_{0,r} = r!\beta E_b$. For every $k = r+1,\dots,D$, every operator in the degree-k step (B_m, $(kI-B)^{-1}$, S_0, G, π_E) is holomorphic at $\rho = r$, so $(\widetilde{w}_k, \widetilde{X}_{i,k-i})_{k=r}^{D}$ obeys the exact canonical degree-k recursion evaluated at $\rho = r$ initialized by $(\widetilde{w}_r, \widetilde{X}_{r,0}, \widetilde{X}_{0,r}) = (\alpha E_a + \beta E_b, r!\alpha E_a, r!\beta E_b)$ and zero at all lower degrees and mixed degree-r indices.

Step 3: Complexified pinch-simplex solutions and Weyl Vandermonde vanishing. Work initially on the nonempty open domain $\Omega = \{(g,\nu) \in \mathbb{C}^2 : \Re g > 2H+1,\ \Re\nu > 0\}$, with independent real variables $(a,\bar{a}) = (Nz+\epsilon_1, Nz+\epsilon_2)$, the open simplex $\Delta_N = \{y \in \mathbb{R}^N_{>0} : \sum_{m=1}^N y_m < 1\}$, and $\delta(z) = \min\big((1-z^2)/(4z),\ z^2(1-z^2)/(4(1+z^2))\big) > 0$. For $0 < \epsilon_1 < \delta(z)$ and $|\epsilon_2| < \delta(z)$, put $w_m = z + \epsilon_1 y_m$, $\Phi_a(w;a,\bar{a}) = (a - \sum_{m=1}^N w_m)^g(\sum_{m=1}^N w_m^{-1} - \bar{a})^g$, and for each sorted four-mode tuple $I = (j_1,\dots,j_N)$,

$$\Psi_{a,I}(a,\bar{a}) = \int_{\Delta_N}\Phi_a(w;a,\bar{a})\prod_{m=1}^N w_m^{j_m}D_z(w_m)^\nu\,\frac{dw_m}{w_m}.$$

Every power base $a - \sum w_m$, $\sum w_m^{-1} - \bar{a}$, $1 - zw_m$, and $1 - z/w_m$ is strictly positive on Δ_N. Direct differentiation gives $\partial_{w_m}\Phi_a = (-\partial_a + w_m^{-2}\partial_{\bar{a}})\Phi_a$, $a\partial_a\Phi_a = g\Phi_a + (\sum w_m)\partial_a\Phi_a$, and $\bar{a}\partial_{\bar{a}}\Phi_a = g\Phi_a + (\sum w_m^{-1})\partial_{\bar{a}}\Phi_a$. For any $p+q < 2H$ and any m, holding $(w_k)_{k\ne m}$ fixed leaves $w_m \in (z, a - \sum_{k\ne m} w_k)$, where $D_z(w_m)^{\nu+1} = 0$ at $w_m = z$ ($\Re(\nu+1) > 1$) and $\partial_a^p\partial_{\bar{a}}^q\Phi_a = 0$ at the upper endpoint ($\Re(g-p) > 1$). Fubini's theorem therefore yields $\int_{\Delta_N}\partial_{w_m}(w_m^j D_z(w_m)^{\nu+1}\partial_a^p\partial_{\bar{a}}^q\Phi_a)\,dw_m = 0$, which reproduces (10.4) verbatim with $t = -\partial_a$ and $u = -\partial_{\bar{a}}$. Consequently Ψ_a satisfies the exact two-dimensional displacement PDE $(L + \mathrm{diag}(\epsilon_1 I, \epsilon_2 I))(\partial_a\Psi_a, \partial_{\bar{a}}\Psi_a)^{\mathsf{T}} = G\Psi_a$, and along $\epsilon_1 = \epsilon_2 = \epsilon$ satisfies the exact normal ODE $\partial_\epsilon\Psi_a = (B/\epsilon + \sum_{m\ge0} B_m\epsilon^m)\Psi_a$.

Divide Ψ_a by the $(a,\bar{a})$-independent Dirichlet constant $C(g,\nu,z) = [N(z^{-1}-z)]^g z^{-N(1+\nu)}(1-z^2)^{N\nu}\Gamma(g+1)\Gamma(\nu+1)^N/\Gamma(\rho+1)$ to form $\widehat{\Psi}_a = \Psi_a/C$. Under $w_m = z + \epsilon_1 y_m$, the remaining holomorphic factor expands uniformly on $\overline{\Delta_N}$ as $\sum_{p,q\ge0} P_{I,p,q}(y;g,\nu,z)\epsilon_1^p\epsilon_2^q$ with $P_{I,0,0} = 1$ and each $P_{I,p,q}$ homogeneous of degree p in y over $\mathbb{Q}(z)[g,\nu]$. Integrating monomials against the normalized Dirichlet measure on Δ_N gives

$$\widehat{\Psi}_a(Nz+\epsilon_1, Nz+\epsilon_2) = \epsilon_1^\rho\sum_{p,q\ge0}c_{p,q}^{(a)}(g,\nu,z)\epsilon_1^p\epsilon_2^q, \qquad c_{0,0}^{(a)} = E_a, \qquad c_{p,q}^{(a)} \in \frac{1}{(\rho+1)_p}\,\mathbb{Q}(z)[g,\nu]^d.$$

Symmetrically, for $0 < \epsilon_2 < \delta(z)$ and $|\epsilon_1| < \delta(z)$, setting $w_m = v_m^{-1}$ with $v_m = z + \epsilon_2 y_m$, $\Phi_b(w;a,\bar{a}) = (\sum w_m - a)^g(\bar{a} - \sum w_m^{-1})^g$, and $\Psi_{b,I} = \int_{\Delta_N}\Phi_b(v^{-1};a,\bar{a})\prod v_m^{-j_m}D_z(v_m)^\nu\,dv_m/v_m$ satisfies the identical $\partial_{w_m}, a\partial_a, \bar{a}\partial_{\bar{a}}$ identities and $D_z(w_m) = D_z(v_m)$, $w_m\partial_{w_m} = -v_m\partial_{v_m}$, so $\widehat{\Psi}_b = \Psi_b/C$ satisfies the exact same displacement PDE and normal ODE with expansion $\widehat{\Psi}_b = \epsilon_2^\rho\sum_{p,q\ge0}c_{p,q}^{(b)}\epsilon_1^p\epsilon_2^q$, $c_{0,0}^{(b)} = E_b$, $c_{p,q}^{(b)} \in (\rho+1)_q^{-1}\mathbb{Q}(z)[g,\nu]^d$.

Now apply $\mathcal{L}_{\det} = \sum_{0\le i+j\le D}(-1)^{i+j}p_{i,j}(z,s)\partial_a^i\partial_{\bar{a}}^j$ to Ψ_a on Ω. In Theorem 10.6's clearing of $(tu)^H\det(F_{i-j})$, every permutation $\sigma \in S_N$ is reduced separately using nonnegative powers of $t = -\partial_a$ and $u = -\partial_{\bar{a}}$, and

each application of (10.4) preserves total degree $\le 2H$ in (t,u). Every single-variable integration-by-parts step therefore holds on Δ_N for $(g,\nu)\in\Omega$, giving

$$\mathcal{L}_{\det}[\Psi_a](a,\bar a)=(-\partial_a)^H(-\partial_{\bar a})^H\int_{\Delta_N}\Phi_a(w;a,\bar a)\left(\sum_{\sigma\in S_N}\operatorname{sgn}(\sigma)\prod_{m=1}^{N}w_m^{m-\sigma(m)}\right)\prod_{m=1}^{N}D_z(w_m)^{\nu}\,\frac{dw_m}{w_m}.$$

By S_N-symmetry of Δ_N, Φ_a, and the product weight, averaging over permutations replaces the inner sum by $\frac{1}{N!}\Delta(w)\Delta(w^{-1})=\frac{(-1)^{\binom{N}{2}}}{N!}(\prod w_k^{-(N-1)})\Delta(w)^2$. Under $w_m=z+\epsilon_1 y_m$, $\Delta(w)^2=\epsilon_1^{N(N-1)}\Delta(y)^2$, $(-\partial_a)^H(-\partial_{\bar a})^H\Phi_a$ supplies ϵ_1^{g-H}, and the measure supplies $\epsilon_1^{N(\nu+1)}$. Dividing by $C(g,\nu,z)$ gives $\mathcal{L}_{\det}[\widehat\Psi_a]=\epsilon_1^{\rho+N(N-1)-H}\Theta_a(\epsilon_1,\epsilon_2)$ with Θ_a holomorphic near $(0,0)$. On the other hand, termwise differentiation yields $\mathcal{L}_{\det}[\widehat\Psi_a]=\epsilon_1^{\rho-2H}\sum_{m,n\ge0}d^{(a)}_{m,n}(g,\nu,z)\epsilon_1^m\epsilon_2^n$, where

$$d^{(a)}_{m,n}(g,\nu,z)=\sum_{\substack{0\le i+j\le 2H\\ m-2H+i\ge0}}(-1)^{i+j}p_{i,j}(z,s)\,(\rho+m-2H+i)^{\underline{i}}\,(n+j)^{\underline{j}}\,c^{(a)}_{m-2H+i,\,n+j}(g,\nu,z)\in\frac{1}{(\rho+1)_m}\,\mathbb{Q}(z)[g,\nu].$$

Comparing powers of ϵ_1 on the open set Ω forces the rational identity $d^{(a)}_{m,n}\equiv0$ in $\mathbb{Q}(z,g,\nu)$ for all $m<H+N(N-1)$ and all $n\ge0$. Symmetrically, $\Delta(v^{-1})\Delta(v)=(-1)^{\binom{N}{2}}(\prod v_k^{-(N-1)})\epsilon_2^{N(N-1)}\Delta(y)^2$ forces $d^{(b)}_{m,n}\equiv0$ for all $n<H+N(N-1)$ and all $m\ge0$.

Step 4: Specialization, residue vanishing, and bidegree proof. Fix $r\in\{1,\dots,D\}$. Because all coefficient denominators $(\rho+1)_p$ and $(\rho+1)_q$ are nonzero at $\rho=r\ge1$, every finite-jet PDE and normal-ODE identity through degree D specializes algebraically from Ω to $\rho=r$. Setting $w_k^{(a)}=\sum_{p+q=k-r}c^{(a)}_{p,q}|_{\rho=r}$, $X^{(a)}_{i,j}=i!j!\,c^{(a)}_{i-r,j}|_{\rho=r}$ ($i\ge r$, else 0) and symmetrically $w_k^{(b)}=\sum_{p+q=k-r}c^{(b)}_{p,q}|_{\rho=r}$, $X^{(b)}_{i,j}=i!j!\,c^{(b)}_{i,j-r}|_{\rho=r}$ ($j\ge r$, else 0), the linear combination $w_k^*=\alpha w_k^{(a)}+\beta w_k^{(b)}$, $X^*_{i,j}=\alpha X^{(a)}_{i,j}+\beta X^{(b)}_{i,j}$ matches $(\widetilde w_k,\widetilde X_{i,j})$ of Step 2 through degree r and satisfies the exact PDE and normal-ODE compatibility relations at every degree $k=r+1,\dots,D$ (so $V_i^*-U_i^*$ and $k!w_k^*-U_k^*-V_0^*-\sum_{i=1}^{k-1}\binom{k}{i}X^*_{i,k-i}$ lie genuinely in $\operatorname{span}(E_a,E_b)$, recovered identically by π_E, with $kI-B|_{\rho=r}$ invertible). By induction on $k=r+1,\dots,D$, $\operatorname{Res}_{\rho=r}(X_{i,j}W_0)=X^*_{i,j}$ for all $i+j\le D$.

Now evaluate $d^{(a)}_{2H-r,0}|_{\rho=r}$ and $d^{(b)}_{0,2H-r}|_{\rho=r}$. For every $N\ge3$ and $r\in\{1,\dots,2H\}$, $2H-r<2H<H+N(N-1)$ (since $N(N-1)-H\ge(N-1)(3N+1)/4\ge5$), and at $\rho=r$, $(r+i-r)^{\underline i}=i!$, $j^{\underline j}=j!$. Therefore

$$\operatorname{Res}_{\rho=r}\big(Q_{N,z}(h,s)W_0\big)=\alpha\,d^{(a)}_{2H-r,0}\Big|_{\rho=r}+\beta\,d^{(b)}_{0,2H-r}\Big|_{\rho=r}=0.$$

Since $W_0\in\mathbb{C}^d$ and $r\in\{1,\dots,D\}$ are arbitrary, and $\partial_h d_D(\rho)|_{\rho=r}=-\prod_{m\ne r}(m-r)\ne0$, every coordinate of $N_{N,z}(h,s)=d_D(\rho)Q_{N,z}(h,s)$ vanishes identically along each hyperplane $L_r(h,s)=0$. Viewing each entry in $(\mathbb{Q}(z)[s])[h]$, the monic-up-to-sign linear factor $L_r(h,s)$ divides $N_{N,z}(h,s)$ in $\mathbb{Q}(z)[h,s]$. Because $L_1,\dots,L_D$ are pairwise non-associate irreducibles in the unique factorization domain $\mathbb{Q}(z)[h,s]$, their product $d_D(\rho)$ divides $N_{N,z}(h,s)$ in $\mathbb{Q}(z)[h,s]^{1\times d}$, proving $Q_{N,z}(h,s)\in\mathbb{Q}(z)[h,s]^{1\times d}$. Since $\mathbb{Q}(z)[h,s]$ is an integral domain and $\deg_h d_D=\deg_s d_D=\deg_{(h,s)}d_D=D$ (leading terms $(-1)^Dh^D$ and N^Ds^D), dividing $N_{N,z}$ by $d_D(\rho)$ subtracts D from each bound of Step 1, proving $\deg_h Q_{N,z}\le D$, $\deg_s Q_{N,z}\le D+H+H_+$, and $\deg_{(h,s)}Q_{N,z}\le D+H+H_+$.

For (ii), both $T_N(h,s;z)$ and $\frac{(1-z^2)^{N^2+2Ns}}{(h+1)_H^2}Q_{N,z}(h,s)W_g(Nz;z)$ are holomorphic on $\{\Re h>-1\}\times\mathbb{C}$ (including at every transverse intersection of $\{\rho=r\}$ with $\{\cos\vartheta(h)=0\}$, where $(h+1)_H^2\ne0$) and agree off $\bigcup_{r=1}^D\{\rho=r\}$ by Theorem 10.6; hence they agree everywhere on $\{\Re h>-1\}\times\mathbb{C}$. Part (iii) follows immediately from $\deg_h Q_{N,z}\le D$, and the shortcut contrast follows because Theorem 23.1's zero-injection shortcut drops arbitrary normal-jet corrections off the resonance hyperplanes: at $N=3,4$ only the h-independent top grade at $r=D-V_N\le1$ can enter, whereas for $N\ge5$ ($D-V_N\ge3$) lower h-dependent grades enter at $1\le r<D-V_N$ and vanish only on the resonance hyperplane $\rho=r$, not off it. □

Computational consistency checks (not part of the proof). Independent exact calculations over the two prime fields $P_1=1{,}000{,}003$ and $P_2=1{,}000{,}033$ confirm every assertion of Theorem 23.1A at ranks $N=3,4,5,6$ ($d=20,35,56,84$; $D=2,4,8,12$) for $(z,s)=(7/19,-41/13)$ and at $N=3,4,5$ for $(z,s)=(11/25,-17/7)$: all D residues $\operatorname{Res}_{\rho=r}(Q_{N,z})$ vanish identically on all d coordinates despite nonzero pre-contraction $\operatorname{Res}(w_r)$, all residue

jets satisfy exact PDE compatibility, and Lagrange interpolation confirms polynomiality at held-out points with observed degrees $\deg_h = 2,4,7,10 \le D$ and $\deg_s = 2,4,7 \le D + H + H_+$ ($N = 3,4,5$). At $N = 5$, testing Theorem 23.1's zero-injection shortcut at $(z,s,h) = (7/19, -41/13, 200)$ confirms that injections are killed for $r = 3,\dots,8$ ($D - V_5 = 3$) but fail at $r = 2$ (on E_b) and $r = 1$ (on both E_a and E_b); on the published rank-five checkpoint $(z,h,s) = (2/7,2,-5)$ of Theorem 10.6, the canonical row reproduces 34402/2401 while the shortcut fails on all 56 entries. Finally, at the previously open rank-five resonances $(z,s) = (2/7,-3)$ ($\nu = -2$, $\rho = h-1$) for $h = 2,3,4$ ($\rho = 1,2,3$), degree-8 Lagrange interpolation of the canonical row matches the direct $U(5)$ Toeplitz determinant identically over both primes (including the exact rational check $U_2(10/7;2/7) = 31582754/4100625$ at $\rho = 1$), whereas the zero-injection shortcut fails on all three.

Theorem 23.2 (readout at simultaneous exceptions and endpoint bounds). On the connection charts of Theorem 10.9 at any rank $N \ge 3$ and any regular exit endpoint $0 < z < 1$ off (10.9), perform the ordinary or derivative physical connection on the compact angular state, then apply the regular canonical row $\ell = \ell_{N,z}(h,s)$ of Theorem 23.1A (which agrees with Theorem 23.1's row at ranks three and four). Normal-jet resonance requires no modification of the connection weights. At a simple exceptional connection order the order derivative is the total derivative of the phase-weighted branch numerator, including differentiated incoming preparation. Equivalently one may first multiply both branches by the same analytic ℓ. In the derivative formula the term differentiating the common row multiplies a zero vector on the physical input. This argument applies at a simultaneous resonance and also along arbitrary analytic tilt slices through it. Any error ϵ in each coordinate of the connected physical state contributes at most $\|\ell\|_1\epsilon$ to the absolute scalar error, before endpoint arithmetic. The executed numerical row one-norm bounds below remain specific to the recorded rank-three and rank-four charts.

On $|h-e| \le 1/64$, $|s-s_c| \le 1/512$, use $(e,s_c) = (3/2,-11/6)$ at rank three, $(2,-3)$ at rank four. These sets contain the intersections with the top normal divisor ($\rho = 2,4$ respectively). The uniform row one-norm bounds at the entry and exit of the established arcs are

Rank	Entry z	Entry bound	Exit z	Exit bound
3	13/50	71.956	2/5	309.385
4	11/25	17979.989	14/25	2.713296×10^9

Proof and computational verification. Theorem 23.1A (and Theorem 23.1 at ranks three and four) gives the same finite physical linear map on each branch at every rank $N \ge 3$ and every regular exit endpoint off (10.9). Theorem 10.9 applied componentwise and holomorphy at the two regular fibres justify the connection and its derivative. Write $Q = \sum_{i,j} q_{ij}(h-e)^i(s-s_c)^j$. The degree bound and rectangular rational interpolation recover these finite row coefficients exactly. The four charts were constructed over $\mathbb{Q}$ and checked at a held-out rational pair. For radii r_h, r_s as above, apply the triangle inequality to the polynomial and use

$$\|\ell\|_1 \le \frac{(1-z^2)^{N^2+2N(s_c-r_s)}}{\prod_{m=1}^{H}(e+m-r_h)^2} \sum_{i,j} \|q_{ij}\|_1 r_h^i r_s^j.$$

The sum and the denominator are rational. Outward rounding of the prefactor and final bound gives the entries in the table. These are error-amplification bounds for physical recovery. □

Checks and failure controls. As a separate test at the four rational endpoints, injecting every possible pair of free coefficients and checking the resulting polynomial rows directly gives 40 exact zero entries per rank-three endpoint and 384 per rank-four endpoint. The grid sizes are fixed by polynomial degrees, and this check uses the original full group inverse rather than the graded equations. At rank four a deliberate omission of the degree-four contribution to the upper degree-one test leaves K. At $z = 14/25$, $s = -49/16 + i/16$, its modulus exceeds 0.0003987. This fault is invisible on the special real tilt $s = -3$.

The missing full normal coordinates can be measured independently. At $s = 1-N$ the one-angle preparation is the Poisson kernel divided by $1-z^2$. Finite Fourier sums for the physical projected Taylor coefficient $(B/\rho)w_\rho$ give, in the (E_a,E_b) basis, $(1148125/388962, -340000/194481)$ at $(N,z,h) = (3,2/5,1)$ and $(77696791142187500/79111575131589, -1313938675000000/538173980487)$ at $(4,14/25,2)$. Zeroing either supplementary coefficient changes that jet. For the same inputs the quotient scalar and the separately expanded original determinant agree in exact rationals, respectively 640625/194481 and

309308841824531555175781250/492170557240509868475469. Dropping the preparation prefactor gives 41/21 and 8302946/268125.

Independent determinant and compact-mode quadratures with 800-bit arithmetic were also run on both sides of each critical radius at $h = 7/4 + i/4$. On the top normal divisor take $s = -7/4 + i/12$ at rank three and $s = -49/16 + i/16$ at rank four. Additional tests displace each tilt by 2^{-20}. All pairs overlap. Resolution matters here. At the rank-four exit, the 32-node full-mode Hermite error propagated through the row exceeds 4.09×10^4, whereas the direct determinant has absolute error below 7.16×10^{-5}. Overlap in this case supplies little discrimination and the wide enclosure fails to exclude the incorrect preparation normalization. In contrast, at the joint integer case the finite polynomial quadratures have zero analytic tail; equality also follows from the exact Poisson computation above. The scripts and receipts include the widths for every tested input.

For the arbitrary-rank degree estimate, a separate exact test uses $z = 7/19$, $s = -41/13$, $(\xi, \eta) = (3/7, -10/9)$, and the basic perturbation direction $(2/5, -2, 1/11, 3/4)$. For both choices of x the first nonzero total degrees at ranks three through nine are $2, 3, 5, 7, 9, 12, 15$, respectively, attaining V_N on these examples. Adding a unit term to the constant outermost Toeplitz mode gives first degrees $1, 2, 3, 5, 7, 9, 12$. This control tests the dependence on the geometric preparation in the determinant. Attainment of the total-degree bound leaves open further cancellations in the final contracted scalar, as the rank-four K calculation illustrates.

A single order contour through two exceptional sets

Theorem 23.3 (two-path scalar recovery on joint order and tilt disks). Use the two polygonal paths of Theorem 10.15. Let $(e, s_\dagger) = (3/2, -11/6)$ at rank three and $(2, -3)$ at rank four. On the independent closed product

$$|h - e| \le r = 1/256, \qquad |s - s_\dagger| \le d = 1/512$$

the physical, unnormalized $T_N(h, s; z_r)$ can be recovered from sixteen order samples, each using independently prepared incoming data and both full radius paths. Uniform errors about the computed value are below 1.334×10^{-30} at rank three and 1.139×10^{-25} at rank four. Eight samples give bounds 9.620×10^{-15} and 3.206×10^{-11}. These are absolute-error guarantees for the finite algorithms. The full sixteen-order runs have not been executed. The construction also works with the original cleared row before any elimination of normal coordinates.

Proof. Put $H = \lfloor (N-1)^2/4 \rfloor$, $u = h - e$ and $v = s - s_\dagger$. The normal exponent is $2H + u - Nv$. The connection vanishes in its denominator at $u = 0$, and the top normal divisor vanishes at $u = Nv$. The polydisk contains both divisors, their intersection, and points with two nonreal exponents on the normal divisor. On the single sampling circle $|u| = a = 1/64$ the top divisor has modulus at least $a - Nd$; each lower one has modulus at least $2H - j - a - Nd$. The ordinary denominators $(h+1)_H$ are bounded away from zero there. The same circle avoids the vanishing sine in Theorem 10.16. Both arc values contribute with their physical phases and the sum of the absolute weights is at most

$$P_a = \frac{e^{\pi a}}{\pi a[2 - \sinh(\pi a)/(\pi a)]} < 21.406.$$

These facts only concern the samples. At the query the algorithm evaluates a polynomial in u and never divides by either exceptional factor.

Keep s fixed in its disk. With $R = 3 - e$, the function $f(u) = T_N(e + u, s; z_r)$ is holomorphic on a neighborhood of $|u| \le R$. On that disk its modulus is bounded by

$$M = \sum_{\sigma = s_\dagger \pm d} \left[T_N(0, \sigma; z_r) + T_N(3, \sigma; z_r) \right].$$

Indeed $0 \le \operatorname{Re}(e + u) \le 3$, $x^{2\operatorname{Re}(e+u)} \le 1 + x^6$, and the sum of the two real preparations bounds the variation of the complex preparation pointwise whether $|\Lambda_N|$ is smaller or greater than one. Integer determinant jets, including all prefactors, give $M < 69.216$ and $M < 8988$, respectively. The proof uses the original Haar scalar to bound the *growth* of the interpoland. Its samples are supplied by the transported full state. If m equally spaced values on the circle each have error at most η, compute the normalized discrete Fourier coefficients of nonnegative indices below m and evaluate the resulting polynomial at u/a. Taylor's formula, Cauchy coefficient bounds, and the alias identity give the error bound

$$M\mathcal{E}(m, a, r, R) + \frac{\eta}{1 - r/a}, \qquad \mathcal{E}(m, a, r, R) = \frac{(r/R)^m + (a/R)^m/[1 - (a/R)^m]}{1 - r/R}.$$

For example, the discrete coefficient at index k adds the terms of indices $k+lm$, $l \geq 1$. Summing their majorants over k gives the second term of $\mathcal{E}$. The exact numerator cancellation and angular compatibility are retained through holomorphy of the physical scalar. Separate unrestricted columns need not have these continuations.

Here the new tilt centers lie outside the physical parameter disks of Theorem 21.12. To bound the full matrices, return to the affine generator and the Euclidean signed contiguous-product proof of Theorem 10.15. Write $U = |e - h_*| + a$, $V = |s_\dagger - s_*| + d$. In each previous complex-time bound D_i at radii $(1, 1/2)$ replace D_i by $D_i \max(1, U, 2V)$: each of its three norm majorants is nonnegative. The denominator, paths and rational frame are parameter-independent. At real time use the previously verified three separate bounds for the logarithmic norm and the two coefficient directions with the new multipliers U, V. In the signed-product recursion the per-panel perturbation is at most $e^{\mu_i}(e^{Up_i+Vq_i} - 1) + \epsilon_i$, with ϵ_i the center-panel error. For the Taylor approximation, add $\sqrt{\binom{N+3}{3}} \exp(D_i \max(1, U, 2V))2^{-m_z}$ for each panel since its verified time-radius ratio is at least two. Applying the same product recursion and telescoping its tails yields the following bounds for either path. All 64 panels and both paths are included.

N	Taylor degree m_z	canonical transfer norm	transfer truncation error	norm of original scalar row on sampling circle
3	420	1.092×10^{9}	5.052×10^{-113}	3.709×10^{6}
4	1260	2.324×10^{75}	2.425×10^{-167}	1.754×10^{15}

For the last column, apply the finite coefficient norm sum of Proposition 21.11 and divide by the lower bounds on the *circle*, including $a - Nd$. This deliberately allows loss of compatibility digits in the row. Exact elimination elsewhere in this section gives much smaller row bounds. Let K, τ, P be the respective certified transfer norm, tail and row norm from the receipt, and put $B = [N(1 + z_l)]^{2(e+a+H)}(1 - z_l)^{2N(-N-s_\dagger-d)}$. This bounds the uniform incoming vector componentwise. Choose $w = 10^{-33}(1 - r/a)/[20(1 + P)(1 + P_a)]$. Compute a dyadic incoming center with error at most $w/(1 + K)$, including its arithmetic, and evaluate each real-time Taylor product with final arithmetic radius at most w per component. The scalar node error is bounded by

$$\eta = PP_a\{Kw/(1 + K) + \tau[B + w/(1 + K)] + w\} + 10^{-33}/20.$$

The final term covers node contraction, and a further $10^{-33}/20$ covers polynomial evaluation. All finite arithmetic can be refined until these absolute tolerances hold, including evaluation of algebraic circle nodes. Positive denominators on the sampled paths establish termination for computable inputs with the specified disk membership.

A finite incoming rule attaining these tolerances can be given without a large tensor mesh. In the Fourier–Mellin rule of Proposition 21.11, now $|N + s| < 2$. Each half-factor binomial coefficient has modulus at most $(2)_j/j! = j + 1$. For $z = z_l$ the modulus of the Fourier coefficient of index $j \geq 0$ is therefore at most $z^j(A + jB_1)$ with $A = (1 + z^2)/(1 - z^2)^3$, $B_1 = (1 - z^2)^{-2}$, by summation of $(k + 1)(k + j + 1)z^{2k}$. The sum of the two tails after index b is at most

$$2z^{b+1}\left[\frac{A + (b + 1)B_1}{1 - z} + \frac{B_1 z}{(1 - z)^2}\right].$$

Use this bound for both Fourier cutoffs and $(1 - z)^{-2(|N+s_\dagger|+d)}$ for the total Fourier mass. Use $g_\pm = e + H \pm a$ in the Mellin and origin bounds. In the inherited deep signed-tail estimate, the largest Bessel order is $N(b + 2)$ and the smallest frequency scale is $\min(1, Nz)$. No conjugation is applied to the complex Fourier preparation. Substituting in the five error estimates of Proposition 21.11 gives the following total analytic angular errors, before arithmetic.

N	Fourier cutoffs	signed-tail order	terminal frequency	Gauss nodes per panel / central degree	panels	analytic input error
3	$150, 75$	100	4098	$85, 66$	518	1.028×10^{-61}
4	$450, 270$	190	65538	$154, 130$	8198	1.165×10^{-133}

The required total incoming errors are at least 4.13×10^{-52} and 4.11×10^{-127} respectively. Rounding is separately tested against the available margin. Sampling several orders at one tilt reuses every finite-frequency Bessel vector. Rank four still requires 1,262,492 such vectors per tilt and a signed-tail convolution at order 190. The budget computation was executed and its conservative cost is substantial. This completes the uniform guarantee. □

Proposition 23.4 (executed rank-four crossing with an order correction). On the rank-four polydisk of Theorem 23.3, an explicit stored approximant has absolute error below 1.403×10^{-8}. It crosses at order two and restores the requested complex order by an angular integral on the outgoing real fibre. It computes the physical scalar over the polydisk. Individual branch values at off-slice orders require the fixed-parameter calculation of Theorem 23.3.

Construction and proof. Use $m = 8$ equally spaced tilts at distance $1/128$ from -3. At each tilt propagate the seven Fourier modes and their seven scaled derivatives along *both* paths on the order-two slice as in the rank-four factorization below. Their products lift to the full 35-component physical column. Both endpoint scalar values on this slice agree by the integer-order identity. These independently initialized sixteen paths give the scalar anchor $T_N(2, s; z_r)$ at each tilt. The remaining observable is explicit. With $D = N(1 + z_r)$ and $x = |S_N|^2/D^2$, integrate

$$F_u(x) = D^4 x^2[(D^2x)^u - 1], \quad F_u'(x) = D^4 x\{2[(D^2x)^u - 1] + u(D^2x)^u\}$$

under the same complex tilt. Its addition to the anchor is exactly $T_N(2 + u, s; z_r)$ and $F_0 = 0$. The subtraction at fixed preparation prevents an independent error in the normalization of the anchor.

Use the degree-135 open Hermite interpolant at $k = 68$ Legendre nodes, integrating its value and slope cardinal polynomials by the directional determinant jets of Section 21. For comparison use $\gamma = 7/4$ and the constant-sign closed/open bracket from (21.6). The quadrature reproduces the subtracted x^2 exactly. For $|u| \le r$, the derivative-product constant including radial scaling is at most

$$|u| D^{2(2+r)} \frac{\prod_{0 \le j < 2k,\ j \ne 2} (|2 - j| + r)}{|(-\gamma)_{2k}|}.$$

This follows by removing just the factor $-u$ before taking absolute values. Integrate the comparator gap against the real tilt $\operatorname{Re} s$ of each sample and multiply by this bound. This treats the variation of the complex preparation and also preserves the exact zero at $u = 0$. Apply the degree-seven tilt Fourier interpolant to the sums of anchor and correction. On the larger tilt circle of radius one and $|h - 2| \le 1$, the positive determinant majorant in the preceding proof, with real tilts $-4, -2$, is below 185643. The tilt alias error is at most 2.582×10^{-12}. The transported anchors and serialized cardinal tables contribute less than 10^{-60}. The corrected angular sample errors, after tilt interpolation, contribute less than $3.591 \times 10^{-6}|u|$. Evaluating the saved approximation with final arithmetic radius below 10^{-12} gives the stated bound, using the unrounded constants in its receipt. User-facing centers must also include decimal formatting error. A 46-node run gave 1.384×10^{-7} by the same calculation.

Executed controls. The 68-node construction took 198.148 seconds at 1300 bits, the 46-node run 61.393 seconds at 1000 bits, on the recorded host. Per sample it checked all 35 lifted entries between the two branches and checked the anchor against a separate determinant. Held-out checks included the joint exceptional point, the phase divisor alone, the exact complex normal divisor $(h, s) = (2 + i/256, -3 + i/1024)$, and two independent boundary inputs. At $(2 + i/256, -3 + 1/512)$ the result is $624.63422528274 + 4.51509766585i$ with absolute error below 1.403×10^{-8} about this displayed center. Removing the order correction is separated from the direct enclosure by more than 4.5151. The independent exit check uses a fresh determinant at a different angular degree. The separate eight-by-eight determinant tables at both entry and exit give uniformly enclosed scalar comparators across each rank's full two-parameter polydisk. At rank three their errors are below 7.026×10^{-5}

and 1.033×10^{-4}; at rank four they are below 9.103×10^{-6} and 2.798×10^{-5}. They also reject removal of the preparation prefactor on the recorded test inputs. These comparators alone supply no evidence of propagation of an arbitrary starting vector. □

One connected tilt region containing all four intersections. The same construction was executed on the larger product

$$|h-2| \le 1/16, \qquad |s+25/8| \le 29/32.$$

It returns the physical scalar at $z_r = .56$ with uniform absolute error below 2.890×10^{-4}. At $h = 2$ the four intersections are $s = -2 - j/4$ for $j = 1, 2, 3, 4$. Each of the corresponding complex normal divisors enters the interior of this region. The complete rank-four exceptional disk of Theorem 21.12 is also contained here, since $|-3.86+.21i+25/8|+1/16 < 29/32$. For this proof take a tilt sampling radius 17/16, 32 equally spaced samples and an analytic tilt radius of five about $-25/8$. On the sampling circle $|4+s| \le 31/16 < 2$, as required by the physical factorization. The analytic radius of five is used only for the scalar Haar growth bound at the real exit z_r. There $-65/8 \le \operatorname{Re} s \le 15/8$ and the two extreme real preparations majorize the variation for every complex tilt in the disk. At this radius the scalar majorant is below 1.449×10^{14}. The alias bound is below 5.320×10^{-8}. The larger tilt interpolation norm is $(1-(29/32)/(17/16))^{-1} = 34/5$. With 38 open Hermite nodes the executed absolute budget before evaluation rounding was below 2.88927×10^{-4}. The 880-bit table build took 160.136 seconds, including 64 radius paths and the angular correction tables. For scale, the real-order moments at $h = 2$ on the two real edges of this tilt disk are approximately 21889.842605 and 67.312930. No positive lower bound for the modulus throughout the complex disk is used.

Separate inexpensive tables improve the error on smaller regions. For $|h-2| \le 1/256$, $|s+2+j/4| \le 1/512$, 46 Hermite nodes and eight tilts give absolute errors below 8.335×10^{-8}, 9.654×10^{-8} and 1.142×10^{-7} for $j = 1, 2, 3$ respectively, including a 10^{-12} final evaluation allowance. The finer $j = 4$ bound is given above. Finally the original disk $|h-2| \le 1/16$, $|s+3.86-.21i| \le 1/16$ has its own executed 16-tilt, 46-Hermite-node table with absolute error below 1.844×10^{-5}, built in 144.673 seconds. These computations vary the order after crossing at $h = 2$. They have their own error budgets; the fixed-parameter 56-order algorithm in Theorem 21.12 remains a separate, unexecuted full query.

Implementation checks on the fixed-parameter alternative. A reduced-size two-order streaming source was compared component by component with the separate single-order integral, and with an independent angular Hermite enclosure, at both ranks. The first cutoff of 66 had too wide a tail to exclude an intentionally misnormalized source. Increasing it to 258 separated the wrong preparation and gave overlap on all correct components. Its rank-four source bound was still larger than two, so this inexpensive test verifies the implementations and normalizations without establishing high input accuracy. On each upper and lower path an off-centre Taylor panel was independently enclosed, testing all 400 or 1225 matrix entries. The connected-region table was independently checked at the four exact intersections, four nonreal exact normal incidences $h = 2 + i/16$, $s = -2 - j/4 + i/64$, and five further old-region and outer-boundary inputs. In each off-slice case omitting the angular order correction was distinguishable from the direct enclosure. These tests complement the finite budget calculations and the physically prepared paths reported separately.

Integer order as a physical invariant subspace

Theorem 23.5 (rank-four propagation on the exceptional order). Take the upper and lower polygons from 11/25 to 14/25 through $1/2 \pm 3i/50$. At $h = 2$, the angularly prepared solution on each path has a representation by seven two-component linear equations, valid for every complex s. Its polynomial readouts give the entire 35-component physical vector and the original scalar at the exit. On the closed disk $|4+s| \le 2$, the scheme below gives uniform absolute approximation errors smaller than 5.055×10^{-68} per physical component and 1.358×10^{-64} for the scalar, including the specified arithmetic allowances. This includes all four normal divisors on this order slice. The theorem concerns the values on the slice. Order derivatives contain additional information.

Proof. Set $a = 4+s$ and use the analytic branches at $z = 0$. For one uniform unit phase w define the coefficients of $(1-zw)^{-a}(1-z/w)^{-a}$ by

$$f_l(z) = \sum_{k \ge 0} \frac{(a)_k (a)_{k+l}}{k!(k+l)!} z^{2k+l}, \qquad f_{-l} = f_l \quad (l \ge 0).$$

Let $D = z\partial_z$. The coefficient ratios, also valid by polynomial continuation when a numerator vanishes, give

$$(D^2 - l^2) f_l = z^2 \{(D + 2a)^2 - l^2\} f_l.$$

The equations have no singularity on either polygon. To specify their output put $A = 4z$, $Z = \sum_{j=1}^{4} w_j$, and define a product linear functional I_z on Laurent monomials by $I_z(w^m) = \prod_j f_{|m_j|}(z)$. The raised tagged states and physical scalar are

$$W_m = I_z \left[w^m \{(A - Z)(A - \sum_j w_j^{-1})\}^4 \right],$$

$$T_4 = (1 - z^2)^{16+8s} \sum_{\pi \in S_4} \operatorname{sgn}(\pi) I_z \left[w^{\pi - \mathrm{id}} \{(A - Z)(A - \sum_j w_j^{-1})\}^2 \right].$$

These formulas follow by expansion of the angular preparation and of the squared Vandermonde in the Weyl integral. Symmetry reduces the two permutations in the latter to one and cancels the factor 4!. The 35 sorted four-mode tags require $0 \le l \le 6$ and the scalar requires $l \le 5$. The source assigns all factors, including their incoming derivatives, before either branch is evaluated. Holomorphy on $|z| < 1$ identifies the two analytic continuations with these readouts by uniqueness. At $h = 2$, each arc state and the physical exit state therefore agree. In the derivative connection of Theorem 10.9, written in regular form in Theorem 10.16, substitution implies $\partial_h W_+ = \partial_h W_-$ for the *total* prepared derivatives. This equality applies at every tilt. It permits an exact replacement of the derivative difference by zero for this particular order and preparation. The equality does not extend to the derivative of the physical exit germ, as the explicit comparison in Theorem 10.17 shows.

For the computational bounds use $U = (f_l, D f_l/6)^t$. In z time its numerator and denominator are

$$B_l(z) = \begin{pmatrix} 0 & 6(1 - z^2) \\ [l^2(1 - z^2) + 4a^2 z^2]/6 & 4az^2 \end{pmatrix}, \qquad q(z) = z(1 - z^2).$$

Divide each leg into eight equal panels of length v in modulus. On the complex disk of radius $R = 1/8$ around every panel centre at its left endpoint one has $.31 < |z| \le .685$, since the endpoints of the polygon have modulus at most .56. Uniformly for all seven modes the elementary row-sum bound gives $\|B_l/q\|_\infty < 83.995 = K_0$. In particular, with $r = .685$ and $A_0 = 2$ an admissible sharper K is the larger of

$$\frac{6(1 + r^2)}{.31(1 - r^2)}, \qquad \frac{[36(1 + r^2) + 4A_0^2 r^2]/6 + 4A_0 r^2}{.31(1 - r^2)}.$$

Taylor coefficients for the linear system are obtained by multiplying its series by q. The left-hand scalar $q(z_0)(k+1)$ never vanishes. Write $t = v/R < .084853$ and use degree $m = 80$. The exact fundamental matrix from a panel's left endpoint has maximum norm e^{KR} on the disk, by integration on each radius. Its Taylor polynomial map at the right endpoint has norm at most $G = e^{Kv} + e^{KR} t^{m+1}/(1 - t) < 2.438$. The true physical solution admits the smaller disk bound $M = (1 - r)^{-4} \max(1, 4r/[6(1 - r)])$. Indeed the two analytic logarithms have absolute values at most $-\log(1 - r)$ and differentiation costs at most $4r/(1 - r)$. The physical Taylor tail is at most $Mt^{81}/(1 - t) < 2.683 \times 10^{-85}$. This separate use of the physical bound avoids treating a general solution with an arbitrary second initial value as an angular integral.

Initialize at .44 by truncating the displayed series at $k = 200$ and differentiating its terms. The half-factor coefficients obey $|(a)_k/k!| \le k + 1$. Both scaled source tails are bounded by $\frac{4}{3}(201 + 7)^3 (.44)^{402} < 5.587 \times 10^{-137}$, because consecutive cubic majorants decrease by a factor smaller than $1/4$. Materialize the rounded midpoint of each pair, charging at most 10^{-100} for its arithmetic ball. Do the same after each panel. If E_j bounds the error in this midpoint from the true input, then $E_{j+1} \le G E_j + Mt^{81}/(1 - t) + 10^{-100}$. All sixteen applications with the unrounded constants above give $E_{16} < 2.895 \times 10^{-79}$. The elementary row and scalar errors follow by telescoping the four one-body factors. Set $F = (1 - .56)^{-4}$, $A_1 = 4(1 + .56)$ and $E = E_{16}$. Before final readout rounding the bounds are respectively

$$4A_1^8 (F + E)^3 E < 5.054 \times 10^{-68}, \qquad 24(1 - .56^2)^{-32}\, 4A_1^4 (F + E)^3 E < 1.358 \times 10^{-64}.$$

The tighter unrounded scalar budget is 1.357163×10^{-64}. Evaluate the readouts on the dyadic centres to rounding radius at most 10^{-86} and charge 10^{-85} for the final averaging and decimal presentation. The stated bounds follow,

also for their physical average. Arb performs all arithmetic comparisons for the fixed inputs. For other exactly represented points in the tilt disk the code increases precision on a rounding-budget failure. This terminates at each rational complex input by positivity of the panel denominator bounds. Higher precision does not change the analytic remainder. The distinct errors on an interval of input tilts additionally depend on variation of the physical answer over that interval.

Independent checks in the original eigenangles. At both real endpoints we also evaluated the Haar observable in its original variables λ_j. For each pair u, v of weak compositions of 2 into four parts, and permutation displacement m, the original numerator contributes the multinomial coefficients, $(1-z^2)^4$, and a product of four integrals

$$\int_{\mathbb{T}} \lambda^{m_j+u_j-v_j}(1-z\lambda)^{s-u_j}(1-z/\lambda)^{s-v_j}\,d\mu(\lambda),$$

where μ is normalized arc length. This uses neither transported state nor Möbius radial readout. Cut each half series at degree 840. Cauchy's coefficient bound on radius .8 is $5^8(.8)^{-k}$ for these exponents. With $q_1 = z/.8$ and $B = 5^8/(1-q_1)$ the total omitted absolute value is bounded by $24 \cdot 4^4 \cdot 8B^8 q_1^{841}$. This bounds the original-angle integral separately for either entrance or exit. All 35 outgoing tagged components were also checked by independent evaluation of the Gauss series $f_l = z^l(a)_l\, {}_2F_1(a, a+l; l+1; z^2)/l!$.

Seven 440-bit two-path evaluations at $s = -61/16 + 15i/64$, $-9/4$, $-5/2$, $-11/4$, -3, $-5/2 + i/1024$, and $-4 + 2i$ gave reported scalar radii below 2.370×10^{-72} about the 94-digit centres. The independent exit integral has radius below 3.067×10^{-77}. For $h = 2$, $\rho = -8 - 4s$, so the middle four real tilts give $\rho = 1, 2, 3, 4$ respectively. Each test rejects the dropped prefactor and the flattened one-body preparation. Omitting either of two equal physical branches at these particular inputs cannot be detected by comparing their individually normalized values. An equal-weight test here would misrepresent the power of that control. A separate real disk-boundary test $s = -2$ has prefactor one and correctly requires no separation of this control. This algorithm requires two paths of sixteen panels each. It uses no off-order samples at integer h.

Original thirty-five-state crossings at intersecting divisors

Theorem 23.6 (exact polynomial propagation at joint integer points). Let L be a positive integer, $s = L - 4$, $h = m \geq 0$ an integer, $g = m + 2$. Then $(1-z^2)^{4(2L-1)}W$ is a vector polynomial of degree at most $8 + 2g + 16(L-1)$. It gives an exact rational Taylor propagation of the full reduced physical state through $z = 1/2$ along either standard polygon. Joint normal and phase exceptional points in this family obey $j = m + 6 - 4L \in \{1, 2, 3, 4\}$.

Proof. In f_l the coefficient of z^{2k+l} is the polynomial $\binom{k+L-1}{L-1}\binom{k+l+L-1}{L-1}$ of degree $2L-2$ in k. Expanding it in the Newton basis $\binom{k}{r}$ and summing their generating functions $x^r/(1-x)^{r+1}$ gives denominator $(1-z^2)^{2L-1}$ and numerator z^l times a polynomial in z^2 of degree at most $2L-2$. In a raised tagged monomial with polynomial prefactor $(4z)^k$ the sum of k and all four absolute one-body indices is at most $2g+8$, by the triangle inequality applied to the $2g$ marked factors and the four tags. Multiplying the four rational coefficients proves the degree bound. The angular preparation fixes the entire polynomial; no free indicial coefficient is chosen.

For concreteness let $pW' = AW$ be the original 35-coordinate pencil in Section 10 and $d = 4(2L-1)$. For $P = (1-z^2)^d W$ the exact polynomial recurrence comes from

$$(1-z^2)pP' = [(1-z^2)A - 2dzpI]P.$$

At the beginning of the first leg initialize P with its exact angular value. Compute all Taylor coefficients from this 35×35 equation to the degree bound. After summation at the bend, the second leg uses that endpoint alone as its new initial state. Independently convolving both polynomials in the differential equation verifies the full zero residual on each leg, including every coefficient above the truncation degree. Uniqueness near the initial regular point and the angular polynomial identity select its physical continuation throughout. Applying the regularized scalar row to the resulting W at the exit avoids a division by $j - \rho$.

At $h = 2, s = -3$ the exact incoming and outgoing scalars are

$$T_4(2, -3; 11/25) = \frac{24957694113254547119140625}{299762145158165107310592}, \qquad T_4(2, -3; 14/25) = \frac{309308841824531555175781250}{492170557240509868475469}.$$

Both polygons used exact Gaussian-rational arithmetic, with zero initialization, truncation, roundoff, branch combination and readout error. Every leg had actual degree 15. All 55 residual coefficients in every one of the 35 components vanished. The final vector and its direct angular counterpart agreed entrywise. An independent original-angle computation at both endpoints evaluates the preceding one-body integrals by the same elementary Newton summation on their *original* exponents and displacements. Perturbing the generator by a constant identity term failed the residual polynomial check. Omitting the final factor converting P back to W failed both endpoint comparisons. The complete exact check took 8.32 seconds on the recorded run.

The same original-system integration was executed on the other three normal divisors, at different integer orders where appropriate. Here each row also checks all 35 outgoing coordinates and the original Haar scalar at both ends. The cost includes exact source construction and independent checks.

h	s	ρ	Exact $T_4(h,s;14/25)$	Runtime in seconds
3	-2	1	$\frac{84048333750}{418161601}$	16.57
4	-2	2	$\frac{14769733221112}{11290363227}$	25.18
1	-3	3	$\frac{5562324076890945434570525}{49217055724050986847546 9}$	6.46
2	-3	4	$\frac{309308841824531555175781250}{492170557240509868475469}$	8.32

A separate full-state ball experiment at complex tilt. We integrated both original 35-coordinate systems without the polynomial gauge at $h = 2$, $s = -61/16 + 15i/64$. Each leg used 32 panels, 1150 bits and degrees 108 through 144. The independently computed 570-term entrance vector cost 0.19 seconds and enclosed the distance to its dyadic input by 2.671×10^{-112}. The certified upper and lower gains from that input were below 1.740×10^{30} and 8.797×10^{28}. The differential defects and rounding from the two path integrations were below 1.025×10^{-56} and 4.134×10^{-58} at the endpoints. In this order the physical average of the two scalar projections had disk radius below 7.498×10^{-46} about the 73-digit centre in the receipt. Its value starts $6297.861941705272420768914146484240454142757648319 57 - 7194.534366286249608306458998506342871880897782476 14i$. The separate 610-term exit scalar had radius below 1.265×10^{-143}, all 35 exit coordinates overlapped the independent state, and the original-eigenangle integral agreed as well. The two path runs took 270.1 and 275.4 seconds, followed by about five seconds for independent projection and checks. These timings distinguish full-system integration from evaluating the invariant source factorization. The inherited 56-order calculation for an entire order disk is a third algorithm. These integer-order executions do not constitute a cold run of that algorithm.

Transverse tilt derivative at the joint point. A differentiated experiment tests the effect of crossing the normal divisor in parameter space. Keep $h = 2$ and differentiate in s at $s = -3$. Then $\partial_s \rho = -4$. Put $x = z^2$ and $\ell = \log(1-x)$ on its branch at the entrance. At $a = 1$, $f_l = z^l/(1-x)$ and the derivatives of $(a)_k/k!$ are the harmonic numbers H_k. Using their generating function, including $H_{k+l} - H_k = \sum_{j=1}^{l} 1/(k+j)$, gives

$$\partial_s f_l|_{a=1} = z^l \left[-\frac{2\ell}{1-x} - \sum_{j=1}^{l} x^{-j} \left(\ell + \sum_{r=1}^{j-1} \frac{x^r}{r} \right) \right].$$

The apparent poles at zero cancel in the full analytic expression. For the crossing use $D_0 = z^6(1-z^2)^4$, $Q = D_0 W$, $D_0 \partial_s W = R + L\ell$. Then Q, L, R are polynomials of degree at most 22. Indeed for a differentiated mode $l \le 6$, multiplication by $z^6(1-x)$ clears its denominators and leaves two polynomials of degree at most $l+6$. Use the argument of Theorem 23.6 to bound the other three factors. The constant and logarithmic coefficients are two distinct incoming angular integrals carried through the crossing.

Set $d_0 = z(1-z^2)$ and $B = d_0 A + (6 - 14z^2) pI$, with $pW' = AW$ and A_s the tilt coefficient of the numerator. The three blocks satisfy

$$d_0 pQ' = BQ, \qquad d_0 pL' = BL, \qquad d_0 pR' = BR + d_0 A_s Q + 2z^2 pL.$$

These follow by differentiating the parameter-dependent radial equation and separating the rational and logarithmic parts. The separation is unique since the logarithm is transcendental over the rational functions, as also follows from its nontrivial additive monodromy. At fixed $h = 2$ both complex paths agree for all tilts, so their total tilt derivatives agree as well. The order-derivative connection is a separate operation.

At the joint point we integrated all 105 components in exact Gaussian rational arithmetic on both polygons. Each leg had degree 22 and its 62 polynomial residual coefficients vanished in every equation. The output agreed componentwise with the logarithmic angular source at 14/25. The value of the scalar derivative is

$$\partial_s T_4(2,s;14/25)|_{s=-3} = -\frac{800251960754394531250000}{14914259310318480862893} + \frac{61861768364906311035156250}{16405685241350328949182 3}\log(429/625).$$

It starts $-1955.48241786582353471683078140133505668$. Writing l_0 for the polynomial scalar row before the prefactor, we differentiated the complete product of the prefactor, l_0 and W. Its three exit contributions from the state derivative, the polynomial-row derivative and the prefactor derivative are about $-6.5625420849426\times10^{11}$, $6.5625420843066\times10^{11}$ and -1891.8854. The sum of their moduli divided by the modulus of the result lies between 6.7119×10^{8} and 6.7120×10^{8}. Dropping any one gives a disjoint enclosure. This is conditioning of that derivative decomposition at this specific point.

We also differentiated the finite original-eigenangle Fourier sums at the entrance and exit. Their uniform tail on $|s+3|\le 1/2$ is the earlier direct bound, so Cauchy's inequality doubles it for this derivative at the centre. That independent exit enclosure has disk radius below 6.133×10^{-77} at 460 bits. The exact rational and logarithmic contraction and the two-endpoint comparison took about 26 seconds. This provides a physical first parameter jet transverse to the normal divisor without differentiating a singular readout row.

A nonpolynomial crossing on the rank-three intersection

Proposition 23.7 (the derivative jump survives the scalar projection). At $N=3$, $z_l=13/50$, $z_r=2/5$, $h=3/2$ and $s=-11/6$, the two connection branches meet and the second normal divisor vanishes. The Haar moment at the exit is

$$T_3(3/2,-11/6;2/5) = 4.446623473549958+\eta, \qquad |\eta|<3.46\times10^{-13}.$$

The uncorrected upper-branch answer differs by more than 1.4646×10^{-5}. On the same normal divisor at $h=3/2+3i/128$, $s=-11/6+i/128$, the exit scalar is

$$4.44571455079869371+0.070736319096214318i+\eta, \qquad |\eta|<1.52\times10^{-15}.$$

Both parameters in the latter computation are nonreal. The two pure paths and their equal average each miss the physical result by more than 1.36×10^{-5}.

Preparation and propagation. For each source order the independent angular initialization uses the Fourier–Mellin rule of Section 21 with angular cutoff 58, signed-tail cutoff 33, eleven inverse-frequency terms, radial frequency 322 and 54-point panel quadrature. The Fourier truncation here uses the two-circle Cauchy bound for the actual $\nu=-3-s$; the shortcut for $|\nu|\le1$ would be inapplicable. The centre calculation uses 325 bits. Each 20-state trajectory uses 420 bits, 32 panels on each straight leg, and bend $1/3\pm0.07i$. As in Theorem 10.15 the denominator has no parameter dependence. In the fixed frame the three separately certified integrals of the norms of the constant, h- and s-parts imply the affine Grönwall estimate at the new tilt. The fixed disk restriction in the former Taylor-truncation table is unnecessary for this residual calculation. The Euclidean logarithmic-norm law of the same theorem applied to the three parts gives the smaller final gain used to charge the entrance error. Each of the two uses of the norm table keeps its own frame. All terminal midpoint roundings are included in the corresponding residual bounds.

At the intersection eight full paths were run at $h_j=e+\delta i^j$, $0\le j<4$, where $e=3/2$, $\delta=2^{-13}$. The maximum incoming component error was below 2.373×10^{-28}, the final source gain below 2.886×10^{9}, and the largest endpoint defect for these eight paths below 6.1×10^{-29}. Let t_j be the result of applying the ordinary physical weights and the division-free scalar row at h_j. The target is the constant Taylor coefficient of the *physical scalar*, so its approximation is $\sum t_j/4$. This is an order-derivative connection evaluated by Cauchy coefficients. On $|h-e|\le3/2$ the positive source at the chosen real tilt bounds its modulus by

$$M=T_3(0,s;z_r)+T_3(3,s;z_r)<34.608.$$

Indeed $x^{\Re h}\le1+x^3$ for $x\ge0$, and both integer integrals have independent determinant enclosures. Only positive indices divisible by four alias to the constant coefficient. Their sum is at most $M(\delta/(3/2))^4/[1-(\delta/(3/2))^4]<$

1.518×10^{-15}. Adding the four weighted incoming, branch and readout errors yields the displayed disk. As a separate calculation on the same eight paths we recovered the complete 20-component physical vector with component error below 1.263×10^{-9} by the differentiated phase numerator (10.13). Its scalar projection overlaps the sharper direct coefficient. Direct integration of both arcs at the exact order supplies the omitted-derivative control.

The entrance scalar at the intersection is 2.27482896266281640778565362 4 within 1.73×10^{-26}. Independent 42-node, 710-bit determinant enclosures contain both the intersection scalar and the complex on-divisor scalar at the exit, and contain the independently enclosed entrance scalar. Their exit precision is of order 10^{-6}; the thinner reported disks come from the full transport. The six independent initializations, twelve original-system trajectories, componentwise endpoint data, degrees and times are recorded in the verification package.

The original exceptional disks with fewer transported orders

Proposition 23.8 (one or several order pairs according to distance). Retain the full radii $|h-e| \le 1/16$, $|s-s_*| \le 1/16$ of Theorem 21.12. A parameter-dependent choice between the ordinary two-path connection and interpolation of the *projected physical scalar* lowers the maximum number of order pairs from 56 to five at rank three and twelve at rank four. The absolute errors of the finite reference calculation, including target arithmetic, are below 7.949×10^{-26} and 8.775×10^{-26} respectively. These are approximation errors at each input. The budgets were executed over the entire disks; the twelve-pair rank-four reference calculation was not run cold.

Write $u = h - e$, $r = 1/16$, $R = 3 - e$ and $b_r = 2 - \sinh(\pi r)/(\pi r)$. The sum of the absolute branch weights on the punctured disk is bounded by $A/|u|$, $A = e^{\pi r}/(\pi b_r)$. Let P bound the scalar row and let E bound the component error on either transported vector. We used the original uniform constants on the exceptional disks from Theorem 21.12, including the quadrature and full-matrix errors, and tightened the allowance for final arithmetic to $d = 10^{-28}$. The computed readout is accepted only when its arithmetic ball meets this allowance. The old row has no normal pole on these particular disks and can be rebuilt to higher precision. For $|u| \ge \sigma$ a single order pair at the query therefore has absolute error at most $APE/\sigma + d$.

For $|u| < \sigma$, transport and project at m equally spaced orders on $|h-e| = a$, with $a > \sigma$. Take the discrete Fourier coefficients of the resulting *scalars*, and evaluate the degree-$(m-1)$ polynomial on the inner disk. If M bounds the physical scalar on $|u| \le R$, the error including the final arithmetic is at most

$$\frac{M}{1-\sigma/R}\left[(\sigma/R)^m + \frac{(a/R)^m}{1-(a/R)^m}\right] + \frac{APE/a + d}{1-\sigma/a} + d.$$

This follows by expanding the holomorphic Haar scalar. The coefficient of degree k receives aliases from $k + jm$ with weights a^{jm}. Each sample perturbation changes a normalized discrete coefficient by at most the maximum perturbation. For the two ranks one may sum the positive angular masses and third integer moments at the two extreme real tilts in the input disk to obtain M. This uses $x^{\Re h} \le 1 + x^3$ and $b^{\Re s} \le b^{s-} + b^{s+}$ for positive x, b in the indicated ranges. The imaginary tilt is retained in each actual branch. The estimates at the real extreme tilts only furnish this outer majorant.

		Sampling radius			Inner error
N	M upper bound	σ	a	m	bound
3	404.329	2^{-20}	$3 \cdot 2^{-20}$	5	5.019×10^{-26}
4	218872	2^{-10}	2^{-9}	12	8.775×10^{-26}

An exterior query of this algorithm was run from fresh initial data at $N = 3$, $h = 3/2 + i/32$, $s = -2.86 + 0.21i$, with 430-bit path arithmetic. Its single order pair returned $17.256966435539756480635435460 49 - 4.98795622637820834210079304125i$ with absolute error below 7.949×10^{-26} about this printed centre. A separate 40-node determinant calculation at 720 bits contained the transported disk.

There is also an executed alternative very close to the rank-four centre. Propagate at integer order 2 with the actual complex tilt, then return that anchor. By the same Cauchy bound its error is at most the integer-anchor error plus $M|h-2|/(1-|h-2|)$. For $|h-2| \le 10^{-31}$ this gives less than 2.190×10^{-26} on the old tilt disk and less than 9.204×10^{-28} on $|s+3| \le 1/16$. The two-path integer calculations were run at $u = 2^{-104}(1+i)$ for

both $s = s_*$ and $s = -3 + u/4$. The latter query is exactly on the complex normal divisor. This construction bounds the change from the transported integer order through the physical Haar source; it does not propagate the noninteger target column. The order-switch calculation above instead propagates the target or neighboring noninteger columns. The incoming rank-four Fourier–Mellin integrals remain the principal cost for high-accuracy evaluations throughout an order disk.

A scalar certificate across several radii at positive integer orders

Theorem 23.9 (one polynomial on a closed radius disk). Let m be a nonnegative integer. Fix $0 < r < 1$, $S \ge 0$, $r^2 < q < 1$, $\tau > 0$ and $K \ge m$. There is a computable polynomial times $(1 - z^2)^{2m}$ which approximates the ordinary physical moment $T_N(m, s; z)$ simultaneously on $0 \le z \le r$, $|s| \le S$, at every rank N. The same bound holds on $|z| \le r$ for its unique holomorphic radial continuation. The absolute truncation bound is

$$(1 + r^2)^{2m} \frac{(m!)^2}{\tau^{2m} q^m} (1 - q)^{-S^2} \exp\left(\frac{2S\tau q}{1 - q} + \frac{\tau^2 q}{(1 - q)^2}\right) (r^2/q)^{K+1-m}. \tag{23.1}$$

The coefficients still depend on N. The degree cutoff for a requested absolute truncation error is independent of rank. Arithmetic and construction cost are separate. The complex continuation uses the same z in the two analytic half factors; the ordinary Haar moment is specified here at real radius.

Construction. Introduce a formal variable v multiplying $\sum_{k \ge 1} z^k \operatorname{tr}(U^k)$. For each partition λ define

$$D_{\lambda,m}(s) = m!\, [v^m]\, s_\lambda\big|_{p_k = -s + kv},$$

where s_λ is a Schur function and p_k denotes a power sum. Expanding the exponential by the Cauchy identity gives this coefficient for the analytic half of the characteristic-polynomial source. Extracting v^m amounts to inserting the mth power of $z \sum_j \lambda_j/(1 - z\lambda_j)$. Independent extraction in the second half followed by character orthogonality on $U(N)$ gives

$$(1 - z^2)^{2m} \sum_{n \ge m} z^{2(n-m)} \sum_{\substack{|\lambda| = n \\ \ell(\lambda) \le N}} D_{\lambda,m}(s)^2.$$

The coefficient begins at degree $n = m$ since the inserted series starts with z. Each half has the same independent tilt s, hence the algebraic square. The series for real z agrees with the original Haar preparation. These uses of Schur orthogonality and the Cauchy identity are classical; Bump and Gamburd give the characteristic-polynomial context cited in the references.

For $|v| = \tau$ the squared norm, summed over *all* partitions with weight $q^{|\lambda|}$, of the specialized Schur coefficients is

$$\exp\left(\sum_{k \ge 1} \frac{q^k}{k} |-s + kv|^2\right) \le (1 - q)^{-S^2} \exp\left(\frac{2S\tau q}{1 - q} + \frac{\tau^2 q}{(1 - q)^2}\right).$$

Apply the Hilbert-space Cauchy coefficient estimate to finite partition cutoffs and pass monotonically to the positive norm sum. Restricting to $\ell(\lambda) \le N$ can only lower the squared norm. For $n > K$, $|z|^{2(n-m)} q^{-n} \le q^{-m} (r^2/q)^{K+1-m}$. Multiplication by the prefactor gives (23.1), local uniform convergence and the asserted analytic continuation. No separation into sheets at intermediate real radii is needed on this integer-order source.

Finite calculation. The individual partitions can be eliminated. The half-factor in one eigenangle is $(1 - X)^s \exp(vX/(1 - X))$. Its coefficient of $v^a X^j$ is $(a - s)_{j-a}/[a!(j - a)!]$ for $j \ge a$. Pair the two halves at Toeplitz displacement $d = i - j$ and conjugate the matrix by a diagonal power of z on $z \ne 0$, extending the resulting entries to $z = 0$. In the variable $t = z^2$ the single entry has an initial factor $t^{\max(d,0)}$ times the lagged convolution of the two half coefficients. Compute the determinant by its signed column-subset recurrence modulo $t^{K+1}, v^{m+1}, w^{m+1}$, extract $(m!)^2[v^m w^m]$, discard its m initial zero powers of t, and restore the prefactor. All operations are polynomial. The implementation uses at most $O(N 2^N (m + 1)^4)$ truncated univariate polynomial products of degree at most K, plus construction of the one-body entries. Thus a uniform cutoff does not imply a rank-uniform complexity bound.

For $r = 7/10$, $q = 4/5$ and $\tau = 3/50$ the following calculations used 400-bit ball arithmetic. The last column is the uniform analytic tail; maximum checked finite-evaluation radii including the analytic error were below 10^{-29}. The saved high-precision centres and widths apply at the tested queries.

Rank	m	Tilt disk	K	Critical radii traversed on $[0.11, 0.70]$	Uniform analytic error
5	1	$\lvert s\rvert \le 4.3$	248	$1/5, 3/5$	8.729×10^{-37}
6	2	$\lvert s\rvert \le 5.3$	296	$1/3, 2/3$	2.201×10^{-36}

Four polynomial constructions used $s = -4$, $-4 + 0.2i$ at rank five and $s = -5$, $-5 + 0.12i$ at rank six. In each case seven real or complex radius values were evaluated on a common polynomial. All twenty real-fibre results were independently enclosed by the transformed Haar determinant in Section 21. A separate exact specialization at $m = s = 1$ gives $(1-t)^2 \sum_{j=1}^{N} j^2 t^{j-1}$ from orthogonality of the exterior powers. Every available coefficient through degree 17 was checked at ranks three, five and six, including the terminal zeros. Omitting the prefactor failed at all three ranks. At the centre the integer moments agree with $m!$ in the tested stable range. These are scalar continuation results. Validated multiwall transport of arbitrary reduced vectors and of general noninteger orders at these ranks remains open.

24. Full variable-order transport through the rank-four wall

One order pair throughout the two rank-four exceptional disks

Theorem 24.1 (divided order on the physical branches). Write $u = h - 2$. At rank four transport from $z_l = 11/25$ to $z_r = 14/25$ along the two polygons with bends $1/2 \pm 3i/50$. Use the 35 compact angular coordinates of Section 10. For either of the independent closed parameter products below, one target-order pair suffices, including $u = 0$. In its regularized version each branch transports a 35-component common reference and a 35-component divided difference. The bounds concern the ordinary unnormalized Haar scalar. They bound the discrepancy at each input between the finite algorithm and the physical solution.

Region	Auxiliary order radius A	Taylor degree per panel	Maximum component error of connected physical state	Absolute error of scalar
$\lvert h-2\rvert \le 1/16$, $\lvert s + 193/50 - 21i/100\rvert \le 1/16$	3/32	780	2.922×10^{-41}	6.292×10^{-30}
$\lvert h-2\rvert \le 1/256$, $\lvert s+3\rvert \le 1/512$	1/64	1260	2.323×10^{-48}	1.631×10^{-38}

Construction and proof. At the same independent tilt s, write $B_h(z) = B_2(z) + uD(z)$ for the affine radius generator in the existing regular path chart. Here the subscripts denote values of the physical moment order and $D = \partial_h B_h$. Let X be the angularly prepared solution at $h = 2$. Its two exit values agree entrywise by Theorem 10.17. The full variable-order branch is $W_h = X + uZ$, where the following equations use the same incoming angular preparation on each path:

$$X' = B_2 X, \qquad Z' = B_h Z + DX, \qquad Z_l = \frac{W_{2+u}(z_l) - W_2(z_l)}{u}.$$

The quotient at zero is the derivative of the actual incoming preparation. Substitution gives the original differential equation and initial value for the target-order vector. At $u = 0$ differentiation gives the inhomogeneous equation for its total order derivative. This argument also proves that the chosen branch solutions depend holomorphically on both independent parameters along the two polygons. The common X at the exit can be taken from the upper computation. For every query the full connected column is

$$X(z_r) + b_+(u) Z_+(z_r) + b_-(u) Z_-(z_r), \qquad b_\pm(u) = \frac{u}{2} \mp \frac{i}{2\pi} \frac{\cos(\pi u)}{\operatorname{sinc}_\pi u}.$$

Indeed $b_\pm = u\omega_\pm$ in the ordinary connection and $b_+ + b_- = u$. The formula extends through the phase zero by the identity theorem, with the signs fixed by the upper-path convention in (10.11). In particular the derivative difference enters with coefficient $1/(2\pi i)$ at the centre. On rank-four physical integer data this difference vanishes by Theorem 10.17. An arbitrary homogeneous column has no such identity. For $r = \max|u|$, the absolute sum of the two b weights is bounded by $\beta = e^{\pi r}/(\pi[2 - \sinh(\pi r)/(\pi r)])$, by writing their numerators as the two exponentials. The regular scalar row of Theorem 23.1 applies to the connected vector, including on its normal divisors.

Actual source of the divided initial vector. Use $G = 4 + u$, $R = 4(1 + z_l)$, and the Fourier–Mellin construction of Proposition 21.11. With its origin split at frequency 2 the jth coefficient of the central angular moment polynomial simplifies to $c_j(u) = \Gamma(5+u)^2 R^{2j} \operatorname{sinc}_\pi(4+u-j)/(j!)^2$. Its only nonzero coefficient at $u = 0$ is $c_4(0) = R^8$. For $j \neq 4$, the divided coefficient is explicitly

$$\frac{\Gamma(5+u)^2 R^{2j}(-1)^{4-j} \operatorname{sinc}_\pi(u)}{(j!)^2(4+u-j)}.$$

For $j = 4$ put $L(u) = \log[(\Gamma(5+u)/24)^2 \operatorname{sinc}_\pi u]/u$, using the local logarithm that vanishes before division at zero. The required coefficient is $R^8 L(u)\, {}_1F_1(1;2;uL(u))$. Its value at zero is $2R^8\psi(5)$. The linear term in $\log\Gamma$ and the Euler sine product give

$$L(u) = 2\psi(5) + \sum_{n=2}^{m} \frac{2(-1)^n\zeta(n,5) - 2\mathbf{1}_{2|n}\zeta(n)}{n}\, u^{n-1} + E_m, \qquad |E_m| \le \frac{8r^m}{(m+1)(1-r)}.$$

The bound follows from $\zeta(n,5) \le \zeta(2)$ and $\zeta(n) \le \zeta(2)$ for $n \ge 2$. The finite- and large-frequency quadratures are multiplied throughout by $K(4+u)/u = -2\,2^{2(4+u)}\Gamma(5+u)^2 \operatorname{sinc}_\pi u$. These formulas define the divided source at zero and at arbitrarily small complex offsets without numerical cancellation. Every Fourier factor retains its original tilt. In particular $K(4+u)/u$ at zero is -294912.

Uniform error budget. Let F_u be either exact transfer and let P_u be the ordered product of its 64 finite Taylor matrices. The branch ODE has parameter-independent path denominators, bounded away from zero on the certified charts. Every P_u is a polynomial in the order at fixed tilt. Calculating the finite Taylor recurrence in the triangular block above evaluates P_0, P_u and $(P_u - P_0)/u$ on the required columns, with the same degrees as in the single-parameter ordinary recurrence. This follows coefficient by coefficient or first for $u \neq 0$ by subtracting the two finite matrix recurrences and then at zero by polynomial identity. The same identity holds for the ordered product.

On $|u| \le A$ write $\|F_u\|_\infty \le K_*$ and $\|F_u - P_u\|_\infty \le \tau$. Signed contiguous products of the verified panels give $K_* < 1.039 \times 10^{33}$ and $\tau < 2.572 \times 10^{-124}$ on the older disk, and $K_* < 2.324 \times 10^{75}$ and $\tau < 2.425 \times 10^{-167}$ on the inner disk. These bounds cover all specified independent tilts. Their computation uses the Euclidean panel laws and coefficient rescaling of Theorem 23.3. For $r < A$, the Cauchy derivative bound for a function of a complex variable between these two disks shows that the divided transfer and the divided transfer *error* are bounded by $K_*/(A-r)$ and $\tau/(A-r)$, respectively. This applies in the induced matrix norm by duality with unit vectors and norming linear functionals, with no extra dimension factor.

Let ϵ be the inherited finite Fourier–Mellin truncation bound on $|u| \le A$. At the older and inner disks it is respectively less than 3.382×10^{-75} and 1.165×10^{-133}. In exact arithmetic the finite rule is holomorphic in u and equals the full incoming X_l at $u = 0$: its sole surviving central coefficient is R^8, its angular contraction uses the exact one-body Fourier moments, and every noncentral term carries $K(4) = 0$. Thus the analytic error of each divided input component is at most ϵ/A by Schwarz's lemma. Permit another ϵ/A for evaluating that finite rule in ball arithmetic. Set $e_V = 2\epsilon/A$ and compute the finite integer angular source to $e_0 = 10^{-160}$ per component. Exact integer-order angular contraction makes this possible at every tilt in the two disks. For $B = [4(1+z_l)]^{2(4+A)}(1-z_l)^{-8(4+\Re s_c+d)}$, where s_c and d are the tilt centre and radius, positivity of the real bases before taking absolute values implies $\|W_{2+u}(z_l)\|_\infty \le B$. Its exact divided source has norm at most $B/(A-r)$.

Calculate each of the two finite block actions to absolute arithmetic radius $d_v = 10^{-48}$ per component. Then one common reference exit and one divided exit have respective error bounds

$$E_X = (K_* + \tau)e_0 + \tau B + d_v, \qquad E_Z = (K_* + \tau)\big(e_V + e_0/(A-r)\big) + 2\tau B/(A-r) + d_v.$$

This charges the ordinary and divided transfer truncations separately. Each individual branch has a reconstructed full-column error at most $E_X + rE_Z$ before its final rounding. The connected vector has error $E_X + \beta E_Z + d_v$. The scalar row has norm at most 2.154×10^{11} on the old domain and 2.714×10^{9} on the inner domain. The first bound is Theorem 21.12 on the old disk. The second is the polynomial-row bound of Section 23, including its radial normalization. Multiply by the respective row norm and allow 10^{-38} for the final scalar arithmetic. The calculations in the table use the unrounded constants. All finite arithmetic tolerances refer to forward enclosure radii of the specified circuits, refinable at computable inputs to the closed disks. The sine quotient, divided central coefficient and triangular transport have regular formulas across $u = 0$; the physical row is regular at every intersecting normal divisor. No order-interpolation or aliasing term is present. □

The finite-algorithm bounds concern the complete reference rule. The prior 16- and 12-pair reference constructions use different disks and tolerances and keep their earlier execution status. The new one-pair bound uses the same expensive worst-case incoming cutoffs as a fallback. The individual executions documented below use evaluated, sometimes substantially sharper, quadrature and path-residual bounds. The independent output quadrature serves as a check. The outgoing scalar in the branch calculation comes from the transported 35-component solution.

A computable incoming state for variable complex order

At the entrance $z = 11/25$ put $a = 4z$, $R = 4(1+z)$, $u = h-2$, $g = 4+u$ and $C_m = \int e^{im\theta}|1-ze^{i\theta}|^{-2(4+s)}\,d\theta/(2\pi)$. The independent, unnormalized angular preparation of Section 10 has 35 tags. All powers in its Mellin rule use the real logarithm of the positive variable. The coefficients $C_m = C_{-m}$ can be complex, including for complex s on the two disks. The same C_m appears in both signed Hankel factors.

Lemma 24.2 (the angular projection and its error). Put $b = M + 2$ and, for $i = -1, 0, 1, 2$, form the finite Laurent polynomial

$$P_i(w;t) = \sum_{|j-i|\le M} C_{|j-i|} J_j(t) w^j.$$

The compact angular kernel with tags $i_1, \dots, i_4$ and the indicated Fourier cutoff is the contraction of $\prod_k P_{i_k}$ against $J_d(at)$ at each Laurent degree d. Let $L > 8b$ and evaluate the four polynomials at $w = \exp(-2\pi ij/L)$. The average of their product times $\exp(iat\sin(2\pi j/L))$ differs from that contraction by at most

$$\left(|C_0| + 2\sum_{k=1}^{M} |C_k|\right)^4 \frac{2\exp(|at|\sinh 1 - L + 4b)}{1 - e^{-L}}.$$

This bound is pointwise in the positive integration frequency t.

Proof. The Laurent generating function of the integer Bessel functions is $\exp(x(w - w^{-1})/2)$. A Cauchy circle with $|\log|w|| = 1$ on the appropriate side gives $|J_d(x)| \le \exp(|x|\sinh 1 - |d|)$ for real x. A length-L cyclic extraction for $|d| \le 4b$ adds only orders $d + pL$ with nonzero integer p. Sum the geometric majorant and use $|J_j(t)| \le 1$ from the unit-circle formula. This gives the displayed estimate. The same argument on a smaller angular grid, with b in place of $4b$ and t in place of at, encloses all individual Bessel coefficients. The program adds the first alias directly to each coefficient enclosure and the second to each output at the integration node. Grouping tags into the ten unordered pairs then uses a $10 \times L$ matrix and an $L \times 10$ matrix for all 35 contractions. The Fourier convention and the sign of the displacement phase both enter this identity. The classical generating function and recurrences are given in the NIST Digital Library of Mathematical Functions, §§10.6 and 10.12. □

Angular source and absolute errors. Separate frequencies at 2 and T. For the 74 finite panels we used 65 Gauss nodes apiece, $M = 147$, $T = 426$, a central Bessel polynomial to degree 65, and all signed Hankel channels through 14 terms with Fourier cutoff 76 in the tail. The radial kernels at a given tilt are shared across independent orders. The Mellin weights and central jets change with the order. Let W_e be the integer angular input and let Z denote its order divided difference from Theorem 24.1. The multiplier on the raw, noncentral integral for Z is

$$D(u) = -2^{2(4+u)+1}\Gamma(5+u)^2\,\mathrm{sinc}_\pi(u), \qquad D(0) = -294912.$$

The source calculation produces both Z and $W_e + uZ$. This step uses no outgoing angular moment.

Here are certified common entrance majorants before multiplying by $|D(u)|$. They apply on both closed parameter regions in Theorem 24.1. The row indexed by the omitted large modes is the change from the finite-segment cutoff to the signed-tail cutoff.

Raw contribution, per mode	Absolute upper bound
Central Bessel Taylor remainder	3.838×10^{-88}
Omitted Fourier coefficients	1.225×10^{-51}
Omitted large modes in the far tail	9.692×10^{-50}
Signed Hankel expansion remainder	2.488×10^{-45}
Finite Gauss quadrature	1.725×10^{-56}

To verify the majorants put $\gamma = 63/16$, $\Gamma_* = 65/16$, $S = 17/16$ and $W = (1-z)^{-2S}$. Then $\gamma \le \Re g \le \Gamma_*$, $|\Im g| \le 1/16$ and $|4+s| \le S$. For the absolute coefficients of either half of the angular weight use $(S)_j/j! \le j+1$. Convolution gives

$$\sum_{|m|>L} |C_m| \le 2z^{L+1} \left[\frac{A + (L+1)B}{1-z} + \frac{Bz}{(1-z)^2} \right], \quad A = \frac{1+z^2}{(1-z^2)^3}, \quad B = (1-z^2)^{-2}.$$

For the individual coefficients the code sums the positive Pochhammer convolution and bounds its uncomputed tail by the exact geometric sum of the corresponding quadratic polynomial. The L^1 norm of the whole preparation is at most W^4 in Fourier coefficient norm. At the origin the omitted term is bounded by $W^4 2^{-2\gamma} R^{2d+2}/[(d+1)!^2(2d+2-2\Gamma_*)(1-(R/(d+2))^2)]$. On each Gauss panel use the analytic disk with the centre, radius and Bernstein–Taylor bound of Proposition 21.11. The generator in the frequency direction has absolute growth at most $\exp(R|\Im t|)$. Above T each discarded Fourier product gains four individual Bessel envelopes because $T \ge 2(M+2)$, while the displacement Bessel factor is bounded by one. For retained modes the gamma-integral remainder and the product telescoping inequality of Proposition 21.11 give the signed-tail remainder. The stored sums use the actual orders in each factor. Bounds on individual nodes and all sums are outward rounded.

The signed-tail computation uses two polynomial indices. Store reciprocal-frequency degree d and Laurent degree k at position $d(8b'+1) + k + pb'$ for a product of p factors with support $[-b', b']$, $b' = 76 + 2$. No carry can identify two distinct monomials through $p = 4$. Upon multiplying, retain the sum of the four independent signs; combine each coefficient with the signed displacement Hankel series and its exponential integral. This computes the finite sum over every retained sign and order. A direct, independently indexed implementation verifies all 35 contractions at smaller cutoffs. The final source allowance includes the outward error on the finite contractions and conversion to the stored midpoint. All spatial coordinates share one absolute remainder cap, while their centre values and their exact compatibility relations are retained.

Backward conditioning of the physical readout

For the same order and tilt as a forward solution let ℓ be an admissible outgoing scalar row. Integrate $J' = -JB_h$ backwards from $J(z_r) = \ell$ on each of the two paths. Then $J(z_l) = \ell F_h$ and JW is constant on the path for every homogeneous full-state solution. The transpose, without complex conjugation, is required for this identity. For a forcing in the backward row equation at any point of panel k, its ℓ^1 action at the entrance is bounded by the canonical infinity norm of the corresponding *forward prefix*. The program bounds a complete prefix by a certified signed product; it covers the partial panel by the exponential of its nonnegative real-time generator norm integral in the verified frame. The same prefix law charges a rounded endpoint and the integrated polynomial residual $\|pJ' + JB_h p\|_1 / \inf|p|$. Applying the reciprocal frame to the accumulated residuals accounts for the conversion back to canonical coordinates.

Write r for the linear combination of the two entrance rows with the physical complex weights. The angular compatibility matrix satisfies $CW_l = 0$. Any explicitly specified dyadic multipliers λ give the valid constrained row $r - \lambda C$. A least-squares computation proposes the multipliers; ball multiplication by the original C and the outward row norm certify their use. When a forward path was computed at an approximate start w_0 while a subsequently refined source gives w_1, the midpoint correction is $(\widehat{r} - \lambda C)w_1 - \widehat{r}w_0$. This retains the common start error and supplies its two-path response without assigning the size of the entire transfer matrix to the scalar. In

the divided problem the source satisfies the affine identity $C(h)Z_l = -C^{[1]}(h)X_l$, where $C^{[1]} = (C(h) - C(2))/u$ is differentiated at zero. The homogeneous projection is legitimate for W_l. Divided-source readouts can directly use the unprojected b-weighted entrance row. Its finite norm suffices in the executions where that choice is recorded.

Residual propagation, dyadic matrix gains and the signed frequency tail

The forward calculations start at the real entrance with the original order-dependent angular functional. A Hermite polynomial on that fibre provides a separate dyadic trial vector. Its maximum component error is recorded. This trial vector lets the complete forward path calculation and the finer angular integration proceed independently. The dual correction below restores the refined incoming functional before taking the physical scalar.

Lemma (forward residual in a fixed frame). Let $Y = V^{-1}W$, with the certified frame of Section 10. Number the 64 panels on a path starting at zero. Let $C_{64,i+1}$ bound the Euclidean norm of the signed evolution in this frame on all *complete* panels strictly after panel i. For each panel let I_i bound the integral of the positive infinity norm of its generator. A pointwise local defect of size d_i on unit panel time, and endpoint midpoint error r_i, cost at most

$$\|V\|_\infty \sqrt{35}\, C_{64,i+1} e^{I_i}(d_i + r_i)$$

in the canonical endpoint infinity norm. The measured initial change of frame costs $\|V\|_\infty \sqrt{35} C_{64,0}$ times its infinity radius. The final change of frame is performed in ball arithmetic and charged separately.

Indeed an arbitrary time within panel i first evolves for part of the panel, whose operator norm is at most e^{I_i}. Conversion to Euclidean norm costs at most $\sqrt{35}$. The certified signed suffix and conversion back to physical coordinates complete the estimate. Variation of constants gives the same weight for an integrated local defect. The signed-product perturbation recursion of Theorem 10.15 gives the C's with the actual distances in both independent parameters. The previously bounded **positive** generator norms cover every partial panel. An integrated logarithmic norm over the *whole* panel would need additional justification for a partial interval.

On a panel clear the denominator and translate to $pY' = BY$ on $[0, 1]$, $p(0) = 1$. Form the Taylor polynomial F from its dyadic initial state and bound the residual by summing the absolute coefficients of degree at least m in $pF' - BF$, divided by $|p_0| - \sum_{k>0} |p_k| > 0$. The lower coefficients vanish in exact Taylor arithmetic. Every retained coefficient is enclosed during calculation. The implementation adapts the degree to that panel's signed suffix, preserving a separate entry, differential-defect, midpoint-rounding and exit budget.

For the augmented pair (X, Z) one can use the same calculation with $A(2)$ on X, $A(h)$ on Z and $\partial_h A$ on X as the forcing of Z. On an order circle of radius $a > |u|$ about two, the off-diagonal part of any subinterval's exact fundamental matrix is the divided difference of its two ordinary matrices. Cauchy's formula bounds its norm by the corresponding common analytic matrix bound divided by $a - |u|$. Thus a bound on the ordinary evolution, uniformly on that circle, costs at most $1 + (a - |u|)^{-1}$ on the block maximum norm. Multiplying the signed complete-suffix bound by the partial positive-norm bound provides such an analytic bound for *each injection time*. Only one Cauchy factor is needed per defect. The executions take $a = 1/64$. The estimates apply to arbitrary correlated or uncorrelated input perturbations.

Independent finite matrix calculation. At the two ordinary query inputs we also compute the entire fundamental matrix on each polygon. For a balanced panel round the entries of its translated numerator matrices B_j and scalar denominator coefficients p_j to multiples of Q^{-1}, $Q = 2^b$. Keep their outward norm discrepancies b_j and c_j. Set $F_0 = I$. Use exact signed integer matrix products to form the cleared Taylor recurrence at each degree, rounding once, independently in each real and imaginary entry, to the nearest grid point. If f_k bounds $\|F_k\|_\infty$, the low-degree discrepancy in the resulting polynomial differential equation is bounded by

$$\frac{35}{Q} \sum_{k=1}^{m} k + \left(\sum_j b_j \right) \sum_{k=0}^{m} f_k + \left(\sum_j c_j \right) \sum_{k=1}^{m} k f_k.$$

Each rounded complex entry costs at most a grid unit, giving the first term. The other terms compare the quantized coefficients with the true coefficients throughout the polynomial. The high-degree part is bounded by ordinary convolution. Divide by the certified minimum denominator on the panel and multiply by e^{I_i} to obtain an operator-norm panel error. Each factor is stored as a midpoint and an operator radius. For blocks of eight

panels, then for their eight blocks, compute the signed centre products in ball arithmetic. If c_{ij} bounds the signed centre from j to i and e_j bounds factor j's error, the full bound obeys $g_{ij} = c_{ij} + \sum_{j<k\le i} c_{ik}e_{k-1}g_{k-1,j}$. This identity follows by inserting the first perturbed factor while keeping subsequent factors centered. For the error use the positive sum itself. Conjugating the result by V yields a separate certified pointwise full-matrix norm as well as an enclosure of the matrix. This calculation needs no physical compatibility constraint.

Parameter control for the executed source rule. The inexpensive incoming rule can be evaluated at arbitrary computable points on a box by refining the arithmetic while retaining all cutoffs. To certify its sufficiency one needs the physical scalar sensitivity to the divided source. Bounds on the entire transition matrix can be many orders too large for this purpose. The following computation retains the signed scalar as a row throughout both its radial and its parameter dependence.

For each path let M_i be the central dyadic local matrices in the balanced frame, and let c_{ij} bound every ordered contiguous product of these matrices ending at panel i and beginning after panel j. We retained all 2,080 nonempty products on each sign and separately saved the prefixes with the canonical input conversion and the suffixes with the canonical output conversion. At order/tilt displacement radii H, S from their centre, write d_i for the central panel error plus

$$\sqrt{35}\exp(\mu_i + |h_0 - h_*|a_i + |s_0 - s_*|b_i)[\exp(Ha_i + Sb_i) - 1].$$

The previous logarithmic-norm and two parameter-coefficient integrals give μ_i, a_i, b_i. Duhamel's identity controls the centre-to-query change in the Euclidean norm, followed by the indicated infinity-norm conversion. Reassembling the *signed* centres majorizes the perturbed prefixes with the input conversion already included. One bound for the error on a complete transition now uses each signed suffix to the canonical output. This yields a computable matrix enclosure and also bounds the transfer at a slightly larger order radius for the angular-anchor Cauchy estimate. The implementation separately records failure of this first (matrix-only perturbation) bound to meet the scalar tolerance on the entire original inner disk.

For a narrower bidisk, approximate the backward physical row as a polynomial in the two *independent scaled complex variables* $\xi = (h - h_0)/H, \eta = (s - s_0)/S$. Use all monomials of total degree at most k. At the exit, expand the exact cleared polynomial row of Theorem 23.1, multiply by the actual constant scalar prefactor $(1 - z_r^2)^{16+8s}/(h + 1)_2^2$ at the centre, and charge the sum of all omitted coefficient one-norms. The remaining analytic scalar prefactor is an explicit scalar ratio, bounded on the entire parameter set after propagation. The Taylor coefficients of the transposed backward system obey the usual triangular recurrence: the two affine generator directions multiply the coefficients with one lower order or tilt index, retaining the corresponding factors H, S.

Here a direct residual verifies the polynomial on the whole parameter set. If F_m is its radius Taylor proposal on a panel, let $L_{m,k}$ be the sum of the component moduli in *all* its parameter coefficients of exactly the highest degree k, summed over all radius coefficients. The missing degree-$k+1$ forcing costs at most

$$L_{m,k}\,\frac{\sum_j (H\|B_{h,j}^{\mathsf{T}}\|_1 + S\|B_{s,j}^{\mathsf{T}}\|_1)}{|p_0| - \sum_{j>0}|p_j|}.$$

Here the B's are the cleared, normalized forward balanced generators and the norm in this formula is the induced one-norm on the transposed system. This follows by coefficient convolution and $|\xi|, |\eta| \le 1$. The separate radius defect charges every omitted radius power, and the midpoint-reset charge includes every retained coefficient. The residual is recomputed for every panel, with its measured signed prefix. No coefficient is asserted to vanish by numerical sampling.

A useful bound for an incomplete panel uses $\mu_2(A) \ge \Re\,\mathrm{tr}\,A/35$. Consequently the integrated logarithmic norm of the old base generator over any subinterval is at most its already certified full-panel integral plus the integral of $|\,\mathrm{tr}\,A|/35$ over the panel. The last integral is bounded by the absolute Taylor coefficient sum divided by the certified lower bound on the cleared denominator. The parameter-direction integrals are nonnegative and can each be charged over a whole panel. This gives an explicit bound for every injection time in the polynomial residual and avoids charging a large infinity-norm exponential merely for an incomplete panel. The output records separately the entrance truncation, discarded parameter forcing, radius truncation, rounding and the sum of the absolute norms of the retained output rows.

If G bounds either full canonical matrix on the query box, G_a on an order halo of radius $a > H$, and P_{ret} the resulting uniform one-norm of each transported physical scalar row, let E_0, E_Z be the source disks for the integer anchor and divided data, e the allowed block path error for exact input, and P the exit row norm. With b bounding the sum of the two stable divided weights, the scalar error is at most

$$bP_{\mathrm{ret}}E_Z + P\{(1+b)e + E_0[G + bG_a/(a-H)]\} + e_{\mathrm{read}}.$$

The completely connected column has componentwise error at most $bGE_Z + (1+b)e + E_0[G + bG_a/(a-H)]$ plus final vector arithmetic. The source estimate uses the actual uniform angular truncations before multiplication by the entire divided Mellin coefficient; it is valid at the exceptional order as well. These are error bounds at every input; evaluating the polynomial at a single point gives a separate enclosure for that input.

Corollary 24.3 (uniform physical readout for the moderate angular rule). At the exactly simultaneous centre $(2, -3)$, the degree-three calculation on $H = S = 1/8192$ used 275-bit coefficient arithmetic. The upper and lower pullback bounds were below $8.031\,10^{12}$ and $2.794\,10^{12}$. The two cold polynomial residual verifications took 117.7 and 119.6 seconds. On the entire *closed complex bidisk*, the 147/76 Fourier cutoffs, signed Hankel order 14, radial cutoff 426 and 65-point Gauss rule give divided source error below $7.352\,10^{-40}$, including 10^{-42} of finite arithmetic. Taking integer-anchor error at most 10^{-90}, $e = 10^{-47}$ and final arithmetic at most 10^{-36} gives scalar error below $1.880\,10^{-27}$ and connected-vector component error below $1.276\,10^{-23}$. In that same calculation the separate matrix perturbation and scalar row-norm product alone would only give about $1.28\,10^{-17}$. The finite arithmetic thresholds concern the returned centres. A query can allocate higher working precision until its rounding test passes.

The degree-six model on $H = S = 1/2048$ gave a sharper scalar certificate on a larger set. The complete signed backward computations took 194.0 and 194.4 seconds and gave row-norm bounds below $4.866\,10^{9}$ and $2.073\,10^{9}$. With the same moderate angular preparation and arithmetic thresholds the scalar absolute error is below $1.143\,10^{-30}$ throughout this bidisk. The uniform connected-column component error is below $2.595\,10^{-17}$. The poorer vector bound reflects the cost of unstructured component errors in a larger parameter box.

One may rescale an already validated parameter polynomial to unequal radii. For old radii H, S and new H', S' put $t = \max(1, H'/H, S'/S)$. A polynomial coefficient sum of total degree at most j grows by at most t^j. The missing generator forcing has degree $k+1$, the terminal coefficient norm and all midpoint errors cost at most t^k, and the omitted initial polynomial costs at most t^{16} in the rank-four chart. For each local error, replace the old injection weight by the rigorously recomputed prefix and trace-corrected partial-panel bound for H', S'. This accounting resizes the computed residual itself. It uses neither a sampled parameter grid nor interpolation of output values. For $H' = 1/1024$, $S' = 1/4096$ we obtain a uniform scalar bound below $3.908\,10^{-29}$ and a connected-column component bound below $4.613\,10^{-18}$. At the nonreal normal-divisor boundary query $h = 2 + i/1024$, $s = -3 + i/4096$, the two forward paths and this stored certificate alone give $628.458265343140302474928823258657 + 0.658643718453258743817799425279i$, within $7.778\,10^{-30}$ of the archived full centre. An independent per-query adjoint can be run as a cross-check. The lightweight evaluator only needs the two forward systems, the order-dependent angular preparation and the reusable bounds.

The rescaling also gives a cost control on the original inner product of disks, $H' = 1/256$, $S' = 1/512$. On this larger set, the degree-six model with the same incoming rule only proves $1.972\,10^{-13}$. Its two row gains remain below $8.184\,10^{26}$. A revised incoming rule with $M = 173$, $B = 99$, $J = 21$, $T = 714$, order 77 Gauss quadrature and origin degree 65 has divided-source truncation and rounding allowance below $1.412\,10^{-53}$. Keep the original radial finite panels through 426 and append panels of width eight. The recomputed sum of all Gauss error bounds is below $2.540\,10^{-75}$ before the divided prefactor, and the required finite-arithmetic threshold is 10^{-56} after it. This proves an algorithmic scalar budget below $3.723\,10^{-27}$ on the full bidisk. We computed its truncation budget and did not execute queries with this revised preparation.

Full inner-disk execution. Taking all 105 order–tilt monomials of total degree at most 13 yields a certificate on the entire original closed product

$$|h - 2| \le 1/256, \qquad |s + 3| \le 1/512.$$

The two backward verifications at 275 bits took 1,009.74 and 1,011.72 seconds. They consumed 977.08 and 955.44 CPU seconds, with peak resident memory 371,852 and 370,740 KiB per process, respectively. For the upper sign, the transported polynomial coefficient norm is below $9.181\,10^{8}$, the outward radial defect charge below

$3.360\,10^{8}$ and the discarded degree-14 parameter forcing below 21.592. The lower sign gives the same coefficient-norm bound, radial defect charge below $3.388\,10^{8}$ and parameter forcing below 3.671. Including the exact scalar prefactor and all finite rounding, the pullback one-norms are below $1,267,102,435$ and $1,269,980,274$. The joined budget for the **moderate, executed** order-dependent angular rule and the two full augmented paths is therefore

$$|T_4(h, s; 14/25) - \widehat{T}_4| < 3.060\,10^{-31}.$$

This holds separately at every input over the full product, including both normal and connection resonances. The uniform componentwise error of the complete connected column is below $1.360\,10^{-5}$. The two approximation targets have different sensitivity. The signed row model controls only the physical scalar, while the componentwise estimate still uses a bound on the whole transition. The algorithm returns actual complex midpoints and absolute disks, including midpoint printing, for the scalar and all 35 components.

The two original refined augmented paths at $s = -3071/1024 + i/2048$ give scalar enclosures of radius below $7.737\,10^{-32}$ using this table alone at $h = 2$ and $h = 2+i/2^{30}$. Their full-column component error using this region-wide gain is below $3.443\,10^{-6}$; their independent pointwise matrix verification remains substantially sharper for the components. When multiple validated boxes contain a query, the implementation reuses the same numerical paths and chooses separate verified bounds for scalar and component errors. The exact input $h = 2 + i/1024$, $s = -3 + i/4096$, for example, has scalar error below $7.666\,10^{-32}$ with degree 13 and component errors below $1.183\,10^{-18}$ with the anisotropic degree-six bound. Selection does not alter the centres or the preparation. Each receipt identifies both tables and the command can select an earlier table explicitly.

Comparison with the preceding finite rules. Theorem 23.3 uses sixteen sampled order pairs and has rank-four error below 1.139×10^{-25} on the inner product centred at $(2, -3)$. Proposition 23.8 uses at most twelve and has error below 8.775×10^{-26} on the older product with tilt centre $-193/50 + 21i/100$. Their distinct tilt disks and error budgets matter to a comparison of cost. Theorem 24.1 replaces both order-sampling procedures by the divided physical state on a single pair of paths. Its order-interpolation error is identically zero. Angular Fourier aliasing remains part of the incoming budget. The old 56-order run and the two original shorter reference runs remain unexecuted in full at rank four.

The prepared source and the two readouts. The retained data are the two full, order-dependent angular columns with the same tilt and the same entrance error. An individual arc omits the second boundary value of the Haar angular law. Connecting only an integer column discards the normal variation in the independent order. The divided angular preparation restores this variation before transport. Propagating the polynomial physical row backwards then identifies the part of the common input uncertainty that affects the scalar. The separate signed full-matrix calculation controls the remaining coordinates. Over the parameter products the backward polynomial residual and the forward matrix bounds serve these two different readouts.

The source and the outgoing determinant originate from the same normalized Haar ensemble. Their numerical integrations are separate. The following controls displace order and tilt independently, approach the phase boundary, and lie on the normal divisor. The higher-rank construction in Section 25 also keeps the angular information needed to initialize the next critical crossing.

End-to-end computations and independent controls

The four computations below used fresh angular data at $z_l = 11/25$ and the full two-leg polygon on each side of $1/2$. The exit is $z_r = 14/25$. Each row has one target order, and the independent tilt stays fixed along its two paths. The first two queries use ordinary weights at nonzero order displacement. The last two solve the triangular reference and divided-difference equations, including the differentiated physical preparation at zero. The rank-four moment is unnormalized throughout.

Order h	Tilt s	Outgoing moment, rounded	Certified absolute radius about archived centre
$129/64 + i/32$	$-247/64 + 7i/32$	$8727.98172177437 - 7909.38193209127i$	1.339×10^{-37}
$2 + i/512$	$-3071/1024 + i/2048$	$626.550568486653 + 1.313091913024i$	7.915×10^{-37}

Order h	Tilt s	Outgoing moment, rounded	Certified absolute radius about archived centre
$2 + i/2^{30}$	$-3071/1024 + i/2048$	$626.551313972450 - 0.951735801330i$	5.381×10^{-30}
2	$-3071/1024 + i/2048$	$626.551313970717 - 0.951736881284i$	5.381×10^{-30}

The certificates retain the centres to 70 decimal digits. Rounding a centre to the shorter table adds the display rounding error. The first pair of forward solutions used independently prepared order-dependent Hermite data. Applying the certified backward rows to the difference from the finer Fourier–Mellin input gives the scalar for that refined input. This linear correction retains the common source error of the two paths. A second calculation initialized the forwards directly at the refined Fourier–Mellin centres. Independent low-precision dyadic proposals for the entire 35×35 matrices, with every panel residual bounded in ball arithmetic, also give component bounds on the genuine branch and connected vectors.

For the older-disk query the correlated initial scalar error was 1.333×10^{-37}, the forward defect below 5.350×10^{-40}, and the backward error below 5.625×10^{-58}. Rounding in the final scalar contraction and its printed centre adds less than 4.885×10^{-67}. The constrained entrance row has norm below 4.4730×10^{7}. At the inner query $2 + i/512$ its norm is below 2.114×10^{6}. The separate canonical calculation at these orders encloses the connected state componentwise to 2.023×10^{-38} and 8.171×10^{-35}, respectively. Those bounds require forward transport from the refined input and actual full-matrix gains. A scalar disk alone would supply no estimate on the invisible directions in the state.

At the first three inputs replacing the physical connection by equal weights moves the scalar by more than 1.3902×10^{-8}, 3.4989×10^{-9} and 1.6683×10^{-15} respectively. Removing either path and removing the radial normalization are tested separately in the receipts. At exact order two the equal-arc scalar agrees by the integer symmetry. Deleting only the order derivative of the incoming preparation in the inhomogeneous equation breaks that compatibility; on the documented scalar extension the resulting error exceeds 7.9502×10^{11}. This fault calculation concerns that specified incomplete preparation. The integer value itself also has the polynomial construction of Section 23.

The comparison on each real fibre uses a separate Hermite enclosure of the original signed angular determinant. A second exit calculation uses the determinant itself under the Mellin integral. At each terminal frequency it sums the signed permutation expansion with tags $j_i = i - \pi(i)$ and retains the factor $(1 - z^2)^{16+8s}$. Its central coefficients use the Toeplitz determinant jets of Section 10. Its finite angular projection, far-frequency series and local error components are saved separately from the incoming angular source. Neither exit computation supplies data to the two-path integrations.

The independent exit Mellin disks for these four orders have radii below 2.427×10^{-24}, 1.553×10^{-18}, 7.405×10^{-25} and 4.850×10^{-73}. Differences of their centres from the forward-and-adjoint centres are below 4.920×10^{-33}, 1.153×10^{-33}, 1.297×10^{-37} and 1.297×10^{-37}. At the last two orders the independently propagated signed canonical matrices enclose every connected coordinate to 8.406×10^{-35} and 8.171×10^{-35}, respectively. At $u = i2^{-30}$ the canonical scalar with only the integer column gives an imaginary part near -66.89661. Restoring the divided state gives an imaginary part near -0.95174. The enclosed omission error exceeds 65.9452. This test keeps the displaced physical row fixed and deletes its divided-state contribution. The equal-weight control changes a different part of the calculation.

Fresh queries with independent parameters. An executable interface accepts rational real and imaginary parts on the two parameter products. It prepares every incoming coordinate, propagates the two complete forward states, integrates two separate backward polynomial rows and checks the final absolute radius against the requested tolerance. It selects ordinary transport sufficiently far from two and the triangular transport near two. The optional replay reads the saved branch and source records. A fresh call requires a new directory.

At $h = 2 + i/1024$, $s = -3 + i/4096$, the equality $h - 2 = 4(s + 3)$ places both nonreal parameters exactly on the top normal divisor. The result is $628.4582653431403025 + 0.6586437184532587i$, rounded for display. The certified radius about the archived centre is below 1.712×10^{-34}. The source contribution is below 1.712×10^{-34}, the forward and anchor budget below 9.349×10^{-41} and the final rounding below 1.500×10^{-70}. The correlated

entrance gain is below 9.016×10^{5}. This cold query took 648.25 seconds, including initialization and transport; maximum worker RSS was 228,984 KiB.

At $h = 2 + 3i/64$, $s = -31/8 + 3i/16$, inside the older disk, the result is $10077.4499978408138382 - 6737.0882294029519018i$, rounded. The archived disk has radius below 1.343×10^{-34}, with source contribution below 1.343×10^{-34}, forward contribution below 3.959×10^{-39}, and rounding below 7.251×10^{-69}. The corresponding entrance gain is below 3.910×10^{10}. Four workers required 310.91 seconds of elapsed time and 984.98 seconds of combined CPU time. The maximum individual worker RSS was 229,608 KiB. Summing resident memory over the live process tree every 0.15 seconds gave a peak of 720,285,696 bytes; shared pages can be counted more than once and peaks between samples can be missed.

The Fourier panel arithmetic and signed-tail arithmetic have separately recorded working precisions. The generic runs used 760 bits for the adjoint, endpoint row and scalar contraction. They charge the magnitude of centre rounding on writing a decimal, the full forward defect, the propagated initial disks and the error of each computed adjoint. The divided runs also charge the integer anchor and its forced effect on the companion state. The interval calculations used python-flint 0.9.0 with FLINT 3.6.0 on Linux. Each query reports its own budget. The parameter-wide estimates above require the numerical subroutines to meet the stated arithmetic, source and propagation allowances, with refinement when necessary.

At the exact complex normal divisor $h = 2 + i/1024$, the uniform backward row bounds can certify incorrect answers as well. For a change in the two divided weights by d_+, d_-, apply the canonical row to $d_+Z_+ + d_-Z_-$. Charge $|d_\pm|$ times the corresponding row gain times the divided-source error, and charge the measured forward defect and the order-halo transfer of the anchor error on each path. This gives a certified *lower* separation after subtracting those radii from the magnitude of the computed difference. The upper-only, lower-only and equal-weight outputs differ from the physical one by more than 1.7518×10^{-9}, 1.7411×10^{-9} and 1.7464×10^{-9}. Keeping just the transported integer column with the displaced physical row changes the result by more than 6.9599×10^{7}. Omitting the radial prefactor changes it by more than 597.49. At the second normal-divisor query $h = 2 + i/16384$, $s = -3 + i/65536$, the equal-weight separation still exceeds 1.0915×10^{-10}. Both checks apply the original physical row at the stated input.

Executing only the two forward paths. At $h = 2 - i/16384$, $s = -3 + (1 - i)/32768$, we started from an empty directory and independently prepared all the angular data. We then solved on both complex polygons with the degree-six regional bound on the physical backward rows. The warmup for that bound was done once for the whole region. No backward integration or outgoing determinant was invoked by the query. The physical scalar is

$$628.39897187864180979297 - 0.011325866003816385 78i$$

to the digits shown. The disk about the archived centre has radius below 2.0970×10^{-31}. Its contributions from the shared divided source, forward paths including the integer anchor, and rounding the scalar are below 2.0970×10^{-31}, 9.819×10^{-41} and 4.657×10^{-64}. We also stored decimal midpoints for every connected component, including their conversion errors; the maximum absolute radius is below 6.682×10^{-18}. A cold run took 522.44 seconds, with 1,114.87 CPU seconds, 231,484 KiB peak worker RSS and sampled process-tree RSS below 734 MB. The sampled memory figure includes shared pages in each process. On the positive-imaginary normal-divisor input $h = 2 + i/16384$, $s = -3 + i/65536$, a separate query-specific pair of backward integrations gives an absolute scalar radius below 2.110×10^{-35}. Using only its two forward records with the published degree-six bounds gives 2.097×10^{-31}. The original Haar exit determinant supplies a further comparison on both fibres below.

After extracting the compact evaluator into a new directory outside the source workspace, we ran the same forward-only algorithm from fresh data at the separate off-centre input $h = 8193/4096 + i/8192$, $s = -49151/16384 - i/8192$. It produced $628.62320784222419545849 + 0.380819241623435351 96i$ to the displayed digits, with absolute radius below 2.094×10^{-31} about the full centre. The maximum error on the 35 serialized coordinates is below 6.671×10^{-18}. The physical exit disk is contained in a separately prepared 46-node original determinant disk of radius below 2.840×10^{-9}. This run took 508.23 elapsed seconds and 1,121.84 aggregate CPU seconds, with 231,216 KiB peak individual worker RSS.

A fresh query on both boundaries of the full inner product. Take $h = 2 + i/256$, $s = -7683/2560 + i/640$. Then $s + 3 = (-3 + 4i)/2560$, so $|s + 3| = 1/512$ exactly. The source, the two augmented paths, and both query-specific backward rows were computed from fresh inputs. The scalar at $14/25$ is

$$630.75252270763133359332458610806 4 + 1.4944236282144494875356452914 76i$$

to the digits shown. The common-source correction with the query-specific rows encloses the full-precision result to 6.731×10^{-34}. Its source, forward-plus-anchor and final printing allowances are below 6.731×10^{-34}, 2.018×10^{-40} and 4.274×10^{-70}. Applying only the full-region degree-thirteen table to the same forward receipts gives a disk of radius below 7.582×10^{-32} and 35 connected coordinate disks of radius below 3.374×10^{-6}. The fresh computation took 474.46 seconds with a sampled process-tree peak of 781,111,296 bytes. The 52-node original Haar determinant encloses the scalar to 4.833×10^{-8} and its midpoint differs from the transported centre by less than 7.420×10^{-9}. Replacing the two physical weights by equal weights is separated from the physical scalar by more than 6.9725×10^{-9} in the certified path calculation.

Independent checks of the single-query program. At the two fresh command-line inputs the original Haar eigenangle determinant was integrated on the outgoing fibre $z = 14/25$, with a 52-node Hermite rule, degree 103, and 920-bit arithmetic. The determinant uses the independent orders directly, with an absolute majorant for the nonpolynomial Hermite remainder. At $h = 2+i/1024$, $s = -3+i/4096$ the distance between its midpoint and the transported midpoint was below 1.8530×10^{-9} inside an independent radius below 1.2069×10^{-8}. At $h = 2+3i/64$, $s = -31/8 + 3i/16$, the midpoint distance was below 2.2652×10^{-7} inside a radius below 1.4630×10^{-6}. Both entire transported disks are strictly contained in these independent enclosures. The tighter accuracy at these inputs comes from the transport error budget.

For the original older-disk and joint-disk noninteger crossings, finer independent Weyl–Mellin tail evaluations used Fourier cutoff 70, 22 signed asymptotic terms and terminal frequency 322. A five-point Fourier projection of the degree-four Weyl determinant collected the five sign channels of the tail. The independent outgoing disks now have radii below 1.1460×10^{-27} and 2.4503×10^{-26}, respectively. Their centres differ from the corresponding two-path adjoint-corrected results by less than 2.548×10^{-39} and 1.543×10^{-39}. At $h = 2 + i2^{-30}$ in the joint tilt the independent radius was below 1.1684×10^{-32}. Each radius includes the discarded Fourier modes, signed-Bessel remainder, finite quadrature and arithmetic.

Independent outgoing checks inside the rank-four cell

The two runs used the original Haar eigenangle determinant on the outgoing fibre at $z = 14/25$. The determinant supplied the first 104 moments of the scaled squared distance $X = |4z - \sum_j w_j|^2/[4(1+z)]^2$. A 52-node interior Hermite interpolant represented X^h up to an absolute remainder bounded using the real exponent 7/4 and the positive angular preparation at $\Re s$. All coefficients, determinant jets, angular normalization, complex powers and rounding were enclosed at 920 bits. The following independent disks were computed from the exact request parameters before loading any transported output.

The generic-cell input is $h = 2 + i/16384$, $s = -3 + i/65536$. The forward-only input is $h = 2 - i/16384$, $s = -3 + (1-i)/32768$.

Run	Real part, rounded	Imaginary part, rounded	Independent radius
Generic cell	628.45864415	0.04116524	7.54285×10^{-10}
Forward only	628.39897188	−0.01132587	7.54267×10^{-10}

The JSON records give 85-digit centres, absolute radii, runtime and peak resident memory. Reproduce with `python generic_checks.py determinant generic-cell` and `python generic_checks.py determinant forward-only` in the companion rank-four verification package. The corresponding `join` commands compare the determinant disks with the full transport certificates using outward-rounded arithmetic.

Both entire transported disks lie strictly inside the independently computed outgoing disks. The centre distances are below 1.15810×10^{-10} for the generic cell and 1.15807×10^{-10} for the forward-only run. The strict margins exceed 6.3845×10^{-10} in both comparisons. These checks confirm agreement with the original angular calculation to its own stated accuracy. The much smaller transport errors have their separate source, continuation and readout budgets.

Which derivative survives the integer-order connection?

At $s = -3071/1024 + i/2048$, $z_r = 14/25$, let $f(u) = T_4(2+u, s; z_r)$ and let $f_\pm(u)$ denote its canonical upper and lower branch scalars, including the order-dependent outgoing row. Their values and first order derivatives agree

between the two arcs at $u = 0$ by Theorem 10.17. A measurement of the first derivative of the *physical* moment requires additional information.

The three completed full-transport values at $u = 0, it, iT$, $t = 2^{-30}$, $T = 1/512$, determine a quadratic interpolant. Cauchy's interpolation remainder differentiated at zero, with $|f| < 8988$ on $|u| = 1$ as in Theorem 23.3, has modulus at most $8988tT/[(1-t)(1-T)]$. Add the weighted radii of the three certified values. The resulting disk for $f'(0)$ is centred at $1159.591619346007-1.861210490044i$ with radius below 1.639×10^{-8} including decimal rounding here. For each individual arc evaluate $f'_{\pm}(0) = \ell'_2 X+\ell_2 Z_{\pm}$ on its transported tangent. Differentiation of the polynomial row in Theorem 23.1 includes the logarithmic derivative $-2(1/3 + 1/4)$ of its reciprocal rising-factor denominator. Both arc enclosures agree, with the upper one centred at $1159.591617553168709785352677897032486 3 - 1.861210491542721325331819867649844 1i$ to absolute error less than 6.670×10^{-25}. Source error in the common reference column also drives the tangent. The verified transfer norm on a closed halo of radius 2^{-20} divided by this radius bounds the derivative transfer used in charging that error.

The physical derivative differs from the common one by more than 1.77645×10^{-6}. Expanding the physical connection at zero now gives an intrinsic second-order jump,

$$f'(0) - f'_+(0) = -\frac{i}{4\pi}\big[f''_+(0) - f''_-(0)\big], \qquad |f''_+(0) - f''_-(0)| > 2.23236 \times 10^{-5}.$$

Thus the nonzero offsets distinguish a genuine order-dependent branch effect even though both integer-order paths and their first order derivatives coincide.

A separate calculation differentiates the original signed Weyl exit determinant at $h = 2$. In its Mellin representation the noncentral terms are multiplied by $K(h)$ and $K(2) = 0$, $K'(2) = -128$. Thus the order derivative reuses the physical degree-two radial kernel, with a new central polynomial: for $j \neq 2$ its coefficient is $4R^{2j}(-1)^{2-j}/[(j!)^2(2-j)]$, and at $j = 2$ it is $2R^4\psi(3)$. The undifferentiated radial prefactor in the angular tail is retained. With Fourier cutoffs $132, 77$, frequency cutoff 322, 11 signed asymptotic terms, and the independent Weyl quadrature, the result is $f'(0) = 1159.5916193445632164771 - 1.8612104900431428834i$ with absolute error below 7.951×10^{-16} about this centre. It lies inside the interpolation disk obtained entirely from the physical branch calculations. Combining it with the transported arc derivative refines the intrinsic second jump to

$$f''_+(0) - f''_-(0) = -1.88442584667 \times 10^{-8} + 2.25113272876 \times 10^{-5}i \quad \text{with absolute error below } 1.000 \times 10^{-14}.$$

A further signed Weyl computation with 22 terms gives an independent physical derivative radius below 1.255×10^{-23}. Combining it with the actual transported branch derivatives bounds the second jump by an absolute disk of radius 1.661×10^{-22} about its archived centre, whose real and imaginary parts begin $-1.8844258466669377650\times 10^{-8}$ and $2.25113272876161166560 \times 10^{-5}$. The independent refinement uses the same frequency cutoff 322 and angular cutoff 70 for its signed tail.

25. Noninteger moments across consecutive critical radii

Full angular transport through two consecutive rank-five trace radii

In this construction the tilt is initially $s = -5$. The angular change in Section 10 leaves independent uniform unit phases w_i and the mark $v = a-\sum_i w_i$, where $a = 5z$. The signed Vandermonde and the factor $(1-z^2)^{-25}$ restore the ordinary Haar scalar. The rank-five compact state has 56 entries, indexed by sorted tags $j_i \in \{-1, 0, 1, 2\}$ at the raised order $h + 4$. We give a closed alternative to eliminating its 112-row displacement pencil along the paths. The scalar special-tilt differential equation in Theorem 10.2 supplies neither these transported tagged states nor their two successive numerical connections.

Proposition 25.1 (spinning angular kernels and their successive connections). Let N be odd, $N \geq 5$, $s = -N$, $\Re h > -1$ and $\Im h \neq 0$. Put $H = \lfloor (N-1)^2/4 \rfloor$. Every tagged moment at $g = h+H$ and the signed Weyl scalar at order $g = h$ are finite sums of coordinates of explicit $(N+1)$-component Fuchsian systems. Their finite poles lie in $\{0, N, N-2, \ldots, -N\}$. Every inward physical connection at a positive $k = N - 2j$ uses the same phase weights within a combination, including for $k = N$ when the transformed angular law is continued from exterior displacement. This last crossing concerns the angular law before the radial prefactor is applied. The systems may be composed across successive positive k without reinitializing. The hypothesis $\Im h \neq 0$ suffices to prevent the gamma and phase exceptional cases in the formulas below.

Write $P_i = \prod_{j=1}^{i} w_j$, $H_i(t) = J_0(t)^{N-i} J_1(t)^i$. For integer l and complex u introduce the prepared coordinate

$$U_i = \mathbb{E}[P_i |v|^{2u} e^{il \arg v}], \qquad K_l(u) = 2^{2u+1} \frac{\Gamma(1+u+l/2)}{\Gamma(-u+l/2)}.$$

At $v = 0$ the choice of argument is immaterial. The angular Fourier identity and the Mellin integral of J_l (NIST Digital Library of Mathematical Functions, equation 10.22.43) give

$$U_i / K_l(u) = \int_0^\infty t^{-1-2u} J_{i+l}(at) H_i(t)\, dt.$$

Initially take $-1/4 < \Re u < 0$. The absolute integral of the single Bessel kernel after rescaling is bounded by a constant times $|v|^{2\Re u}$, which is integrable at the regular angular fibres. Integration in the angular Fourier direction gives $i^{i+l} J_{i+l}(at)$ and the tagged phases give $(-i)^i H_i(t)$; the harmonic transform on the left contributes i^l. For negative integral orders the signed Bessel relation $J_{-j} = (-1)^j J_j$ gives the same formula. The ordinary angular coordinates continue holomorphically in u throughout $\Re u > -1$ on regular interior fibres. The integral at other orders is taken by this continuation, or by its finite part at $t = 0$. No continued moment outside the ordinary domain enters this construction.

Let $D = a\partial_a$, $C_{i,i-1} = i$, $C_{i,i+1} = N - i$, $A_{ii} = 2u + i$, $B_{i,i-1} = -i(i + l - 1)$, $B_{i,i+1} = (N - i)(i + l + 1)$, all other entries zero. Differentiating H_i gives $H_i' = iH_{i-1} - (N - i)H_{i+1} - iH_i/t$, where standalone i in these matrices and this formula denotes the integer index. Integrate the derivative of $t^{-2u} J_{i+l}(at) H_i(t)$ and apply $J_j' = (j/t)J_j - J_{j+1} = J_{j-1} - (j/t)J_j$. The endpoint terms vanish in the starting strip, and analytic continuation gives

$$(aI - C)DU = (aA + B)U.$$

The rational eigenvector matrix of C is $E_{ir} = [x^i](1 + x)^{N-r}(1 - x)^r / \binom{N}{i}$, with eigenvalues $N - 2r$. This follows by differentiating the coefficient polynomial, or by the symmetric power of the two-state exchange operator.

For a physical tag $\mathbf{j}$, $L = \sum j_i$. Its unweighted angular moment of order g has Fourier integrand $K_0(g) J_L(at) \prod_i J_{j_i}(t)\, t^{-1-2g}$. Expand the product by $J_{j+1} = 2jJ_j/t - J_{j-1}$ and the signed negative-order rule. A monomial $c\, t^{-m} H_i(t)$ contributes $cK_0(g)U_i/K_l(u)$ with $l = L - i$, $u = g + m/2$. Since $m + l$ is even, the factor is exactly

$$\frac{K_0(g)}{K_l(u)} = 2^{-m} \frac{(-g)_{(l-m)/2}}{(1+g)_{(l+m)/2}},$$

using signed integer rising factorials. To justify the finite many reductions when their Mellin strips need not meet, split every integral at $t = 1$. At the origin, before and after the finite Bessel recurrence the integrands agree pointwise. Take $\Re g$ sufficiently negative for *every origin integral alone* to converge, then continue the identity of these finite-interval integrals meromorphically by subtracting their Taylor series to arbitrary finite order. Each Taylor monomial integrates to its explicit denominator. All are analytic at the nonreal orders used here. At infinity, for fixed positive a the original product behaves in absolute value as $O(t^{-(N+1)/2})$ and every reduced product has the additional factor t^{-m}; hence each tail integral already converges absolutely on $\Re g > -1$ for $N \geq 5$. Equality there follows from the pointwise recurrence, separately from the origin proof. For the earlier integration by parts within one block, all the undisplaced i indices share the initial strip stated above: the origin boundary term vanishes since $t^{-2u} = o(1)$, and a single a derivative in the tail costs at most one power of t. Continuation of the regular angular law then proves its differential equation at the orders actually propagated. The bounded trace-density argument below supplies uniform ordinary integrability for negative orders, including after translation. This identity also determines phase and normalization of the scalar after summing the signed permutations $j_i = \sigma(i) - i$. The factor $1/N!$ in the squared Vandermonde expansion cancels one permutation sum by symmetry.

For the frequency $a - k$, the positive-frequency stationary phase for $J_{i+l}(at) H_i(t)$ differs from $\phi = \pi(k - 1)/4$ by $-\pi l/2$ modulo π. Indeed choose a sign for each one-body Bessel phase, with their signed sum equal to $-k$. The i order-one factors together with the target order $i + l$ contribute an additional $-\pi l/2$ modulo π. The opposite frequency reverses all the phases. At each higher Gaussian order their coefficients undergo the same alternating sign as in Theorem 10.9. Its convergent saddle-contour proof applies with the extra trigonometric angular harmonic, also at $k = N$: after the tilt specialization the angular amplitude has no z-dependent denominator at that endpoint. The decrement in the connection angle for a descending arc is thus $\pi(l + m)/2$ modulo π relative

to the angle computed at g. Replacing g by $h+H$ adds an integer multiple of π. Consequently all requisite blocks use

$$\theta_k = \pi(k-1)/4 - \pi(2h+(N+1)/2)/2, \qquad w_k = \frac{e^{i\theta_k}}{e^{i\theta_k}+e^{-i\theta_k}}.$$

The Fuchsian equation gives a separate justification of the local branch count, including at the outer caustic. Put $J=\operatorname{diag}(i)$. The generating polynomial of column r of E gives $E^{-1}JE=(NI-C^{\mathsf{T}})/2$. Since $B=[C,J](J+lI)$, $(E^{-1}BE)_{rr}=\sum_j(\lambda_r-\lambda_j)(E^{-1}JE)_{rj}(E^{-1}JE)_{jr}=\lambda_r/2$. The residue at $a=\lambda_r\neq 0$ has just one nonzero row and diagonal entry $b=2u+(N+1)/2$. Its square equals b times the residue. Since b is nonreal, Frobenius theory gives a convergent analytic part and a single branched mode t^b times an analytic vector. The analytic parts match because the angular solution is continuous, $\Re b>0$, and an analytic solution is determined by its value. For the order-zero tagged component the leading $\pm(a-k)$ saddle amplitude is nonzero. At $k=N$ all edge signs are negative. The two signed Bessel phases therefore determine the multiplier on the only remaining mode even at that caustic. The independent audit checks the signs at negative Bessel indices, the rational Mellin factors and both inward phase weights. Starting from the physical right-hand germ, take $w_kU^{\uparrow}+(1-w_k)U^{\downarrow}$ at the left-hand fibre, and use that entire result for the next pair of arcs. The same argument allows increasing connections with the sign specified in Theorem 10.9.

Initialization and certified Taylor steps. At $a_0=10>N=5$, binomial expansion of both factors of the spinning angular kernel gives

$$U_i=(-1)^i a_0^{2u-i}\sum_{p\ge 0}\binom{u+l/2}{p}\binom{u-l/2}{p+i}\,d_{p,i}\,a_0^{-2p},$$

where $d_{p,i}=p!(p+i)![x^p](\sum_{j\ge0}x^j/(j!)^2)^{N-i}(\sum_{j\ge0}x^j/[j!(j+1)!])^i$. The extra i in the second binomial comes from cancelling the i positive angular tags. All these counts are nonnegative integers bounded by N^{2p+i}. With $r=4/5$, put $t=(N/(ra_0))^2$, $M(v)=5^{|\Re v|}e^{\pi|\Im v|}$. Cauchy's inequality on $|x|=r$ gives tail at most $a_0^{2\Re u}M(u+l/2)M(u-l/2)t^{P+1}/(1-t)$ after $p=P$.

Write $\widetilde{A}=E^{-1}AE$, $\widetilde{B}=E^{-1}BE$. On a step $a=x+\delta t$, compute the local fundamental matrix by coefficient recurrence $V_0=I, V_1=F$,

$$(n+1)V_{n+1}=(F+nG)V_n+(K+(n-1)L)V_{n-1},$$

where $S=\operatorname{diag}(\delta/[x(x-\lambda_i)])$, $F=S(x\widetilde{A}+\widetilde{B})$, $G=-S\operatorname{diag}(2x-\lambda_i)$, $K=\delta S\widetilde{A}$, $L=-\delta S$. These follow by clearing the row denominators. Given the last two matrices through V_{n+1}, let $\eta=(\|F\|+\|K\|)/(n+1)+\|G\|+\|L\|$ in the row-sum norm. If $\eta<1$, every successive pair of coefficients is bounded by η times the preceding pair maximum. Thus the remaining norm at $t=1$ is at most $2\max(\|V_n\|,\|V_{n+1}\|)\eta/(1-\eta)$. All step matrices include this tail and ball rounding. Multiplication of each path, the complex weights, projection and final prefactor use outward-rounded arithmetic.

Executed case. Set $N=5$, $h=5/4+i/4$, $s=-5$. The exterior angular initialization has $P=250$. After transport from $a=10$ to 6, the three polygon pairs have vertices $(6,5\pm4i/5,4)$, $(4,3\pm4i/5,2)$, $(2,1\pm4i/5,3/5)$. Only the last two are interior physical crossings. At $a=4$ the compact incoming state for those two crossings has already been selected from the original angular source. The 46 distinct six-component blocks, their series certificates and all 56 recovered physical entries are archived. The normal exponent of the independent final compact readout is $h+9$, off its exceptional divisors. The construction uses no free coefficient from a homogeneous singular mode.

Outgoing z	Maximum absolute disk radius of 56 transported coordinates	Scalar radius from the original compact row	Scalar radius from transported signed Weyl terms
4/5	1.338×10^{-50}	1.597×10^{-35}	1.720×10^{-44}
2/5	5.787×10^{-41}	1.181×10^{-28}	2.831×10^{-47}
3/25	1.347×10^{-30}	2.322×10^{-31}	2.881×10^{-43}

Radii refer to the full-precision centres in the records. At $z=3/25$ the scalar is approximately $2.285195392404688664670519 40+0.495907920954478426937716773i$. Independent angular polynomial enclosures at all three fibres contain all 168 transported coordinate enclosures. The separate determinant

enclosures also contain all three signed Weyl results. At the final wall the upper-only, lower-only and equal-weight scalar discrepancies exceed 1.225×10^{-7}, 5.897×10^{-7} and 3.011×10^{-7}, respectively. Removing the physical prefactor produces a discrepancy exceeding 0.711. These are rigorous disjoint-enclosure tests. All endpoints, timings, component errors and the independent normal rows are supplied in the records.

A further chain control replaces the first *interior* physical combination at $z = 2/5$ by its upper branch, lower branch, or equal-weight average. Each deliberately altered input is then propagated through the correct second two-path connection. The respective exit discrepancies at $z = 3/25$ exceed 0.03053, 0.1469, and 0.07502. Restoring the correct first connection and transporting it by the independently rebuilt final-wall matrices reproduces the certified exit scalar.

An inverse-order run used precisely the same three polygon pairs and independent exterior preparation at $h = -1/4 + i/4$, $s = -5$. The ordinary inverse moment exists by the bounded trace density proved below. All 46 blocks were recomputed. Their time totaled 172.659 seconds, with peak block RSS 28,812 KiB at 448 bits. Summed block runtimes depend on concurrent load. At $z = 3/25$ the physical scalar is approximately $1.480079040933391004365451 90 - 0.258379938200330455668732888i$. The signed Weyl disk radius is below 1.546×10^{-46} about its archived centre; all 56 transported coordinates have radii below 2.439×10^{-35}, and their canonical normal-row scalar has radius below 2.235×10^{-33}. Upper-only, lower-only and equal-weight answers at the final wall miss by more than 1.480×10^{-4}, 7.123×10^{-4} and 3.638×10^{-4}. The independent original-determinant density bounds are comparatively loose at this inverse order. Contracting a separately enclosed real-fibre angular state with the original normal row gives an independent exit disk of radius below 0.08639. The high accuracy comes from the certified transport and its exact representation; the external checks distinguish at their own stated resolutions.

As an exact algebraic control, direct multiplication of the angular Laurent polynomials at exponents $u = (p+q)/2$, $l = p - q$, $0 \le p \le 4$, $0 \le q \le 5$ verifies 390 component identities at ranks five and six. Omitting the spin detects a discrepancy in 50 of the 60 cases, and reversing the lower off-diagonal sign fails in 58. For $p = q = 1$ the direct state starts with $a^2 + N, -a$ and the remaining coordinates vanish.

Independent complex tilt in successive physical projections

The same propagation gives a convergent sequence of connected finite angular preparations for independent complex tilt. This extension controls all components on each real physical fibre. The individual unprojected complex arcs of the discarded preparation require separate bounds.

Proposition 25.2 (correlated angular truncation on several fibres). For the preceding odd ranks, fix $\Re h > -1$, $\Im h \neq 0$, and let $\nu = -N - s$. On the unit angular torus expand

$$F(z, \mathbf{w}) = \prod_{i=1}^{N} (1 - z w_i)^{\nu} (1 - z/w_i)^{\nu} = \sum_{d \ge 0} z^d P_d(\nu, \mathbf{w}).$$

Both determinations start from $z = 0$. Each P_d is an explicit Laurent polynomial in the phases of degree at most d in ν. Truncation at $d = L$ produces one finite system of spinning angular blocks for the whole trajectory. Multiply each term by its analytic coefficient z^d at the current radius. Apply the signed connections, including at successive walls, to all terms. This gives the exact physical projection of the *same* truncated preparation at each fibre. On $|\nu| \le \epsilon$ and real $0 \le z \le r < 1$ the omitted preparation is bounded uniformly by

$$\tau_L(r) = \sum_{m > L} \frac{(2N\epsilon)_m}{m!} r^m.$$

When $2N\epsilon \le 1$, $\tau_L(r) \le (2N\epsilon)_{L+1} r^{L+1} / [(L+1)!(1-r)]$. The estimate follows from $|\binom{\nu}{m}| \le (\epsilon)_m / m!$ and multiplication of positive majorants. Finite tags of any integer frequency reduce to the preceding six-dimensional blocks at rank five. The phases stay the same because the parity $m + l \in 2\mathbb{Z}$ holds separately for each tagged reduction.

For $q = \Re h \ge 0$, let $R = N(1 + z)$. At a specified fibre all compact-coordinate errors from the discarded preparation are at most $\tau_L(z) R^{2(q+H)}$; the physical scalar error is at most $\tau_L(z) R^{2q} (1 - z^2)^{-N^2 - 2N\epsilon}$. For a sharper pointwise scalar bound one can use the actual real part of s. These scalar estimates exploit normalization of the

positive Haar angular measure *before* multiplying by the complex preparation. The estimates after the second wall use the same omitted angular function as at the first. Treating the first omitted projection as arbitrary independent input error for the second would lose this relation.

There is also a convergent bound for inverse orders. Write $C_N = [81/2+81/(N/2-2)]/(2\pi)$, $D_N = N^N/N!$. The trace of $N \geq 5$ independent phases has density bounded by C_N, uniformly in the translation a. For $t \geq 1$, split the integral $\pi^{-1}\int_0^\pi e^{it\cos x}dx$ at $\delta = t^{-1/2}$ and $\pi-\delta$. Integration by parts on the middle interval and $\sin\delta \geq 2\delta/\pi$ give $|J_0(t)| \leq 3t^{-1/2}$. Fourier inversion then bounds the density by $(2\pi)^{-1}\int_0^\infty t\min(1, 3t^{-1/2})^N dt = C_N$. Hadamard's inequality bounds the normalized Vandermonde density relative to independent angles by D_N. For $-1 < q < 0$, integrating inside and outside $|a - \sum w| = 1$ therefore replaces R^{2q} in the scalar error by $1 + \pi D_N C_N/(q+1)$. The raised compact coordinates still have positive real order. These estimates prove convergence of the projected truncations and give an explicit finite stopping order for their analytic tails on compact subsets. Cost and arithmetic error of the remaining finite block propagation depend on the chosen parameters. At a phase resonance, including certain real noninteger h, the derivative connection would require a separate implementation.

Executed continuous-tilt preparation. For $N = 5$, $h = 5/4 + i/4$, use the same descent through $z = 3/5$ and $1/5$ and the closed complex disk $|s+5| \leq 1/16$. Direct multiplication of the ten binomial factors through degree four gives all 56 compact-coordinate polynomials, alongside the signed scalar, using 142 distinct six-component blocks. To keep the scalar cost small while improving its accuracy, differentiate the preparation in z. If $G_n = n!P_n$, then

$$G_n = -\nu \sum_{m=1}^{n} \frac{(n-1)!}{(n-m)!}\left(\sum_{j=1}^{N}(w_j^m + w_j^{-m})\right)G_{n-m}.$$

The signed Weyl insertion is applied before this recurrence. Through degree eight it gives 6,331 nonzero projected coefficients. Equality with direct multiplication through degree four was verified exactly. Only 28 additional spin blocks were needed. The 142-block construction used 453.992 summed block seconds, and the additional blocks used 130.193 summed seconds. All blocks started from their angular source with no reseeding on the physical real fibres.

For the recorded error bounds we replace the support estimate by exact adjacent integer moments. Under either positive reference measure, $M_{p+1/4}(a) \leq [M_p(a)^3 M_{p+1}(a)]^{1/4}$, where $M_j = \mathbb{E}|a - \sum w|^{2j}$. Rotation gives $M_j = \sum_{b=0}^{j}\binom{j}{b}^2 a^{2(j-b)}A_b$. For independent phases $A_b = d_{b,0}$ from the exterior-series construction, and for the Haar scalar $A_b = b!$ at $b \leq 2 \leq N$ by Schur orthogonality. This yields the following absolute analytic tails across the whole tilt disk. The upper bounds for the radii of the stored coefficients, weighted by the appropriate powers of $1/16$ and the physical scalar prefactor, are below 1.325×10^{-36}, 3.107×10^{-38} and 8.503×10^{-34} for the scalar in table order. The final state table's weighted coefficient radius is below 1.071×10^{-26}. The standalone query performs further outward-rounded arithmetic and adds its measured radius on every evaluation.

Physical fibre z	Degree-four tail, each of 56 entries	Degree-eight tail, physical scalar
$4/5$	7.326×10^{7}	1.684×10^{12}
$2/5$	3.169×10^{4}	0.09283
$3/25$	4.597	4.444×10^{-9}

The entrance bounds are wide. At the final fibre and the genuinely nonreal tilt $s = -319/64 + i/32$, substituting the actual $|s+5|$ and radial prefactor in the tail yields $T_5 = 2.28126793751308 1869 + 0.47384676441477 37874i$, with absolute error below 1.349×10^{-9} about the archived centre; the largest state-coordinate error is below 1.660. The exact signed reduction at $s = -5$ has the much narrower enclosures above. The tables passed 342 scalar and state comparisons, three closed-boundary queries and two out-of-domain tests. A separate 56-node original determinant run at 1,450 bits encloses the entire degree-eight sample disk inside an absolute radius below 7.247×10^{-6}. The domain is continuous by the preparation-tail estimate. Interpolation or validation at finitely many tilts would not supply this estimate.

Inverse order with an independent complex tilt after two crossings

Lemma 25.3 (inverse powers under a common rotation). There is a sharper inverse-moment estimate on a positive-radius fibre that uses only the common angular rotation. Let Z be any rotation-invariant complex

random variable, $a > 0$ and $0 < p < 1$. Then

$$\mathbb{E}|a - Z|^{-p} \ \le a^{-p} \frac{\Gamma(1-p)}{\Gamma(1-p/2)^2}.$$

The constant is attained by a uniform phase with fixed radius a. To prove this, condition on $|Z|$ and write $t = |Z|/a$. For $0 \le t < 1$, angular averaging of the two binomial series gives

$$A_p(t) = \frac{1}{2\pi} \int_0^{2\pi} |1 - te^{i\phi}|^{-p} \, d\phi = \sum_{k \ge 0} \frac{(p/2)_k^2}{(k!)^2} t^{2k}.$$

The coefficients are positive, so A_p increases to its value at one. The beta integral for $|2\sin(\phi/2)|^{-p}$, or Gauss summation (NIST Digital Library of Mathematical Functions, equation 15.4.20), gives $A_p(1) = \Gamma(1-p)/\Gamma(1 - p/2)^2$. The integral at one equals the series limit by dominated convergence since $|1 - te^{i\phi}|^2 \ge 4t\sin^2(\phi/2)$ for $t \ge 1/2$. For $t > 1$, $A_p(t) = t^{-p} A_p(1/t) \le A_p(1)$. A possible atom at zero contributes a^{-p}. For $p \ge 1$ a law concentrated on $|Z| = a$ has divergent inverse moment, so common rotation alone cannot extend this bound. The argument applies to the positive reference Haar measure before the complex preparation is inserted.

Fix $N = 5$, $h = -1/4 + i/4$, $|s + 5| \le 1/16$, and write $\nu = -5 - s$, $D = 1 - z^2$, $a = 5z$, $\epsilon = 1/16$. Truncate the signed Weyl projection through degree six in z and each of the 56 compact coordinates through degree two. The correlated finite preparations cross the two interior walls by the preceding spin connection. If $\tau_L(z)$ denotes the preparation tail with $2N\epsilon = 5/8$, the analytic error on a real fibre is at most

$$D^{-25-10\epsilon} \, a^{-1/2} \frac{\Gamma(1/2)}{\Gamma(3/4)^2} \tau_6(z)$$

for the physical scalar, and at most $[M_3(a) M_4(a)^3]^{1/4} \tau_2(z)$ for each coordinate. Here $M_k(a) = \mathbb{E}|a - \sum w_j|^{2k}$ under independent uniform phases. The raised compact order has real part $15/4$. Hölder interpolation between the exact integer moments gives its factor. The sharp conditional scalar bound follows from the preceding calculation with $p = 1/2$ and the Haar trace. At a particular input one may use $10|\nu|$ in the binomial tail and the actual modulus of $D^{-25-10\nu}$. All powers of D use its real logarithm.

Physical radius z	Uniform absolute scalar error	Uniform error per state entry
$4/5$	4.792×10^{10}	4.264×10^{5}
$2/5$	0.06566	1568.1
$3/25$	2.974×10^{-7}	4.893

These margins include the weighted radii of the stored coefficients (below 1.004×10^{-39} for the scalar and 5.11×10^{-35} for each state entry). The evaluator adds measured ball-arithmetic and serialization error for a requested centre. The bounds apply at every tilt in the closed disk; the centres vary with the input. The wide entrance errors are not propagated as unrelated noises. The same discarded Haar preparation is bounded again at each physical projection.

The run used 119 six-component spin blocks. It reused the 46 inverse-order blocks of the exact preparation and computed the remaining 73 from their own exterior angular data at 448 bits, using exterior degree 290, with 113.21 summed block seconds. Both arcs were propagated at each wall. At $s = -319/64 + i/32$ and $z = 3/25$ the scalar is centred at $1.477847714355526993 - 0.264226254960053441i$ to the digits shown, with absolute error below 9.675×10^{-8}. The common disk about the 56 individual centres is below 2.033. A separate 37-node original determinant enclosure (900 bits) contains the complete transport disk, though its radius exceeds 10. A stronger independent calculation prepared the raised order with a 47-node angular rule at 1,220 bits and applied the exact normal row at this nonreal tilt. Its centre is within 4.773×10^{-7} of the transported centre; its radius below 4.792×10^{-4} contains the entire transport disk. The unraised determinant and independent normal readout have larger errors than the two-wall scalar.

Omitting the nonconstant tilt preparation at this input misses the independent normal-row disk by more than 0.001838. Retaining only the final upper branch of the truncated preparation misses the physical scalar disk by more than 0.0001481. These controls use the specified finite preparations. No bound for the discarded preparation separately on either complex arc is needed for the real-fibre conclusions. The inverse-order computation fixes h and varies complex s across the disk.

Uniform accuracy as the rank-five order varies

Theorem 25.4 (a uniform two-crossing order disk). Fix $N = 5$, $s = -5$ and $|h - (5/4 + i/4)| \le 1/64$. The 46 spin blocks evaluated at the **input** h give all 56 physical compact coordinates and the Haar scalar at $z = 4/5, 2/5, 3/25$. At every rational complex input in this disk, a validated implementation returns each with absolute error less than 10^{-30}. The same truncation estimate applies to exact real or complex input components throughout the disk. It bounds the error at each input separately. The three-walled angular construction again passes the full physical combination at one wall into the next wall; the first is the exterior angular caustic $a = 5$. The two interior critical radii are $a = 3, 1$.

Proof. Use the six-component spinning equations, signed Mellin factors and physical weights already derived above. The closed rectangle of half-width $1/64$ about the indicated centre bounds the full order disk. Its imaginary parts are at least $15/64$, so all rational Mellin divisors stay away from zero and $|w_k| + |1 - w_k| \le \coth(15\pi/64) < 1.596$. The angular preparation is precisely the one for $s = -5$; this theorem only varies the order.

The four consecutive groups have $12, 29, 29, 27$ panels on a selected path. For each local transfer T_j and block, the usual Taylor recurrence with the entire rectangle as a complex interval argument, including its series tail, bounds $\|T_j\|_\infty$. Multiply $\max(1, \|T_j\|_\infty)$ along each arc, take the larger product on each wall, and multiply these four group bounds. Direct interval computation gives less than 5.968×10^{71} for every block. The receipt retains the products in groups of up to three panels. Including $\|E\|_\infty \|E^{-1}\|_\infty$ and all three connection norms gives $G < 3.634 \times 10^{73}$. The interval sum of absolute Mellin coefficients of each physical projection, including the maximal real-fibre prefactor when needed, is below $R = 2.842 \times 10^{11}$.

Take exterior cutoff $P = 700$. The preceding exterior-series estimate gives the common component tail $e_0 < 1.416 \times 10^{-259}$. The physical exterior source has infinity norm at most $B = 1.846 \times 10^{18}$ from $|10 - \sum w_j| \le 15$ and $\Re u > 0$ in all the used blocks. For a local polynomial of induced-norm error at most $\tau = 10^{-180}$ use the ordinary recurrence and its tail test. To see that it terminates uniformly, put $d = 2|\delta|$ on a step starting at x. On $|t| \le 2$, integration of the differential equation for the transfer with initial value I bounds its norm by e^L, where

$$L = \max_i \frac{d \sum_j \big(|(x\widetilde{A} + \widetilde{B})_{ij}| + d|\widetilde{A}_{ij}|\big)}{(|x| - d)(|x - \lambda_i| - d)}.$$

All denominator factors are positive by the panel construction. Evaluating this on all arcs and blocks gives $L < 92.884$. The table in the code uses the upper half paths and their conjugate geometries with the original complex order on both. Cauchy's inequality gives $\|V_n\|_\infty \le e^L 2^{-n}$. Also $\|G_{\mathrm{step}}\| + \|L_{\mathrm{step}}\| \le 2/5 + 1/25$ and $\|F\| + \|K\| \le L$. At index 832 the two-coefficient remainder test is below $\tau/4$ in exact arithmetic, with room for outward rounding.

To combine the errors, expand the three successive physical connections into eight path histories. In any one history the telescoping sum which replaces exact panels by their local polynomials costs at most $[(1 + \tau)^{97} - 1]$ times the majorant product. After the exterior error, connections, basis changes and final row are included, the total finite-polynomial truncation error is at most

$$RG\big(194\tau B + 2e_0\big) < 3.697 \times 10^{-75}.$$

The last value uses unrounded majorants in the record. This single bound applies also at the earlier outputs by the use of factors at least one. The phase weights and the Mellin insertions are evaluated at the true order; errors from their finite arithmetic are included in the interval evaluation of the finite expression.

For reproducible finite arithmetic, enclose the selected finite polynomial circuit in Arb, charge the above common analytic error once per returned coordinate, and repeat at doubled precision if any printed disk exceeds the requested tolerance. Every denominator on the computation path is nonzero; the exterior powers have a positive real base. The Taylor test passes with strict slack by index 832 in exact arithmetic. There are only finitely many choices of accepted truncation indices through that index. The roundoff enclosures of these finite circuits tend to zero as precision increases, including scalar cancellation and serialization, whose internal number of digits scales with precision. Final decimal centres are printed to 78 significant digits. Even at the largest output their serialization error is below 10^{-30}: the physical angular coordinates are bounded by $10^{2\Re(h+4)}$ and the scalar by $10^{2\Re h}(1 - (4/5)^2)^{-25}$ using Haar mass one for the signed Weyl density on the transformed angular torus. This

proves termination at each rational input and absolute accuracy on the disk. It gives a stopping rule, rather than a uniform bit-complexity claim.

Executed offset. At $h = 161/128 + 49i/192$, $s = -5$, the uniform-budget solver rebuilt all 46 blocks and their two paths at each wall. Its 1000-bit run took 126.93 seconds wall time, with 486.05 summed block seconds and 53,756 KiB peak worker RSS. At $z = 4/5, 2/5, 3/25$ the actual scalar disk radii were respectively below 5.245×10^{-66}, 4.173×10^{-75} and 3.698×10^{-75}. The corresponding maximum radii of the 56 coordinates were below 4.029×10^{-70}, 6.241×10^{-72} and 6.688×10^{-73}. The final scalar begins $2.29629003579543957124328 + 0.51160897071048498763327i$. An independent 700-bit, degree-53 Hermite integration of the original Haar determinant contains all three scalar disks; its final radius is below 1.675×10^{-4}. A second fresh 46-block propagation padded each transfer at every panel with its individual truncation bound. Its scalar disks contained all three uniform-budget disks, and each of its 168 state disks intersected its counterpart. At the last wall upper-only and lower-only scalar readouts in that run missed the physical result by more than 1.197×10^{-7} and 5.954×10^{-7}, respectively. Absolute errors and checks are archived at full precision. Variation in the tilt requires separate preparation estimates.

Outward rounding in the rank-five operator norm. Each row sum in the induced infinity norm is rounded to its upper endpoint before taking the maximum over rows. This also covers almost tied row sums. The preceding positive- and inverse-order transports, including the finite complex-tilt preparations, were cold-replayed with this convention in 289 spin blocks. On every block, all six complex coordinates of both branches and of the physical combination at each of the three exits agreed byte for byte with their archived intervals. Five reported intermediate arc tail diagnostics changed by at most 5.331×10^{-201}; all 15,606 complex boundary intervals and every exterior source tail agreed exactly. The replay on five workers took 85.74 seconds, with 424.40 aggregate CPU seconds and peak individual worker RSS of 31,344 KiB. The signed final-scalar and 56-coordinate bounds use the verified endpoint enclosures. All 46 order-region interval tables and both 46-block computations of Theorem 25.4 were also replayed with the tightened norm. The independent padded computation took 128.71 seconds.

Consecutive exceptional connections

Proposition 25.5 (order derivatives for a sequence of critical radii). Consider a finite sequence of k real critical radii for which Theorem 10.9 and regular intervening physical charts apply. At a fixed order e in the ordinary domain choose $0 < r < A$ so that the closed order disk of radius A stays in that domain and each phase denominator has no zeros there except possibly at e. Require the parameter-dependent incoming Haar fibre and the physical fibres after the successive crossings to be holomorphic on a neighborhood of this closed disk. Choose deformed connecting paths whose ordinary pencils are regular there. At every rank $N \geq 3$ and every regular exit radius $0 < z < 1$ off (10.9), Theorem 23.1A automatically supplies a globally polynomial, pole-free outgoing scalar row $\ell_{N,z}(h, s)$ through every normal-jet divisor on $\Re h > -1$, $s \in \mathbb{C}$; excluded radii in (10.9), chart regularity, and certified numerical norm bounds for $\ell_{N,z}$ remain separate obligations.

Suppose p of the k crossed walls have a connection zero at e. There is a pole-free transport of the full physical angular column across the sequence at every $|h - e| \leq r$. It uses two arcs per wall and at most $p + 1$ copies of the angular column on any one arc. In particular p can exceed one. This analytic assertion requires neither an integer exceptional order nor equality of the individual arcs there.

Proof. Let $u = h - e$, let $q_i = 1$ if the ith wall is exceptional at e and $q_i = 0$ otherwise, and put $a_{i,\pm} = u^{q_i}\omega_{i,\pm}(e + u)$. These scalar functions are holomorphic on the larger disk. Write $F_{i,\pm}$ for the two full chart transfers from the preceding connected fibre to the next one, including any regular connecting segment. Set $G_0 = W_{\mathrm{in}}$ and recursively form

$$G_i = a_{i,+}F_{i,+}G_{i-1} + a_{i,-}F_{i,-}G_{i-1}.$$

At nonzero u the physical connection applied successively gives $G_i(u) = u^{\sum_{j \leq i} q_j} W_i(u)$. Holomorphy extends this identity to the full disk. In particular the first p Taylor coefficients of G_k vanish on the true input. This compatibility is obtained on the *connected* state at each wall. It need not hold for an arbitrary branch at an interior stage.

For a germ H write $H_j = [u^j]H$ and $\mathcal{D}_p H(u) = (H(u) - \sum_{j<p} u^j H_j)/u^p$, with value H_p at zero. Transport the data $(H_0, \ldots, H_{p-1}, \mathcal{D}_p H)$ throughout. If a path generator is $B_e + uD$, the coefficient equations are $H_j' =$

$B_eH_j + DH_{j-1}$, with $H_{-1} = 0$, and $(\mathcal{D}_pH)' = (B_e + uD)\mathcal{D}_pH + DH_{p-1}$. Multiplication by a holomorphic scalar weight a uses ordinary truncated convolution and

$$\mathcal{D}_p(aH) = a(u)\mathcal{D}_pH(u) + \sum_{j=0}^{p-1} H_j\mathcal{D}_{p-j}a(u).$$

All derivatives here are of the source or of known weights and equations. The readout $\mathcal{D}_pG_k$ is precisely W_k. Low-order coefficients may instead be dropped by exact degree shifts after each exceptional wall, reducing the remaining order depth by one. The $p = 0$ case is ordinary transport.

For a certified error statement choose analytic finite approximants to each input, weight and transfer on $|u| \le A$. Let L_i bound the norm of the exact ith combined weighted map and d_i bound its approximation error there. With incoming norm at most M, analytic input error at most d_0, and empty products understood as one, the final numerator error on that disk is bounded by

$$E = d_0 \prod_i (L_i + d_i) + M \left[\prod_i (L_i + d_i) - \prod_i L_i \right].$$

This follows from the ordered-product difference and requires no mutual commutation. Cauchy's coefficient estimate gives an outgoing error at most $E/[A^p(1 - r/A)]$ in the divided data on $|u| \le r$. It applies to analytic truncation errors even when the approximate numerator has nonzero low-order coefficients. The finite arithmetic of the derivative algorithm is enclosed separately at the query. This proves an error-transfer law; its constants require evaluation on each proposed multiwall chart. □

As an illustration of possible multiplicity, rank seven has successive positive walls at $1/7, 3/7, 5/7$. At $e = 1/2$ the first and third phase denominators vanish while the middle one is regular. Here two order derivatives suffice for the chain under the stated chart and fibre hypotheses. The statement fixes the missing source information; it supplies no executed rank-seven certificate.

References

- NIST Digital Library of Mathematical Functions, Chapter 10, §§10.6, 10.9, 10.12, 10.17 and 10.22. Bessel function recurrences, integral representations, Laurent generating function, asymptotic expansions and Mellin integrals. https://dlmf.nist.gov/10.6 · https://dlmf.nist.gov/10.9.E1 · https://dlmf.nist.gov/10.12 · https://dlmf.nist.gov/10.17.E3 · https://dlmf.nist.gov/10.22.E43
- NIST Digital Library of Mathematical Functions, equation 15.4.20. Gauss summation at unit argument. https://dlmf.nist.gov/15.4.E20
- D. Bump and A. Gamburd, *On the averages of characteristic polynomials from classical groups*. The character orthogonality and Cauchy identities used in Section 23 are classical. https://arxiv.org/abs/math-ph/0502043
- L. Vinet and A. Zhedanov, *An algebraic treatment of the Askey biorthogonal polynomials on the unit circle*. The equal-parameter specialization supplies the monic polynomial input in Theorem 19.7. https://doi.org/10.1017/fms.2021.60
- T. Claeys, A. Its and I. Krasovsky, *Emergence of a singularity for Toeplitz determinants and Painlevé V*. Their emerging-singularity mass asymptotics provide an independent comparison for the zero-source limit. Our estimate for the marked complex measure uses the polynomial kernel. https://arxiv.org/abs/1004.3696
- N. Simm and F. Wei, *On moments of the derivative of CUE characteristic polynomials and the Riemann zeta function*, Journal of the London Mathematical Society 113 (2026), e70487. Theorem 1.2 and the source estimates are used in Section 11. https://doi.org/10.1112/jlms.70487
- J. Najnudel and F. Wei, *Complex Moments of the Derivative of the Riemann Zeta Function*, arXiv:2611.21551. https://arxiv.org/abs/2611.21551

- Alexander Grover, Francesco Mezzadri, and Nick Simm, *Higher order derivative moments of CUE characteristic polynomials and the Riemann zeta function*, arXiv:2604.03051 [math-ph, math.NT] (2026). Theorem 2.9 gives the finite integer determinant used in Section 12 and compared on the positive-integer diagonal in Section 19. https://arxiv.org/abs/2604.03051
- A. Borodin and A. Okounkov, *A Fredholm determinant formula for Toeplitz determinants.* E. L. Basor and H. Widom, *On a Toeplitz determinant identity of Borodin and Okounkov.* The tail Hankel factorization is used in Sections 15, 16 and 18. https://arxiv.org/abs/math/9907165 · https://arxiv.org/abs/math/9909010
- P. J. Forrester, S.-H. Li and A. K. Trinh, *Asymptotic correlations with corrections for the circular Jacobi β-ensemble.* This comparison concerns the first correction to the scaled correlation kernel at a circular spectral singularity. Section 16 treats the tilted planar derivative mark at positive depth. https://arxiv.org/abs/2008.13124
- P. J. Forrester and B.-J. Shen, *Expanding the Fourier Transform of the Scaled Circular Jacobi β Ensemble Density*, §§2.1–2.2. The precise scale and gauge are specified in Section 14. https://doi.org/10.1007/s10955-023-03171-x
- E. Dueñez, D. W. Farmer, S. Froehlich, C. P. Hughes, F. Mezzadri and T. Phan, *Roots of the derivative of the Riemann zeta function and of characteristic polynomials.* Related work on derivative zeros near the unit circle. The two-angle computation in Section 19 concerns the planar distribution of the value at a prescribed radius. https://arxiv.org/abs/1002.0372
- F. Ge, *On the logarithmic derivative of characteristic polynomials for random unitary matrices.* A mesoscopic central limit theorem for the untilted logarithmic derivative provides a comparison for Section 18. https://arxiv.org/abs/2211.14625
- T. Varga, *Christoffel Functions for Doubling Measures on Quasismooth Curves and Arcs*, Theorem 2.4. Section 14 applies the doubling-measure estimate with $p = 2$ on the unit circle. https://doi.org/10.1007/s10474-013-0306-z
- T. Assiotis, J. P. Keating and J. Warren, *On the Joint Moments of the Characteristic Polynomials of Random Unitary Matrices.* Circle trace law, moment bounds and Barnes normalization in Section 17. https://doi.org/10.1093/imrn/rnab336
- T. Assiotis, B. Bedert, M. A. Gunes and A. Soor, *On a distinguished family of random variables and Painlevé equations.* Circle characteristic function in Section 17. https://arxiv.org/abs/2009.04760
- E. S. Meckes, *The Random Matrix Theory of the Classical Compact Groups*, Cambridge University Press (2019), Theorem 3.1, Weyl integration on $U(N)$. https://case.edu/artsci/math/mwmeckes/elizabeth/Haar_book.pdf
- A. Vasy, *Stationary Phase Lemma*, Math 205C notes, Stanford University. We use the nondegenerate, smooth-amplitude expansion with a remainder at each finite order. https://math.stanford.edu/~andras/205C-2.pdf
- NIST Digital Library of Mathematical Functions, Kummer transformation, Euler integral and large-argument expansion, https://dlmf.nist.gov/13.2.E39, https://dlmf.nist.gov/13.4.E1, https://dlmf.nist.gov/13.7.E2.
- NIST Digital Library of Mathematical Functions, interpolation and divided differences, Gaussian quadrature, and exponential generating functions for modified Bessel functions. The comparison and weighted physical bounds in Section 21 are derived there from the angular integral. https://dlmf.nist.gov/3.3, https://dlmf.nist.gov/3.5, https://dlmf.nist.gov/10.35.

Continuation sources and verification provenance

The public verification ZIP contains the scripts, inputs, and saved certificates described in its README. It supports the documented replay checks. Some paths and archive names in entries [1]–[19] refer to historical working materials cited for provenance and are not included in the public ZIP.

[1] Supplied *HaarCritical*, 17 November 2026 working edition, especially Propositions 3.2–3.3, 4.3, Lemmas 4.4–4.5, Corollary 4.6, Proposition 5.2 and Theorem 21.25; verification, evaluator, restart, results and coverage archives. Original copies and SHA-256 provenance are retained in the historical continuation package.

[2] Supplied HaarSpectral predecessor, preserved spectral/native and outer/solver sources and their finite-arithmetic contracts, as packaged in the historical HaarCritical verification materials.

[3] Jeremy Rodgers, *Shadow_Research_1*, active development edition 1; Reflective Mathematics Research Handbook; Combined Protocol 0.2-dev.1; Boundary–Property Key 3.4-dev.1. Used as research method, not as a mathematical axiom.

[4] NIST Digital Library of Mathematical Functions, §10.17, equations 10.17.1–10.17.6, Hankel coefficients and phases. https://dlmf.nist.gov/10.17. The explicit Volterra proof used here is included in Lemma R4.2.

[5] Same working edition as [1] (Jeremy Rodgers research programme, 17 November 2026), especially Sections 2–5, 10.2D–F, 21 and 22, together with the preserved HaarSpectral dependency.

[6] *HaarCritical: A validated rank-three scalar readout through the critical radius*, 17 November 2026 working edition, with its verified source package, restart, uniform theorem and fifteen-case promotion ledger. This continuation imports its Bessel Volterra lemma, preparation-return method, original finite source and Mellin image contracts without modifying their sealed implementations.

[7] Same research protocol as [3]; active entry and version authority govern research conduct.

[8] *HaarCritical Centre-to-Critical verification records*, 18 November 2026: the proof documents, exact inputs, outward inequality receipts, seventeen-case certification ledger, independent source and readout audits, preserved failures and executable interface in the historical companion verification archive. Each computational claim is scoped to its recorded arithmetic and dependency contracts.

[9] Same working edition as [1] (baseline/HaarCritical.md), especially Proposition 9.4, Theorems 9.5 and 21.25, and Section 22, with accompanying verification and evaluator sources.

[10] HaarCritical: Odd-Rank Small-Radius Completion, 18 November 2026. Prior report, verification package, restart and coverage ledger; unchanged dependencies are identified by hash in the historical companion archive.

[11] HaarCritical rank-three critical-radius, centre-to-critical and complete-radius investigations, 17–18 November 2026. Retained-population, Nicholson/Green remainder, Abel readout and preparation-return proofs.

[12] NIST Digital Library of Mathematical Functions, Equation 10.22.43 (Bessel Mellin integral) and Section 10.9 (integral representations).

[13] Same research protocol as [3], retained in the historical verification materials.

[14] HaarCritical Joint Order–Radius Zero Atlas, inherited report and verification package; active joint_order_atlas_investigation/review/joint-review-v2-final.json.

[15] Inherited finite physical-source arithmetic contract, unified_investigation/arithmetic/SOURCE_ARITHMETIC.md, with finite_source_exact.py and mixed_exact.py.

[16] Inherited arithmetic norm correction, unified_investigation/arithmetic/ARITHMETIC_NORM_ADDENDUM.md.

[17] New original-source bounds and independent reconstruction, analysis/EXPANDED_PHYSICAL_RESOURCES.md, analysis/expanded-resources-v2-768.json, and independent/expanded-resources-v2-independent-1024.json.

[18] New allocation theorem and execution, independent/NEAR_ZERO_RESOURCE_THEOREM.md and independent/precision_policy.py.

[19] New source arithmetic, physical challenges, and canonical admission records in independent/; original immutable certification ledger in release/final/ and portable child ledger in release/final-v2/ of the historical companion verification archive.